University of Wisconsin Milwaukee
UWM Digital Commons

Theses and Dissertations

5-1-2019

Design and Synthesis of Achiral and Chiral Imidazodiazepine (IMDZ) GABA(A)R Subtype Selective Ligands for the Treatment of CNS Disorders, as well as Asthma

Guanguan Li
University of Wisconsin-Milwaukee

Follow this and additional works at: https://dc.uwm.edu/etd

Part of the Biochemistry Commons, and the Chemistry Commons

Recommended Citation

Li, Guanguan, "Design and Synthesis of Achiral and Chiral Imidazodiazepine (IMDZ) GABA(A)R Subtype Selective Ligands for the Treatment of CNS Disorders, as well as Asthma" (2019). *Theses and Dissertations*. 2093.
https://dc.uwm.edu/etd/2093

This Dissertation is brought to you for free and open access by UWM Digital Commons. It has been accepted for inclusion in Theses and Dissertations by an authorized administrator of UWM Digital Commons. For more information, please contact open-access@uwm.edu.

DESIGN AND SYNTHESIS OF ACHIRAL AND CHIRAL IMIDAZODIAZEPINE (IMDZ) GABA(A)R SUBTYPE SELECTIVE LIGANDS FOR THE TREATMENT OF CNS DISORDERS, AS WELL AS ASTHMA

by

Guanguan Li

A Dissertation Submitted in

Partial Fulfillment of the

Requirements for the Degree of

Doctor of Philosophy

in Chemistry

at

The University of Wisconsin-Milwaukee

May 2019

ABSTRACT

DESIGN AND SYNTHESIS OF ACHIRAL AND CHIRAL IMIDAZODIAZEPINE (IMDZ) GABA(A)R SUBTYPE SELECTIVE LIGANDS FOR THE TREATMENT OF CNS DISORDERS, AS WELL AS ASTHMA

by

Guanguan Li

The University of Wisconsin-Milwaukee, 2019
Under the Supervision of Professor James M. Cook

Gamma-aminobutyric acid type A receptors ($GABA_AR$) are transmembrane pentameric ligand-gated chloride ion channels that respond to GABA, the major inhibitory neurotransmitter in the central nervous systems (CNS). The benzodiazepines (BZDs) bind at the extracellular interface of the α+γ2-subunits of $GABA_AR$. The binding of ligands at different subunits of $GABA_A$ receptors specifically at $\alpha_{1\text{-}6}\beta_{2/3}\gamma_2$ ion channels, can affect a wide variety of brain functions. The α1-subtype selective ion channels of $GABA_ARs$ are involved in the sedative, ataxic, amnesic, anticonvulsant and addictive effects, which should be avoided, with the exception of the anticonvulsant effects, when designing ligands for this BZ allosteric modulatory site. The α2/3-containing $GABA_ARs$ have been implicated by many, in the anxiolytic, anticonvulsant, and antinociceptive activities. At higher doses, muscle relaxation may be mediated by interaction at α3 subtypes. It is known that α5-containing $GABA_ARs$ are involved in cognition, as well as learning and memory processes. The disruption of GABA activity at α5 subtypes on $GABA_AR$ plays a role in the pathophysiology of CNS disorders such as schizophrenia, major

depressive disorder (MDD), bipolar disorder and certain anxiety disorders such as OCD. The α5 subtypes in the lung play a major role in potential new treatments for asthma.

Based on the "privileged imidazodiazepine (IMZD) structures" derived from the unified pharmacophore model of Milwaukee, the design, synthesis and biological activities of more than 120 novel chiral $GABA_AR$ α2/α3/α5 or α5 subtype selective imidazodiazepines (IMDZs) related to SH-053-2'F-*R*-CH_3, and its enantiomer SH-053-2'F-*S*-CH_3, as well as the key achiral ligand Hz-166 are described. The goal of this research is to develop new analogs with improved metabolic stability that also retain the desired biological properties with little or no side effects for the treatment of CNS disorders, as well as asthma.

Several compounds from the α5 subtype selective group are anxiolytic, antidepressant, as well as pro-cognitive, and are targeted toward the treatment of major depressive disorders. About 20 grams of one lead compound **(**GL-II-73), and more than 80 analogs were designed, synthesized and evaluated. The α5 selective chiral lead amide, GL-II-73, looks very good in rodent models for the treatment of depression. It exhibited an excellent pharmacokinetic profile, as well as anti-depressant and anxiolytic activities in mice. This antidepressant effect has been realized with no side effects such as sedation nor motor impairment that benzodiazepine drugs would normally effect. In addition, the much sought after improved cognitive effects were clear in mice; this is a key in treating depression or schizophrenia. Examination of the data in the most recent study indicated that the administration of a single dose of GL-II-73 within 30 minutes could reverse the stress-induced or normal aging-related working memory deficits in old mice back up to 80-90 %, which is almost at the level of a young mouse. Whereas the old mice or stressed young mice will normally perform at about a level of 50-60 %. Furthermore, the brain cells, which had shrunk in older mice associated with aging, grew back (dendrites and spines) to a level that is similar to the

young mice. This is extremely exciting and occurred after two months of the administration of GL-II-73 to the old mice in their drinking water. These results were presented by our collaborator, Dr. Etienne Sibille in an interview with the BBC, but also resulted in three papers and two patents. It is hoped the CAMH group of Sibille can push this project forward to human trials within two years as proposed. Additional research on these key compounds by several groups is ongoing. One can imagine the use of GL-II-73 or analogs in other neurodegenerative diseases of the CNS.

After evaluation of a series of novel IMDZs that were α5 subtype selective for the treatment of asthma, one compound MIDD0301 (originally named GL-II-93) was found to be orally active and also as an inhalant in rodent asthma models. Ligand MIDD0301 was active in the airway smooth muscle (ASM) relaxation assay, in the airway hyper-responsiveness model, in the human and guinea pig tracheal bath assays. Moreover, it does not induce any immunotoxicity in animal models. Taken together this data suggests that this novel ligand can be a potential candidate for the treatment of asthma. About 50 grams of the ligand has been synthesized in good yield to support all the different biological assays from our collaborators. Furthermore, the large scale total synthesis of MIDD0301 was presented to the Alcami Corporation for a proposed kilogram scale synthesis of GMP material for further research on toxicity and safety. This research has resulted in three new publications over the last year. This compound provided some of the impetus to found a new company, Panthergenics, to try to get it through the FDA. Dr. Arnold and Dr. Stafford founded the company via UW-Milwaukee.

In regard to the design of new α2/3 subtype selective agents to treat anxiety disorders, neuropathic pain and epilepsy, an improved large scale synthesis of Hz-166, MP-III-080, and KRM-II-81 was executed. These ligands are anxiolytic, anticonvulsant and antinociceptive agents. They were prepared under milder conditions and with much improved yields. Moreover, an

alternative reduction process, which was developed for the synthesis of the key aldehyde intermediate from the ethyl ester, was optimized. This new process overcame the long-standing problem of imine reduction in good yield. These methods can be employed for larger scale reactions. In addition, there is no need for column chromatography for most of the compounds, which provided a much more practical route. With the improved synthesis, large quantities of these three α2/3-subtype selective $GABA_ARs$ PAMs, which exhibited anxiolytic, anticonvulsant and antinociceptive effects in many animal tests, can be supplied with high-efficiency and quality to our collaborators. The large-scale synthesis and the analog research will permit investigation of ADME toxicity and for other behavior assays including those in primates. Studies in animal models for anxiety and epilepsy, as well as for neuropathic pain require gram quantities of compounds, which can now be provided. This will also permit the execution of long-term safety studies in order to approach the FDA.

TO

my father Mr. Qing Li,

my mother Mrs. Jianping Du,

and my family

TABLE OF CONTENTS

LIST OF FIGURES xxiii
LIST OF TABLES lx
LIST OF SCHEMES lxiv
LIST OF ABBREVIATIONS lxvi
Chapter 1. Introduction 1
1.1. The $GABA_A$ receptors 1
1.2. Benzodiazepines (BZD) 4
1.3. Modulation of BZDs on the Pharmacological Effects of $GABA_AR$ 7
1.4. Molecular Modeling – Pharmacophore Model 11
1.5. Research Objectives 18
Chapter 2. Design and Synthesis of Chiral α2/α3/α5 or α5 Subtype Selective Ligands and Their Use for the Treatment of Schizophrenia, Major Depressive Disorder as well as Asthma 19
2.1. Introduction of Chirality in Drug Design 19
2.2. Schizophrenia and Major Depressive Disorder (MDD) 22
2.2.1. Introduction 22
2.2.2. Background 23
2.2.3. Chemistry and Results 25
2.2.3.1. Comparison of Enantiomers 25
2.2.3.1.1. Synthesis of SH-053-2'F-*R*-CH_3 (1) and SH-053-2'F-*S*-CH_3 (2) 25
2.2.3.1.2. Biology on the *R* and *S* Enantiomers 29
2.2.3.2. Analogs of the *S*-isomer 32
2.2.3.2.1. Synthesis of Analogs of SH-053-2'F-*S*-CH_3 (2) 32
2.2.3.2.2. Biological Activity: Metabolism, Cytotoxicity and Rotarod Studies 39
2.2.3.3. Analogs of the R-isomer 46
2.2.3.3.1. Medicinal Chemistry Strategy of Analog Search in the (*R*)-CH_3 Series 47
2.2.3.3.2. A Study of the Biology of MP-III-022, a Potent Analog of SH-053-2'F-*R*-CH_3 (1) 52
2.2.3.3.3. Synthesis of the Analogs of SH-053-2'F-*R*-CH_3 (1) 55
2.2.3.4. Biological Screening for the Selection of Lead Compounds 66

2.2.3.4.1. Study of Metabolism 66
2.2.3.4.1.1. *In Vitro* Metabolic Stability in HLM and MLM 66
2.2.3.4.1.2. Proposed Possible Metabolites 70
2.2.3.4.1.3. P450 Inhibition 73
2.2.3.4.2. Cytotoxicity Study 74
2.2.3.4.3. Evaluation of the CNS Effects 79
2.2.3.4.3.1. Rotarod Test *via* Oral Gavage 79
2.2.3.4.3.2. Rotarod Test *via* I.P. Administration 83
2.2.3.4.3.3. Spontaneous Locomotor Activity 95
2.2.3.4.4. Receptor Binding Studies 100
2.2.3.4.5. Potentiation at $GABA_ARs$ 109
2.2.3.4.6. Studies of Pharmacokinetics 115
2.2.3.5. Schizophrenia 120
2.2.3.5.1. Neuroinflammatory Effects and Schizophrenia 120
2.2.3.5.2. Behavioral Studies in an Animal Models of Schizophrenia 126
2.2.3.6. Depression 132
2.2.3.6.1. Elevated Plus Maze to Determine Anxiolytic Effects 132
2.2.3.6.2. The Forced Swim Test to Assess Antidepressant Properties of the Ligands 134
2.2.3.6.3. Evaluation of Spatial Working Memory by the Y-maze Test 137
2.2.3.6.3.1. Reversal of Stress-Induced Working Memory Deficits 138
2.2.3.6.3.2. Reversal of Age-Induced Working Memory Deficits in the Y-maze Task 147
2.2.3.6.3.3. The Effect of Blockade of the α1 and α5 Bz/GABA(A) Subtypes 150
2.2.3.6.4. The Lead Compound GL-II-73 on the Study of the Effects of Morphology of Mice Brain (CONFIDENTIAL UNPUBLISHED DATA) 152
2.2.4. Discussion 158
2.2.5. Conclusion 168
2.2.6. Methods 170
2.2.6.1. Catalepsy Assay (Nicholas J. Raddatz and Dr. David A. Baker, Marquette University) 170

2.2.6.2. Prepulse Inhibition (Nicholas J. Raddatz and Dr. David A. Baker, Marquette University) 171

2.2.6.3. Seizure Protection in the 6 Hz Electroshock Assay (ETSP) 172

2.2.6.4. Ataxic Assessment in the Rotorod Assay (ETSP) 173

2.2.6.5. Microsomal Stability Assay (Revathi Kodali, UWM) 173

2.2.6.6. Cytotoxicity Assay (Dr. Michael R. Stephen, UWM) 174

2.2.6.7. Rotorod Assay via Oral Gavage (Nick Zahn, and Alec Huber, UWM) . 175

2.2.6.8. Rotorod Assay via I.P. Administration (Dr. Aleksandra Vidojevic and Dr. Miroslav Savic, University of Belgrade) 175

2.2.6.9. Spontaneous Locomotor Activity (Dr. Aleksandra Vidojevic and Dr. Miroslav Savic, University of Belgrade) 176

2.2.6.10. Grip Strength (Dr. Aleksandra Vidojevic and Dr. Miroslav Savic, University of Belgrade) 176

2.2.6.11. Binding Studies (PDSP) 177

2.2.6.12. KOR Stimulation Response Test (Dr. Petra Scholze, University of Vienna) 179

2.2.6.13. Electrophysiological Recordings (Dr. Fisher, University of South Carolina School of Medicine) 179

2.2.6.14. Pharmacokinetic Studies (Dr. Aleksandra Vidojevic and Dr. Miroslav Savic, University of Belgrade) 180

2.2.6.15. Griess Assay and Toxicity Assay (Amanda Nieman, UWM) 182

2.2.6.16. Anti-Schizophrenic-like Behavioral Study Induced by MK-801 (Dr. Aleksandra Vidojevic and Dr. Miroslav Savic, University of Belgrade) 183

2.2.6.17. Anxiety-Like Behaviors in the Elevated Plus Maze (Dr. Thomas D. Prevot and Dr. Etienne Sibille, CAMH) 184

2.2.6.18. Antidepressant Predictability via Forced Swim Test (Dr. Thomas D. Prevot and Dr. Etienne Sibille, CAMH) 184

2.2.6.19. Cognitive Flexibility via Y-Maze Test (Dr. Thomas D. Prevot and Dr. Etienne Sibille, CAMH) 185

2.2.6.20. A Golgi-Cox Study (Dr. Thomas D. Prevot and Dr. Etienne Sibille, CAMH) 187

2.2.7. Experimental 191

2.2.7.1. *Tert*-Butyl-(*R*)-(1-((4-bromo-2-(2-fluorobenzoyl)phenyl)amino)-1-oxoprop an-2-yl) carbamate (4) 191

2.2.7.2. (*R*)-7-Bromo-5-(2-fluorophenyl)-3-methyl-1,3-dihydro-2*H*-benzo[*e*][1,4] diazepin-2-one (5) 193

2.2.7.3. Ethyl (*R*)-8-bromo-6-(2-fluorophenyl)-4-methyl-4*H*-benzo[*f*]imidazo[1,5-*a*] [1,4] diazepine-3-carboxylate (SH-I-047, 6) 194

2.2.7.4. Ethyl (*R*)-6-(2-fluorophenyl)-4-methyl-8-((trimethylsilyl)ethynyl)-4*H*-benz o[*f*]imi dazo[1,5-*a*][1,4]diazepine-3-carboxylate (7) 195

2.2.7.5. Ethyl (*R*)-6-(2-fluorophenyl)-4-methyl-8-((triisopropylsilyl)ethynyl)-4*H*-be nzo[*f*] imidazo[1,5-*a*][1,4]diazepine-3-carboxylate (8) 196

2.2.7.6. Ethyl (*R*)-8-ethynyl-6-(2-fluorophenyl)-4-methyl-4*H*-benzo[*f*]imidazo[1,5*a*] [1,4] diazepine-3-carboxylate (SH-053-2'F-*R*-CH_3, 1) 197

2.2.7.7. *Tert*-Butyl (*S*)-(1-((4-bromo-2-(2-fluorobenzoyl)phenyl)amino)-1-oxopropa n-2-yl) carbamate (9) 199

2.2.7.8. (*S*)-7-Bromo-5-(2-fluorophenyl)-3-methyl-1,3-dihydro-2*H*-benzo[*e*][1,4]diazepin-2-one (SH-I-048A, 10) 199

2.2.7.9. Ethyl (*S*)-8-bromo-6-(2-fluorophenyl)-4-methyl-4*H*-benzo[*f*]imidazo[1,5-*a*] [1,4] diazepine-3-carboxylate (SH-I-48B, 11) 200

2.2.7.10. Ethyl (*S*)-6-(2-fluorophenyl)-4-methyl-8-((trimethylsilyl)ethynyl)-4*H*-benz o[*f*]imi dazo[1,5-*a*][1,4]diazepine-3-carboxylate (SH-I-055, 12) 201

2.2.7.11. Ethyl (*S*)-8-ethynyl-6-(2-fluorophenyl)-4-methyl-4*H*-benzo[*f*]imidazo[1,5-*a*] [1,4] diazepine-3-carboxylate (SH-053-2'F-*S*-CH_3, 2) 202

2.2.7.12. (*S*)-Ethyl-8-cyclopropyl-6-(2-fluorophenyl)-4-methyl-4*H*-benzo[*f*]imidazo[1,5-*a*][1,4]diazepine-3-carboxylate (GL-I-78, 13) 203

2.2.7.13. (*S*)-Methyl-8-bromo-6-(2-fluorophenyl)-4-methyl-4*H*-benzo[*f*]imidazo[1,5-*a*][1,4]diazepine-3-carboxylate (MP-III-059, 14) 204

2.2.7.14. (*S*)-Methyl-8-ethynyl-6-(2-fluorophenyl)-4-methyl-4*H*-benzo[*f*]imidazo[1,5-*a*][1,4]diazepine-3-carboxylate (MP-III-021, 16) 206

2.2.7.15. (*S*)-Propyl-8-ethynyl-6-(2-fluorophenyl)-4-methyl-4*H*-benzo[*f*]imidazo[1,5-*a*][1,4]diazepine-3-carboxylate (GL-I-32, 17) 207

2.2.7.16. (*S*)-Isopropyl-8-ethynyl-6-(2-fluorophenyl)-4-methyl-4*H*-benzo[*f*]imidazo[1,5-*a*][1,4]diazepine-3-carboxylate (GL-I-31, 18) 208

2.2.7.17. (*S*)-*tert*-Butyl-8-ethynyl-6-(2-fluorophenyl)-4-methyl-4*H*-benzo[*f*]imidazo[1,5-*a*][1,4]diazepine-3-carboxylate (GL-I-30, 19) 209

2.2.7.18. (*S*)-*tert*-Pentyl-8-ethynyl-6-(2-fluorophenyl)-4-methyl-4*H*-benzo[*f*]imidazo[1,5-*a*][1,4]diazepine-3-carboxylate (GL-I-33, 20) 210

2.2.7.19. (*S*)-8-Ethynyl-6-(2-fluorophenyl)-4-methyl-4*H*-benzo[*f*]imidazo[1,5-*a*][1,4]diazepine-3-carboxylic acid (SH-05 3-2'F-*S*-CH_3-acid, 23) 211

2.2.7.20. (*S*)-2,2,2-Trifluoroethyl-8-ethynyl-6-(2-fluorophenyl)-4-methyl-4*H*-benzo[*f*]imidazo[1,5-*a*][1,4]diazepine-3-carboxylate (GL-I-36, 21) 213

2.2.7.21. (*S*)-Cyclopropyl-8-ethynyl-6-(2-fluorophenyl)-4-methyl-4*H*-benzo[*f*]imidazo[1,5-*a*][1,4]diazepine-3-carboxylate (GL-I-38, 22) 214

2.2.7.22. (*S*)-S-Ethyl-8-ethynyl-6-(2-fluorophenyl)-4-methyl-4*H*-benzo[*f*]imidazo[1,5-*a*][1,4]diazepine-3-carbothioate (GL-I-77, 24) 215

2.2.7.23. (*S*)-8-Ethynyl-6-(2-fluorophenyl)-N,4-dimethyl-4*H*-benzo[*f*]imidazo[1,5-*a*][1,4]diazepine-3-carboxamide (MP-III-023, 25) 216

2.2.7.24. (*S*)-N-Ethyl-8-ethynyl-6-(2-fluorophenyl)-4-methyl-4*H*-benzo[*f*]imidazo[1,5-*a*][1,4]diazepine-3-carboxamide (GL-I-43, 26) 217

2.2.7.25. (*S*)-N-Cyclopropyl-8-ethynyl-6-(2-fluorophenyl)-4-methyl-4*H*-benzo[*f*]imidazo[1,5-*a*][1,4]diazepine-3-carboxamide (GL-I-55, 27) 218

2.2.7.26. (*S*)-8-Ethynyl-6-(2-fluorophenyl)-N-isopropyl-4-methyl-4*H*-benzo[*f*]imidazo[1,5-*a*][1,4]diazepine-3-carboxamide (GL-I-57, 28) 218

2.2.7.27. (*S*)-N-(*tert*-Butyl)-8-ethynyl-6-(2-fluorophenyl)-4-methyl-4*H*-benzo[*f*]imidazo[1,5-*a*][1,4]diazepine-3-carbox- amide (GL-I-41, 29) 219

2.2.7.28. (*S*)-8-Ethynyl-6-(2-fluorophenyl)-N,N,4-trimethyl-4*H*-benzo[*f*]imidazo[1,5-*a*][1,4]diazepine-3-carboxamide (GL-I-54, 30) 220

2.2.7.29. (*S*)-5-(8-Ethynyl-6-(2-fluorophenyl)-4-methyl-4*H*-benzo[*f*]imidazo[1,5-*a*][1,4]diazepin-3-yl)-3-methyl-1,2,4-oxadiazole (GL-I-65, 31) 222

2.2.7.30. (*S*)-3-Ethyl-5-(8-ethynyl-6-(2-fluorophenyl)-4-methyl-4*H*-benzo[*f*]imidazo[1,5-*a*][1,4]diazepin-3-yl)-1,2,4-oxadiazole (GL-I-66, 32) 223

2.2.7.31. (*S*)-5-(8-Ethynyl-6-(2-fluorophenyl)-4-methyl-4*H*-benzo[*f*]imidazo[1,5-*a*][1,4]diazepin-3-yl)-3-isopropyl-1,2,4-oxadiazole (GL-I-81, 33) 224

2.2.7.32. (*S*)-8-Ethynyl-6-(2-fluorophenyl)-4-methyl-4*H*-benzo[*f*]imidazo[1,5-*a*][1,4]diazepine-3-carbonitrile (MP-III-018.A, 34) 224

2.2.7.33. (*R*)-8-Ethynyl-6-(2-fluorophenyl)-N,4-dimethyl-4*H*-benzo[*f*]imidazo[1,5-*a*][1,4]diazepine-3-carboxamide (MP-III-022, 35) 226

2.2.7.34. (*R*)-8-Ethynyl-6-(2-fluorophenyl)-4-methyl-4*H*-benzo[*f*]imidazo[1,5-*a*][1,4]diazepine-3-carboxylic acid. (SH-053-2'F-*R*-CH_3-acid, 68) 227

2.2.7.35. (*R*)-8-Ethynyl-6-(2-fluorophenyl)-*N*,*N*,4-trimethyl-4*H*-benzo[*f*]imidazo[1,5-*a*][1,4]diazepine-3-carboxam (GL-II-73, 36) 228

2.2.7.36. (*R*)-*N*-Ethyl-8-ethynyl-6-(2-fluorophenyl)-4-methyl-4*H*-benzo[*f*]imidazo[1,5-*a*][1,4]diazepine-3-carboxamide (GL-II-74, 37) 229

2.2.7.37. (*R*)-*N*-Cyclopropyl-8-ethynyl-6-(2-fluorophenyl)-4-methyl-4*H*-benzo[*f*]imidazo [1,5-*a*][1,4]diazepine-3-carboxamide (GL-II-75, 38) 229

2.2.7.38. (*R*)-8-Ethynyl-6-(2-fluorophenyl)-*N*-isopropyl-4-methyl-4*H*-benzo[*f*] imidazo[1,5-*a*][1,4]diazepine-3-carboxamide (GL-III-66, 39) 230

2.2.7.39. (*R*)-(8-Ethynyl-6-(2-fluorophenyl)-4-methyl-4*H*-benzo[*f*]imidazo[1,5-*a*][1,4] diazepin-3-yl)(pyrrolidin-1-yl)methanone (GL-II-76, 40) 231

2.2.7.40. (*R*)-8-Ethynyl-6-(2-fluorophenyl)-*N*,4-dimethyl-4*H*-benzo[*f*]imidazo[1,5-*a*][1,4] diazepine-3-carbothioamide (GL-III-84, 41) 233

2.2.7.41. (*R*)-8-Ethynyl-6-(2-fluorophenyl)-*N*,*N*,4-trimethyl-4*H*-benzo[*f*]imidazo[1,5-*a*][1,4] diazepine-3-carbothioamide (GL-III-85, 42) 234

2.2.7.42. (*R*)-*N*-Ethyl-8-ethynyl-6-(2-fluorophenyl)-4-methyl-4*H*-benzo[*f*]imidazo[1,5-*a*] [1,4]diazepine-3-carbothioamide (GL-III-86, 43) 235

2.2.7.43. (*R*)-*N*-Cyclopropyl-8-ethynyl-6-(2-fluorophenyl)-4-methyl-4*H*-benzo[*f*]imidazo [1,5-*a*][1,4]diazepine-3-carbothioamide (GL-III-87, 44) 235

2.2.7.44. (*R*)-8-Bromo-6-(2-fluorophenyl)-*N*,*N*,4-trimethyl-4*H*-benzo[*f*]imidazo[1,5-*a*][1,4]diazepine-3-carboxamide (GL-III-69, 45) 236

2.2.7.45. (*R*)-8-Bromo-*N*-ethyl-6-(2-fluorophenyl)-4-methyl-4*H*-benzo[*f*]imidazo[1,5-*a*][1,4]diazepine-3-carboxamide (GL-III-67, 46) 237

2.2.7.46. (*R*)-8-Cyclopropyl-6-(2-fluorophenyl)-*N*,*N*,4-trimethyl-4*H*-benzo[*f*]imidazo[1,5-*a*][1,4]diazepine-3-carboxamide (GL-III-70, 47) 238

2.2.7.47. (*R*)-8-Cyclopropyl-*N*-ethyl-6-(2-fluorophenyl)-4-methyl-4*H*-benzo[*f*]imidazo[1,5-*a*][1,4]diazepine-3-carboxamide (GL-III-68, 48) 239

2.2.7.48. 8-Bromo-6-(2-fluorophenyl)-*N*-methyl-4*H*-benzo[*f*]imidazo[1,5-*a*][1,4]diazepine-3-carboxamide (RV-II-04, 49) 240

2.2.7.49. (*R*)-*Tert*-Butyl(1-((4-bromo-2-picolinoylphenyl)amino)-1-oxopropan-2-yl)carb amate (GL-II-04, 71) 241

2.2.7.50. (*R*)-7-Bromo-3-methyl-5-(pyridin-2-yl)-1*H*-benzo[*e*][1,4]diazepin-2(3*H*)-one (GL-II-05, 72) 242

2.2.7.51. (*R*)-Ethyl 8-bromo-4-methyl-6-(pyridin-2-yl)-4*H*-benzo[*f*]imidazo[1,5-*a*][1, 4]diazepine-3-carboxylate (GL-II-06, 73) 243

2.2.7.52. (*R*)-Ethyl 4-methyl-6-(pyridin-2-yl)-8-((trimethylsilyl)ethynyl)-4*H*-benzo[*f*] imidazo[1,5-*a*][1,4]diazepine-3-carboxylate (GL-II-18, 74) 244

2.2.7.53. (*R*)-Ethyl 8-ethynyl-4-methyl-6-(pyridin-2-yl)-4*H*-benzo[*f*]imidazo[1,5-*a*][1, 4]dia zepine-3-carboxylate (GL-II-19-2'N-*R*-CH_3, 75) 245

2.2.7.54. (*R*)-8-Ethynyl-*N*,4-dimethyl-6-(pyridin-2-yl)-4*H*-benzo[*f*]imidazo[1,5-*a*][1,4] diazepine-3-carboxamide (GL-II-31, 50) 246

2.2.7.55. (*R*)-5-(8-Ethynyl-4-methyl-6-(pyridin-2-yl)-4*H*-benzo[*f*]imidazo[1,5-*a*] [1,4]diaze pin-3-yl)-3-methyl-1,2,4-oxadiazole (GL-II-33, 51) 247

2.2.7.56. 5-(8-Ethynyl-6-(2-fluorophenyl)-4*H*-benzo[*f*]imidazo[1,5-*a*][1,4]diazepin-3-yl)-3-methyl-1,2,4-oxadiazole (GL-III-23, 52) 248

2.2.7.57. (R)-5-(8-Bromo-4-methyl-6-(pyridin-2-yl)-4*H*-benzo[*f*]imidazo[1,5-*a*][1,4] diazepin-3-yl)-3-methyl-1,2,4-oxadiazole (GL-II-54, 53)..... 249

2.2.7.58. (*R*)-5-(8-Cyclopropyl-4-methyl-6-(pyridin-2-yl)-4*H*-benzo[*f*]imidazo[1,5-*a*][1,4] diazepin-3-yl)-3-methyl-1,2,4-oxadiazole (GL-III-64, 54) 250

2.2.7.59. (*R*)-5-(8-Ethynyl-6-(2-fluorophenyl)-4-methyl-4*H*-benzo[*f*]imidazo[1,5-*a*][1,4] diazepin-3-yl)-3-isopropyl-1,2,4-oxadiazole (MP-IV-010, 57)..... 251

2.2.7.60. (*R*)-5-(8-Bromo-6-(2-fluorophenyl)-4-methyl-4*H*-benzo[*f*]imidazo[1,5-*a*][1,4] diazepin-3-yl)-3-methyl-1,2,4-oxadiazole (GL-III-60, 58) 252

2.2.7.61. (*R*)-5-(8-Bromo-6-(2-fluorophenyl)-4-methyl-4*H*-benzo[*f*]imidazo[1,5-*a*][1,4] diazepin-3-yl)-3-ethyl-1,2,4-oxadiazole (GL-III-98, 59) 253

2.2.7.62. (*R*)-5-(8-Bromo-6-(2-fluorophenyl)-4-methyl-4*H*-benzo[*f*]imidazo[1,5-*a*][1,4] diazepin-3-yl)-3-isopropyl-1,2,4-oxadiazole (GL-IV-01, 60) 254

2.2.7.63. (*R*)-5-(8-Cyclopropyl-6-(2-fluorophenyl)-4-methyl-4*H*-benzo[*f*]imidazo [1,5-*a*][1,4]diazepin-3-yl)-3-methyl-1,2,4-oxadiazole (GL-III-63, 61)…….. 255

2.2.7.64. (*R*)-5-(8-Cyclopropyl-6-(2-fluorophenyl)-4-methyl-4*H*-benzo[*f*]imidazo[1,5-*a*][1,4]diazepin-3-yl)-3-ethyl-1,2,4-oxadiazole (GL-IV-03, 62) 256

2.2.7.65. (*R*)-5-(8-Cyclopropyl-6-(2-fluorophenyl)-4-methyl-4*H*-benzo[*f*]imidazo[1,5-*a*][1,4]diazepin-3-yl)-3-isoproyl-1,2,4-oxadiazole (GL-IV-04, 63)……..... 257

2.2.7.66. (*R*)-8-Bromo-6-(2-fluorophenyl)-4-methyl-4*H*-benzo[*f*]imidazo[1,5-*a*][1,4]diaze pine-3-carbaldehyde (GL-III-35, 78)..... 258

2.2.7.67. (*R*)-5-(8-Bromo-6-(2-fluorophenyl)-4-methyl-4*H*-benzo[*f*]imidazo[1,5-*a*][1,4]diaze pin-3-yl)oxazole (GL-III-36, 78)..... 260

2.2.7.68. 5-(8-Bromo-6-(2-fluorophenyl)-4-methyl-6H-benzo[f]imidazo[1,5-a][1,4]diazepin -3-yl)oxazole (GL-III-36A/76A, 79)..... 261

2.2.7.69. (*R*)-5-(6-(2-Fluorophenyl)-4-methyl-8-((trimethylsilyl)ethynyl)-4*H*-benzo[*f*]imida zo[1,5-*a*][1,4]diazepin-3-yl)oxazole (GL-III-72, 80) 262

2.2.7.70. (*R*)-5-(8-Ethynyl-6-(2-fluorophenyl)-4-methyl-4*H*-benzo[*f*]imidazo[1,5-*a*][1,4]dia zepin-3-yl)oxazole (GL-III-73, 66)..... 263

2.2.7.71. (*S*)-8-Bromo-6-(2-fluorophenyl)-4-methyl-4*H*-benzo[*f*]imidazo[1,5-*a*][1,4]diaze pine-3-carbaldehyde (GL-III-75, 81)..... 264

2.2.7.72. (*S*)-5-(8-Bromo-6-(2-fluorophenyl)-4-methyl-4*H*-benzo[*f*]imidazo[1,5-*a*][1,4]diaze pin-3-yl)oxazole (GL-III-76, 65)..... 265

2.2.7.73. (*S*)-5-(6-(2-Fluorophenyl)-4-methyl-8-((trimethylsilyl)ethynyl)-4*H*-benzo[*f*]imida zo[1,5-*a*][1,4]diazepin-3-yl)oxazole (GL-III-77, 82) 266

2.2.7.74. (*S*)-5-(8-Ethynyl-6-(2-fluorophenyl)-4-methyl-4*H*-benzo[*f*]imidazo[1,5-*a*][1,4]dia zepin-3-yl)oxazole (GL-III-78, 67) 267

2.3. Asthma 268

2.3.1. Introduction 268

2.3.2. Background 271

2.3.3. Chemistry and Results 278

2.3.3.1. SH-053-2'F-*R*-CH$_3$-acid (Follow-up Experiments) 278

2.3.3.2. GL-II-93 (MIDD0301) 284

2.3.3.2.1. Development and Synthesis 284

2.3.3.2.2. Efficacy on α1-5 GABA$_A$R Subtypes and Receptor Binding 286

2.3.3.2.3. Pharmacokinetic Study, CNS Exposure as well as Cytotoxicity 290

2.3.3.2.4. The Relaxation of Contracted Smooth Muscle *Ex Vivo* and *In Vivo* ... 294

2.3.3.2.5. Effects on Asthmatic Properties of Acid 85 299

2.3.3.2.6. Immunotoxicity (Evaluation over a 28-Day Period) with Acid 85 309

2.3.3.2.7. Stability Studies 315

2.3.3.3. Analog Research on GL-II-93 330

2.3.3.3.1. Synthesis of Analogs 330

2.3.3.3.2. Evaluation of GL-II-93 Analogs, to Date 339

2.3.4. Discussion 343

2.3.5. Conclusion 348

2.3.6. Methods 349

2.3.6.1. ASM Relaxation of SH-053-2'F-R-CH3-acid (Dr. Emala, Columbia University)[99] 349

2.3.6.2. Evaluation of AHR of SH-053-2'F-*R*-CH$_3$-acid (Dr. Gloria Forkuo, UWM)[99]…. 350

2.3.6.3. Pharmacokinetic Study of SH-053-2'F-*R*-CH$_3$-acid (Revathi Kodali, UWM)[99]….. 351

2.3.6.4. The Rotarod Study of SH-053-2'F-*R*-CH$_3$-acid (Revathi Kodali, Nick Zahn, and Alec Huber, UWM)[99] 353

2.3.6.5. Patch Clamp Studies of GL-II-93 (Dr. Fisher, University of South Carolina School of Medicine)[187] 354

2.3.6.6. Pharmacokinetic Study of GL-II-93 (Dr. Arnold, UWM)[187] 355

2.3.6.7. Liver Microsomal Stability Study of GL-II-93 (Revathi Kodali, UWM)[187]…… 356

2.3.6.8. Evaluation of Mouse Plasma Binding of GL-II-93 (M. S. Rashid Roni, UWM)[187]…. 357

2.3.6.9. Quantification of GL-II-93 by LCMS/MS (M. S. Rashid Roni, UWM)[189]…….. 357

2.3.6.10. Rotarod Assay of GL-II-93 (Dr. Arnold, UWM)[187] 358

2.3.6.11. Cytotoxicity Study of GL-II-93 (Dr. Michael R. Stephen, UWM) 358

2.3.6.12. *Ex Vivo* Guinea Pig Tracheal Ring Organ Bath Induced by Substance P (Dr. Emala, Columbia University)[188] 359

2.3.6.13. *Ex Vivo* Guinea Pig Tracheal Ring Organ Bath with Histamine (Dr. Emala, Columbia University)[188]..... 359

2.3.6.14. *Ex Vivo* Human Tracheal Airway Smooth Muscle Strip Organ Bath (Dr. Emala, Columbia University)[188] 361

2.3.6.15. *Ex Vivo* Mouse Precision-Cut Lung Slice Experiments (Dr. Emala, Columbia University)[188]..... 361

2.3.6.16. Evaluation of GL-II-93 on AHR (Dr. Gloria Forkuo, UWM)[187]..... 362

2.3.6.17. Evaluation of *In Vivo* Mouse Airway Resistance (Dr. Emala, Columbia University)[188] 363

2.3.6.18. Quantification of Airway Inflammatory Cells (Dr. Gloria Forkuo, UWM)[187]…..... 363

2.3.6.19. EdU Staining (Dr. Gloria Forkuo, UWM)[187] 364

2.3.6.20. Histopathological Analysis of Lung Sections (Dr. Gloria Forkuo, UWM)[187]…..... 365

2.3.6.21. Expression of Cytokines (Dr. Gloria Forkuo, UWM)[187] 366

2.3.6.22. The 28-Day Immunotoxicity Study of GL-II-93 (Nick Zahn, UWM)[189]. 366

2.3.6.23. Effect of GL-II-93 on DNP-KLH Immunization (Nick Zahn, UWM)[189] 367

2.3.6.24. Study of GL-II-93 on Lymphoid Organs and Peyer's Patches (Nick Zahn, UWM)[189]……..368

2.3.6.25. The experiment of H&E-Staining (Wisconsin Children's Research Institute)[189]..... 368

2.3.6.26. DNP IgG Quantification (Nick Zahn, UWM)[189]..... 368

2.3.6.27. Cytotoxicity Study of GL-II-93 Analogs (Dr. Michael R. Stephen, UWM)……..... 369

2.3.6.28. Evaluation of AHR of GL-III-43 (Dr. Gloria Forkuo, UWM) 369

2.3.6.29. Patch Clamp Study of GL-III-54 (Dr. Fisher, University of South Carolina School of Medicine) 369

2.3.6.30. Relaxation of ASM by GL-III-54 in Guinea Pig Tracheal Rings with Substance P (Dr. Emala, Columbia University) 369

2.3.7. Experimental 370

2.3.7.1. (*R*)-8-Ethynyl-6-(2-fluorophenyl)-4-methyl-4*H*-benzo[*f*]imidazo[1,5-*a*][1,4]diazepine-3-carboxylic acid. (SH-053-2'F-*R*-CH_3-acid, 68) 370

2.3.7.2. (*R*)-8-Bromo-6-(2-fluorophenyl)-4-methyl-4*H*-benzo[*f*]imidazo[1,5-*a*][1,4]diazepine-3-carboxylic acid (GL-II-93, 85) 371

2.3.7.3. Sodium (*R*)-8-bromo-6-(2-fluorophenyl)-4-methyl-4*H*-benzo[*f*]imidazo[1,5-*a*][1,4]diazepine-3-carboxylate (GL-IV-18, 89) 372

2.3.7.4. (*R*)-5-(1-Aminoethyl)-1-(4-bromo-2-(2-fluorobenzoyl)phenyl)-1*H*-imidazole-4-carboxylic acid (GL-IV-19, 90) 372

2.3.7.5. (*S*)-8-Bromo-6-(2-fluorophenyl)-4-methyl-4*H*-benzo[*f*]imidazo[1,5-*a*][1,4]diazepine-3-carboxylic acid (GL-III-20, 91) 373

2.3.7.6. 8-Ethynyl-6-(2-fluorophenyl)-4*H*-benzo[*f*]imidazo[1,5-*a*][1,4]diazepine-3-carboxylic acid (GL-II-79, 93) 374

2.3.7.7. (*R*)-8-Bromo-4-methyl-6-(pyridin-2-yl)-4*H*-benzo[*f*]imidazo[1,5-*a*][1,4]diazepine-3-carboxylic acid (GL-II-51, 94) 375

2.3.7.8. (*R*)-8-Ethynyl-4-methyl-6-(pyridin-2-yl)-4*H*-benzo[*f*]imidazo[1,5-*a*][1,4]diazepine-3-carboxylic acid (GL-II-30, 95) 376

2.3.7.9. (*R*)-*Tert*-Butyl(1-((4-chloro-2-(2-fluorobenzoyl)phenyl)amino)-1-oxopropan-2-yl)carbamate (GL-III-51, 98) 376

2.3.7.10. (*R*)-7-Chloro-5-(2-fluorophenyl)-3-methyl-1*H*-benzo[*e*][1,4]diazepin-2(3*H*)-one (GL-III-52, 99) 378

2.3.7.11. (*R*)-Ethyl-8-chloro-6-(2-fluorophenyl)-4-methyl-4*H*-benzo[*f*]imidazo[1,5-*a*][1,4]diazepine-3-carboxylate (GL-III-53, 100) 379

2.3.7.12. (*R*)-8-Chloro-6-(2-fluorophenyl)-4-methyl-4*H*-benzo[*f*]imidazo[1,5-*a*][1,4]diazepine-3-carboxylic acid (GL-III-54, 87) 380

2.3.7.13. (*R*)-Ethyl-cyclopropyl-6-(2-fluorophenyl)-4-methyl-4*H*-benzo[*f*]imidazo[1,5-*a*][1,4]diazepine-3-carboxylate (GL-III-42, 101) 381

2.3.7.14. (*R*)-8-Cyclopropyl-6-(2-fluorophenyl)-4-methyl-4*H*-benzo[*f*]imidazo[1,5-*a*][1,4]diazepine-3-carboxylic acid (GL-III-43, 86) 382

2.3.7.15. (*R*)-6-(2-Fluorophenyl)-8-hydroxy-4-methyl-4*H*-benzo[*f*]imidazo[1,5-*a*][1,4]diazepine-3-carboxylic acid (GL-IV-14, 88) 383

2.3.7.16. (*R*)-8-Bromo-6-(2-fluorophenyl)-4-methyl-3-(1*H*-tetrazol-5-yl)-4*H*-benzo[*f*]imidazo[1,5-*a*][1,4]diazepine (GL-IV-21, 96) 384

Chapter 3. Design and Synthesis of Achiral α2/α3 Subtype-Selective Ligands and Their Use for the Treatment of Anxiety, Epilepsy, and Neuropathic Pain 385

3.1. Introduction 385

3.2. Synthesis α2/α3 Subtype Selective Ligands 389

3.3. Results and Discussion of Biological Studies on KRM-II-81 (77) 397

3.3.1. Anxiety 400

3.3.2. Epilepsy 404

3.3.2.1. Acute Seizure Models 405

3.3.2.2. Chronic Seizure Models 411

3.3.2.3. Evaluation of Seizure Protection in Resistant Epileptic Human Cortical Tissue 417

3.3.3. Activity of 1,3-oxazole (77) in Different Types of Pain Models 420

3.3.3.1. Visceral Pain Model 421

3.3.3.2. Inflammatory Pain Models 424

3.3.3.3. Neuropathic Pain Model 429

3.3.4. Depression 434

3.3.5. Evaluation of the Lack of Side Effects in Other Animal Models 435

3.3.5.1. Respiratory Depression Effects 435

3.3.5.2. Drug Abuse Liability 436

3.3.5.3. No Motor Impairment in the Rotarod Study 439

3.4. Conclusion 442

3.5. Methods 443

3.5.1. Dorsal Root Ganglion Electrophysiology (Dr. Kevin Freeman, University of Mississippi Medical Center) 443

3.5.2. Marble Burying Assay (CRO) 444

3.5.3. Vogel Conflict Assay (Dr. Jeffrey M. Witkin, Wikin Consulting) 444

3.5.4. 6 Hz 44mA Seizure Model (ETSP) 445

3.5.5. Maximal Electroshock Seizure (MES) Model (ETSP) 446

3.5.6. Inverted Screen Test (ETSP) 446

3.5.7. Pentylenetetrazole (PTZ)-Induced Seizures (ETSP) 447

3.5.8. Pentylenetetrazole (PTZ)-Induced Seizure Threshold (ETSP) 447

3.5.9. Corneal Kindled Mouse Model (ETSP) 448

3.5.10. Lamotrigine (LTG)-Resistant Amygdala Kindled Rat Model (ETSP) 448

3.5.11. Model of Mesial Temporal Lobe Epilepsy (ETSP) 449

3.5.12. Chronic Post-SE (KA) Spontaneously Seizing Rats: Stage 1 with IP Administration (ETSP) 449

3.5.13. Evaluation of Seizure Protection in Resistant Epileptic Human Brain Tissue (Dr. Jeffrey M. Witkin, Wikin Consulting) 450

3.5.14. Acetic Acid and Lactic Acid-Induced Writhing Model (Dr. Lakeisha A. Lewter and Jun-Xu Li, University at Buffalo) 451

3.5.15. CFA-Induced Inflammatory Pain Model by the Von Frey Test (Dr. Lakeisha A. Lewter and Jun-Xu Li, University at Buffalo) 451

3.5.16. Formalin Assay (Dr. Jeffrey M. Witkin, Wikin Consulting) 453

3.5.17. SNL-Induced Hyperalgesia Model of Neuropathic Pain (Dr. Jeffrey M. Witkin, Wikin Consulting) 454

3.5.18. Chemotherapy Induced Neuropathic Pain (CINP) Models (Dr. Bronwyn Kivell, Victoria University of Wellington) 454

3.5.19. Respiratory Depression (Dr. Kevin Freeman, University of Mississippi Medical Center)... 456

3.5.20. Pain-Depressed Intracranial Self-Stimulation (ICSS model, Dr. Megan Moerke and Dr. Steve Nuggus, Virginia Commonwealth University 457

3.6. Experimental 458

3.6.1. 7-Bromo-5-(pyridin-2-yl)-1*H*-benzo[*e*][1,4]diazepin-2(3*H*)-one (104) 458

3.6.2. Ethyl-8-bromo-6-(pyridin-2-yl)-4*H*-benzo[*f*]imidazo[1,5-*a*][1,4] diazepine-3-carboxyl ate (105) 459

3.6.3. Ethyl-6-(pyridin-2-yl)-8-((trimethylsilyl)ethynyl)-4*H*-benzo[*f*] imidazo[1,5*a*]-[1,4]dia zepine-3-carboxylate (106) 461

3.6.4. Ethyl-8-ethynyl-6-(pyridin-2-yl)-4*H*-benzo[*f*]imidazo[1,5-*a*][1,4] diazepine-3-carboxy late (HZ-166, 76) 462

3.6.5. 3-Ethyl-5-(8-ethynyl-6-(pyridin-2-yl)-4*H*-benzo[*f*]imidazo[1,5-*a*] [1,4]diazepin-3-yl)-1,2,4-oxadiazole (MP-III-080, 102). 463

3.6.6. 8-Ethynyl-6-(pyridin-2-yl)-4*H*-benzo[*f*]imidazo[1,5-*a*][1,4] diazepine-3-carbaldehyde (GL-III-13, 107) 465

3.6.7. 5-(8-Ethynyl-6-(pyridin-2-yl)-4*H*-benzo[*f*]imidazo[1,5-*a*][1,4] diazepin-3-yl)oxazole (KRM-II-81, 77). 466

References. 468

Appendix… 505

Appendix I: HPLC/PDA 505

Appendix II: PDSP Data 513

Table 35. PDSP compound list. 513

Table 36. PDSP primary binding data for 5-HT1A, 5-HT1B, 5-HT1D, 5-ht1e, 5-HT2A, and 5-HT2B. 517

Table 37. PDSP primary binding data for 5-HT2C, 5-HT3, 5-ht5a, 5-HT6, 5-HT7, and Alpha1A. 522

Table 38. PDSP primary binding data for Alpha1B, Alpha1D, Alpha2A, Alpha2B, Alpha2C, and Beta1. 526

Table 39. PDSP primary binding data for Beta2, Beta3, BZP Rat Brain Site, Calcium Channel, D1, and D2. 531

Table 40. PDSP primary binding data for D3, D4, D5, DAT, DOR, and GABAA. 536

Table 41. PDSP primary binding data for H1, H2, H3, H4, HERG binding, and KOR. 541

Table 42. PDSP primary binding data for M1, M2, M3, M4, M5, and mGlur5. 545

Table 43. PDSP primary binding data for MOR, NET, NMDA, Oxytocin, PBR, and SERT. 550

Table 44. PDSP primary binding data for Sigma 1, Sigma 1 GP, Sigma 2, Sigma 2 PC12, V1A, V1B, and V2. 554

Table 45. PDSP secondary binding data for 5-HT1A, 5-HT1B, 5-HT1D, 5-ht1e, 5-HT2A, and 5-HT2B. 559

Table 46. PDSP secondary binding data for 5-HT2C, 5-HT3, 5-ht5a, 5-HT6, 5-HT7, and Alpha1A. 564

Table 47. PDSP secondary binding data for Alpha1D, Alpha2A, Alpha2B, Alpha2C, Beta1, and Beta2. 569

Table 48. PDSP secondary binding data for Beta3, BZP Rat Brain Site, D1, D3, D5, and DAT. 574

Table 49. PDSP secondary binding data for DOR, H1, H2, H3, H4, and HERG binding..... 578

Table 50. PDSP secondary binding data for KOR, M1, M2, M3, M4, M5 and mGlur5. 584

Table 51. PDSP secondary binding data for MOR, NET, NMDA, PBR, Sigma 1, Sigma 2, and Sigma 2 PC12. 589

Appendix III: The master data file for anti-depression project 596

Table 52. Pharmacokinetic parameters in mice and rats calculated for GL-II-73, GL-II-74, GL-II-75, RV-II-04, GL-II-31, MP-III-023, GL-I-54, GL-III-23, GL-II-33, GL-II-54 and GL-I-65. 596

Table 53. PK parameters for GL-III-68 and GL-III-70. 605

Table 54. Summary table (occupancy, efficacy, binding) 624

Table 55. Summary table (microsomal stability, FST, Y-maze) 626

Appendix IV: Additional Data for Anti-schizophrenic like Behavioral Study Induced by MK-801 633

Total immobile episodes 633

Maximum speed (m/s) 634

Rotations of the animal's body 635

Clockwise rotations of the animal's body 636

Anticlockwise rotations of the animal's body 637

Total freezing episodes 638

Total time freezing (s) 639

Total distance travelled (m) 640

Average speed (m/s) 642

Total time mobile (s) 644

Total time immobile (s) 646

Total mobile episodes 648

Total immobile episodes 650

Maximum speed (m/s) 652

Rotations of the animal's body 654

Clockwise rotations of the animal's body 656

Anticlockwise rotations of the animal's body 658

Total freezing episodes 660

Total time freezing (s) 662

Table 57. Raw data of anti-schizophrenia model. 663

Appendix V: NIH Epilepsy Therapy Screening Program (ETSP) Test Results of KRM-II-81 681

Appendix VI: Metabolites Study from Eli Lilly of KRM-II-81 and MP-III-080 699

Report 1. *In Vitro* Metabolism of Compound (KRM-II-81) LSN3310515 in Mouse Hepatocytes 699

Report 2. *In Vitro* Metabolism of Compound (KRM-II-81) LSN3310515 in Rat, Monkey and Human Hepatocytes 709

Report 3. *In Vitro* Metabolism of Compound (MP-III-080) LSN3310516 in Mouse Hepatocytes 719

Report 4. *In Vitro* Metabolism of Compound (MP-III-080) LSN3310516 in Rat, Monkey and Human Hepatocytes 729

Appendix VII: Kinetic and Stability Studies of GL-II-93 in Acidic and Basic Condition…… 739

1. 2D NMR experiment (DCl addition) 739

2. The area (lg)-time curve of DCl addition at pH = 2 741

3. The intensity (lg)-time curve of DCl addition at pH = 2 745

4. DCl addition t1/2 list [area (lg)-time curve] 748

5. DCl addition t1/2 list [intensity (lg)-time curve] 749

6. 2D NMR experiment (NaOD addition) 749

7. The area (lg)-time curve of NaOD addition at pH = 8 752

8. The intensity (lg)-time curve of NaOD addition at pH = 8 759

9. NaOD addition t1/2 list [area (lg)-time curve] 766

10. NaOD addition t1/2 list [intensity (lg)-time curve] 767

Appendix VIII: BZD-related drugs reduced methamphetamine-related behaviors in rats via BZD-induced TSPO activation 768

1. 2016 poster (Ro5-4846) 775

2. 2018 poster (Ro5-4846) 777

Appendix IX: Angelman syndrome (in collaboration with Kiyoshi Egawa, Japan) 779

Appendix X: Modulating GABAA receptors in medulloblastoma with BZD derivatives…….. 785

1. Poster: Targeting medulloblastoma with benzodiazepines delivered using tunable biodegradable hydrogels 785

2. Poster: Understanding the mechanism of benzodiazepine mediated cell death in GABRA5 overexpressing medulloblastomas 786

3. Poster: Modulating $GABA_A$ receptors in medulloblastoma with benzodiazepine derivatives induces cell death 787

4. Paper: Modulating native -GABAA receptors in medulloblastoma with positive allosteric benzodiazepine-derivatives induces cell death 788

Appendix XI: Additional poster presentations..... 802

1. Poster: Novel α5 selective benzodiazepine site ligands 802

2. Poster: Design and synthesis of anxiolytic, anticonvulsant and antinociceptive benzodiazepine/GABA(a)ergic receptor subtype selective ligands as potential nonsedating treatment for anxiety disorders, epilepsy and pain disorders (ACS 2018) 803

CURRICULUM VITAE..... 806

LIST OF FIGURES

Figure 1. A proposed $GABA_AR$ subunit topology. The extracellular domain starts with the N-terminal end, and the M1-M4 are regions within the membrane. (Modified from the Figure in Burt, et al. [17] and Clayton, et al.)[18] 2

Figure 2. The schematic representations of $GABA_AR$, the ligand-gated chlorine ion channel in longitudinal vision (A) and cross-sectional vision (B). The number 1-4 represents the M1-M4 transmembrane domains. The domain M2 contributes to most of the pore lining within the lipid bilayer membrane. (Modified from the Figure in Keramidas et al.[19], and Clayton et al.)[18] 3

Figure 3. The arrangement of the $\alpha 1\beta 3\gamma 2$ $GABA_AR$ subtypes as viewed from the synaptic cleft. The binding sites of GABA are located at the interfaces between β^+ and α^- subunits and the BZD binding site is located at the interface of the $\alpha^+\gamma^-$ subunits. The + represents the loop C of each subunit. (Modified from the Figure in Clayton, et al.[18] and Ernst, et al.)[27] 4

Figure 4. The structures of common BZDs: diazepam, chlordiazepoxide, imidazodiazepine (IMDZ) midazolam and flumazenil. The atoms are labeled for both BZDs and IMDZs. Diazepam, chlordiazepoxide, and midazolam can bind only to the DS sites, whereas flumazenil can bind to both the DS and DI sites. 6

Figure 5. The membrane potential overtime when a depolarizing stimulus initiates a nerve signal. A hyperpolarized state indicates a potential further away from the threshold potential. (Modified from the Figure in the Ph.D. thesis of Terry Clayton)[64] 10

Figure 6. The locations of the descriptors and areas of the Milwaukee-Unified Pharmacophore /Receptor Model for BZD at $GABA_AR$ BzR. Depicted here is pyrazolo[3,4-c]quinolin-

3-one CGS-9896 as a dotted line, a diazadiindole as a thin line, and diazepam as a thick line aligned within the unified pharmacophore/receptor model for the BzR. H_1 and H_2 stand for the hydrogen bond donor sites within the BzR, while A_2 stands for a hydrogen bond acceptor site that may be necessary for potent inverse agonist activity in vivo. L_1, L_2, L_3, and L_{Di} represent the four lipophilic regions and S_1, S_2, and S_3 represent the regions of negative steric repulsion. LP stands for the lone pair of electrons on the nitrogen (N) or oxygen (O) atoms of the ligands. (Modified from the Figure in Clayton et al.)[18] 13

Figure 7. Overlap images between the induced volumes derived from receptor subtype selective ligands: a) α1 and α2 subtypes; b) α2 and α3 subtypes; c) α4 and α6 subtypes; d) α1 and α6 subtypes; e) α1 and α5 subtypes; f) diazepam and the descriptors of the unified pharmacophore model in the included volume of the α1 subtype. The yellow color represents overlapping induced volumes, and each grid measures 4 Å in width and height.[67] 14

Figure 8. Bz/$GABA_AR$ in vitro binding data of diazepam and QH-II-066. (Modified from the Figure in the Ph. D. thesis of M. Poe and T. Clayton) [65, 78] 15

Figure 9. The structures of enantiotopic chiral imidazodiazepine (IMDZ) ligands 1 and 2. 16

Figure 10: Ligand occupation of SH-053-2'F-R-CH_3 (**1**) and SH-053-2'F-S-CH_3 (**2**) in the α5 and α2 pharmacophore/receptor models. (Modified and reproduced from that reported by Clayton et al.)[67] 17

Figure 11. The structures of both enantiomers of thalidomide. 20

Figure 12. Impact of **1** or **2** treatment (30 mg/kg, i.p.) on cataleptic behavioral. Haloperidol, but not **1** nor **2** produced a significant cataleptic response at 30, 60, and 120 minutes post-

injection. The data are expressed as the mean (+SEM) time (sec) subjects spent with both front paws on an elevated bar; *p<0.001, the difference from controls receiving vehicle alone. 31

Figure 13. Impact of **1** or **2** treatment (30 mg/kg, IP) on prepulse inhibition. Ligand **2**, but not **1** reversed the PPI deficits induced by PCP when given one hour before testing. The data are expressed as the mean (+SEM) percent prepulse inhibition of the startle response to an auditory stimulus when preceded by a nonstartle-eliciting auditory cue at 5, 10, and 15 decibels. Disruption of prepulse inhibition was obtained in rats by an acute injection of phencyclidine (PCP·HCl, 1.5 mg/kg, SC) ten minutes prior to testing; *p<0.05, difference from controls receiving phencyclidine with 0 mg/kg drug pretreatment. 31

Figure 14. Impact of **1** or **2** treatment on anticonvulsant effects. A) Mice were dosed i.p. with either **1** (150 mg/kg) or **2** (100 mg/kg) and a 6 Hz shock by a corneal electrode was administered at various time points, and the animal observed for convulsions. Ligand **2** was able to protect some subjects while **1** was not able to protect mice from electroshock-induced seizures. B) In the rotarod assay, mice were dosed i.p. with **1** or **2** (100 mg/kg) 30 minutes prior to testing on a rotating rod (6 rpm). Mice that fell 3 times during a 1-minute trial were deemed toxic (ataxic or sedated). Also there was no indication of toxicity nor sedation in rhesus monkeys at 10 mg/kg (Fischer, et al, 2010).[83] 31

Figure 15. Chiral analogs and bioisosteres of the lead compound S-isomer **2**. 33

Figure 16. Effect of analogs of **2** on sensorimotor coordination. Mice were placed on the rotarod at three separate time points of 10, 30, and 60 minutes after each oral gavage drug

administration at 40 mg/kg. Their performance on the rotarod for 3 minutes was recorded and analyzed. After a second fall, it would be considered a fail, and that time point would be recorded..... 45

Figure 17. Medicinal chemistry strategy of analog research from the parent compound **1**, based on previous work on the C(4)-S-CH_3 isomer and the C(4) achiral analogs..... 47

Figure 18. The electrophysiological response of **35** (A) and **1** (B) . The GABA EC3 (3% of the maximal GABA current) measurement was illustrated on the concentration-response curves at $\alpha_{1\text{-}3,5}\beta3\gamma2$ $GABA_A$Rs of rat recombinant receptors. The dose range of **35** (MP-III-022) to provide a selective potentiation at α5 was 1-10 mg/kg, whereas it was 10-200 mg/kg for compound 1. (Modified from the Figure in Stamenić et al.)[121] 53

Figure 19. The proposed mechanism for the formation of the byproduct **79** from workup of the van Leusen reaction; an effect of tosic acid on the [N(5)-C(6)] imine to [N(5)-C(4)] imine rearrangement (tautomerism)..... 64

Figure 20. Proposed metabolites of key dimethyl amide **36** (GL-II-73). 73

Figure 21. The CYP3A4 inhibition of GL-II-73 (**36**). Not much effect even at 50 μM. This is an important result. Unpublished data. 74

Figure 22. The effect of amides from the R-series (**36-40**) and the S-series (**25-30**) on the sensorimotor coordination on the rotarod in vivo. Swiss Webster mice received an oral gavage of the compound at 40 mg/kg or diazepam (5 mg/kg i.p.) and were placed on a rotarod at 15 rpm for 3 minutes, and the performance was recorded after 10, 30 and 60 minute time points after drug administration. A fail was assigned to a mouse if they have fallen twice within 3 minutes. The latency to fall is presented as mean ± SEM (n

= 9). The vehicle was used as the negative control, and diazepam as the positive control. Unpublished data. 80

Figure 23. The effect of thioamides from the R-series (**41-44**), the amides with either a Br or a cyclopropyl group at the C(8) position (**45-48**), an achiral C(Br) methyl amide (**49**), as well as a methyl amide (**50**) in the 2'N series on the sensorimotor coordination assay on the rotarod assay in vivo. Swiss Webster mice received an oral gavage of the compound at 40 mg/kg or diazepam (5 mg/kg i.p.) and were placed on a rotarod at 15 rpm for 3 minutes, and the performance was recorded after 10, 30 and 60 minute time points (additional time points at 120 and 240 minutes for the thioamides) after drug administration. A fail was assigned to a mouse if they had fallen twice within 3 minutes. The latency to fall is presented as mean ± SEM (n = 7-8). The vehicle was used as the negative control, and diazepam as the positive control. Unpublished data. 81

Figure 24. The effect of oxadiazoles on the sensorimotor coordination on the rotarod test in vivo. The Swiss Webster mice received an oral gavage of the compound at 40 mg/kg or diazepam (5 mg/kg i.p.) and were placed on a rotarod at 15 rpm for 3 minutes, and the performance was recorded after 10, 30 and 60 minute time points (additional time points at 120 and 240 minutes for later compounds) after drug administration. A fail was assigned to a mouse if they had fallen twice within 3 minutes. The latency to fall was presented as mean ± SEM (n =7-8). The vehicle was used as the negative control, and diazepam as the positive control. Unpublished data. 82

Figure 25. The effect of 1,3-oxazoles on the sensorimotor coordination on the rotarod test in vivo. The Swiss Webster mice received an oral gavage of the compound at 40 mg/kg or diazepam (5 mg/kg i.p.) and were placed on a rotarod at 15 rpm for 3 minutes, and the

performance was recorded after 10, 30 and 60 minute time points after drug administration. A fail was assigned to a mouse if they had fallen twice within 3 minutes. The latency to fall is presented as mean ± SEM (n = 4-7). The vehicle was used as the negative control, and diazepam as the positive control. Unpublished data. 83

Figure 26. The effect of GL-II-73 (**36**), GL-II-74 (**37**) and GL-II-75 (**38)**, all dosed i.p. at 10 mg/kg, on the average time on the rotarod 20 minutes after administration of the drug in mice. All data are presented as the mean ± S.E.M. Number of animals per treatment group (Vehicle, GL-II-73, GL-II-74, and GL-II-75) was 5, 7, 12 and 9, respectively. **p < 0.01 and ***p < 0.001 compared to Vehicle, ###p < 0.001 compared to GL-II-73 (36). Unpublished data. 84

Figure 27. The effects of increasing doses of MP-III-022 (a), GL-II-73 (b), GL-II-74 (c) and GL-II-75 (d) on the rotarod performance assessed 20 minutes and 1 hour after i.p. administration in male C57/BL6 mice (n = 1–4 per treatment). The doses administered were 5, 10, 15 and 20 mg/kg for MP-III-022; 10, 15, 20, 30, 45, 60 and 90 mg/kg for GL-II-73; 5, 10, 15 and 20 mg/kg for GL-II-74 and 3, 5, 10, 15 and 20 mg/kg for GL-II-75. Additionally, the reliably incapacitating dose of each of the ligands was co-administered with flumazenil at a dose of 15 mg/kg and that influence on the rotarod performance was also observed. 87

Figure 28. The observed effect of GL-III-66 (**39**), GL-III-67 (**46**), GL-III-70 (**47**), GL-III-68 (**48**), GL -III-64 (**54**), GL-III-60 (**58**), and GL-III-63 (**61**) dosed i.p. at 20, 30 and 40 mg/kg on average time on the rotarod 20 minutes after administration of ligand to the rats. All data are presented as the mean ± S.E.M. (n = 3). Unpublished data. 90

Figure 29. The observed effect of GL-III-66 (**39**), GL-III-67 (**46**), GL-III-70 (**47)**, GL-III-68 (**48**), GL -III-64 (**54**), GL-III-60 (**58**), and GL-III-63 (**61**) dosed intraperitoneally at 20, 30 and 40 mg/kg on muscle strength right after the rotarod testing. All data are presented as the mean ± S.E.M. Number of animals per treatment group was 3, 2, 3, 1, respectively in the order of the treatments in the Figure. Unpublished data. 94

Figure 30. The effect of GL-II-73 (**36**), GL-II-74 (**37**) and GL-II-75 (**38**), all dosed i.p. at 10 mg/kg, on spontaneous locomotor activity during 60 minutes of recording in mice. All data are presented as the mean±S.E.M. Number of animals per treatment group was 7, with the exception of GL-II-73 (n=6). ++P<0.01 between GL-II-74 and GL-II-75 groups..... 96

Figure 31. The effect of GL-II-73 (**36**), GL-II-74 (**37**) and GL-II-75 (**38**), all dosed i.p. at 10 mg/kg, on distance traveled in 5-min bins during recording on the locomotor activity test in mice. All data are presented as the mean±S.E.M. *P<0.05, **P<0.01 and ***P<0.001 versus SOL group. 96

Figure 32. The effect of RV-II-04 (**49**), GL-II-31 (**50**), MP-III-023 (**25**), GL-I-54 (**30**), GL-III-23 (**52**), GL-II-33 (**51**), GL-II-54 (**53**) and GL-I-65 (**31**), all dosed i.p. at 10 mg/kg, on spontaneous locomotor activity during 60 min of recording in rats. All data are presented as the mean±S.E.M. Number of animals per treatment group was 5, with the exception of **51, 53 and 52**, and SOL (n=6). **P<0.01 and ***P<0.001 versus SOL group. Other differences were not presented; in general, the animals treated with **49** were sedated when compared to all other groups, with the exception of 25. Unpublished data. 97

Figure 33. The effect of RV-II-04 (**49**), GL-II-31 (**50**), MP-III-023 (**25**), GL-I-54 (**30**), GL-III-23 (**52**), GL-II-33 (**51**), GL-II-54 (**53**) and GL-I-65 (**31**), all dosed i.p. at 10 mg/kg, on

distance traveled in 5-min bins during recording in the locomotor activity test in rats. All data are presented as the mean±S.E.M. Statistical significances were not presented. Unpublished data. 97

Figure 34. The effect of GL-III-66 (**39**), GL-III-67 (**46**), GL-III-70 (**47**), GL-III-68 (**48**), GL -III-64 (**54**), GL-III-60 (**58**), and GL-III-63 (**61**), dosed intraperitoneally at 10 mg/kg (dark symbols) and 15 mg/kg (light symbols), on total distance travelled (A) and % of time in the central zone (B) during 60 min of recording in rats. All data are presented as the mean ± S.E.M. Number of animals per treatment group was 4 (10 mg/kg) and 6, 6, 7, 6, 8, 6, 7, 6 (15 mg/kg), respectively to the order of the ligands in Figure 34. Unpublished data. 99

Figure 35. Efficacy data of **36** (a), **37** (b), **38** (c) and **39** (d) at 100 nM or 1 μM for α1-6-containing $GABA_A$Rs. Comparison of α1β1γ2 and α1β3γ2 for **36** (e), **37** (f), **38** (g) and **39** (h) at 100 nM or 1 μM. The EC_{3-5} GABA value is presented in percentage of response to GABA alone. * $p < 0.05$, ** $p < 0.01$, and *** $p < 0.001$ compared to 100%; + $p < 0.05$ compared to α5β3γ2; # $p < 0.05$ compared to α1β3γ2. The estimated free brain concentrations were illustrated on the dose-response curves for the approximated electrophysiological responses of **36** (i), **37** (j), **38** (k), and DZP (l). (Adopted from the figure in Prevot et al.)[117] 111

Figure 36. Efficacy data of GL-II-73, GL-III-67, GL-III-68, GL-III-70, GL-III-84, GL-III-85, GL-III-86, GL-III-87, GL-II-33, GL-II-54 and GL-I-65 at 100 nM for α1,2,3,5-containing $GABA_A$Rs. Unpublished data. 113

Figure 37. Efficacy data of GL-II-73, GL-III-67, GL-III-68, GL-III-70, GL-III-84, GL-III-85, GL-III-86, GL-III-87, GL-II-33, GL-II-54 and GL-I-65 at 1 μM for α1,2,3,5-containing $GABA_A$Rs. Unpublished data. 114

Figure 38. Efficacy data of (R) **64** (GL-III-36), (S) **65** (GL-III-76), (R) **66** (GL-III-73), (S) **67** (GL-III-78), and **79** (GL-III-76A) at 100 nM for α1-5-containing $GABA_A$Rs. Unpublished data. 114

Figure 39. Efficacy data of (R) **64** (GL-III-36), (S) **65** (GL-III-76), (R) **66** (GL-III-73), (S) **67** (GL-III-78), and **79** (GL-III-76A) at 1 μM for α1-5-containing $GABA_A$Rs. Unpublished data. 115

Figure 40. Plasma and brain concentration-time profiles of **36** (a), **37** (b), **38** (c), and DZP (d) after 10 mg/kg i.p. administration in male C57BL/6 mice (n = 3 per time point). (Adopted from the **Figure** in Prevot et al.)[117] 118

Figure 41. NO production via the Griess assay. Test compounds were screened at 50 μM with 1 μM GABA in mouse microglia activated with 150 U/mL IFNγ and 50 ng/mL LPS, along with 100 nM dexamethasone as a positive control and 1 mM CBT as the cytotoxicity control. Unpublished data. 122

Figure 42. Cytotoxicity via the Cell-Titer Glo Assay. Control compounds dexamethasone and CBT were run at concentrations of 100 nM and 1 mM respectively. Unpublished data. 123

Figure 43. Dose-response of the active compounds from the Griess assay. The test compounds were screened at 50 μM with 1 μM GABA in mouse microglia activated with 150 U/mL IFNγ and 50 ng/mL LPS, along with 100 nM dexamethasone as a positive control and 1 mM CBT as a cytotoxicity control. Unpublished data. 123

Figure 44. NO production via the Griess assay for the oxazole compounds as well as the $GABA_AR$ antagonist picrotoxin at 50, 100 μM and flumazenil at 500 nM. Test compounds **64** (GL-III-36), **65** (GL-III-76), **66** (GL-III-73), **67** (GL-III-78), **69** (GL-III-76A), **80** (GL-III-72) and **82** (GL-III-77), were screened at 50 μM with 1 μM GABA in mouse microglia activated with 150 U/mL IFNγ and 50 ng/mL LPS, along with 100 nM dexamethasone as a positive control and 1 mM CBT as a cytotoxicity control. Unpublished data. 125

Figure 45. Cytotoxicity via the Cell-Titer Glo Assay for oxazole compounds **64** (GL-III-36), **65** (GL-III-76), **66** (GL-III-73), **67** (GL-III-78), **69** (GL-III-76A), **80** (GL-III-72) and **82** (GL-III-77), as well as $GABA_AR$ antagonist picrotoxin at 50, 100 μM and flumazenil at 500 nM. Control compounds dexamethasone and CBT were run at concentrations of 100 nM and 1 mM respectively. Unpublished data. 125

Figure 46. Total distance traveled in the MK-801-induced hyper-locomotor model. The data analyzed has been limited in the following way: Treatment = SAL + SOL, SAL + GL-III-36 10 mg/kg, SAL + GL-III-73 10 mg/kg, SAL + GL-III-76 10 mg/kg, SAL + GL-III-78 10 mg/kg, MK-801 0.32 mg/kg + SOL, MK-801 0.32 mg/kg + GL-III-36 10 mg/kg, MK-801 0.32 mg/kg + GL-III-73 10 mg/kg, MK-801 0.32 mg/kg + GL-III-76 10 mg/kg or MK-801 0.32 mg/kg + GL-III-78 10 mg/kg and Trial = Habituation trial or MK-801 challenge trial. Unpublished data..... 128

Figure 47. Average speed in the MK-801-induced hyper-locomotor model. The data analyzed has been limited in the following way: Treatment = SAL + SOL, SAL + GL-III-36 10 mg/kg, SAL + GL-III-73 10 mg/kg, SAL + GL-III-76 10 mg/kg, SAL + GL-III-78 10 mg/kg, MK-801 0.32 mg/kg + SOL, MK-801 0.32 mg/kg + GL-III-36 10 mg/kg, MK-

801 0.32 mg/kg + GL-III-73 10 mg/kg, MK-801 0.32 mg/kg + GL-III-76 10 mg/kg or MK-801 0.32 mg/kg + GL-III-78 10 mg/kg and Trial = Habituation trial or MK-801 challenge trial. Unpublished data..... 129

Figure 48. Total time immobile in the MK-801-induced hyper-locomotor model. The data analyzed has been limited in the following way: Treatment = SAL + SOL, SAL + GL-III-36 10 mg/kg, SAL + GL-III-73 10 mg/kg, SAL + GL-III-76 10 mg/kg, SAL + GL-III-78 10 mg/kg, MK-801 0.32 mg/kg + SOL, MK-801 0.32 mg/kg + GL-III-36 10 mg/kg, MK-801 0.32 mg/kg + GL-III-73 10 mg/kg, MK-801 0.32 mg/kg + GL-III-76 10 mg/kg or MK-801 0.32 mg/kg + GL-III-78 10 mg/kg and Trial = Habituation trial or MK-801 challenge trial. Unpublished data..... 130

Figure 49. Total time mobile in the MK-801-induced hyper-locomotor model. The data analyzed has been limited in the following way: Treatment = SAL + SOL, SAL + GL-III-36 10 mg/kg, SAL + GL-III-73 10 mg/kg, SAL + GL-III-76 10 mg/kg, SAL + GL-III-78 10 mg/kg, MK-801 0.32 mg/kg + SOL, MK-801 0.32 mg/kg + GL-III-36 10 mg/kg, MK-801 0.32 mg/kg + GL-III-73 10 mg/kg, MK-801 0.32 mg/kg + GL-III-76 10 mg/kg or MK-801 0.32 mg/kg + GL-III-78 10 mg/kg and Trial = Habituation trial or MK-801 challenge trial. Unpublished data..... 131

Figure 50. Anxiolytic-like properties of novel ligands 36-38 as compared to DZP. Potential anxiolytic IMDZ ligands (a) GL-II-73 (**36**), (b) GL-II-74 (**37**), and (c) GL-II-75 (**38**) at 5 or 10 mg/kg and DZP (1.5 mg/kg; d) were assessed in mice (50% females) in the EPM test. Mice received either vehicle or the test compound **36** (n(0) = 13, n(5) = 13, and n(10) = 14), **37** (n(0) = 14, n(5) = 13, and n(10) = 14), **38** (n(0) = 13, n(5) = 14, and n(10) = 13), or DZP (n(0) = 11 and n(1.5) = 10) 30 min before testing. Possible

anxiolytic effects were indicated by an increase in time spent in the open arms of the EPM. Sex was not significant factor ($p \geqslant 0.17$) as a cofactor. (Modified from the figure in Prevot et al.)[117] 132

Figure 51. Anxiolytic-like properties of the ligands of GL-III series and the NAM (MRK-016) in the elevated plus maze at 10 mg/kg, i.p. administration. Unpublished data. 133

Figure 52. Antidepressant properties of 36-38. Potential antidepressant effect of IMDZ ligands **36** (a), **37** (b), and **38** (c) at 1, 5 or 10 mg/kg and DZP (1.5 mg/kg; d) was assessed in male mice in the FST after i.p administration. An inescapable transparent tank filled with water was used to place the mice (25 cm, 26 ± 1 °C) for 6 minutes. The minimum amount of movement for staying afloat indicated the immobility, between 2-6 min testing period. and the sixth minute of testing. (**36**: n(0) = 8, n(1) = 8, n(5) = 6, and n(10) = 8; **37**: n(0) = 8, n(1) = 8, n(5) = 8, and n(10) = 8; **38**: n(0) = 8, n(1) = 8, n(5) = 8, and n(10) = 9) or DZP (n(0) = 12 and n(1.5) = 12). The potential antidepressant-like profile was indicated by any significant decrease of immobility induced by the test compound. * $p < 0.05$, ** $p < 0.01$, and *** $p < 0.001$ compared to vehicle. All values are represented as mean ± standard error of the mean. (Modified from the Figure in Prevot et al.)[117] 135

Figure 53. Effect of **53** (GL-II-54) and **30** (GL-I-54) on time spent immobile in the FST. The ligand **53** (A) at 10 mg/kg, and the ligand **30** (B) at 5 mg/kg i.p. administered (24, 20, 1 h before testing) induced a significant antidepressant-like action when compared to the vehicle group (n = 9). *p<0.05 and ***p<0.001 when compared to the vehicle group. Unpublished data. 136

Figure 54. Pro-cognitive effect of ligands **36-38** on working memory impairment induced by stress. The spontaneous alternation Y-maze task was employed to determine the effects on working memory using a 90-second intertrial interval. The cognitive deficit was introduced by exposing mice to daily CRS, 1 h twice a day for 1 week before the experiment. Young mice (50% females) received i.p. administrated vehicle or 1, 5, or 10 mg/kg of **36** (a; n(0-NS) = 10, n(0-S) = 10, n(1) = 5, n(5) = 10, n(10) = 12), for **37** (b; n(0-NS) = 8, n(0-S) = 8, n(1) = 4, n(5) = 10, n(10) = 4), **38** (c; n(0-NS) = 8, n(0-S) = 8, n(1) = 6, n(5) = 4, n(10) = 9), and DZP (d; n(0-NS) = 6, n(0-S) = 6, n(1.5) = 6) 30 min prior testing. * $p < 0.05$, ** $p < 0.01$, *** $p < 0.001$ compared to "No stress vehicle." Effect of the ligand: $ $p < 0.05$ compared to "Stress vehicle" (Adopted from the figure in Prevot et al.)[117] 139

Figure 55. Effect of **36-38** and DZP on alternation rate in a spontaneous alternation Y-maze task to evaluate the potential cognitive deficit under baseline conditions induced by test compounds at 5 or 10 mg/kg, or 1.5mg/kg of DZP in non-CRS mice. Prior to 30 min for the test, the i.p. injection of PAM or DZP was administrated. A reduced alternation rate was only seen in mice treated with 10 mg/kg of **37**, as compared to DZP. **$p<0.001$ compared to the "No Stress-Vehicle" group. (Adopted from the figure in Prevot et al.)[117] 140

Figure 56. Effect of **30** (GL-I-54) on the percent alternation rate in the Y-maze spatial alternation task assessing working memory in mice. Mice subjected to CRS were injected with **30** (0, 1, 5, 10 mg/kg) i.p. 30 min before testing). ANOVA revealed statistical significance on the overall effect of stress and treatment with **30** at 5 and 10 mg/kg. Differences

between groups were tested using the posthoc analysis of Scheffe (**p<0.01 compared to the “Control-Vehicle” group) n=5-9. Unpublished data..... 141

Figure 57. Effect of the racemic mixture of **36/30** (GL-II-73/GL-I-54) on percent alternation rate in the Y-maze spatial alternation task assessing working memory in mice. Mice subjected to CRS were injected with the racemic mixture solution (10 mg/kg, ip., 5 mg/kg each enantiomer, 30 min before testing) or vehicle. ANOVA revealed statistical significance on the overall effect of manipulation. Differences between groups were tested using the posthoc analysis of Scheffe (***p<0.001 compared to the “Control-Vehicle” group / $$p<0.01 compared to the “CRS-Vehicle” group). n=4-5. Unpublished data. 142

Figure 58. The effect of GL-I-65 (A) and GL-II-33 (B) on the percent alternation rate in the Y-maze spatial alternation task assessing working memory in mice. The mice subjected to the CRS were injected with GL-I-65 or GL-II-33 (10 mg/kg, i.p., 30 min before testing). ANOVA revealed statistical significance on the overall effect of manipulation. The CRS animals showed a significant reduction of working memory performance and the CRS mouse group injected with GL-I-65 were not statically different from the control-vehicle group. Differences between groups were tested using the posthoc analysis of Scheffe (*p<0.05 compared to the “control-vehicle” group) n=9-11, n =4-5 for GL-I-65 and GL-II-33, respectively. (CRS = chronic restraint stress) Unpublished data. 143

Figure 59. The effects of GL-III-70 (**47**) on the percent alternation rate in the Y-maze spatial alternation task assessing working memory in mice. The chronic restraint stress (CRS) paradigm was used to induce a working memory deficit in young (2-3 months) mice.

The mice were injected with GL-III-70 (0, 1, 3, or 10 mg/kg) i.p. 30 min before testing. ANOVA revealed statistical significance on the overall effect of the treatment ($F(4,46)=15.008$; $p<0.0001$). Differences between groups were detected using post-hoc Scheffe analysis (**$p<0.01$ and ***$p<0.001$ compared to the "Control-Vehicle" group / \$$p<0.05$ and \$\$\$$p<0.001$ compared to the "CRS-Vehicle" group). Unpublished data. 144

Figure 60. The pro-cognitive efficacies of GL-III-70 (10mg/kg) and the NAM MRK-016 in the Y-maze alternation task. Statistical data not shown, unpublished data. 145

Figure 61. The potential pro-cognitive effect of **36** (GL-II-73) and **38** (GL-II-75) in the age-induced Y-maze task. The same experimental protocol was used for old mice but with a shorter interval to 1 minute. Old male mice were treated with either vehicle or test compound **36** (E; n(0-Young) = 5, n(0-Old) = 5, n(5) = 6) or 38 (F; n(0-Young) = 5, n(0-Old) = 5, n(5) = 4). The significance was obtained by comparing the treated group with the young and old vehicle control groups. The significance was not achieved with a sex cofactor. ($p \geqslant 0.49$). Results are shown as the mean of the percentage of alternation ± SEM. Effect of age: ++ $p < 0.01$ or +++ $p < 0.001$ compared to "Young vehicle." Effect of the ligand: \$ $p < 0.05$ compared to "Stress vehicle" or "Old vehicle." (Adopted from the figure in Prevot et al.)[117]..... 147

Figure 62. The pro-cognitive effect assessment of **36** (GL-II-73) and **38** (GL-II-75) on stress-induced and age-related working memory deficits. Effects of **36** (a, c) and **38** (b, d) were evaluated in young (a, b) and old (c, d) male mice via the sub-chronic administration (p.o.) in the drinking water for 10 consecutive days in the Y-maze task. Prior to the experiment, cognitive impairment in young mice was induced by CRS

exposure for 7 days. The young mice were treated sub-chronically with **36** (n(0-NS) = 6, n(0-S) = 5, n(30) = 6) or **38** (n(0-NS) = 5, n(0-S) = 5, n(30) = 6) dosed at 30 mg/kg. The old mice mice were treated sub-chronically with **36** (n(0-Young) = 5, n(0-Old) = 6, n(30) = 4) or **38** (n(0-Young) = 6, n(0-Old) = 5, n(30) = 5) dosed at 30 mg/kg. The results are presented as the mean of the percentage of alternation ± SEM. Effect of the stress: * $p < 0.05$, ** $p < 0.01$, and *** $p < 0.001$ compared to "No stress vehicle." Effect of the ligand: $$$ $p < 0.001$ compared to "Stress vehicle" or "Old vehicle." (Adopted from the figure in Prevot et al.)[117] 149

Figure 63. Flumazenil blocks the effects of **36** (GL-II-73) on percent alternation rate in the Y-maze spatial alternation task assessing working memory in mice. The chronic restraint stress (CRS) paradigm was used to induce a working memory deficit in young (2-3 months) animals. The animals were injected with vehicle, **36** (10 mg/kg) or a combination of **36** (10 mg/kg) and flumazenil (10 mg/kg) i.p. 30 min before testing. ANOVA revealed statistical significance on the overall effect of the treatment. Differences between groups were detected using post-hoc Scheffe analysis (**p<0.01 and ***p<0.001 compared to the "control-vehicle" group / $p<0.05 and $$p<0.01 compared to the "CRS-vehicle" group). n=4-6. Unpublished data. 151

Figure 64. βCCt blocks the effects of **36** (GL-II-73) on percent alternation rate in the Y-maze spatial alternation task assessing working memory in mice. The chronic restraint stress (CRS) paradigm was used to induce a working memory deficit in young (2-3 months) animals. The animals were injected with vehicle, **36** (10 mg/kg) or a combination of **36** (10 mg/kg) and βCCt (10 mg/kg) i.p. 30 min before testing. ANOVA revealed statistical significance on the overall effect of the treatment. The differences between

groups were detected using post-hoc Scheffe analysis (**p<0.01 and ***p<0.001 compared to the "Control-Vehicle" group / $p<0.05 and $$p<0.01 compared to the "CRS-vehicle" group). n=5-6. Unpublished data. 151

Figure 65. Xli-093 blocks the effects of **36** (GL-II-73) on the percent alternation rate in the Y-maze spatial alternation task assessing working memory in mice. The chronic restraint stress (CRS) paradigm was used to induce a working memory deficit in young (2-3 months) animals. The animals were injected with vehicle, **36** (10 mg/kg) or a combination of **36** (10 mg/kg) and XLi-093 (10 mg/kg) i.p. 30 min before testing. ANOVA revealed statistical significance on the overall effect of the treatment. Differences between groups were detected using post-hoc Scheffe analysis (**p<0.01 and ***p<0.001 compared to the "control-vehicle" group / $p<0.05 and $$ p<0.01 compared to the "CRS-vehicle" group). n=5-6. Unpublished data. 152

Figure 66. Alternation rate in the age-related model of cognitive dysfunction in the Y-maze task in young, old and old+treatment groups. (CONFIDENTIAL unpublished data)..... 154

Figure 67. Representative images of PFC pyramidal cells between groups (young, old, and old+treatment). Compared to young mice (A), all aged mice showed reductions in spine counts of pyramidal cells (the box in lower panels of A-C). It was noted that old+treatment mice showed a higher spine count than old mice [Scale bars: 5 um]. Note: The quantitation of spine subtypes was not included in the current study. (CONFIDENTIAL unpublished data) 155

Figure 68. Comparison of total dendritic lengths of pyramidal cells as well as the break-down analysis between young, old, and old+treatment groups. (CONFIDENTIAL unpublished data)..... 156

Figure 69. Comparison of total spine counts of pyramidal cells as well as the break-down analysis between young, old, and old+treatment groups. (CONFIDENTIAL unpublished data) 157

Figure 70. Comparison of overall spine density of pyramidal cells as well as the break-down analysis between young, old, and old+treatment groups. (CONFIDENTIAL unpublished data) 158

Figure 71. Anatomic structure of the normal and asthmatic bronchial wall. The asthmatic bronchial wall exhibits a series of pathological effects such as swelling, decreased lumen diameter, airway remodeling, infiltration of immune cells, mucus overproduction, goblet cell hyperplasia, ASM thickening, and contracting.[163, 167-170] (Drawing by Guanguan Li on iPad Pro, App: OneNote, version 16.11) 269

Figure 72. The structures of short-acting β2 agonist (salbutamol), corticosteroid (cortisol), and long-term β2 agonist (salmeterol). 271

Figure 73. The structures of the α4 selective ligands, CMD-45, XHe-III-74, XHe-III-74EE (ethyl ester) and XHe-III-74A (acid). 273

Figure 74. The structures of Hz-166 (**76**), SH-I-048A (**10**) and α5 subtype selective ligands SH-053-2'F-R-CH_3 (**1**), SH-053-2'F-R-CH_3-acid (**68**), MP-III-004 (**83**), MP-III-058 (**84**), that were evaluated in an organ bath assay for the effect of bronchorelaxation on guinea pig tracheal rings, and the study of electrophysiology. 275

Figure 75. The oocyte efficacy of the Hz-166 (**76**), SH-I-048A (**10**), and the α5 subtype selective ligands. Concentration curves on $GABA_AR$ using an EC_3 GABA concentration (n = 3 – 5). (Unpublished results from the Ph. D. thesis of M. Poe, in collaboration with Dr. Ernst's group.)[120] 276

Figure 76. The results of Hz-166 (**76**), SH-I-048A (**10**) and α5 subtype selective ligands on the airway muscle relaxation effects from the precontracted guinea pig tracheal rings induced by substance P (1 μM). This was followed by vehicle (0.1% EtOH) or a test ligand (50 μM) in an organ bath, and the muscle force was measured. ** and *** represent p< 0.01 and 0.001 as compared to vehicle control, respectively; $$$ p< 0.001 compared to SH-053, n = 6-17. SH-053 = SH-053-2'F-R-CH_3; SH-053 Acid = SH-053-2'F-R-CH_3-acid. (Unpublished results from the Ph. D. thesis of M. Poe, in collaboration with Dr. Ernst's group)[120] 277

Figure 77. The contractile force of ASM measurement in the presence of **68**. (A) The human tracheal airway smooth muscle strips were contracted with an EC_{50} concentration of acetylcholine (Ach) and then treated with 100 μM of the acid **68** or the vehicle 0.2% ethanol. The muscle force was measured at 15, 30, 45, and 60 minute time points after addition of **68**. The percent of the initial Ach-induced contractile force was presented as shown. Individual muscle strips were used from at least seven humans. (B) Guinea pig tracheal rings were contracted with 1 μM substance P and then treated with different concentrations of **68**. The percent of remaining contractile force was measured at 30 min and expressed as compared to the initial substance P-induced contractile force as a percent of control (N = 3). *, ** and *** represents $p < 0.05$, $p < 0.01$ and $p < 0.001$, respectively, as compared to the vehicle control. (Modified from the figure in Forkuo et al.)[99] 280

Figure 78. Effect of **68** on AHR. The sRaw was measured at an increasing dose of MCh by a DSI's Buxco FinePointe noninvasive airway mechanics instrument. Ligand **68** was orally administered in ova s/c BALB/c mice at 100 mg/kg twice daily for 5 days. Data

represent mean ± SEM (n=10). *, **, and *** represents significance $p < 0.05$, $p < 0.01$, and $p < 0.001$, respectively, as compared to the vehicle control. a5-acid = **68** (Modified from the Figure in Forkuo et al.)[99] 281

Figure 79. The pharmacokinetic data of **68** in blood, lungs, and brain in mice. The time-dependent systemic distribution of **68** was determined at 25 mg/kg via oral gavage. (Modified from the Figure in Forkuo et al.)[99] 282

Figure 80. The effect of **68** on sensorimotor coordination in vivo. The Swiss Webster mice received a single intragastric gavage of the ligand at 100 mg/kg or diazepam (5 mg/kg i.p.) and were placed on a rotarod at 15 rpm for 3 minutes, and the performance was recorded after 10, 30 and 60 minute time points of drug administration. A fail was assigned to a mouse if they had fallen twice within 3 minutes. The latency to fall is presented as mean ± SEM (n = 9). The vehicle was used as the negative control, and diazepam as the positive control. a5-acid = **68**. (Modified from the Figure in Forkuo et al.)[99] 283

Figure 81. Development of GL-II-93 (**85**) and its key features, as compared to the previous ligands in this series 285

Figure 82. The potentiation of GL-II-93 (**85**) at α-containing $GABA_AR$s. The transiently transfected HEK-293T cells with α subunits with β3 and γ2L subunits of $GABA_AR$ were used to measure the average enhancement of current evoked to GABA by 0.1 μM or 1 μM 85 by patch clamp. Data represented mean ± SEM (n = 5). (Adopted from the figure in Forkuo et al.)[187] 287

Figure 83. The pharmacokinetic data of GL-II-93 (**85**) in blood, lungs, and brain in mice. The time-dependent systemic distribution of GL-II-93 was determined at 25 mg/kg via oral gavage. (Adopted from the figure in Forkuo et al.)[187] 291

Figure 84. The incremental rotarod study of GL-II-93 (**85**) in mice. The Swiss Webster mice received a single intragastric gavage of GL-II-93 at an increased dosage 50-800 mg/kg rate or diazepam (5 mg/kg ip) and were placed on a rotarod at 15rpm for 3 minutes, and the performance was recorded after 10, 30 and 60 minutes. A fail was assigned to a mouse if they had fallen twice within 3 minutes. The latency to fall is presented as mean ± SEM (n = 9). The vehicle was used as the negative control and diazepam as positive control..... 293

Figure 85. In vitro cytotoxicity data of GL-II-93 (**85**). GL-II-93 was incubated with HEK293T cells and HEPG2 cells, respectively, for 48 hours followed by detection of cell viability using a Cell-Titer Glo (Promega). The results were normalized using DMSO as a negative control and 3-dibutylamino-1-(4-hexyl-phenyl)-propan-1-one (150 mM in DMSO final concentration, as a positive control. Data was determined by three independent experiments carried out in quadruplet. 294

Figure 86. The GL-II-93 (**85**) relaxed the contracted muscle induced by substance P ex vivo. Muscle force in guinea pig ASM contracted with 1 μM substance P. GL-II-93 (25−100 μM) significantly produced a relaxation of substance P induced contraction of guinea pig tracheal rings, as compared to vehicle (0.1% DMSO). Muscle force is presented as a percent of the first muscle force remaining at different time points. The significance was determined by a two-way ANOVA repeated measures analysis. *, **, and ***

represents p < 0.05, 0.01, or 0.001, respectively, as compared to vehicle (n = 33). (Adopted from the Figures in Forkuo et al.)[187] 296

Figure 87. The GL-II-93 (**85**) relaxed the contracted muscle induced by histamine ex vivo. A: The contractile force of the guinea pig tracheal ring was presented as a percentage remaining versus time in an organ bath. The tracheal rings were exposed to 10 μM histamine, which was used to induce a rapid contractile force. Once a stable peak was achieved, GL-II-93, or DMSO as vehicle control, was added. B: GL-II-93 presented a dose-dependent decrease in the contractile force, and the significant effect was observed at 25, 50, and 100 μM at 15 minutes, as compared to the control DMSO. The significance was determined by a two-way ANOVA repeated measures analysis (n=6-9), $p<0.05$. (Adopted from the figure in Yocum et al.)[188] 297

Figure 88. The human tracheal ASM strips were relaxed by GL-II-93 ex vivo. A: The contractile force of guinea pig tracheal ring was presented as a percentage remaining versus time in the organ bath. The tracheal rings were exposed to 10 μM of histamine. Once a stable peak was achieved, 100 μM GL-II-93 or DMSO as vehicle control, was added. B: The GL-II-93 at 100 uM relaxed ASM contractile force significantly by 30 minutes, as compared to the control DMSO. The significance was determined by a two-way ANOVA repeated measures analysis(n=6-10), *, and ** indicated $p<0.05$ and $p<0.01$, respectively. (Adopted from the Figure in Yocum et al.)[188] 298

Figure 89. The mouse peripheral airways in PCLS was relaxed by GL-II-93 ex vivo. The 100 nM MCh was used to induce the contraction of the peripheral airways of an A/J mouse lung slices, which was exposed to 100 μM GL-II-93 subsequently, while the microscopy image of airway luminal was recorded continuously. A: The still photos tracing of

airway luminal was presented over time during the experiments. B: The percentage of the overtime tracing of airway luminal area during the experiment. C: A significant reduction of MCh-induced ASM contraction was observed with GL-II-93 treatment. *** indicates p<0.001, (n=3). (Adopted from the Figure in Yocum et al.)[188] 299

Figure 90. The examination of orally administered GL-II-93 and salmeterol on AHR. The sRaw was measured at an increasing dosage of MCh on a DSI's Buxco FinePointe noninvasive airway mechanics instrument. A, B, C: GL-II-93 was orally administered in ova s/c BALB/c mice twice daily for 5 days at a dosage of 100, 50, and 20 mg/kg, respectively. D: Salmeterol was administrated at 1 mg/kg twice daily for 5 days. Data represent mean ± SEM (n=10). The significance was determined by a two-way ANOVA repeated measures analysis. *, **, and *** represents significance $p < 0.05$, $p < 0.01$, and $p < 0.001$, respectively. (Adapted from the figure in Forkuo et al.)[187] 300

Figure 91. The bronchoconstriction in mice was reduced by GL-II-93 (**85**) treatment in vivo. The A/J mice were given an inhaled, MCh challenge, anesthetized and mechanically ventilated, then the mice received nebulized GL-II-93 at 5 mM, for 10 s nebulization (50 % duty cycle) or 25% ethanol in PBS as vehicle control. The resistance of mice receiving GL-II-93 was significantly reduced in regard to airway resistance during the MCh challenge with an increasing concentration. Data represent mean ± SEM (n=6). The significance was determined by a two-way ANOVA repeated measures analysis, * indicated p<0.05. (Adopted from the Figure in Yocum et al.)[188] 301

Figure 92. The concentrations of GL-II-93 (**85**) in serum, lung, and brain in mice after inhalation, was followed by the airway resistance assay. The concentration of GL-II-93 was determined in the serum, lung, and brain tissues from the A/J mice with GL-II-93

treatment after inhalation at 30 min. The mean concentrations (n=6 mice) were 412.8±44.8 ng/g in the lung, whereas 9.6±3.0 ng/g in the brain. (Adopted from the figure in Yocum et al.)[188] 302

Figure 93. The influence of GL-II-93 and salmeterol on airway inflammatory cells. The vehicle, GL-II-93 (20, 50, or 100 mg/kg), or salmeterol (1 mg/kg) were orally administrated in the ova s/c mice twice daily for 5 days. BALF was obtained from each animal and analyzed for by flow cytometry (A) Quantification of total inflammatory cells using anti-CD45 APC antibody, (B) CD4+ T cell, (C) F4/80+ cell, and (D) Siglec F+ cell. Data represent mean ± SEM (n = 10). The significance was determined by a two-way ANOVA repeated measures analysis. *, **, and *** indicated the significance $p < 0.05$, $p < 0.01$, and $p < 0.001$, respectively, as compared to vehicle control. (Adopted from the figure in Forkuo et al.)[187] 304

Figure 94. The effect of GL-II-93 treatment on the cellular difference of the asthmatic mouse lung. The EdU was injected i.p. into the mice lungs and they were harvested after 4 h. A fluorescent azide was applied to the lung section with “Click” chemistry to produce the conjugation of EdU to visualize cells that underwent the dividing stage in a 4 hour-period (column 1). The Hoechst 33342 (column 2) was used to counterstain the sections, and the images were superimposed images as shown in column 3. The lung images of control mice were shown in Row 1. The images of vehicle-treated ova s/c mice are presented in Row 2. The images of GL-II-93 (100 mg/kg) treated ova s/c mice were shown in Row 3. (Adopted from the figure in Forkuo et al.)[187] 306

Figure 95. The effect on mucin production with GL-II-93 or salmeterol treatment. A: Images of lungs in control mice, ova s/c mice, salmeterol treated mice at 1 mg/kg, and GL-II-93

treated mice at 100 mg/kg twice daily for 5 days. Scale bar indicates 100 μm. Periodic acid fluorescent Schiff's stain agent was used to color the slides, and green represented the airway epithelium green, and mucin is in red. B: The mucin volume density of each group was measured. Data represent the mean ± SEM (n = 6). The significance was determined by a two-way ANOVA repeated measures analysis. (Adopted from the figure in Forkuo et al.)[187] 307

Figure 96. The evaluation of cytokine expression with GL-II-93 treatment in the lung. The quantification of mouse Th1/Th2/Th17 cytokines in mouse tissue homogenates was determined by applying the BD mouse Th1/Th2/Th17 cytometric bead array kit. Ova s/c mice were treated orally with 100 mg/kg GL-II-93 or vehicle twice a day for 5 days. The significance was determined by a two-way ANOVA repeated measures analysis. *, **, and *** represented the significance $p < 0.05$, $p < 0.01$, and $p < 0.001$, respectively. Data represent mean ± SEM (n = 10). (Adopted from the figure in Forkuo et al.)[187] 308

Figure 97. The effect of GL-II-93 on the average mouse body weights during the 28-day study. Peanut butter without or with 100 mg/kg MIDD0301 was administrated orally twice daily in both male and female Swiss Webster mice at the age of 8 weeks in a separate container. Mice without GL-II-93 treatment stayed in the same containers. Body weights were measured every week. Data represent mean ± SEM (n = 5). The significance was determined by a two-way ANOVA repeated measures analysis. *, and **, represented the significance $p < 0.05$, and $p < 0.01$, respectively. (Adopted from the figure in Zahn et al.)[189] 310

Figure 98. Evaluation of average body-weight with DNP-KLH immunization. Peanut butter without or with 100 mg/kg GL-II-93, or peanut butter + prednisone (5 mg/kg daily) was administrated orally twice daily to both male and female Swiss Webster mice at the age of 6 weeks in a separate container. DNP-KLH immunization was applied on days 1 and 21 for these 3 groups. Body weights were measured on day 14 and 28. Data represent mean ± SEM (n = 5). The significance was determined by a two-way ANOVA repeated measures analysis. *** indicates P < 0.001. (Adopted from the figure in Zahn et al.)[189]..... 311

Figure 99. Effect of 28 days of treatment of GL-II-93 on lymphoid organs and Peyer's patches from Swiss Webster mice immunized with DNP-KLH. Peanut butter without or with 100 mg/kg MIDD0301, or peanut butter + prednisone (5 mg/kg daily) was administrated orally twice daily in both female (A-C) and male (D-F) Swiss Webster mice at the age of 6 weeks. The DNP-KLH immunization was applied on days 1 and 21 for these 3 groups. After the 28 day test period, organs were obtained and weighed, and small intestines were dissected for the counting of Peyer's patches. Data represent mean ± SEM (n = 5). The significance was determined by a two-way ANOVA repeated measures analysis. *, **, and *** represented the significance $p < 0.05$, $p < 0.01$, and $p < 0.001$, respectively. (Adopted from the figure in Zahn et al.)[189] 312

Figure 100. The mouse spleens (A-H, 40x) and thymus (I-P, 100x) H&E staining. A and I) male mice, peanut butter; B and J) female mice, peanut butter; C and K) DNP-KLH-immunized male mice, peanut butter; D and L) DNP-KLH-immunized female mice, peanut butter; E and M) DNP-KLH-immunized male mice, peanut butter with 100 mg/kg GL-II-93 twice daily for 28 days; F and N) DNP-KLH-immunized female mice,

peanut butter with 100 mg/kg GL-II-93 twice daily for 28 days. G and O) DNP-KLH-immunized male mice, peanut butter with 5 mg/kg prednisone daily for 28 days; H and P) female DNP-KLH-immunized mice, peanut butter with 5 mg/kg prednisone daily for 28 days. (Adopted from the figure in Zahn et al.)[189] 314

Figure 101. The mouse serum DNP IgG. The peanut butter without or with 100 mg/kg GL-II-93, or peanut butter + prednisone 5 mg/kg daily was administrated orally twice daily in both female (A) and male (B) Swiss Webster mice. The DNP-KLH immunization applied on days 1 and 21, and quantification of DNP-specific IgG was measured on day 28. Data represent mean ± SEM (n = 5). The significance was determined by a two-way ANOVA repeated measures analysis. ** represented the significance $p < 0.01$. (Adopted from the figure in Zahn et al.)[189] 315

Figure 102. A, B, C, D: The mass spectra of GL-IV-19 (**90**) in 4-time points, respectively and examination of them indicated the conversion of GL-IV-19 to GL-II-93 took place in a time-dependent manner. The equilibrium was reached at 1 h, as compared to longer reaction times, which was very similar, data not shown here. 318

Figure 103. A, B, C: The mass spectra of GL-IV-19 (**90**) in DMSO at 0.5 min, 1 min, and 6 h time points, respectively. It indicated the conversion of GL-IV-19 to GL-II-93 in a time-dependent manner. The equilibrium was reached at 6 h, as compared to longer time points, data not shown here. 319

Figure 104. The ^{1}H NMR spectra comparison of GL-II-93 **85** (upper spectra in red) and GL-IV-19 90 (lower spectra in blue). The doublet of the C(4)-methyl group was shifted from 1.2 ppm to 1.4 ppm (two double are the rotamers of the methyl group in 90), and quartet of the C(4)-hydrogen atom from 6.4 ppm to 4.2 ppm. The peaks disappeared in the

spectra of 90 as indicated by yellow arrows, whereas the peak that appeared was colored in green. The DMSO peak was at 2.5 ppm; the D_2O peak was at 4.8 ppm. 320

Figure 105. The ^1H NMR spectra for the equilibrium study of the conversion from GL-II-93 (**85**) into the open ring form GL-IV-19 (**90**) with a increased volume of DCl (5.125 M) from bottom to the top the spectra follow this order: 0, 0.1, 1, 2, 3, 4, 5, 8, 11, 21 μL. ... 321

Figure 106. The area-concentration curve of the C(4) methyl group at (A) 1.4 ppm (the peak for the second rotamer was due to higher intensity), and (B) 1.2 ppm for the right panel under acidic conditions. 322

Figure 107. The ^1H NMR spectrum of 13 spectra in the kinetic study at pH = 2. The spectra were selected to show the obvious peak changes at specific time points. The bottom spectrum is the ^1H NMR spectrum of GL-II-93 (**85**) in the DMSO/ D_2O mixture, and the spectra with an increase of time points at 1, 2, 3, 4, 5, 6, 7, 8, 9, 11, 15, 20, 30, 40, 50, 62 minute time points in order from bottom to the top. As described above, the peaks for the C(4) methyl group and hydrogen atom were shifted from the position indicated with red arrows (peak decreased at 1.2 ppm and 6.4 ppm) to the position with green arrows (peak appeared at 1.4 ppm and 4.2 ppm). 323

Figure 108. The area (lg)-time curve for the C(4) methyl group of GL-II-93 (**85**) at pH = 2. The panel on the left is the rotamer appearing at 1.4 ppm, and the right-hand panel is for the disappearing methyl group peak originally at 1.2 ppm. The half-life for these two peaks is 1201 seconds and 1189 seconds, respectively. 324

Figure 109. The ^1H NMR spectra of equilibrium study of the conversion from 1 mg/mL of GL-IV-19 (**90)** to the original form GL-II-93 (**85**) or its sodium salt GL-IV-18 (**89**) with an increased volume of NaOD (7.23 M) from bottom to the top spectra as following order:

0, 0.001, 0.005, 0.01, 0.02, 0.05, 0.075, 0.1, 0.2, 0.5, 1, 2 μL.The pH after each addition was indicated..... 325

Figure 110. The ^{1}H NMR spectra of GL-IV-19 (**90**) in the DMSO/D_2O mixture and DMSO only. The pH in the mixture was about 4, and the peak of the product GL-II-93 (**85**) at 1.2 ppm had started to appear in the mixture, whereas this was not observed in the solution of DMSO only..... 326

Figure 111. In panel A is represented the area-concentration curve of the C(4) methyl group at 1.4 ppm (the peak for the second rotamer due to higher intensity), and panel B represents 1.2 ppm under basic conditions. The red dot on the Y-axis represented the trials without any addition of base but just in the mixture of DMSO and D_2O. 327

Figure 112. The ^{1}H NMR of 13 spectra in the kinetic study at pH = 8. The spectra were selected to show the obvious peak changes at time points. The spectra were presented with an increase in time point at 1, 9, 20, 30, 40, 50, 60, 80, 100, 120, 140, 160, 180 minutes in order from bottom to the top. As described above, the peaks of the C(4) methyl group and the C(4) hydrogen atom were shifted as indicated with green arrows (peak decreased at 1.2 ppm and 6.4 ppm) to the position with red arrows (peak appeared at 1.4 ppm and 4.2 ppm). 329

Figure 113. The area (lg)-time curve for the C(4) methyl group of GL-IV-19 (**90**) at pH = 8, the left panel is for the disappearing rotamer at 1.4 ppm, and the right panel is for the appearing methyl group peak originally at 1.2 ppm. The half-life for these two peaks is 8006 seconds and 8262 seconds, respectively. 329

Figure 114. Analogs of **85** by modification of the substituents at the C(3), C(4), C(8) and 2'X positions. 331

Figure 115. The effect of GL-III-43 (**86**) on AHR, orally administered. The sRaw was measured at an increasing dosage of MCh by a DSI's Buxco FinePointe noninvasive airway mechanics instrument. GL-III-43 was orally administered in ova s/c BALB/c mice at 100 mg/kg twice daily for 5 days. Data represent mean ± SEM (n=10). *** represents significance $p < 0.001$. 340

Figure 116. Potentiation of GL-III-54 and GL-II-93 in comparison at α_{1-5}-containing $GABA_ARs$. The transiently transfected HEK-293T cells with α subunits of $GABA_AR$ were used to measure the average enhancement of current evoked to GABA EC3 by 0.1 μM or 1 μM GL-III-54 and GL-II-93 by patch clamp. Data represented mean ± SEM (n = 5).... 341

Figure 117. The ASM contractile force in guinea pig tracheal rings contracted with 1uM substance P and then treated with 25, 50 or 100 μM GL-II-93 (**85**) or GL-III-54 (**87**) in comparison. Data are expressed as the amount of muscle force remaining at 15, 30, 45 and 60 minutes, as compared to the initial substance P-induced contractile force. *, **, *** represented the significance $p < 0.05, 0.01, 0.001$ as compared to vehicle control (0.1% DMSO), respectively. $, $$, $$$ represents $p< 0.05, 0.01, 0.001$ compared to 100 μM GL-III-54, respectively. The significance was determined by a two-way ANOVA repeated measures analysis with Bonferroni selected post-test comparisons n = 7 for GL compounds or 14 for vehicle controls. 343

Figure 118. Structure of Hz-166 (**76**), MP-III-080 (**102**), and KRM-II-81 (**77**)..... 387

Figure 119. The dose-responsive efficacy data of KRM-II-81 (**77**) at α1,2,3,5-containing GABAARs. EC3–5 GABA value is presented in percentage of response to GABA alone. 399

Figure 120. The effect of KRM-II-81 (**77**) on the potentiation of native GABA currents in cultured DRG neurons. A: Manual patch clamp recording of currents activated by saturating GABA concentration (1mM), and by EC10 concentration of GABA (5μM) and 10 μM of **77**. GABA current activated with a low concentration of 5μM GABA was enhanced by 10μM of **77**. B: Dose-response curve of **77** on currents activated with 5 μM GABA (EC10). The potentiation is represented as % of increase produced by saturating GABA-activated current. All values shown are mean ± SEM (n=4). (Adopted from Figure in Witkin et al., 2019) [245] 400

Figure 121. The evaluation of the anxiolytic-like activity of chlordiazepoxide and KRM-II-81 (**77**) in the marble burying assay. Male NIH Swiss Webster mice (n = 10) were administrated i.p. with either vehicle or chlordiazepoxide (CDAP) and KRM-II-81 (**77**) at 30 mg/kg 30 min prior to testing. The rotarod assay was performed (spinning at 4 rpm) for the assessment of motor impairment. Mice that fall off twice are scored as failures. Data were analyzed using ANOVA. Dunnett's test: (∗) $P < 0.05$ vs vehicle. 402

Figure 122. The Vogel Conflict assessment of anxiolytic-like properties with male Sprague-Dawley rats (n = 6-8). A. The evaluation of Hz-166 (76) and anxiolytic chlordiazepoxide (CDAP) administrated i.p. at 30 mg/kg and 20 mg/kg, respectively; B The dose response of KRM-II-81 (**77**) as compared to CDAP at 20 mg/kg. All compounds were administered 30 minutes prior to testing. Results were analyzed using ANOVA. Each point represents the mean + SEM of 6-8 rats. * $p<0.05$, significantly different than vehicle control. (Dunnett's test: * $P < 0.05$; Student t-test: ** $P < 0.05$). (Modified from the Figure in Poe et al.) [107] 403

Figure 123. The evaluation of the anticonvulsant activity of Diazepam, HZ-166 (**76**) and KRM-II-81 (**77**) in the MES assay. Male CD-1 mice (n = 10) were administrated i.p. 30 minutes prior to being tested with either vehicle (1% CMC), diazepam (1, 3 or 6 mg/kg), KRM-II-81 (3, 10 or 30 mg/kg) or HZ-166 (3, 10 or 30 mg/kg). Analyzed using ANOVA (Dunnett's test versus vehicle: * P < 0.05). (Adopted from Figure in Witkin, et al) [253] 407

Figure 124. The anticonvulsant effects of Hz-166 (**76**), KRM-II-81 (**77**), and diazepam against (A) pentylenetetrazole (PTZ)-induced seizures (35 mg/kg, s.c.) and (B) their motor performances on an inverted screen in rats. Data represent mean ± SEM (n=5-8). Significant probability was analyzed by Fisher's Exact Probability test (*: $p<0.05$). For the motor score, n = 5 (diazepam, 3 mg/kg) or 8 (all other data) rats, 0=climbed over to the top of the screen, 1= hanging on to screen, 2= fell off. Data were analyzed by ANOVA followed by Dunnett's test with * $p<0.05$. PTZ alone produced convulsions in 96 ± 4%. The baseline motor scores were 0.12 ± 0.8. (Adopted from Figure in Witkin et al.) [253] 409

Figure 125. The threshold measurement of Hz-166 (**76**), KRM-II-81 (**77**), and diazepam (DZP) against PTZ-induced seizures. The threshold procedure (B) dosed diazepam, KRM-II-81, HZ-166 or valproic acid 30 minutes prior to an i.v. infusion of pentylenetetrazole until convulsions were observed in rats, n = 8. Analyzed using ANOVA (Dunnett's test: * P < 0.05). (Modified from Figure in Witkin, et al) [253] 410

Figure 126. The effect of KRM-II-81 (**77**) in lamotrigine (LTG)-resistant amygdala-kindled rat model. (A)The percentage of seizure protection by **77** at the doses of 1, 5, 10, 20, and 40 mg/kg, (B) the seizure severity score of vehicle and **77** at 40 mg/kg, (C) the seizure

duration of vehicle and 77 at 40 mg/kg, The average seizure scores ± S.E.M.and afterdischarge duration is noted, as are the number of animals protected from seizure (defined as a Racine score < 3) over the number of animals tested. (Unpublished data) 414

Figure 127. The effect of KRM-II-81 (**77**) in the SE-induced spontaneous recurrent seizures model in rats. During the test period, a baseline seizure rate is determined in week 1. An initial group of 12 rats enrolled in Stage 1 chronic monitoring were split into two (N=6/group) treatment groups. During week 2, the first group of rats was administrated with 20 mg/kg of KRM-II-81 (77) over 5 days, Monday-Friday. Once the treatment is completed in week 2, rats will be monitored during week 3 with only vehicle treatment. Similar to the first group (n = 6), the second group (n = 6) receives vehicle first, followed by the treatment of **77**. Each data represents a seizure event. * $p<0.05$ as compared to the vehicle group. (Unpublished data) 417

Figure 128. Functional blockade of the epileptic phenomenon in cortical slices of KRM-II-81 (**77**) from juvenile epileptic patients. Data of network firing rate frequency (Hz) was collected for 1 hour under each condition (unfilled circle EACSF, no **77** treatment; filled circle EACSF + 30 µM of **77**) with either 10 µM of picrotoxin (left panel) or 50 µM AP-4 (right panel) as a neuronal stimulant. A 60-microelectrode array was used for recording. (paired t-test: $P < 0.05$). (Adopted from the Figure in Witkin et al.). 419

Figure 129. The assessment of antinociceptive effects of morphine, KRM-II-18B, and KRM-II-81 on (A) 0.6% acetic acid and (B) 0.32% lactic acid-induced writhing (n = 6−8 per group) observed in the 25 min observation period. *$P < 0.05$, ***$p < 0.001$. (Adopted from Figure in Lewter et al.) [236] 423

Figure 130. The assessment of flumazenil on the antinociceptive effects of KRM-II-18B- and KRM-II-81 in the acid-induced writhing model (n = 6−8 per group). Bars represent the mean and error bars show SEM. *P < 0.05, ***p < 0.001. (Adopted from Figure in Lewter et al.) [236] 424

Figure 131. The withdrawal threshold by KRM-II-81 (**77**) treatment in the CFA-induced inflammatory pain in von Frey test in rats (n = 6) at 1.78, 3.2, 5.6 mg/kg up to 270 minutes test period. Each point represents the mean + SEM of 6 rats. (Lewter, L., Cook, J.M. Li, J. The Behavioral effects of novel GABA(A) receptor positive allosteric modulators in rats. Biology, Behavior, and Chemistry Meeting, San Antonio, TX.,Mar. 2016) 425

Figure 132. The assessment of flumazenil on the antinociceptive effects of KRM-II-81 (**77**) in CFA-induced inflammatory pain in rats (n = 6). The filled circle represented the PAM (5.6 mg/kg) + flumazenil group. The unfilled circles represent the PAM + saline group. The effect of KRM-II-81 (77) was completely blocked by flumazenil at 10 mg/kg. (Lewter, L., Cook, J.M. Li, J. The Behavioral effects of novel GABA(A) receptor positive allosteric modulators in rats. Biology, Behavior, and Chemistry Meeting, San Antonio, TX.,Mar. 2016) 426

Figure 133. The evaluation of possible tolerance to the antinociceptive effects of KRM-II-81 (**77**) was conducted in rats (n=6) that received 5.6 mg/kg (i.p.) of KRM-II-81 twice a day for 11 consecutive days in CFA-induced inflammatory pain in von Frey test.Starting two days after CFA treatment, rats (n=6) were given 5.6 mg/kg of KRM-II-81, twice a day, for 11 consecutive days. On days 0, 4, and 8 rats will only receive P.M. injections due to the mechanical hyperalgesia test done in the A.M. (Unpublished data)..... 427

Figure 134. The assessment of antinociceptive effect of KRM-II-81 (**77**) in the formalin assay by reducing the paw-withdrawal thresholds. KRM-II-81 was given by i.p. injection to rats at a dose of 1-, 30, and 100 mg/kg, the positive control tramadol at 80 mg/kg. **77** (30 min prior) significantly reduced the nociceptive responses in the late phase at the dose of 30 mg/kg, whereas 100 mg/kg for the early stage. As a positive control, tramadol was active in both phases. Each point represents the mean±SEM of the same 8 rats *p<.05 compared to vehicle. (Modified from Figure in Witkin et al.) [245] 428

Figure 135. The assessment of KRM-II-81 (**77**) and gabapentin in the spinal (L5/6) nerve-ligation-induced neuropathic pain via the von Frey filament assay. Male Sprague-Dawley rats (n = 5) were administrated i.p. either vehicle, **77** (30 mg/kg), or gabapentin (50 mg/kg) and 30 minutes before testing. Analyzed using ANOVA (Dunnett's test: * P < 0.05). (Adopted from the Figure in Witkin et al, 2019) 430

Figure 136. The assessment of KRM-II-81 (**77**) and gabapentin in the chronic spinal (L5/6) nerve-ligation-induced neuropathic pain in the von Frey filament assay under conditions of sensitization training. Male Sprague-Dawley rats (n = 5) were administrated p.o. either vehicle, **77** (10, 30, or 100 mg/kg), or gabapentin (75 mg/kg) and 30 minutes before testing. Analyzed using ANOVA (Dunnett's test: * P < 0.05). 431

Figure 137. Acute dose-response effects of KRM-II-81 and MP-III-80 on (A) mechanical hyperalgesia and (B) thermal allodynia (n = 4). Veh represents mean of measurements from paclitaxel pre-treated animals in the vehicle dose response group (Mean ± SEM). 432

Figure 138. Effects of daily KRM-II-81 and MP-III-80 administration on chronic neuropathic pain (Day 18-40). Data for days 18-40 represent measurements of (A) mechanical

hyperalgesia and (B) thermal allodynia (n = 4) 30 minutes after KRM-II-81, MP-III-80 or Vehicle administration. Ptx – Paclitaxel pre-treatment group, Veh – Vehicle pre-treatment or treatment groups. Error bars - ±SEM 433

Figure 139. Effects of daily KRM-II-81 and MP-III-80 administration on chronic neuropathic pain (Day 19-39). Data for days 19-39 represent measurements of (A) mechanical hyperalgesia and (B) thermal allodynia (n = 4) before KRM-II-81, MP-III-80 or vehicle administration. Ptx – Paclitaxel pre-treatment group, Veh – Vehicle pre-treatment or treatment groups..... 433

Figure 140. The antidepressant effect of KRM-II-81 (**77**) in male NIH Swiss mice in the FST. Mice were injected i.p. with vehicle (1% HEC, 0.25% Tween 80, 0.05% antifoam), KRM-II-81 (3, 10 or 30 mg/kg) or imipramine (15 mg/kg), n=6. *p < 0.05; ***p < 0.0001 as compared to vehicle by Dunnett's test. 435

Figure 141. The effect comparison with administration i.p. of KRM-II-81 (30 min prior) and alprazolam (15 min prior) on measures of respiration in rats. a) Respiration rate, b) Tidal Volume c) Minute Volume / Kg. Data are means±S.E.M. (n = 8). *p < 0.05. (Adopted from Figure in Witkin et al., 2019)[245]..... 436

Figure 142. Drug discrimination assessment of increasing dose (3.2, 5.6, 10, 17.8, 32 mg/kg) of KRM-II-81 (**77**) as compared to the known drug of abuse, midazolam at 3.2 mg/kg. Upper panel, midazolam lever responding percentage; lower panel, responses per second. KRM-II-81 at 5.6 mg/kg does not substitute for midazolam in the drug discrimination assay..... 438

Figure 143. The effects of ketorolac (n=6), KRM-II-81 (n=8) or diazepam (n=6) effects on ICSS in the absence of the acid noxious stimulus in rats. Top panels show frequency-rate

curves. Significance ($p<0.05$) is indicated by filled symbols, as compared to vehicle. Bottom panels show the total stimulations earned across all frequencies expressed as a baseline % for each frequency-rate curve on the top. Upward arrows indicate a significant increase in ICSS. All points and bars represent mean (± S.E.M.). (Adopted from the Figure in Moerke et al., 2018)..... 439

Figure 144. The observation of possible tremors of KRM-II-81 (**77**) administrated p.o. at 120 mg/kg for 24 hours, n = 9. 440

Figure 145. The observation of righting reflex of KRM-II-81 (**77**) administrated p.o. at 120 mg/kg for 24 hours, n = 9. 440

Figure 146. The observation of sedation of KRM-II-81 (**77**) administrated p.o. at 120 mg/kg for 24 hours, n = 9, on rotarod test. 441

LIST OF TABLES

Table 1. The CNS effects at $GABA_A$ $\alpha_{1-6}\beta_{1-3}\gamma_2$ receptor subtypes.[18, 46-58] Presented at the Mona Symposium (2014), University of the West Indies.[59] Earlier reported, in part, by Mckernan et al. (ACNP). 7

Table 2. In vitro liver microsomal stability of **1** and **2**..... 25

Table 3. In vitro microsomal stability of analogs of SH-053-2'F-S-CH_3 (**2**). 39

Table 4. In vitro cytotoxicity of SH-053-2'F-S-CH_3 (**2**) analogs. 42

Table 5. Amide and thioamide analogs derived from SH-053-2'F-R-CH_3 (**1**). 49

Table 6. Oxadiazole derivatives related to the α5 subtype selective PAM, SH-053-2'F-R-CH_3 (**1**). 51

Table 7. The 1,3-oxazole analogs related to the α5 subtype selective PAM, SH-053-2'F-R-CH_3 (**1**). 52

Table 8. The binding affinity of **1** and **35**; the K_i values are reported in nM.[83, 121] 53

Table 9. Metabolic stability of amides and oxadiazoles. Unpublished data. (R-CH_3 isomers) ... 67

Table 10. Metabolic stability of amides and oxadiazoles. (S-CH_3 isomers)..... 67

Table 11. Cytotoxicity data of all synthesized analogs from both *R* and *S* enantiomeric series, as well as achiral analogs with different modifications at four proposed positions: C(3), C(4), C(8), and 2'-phenyl position. Unpublished data. 74

Table 12. Binding affinities at hERG, only the TMS-acetylene compounds among the entire compound library have slight affinity to hERG (PDSP). Unpublished data. 101

Table 13. Binding affinities at peripheral benzodiazepine receptor (PBR) for the novel compounds (PDSP). Unpublished data. 103

Table 14. KOR binding affinity from the primary binding assay. Unpublished data. (PDSP).. 105

Table 15. Selective compounds for KOR stimulation response..... 108

Table 16. K_i values for all three compounds at α1/2/3/5β3γ2 receptors. 108

Table 17. Antidepressant effect of all test compounds in the FST. Unpublished data. 137

Table 18. Summary of all compounds tested in the Y-maze task. Unpublished data. 146

Table 19. Summary of morphological analysis of young, old, old-treated mice in the prefrontal cortex (PFC) between groups. (CONFIDENTIAL unpublished data) 153

Table 20. Comparison of the essential pharmacological features of SH-053-2'F-R-CH_3 (**1**) and SH-053-2'F-R-CH_3-acid (68).[99] 279

Table 21. Primary and secondary binding assay for GL-II-93 in a panel of CNS receptors, channels, and transporters. (PDSP code for GL-II-93 is 50109) 288

Table 22. Summary of microsomal stability studies for GL-II-93. 291

Table 23. Summary of plasma protein binding in mice. 292

Table 24. The solubility of GL-IV-19, GL-II-93 and GL-IV-18. 316

Table 25. The binding affinity at α1-6β3γ2 $GABA_AR$ BzR. Measurements were generated in duplicate. K_i values are reported in nM. (Modified from the Figure in Fischer et al.)[83] 332

Table 26. Efficacy at α1-3,5β3γ2 $GABA_ARs$ as % of the control current at the concentration of 0.1 and 1 μM. Data are presented as 0.1μM/1 μM. (Modified from the Figure in Fischer et al.)[83] Data determined in the laboratory of Dr. Sieghart with an EC_3 GABA. 333

Table 27. Cytotoxicity of GL-II-93 (85) analogs. 339

Table 28. Optimization of reduction conditions to form aldehyde **107**. 395

Table 29. The effects of KRM-II-81 (**77**) p.o. in the 6 Hz seizure model and the motor effects. (Adopted from Figure in Witkin, et al) [253] 406

Table 30. Protective indices (PI) for DZP and **77.** (Modified from Figure in Witkin et al.) 411

Table 31. The effect of KRM-II-81 in a corneal kindled mouse model. (Unpublished data).... 412

Table 32. The effect of KRM-II-81 (**77**) at 15 mg/kg on in MTLE mice model. (Unpublished data) 415

Table 33. The effect of KRM-II-81 (**77**) at 30 mg/kg on in MTLE mice model. (Unpublished data) 415

Table 34. Pre-clinical results of KRM-II-81 (**77**) in different animal models of epilepsy as well as in human cortical epileptic tissue. (Adopted from Table in Witkin et al. 2019) 419

Table 35. PDSP compound list. 513

Table 36. PDSP primary binding data for 5-HT1A, 5-HT1B, 5-HT1D, 5-ht1e, 5-HT2A, and 5-HT2B..... 517

Table 37. PDSP primary binding data for 5-HT2C, 5-HT3, 5-ht5a, 5-HT6, 5-HT7, and Alpha1A. 522

Table 38. PDSP primary binding data for Alpha1B, Alpha1D, Alpha2A, Alpha2B, Alpha2C, and Beta1. 526

Table 39. PDSP primary binding data for Beta2, Beta3, BZP Rat Brain Site, Calcium Channel, D1, and D2. 531

Table 40. PDSP primary binding data for D3, D4, D5, DAT, DOR, and GABAA..... 536

Table 41. PDSP primary binding data for H1, H2, H3, H4, HERG binding, and KOR. 541

Table 42. PDSP primary binding data for M1, M2, M3, M4, M5, and mGlur5. 545

Table 43. PDSP primary binding data for MOR, NET, NMDA, Oxytocin, PBR, and SERT... 550

Table 44. PDSP primary binding data for Sigma 1, Sigma 1 GP, Sigma 2, Sigma 2 PC12, V1A, V1B, and V2. 554

Table 45. PDSP secondary binding data for 5-HT1A, 5-HT1B, 5-HT1D, 5-ht1e, 5-HT2A, and 5-HT2B..... 559

Table 46. PDSP secondary binding data for 5-HT2C, 5-HT3, 5-ht5a, 5-HT6, 5-HT7, and Alpha1A. 564

Table 47. PDSP secondary binding data for Alpha1D, Alpha2A, Alpha2B, Alpha2C, Beta1, and Beta2. 569

Table 48. PDSP secondary binding data for Beta3, BZP Rat Brain Site, D1, D3, D5, and DAT. 574

Table 49. PDSP secondary binding data for DOR, H1, H2, H3, H4, and HERG binding. 578

Table 50. PDSP secondary binding data for KOR, M1, M2, M3, M4, M5 and mGlur5. 584

Table 51. PDSP secondary binding data for MOR, NET, NMDA, PBR, Sigma 1, Sigma 2, and Sigma 2 PC12. 589

Table 52. Pharmacokinetic parameters in mice and rats calculated for GL-II-73, GL-II-74, GL-II-75, RV-II-04, GL-II-31, MP-III-023, GL-I-54, GL-III-23, GL-II-33, GL-II-54 and GL-I-65. 596

Table 53. PK parameters for GL-III-68 and GL-III-70. 605

Table 54. Summary table (occupancy, efficacy, binding)..... 624

Table 55. Summary table (microsomal stability, FST, Y-maze) 626

Table 56. Summary table (Y-maze, SLA, RR, EPM). 629

Table 57. Raw data of anti-schizophrenia model. 663

Table 58. Raw data of anti-schizophrenia model. Continued. 671

LIST OF SCHEMES

Scheme 1. Synthesis of SH-053-2'F-R-CH_3 (**1**). 28

Scheme 2. Synthesis of SH-053-2'F-S-CH_3 (**2**). 29

Scheme 3. Synthesis of 8-cyclopropyl-4-(S-CH_3) imidazodiazepine **13** from bromide **14**.[48]..... 34

Scheme 4. Synthesis of methyl esters **14** and **16** from ethyl ester **15** or **2**, respectively.[48] 35

Scheme 5. Synthesis of esters **17-20** from ethyl ester **2** via transesterification.[110] 35

Scheme 6. Synthesis of analogs **21-30.** 37

Scheme 7. Synthesis of oxadiazoles **31-33**..... 38

Scheme 8. Synthesis of the C(3)-substituted nitrile **34.** 39

Scheme 9. Synthesis of the C(8)-ethinyl amide analogs **35-40** of the parent ethyl ester **1** (SH-053-2'F-R-CH_3). 56

Scheme 10. Synthesis of the C(8)-ethinyl thioamide analogs **41-44** from corresponding amides **35-38.** 57

Scheme 11. Synthesis of C(8)-bromo amides **45-46** and C(8)-cyclopropyl amides **47-48** from SH-I-47 (**6**).[82, 120] 58

Scheme 12. Synthesis of analogs in the 2'N-R-CH_3 series..... 60

Scheme 13. Synthesis of 1,2,4-oxadiazole analogs **51-63** with the C(8)-ethinyl, bromo or cyclopropyl group in the 2'F or 2'N pendant phenyl series..... 61

Scheme 14. Synthesis of the 2'F-R-CH_3 chiral 1,3-oxazole GL-III-73 (**66**). 65

Scheme 15. Synthesis of GL-II-93 (**85**). 286

Scheme 16. A. The structure of EdU. B. The "click" chemistry between EdU labeled DNA and Alexa Fluor 488 azide. The alkyne of EdU reacted with the azide in the presence of a copper catalyst to form a detectable triazole ring. 305

Scheme 17. Synthesis of the keto (ring-opened) form GL-IV-19 (**90**) and the sodium salt form GL-IV-18 (**89**) from GL-II-93 (**85**). 316

Scheme 18. Synthesis of GL-III-20 (**91**) and SH-053-2'F-S-CH_3-acid (**23**) from the corresponding ethyl esters in the 2'F-S-CH_3 series..... 331

Scheme 19. Synthesis of GL-III-19 (**92**) and GL-II-79 (**93**) negative controls from the corresponding ethyl esters in the achiral 2'F series..... 333

Scheme 20. Synthesis of GL-II-51 (**94**) and GL-II-30 (**95**) from the corresponding ethyl esters in the 2'N-*R*-CH_3 series..... 334

Scheme 21. Synthesis of GL-III-54 (**87**); the C(8)-Cl analog of **85**..... 335

Scheme 22. Synthesis of GL-III-43 (**86**); the C(8)-cyclopropyl analog of **85**. 336

Scheme 23. Synthesis of GL-IV-14 (88); the C(8)-OH analog of **85.** 337

Scheme 24. Synthesis of GL-IV-21 (96); tetrazole analog of **85.** 339

Scheme 25. Optimized total synthesis of Hz-166 (**76**)..... 390

Scheme 26. Synthesis of MP-III-080 (**102**) from Hz-166 (**76**). 392

Scheme 27. Attempts to prepare aldehyde (**4**) from Hz-166 (**1**). 394

Scheme 28. The optimized synthesis of oxazole **77** with a significantly improved overall yield. 397

LIST OF ABBREVIATIONS

ACh	acetylcholine
AHR	airway hyperresponsiveness
AP-4	4-Aminopyridine
ASM	airway smooth muscle
BALF	bronchoalveolar lavage fluid
BBB	blood-brain-barrier
BQL	below the quantification limit
BZD	benzodiazepine
BzR	benzodiazepine receptor
CFA	complete Freund's adjuvant
CDAP	chlordiazepoxide
CINP	Chemotherapy-induced neuropathic pain
CMC	carboxymethyl cellulose
CNS	central nervous system
COPD	chronic obstructive pulmonary disease
CRS	chronic restraint stress
DI	diazepam-insensitive
DLM	dog liver microsomes
DNP-KLH	dinitrophenyl hapten-keyhole limpet hemocyanin
DS	diazepam-sensitive
ETSP	Epilepsy Therapy Screening Program
FDA	Food and Drug Administration

FST	forced swim test
GABA	gamma-aminobutyric acid
$GABA_AR$	gamma-aminobutyric acid type A receptors
$GABA_BR$	gamma-aminobutyric acid type B receptors
GINA	Global Initiative for Asthma
hERG	human Ether-à-go-go-Related Gene
HEK	human embryonic kidney cells
HDM	house dust mite
HLM	human liver microsomes
HPLC	high-performance liquid chromatography
ICSS	ICSS
IMDZ	imidazodiazepine
IgG	immunoglobulin G
IP	intraperitoneal
IV	intravenously
KA	kainic acid
KOR	kappa opioid receptors
LABA	long-acting β_2 agonist
LR	Lawesson's reagent
LTG	lamotrigine
MAM	methylazoxymethanol acetate
MCh	methacholine
MDD	major depressive disorder

MED	minimal effective dose
MES	maximal electroshock
MLM	mouse liver microsomes
MOE	Molecular Operating Environment
MPE	maximum possible effect
MRM	multiple reaction monitoring
MTD	minimal toxic dose
mTLE	mesial temporal lobe epilepsy
MW	molecular weight
NAM	negative allosteric modulator
NIMH	National Institute of Mental Health
NO	nitric oxide
NMDA	*N*-methyl-D-aspartate
Ova s/c	ovalbumin sensitized challenged
PAM	positive allosteric modulator
PBR	peripheral benzodiazepine receptor
PCLS	precision-cut lung slice
PCP	phencyclidine
PDSP	Psychoactive Drug Screening Program
PEG	polyethylene glycol
PFC	mouse prefrontal cortex
PI	protective indices
PK	pharmacokinetics

PPI	prepulse inhibition
PTZ	pentylenetetrazole
PWT	paw withdrawal threshold
PO	oral administration
RLM	rat liver microsomes
SABA	short-acting β_2 agonist
SAR	structure-activity relationship
scMET	subcutaneous pentylenetetrazole
SE	severe epilepsy
SEM	standard error of the mean
SLA	spontaneous locomotor activity
SNL	sciatic nerve ligation
SSRI	selective serotonin reuptake inhibitors
sRaw	specific airway resistance
SST	somatostatin
TLC	thin-layer chromatography
TLE	temporal lobe epilepsy
TPE	time of peak effect
TSPO	translocator protein
UCMS	unpredictable chronic mild stress

ACKNOWLEDGMENTS

First and foremost, I would like to express my sincere gratitude to my advisor Professor James M. Cook for the opportunity to allow me to be the leader on several projects. His generous support professionally and personally, and outstanding guidance on my research as well as my papers and thesis writing. Also, I am grateful for his invaluable suggestions for job applications, as well as continuous encouragement to complete my doctorate in synthetic medicinal chemistry throughout the years on this marvelous journey. In addition, Dr. Cook gave me a chance to gain experience in grant and patent writing to further my development during my time at the UW-Milwaukee. This will be of critical value in my future career. I would also like to thank the members in my doctoral committee, Professor's Arnold, Schwabacher, Pacheco, and Moran for giving great graduate lectures of the beautiful world of chemistry, their helpful suggestions, instructive discussions, and advice not only on my course and research work, but also on my future career plans.

I would like to express my gratitude to our numerous collaborators, and it was a pleasure working with them. I have benefitted greatly and gained significant knowledge in various fields through the insightful discussions with each individual, especially Dr. Etienne Sibille (CAHM, University of Toronto, Canada), Miroslav Savić (University of Belgrade, Serbia), Dr. Petra Scholze and Dr. Ernst Margot (Medical University of Vienna, Austria), Dr. Catherine Belzung (University of Tours, France), Dr. Jeff Witkin (Eli Lilly and Company, USA), Dr. Donna M. Platt (Mississippi Medical School, USA), Dr. Jun-Xu Li (University at Buffalo, USA), Dr. Soma Sengupta (Emory University, USA), Dr. Charles W. Emala (Columbia University, USA) Dr. John Chan and Dr. Jyoti Sengupta (Medical College of Wisconsin, USA). A special thanks to Dr. Leggy A. Arnold and Dr. Stafford (UW-Milwaukee, USA) for their generous support, helpful advice and

encouragement at the biweekly asthma meetings as well as their excellent suggestions on the presentation of the GMP synthesis ideas to the Alcami Corporation.

I am thankful for the past and present members of the Cook group. It has been a great pleasure to be a part of this excellent group. I thank the former members in the group, Dr. German Fonseca, Dr. Sundari Rallapalli, Dr. Ashwini Verma, Dr. Ranjit Verma, and Ms. Poonam Biawat for their wise guidance at the time when I first joined the group. I would like to thank Dr. Michael Rajesh and Dr. Kashi Reddy Methuku for their help on my studies on the mechanism, reaction optimization, as well as a detailed explanation for biological assays. I would also like to thank Dr. Lalit Golani, for his help and patience on training me on molecular modeling. I thank my seniors Dr. Michael Poe and Dr. Chris Witzigmann for their great help on introducing me to many research techniques and skills in organic chemistry, which benefited me throughout my Ph.D. years here. Last but not the least, I sincerely thank Dr. V. V. N. Phani Babu Tiruveedhula and Dr. Tofique Rahman for their great company, support, discussions, and advice after work hours in the laboratory for the past seven years, which made my work late at night much fun and fruitful. This will be one of the greatest memories in my life.

I am very grateful to my colleagues. I thank Rajwana and Zubair for their help during my first two years of course work and later help on research. A special thanks to Dan for sharing his insightful ideas and excellent lab skills, as well as the generous ride and company for the trip to the H. C. Brown lectures at Pardue University. I would also like to thank all the current group member Farjana Rashid, Taukir Ahmed, Yeunus Mian, Kamal Pandey, Prithu Mondal, Nicholas Lewandowski and Sepideh Rezvanian for creating such an amicable atmosphere in helping each other as much as one can in this group and for bringing extra fun (FOOD) for our Saturday group meetings.

I would like to acknowledge the financial and academic support of the Department of Chemistry at UW-Milwaukee, the UW-Milwaukee Graduate School, and the National Institutes of Health (NIH). I gratefully acknowledge the Sosnovsky Award for Excellence in Graduate Research, which boosted my confidence and inspired me to work harder. I thank the Late Professor George Sosnovsky for sponsoring the Sosnovsky Award. I express deep gratitude to Dr. Frank H Holger for his invaluable help for NMR, and Mr. Neal Korfhage for the design and fabrication of very specialized glassware. I sincerely thank Dr. Mark Wang for performing and teaching me the techniques of LCMS and HRMS analysis. I greatly appreciate Dr. Anna Benko for her outstanding expertise and support during the last couple of years for help with mass spectroscopy. I would also like to thank Dr. Shama Mirza for her help in the analysis of mass spectra. I would also like to thank Mr. Kevin Blackburn, Ms. Elise D. Nicks, Ms. Wendy Grober, Ms. Shelley Hagen, Ms. Mary Eckert, and Ms. Goldie Gibbs for being there for me whenever I needed help.

I would like to extend my special thanks to my friends: Dr. Fang du, Dr. Lanlan Han, Dr. Yongtao Zhu, Mrs. Wei Zhou, Mr. Peng Geng, Mrs Yuting Tan in Milwaukee as well as all my friends in China, especially Ms. Yaxing Li and Mrs. Lu Shen, who has helped, supported and accompanied me, and shared the joyful time with me on this great journey.

Finally, I want to thank my family. I thank my cousin Dr. Jinxin Li for his visit last year, and my cousin Mr. Zimo Li and my aunt Mrs. Andao Tian for their help and support when I first stepped onto this brand-new but strange land years ago. I would like to give special thanks to my uncle Dr. Jin Li, who has encouraged and supported me with his stories and advice since I was a kid. I could not ever image I could pursue my Ph. D. studies one day in the U.S. without him. Lastly, I would like to express my love sincerely to my dearest father Mr. Qing Li and my mother Mrs. Jianping Du, to which this whole thesis is dedicated to for all their unconditional love,

invaluable support and encouragement throughout my life from day one, and especially for their great company during the last three months when I was writing my Ph. D. thesis. I will never forget and will always be grateful for the 3 A.M. strong tea service, every delicious hot meal, each trustful eyesight, and all the sweet and encouraging words from them physically, mentally and emotionally. I would never be able to accomplish this hard task without their help, support, respect, blessing, and trust. They have made my last few months in Milwaukee one of the best times of my life.

Chapter 1. Introduction

1.1. The $GABA_A$ receptors

In the central nervous system (CNS) in the mammalian brain, gamma (γ)-amino butyric acid (GABA), the chief inhibitory neurotransmitter, is principally responsible for the inhibition of excess decrease in the neuronal activity.[1] The inhibitory effect of GABA can be triggered *via* binding to GABA receptors, which are composed of two major classes: $GABA_A$ receptors ($GABA_AR$) and $GABA_B$ receptors ($GABA_BR$). The $GABA_A$-rho receptors, previously named $GABA_C$ receptors, are now classified into $GABA_A$ receptors as a subclass due to the composition of ρ (rho) subunits related to $GABA_AR$. This subclass is not discussed here.[2] The $GABA_ARs$ are contained in fast-acting transmembrane ligand-gated chloride ion channels. Upon activation, $GABA_AR$ causes a conformational change in the ion channel permitting chloride ions to pass through the pentameric channel, which results in the hyperpolarization of the gradient, which reduces neuronal transmission.[3] Whereas the slow-acting $GABA_BR$ are members of the G-protein coupled receptor family and are linked to the mediation of the activity of potassium and calcium channels.[4] The accumulating evidence has long indicated that disruption of the proper function of $GABA_AR$ is associated with a wide variety of CNS disorders, such as schizophrenia,[5] major depressive disorder (MDD),[6] anxiety,[7] epilepsy[8] as well as neuropathic pain.[9]

To study the relationship between the function of $GABA_AR$ and different CNS disorders, a large body of research has been conducted to explore the structures and activities of $GABA_ARs$. The leading cause of different pharmacological effects is the multiplicity of the specific combination of $GABA_AR$ subunits.[10] In humans, there is a total of 19 subunit isoforms (α1-6, β1-3, γ1-3, δ, ε, π, θ, ρ1-3).[11] The minimal requirement of the most common and well investigated

$GABA_AR$ is the combination of α, β and γ subunits (α1-6β1-3γ2) in a stoichiometric ratio of 2:2:1.[2] This is required for a fully functional allosteric effect of benzodiazepines at the α and γ interface.

Immunocytochemistry studies have been employed by Wisden et al.[12] to determine the occurrence of $GABA_AR$ in the CNS of rodents, as well as the distribution of different assemblies of $GABA_AR$. It has been well documented that α1 β1-3 and γ2 are highly expressed throughout the brain both synaptically and extrasynaptically.[13] The most abundant combination of $GABA_AR$ in the rat brain is α1β2γ2, which accounts for at least 60 % of total $GABA_AR$.[13-15] The α2 and α3 containing $GABA_ARs$ have similarly high prevalence and account for approximately 20-30 % of $GABA_AR$ in rat brain.[13-15] The α5 containing $GABA_AR$ are localized predominately in the cortex, and the hippocampus, and represent about 5 % of the total $GABA_AR$. This prevalence is much lower, as compared to other subtype assembles in rat brain.[13-16] Moreover, $GABA_ARs$ are not restricted to the CNS; a large amount of evidence indicates that $GABA_AR$ can also be found in other tissues outside of brain including the lungs, stomach, heart sinus node, intestines, etc. [1]

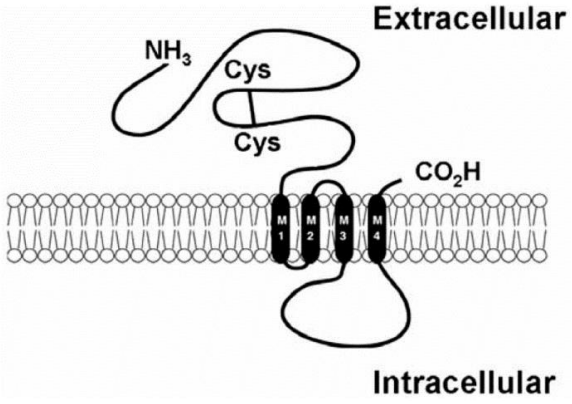

Figure 1. A proposed $GABA_AR$ subunit topology. The extracellular domain starts with the N-terminal end, and the M1-M4 are regions within the membrane. (Modified from the Figure in Burt, et al. [17] and Clayton, et al.)[18]

The approximate molecular mass of $GABA_AR$ subunits is ~50 kD, and the structure of the receptors exhibit high homology. Each subunit contains four transmembrane domains M1-M4,

embedded in the lipid bilayer of its neuron. Both the C- and N- terminal of the subunit are located in the extracellular region, which includes potential glycosylation sites and a "cys-loop" formed by a disulfide bond at the N-terminal end. The large intracellular region is located between domain 3 and 4, which is responsible for the regulation of $GABA_AR$ at possible phosphorylation sites (Figure 1). Five monomeric subunits can arrange in a ring to form the hetero- or homo- pentameric chloride channel (Figure 2).[17-19]

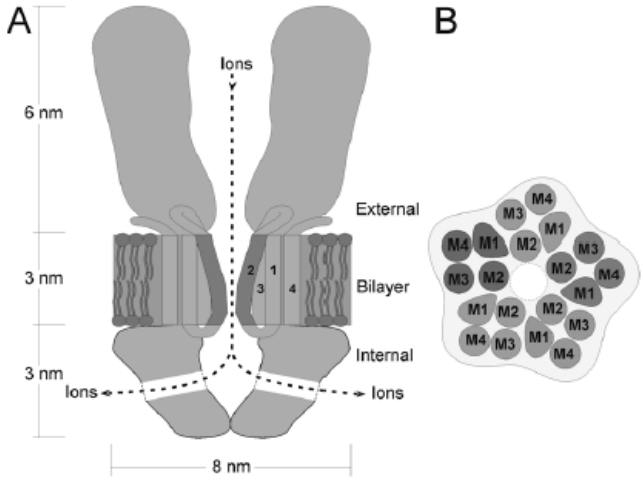

Figure 2. The schematic representations of $GABA_AR$, the ligand-gated chlorine ion channel in longitudinal vision (A) and cross-sectional vision (B). The number 1-4 represents the M1-M4 transmembrane domains. The domain M2 contributes to most of the pore lining within the lipid bilayer membrane. (Modified from the Figure in Keramidas et al.[19], and Clayton et al.)[18]

It has been well studied that besides the two binding sites for GABA, $GABA_ARs$ contain a series of other binding sites for psychoactive compounds including benzodiazepines, barbiturates, anesthetics, neurosteroids, ethanol, etc., at the synapse and inside the channel as well.[1-2, 10, 14, 18] The view from the extracellular region of the clockwise-arranged αβαβγ subunits illustrates the binding sites of $GABA_AR$ (Figure 3). GABA binds at the two interfaces of the $\alpha^-\beta^+$ subunits, whereas the benzodiazepines bind at the interface of the $\gamma^-\alpha^+$ subunits.[1-2, 7, 18] The interface of $\beta^-\alpha^+$

is also the binding site of newly discovered subtype-selective target CGS 9895 by Seighert, Ernst, Cook et al.[18, 20-21] More recently Knutson et al, have shown this receptor can be alpha 6 subtype selective.[22-24] In addition, drugs such as barbiturates[1-2, 15] and ethanol,[25-26] can also bind in the interior portion of the ion channel, which not only enhance the response of GABA but also opens the chloride ion pore directly to a degree, which results in the addiction potential or even death.[1-2, 10, 14-17]

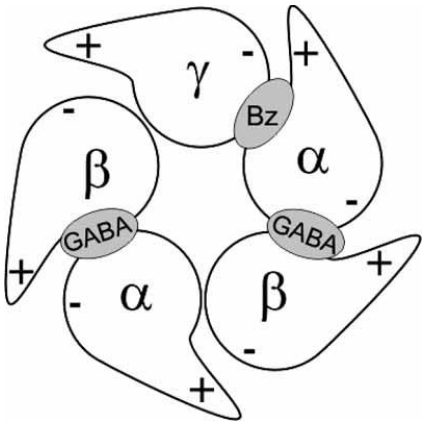

Figure 3. The arrangement of the α1β3γ2 $GABA_AR$ subtypes as viewed from the synaptic cleft. The binding sites of GABA are located at the interfaces between β^+ and α^- subunits and the BZD binding site is located at the interface of the $\alpha^+\gamma^-$ subunits. The + represents the loop C of each subunit. (Modified from the Figure in Clayton, et al.[18] and Ernst, et al.)[27]

1.2. Benzodiazepines (BZD)

Benzodiazepines (BZDs), as a class of psychoactive drugs, were first discovered in 1955 by Leo Sternbach. The first and most successful BZD drug, diazepam, was marketed as Valium in 1963.[28] Due to their potent activity, low toxicity[29], minimal drug-drug interactions in the liver,[30] rapid penetration across the blood-brain barrier (BBB), rapid absorption from the gastrointestinal tract, and ready distribution in the brain,[31-33] BZDs have been prescribed for the treatment of a series of CNS disorders such as anxiety, seizures, and insomnisia[28, 34] for over 50 years. Traditional

BZDs share a core structure of a benzene ring fused with a seven-membered diazepine ring, together with a pendant phenyl C ring (Figure 4).[35]

Classical 1,4-benzodiazepines such as diazepam (Figure 4) and alprazolam exhibit a high affinity for Bz/$GABA_AR$ non-selectively at the benzodiazepine binding site (BzR), at the interface of the $\gamma^-\alpha^+$ subunits.[1-2, 7, 18] Therefore, the α and γ subunits are much more critical than β subunits in terms of the influence on the pharmacological effects of BZDs.[36] It has been illustrated that BZDs interact with $\alpha_{1\text{-}3,5}\beta_{2/3}\gamma_2$ $GABA_AR$ subtypes, but exhibit fewer effects at $\gamma_{1,3}$ subtypes.[37] Besides the major diazepam-sensitive (DS) $GABA_AR$ subtypes, two other subtypes, α4- and α6-containing $GABA_AR$, account for a much less percentage in the brain,[38] as compared to the DS $GABA_AR$ subtypes. It has been demonstrated that the binding pocket of diazepam-insensitive (DI) subtypes is not able to tolerate the pendent phenyl C ring of BZD ligands, such as the 1,4-benzodiazepine diazepam and the imidazodiazepine (IMDZ) midazolam (Figure 4).[39-40] However, drugs such as flumazenil (Figure 4), which lack the pendent phenyl C ring, can bind to all 6 major subtypes at both DS and DI sites.[11]

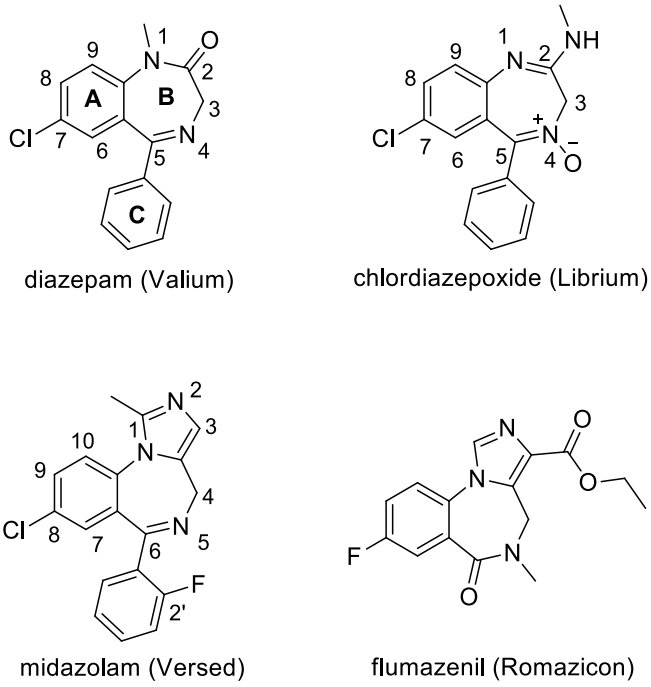

Figure 4. The structures of common BZDs: diazepam, chlordiazepoxide, imidazodiazepine (IMDZ) midazolam and flumazenil. The atoms are labeled for both BZDs and IMDZs. Diazepam, chlordiazepoxide, and midazolam can bind only to the DS sites, whereas flumazenil can bind to both the DS and DI sites.

In the absence of GABA, a BZD itself is not able to modulate $GABA_AR$ directly.[41] Once a BZD is bound to $GABA_AR$ ion channel, the affinity of GABA to $GABA_AR$ is enhanced, which results in a much higher frequency of the chloride ion channel opening and hyperpolarization of the membrane potential.[42] This results in inhibition of neuronal firing which is responsible for a series of pharmacological properties; for instance, anxiolytic, ataxic, amnesic, and sedative effects, as well as anticonvulsant effects, etc., which permits the use of BZDs for a variety of CNS disorders including GAD, SAD, PTSD, status epilepticus, and panic disorders. However, despite all the advantages, BZDs do, unfortunately, produce a series of adverse effects that are due to the simultaneous non-selective binding and efficacy at many $GABA_ARs$.[2, 28] The common side effects of BZDs include sedation, ataxia, amnesia, addiction, fatigue, dependence, withdraw issues, muscle-relaxation, and tolerance to the antinociceptive and anticonvulsant effects.[43-45] Therefore,

there is a large unmet medical need for improved BZDs that could retain the desired pharmacological properties, but be devoid of the unnecessary side effects for better treatment of a series of CNS disorders.

1.3. Modulation of BZDs on the Pharmacological Effects of $GABA_AR$

The converging lines of evidence have demonstrated that the pharmacological effects of the $GABA_ARs$ depend on modulation of receptor subtypes, principally due to the type of α_x subunits. Due to the pioneering work of Mohler, Sieghart, McKernan, Sigel, Seeburg, Squires, and Haefely, the identification of the associated effect for each subunit was achieved by using receptor binding, pharmacology and a molecular genetic approach, which introduced a point mutation into a specific α subunit. This involved replacement of the histidine amino acid (AA) by an arginine AA in the α1 subunit (α1His101Arg),[46] α2His101Arg, α3His126Arg,[47] and α5His105Arg.[48] The rodents which contained the specific mutations above were treated with diazepam, and the change of the behavioral response (or lack thereof) was considered to be mediated by the mutated subunits as compared to the wild-type animals.[46-48] The pharmacological effects of different subtypes are presented in Table 1, which is summary of many years of work by Mohler, Rudolph, McKernan, Sieghart, Siegel et al.

Table 1. The CNS effects at $GABA_A$ $\alpha_{1\text{-}6}\beta_{1\text{-}3}\gamma_2$ receptor subtypes.[18, 46-58] Presented at the Mona Symposium (2014), University of the West Indies.[59] Earlier reported, in part, by Mckernan et al. (ACNP).

Subtype	Associated Effect
α1	Sedation, anterograde amnesia, ataxia, some anticonvulsant action, addiction, dependence, as well as involved in the development of tolerance, and muscle relaxation
α2	**Anxiolytic**, **anticonvulsant action**, **antihyperalgesic effects**

α3	Some **anxiolytic action**, **some antinociceptive effects,** anticonvulsant action at higher doses, some muscle relaxation at higher doses
α4	Diazepam-insensitive (DI) site, important in lung disorders in the periphery
α5	Cognition, learning, temporal and spatial memory (maybe memory component of anxiety); schizophrenia, depression and in the peripheral-asthma
α6	Diazepam-insensitive (DI) site, important in Tic disorders, Tourette's syndrome, migraine, trigerminal or a facial pain and perhaps schizophrenia

Pharmacology indicated in red was discovered by pharmacologists in collaboration with the Milwaukee group. Presented at the ASPECT meeting, Cook et al. April 9th, Orlando FL.

The α1-containing $GABA_AR$s have been found to mediate sedative effects, anterograde amnesia, ataxia, development of tolerance, addiction, dependence, and some anticonvulsant action, as well as muscle relaxation.[46, 50] The α2-containing $GABA_AR$s play a prominent role in anxiolytic, antinociceptive and some anticonvulsant effects;[47, 51] perhaps some hypnotic effects and some muscle relaxation at higher doses. Much of the antihyperalgesic effects from the $GABA_AR$, however, occur in the spinal cord, as confirmed by a triple-point mutation study, as well as other work by Zeilhofer, Cook et al. using ligand Hz-166.[49, 55] The α3-containing $GABA_AR$s are possibly involved in the anxiolytic-like effects, anticonvulsant action, antinociceptive effects and muscle relaxation at higher doses.[47, 51-53] The α5-containing $GABA_AR$s contribute to cognition, memory, and spatial learning, as well as a possible memory component of anxiety.[48, 54] The α4- and α6-containing $GABA_AR$ are DI subtypes that lack the large binding pocket for the pendant C ring of some BZDs, especially 1,4-benzodiazepines and IMDZs, therefore, no corresponding ataxic or sedative CNS effect is associated with these two subtypes.[39-40] Recent studies have shown that not only α5- but also α4-containing $GABA_AR$s are expressed in the peripheral nervous system (PNS), notably in lungs,[56-58] which provided another possible treatment for asthma using BZDs. Recently, Knutson et al. have shown that the α6 Bz/GABAergic subtypes, at the PQ site, are involved in

migraine, trigeminal pain, Tic diseases such as Tourette's syndrome, OCD and perhaps schizophrenia.[22-24]

In addition to the multiplicity of receptor subtypes, the chloride ion influx plays an essential role in the pharmacological effects of $GABA_AR$s in the CNS from the allosteric modulation of GABA. BZDs such as diazepam bind to the $GABA_AR$ BZD allosteric site on the ion channel and lock it into an agonist conformation. This action increases the orthosteric binding of GABA to the ion channel. Once bound to GABA, the receptor changes conformation within the membrane, which increases the frequency of opening of the chloride ion channel. This effect results eventually in a decrease in the membrane potential (Figure 5). This hyperpolarization of the neurons further inhibits neuronal transmission, which results in sedative, anxiolytic, hypnotic, amnesic, and anticonvulsant in the CNS, as well as muscle relaxant effects. BzR ligands are not able to influence the intrinsic chloride ion channel in the absence of GABA; however, they can mediate the ion influx and change the opening frequency of the complex as allosteric modulators.[60-62] The BZDs that are able to interact with $GABA_A$/BzR fall into three categories: agonist, inverse agonist, and antagonist. BZD agonists, termed positive allosteric modulators (PAM), are the compounds that can increase the chloride ion influx and further enhance the actions of GABA. It should be noted that BZD PAMs do not bind at the GABA binding site as other agonists by definition. On the other hand, the inverse agonists, termed negative allosteric modulators (NAM) bind to the BZD site and elicit the opposite effect and reduce the GABA-induced chloride ion influx. This results in the depolarization of the membrane and increases the chance of neuronal firing activity. In addition to the full agonists and inverse agonists, the compounds that elicit variable efficacy in between the maximum enhancement or reduction as a partial effect are considered as partial agonists and partial inverse agonists,[10] respectively. The third type of BZDs (antagonists)[2] do not enhance nor impair

the action of GABA, which results in no pharmacological effect. However, these antagonists block the interaction of PAMs and NAMs at the BzR site because of their more potent binding affinity for BzR sites over other BZD ligands.[18] Consequently, because of the ability to occupy the BzR site and restrict the binding of other BZDs, antagonists such as flumazenil, βCCt and 3PBC are commonly used to reverse the effects of a BZD-mediated response. Flumazenil, for more than 40 years, has been employed as an antidote to reverse BZD overdose.[63]

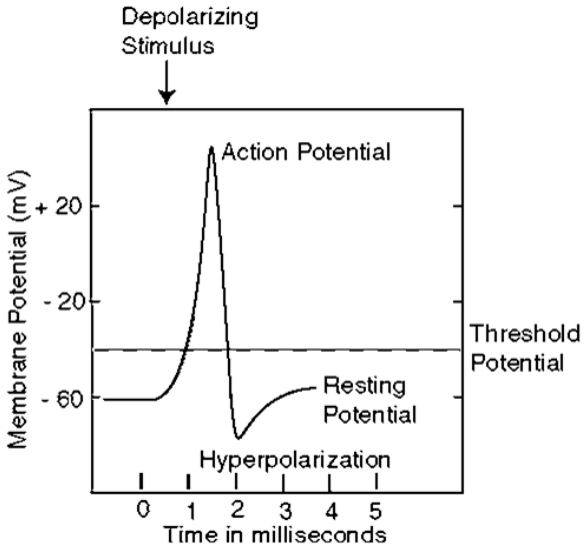

Figure 5. The membrane potential overtime when a depolarizing stimulus initiates a nerve signal. A hyperpolarized state indicates a potential further away from the threshold potential. (Modified from the Figure in the Ph.D. thesis of Terry Clayton)[64]

The concept of the multiplicity of $GABA_AR$ subtypes and BZD allosteric modulation are essential for the understanding of the complex pharmacological effects from $GABA_AR$, as well as a guide for further ligand design for the treatment of different CNS disorders. For instance, ligands that are α1 subtype selective agonists can be used as hypnotic and sedative agents. On the other hand, α1 subtype selective antagonists are suitable for reversing the hypnotic, ataxic, amnesic or sedative effects as well as the respiratory depression of clinical BZDs. Most importantly, ligands which exhibit α2/3/5 or α2/3 subtype selective agonist or partial agonist activity with α1 subtype

antagonist effects, or inverse agonists, or no α1 subtype efficacy at all, can elicit desirable effects to treat anxiety disorders, convulsions, diabetic neuropathy, neuropathic pain, inflammatory pain, complex regional pain disorders, fibromyalgia, and panic disorders etc. with little or no sedative effects from α1 subtype efficacy. Furthermore, α5 subtype selective inverse agonists have been shown to be effective in improving learning and memory deficits without causing unwanted side effects from inverse agonist effects (anxiety, convulsions) at the α1 subtype. Thus, the variable efficacy at different subtypes can be employed, accordingly, to develop a specific spectrum of pharmacological effects.

1.4. Molecular Modeling – Pharmacophore Model

Although BZDs posses a series of important CNS pharmacological effects clinically, the further improvement and design of novel BZDs in recent years has been hampered due to the failure of numerous attempts to crystallize the transmembrane protein $GABA_AR$, especially the most critical recombinants of $\alpha_{1\text{-}6}\beta_{1\text{-}3}\gamma_2$. Consequently, previous to the solution of the structure of the α1β3γ2 ion channel this year by electron microscopy, fragment-based molecular modeling, and structure-activity relationship (SAR) studies were considered the best two methods to investigate the overall effects of BZDs, as well as to develop new drugs which have more selectivity to treat specific diseases.

Over the past few decades, based on *in vitro* binding affinities at BzR subtypes of more than 150 BZD ligands including all three types: agonists, inverse agonists, and antagonists,[18, 65-67] the Unified Pharmacophore/Receptor Model has been developed[18, 65-66] in Milwaukee.[67] Subtype selective ligands for each $\alpha_{1\text{-}6}\beta_{2/3}\gamma2$ $GABA_AR$ from 15 classes of structural families such as

BZDs,[68-69] β-carbolines,[70-72] triazolopyrimidines,[73] pyridodiindoles,[74-75] imidazopyridines[76], and pyrazoloquinolines.[77] were overlaid on a planar template ligand within the BZD binding site to generate the approximate binding pockets. Illustrated in Figure 6 are the locations and descriptors of the two-dimensional representation of the comprehensive pharmacophore model. The model consisted of four critical descriptors used as anchor points and assigned as H_1 (Y210), H_2 (H102), A_2 (T142) and L_1, where H_1 and H_2 represent two hydrogen bond donor sites on the protein, A_2 represents one hydrogen bond acceptor site important for inverse agonist action *in vivo*, and L_1 represents a lipophilic pocket. In addition, there are three additional lipophilic regions (L_2, L_3, and L_{Di}), where the interactions between the ligand and the protein are mediated by van der Waals interactions, as well as p – π and π – π stacking. Moreover, three negative steric repulsive regions (S_1, S_2, and S_3) have been proposed as well, which represents the proteins themselves. The extracellular domain lines in the region of carbon atoms 6 and 7 in the L_{Di} region.[18, 65-66]

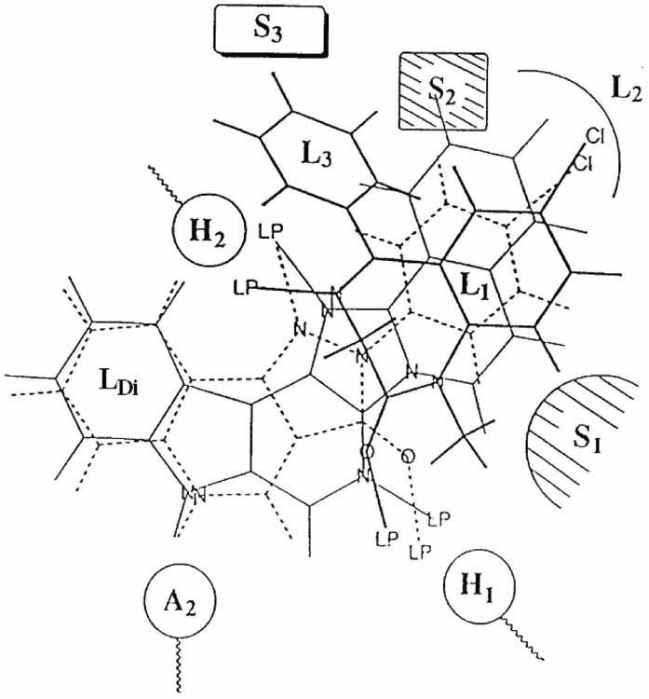

Figure 6. The locations of the descriptors and areas of the Milwaukee-Unified Pharmacophore/Receptor Model for BZD at $GABA_AR$ BzR. Depicted here is pyrazolo[3,4-c]quinolin-3-one CGS-9896 as a dotted line, a diazadiindole as a thin line, and diazepam as a thick line aligned within the unified pharmacophore/receptor model for the BzR. H_1 and H_2 stand for the hydrogen bond donor sites within the BzR, while A_2 stands for a hydrogen bond acceptor site that may be necessary for potent inverse agonist activity in vivo. L_1, L_2, L_3, and L_{Di} represent the four lipophilic regions and S_1, S_2, and S_3 represent the regions of negative steric repulsion. LP stands for the lone pair of electrons on the nitrogen (N) or oxygen (O) atoms of the ligands. (Modified from the Figure in Clayton et al.)[18]

From the ligand docking study at the BzR via use of the pharmacophore model, several important trends were proposed to explain the relationship between subtype selectivity and the ligand structure (Figure 7), which were extremely valuable for the future ligand design and modification.[18] 1. There is a slight difference between the induced volumes of α1 and α2 subtypes in the region L_2. 2. The included volume demonstrated that the size, lipophilicity, and shape of the binding pocket of the α2 and α3-containing $GABA_AR$ subtypes are very similar to each other. 3. The examination of the induced volume of the α4, and α6 subtypes indicated that the volume of the α4 subtype is smaller than that of α6 subtype, especially in the L_2 and L_{Di} regions. 4. By viewing the overlap of the included volume of the α1 subtypes vs the α4 and α6 subtypes, it is clear that the L3 lipophilic pocket is almost non-existent in α4 and α6 subtypes. This explains why these two subtypes are DI sites, as compared to other subtypes since they lack the binding pocket for the pendant phenyl ring present in most of the BZDs and IMDZs. 5. The volume of the L_2 region in α5 subtypes is somewhat larger than in the α1 subtypes as well as the α2 and α3 subtypes. This is an important feature for α5 subtype-selectivity with decreased binding at α1 subtypes. For instance, a switch from a chlorine atom (diazepam) to an ethinyl group (QH-II-66) at the C(7) position (Figure 8),[65, 78] altered the ratio of α5 over α1 subtypes from 1.27 to 11.22, which significantly increased the selectivity at the α5 subtype in comparison to the binding affinity of the α1 subtype at the same time and led to a potential anticancer drug, QH-II-66. Furthermore, a recent study by Mohler et al. has demonstrated that the development of tolerance to the antinociceptive effects of

BZD's resulted from the coupling of α1 to α5 subtypes.[79] Therefore, the strategy of limiting the binding affinities and efficacy at both these subtypes has provided a series of compounds that exhibited antinociceptive activity with no observation of the development of tolerance in agreement with the effect proposed by Mohler [80-82] in the area of anticonvulsant drugs. **Recall that clinical BZDs are active against status epilepticus in humans for about 3 days, whereas α2/α3 subtype selective ligands appear to be devoid of the development of tolerance in convulsions and pain in animal models (ASPECT talk, April 9th 2019, Orlando, FL)**

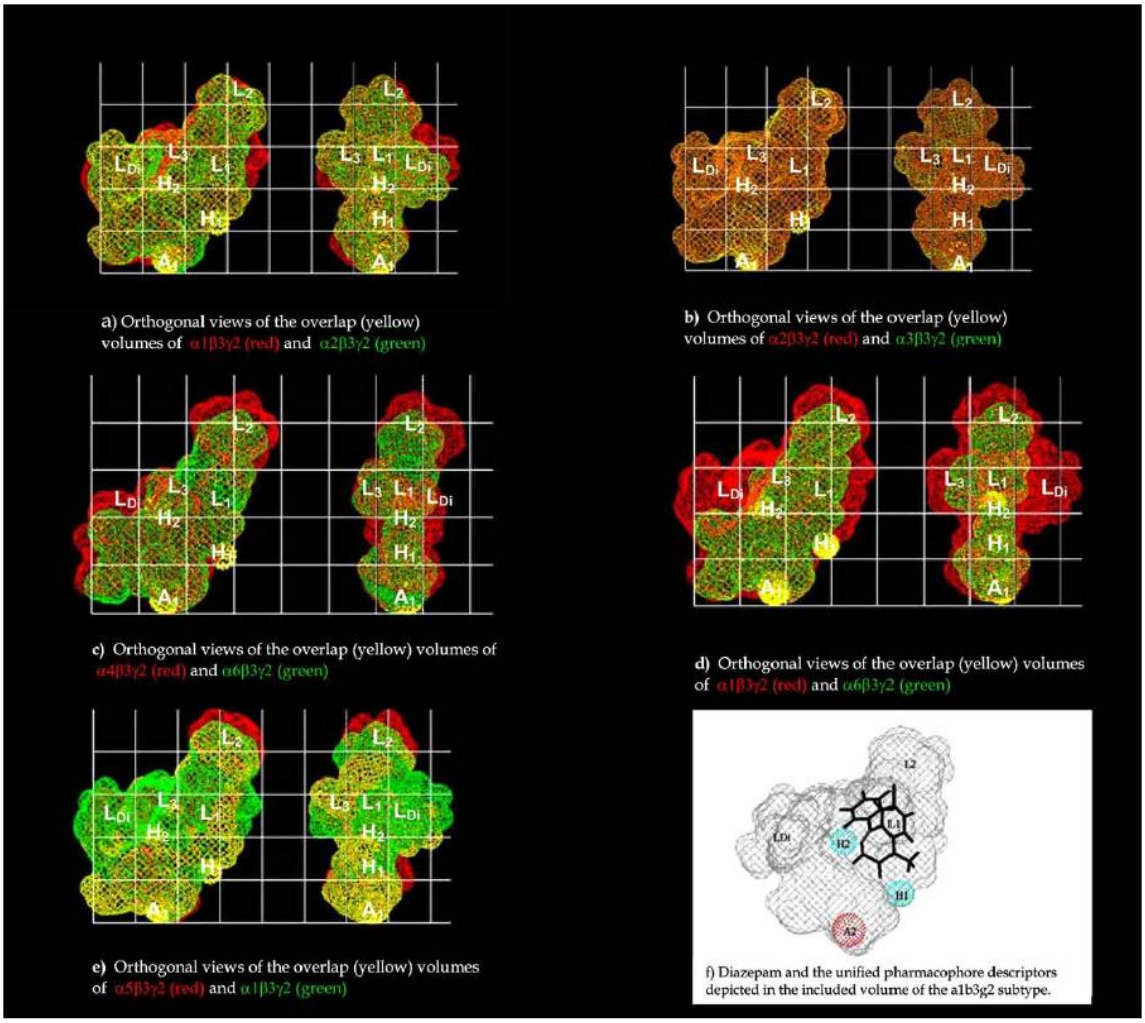

Figure 7. Overlap images between the induced volumes derived from receptor subtype selective ligands: a) α1 and α2 subtypes; b) α2 and α3 subtypes; c) α4 and α6 subtypes; d) α1 and α6 subtypes; e) α1 and α5 subtypes; f) diazepam and the descriptors of the unified pharmacophore model in the included volume of the α1 subtype. The yellow color represents overlapping induced volumes, and each grid measures 4 Å in width and height.[67]

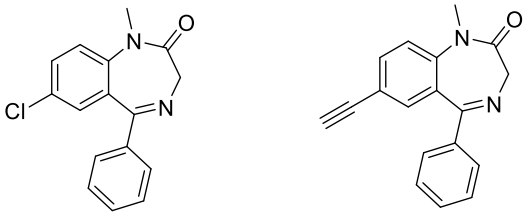

diazepam QH-II-066

Bz/$GABA_A$ receptor binding data (K_i = nM)

	α1	α2	α3	α5	α1/α5	Change in Selectivity
diazepam	14	20	15	11	1.27	8.83
QH-II-066	76.3	42.1	47.4	6.8	11.22	

Figure 8. Bz/$GABA_AR$ in vitro binding data of diazepam and QH-II-066. (Modified from the Figure in the Ph. D. thesis of M. Poe and T. Clayton) [65, 78]

Over the past few years, the updated pharmacophore model and homology model for α5 $GABA_AR$ subtypes has been published by Clayton, et al. in 2015.[67] In addition to the binding affinities and updated compound library, a new lipophilic region L_4 was identified with the chiral methyl enantiomers at the C(4) position from the IMDZ class: the α5 subtype-selective ligand SH-053-2'F-*R*-CH_3 (**1**), and its enantiomer the α2/3/5 subtype-selective ligand SH-053-2'F-*S*-CH_3 (**2**),[83] see Figure 9. This recent work indicated that the new binding pocket (L_4) was only located in the α5 subtype, and was not present in the α2 or α3 subtypes. Both enantiomers (R and S) can fit in the binding pocket of the α5 subtype (see included volume). However, the pendant phenyl ring of the R-isomer (**1**) did not fit in the binding pockets of the α2 nor α3 subtypes. This phenyl group protruded outside of the included volume, which resulted in no efficacy for the *R*-CH_3 isomer at α2 nor α3 subtypes (Figure 10). On the other hand, the *S*-isomer (**2**) was very well accommodated in all three α2, α3, and α5 subunits, since α2 and α3 subunits share a similar shape and size. Taken together, the results from the pharmacophore model are consistent with the efficacy data of the α2/3/5 subtype-selective ligand (**2**).[67]

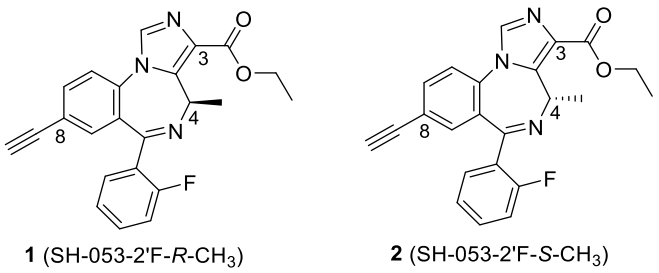

Figure 9. The structures of enantiotopic chiral imidazodiazepine (IMDZ) ligands 1 and 2.

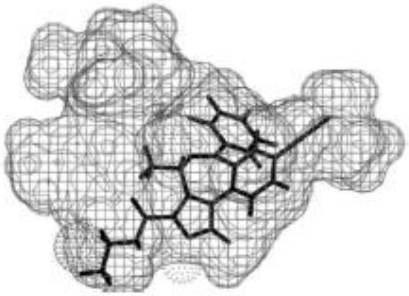

SH-053-2′F-S-CH_3 **2** fits the pharmacophore in the included volume of the alpha 2 subtype

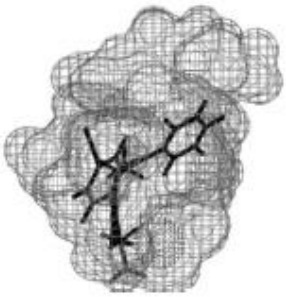

The left image of figure rotated 90°. It can be clearly seen that **2** fits within the included volume

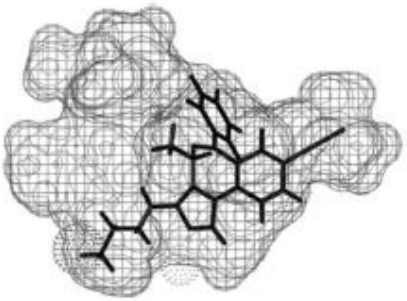

SH-053-2′F-R-CH_3 **1** does not fit the pharmacophore in the included volume of the alpha 2 subtype

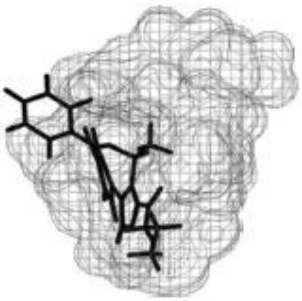

The left image of figure rotated 90°. It can be clearly seen that the conformation of **1** is such that the pendant 6-phenyl sticks outside the included volume

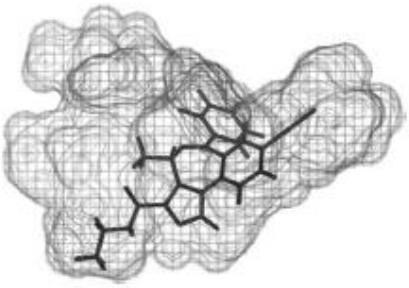

SH-053-2′F-S-CH_3 **2** fits the pharmacophore in the included volume of the alpha 5 subtype

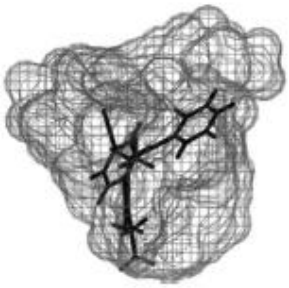

The left image of figure rotated 90°. It can be clearly seen that **2** fits within the included volume

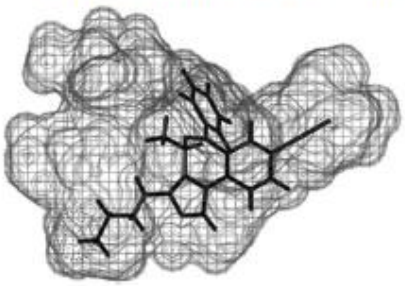

SH-053-2′F-R-CH_3 **1** fits the pharmacophore in the included volume of the alpha 5 subtype

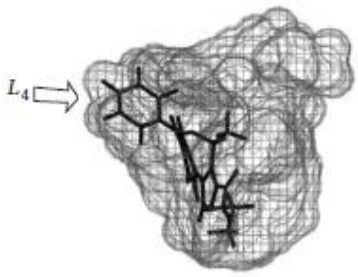

The left image of figure rotated 90°. It can be clearly seen that **1** fits within the included volume

Figure 10: Ligand occupation of SH-053-2'F-*R*-CH_3 (1) and SH-053-2'F-*S*-CH_3 (2) in the α5 and α2 pharmacophore/receptor models. (Modified and reproduced from that reported by Clayton et al.)[67]

1.5. Research Objectives

With the aid of the unified pharmacophore model, the first goal of this research was to design and synthesize a series of novel optically active BZD compounds that have good or better binding affinity and efficacy at BzR, but are devoid of the BZD side effects by reducing the efficacy or affinity at the α1 subtypes. It was also desirable to reduce the efficacy at both α1 and α5 subtypes to limit the development of tolerance.[80-82] The new ligands were not only employed in the study of the SAR but also in the pharmacological effects of the potential drugs on individual or a combination of $GABA_AR$ subtypes. The ligands necessarily had to be evaluated in different *in vitro* assays and *in vivo* animal models to further determine their effectiveness in the treatment of diseases such as asthma, schizophrenia, MDD, anxiety, epilepsy as well as pain disorders. In addition to the development of potential new drugs, the second goal of the research was to improve the synthesis of several key compounds on a larger scale for better yields, as compared to the previous routes. This was necessary in order to provide an efficient and consistent supply of the ligands for studies of the pharmacology in larger animals for the treatment of a series of CNS disorders.

Chapter 2. Design and Synthesis of Chiral α2/α3/α5 or α5 Subtype Selective Ligands and Their Use for the Treatment of Schizophrenia, Major Depressive Disorder as well as Asthma

2.1. Introduction of Chirality in Drug Design

Chirality, a geometric property, is a universal phenomenon that exists in microscopic objects at the molecular level, and in macroscopic objects as well, such as proteins, and key components of living creatures in nature. A chiral object has two forms, termed enantiomers. These asymmetric enantiomers are non-superimposable mirror-images to each other.[84-86] It is well known that chirality plays an essential role not only in the field of chemistry but also in people's daily life. The concept of chirality has widely been applied to flavors, agricultural agents and especially medications. Long before the development of the pharmaceutical industry or even the knowledge of chirality, medicines were usually given as a single enantiomer, since they were derived from crude extracts or semi-synthetically from plants or animals without enantiomeric purification.[84] However, since the rapid development of total synthesis in the pharmaceutical industry in the 1950s, most of the drugs at that time were racemic. This was due to optically inactive starting materials and racemic preparations. There were also less restrictions by the federal governmental, the Food and Drug Administration (FDA). The thalidomide tragedy[87] raised the concern of chirality in drug development and at the FDA. The (*S*)-enantiomer of thalidomide caused a series of severe birth-deficits, and unfortunately, use of the pure (*R*)-isomer itself would not prevent the problem, due to the spontaneous racemization in the body (Figure 11).[85-86] Since the 1990s, the FDA announced a series of regulations for the requirement of stereochemically pure drug submissions, which significantly reduced the use of racemates for the treatment of diseases

to avoid possible issues. However, these restrictions also raised the cost of drug development significantly.

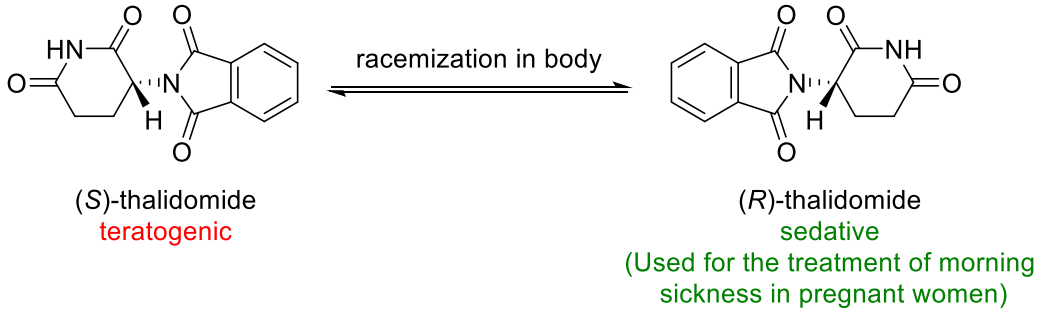

Figure 11. The structures of both enantiomers of thalidomide.

In addition to the brief history of chiral drugs, clinical studies have also clearly illustrated that the enantiomers of a racemic drug usually exhibited differences in activity, metabolism, pharmacokinetics (PK), toxicity, absorption, excretion, etc., and most importantly in potency. One enantiomer maybe pharmacologically active, whereas the other enantiomer may be inactive, have the same effect, a different phenotype or a completely opposite effect,[86] as well as an important antagonist at this receptor. Furthermore, the "chiral switch" might be used as a strategy to extend patent life and establish an improved profile for previously developed racemic drugs,[84] which was illustrated clearly by the development and use of a pure enantiomer of Prozac in the clinic by Sepracor to overcome the Lilly patent.

Since more and more evidence has demonstrated the importance of chirality in different fields, the synthesis of stereoselective compounds has become a popular topic worldwide. In recent years many methods have been developed and employed for production and separation of the enantiopure compounds, including enantioselective catalysis, internal asymmetric induction, external asymmetric acid-base reactions for the resolution of diastereomeric salts, and chiral high-performance liquid chromatography (HPLC).[88-89]

Taken together these facts suggest that it is very important to keep chirality in mind while designing new ligands. Over the past decades, based on the Milwaukee-unified pharmacophore model,[18, 65-67] a series of enantiopure ligands have been designed, synthesized and studied in different *in vitro* assays and *in vivo* animal models. According to the data up to date, it has been well demonstrated that the *R* and *S* 4-substituted chiral IMZDs exhibit different subtype selectivity at Bz/GABA(A)ergic receptors. It has been shown that the ligands which contain a chiral (*S*)-methyl group at the C(4) position of the IMDZ tend to be α2/3/5 subtype selective ligands, whereas the (*R*)-isomers are α5 subtype selective ligands.[83] This is an important finding by the group in Milwaukee. Based on the different subtype selectivity profiles, the two enantiomers behaved differently in animal models, as expected, and exhibited completely opposite metabolic rates on human liver microsomes (HLM).[90] This will be further discussed in later chapters. In this vein, one specific goal for this research was to design and synthesize a series of novel stereospecific enantiomers for the application to different disorders, such as schizophrenia, MDD, anxiety, epilepsy, pain as well as asthma depending on their subtype selectivities. This early strategy focused entirely on ligands that interacted with α2, α3 or α5 subtypes, with little or no efficacy or affinity at α1 subtypes.

2.2. Schizophrenia and Major Depressive Disorder (MDD)

Section 2.2.2. to Section 2.2.3.2. of this dissertation have been adopted from the following article:

- Li, G.; Stephen, M. R.; Kodali, R.; Zahn, N. M.; Poe, M. M.; Tiruveedhula, V. V. N. P. B.; Huber, A. T.; Schussman, M. K.; Qualmann, K.; Panhans, C. M.; Raddatz, N. J.; Baker, D. A.; Prevot, T. D.; Banasr, M.; Sibille, E.; Arnold, L. A.; Cook, J. M., Synthesis of chiral GABAA receptor subtype selective ligands as potential agents to treat schizophrenia as well as depression. *ARKIVOC* **2018**, *iv*, 158-183.

2.2.1. Introduction

Schizophrenia is one of the most complex central nervous system (CNS) disorders known. Approximately 1% of the population worldwide[91] is affected by this disease. The symptoms fall into three broad categories: positive symptoms including hallucinations and delusions; negative symptoms such as the blunted affect, social dysfunction and lack of motivation or pleasure in daily life, and cognitive abnormalities. For instance, in the disruption of cognition, symptoms such as impairments in working memory, verbal memory, attention and executive deficits, which can lead to severe emotional distress, are prominent.[91] The treatments commonly used to manage positive symptoms are typical and atypical antipsychotic drugs, which target and block the over-activation of dopamine receptors[92] in patients with schizophrenia. In fact, the drugs prescribed, to date, only reduce the positive symptoms in the majority of schizophrenia patients. They are often not effective especially in patients with negative symptoms and cognitive abnormalities.[93] Moreover, the antipsychotics in many patients induce adverse effects such as tolerance, addiction, sedation, drug-resistance, weight gain and liver toxicity.[94] The lack of proper medications and limited

efficient psychosocial therapy together increase the psychological and financial burden rapidly not only for the patients and their family but also for society as a whole. Consequently, there is an urgent clinical need for novel drug candidates that can address all aspects of schizophrenia including the alleviation of the negative and cognitive symptoms with decreased side effects.

2.2.2. Background

It is well known that asymmetry plays an essential role in physiological processes; therefore, a large number of drugs are chiral molecules, in which one enantiomer of a drug may have the desired beneficial effect, while the other enantiomer may cause serious adverse effects.[88-89] This was observed with thalidomide.[87] Based on our earlier established BZD/$GABA_A$ pharmacophore model[18] that was developed by ligand binding data, a series of chiral molecules have been designed, synthesized and studied. Ligand SH-053-2'F-*R*-CH_3 (**1**) was the lead stereospecific $GABA_AR$ α5-subtype selective positive allosteric modulator (PAM) because of the chiral (*R*)-methyl group at the C-4 position of the imidazodiazepine (IMDZ) nucleus, as shown in Figure 9. This resulted in increased potency at α5 $GABA_A$ receptor subtypes, accompanied by a concomitant decrease at the α1, α2, and α3 subtypes. This α5-selective ligand has been reported to successfully alleviate the hyperactivity of the dopamine system induced by amphetamine in the methylazoxymethanol acetate model (MAM) of schizophrenia.[95-96] Moreover, this ligand **1** in an animal behavioral model of depression exhibited anxiolytic and antidepressant effects in female mice that were exposed to unpredictable chronic mild stress (UCMS) in a sex-dependent manner. The effects on male mice in the same paradigm were very weak or none at all.[97] Furthermore, analogs of 4(*R*)-CH_3 enantiomer **1**, such as the methyl amide MP-III-022 (**35**),[98] the carboxylic

acid SH-053-2'F-*R*-CH_3-acid[99], etc., which are more potent at the α5-subtypes than **1**, have also been investigated and undergone a number of behavioral studies.[56, 58]

In order to study how the chirality at the C-4 position of IMDZ could affect the pharmacological response, the enantiomer of **1**, SH-053-2'F-*S*-CH_3 (**2**) was synthesized.[82] As expected, these two enantiomers exhibited vastly different GABAergic efficacy and binding affinity at Bz/GABA(A) receptor sites. Ligand **2** was found to be an α2-, α3-, α5-β3γ2 subtype selective IMDZ, while **1** was an α5 subtype selective ligand. Since **1** and **2** both target the α5-subunit, they have been assayed in several behavioral models. Examination of the results revealed **2** exerted anxiolytic effects in both rhesus monkeys[100] and rats[101], while **1** had only a minimal anxiolytic effect when much higher doses were applied. Interestingly **2** also successfully mitigated the amphetamine-induced hyperactivity in a poly (I:C) animal model of schizophrenia.[102]

The results of these studies indicated that both enantiomers might be useful in the treatment of the symptoms of schizophrenia, while the α2/3/5 agonist **2** exhibited the potential for the treatment of conditions comorbid with schizophrenia, such as anxiety, which commonly coexists in patients with schizophrenia. Unfortunately, during other studies, ligand **2** was shown to be metabolized at a very high rate *in vitro* in the presence of human liver microsomes (HLM);[103] 3% of **2** remaining after incubation at 37 ^oC for 30 minutes, while ligand **1** was stable in HLM with 100% remaining under the same conditions, as presented in Table 2. The principal aim of this research was to improve the metabolic stability of the ester functional group while retaining the properties potentially useful for the treatment of schizophrenia and depression. Schizophrenia and some forms of depression (bipolar I disorder and perhaps major depressive disorder) are linked both genetically and etiologically. Herein we present the synthesis and characterization of novel analogs of SH-053-2'F-*S*-CH_3 (**2**) including esters, thioesters, amides, carboxylic acids and the

ester bioisostere oxadiazoles at the C(3) position together with modifications at the C(8) position. The newly designed ligands were prepared and investigated in *in vitro* metabolism studies, cytotoxicity assays and *in vivo* in mice with a rotarod study to identify ligands with a lower systematic clearance rate, low toxicity, little or no sedative/ataxia activity, which might be useful in the management of the symptoms schizophrenia[18] and depression.[96] This go/no-go point is important for the development of a safe treatment for schizophrenia and depression that can occur at any age.

Table 2. In vitro liver microsomal stability of 1 and 2.

Ligand	Liver microsomal stability (%-remaining) *Conditions*: 4 µM compound, 37 °C, 30 minutes			
	HLM[a]	DLM[b]	MLM[c]	RLM[d]
SH-053-2'F-*R*-CH_3 (**1**)	100.0	90.3	59.1	5.4
SH-053-2'F-*S*-CH_3 (**2**)	2.3	90.7	66.5	6.0

[a] Human liver microsomes (HLM), [b] dog liver microsomes (DLM), [c] mouse liver microsomes (MLM), and [d] rat liver microsomes (RLM).

2.2.3. Chemistry and Results

2.2.3.1. Comparison of Enantiomers

2.2.3.1.1. Synthesis of SH-053-2'F-*R*-CH_3 (1) and SH-053-2'F-*S*-CH_3 (2)

Both enantiomers were resynthesized on a large scale for the SAR of the analogs. The preparation of both **1** and **2** followed the same synthetic route with similar yields. The chirality difference was achieved by using *N*-Boc-D-alanine for the chiral building block of the *R*-isomer (**1**), whereas *N*-Boc-L-alanine was employed for the *S*-enantiomer (**2**), as demonstrated in Scheme 1 and Scheme 2, respectively.

For the amidation reaction, *N*-Boc-D-alanine was coupled with the commercially available (2-amino-5-bromophenyl)(2-fluorophenyl)methanone **3** by using a dehydrating agent N,N'-dicyclohexylcarbodiimde (DCC) to afford amide **4** in 97 % yield on a **150-gram scale**. Note, **DCC should be first dissolved in DCM to form a homogenous solution, which was then added dropwise to the mixture of alanine and benzophenone 3 in DCM at 0 ˚C**. If DCC was added in one portion or at rt, a dimerization to a dimer of DCC urea would occur due to the concentration of DCC. Moreover, the quality of DCC also affected the yield of this reaction significantly. The DCC should be stored properly to avoid moisture and the solvent should be anhydrous. The reaction progress was monitored by HPLC/PDA (Shimadzu LCMS 2020 instrument) and the molecular mass of the unwanted dimer (m/z 450) was observed in the mass spectra when an improper addition operation was carried out; see Appendix A for the HPLC/PDA Analysis Report for details. The Boc-deprotection step was carried out by stirring the amide **4** in a saturated solution of HCl gas in DCM at 0 ˚C for 1 hour, and this was followed by the cyclization to the 7-membered ring in the 3:2 ratio of methanol and water mixture after adjusting the pH to 8.5 with 2 N aq NaOH solution. The desired 1, 4-benzodiazepine **5** precipitated out of the solution in 73 % yield. A mild exotherm was observed, as expected, during the slow addition of a saturated aq $NaHCO_3$ solution workup. The recrystallization of the benzodiazepine **5** was conducted in a mixture of EtOAc and hexanes in a ratio of 1:9 after adding seed crystals. The imidazole ring was prepared by the treatment of the benzodiazepine **5** with potassium *t*-butoxide and diethyl chlorophosphate at -50 ˚C, and this was followed by addition of ethyl isocyanoacetate and a second portion of potassium *t*-butoxide at -78 ˚C. This gave the desired IMZD **6** in 75 % yield. The majority of this bromide **6** can be recrystallized from methyl t-butyl ether or EtOAc after cooling from 60 ˚C. An additional portion was obtained by purification of the mother liquor by flash

column chromatography (silica gel, EtOAc:hexane, 3:2). This chiral bromide **6** was then reacted with trimethylsilylacetylene in the presence of a palladium catalyst *via* a Heck-type coupling reaction to obtain the TMS-analog **7** in 78 % yield, or *via* an alternative coupling reaction by mixing the TIPS-acetylene, palladium acetate, tri(O-tolyl)phosphine and the bromide **6** in one pot under refluxing conditions for 4 hours. This second procedure gave the TIPS acetylene analog **8** in an improved yield (86 %). **This latter Greg Fu-type process was easier to handle for no degassing was needed, and the catalyst was generated *in situ*. Moreover, the TIPS-product 8 has a higher Rf value than the TMS-analog, which resulted in a much easier purification by flash column chromatography, as compared to the purification of the TMS-analog 7.** The fluoride-mediated desilylation was executed by stirring **7** or **8** with tetra-*n*-butylammonium fluoride in THF to provide **1** (SH-053-2'F-*R*-CH_3) in 96 % or 90 % yield, respectively, as shown in Scheme 1. The *S*-isomer SH-053-2'F-*S*-CH_3 **2** was prepared by utilizing the same route but with *N*-Boc-L-alanine in place of *N*-Boc-D-alanine in the first step. The yield of each step was similar to that observed with the *R*-isomer, as demonstrated in Scheme 2.

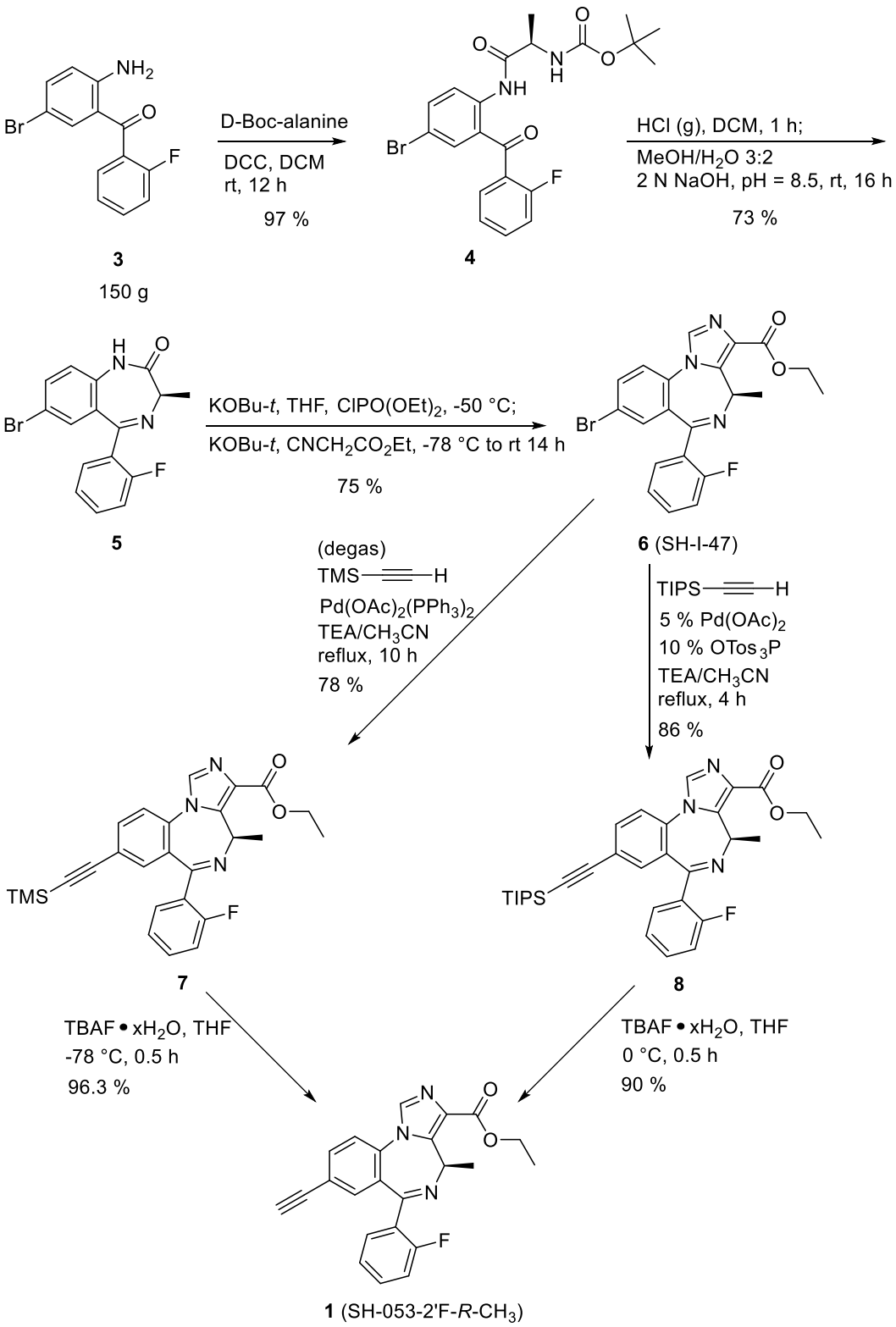

Scheme 1. Synthesis of SH-053-2'F-*R*-CH$_3$ (1).

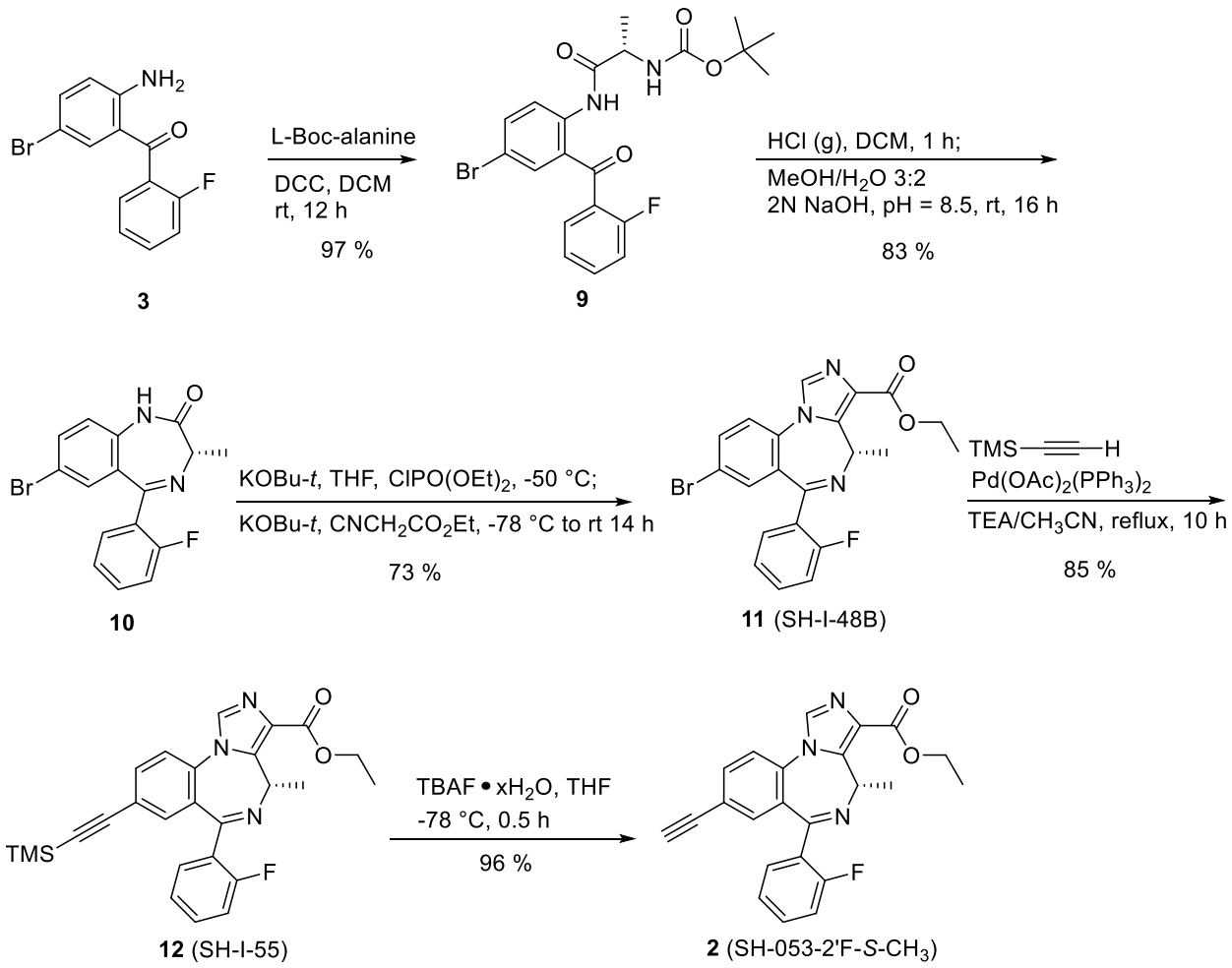

Scheme 2. Synthesis of SH-053-2'F-S-CH$_3$ (2).

2.2.3.1.2. Biology on the *R* and *S* Enantiomers

The characterization of the biology of lead compound **2** was carried out simultaneously with the synthesis and assessment of novel analogs. Due to the ability of **2** to potentiate the α5 containing $GABA_AR$ as well as the α2 and α3 subtypes, while inactive at the α1 containing $GABA_AR$, which mediates sedation and other adverse effects, ligand **2** was evaluated in behavioral models in direct comparison with its enantiomer **1**. For cataleptic behavior in the studies of schizophrenia,[104] the control antipsychotic, haloperidol, elicited a significant cataleptic response.

In contrast, both the C(4)-methyl substituted ligands **1** and **2** did not show any signs of the catalepsy (side effect) in comparison to the vehicle, as illustrated in Figure 12. Moreover, in the prepulse inhibition (PPI) assay, which was used as a classical animal model of schizophrenia, the *S*-isomer **2** significantly reversed the PPI deficit induced by phencyclidine hydrochloride (PCP), an *N*-methyl-D-aspartate (NMDA) antagonist.[105] Ligand **1** did antagonize the deficit compared to the vehicle but failed to reach a significant effect at the same dosage, as depicted in Figure 13. However, the results on PPI with the *R*-isomer **1** were trending toward significance but would have required a larger number of animals to reach significance which was cost limiting. Additionally, in the 6 Hz electroshock (3 seconds duration) assay, both ligands were evaluated for their ability to protect against epileptic seizures. As shown in Figure 14, ligand **2** was able to protect mice from the electroshock-induced seizures at all time points (1/4, 1/2, 1, 2, and 4 hours), which was predicted due to the activation of α2 and α3 subtypes (Figure 14A) as well as α5 subtypes. However, the *R*-enantiomer (α5) **1** was not effective at any time at a relatively higher dose in the 6 Hz paradigm. For the rotarod (n=8) assay, neither **1** nor **2** produced any ataxia or sedation at 100 mg/kg i.p. in mice (Figure 14B). This was in complete agreement with the poor efficacy at α1β3γ2 Bz/GABAergic subtypes previously reported.[83]

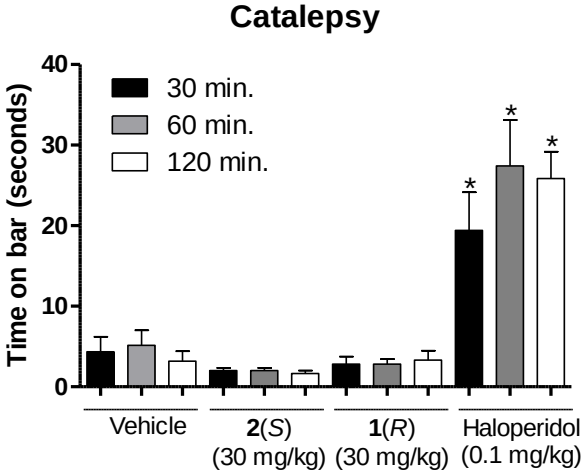

Figure 12. Impact of 1 or 2 treatment (30 mg/kg, i.p.) on cataleptic behavioral. Haloperidol, but not 1 nor 2 produced a significant cataleptic response at 30, 60, and 120 minutes post-injection. The data are expressed as the mean (+SEM) time (sec) subjects spent with both front paws on an elevated bar; *p<0.001, the difference from controls receiving vehicle alone.

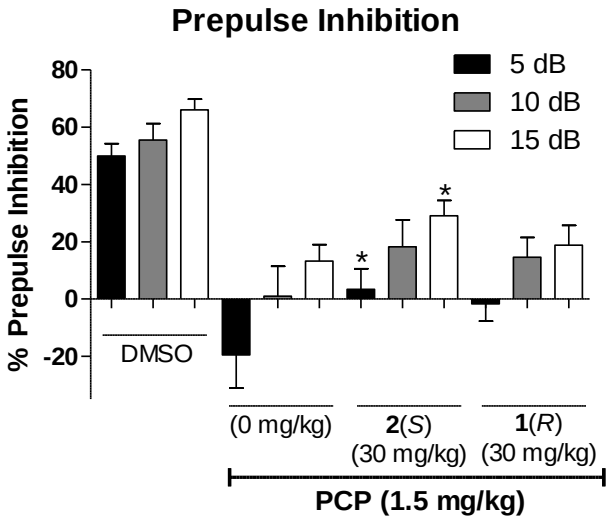

Figure 13. Impact of 1 or 2 treatment (30 mg/kg, IP) on prepulse inhibition. Ligand 2, but not 1 reversed the PPI deficits induced by PCP when given one hour before testing. The data are expressed as the mean (+SEM) percent prepulse inhibition of the startle response to an auditory stimulus when preceded by a nonstartle-eliciting auditory cue at 5, 10, and 15 decibels. Disruption of prepulse inhibition was obtained in rats by an acute injection of phencyclidine (PCP·HCl, 1.5 mg/kg, SC) ten minutes prior to testing; *p<0.05, difference from controls receiving phencyclidine with 0 mg/kg drug pretreatment.

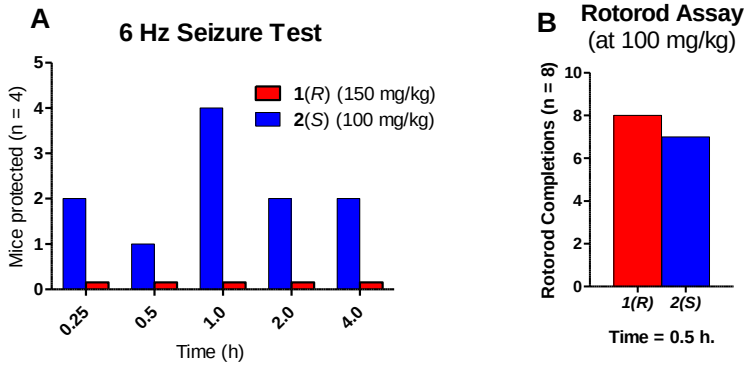

Figure 14. Impact of 1 or 2 treatment on anticonvulsant effects. A) Mice were dosed i.p. with either 1 (150 mg/kg) or 2 (100 mg/kg) and a 6 Hz shock by a corneal electrode was administered at various time points, and the animal observed for convulsions. Ligand 2 was able to protect some subjects while 1 was not able to protect mice from electroshock-induced seizures. B) In the rotarod assay, mice were dosed i.p. with 1 or 2 (100 mg/kg) 30 minutes prior to testing on a rotating rod (6 rpm). Mice that fell 3 times during a 1-minute trial were deemed

toxic (ataxic or sedated). Also there was no indication of toxicity nor sedation in rhesus monkeys at 10 mg/kg (Fischer, et al, 2010).[83]

2.2.3.2. Analogs of the *S*-isomer

2.2.3.2.1. Synthesis of Analogs of SH-053-2'F-*S*-CH_3 (2)

Previously, evidence from the ligand-based $GABA_AR$ pharmacophore/receptor model and SAR[18, 67] have indicated that subtle changes in the IMDZ substituents will affect the BzR/GABA(A)R subtype selectivity dramatically. For instance, the loss of the chiral methyl group at the C(4) position will decrease the α5-subtype selective efficacy, while the efficacy at α2/α3-β3γ2 GABA(A)ergic subtypes will increase dramatically. Efficacy at the α1 subtype will increase with a 2'-F substituent on the C(6) pendent phenyl ring, but the 2'-N and 2'-H analogs remain α2/α3 subtype selective. It has also been shown that the α5 selectivity can be modified by the presence of different lipophilic groups at the C(8) position. Analogs, which have been optimized at the C(3) position demonstrated higher affinity and potency at α5-[106] or α2/3-[107-109] subtypes, which led to better and longer physiological effects. For these reasons, the C(3) and C(8) positions are considered to be the optimal regions for ligand improvement. To evaluate the modification of the lead compound **2** at these two positions, a series of novel analogs were designed, synthesized and characterized, as summarized in Figure 15.

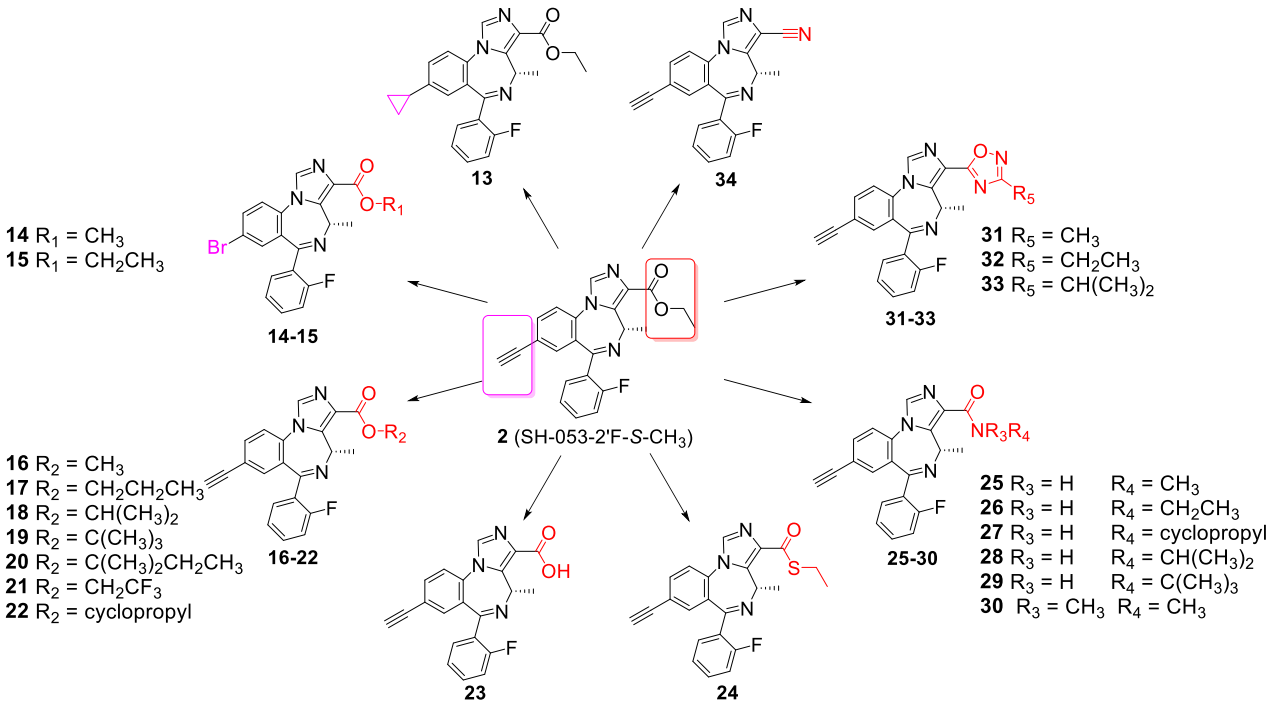

Figure 15. Chiral analogs and bioisosteres of the lead compound *S*-isomer 2.

As mentioned earlier, the C(8)-acetylene and C(4) methyl function were found to enhance the α5-subtype selectivity, therefore a cyclopropyl group, which is commonly incorporated into biologically active materials, was introduced into the parent compound **2** as a substituent to extend the SAR. As a result of its flexible rotation at the C(8) position, it should fill a similar volume of electron density as the ethynyl moiety. Consequently, it might be expected to exhibit parallel physiological effects and enhanced subtype selectivity due to similar interactions in the lipophilic binding pocket (L2, see Figure 6).[87] Moreover, the metabolism by liver microsomes would be expected to be different for a cyclopropyl substituent as compared to an ethynyl functional group. Hence, the C(8)-substituted cyclopropyl analog GL-I-78 (**13**) was prepared based on this hypothesis. The cyclopropyl ligand **13** was synthesized from cyclopropyl boronic acid *via* a Suzuki-coupling reaction[110] with the aryl bromide SH-I-48B (**15**), whose synthesis had been previously described. [48] The coupling reaction was carried out in the presence of potassium

phosphate and a 10 mol% Pd-catalyst, bis(triphenylphosphine)palladium(II) diacetate, in toluene at 100 °C for 12 hours. This process was executed in good yield (82%), as shown in Scheme 3.

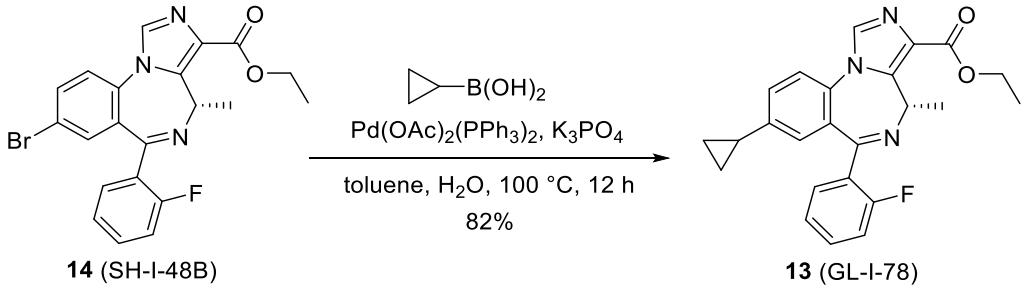

Scheme 3. Synthesis of 8-cyclopropyl-4-(S-CH_3) imidazodiazepine 13 from bromide 14.[48]

Based on the results described previously, the ethyl ester **2** was rapidly degraded in the HLM, which suggested modification of the ester might play an essential role in metabolism, as well as efficacy, as compared to the lead compound **2**. Therefore, a series of esters, which contained different alkyl groups other than ethyl were synthesized. The synthesis of the C(8)-bromo methyl ester MP-III-059 (**14**) and the C(8)-ethynyl methyl ester MP-III-021 (**16**) were achieved in the presence of sodium methoxide in methanol in good yields, as depicted in Scheme 4. The majority of the reactions were carried out *via* a transesterification process[111] with pieces of freshly cut lithium rod in the presence of alcohols in THF at 40 °C for 0.5 hours to generate the corresponding alkoxides. To this solution, ester **2** was added**,** which had been dissolved in dry THF, and full conversion was observed after 15 to 30 minutes. New ester analogs generated via this general route were: propyl ester GL-I-32 (**17**), isopropyl ester GL-I-31 (**18**), *t*-butyl ester GL-I-30 (**19**) and 2-methyl butyl ester GL-I-33(**20**), respectively. The yields were good to excellent (77-97%), as illustrated in Scheme 5. However, the trifluoroethyl ester GL-I-36 (**21**), and the cyclopropyl ester GL-I-38 (**22**) were not obtained under these conditions due to electronic and steric effects. As a result, both analogs were prepared by an alternate procedure. The ester **2** was

saponified to form the carboxylic acid, SH-053-2'F-*S*-CH_3-acid (**23**), with sodium hydroxide in ethanol at reflux for 1 hour in nearly quantitative yield (99%) after acidic workup, as illustrated in Scheme 6. The subsequent reactions for the synthesis of ester **21** and **22** were conducted with thionyl chloride in dichloromethane at reflux to give the acyl chloride, which was converted into ester **21** and **22** on addiction of 2,2,2-trifluoroethanol and cyclopropanol, respectively. Additionally, it must be pointed out that the acid **23** was synthesized not only because it was an important intermediate for the majority of the analogs, but also because the enantiomer (*R*)-CH_3 carboxylic acid in the C(4)*R*-isomer series significantly increased the α*5*-subtype selectivity and potency.[98] It was hoped that the acid **23** in the C(4)*S*-isomer series might effect a similar increase in the selectivity and potency at the α*2*/α*3*/α*5*-subtypes.

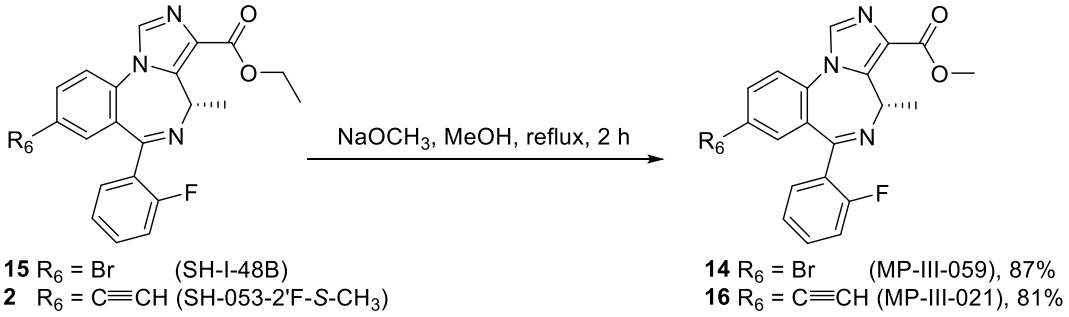

Scheme 4. Synthesis of methyl esters 14 and 16 from ethyl ester 15 or 2, respectively.[48]

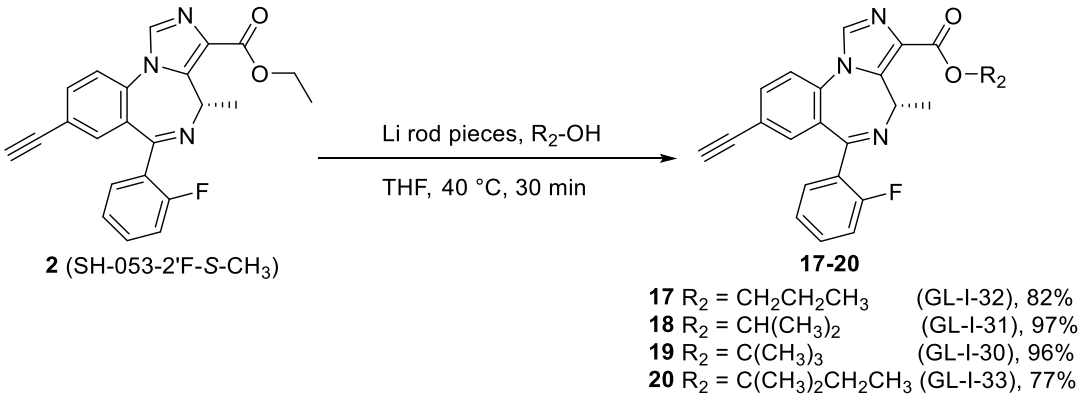

Scheme 5. Synthesis of esters 17-20 from ethyl ester 2 via transesterification.[110]

In a previous study, it was shown that a heteroatom attached directly to the carbonyl at C(3) would affect the $GABA_AR$ subtype selectivity. For example, a thioester function at C(3) in the 2'N series exerted no efficacy at the α1-subtype even at higher concentrations in comparison with the corresponding oxygen substituted ester, but with a slightly higher preference for the α3-subtype.[112] Therefore, it was decided to replace the oxygen atom in lead compound **2** at the C(3) position with a sulfur atom. The thioethyl ester GL-I-77 (**24**) was synthesized from the carboxylic acid **23** following the general procedure as mentioned below in Scheme 6 with ethanethiol as the nucleophile.

Besides the slight changes in steric effects, as compared to lead ester **2**, the amide analogs are well-known stable replacements for metabolically labile ester moieties. The amides were considered to be important replacements for ester functions to improve the *in vivo* stability, as well as the bioavailability when compared to the stability of esters. To evaluate the potential activity of the amides in regard to future SAR, a series of amide analogs **25-30** were synthesized to enable a comparison between esters and amides in regard to *in vitro* metabolic stability, cytotoxicity and *in vivo* locomotor activity. The methyl amide MP-III-023 (**25**) was prepared by the direct amidation of ethyl ester **2** in the presence of methylamine in dichloromethane in a sealed tube. As indicated in Scheme 6, the rest of the amide analogs were synthesized from carboxylic acid **23** *via* an acyl chloride intermediate, using the corresponding primary or secondary amine as the nucleophile. This process gave the ethyl amide GL-I-43 (**26**), cyclopropyl amide GL-I-55 (**27**), isopropyl amide GL-I-57 (**28**), *t*-butyl amide GL-I-41 (**29**) and dimethyl amide GL-I-54 (**30**), respectively, in good to excellent yields (71-88%), as shown in Scheme 6.

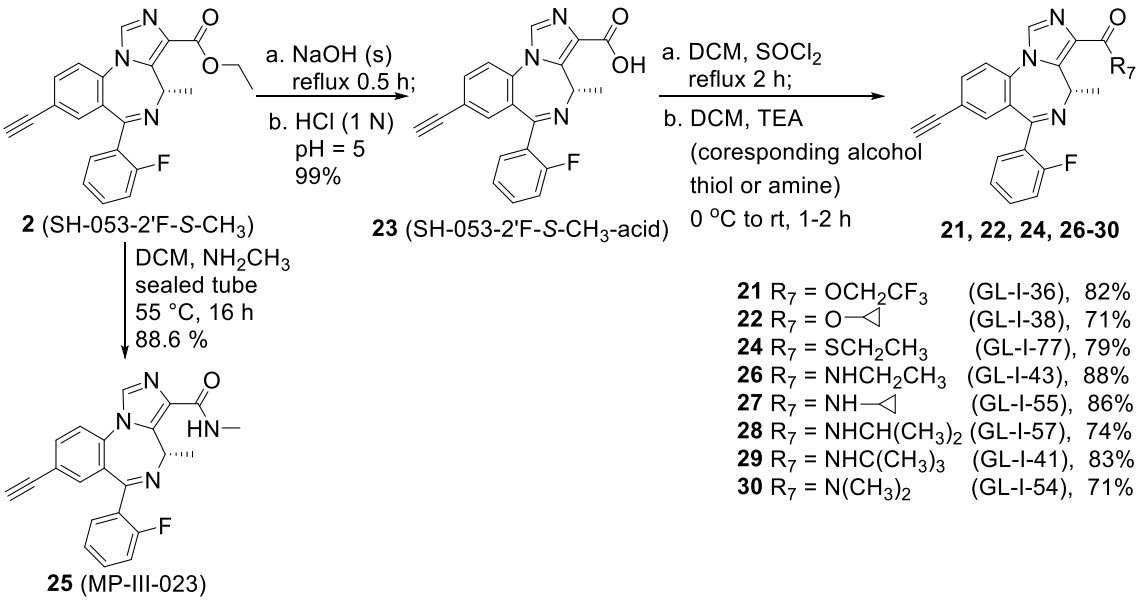

Scheme 6. Synthesis of analogs 21-30.

Ester bioisosteres have been utilized commonly in drug design in order to render them metabolically more stable than the corresponding esters with less adverse effects and to provide better clinical candidates.[113] The previous results [98,114] indicated that replacement of ester functions by substituted 1,2,4-oxadiazoles significantly increased the *in vitro* and *in vivo* stability, as well as slightly improved the hydrophilicity of the ligands. Moreover, the efficacy at BZD receptors was enhanced, as compared to the corresponding ester ligands as well. Encouraged by this previous evidence, the substituted 1,2,4-oxadiazoles **31-33** were designed and synthesized from lead **2**. The condensation of the ethyl ester **2** and corresponding amidoximes in the presence of sodium hydride in THF was employed to prepare the C(3)-substituted oxadiazole ligands, respectively. This route was successfully applied previously with achiral ligands at the C(4) position.[113] However, the desired oxadiazoles with the C(4) chiral methyl group were obtained only in moderate yield (30-40%). The reason for this low yield was the formation of a byproduct (50-60% yield), in which the C(5)-C(6) imine bond isomerized to the C(4)-C(5) position. As a result, the chirality at the C(4)

position was lost. To overcome this problem, the amount of strong base, sodium hydride, which could readily lead to isomerization of the imine bond, was reduced from 4 equivalents to 1.1 equivalents. In addition, the amidoxime was stirred longer with NaH before the ester was added to the mixture. This process gave methyl oxadiazole GL-I-65 (**31**), ethyl oxadiazole GL-I-66 (**32**) and isopropyl oxadiazole GL-I-81 (**33**) in improved yields of 79-85%, respectively, as depicted in Scheme 7. Moreover, the chirality remained intact.

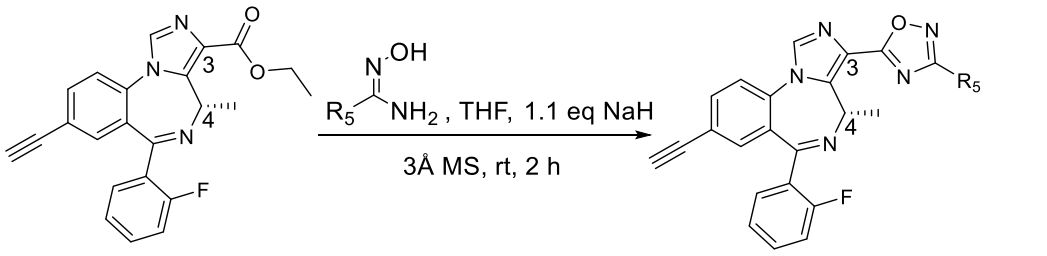

2 (SH-053-2'F-*S*-CH_3)

31 $R_5 = CH_3$ (GL-I-65), 85%
32 $R_5 = CH_2CH_3$ (GL-I-66), 79%
33 $R_5 = CH(CH_3)_2$ (GL-I-81), 82%

Scheme 7. Synthesis of oxadiazoles 31-33.

To explore the extent of flexibility of the hydrogen-bond acceptor in the binding pocket designed H1 in the pharmacophore/receptor model (see Figure 6),[98] it was decided to synthesize the linear nitrile at the C(3) position. This substituted group sometimes is employed to increase water solubility of a ligand and has been used to reduce the possible oxidative metabolism by the liver in clinical studies.[115] **The nitrile MP-III-018.A (34) was produced from the ester 2 via reaction with dimethyl aluminum amine[116] in xylene at 80 °C in 75% yield, as shown in Scheme 8.** The dimethylaluminum amine was prepared freshly by adding trimethylaluminum into a solution of dichloromethane,[45] which had been saturated with ammonia gas.

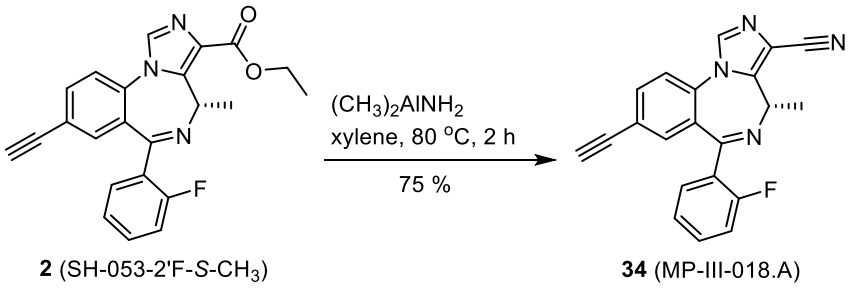

Scheme 8. Synthesis of the C(3)-substituted nitrile 34.

2.2.3.2.2. Biological Activity: Metabolism, Cytotoxicity and Rotarod Studies

The parent compound **2**, which was prepared in the last section, and its analogs were then assayed for metabolic stability *in vitro* on HLM and mouse liver microsomes (MLM) to identify the most stable analogs and the possible trend of steric effects with respect to metabolic stability. Moreover, it was important to evaluate stability in both species with respect to applied animal models and future treatment with of humans with such a diverse array of functional groups at C(3). The results of this study are shown in Table 3.

Table 3. In vitro microsomal stability of analogs of SH-053-2'F-*S*-CH$_3$ (2).

Entry		Structure at C(3) with C(8)-ethynyl	Microsomal stability (HLM) after 2 hr		Microsomal stability (MLM) after 2 hr	
			Half-life (min)	% remaining	Half-life (min)	% remaining
2	ester	$CO_2CH_2CH_3$	< 5[b]	< 5.0[b]	155 ± 9[d]	78.0 ± 0.2[d]
13		$CO_2CH_2CH_3$[e]	< 5[b]	< 5.0[b]	46 ± 3	16.0 ± 0.4
14		CO_2CH_3[f]	10 ± 1[d]	2.0 ± 0.3[d]	116 ± 13	41.0 ± 0.6
15		$CO_2CH_2CH_3$[f]	< 5[b]	< 5.0[b]	< 5[b]	< 5.0[b]
16		CO_2CH_3	119 ± 21[d]	43.0 ± 0.4[d]	216 ± 28	62.0 ± 0.5
17		$CO_2CH_2CH_2CH_3$	< 5[c]	< 5.0[c]	24 ± 0[d]	12.0 ± 0.2[d]
18		$CO_2CH(CH_3)_2$	57 ± 2[d]	47.0 ± 0.2[d]	227 ± 16[d]	83.0 ± 0.1[d]
19		$CO_2C(CH_3)_3$	514 ± 115[d]	89.0 ± 0.2[d]	196 ± 20[d]	78.0 ± 0.2[d]
21		$CO_2CH_2CF_3$	< 5[a]	< 5.0[a]	< 5[b]	< 5.0[b]

22		CO_2-cyclopropyl	< 5[a]	< 5.0[a]	19 ± 2[d]	11.0 ± 0.2[d]
23	acid	COOH	358 ± 56	74.0 ± 0.4	139 ± 11[d]	54.0 ± 0.3[d]
24	thioester	$COSCH_2CH_3$	101 ± 19	28.0 ± 0.3	46 ± 6	9.0 ± 0.5
25	amide	$CONHCH_3$	**1780 ± 39**	**92.0 ± 0.3**	**845 ± 5**	**86.0 ± 0.2**
26		$CONHCH_2CH_3$	**1978 ± 50**	**93.0 ± 0.3**	**1961 ± 46**	**92.0 ± 0.3**
27		CONH-cyclopropyl	**1625 ± 803[d]**	**89.0 ± 0.4[d]**	**320 ± 34[d]**	**72.0 ± 0.3[d]**
28		$CONHCH(CH_3)_2$	107 ± 10	38.0 ± 0.5	28 ± 0	75.0 ± 0.3
29		$CONHC(CH_3)_3$	205 ± 14	63.0 ± 0.3	142 ± 9	52.0 ± 0.3
30		$CON(CH_3)_2$	59 ± 5[d]	41.0 ± 0.9[d]	24 ± 2[d]	19.0 ± 0.9[d]
31	1,2,4-oxadiazole	3-CH_3	**866 ± 213**	**86.0 ± 0.3**	**443 ± 66**	**81.0 ± 0.4**
32		3-CH_2CH_3	563 ± 123	80.0 ± 0.4	213 ± 17	63.0 ± 0.3
33		3-$CH(CH_3)_2$	**2584 ± 1920**	**91.0 ± 0.3**	**500 ± 109**	**79.0 ± 0.5**
34	nitrile	CN	41 ± 5	9.0 ± 0.3	58 ± 6	17.0 ± 0.6

[a] Compound was not detected after 10 minutes. [b] Compound was not detected after 20 minutes. [c] Compound was not detected after 30 minutes. [d] Compound was assessed at 1-hour pre-incubation time. [e] C(8)-cyclopropyl. [f] C (8)-bromo.

The lead compound **2**, as mentioned before, was found to be rapidly metabolized on HLM with less than 5% remaining after 20 minutes, while **2** exhibited good stability for MLM with 78% remaining after 1 hour. Among the ester analogs, **13-19, 21**and **22,** an increasing trend in metabolic stability in HLM was observed as the size of the alkyl chain of the ester function increased. However, esters bearing a linear 2-3 carbon chain (**13, 15, 17, 21,** and **22**), regardless of the functional group at the C(8) position (-bromo, -cyclopropyl or -ethynyl), were metabolized very rapidly with less than 5% remaining after 10, 20, and 30 minutes in HLM. A similar trend was observed for MLM; however, the C(8)-bromo and -cyclopropyl replacement of the ethynyl group decreased the metabolic stability (see **2** vs **13**, **15**; **14** vs **16**). It is important to point out that the introduction of an ester function with a longer carbon atom side chain or a terminal CF_3 group reduced the metabolic stability significantly, as shown in Table 3; both ligands **15** and **21** were not detected anymore after 20 minutes in HLM or MLM, respectively. Most of the esters are only slightly more stable in MLM, as compared to HLM, which suggests that longer lipophilic linear

alkyl chains in the ester functional group should be avoided in the ligand design. The carboxylic acid **23** was slightly more stable, as compared to the esters. The stability of thioethyl ester **24** for HLM was improved slightly compared to ethyl ester **2**, which suggests a sulfur atom in place of an oxygen atom would provide greater metabolic stability. Electronegativity might play a role here. The nitrile **34** was metabolized at a rapid rate with only 9% and 16% of **34** remaining after two hours in HLM and MLM, respectively. As expected, the amide analogs enhanced the metabolic stability remarkably in both HLM and MLM. Unlike the esters, the trend regarding steric effects on the rate of metabolism of the amides was opposite to the esters; ligand, which contained bulkier substituents, were less metabolically stable. Presumably, bulkier esters are more lipophilic and react faster with CYP450 enzymes of the liver microsomal extract. The ethyl amide **26** exhibited the best stability with more than 92% of **26** remaining after 2 hours, as well as the longest half-life for both types of liver microsomes among all the amides. The isopropyl amide **28** was the only ligand, whose metabolism was a little inconsistent, as a result, the isopropyl ester **18** and amide **28** shared a similar metabolic pattern. As expected, the replacement of the ester moiety with the oxadiazole bioisosteres **31-33** significantly improved the metabolic stability over a two-hour period of incubation in both HLM and MLM. It was notable that the isopropyl oxadiazole **33** exhibited the longest half-life (2584 minutes), as compared to all the analogs investigated in the SH-053-2'F-*S*-CH_3 (**2**) series. **In brief, it is clear that the amides and substituted oxadiazole functionality at the C(3) position provide the desired ligands with longer half-life values, as compared to other functional groups. Further evaluation of these analogs involved a study of potential cytotoxicity in both HEPG2 (liver) and HEK293 (kidney) cell lines, as summarized in Table 4.**

Table 4. In vitro cytotoxicity of SH-053-2'F-*S*-CH_3 (2) analogs.

Entry		Structure at C(3) with C(8)-ethynyl	HEK293 LD_{50} (μM)[a]	HEPG2 LD_{50} (μM)[a]
2	ester	$CO_2CH_2CH_3$	28.0 ± 4.1	**73.5 ± 14.4**
13		$CO_2CH_2CH_3$[b]	**58.0 ± 6.0**	**87.0 ± 6.6**
14		CO_2CH_3[c]	**98.5 ± 7.9**	**136.8 ± 6.3**
15		$CO_2CH_2CH_3$[c]	**187.0 ± 49.7**	**>400**
16		CO_2CH_3	**68.2 ± 4.3**	**136.6 ± 6.3**
17		$CO_2CH_2CH_2CH_3$	**53.2 ± 4.4**	**56.3 ± 4.0**
18		$CO_2CH(CH_3)_2$	48.9 ± 4.4	39.9 ± 2.8
19		$CO_2C(CH_3)_3$	12.3 ± 1.6	21.4 ± 1.9
20		$CO_2C(CH_3)_2CH_2CH_3$	17.2 ± 1.6	17.1 ± 1.4
21		$CO_2CH_2CF_3$	**138.1 ± 31.8**	**>400**
22		CO_2-cyclopropyl	35.8 ± 3.3	**85.1 ± 3.8**
23	acid	COOH	**>400**	**>400**
24	thioester	$COSCH_2CH_3$	20.5± 4.7	30.2 ± 9.7
25	amide	$CONHCH_3$	**>200**	**>200**
26		$CONHCH_2CH_3$	**95.5 ± 12.6**	**65.4 ± 7.3**
27		CONH-cyclopropyl	**63.8 ± 3.0**	**93.5 ± 5.7**
28		$CONHCH(CH_3)_2$	**80.2 ± 11.1**	**56.9 ± 4.8**
29		$CONHC(CH_3)_3$	33.6 ± 3.0	43.4 ± 4.0
30		$CON(CH_3)_2$	**>400**	**>400**
31	1,2,4-oxadiazole	3-CH_3	**69.3 ± 2.3**	**>180**
32		3-CH_2CH_3	46.9 ± 6.6	35.1 ± 3.7
33		3-$CH(CH_3)_2$	32.5 ± 7.6	21.7 ± 1.8
34	nitrile	CN	**81.6 ± 6.7**	**57.1 ± 5.6**

[a] Compounds were incubated at different concentrations with the specific cells for 48 h, followed by detection of cell viability using a Cell-Titer Glo (Promega). The results were normalized using DMSO (negative control) and 3-dibutylamino-1-(4-hexyl-phenyl)-propan-1-one (150 mM in DMSO final concentration, positive control). Data were acquired by three independent experiments carried out in quadruplet. [b] C(8)-cyclopropyl. [c] C(8)-bromo.

Examination of the cell viability assay indicated that ligands with a C-3 carboxylic acid substituent of the *S*-isomer analog **23** or dimethyl amide **30** moiety were non-toxic even at 400 μM (LD_{50} > 400 μM) in the presence of HEK293 and HEPG2 cells. Esters represented by C(8)-bromo ethyl ester **15** and trifluoroethyl ester **21** were non-toxic at doses higher than 400 μM (LD_{50} > 400 μM) for the HEPG2 cells, and they exhibited an LD_{50} of 187 μM and 138 μM in HEK293 cells,

respectively. They were non-toxic at any clinically important level. The methyl amide **25** was non-toxic at concentrations of 200 μM for both cell lines. The esters **13, 14, 16, 17,** amides **26-28**, methyl oxadiazole **31** and nitrile **34**, were safe at lower concentrations with LD_{50} values of >50 μM for both cell lines. Usually, these ligands *in vivo* potentiate the $GABA_AR$s at nanomolar concentrations, consequently the cytotoxicity concentration with LD_{50} values at 50 μM would be far above the clinical concentrations of the ligands used in patients. Ligands with moderate cytotoxicity (30 μM <LD_{50} <50 μM) were ligands with the isopropyl ester **18**, cyclopropyl ester **22**, *t*-butyl amide **29** and ethyl oxadiazole **32**. Ligands that exhibited cytotoxicity (LD_{50} <30 μM) for HEK293 kidney cells were ethyl ester **2**, *t*-butyl ester **19**, 2-methyl butyl ester **20**, thioethyl ester **24**, and isopropyl oxadiazole **33**. These data revealed that increasing the size of the substituent of the oxadiazole moiety may increase cytotoxicity; most of the esters are considered to be cytotoxic if given at very high doses (much higher than any therapeutic dose), unless a different group at C(8) was introduced (see **13-15**). The trifluoroethyl ester was fairly cytotoxic perhaps because the trifluoroethanol group is a much better leaving group and maybe toxic itself. *In vitro* toxicity can be used as a measure to estimate *in vivo* toxicity, however, variations can occur. For instance, lead compound **2** exhibited a fairly low LD_{50} value, however it was not toxic *in vivo* in a number of pharmacological assays in mice, rats and primates. The cytotoxicity assays indicated which analogs were the least cytotoxic but were not potent enough (nM) in regard to cytotoxicity to rule out further pharmacological studies in models of schizophrenia or depression.

To assess the possibility of undesired CNS side effects (α1-mediated), a locomotor coordination study of each analog was conducted by placing mice on a rotating rod for a maximum of 3 minutes after oral administration by gavage at a dose of 40 mg/kg (Figure 16). The mice were also observed for loss of righting reflex, an indication of undesired CNS effects. Most of the mice

treated with the compounds exhibited no sedation or ataxia, nor loss of righting reflection vs the control diazepam. Most of the compounds exhibited sensorimotor steadiness at all three time-points, which indicated no sedative/ataxic effects. However, some amides did exhibit some sensorimotor deficits. The methyl amide **25** and ethyl amide **26** effected severe motor impairment, while the cyclopropyl amide **27** and dimethyl amide **30** exhibited only minor motor impairment. The bulkier isopropyl amide **28** and *t*-butyl amide **29** did not show any motor impairment. These results suggested that these particular amides, which produced sedation/ataxia, are sedating presumably, because of some efficacy at the α1-$GABA_AR$ subtype. In regard to the pharmacological effects of the amide side chain, it is obvious that a smaller alkyl chain promoted a more sedating effect. This effect presumably did not result from metabolism nor cytotoxicity since these two assays indicated that the amides with smaller substituents were highly stable and non-toxic.

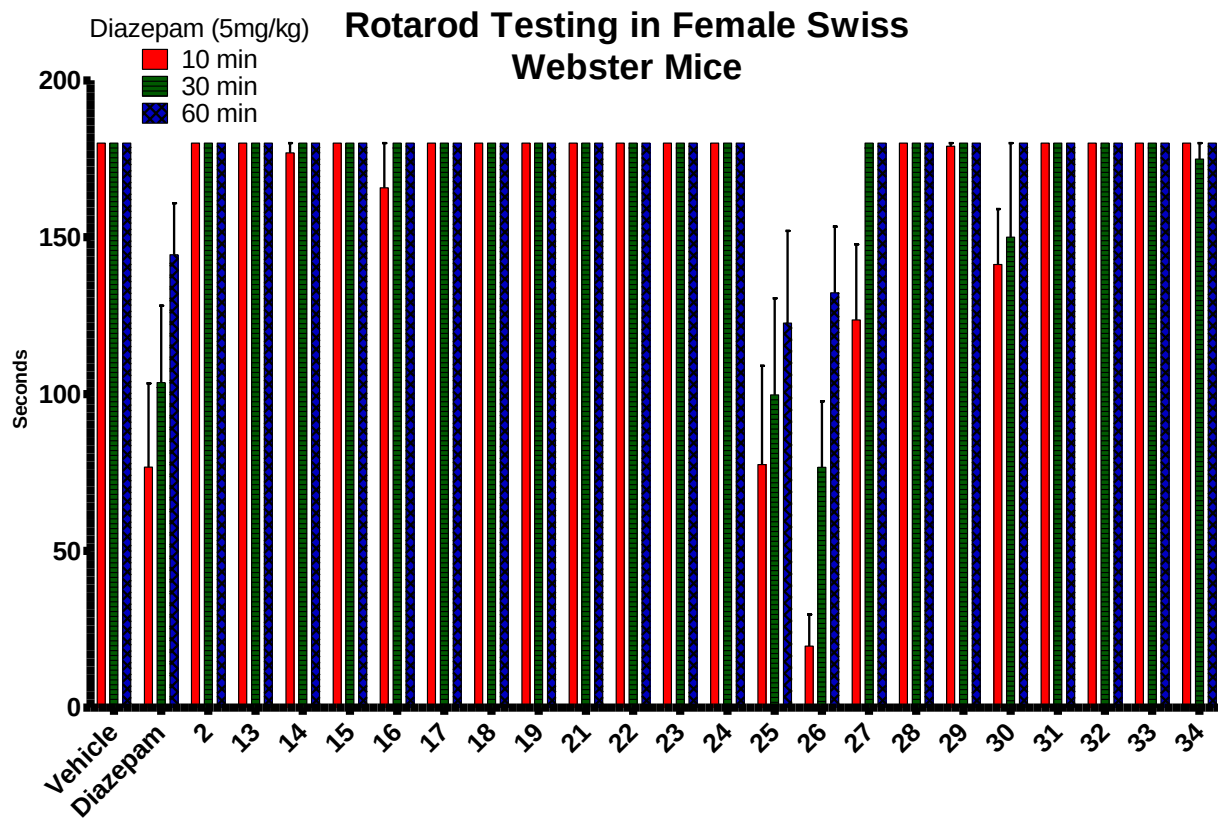

Figure 16. Effect of analogs of 2 on sensorimotor coordination. Mice were placed on the rotarod at three separate time points of 10, 30, and 60 minutes after each oral gavage drug administration at 40 mg/kg. Their performance on the rotarod for 3 minutes was recorded and analyzed. After a second fall, it would be considered a fail, and that time point would be recorded.

After examination of all the results for the series of C(4)-*S*-CH_3 substituted enantiomers described above, the best two compounds, which exhibited excellent stability, minimal or no toxicity and did not exhibit motor impairments, were cyclopropyl amide GL-I-55 (**27**) and methyl oxadiazole GL-I-65 (**31**). Moreover, it was suggested that the bioisosteres GL-I-66 (**32**) and GL-I-81 (**33**), which were very metabolically stable and exhibited no sensorimotor impairment, will need to be administrated at low concentrations in behavioral studies to avoid adverse chronic side effects. Amides **25** and **26** exerted excellent stability and no cytotoxicity, however, these two ligands were sedating at 40 mg/kg p.o. Esters (**13-19**) including the lead compound **2** exhibited either cytotoxicity or were metabolically less stable in the presence of HLM and MLM. Thioester

24, isopropyl amide **27** and nitrile **34** were not metabolically stable enough to encourage further studies. The carboxylic acid **23** exhibited excellent properties in all three assays, however, the acid functionality will prevent the penetration through the blood-brain barrier, which was demonstrated for the *R* enantiomer.[98] This property is not suitable for the treatment of schizophrenia and depression. The cognitive deficits developed in these two disease states are still poorly managed with current drugs. Although the data is only preliminary, the *S*-CH_3 ligand **31** demonstrated pro-cognitive effects (C+) in the Y-maze paradigm at CAMH. The *S*-CH_3 ligand GL-I-54 (**30**) was active in the antidepressant assay (forced swim test) and pro-cognitive (A++ and C++) assay.[117] However, **30** was metabolized fairly rapidly in HLM, as shown in Table 3. **To date, these two ligands, dimethyl amide GL-I-54 (30) and methyl oxadiazole GL-I-65 (31), along with cyclopropyl amide GL-I-55 (27) in this *S*-enantiomeric series seemed to be the best candidates for additional preclinical behavioral testing** (data described in the later biological screening sections 2.2.3.4.), while in the *R*-CH_3 series (α5 subtype selective series) a number of ligands have demonstrated promising pharmacological effects for the treatment of schizophrenia and depression.[18, 67, 83, 95-96, 117]

2.2.3.3. Analogs of the R-isomer

As mentioned above, in addition to the studies of SH-053-2'F-*S*-CH_3 (**2**) and its (*S*)-analogs, the research on the SH-053-2'F-*R*-CH_3 (**1**) series was ongoing at the same time, due to its α5-$GABA_AR$ subtype selectivity as compared to the other series of IMDZs. It was felt that the (*R*)-isomers might provide a better lead to further study the effect on cognitive effects, learning process, and working memory from the interactions with α5-$GABA_ARs$ and Tony Grace and others have

shown in MAM rats, SH-053-2'F-*R*-CH_3 (**1**) was a better ligand in models of schizophrenia[95-96, 98] and depression.[97, 118-119]

2.2.3.3.1. Medicinal Chemistry Strategy of Analog Search in the (*R*)-CH_3 Series

In order to perform a comprehensive SAR study, the design of analog of the α5 subtype selective parent compound **1** was based on the pharmacological data collected from previous studies carried out at Milwaukee.[18, 66-67, 82-83, 95-97, 120] There are four positions in the molecule that can be modified, as depicted in Figure 17, depending on the requirement of specific subtype selectivity and pharmacokinetic profile in addition to the use of the unified BzR/GABA(A) pharmacophore model.

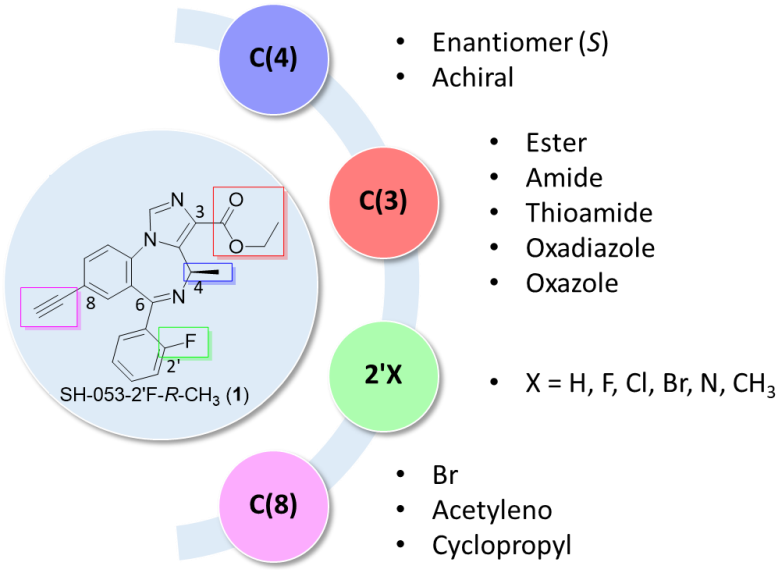

Figure 17. Medicinal chemistry strategy of analog research from the parent compound 1, based on previous work on the C(4)-*S*-CH_3 isomer and the C(4) achiral analogs.

Without the chiral substituent at the C(4) position, the IMDZ acts preferentially as PAMs at α2 and α3-subtypes. The α5 subtype selectivity can be improved by introducing a chiral methyl

function at the C(4) position of the basic "privileged framework." The *R*-isomer was known to be more α5 subtype selective, whereas the enantiomeric *S*-methyl group usually leads to an α2/3/5 subtype selective ligand, as mentioned, with better binding affinity and potency than the *R*-isomers.[18, 67, 83]

The BZD binding pocket of α1 subtypes appears from molecular modeling to be smaller than the α5 binding site,[18, 67] therefore, a larger group at the C(8) position would exhibit less or no binding at α1β3γ2 subtypes, such as an ethinyl and a cyclopropyl group.[67] On the other hand, the smaller group at the C(8) position, would increase the binding affinity and efficacy at all subtypes, which results in sedation and ataxia. Therefore, the best scenario is to achieve the balance so that the size of the substituent at the C(8) position is large enough to retard high affinity at α1 subtypes, but not too large so as to lose high potency at the desired subtypes.

By changing the atoms at the 2' prime position at the C(6) pendant phenyl ring of the IMDZ, the subtype selective varies accordingly. The IMDZs bearing a 2' halogen atom such as Cl and F usually exhibited more potent binding affinity at all subtypes, as compared to the 2'H compounds. The ligands in the 2'N series exhibited the least binding affinity, as compared to other 2' phenyl substituents, hence the binding affinity order influenced by the atom at 2 prime position would be Cl, F > H > N. However, the efficacy profile of each ligand is not always proportional to the binding affinity. Therefore, both factors should be taken into consideration other than just focusing on improving one parameter while designing new compounds.

Aside from the modifications at the C(4), C(8), and 2' phenyl position, different functionality at the C(3) position can provide a distinct influence on the PK profile and induce a variety of behavioral effects in animal models. As previously described in the research on the analog of the *S*-isomer **2**,[90] the presence of a linear ester functional group at the C(3) position

increased the metabolic rate of hydrolysis by the microsomes in the liver. In contrast, the branched ester group can improve the stability of the molecule but also increase the cytotoxicity. The amide groups at the C(3) position are usually much more metabolically stable and less cytotoxic than the corresponding esters. However, the stability trend is opposite to the esters in that the branched chain amides exhibited reduced stability as compared to the linear functionalized amides. Moreover, the smaller size amides might exert mild sedative effects in the rotarod study based on the effects in the C(4)-*S*-CH_3 enantiomeric isomers. The thioamides as isosteres of amides, the oxadiazole and oxazole bioisosteres of esters are commonly used to improve the metabolic stability, PK (solubility-hydrophilicity), as well as pharmacological activity in drug discovery. The carboxylic acid of the parent compound **1** (SH-053-2'F-*R*-CH_3) was not able to pass through the BBB, therefore, this type of analogs was not studied for the treatment of CNS disorders since the ligands are required to penetrate the BBB to affect brain function. However, those compounds were used in the treatment of asthma since they had no CNS effects because there was no penetration through the BBB.

Based on the strategy involved in medicinal chemistry, a series of IMDZ analogs of the (*R*)-enantiomer **1** were designed, synthesized and evaluated in varies animal models. Since most of the esters were metabolized rapidly in rodents, therefore, the synthetic strategy concentrated on the more stable analogs, such as the amide, oxadiazole and oxazole analogs, as summarized in Tables 5, 6, and 7.

Table 5. Amide and thioamide analogs derived from SH-053-2'F-*R*-CH_3 (1).

Other change	Alkyl group on the nitrogen atom					
	Methyl	**Dimethyl**	**Ethyl**	**Cyclopropyl**	**Isopropyl**	**Larger group**
2'F-*R*	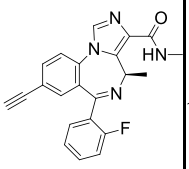 **35** (MP-III-022)	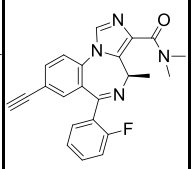 **36** (GL-II-73)	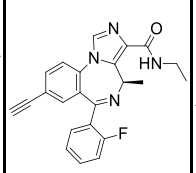 **37** (GL-II-74)	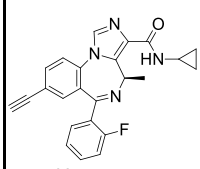 **38** (GL-II-75)	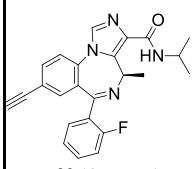 **39** (GL-III-66)	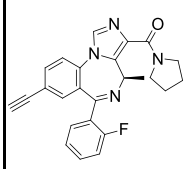 **40** (GL-II-76)
2'F-*S*	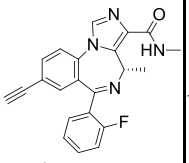 **25** (MP-III-023)	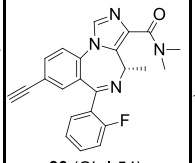 **30** (GL-I-54)	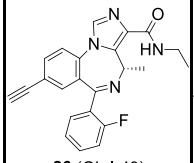 **26** (GL-I-43)	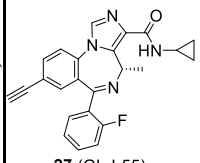 **27** (GL-I-55)	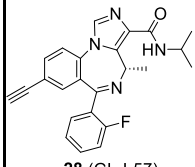 **28** (GL-I-57)	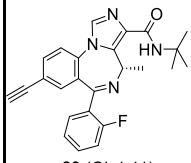 **29** (GL-I-41)
Thio amide (*R*)	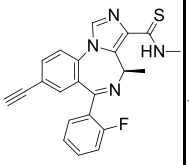 **41** (GL-III-84)	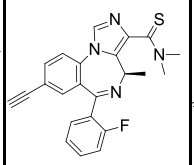 **42** (GL-III-85)	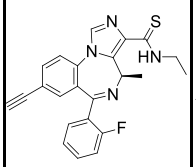 **43** (GL-III-86)	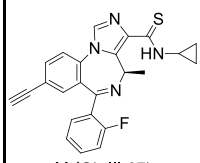 **44** (GL-III-87)		
C(8)-Br	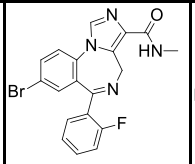 **49** (RV-II-04) achiral	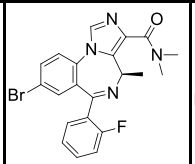 **45** (GL-III-69)	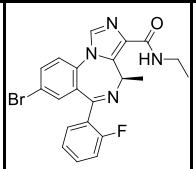 **46** (GL-III-67)			
C(8)-cyclopropyl		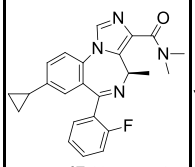 **47** (GL-III-70)	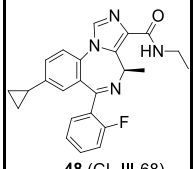 **48** (GL-III-68)			
2'N-*R*	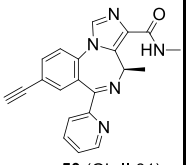 **50** (GL-II-31)					

- **The first row of amides are direct amide analogs of SH-053-2'F-*R*-CH_3 (1), with different alkyl groups on the amide nitrogen atom depicted in the order of increasing the size of the alkyl group from methyl to a larger group.**
- **The second row of amides are the *S*-enantiomers of the amides in the first row (*R*-series), except the *S*-*t*-butyl amide, whereas the pyrrolidine amide had the largest alkyl size in the *R* series.**
- **The third row of amides are the thioamide analogs of the corresponding amide in the first row.**
- **The fourth row are the amides with a C(8)-bromo functional group instead of ethinyl. Note, RV-II-04 is an achiral amide without a chiral methyl group at the C(4) position, as compared to other amides.**
- **The fifth row are the amides bearing a C(8)-cyclopropyl group.**

- **All amides listed above are the amides in the 2'F series, except the amide in the last row, which is in 2'N-*R* amide.**

Table 6. Oxadiazole derivatives related to the α5 subtype selective PAM, SH-053-2'F-*R*-CH_3 (1).

	Methyl		Ethyl	Isopropyl
	2'N	2'F	2'F	2'F
2'F-*R*-oxadiazole	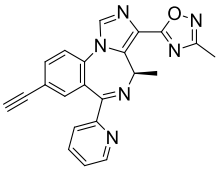 **51** (GL-II-33)	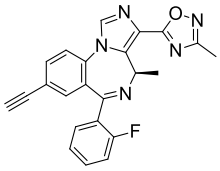 **55** (MP-IV-004)	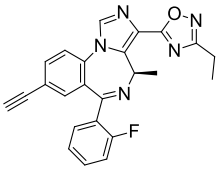 **56** (MP-IV-005)	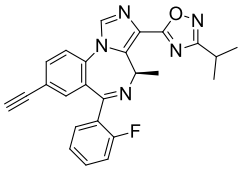 **57** (MP-IV-010)
2'F-*S*-oxadiazole	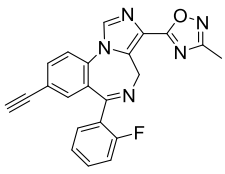 **52** (GL-III-23) achiral	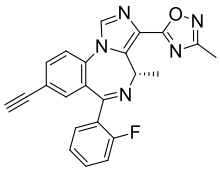 **31** (GL-I-65)	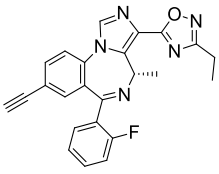 **32** (GL-I-66)	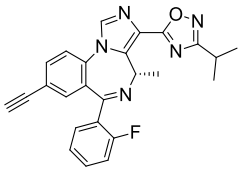 **33** (GL-I-81)
C(8)-Br-oxadiazole	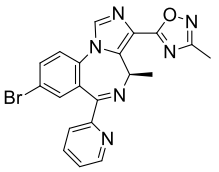 **53** (GL-II-54)	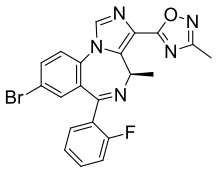 **58** (GL-III-60)	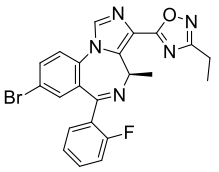 **59** (GL-III-98)	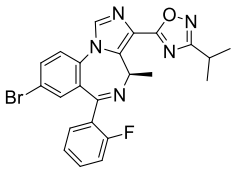 **60** (GL-IV-01)
C(8)-cyclopropyl-oxadiazole	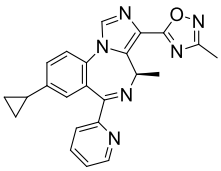 **54** (GL-III-64)	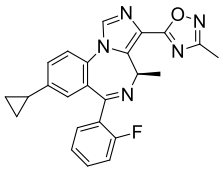 **61** (GL-III-63)	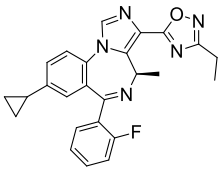 **62** (GL-IV-03)	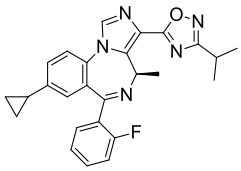 **63** (GL-IV-04)

- **The first two columns of oxadiazole analogs are all methyl substituted on the oxadiazole ring, the first column is the oxadiazoles from the 2'N-*R* series, whereas the 2'F-*R* series is in the second column.**
- **The third and fourth columns are for the oxadiazoles with ethyl and isopropyl groups, respectively.**
- **The first row contains the oxadiazoles in the *R*-isomer series.**
- **The second rows are the *S*-enantiomers of the corresponding oxadiazoles in the first row, except 52, which is an achiral methyl oxadiazole.**
- **The third row are the oxadiazoles with a C(8)-bromo substituent instead of ethinyl group, as compared to the first row of ligands.**
- **The fourth row are the oxadiazoles bearing a C(8)-cyclopropyl group.**

Table 7. The 1,3-oxazole analogs related to the α5 subtype selective PAM, SH-053-2'F-*R*-CH$_3$ (1).

	2'F-R	2'F-S
C(8)-Br-oxazole	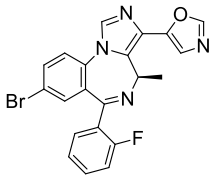 **64** (GL-III-36)	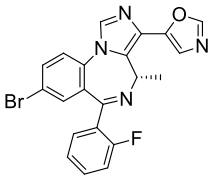 **65** (GL-III-76)
C(8)-acetylene-oxazole	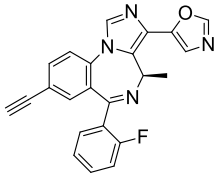 **66** (GL-III-73)	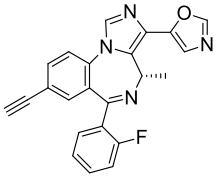 **67** (GL-III-78)

- **The first row are the oxazoles bearing a C(8)-bromo atom in both *R* and *S* enantiomers.**
- **The second row are the oxazoles with a C(8)-ethinyl group in both the *R* and *S* enantiomers.**

2.2.3.3.2. A Study of the Biology of MP-III-022, a Potent Analog of SH-053-2'F-*R*-CH$_3$ (1)

The methyl amide analog of **1**, MP-III-022 (**35**), which was first synthesized by Michael Poe, was found to be a much more potent α5-GABA$_A$R PAM in regard to receptor efficacy than the parent compound **1** at all concentrations,[121] as illustrated in Figure 18. The binding affinity of the amide **35** at α5 subtypes was 55 nM,[83, 121] which was nearly one half of the Ki value of **1,** as shown in Table 8, and was much more selective as compared to other subtypes in agreement with the electrophysiological response. To achieve substantial α5 selectivity without potentiating other subtypes, the administrative dose range was determined by Savic et al.[121] to be 1-10 mg/kg by measurement of the compound concentration in the rat brain, whereas the range of parent compound **1** was 10-200 mg/kg. As a result of better α5 subtype selectivity, the amide **35** was resynthesized via direct amidation of ethyl ester **1** in the presence of methylamine in

dichloromethane. The same procedure had been used for the methyl amide of the *S*-isomer [90] and the *R*-CH_3 amide (**35**) was subjected to further biological evaluation.

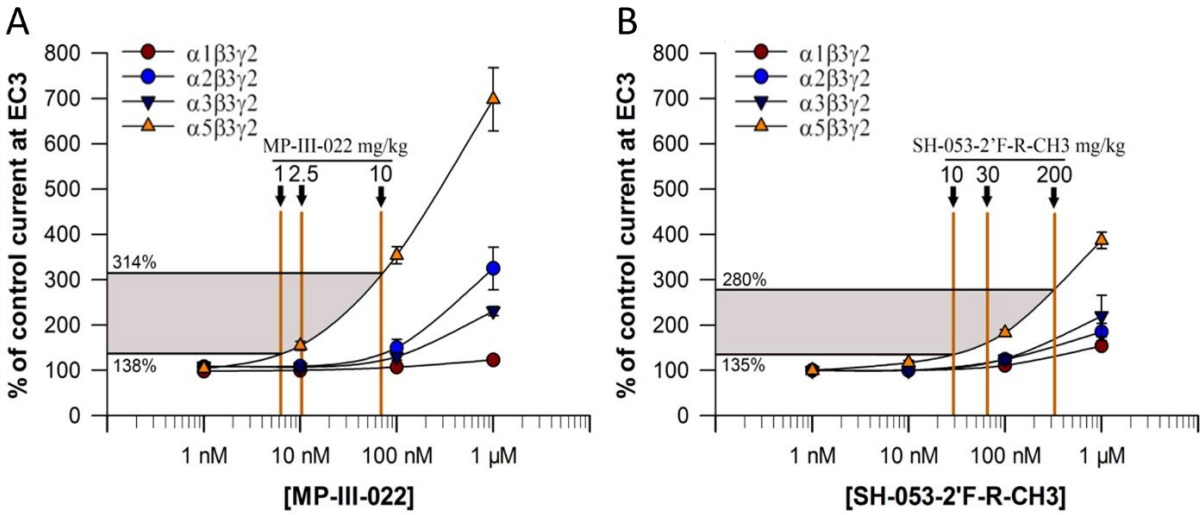

Figure 18. The electrophysiological response of 35 (A) and 1 (B) . The GABA EC3 (3% of the maximal GABA current) measurement was illustrated on the concentration-response curves at $\alpha_{1\text{-}3,5}\beta3\gamma2$ $GABA_A$Rs of rat recombinant receptors. The dose range of 35 (MP-III-022) to provide a selective potentiation at α5 was 1-10 mg/kg, whereas it was 10-200 mg/kg for compound 1. (Modified from the Figure in Stamenić et al.)[121]

Table 8. The binding affinity of 1 and 35; the K_i values are reported in nM.[83, 121]

Compound	**α1**	**α2**	**α3**	**α5**
SH-053-2'F-R-CH_3 (**1**)[83]	759.1	948.2	768.8	95.2
MP-III-022 (**35**)[121]	850	360	660	55

The methyl amide **35** (MP-III-022) did not induce spontaneous hyperlocomotor activity at the **highest α5 selective dose at 10 mg/kg**, only slight hyperlocomotor was observed at **the lowest non-selective dose (15 mg/kg),**[121] which might result from the slight potentiation of α2/3, but not from α1 subtypes. However, **35** did not present any effect on wild-type rats during the amphetamine-induced locomotor stimulation assay,[121] whereas the parent compound **1** exhibited a significant suppression of the locomotor response induced by amphetamine in MAM rats, which

demonstrated an anti-psychotic property.[96] Moreover, the lack of activity in the elevated plus maze assay indicated that amide **35** did not possess any anxiolytic property in this assay.

Recently, the ligand **35** (MP-III-022) was evaluated in the lipopolysaccharide (LPS) - induced maternal immune activation model; it is a common model for research on the onset schizophrenia. It was illustrated that amide **35** at a dose of 2 mg/kg daily, i.p. prevented the deficit locomotor activity due to prenatal maternal immune activation by LPS (100 μg/kg, i.p.), as well as the diminished reactivity to amphetamine (0.5 mg/kg, i.p.) in adult female mice to a certain extent, but not in male mice.[122] During the examination of the LPS-induced immune response by cytokine (IL-6) expression after 6 hours of the LPS treatment, the GABA concentration was significantly increased in the whole fetal brain, whereas a significant decrease of glutamate concentration was also observed at the same time. The imbalance of GABA/glutamate can profoundly influence the development of the GABAergic system, especially in the fetal brain even for just a few hours. The observation that **the locomotor reactivity in the LPS-induced immune activation in female adult mice has been improved with the treatment with α5 PAM 35, might provide a novel strategy for the early prevention of schizophrenia with the intervention via use of α5 $GABA_AR$ subtypes.** Therefore, taken together with the previous pharmacological activity,[97, 118, 122] potentiation at α5 subtypes, and the most recent published results from the research based on the models of schizophrenia, a series of IMDZ analogs were designed and synthesized for further study on the influence of α5-containing $GABA_ARs$ for schizophrenia, as well as depression. This was based on the structure of the α5 subtype selective ethyl ester **1** and its more potent methyl amide analog **35**.

2.2.3.3.3. Synthesis of the Analogs of SH-053-2'F-*R*-CH_3 (1)

In order to explore the SAR of amides with different alkyl substituents in addition to the methyl amide **35**, the first set of C(8)-ethinyl-C(3)-amide analogs of the parent compound **1** were designed and synthesized following the general procedure of amide synthesis in the (*S*)-CH_3 series (Li, Arkivoc 2018).[90] First, the ethyl ester **1** was hydrolyzed to the carboxylic acid SH-053-2'F-*R*-CH_3-acid (**68**) by treatment with sodium hydroxide in ethanol and this was followed by adjusting the pH to 5 with a cold aq 1 M solution of HCl, which gave the desired acid **68** as a white precipitate. The acid **68** was then treated with thionyl chloride to form the intermediate acyl chloride, and this was followed by the addition of the corresponding amines (individually) to yield the dimethyl amide GL-II-73 (**36**), ethyl amide GL-II-74 (**37**), cyclopropyl amide GL-II-75 (**38**), isopropyl amide GL-III-66 (**39**), and pyrrolidine amide GL-II-76 (**40**) in good yield (70-82 %), respectively, as illustrated Scheme 9. The synthesis of the corresponding amides in the *S*-isomer series: the methyl amide MP-III-023 (**25**), dimethyl amide GL-I-54 (**30**), ethyl amide GL-I-43 (**26**), cyclopropyl amide GL-I-57 (**27**), and isopropyl amide GL-I-41 (**28**), were described in the previous section and employed as a model for the synthesis of the *R*-CH_3 substituted analogs here.

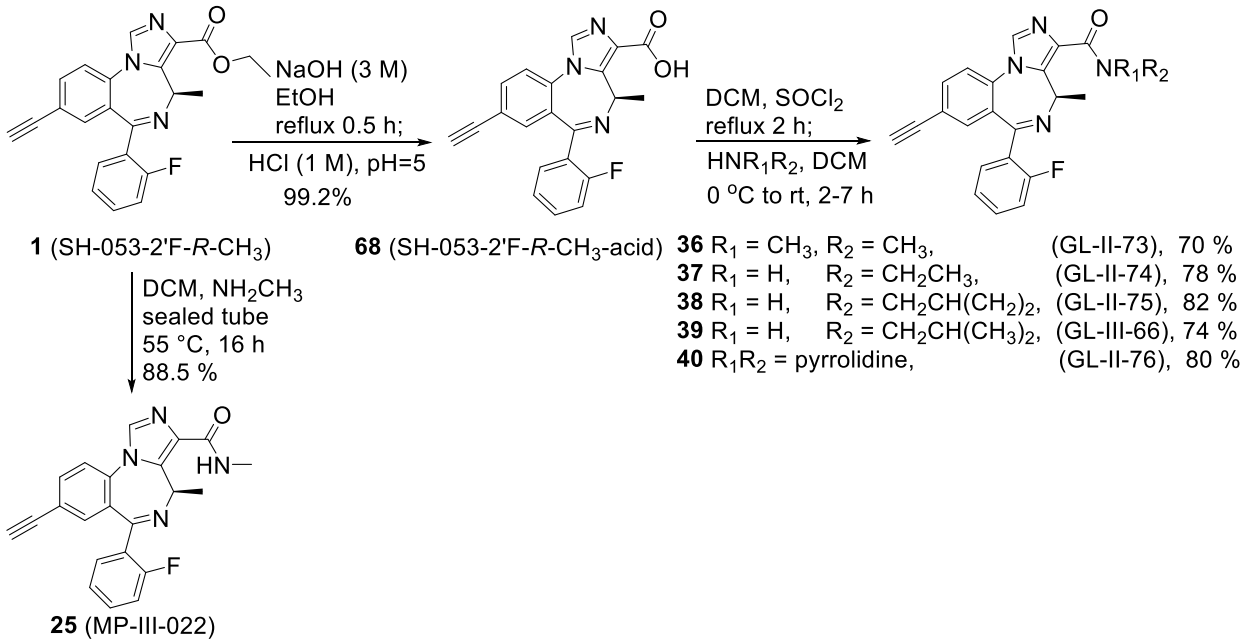

Scheme 9. Synthesis of the C(8)-ethinyl amide analogs 35-40 of the parent ethyl ester 1 (SH-053-2'F-*R*-CH$_3$).

The thioamides are known as one of the isosteres of amides. Due to the reduced electronegativity and larger atomic size of a sulfur atom, the C=S carbon is less electron deficient and less prone to undergo attack by an electron-rich nucleophile as compared to an amide C=O. The larger and uncharged sulfur atom is able to accept more charge density to transfer from the nitrogen atom in a thioamide, as compared to an amide moiety.[123] Moreover, from the ground state to the transition state, the rotational barrier of the C-N bond is larger in a thioamide than amide,[124] which results from the relatively larger dipole moment in a thioamide. With a higher polarity, thioamides are much better H-bond donors than the corresponding amides due to less electronegativity on the sulfur atom and higher electron density as compared to the C-N bond. On the other hand, amides are better H-bond acceptors than thioamides. In order to study the electronic effect at the C(3) position on stability, the thioamide family was prepared. This would lead to the direct SAR comparison between amides and thioamides. Therefore, several thioamides were prepared by using Lawesson's reagent (LR)[125-126] in refluxing THF; the four amides **35-38** were

converted into their corresponding thio-derivatives, respectively: the methyl thioamide GL-III-84 (**41**), dimethyl thioamide GL-III-85 (**42**), ethyl thioamide GL-III-86 (**43**), and methyl thioamide GL-III-87 (**44**), as presented in Scheme 10. ***Caution, LR has a very unpleasant sulfur smell, it should be handled carefully in a fume hood.*** After removing the solvent from the mixture, the residue was dissolved in DCM and loaded onto a silica gel flash column. The LR byproduct was flashed off with 2:3 EtOAc and hexanes in the first fraction as a cloudy white solution. The thioamide was purified in later fractions from the same flash column.

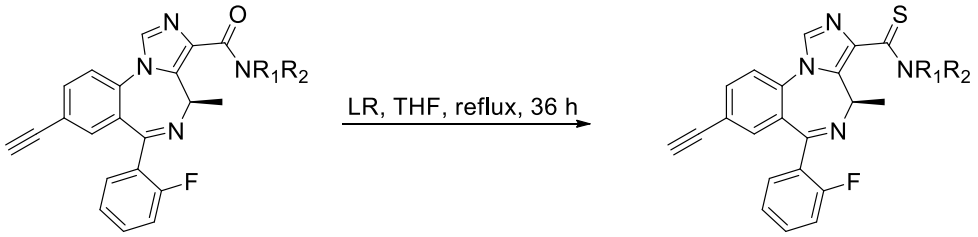

35 R_1 = H, R_2 = CH_3, (MP-III-022)
36 R_1 = CH_3, R_2 = CH_3, (GL-II-73)
37 R_1 = H, R_2 = CH_2CH_3, (GL-II-74)
38 R_1 = H, R_2 = $CH_2CH(CH_2)_2$, (GL-II-75)

41 R_1 = H, R_2 = CH_3, (GL-III-84), 60 %
42 R_1 = CH_3, R_2 = CH_3, (GL-III-85), 70 %
43 R_1 = H, R_2 = CH_2CH_3, (GL-III-86), 62 %
44 R_1 = H, R_2 = $CH_2CH(CH_2)_2$, (GL-III-87), 64 %

Scheme 10. Synthesis of the C(8)-ethinyl thioamide analogs 41-44 from corresponding amides 35-38.

Due to the more potent binding affinity from the C(8)-bromo substituent at lower concentrations in same cases, as compared to the ethinyl group, the synthesis of the C(8)-bromo amides were also prepared from the C(8)-bromo ethyl ester SH-I-047 (**6**). This required the same general synthetic procedure for the amides, with the corresponding amine, to form the C(8)-bromo dimethyl amide GL-III-69 (**45**) and the C(8)-bromo ethyl amide GL-III-67 (**46**), respectively, as indicated in Scheme 11. As previously mentioned, the C(8)-cyclopropyl group can flexibly rotate and should have a similar volume of electron density as the ethinyl group. This similar electron density profile might result in parallel pharmacological effects. Furthermore, the metabolism of the cyclopropyl group would be expected to be different from the C(8)-ethinyl or Br groups.

Therefore, based on these hypotheses, the C(8)-cyclopropyl analogs were prepared *via* a Pd catalyzed Suzuki cross-coupling reaction process with the cyclopropyl boronic acid and the corresponding C(8)-bromo amido analogs to yield the C(8)-cyclopropyl dimethyl amide GL-III-70 (**47**) and the C(8)-cyclopropyl ethyl amide GL-III-68 (**48**), respectively, as shown in Scheme 11.

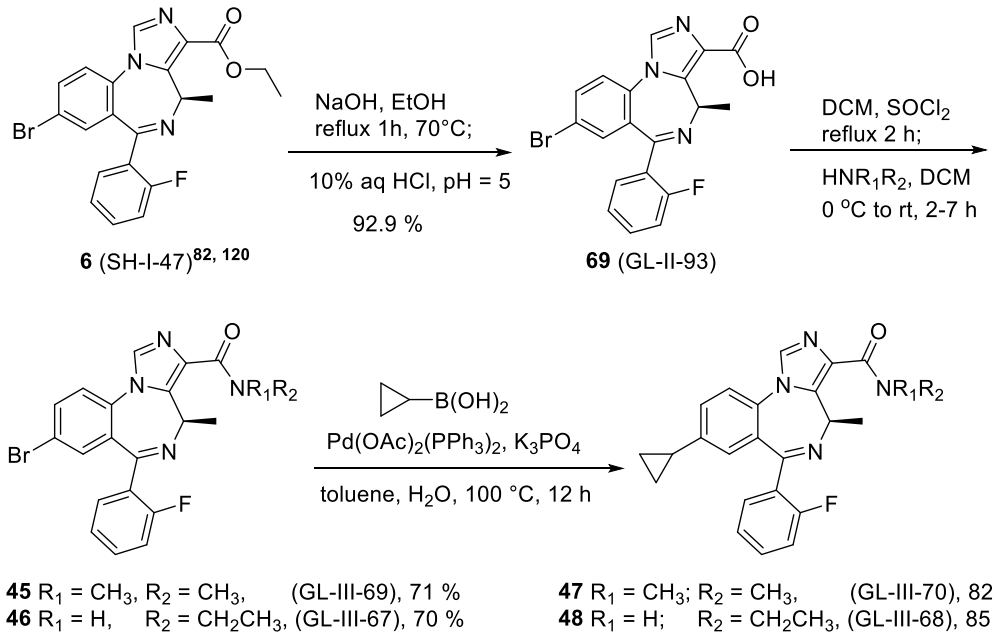

6 (SH-I-47)[82, 120] **69** (GL-II-93)

45 $R_1 = CH_3$, $R_2 = CH_3$, (GL-III-69), 71 %
46 $R_1 = H$, $R_2 = CH_2CH_3$, (GL-III-67), 70 %
47 $R_1 = CH_3$; $R_2 = CH_3$, (GL-III-70), 82 %
48 $R_1 = H$; $R_2 = CH_2CH_3$, (GL-III-68), 85 %

Scheme 11. Synthesis of C(8)-bromo amides 45-46 and C(8)-cyclopropyl amides 47-48 from SH-I-47 (6).[82, 120]

In addition to the 2'F series, the analogs in the chiral 2'N series were synthesized as well to compare the SAR between the two series. The 2'N-*R* ethyl ester was prepared via the same route employed for esters **1** and **2**, except the 2'-pyridyl ketone **70** was substituted for the 2'F benzophenone in the first step. The synthesis is illustrated in Scheme 12. The intermediate amide **71** was obtained from the amidation reaction, which employed the coupling reagent (DCC) in 99.2 % yield on a 100-gram scale. The Boc-deprotection of the amide **71** was carried out in a saturated solution of HCl (gas) solution in DCM at 0 ˚C. The mixture was stirred for one hour and this was

then followed by the cyclization to the 7-membered ring. The crystallization was carried out in the 1:1 mixture of methanol and water after adjusting the pH to 9 by addition of 2 N aq NaOH solution. The desired 1, 4-benzodiazepine **72** precipitated out of the solution in 94 % yield. The recrystallization of the benzodiazepine **72** was conducted in a mixture of EtOAc and hexanes in a ratio of 1:1, after adding seed crystals. The imidazole ring was added on to **72** by treating benzodiazepine **72** with potassium *t*-butoxide and diethyl chlorophosphate at -50 ˚C, and this was followed by addition of ethyl isocyanoacetate and a second portion of potassium *t*-butoxide at -78 ˚C. This addition reaction was carried out in 68 % yield on a 150-gram scale. The majority of the bromide **73** can be recrystallized after cooling from 60 ˚C to room temperature. The material left in the mother liquor was purified by flash column chromatography (silica gel, EtOAc: hexane, 3:2). This bromide **73** was then reacted with trimethylsilylacetylene in the presence of a palladium catalyst *via* a Heck-type coupling reaction to obtain the TMS-analog **74** in 90 % yield. The fluoride-mediated desilylation was carried out by treatment of **74** with tetra-*n*-butylammonium fluoride to provide **75** (GL-II-19-2'N-*R*-CH_3) in 95 % yield, as shown in Scheme 12. The methyl amide of **75** was prepared via direct amidation in a similar fashion to amide **25** prepared earlier [90] to achieve the desired methyl amide **50** in 72 % yield.

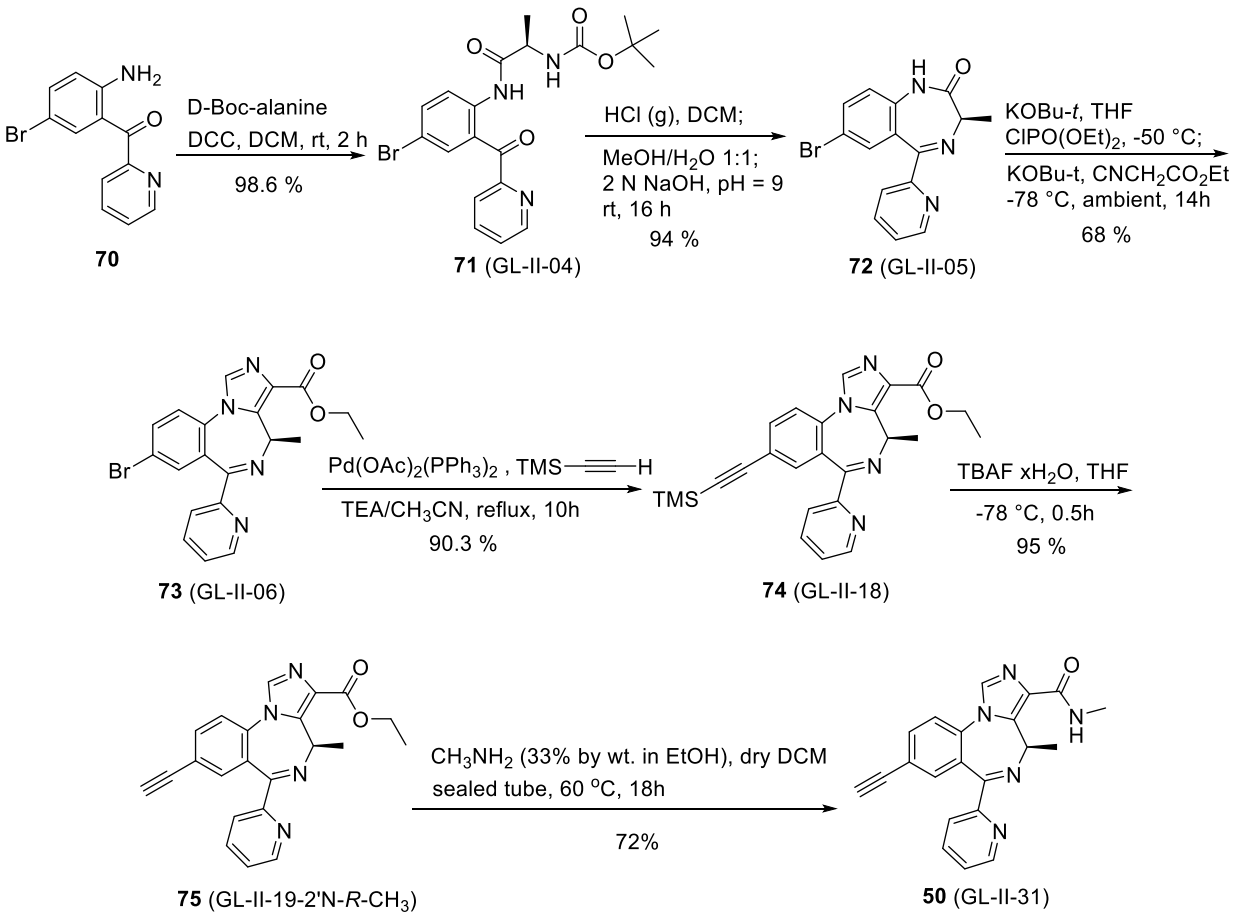

Scheme 12. Synthesis of analogs in the 2'N-*R*-CH$_3$ series.

As a common ester bioisostere, 1,2,4-oxadiazoles in the 2'F-*R*-CH$_3$ and 2'N-*R*-CH$_3$ series were synthesized either from the C(8)-ethinyl or bromo ethyl ester, respectively. The general procedure employed here for the synthesis of 1,2,4-oxadiazoles was executed with different substituted oximes to form the corresponding analogs: 2'N-*R*-CH$_3$ series: C(8)-ethinyl methyl oxadiazole GL-II-33 (**51**), 2'N-*R*-CH$_3$-C(8)-bromo methyl oxadiazole GL-II-54 (**53**); 2'F-*R*-CH$_3$-C(8)-ethinyl series: methyl oxadiazole MP-IV-004 (**55**), ethyl oxadiazole MP-IV-005 (**56**), isopropyl oxadiazole MP-IV-010 (**57**); 2'F-*R*-CH$_3$ C(8)-bromo series: methyl oxadiazole GL-III-60 (**58**), ethyl oxadiazole GL-III-98 (**59**), isopropyl oxadiazole GL-IV-01 (**60**), as illustrated in Scheme 13. The cyclopropyl oxadiazole was prepared *via* a Suzuki Pd-mediated cross-coupling

reaction with cyclopropyl boronic acid and the corresponding C(8)-bromo oxadiazoles to yield the analogous C(8)-cyclopropyl oxadiazole analogs: 2'N methyl oxadiazole GL-III-64 (**54**); 2'F-*R*-CH_3-C(8)-cyclopropyl series: methyl oxadiazole GL-III-63 (**61**), ethyl oxadiazole GL-IV-03 (**62**), isopropyl oxadiazole GL-IV-04 (**63**). The achiral methyl 2'F-C(8)-ethinyl oxadiazole GL-III-23 (**52**) was synthesized from JY-XHe-053 with the methyl oxime (Scheme not shown). The synthesis of oxadiazoles from the *S*-CH_3 enantiomeric series **31-33** were described in the previous section.

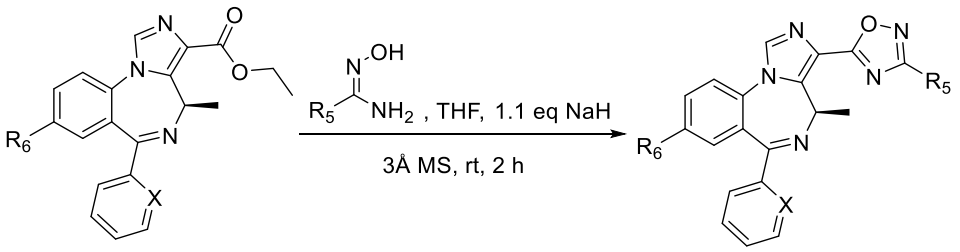

75 R_6 = ≡, X = N, (GL-II-19-2'N-*R*-CH_3)
73 R_6 = Br, X = N, (GL-II-05)
1 R_6 = ≡, X = CF, (SH-053-2'F-*R*-CH_3)
6 R_6 = Br, X = CF, (SH-I-047)

51 R_6 = ≡, X = N, R_5 = CH_3, (GL-II-33), 85 %
53 R_6 = Br, X = N, R_5 = CH_3, (GL-II-54), 85 %
55 R_6 = ≡, X = CF, R_5 = CH_3, (MP-IV-004), 85 %
56 R_6 = ≡, X = CF, R_5 = CH_2CH_3, (MP-IV-005), 79 %
57 R_6 = ≡, X = CF, R_5 = $CH(CH_3)_2$, (MP-IV-010), 82 %
58 R_6 = Br, X = CF, R_5 = CH_3, (GL-III-60), 85 %
59 R_6 = Br, X = CF, R_5 = CH_2CH_3, (GL-III-98), 79 %
60 R_6 = Br, X = CF, R_5 = $CH(CH_3)_2$, (GL-IV-01), 82 %

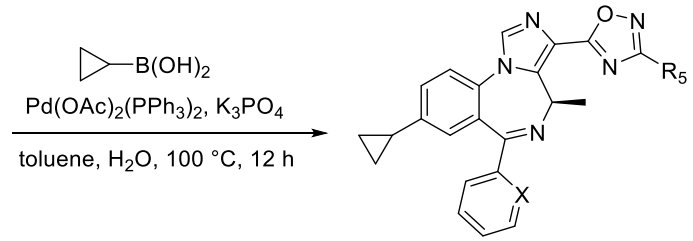

54 X = N, R_5 = CH_3, (GL-III-64), 85 %
61 X = CF, R_5 = CH_3, (GL-III-63), 85 %
62 X = CF, R_5 = CH_2CH_3, (GL-IV-03), 79 %
63 X = CF, R_5 = $CH(CH_3)_2$, (GL-IV-04), 82 %

Scheme 13. Synthesis of 1,2,4-oxadiazole analogs 51-63 with the C(8)-ethinyl, bromo or cyclopropyl group in the 2'F or 2'N pendant phenyl series.

In addition to the traditional 1,2,4-oxadiazole, bioisosteres, the 1,3-oxazoles are unique bioisosteres and possess a very similar electron density map to that of an ester. It has been reported

that the molecules containing the 1,3-oxazole moiety exhibited the desired pharmacological effects in animal models with better therapeutic and PK profiles.[127-129] Furthermore, the 1,3-oxazoles should be easier to patent than the often used 1,2,4-oxadiazoles.

The 1,3-oxazole analog of α2/3 PAM Hz-166 (**76**), termed KRM-II-81 (**77**) is an achiral and very selective α2 and α3 subtype selective IMDZ $GABA_AR$ ligand, which has proven to be active in models of anxiety, epilepsy, pain, and depression, which will be discussed in detail in the last chapter. The success of 1,3-oxazole **77** directed attention to this fairly unique moiety in regard to analogs in the chiral series in order to improve the duration of action, which should be a better candidate for both schizophrenia and depression. In addition, it might provide some anxiolysis which would be important since anxiety is always comorbid with for these two CNS disorders.

However, the synthesis of the 1,3-oxazole in the chiral series met with a number of difficulties. The standard route employed previously, not only encountered [N(5)-C(6)] imine bond reduction of the C(3) ester function on attempts to prepare the C(3) aldehyde with DIBAL, which was a similar problem observed in the synthesis of **77**, but also underwent [N(5)-C(6)] imine to [N(5)-C(4)] imine migration to the C(4)-N(5) position. This resulted in the loss of the correct chirality at the C(4) position. The problem of imine reduction and isomerization was resolved and was published (Li, SYNTHESIS, 2018)[130] by using a more hindered reducing reagent than DIBAL. The potassium diisobutyl-t-butoxy aluminum hydride (PDBBA) solution was prepared and found to reduce the C(3) ester to the desired aldehyde, but did not reduce the [N(5)-C(6)] imine moiety due to the bulky steric size of the PDBBA reagent. The details of this reaction will be presented in the last chapter. It was felt once the aldehyde GL-III-35 (**78**) had been formed readily, the remaining synthesis would go smoothly. On the contrary, the van Leusen reaction in the chiral series was not as simple as in the achiral series. During the reaction, in the chiral series, the

majority of the product was the desired 1,3-oxazole GL-III-36 (**64**), on analysis by TLC (silica gel). However, after the reaction mixture was worked up, a large portion of the desired oxazole were converted into another compound (45 %), which proved to be the [N(5)-C(6)] imine migration byproduct GL-III-36A (**79**) without the correct chirality at the C(4) position (NMR and LCMS).

To find the cause of the unexpected formation of the byproduct, the reaction was conducted exactly the same way as the first time; however, the reaction mixture was monitored very carefully after each workup step (analysis by TLC). With the help of TLC, analysis of this data indicated that the conversion was complete but the isomerization occurred during the removal of methanol at 50 degrees under reduced pressure. Presumably, as the solvent became more concentrated, the tosic acid concentration increased while reducing the solvent volume at higher temperature. The imine bond was hydrolyzed by the concentrated tosic acid to the keto form. When the imine was regenerated by cyclization, the deprotonation of the iminium ion in the transition state would most likely take place in two directions, as illustrated in Figure 19. It would occur either from the proton on the imine nitrogen atom or the proton from the chiral carbon atom. Apparently, the deprotonation of the latter case requires more energy than the direct deprotonation from the nitrogen atom. However, the byproduct **79** presumably would be more stable than the desired product **64** due to better electron delocalization into the adjacent imidazole ring system. This energy barrier can be reached by applying heat, which occurred while reducing the solvent volume on heating the solution to 50 degrees centigrade. Once the energy overcame the transition state barrier, the more stable byproduct **79** would likely form than the less stable desired product **64**. The proposed mechanism is demonstrated in Figure 19.

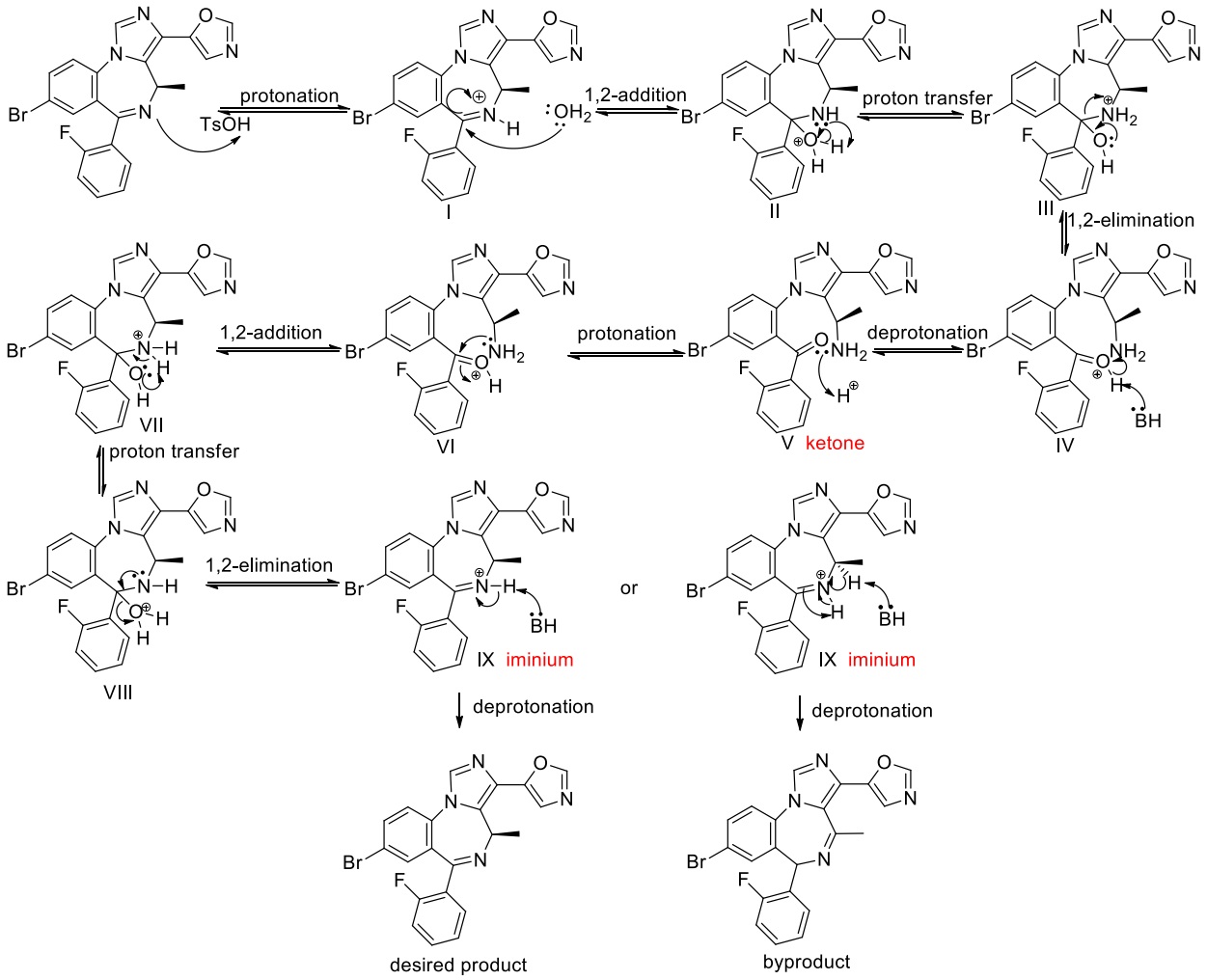

Figure 19. The proposed mechanism for the formation of the byproduct 79 from workup of the van Leusen reaction; an effect of tosic acid on the [N(5)-C(6)] imine to [N(5)-C(4)] imine rearrangement (tautomerism).

It is also possible the concentrated tosic acid protonated the imine nitrogen atom and with heat the chiral proton was lost to provide the more stable C(4)-N(5) double bond.

To avoid the byproduct formation, 4 more equivalents of base and a large amount of water were added after the reaction during workup, which was completed at room temperature. The mixture was stirred for an extra one hour to neutralize the tosic acid. The temperature was also reduced, while removing the solvent, to 40 degrees to lower the possible energy for byproduct formation. The product yield was improved to 82 %, as compared to 50 % for the initial reaction,

with an only a trace of byproduct observed. The C(8)-bromo 1,3-oxazole was converted into the TMS analog GL-III-72 (**80**) with ease and this was followed by removal of the trimethylsilyl function to furnish the C(8)-ethinyl-C(3)-1,3-oxazole, which overcame a long-standing problem, as presented in Scheme 14. In the *S*-CH_3 series, the C(8)-bromo ethyl ester was reduced to the desired aldehyde GL-III-75 (**81**). The 1,3-oxazole C(8)-bromo GL-III-76 (**65**) were prepared via the same simplified route from aldehyde **81**. The olefinic byproduct GL-III-76A in the *S*-CH_3 series was identical to the **79** from the *R*-CH_3 series**.** The C(8)-TMS-acetylene was introduced to form the TMS-analog (**82**), after deprotection of which, the C(8)-ethinyl GL-III-78 (**67**) was achieved. **Simply be aware of the tosic acid during workup.**

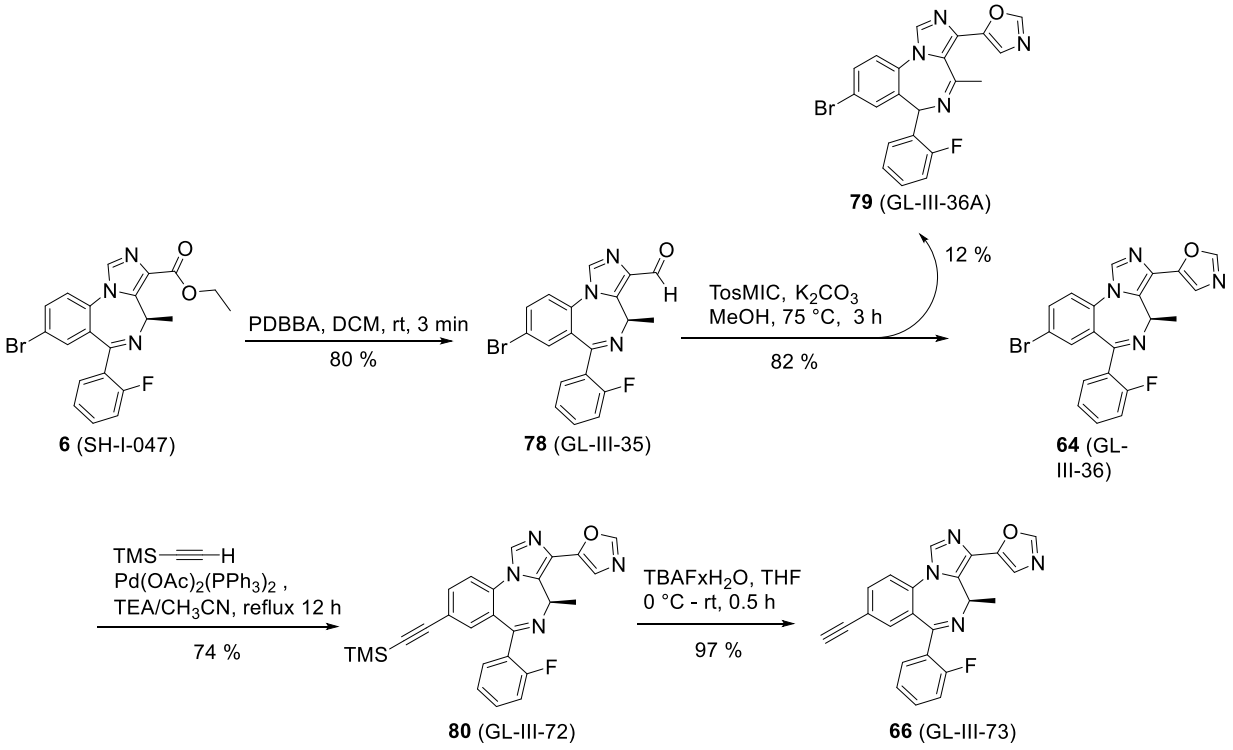

Scheme 14. Synthesis of the 2'F-*R*-CH_3 chiral 1,3-oxazole GL-III-73 (66).

2.2.3.4. Biological Screening for the Selection of Lead Compounds

In order to select the lead compounds, a series of biological screenings, such as metabolism studies in HLM and MLM, cytotoxicity assays, rotarod tests, receptor binding studies, electrophysiology recording assays as well as PK studies, were performed with all newly designed IMDZs before behavioral studies in critical animal models. Only the compounds that were metabolically stable, non-toxic, and subtype-selective with good PK profiles but devoid of other possible receptor interactions, such as hERG or PBR, would be further investigated. This would be executed in specific disease-related animal models to reduce the possible failure of candidates in the later drug development stages.

2.2.3.4.1. Study of Metabolism

2.2.3.4.1.1. *In Vitro* Metabolic Stability in HLM and MLM

The first sets of the *R*-CH_3 amide and oxadiazole analogs were assayed for metabolic stability *in vitro* on HLM and MLM at 10 μM concentration (see Table 9). After 2-hours of incubation at 37 degrees, the most stable analogs were determined, and a possible trend of steric effects with respect to metabolic stability was determined. The half-life and percent remaining of the compound at the end of two hours for the *R*-CH_3 isomers are presented in Table 9, while those half-lives for the corresponding *S*-CH_3 enantiomers can be found in Table 10.

Table 9. Metabolic stability of amides and oxadiazoles. Unpublished data. (*R*-CH_3 isomers)

Type	2'	Code (R)	Half-life (min) (HLM)	% left after 2 hr. (HLM)	Half-life (min) (MLM)	% left after 2 hr. (MLM)
Methyl	F	**49** (RV-II-04) (Br)	595 ± 157	80.2 ± 0.4	302 ± 33	73.7 ± 0.30
Methyl	N	**50** (GL-II-31)	1870 ± 765	92 ± 0.32	1840 ± 590	93.17 ± 0.24
Methyl	F	**35** (MP-III-022)	141 ± 18 (At 1 hr.)	69.35 ± 0.36 (At 1 hr.)	164.3 ± 9.8 (At 1 hr.)	76.55 ± 0.15 (At 1hr.)
Ethyl	F	**37** (GL-II-74)	403 ± 40	82 ± 0.52	72 ± 6.7	32.1 ± 0.54
Cyclopropyl	F	**38** (GL-II-75)	163 ± 12	61.9 ± 0.9	106 ± 8	50 ± 0.55
t-butyl /pyrrolidine	F	**40** (GL-II-76) (pyrrolidine)	86 ± 7.12	40 ± 0.47	33 ± 1.46	7.3 ± 0.62
Dimethyl	F	**36** (GL-II-73)	280 ± 31	73.34 ± 0.6	472.7 ± 56	81.6 ± 0.27
Methyl	N	**51** (GL-II-33)	2586 ± 1106	95.3 ± 0.2	500 ± 66	82 ± 0.26
Methyl	N	**53** (GL-II-54) (Br)	404 ± 61	76 ± 0.2	2331 ± 1112	93.6 ± 0.24
Methyl	F	**52** (GL-III-23) (non chiral)	504.2 ± 77	82 ± 0.3	1324 ± 316	92 ± 0.2
Methyl	F	**55** (MP-IV-004) (MP-IV-004)*		ND 86.4		ND 74.3
Ethyl	F	**56** (MP-IV-005) (MP-IV-005)*		ND 89.3		ND 51.3
Isopropyl	F	**57** (MP-IV-010)*		74.3		26.6

- **Data presented in half-life (minute) and % remaining after 2 hours of incubation, respectively for both HLM and MLM.**
- **Data of compound without the star * were obtained from Dr. Arnold's group by Revathi Kodali. All ligands were incubated with human liver microsomes (HLM) or mouse liver microsomes (MLM) for 2 h (except for MP-III-022 incubated for 1 h) at 37 ºC at a final concentration of 10 µM. The percentage of compound remaining after incubation was measured by LC-MS/MS.**
- **Data with a star * was obtained from Eli Lilly. The assay was performed with Hep microsomes at 4 µM for 30 min at 37 ºC.**
- **Different alkyl groups on the amide nitrogen atoms or oxadiazole rings are listed in the first column. Examination of the data in the second column indicates the 2 prime substituents, the compounds are either from the 2'F or the 2'N series.**
- **Amides are in red rectangles, oxadiazoles are depicted in yellow.**
- **ND: not determined.**

Table 10. Metabolic stability of amides and oxadiazoles. (*S*-CH_3 isomers)

Type	2'	Code (S)	Half-life (min) (HLM)	% left after 2 hr. (HLM)	Half-life (min) (MLM)	% left after 2 hr. (MLM)
Methyl	N					
Methyl	F	**25** (MP-III-023)	1790 ± 40	91.6 ± 0.35	846 ± 5	84.6 ± 0.21
Ethyl	F	**26** (GL-I-43)	1978 ± 55	93.2 ± 0.27	1970 ± 46	93 ± 0.3
Cyclopropyl	F	**27** (GL-I-55)	1625 ± 803	89 ± 0.35	320.5 ± 34	72.5 ± 0.3
t-butyl /pyrrolidine	F	**29** (GL-I-41) (*t*-butyl)	205 ± 14	63.5 ± 0.27	141.5 ± 8	51 ±0.34
Dimethyl	F	**30** (GL-I-54)	100 ± 4.5	36.4 ± 2	53 ± 10	15 ± 3
Methyl	N					
Methyl	N					
Methyl	F					
Methyl	F	**31** (GL-I-65) (GL-I-65)*	866 ± 213	86.4 ± 0.3 88.4	443 ± 67	81 ± 0.42 80.7
Ethyl	F	**32** (GL-II-66) (GL-I-66)*	564.4 ±123.5	80.5±0.4 76.1	217 ±17	63 ±0.34 64.9
Isopropyl	F	**33** (GL-I-81)	2584 ± 1920	91.0 ± 0.3	500 ± 109	79.0 ± 0.5

- **Data presented in half-life (minute) and % remaining after 2 hours of incubation, respectively for both HLM and MLM.**
- **Data of compound without the star * were obtained from Dr. Arnold's group by Revathi Kodali. All ligands were incubated with human liver microsomes (HLM) or mouse liver microsomes (MLM) for 2 h at 37 ºC at a final concentration of 10 µM. The percentage of compound remaining after incubation was measured by LC-MS/MS.**
- **Data with a star * was obtained from Eli Lilly. The assay was performed with Hep microsomes at 4 µM for 30 min at 37 ºC.**
- **Different alkyl groups on the amide nitrogen or oxadiazole ring are listed in the first column. Examination of the data in the second column indicates the 2 prime substituents, the compounds are either from the 2'F or the 2'N series.**
- **Amides are in red rectangles, oxadiazoles are depicted in yellow.**

In the amide family, on human liver microsomes (HLM), the methyl amides **50** and **25** are more stable with more than 90 % remaining after 2 hours of incubation. In comparison, the stability

of the methyl amide of the enantiomeric *R*-CH_3 series **35**, as compared to the *S*-isomer **25**, the *S*-methyl amide **25** was more stable than the *R* enantiomer **35,** which is reversed in the case of the dimethyl amide **36** (*R*) and **30** (*S*) in regard to the structural configurations: the *R*-isomer **36** was more stable than the *S* enantiomer **30,** with 73.4 % and 36.4 % remaining after 2 hours in HLM, respectively. All other compounds were more stable than 60% except the *R*-pyrrolidine amide **40,** which was less stable after 2 hours of incubation. In MLM, the lower stability was observed for **29, 30, 37, 38,** and **40,** while other compounds were more stable than 60% after 2 hours of incubation and **methyl amide in the 2'N-*R*-CH_3 50 was much more stable with 93 % remaining after 2 hours.**

In both HLM and MLM after two hours, the oxadiazole analogs were stable above 80%, and a higher stability of 95 % was observed in case of MLM for ligand **51**. The oxadiazoles **52** and **53** were more stable in MLM with more than 90 % remaining after 2 hours of incubation. In terms of stability trends, oxadiazoles, as expected, are much more stable than amides and the stability tends to decrease with increasing alkyl chains for amides and oxadiazoles in both enantiomeric series in HLM as well as MLM. The more lipophilic compounds are attacked much more readily by CYP enzymes, as expected. The ligands are more lipophilic but also contain more CH_2 or benzylic CH_2 groups to be attacked by CYP enzymes. Moreover, the higher metabolic stability (> 90 % remaining) and longer half-life were observed in more polar 2'N series than the analogs in the 2'F series. The compounds that exhibited moderate to high metabolic stability appeared to be the less lipophilic compounds and were considered for the next stages of the investigation.

2.2.3.4.1.2. Proposed Possible Metabolites

It is critical to understand the possible pathways of the metabolism of these IMDZs for a suitable duration of action depending on this necessary requirement. The study of the metabolism of BZD and BZD-related compounds is well known, and it is desirable to understand it at a deeper, perhaps, molecular level as possible. With accumulating evidence, along with the possible metabolism of the tricyclic BZD such metabolism of IMDZ includes cytochrome P450 oxidation and then further glucuronidation for excretion.[131] Using the dimethyl amide GL-II-73 (**36**) as an example, the metabolism of amide analogs of IMDZ might undergo the following possible pathways, as illustrated in Figure 20.

The ligand may undergo an aromatic hydroxylation by P450, and a hydroxyl group can be introduced in ring A or ring C at the two positions as indicated in **I** and **II**.[132] The *N*-oxidation might occur at the imine nitrogen atom to form the metabolite **III**.[133] The C-4 hydroxylation was reported to lead to an active metabolite by CYP3A4 and CYP2A19, and this was followed with OH-glucuronidation.[134] However, because there is a chiral methyl group at the C(4) position, it is not clear whether the traditional hydroxylation would still occur at that position (**IV**) or it would be at the C(4)methyl group (**V**). The chirality would also affect the metabolic process at this position. The *N*-dealkylation processes of the C(3) amide would result in a carbinol-amide as an intermediate (**VI**) catalyzed by P450, followed by facile elimination of an aldehyde moiety to yield a secondary amide (**VII**), which would substantially undergo the same process to form another carbinol-amide intermediate (**VIII**), and then further provide a primary amide (**IX**).[135] The ethinyl group can be metabolized by P450 enzymes with two mechanisms. One is to form an oxirene (**X**), which is very difficult but might be followed by heme- or apoprotein alkylation. An alternative mechanism would be to produce a reactive ketene intermediate (**XI**) by a 1,2-hydrogen shift of the

terminal hydrogen to the adjacent carbon of the triple bond by P450 oxidation. The ketene might then proceed to two fates: either undergo the heme alkylation by P450s and/or apoprotein (**XII**), or react with the surrounding water to yield a carboxylic acid metabolite (**XIII**), which can bind with proteins (**XIV**).[136] If the compound is administrated orally, at gastric acid pHs (pH = 1.5-3.5), imine hydrolysis may first occur to form the iminium ion (**XVI**) before it is distributed to the liver and it could also form salts with the nitrogen from the imidazole ring (**XV**). However, the unstable iminium ion would favor the reformation of the 7-membered ring at physiologic pH. Last but not least, since GL-II-73 is an amide, it can be hydrolyzed to its carboxylic acid metabolite by peptidases or hydrolysis (**XVII**).

Possible metabolites of GL-II-73 (**36**)

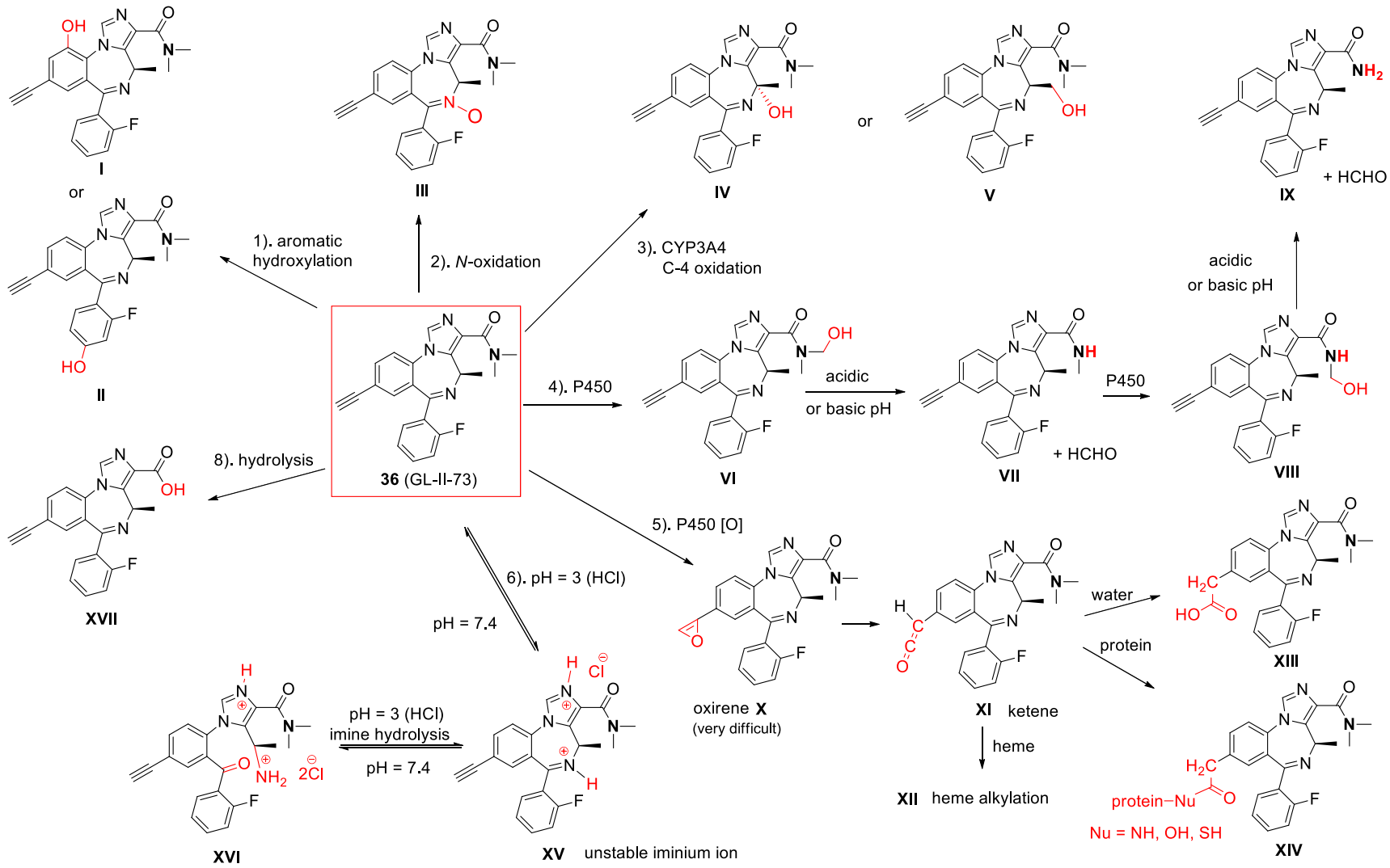

Figure 20. Proposed metabolites of key dimethyl amide 36 (GL-II-73).

2.2.3.4.1.3. P450 Inhibition

Cytochrome P450-drug interactions is one of the key factors that raises concerns during drug development. Therefore, it is important to study if there is any possible P450 inhibitions or toxicity induced from the drug candidate. The P450 inhibition study for one of the key compounds GL-II-73 (**36**) was carried out via a commercially available kit (Vivid® P450 Metabolism assays). The Vivid® substrates are blocked dyes that can be metabolized by P450 oxidation, which results in high fluorescence. If a test compound is a P450 inhibitor, the production of the fluorescent metabolite of the blocked dyes would be prevented. The test compound is added to a mixture of NADPH and P450, followed by the addition of the substrate. The red fluorescence signal indicates the degree of P450 inhibition. The results of the CYP3A4 inhibition of GL-II-73 is presented in Figure 21. At both 10 and 50 μM high concentrations, dimethyl amide **36** only exhibited very little inhibition, and its fluorescence signal was nearly the same as the vehicle, which confirmed that this ligand **36** did not inhibit in CYP3A4 enzymes to any appreciable degree. Since CYP3A4 is the most abundant and relevant CYP450 for interactions, this result is very important. However, other CYP450 enzymes such as CYP2C9 and CYP2D6 will also need to be assayed with GL-II-73 (**36**) in the future due to their major role of oxidation and detoxification in the liver.

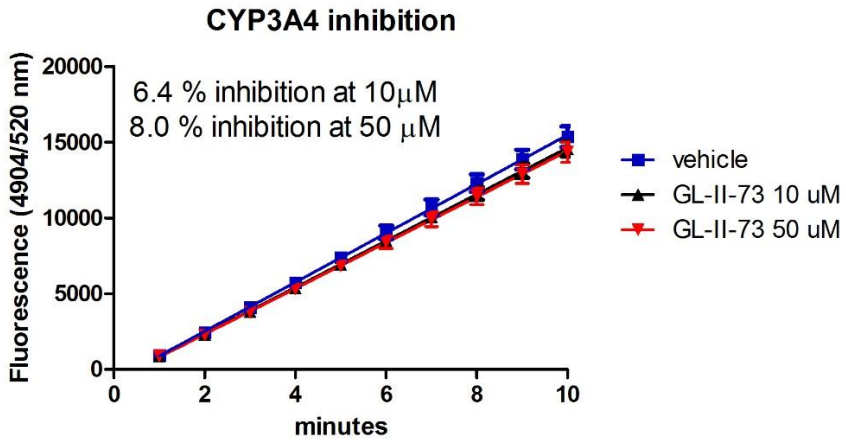

Figure 21. The CYP3A4 inhibition of GL-II-73 (36). Not much effect even at 50 μM. This is an important result. Unpublished data.

2.2.3.4.2. Cytotoxicity Study

The cytotoxicity assay was performed in both human embryonic kidney cells (HEK293T) and human liver cancer cell lines (HEPG2) to investigate the toxicity of all analogs at the cellular level for the selection of safe lead compounds. The results are shown in Table 11.

Table 11. Cytotoxicity data of all synthesized analogs from both *R* and *S* enantiomeric series, as well as achiral analogs with different modifications at four proposed positions: C(3), C(4), C(8), and 2'-phenyl position. Unpublished data.

Genus: C(3)	#	Code	2' X	C(3)-substituents	C(4)	C(8)	HEK293 LD_{50}	HEPG2 LD_{50}
Thio-amide	**42**	GL-III-84	F	Methyl	R	Acetylene		>400
	43	GL-III-85	F	Dimethyl	R	Acetylene		>400
	44	GL-III-86	F	Ethyl	R	Acetylene		>400
	45	GL-III-87	F	Cyclopropyl	R	Acetylene		>400
Amide	**35**	MP-III-022	F	Methyl	R	Acetylene	>200	>200
	25	MP-III-023	F	Methyl	S	Acetylene	>200	>200

	36	GL-II-73	F	Dimethyl	R	Acetylene	>200	>400
	37	GL-II-74	F	Ethyl	R	Acetylene	>50	>200
	38	GL-II-75	F	Cyclopropyl	R	Acetylene	>50	>200
	39	GL-III-66	F	Isopropyl	R	Acetylene		>240
	40	GL-II-76	F	Pyrrolidine	R	Acetylene	>100	>400
	30	GL-I-54	F	Dimethyl	S	Acetylene	>400	>400
	26	GL-I-43	F	Ethyl	S	Acetylene	>100	>60
	27	GL-I-55	F	Cyclopropyl	S	Acetylene	>60	>90
	28	GL-I-57	F	Isopropyl	S	Acetylene	>80	>50
	29	**GL-I-41**	**F**	**t-Butyl**	**S**	**Acetylene**	**>30**	**>40**
	49	RV-II-04	F	Methyl	A*	Br	>200	>200
	45	GL-III-69	F	Dimethyl	R	Br		>400
	46	GL-III-67	F	Ethyl	R	Br		>240
	47	GL-III-70	F	Dimethyl	R	Cyclopropyl		>400
	48	GL-III-68	F	Ethyl	R	Cyclopropyl		>400
	50	GL-II-31	N	methyl	R	Acetylene	>400	>400
Ester	**73**	GL-II-05	N	Ethyl ester	R	Br		>400
	74	GL-II-18	N	Ethyl ester	R	TMS-Acetylene		>400
	75	GL-II-19	N	Ethyl ester	R	Acetylene		>400
Oxadia-zole	**51**	GL-II-33	N	Methyl	R	Acetylene	>400	>400
	53	GL-II-54	N	Methyl	R	Br	>400	>400

	54	GL-III-64	N	Methyl	R	Cyclopropyl		>400
	55	MP-IV-004	F	Methyl	R	Acetylene		
	56	MP-IV-005	F	Ethyl	R	Acetylene		>400
	57	**MP-IV-010**	**F**	**Isopropyl**	**R**	**Acetylene**		**>30**
	52	GL-III-23	F	Methyl	A*	Acetylene	>100	>100
	31	GL-I-65	F	Methyl	S	Acetylene	>50	>100
	32	**GL-I-66**	**F**	**Ethyl**	**S**	**Acetylene**	**>40**	**>30**
	33	**GL-I-81**	**F**	**Isopropyl**	**S**	**Acetylene**	**>30**	**>20**
	58	GL-III-60	F	Methyl	R	Br		>400
	59	GL-III-98	F	Ethyl	R	Br		>120
	60	GL-IV-01	F	Isopropyl	R	Br		>400
	61	GL-III-63	F	Methyl	R	Cyclopropyl		>100
	62	**GL-IV-03**	**F**	**Ethyl**	**R**	**Cyclopropyl**		**>30**
	63	GL-IV-04	F	Isopropyl	R	Cyclopropyl		>400
Oxazole	**78**	GL-III-35	F	aldehyde	R	Br		>400
	64	GL-III-36	F	No substituent	R	Br		>400
	80	GL-III-72	F	No substituent	R	TMS-Acetylene		>400
	66	GL-III-73	F	No substituent	R	Acetylene		>400
	81	GL-III-75	F	aldehyde	S	Br		>240
	65	GL-III-76	F	No substituent	S	Br		>400
	79	GL-III-76A	F	No substituent	S	Br		>50

	82	GL-III-77	F	No substituent	S	TMS-Acetylene		>400
	67	GL-III-78	F	No substituent	S	Acetylene		>240

- **Ligands was incubated with HEK293T cells and HEPG2 cells, respectively, for 48 hours followed by detection of cell viability using a Cell-Titer Glo (Promega). The results were normalized using DMSO as a negative control and 3-dibutylamino-1-(4-hexyl-phenyl)-propan-1-one (150 mM in DMSO final concentration, as a positive control). Data was determined by three independent experiments carried out in quadruplet.**
- **The LD_{50} values in HEK293 and HEPG2 cell lines of each compound was presented in the last two columns, respectively.**
- **The first column indicates the genus of each compound.**
- **The columns from left to right indicates the difference at the 2 prime, C(3), C(4), and C(8), respectively.**
- **Most of the compounds are non-toxic, only the compounds with LD_{50} values less than 50 µM were depicted in red.**
- **The ligands that are depicted in red and cytotoxic at less than 50 µM raise some concerns.**

The LD_{50} values in HEPG2 cell lines for most of the compounds were greater than 200 µM in all series indicating these compounds are safe and not cytotoxic. Some of the compounds that exhibited an LD_{50} value higher than 100 µM are safe to use, but the concentration in the clinic should not be above 100 µM to avoid any possible cytotoxicity. In-depth, toxicity assays must be run for ADME as well. The compounds that have an LD_{50} value between 30 to 50 µM might show moderate cytotoxicity, such as compounds **28, 29, 32**, and **79**. However, since the pharmacological range of potentiation at $GABA_AR$ is at nanomolar concentrations, this indicates even 30 µM is far greater than the concentration that could induce cytotoxicity. On the other hand, if the compound has an LD_{50} value below 30 µM, as ligand **33**, it would not be carried on for further studies. The LD_{50} value of the same compound most of the time is lower in the kidney HEK293 cell lines than the liver HEPG2 cell lines, which is not difficult to understand since more metabolic enzymes are located in the liver rather than the kidney. However, the LD_{50} value in HEK293 cells should be considered more carefully than the value in HEPG2 in order to avoid possible cytotoxicity that

could cause kidney failure. Notably, most of the compounds with moderate cytotoxicity are from the *S*-series, which comprise the compounds mentioned above. The desired *R*-isomers are much safer to use than the natural *S* enantiomeric analogs. The more the branched the alkyl chain, the more cytotoxicity was observed again providing a more lipophilic ligand with more sites for radical oxidation as well, as compared to compounds with smaller alkyl chains.

Therefore, the summary of the cytotoxicity of the analogs in all the different series can be described by the following bullet points: 1. The thioamides improved the safety profile of the corresponding amides up to a non-toxic level. 2. The safety trend among different types of analogs is as follow: thioamide > unsubstituted oxazole > oxadiazole > amide. Since esters are hydrolyzed rapidly in the liver, they were not included in the above comparison. 3. The analogs in the 2'N series provided a much better safety profile than the analogs in 2'F series. 4. The larger alkyl substituents should be given less consideration due to the observation of cytotoxicity from the larger size of the alkyl group. 5. The *R*-isomer analogs are much safer to use than the α2/α3/α5 *S*-isomers. However, the latter *S*-series exhibits better binding efficacy but with less α5 subtype selectivity. When designing new ligands, the possible cytotoxicity from the *S*-isomers should always be kept in mind. 6. The imine-migration byproduct, [N(5)-C(4) olefin] with no chirality significantly decreased the LD_{50} value of the corresponding oxazole, which indicated a structure with the wrong backbone with no chirality could introduce cytotoxicity and should not be taken to the next level of study in the series described here. 7. The different substituents at the C(8) position did not change the cytotoxicity profile. 8. The HEK293 kidney cell line usually provides a lower LD_{50} value than the liver HEPG2 cell line, thus the kidney LD_{50} value should be considered of higher priority when go/no-go decisions in drug design are made in the series described here.

2.2.3.4.3. Evaluation of the CNS Effects

This CNS screen delineates their influence on motor activity with an aim to preliminary evaluation of the appropriateness of these ligands for further research.

2.2.3.4.3.1. Rotarod Test *via* Oral Gavage

In order to compare the sensorimotor coordination of the amides in the *R*-series with the *S*-series, all amide analogs with different substituents at C(3), C(4), (8) and 2' phenyl positions were assessed on the rotarod test. The results are shown in Figures 22-25.

The comparison of the effects from the amides demonstrated that the *S*-amides at the C(4) exhibited more sedative effects than the corresponding *R*-CH_3 substitute amides. Most of the amides in the *S*-series including diazepam as the positive control (5 mg/kg), elicited the greatest impairment of sensorimotor steadiness at 10 minutes, followed by 30 and 60 minutes on the rotarod. Several of the compounds were not soluble in the vehicle (10 % DMSO, 50 % PBS, 40 % propylene glycol,) and could not be tested. Consequently, all compounds were subsequently administered via oral gavage at 40 mg/kg in a vehicle of 2 % polyethylene glycol and 2.5 % hydroxypropylmethylcellulose solution. The compounds that caused the most severe motor impairment were *S*-isomers **25, 26** and **30**. As previously described, the more the steric size of the groups on the amides, the less sensorimotor impairment in the *S*-series. None of the compounds in the *R*-series exhibited cytotoxicity nor sensorimotor impairment regardless of the alkyl branches on the amide, as illustrated in Figure 22. The thioamides did not induce any sedative effects on mice at all 5-time points, expect dimethyl thioamide **42,** whereas in two fell off the rotarod in the first 10 minutes. The C(8)-bromo-dimethyl amide **45** and the C(8)-cyclopropyl ethyl amide **48,** as well as the 2'N-*R* methyl amide **50** did not exhibit any sedation nor ataxia at all time points. The

C(8)-bromo-ethyl amide **46** and the C(8)-cyclopropyl dimethyl amide **47** exerted moderate sensorimotor deficits as compared to other compounds. Only one compound, the C(8)-bromo-methyl amide **49** in the achiral 2'F series showed severe motor impairment, and it was worse even than the positive control diazepam, as shown in Figure 23. These results indicated that the (*R*) chirality at the C(4) position was important to reduce sedation and ataxia. Moreover, as shown before, the combination of the achiral ligand with a C(8)-bromine atom might want to be avoided while designing new ligands.

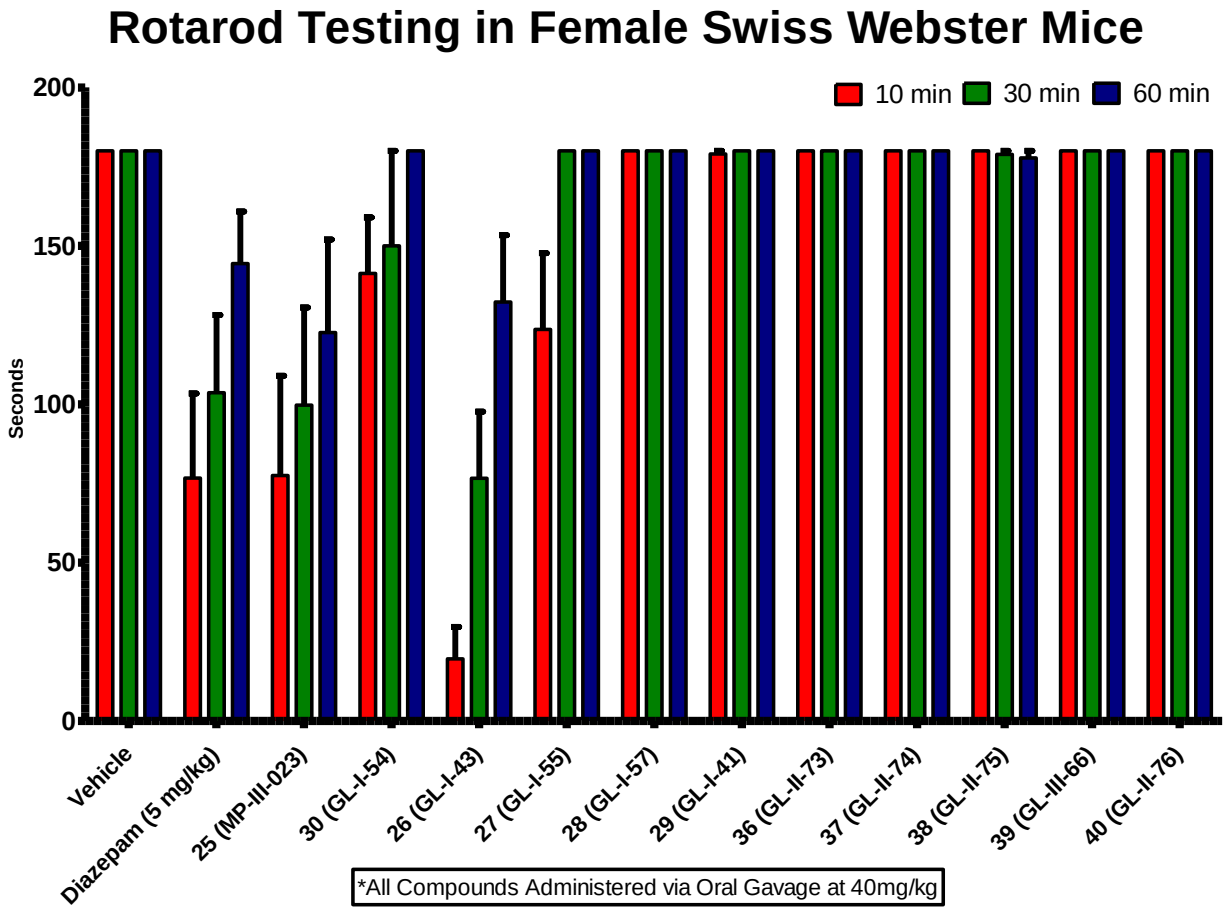

Figure 22. The effect of amides from the *R*-series (36-40) and the *S*-series (25-30) on the sensorimotor coordination on the rotarod *in vivo*. Swiss Webster mice received an oral gavage of the compound at 40 mg/kg or diazepam (5 mg/kg i.p.) and were placed on a rotarod at 15 rpm for 3 minutes, and the performance was recorded after 10, 30 and 60 minute time points after drug administration. A fail was assigned to a mouse if they have fallen twice within 3 minutes. The latency to fall is presented as mean ± SEM (n = 9). The vehicle was used as the negative control, and diazepam as the positive control. Unpublished data.

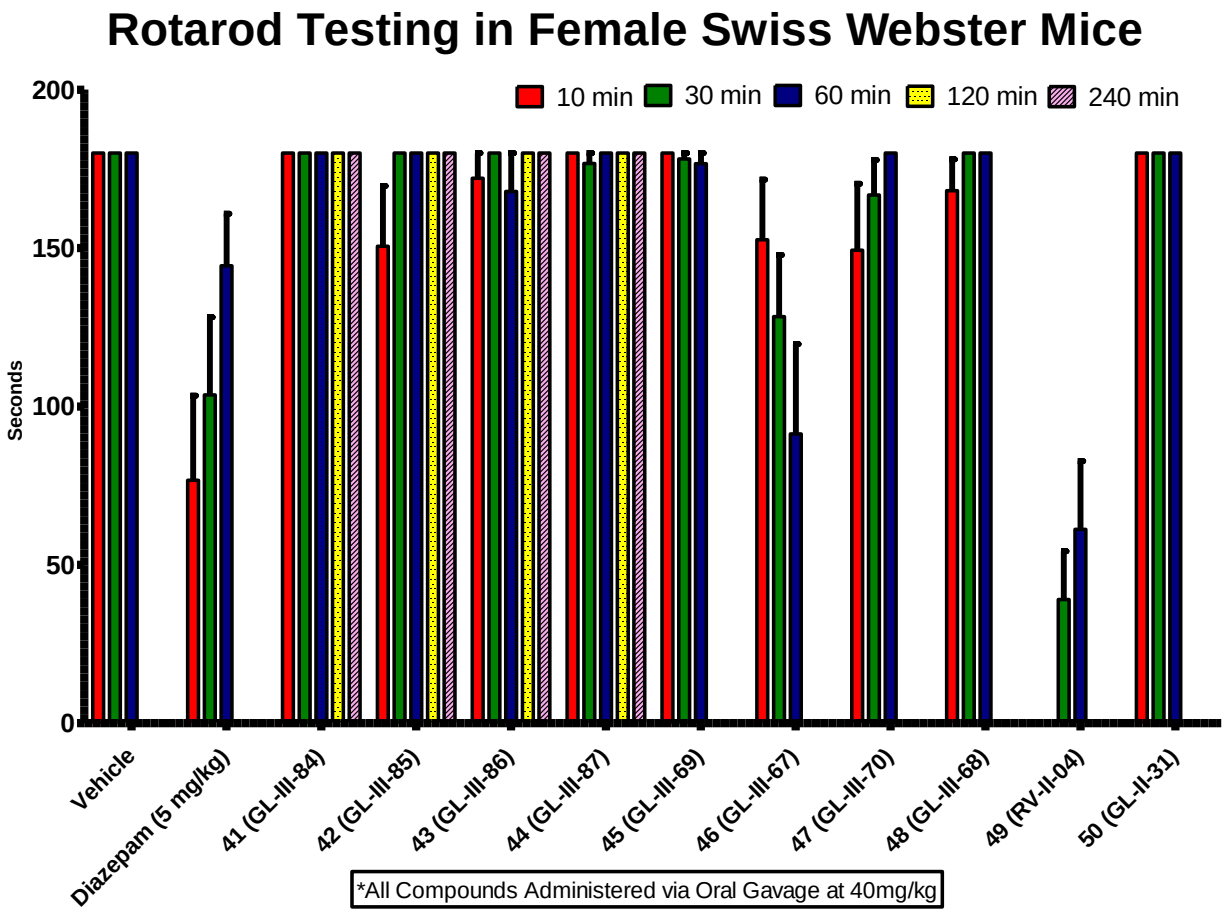

Figure 23. The effect of thioamides from the *R*-series (41-44), the amides with either a Br or a cyclopropyl group at the C(8) position (45-48), an achiral C(Br) methyl amide (49), as well as a methyl amide (50) in the 2'N series on the sensorimotor coordination assay on the rotarod assay *in vivo*. Swiss Webster mice received an oral gavage of the compound at 40 mg/kg or diazepam (5 mg/kg i.p.) and were placed on a rotarod at 15 rpm for 3 minutes, and the performance was recorded after 10, 30 and 60 minute time points (additional time points at 120 and 240 minutes for the thioamides) after drug administration. A fail was assigned to a mouse if they had fallen twice within 3 minutes. The latency to fall is presented as mean ± SEM (n = 7-8). The vehicle was used as the negative control, and diazepam as the positive control. Unpublished data.

The 1,2,4-oxadiazoles in all series did not exhibit any locomotor impairment regardless of any modification at different positions in the molecule at all time points, as shown in Figure 24. Whereas the other bioisostere, the 1,3-oxazoles exhibited slight sensorimotor steadiness than the oxadiazole analogs, except the *R*-C(8)-bromo oxazole **64** and *S*-C(8)-ethinyl oxazole **67**, as presented in Figure 25. In the *S*-series, all Br analogs are more sedating than the ethinyl oxazoles,

which might occur due to the electronegative character of the Br atom as opposed to an electron rich than ethinyl group, which probably lead to a stronger agonist interaction at alpha 1 subtypes. However, contradictory results were observed in the R-enantiomer series: the C(8)-ethinyl ligand is slightly more sedating than Br analog. One may need to repeat the rotarod experiment for further confirmation.

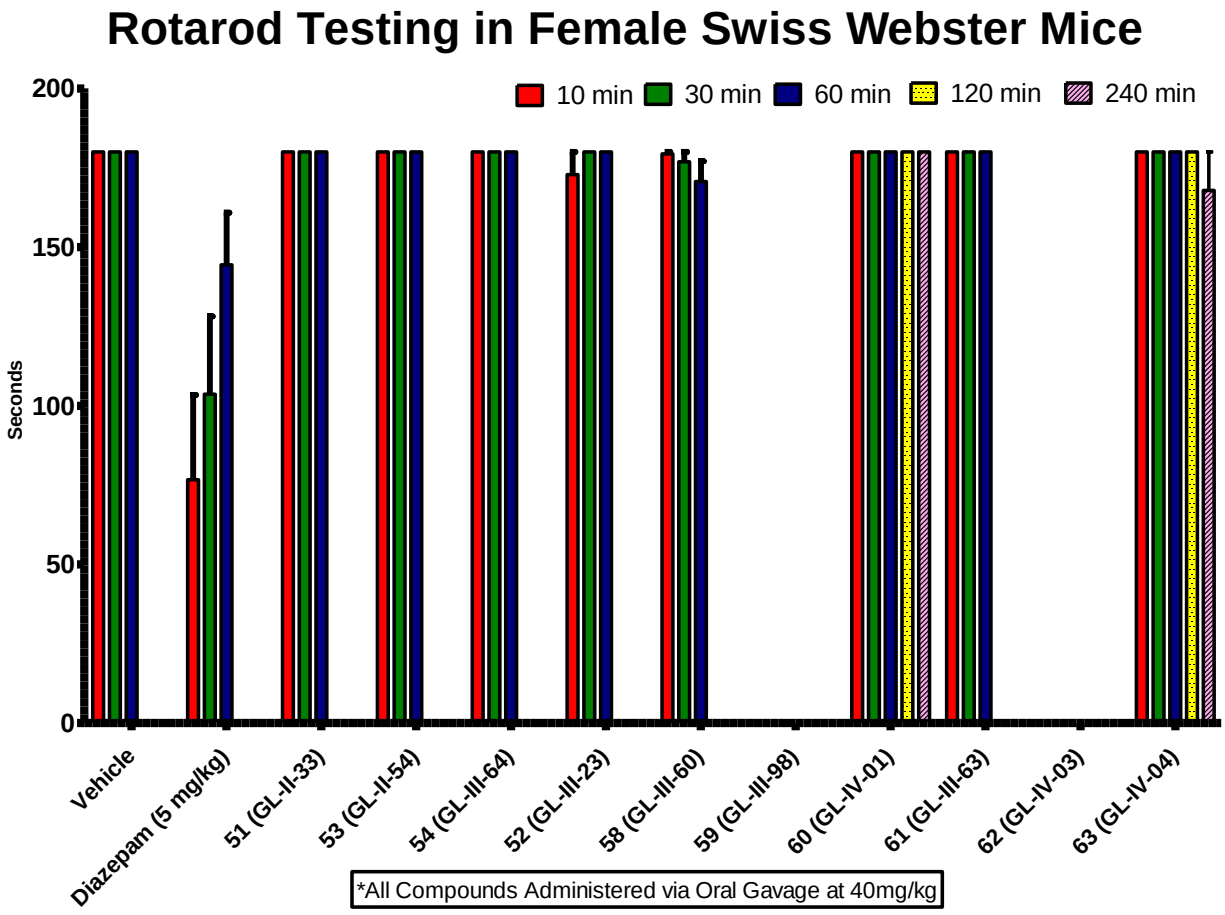

Figure 24. The effect of oxadiazoles on the sensorimotor coordination on the rotarod test *in vivo*. The Swiss Webster mice received an oral gavage of the compound at 40 mg/kg or diazepam (5 mg/kg i.p.) and were placed on a rotarod at 15 rpm for 3 minutes, and the performance was recorded after 10, 30 and 60 minute time points (additional time points at 120 and 240 minutes for later compounds) after drug administration. A fail was assigned to a mouse if they had fallen twice within 3 minutes. The latency to fall was presented as mean ± SEM (n =7-8). The vehicle was used as the negative control, and diazepam as the positive control. Unpublished data.

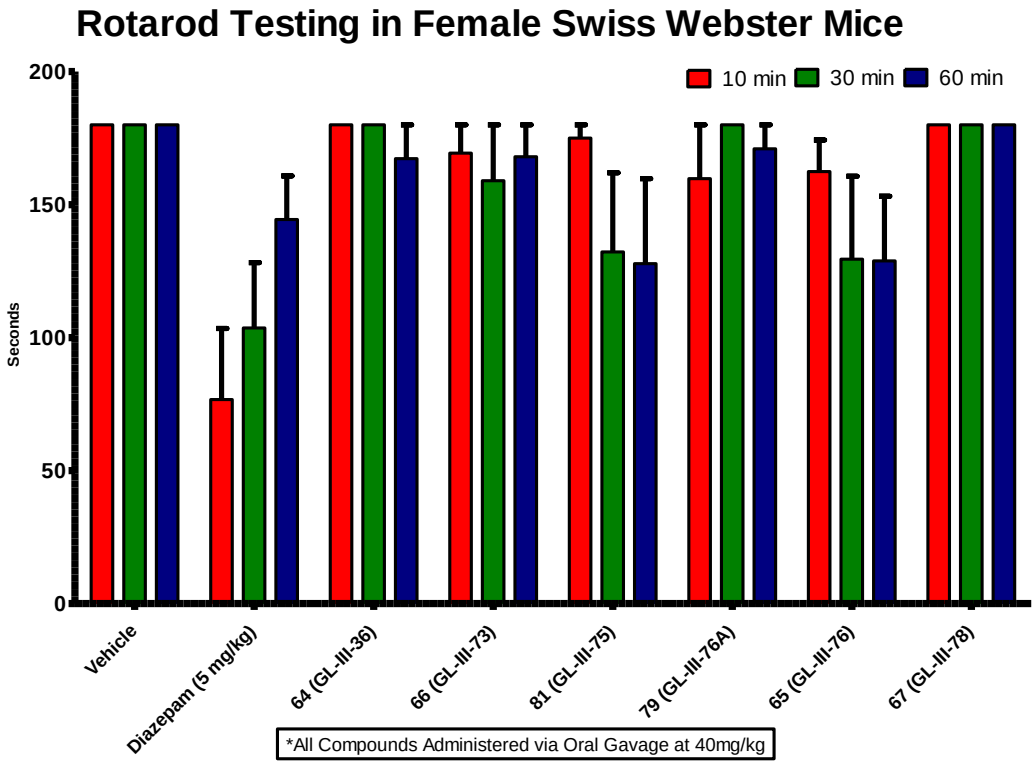

Figure 25. The effect of 1,3-oxazoles on the sensorimotor coordination on the rotarod test *in vivo*. The Swiss Webster mice received an oral gavage of the compound at 40 mg/kg or diazepam (5 mg/kg i.p.) and were placed on a rotarod at 15 rpm for 3 minutes, and the performance was recorded after 10, 30 and 60 minute time points after drug administration. A fail was assigned to a mouse if they had fallen twice within 3 minutes. The latency to fall is presented as mean ± SEM (n = 4-7). The vehicle was used as the negative control, and diazepam as the positive control. Unpublished data.

2.2.3.4.3.2. Rotarod Test *via* I.P. Administration

In addition to the oral administration, the rotarod test of these compounds was also tested via i.p. administration at 10 mg/kg in mice for 20 minutes. The results for the first batch of amide analogs GL-II-73, 74, and 75 (**36, 37,** and **38**) of the parent compound **1** and the methyl amide **35** are presented in Figure 26. It is clear that a different route of administration can exhibit totally different results. The dimethyl amide **36** did not exhibit any sedation nor ataxia on the rotarod performance; however, **37** and **38** exerted impairment of locomotor coordination, which was not seen in the rotarod test with oral gavage. Also examination of the results indicated that the larger alkyl substituents on the amide group, presumably, would increase the CNS effects by passing

through the BBB more rapidly than smaller chain amides due to the higher lipophilicity. Moreover, the i.p. injection allowed the ligands to bypass first-metabolism in the stomach and directly act on the brain much faster than the oral administration. However, **36** did not induce any sedative effect or ataxia or any locomotor impairment by both routes of administration, which is very important.

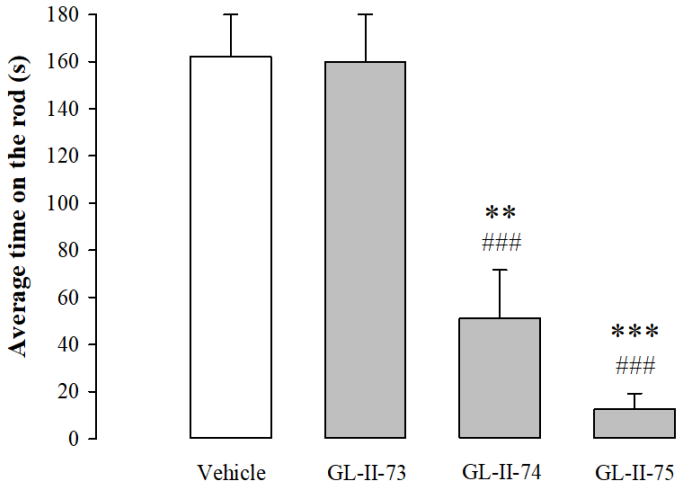

Figure 26. The effect of GL-II-73 (36), GL-II-74 (37) and GL-II-75 (38), all dosed i.p. at 10 mg/kg, on the average time on the rotarod 20 minutes after administration of the drug in mice. All data are presented as the mean ± S.E.M. Number of animals per treatment group (Vehicle, GL-II-73, GL-II-74, and GL-II-75) was 5, 7, 12 and 9, respectively. **p < 0.01 and ***p < 0.001 compared to Vehicle, ###p < 0.001 compared to GL-II-73 (36). Unpublished data.

In order to assess the dose-dependent influence of amides **35-38** on motor coordination, as well as the capability of flumazenil to prevent rotarod incapacitation induced by the lowest fully effective dose of those ligands, the rotarod assay was performed in adult male C57/BL6 mice (n=55). Examination of the data in Figure 27 illustrates the latencies to fall from the rotating rod recorded in mice injected i.p. with the tested ligands, on their own and in combination with flumazenil, the non-selective antagonist of the benzodiazepine binding site of $GABA_AR$s. It can be observed that all compounds exhibited a similar dose-dependance effect on the time that the animals were able to stay: with the increase of the dose the locomotor impairment was more significant. Importantly, the reliably incapacitating dose of all ligands, **35**, **37** and **38**, was 10 mg/kg,

and their impairing effect was prone to prevention by the administration of flumazenil. On the other hand, **36** displayed a much wider margin of safety, and the incapacitating effect of 90 mg/kg dose (i.p.) was also prevented by the co-administration of flumazenil. This indicated that impairing the effects of the novel ligands on motor performance are mediated by the BZD binding site of $GABA_AR$s.

a)

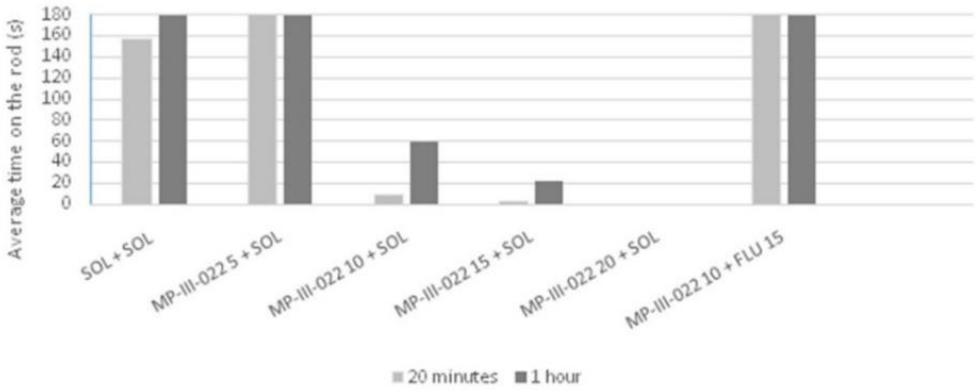
Average time on the rod (s)
180
160
140
120
100
80
60
40
20
0
SOL + SOL
MP-III-022 5 + SOL
MP-III-022 10 + SOL
MP-III-022 15 + SOL
MP-III-022 20 + SOL
MP-III-022 10 + FLU 15
20 minutes
1 hour

b)

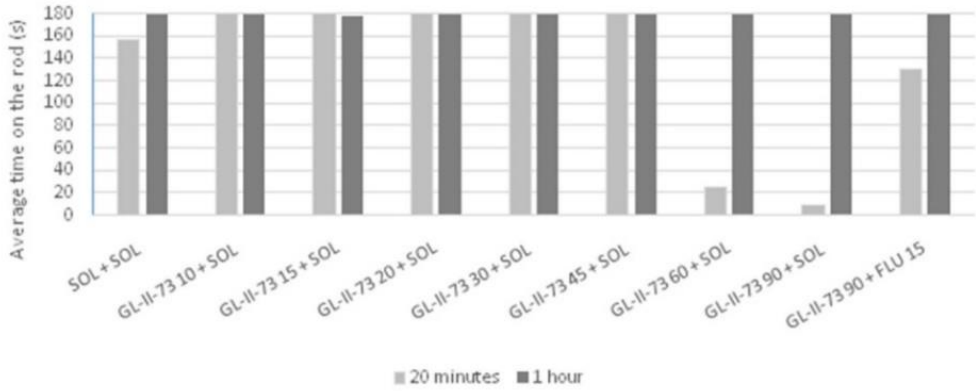
Average time on the rod (s)
180
160
140
120
100
80
60
40
20
0
SOL + SOL
GL-II-73 10 + SOL
GL-II-73 15 + SOL
GL-II-73 20 + SOL
GL-II-73 30 + SOL
GL-II-73 45 + SOL
GL-II-73 60 + SOL
GL-II-73 90 + SOL
GL-II-73 90 + FLU 15
20 minutes
1 hour

c)

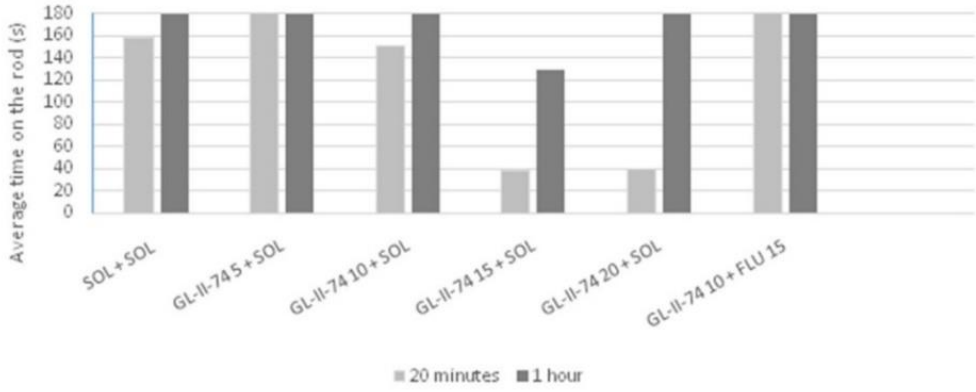
Average time on the rod (s)
180
160
140
120
100
80
60
40
20
0
SOL + SOL
GL-II-74 5 + SOL
GL-II-74 10 + SOL
GL-II-74 15 + SOL
GL-II-74 20 + SOL
GL-II-74 10 + FLU 15
20 minutes
1 hour

d)

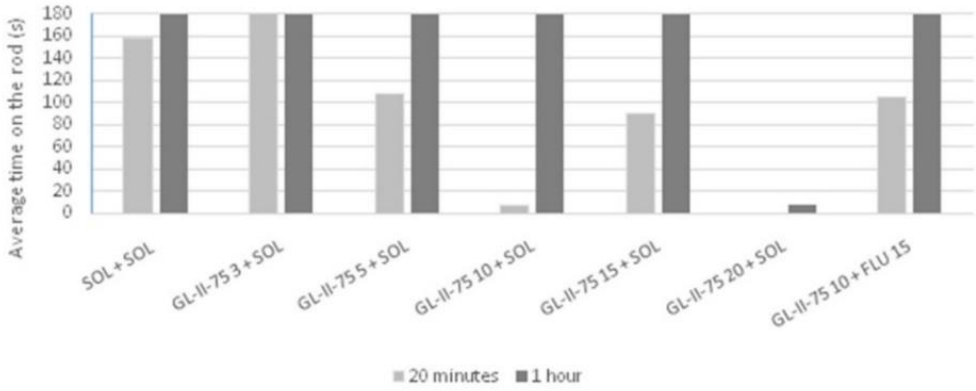
Average time on the rod (s)
180
160
140
120
100
80
60
40
20
0
SOL + SOL
GL-II-75 3 + SOL
GL-II-75 5 + SOL
GL-II-75 10 + SOL
GL-II-75 15 + SOL
GL-II-75 20 + SOL
GL-II-75 10 + FLU 15
20 minutes
1 hour

Figure 27. The effects of increasing doses of MP-III-022 (a), GL-II-73 (b), GL-II-74 (c) and GL-II-75 (d) on the rotarod performance assessed 20 minutes and 1 hour after i.p. administration in male C57/BL6 mice (n = 1–4 per treatment). The doses administered were 5, 10, 15 and 20 mg/kg for MP-III-022; 10, 15, 20, 30, 45, 60 and 90 mg/kg for GL-II-73; 5, 10, 15 and 20 mg/kg for GL-II-74 and 3, 5, 10, 15 and 20 mg/kg for GL-II-75. Additionally, the reliably incapacitating dose of each of the ligands was co-administered with flumazenil at a dose of 15 mg/kg and that influence on the rotarod performance was also observed.

The rotarod test with i.p. administration was performed for another batch of novel ligands GL-III-66 (**39**), GL-III-67 (**46**), GL-III-70 (**47**), GL-III-68 (**48**), GL -III-64 (**54**), GL-III-60 (**58**), and GL-III-63 (**61**), as presented in Figure 28 with the dose-response values. No consistent incapacitating doses of any of the ligands tested were observed, except of ligands **39** and **46**. When given at a dosage of 40 mg/kg and 20 mg/kg, respectively, these two ligands decreased the average time on the rotarod and incapacitated an animal. No sedation nor motor impairment was observed with other test compounds. As expected, the amides (**39, 46, 47** and **48**) produced slightly more motor incapacitation than the oxadiazole analogs (**54, 58,** and **61**).

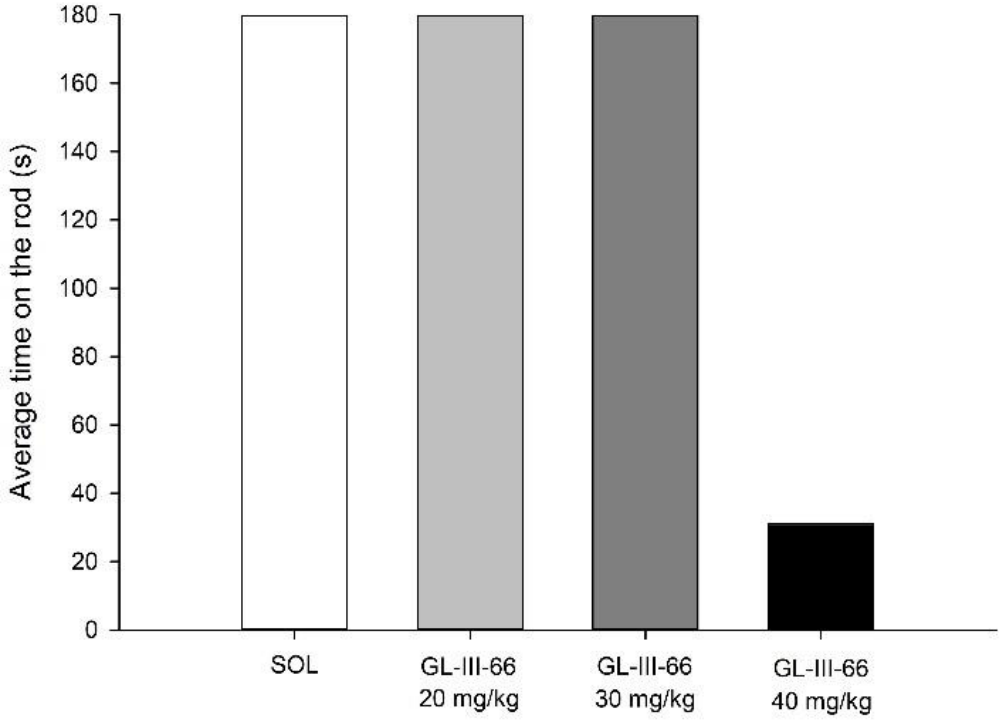

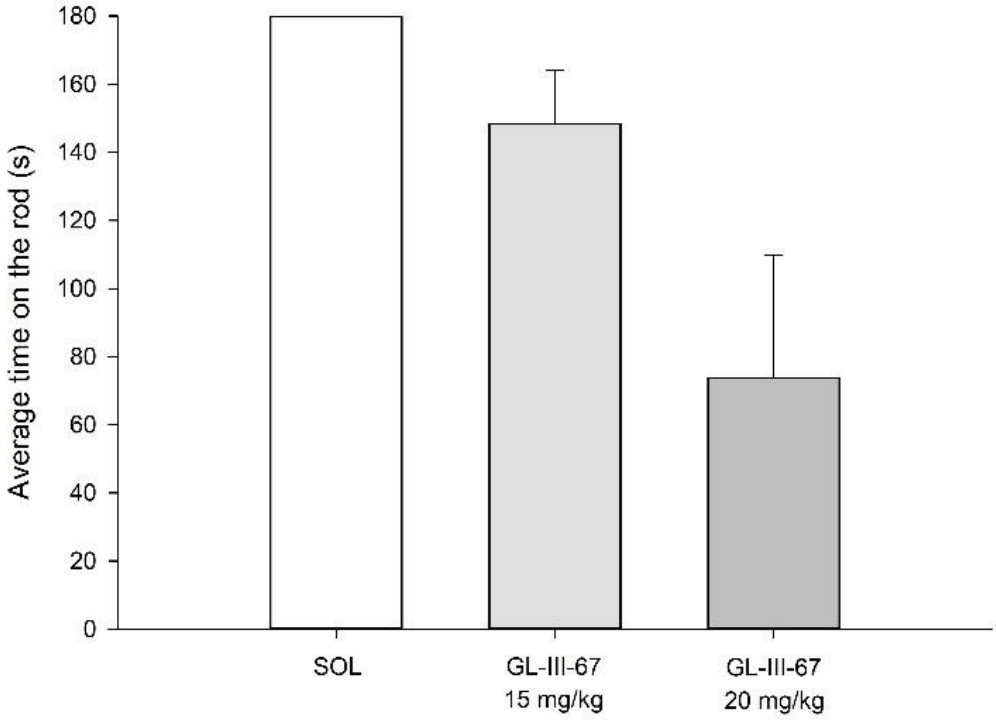
Average time on the rod (s)
180
160
140
120
100
80
60
40
20
0
SOL
GL-III-67
15 mg/kg
GL-III-67
20 mg/kg

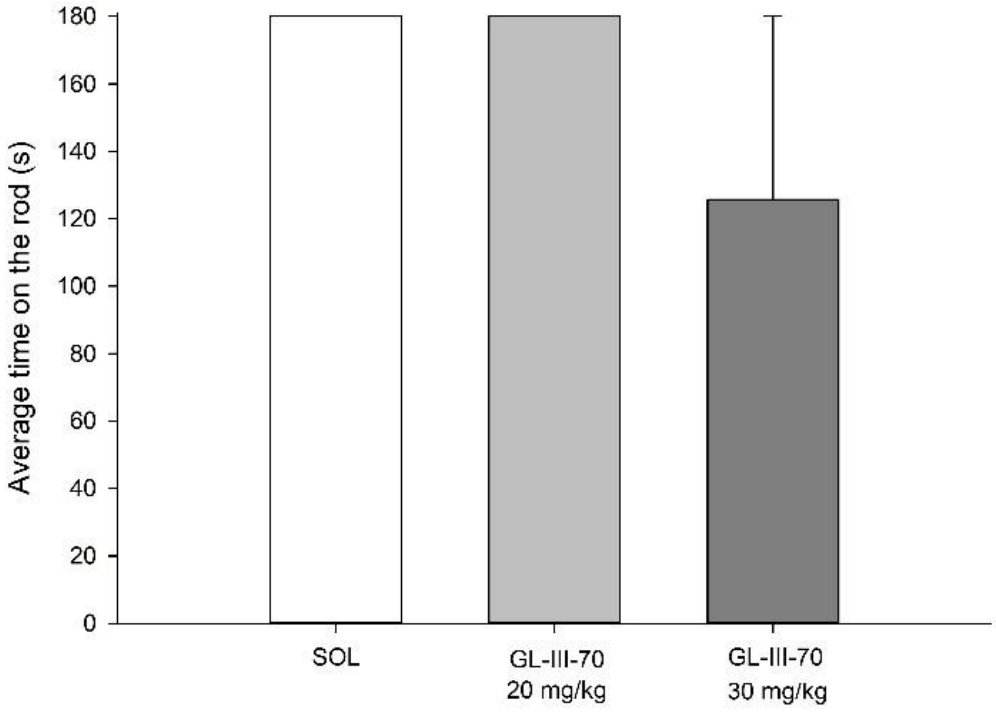
Average time on the rod (s)
180
160
140
120
100
80
60
40
20
0
SOL
GL-III-70
20 mg/kg
GL-III-70
30 mg/kg

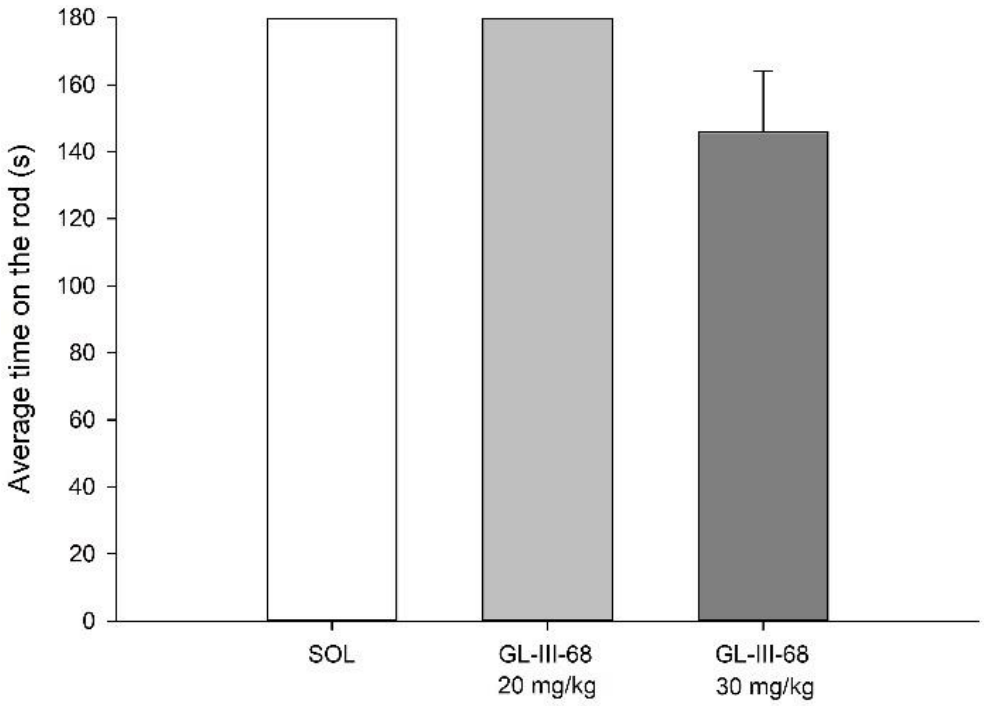
Average time on the rod (s)
180
160
140
120
100
80
60
40
20
0
SOL
GL-III-68
20 mg/kg
GL-III-68
30 mg/kg

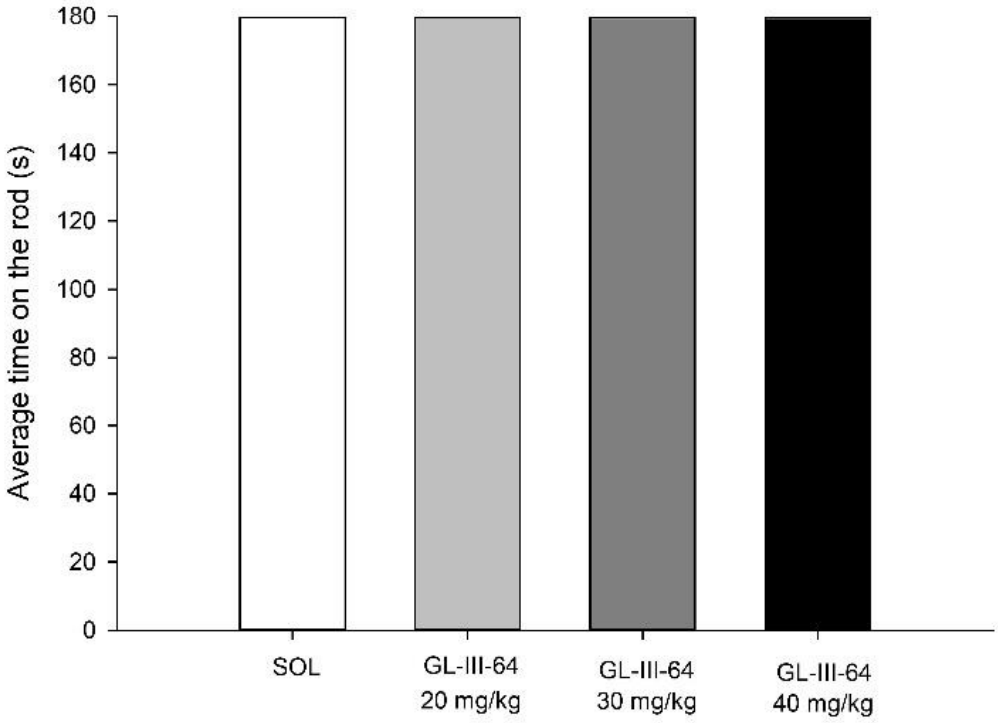
Average time on the rod (s)
180
160
140
120
100
80
60
40
20
0
SOL
GL-III-64
20 mg/kg
GL-III-64
30 mg/kg
GL-III-64
40 mg/kg

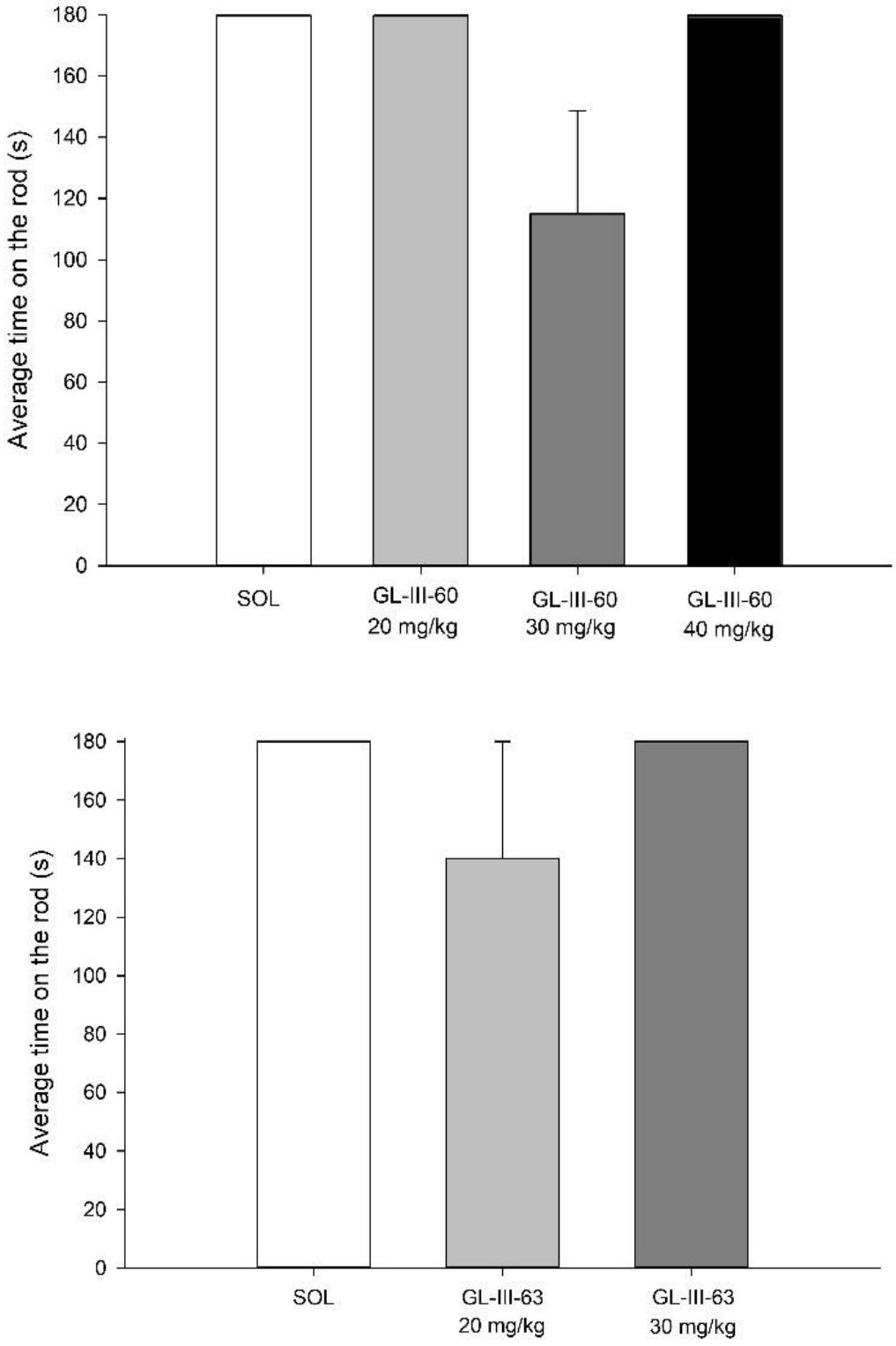

Figure 28. The observed effect of GL-III-66 (39), GL-III-67 (46), GL-III-70 (47), GL-III-68 (48), GL -III-64 (54), GL-III-60 (58), and GL-III-63 (61) dosed i.p. at 20, 30 and 40 mg/kg on average time on the rotarod 20 minutes after administration of ligand to the rats. All data are presented as the mean ± S.E.M. (n = 3). Unpublished data.

Immediately after the test on the rotarod, rats underwent the grip strength test with compounds GL-III-66 (**39**), GL-III-67 (**46**), GL-III-70 (**47**), GL-III-68 (**48**), GL -III-64 (**54**), GL-III-60 (**58**), and GL-III-63 (**61**). The muscle strength was assessed by the grip strength meter. When pulled by the tail, the rat grasps the trapeze connected to a force transducer, and the apparatus measures the peak force of experimenter's pull (in grams) necessary to overcome the strength of the animal's forelimb grip. Each animal was given three consecutive trials, and the median value of three readings was reported. Results of the grip strength test (normalized against the animals' body weight) are given in Figure 29. There are no consistent differences in the peak force of the experimenter's pull necessary to overcome the strength of the animals' grip after treatment, except after administration of **46**. Given in a dose of 20 mg/kg or higher, **46** might reduce the muscle strength and produce muscle relaxation, however, further test with a bigger sample is required.

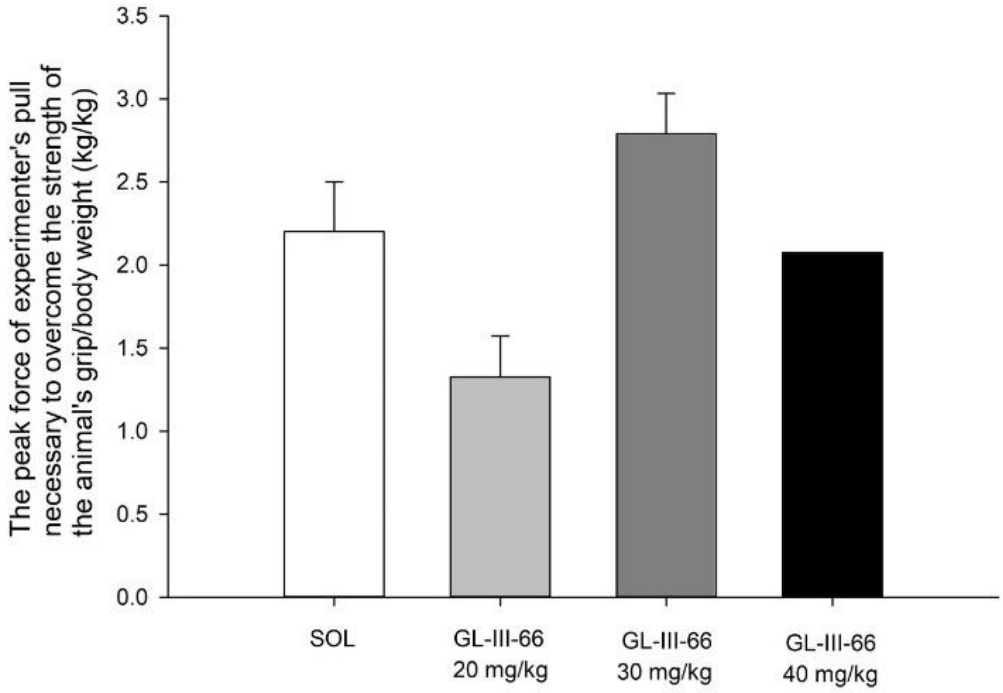

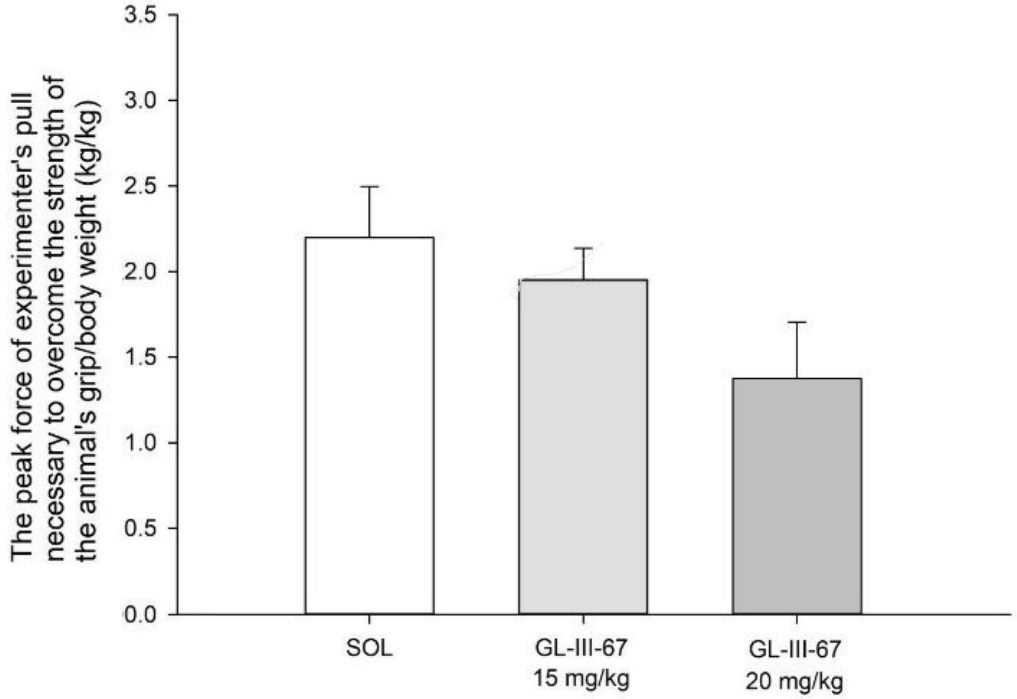
The peak force of experimenter's pull necessary to overcome the strength of the animal's grip/body weight (kg/kg)
3.5
3.0
2.5
2.0
1.5
1.0
0.5
0.0
SOL
GL-III-67 15 mg/kg
GL-III-67 20 mg/kg

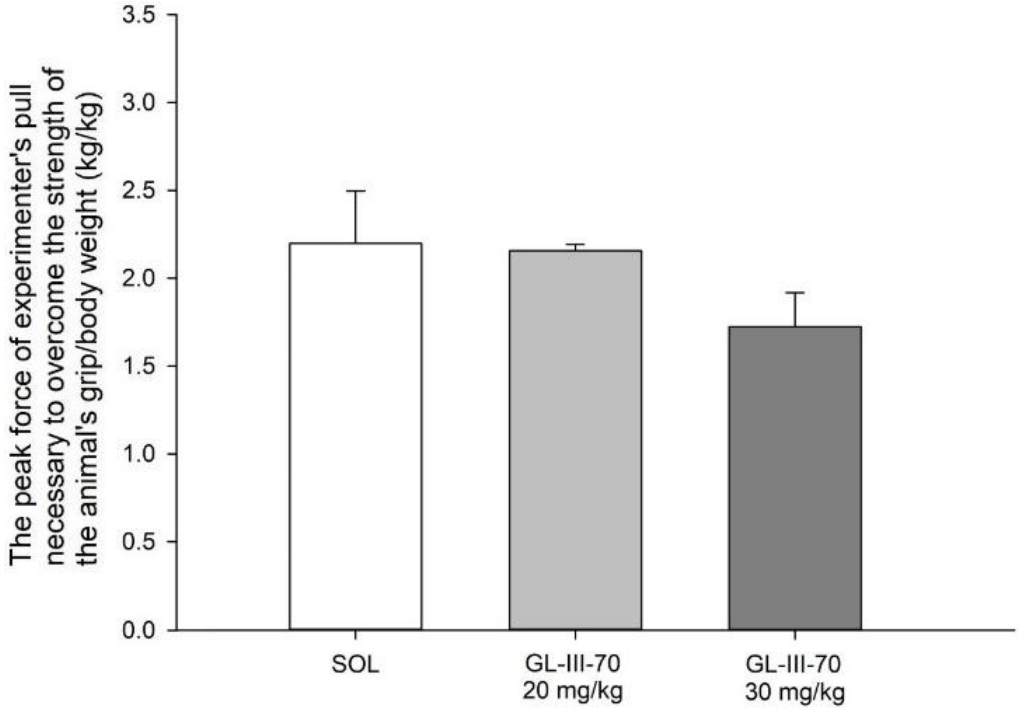
The peak force of experimenter's pull necessary to overcome the strength of the animal's grip/body weight (kg/kg)
3.5
3.0
2.5
2.0
1.5
1.0
0.5
0.0
SOL
GL-III-70 20 mg/kg
GL-III-70 30 mg/kg

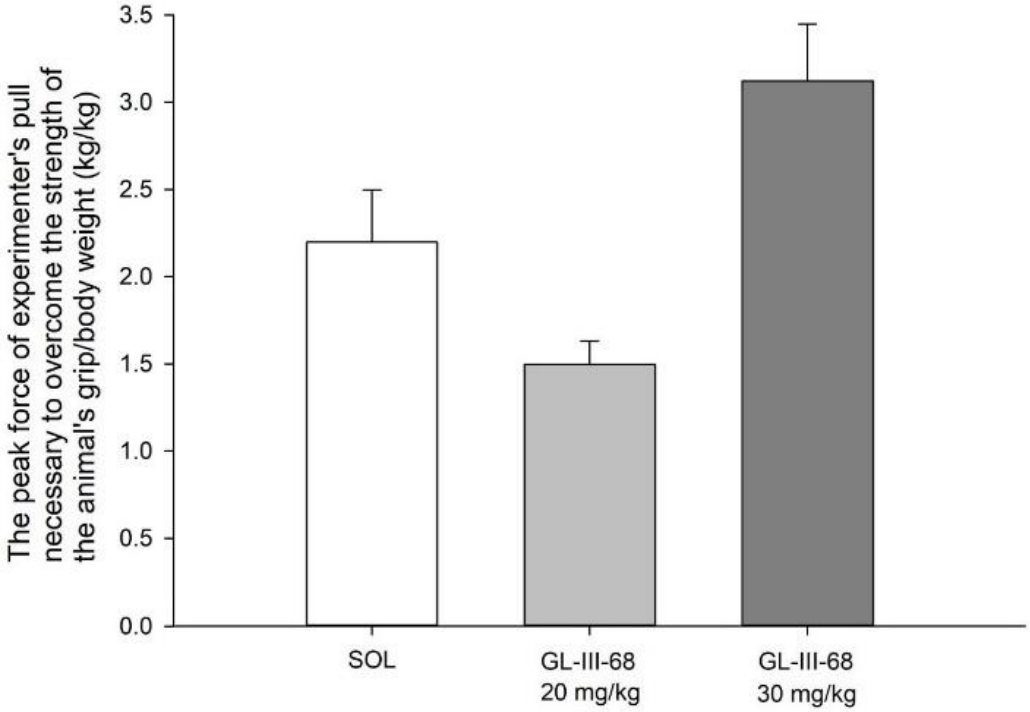
The peak force of experimenter's pull necessary to overcome the strength of the animal's grip/body weight (kg/kg)
3.5
3.0
2.5
2.0
1.5
1.0
0.5
0.0
SOL
GL-III-68 20 mg/kg
GL-III-68 30 mg/kg

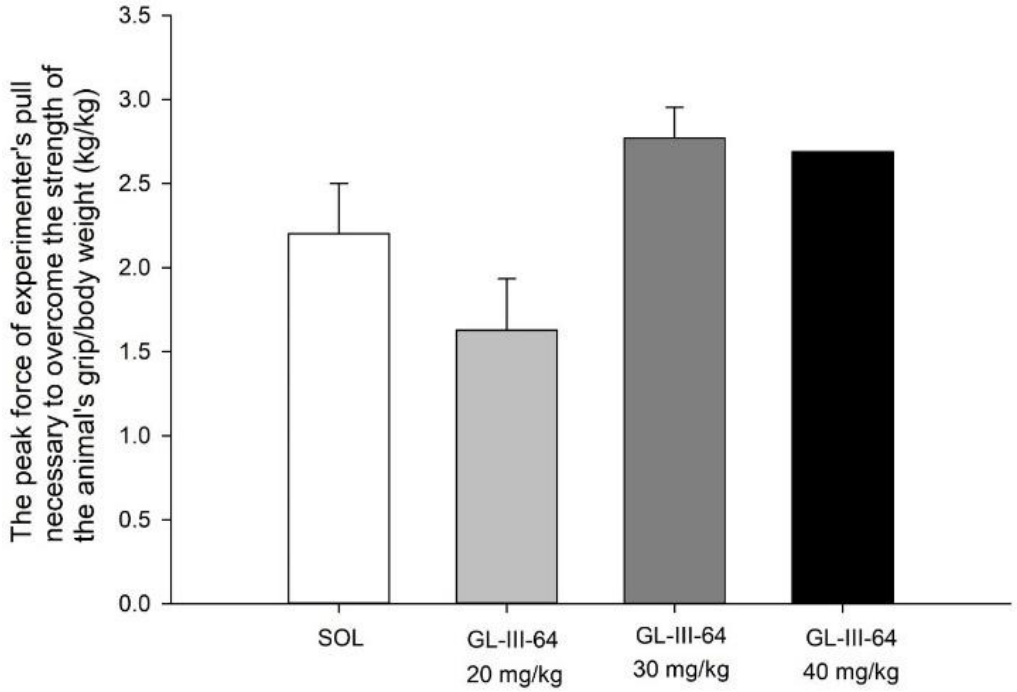
The peak force of experimenter's pull necessary to overcome the strength of the animal's grip/body weight (kg/kg)
3.5
3.0
2.5
2.0
1.5
1.0
0.5
0.0
SOL
GL-III-64 20 mg/kg
GL-III-64 30 mg/kg
GL-III-64 40 mg/kg

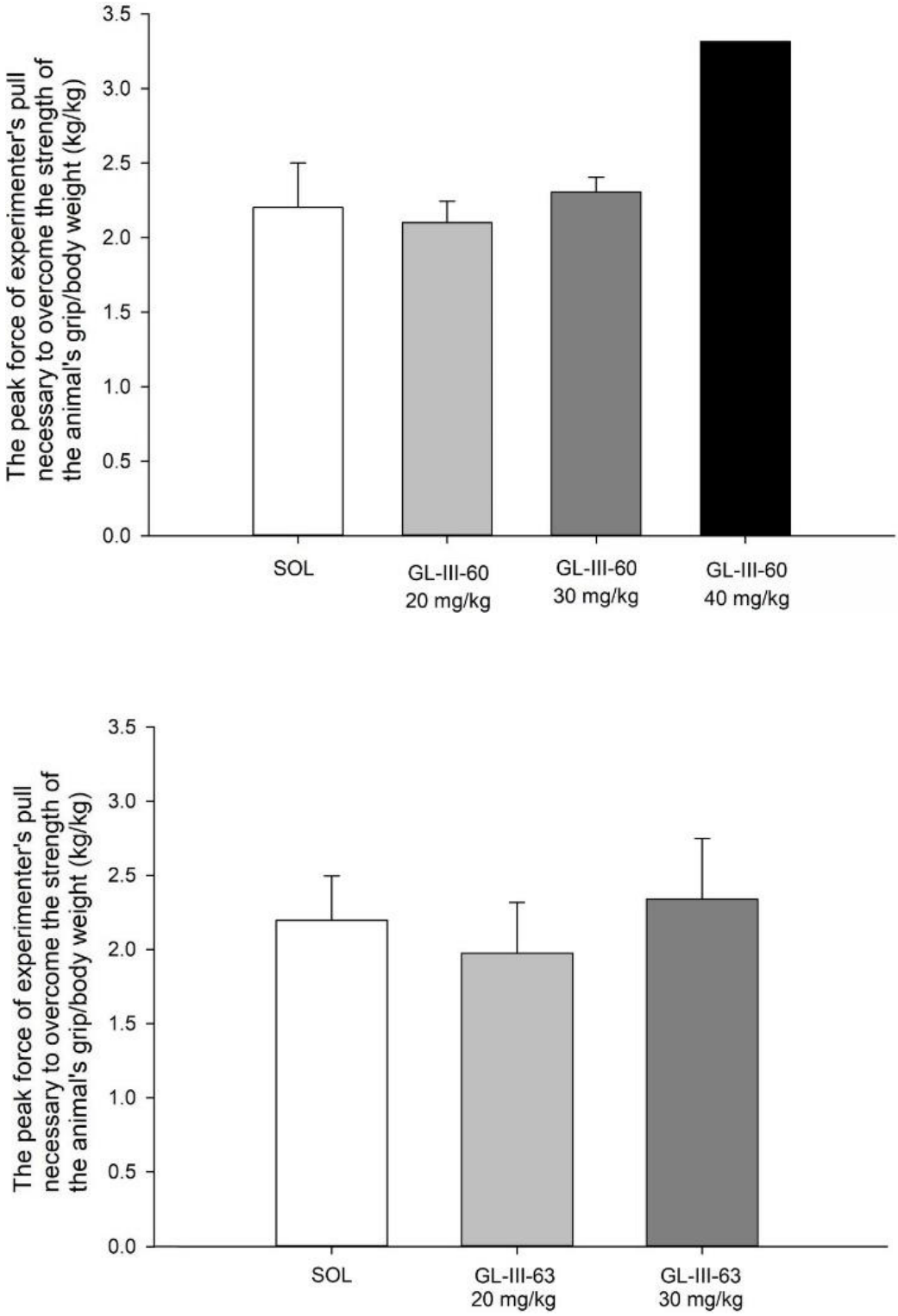

Figure 29. The observed effect of GL-III-66 (39), GL-III-67 (46), GL-III-70 (47), GL-III-68 (48), GL -III-64 (54), GL-III-60 (58), and GL-III-63 (61) dosed intraperitoneally at 20, 30 and 40 mg/kg on muscle strength right after the rotarod testing. All data are presented as the mean ± S.E.M. Number of animals per treatment group was 3, 2, 3, 1, respectively in the order of the treatments in the Figure. Unpublished data.

2.2.3.4.3.3. Spontaneous Locomotor Activity

The influence of **36-38** on spontaneous locomotor activity (SLA) was assessed in adult male C57/BL6 mice (n=27). The overall distances traveled during 60 minutes of recording are presented in Figure 30, while examination of Figure 31 shows distances traveled in 5-min bins. The locomotor effect of **36** was identical with the control, which indicates no locomotor impairment induced by this compound. However, an apparent hyperlocomotor effect of **37** versus SOL group was not significant despite a nominal P value of 0.021, because no significant difference was found between the two means that enclose that comparison; the only significant difference in post hoc analysis was that between the groups treated with **37** and **38**. The hyperlocomotor response was observed with the treatment of **37** in time intervals 0-5 minute and 50-55 minute. The compound **38** exhibited a similar stimulant-like effect in the first 5 minutes of the trials, while with a consistent hypolocomotion response was observed with **38** in the 15-40 minute period.

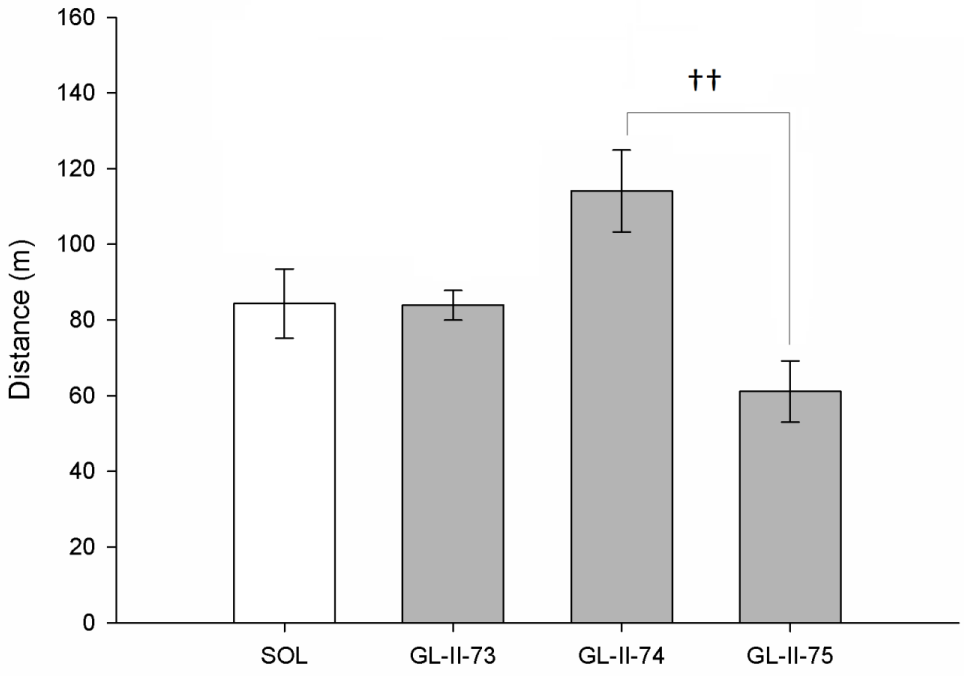

Figure 30. The effect of GL-II-73 (36), GL-II-74 (37) and GL-II-75 (38), all dosed i.p. at 10 mg/kg, on spontaneous locomotor activity during 60 minutes of recording in mice. All data are presented as the mean±S.E.M. Number of animals per treatment group was 7, with the exception of GL-II-73 (n=6). ++P<0.01 between GL-II-74 and GL-II-75 groups.

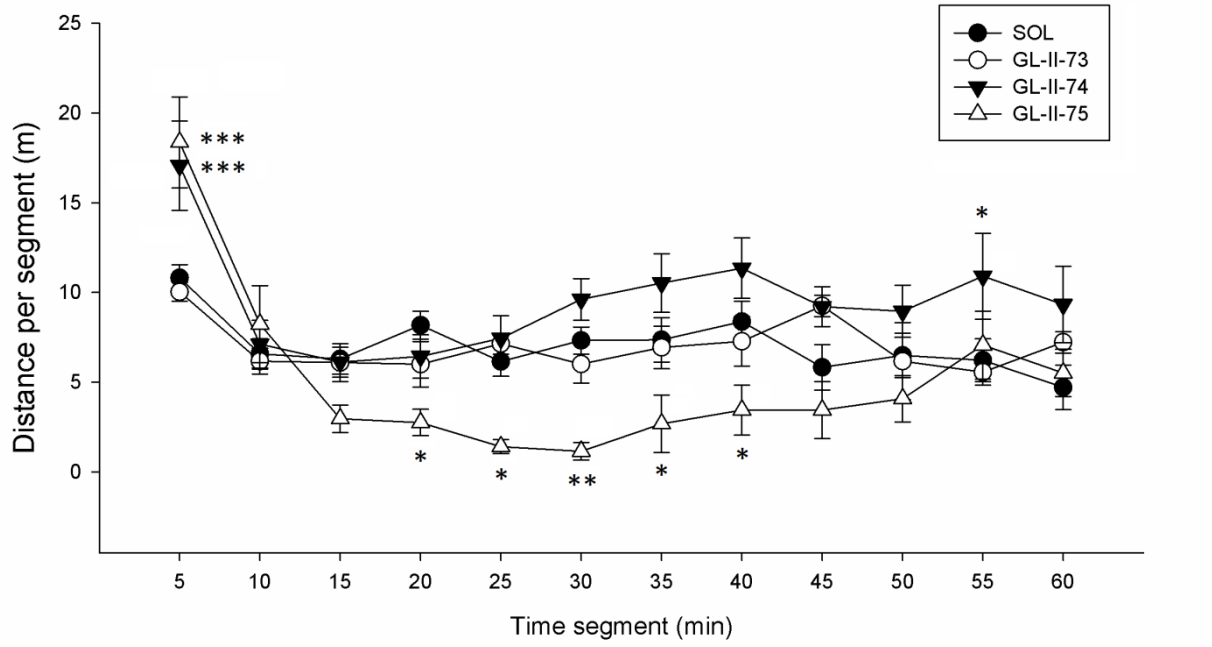

Figure 31. The effect of GL-II-73 (36), GL-II-74 (37) and GL-II-75 (38), all dosed i.p. at 10 mg/kg, on distance traveled in 5-min bins during recording on the locomotor activity test in mice. All data are presented as the mean±S.E.M. *P<0.05, **P<0.01 and ***P<0.001 versus SOL group.

The influence of RV-II-04 (**49**), GL-II-31 (**50**), MP-III-023 (**25**), GL-I-54 (**30**), GL-III-23 (**52**), GL-II-33 (**51**), GL-II-54 (**53**) and GL-I-65 (**31**), all dosed at 10 mg/kg (i.p.), on the SLA was assessed in adult male Wistar rats weighing 350-400 g (n=48). The overall distances traveled during 60 minutes of recording are presented in Figure 32, while examination of Figure 33 shows distances traveled in 5-min bins. According to the post hoc test, **25**, and especially **49** induced profound sedation during nearly the whole period of recording. In the vast majority of bins, the animals treated with **49** or **25** traveled lower distance than SOL. Other compounds did not induce a significant SLA impairment.

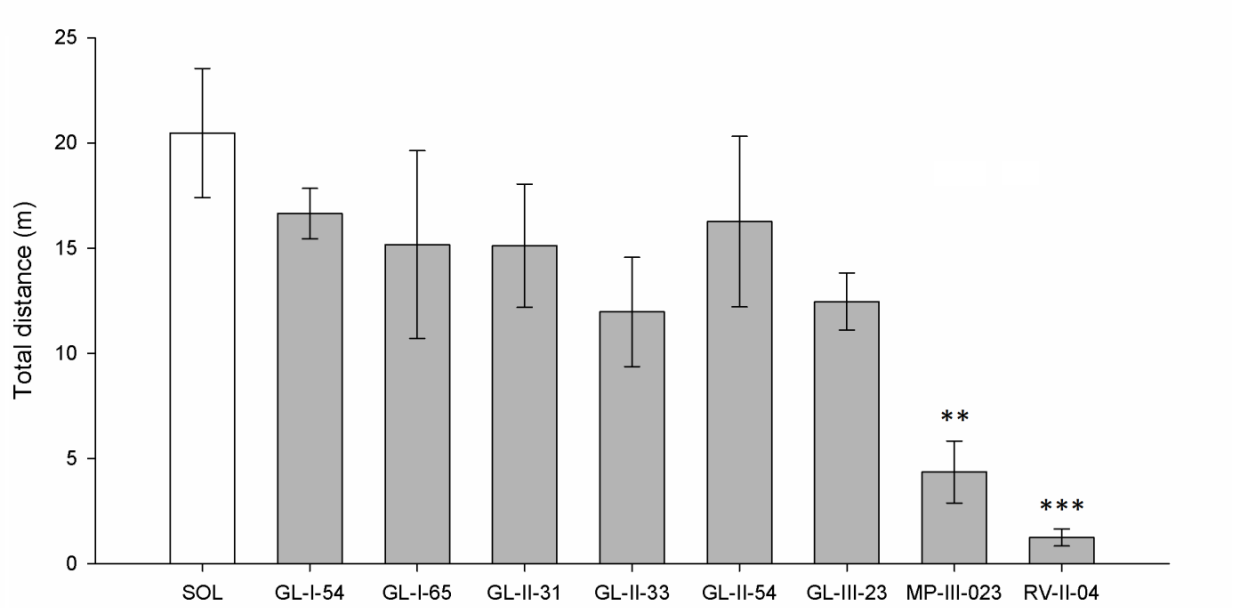

Figure 32. The effect of RV-II-04 (49), GL-II-31 (50), MP-III-023 (25), GL-I-54 (30), GL-III-23 (52), GL-II-33 (51), GL-II-54 (53) and GL-I-65 (31), all dosed i.p. at 10 mg/kg, on spontaneous locomotor activity during 60 min of recording in rats. All data are presented as the mean±S.E.M. Number of animals per treatment group was 5, with the exception of 51, 53 and 52, and SOL (n=6). **P<0.01 and ***P<0.001 versus SOL group. Other differences were not presented; in general, the animals treated with 49 were sedated when compared to all other groups, with the exception of 25. Unpublished data.

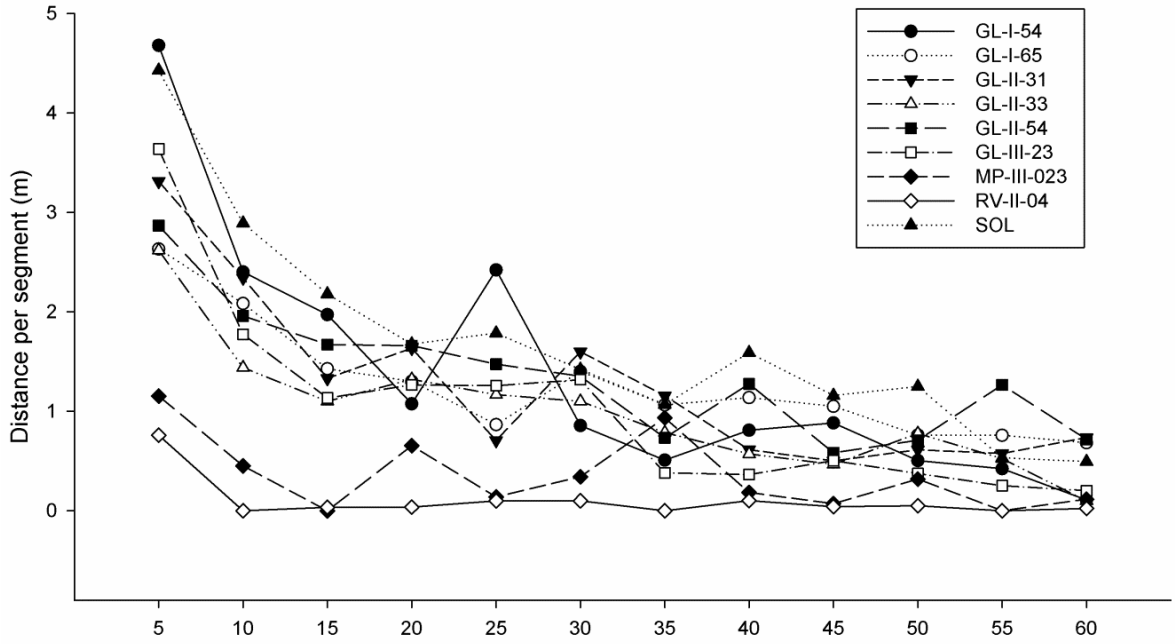

Figure 33. The effect of RV-II-04 (49), GL-II-31 (50), MP-III-023 (25), GL-I-54 (30), GL-III-23 (52), GL-II-33 (51), GL-II-54 (53) and GL-I-65 (31), all dosed i.p. at 10 mg/kg, on distance traveled in 5-min bins during

recording in the locomotor activity test in rats. All data are presented as the mean±S.E.M. Statistical significances were not presented. Unpublished data.

Another series of novel ligands as putative selective modulators of $GABA_ARs$, which effect the α5 subunit are GL-III-66 (**39**), GL-III-67 (**46**), GL-III-70 (**47**), GL-III-68 (**48**), GL -III-64 (**54**), GL-III-60 (**58**), and GL-III-63 (**61**). These ligands were assessed in the SLA by Savic et al. The total distance traveled during 60 minutes of recording are presented in Figure 34A, while Figure 34B shows the % of time in the central zone over the same time period. Although there was no statistical significances in these assays, certain differences between groups can be observed (most prominent difference occurred between the control and the ligand **39**). It was observed a decrease in both total distance traveled and % of time in the central zone after administration of 15 mg/kg of **39**. It implies that this ligand, given in doses higher than 15 mg/kg, might have the potential to produce sedative and/or anxiogenic effects. The observed difference between the control values of total distance traveled in animal groups receiving 10 and 15 mg/kg can be ascribed to the differences in animal weight.

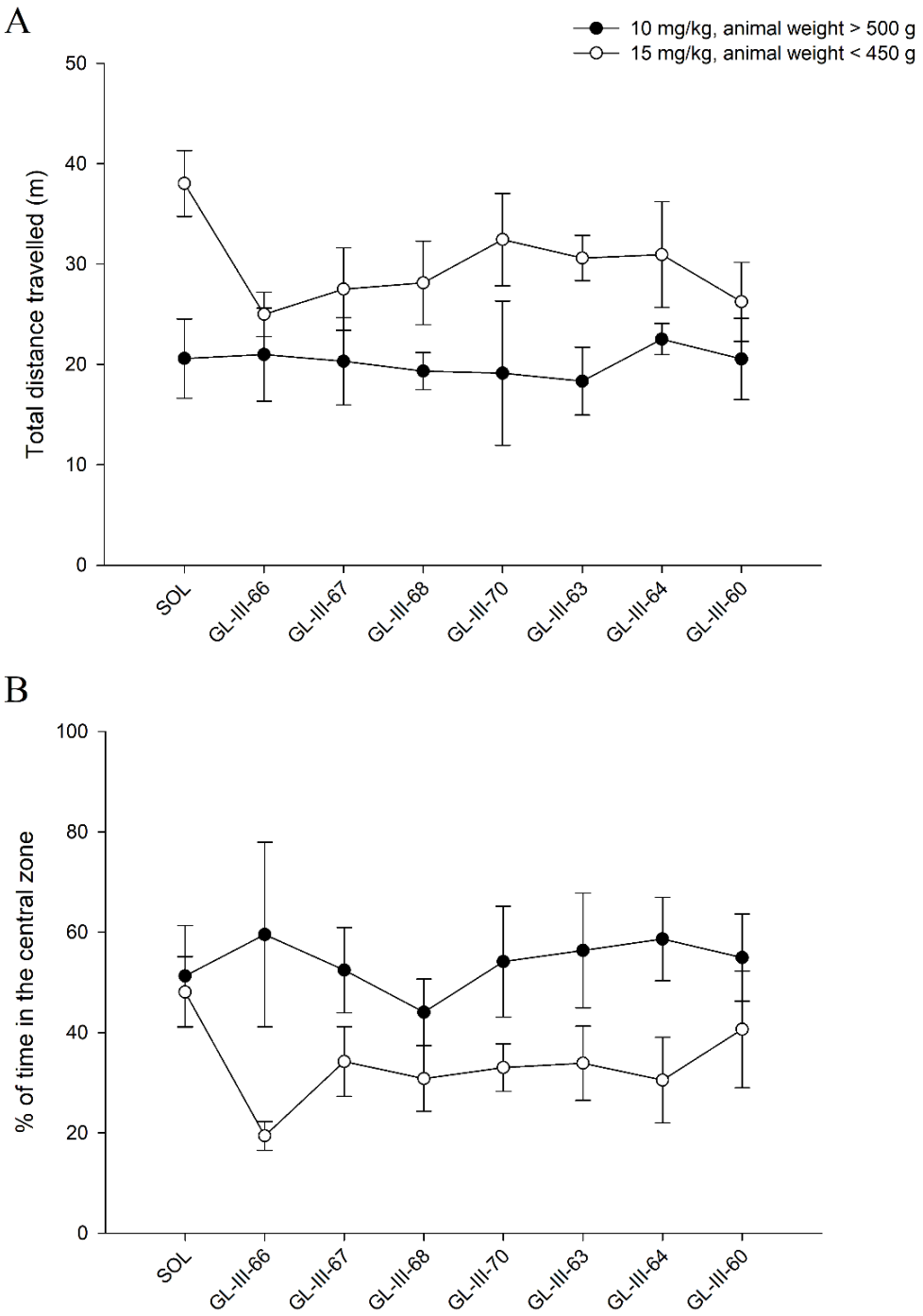

Figure 34. The effect of GL-III-66 (39), GL-III-67 (46), GL-III-70 (47), GL-III-68 (48), GL -III-64 (54), GL-III-60 (58), and GL-III-63 (61), dosed intraperitoneally at 10 mg/kg (dark symbols) and 15 mg/kg (light symbols), on total distance travelled (A) and % of time in the central zone (B) during 60 min of recording in rats. All data are presented as the mean ± S.E.M. Number of animals per treatment group was 4 (10 mg/kg) and 6, 6, 7, 6, 8, 6, 7, 6 (15 mg/kg), respectively to the order of the ligands in Figure 34. Unpublished data.

The results of the effects of i.p. and orally administered novel ligands on motor performance in mice and rats shared a similar effect pattern and illustrated that some of them possess a clear potential to induce sedative and/or locomotor impairment, which is commonly seen as characteristics for BZD-like drugs, such as ligands **25** and **49**. The isopropyl amide **39** might exhibit sedative and anxiogenic potential in rats at a dose higher than 15 mg/kg in the spontaneous locomotor activity assay and ataxic potential at a dose higher than 40 mg/kg in rotarod test. The bromo ethyl amide **46** might exert muscle relaxation in rats when given in a dose higher than 20 mg/kg, as measured, in grip strength test. Other compounds in this behavioral study were pharmacologically inert over a wide dose range, like **36, 37** and **38**, and as such can be considered as ligands possibly more silent at α1 $GABA_A$Rs and also more selective for α5 $GABA_A$Rs. The motor-impairing potential of certain ligands was slight, and the present set of data emphasizes the wide margin of safety from the prospect of unwanted motor-impairing effects of the dimethyl amide **36,** oxadiazoles **54, 58** and **61**. Taken together, it can be concluded from examination of these data that all other ligands except **25, 26, 35, 39, 46** and **49** might represent suitable candidates for examination of the effects mediated by α5 $GABA_A$Rs. Most of all the anxiolytic, pro-cognitive and antidepressant effects were fully devoid of adverse motor effects at doses effective in distinct animal models of human psychopathology.

2.2.3.4.4. Receptor Binding Studies

In order to understand if any other receptor interactions would occur throughout the body, all of the novel ligands were sent to the National Institute of Mental Health (NIMH) Psychoactive Drug Screening Program (PDSP) to screen the ligands on a series of CNS receptors, ion channels, and transporters to determine if any possible receptor bindings interaction occurred (Dr. Bryan

Roth, UNC).[137] A primary binding assay was conducted first to determine if there was any significant inhibition (over 50%), which one would consider as a hit and would be further tested in the secondary binding assay to obtain a Ki (nM) value.

As shown in Appendix B, most of the compounds have exhibited inhibition at BzR rat brain synaptosomal membranes in the primary PDSP binding assay, which indicates binding affinity at $GABA_ARs$; however, these data were not able to indicate the binding affinity at different Bz alpha-subtypes. In addition, the test compounds did not bind to either calcium channels, which indicated no disruption of any physiological events on cardiac and smooth muscle cells,[138] or NMDA receptors to affect any possible synaptic organization or plasticity.[139] It was noticed that only the compounds with a C(8) TMS-acetylene group exerted a slightly undesired binding to hERG regardless of other modifications in the backbone structure, such as changes at the 2' phenyl position, or any different moieties at the C(3) position. The structures and the corresponding Ki values are shown in Table 12.

Table 12. Binding affinities at hERG, only the TMS-acetylene compounds among the entire compound library have slight affinity to hERG (PDSP). Unpublished data.

PDSP Code	Cook Code	Structure	Binding affinity at hERG	
			% inhibition (primary)	Ki in nM (secondary)
42639	GL-II-18	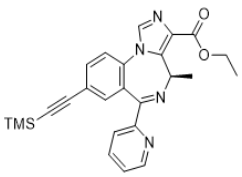	58.5	>10000
50095	SH-I-060	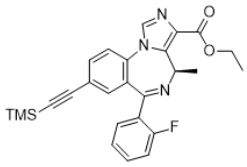	69.1	1658

50099	SH-I-055	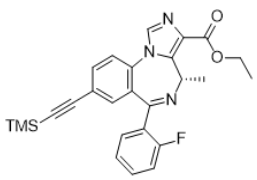	68.5	1268
50117	GL-I-63	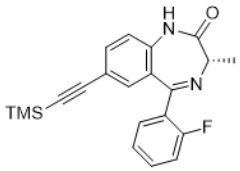	63.8	>10000
50129	GL-III-72	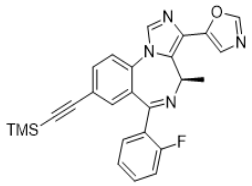	44	ND: Less than 50 % inhibition in the 1^{o} screen
50158	GL-III-77	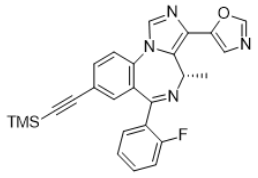	57.4	659

The peripheral benzodiazepine receptor (PBR), later renamed as translocator protein (TSPO), was also selected for screening in regard to binding affinity. PBRs are responsible for numerous biological process, such as the regulation of neurological damage, cellular proliferation, apoptosis, transportation of anions for mitochondrial transmembrane potential, as well as regulation of steroidogenesis and heme biosynthesis.[140] There are some compounds that exhibited binding affinity at PBR, as shown in Table 13 for the selected novel compounds, which have a wide variety of functional groups at different positions. Most of them have a Ki value in the range of 300-3800 nM, except **54** (GL-III-64). **This oxadiazole 54 exhibited a high affinity at PBR in**

the nanomolar range (29 nM), which is even more potent than the classical achiral BZD, Ro5-4846 (53 nM) that was reported to stimulate steroidogenesis.[141] Since **54** is a metabolically stable bioisostere devoid of any CNS effects, it might be an interesting ligand for exploration of its pharmacological effects, in addition to the current lead compounds with the aid of further confirmation of its effect in a functional assay.

Table 13. Binding affinities at peripheral benzodiazepine receptor (PBR) for the novel compounds (PDSP). Unpublished data.

PDSP code	Cook code	Structure	Binding affinity at PBR	
			% inhibition (primary)	Ki in nM (secondary)
42638	GL-II-06	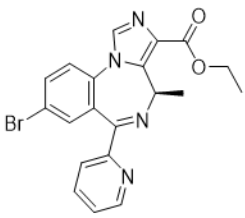	76.4	591.5
42640	GL-II-19	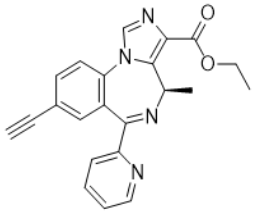	73.5	1397.5
42642	GL-II-31	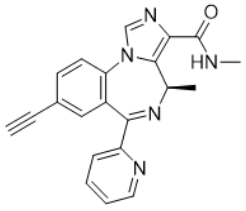	70.2	734.5
42643	GL-II-32	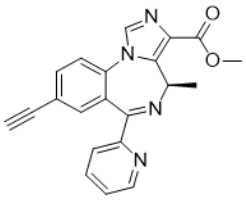	50	3787.5

42648	GL-II-54	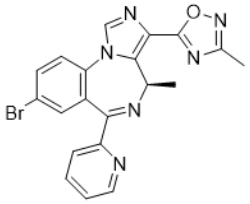	97.2	397
42659	GL-I-33	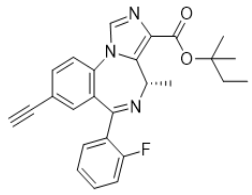	74.7	1791
42667	GL-I-78	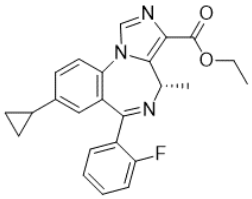	83.4	595
50132	GL-III-42	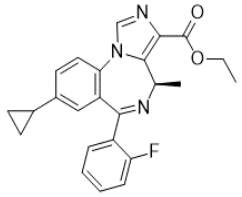	72.1	966
50137	GL-III-60	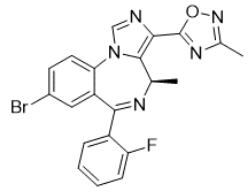	61	2389
50138	GL-III-63	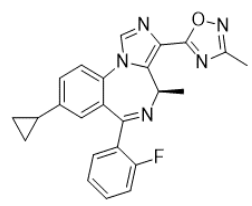	60	364

50139	**GL-III-64**	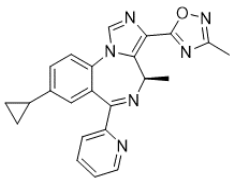	**55.1**	**29**
50142	GL-III-68	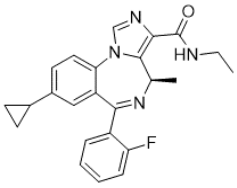	61	1273
42633	**Ro5-4846**	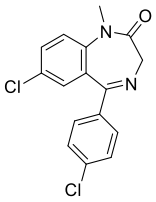	**83.7**	**53**

Besides the binding affinity at the receptors illustrated above, it is interesting to see that most of the IMDZs were not only potent enough to inhibit the BzD rat brains site, but also exhibit inhibition at kappa opioid receptors (KOR). Such compounds are not limited to a certain functional group, oxadiazole, oxazoles, esters, and amides have all exerted different affinities at KOR, as listed in Table 14. All S-isomer analogs have higher affinity at KOR than the corresponding R-isomer analogs. Other trends are increasing affinity in the following order: ester > amide/ oxadiazole/oxazole; 2'F > 2'N; large alkyl group size > small.

Table 14. KOR binding affinity from the primary binding assay. Unpublished data. (PDSP)

PDSP Code	Cook Code	Binding affinity at KOR	
		% Inhibition (primary)	Ki in nM (secondary)
30611	SH-053-2'F-R-CH3	90.9	240
30612	SH-053-2'F-S-CH3	95.7	90
30613	MP-III-004	80.3	599

30614	MP-III-021	97.5	122
30615	MP-III-019	45.5	3367
30616	MP-III-018.A	71.1	1182
30617	MP-III-022	87	381
30618	MP-III-023	96.1	119
30619	SH-I-85	95.6	162
37719	MP-III-018.B	50.9	3072
37720	MP-III-019.B	62.1	2621
37721	MP-IV-004	86	637
37722	GL-I-65	88.4	222
37723	MP-IV-005	89.3	380
37724	GL-I-66	91.7	296
37725	MP-IV-010	93.6	149
37726	GL-I-81	92.9	127
42633	Ro5-4846	57.5	1323
42638	GL-II-06	78.8	401
42644	GL-II-33	88.8	193
42648	GL-II-54	80	504
42656	GL-I-30	94.9	27
42657	GL-I-31	94.2	65
42658	GL-I-32	94.5	64
42659	GL-I-33	93.7	34
42660	GL-I-38	95.2	68
42661	GL-I-36	84.9	411
42662	GL-I-43	95.2	102
42663	GL-I-41	97	39
42664	GL-I-55	93.1	150
42665	GL-I-54	77.9	788
42666	GL-I-77	95	125
42667	GL-I-78	95.7	48
50094	SH-I-047	82.4	110
50096	MP-III-058	83.6	249
50098	SH-I-048B	95.2	63
50104	GL-II-73	58.1	1402
50105	GL-II-74	86	229
50106	GL-II-75	80.9	354
50107	GL-II-76	80.4	418
50125	GL-III-35	77	912
50126	GL-III-36	87.8	253
50127	GL-III-36A	62	2398
50130	GL-III-73	74.3	452
50132	GL-III-42	86.1	213
50133	GL-III-43	50.2	1927

50135	GL-III-53	91.7	227
50137	GL-III-60	87.4	391
50138	GL-III-63	77.5	796
50139	GL-III-64	60.2	2640
50140	GL-III-66	62.9	241
50141	GL-III-67	87.3	181
50142	GL-III-68	88.3	212
50143	GL-III-69	75.1	627
50144	GL-III-70	67.7	1080
50145	GL-III-75	61.2	1569
50146	GL-III-76	83.2	460
50149	GL-III-78	74.1	571

It seems as though as long as the ligand contains a chiral methyl group at the C(4) position, the ligand will bind to KOR at a certain extent, although it will not be potent affinity. Since KOR agonists are a big concern in drug addiction, it is important to know if these IMDZs function as agonists or antagonists at KOR. If they turned out to be potent KOR agonists, the compounds would have been dropped from the next screening panel for other behavioral studies. However, if they acted as antagonists or very weak agonists, the activity would be much less of concern. Therefore, the secondary assay was conducted to determine the function for these ligands. The results are shown in Table 15. The test compounds have weak kappa agonist activity since the potencies are at micromolar concentrations. For comparison, if a compound was a kappa agonist with potent activity, the nanomolar potency would be the range to focus on. In Table 15, two kappa compounds Salvinorin A and U-50488 were used as controls to ensure the assays were functioning correctly. Both Salvinorin A and U-50488 exhibited nanomolar potencies, which means that not very much of those compounds are needed to stimulate a response to the kappa opioid receptor. However, the selected test compounds were in a range of micromolar concentration for the stimulation response, which indicated that these compounds have some kappa activity, but their activity at the kappa receptor is considered fairly weak and inconsequential.

Table 15. Selective compounds for KOR stimulation response.

Test cpd	Potency (μM)	Potency (SEM)	Efficacy (%)	Efficacy (SEM)	n
Salvinorin A	0.0000341	8.64E-06	100.9	0.3687	3
30 (GL-I-54)	3.689	0.3098	112	1.021	3
31 (GL-I-65)	0.9739	0.4672	105.5	2.967	3
51 (GL-II-33)	6.25	3.737	119.1	31.57	2
53 (GL-II-54)	1.573	0.3111	107.4	1.754	3
36 (GL-II-73)	1.511	0.3532	104.4	1.441	3
37 (GL-II-74)	0.1236	0.04516	101.3	0.09095	3
38 (GL-II-75)	0.3157	0.0704	102.7	0.8377	3
U50488	0.0001509	8.01E-05	99.34	0.2595	3

Several key compounds were tested in further binding assays at α1/2/3/5-$GABA_A$Rs. As shown in Table 16, the results indicated that all three amides **36, 37** and **38** exhibited more potent selective-affinity to the α5-subtypes as PAMs than other α-subtypes, whose Ki values were 6-15 fold more potent, as compared to the other subtypes. Notably, the dimethyl amide **36** exhibited the least potent affinities with Ki values in a low μM range, as compared to **37** and **38**. The cyclopropyl amide **38** had an overall low potency but a similar binding pattern than the positive control DZP. In contrast to these new ligands, DZP demonstrated a potent but non-subtype selective-affinity at all α-subtypes.

Table 16. K_i values for all three compounds at α1/2/3/5β3γ2 receptors.

	α1β3γ2	α2β3γ2	α3β3γ2	α5β3γ2
36 (GL-II-73)	55 ± 4μM	30 ± 5 μM	63 ± 7μM	5 ± 2 μM***
37 (GL-II-74)	1060 ± 100 nM	809 ± 130nM	1250 ± 51nM	83 ± 12nM***
38 (GL-II-75)	542 ± 88 nM	789 ± 130 nM	480 ± 62 nM	79 ± 2 nM**
DZP	22.4 ± 5.4 nM	13.4 ±1.1 nM	20.4 ± 2.8 nM	12.1 ± 1.2 nM

Significance towards 1 3 2 ; *:p<0.05,:p<0.01,***:p<0.001. Values determined by Dr. Janet Fisher on HEK cells, University of South Carolina.**

2.2.3.4.5. Potentiation at $GABA_ARs$

To investigate the effects of novel IMDZs on $GABA_ARs$, the potentiation of GABA signaling at α1-6β3γ2 containing recombinant $GABA_ARs$ has been assessed at 100 nM and 1 μM concentration, as compared to the response to GABA alone.

As shown in Figure 35 a-d, at 100 nM, electrophysiological traces at α5β3γ2 $GABA_ARs$ showed that **37** and **38** exhibited a significant allosteric modulation with α5 Bz/GABA(A) subtypes, respectively 169.9% and 182.4% potentiation of the percentage of response to GABA alone. At this concentration, **36** and **39** exhibited a lower potentiation at α5β3γ2 $GABA_ARs$. The compound **38** also exhibited high potentiation at α1, α2, and α3 receptor subtypes, characterized by the potentiation of the response of GABA alone above 180% for each subunit (203%, 194% and 183% for α1, α2, and α3 respectively). The percentage of response to GABA with co-application of diazepam (DZP) was also assessed, and the potentiation obtained at each $GABA_AR$ subtype (α1-6β3γ2) was very similar but slightly more potent to the obtained for **38**. It appeared that the compound GL-II-75 might share electrophysiological properties with DZP. At 1μM concentration, all compounds tested elicited a significant allosteric modulation at the α5β3γ2 GABAA receptor, with potentiation values obtained around and higher than 250%. The potentiation of **36** and **37** at α1, α2, and α3 were lower than α5, which indicated that these two ligands were more α5 preferred. Again, at 1μM, **38** also exhibited high potentiation of α1, α2 and α3 subunits (>300%) while the other compounds had a moderate efficacy (<200%) to these subunits. As expected, none of the compounds potentiated receptors containing α4 or α6 subunits. (Figure 35 a-d), suggesting a similar subtype dependent response as DZP at BZR. A similar potentiation at $GABA_ARs$ with β1 or β3 subtypes were observed for **36-39**, indicating that there was no significant impact between different β subunits on the efficacy of the novel compounds, as presented in Figures 35 e-h.

Based on the estimated free brain concentration, it appeared that the doses of 1 mg /kg and 10 mg/kg used for behavioral assessments elicited a different pattern of $GABA_AR$ potentiation. With **36, 37 or 38** administered at 1 mg/kg, neither α5 nor α1 were potentiated (less than 120 %). However, at 10mg/kg, the potentiation of α1 and α5 were significant for all compounds. At this dose, **36** exhibited a moderate to strong α5 potentiation (180%) as well as a slight potentiation at α1 (130%). This pattern of potentiation was even greater with **37** that exhibited 275% at α5 and 155% at α1. However, **38** elicited a stronger potentiation at α1 (280%) than α5 (240%), which is very similar to the pattern of DZP. Altogether, these results confirmed that each compound had allosteric modulation effects at α5-containing $GABA_ARs$, as well as α1, α2, and α3. Nevertheless, at 10 mg/kg, the potentiation at α1 subtypes of **36, 37** and **38** was lower than that of DZP at 1.5 mg/kg, as demonstrated in Figure 35 i-l, since a low free fraction in brain tissue was observed.[117]

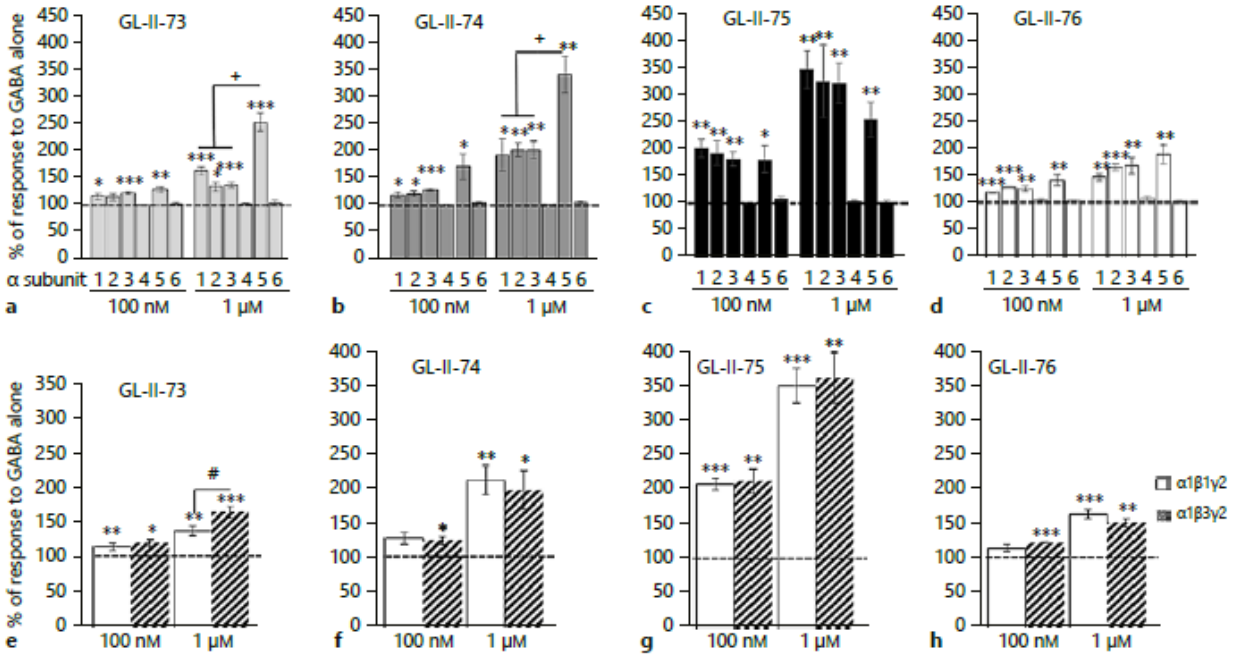

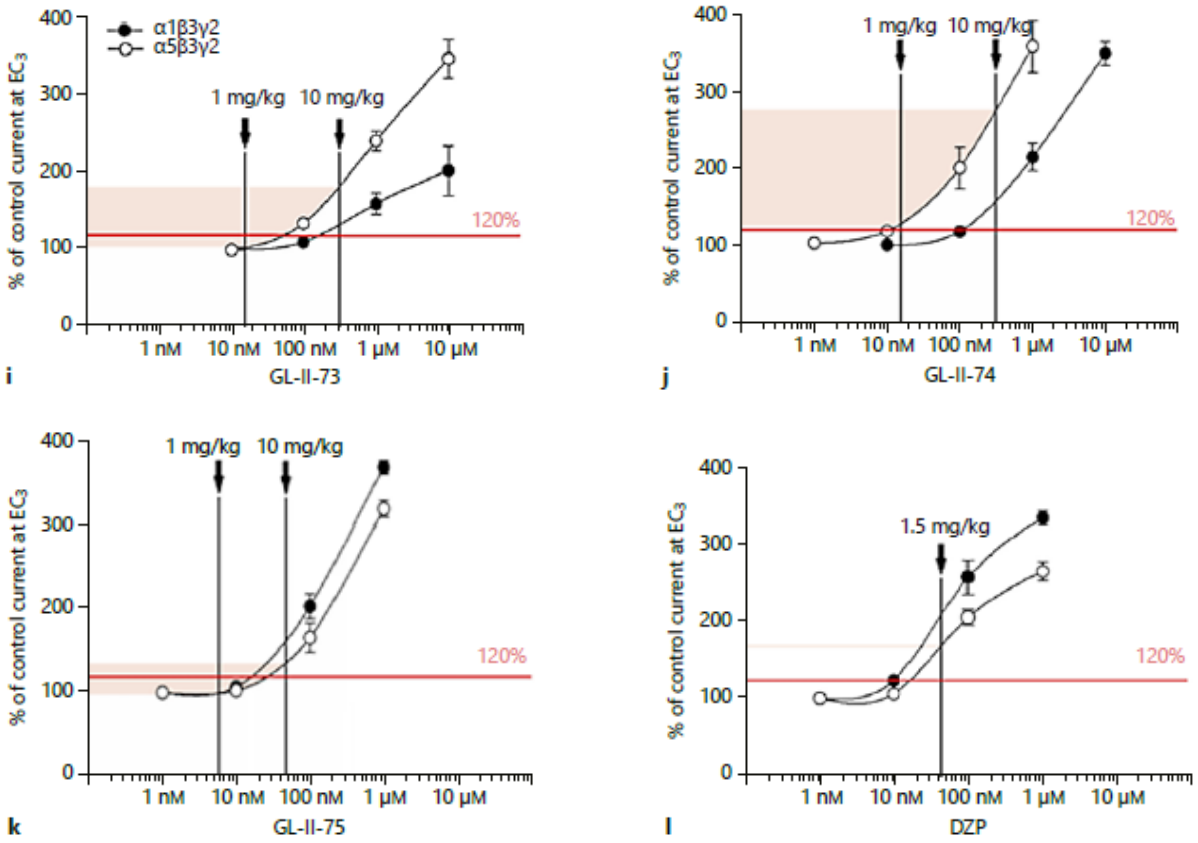

Figure 35. Efficacy data of 36 (a), 37 (b), 38 (c) and 39 (d) at 100 nM or 1 μM for α1-6-containing $GABA_ARs$. Comparison of α1β1γ2 and α1β3γ2 for 36 (e), 37 (f), 38 (g) and 39 (h) at 100 nM or 1 μM. The EC_{3-5} GABA value is presented in percentage of response to GABA alone. * p < 0.05, ** p < 0.01, and *** p < 0.001 compared to 100%; + p <0.05 compared to α5β3γ2; # p < 0.05 compared to α1β3γ2. The estimated free brain concentrations were illustrated on the dose-response curves for the approximated electrophysiological responses of 36 (i), 37 (j), 38 (k), and DZP (l). (Adopted from the figure in Prevot et al.)[117]

Besides the amide analogs **36-39,** a series of other amides, thioamides, and oxadiazoles were assessed for their potentiation at α1,2,3,5-containing $GABA_ARs$ at 100 nM (Figure 36) and 1 μM (Figure 37), as compared to **36** (GL-II-73). The % response value at α4 subtypes was nearly at the baseline, which indicated all those analogs did not potentiate α4-containing $GABA_ARs$ (data was not shown). Among all the test compounds, the C(8)-bromo ethyl amide **46** (GL-III-67) exhibited the greatest potentiation at all subtypes, however, with slightly more potentiation at α1 receptors at 100 nM and a slight preference for α5 receptors at 1 μM concentration. As previously demonstrated on the rotarod studies, this ligand exhibited a slight sedative effect, which was now

confirmed by the potentiation at α1-subtypes at lower concentrations. A cyclopropyl group at the C(8) position significantly reduced the potentiation at all subtypes as illustrated via a direct comparison of amide **36** to **47** (GL-III-70), and **46** to **48** (GL-III-68). The C(8)-cyclopropyl dimethyl amide **47** lost almost all the efficacy at all subtypes at 100 nM, and only a slightly potentiation was observed at 1 μM with more efficacy at α1 subtypes than the other subtypes. The potentiation elicited by the C(8)-cyclopropyl methyl amide **48** was less than the C(8)-bromo compound after the introduction of the C(8)-cyclopropyl group. However, it still exhibited a similar pattern of efficacy as ligand **46,** but even much lower efficacy at 1 μM. In the thioamide series, with the exception of the dimethyl thioamide **42** (GL-III-85), which demonstrated almost no potentiation at all subtypes at both concentrations, the other three thioamides: methyl thioamide **41** (GL-III-84), ethyl thioamide **43** (GL-III-86) and cyclopropyl thioamide **44** (GL-III-87) all exhibited better potentiation than **36** at all subtypes, especially at α2 and α3 subtypes. At 100 nM, they shared a similar efficacy pattern to that of **38** (GL-II-75) with a slight preference for α1 subtypes, similar to the pattern for **37** at 1 μM. In regard to the oxadiazole series, the methyl oxadiazole **31** (GL-I-65) in the 2'F-S-series, elicited a stronger potentiation than **36** with a similar potentiation profile to that of **38** at 100 nM, and to the profile of **36** at 1 μM. The C(8)-ethinyl methyl oxadiazole **51** (GL-II-33) and its C(8)-bromo analog **53** (GL-II-54) in the 2'N-*R*-series, exhibited only slight efficacy at 100 nM, and only at 1 μM did they significant produce the potentiation at $GABA_AR$s. At this concentration, the ligand **51** exhibited an efficacy profile similar to **38** with more efficacy at α1 subtypes, whereas, the bromo analog **53** resembled the more efficacy at the α5- preferring ligand **36.**

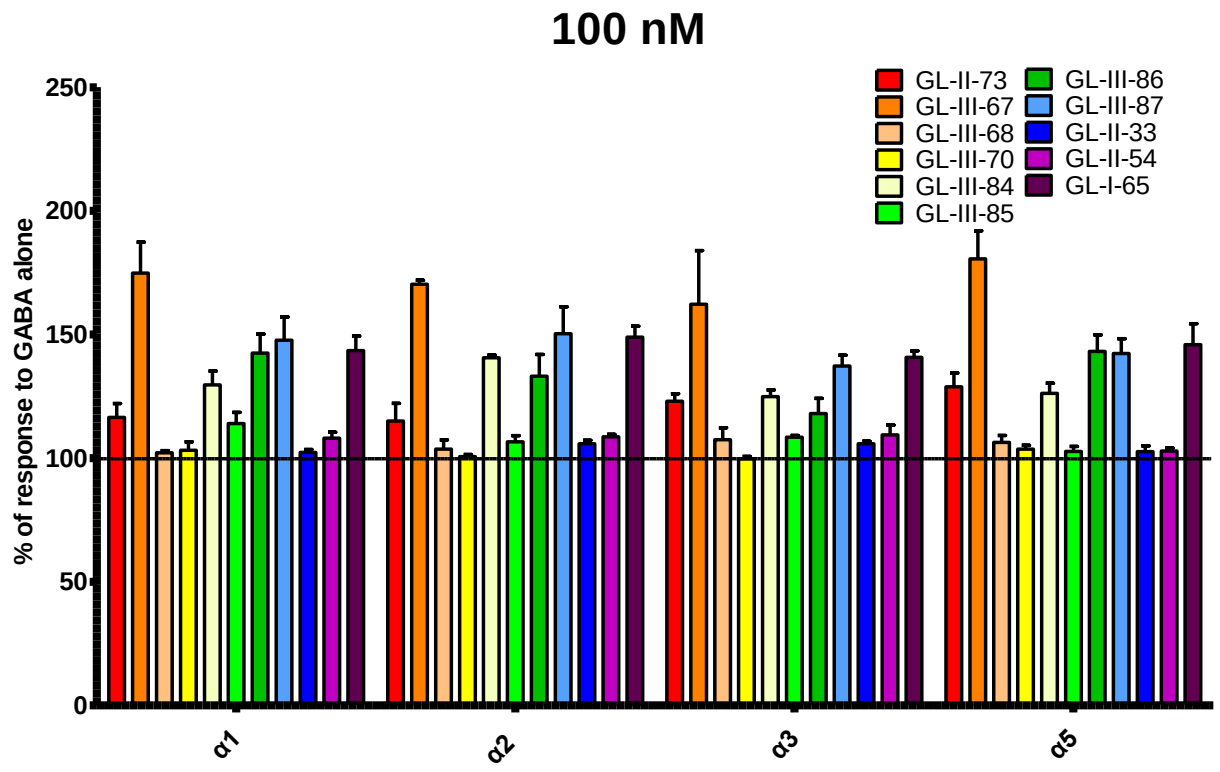

Figure 36. Efficacy data of GL-II-73, GL-III-67, GL-III-68, GL-III-70, GL-III-84, GL-III-85, GL-III-86, GL-III-87, GL-II-33, GL-II-54 and GL-I-65 at 100 nM for α1,2,3,5-containing GABA$_A$Rs. Unpublished data.

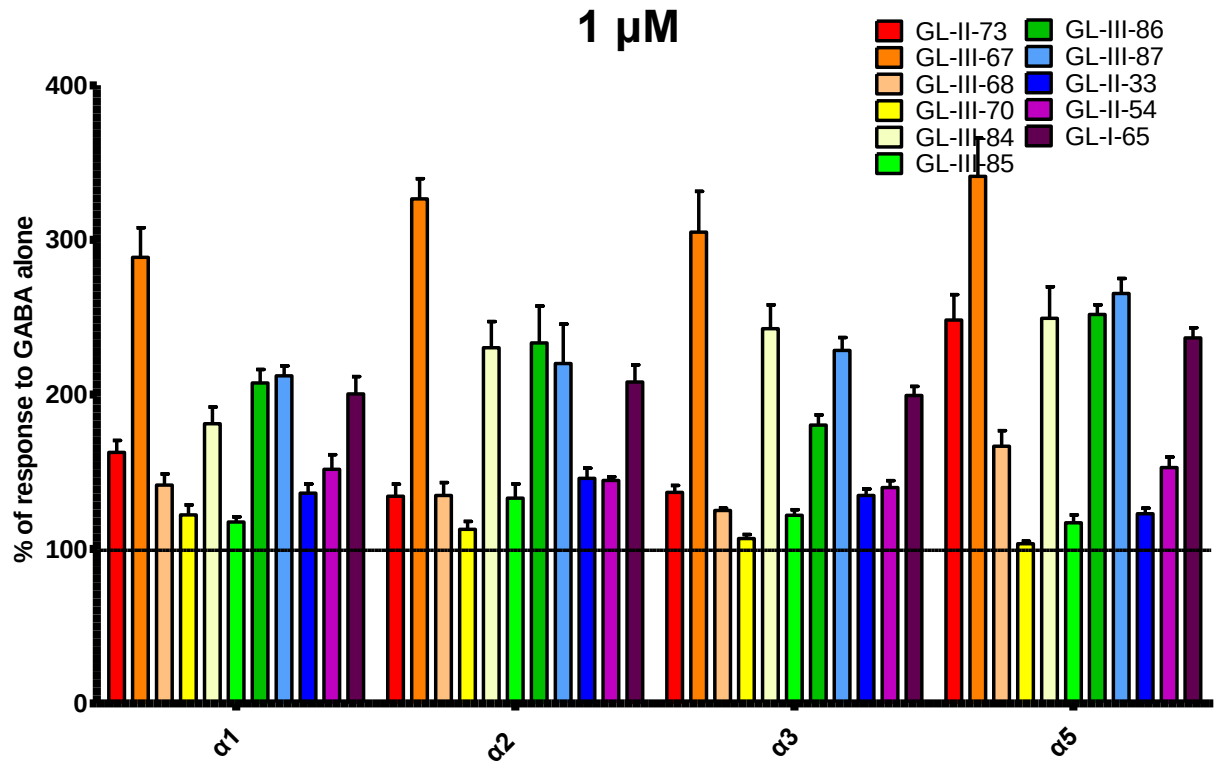

Figure 37. Efficacy data of GL-II-73, GL-III-67, GL-III-68, GL-III-70, GL-III-84, GL-III-85, GL-III-86, GL-III-87, GL-II-33, GL-II-54 and GL-I-65 at 1 μM for α1,2,3,5-containing GABA$_A$Rs. Unpublished data.

In addition to the ester, amide, and oxadiazole moieties at the C(3) position of the targe, several chiral oxazole analogs **64** (GL-III-36), **65** (GL-III-76), **66** (GL-III-73), **67** (GL-III-78), and **79** (GL-III-76A) were also assessed for their potentiation at α1-5 GABA$_A$Rs at 100 nM and 1 μM concentrations, as illustrated in Figures 38 and 39, respectively. As expected, there was no efficacy at α4 subtypes for all IMDZ compounds. However, the distinct difference between *R* and *S*-isomers was observed. The *S*-analogs elicited a stronger non-subtype selective potentiation at α1/2/3/5 subtypes at both concentrations at 100 nM and 1 μM. The C(8)-bromo analogs were more potent than the corresponding ethinyl analogs in the *S*-series. However, efficacy in the *R*-series was visible only at 100 nM. The *R*-analogs tended to elicit a slightly higher α5 preference than at the other subtypes at 100 nM, but lost selectivity at 1 μM. Moreover, **65** exhibited the highest potentiation at both concentrations for all subtypes, as compared to the other compounds. Notably, **65** exerted the most potent α2 subtype selectivity at 1 μM than at the other subtypes.

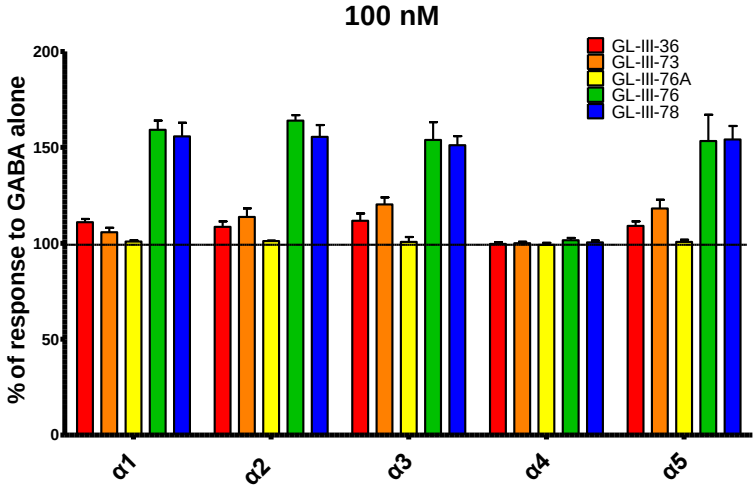

Figure 38. Efficacy data of (*R*) 64 (GL-III-36), (*S*) 65 (GL-III-76), (*R*) 66 (GL-III-73), (*S*) 67 (GL-III-78), and 79 (GL-III-76A) at 100 nM for α1-5-containing GABA$_A$Rs. Unpublished data.

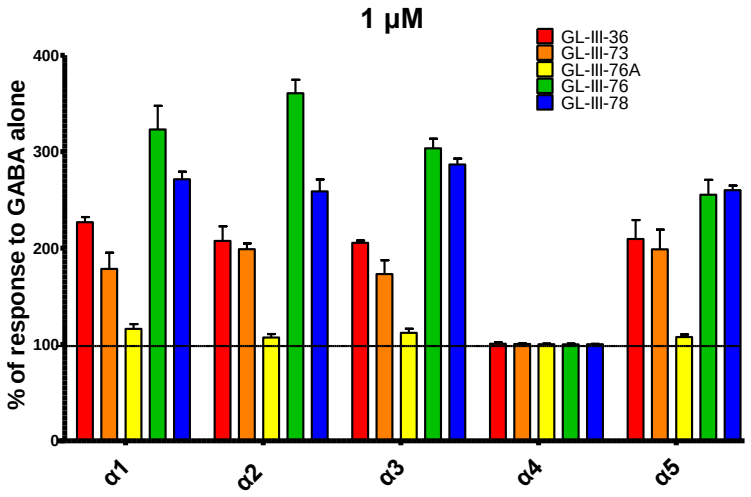

Figure 39. Efficacy data of (*R*) 64 (GL-III-36), (*S*) 65 (GL-III-76), (*R*) 66 (GL-III-73), (*S*) 67 (GL-III-78), and 79 (GL-III-76A) at 1 µM for α1-5-containing $GABA_A$Rs. Unpublished data.

2.2.3.4.6. Studies of Pharmacokinetics

The pharmacokinetic studies of the first batch of test compounds **36-38** and DZP were carried out after 10 mg/kg i.p. administration to mice, as presented in Figures 40 a–d. The brain and plasma free fractions for **36** were 12.14 and 20.39 %, 4.49 and 6.34 % for **37**, 1.34 and 5.08 % for **38**, and 6.38 and 16.25 % for DZP, respectively. The half-life for the test compounds indicated that the ethyl amide **37**, as well as DZP, are the most stable compounds in mouse plasma, as compared to all the other ligands, while **36** exhibited the highest stability in the mouse brain. The ligand DZP and **37** reached the Cmax in the brain in 5 minutes, whereas it took 10 and 20 minutes for **36** and **38** to obtain a similar free fraction, respectively. The ligand **37** presented the highest maximum brain concentration over the other two compounds, suggesting an optimization might be applied for dosage in the brain. The brain-to-plasma partition coefficient values (Kp) for **37** indicated that it exhibited excellent brain permeability, as compared to the other two ligands. The ratio of unbound brain to unbound plasma ligand concentration values (Kp,uu), which measures the net transport through the BBB, further demonstrated similar results those as obtained from the

Kp value. This brain penetration efficiency suggested that **36** may be subject to an efflux transport mechanism at the BBB. The ligands **37** and **38** exhibited a much higher AUC in the brain than DZP, whereas **36** was slightly lower but was similar to DZP. The PK studies illustrated that all 3 ligands have good brain penetration in an efficient manner with the following order: DZP > **37** > **38** > **36**. Accordingly, all of these compounds were further evaluated for *in vivo* behavioral activity by Savic et al.

a

GL-II-73

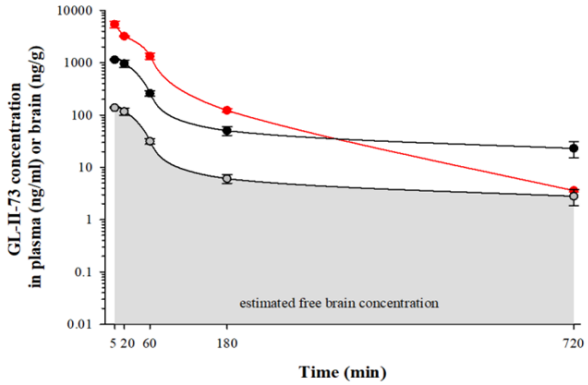

	Plasma	Brain	
C_{max}	5384.54 ± 838.04	1195.94 ± 51.75	(ng/ml)
T_{max}	5.00 ± 0	10.00 ± 5.00	(min)
AUC_{0-12}	4620.09 ± 323.21	1311.86 ± 85.86	(ng*h/ml)
$AUC_{0-\infty}$	4626.35 ± 322.80	1397 ± 119.3	(ng*h/ml)
T½	72.06 ± 1.44	146.58 ± 12.30	(min)
ß	0.0096 ± 0.0002	0.0048 ± 0.0004	(1/min)
K_p	0.30 ± 0.04		
$K_{p,uu}$	0.18 ± 0.02		

b

GL-II-74

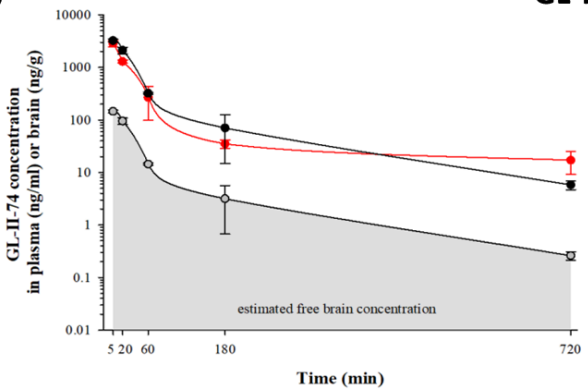

	Plasma	Brain	
C_{max}	2840.74 ± 404.87	3246.23 ± 184.90	(ng/ml)
T_{max}	5.00 ± 0.00	5.00 ± 0.00	(min)
AUC_{0-12}	2053.17 ± 197.11	2218.83 ± 177.52	(ng*h/ml)
$AUC_{0-\infty}$	2102.62 ± 298.38	2231.62 ± 177.69	(ng*h/ml)
T½	110.70 ± 10.00	87.96 ± 4.14	(min)
ß	0.0064 ± 0.0006	0.0079 ± 0.0004	(1/min)
K_p	1.14 ± 0.27		
$K_{p,uu}$	0.81 ± 0.19		

c

GL-II-75

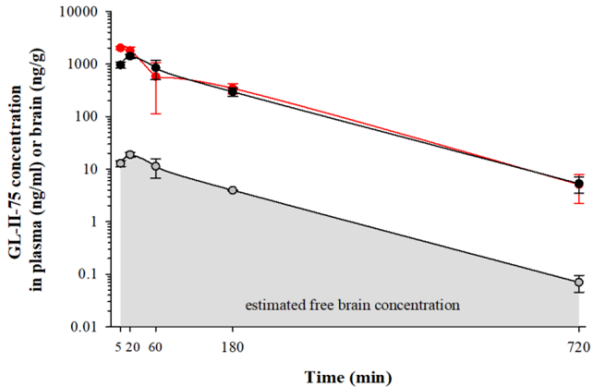

	Plasma	Brain	
C_{max}	2151.323 ± 81.07	1410.23 ± 136.71	(ng/ml)
T_{max}	15.00 ± 5.00	20.00 ± 0.00	(min)
AUC_{0-12}	4845.31 ± 118.92	3895.8 ± 114.08	(ng*h/ml)
$AUC_{0-\infty}$	4856.48 ± 111.76	3907.26 ± 112.51	(ng*h/ml)
T½	80.34 ± 9.54	86.16 ± 5.52	(min)
ß	0.0089 ± 0.001	0.0081 ± 0.0005	(1/min)
K_p	0.80 ± 0.04		
$K_{p,uu}$	0.21 ± 0.01		

d

DZP

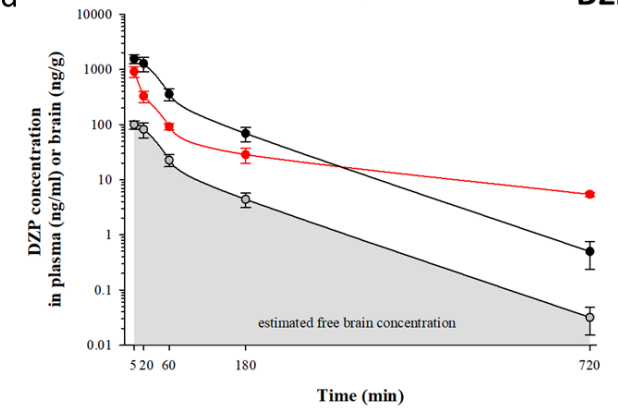

	Plasma	Brain	
C_{max}	909.43 ± 193.20	1555.05 ± 270.87	(ng/ml)
T_{max}	5.00 ± 0.00	5.00 ± 0.00	(min)
AUC_{0-12}	567.41 ± 73.38	1638.94 ± 221.92	(ng*h/ml)
$AUC_{0-\infty}$	583.08 ± 71.57	1778.29 ± 255.93	(ng*h/ml)
T½	118.80 ± 5.40	63.78 ± 3.12	(min)
ß	0.0059 ± 0.0003	0.0109 ± 0.0006	(1/min)
K_p	3.06 ± 0.35		
$K_{p,uu}$	1.20 ± 0.14		

Figure 40. Plasma and brain concentration-time profiles of 36 (a), 37 (b), 38 (c), and DZP (d) after 10 mg/kg i.p. administration in male C57BL/6 mice (n = 3 per time point). (Adopted from the figure in Prevot et al.)[117]

In addition to ligands **36-38**, several amides **49** (RV-II-04), **50** (GL-II-31), **25** (MP-III-023), **30** (GL-I-54), **39** (GL-III-66), **46** (GL-III-67), **47** (GL-III-70), and **48** (GL-III-68), and oxadiazole analogs **52** (GL-III-23), **51** (GL-II-33), **53** (GL-II-54), **54** (GL-III-64), **58** (GL-III-60), **61** (GL-III-63), and **31** (GL-I-65) were also evaluated for their PK profiles in mice and rats after i.p. dosing at 3 mg/kg. The data is presented in Appendix C: Tables 1 and 2, Figures 1-18.

By comparing the AUC and C_{max} values in plasma from the respective concentration-time profiles of all test compounds (see Appendix C Figures 1-18), the examination of the data illustrated the potential for systemic exposure was generally quite high, regardless of the route of administration routes. The AUC values from time 0 to 12 h or infinite time post-dosing values in both plasma and brain indicated around a 2-fold greater exposure of animals to **54, 58,** and **61**, as compared to the other ligands. Moreover, the calculated Kp values (1.15 for **49**, 0.33 for **50**, 1.15 for **25**, 0.19 for **30**, 2.37 for **52**, 1.46 for **51**, 1.17 for **53** and 1.29 for **31)** indicated that all ligands exhibited good brain penetration after i.p. administration in mice, which is critical for research in any *in vivo* animal model. Generally, the values of Kp close to or greater than one unity indicate excellent brain penetration of the test compound. In order to compare concentrations obtained *in vivo* and *in vitro*, it is illustrative to express the kinetic results in molar beside the weight concentrations. After i.p. dosing at 3 mg/kg in mice, compounds **50, 51, 31,** and **39** reached moderate to high submicromolar concentrations; compounds **30, 53, 47,** and **48** reached high submicromolar to low micromolar values, while compounds **49, 25, 52, 39, 54, 58,** and **61** reached micromolar concentrations in brain tissue, and similar results were obtained in rat brain.

All of the test compounds are orally active, which is usually considered as an optimal delivery route for active CNS drugs. The calculated F values (oral bioavailability) after i.p. administration in mice are as follows: 1.25 for **49**, 1.43 for **50**, 1.08 for **25**, 0.74 for **30**, 2.88 for **52**, 3.77 for **51**, 1.24 for **53** and 3.17 for **31**. Usually a relatively high bioavailability is expected for the BZD-like compounds; however, if the F values were above unity, it might suggest that the compound after i.v. injection may have undergone precipitation or crystallization, which would be connected with a probable rupture of the tail vein, while administering the volume of about 0.3 mL. This would be due to the low solubility of the ligands under study. On the other hand, the calculated F value for **36** after iv. or p.o. administration at the 3 mg/kg dose in rats was 0.33, not near a value of unity.

The elimination half-time ($t_{1/2}$) after **i.p. administration of the test compounds in mice plasma** was in the range between 0.53 h (for **38**) and 8.89 h (for **39**). A relatively wide range of half-life values suggests that most of the compounds would be appropriate for a repeated-dose treatment with a $t_{1/2}$ longer than 1 hour, while those with $t_{1/2} < 1$ hour (**38** and **30**) would be more applicable for short-acting agents. Nonetheless, the elimination from mouse brain tissue after i.p. administration tends to be consistently above 1 h (a $t_{1/2}$ was calculated slightly less than 1 hour only for **49**, **25** and **30**), which further confirmed that most of the compounds meet the requirements for a potential CNS-active drug. Qualitatively, a similar pattern was observed from the PK data obtained by other administration routes (i.v. or p.o.) in mice. With regard to the data from rat plasma and brain, the elimination half-lives are usually slightly longer than in mice, as expected. The $t_{1/2}$ of the test compounds in both plasma and brain are consistently higher than 2 h after i.p. administration in rats in the case of **50-53 and 31**; the pharmacokinetic profiles of **36-38**, and later analogs after i.p. administration in rats are have yet to be determined.

Taken together, it can be concluded that **31, 36, 51, 53, 54, 58,** and **61** probably represent suitable candidates for further evaluation of the effects mediated by α5 or α2/3/5-containing $GABA_ARs$, *in vivo* in regard to anxiolytic, pro-cognitive and antidepressant effects.

2.2.3.5. Schizophrenia

2.2.3.5.1. Neuroinflammatory Effects and Schizophrenia

In recent years, the accumulation of a large amount of evidence has suggested the importance of the link between multiple inflammation processes and neuropsychiatric/ neurodegenerative disorders such as schizophrenia, depression, Alzheimer's disease, and Autism spectrum disorders (ASD).[142-146] The immune responses to oxidative stress and neuroinflammation might be applied to represent the abnormal aging process, as well as mental impairments.[142] The primary immune cells in the CNS are microglia, which represent a majority of cell types in the brain. Microglia are involved in numerous critical processes such as regulation of the immune response and neuroinflammation, and cytotoxicity through the release of oxidative secreta and cytokines, which induce nitric oxide (NO)-synthase, etc. Upon activation of microglia, nitric oxide (NO)-synthase produces an increase in the amount of NO in the brain, which leads to a toxic neuronal effect and a decrease in the function of natural killer (NK) cells. The observation of NK reduction was reported in postmortem studies on schizophrenia patients, whereas not in bipolar depression patients.[146]

Up to date, only the α1, α3, and β1-containing $GABA_ARs$ have been identified in glia.[147] In order to evaluate effect of the IMDZs on the modulation of the inflammatory response from microglia, the first set of α2/3 and α2/3/5 subtype selective ligands with a higher preference at α3

subtypes were tested in the Griess assay in $GABA_AR$-containing immortalized microglia to determine for their influence on NO production at 50 μM in combination with 1 μM GABA, along with 100 nM dexamethasone as positive control and 1 mM CBT as a cytotoxicity control (Figure 41). GABA alone was not capable of reducing NO levels, however, 8 out of the first 19 compounds studies elicited significant reductions in NO production (at 50 μM). Other compounds, which did not show a significant reduction in NO production or demonstrated toxicity were eliminated from consideration. The active compounds were further investigated subsequently for dose-response effects in a range of 1 nM – 50 μM, as depicted in Figure 43. This NO reduction was not the result from toxicity, except with ligand **32** (GL-I-66), which showed slight cytotoxicity (Figure 42), as compared to other active compounds. It is interesting that the α2/3 or α3 subtype selective ligands such as **84** (KRM-II-81), **85** (MP-III-080), etc. did not decrease NO production. On the other hand, the C(4) chiral methyl analogs, which were expected to have characteristics compatible with α5 subtype selective ligands, were the only compounds that exhibited the desired effects. None of the effects on NO were observed in the achiral series. For instance, the achiral 2'F oxadiazole did not reduce NO production, whereas the *R*-chiral analog **55** (MP-IV-004) did. Moreover, the *R*-chiral analogs exhibited a better reduction of NO in the Griess assay than the corresponding *S*-chiral analogs, as seen in the comparison of **55** vs. **31.** Comparison of the size of the alkyl group on the oxadiazole ring (*R*-series: **55 vs. 56 vs. 57;** and *S*-series: **31 vs. 32 vs. 33**), it was obvious a larger group on the bioisostere portion produced more NO reduction regardless of the *R* or *S* chirality. In addition, the C(8) substituents influenced the NO reduction greatly, and it followed the trend of decreasing activity: cyclopropyl > Br > acetylene, regardless of the 2' prime pendent phenyl substituent. The trend can be seen in the 2'N series: **54 > 53 > 51** or in the 2'F series: **61 > 58 >**

55. The isopropyl oxadiazole MP-IV-010 (**57**) exhibited the highest efficacy in the Griess assay, and therefore, was chosen as the lead compound for further evaluation.

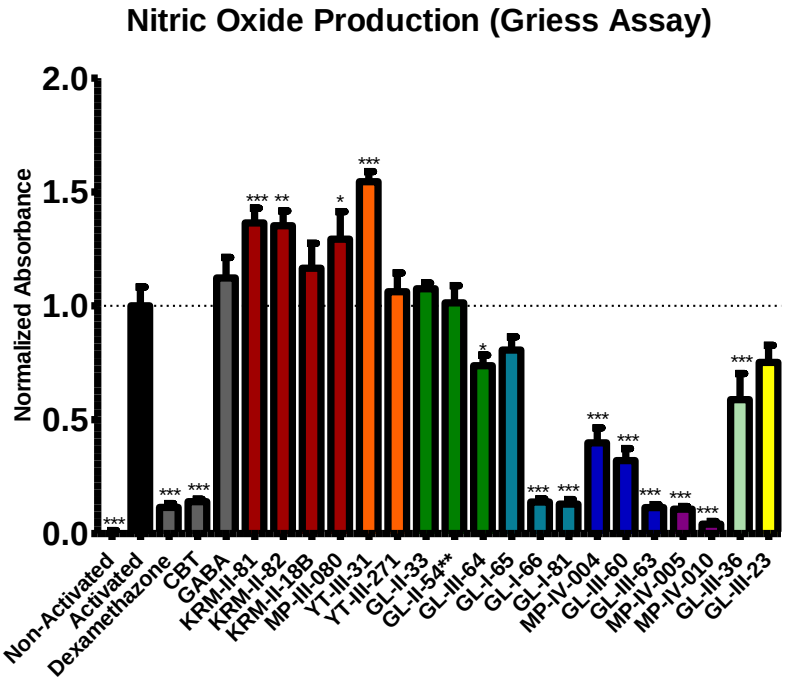

Figure 41. NO production via the Griess assay. Test compounds were screened at 50 µM with 1 µM GABA in mouse microglia activated with 150 U/mL IFNγ and 50 ng/mL LPS, along with 100 nM dexamethasone as a positive control and 1 mM CBT as the cytotoxicity control. Unpublished data.

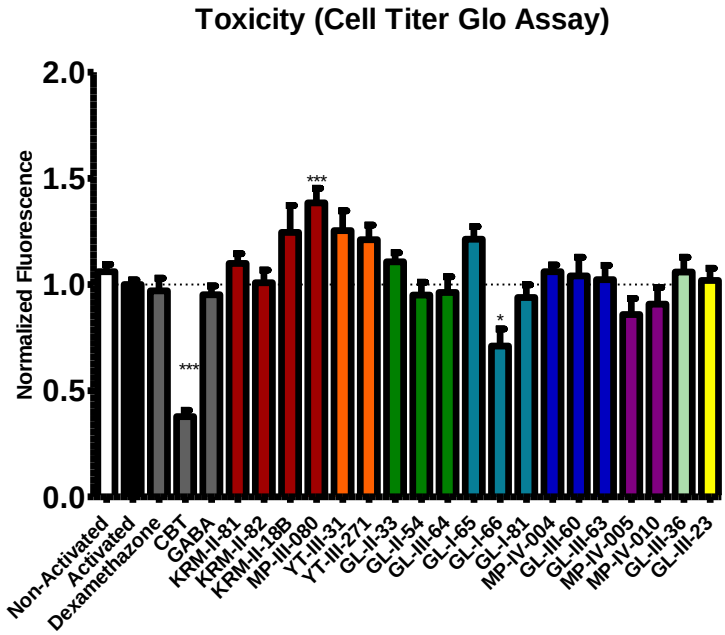

Figure 42. Cytotoxicity via the Cell-Titer Glo Assay. Control compounds dexamethasone and CBT were run at concentrations of 100 nM and 1 mM respectively. Unpublished data.

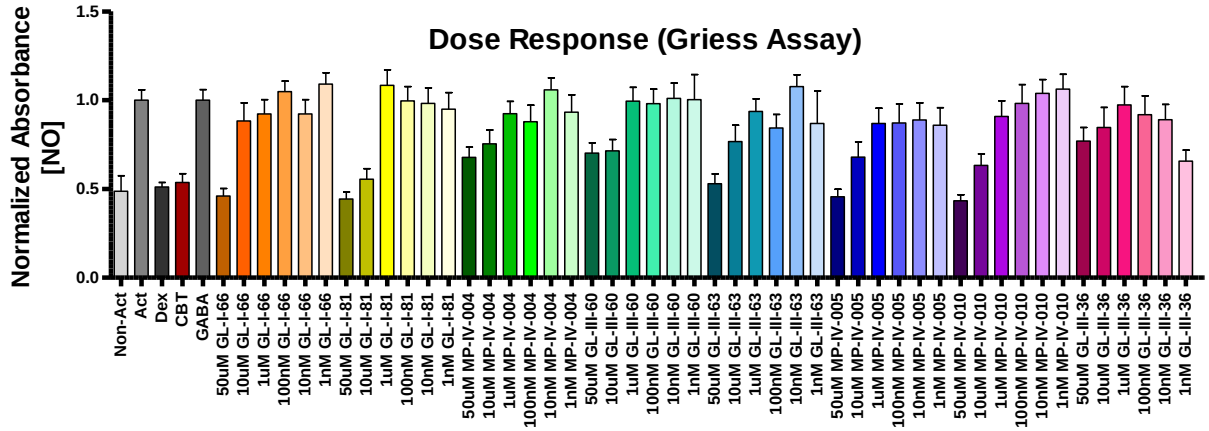

Figure 43. Dose-response of the active compounds from the Griess assay. The test compounds were screened at 50 µM with 1 µM GABA in mouse microglia activated with 150 U/mL IFNγ and 50 ng/mL LPS, along with 100 nM dexamethasone as a positive control and 1 mM CBT as a cytotoxicity control. Unpublished data.

In addition to the first series of compounds that were assayed, the chiral oxazoles **64** (GL-III-36), **65** (GL-III-76), **66** (GL-III-73), **67** (GL-III-78), **69** (GL-III-76A), **80** (GL-III-72) and **82** (GL-III-77), were also evaluated to provide a better SAR. As illustrated in Figure 44, the C(8)-bromo or cyclopropyl analogs **64, 65, 66,** and **67** did not reduce the NO production, indicating they were not active in the Griess assay. A significant reduction in NO was seen with both the *R* and *S* C(8)-TMS-ethinyl analogs **80** and **82**, which were nearly as potent as the lead compound **57**. However, as previously described, all analogs contain the TMS-acetylene function at the C(8) position bind, albeit weakly to hERG channels. Due to cytotoxicity, which was confirmed in the toxicity assay, as shown in Figure 45, these TMS-acetylene oxazoles were the only two compounds that produced toxicity. Therefore they were eliminated from further studies. Interestingly, **79** (GL-III-76A), the imine migration byproduct of **66**, exhibited a significant reduction of NO with no cytotoxicity observed. Notably, from the electrophysiological recording assay of these oxazole

compounds, **79** was the only one that did not potentiate any $GABA_AR$ subtypes at all concentration, which suggested that **79** could affect NO production but not through a $GABA_AR$ mechanism, or this ligand acts as a $GABA_AR$ antagonist.

All of the test compounds exhibited binding affinity to the BzD rat brain sites, as demonstrated by an examination of the PDSP data. When picrotoxin and flumazenil, which are non-competitive antagonists of $GABA_AR$ were introduced into the Griess assay along with **57**, the effect on NO levels was expected to be diminished or reversed. However, the results were not as predicted; the NO production was still significant, as illustrated in Figure 44. This result together with the evidence on ligand **79** suggests that **57** may not be acting through the $GABA_AR$, or only partially through $GABA_AR$ in the microglia. According to the PDSP binding data, these ligands also bound to KOR weakly most notably as well as the Sigma2 receptors, and further investigation is planned to determine the mechanism of action of **57**.

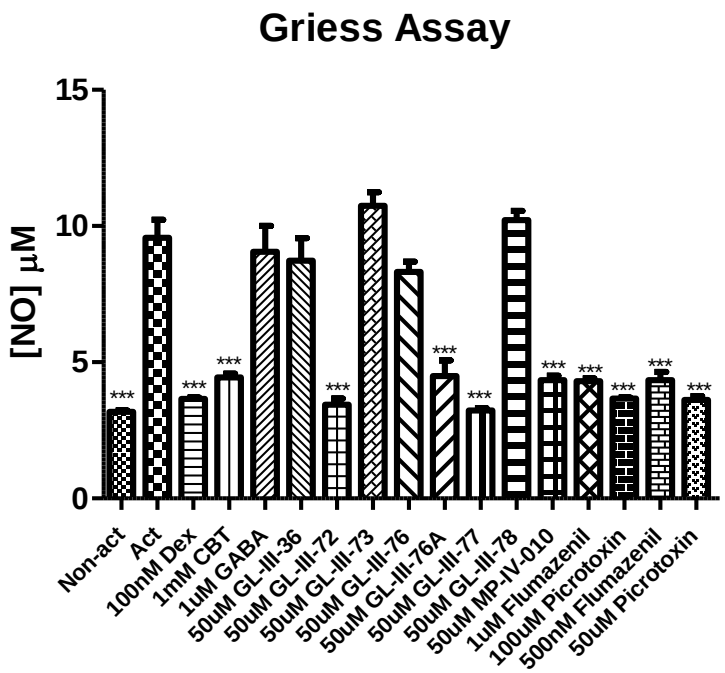

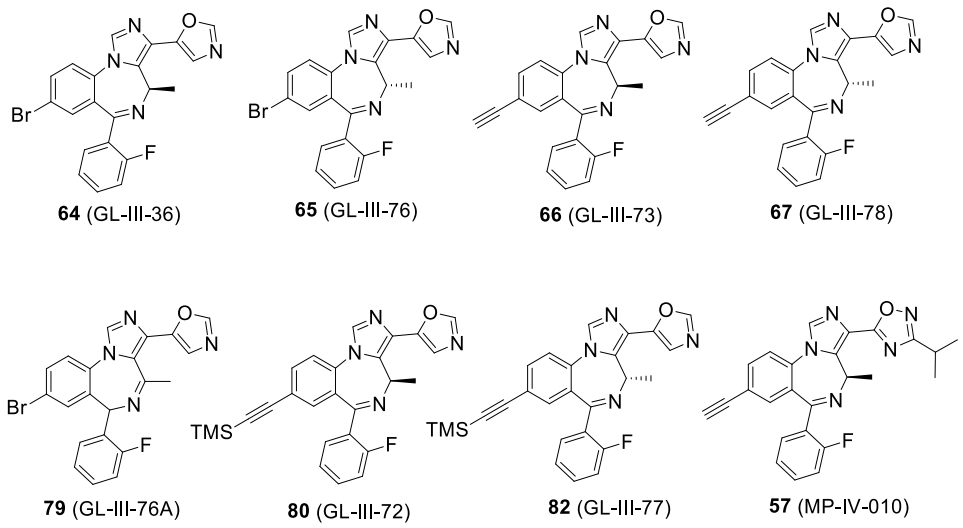

Figure 44. NO production via the Griess assay for the oxazole compounds as well as the GABA$_A$R antagonist picrotoxin at 50, 100 µM and flumazenil at 500 nM. Test compounds 64 (GL-III-36), 65 (GL-III-76), 66 (GL-III-73), 67 (GL-III-78), 69 (GL-III-76A), 80 (GL-III-72) and 82 (GL-III-77), were screened at 50 µM with 1 µM GABA in mouse microglia activated with 150 U/mL IFNγ and 50 ng/mL LPS, along with 100 nM dexamethasone as a positive control and 1 mM CBT as a cytotoxicity control. Unpublished data.

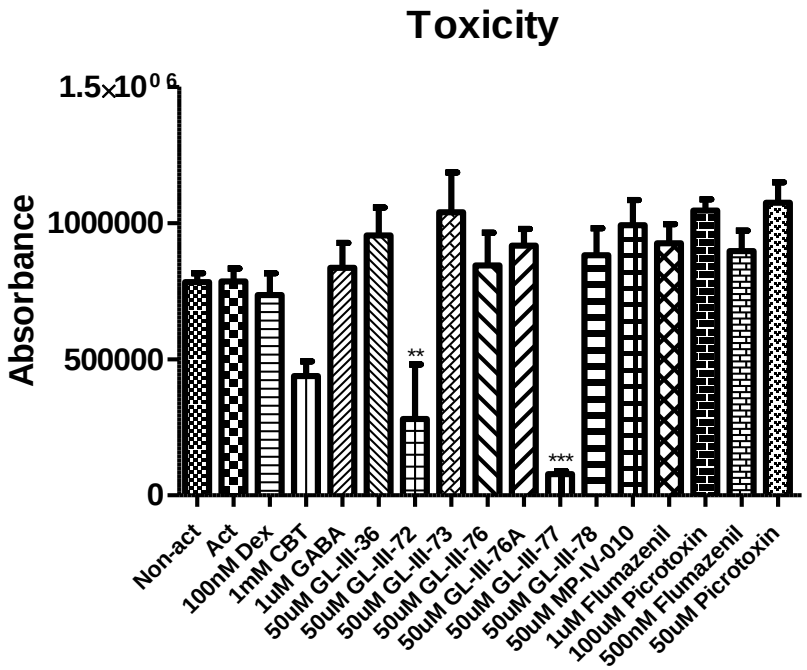

Figure 45. Cytotoxicity via the Cell-Titer Glo Assay for oxazole compounds 64 (GL-III-36), 65 (GL-III-76), 66 (GL-III-73), 67 (GL-III-78), 69 (GL-III-76A), 80 (GL-III-72) and 82 (GL-III-77), as well as GABA$_A$R antagonist picrotoxin at 50, 100 µM and flumazenil at 500 nM. Control compounds dexamethasone and CBT were run at concentrations of 100 nM and 1 mM respectively. Unpublished data.

2.2.3.5.2. Behavioral Studies in an Animal Models of Schizophrenia

To study the neurobiological basis of schizophrenia, a series of animal models have been developed and applied during the past decades for further design of novel drugs. All currently available animal models of schizophrenia can be classified into four categories: neurodevelopmental models during the perinatal period such as MAM and post-weaning social isolation; drug-induced pharmacological models such as amphetamine- or PCP-induced models; lesion models such as neonatal ventral hippocampal lesions; or genetic manipulation models using knock-out mice.[148] Several IMDZs synthesized in the Milwaukee research lab were evaluated in the previously utilized animal models for their effects on the potential treatment of schizophrenia, such as the MAM model,[95-96] the amphetamine-induced hyperactivity in poly (I:C) animal model[102] as well as the PPI of the acoustic model.[90]

Recently, another drug-induced pharmacological model, the NMDA antagonist MK-801-induced hyper-locomotor model, was applied as an activity to combat model for the selection of novel ligands that possess the symptoms of schizophrenic. It has been reported that reduction of the parvalbumin-immunoreactive GABAergic interneurons is related to the onset of schizophrenia during the neurodevelopmental process.[149] The proliferation of these interneurons is affected by glutamate through the mediation of NMDA receptors, the major excitatory neurotransmitter receptors. By blocking the NMDA receptors, the neurodevelopment of the GABAergic system would be influenced, which would further lead to a hyperlocomotive response to the noncompetitive NMDA receptor antagonists such as PCP or MK-801, as well as dopamine receptor agonists such as methamphetamine.[150]

The aim of this preclinical study was to assess the putative anti-schizophrenic-like properties of four novel α5-containing GABA (A) receptor PAM, **64** (GL-III-36), **65** (GL-III-76),

66 (GL-III-73), and **67** (GL-III-78), by measuring their influence on MK-801-induced hyperlocomotion as an animal model of schizophrenia, as well as evaluation on basal motor activity in the spontaneous locomotor activity assay (SLA) in C57BL6 mice, as a measure of anxiolysis.

In regards the behavioral parameter, total distance traveled in the SLA, as shown in Figure 46, all the ligands are brain-penetrant and behaviorally active, but with pretty different types of their respective interactions with MK-801. It can be concluded that **66** did not influence the MK-801-induced hyperlocomotion, ligands **64** and **67** partially decreased this effect; however, ligand **65** managed to completely reduce the hyperlocomotor and bring it down to the level of the control animals. None of the compounds alone produced significant sedation when compared to controls.

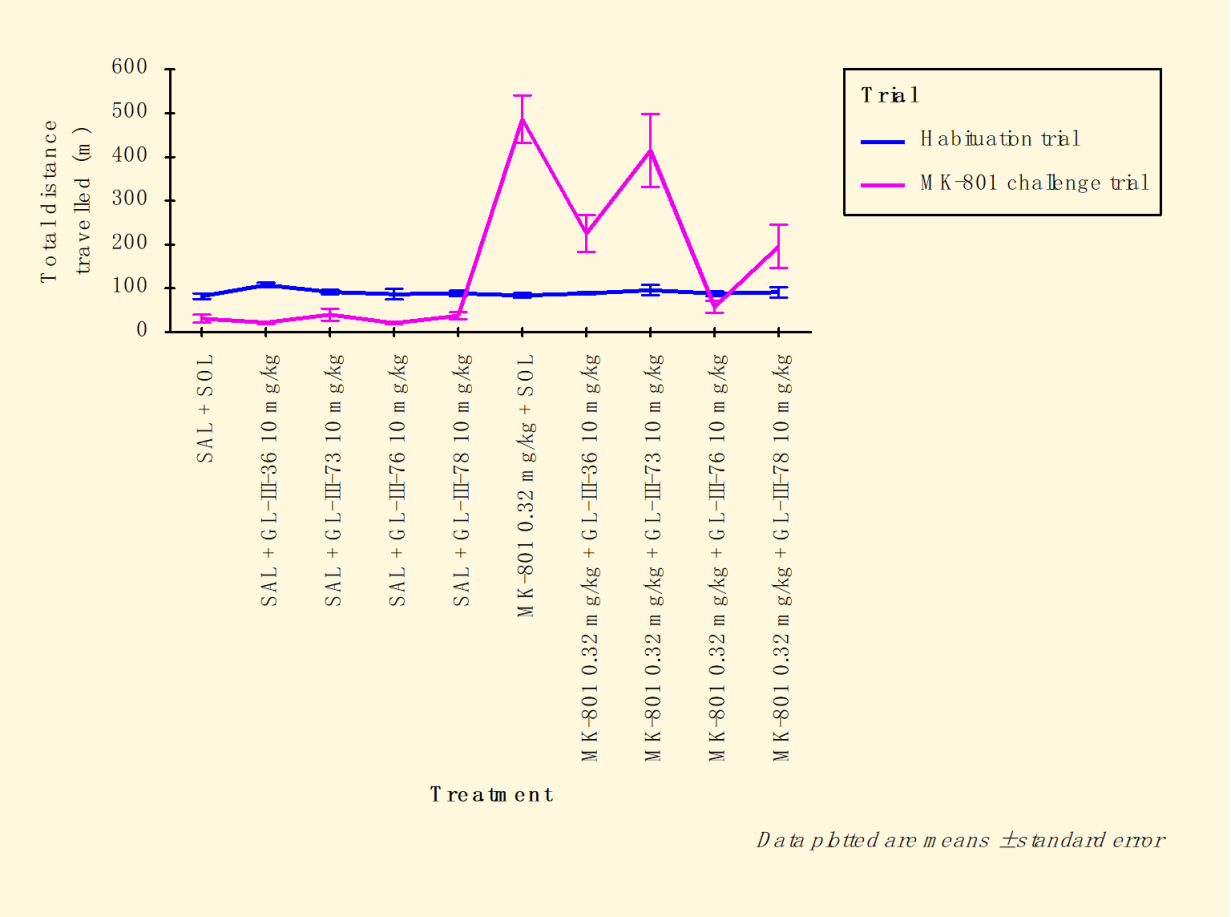

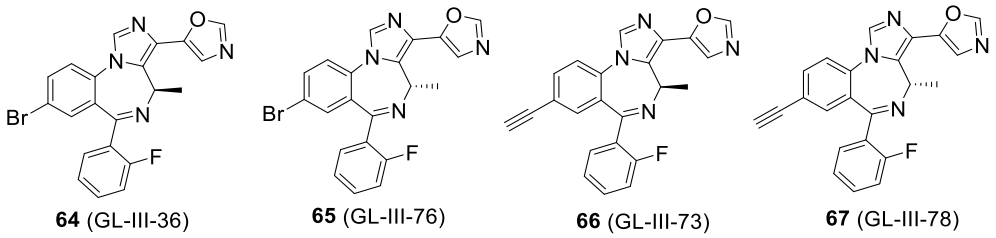

Figure 46. Total distance traveled in the MK-801-induced hyper-locomotor model. The data analyzed has been limited in the following way: Treatment = SAL + SOL, SAL + GL-III-36 10 mg/kg, SAL + GL-III-73 10 mg/kg, SAL + GL-III-76 10 mg/kg, SAL + GL-III-78 10 mg/kg, MK-801 0.32 mg/kg + SOL, MK-801 0.32 mg/kg + GL-III-36 10 mg/kg, MK-801 0.32 mg/kg + GL-III-73 10 mg/kg, MK-801 0.32 mg/kg + GL-III-76 10 mg/kg or MK-801 0.32 mg/kg + GL-III-78 10 mg/kg and Trial = Habituation trial or MK-801 challenge trial. Unpublished data.

The average speed in the MK-801-induced hyper-locomotor paradigm is another behavioral parameter that demonstrated similar results as did the total distance traveled. The *R*-isomer analogs **64** and **66** exhibited a higher average speed than the corresponding *S*-isomer analogs **65** and **67**. Furthermore, the C(8)-bromo ligands indicated a lower average speed than the ethinyl analogs in both series of assays. In summary, a similar pattern was observed in both parameters, that **65** brought the speed level down to nearly the same level as the control animals, as presented in Figure 47.

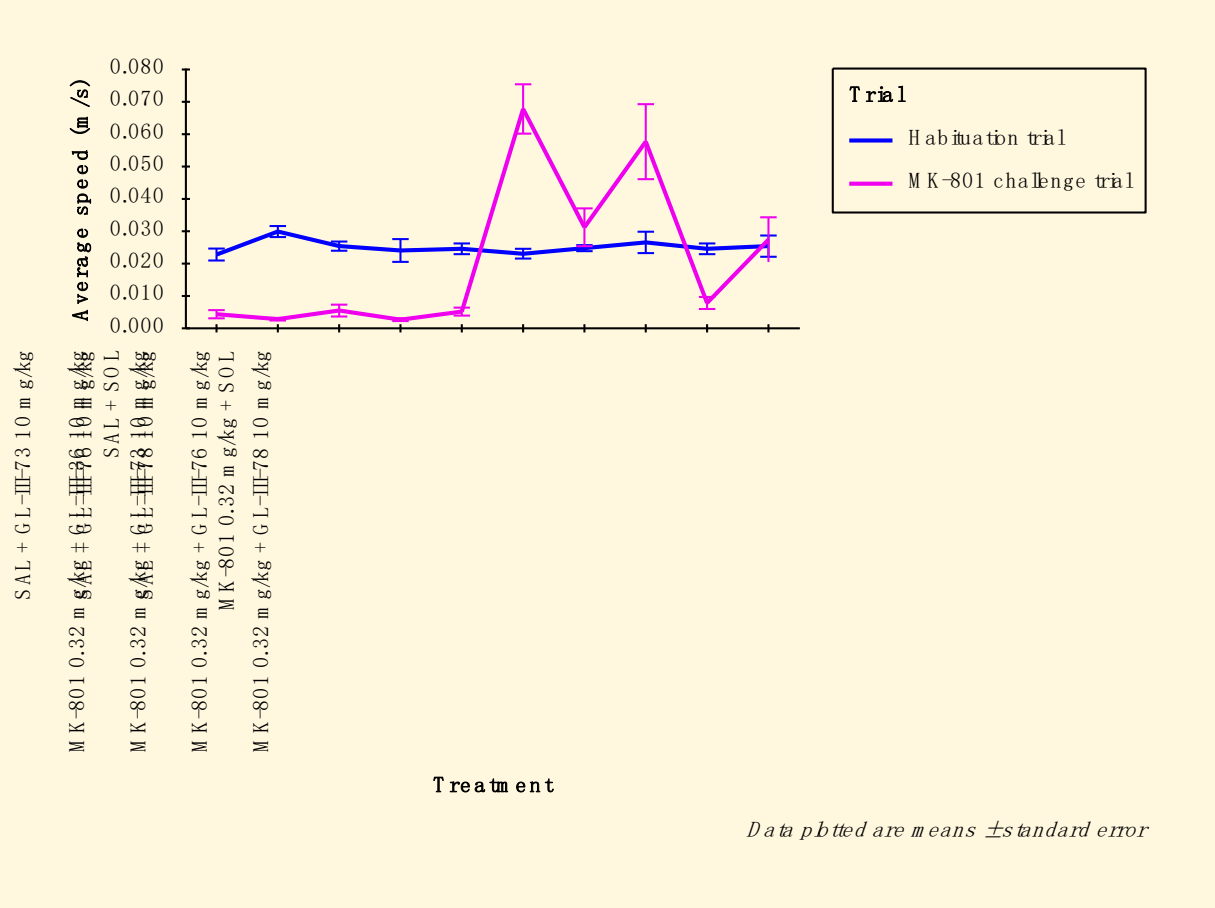

Figure 47. Average speed in the MK-801-induced hyper-locomotor model. The data analyzed has been limited in the following way: Treatment = SAL + SOL, SAL + GL-III-36 10 mg/kg, SAL + GL-III-73 10 mg/kg, SAL + GL-III-76 10 mg/kg, SAL + GL-III-78 10 mg/kg, MK-801 0.32 mg/kg + SOL, MK-801 0.32 mg/kg + GL-III-36 10 mg/kg, MK-801 0.32 mg/kg + GL-III-73 10 mg/kg, MK-801 0.32 mg/kg + GL-III-76 10 mg/kg or MK-801 0.32 mg/kg + GL-III-78 10 mg/kg and Trial = Habituation trial or MK-801 challenge trial. Unpublished data.

The results on total time immobile in the MK-801-induced hyper-locomotor model, again, is consistent with other behavioral parameters. The MK-801 induced hyperlocomotor activity was reduced by all four ligands, which resulted in increasing the time immobile, as compared to the MK-801 challenged animals, as depicted in Figure 48. The *S*-C(8)-bromo oxazole **65** exhibited the longest time immobile, as compared to the other three ligands, which almost reached control levels. The total time animals were mobile was the opposite to the total time immobile, which aligned well to the total distance traveled. Ligand oxazole **65** experienced the least mobile time and shared the same pattern as in other parameters, as shown in Figure 49.

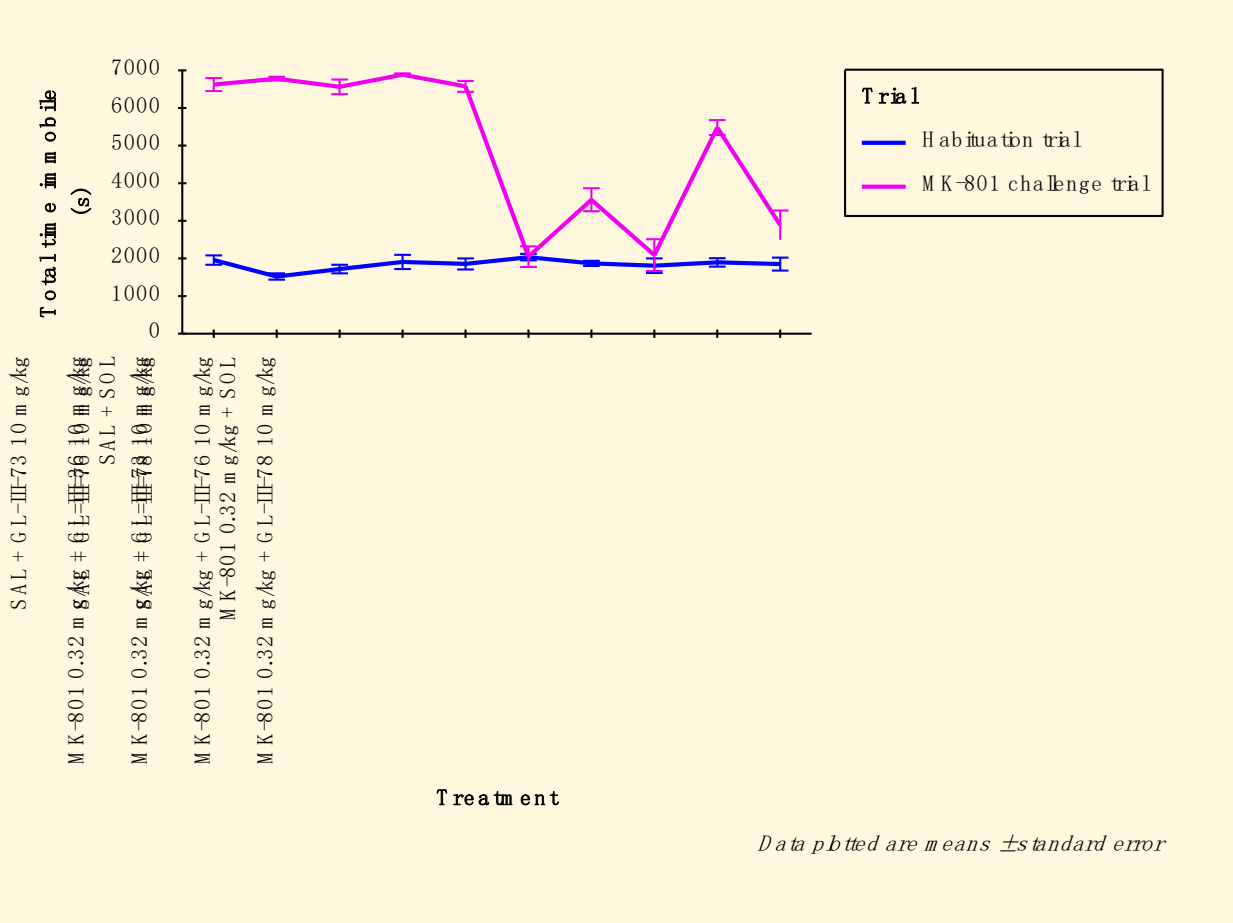

Figure 48. Total time immobile in the MK-801-induced hyper-locomotor model. The data analyzed has been limited in the following way: Treatment = SAL + SOL, SAL + GL-III-36 10 mg/kg, SAL + GL-III-73 10 mg/kg, SAL + GL-III-76 10 mg/kg, SAL + GL-III-78 10 mg/kg, MK-801 0.32 mg/kg + SOL, MK-801 0.32 mg/kg + GL-III-36 10 mg/kg, MK-801 0.32 mg/kg + GL-III-73 10 mg/kg, MK-801 0.32 mg/kg + GL-III-76 10 mg/kg or MK-801 0.32 mg/kg + GL-III-78 10 mg/kg and Trial = Habituation trial or MK-801 challenge trial. Unpublished data.

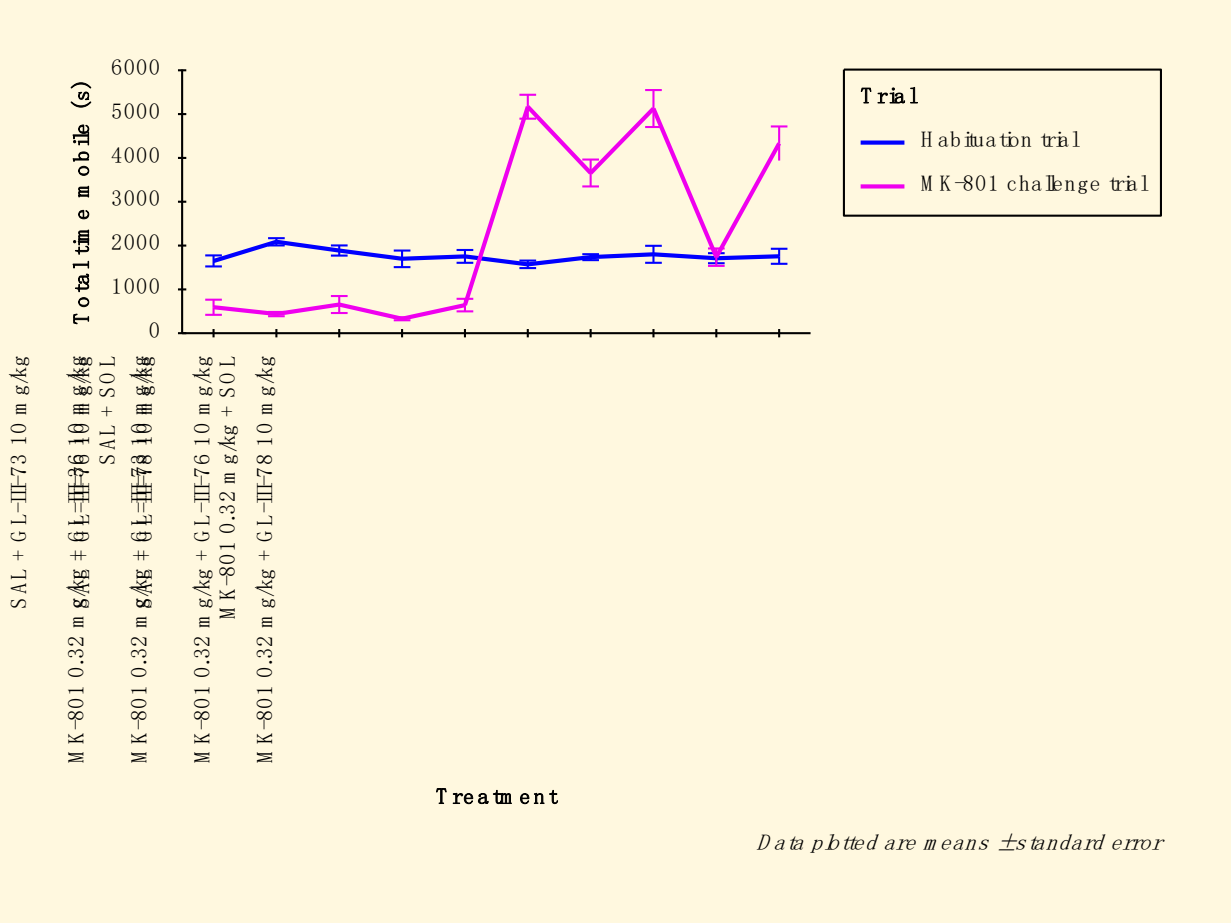

Figure 49. Total time mobile in the MK-801-induced hyper-locomotor model. The data analyzed has been limited in the following way: Treatment = SAL + SOL, SAL + GL-III-36 10 mg/kg, SAL + GL-III-73 10 mg/kg, SAL + GL-III-76 10 mg/kg, SAL + GL-III-78 10 mg/kg, MK-801 0.32 mg/kg + SOL, MK-801 0.32 mg/kg + GL-III-36 10 mg/kg, MK-801 0.32 mg/kg + GL-III-73 10 mg/kg, MK-801 0.32 mg/kg + GL-III-76 10 mg/kg or MK-801 0.32 mg/kg + GL-III-78 10 mg/kg and Trial = Habituation trial or MK-801 challenge trial. Unpublished data.

The examination of these results suggests that oxazole **65** exhibited strong anti-schizophrenic-like activity in the murine model of MK-801 induced hyperlocomotion, while devoid of sedative properties. It is planned to run a basic kinetic study on these four ligands. It appears that **65** may be especially interesting with respect to its potential development as an anti-psychotic drug. However, behavioral parameters total mobile/immobile episodes and rotations of the animal's body require further analysis. The statistical data and related figures are included in Appendix IV.

2.2.3.6. Depression

2.2.3.6.1. Elevated Plus Maze to Determine Anxiolytic Effects

The elevated plus maze (EPM) is a one of the most commonly used anxiety behavioral models that employed to screen most GABA-related putative anxiolytic compounds, such as IMDZs. Based on the rodents' nature to avoid open spaces indicating anxiety, the anxiolytic effect is determined if the rodent spends more time in the open space, which is used to calculate the percentage of time in the open arms of EPM over the total time.[151] Animals who are anxious do not go out and explore the open spaces in the arms of the EPM.

The key chiral ligands **36, 37, 38,** and the control DZP were evaluated in the EPM assay for observation of anxiolytic properties. The test results are presented in Figure 50. As shown, administration of amides **36** and **37** demonstrated a significant increase in time spent in the open arms of the maze after i.p. administration of 10 mg/kg ($p < 0.03$), whereas ligand **38** did demonstrate an increase but it did not reach significance ($p = 0.07$). The well-known anxiolytic DZP induced a significant increase of time spent in the open arm spaces ($p = 0.02$) at 1.5 mg/kg, as expected.

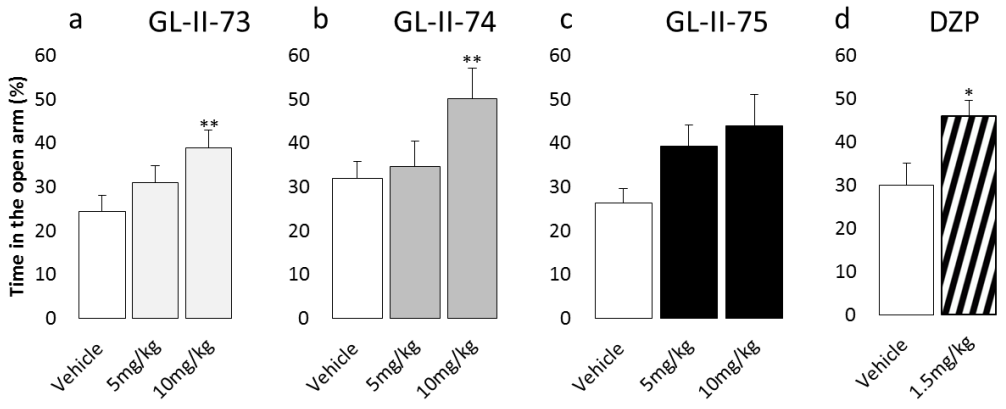

Figure 50. Anxiolytic-like properties of novel ligands 36-38 as compared to DZP. Potential anxiolytic IMDZ ligands (a) GL-II-73 (36), (b) GL-II-74 (37), and (c) GL-II-75 (38) at 5 or 10 mg/kg and DZP (1.5 mg/kg; d) were assessed in mice (50% females) in the EPM test. Mice received either vehicle or the test compound 36

(n(0) = 13, n(5) = 13, and n(10) = 14), 37 (n(0) = 14, n(5) = 13, and n(10) = 14), 38 (n(0) = 13, n(5) = 14, and n(10) = 13), or DZP (n(0) = 11 and n(1.5) = 10) 30 min before testing. Possible anxiolytic effects were indicated by an increase in time spent in the open arms of the EPM. Sex was not significant factor (p ≥0.17) as a cofactor. (Modified from the figure in Prevot et al.)[117]

The related analogs synthesized later included **31, 36-38: 39** (GL-III-66), **46**(GL-III-67), **47** (GL-III-70), **48** (GL-III-68), **54** (GL-III-64), **58** (GL-III-60), and **61** (GL-III-63). These analogs were also evaluated for their potential anxiolytic effects in the EPM. Together with the test compounds, an α5 selective NAM, MRK-016, was also included in the screening panel to determine whether this antidepressant compound possessed any anxiolytic effects. The test results are presented in Figure 51. After 10 mg/kg i.p. administration of the test compounds, only the C(8)-bromo ethyl amide **48** induced a significant anxiolytic-like effect in the EPM, as opposed to all the other test compounds including MRK-016.

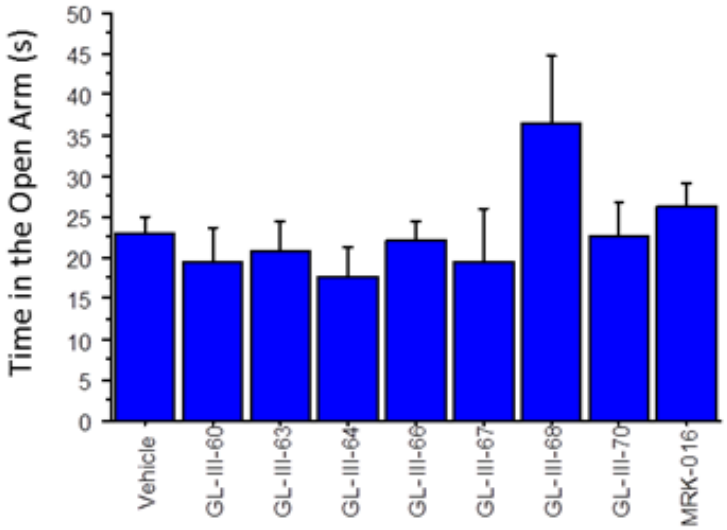

Figure 51. Anxiolytic-like properties of the ligands of GL-III series and the NAM (MRK-016) in the elevated plus maze at 10 mg/kg, i.p. administration. Unpublished data.

2.2.3.6.2. The Forced Swim Test to Assess Antidepressant Properties of the Ligands

The forced swim test (FST) is a widely used behavioral assay for the assessment of potential antidepressant-like properties of test compounds in rodents. The antidepressant effect in the FST is characterized by a decrease in the time spent immobile and as compared to the movement for the animal to stay afloat in an inescapable transparent tank. The tank is filled with water to a level that the animal is not capable of standing at the bottom or escaping. The escape related behavior of the animal is recorded and analyzed. The success of the FST results from its straightforward and easy handling procedure, also a minimum requirement for specialized equipment, and the reduced unwarranted stress to the animals. Therefore, the selective compounds from the first batch, which possessed good PK value, decreased CNS side effect, low cytotoxicity, stable metabolism, as well as a good $GABA_AR$ efficacy and binding profile, were evaluated in the FST for their potential antidepressant-like activity. This is a very select group of compounds.

The first batch of ligands, amides **36-38** all exhibited an antidepressant effect in the FST by reducing the time spend immobile of the animals in the water tank, which represented an antidepressant property of the test compounds, as depicted in Figure 52. The dimethyl amide **36** significantly reduced the immobility at 10 mg/kg, whereas the other two amides **37** and **38** started to show the antidepressant effect at a lower dosage of 5 mg/kg. In contrast, the classic non-selective DZP significantly increased the immobility, which is probably a result of its hyperlocomotor side effects of sedation and ataxia since it greatly potentiates α1-containing $GABA_ARs$ greatly, therefore it is possible the antidepressant effect was precluded. It is now known this is true. Witkin, Babu et al. demonstrated if given diazepam admixed with the α1 preferring antagonist bCCt, the mixture is antidepressant in the FST (paper published).

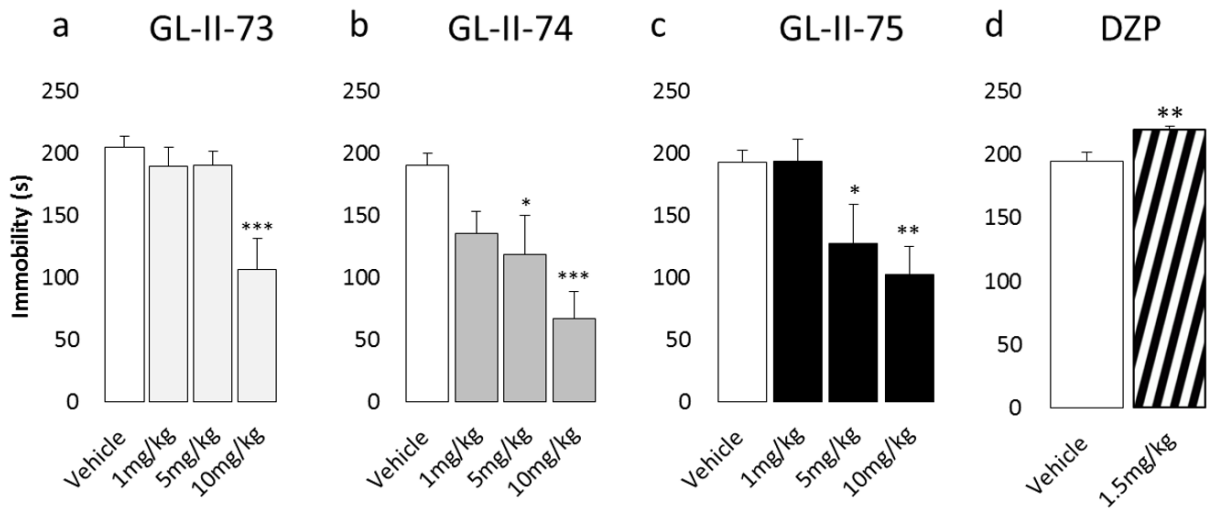

Figure 52. Antidepressant properties of 36-38. Potential antidepressant effect of IMDZ ligands 36 (a), 37 (b), and 38 (c) at 1, 5 or 10 mg/kg and DZP (1.5 mg/kg; d) was assessed in male mice in the FST after i.p administration. An inescapable transparent tank filled with water was used to place the mice (25 cm, 26 ± 1 °C) for 6 minutes. The minimum amount of movement for staying afloat indicated the immobility, between 2-6 min testing period. and the sixth minute of testing. (36: n(0) = 8, n(1) = 8, n(5) = 6, and n(10) = 8; 37: n(0) = 8, n(1) = 8, n(5) = 8, and n(10) = 8; 38: n(0) = 8, n(1) = 8, n(5) = 8, and n(10) = 9) or DZP (n(0) = 12 and n(1.5) = 12). The potential antidepressant-like profile was indicated by any significant decrease of immobility induced by the test compound. * p < 0.05, ** p < 0.01, and *** p < 0.001 compared to vehicle. All values are represented as mean ± standard error of the mean. (Modified from the Figure in Prevot et al.)[117]

The second batch of oxadiazoles and amides were evaluated for their antidepressant effects as well. However, only two ligands exerted the desired effect. Please see Table 17 for the results of the FST on all test compounds assayed to date. The C(8)-bromo methyl oxadiazole in the 2'N series **53** (GL-II-54) exhibited a decrease in immobility at 10 mg/kg, as presented in Figure 53 A. The enantiomer of **36** (GL-II-73), the dimethyl amide in the *S* series **30** (GL-I-54), significantly reduced the time spent immobile at a lower dose, 5 mg/kg, as compared to the control vehicle, as shown in Figure 53 B.

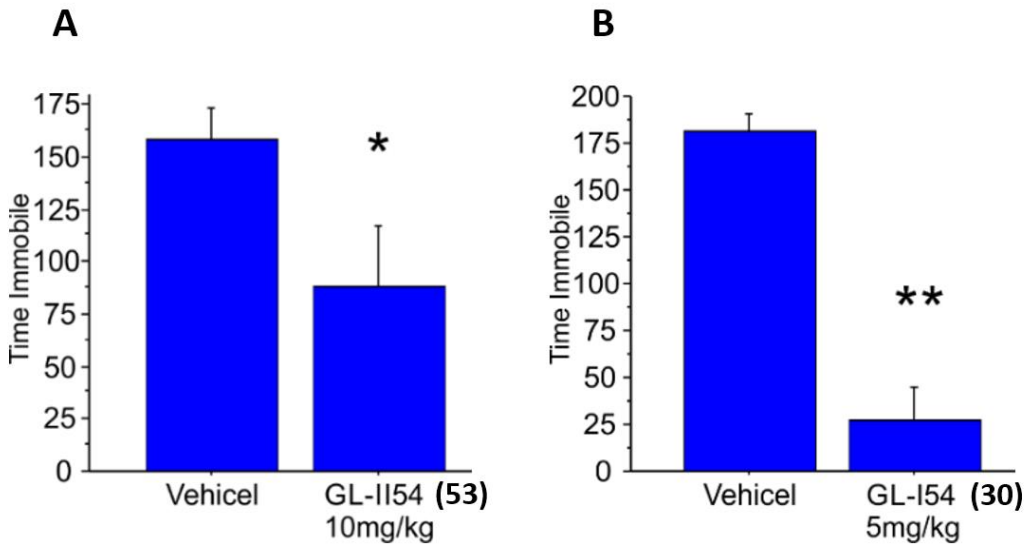

Figure 53. Effect of 53 (GL-II-54) and 30 (GL-I-54) on time spent immobile in the FST. The ligand 53 (A) at 10 mg/kg, and the ligand 30 (B) at 5 mg/kg i.p. administered (24, 20, 1 h before testing) induced a significant antidepressant-like action when compared to the vehicle group (n = 9). *p<0.05 and ***p<0.001 when compared to the vehicle group. Unpublished data.

The results of all the compounds that were assessed in the FST, are summarized in Table 17. The parent compound **1,** which is the first reported antidepressant IMDZ, showed the desired effect at 30 mg/kg due, presumably, to its good α5 subtype selectivity. The *S*-isomer **2,** the enantiomer of **1**, did not show any effect due to the fast-metabolic rate of this ligand. The first amide analog prepared **35** had an improved α5 subtype preference and demonstrated a better antidepressant effect at a lower dosage 10 mg/kg, as compared to the lead compound **1.** The enantiomer of **35**, the *S*-methyl amide **25**, did not produce an antidepressant effect due to the sedative effect by **25** on the animal. The amides **36-38** from the *R* series, as described above, significantly reduced the immobility, as well as did the *S*-isomer, dimethyl amide **30**. The other amides **49** and **50** did not display any effect due to the sedating side effects or they were just inactive. The only oxadiazole that exhibited an antidepressant property was **53** (GL-II-54), the C(8)-bromo methyl oxadiazole in the 2'N series (10 mg/kg).

Table 17. Antidepressant effect of all test compounds in the FST. Unpublished data.

Genus	Compound	Forced Swim Test Result			
		Dose	Admin. route	Observation	Global Effect
Ester	**1** (SH-053-2'F-R-CH3)	30 mg/kg	ip	Antidepressant	**Antidepressant +**
	2 (SH-053-2'F-S-CH3)	ND (fast metabolism)			
Amide	**35** (MP-III-022)	10 mg/kg	ip	Antidepressant	**Antidepressant +**
	25 (MP-III-023)	10 mg/kg	ip	SEDATION	SEDATION
	36 (GL-II-73)	1 mg/kg	ip	No effect	**Antidepressant +**
		5 mg/kg		No effect	
		10 mg/kg		Antidepressant	
	30 (GL-I-54)	5 mg/kg	ip	Antidepressant	**Antidepressant ++**
	37 (GL-II-74)	1 mg/kg	ip	No effect	**Antidepressant ++**
		5 mg/kg		Antidepressant	
		10 mg/kg		Antidepressant	
	38 (GL-II-75)	1 mg/kg	ip	No effect	**Antidepressant ++**
		5 mg/kg		Antidepressant	
		10 mg/kg		Antidepressant	
	40 (GL-II-76)	ND (low brain fraction)			
	49 (RV-II-04)	10 mg/kg	ip	SEDATION	SEDATION
	50 (GL-II-31)	10 mg/kg	ip	No effect	No effect
Oxadiazole	**31** (GL-I-65)	10 mg/kg	ip	No effect	No effect
	51 (GL-II-33)	10 mg/kg	ip	No effect	No effect
	52 (GL-III-23)	10 mg/kg	ip	No effect	No effect
	53 (GL-II-54)	10 mg/kg	ip	Antidepressant	**Antidepressant +**

ND: not determined. Significance was indicated by + or ++.

2.2.3.6.3. Evaluation of Spatial Working Memory by the Y-maze Test

During the past few decades, altered GABAergic function has been continually reported in related to aging, as well as neurodegenerative and psychiatric disorders. Somatostatin (SST) co-expressed GABA interneuron deficits are associated with MDD, other mood symptoms, and cognition.[152] Since SST signaling occurs partially through the $GABA_AR$s system in the prefrontal cortex in the CNS. This implicates GABA in systems in the regulation of mood and cognition.[153] Therefore, it is hypothesized that an enhancement of the response of $GABA_AR$s might have the

potential to improve cognitive dysfunction, which is a key feature that is usually disrupted in patients with depression, schizophrenia, and neurodegenerative diseases. The spontaneous alternation Y-maze is broadly used for the evaluation of short-term spatial working memory by utilizing the exploratory nature of rodents. A series of IMDZs were assessed in the Y-maze test for their potential pro-cognitive effects.

2.2.3.6.3.1. Reversal of Stress-Induced Working Memory Deficits

Adult mice subjected to chronic restraint stress (CRS) are known to undergo working memory impairment, which can be identified in the spontaneous alternation Y-maze task. The injection of vehicle or test compounds **36-38** can be administrated at different doses, as demonstrated in Figure 54. The mice exposed to CRS exhibited a reduction of alternation rates, as compared to the vehicle control mice. The alternation rate of the 10 mg/kg **36-**treated animal was significantly brought back up to a similar level of the non-CRS vehicle control mice. ($p = 0.01$). However, at the lower dose of 1-5 mg/kg of amide **36** administrated to mice, did not have an effect on the CRS mice. On the contrary, the administration of **37** reduced the alternation rate of mice at 5 and 10 mg/kg, which indicated it was inactivity on working memory at these doses ($p > 0.97$). The alternation rate in mice treated with **38** was reversed to the level of the vehicle control group at 5 and 10 mg/kg ($p < 0.045$), which indicated it was active in this Y-maze assay. The cognitive deficits were not restored with the treatment of DZP at 1.5 mg/kg, as expected ($p = 0.94$). In a parallel experiment, the baseline effect in non-CRS mice was tested, as depicted in Figure 55. The ligands **36 and 38** did not induce any effect on the alternation rates at both 5 and 10 mg/kg. However, a decrease in the alternation rate was observed in the animals on the administration of

10 mg/kg of **37** or 1.5 mg/kg of DZP, which would indicate a detrimental influence on working memory or sedation, both of which could be elicited by a PAM interaction at $\alpha1\beta3\gamma2$ subtypes.

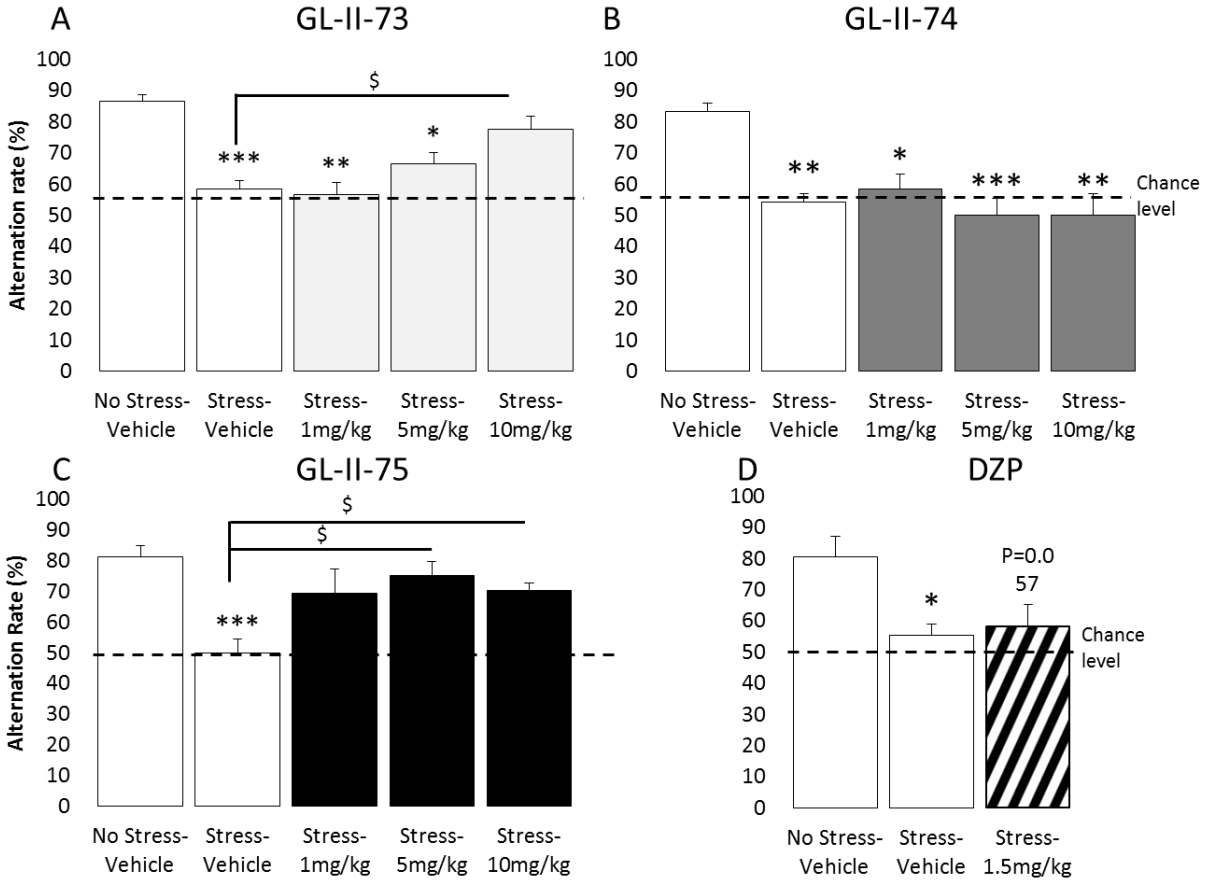

Figure 54. Pro-cognitive effect of ligands 36-38 on working memory impairment induced by stress. The spontaneous alternation Y-maze task was employed to determine the effects on working memory using a 90-second intertrial interval. The cognitive deficit was introduced by exposing mice to daily CRS, 1 h twice a day for 1 week before the experiment. Young mice (50% females) received i.p. administrated vehicle or 1, 5, or 10 mg/kg of 36 (a; n(0-NS) = 10, n(0-S) = 10, n(1) = 5, n(5) = 10, n(10) = 12), for 37 (b; n(0-NS) = 8, n(0-S) = 8, n(1) = 4, n(5) = 10, n(10) = 4), 38 (c; n(0-NS) = 8, n(0-S) = 8, n(1) = 6, n(5) = 4, n(10) = 9), and DZP (d; n(0-NS) = 6, n(0-S) = 6, n(1.5) = 6) 30 min prior testing. * $p < 0.05$, ** $p < 0.01$, *** $p < 0.001$ compared to "No stress vehicle." Effect of the ligand: $ $p < 0.05$ compared to "Stress vehicle" (Adopted from the figure in Prevot et al.)[117]

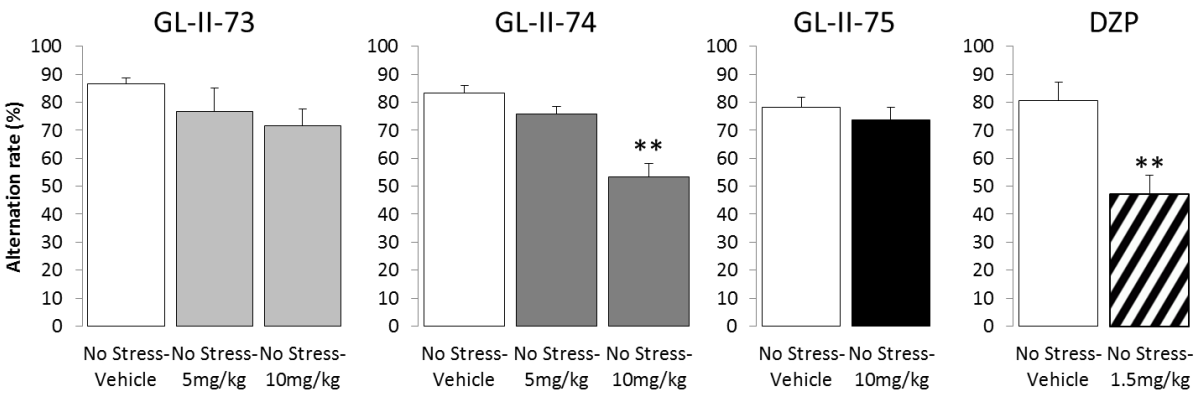

Figure 55. Effect of 36-38 and DZP on alternation rate in a spontaneous alternation Y-maze task to evaluate the potential cognitive deficit under baseline conditions induced by test compounds at 5 or 10 mg/kg, or 1.5mg/kg of DZP in non-CRS mice. Prior to 30 min for the test, the i.p. injection of PAM or DZP was administrated. A reduced alternation rate was only seen in mice treated with 10 mg/kg of 37, as compared to DZP. **p<0.001 compared to the "No Stress-Vehicle" group. (Adopted from the figure in Prevot et al.)[117]

In addition to the amide ligands **36-38,** several of their analogs were also evaluated in the Y-maze test for possible pro-cognitive effects. The enantiomer of **36, 30** (GL-I-54) restored the alternation rates at 5 and 10 mg/kg, which is very similar to the data for **36**, as presented in Figure 56**.** Although CRS animals administered with **30** at 5 and 10 mg/kg were not statistically different from the CRS vehicle groups, they were also not statistically different from the vehicle control group either. However, administration of the *S*-dimethyl amide **30** at 10 mg/kg was significant when using the Student post hoc test (p=0.02).

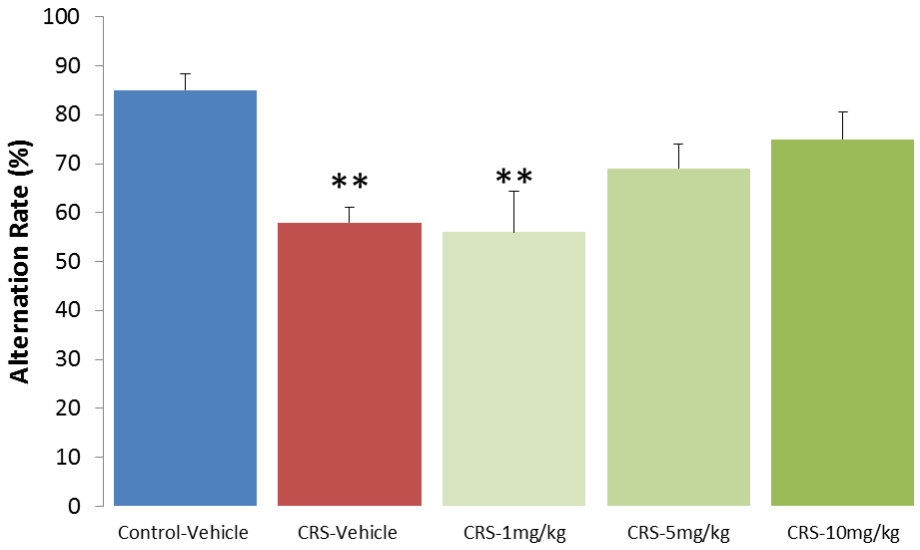

Figure 56. Effect of 30 (GL-I-54) on the percent alternation rate in the Y-maze spatial alternation task assessing working memory in mice. Mice subjected to CRS were injected with 30 (0, 1, 5, 10 mg/kg) i.p. 30 min before testing). ANOVA revealed statistical significance on the overall effect of stress and treatment with 30 at 5 and 10 mg/kg. Differences between groups were tested using the posthoc analysis of Scheffe (p<0.01 compared to the "Control-Vehicle" group) n=5-9. Unpublished data.**

The results of administration of the racemic mixture of **36 + 30** on CRS-mice demonstrated significant differences between groups (ANOVA: F(2,10)=16.82; p=0.0006). The CRS animals exhibited a significant reduction in working memory and the CRS mouse group injected with the racemic mixture (**36 + 30**) were statistically different from the CRS-vehicle group, as indicated in Figure 57. Administration of the racemic mixture of **36+30** (GL-II-73 and GL-I-54) produced a reversal of the cognitive impairment induced by CRS. This effect (p=0.003) was more significant than that of the pure amide **36** alone (p = 0.01), at the same dose (10 mg/kg), as compared to the CRS-vehicle group, which can result from the fast-acting profile of **30.** This data suggested an alternative approach, using the mixture of *R* and *S* dimethyl amide (**36** and **30**), to achieve a more significant effect on the alternation rate in the Y-maze task.

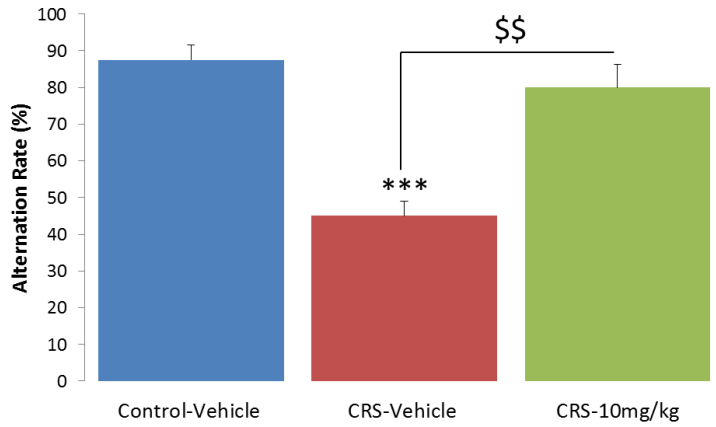

Figure 57. Effect of the racemic mixture of 36/30 (GL-II-73/GL-I-54) on percent alternation rate in the Y-maze spatial alternation task assessing working memory in mice. Mice subjected to CRS were injected with the racemic mixture solution (10 mg/kg, ip., 5 mg/kg each enantiomer, 30 min before testing) or vehicle. ANOVA revealed statistical significance on the overall effect of manipulation. Differences between groups were tested using the posthoc analysis of Scheffe (*p<0.001 compared to the "Control-Vehicle" group / $$p<0.01 compared to the "CRS-Vehicle" group). n=4-5. Unpublished data.**

Besides amide analogs related to GL-II-73 (**36**), oxadiazoles were also assessed in the Y-maze test. Analysis of the data showed significant differences between groups for **31** (GL-I-65) and **51** (GL-II-33) at 10 mg/kg, respectively (ANOVA: **31** $F(2,28)=5.38$; $p=0.0105$, **51** $F(2,11)=4.2$; $p=0.0439$), as presented in Figure 58. Scheffe post hoc analysis revealed decreased performance in the CRS-vehicle treated animals (**31:** $p=0.012$; **51** $p=0.05$) and an increase in alternation rate after **31** or **51** (10 mg/kg) not significantly from the control-vehicle group, which indicated a pro-cognitive effect. Although **31** and **51** mouse groups were not statistically different from the CRS-vehicle mouse group using the Scheffe post hoc analysis ($p=0.12$, $p=0.16$), a significant effect was detected when using the Student post hoc test ($p=0.04$, $p=0.06$).

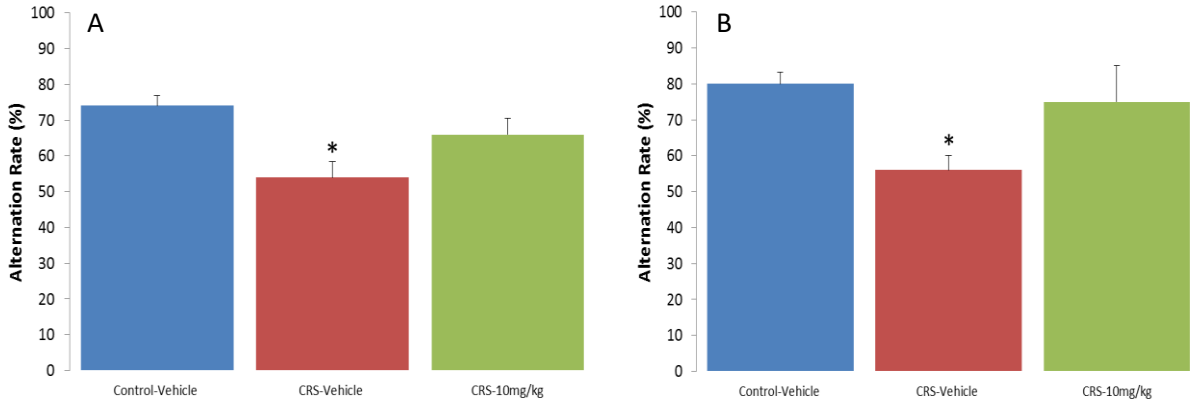

Figure 58. The effect of GL-I-65 (A) and GL-II-33 (B) on the percent alternation rate in the Y-maze spatial alternation task assessing working memory in mice. The mice subjected to the CRS were injected with GL-I-65 or GL-II-33 (10 mg/kg, i.p., 30 min before testing). ANOVA revealed statistical significance on the overall effect of manipulation. The CRS animals showed a significant reduction of working memory performance and the CRS mouse group injected with GL-I-65 were not statically different from the control-vehicle group. Differences between groups were tested using the posthoc analysis of Scheffe (*p<0.05 compared to the "control-vehicle" group) n=9-11, n =4-5 for GL-I-65 and GL-II-33, respectively. (CRS = chronic restraint stress) Unpublished data.

The effects of **39, 46-48, 54, 58,** and **61** (GL-III-60/63/64/66/67/68/70) were assessed in the Y-maze alternation task, as shown in Figure 59. Two of the test compounds, **48** (GL-III-68), and (**58**) GL-III-60 had potential pro-cognitive effects in the stressed-induced working memory deficit, which requires further testing to be validated. The C(8)-cyclopropyl dimethyl amide **47** (GL-III-70), was confirmed with its pro-cognitive effect at different doses from 1, 5, and 10 mg/kg. Importantly, ligand **47** significantly reversed the alternation rates of the treated mice group, as compared to the CRS-vehicle treated mice and brought them back to the level of the non-CRS treated vehicle control group.

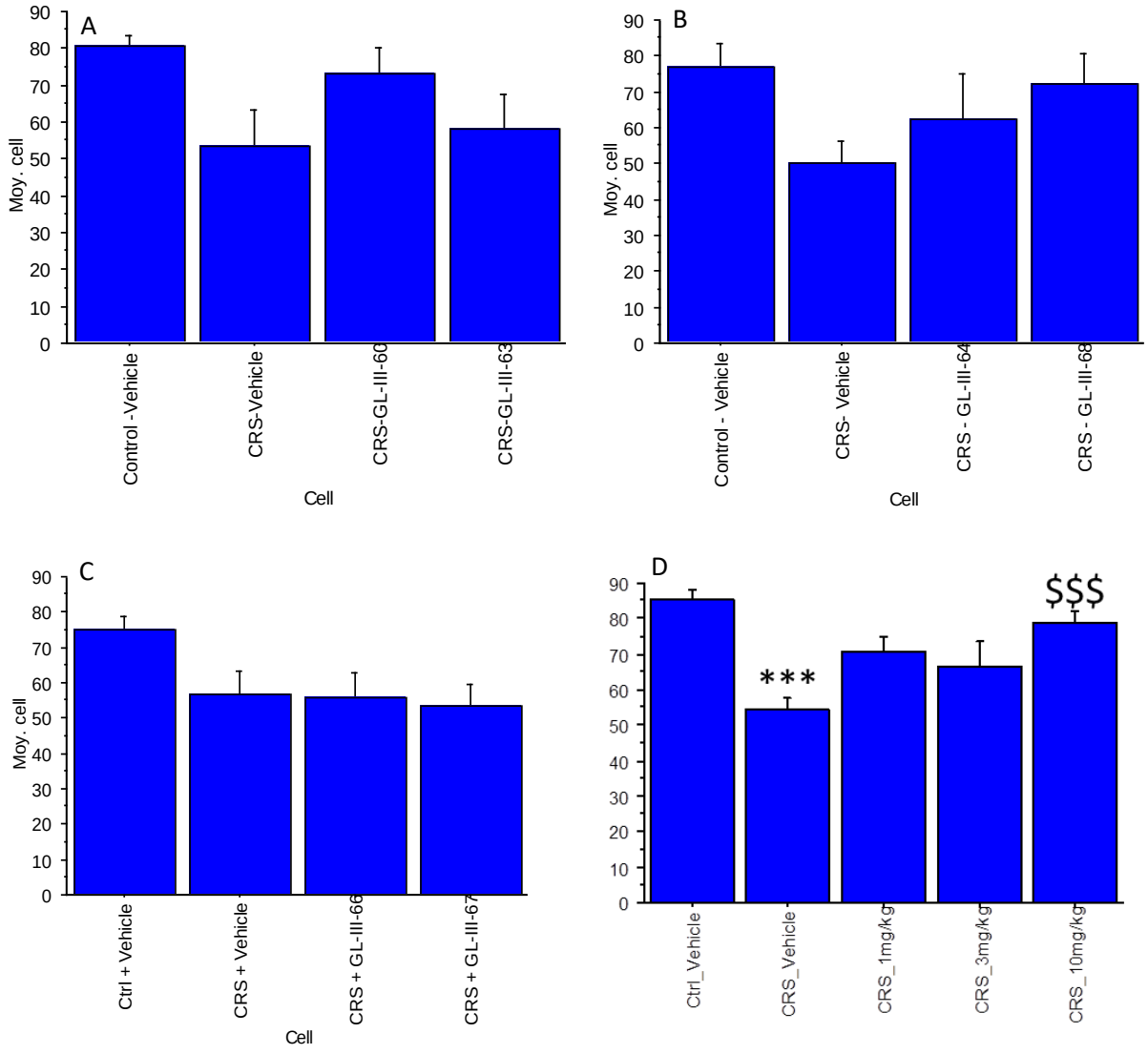

Figure 59. The effects of GL-III-70 (47) on the percent alternation rate in the Y-maze spatial alternation task assessing working memory in mice. The chronic restraint stress (CRS) paradigm was used to induce a working memory deficit in young (2-3 months) mice. The mice were injected with GL-III-70 (0, 1, 3, or 10 mg/kg) i.p. 30 min before testing. ANOVA revealed statistical significance on the overall effect of the treatment ($F(4,46)=15.008$; $p<0.0001$). Differences between groups were detected using post-hoc Scheffe analysis ($p<0.01$ and ***$p<0.001$ compared to the "Control-Vehicle" group / \$$p<0.05$ and \$\$\$$p<0.001$ compared to the "CRS-Vehicle" group). Unpublished data.**

This ligand **47** was further assessed in a parallel experiment with respect to the α5 NAM MRK-016. Both **47** and MRK-016 alone did not exhibit an effect as compared to the vehicle group, however, administration of both compounds significantly restored the alternation rates in the CRS-

mice to a similar level to the non-CRS vehicle group, as shown in Figure 60. This indicated ligand **47** might share a similar effect in Y-maze task as MRK-016.

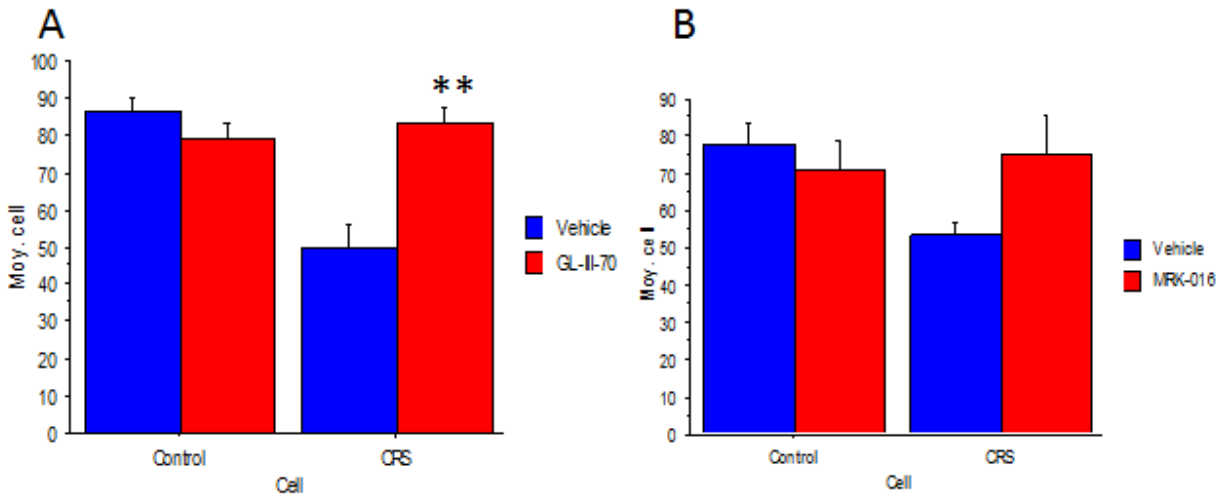

Figure 60. The pro-cognitive efficacies of GL-III-70 (10mg/kg) and the NAM MRK-016 in the Y-maze alternation task. Statistical data not shown, unpublished data.

As summarized in Table 18, the compounds described above were all active in the Y-maze test induced by CRS, however, the rest of the compounds in the screening panel did not restore the alternation rates after 5 or 10 mg/kg drug treatment. Two of the active compounds in the FST, such as **35** (MP-III-022) and **53** (GL-II-54), did not show any effect in the Y-maze test. Therefore, they were placed lower on the lead compound list, since cognitive dysfunction is one of the critical features in patients with depression or schizophrenia, it would be nice to successfully treat. On the other hand, the compounds only active in Y-maze test but not the FST, such as **31** (GL-I-65) and **51** (GL-II-33) would also put lower on the list of lead compounds because they were inactive in the FST. Indeed, several newer compounds have not been tested in the FST and will be evaluated for their antidepressant effect first, then based on those results the go/no go decision of whether to be studied on the next stage will be made. The compound **30** (GL-I-54) was active in both the FST and Y-maze but was not chosen because of the rapid metabolism rate in mice, only 19 % remaining

after 2 hours of incubation in the MLM. Therefore, only two compounds, **36** (GL-II-73) and **38** (GL-II-75) were carried on for future evaluation due to their desired pharmacological properties including antidepressant effects as well as an overall pro-cognitive effect.

Table 18. Summary of all compounds tested in the Y-maze task. Unpublished data.

Genus	Compound	Y-Maze Result			
		Dose	Admin. route	Observation	Global Effect
Ester	**1** (SH-053-2'F-R-CH3)	30 mg/kg	ip	No effect	No effect
	2 (SH-053-2'F-S-CH3)	ND (fast metabolism)			
Amide	**35** (MP-III-022)	5 mg/kg	ip	No effect	No effect
	25 (MP-III-023)	5 mg/kg	ip	No effect	No effect
	36 (GL-II-73)	1 mg/kg	ip	No effect	**Pro-cognitive +**
		5 mg/kg		No effect	
		10 mg/kg		Pro-cognitive	
		20 mg/kg		Pro-cognitive	
	30 (GL-I-54)	1 mg/kg	ip	No effect	**Pro-cognitive ++**
		5 mg/kg		Slight pro-cog	
		10 mg/kg		Pro-cognitive	
	37 (GL-II-74)	1 mg/kg	ip	No effect	No effect
		5 mg/kg		No effect	
		10 mg/kg		No effect	
	38 (GL-II-75)	1 mg/kg	ip	No effect	**Pro-cognitive ++**
		5 mg/kg		Pro-cognitive	
		10 mg/kg		Pro-cognitive	
	39 (GL-III-66)	10 mg/kg	ip	No effect	No effect
	40 (GL-II-76)	10 mg/kg	ip	No effect	No effect
	46 (GL-III-67)	10 mg/kg	ip	No effect	No effect
	47 (GL-III-70)	1 mg/kg	ip	Slight pro-cog	**Pro-cognitive ++**
		3 mg/kg		Slight pro-cog	
		10 mg/kg		Pro-cognitive	
	48 (GL-III-68)	10 mg/kg	ip	Pro-cognitive	**Pro-cognitive +**
	49 (RV-II-04)	5 mg/kg	ip	No effect	No effect
	50 (GL-II-31)	10 mg/kg	ip	No effect	No effect
Oxadiazole	**31** (GL-I-65)	10 mg/kg	ip	Pro-cognitive	**Pro-cognitive +**
	51 (GL-II-33)	10 mg/kg	ip	Pro-cognitive	**Pro-cognitive +**
	52 (GL-III-23)	10 mg/kg	ip	No effect	No effect
	53 (GL-II-54)	10 mg/kg	ip	No effect	No effect
	54 (GL-III-64)	10 mg/kg	ip	Slight pro-cog	Slight pro-cog
	58 (GL-III-60)	10 mg/kg	ip	Pro-cognitive	**Pro-cognitive +**

	61 (GL-III-63)	10 mg/kg	ip	No effect	No effect

ND: not determined. Significance was indicated by + or ++.

2.2.3.6.3.2. Reversal of Age-Induced Working Memory Deficits in the Y-maze Task

According to the results of the antidepressant effects from the FST and the stress-induced working memory deficits in the Y-maze task, **36** (GL-II-73) and **38** (GL-II-75) were further evaluated in the Y-maze task but induced by age on old male mice. The significant difference was observed among three groups, young, old, and drug-treated old mice group by ANVOAs ($F > 12.3$; $p < 0.0015$), as illustrated in Figure 61. The alternation rates of 22-month old mice were significantly lower than the young mice control group to the chance level, indicating the deleterious effects of cognition. The spatial working memory deficits were significantly restored on the administration of 5 mg/kg of **36** or **38**, to a level almost indistinguishable from the vehicle control group in young mice, as compared to the vehicle control group in old mice. ($p < 0.03$)

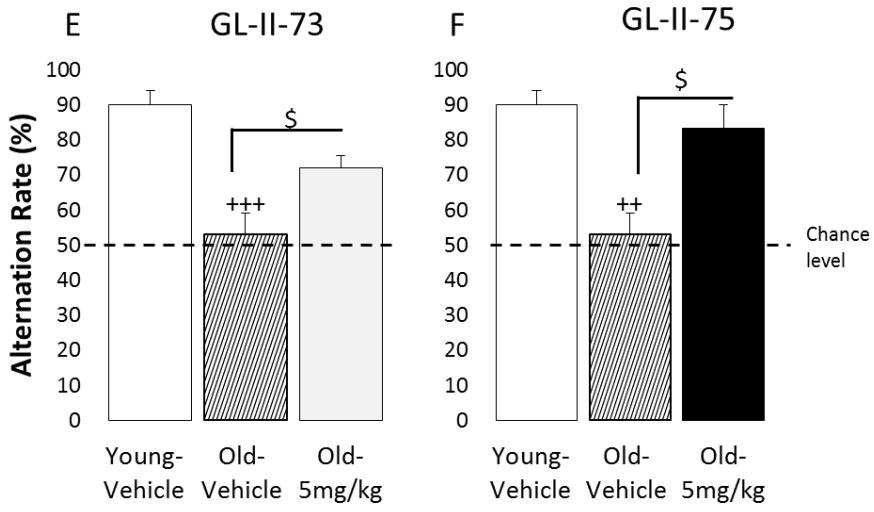

Figure 61. The potential pro-cognitive effect of 36 (GL-II-73) and 38 (GL-II-75) in the age-induced Y-maze task. The same experimental protocol was used for old mice but with a shorter interval to 1 minute. Old male mice were treated with either vehicle or test compound 36 (E; n(0-Young) = 5, n(0-Old) = 5, n(5) = 6) or 38 (F; n(0-Young) = 5, n(0-Old) = 5, n(5) = 4). The significance was obtained by comparing the treated group with the young and old vehicle control groups. The significance was not achieved with a sex cofactor. ($p \geq 0.49$). Results are shown as the mean of the percentage of alternation ± SEM. Effect of age: ++ $p < 0.01$ or +++ $p < 0.001$

compared to "Young vehicle." Effect of the ligand: $ p < 0.05 compared to "Stress vehicle" or "Old vehicle." (Adopted from the figure in Prevot et al.)[117]

The two test compounds, **36** (GL-II-73) and **38** (GL-II-75) that restored the working memory deficits induced by CRS with a single acute i.p. injection, were further evaluated for their pro-cognitive properties in the CRS-induced Y-maze task via sub-chronic administration (p.o.) in drinking water over a period of 10 consecutive days in both young and old mice. The detrimental effects on working memory were observed that were induced by either CRS or age, as compared to the no-stress group and young vehicle group, respectively. The test compounds were diluted in water for a 30 mg/kg dose to match the brain concentration of the compound with an i.p. injection at 10 mg/kg. This solution was prepared fresh daily for administration for 10 consecutive days. From the test results, as presented in Figure 62 A and B, only compound **36** (GL-II-73) exhibited a significant reversal of alternation rates in the Y-maze in young adult mice, whereas treatment with **38** (GL-II-75) did display a slight reversal, but not at the level of significance. In the experiment with the old mice, as demonstrated in Figures 62 C and D, after sub-chronic administration of both compounds, again, **36** produced a profound pro-cognitive effect in old mice group, as compared to the old vehicle group, and even improved the cognition of the young vehicle group slightly. On the other hand, **38** exhibited a similar alternation rate as the old vehicle control group, which indicated it failed to restore the normal age-related working memory deficits in old mice.

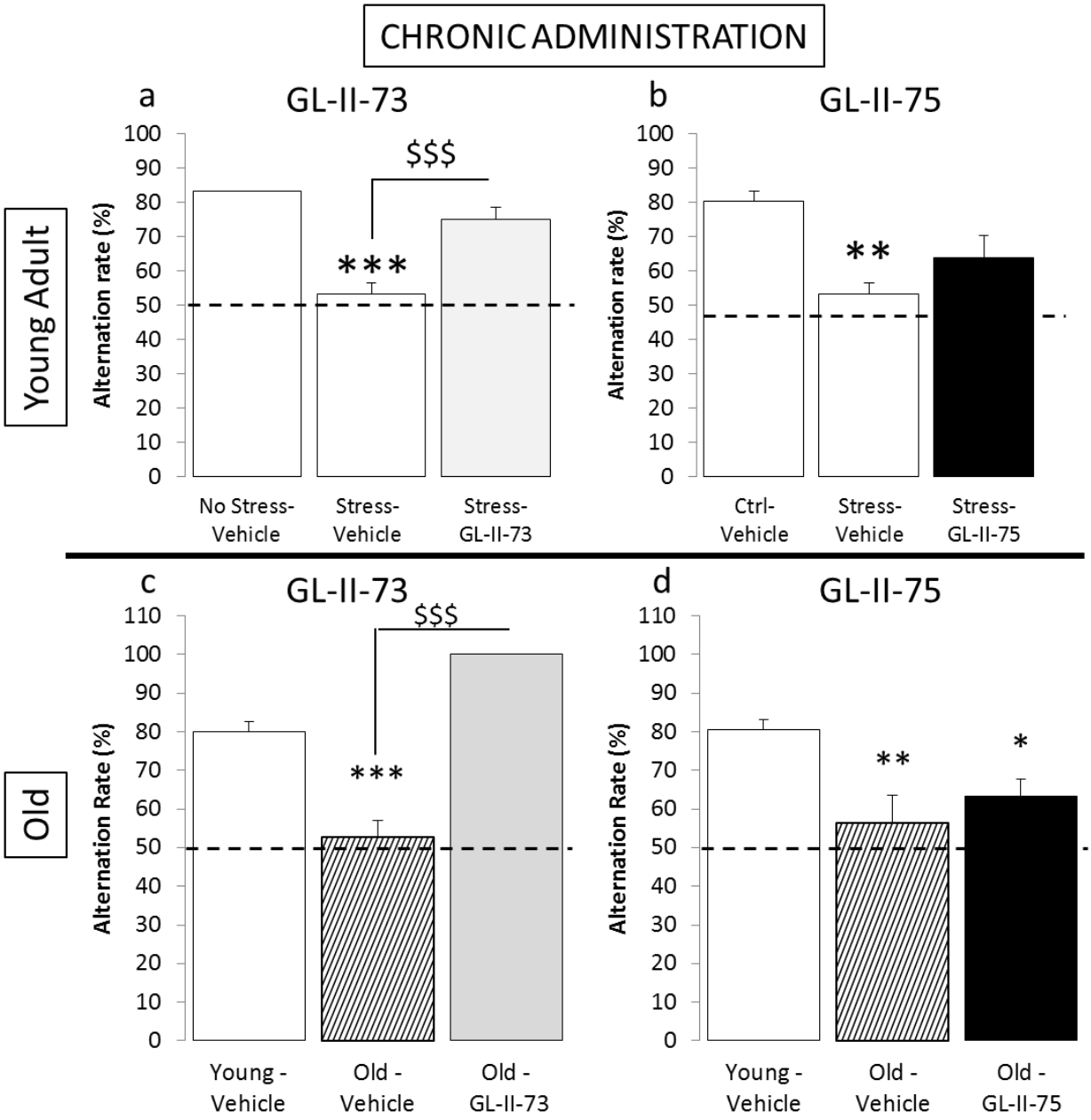

Figure 62. The pro-cognitive effect assessment of 36 (GL-II-73) and 38 (GL-II-75) on stress-induced and age-related working memory deficits. Effects of 36 (a, c) and 38 (b, d) were evaluated in young (a, b) and old (c, d) male mice via the sub-chronic administration (p.o.) in the drinking water for 10 consecutive days in the Y-maze task. Prior to the experiment, cognitive impairment in young mice was induced by CRS exposure for 7 days. The young mice were treated sub-chronically with 36 (n(0-NS) = 6, n(0-S) = 5, n(30) = 6) or 38 (n(0-NS) = 5, n(0-S) = 5, n(30) = 6) dosed at 30 mg/kg. The old mice mice were treated sub-chronically with 36 (n(0-Young) = 5, n(0-Old) = 6, n(30) = 4) or 38 (n(0-Young) = 6, n(0-Old) = 5, n(30) = 5) dosed at 30 mg/kg. The results are presented as the mean of the percentage of alternation ± SEM. Effect of the stress: * $p < 0.05$, ** $p < 0.01$, and *** $p < 0.001$ compared to "No stress vehicle." Effect of the ligand: $$$ $p < 0.001$ compared to "Stress vehicle" or "Old vehicle." (Adopted from the figure in Prevot et al.)[117]

2.2.3.6.3.3. The Effect of Blockade of the α1 and α5 Bz/GABA(A) Subtypes

The antagonist experiments were carried out in order to investigate the mechanism of the beneficial effects of **36** (GL-II-73), by antagonizing one subunit or the other to determine if that abolished the pro-cognitive effects and antidepressant actions of **36**. The ligands chosen to conduct the experiment were flumazenil, βCCt, and Xli-093 in combination with the pro-cognitive ligand **36** due to their specific effects as selective antagonists, as well as the selective antagonist flumazenil. Because flumazenil is a non-selective antagonist of $GABA_ARs$, as a competitive antagonist to reverse the effects of BZD by blocking the **BzR binding site**. It was used to block all subtypes in the experiment. Previously, it has been reported the cognitive impairment, induced by the non-subtype selective DZP, was reversed to the control level by administration of the α1 antagonist beta-CCt (βCCt) at the doses of 5 and 15 mg/kg, but was potentiated by the α5 antagonist Xli-093 at 10 mg/kg, indicating both α1 and α5 subtypes might be involved in the cognitive process.[118] Therefore, βCCt and Xli-093 were also selected to antagonize the effects on **α1 and α5 subtypes**, respectively.

The experiment was conducted using the general Y-maze protocol but with an administration of a mixture. Animals were subjected to CRS to induce a cognitive deficit in working memory prior to the antagonist experiment. Mice were then treated with vehicle, **36** (10 mg/kg) or a combination of **36** at 10 mg/kg and flumazenil, or βCCt, or Xli-093 (10 mg/kg), i.p., respectively. The antagonist results are shown in Figures 63, 64, and 65 for the effects of the three different combinations, respectively. By blocking the BzR binding site at the $GABA_ARs$ with the non-selective flumazenil, this prevented **36** from exerting its beneficial action on cognitive performance, which demonstrated that the efficacy of **36** was mediated by acting at the BZD site of $GABA_ARs$. By blocking the α1 or α5-$GABA_ARs$, by administrating the mixture of **36** with βCCt,

or **36** with Xli-093, respectively, this had a similar abolishing antagonist effect of **36** on working memory deficits. The effects of **36** diminished back down to the chance level, which suggests that both receptor subtypes are required to exhibit an effect on cognitive functions.

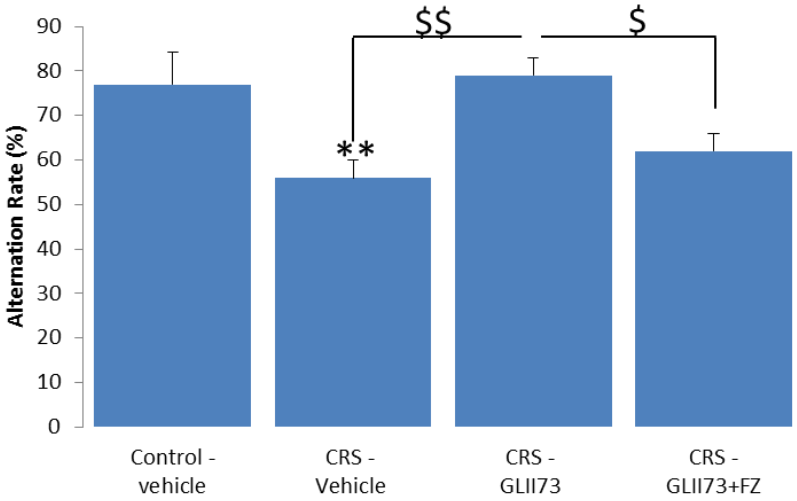

Figure 63. Flumazenil blocks the effects of 36 (GL-II-73) on percent alternation rate in the Y-maze spatial alternation task assessing working memory in mice. The chronic restraint stress (CRS) paradigm was used to induce a working memory deficit in young (2-3 months) animals. The animals were injected with vehicle, 36 (10 mg/kg) or a combination of 36 (10 mg/kg) and flumazenil (10 mg/kg) i.p. 30 min before testing. ANOVA revealed statistical significance on the overall effect of the treatment. Differences between groups were detected using post-hoc Scheffe analysis (p<0.01 and ***p<0.001 compared to the "control-vehicle" group / $p<0.05 and $$p<0.01 compared to the "CRS-vehicle" group). n=4-6. Unpublished data.**

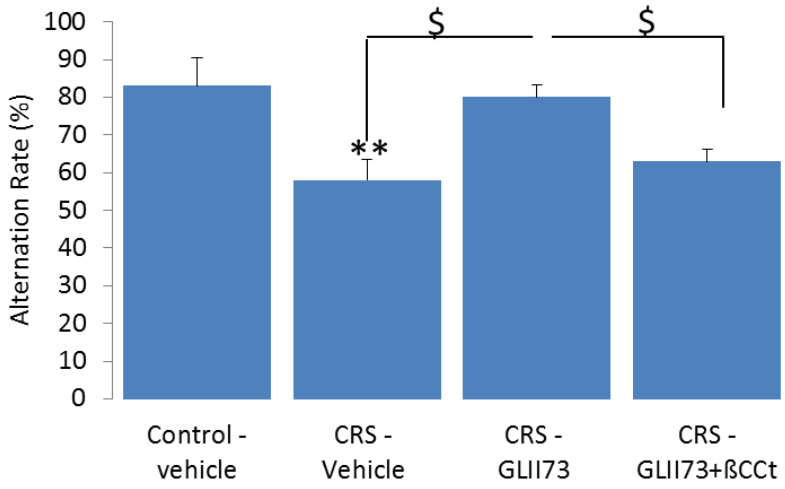

Figure 64. βCCt blocks the effects of 36 (GL-II-73) on percent alternation rate in the Y-maze spatial alternation task assessing working memory in mice. The chronic restraint stress (CRS) paradigm was used to induce a working memory deficit in young (2-3 months) animals. The animals were injected with vehicle, 36 (10 mg/kg)

or a combination of 36 (10 mg/kg) and βCCt (10 mg/kg) i.p. 30 min before testing. ANOVA revealed statistical significance on the overall effect of the treatment. The differences between groups were detected using post-hoc Scheffe analysis (p<0.01 and ***p<0.001 compared to the "Control-Vehicle" group / $p<0.05 and $$p<0.01 compared to the "CRS-vehicle" group). n=5-6. Unpublished data.**

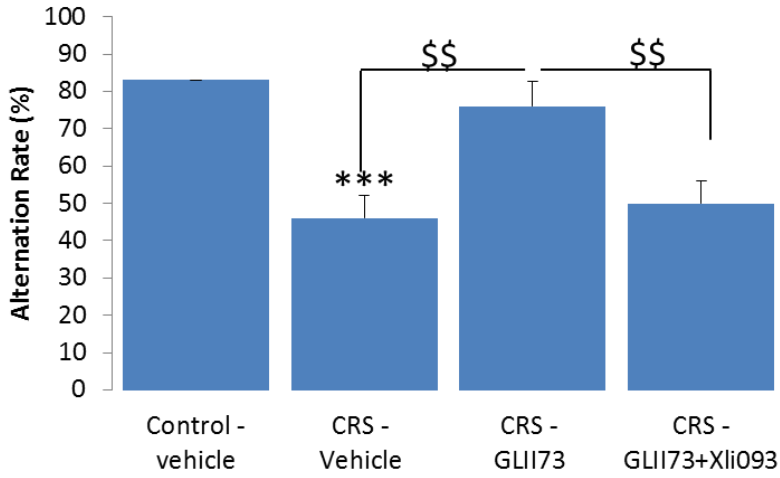

Figure 65. Xli-093 blocks the effects of 36 (GL-II-73) on the percent alternation rate in the Y-maze spatial alternation task assessing working memory in mice. The chronic restraint stress (CRS) paradigm was used to induce a working memory deficit in young (2-3 months) animals. The animals were injected with vehicle, 36 (10 mg/kg) or a combination of 36 (10 mg/kg) and XLi-093 (10 mg/kg) i.p. 30 min before testing. ANOVA revealed statistical significance on the overall effect of the treatment. Differences between groups were detected using post-hoc Scheffe analysis (p<0.01 and ***p<0.001 compared to the "control-vehicle" group / $p<0.05 and $$ p<0.01 compared to the "CRS-vehicle" group). n=5-6. Unpublished data.**

2.2.3.6.4. The Lead Compound GL-II-73 on the Study of the Effects of Morphology of Mice Brain (CONFIDENTIAL UNPUBLISHED DATA)

To visualize the changes in brain morphology after treatment with amide **36** (GL-II-73) in the normal age-related cognitive deficit of memory loss in Y-maze alternation task, a Golgi-cox study was conducted by the morphological analysis of pyramidal cells in Layers II/III of the mouse prefrontal cortex (PFC) between young, old and old-treatment groups.

In short, mice, which were the 22 months old, were treated with freshly-prepared solutions of 30 mg/kg **36** (GL-II-73) in the drinking water daily for 8 weeks. After which the mice were

tested behaviorally in the Y maze alternation task, as described in the previous section. The mice were then euthanized using the cervical dislocation method, and the brains were harvested and stained for 2 weeks in Golgi staining solution. After a rinse and section, the sample included the basal and apical dendrites of pyramidal cells in Layers II/III of PFC and they were imaged and analyzed by a microscope. The details are in Methods Section 2.2.6.20.

The quantitative data of the study of morphology included dendrograms, spine density x branch orders and Sholl analysis. The summary of the quantitative morphology of Layers II/III of pyramidal cells of PFC is presented in Table 19.

Table 19. Summary of morphological analysis of young, old, old-treated mice in the prefrontal cortex (PFC) between groups. (CONFIDENTIAL unpublished data)

Brain ID	QTY of Samples	Total of dendritic segments	Total dendritic lengths (um)	Total of spine counts	Overall spine density
Young	4	629	68,973	79,195	1.15
Old	4	593	58,069	53,227	0.92
Old+Treatment	4	666	66,656	67,107	1.01
Total:	***12***	***1,888***	***193,698***	***199,529***	

A. Behavioral Efficacy

As described in the previous section,[117] mice were tested in the Y-maze spontaneous alternation task. ANOVA analysis revealed a significant difference between groups ($F(2;25)=11.34$; $p<0.001$) in the alternation rates. Post hoc analysis presented a significant reduction in alternation rate in the normal aging groups ($p<0.001$) and the **36** treated old mice group significantly reversed the age-related working memory deficits by increasing the alternation rates. ($p<0.01$), as presented in Figure 66.

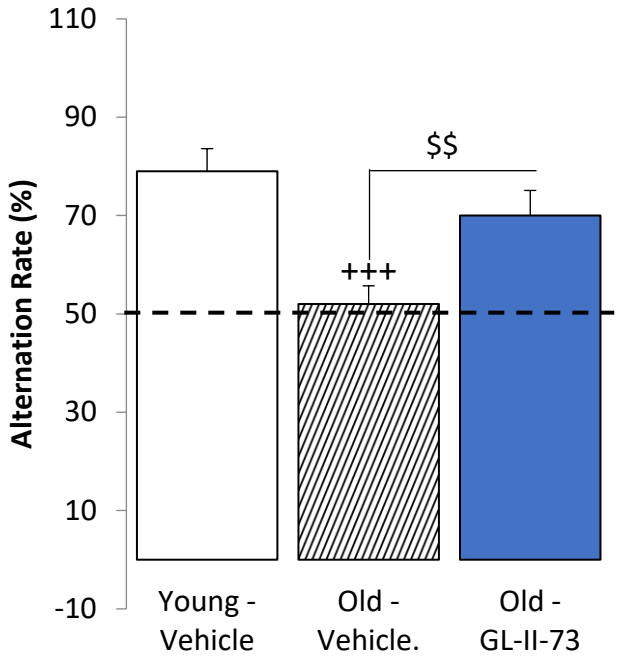

Figure 66. Alternation rate in the age-related model of cognitive dysfunction in the Y-maze task in young, old and old+treatment groups. (CONFIDENTIAL unpublished data)

B. Morphological characterization

The representative images, as shown in Figure 67, are a dendritic segment of pyramidal cells of young, old, and old+treatment groups, respectively. In the following qualitative observations: young mice exhibited more arborizations of the dendritic morphology than old and old+treatment mice (Upper panel of Figure 67. A-C). Moreover, the spine counts were much higher in young mice than old and old+treatment (**36**) mice (lower panel of Figure 67. A-C). Notably, old+treatment mice exhibited a higher spine count than old mice (the box). The quantitative comparisons of dendritic lengths, total spine counts and overall spine density between groups are demonstrated below.

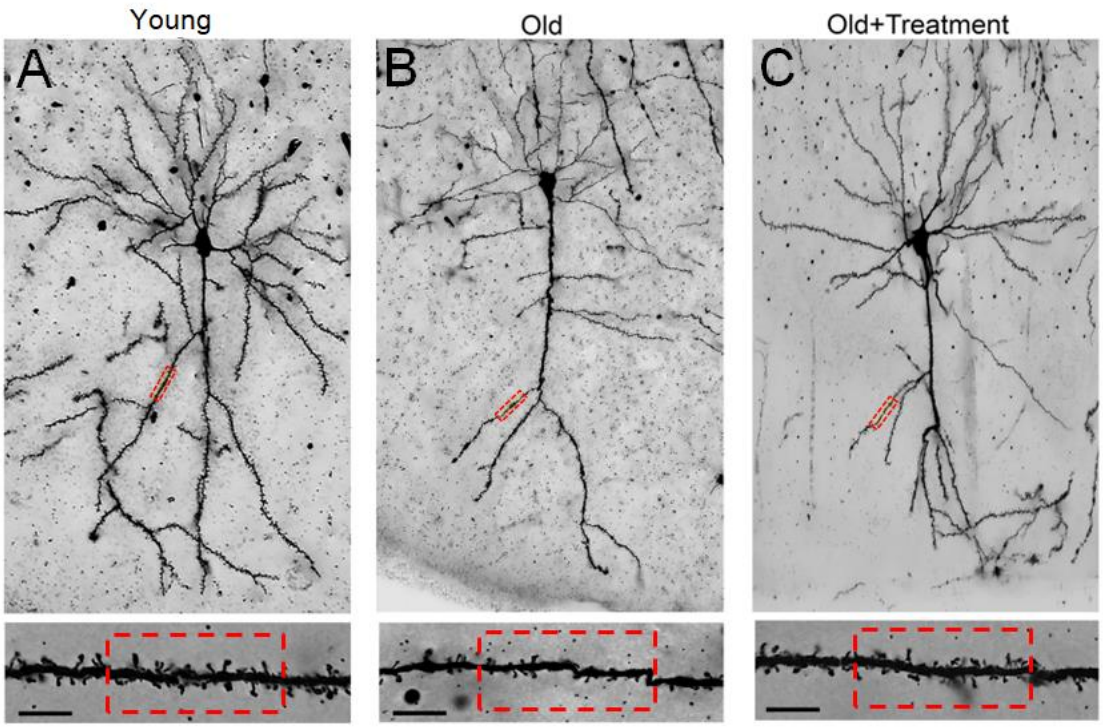

Figure 67. Representative images of PFC pyramidal cells between groups (young, old, and old+treatment). Compared to young mice (A), all aged mice showed reductions in spine counts of pyramidal cells (the box in lower panels of A-C). It was noted that old+treatment mice showed a higher spine count than old mice [Scale bars: 5 um]. Note: The quantitation of spine subtypes was not included in the current study. (CONFIDENTIAL unpublished data)

C. Analysis of Morphological

Examination of the data in Figure 68A for the total dendritic lengths, a significant decrease was observed in old mice, as compared to young mice ($p<0.05$), whereas there was no difference found in old+treatment mice ($p>0.05$). As illustrated in Figure 68B in the break-down analysis of total apical and basal dendrites, it did not show any difference in the basal dendrite between young, old, and old+treatment groups (Figure 68B, $p>0.05$). However, in the apical dendrites, higher total dendritic lengths of apical dendrites were observed in both young and old+treatment mice groups, as compared to that in old mice, respectively ($p<0.05$). Not any difference between young and old+treatment mice was observed ($p>0.05$).

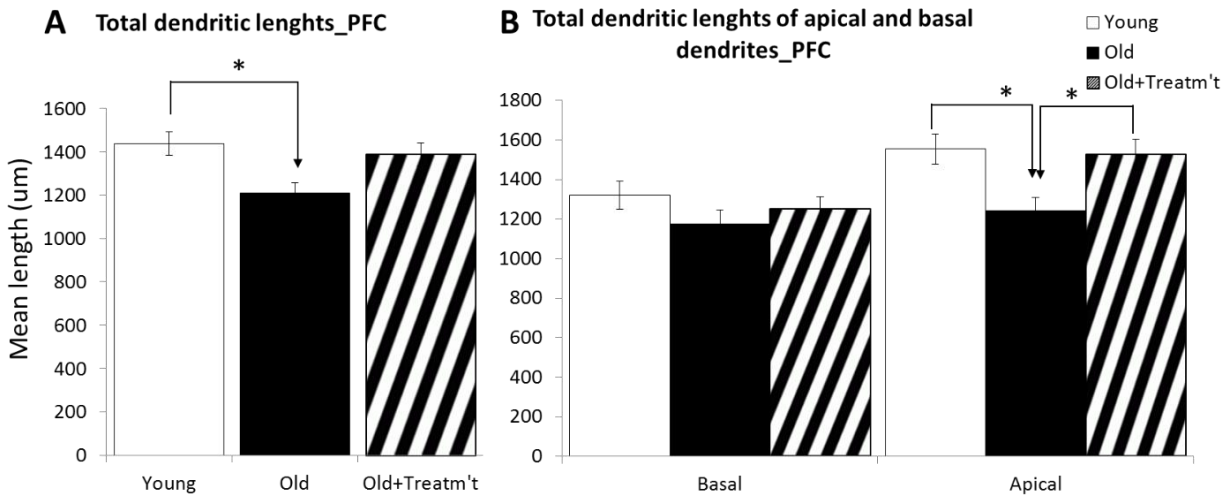

Figure 68. Comparison of total dendritic lengths of pyramidal cells as well as the break-down analysis between young, old, and old+treatment groups. (CONFIDENTIAL unpublished data)

As shown in Figure 69A in the analysis of total spine counts, a significant decrease of total spine counts was found in old mice, as compared to young mice, respectively ($p<0.05$). In addition, the spine counts were higher in the old+treatment mice than old mice ($p<0.05$). In the break-down analysis of total spine counts of apical and basal dendrites, a significant reduction was observed only in old mice in comparison with young mice, as presented in Figure 69B ($p<0.05$). In the apical dendrites, the spine counts in old mice were significantly lower than both young and old+treatment mice, respectively ($p<0.05$). There were not any differences found in both basal and apical dendrites between young and old+treatment mice. ($p>0.05$)

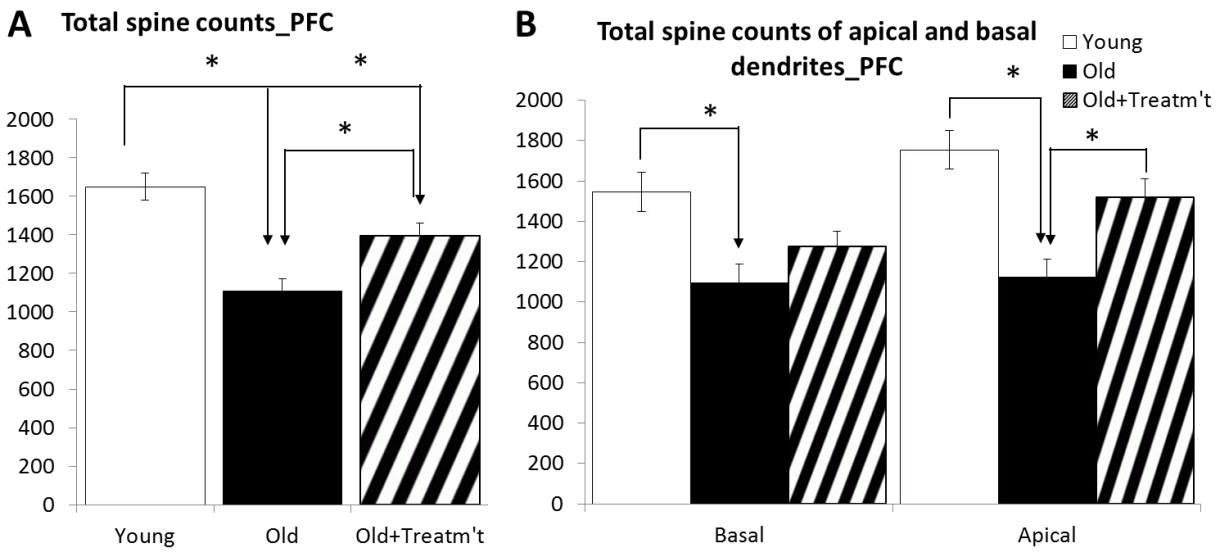

Figure 69. Comparison of total spine counts of pyramidal cells as well as the break-down analysis between young, old, and old+treatment groups. (CONFIDENTIAL unpublished data)

As demonstrated in Figure 70A for the analysis of overall spine density, a significant decrease in spine density of old and old+treatment mice was found in comparison with young mice, respectively ($p<0.05$). In addition, a higher density in old+treatment mice was observed than old mice ($p<0.05$)*. In the break-down analysis of the overall spine density of apical and basal dendrites, a significant reduction was observed only in Old mice in comparison with young mice, as presented in Figure 70B ($p<0.05$). In the apical dendrites, a higher density in young mice was found than both old and old+treatment mice, respectively ($p<0.05$). There were not any differences found in the spine density of both basal and apical dendrites between old and old+treatment mice. ($p>0.05$), which was likely due to the sample size being compromised by the break-down analysis.

*It was noted that the p-value was on the margin of statistical significance, given the sample size (n=4 per group) in the current study.

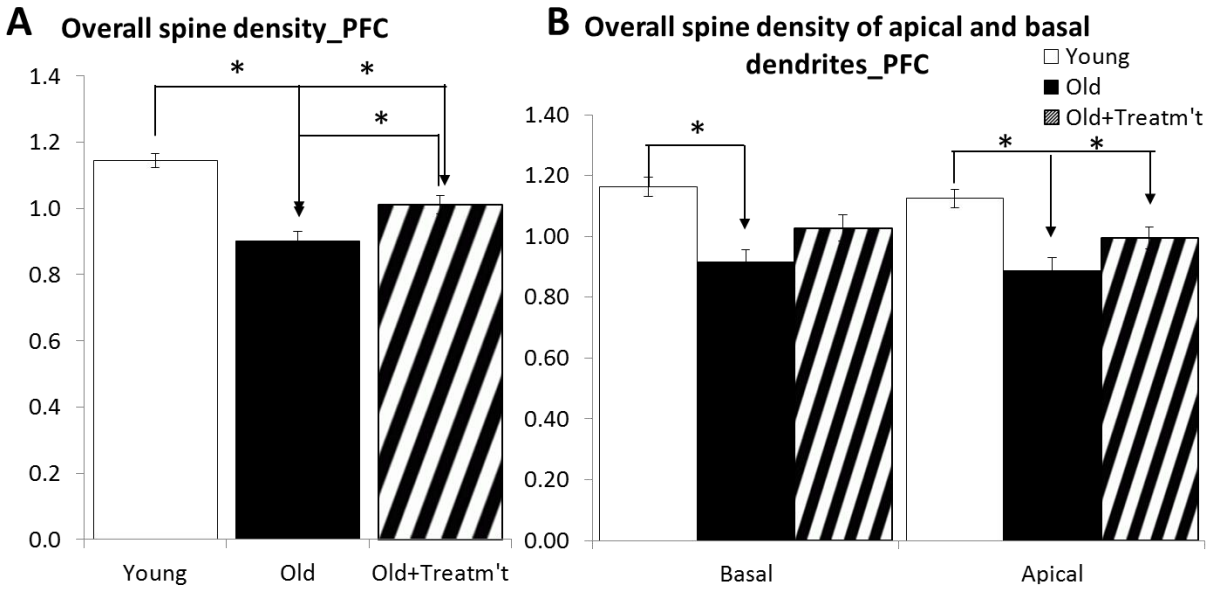

Figure 70. Comparison of overall spine density of pyramidal cells as well as the break-down analysis between young, old, and old+treatment groups. (CONFIDENTIAL unpublished data)

2.2.4. Discussion

It is clear that ligand design to target specific $GABA_AR$ subtypes without adverse effects is very difficult, in part, due to the absence of crystal structures for the α2β3γ2, α3β3γ2 and α5β3γ2 ion channels, as well as the diversity of the receptor subunit expression in different regions of the brain. Although an electron microscopy structure has been reported for a pentameric GABA ion channel for α1β3γ2 $GABA_ARs$, the lack of a similar structure of the α5β3γ2 subunit with diazepam or an α5 subtype-selective ligand in the binding site renders ligand design difficult except for the use of the Milwaukee-based unified pharmacophore/receptor model and the α5 homology model.[154] In the present research, a number of ligands have been successfully designed and synthesized with the C(4) *S*-CH_3 stereochemistry. This series of esters, amides, and bioisosters of the lead compound **2** are devoid of the liable ester functionality at C(3) to enhance metabolic stability**.** The synthesis of these analogs, importantly, were inexpensive and straightforward with

improved yields over the previous routes.[43] More importantly, these reactions can be easily scaled up to gram quantities. The novel ligands **8c** and **9a** are metabolically stable in the presence of human and mouse liver microsomes and exhibit excellent safe cytotoxicity (LD_{50}) values. Furthermore, the ligands do not induce sedative effects, which is a major problem of classical benzodiazepine drugs. Taken together, this research on the *S*-CH_3 enantiomers have provided several novel ligands that possess good safety and metabolic profiles for further *in vivo* behavioral testing in animal models in both schizophrenia and depression.[23-25, 31-32] The *in vivo* activity of **8c** and **9a** in models of schizophrenia and depression is ongoing and preliminary studies look very promising.[50]

Behavioral Study in Animal Models of Schizophrenia

According to the efficacy data of the four ligands **64, 65, 66 and 67**, as illustrated in Figures 38 and 39 , it is clear that both of the *S*-isomer analogs at 100 nM concentration elicited a stronger receptor potentiation than the *R*-isomer, and the C(8)-bromine atom slightly increased the potentiation at all subtypes irregardless of chirality at the C(4) position. Moreover, ligand **65** exhibited the highest potentiation at both concentrations for all subtypes especially at the α2 subtypes at 1 μM, as compared to the other 5 GABA/Bz subtypes. Due to the more potent efficacy of **65**, the behavioral effects of this compound were more profound than those from the other three less potent oxazole analogs. Ligand **65** reduced the hyperlocomotion induced by MK-801 to almost a control level with a 10 mg/kg dose of **65**. Although the efficacy of four ligands was very similar to that of DZP, it was much less potent than DZP and would be less prone possible to induce severe sedative effect. However, data from the rotarod study, as shown in Figure 25, revealed that ligand **65** did produce a slight sedative effect at 40 mg/kg via oral gavage. However, a similar effect was not observed in studies in a model of schizophrenia. The discrepancy should not be overestimated

due to the dose, which was much higher in the rotarod study. Moreover, the dose of 10 mg/kg was potent enough to achieve a significant reduction of the hyperlocomotion induced by MK-801 in a schizophrenia-relevant model. Therefore, the high dose, which produced slight sedation at 40 mg/kg, would not be reached to provide a desired pharmacological engagement effect for schizophrenia. Since **65** was a very potent ligand, with the aid of later PK study, the dose could be further optimized to reduce any possible side effects. Importantly, it should not be overlooked that the high potentiation of **65** at α1 could confound the anti-anxiety and anti-schizophrenia effects in animal models. Therefore, a binding assay is needed on **65** to determine the affinity at all subtypes for further evaluation of **65** in a go no go sense.

EPM for anxiolytic effects

All three target amides **36-38** were tested for their potential anxiolytic properties *in vivo*. The amides **36, 37** as well as the control DZP illustrated a similar and significant anxiolytic effect in the animal model, as shown in Figure 50, irregardless of their different efficacy profiles. Ligand **38** exhibited a non-significant anxiolytic effect but with a strong trend ($p = 0.07$) toward anxiolysis. It is noticed that ligand **38** from efficacy studies in HEK cells elicited a much stronger potentiation at α1 subtypes even at 100 nM, as compared to the other subtypes as well as to **36** and **37.** The lack of a significant anxiolytic effect observed in EMP of ligand **38** may be the result of reduced locomotor activity 30 minutes after the treatment dose, due to the possible sedative effects from potentiation of α1 subtypes, which might confound or even override the anxiolytic effects of **38**.

Antidepressant effects evaluated by the forced swim test (FST)

All three amides **36-38** from the first batch exhibited antidepressant properties without any observation of locomotor impairment at doses up to 10 mg/kg after i.p. administration after 1 hour.

However, the cyclopropyl amide **38** displayed a hypolocomotor activity up to 40 minutes after i.p. administration, which was, presumably, due to its potent efficacy at α1 $GABA_A$Rs and led to a slightly sedative effect at 10 mg/kg. This hypolocomotor effect washed out over time, indicating the brain concentration of this ligand was decreased presumably by metabolism or expulsion from the brain by some p-glycoprotein or diffusion. The other two amides **36** and **37** were less potent in regard to α1 subtypes at a dose of 10 mg/kg as compared to **38**; the tendency for a hypolocomotor impairment was relatively lower than in ligand **38**. Unlike the three amides, the non-selective DZP, on the contrary, increased the immobility, suggesting it is not antidepressant or it induced a depressant behavioral activity because of efficacy at the α1 sedating/ ataxic subtypes. In fact, there is proof of this effect. Witkin, Li, Babu, et al. gave a mixture of the α1 preferring antagonist bCCt admixed with diazepam and this formulation was antidepressant in the FST.

In addition to ligands **36-38,** another two compounds **53** and **30** in the *S*-series also elicited an antidepressant effect in the FST. The ligand **53** shared a similar pattern as compound **36** and **37** at 10 mg/kg, on the other hand, the ligand **30** exhibited the most significant antidepressant effect in the FST among all the compounds tested at a lower dose (5 mg/kg). The efficacy profile of **53** was similar to that of **36,** but it was much less potent and less selective, which may be the reason on the antidepressant effect, was less significant than amide **36**. As expected, the compounds from the 2'N series usually are less potent in efficacy at all subtypes than the 2'F analogs. However, the ability of a compound to induce an antidepressant effect may require activity at α5 subtypes, but not a very potent effect. A lot of PK work is left to be done to understand this. From the PK study, the ligand **53** reached a much larger value of AUC in the brain than most of the test compounds at only 3 mg/kg **53,** which might also confound the physiological effects at the other subtypes. The case of enantiomer **30**, might be slightly different than the compounds discussed above. This ligand

is from the *S*-series, whereas all other compounds that have an antidepressant effect are from the *R*-series. It has been shown that the efficacy and binding affinity is much better in the *S*-series of compounds, as compared to the *R*-series. Therefore, although the efficacy of **30** was not evaluated yet, **it can be predicted that this ligand will be much potent than its amide enantiomer 36**. As a consequence, the S-isomer **30** would be expected to induce a much more significant antidepressant effect at a lower dose as confirmed with the FST. Another factor that complicates the biology is that all of the FST active-compounds, *S*-enantiomer **30** has the shortest half-life. It was less than 1 hour and a short Tmax (5 minutes) than most of the compounds in the brain, indicating a rapid metabolic rate and brain penetration, which might help to explain its fast-acting ability and profound effect as compared to the other relatively stable antidepressant compounds. It is important to make a longer-acting form of *S*-**30**.

Based on the results from the FST, the active compounds above displayed antidepressant properties, which were different from DZP. Further studies on antidepressant effect are still necessary by applying other genetic models.

Analysis of spatial working memory (cognitive effect) via the use of the Y-maze

Among the 22 ligands that were tested, 10 of them have shown moderate to excellent pro-cognitive properties in the stress-induced working memory deficits assay using the Y-Maze. The parent compound ethyl ester **1** (SH-053-2'F-*R*-CH_3) was not active at 30 mg/kg in male mice, and the positive result on female mice was not able to repeat, thus overall it was counted as an inactive compound in Y-maze task. The α5 subtype-selective ligand, **35** (MP-III-022), which did not show any potency at α1 BzR, was only active in the FST but not the Y-maze cognition task. The enantiomers of both compounds, **2** (SH-053-2'F-*S*-CH_3) and **25** (MP-III-023), were inactive in both assays, due to rapid metabolism and sedative effects, respectively. The isopropyl amide **39**

(GL-III-66) did not show any effect in the Y-maze task. The ligand exhibited sedative and anxiogenic effects at the 15 mg/kg, suggesting possible sedative effects at 10 mg/kg, which, presumably could have suppressed the alternation rates in the Y-maze task. The ligand **40** (GL-II-76) exhibited very slight α5 subtype selective efficacy, which was similar but less potent as compared to **36**. However, **40** was not tested in any animal models because of the fast-metabolic rate in MLM, which then led to a low brain fraction from the PK study by Savic et al., which suggests an amide with larger *N*-alkyl side chain might reduce the metabolic stability. This ligand **40** is more lipophilic and has more sites to undergo CYP450 radical oxidation. Any achiral ligands, such as the methyl amide **49** (RV-II-04) and the methyl oxadiazole **52** (GL-III-23), did not display any pro-cognitive activity in the Y-maze task, regardless of the C(3) functional group. This again implicates α5 subtypes or a chiral *R*-CH_3 function for this approach to depression or schizophrenia. The methyl amide in the 2'N series **50** (GL-II-31) was not active in both the FST nor the Y-maze task, which may be due to the very low solubility of **50** and low brain fraction in mice.

Interestingly, the introduction of the C(8)-cyclopropyl group nearly abolished the efficacy at all subtypes at both 100 nM and 1 μM concentrations in Figure 36 and 37, as compared to the corresponding dimethyl amide **36** (GL-II-73) and ethyl amide **37** (GL-II-74). The expected reduction of the desired pro-cognitive effect, on the other hand, was NOT observed. On the contrary, the dimethyl C(8)-cyclopropyl analog **47** (GL-III-70), began to show the increased alternation rates at 1 mg/kg, at which dose **36** was not active. By replacing the acetylene by a C(8) cyclopropyl group, the C(8) cyclopropyl ethyl amide **48** (GL-III-68) exhibited pro-cognitive effects, whereas the acetylene ethyl amide **37** did not show any effect in the Y-maze task. The ligand **46** (GL-III-67), the bromo analog of **37**, shared a similar but much stronger efficacy profile as **37**, but **46** was also not active in the stress-induced working memory deficits assay just like **37.**

In the oxadiazole series, the ligands, which were not active in the Y-maze task, are the achiral methyl oxadiazole **52** (GL-III-23), the oxadiazole **53** (GL-II-54) with an antidepressant property, and one cyclopropyl oxadiazole in the 2'F series **61** (GL-III-63). The other oxadiazoles exhibited moderate to good pro-cognitive effects in the Y-maze task. In the 2'N series, the introduction of a C(8) cyclopropyl group in ligand **54** (GL-III-64) reduced slightly the pro-cognitive effect, as compared to the acetylene analog **51** (GL-II-33), which may result from the decrease of the potency at all subtypes with a C(8) cyclopropyl group in place of an acetylene. As described above, the cyclopropyl group increased the pro-cognitive effects in the amides but decreased the effect in oxadiazoles. The lack of results from the ethinyl analog **55** (MP-IV-004) in the 2'F series, as compared to the cyclopropyl analog **61** (GL-III-63), which was precognitive, is difficult to resolve. If all cyclopropyl oxadiazoles are less potent than the acetylene substituted oxadiazoles regardless of the 2'X substituent, the desired activity in **55** might have been expected. Although the cyclopropyl analog **61** was inactive, its enantiomer **31** (GL-I-65) and the bromo analog **58** (GL-III-60) exhibited the increase of the alternation rates in the Y-maze test. It is not possible to resolve the SAR above without more data including binding affinity.

In summary, in the stress-induced working memory impairment (Y-maze) task, several compounds have shown the desired effect by increasing the alternation rates of the stressed animal in the Y-maze assay. Only three compounds were active in both the Y-maze and the FST test: **30** (GL-I-54), **36** (GL-II-73), and **38** (GL-II-75). The compound **30** was not further investigated in the aging-related Y-maze task due to the rapid rate of metabolism, but this potent ligand **30** can be applied as a short-acting agent in the requested condition. **However, it is reasonable to replace the C(3) moiety with a more metabolically stable group with a similar bioisosteric function to the C(3) amide.** Only 2 out of the 22 compounds were carried on for the Y-maze experiment

in young and old mice to determine their pro-cognitive effect. The dimethyl amide **36** successfully reversed the memory deficits in normal aging old mice to a level similar to that of young mice in a 10-days sub-chronic administration in the Y-maze test. Moreover, in the group of young mice, the pro-cognitive effect of **36** was maintained in the Y-maze when cognition deficits had been induced by CRS, whereas, the ligand **38** did not show a significant effect in these experiments.

The implications of α5-$GABA_A$Rs on cognitive processes have been investigated substantially during the past decades that the cognitive learning processes and anxiety might be mediated by α5 $GABA_A$Rs.[155-156] The present results from the FST and Y-maze task on the novel IMDZs suggested that the pro-cognitive effects might not only be mediated by α5 subtypes, but also accompanied by slight activation at α1 receptors as well. The compounds, according to the HEK efficacy studies of Janet Fisher did, potentiate both α5 and some α1 subtypes, such as **36** (GL-II-73) and **38** (GL-II-75). They demonstrated the desired antidepressant effect and pro-cognitive effect without sedation. It is the ligand **36,** which exhibited moderate activation at $GABA_A$Rs subtypes, restored working memory deficits in the sub-chronic administrative Y-maze task, not the non-selective but more potent ligand **38**. On the other hand, the classical non-selective high-affinity DZP did not reverse the working memory deficits and even induced cognitive impairment, as compared to the chance level. This is because of the sedating effects from efficacy at α1 receptors always present with diazepam. This impairment can be reversed by blocking the potentiation at α1-subtypes or became worse by blocking the activation of α5 subtypes.[118] Thus, in order to further unmask this low-affinity, and moderate-efficacy mechanism, blockade experiments not only at the α1-subtypes but also at the α5-subtypes must be carried out. In addition, antagonism of all BzR subtypes could also be done. Antagonist studies were conducted by using the antagonist Xli-093 (α5 blockade), the antagonist βCCt (α1 blockade), and the antagonist

flumazenil (BZD receptor sites blockade). In short, all three of them abolished the pro-cognitive effects of **36** in the stress-induced working memory assay using the Y-Maze, when combined one at a time with **36**. This was quite interesting and unexpected. It may be true that efficacy is required for a small amount of PAM efficacy at α1 subtypes in combination with α5-PAM for pro-cognitive effects.

Does this hypothesis help to rationalize why the α5 subtype selective ligands exhibit no or much less activation at α1 subtypes, such as **1** (SH-053-2'F-*R*-CH_3), **35** (MP-III-022), as well as the novel ligand **37** (GL-II-74), which only exhibited the antidepressant effects in the FST, but not the cognitive effect the in Y-maze? This hypothesis in regard to the α5/α1 binding and efficacy for cognition is a very interesting point, but also one that is very difficult to untangle. Certainly, a "titration" experiment is reasonable to conduct by a combination of a selective an α5-PAM with a selective α1-PAM to determine if the activity of **36** can be mimicked. However, the combination of any two ligands introduces additional unknowns, therefore, the behavioral tests in double α2/α3 knock-in mice would be one realistic way to test the idea in regard to the concordant beneficial effect via α1 and α5 $GABA_AR$ subtypes. On the other hand, the alternative approach 'genuinely mine' is to combine MP-III-022 and WYS8, the latter of which is one of the most selective α1 compounds that is known and might be used as an α1 partial agonist.[157-158] It would definitely be a challenge to titrate the doses of MP-III-022 and WYS8, but since these two compounds have been studied, therefore, they are 'manageable'. To date, WYS8 was only been tested in rats. A PK study in mice is necessary, especially for the free fraction of the mixture at 100 nM. One needs to design the experiment to determine how to combine the two ligands with an aim to obtain minimal activity at α1 and potent α5 activity and selectivity. If the result of this combination confirmed that the dual moderate α1/5 combination is indeed beneficial (anxiolytic, antidepressant, and pro-

cognitive), it would be both, novel and non-obvious, and may even be an excellent candidate for clinical trials. Certainly it would help to define the actual mechanism of action of important ligand GL-II-73 (**36**).

*The study of the effects of **36** (GL-II-73) on brain morphology*

The results presented here, provided evidence of a significant difference in morphological properties of Layers II/III pyramidal cells of PFC between young, old, and old+treatment mice. In general, a significant decrease in spine morphology of pyramidal cells, including total dendritic lengths, total spine counts and overall spine density, was found in old mice in comparison with young mice. Notably, old+treatment mice exhibited a relatively higher spine density ($p=0.0457$) than old mice, although further confirmation of this finding is recommended and might require a larger sample size of mice brains. More importantly, it will be informative for future studies to examine the drug efficacy/effects upon the morphology of spine subtypes (thin, stubby, mushroom, etc.) between groups.

Accordingly, these recent findings confirmed the difference in spine morphology between young, old and **36** (GL-II-73) treated old mice in the prefrontal cortex. Importantly, the aging-induced dendritic shrinkage in the old mice was reversed to 80-90 % of the level of the young mice after 8 weeks of **36** administrated in the mice's daily drinking water. This suggests (with GL-II-73) a feasible drug treatment program to administer the α5 selective PAM of $GABA_ARs$ to reverse the loss of spine and dendrites morphology in aging-related diseases including Alzheimer's disease, depression, and schizophrenia.

2.2.5. Conclusion

Based on the structure and activity of the parent chiral compounds **1** (SH-053-2'F-*R*-CH_3) and its enantiomer **2** (SH-053-2'F-*R*-CH_3), a series of analogs, including those substitution with very different functional groups such as esters, amides, thioamides, oxadiazoles and oxazoles, were designed, synthesized and evaluated in *in vitro* studies to determine their metabolism, cytotoxicity, receptor binding affinity, and efficacy at different $GABA_A$Rs subtypes. The compounds that possessed the desired *in vitro* profile were selected from the above assays and carried out for the further investigation in *in vivo* animal models. This was done to determine the PK profiles, to identify possible CNS side effects, and potential useful pharmacological effects, such as anti-inflammatory, anti-schizophrenic, anxiolytic, antidepressant and pro-cognitive effects.

The data, up to date, indicated several possible compounds for different diseases among all the analogs evaluated and some may have clinical potential at this time point (May 2019). The isopropyl oxadiazole **57** (MP-IV-010) exhibited the most significant reduction of nitric oxide in the Griess assay to the control level without any CNS side effects nor profound cytotoxicity, consequently, it was selected as the lead anti-neuroinflammatory compound. In addition, the C(8)-bromo oxazole **65** (GL-III-76) in the 2'F series was the ligand that presented the strongest anti-schizophrenic-like activity in the murine model of MK-801 induced hyperlocomotion, while being devoid of sedative properties, which suggests a candidate for further studies and perhaps for the treatment of schizophrenia. Moreover, three compounds, *S*-dimethyl amide **30** (GL-I-54), *R*-dimethyl amide **36** (GL-II-73) and *R*-cyclopropyl amide **38** (GL-II-75), exhibited both antidepressant and pro-cognitive effects and the latter two compounds elicited anxiolytic effects as well. The ligand **30** can be applied as a short-acting agent for acute use due to its fast distribution in the brain and rapid metabolic rate in depression, but perhaps a longer-lived C(3) bioisostere can

be found to replace the amide. The other two ligands **36** and **38** are chosen to be the lead compounds for depression due to their significant potency. The most recent finding demonstrated that the dimethyl amide **36**, not only was active in reversing the stress-induced working memory deficits in young mice, but also restored the normal aging-induced dendritic shrinkage in the old mice to nearly a level (80-90 %) that is normally only seen in young mice. This effect was in the prefrontal cortex, which suggests a novel therapy for depression and aging-related diseases by using α5-$GABA_AR$ PAM with an interesting low-efficacy and low-affinity profile, unlike the classical high-potent drugs. This is a very important result in terms of depression, schizophrenia, Alzheimer's disease, and age-associated memory loss. These results have gained a lot of attention throughout the world. It was presented at the AAAS meeting and engendered a lot of press, including The New Daily, The Guardian as well as an interview with the BBC-TV World News. Now the GL-II-73 antidepressant project has been moved forward to other studies on larger animals such as dogs, and more work is underway at this time to develop better α5-subtype preferred anxiolytic, antidepressant and pro-cognitive ligands. In turn studies on the exact mechanism of GL-II-73 on the regrowth of dendrites and spines is underway. The mechanism of action on this novel and potential pharmacological approach for the treatment of schizophrenia, depression and other neurodegenerative, aging-related brain disorders such as Alzheimer's disease is the object of further research at this moment.

2.2.6. Methods

2.2.6.1. Catalepsy Assay (Nicholas J. Raddatz and Dr. David A. Baker, Marquette University)

Animals

Male Sprague Dawley rats (350-450 g) were singly housed and kept on a reverse 12 hr dark/light cycle (lights on 7:00 pm) with food and water provided ad libitum. The behavioral testing occurred between the hours of 9:00 am, and 4:00 pm with all animals individually handled a minimum of five minutes each for two days prior to the testing days.

Drugs

SH-053-2'F-*R*-CH_3 (**1**), SH-053-2'F-*S*-CH_3 (**2**), and haloperidol (Sigma-Aldrich, St. Louis, MO) were dissolved in dimethyl sulfoxide to a final concentration of 30 and 0.1 mg/mL, respectively. Dimethyl sulfoxide, while not an ideal vehicle for animal behavioral work, is an acceptable formulation for rats (Gad et al., 2006). The phencyclidine hydrochloride (NIDA Drug Supply Program, Research Triangle, NC) was dissolved in saline at a concentration of 1.5 mg/mL.

Catalepsy assay[104]

Catalepsy was tested as per the methods reviewed by Sanberg et al. (1988). In short, the subjects were placed in a test box that has an open top and a stainless steel floor and grey plastic walls (34.50 cm x 19.60 cm x 23.00 cm). The box contains a stainless steel bar 1.25 cm in diameter laterally mounted 12.50 cm above the floor and 8.50 cm from one end of the box. Haloperidol (0.1 mg/kg), SH-053-2'F-S-CH3, SH-053-2'F-R-CH3 (30 mg/kg), or vehicle was administered intraperitoneally, and subjects were tested at 30, 60, and 120 min post-injection with a maximum

of five trials per session. The time (seconds) was measured from the placement of the subject's front paws on the bar until one paw moves or slips from the bar. A maximum of five consecutive trials was attempted. Criteria time for a completed trial is between ten seconds and five minutes. After five trials, if the subject had not remained on the bar for a minimum of five seconds, the longest time of the five trials was recorded.

2.2.6.2. Prepulse Inhibition (Nicholas J. Raddatz and Dr. David A. Baker, Marquette University)

The prepulse inhibition of acoustic[105] was run according to the method of Bakshi and Geyer (1995). The subjects were placed on a platform in a sound-attenuating chamber (10.875"x14"x19.5"; Hamilton-Kinder, CA) that rested on a motion sensing plate. A matching session was conducted to determine the magnitude of the startle response for each subject. This session consisted of a five minute habituation period followed by 20 trials; 17 trials involving the presentation of a single auditory stimulus (pulse stimulus; 50 dB above a 60 dB background noise) and three trials in which a prepulse stimulus (10 dB above background) was presented 100 milliseconds before the auditory pulse stimulus. Subjects were then assigned to the various treatment groups based on the magnitude of their startle response. At least one day later, an experimental session was conducted to assess sensorimotor gating. Subjects were given an intraperitoneal injection of SH-053-2'F-*S*-CH_3, SH-053-2'F-*R*-CH_3 (30 mg/kg), or vehicle 60 min before testing, followed by subcutaneous injection of either phencyclidine hydrochloride (1.5 mg/kg) or saline ten minutes prior to testing. In the experimental session, after a five or ten minute habituation period, subjects received 58 discrete trials; 26 trials during which the pulse stimulus (50 dB above background) was presented alone, 8 trials each in which the pulse stimulus was preceded by a pre-pulse stimulus (5, 10, or 15

dB above background) and 8 background trials with no pulse and only background noise. The first 6 pulse alone trials were not included in the average startle stimulus to achieve a relatively stable level of startle reactivity. The percent of prepulse inhibition was determined as 100-(average prepulse startle response/average startle stimulus alone)*100.

Statistical comparisons in each experiment were analyzed using a repeated measures analysis of variance (ANOVA) with drug treatment as between-subject variables and time of prepulse intensity as within-subjects variables for catalepsy and prepulse inhibition, respectively. Significant interactions and main effects were further analyzed using a Fisher LSD post hoc test ($p<0.05$).

2.2.6.3. Seizure Protection in the 6 Hz Electroshock Assay (ETSP)

Adult male CF1 mice (18-25 g) were pretreated intraperitoneally (i.p.) with the test compound at either 100 or 150 mg/kg. Each treatment group (n = 4 mice/group) was examined for anticonvulsive effects at one of five time points (1/4, 1/2, 1, 2, and 4 hr) after treatment with the test compound. Following pretreatment, each mouse received a drop of 0.5% tetracaine hydrochloride applied to each eye. The mouse was then challenged with the low-frequency (6 Hz) stimulation for 3 sec delivered through corneal electrodes. The low-frequency (6 Hz), long-duration (3 sec) stimuli are initially delivered at 32 mA intensity. Animals are manually restrained and released immediately following the stimulation and observed for the presence or absence of seizure activity. If the test compound is effective in the 6 Hz screen, mice were assessed in a dose-response using 5, 15, 30 and 60 mg/kg i.p. doses to determine the ED_{50} value.

2.2.6.4. Ataxic Assessment in the Rotorod Assay (ETSP)

Adult mice were dosed (i.p.) 30 minutes prior to being placed on a rotating rod at a speed of 6 rpm.[159] The ligand was considered toxic (sedating/ataxia) if the animal fell off this rotating rod three times during a 1-min period. In addition to minimal motor impairment, animals may exhibit a circular or zigzag gait, abnormal body posture and spread of the legs, tremors, hyperactivity, lack of exploratory behavior, somnolence, stupor, catalepsy, loss of righting response and changes in muscle tone and are noted accordingly by the observer. Toxicity equates to sedation and/or ataxia.

2.2.6.5. Microsomal Stability Assay (Revathi Kodali, UWM)

The 4 µL of 1 mM test compound at a final concentration of 10 µM was dissolved in DMSO/ACN/ methanol/ ethanol and was preincubated at 37 °C for 5 minutes on a digital heating shaker dry bath (Fischer Scientific, Pittsburgh, PA) in a mixture containing 282 µL of water, 80 µL of phosphate buffer (0.5 M, pH 7.4), 20 µL of NADPH Regenerating System Solution A (BD Bioscience, San Jose, CA) and 4 µL of NADPH Regenerating System Solution B (BD Bioscience, San Jose, CA) in a total volume of 391.2 µL. Following the preincubation, the reaction progress was initiated by addition of 8.8 µL of either human liver microsomes (BD Gentest, San Jose, CA), or mouse liver microsomes (Life technologies, Rockford, IL), at a protein concentration of 0.5 mg/mL. Aliquots of 50 µL were taken at time intervals of 0 (without microsomes), 10, 20, 40, 60, 90 and 120 minutes. Each aliquot was added to 100 µL of cold acetonitrile solution containing 1 µM/2 µM internal standard (Verapamil or 4,5-diphenyl imidazole). This was followed by sonication for 10 seconds and centrifugation at 10,000 rpm for 5 minutes. The 100 µL of the supernatant was transferred into Spin-X HPLC filter tubes (Corning Incorporated, NY) and centrifuged at 13,000 rpm for 5 minutes.

The filtrate was diluted 100-fold and subsequently analyzed by LC-MS/MS with a Shimadzu LCMS 8040, (Shimadzu Scientific Instruments, Columbia, MD). The ratio of the peak areas of the internal standard and test compound was calculated for every time point, and the natural log of the ratio was plotted against time to determine the linear slope (k). The metabolic rate (k*C0/C), half-life (0.693/k), and internal clearance (V*k) were calculated, where k was the slope, C0 was the initial concentration of test compound, C was the concentration of microsomes, and V was the volume of incubation in µL per microsomal protein in mg. All experiments were repeated three times in duplicates.

2.2.6.6. Cytotoxicity Assay (Dr. Michael R. Stephen, UWM)

The human liver hepatocellular carcinoma (HEPG2) and human embryonic kidney 293T (HEK293T) cell lines were purchased (ATCC) and cultured in 75 cm^2 flasks (CellStar). Cells were grown in DMEM/High Glucose (Hyclone, #SH3024301) media to which non-essential amino acids (Hyclone, #SH30238.01), 10 mM HEPES (Hyclone, #SH302237.01), 5 x 106 units of penicillin and streptomycin (Hyclone, #SV30010), and 10% of heat-inactivated fetal bovine serum (Gibco, #10082147) were added. The cells were harvested using 0.05% Trypsin (Hyclone, #SH3023601), washed with PBS, and dispensed into sterile white, optical bottom 384-well plates (NUNC, #142762). After two hours, the small molecule solutions were transferred with a Tecan Freedom EVO liquid handling system equipped with a 100 nL pin tool (V&P Scientific). The controls were 3-dibutylamino-1-(4-hexyl-phenyl)-propan-1-one (25 mM in DMSO, positive control) and DMSO (negative control). The cells were incubated for 48 hours, and this was followed by the addition of CellTiter-Glo™, a luminescence-based cell viability assay (Promega, Madison, WI). All luminescence readings were performed on a Tecan Infinite M1000 plate reader.

The assay was carried out in quadruplet with three independent runs. The data was normalized to the controls and analyzed by nonlinear regression (GraphPad Prism).

2.2.6.7. Rotorod Assay via Oral Gavage (Nick Zahn, and Alec Huber, UWM)

Swiss Webster mice were trained to maintain balance at a constant speed of 15 rpm on the rotarod apparatus (Omnitech Electronics Inc., Nova Scotia, Canada) until mice could perform for 3 minutes for three consecutive trials. Separate groups of nine mice received oral gavage of vehicle (2% hydroxypropyl methylcellulose and 2.5% polyethylene glycol) or compounds (40 mg/kg) in a volume of 200 μL. The control compound diazepam was given as an i.p. injection at 5 mg/kg in 10% DMSO, 40% propylene glycol, and 50% PBS. The mice were placed on the rotarod at three separate time points of 10, 30, and 60 minutes after each oral gavage drug administration. A fail was classified for each mouse falling twice prior to 3 minutes, as it is common for a mouse injected with a vehicle to occasionally fall once. Hence after a second fall, it would be considered a failure, and that time point would be recorded.

2.2.6.8. Rotorod Assay via I.P. Administration (Dr. Aleksandra Vidojevic and Dr. Miroslav Savic, University of Belgrade)

The rotarod test (Ugo Basile, Comerio, Italy) measured the capacity of the animal to maintain itself on the rod revolving 15 rpm, as a qualitative phenomenon. The test was performed in animals that received 15 mg/kg of treatment in SLA i.p. with eight days of washout period. Two days before testing, rats or mice were trained in three sessions in a row with each session lasting 180 s (with a pause of 30 minutes between them). On the test day, the selection was made and rats fulfilling the

criteria of maintaining themselves on the rod for 180 s without falling off (N = 40) were included in the test. Rats or mice were tested 20 minutes after the application of corresponding treatment dosed at 3, 5, 10, 15, 20, 30, 45, 60 and 90 mg/kg (N = 1-3 per treatment), depending on the test compounds. The latency to fall from the rod was recorded manually by an experimenter blind to the treatment assignment. The animals were given two trials and the higher value of the two (in sec) was used for further observation. Graphical analysis was performed in SigmaPlot 12 software (Systat, USA).

2.2.6.9. Spontaneous Locomotor Activity (Dr. Aleksandra Vidojevic and Dr. Miroslav Savic, University of Belgrade)

All compounds were tested on spontaneous locomotor activity (SLA) to determine the influence of the ligands in young mice (n=27). A white and opaque Plexiglas chamber (40×25×35 cm) was used as the apparatus under dim red light (20 lux). The mouse was injected i.p. with either vehicle or test compounds and placed immediately in the center of the chamber. Animal activity was recorded by a digital camera above the apparatus. ANY-maze Video Tracking System software (Stoelting Co, Wood Dale, IL, USA) was used to track and analyze the animal activity for a total of 60 min. The 70% ethanol was used to clean the chambers after each trial.

2.2.6.10. Grip Strength (Dr. Aleksandra Vidojevic and Dr. Miroslav Savic, University of Belgrade)

Rats were tested in the grip strength test after the rotarod assay. A grip strength meter (Ugo Basile, Milan, Italy, model 47105) was used to assess muscle strength. The rat grasped the trapeze that

was connected to a force transducer when the tail was pulled. This apparatus measured the peak force of pull (in grams) that was necessary to overcome the strength of the animal's forelimbs grip. Each rat was given 3 consecutive trials, and the median value was normalized against the body weight, which was used for further observation. Graphical analysis was performed in SigmaPlot 12 software (Systat, USA).

2.2.6.11. Binding Studies (PDSP)

The HEK-293 cells were used to conduct the binding studies following the methods as previously described. Human embryonic kidney (HEK) 293 cells (AmericanType Culture Collection ATCCs CRL-1574™) were maintained in Dulbecco's modified Eagle medium (DMEM, high glucose, GlutaMAX™ supplement, Gibco61965-059, ThermoFisher, Waltham, Massachusetts, USA) supplemented with MEM (Non-Essential Amino Acids Gibco 11140-035, ThermoFisher, Waltham, Massachusetts, USA), 100U/ml Penicillin-Streptomycin (Gibco 15140-122, ThermoFisher, Waltham, Massachusetts, USA), and 10% fetal calf serum (Sigma-AldrichF7524, St. Louis, Missouri, USA) in 10 cm Cell culture dishes (Cell+, Sarstedt, Nürnbrecht, Germany) at 37 °C and 5% CO_2. HEK293 cells were transfected with cDNAs encoding rat $GABA_AR$ subunits that were subcloned into pCI expression vectors. The 3 mg of α(1,2,3 or 5): 3 mg of β3 and 15 mg of γ2 per 10 cm dish were used as the ratio of plasmids, which was employed for the transfection with the calcium phosphate precipitation method (Chen and Okayama,1987). After transfection for 4–6 h, the medium was changed. The cells were harvested 72 days after transfection by scraping into phosphate buffered saline. After centrifugation (10 min,12000 g, 4°C) cells were resuspended in TC50 (50 mM Tris-citrate pH¼7.1), homogenized with an Ultra-Turraxs (IKA, Staufen,

Germany) and centrifuged (20 min,50000 g). The membranes were washed 3 times in TC50 as described above and frozen at -20 °C until use. The frozen membranes were then thawed, re-suspended in TC50 and incubated for 90 min at 4°C in a total of 500 mL of a solution containing 150 mM NaCl, 50 mM Tris/citrate buffer, pH=7.1, and 2 nM [3H]-Flunitrazepam (Perkin Elmer New England Nuclear, Waltham, Massachusetts, USA) in the absence or presence of either 5 mM diazepam (Nycomed, Opfikon, Switzerland) (to determine unspecific binding) or various concentrations of test compounds (dissolved in DMSO, final DMSO concentration 0.5 %). Membranes were filtered through Whatman GF/B filters, and the filters were rinsed twice with 4 mL of ice-cold 50 mM Tris/citrate buffer. The filters were transferred to scintillation vials and subjected to scintillation counting after the addition of 3 mL Rotiszint Eco plus liquid scintillation cocktail. The non-specific binding, which was determined in the presence of 5 mM DZP, was subtracted from the total [3H]-flunitrazepam binding to determine specific binding. In order to determine the equilibrium binding constant KD of 3H-Flunitrazepam for the various receptor-subtypes, membranes were incubated with various concentrations of 3H-flunitrazepam in the absence or presence of 5 mM DZP. The saturation binding experiments were analyzed by using the equation Y=Bmax*X/(KD+X). The non-linear regression analysis of the displacement curves used the equation: log(inhibitor) vs. response-variable slope with Top = 100 % and Bottom = 0 % Y = 100/(1+10^((logIC50-x)*Hill-slope)). Both analyses were performed using GraphPad Prism (LaJolla California USA). The drug concentrations which resulted in half-maximal inhibition of specific 3H-flunitrazepam binding (IC50) were converted to K_i values by using the Cheng-Prusoff relationship (Cheng and Prusoff, 1973) $K_i = IC_{50}/(1+(S/K_D))$ with S being the concentration of the radioligand (2 nM).

2.2.6.12. KOR Stimulation Response Test (Dr. Petra Scholze, University of Vienna)

The HitHunter Chinese hamster ovary cells (CHO-K1) stably expressing the human κ-opioid receptor (OPRK1, catalog no. 95-0088C2) were purchased from DiscoverX Corp. (Fremont, CA). The cells were maintained in F-12 media with 800 μg/mL geneticin (Mirus Bio, Madison, WI), 10% fetal bovine serum (Life Technologies, Grand Island, NY), and 1% penicillin/streptomycin/L-glutamine (Life Technologies). All cells were grown at 37 °C and in 5% CO_2 in a humidified incubator. The data of forskolin-induced cAMP accumulation were analyzed using nonlinear regression analysis in GraphPad Prism 5.0 software (GraphPad, La Jolla, CA) to generate sigmoidal dose-response curves for the cAMP accumulation assay. The cAMP accumulation data were normalized to vehicle and forskolin only control values. All ligands were tested in parallel assays in triplicate in $\geqslant$ 2 individual experiments. The EC_{50} and E_{max} values were reported as the means ± SEM and were represented by the average of each experiment following nonlinear regression analysis. This method was reported in Riley, A. P.; Groer, C. E.; Young, D.; Ewald, A. W.; Kivell, B. M.; Prisinzano, T. E. Synthesis and kappa-opioid receptor activity of furan substituted salvinorin A analogs. J. Med. Chem. 2014, 57, 10464−10475; and Crowley, R.S., et. al. Synthetic Studies of Neoclerodane Diterpenes from Salvia divinorum: Identification of a Potent and Centrally Acting μ Opioid Analgesic with Reduced Abuse Liability J. Med. Chem., 2016, 59 (24), pp 11027–11038.

2.2.6.13. Electrophysiological Recordings (Dr. Fisher, University of South Carolina School of Medicine)

The electrophysiological recordings were performed following the methods described in Alexeev et al. The full-length cDNAs for $GABA_AR$ subtypes (generously provided by Dr. David Weiss, the University of Texas Health Science Center, San Antonio, TX and Dr. Robert Macdonald, Vanderbilt University) in mammalian expression vectors were transiently transfected into HEK-293T cell lines (GenHunter, Nashville, TN). All subtypes were rat clones except for α2, which was a human clone. The cells were transiently transfected using calcium phosphate precipitation. The plasmids encoding $GABA_AR$ subtype cDNAs were added to the cells in 1:1:1 ratio (α:β:γ) of 2 μg each. The cells were patch-clamped at −50 mV in the whole-cell recording configuration. GABA was diluted into the bath solution from freshly made or frozen stocks in water. The test compounds were dissolved in DMSO and diluted into a bath solution with the highest DMSO level applied to cells of 0.01%. The solutions containing GABA or GABA + compounds were employed to cells for 5 s using a 3-barrelled solution delivery device controlled by a computer-driven stepper motor (SF-77B, Harvard Apparatus, Holliston, MA, open tip exchange time of < 50 ms). There was a continuous flow of external solution through the chamber. An Axon 200B (Foster City, CA) patch clamp amplifier was used to record the currents. The whole-cell currents were analyzed using the programs Clampfit (pClamp9 suite, Axon Instruments, Foster City, CA) and Prism (GraphPad, San Diego, CA). The concentration-response data was fit with a four-parameter logistic equation $\text{current} = \frac{\text{minimum current} + (\text{maximum current} - \text{minimum current})}{1 + (10(\log EC50 - \log(\text{modulator}))n)}$ where n represents the Hill number. All fits were made to normalized data with current expressed as a percentage of the response to GABA alone for each cell.

2.2.6.14. Pharmacokinetic Studies (Dr. Aleksandra Vidojevic and Dr. Miroslav Savic, University of Belgrade)

Young mice (n = 15) were divided into 5 groups; each group contained 3 animals and corresponded to predetermined time intervals (5, 20, 60, 180, and 720 min). The mice were administrated (i.p.) with test compounds at the 10 mg/kg dose (a volume of 10 mL/kg). The brain concentrations were measured 20 min after i.p. injection at the dose of 1 mg/kg, as well as after 3 i.p. injections, administered 24 h, 20 h and 1 h prior to the measurement of concentration.

The mice were anesthetized with ketamine solution (10% Ketamidor, Richter Pharma Ag, Wels Austria, dosed at 100 mg/kg i.p.) at the appropriate time intervals. The blood samples were then collected via cardiac puncture of mice in heparinized syringes, and the plasma samples were obtained after centrifuging at 800 rcf for 10 min. Mice were decapitated, and brains were weighed, which were homogenized in 1.25 mL of methanol and centrifuged at 3400 rcf for 20 min. The compounds were extracted from plasma and supernatants of brain tissue homogenates by solid phase extraction, using Oasis HLB cartridges (Waters Corporation, Milford, Massachusetts). The procedure of sample preparation and determination of concentration by ultraperformance liquid chromatography-tandem mass spectrometry (UPLC–MS/MS) with Thermo Scientific Accela 600 UPLC system connected to a Thermo Scientific TSQ Quantum Access MAX triple quadrupole mass spectrometer (Thermo Fisher Scientific, San Jose, California), equipped with the electrospray ionization (ESI) source, has been already described in detail. The non-compartmental pharmacokinetic analysis was performed using PK functions for Microsoft Excel software (by Joel Usansky, Atul Desai, and Diane Tang-Liu were), while graphs were constructed in commercial statistical software Sigma Plot 12 (Systat Software Inc., USA).

In vitro hydrolytic stability study in plasma

The hydrolytic stability of the test compounds was conducted in vitro at 37 °C, and the blank mouse plasma was used to spike with the respective compound as well as the internal standard

(SH-I-048A; synthesized at the Department of Chemistry and Biochemistry, University of Wisconsin–Milwaukee, USA).

Plasma protein and brain tissue binding studies

The rapid equilibrium dialysis assay determined the free fraction of GL-II-73, GL-II-74, and GL-II-75 in mouse plasma and brain tissue was the same as in the previously described method. The free concentrations in the brain for GL-II-73, GL-II-74, and GL-II-75 were calculated by multiplying the total brain concentrations obtained with the appropriate free fractions determined by rapid equilibrium dialysis (12.14%, 4.49% and 1.34%, respectively).

2.2.6.15. Griess Assay and Toxicity Assay (Amanda Nieman, UWM)

The 80 μL of non-activated mouse microglia (1x106 cells/mL) were plated in sterile 384 well plates. The culture, which remained, was activated with 50 ng/mL LPS and 150 U/mL IFNγ and distributed into the 384 well plates. The 0.1 μL of 800 μM GABA diluted in MilliQ water (final concentration of 1 μM), and appropriate concentrations of compounds of interest diluted in DMSO were added via a TECAN automated liquid handling robot. The assay plate was incubated for 24 h at 37 °C, spun down, and 40 μL of supernatant was removed to a new plate for analysis by the Griess Assay (Promega, Madison, WI). Absorbance at 530 nM was read using a TECAN Infinite M1000 plate reader. The remaining 40 μL containing cells was analyzed for toxicity by the Cell Titer-Glo Assay (Promega, Madison, WI). Luminescence was read using a TECAN Infinite M1000 plate reader.

2.2.6.16. Anti-Schizophrenic-like Behavioral Study Induced by MK-801 (Dr. Aleksandra Vidojevic and Dr. Miroslav Savic, University of Belgrade)

The SLA was performed in 10 ± 2 week-old male naïve C57BL/6 mice (N = 64) in the apparatus which consisted of four white and opaque Plexiglas chambers (40×25×35 cm) under dim red light (20 lux). A digital camera mounted above the apparatus recorded the animal's activity, which was analyzed using ANY-maze Video Tracking System software (Stoelting Co, Wood Dale, IL, USA). A test was conducted in two stages. The first stage ("Habituation") started when a single mouse was placed in the center of the chamber in order to habituate for 60 min; immediately after the appropriate treatment was administered and the animal's activity was recorded for an additional 120 minutes (second stage; "MK-801 challenge"). The testing of animals was balanced for the time of the day (am or pm), treatment and chamber. The chambers and the upper surface of the stand were cleaned with 70 % ethanol after every test.

The dose of MK-801, which robustly induces hyperlocomotion, was determined after reviewing the literature (Kalinichev et al. 2008., the text of the article is in the attachment), while the dose of compounds was chosen based on the laboratory experience. The MK-801 was applied as a maleate (Tocris Bioscience, Bristol, UK) in a dose of 0.32 mg/kg and compounds (synthesized at the University of Wisconsin-Milwaukee, Milwaukee, USA) were dosed at 10 mg/kg. The dosage form of MK-801 maleate was prepared by dissolving it in the saline (SAL), while the compounds were readily suspended in the solvent (SOL) containing 85% distilled water, 14% propylene glycol and 1% Tween 80 with the aid of sonication. The treatments administered were: SAL in the combination with SOL as a different injection administered immediately after the first one at the animal's counter site (SOL + SOL), then SAL + GL-III-36, SAL + GL-III-73, SAL + GL-III-76, SAL + GL-III-78, MK-801 + SOL, MK-801 + GL-III-36, MK-801 + GL-III-73, MK-801 + GL-

III-76 and MK-801 + GL-III-78. The treatments were applied intraperitoneally in a total volume of 20 ml/kg (10 mL/kg each injection).

2.2.6.17. Anxiety-Like Behaviors in the Elevated Plus Maze (Dr. Thomas D. Prevot and Dr. Etienne Sibille, CAMH)

The anxiety-like behaviors from the test compounds were assessed by the use of the elevated plus maze (EPM) in rodents. The maze is made of four white Plexiglas arms, which included two open arms (29x7 cm), and two enclosed arms (29x7x17 cm). These four arms formed a cross shape with the two open arms opposite each other. The maze is 90 cm above the floor and illuminated at 100 lux. Prior to test 30 minutes, the young male and female (50 %) mice (Jackson Laboratories) were administrated i.p. with either vehicle, 5 or 10 mg/kg dose of test compound or 1.5mg/kg of DZP. The mice were placed in the center of the platform individually, and they were facing an open arm, then allowed to explore the maze for 10 min. The animal activity was recorded with a digital camera and analyzed using ANY-maze Video Tracking System software (Stoelting Co, Wood Dale, IL, USA). The time in the open arm was used to calculate the percentage of time in the open arm by the following formula: the % time in open arm = (time in the open arm)/(total time) x 100.

2.2.6.18. Antidepressant Predictability via Forced Swim Test (Dr. Thomas D. Prevot and Dr. Etienne Sibille, CAMH)

Under normal housing conditions (12 h light ON cycle starting at 7am / water and food ad libitum), the 8 weeks-old C57Bl/6 male mice (Jackson Laboratories) were group housed (4-5 mice/cage) for one week. All drugs were dissolved in a vehicle solution containing 14% propylene glycol

(Sigma Aldrich), 1% Tween 80 (Sigma Aldrich) and 85% H_2O. The working solutions (20 mg/mL) was injected i.p. with vehicle or αPAM in mice at doses of 1, 5 or 10 mg/kg. After the injection for 1 h, mice were placed in an inescapable transparent tank filled with water (25 cm, 25-26 ^oC) to a level, where they are unable to touch the bottom and unable to escape. Animal activity was recorded for a period of 6 min for the immobile time in the tank. Compounds that reduced the time spent immobile in the FST are considered to have potential antidepressant effects.

2.2.6.19. Cognitive Flexibility via Y-Maze Test (Dr. Thomas D. Prevot and Dr. Etienne Sibille, CAMH)

Young animals and chronic stress procedure: the C57/Bl6 mice, males, and females were ordered from Jackson Laboratories at 8 weeks old and were kept in normal housing conditions (12 h light ON cycle starting at 7am / water and food ad libitum) for one week. During this week, animals were singly housed and handled to reduce the anxiety-like response toward the experimenter. To induce a working memory deficit, mice were subjected to a chronic restraint stress protocol (CRS). They were placed in a 50ml falcon® tube, twice a day, for 1 h during their diurnal cycle. The time of occurrence of the stress was randomized every day to avoid predictability. The CRS was not applied on testing days. The Y-maze test occurred 15 h minimum after the last stressor.

Testing in young versus old Animals testing: C57/Bl6 male mice males were ordered from Jackson Laboratories at 10 months-old and were kept in normal housing conditions (12 h light ON cycle starting at 7am / water and food ad libitum) until they reached the age of 22 months. A younger cohort of 8 week old animals was used as controls for the experiment. Before testing, animals were

handled to reduce the anxiety-like response toward the experimenter. Normal aging induced-working memory deficits were assessed using the Y-maze test, as described below.

Y-maze Protocol: The mice were first habituated to the Y-maze apparatus and distal cues during 2 consecutive days over a 10 min free exploration session (one session per day). The next day, animals performed a training session consisting of seven successive trials separated by a 30 s inter-trial interval (ITI); during this training session, mice were familiarized with the experimental procedure (opening and closing of the doors and confinement into the goal arms). For each trial, the mice remained in the start-box for a 30 s ITI. Then, the door was opened, and the mouse was allowed to enter freely one of the two goal arms; the chosen arm was closed, and the choice was recorded. After a 30 s confinement period into the chosen arm, the mouse was removed and brought back to the start-box for a second trial identical to the first one and this procedure was repeated over the series of trials.

The same general procedure used in the training session was implemented 24 h later, except that the ITI was lengthened to 90 s. For this experiment, animals were acutely injected i.p. with vehicle or an α PAM, 30 min before the beginning of the test. To dissociate memory deficits from an eventual progressive loss of motivation to alternate over the series, an 8th trial was added to the series which was separated from the 7th trial by a shorter ITI (5 s). All animals failing to alternate at the 8th trial were excluded. The mean alternation rate was calculated and was expressed in percentage (number of alternation done by the animal / total number of alternation possible × 100) ± SEM. The percentage of alternation during the entire task was considered as an index of working memory performance (50% of it being a random alternation rate). A factorial ANOVA was applied to the data to reveal differences between groups. If the ANOVA was significant for group effect

($p<0.05$), Scheffe post-hoc analysis was conducted to identify which groups are different from each other.

Drug preparation and administration: All drugs were diluted in a vehicle solution containing 85% H_2O, 14% propylene glycol (Sigma Aldrich) and 1% Tween 80 (Sigma Aldrich). The working solutions (10 mg/mL) and injected i.p. to the mice. For all Y-maze experiments, animals were acutely injected i.p. with vehicle or α PAM at the dose of 1, 5, 10 or 20 mg/kg, 30 min before the beginning of the test.

2.2.6.20. A Golgi-Cox Study (Dr. Thomas D. Prevot and Dr. Etienne Sibille, CAMH)

The old (22 months old) and young (2 months) C57BL/6 male mice (Charles River) were used in this study. A subset of old mice received the compound GL-II-73 for 8 weeks in the drinking water at the concentration of 30 mg/kg. Prior to administration of the compound to the animals, the average volume consumed was measured to obtain the daily consumption of 8 mL per day. Based on this assessment, the compound was prepared in drinking water and provided fresh to the animals every other day. The group details are as follow: Young (N=9); Old (N=13) and Old+Treatment (N=6).

The mice were then behaviorally tested in the Y maze alternation task, as described in Prevot et al. (2019), prior to euthanasia using the cervical dislocation method. The brains were harvested and soaked in Golgi staining solution (provided by the CRO) for 2 weeks. The brains were then rinsed and kept in 30% sucrose solution for shipment to the CRO. Brains were sectioned using a cryostat, and coronal sections were mounted on a slice. The slides included serial coronal sections that covered the anterior-to-posterior axis of the brain. The sampling of ROIs included the basal and apical dendrites of pyramidal cells in Layers II/III of PFC. The ROIs were then chosen and analyzed using a stereology-based software, termed NeuroLucida, v10 (Microbrightfield, VT), installed on a Dell PC workstation that controlled Zeiss Axioplan 2 image microscope with

Optronics MicroFire CCD camera (1600 x 1200) digital camera, motorized X, Y, and Z-focus for high-resolution image acquisition and digital quantitation.

I. Sample selection criteria:

The sampling process was conducted as follows: The investigators first 1) previewed the entire rostrocaudal axis of ROIs, under low-mag Zeiss objectives (10x and 20x), 2), then compared and located those with the least truncations of distal dendrites as possible under high-mag Zeiss objectives (40x and 63x), 3), and then 4) used a Zeiss 100x objective with immersion oil to perform 3D dendritic reconstruction, followed by counting of the spines throughout the entire dendritic trees. The criteria for selecting candidate neurons for analysis were based on i) visualization of a completely filled soma with no overlap of neighboring soma and completely filled dendrites, ii) the tapering of most distal dendrites; iii) the visualization of the complete 3-D profile of dendritic trees using the 3-D display of imaging software. Neurons with incomplete impregnation and/or neurons with truncations due to the plane of sectioning were not collected. Moreover, cells with dendrites labeled retrogradely by impregnation in the surrounding neuropil were excluded (derived from Wu et al. [2004], PNAS).

With the systematic registration and digital monitoring, the software was able to accurately record every step of the tracing/contouring and generate a 3D reconstructed dendritic morphology for subsequent spine counting. Automatic navigation of the digital probes with registered x-y-z coordinates of each 2D image stack was able to create a complete 3D digital profile for the dendrograms, spine density, and Sholl analysis (see below).

II. Spine sampling criteria & quantitative analysis:

i) Spine sampling: Only spines orthogonal to the dendritic shaft were readily resolved and included in this analysis, whereas spines protruding above or beneath the dendritic shaft were not sampled (see below). This principle remained consistent throughout the course of the analysis. Also, due to the inevitable truncations of most distal ends of the sections and shrinkage after the impregnation process and optical limit to resolving most distal dendrites in the deep z-axis. This process under-estimates the actual dendritic lengths and spine numbers would be expected. The above limitations, however, did not affect the comparison of morphological properties between animals in the current study.

Schematic diagram of spine sampling:

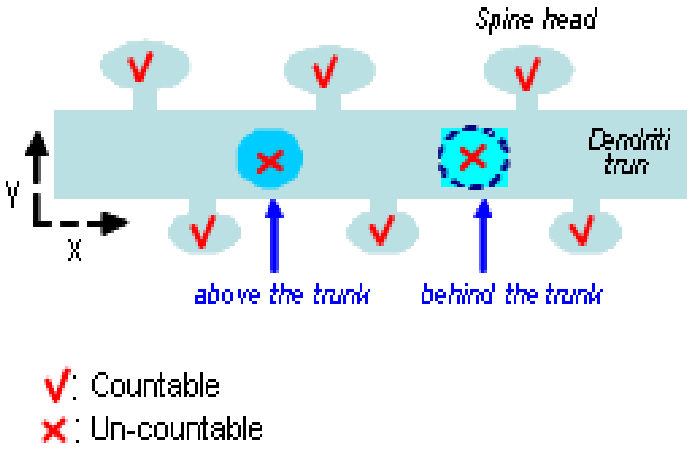

√: Countable
×: Un-countable

ii) Quantitative analysis: After tracing and spine counting, the raw data were extrapolated and quantitated using the NeuroExplorer program (Microbrightfield, VT). In addition, to further investigate the change in spine morphology, Sholl analysis was performed to characterize the spine properties in reference to a series of concentric circles (spheres in 3D) around the soma of the sampled neurons. Within each sphere, various measures were obtained, including 1) Frequency of intersections (or dendritic ramification) and 2) Spine density based on every 30um interval or concentric circle from the soma (see "Schematic diagram" below). *Note: Frequency of intersections represents the intersections or ramifications of dendritic processes interacting with the concentric rings from the soma of pyramidal cells.*

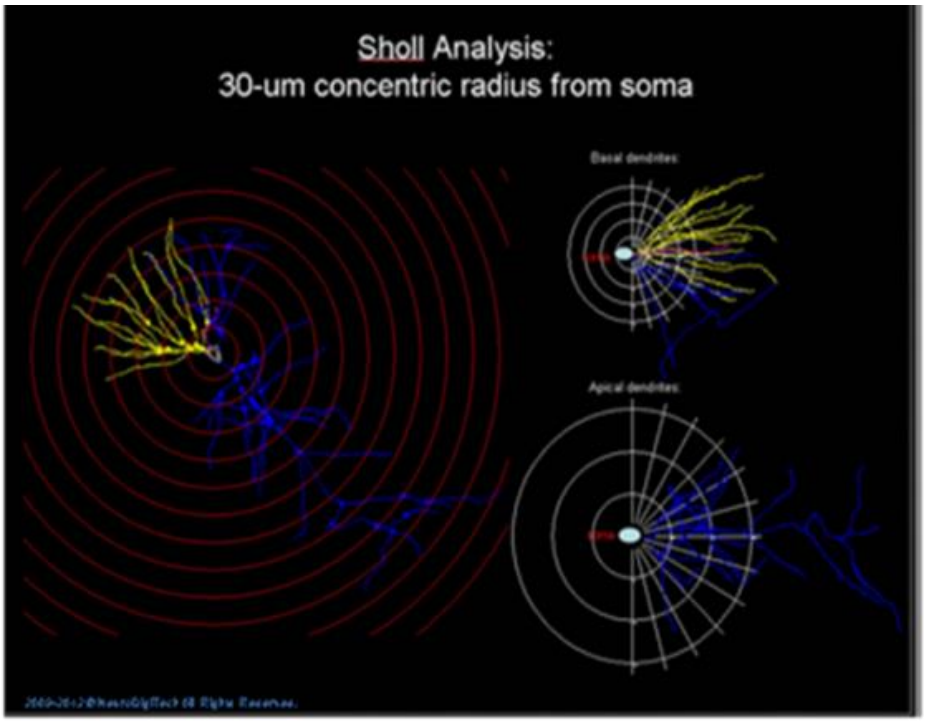

Schematic diagram of *Sholl* analysis.

After completion, the digital profile of neuron morphology was extrapolated and transported to a multi-panel computer workstation for quantitative analysis, including the dendrograms, spine counts, and Sholl analyses.

2.2.7. Experimental

All reactions were carried out in oven-dried round-bottom flasks and cooled under an argon atmosphere. All organic solvents and chemicals were purchased from commercial suppliers, then further dried and purified with the PURESOLV Solvent Purification System (Innovative Technology, Inc.) and KNF LABOPORT diaphragm laboratory vacuum pumps. Reactions were analyzed and monitored on TLC plates from Dynamic Adsorbents Inc. under a fluorescence indicator (UV_{254}). The purification of some compounds were completed by column chromatography on silica gel (230-400 mesh, Dynamic Adsorbents) using a glass column. The melting points were determined on a Stuart melting point SMP3 apparatus manufactured by Barloworld Scientific US Ltd. The ^{1}H and ^{13}C NMR spectra were obtained on a Bruker Spectrospin 300 MHz or 500 MHz instruments in $CDCl_3$ or DMSO-d_6. Chemical shifts were reported in δ (ppm) relative to TMS as an internal standard. The NMR multiplicities are presented as follows: singlet (s), broad singlet (br s), doublet (d), triplet (t), quartet (q), and multiplet (m). The determination of compound purity (> 95%) was performed by HPLC-MS on a Shimadzu LCMS-2020, and HRMS was performed on a Shimadzu LCMS-IT-TOF at the Milwaukee Institute for Drug Discovery in the Shimadzu Laboratory for Advanced and Applied Analytical Chemistry.

2.2.7.1. *Tert*-Butyl-(*R*)-(1-((4-bromo-2-(2-fluorobenzoyl)phenyl)amino)-1-oxopropan-2-yl) carbamate (4)

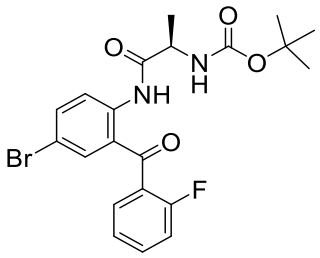

4

The (2-amino-5-bromophenyl)(2-fluorophenyl)methanone **3** (150 g, 510.0 mmol) and Boc-D-alanine (160 g, 845.6 mmol) were dissolved in dry DCM (500 mL) and stirred at 0 ^{o}C. Then dicyclohexylcarbodiimide (DCC; 186.9 g, 905.8 mmol) was dissolved in dry DCM (250 mL) to form a homogenous solution, which was added to the former mixture dropwise over a 30 min period at 0 ^{o}C. The solution was allowed to stir for 22 h at rt. The dicyclohexyl urea byproduct which was formed was filtered off and washed with DCM until the solid was colorless. The organic layers were combined and concentrated under reduced pressure. The crude solid was dissolved in hexane at 45 ^{o}C, and the Boc analog **4** was recrystallized when cooled down to rt after adding seed crystals. The crystals were further washed with hexane to afford the majority of Boc analog **4.** The filtrate was combined, concentrated and purified on a flash column chromatography (silica gel, DCM/hexane 1:1) to yield additional amide **4** (230 g, 97 %): **^{1}H NMR** (300 MHz, $CDCl_3$) δ 11.68 (s, 1H), 8.71 (d, *J* = 9.0 Hz, 1H), 7.69 (dd, *J* = 9.0, 2.3 Hz, 1H), 7.64 – 7.53 (m, 2H), 7.51 – 7.42 (m, 1H), 7.35 – 7.27 (m, 1H), 7.21 (t, *J* = 9.1 Hz, 1H), 5.13 (s, 1H), 4.37 (s, 1H), 1.52 (d, *J* = 7.2 Hz, 3H), 1.45 (s, 9H); **^{13}C NMR** (75 MHz, $CDCl_3$) δ 195.47 (s), 172.42 (s), 159.56 (d, *J* = 253.2 Hz), 155.28 (s), 139.68 (s), 137.97 (s), 135.97 (d, *J* = 1.9 Hz), 133.62 (d, *J* = 8.4 Hz), 130.31 (d, *J* = 2.4 Hz), 126.77 (d, *J* = 14.5 Hz), 124.51 (s), 124.46 (s), 122.63 (s), 116.55 (d, *J* = 21.4 Hz), 114.95 (s), 80.26 (s), 51.86 (s), 28.26 (s), 18.58 (s); **HRMS** (ESI/IT-TOF) m/z: $[M + H]^+$ Calcd for $C_{21}H_{23}BrFN_2O_4$ 465.0820; found 465.0845. This was used in the next step without further characterization. The spectral data for **4** was identical to the literature.[160]

2.2.7.2. (*R*)-7-Bromo-5-(2-fluorophenyl)-3-methyl-1,3-dihydro-2*H*-benzo[*e*][1,4]diazepin-2-one (5)

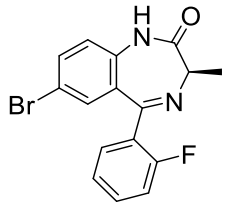

5

Amide **4** (221.6 g, 467.2 mmol) was dissolved in dry DCM (1 L) and cooled to 0 ^{o}C. Anhydrous HCl (g) was slowly added until the solution was saturated, about 2 h, and the solution was allowed to stir overnight at rt. The reaction mixture was then washed with a sat aq solution of $NaHCO_3$ (2 x 500 mL) and water (2 x 300 mL). ***A mild exotherm was observed during the addition of a saturated aq $NaHCO_3$ workup.*** The organic layer was concentrated under reduced pressure and the oil which resulted was dissolved in methanol-water (3:2, 1.7 L) while the pH was adjusted to 8.5 using a solution of 1 M aq NaOH. The reaction mixture was allowed to stir at rt overnight. The solution was concentrated under reduced pressure and water (100 mL) was added. The solution was extracted with DCM and the organic layer was washed with brine, dried (Na_2SO_4), and concentrated under reduced pressure. The recrystallization of the benzodiazepine **5** was conducted in the mixture of EtOAc and hexanes in a ratio of 1:9 after adding seed crystals. The crystals were washed with a solution of EtOAc and hexanes (1:9), and the filtrate was combined, concentrated and purified on a flash column chromatography (silica gel, EtOAc/hexane 1:2) to yield the additional benzodiazepine **5** (129 g, 78.5 %): **[α]** $^{26}_{D}$ = -169.1 (c 0.71, EtOAc); **^{1}H NMR** (300 MHz, $CDCl_3$) δ 9.66 (s, 1H), 7.64 – 7.53 (m, 2H), 7.45 (dq, *J* = 6.3, 1.6 Hz, 1H), 7.36 (d, *J* = 1.9 Hz, 1H), 7.24 (t, *J* = 7.5 Hz, 1H), 7.12 (d, *J* = 8.7 Hz, 1H), 7.05 (t, *J* = 9.0 Hz, 1H), 3.80 (q, *J* = 6.5

Hz, 1H), 1.79 (d, *J* = 6.5 Hz, 3H); **^{13}C NMR** (75 MHz, $CDCl_3$) δ 172.30 (s), 164.48 (s), 160.43 (d, *J* = 251.9 Hz), 136.47 (s), 134.70 (s), 132.14 (d, *J* = 8.6 Hz), 132.06 (d, *J* = 2.0 Hz), 131.54 (d, *J* = 2.4 Hz), 130.11 (s), 127.12 (d, *J* = 12.4 Hz), 124.41 (d, *J* = 3.6 Hz), 122.89 (s), 116.48 (s), 116.28 (d, *J* = 21.6 Hz), 58.84 (s), 16.94 (s); **HRMS** (ESI/IT-TOF) m/z: $[M + H]^+$ Calcd for $C_{16}H_{13}BrFN_2O$ 347.0190; found 347.0181. The spectral data for **5** were identical to the literature.[160]

2.2.7.3. Ethyl (*R*)-8-bromo-6-(2-fluorophenyl)-4-methyl-4*H*-benzo[*f*]imidazo[1,5-*a*][1,4] diazepine-3-carboxylate (SH-I-047, 6)

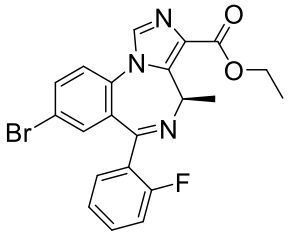

6 (SH-I-47)

The 1,4-benzodiazepine **5** (100 g, 288 mmol) was dissolved in dry THF (1.4 L) and cooled to -35 ^oC. The K-*t*-BuO (38.8 g, 345.6 mmol) was then added in one portion and the solution was allowed to warm to rt where the temperature was held for 30 min. The reaction was then cooled to -50 ^oC and diethyl chlorophosphate (70.8 g, 403.3 mmol) was added. The solution was allowed to warm to rt and the temperature was held there for 1 hour. The reaction was then cooled to -78 ^oC and ethyl isocyanoacetate (45.6 g, 403.3 mmol) was added, followed by a second portion of K-*t*-BuO (38.8 g, 345.6 mmol). The reaction was allowed to warm to rt and stirred overnight. The reaction was quenched by addition of a cold sat aq solution of $NaHCO_3$ (1 L) and extracted with EtOAc.

The organic layers were combined and washed with brine (2 x 250 mL), dried (Na_2SO_4) and the solvent was removed under reduced pressure to afford a brown solid. The majority of the bromide **6** can be crystallized in methyl t-butyl ether or EtOAc after cooling from 60 ˚C, and the additional portion was purified with flash column chromatography (silica gel, EtOAc:hexane, 3:2) to afford pure IMDZ **6** as an off-white solid (95.6 g, 75%): **[α]** $^{26}_{D}$ = -10.9 (c 0.53, EtOAc); **^{1}H NMR** (300 MHz, $CDCl_3$) δ 7.90 (s, 1H), 7.67 (d, *J* = 8.4 Hz, 1H), 7.55 (t, *J* = 7.3 Hz, 1H), 7.46 (d, *J* = 8.6 Hz, 1H), 7.44 – 7.33 (m, 2H), 7.20 (t, *J* = 7.5 Hz, 1H), 6.98 (t, *J* = 9.3 Hz, 1H), 6.66 (q, *J* = 7.1 Hz, 1H), 4.71 – 3.81 (m, 2H), 1.36 (t, *J* = 7.1 Hz, 3H), 1.24 (d, *J* = 7.3 Hz, 3H); **^{13}C NMR** (75 MHz, $CDCl_3$) δ 162.89 (s), 162.63 (s), 160.04 (d, *J* = 250.7 Hz), 141.51 (s), 134.87 (s), 134.82 (s), 133.62 (s), 132.94 (s), 132.07 (d, *J* = 8.2 Hz), 131.17 (s), 131.05 (s), 129.50 (s), 128.38 (d, *J* = 12.4 Hz), 124.52 (d, *J* = 3.5 Hz), 123.73 (s), 120.89 (s), 116.17 (d, *J* = 21.5 Hz), 60.73 (s), 50.07 (s), 14.84 (s), 14.40 (s); **HRMS** (ESI/IT-TOF) m/z: $[M + H]^+$ Calcd for $C_{21}H_{18}BrFN_3O_2$ 442.0561; found 442.0563. The spectral data for **6** were identical to the literature.[160]

2.2.7.4. Ethyl (*R*)-6-(2-fluorophenyl)-4-methyl-8-((trimethylsilyl)ethynyl)-4*H*-benzo[*f*]imidazo[1,5-*a*][1,4]diazepine-3-carboxylate (7)

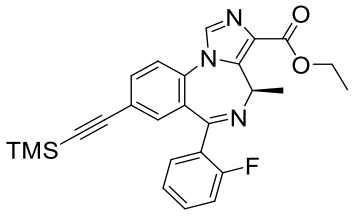

7

The IMDZ **6** (55 g, 124.4 mmol) was dissolved in triethylamine (400 mL) and acetonitrile (550 mL). Trimethylsilylacetylene (18.3 g, 186.5 mmol) and bis(triphenylphosphine)-palladium (II) acetate (5.12 g, 6.8 mmol) were added. A reflux condenser was attached and the mixture was

degassed under vacuum with argon; this process was repeated four times. The reaction mixture was heated to reflux under argon and stirred for 8 hours. The solution was cooled to rt, filtered through celite, and washed with EtOAc. The filtrate was concentrated under reduced pressure. The black residue which resulted was purified by a wash column (silica gel, EtOAc/hexanes 1:1) to afford the TMS-analog **7** as an off-white solid (44.6 g, 77.7 %): **[α]** $^{26}_{D}$ = +28.2 (c 0.48, EtOAc); **^{1}H NMR** (300 MHz, $CDCl_3$) δ 7.93 (s, 1H), 7.66 (d, *J* = 7.9 Hz, 1H), 7.59 (t, *J* = 7.3 Hz, 1H), 7.53 (d, *J* = 8.3 Hz, 1H), 7.44 (td, *J* = 7.3, 1.6 Hz, 1H), 7.36 (s, 1H), 7.24 (dd, *J* = 10.9, 4.1 Hz, 1H), 7.04 (t, *J* = 9.2 Hz, 1H), 6.68 (q, *J* = 7.2 Hz, 1H), 4.53 – 4.23 (m, 2H), 1.41 (t, *J* = 7.1 Hz, 3H), 1.25 (d, *J* = 7.3 Hz, 3H), 0.23 (s, 9H); **^{13}C NMR** (75 MHz, $CDCl_3$) δ 163.34 (s), 162.94 (s), 160.14 (d, *J* = 250.6 Hz), 141.69 (s), 135.16 (s), 134.80 (s), 134.12 – 133.69 (m), 133.40 (s), 131.85 (d, *J* = 8.3 Hz), 131.20 (s), 129.60 (s), 129.48 (s), 128.76 (d, *J* = 13.2 Hz), 124.43 (d, *J* = 3.4 Hz), 122.67 (s), 122.10 (s), 116.22 (d, *J* = 21.5 Hz), 102.50 (s), 97.31 (s), 60.74 (s), 50.08 (s), 14.76 (s), 14.42 (s), -0.26 (s); **HRMS** (ESI/IT-TOF) m/z: $[M + H]^+$ Calcd for $C_{26}H_{27}FN_3O_2Si$ 460.1851; found 460.1833. The spectral data for **7** were identical to the literature.[160]

2.2.7.5. Ethyl (*R*)-6-(2-fluorophenyl)-4-methyl-8-((triisopropylsilyl)ethynyl)-4*H*-benzo[*f*]imidazo[1,5-*a*][1,4]diazepine-3-carboxylate (8)

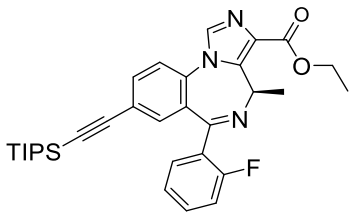

8

Tri(O-tolyl)phosphine (1.94 g, 6.38 mmol) was suspended in ACN (200 mL), and then $Pd(OAc)_2$ (0.72 g, 3.2 mmol) was added under Ar at rt to form an orange cloudy solution. The mixture was

allowed to stir at rt for 40 min untill the color of the solution turned yellow, which was an indication for the formation of the Pd complex generated *in situ*. TIPS-acetylene and the bromide **6** were suspended in ACN (250 mL), which was added to the former mixture, and this was followed by addition of TEA. The mixture was stirred until the starting material **6** was consumed, as indicated by TLC (silica gel), in about 4 h. The reaction mixture was cooled down to rt, and the solvent was removed to 1/4th of the original volume. The solid, which resulted, was filtered off and washed with EtOAc. The filtrate was combined and concentrated under reduced pressure. The residue which resulted was purified by a wash column (silica gel, EtOAc/hexanes 2:3) to afford pure triisopropylsilyl analog **8** (29.9 g, 86.0 %): ^{1}H NMR (300 MHz, $CDCl_3$) δ 7.90 (s, 1H), 7.58 (dd, *J* = 19.5, 7.9 Hz, 2H), 7.51 (d, *J* = 8.3 Hz, 1H), 7.36 (dt, *J* = 7.4, 6.1 Hz, 1H), 7.28 (s, 1H), 7.17 (t, *J* = 7.5 Hz, 1H), 6.96 (t, *J* = 9.3 Hz, 1H), 6.63 (q, *J* = 7.0 Hz, 1H), 4.47 – 4.20 (m, 2H), 1.33 (t, *J* = 7.1 Hz, 3H), 1.21 (d, *J* = 8.3 Hz, 3H), 1.03 (s, 21H); ^{13}C NMR (75 MHz, $CDCl_3$) δ 163.29 (s), 162.88 (s), 160.09 (d, *J* = 250.6 Hz), 141.60 (s), 135.26 (s), 134.87 (s), 134.01 (s), 133.28 (s), 131.79 (d, *J* = 8.8 Hz), 131.17 (s), 130.84 (ddd, *J* = 261.9, 259.9, 12.8 Hz), 129.52 (s), 129.40 (s), 124.36 (s), 122.91 (s), 122.14 (s), 116.03 (d, *J* = 21.5 Hz), 104.58 (s), 94.01 (s), 60.62 (s), 50.05 (s), 18.52 (s), 14.77 (s), 14.36 (s), 11.14 (s); **HRMS** (ESI/IT-TOF) m/z: $[M + H]^+$ Calcd for $C_{32}H_{39}FN_3O_2Si$ 544.2790; found 544.2785.

2.2.7.6. Ethyl (*R*)-8-ethynyl-6-(2-fluorophenyl)-4-methyl-4*H*-benzo[*f*]imidazo[1,5-*a*][1,4] diazepine-3-carboxylate (SH-053-2'F-*R*-CH_3, 1)

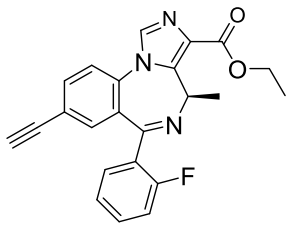

1 (SH-053-2'F-*R*-CH_3)

The intermediate **7** (44.4 g, 96.6 mmol) was dissolved in THF (400 mL) and cooled to -78 ^{o}C. This was treated with tetrabutylammonium fluoride hydrate (1 M solution in THF, 145 mmol), and this was followed by water (45 mL). The reaction mixture was stirred until the starting material was consumed as indicated by TLC (silica gel), about 1 h. The reaction mixture was allowed to warm to rt, and water (200 mL) was slowly added. The solution was extracted with EtOAc and the organic extracts were combined, washed with brine, dried (Na_2SO_4), and the solvent was removed under reduced pressure. The residue which resulted was purified by a wash column (silica gel, EtOAc/hexanes 1:1) to afford pure ethyl ester **1** as a white powder (36 g, 96.3 %). The deprotection of the triisopropylsilyl analog **8** (27.2 g, 50.0 mmol) followed the same procedure as the deprotection of the trimethylsilyl analog **7** to produce the same product ethyl ester **1** (17.4 g, 89.8 %): **[α]** $^{26}_{D}$ = +20.9 (c 0.89, EtOAc); **^{1}H NMR** (300 MHz, $CDCl_3$) δ 7.93 (s, 1H), 7.69 (d, *J* = 8.1 Hz, 1H), 7.57 (t, *J* = 9.6 Hz, 2H), 7.48 – 7.36 (m, 2H), 7.24 (t, *J* = 7.5 Hz, 1H), 7.02 (t, *J* = 9.3 Hz, 1H), 6.69 (q, *J* = 7.1 Hz, 1H), 4.54 – 4.27 (m, 2H), 3.15 (s, 1H), 1.40 (t, *J* = 7.1 Hz, 3H), 1.27 (d, *J* = 7.2 Hz, 3H). **^{13}C NMR** (75 MHz, $CDCl_3$) δ 163.20 (s), 162.91 (s), 160.08 (d, *J* = 252.0 Hz), 141.64 (s), 135.17 (s), 134.86 (s), 134.49 (s), 133.88 (s), 131.93 (d, *J* = 8.2 Hz), 131.17 (s), 129.59 (s), 129.50 (s), 128.64 (d, *J* = 12.6 Hz), 124.47 (d, *J* = 3.3 Hz), 122.23 (s), 121.62 (s), 116.16 (d, *J* = 21.5 Hz), 81.40 (s), 79.78 (s), 60.75 (s), 50.07 (s), 14.85 (s), 14.41 (s); **HRMS** (ESI/IT-TOF) m/z: $[M + H]^+$ Calcd for $C_{23}H_{19}FN_3O_2$ 388.1456; found 388.1439. The spectral data for (*R*)-**52** were in excellent agreement with the literature.[160]

2.2.7.7. *Tert*-Butyl (*S*)-(1-((4-bromo-2-(2-fluorobenzoyl)phenyl)amino)-1-oxopropan-2-yl) carbamate (9)

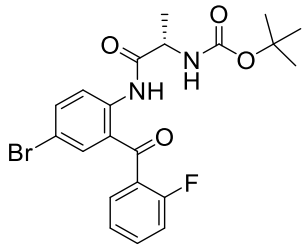

9

The carbamide **9** was synthesized as described in 2.2.7.1, with **3** (100 g, 340.0 mmol), the Boc-L-alanine (90 g, 467.0 mmol) and DCC (100 g, 484.7 mmol) were employed to afford **9** (144 g, 91 %): **^{1}H NMR** (300 MHz, $CDCl_3$) δ 11.67 (s, 1H), 8.70 (d, *J* = 9.0 Hz, 1H), 7.67 (dd, *J* = 9.0, 2.3 Hz, 1H), 7.68 – 7.56 (m, 2H), 7.53 – 7.44 (m, 1H), 7.34 – 7.28 (m, 1H), 7.22 (t, *J* = 9.1 Hz, 1H), 5.13 (s, 1H), 4.33 (s, 1H), 1.51 (d, *J* = 7.2 Hz, 3H), 1.42 (s, 9H); **^{13}C NMR** (75 MHz, $CDCl_3$) δ 195.46 (s), 172.43 (s), 159.59 (d, *J* = 253.2 Hz), 155.27 (s), 139.64 (s), 137.98 (s), 135.96 (d, *J* = 1.9 Hz), 133.61 (d, *J* = 8.4 Hz), 130.33 (d, *J* = 2.4 Hz), 126.78 (d, *J* = 14.5 Hz), 124.50 (s), 124.45 (s), 122.61 (s), 116.52 (d, *J* = 21.4 Hz), 114.93 (s), 80.27 (s), 51.85 (s), 28.25 (s), 18.57 (s); **HRMS** (ESI/IT-TOF) m/z: $[M + H]^+$ Calcd for $C_{21}H_{23}BrFN_2O_4$ 465.0820; found 465.0841. This material was used in the next step without further characterization. The spectral data for **9** were identical to the literature.[160]

2.2.7.8. (*S*)-7-Bromo-5-(2-fluorophenyl)-3-methyl-1,3-dihydro-2*H*-benzo[*e*][1,4]diazepin-2-one (SH-I-048A, 10)

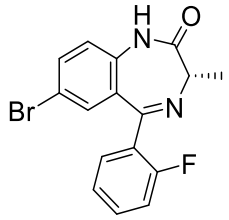

10

The 1,4-benzodiazepine **10** was synthesized, as described in 2.2.7.2, by using carbamide **9** (135 g, 290.1 mmol) as the starting material to afford **10** (83 g, 83 %): **[α]** $^{26}_{D}$ = +168.8 (c 0.73, EtOAc);); **^{1}H NMR** (300 MHz, $CDCl_3$) δ 9.65 (s, 1H), 7.63 – 7.52 (m, 2H), 7.46 (dq, *J* = 6.3, 1.6 Hz, 1H), 7.35 (d, *J* = 1.9 Hz, 1H), 7.24 (t, *J* = 7.5 Hz, 1H), 7.14 (d, *J* = 8.7 Hz, 1H), 7.03 (t, *J* = 9.0 Hz, 1H), 3.82 (q, *J* = 6.5 Hz, 1H), 1.77 (d, *J* = 6.5 Hz, 3H); **^{13}C NMR** (75 MHz, $CDCl_3$) δ 172.31 (s), 164.49 (s), 160.47 (d, *J* = 251.9 Hz), 136.46 (s), 134.71 (s), 132.15 (d, *J* = 8.6 Hz), 132.07 (d, *J* = 2.0 Hz), 131.56 (d, *J* = 2.4 Hz), 130.12 (s), 127.11 (d, *J* = 12.4 Hz), 124.43 (d, *J* = 3.6 Hz), 122.87 (s), 116.49 (s), 116.27 (d, *J* = 21.6 Hz), 58.85 (s), 16.93 (s); **HRMS** (ESI/IT-TOF) m/z: $[M + H]^+$ Calcd for $C_{16}H_{13}BrFN_2O$ 347.0190; found 347.0187. The spectral data for **10** were identical to that found in the literature.[160]

2.2.7.9. Ethyl (*S*)-8-bromo-6-(2-fluorophenyl)-4-methyl-4*H*-benzo[*f*]imidazo[1,5-*a*][1,4] diazepine-3-carboxylate (SH-I-48B, 11)

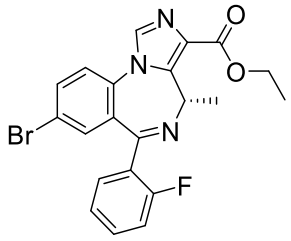

11 (SH-I-48B)

The IMDZ **11** was synthesized as described in section 2.2.7.3, by using 1,4-benzodiazepine **10** (70 g, 201.6 mmol) as the starting material to afford **11** (65 g, 73 %): **[α]** $^{26}_{D}$ = +10.6 (c 0.53, EtOAc); **^{1}H NMR** (300 MHz, $CDCl_3$) δ 7.92 (s, 1H), 7.66 (d, *J* = 8.4 Hz, 1H), 7.56 (t, *J* = 7.3 Hz, 1H), 7.44 (d, *J* = 8.6 Hz, 1H), 7.45 – 7.34 (m, 2H), 7.25 (t, *J* = 7.5 Hz, 1H), 6.99 (t, *J* = 9.3 Hz, 1H), 6.65 (q, *J* = 7.1 Hz, 1H), 4.74 – 3.83 (m, 2H), 1.32 (t, *J* = 7.1 Hz, 3H), 1.23 (d, *J* = 7.3 Hz, 3H); **^{13}C NMR** (75 MHz, $CDCl_3$) δ 162.88 (s), 162.65 (s), 160.06 (d, *J* = 250.7 Hz), 141.55 (s), 134.89 (s), 134.83 (s), 133.61 (s), 132.95 (s), 132.04 (d, *J* = 8.2 Hz), 131.16 (s), 131.04 (s), 129.52(s), 128.33 (d, *J* = 12.4 Hz), 124.55 (d, *J* = 3.5 Hz), 123.71 (s), 120.88 (s), 116.16 (d, *J* = 21.5 Hz), 60.75 (s), 50.05 (s), 14.85 (s), 14.41 (s); **HRMS** (ESI/IT-TOF) m/z: $[M + H]^+$ Calcd for $C_{21}H_{18}BrFN_3O_2$ 442.0561; found 442.0568. The spectral data for **11** were identical to the literature.[160]

2.2.7.10. Ethyl (*S*)-6-(2-fluorophenyl)-4-methyl-8-((trimethylsilyl)ethynyl)-4*H*-benzo[*f*]imidazo[1,5-*a*][1,4]diazepine-3-carboxylate (SH-I-055, 12)

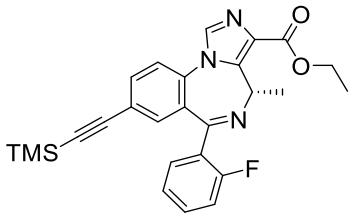

12 (SH-I-55)

The TMS-protected acetylene **12** was synthesized as described in 2.2.7.4., by using IMDZ **11** (30 g, 67.8 mmol) as the starting material to afford **12** (26.5 g, 85.0 %): **[α]** $^{26}_{D}$ = -27.8 (c 0.46, EtOAc); **^{1}H NMR** (300 MHz, $CDCl_3$) δ 7.94 (s, 1H), 7.68 (d, *J* = 7.9 Hz, 1H), 7.56 (t, *J* = 7.3 Hz, 1H), 7.51 (d, *J* = 8.3 Hz, 1H), 7.48 (td, *J* = 7.3, 1.6 Hz, 1H), 7.37 (s, 1H), 7.26 (dd, *J* = 10.9, 4.1 Hz, 1H), 7.06 (t, *J* = 9.2 Hz, 1H), 6.68 (q, *J* = 7.2 Hz, 1H), 4.52 – 4.21 (m, 2H), 1.42 (t, *J* = 7.1 Hz, 3H), 1.24 (d, *J* = 7.3 Hz, 3H), 0.22 (s, 9H); **^{13}C NMR** (75 MHz, $CDCl_3$) δ 163.37 (s), 162.96 (s), 160.16 (d, *J* = 250.6 Hz), 141.68 (s), 135.14 (s), 134.81 (s), 134.13 – 133.67 (m), 133.43 (s), 131.86 (d, *J* = 8.3 Hz), 131.21(s), 129.61 (s), 129.49 (s), 128.77 (d, *J* = 13.2 Hz), 124.42 (d, *J* = 3.4 Hz), 122.68 (s), 122.11 (s), 116.23 (d, *J* = 21.5 Hz), 102.55 (s), 97.31 (s), 60.75 (s), 50.09 (s), 14.71 (s), 14.41 (s), -0.26 (s); **HRMS** (ESI/IT-TOF) m/z: $[M + H]^+$ Calcd for $C_{26}H_{27}FN_3O_2Si$ 460.1851; found 460.1830. The spectral data for **12** were identical to the literature.[160]

2.2.7.11. Ethyl (*S*)-8-ethynyl-6-(2-fluorophenyl)-4-methyl-4*H*-benzo[*f*]imidazo[1,5-*a*][1,4]diazepine-3-carboxylate (SH-053-2'F-*S*-CH$_3$, 2)

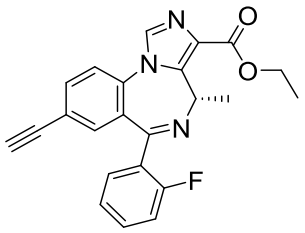

2 (SH-053-2'F-*S*-CH_3)

The ethyl ester SH-053-2'F-R-CH_3 **2** was synthesized as described in section 2.2.7.6., by using the benzodiazepine **12** (18.4 g, 40.0 mmol) as the starting material to afford **2** (14.9 g, 96 %): mp 218-220 °C; **[α]** $^{26}_{D}$ = -21.5 (c 0.89, EtOAc); **^{1}H NMR** (300 MHz, $CDCl_3$) δ 7.97 (s, 1H), 7.71 (d, *J* = 8.2 Hz, 1H), 7.61 (dd, *J* = 15.0, 7.8 Hz, 2H), 7.46 (dd, *J* = 14.2, 7.1 Hz, 2H), 7.25 (t, *J* = 7.5 Hz, 1H), 7.05 (t, *J* = 9.3 Hz, 1H), 6.71 (q, *J* = 7.0 Hz, 1H), 4.67 – 4.05 (m, 2H), 3.16 (s, 1H), 1.42 (t, *J* = 7.1 Hz, 3H), 1.29 (d, *J* = 7.2 Hz, 3H). **^{13}C NMR** (75 MHz, $CDCl_3$) δ 163.95 (s), 162.69 (s), 160.12 (d, *J* = 252.3 Hz), 141.32 (s), 135.61 (s), 134.97 (s), 134.52 (s), 134.21 (s), 132.44 (d, *J* = 8.2 Hz), 131.35 (d, *J* = 2.1 Hz), 129.49 (s), 129.16 (s), 127.98 (s), 124.58 (d, *J* = 3.5 Hz), 122.39 (s), 121.85 (s), 116.27 (d, *J* = 21.4 Hz), 81.28 (s), 79.92 (s), 60.92 (s), 49.85 (s), 14.92 (s), 14.41 (s); **HRMS** (ESI/IT-TOF) m/z: $[M + H]^+$ Calcd for $C_{23}H_{19}FN_3O_2$ 388.1456; found 338.1448. The spectral data for **2** were in excellent agreement with the literature.[160]

2.2.7.12. (*S*)-Ethyl-8-cyclopropyl-6-(2-fluorophenyl)-4-methyl-4*H*-benzo[*f*]imidazo[1,5-*a*][1,4]diazepine-3-carboxylate (GL-I-78, 13)

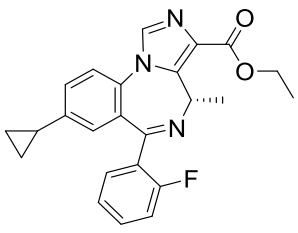

13 (GL-I-78)

To a solution of the bromo ethyl ester **11** (5.0 g, 11.3 mmol) in toluene (100 mL) and water (14.5

mL), cyclopropyl boronic acid (4.9 g, 57.0 mmol), potassium phosphate (10.3 g, 48.6 mmol) and bis(triphenylphosphine)palladium(II) diacetate (0.85 g, 1.13 mmol) were added under argon. A reflux condenser was attached and the mixture was degassed under vacuum with argon; this process was repeated four times. The mixture was stirred and heated to 100°C. After 12 h the reaction was completed on analysis by TLC (silica gel) and it was then cooled to rt. Water (10 mL) was added and the mixture was extracted with EtOAc (3 × 15 mL), after which the filtrate was washed with brine (10 mL), dried (Na_2SO_4) and concentrated under reduced pressure. The black residue which resulted was purified by a wash column (silica gel, EtOAc/hexane 7:3) to afford the desired 8-cyclopropyl-imidazodiazepine **13** as a white solid (3.74 g, 82%): mp 106-108 °C; **$[\alpha]_D^{25}$** = +65.34 (*c* 0.81, $CHCl_3$); **^{1}H NMR** (300 MHz, $CDCl_3$): δ 7.88 (s, 1H), 7.54 (t, *J* = 7.0 Hz, 1H), 7.48 – 7.32 (m, 2H), 7.19 (t, *J* = 7.6 Hz, 2H), 7.08 – 6.85 (m, 2H), 6.63 (q, *J* = 6.9 Hz, 1H), 4.34 (dd, *J* = 14.4, 7.1 Hz, 2H), 2.11 (d, *J* = 7.0 Hz, 1H), 1.91 – 1.72 (m, *J* = 4.0 Hz, 1H), 1.37 (t, *J* = 7.1 Hz, 3H), 1.23 (d, *J* = 7.0 Hz, 2H), 0.95 (d, *J* = 8.1 Hz, 2H), 0.59 (dd, *J* = 10.1, 4.6 Hz, 2H); **^{13}C NMR** (75 MHz, $CDCl_3$): δ 164.15 (s), 163.09 (s), 160.10 (d, J_{C-F} = 250.1 Hz), 143.86 (s), 141.56 (s), 134.84 (s), 132.06 (s), 131.65 (s), 131.54 (s), 131.20 (d, J_{C-F} = 1.3 Hz), 129.16 (d, J_{C-F} = 12.8 Hz), 129.08 (d, J_{C-F} = 9.4 Hz), 128.44 (s), 127.85 (s), 124.30 (d, J_{C-F} = 3.3 Hz), 121.93 (s), 115.97 (d, J_{C-F} = 21.6 Hz), 60.58 (s), 50.03 (s), 15.02 (s), 14.62 (s), 14.42 (s), 9.88 (s); **HRMS** (ESI/IT-TOF) m/z: $[M + H]^+$ Calcd for $C_{24}H_{23}FN_3O_2$ 404.1769; found 404.1766.

2.2.7.13. (*S*)-Methyl-8-bromo-6-(2-fluorophenyl)-4-methyl-4*H*-benzo[*f*]imidazo[1,5-*a*][1,4]diazepine-3-carboxylate (MP-III-059, 14)

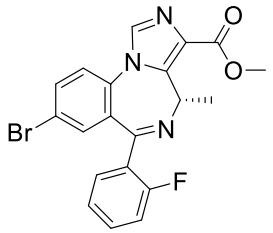

14 (MP-III-059)

The ethyl ester SH-053-2'F-*S*-CH_3 **2** (2.0 g, 4.52 mmol) was dissolved in methanol (120 mL). Sodium methoxide (0.98 g, 18.1 mmol) was added in one portion and the solution was heated to reflux. The reaction mixture was monitored on analysis by TLC (silica gel, EtOAc/hexane 4:1) until the starting material had been consumed. This took about 30 min. The reaction mixture was cooled to rt and then quenched with a saturated aq solution of $NaHCO_3$ (20 mL). Water (50 mL) was then added to the solution and the methanol was removed under reduced pressure. The product was extracted with EtOAc (3 x 100 mL) and the organic layers were combined, washed with brine (50 mL) and dried (Na_2SO_4). The solution was concentrated under reduced pressure. The solid, which resulted, was purified by flash column chromatography (silica gel, EtOAc/hexane 4:1) which provided pure methyl ester **14** as an off-white solid (1.68 g, 87% yield): mp 194-195 °C; $\mathbf{[\alpha]_D^{25}}$ = –4.55 (*c* 0.22, $CHCl_3$); **^{1}H NMR** (300 MHz, $CDCl_3$): δ 7.92 (s, 1H), 7.70 (d, *J* = 8.5 Hz, 1H), 7.57 (t, *J* = 7.0 Hz, 1H), 7.51 – 7.36 (m, 3H), 7.23 (t, *J* = 7.5 Hz, 1H), 7.02 (t, *J* = 9.3 Hz, 1H), 6.67 (q, *J* = 7.2 Hz, 1H), 3.89 (s, 3H), 2.13 (d, *J* = 7.3 Hz, 1H), 1.26 (d, *J* = 7.3 Hz, 2H); **^{13}C NMR** (75 MHz, $CDCl_3$): δ 163.29 (s), 162.70 (s), 160.06 (d, $J_{C\text{-}F}$ = 251.3 Hz), 141.56 (s), 134.89 (s), 133.57 (s), 133.01 (s), 132.18 (s), 132.07 (s) 131.18 (d, $J_{C\text{-}F}$ = 2.0 Hz), 131.10 (s), 129.22 (s), 128.35 (d, $J_{C\text{-}F}$ = 12.5 Hz), 124.56 (d, $J_{C\text{-}F}$ = 3.4 Hz), 123.69 (s), 120.98 (s), 116.21 (d, $J_{C\text{-}F}$ = 21.4 Hz), 51.86 (s), 50.04 (s), 14.86 (s); **HRMS** (ESI/IT-TOF) m/z: $[M + H]^+$ Calcd for $C_{20}H_{16}BrFN_3O_2$ 428.0404; found 428.0402.

2.2.7.14. (*S*)-Methyl-8-ethynyl-6-(2-fluorophenyl)-4-methyl-4*H*-benzo[*f*]imidazo[1,5-*a*][1,4]diazepine-3-carboxylate (MP-III-021, 16)

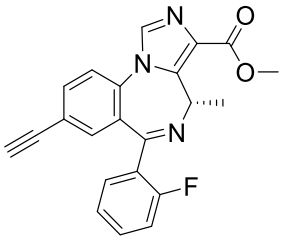

16 (MP-III-021)

The ethyl ester SH-053-2'F-*S*-CH_3 **2** (150 mg, 0.387 mmol) was dissolved in MeOH (20 mL). Sodium methoxide (84 mg, 1.55 mmol) was added in one portion and the solution was heated to reflux. The reaction mixture was monitored by analysis by TLC (silica gel, EtOAc/hexane 4:1) until the starting material had been consumed. This took about 30 min. The reaction mixture was cooled to rt and then quenched with a saturated aq solution of $NaHCO_3$ (4 mL). Water (10 mL) was then added to the solution and the methanol was removed under reduced pressure. The methyl ester **16** was then extracted with EtOAc (3 x 40 mL). The organic layers were combined, washed with brine (10 mL) and dried (Na_2SO_4). The solution was concentrated under reduced pressure. The solid, which resulted, was purified by flash column chromatography (silica gel, EtOAc/hexane 4:1) which provided pure methyl ester **16** as an off-white solid (117 mg, 81% yield): mp 119-120 °C; **$[\alpha]_D^{25}$** = +6.00 (*c* 2.0, $CHCl_3$); **^{1}H NMR** (300 MHz, $CDCl_3$): δ 7.96 (s, 1H), 7.71 (d, *J* = 8.3 Hz, 1H), 7.59 (t, *J* = 9.5 Hz, 2H), 7.49-7.40 (m, 2H), 7.29-7.21 (m, 1H), 7.04 (t, *J* = 9.3 Hz, 1H), 6.69 (q, *J* = 7.2 Hz, 1H), 3.92 (s, 3H), 3.16 (s, 1H), 2.16 (d, *J* = 7.3 Hz, 1H), 1.29 (d, *J* = 7.1 Hz, 2H); **^{13}C NMR** (75 MHz, $CDCl_3$): δ 163.71 (s), 161.17 (s), 161.16 (d, J_{C-F} = 251.1 Hz), 141.47 (s), 135.49 (s), 135.01 (s), 134.46 (s), 134.13 (s), 132.30 (d, J_{C-F} = 7.1 Hz), 131.30 (s), 129.30(s), 129.21 (s), 128.58 (d, J_{C-F} = 9.4 Hz), 124.58 (d, J_{C-F} = 3.2 Hz), 122.33 (s), 121.83 (s), 116.40 (d, J_{C-F} = 21.2 Hz), 81.31 (s), 79.90 (s), 51.93 (s), 49.88 (s), 14.92 (s); **HRMS** (ESI/IT-TOF) m/z: [M

+ H]$^+$ Calcd for $C_{22}H_{17}FN_3O_2$ 374.1299; found 374.1307.

General procedure for the synthesis of esters (17-20)

The ethyl ester SH-053-2'F-*S*-CH_3 **2** (200 mg, 0.52 mmol) was stirred in dry THF (20 mL) in an oven-dried flask under an argon atmosphere at 40 °C. Simultaneously, the corresponding anhydrous alcohol R_2-OH (5 mL) was stirred in a separate oven-dried flask under argon at 40 °C. Small pieces of freshly cut Li rod (excess) were quickly added to the dry alcohol solution, and the suspension was stirred for 30 min under argon. The ethyl ester solution was then added to the alcohol/lithium mixture, and the reaction was monitored on analysis by TLC (silica gel) until the starting material had been consumed. This took 30-45 min. The reaction mixture was then quenched with a saturated aq solution of $NaHCO_3$ aq (15 mL), and the product was extracted with EtOAc (3 x 20 mL). The organic layers were combined, washed with brine (20 mL), dried (Na_2SO_4) and the solvent was removed under reduced pressure. The solid, which resulted, was purified by flash column chromatography to afford the corresponding pure esters **17-20**.

2.2.7.15. (*S*)-Propyl-8-ethynyl-6-(2-fluorophenyl)-4-methyl-4*H*-benzo[*f*]imidazo[1,5-*a*][1,4]diazepine-3-carboxylate (GL-I-32, 17)

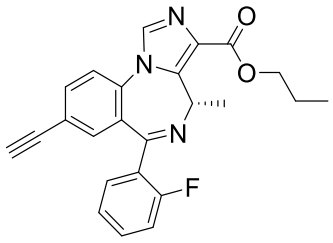

17 (GL-I-32)

The ester **17** was prepared from **2** following the general procedure for esters with dry 1-propanol. The crude residue was purified by flash column chromatography (silica gel, EtOAc/hexane 7:3) to yield the pure propyl ester **17** as a white powder (0.17 g, 82%): mp 204-205 °C; **$[\alpha]_D^{25}$** = +5.26 (*c* 0.19, $CHCl_3$); **^{1}H NMR** (300 MHz, $CDCl_3$): δ 7.95 (s, 1H), 7.71 (d, *J* = 7.8 Hz, 1H), 7.59 (dd, *J* = 15.9, 7.7 Hz, 2H), 7.46 (dd, *J* = 14.0, 6.5 Hz, 2H), 7.31 – 7.22 (m, 1H), 7.05 (t, *J* = 9.2, 1H), 6.71 (q, *J* = 6.6 Hz, 1H), 4.42 – 4.22 (m, 2H), 3.16 (s, 1H), 1.94 – 1.76 (m, 2H), 1.29 (d, *J* = 6.8 Hz, 3H), 1.03 (t, *J* = 7.4 Hz, 3H); **^{13}C NMR** (75 MHz, $CDCl_3$): δ 163.23 (s), 163.02 (s), 160.11 (d, J_{C-F} = 250.9 Hz), 141.64 (s), 135.18 (s), 134.88 (s), 134.54 (s), 133.93 (s), 131.95 (d, J_{C-F} = 8.3 Hz), 131.19 (s), 129.63 (s), 129.59 (s), 128.66 (d, J_{C-F} = 11.6 Hz), 124.49 (d, J_{C-F} = 3.4 Hz), 122.21 (s), 121.62 (s), 116.21 (d, J_{C-F} = 21.4 Hz), 81.43 (s), 79.70 (s), 66.38 (s), 50.14 (s), 22.09 (s), 14.88 (s), 10.49 (s); **HRMS** (ESI/IT-TOF) m/z: $[M + H]^+$ Calcd for $C_{24}H_{21}FN_3O_2$ 402.1612; found 402.1615.

2.2.7.16. (*S*)-Isopropyl-8-ethynyl-6-(2-fluorophenyl)-4-methyl-4*H*-benzo[*f*]imidazo[1,5-*a*][1,4]diazepine-3-carboxylate (GL-I-31, 18)

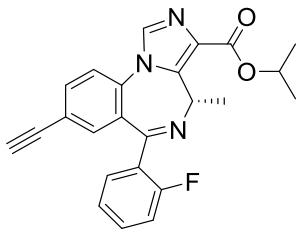

18 (GL-I-31)

The isopropyl ester **18** was prepared from **2** following the general procedure for esters with dry isopropanol. The crude residue was purified by flash column chromatography (silica gel, EtOAc/hexane 3:7) to yield the pure isopropyl ester **18** as a white powder (0.20 g, 97%): mp 231-232 °C; **$[\alpha]_D^{25}$** = +14.89 (*c* 0.94, $CHCl_3$); **^{1}H NMR** (300 MHz, $CDCl_3$): δ 7.93 (s, 1H), 7.69 (d, *J* = 8.2 Hz, 1H), 7.58 (dd, *J* = 16.6, 7.7 Hz, 2H), 7.44 (dd, *J* = 14.2, 6.6 Hz, 2H), 7.25 (t, *J* = 7.5 Hz, 1H), 7.04 (t, *J* = 9.2 Hz 1H), 6.70 (q, *J* = 7.0 Hz, 1H), 5.36 – 5.20 (m, 1H), 3.15 (s, 1H), 1.40 (dd, *J* = 9.4, 6.4 Hz, 6H), 1.28 (d, *J* = 7.0 Hz, 3H); **^{13}C NMR** (75 MHz, $CDCl_3$): δ 163.19 (s), 162.52 (s), 160.12 (d, J_{C-F} = 251.9 Hz), 141.63 (s), 135.16 (s), 134.76 (s), 134.57 (s), 133.92 (s), 131.92 (d, J_{C-F} = 8.7 Hz), 131.18 (s), 129.87 (s), 129.62 (s), 128.73 (d, J_{C-F} = 6.0 Hz), 124.48 (d, J_{C-F} = 3.4 Hz), 122.20 (s), 121.60 (s), 116.19 (d, J_{C-F} = 21.5 Hz), 81.44 (s), 79.67 (s), 68.26 (s), 50.14 (s), 21.95 (s), 14.85 (s); **HRMS** (ESI/IT-TOF) m/z: $[M + H]^+$ Calcd for $C_{24}H_{21}FN_3O_2$ 402.1612; found 402.1610.

2.2.7.17. (*S*)-*tert*-Butyl-8-ethynyl-6-(2-fluorophenyl)-4-methyl-4*H*-benzo[*f*]imidazo[1,5-*a*][1,4]diazepine-3-carboxylate (GL-I-30, 19)

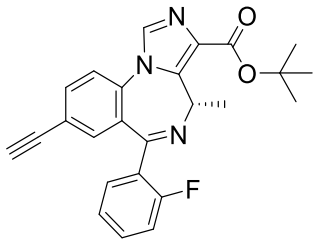

19 (GL-I-30)

The *t*-butyl ester **19** was prepared from **2** following the general procedure for esters with dry *t*-butanol. The crude residue was purified by flash column chromatography (silica gel, EtOAc/hexane 3:7) to yield the pure *t*-butyl ester **19** as a white powder (0.21 g, 96%): mp 214-215 °C; $\mathbf{[\alpha]_D^{25}}$ = + 15.29 (*c* 0.85, $CHCl_3$); **^{1}H NMR** (300 MHz, $CDCl_3$): δ 7.92 (s, 1H), 7.69 (d, *J* = 7.3 Hz, 1H), 7.65 – 7.51 (m, 2H), 7.45 (dd, *J* = 15.0, 6.9 Hz, 2H), 7.28 – 7.21 (m, 1H), 7.05 (t, *J* = 9.3 Hz, 1H), 6.67 (q, *J* = 6.9 Hz, 1H), 3.15 (s, 1H), 1.63 (s, 9H), 1.28 (d, *J* = 7.3 Hz, 3H); **^{13}C NMR** (75 MHz, $CDCl_3$): δ 163.17 (s), 162.24 (s), 160.12 (d, J_{C-F} = 250.7 Hz), 141.19 (s), 135.14 (s), 134.69 (s), 134.58 (s), 133.91 (s), 131.91 (d, J_{C-F} = 8.2 Hz), 131.16 (s), 130.85 (s), 129.59 (s), 128.73 (d, J_{C-F} = 13.1 Hz), 124.49 (d, J_{C-F} = 3.5 Hz), 122.22 (s), 121.50 (s), 116.21 (d, J_{C-F} = 21.4 Hz), 81.51 (s), 79.60 (s), 50.23 (s), 28.33 (s), 21.97 (s), 14.85 (s); **HRMS** (ESI/IT-TOF) m/z: $[M + H]^+$ Calcd for $C_{25}H_{23}FN_3O_2$ 416.1769; found 416.1768.

2.2.7.18. (*S*)-*tert*-Pentyl-8-ethynyl-6-(2-fluorophenyl)-4-methyl-4*H*-benzo[*f*]imidazo[1,5-*a*][1,4]diazepine-3-carboxylate (GL-I-33, 20)

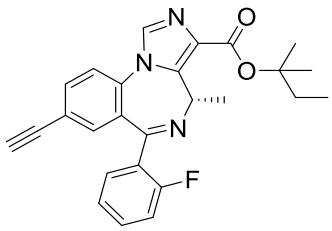

20 (GL-I-33)

The 2-methylbutyl ester **20** was prepared from **2** following the general procedure for esters with dry 2-methylbutan-2-ol. The crude residue was purified by flash column chromatography (silica gel, EtOAc/hexane 1:1) to yield the pure 2-methylbutyl ester **20** as a white powder (0.17 g, 77%): mp 94-96 °C; $\mathbf{[\alpha]_D^{25}}$ = +34.15 (*c* 0.41, $CHCl_3$); **^{1}H NMR** (300 MHz, $CDCl_3$): δ 7.92 (s, 1H), 7.69 (d, *J* = 8.1 Hz, 1H), 7.66 – 7.50 (m, 2H), 7.45 (dd, *J* = 16.3, 8.6 Hz, 2H), 7.29 – 7.19 (m, 1H), 7.05 (t, *J* = 9.2 Hz, 1H), 6.66 (q, *J* = 7.2 Hz, 1H), 3.15 (s, 1H), 1.98 (q, *J* = 7.4 Hz, 2H), 1.59 (s, 6H), 1.28 (d, *J* = 3.6 Hz, 3H), 0.99 (t, *J* = 7.5 Hz, 3H); **^{13}C NMR** (75 MHz, $CDCl_3$): δ 163.17 (s), 162.15 (s), 160.11 (d, J_{C-F} = 250.2 Hz), 141.12 (s), 135.15 (s), 134.68 (s), 133.89 (s), 131.96 (s), 131.85 (s), 131.16 (d, J_{C-F} = 1.6 Hz), 130.80 (s), 129.58 (s), 128.71 (d, J_{C-F} = 13.2 Hz), 124.49 (d, J_{C-F} = 3.4 Hz), 122.24 (s), 121.49 (s), 116.20 (d, J_{C-F} = 21.5 Hz), 84.17 (s), 81.48 (s), 79.61 (s), 50.24 (s), 33.47 (s), 25.91 (s), 25.73 (s), 14.91 (s), 8.47 (s); **HRMS** (ESI/IT-TOF) m/z: $[M + H]^+$ Calcd for $C_{26}H_{25}FN_3O_2$ 430.1925; found 430.1928.

2.2.7.19. (*S*)-8-Ethynyl-6-(2-fluorophenyl)-4-methyl-4*H*-benzo[*f*]imidazo[1,5-*a*][1,4]diazepine-3-carboxylic acid (SH-05 3-2'F-*S*-CH_3-acid, 23)

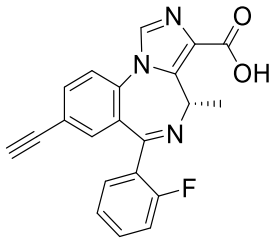

23 (SH-053-2'F-*S*-CH_3-acid)

The ethyl ester SH-053-2'F-*S*-CH_3 **2** (5.0 g, 12.91 mmol) was dissolved in EtOH (200 mL), after which sodium hydroxide pellets (4.1 g, 103.25 mmol) were added to the solution. This reaction mixture was heated to 55 ˚C for 0.5 h and the EtOH was removed under reduced pressure. Water (50 mL) was added to the residue to form an aq solution, which was then stirred at 0 ˚C for 10 min and then aq HCl (1 M) was added dropwise to the solution until the pH was 5 (pH paper). A pale white precipitate which formed, was left in the solution for 10 min and was then collected by filtration, washed with cold water and the aq layer also allowed to stand at rt for 10 h to yield additional acid **23**. The combined solids were dried under vacuum for 7 h to provide pure acid **23** as a white powder (4.6 g, 99%): mp 217-218 °C; **$[\alpha]_D^{25}$** = -14.58 (*c* 0.48, $CHCl_3$); **^{1}H NMR** (300 MHz, DMSO-d^6): δ 8.36 (s, 1H), 7.92 (d, *J* = 7.9 Hz, 1H), 7.79 (d, *J* = 7.2 Hz, 1H), 7.55 (dt, *J* = 7.8, 6.5 Hz, 2H), 7.32 (t, *J* = 7.4 Hz, 1H), 7.21 (t, *J* = 9.3 Hz, 2H), 6.61 (d, *J* = 7.6 Hz, 1H), 4.36 (s, 1H), 1.13 (d, *J* = 6.6 Hz, 3H); **^{13}C NMR** (75 MHz, DMSO-d^6): δ 164.63 (s), 162.92 (s), 159.85 (d, J_{C-F} = 242.7 Hz), 141.08 (s), 136.73 (s), 135.57 (s), 134.68 (d, J_{C-F} = 2.7 Hz), 133.19 (s), 133.14 (s), 132.64 (d, J_{C-F} = 6.1 Hz), 131.89 (s), 129.36 (d, J_{C-F} = 2.3 Hz), 128.85 (d, J_{C-F} = 8.2 Hz), 125.14 (d, *J* = 3.0 Hz), 123.98 (s), 121.15 (s), 116.39 (d, J_{C-F} = 20.3 Hz), 83.42 (s), 81.97 (s), 49.82 (s), 15.02 (s); **HRMS** (ESI/IT-TOF) m/z: $[M + H]^+$ Calcd for $C_{21}H_{15}FN_3O_2$ 360.1143; found 360.1142.

General procedure for the synthesis of esters/thioester/amides (21, 22, 7, 26-30)

A mixture of the acid SH-053-2'F-*S*-CH_3-acid **23** (200 mg, 0.56 mmol), thionyl chloride (0.407 mL, 5.6 mmol) and dry DCM (20 mL) was placed in an oven dried round bottom flask under argon. This suspension, which formed, was allowed to reflux at 60 ˚C for 1 h under argon. The absence of the starting material was confirmed on analysis by TLC (silica gel). The organic solvent and excess thionyl chloride were removed under reduced pressure on a rotovapor. This procedure was repeated five times with dry DCM (15 mL). The yellow residue, which remained was dissolved in dry DCM (20 mL) and cooled to 0 ˚C for 10 min under argon. Then the appropriate nucleophilic alcohol/thiol/amine (5.6 mmol), followed by triethylamine (0.78 mL, 5.6 mmol) was added to the reaction mixture at 0˚C and the mixture (individually) was then allowed to warm to rt and stirred for 1-2 h. After the completion of the reaction by TLC (silica gel), the solvent was removed under reduced pressure. The residue was treated with ice cold water (15 mL) and extracted with DCM (3 x 20 mL). The combined organic layer was washed with brine (20 mL) and dried (Na_2SO_4). The solvent was removed under reduced pressure and the residue was purified by column chromatography to yield the corresponding pure esters, thioesters or amides described below:

2.2.7.20. (*S*)-2,2,2-Trifluoroethyl-8-ethynyl-6-(2-fluorophenyl)-4-methyl-4*H*-benzo[*f*]imidazo[1,5-*a*][1,4]diazepine-3-carboxylate (GL-I-36, 21)

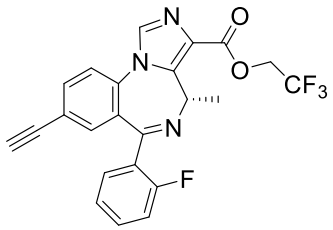

21 (GL-I-36)

The trifluoroethyl ester **21** was prepared from carboxylic acid **23** following the general procedure for esters/thioester/amides with dry 2,2,2-trifluoroethanol as the nucleophile. The crude residue

was purified by flash column chromatography (silica gel, EtOAc/hexane 2:3) to yield the pure trifluoroethyl ester **21** as a white powder (0.20 g, 82%): mp 226-227 °C; **[α]$_D^{25}$** = +9.43 (*c* 0.53, $CHCl_3$); **^{1}H NMR** (300 MHz, $CDCl_3$): δ 7.98 (s, 1H), 7.69 (d, *J* = 7.9 Hz, 1H), 7.57 (d, *J* = 7.9 Hz, 2H), 7.50 – 7.36 (m, 2H), 7.23 (t, *J* = 7.3 Hz, 1H), 7.01 (t, *J* = 8.9 Hz, 1H), 6.60 (q, *J* = 7.0 Hz, 1H), 4.88 – 4.54 (m, 2H), 3.16 (s, 1H), 1.26 (d, *J* = 6.9 Hz, 3H); **^{13}C NMR** (75 MHz, $CDCl_3$): δ 163.41 (s), 161.09 (s), 160.07 (d, J_{C-F} = 250.9 Hz), 143.06 (s), 135.54 (s), 135.29 (s), 134.19 (s), 133.89 (s), 132.08 (d, J_{C-F} = 8.1 Hz), 131.16 (s), 129.61 (s), 128.45 (d, J_{C-F} = 12.7 Hz), 127.72 (s), 124.53 (d, J_{C-F} = 3.2 Hz), 123.04 (q, J_{C-F} = 276.5 Hz), 122.31 (s), 121.95 (s), 116.20 (d, J_{C-F} = 21.4 Hz), 81.27 (s), 79.99 (s), 60.15 (q, J_{C-F} = 36.9 Hz), 50.10 (s), 14.70 (s); **HRMS** (ESI/IT-TOF) m/z: $[M + H]^+$ Calcd for $C_{23}H_{16}F_4N_3O_2$ 442.1173; found 442.1176.

2.2.7.21. (*S*)-Cyclopropyl-8-ethynyl-6-(2-fluorophenyl)-4-methyl-4*H*-benzo[*f*]imidazo[1,5-*a*][1,4]diazepine-3-carboxylate (GL-I-38, 22)

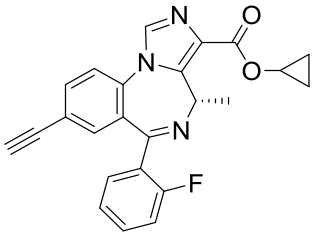

22 (GL-I-38)

The cyclopropyl ester **22** was prepared from the carboxylic acid **23** following the general procedure for esters/thioester/amides with dry cyclopropanol as the nucleophile. The crude residue was purified by flash column chromatography (silica gel, EtOAc/hexane 3:2) to yield the pure cyclopropyl ester **22** as a white powder (0.16 g, 71%): mp 230-231 °C; **[α]$_D^{25}$** = +11.38 (*c* 1.23, $CHCl_3$); **^{1}H NMR** (300 MHz, $CDCl_3$): δ 7.92 (s, 1H), 7.67 (d, *J* = 7.4 Hz, 1H), 7.55 (d, *J* = 7.9

Hz, 2H), 7.49 – 7.32 (m, 2H), 7.22 (t, *J* = 7.0 Hz, 1H), 7.00 (t, *J* = 8.6 Hz, 1H), 6.64 (q, *J* = 6.6 Hz, 1H), 4.38 – 4.21 (m, 1H), 3.15 (s, 1H), 1.24 (d, *J* = 5.6 Hz, 3H), 0.87 (d, *J* = 7.1 Hz, 2H), 0.77 (d, *J* = 5.5 Hz, 2H); **^{13}C NMR** (75 MHz, $CDCl_3$): δ 163.77 (s), 163.25 (s), 160.06 (d, J_{C-F} = 250.6 Hz), 141.87 (s), 135.20 (s), 134.93 (s), 134.39 (s), 133.88 (s), 131.97 (d, J_{C-F} = 9.0 Hz), 131.15 (s), 129.58 (s), 129.04 (s), 128.60 (d, J_{C-F} = 11.4 Hz), 124.49 (d, J_{C-F} = 3.1 Hz), 122.25 (s), 121.69 (s), 116.17 (d, J_{C-F} = 21.5 Hz), 81.37 (s), 79.85 (s), 50.02 (s), 49.32 (s), 14.82 (s), 5.22 (s); **HRMS** (ESI/IT-TOF) m/z: $[M + H]^+$ Calcd for $C_{24}H_{19}FN_3O_2$ 400.1456; found 400.1453.

2.2.7.22. (*S*)-S-Ethyl-8-ethynyl-6-(2-fluorophenyl)-4-methyl-4*H*-benzo[*f*]imidazo[1,5-*a*][1,4]diazepine-3-carbothioate (GL-I-77, 24)

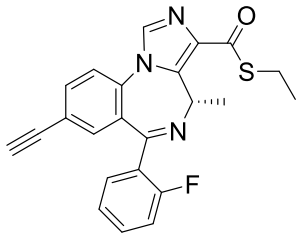

24 (GL-I-77)

The thioester **24** was prepared from the carboxylic acid **23** following the general procedure for esters/thioester/amides with dry ethanethiol as the nucleophile. The crude residue was purified by flash column chromatography (silica gel, EtOAc/hexane 2:3) to yield the pure thioethyl ester **24** as a white powder (0.18 g, 79%): mp 210-211 °C; **$[\alpha]_D^{25}$** = +21.43 (*c* 0.98, $CHCl_3$); **^{1}H NMR** (300 MHz, $CDCl_3$): δ 7.91 (s, 1H), 7.69 (d, *J* = 8.1 Hz, 1H), 7.64 – 7.50 (m, 2H), 7.48 – 7.38 (m, 2H), 7.24 (t, *J* = 7.3 Hz, 1H), 7.02 (t, *J* = 9.1 Hz, 1H), 6.65 (q, *J* = 14.0, 6.8 Hz, 1H), 3.16 (s, 1H), 3.09 – 2.89 (m, 2H), 1.33 (t, *J* = 7.4 Hz, 3H), 1.26 (d, *J* = 6.8 Hz, 3H); **^{13}C NMR** (75 MHz, $CDCl_3$): δ 187.81 (s), 163.16 (s), 160.11 (d, J_{C-F} = 250.3 Hz), 138.17 (s), 135.44 (s), 135.17 (s), 134.48 (s),

134.34 (s), 133.95 (s), 131.97 (d, J_{C-F} = 8.9 Hz), 131.23 (s), 129.66 (s), 128.61 (d, J_{C-F} = 11.7 Hz), 124.49 (d, J_{C-F} = 3.4 Hz), 122.19 (s), 121.76 (s), 116.17 (d, J_{C-F} = 21.5 Hz), 81.41 (s), 79.78 (s), 49.85 (s), 22.56 (s), 14.79 (s); **HRMS** (ESI/IT-TOF) m/z: $[M + H]^+$ Calcd for $C_{23}H_{19}FN_3OS$ 404.1227; found 404.1229.

2.2.7.23. (*S*)-8-Ethynyl-6-(2-fluorophenyl)-N,4-dimethyl-4*H*-benzo[*f*]imidazo[1,5-*a*][1,4]diazepine-3-carboxamide (MP-III-023, 25)

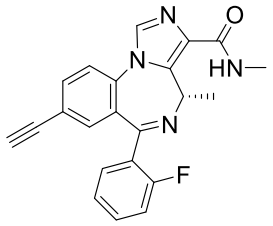

25 (MP-III-023)

The ethyl ester SH-053-2'F-*S*-CH_3 **2** (2 g, 5.2 mmol) was dissolved in DCM (10 mL) and was added to a sealed vessel fitted with a septum at -30 °C and treated with methyl amine (20 mL, 33% wt solution in EtOH). The vessel was sealed with a screw-cap and stirred at 55 °C for 18 h. The solution was then cooled to rt and the methyl amine and ethanol were removed under reduced pressure. The residue, which resulted, was purified by flash column chromatography (silica gel, EtOAc) to afford the pure methyl amide **25** as a pale white powder (1.7 g, 88.6 %): mp 136-137 °C; $[\alpha]_D^{25}$ = -11.54 (*c* 2.34, $CHCl_3$); **^{1}H NMR** (300 MHz, $CDCl_3$): δ 7.84 (s, 1H), 7.69 (d, *J* = 8.1 Hz, 2H), 7.64 (t, *J* = 7.0 Hz, 1H), 7.54 (d, *J* = 8.3 Hz, 1H), 7.44 (dd, *J* = 14.1, 7.1 Hz, 1H), 7.25 (t, *J* = 7.5 Hz, 1H), 7.17 (s, 1H), 7.03 (t, *J* = 9.3 Hz, 1H), 6.91 (q, *J* = 6.5 Hz, 1H), 3.15 (s, 1H), 2.97 (d, *J* = 5.0 Hz, 3H), 1.27 (d, *J* = 7.0 Hz, 3H); **^{13}C NMR** (75 MHz, $CDCl_3$) δ 163.41 (s), 162.86 (s), 161.81(d, J_{C-F} = 250.8 Hz), 138.68 (s), 135.31 (s), 134.58 (s), 134.14 (s), 133.46 (s), 132.28 (s), 132.26 (d, J_{C-F} = 6.4 Hz), 131.47 (s), 129.47 (s), 128.36 (d, J_{C-F} = 10.0 Hz), 124.54 (d, J_{C-F} =

3.5 Hz), 122.24 (s), 121.69 (s), 116.28 (d, J_{C-F} = 21.5 Hz), 81.42 (s), 79.76 (s), 49.66 (s), 25.67 (s), 15.06 (s); **HRMS** (ESI/IT-TOF) m/z: $[M + H]^+$ Calcd for $C_{22}H_{18}FN_4O$ 373.1459, found: 373.1462.

2.2.7.24. (*S*)-N-Ethyl-8-ethynyl-6-(2-fluorophenyl)-4-methyl-4*H*-benzo[*f*]imidazo[1,5-*a*][1,4]diazepine-3-carboxamide (GL-I-43, 26)

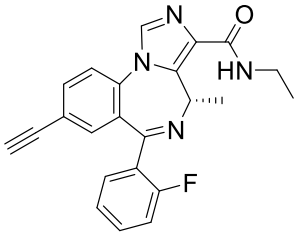

26 (GL-I-43)

The ethyl amide **26** was prepared from the carboxylic acid **23** following the general procedure for esters/thioester/amides with dry ethylamine as the nucleophile. The crude residue was purified by flash column chromatography (silica gel, EtOAc/hexane 1:1) to yield the pure ethyl amide **26** as a white powder (0.18 g, 88%): mp 208-209 °C; **$[\alpha]_D^{25}$** = -13.33 (*c* 0.6, $CHCl_3$); **^{1}H NMR** (300 MHz, $CDCl_3$): δ 7.97 (s, 1H), 7.69 (dd, *J* = 16.7, 7.9 Hz, 2H), 7.58 (d, *J* = 8.2 Hz, 1H), 7.46 (dd, *J* = 13.4, 7.2 Hz, 2H), 7.27 (t, *J* = 7.4 Hz, 2H), 7.04 (t, *J* = 9.3 Hz, 1H), 6.93 (q, *J* = 7.2 Hz, 1H), 3.55 – 3.37 (m, 2H), 3.16 (s, 1H), 1.29 (d, *J* = 7.2 Hz, 3H), 1.23 (t, *J* = 7.3 Hz, 3H); **^{13}C NMR** (75 MHz, $CDCl_3$): δ 162.82 (s), 162.51 (s), 160.10 (d, J_{C-F} = 250.5 Hz), 138.79 (s), 134.97 (s), 134.70 (s), 133.88 (s), 133.39 (s), 131.82 (d, J_{C-F} = 4.8 Hz), 131.75 (s), 131.35 (d, J_{C-F} = 1.5 Hz), 129.76 (s), 128.84 (d, J_{C-F} = 11.9 Hz), 124.45 (d, J_{C-F} = 3.4 Hz), 122.06 (s), 121.37 (s), 116.06 (d, J_{C-F} = 21.5 Hz), 81.54 (s), 79.55 (s), 49.88 (s), 33.71 (s), 15.02 (s); **HRMS** (ESI/IT-TOF) m/z: $[M + H]^+$ Calcd for $C_{23}H_{20}FN_4O$ 387.1614; found 387.1614.

2.2.7.25. (*S*)-N-Cyclopropyl-8-ethynyl-6-(2-fluorophenyl)-4-methyl-4*H*-benzo[*f*]imidazo[1,5-*a*][1,4]diazepine-3-carboxamide (GL-I-55, 27)

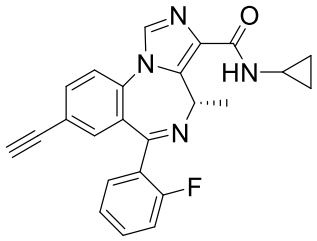

27 (GL-I-55)

The cyclopropyl amide **27** as prepared from the carboxylic acid **23** following the general procedure for esters/thioester/amides with dry cyclopropylamine as the nucleophile. The crude residue was purified by flash column chromatography (silica gel, EtOAc/hexane 1:1) to yield the pure cyclopropyl amide **27** as a white powder (0.19 g, 86%): mp 225-226 °C; $[\alpha]_D^{25}$ = -11.77 (*c* 0.17, $CHCl_3$); **^{1}H NMR** (300 MHz, $CDCl_3$): δ 8.00 (s, 1H), 7.69 (dd, *J* = 16.5, 8.1 Hz, 2H), 7.58 (d, *J* = 8.3 Hz, 1H), 7.46 (dd, *J* = 14.0, 6.8 Hz, 3H), 7.27 (t, *J* = 7.3 Hz, 1H), 7.04 (t, *J* = 9.3 Hz, 1H), 6.93 (q, *J* = 7.2 Hz, 1H), 3.17 (s, 1H), 2.85 (dq, *J* = 10.6, 3.6 Hz, 1H), 1.30 (d, *J* = 7.3 Hz, 3H), 0.89 – 0.73 (m, 2H), 0.69 – 0.50 (m, 2H); **^{13}C NMR** (75 MHz, $CDCl_3$): δ 164.02 (s), 162.83 (s), 160.12 (d, J_{C-F} = 249.8 Hz), 138.93 (s), 134.96 (s), 134.66 (s), 133.91 (s), 133.36 (s), 131.82 (d, J_{C-F} = 8.3 Hz), 131.59 (s), 131.37 (s), 129.79 (s), 128.84 (d, J_{C-F} = 11.4 Hz), 124.46 (d, J_{C-F} = 3.3 Hz), 122.04 (s), 121.42 (s), 116.07 (d, J_{C-F} = 21.5 Hz), 81.53 (s), 79.53 (s), 49.89 (s), 22.09 (s), 15.00 (s), 6.55 (s), 6.51 (s); **HRMS** (ESI/IT-TOF) m/z: $[M + H]^+$ Calcd for $C_{24}H_{20}FN_4O$ 399.1616; found 399.1618

2.2.7.26. (*S*)-8-Ethynyl-6-(2-fluorophenyl)-N-isopropyl-4-methyl-4*H*-benzo[*f*]imidazo[1,5-*a*][1,4]diazepine-3-carboxamide (GL-I-57, 28)

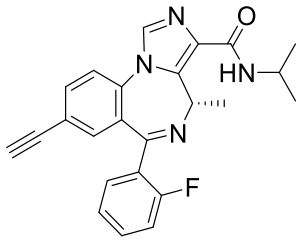

28 (GL-I-57)

The isopropyl amide **28** was prepared from the carboxylic acid **23** following the general procedure for esters/thioester/amides with dry isopropylamine as the nucleophile. The crude residue was purified by flash column chromatography (silica gel, EtOAc/hexane 2:3) to yield the pure isopropyl amide **28** as a white powder (0.16 g, 74%): mp 238-239 °C; **$[\alpha]_D^{25}$** = -6.19 (*c* 2.1, $CHCl_3$); **^{1}H NMR** (300 MHz, $CDCl_3$): δ 7.81 (s, 1H), 7.62 (dd, *J* = 17.0, 7.9 Hz, 2H), 7.51 (d, *J* = 8.3 Hz, 1H), 7.46 – 7.33 (m, 2H), 7.21 (t, *J* = 7.5 Hz, 1H), 7.02 – 6.94 (m, 2H), 6.88 (q, *J* = 6.9 Hz, 1H), 4.21 (dq, *J* = 13.4, 6.6 Hz, 1H), 3.14 (s, 1H), 1.22 (dd, *J* = 13.5, 7.2 Hz, 9H); **^{13}C NMR** (75 MHz, $CDCl_3$): δ 162.83 (s), 161.78 (s), 158.43 (s), 138.78 (s), 134.98 (s), 134.69 (s), 133.85 (s), 133.35 (s), 131.85 (s), 131.74 (s), 131.35 (s), 129.73 (s), 128.83 (d, J_{C-F} = 12.7 Hz), 124.43 (d, J_{C-F} = 3.3 Hz), 122.08 (s), 121.36 (s), 116.04 (d, J_{C-F} = 21.6 Hz), 81.53 (s), 79.62 (s), 49.87 (s), 40.69 (s), 22.93 (s), 22.85 (s), 15.00 (s); **HRMS** (ESI/IT-TOF) m/z: $[M + H]^+$ Calcd for $C_{24}H_{22}FN_4O$ 401.1772; found 401.1776.

2.2.7.27. (*S*)-N-(*tert*-Butyl)-8-ethynyl-6-(2-fluorophenyl)-4-methyl-4*H*-benzo[*f*]imidazo[1,5-*a*][1,4]diazepine-3-carbox- amide (GL-I-41, 29)

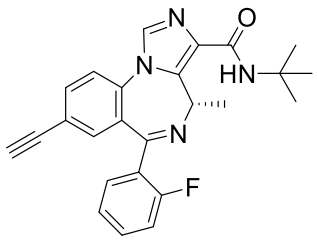

29 (GL-I-41)

The *t*-butyl amide **29** was prepared from the carboxylic acid **23** following the general procedure for esters/thioester/amides with dry *t*-butylamine as the nucleophile. The crude residue was purified by flash column chromatography (silica gel, EtOAc/hexane 1:1) to yield the pure *t*-butyl amide **29** as a white powder (0.19 g, 83%): mp 136-137 °C; $\mathbf{[\alpha]_D^{25}}$ = +8.7 (*c* 0.23, $CHCl_3$); **^{1}H NMR** (300 MHz, $CDCl_3$): δ 7.80 (s, 1H), 7.65 (dd, *J* = 15.1, 7.7 Hz, 2H), 7.51 (d, *J* = 8.3 Hz, 1H), 7.44 (dd, *J* = 10.1, 7.6 Hz, 2H), 7.24 (t, *J* = 7.5 Hz, 1H), 7.02 (dd, *J* = 15.8, 5.8 Hz, 2H), 6.87 (q, *J* = 7.1 Hz, 1H), 3.15 (s, 1H), 1.46 (s, 9H), 1.27 (d, *J* = 7.2 Hz, 3H); **^{13}C NMR** (75 MHz, $CDCl_3$): δ 162.84 (s), 162.11 (s), 160.15 (d, J_{C-F} = 250.3 Hz), 138.60 (s), 134.97 (s), 134.76 (s), 133.85 (s), 133.02 (s), 132.59 (s), 131.84 (d, J_{C-F} = 7.8 Hz), 131.39 (d, J_{C-F} = 2.4 Hz), 129.81 (s), 128.79 (d, J_{C-F} = 11.8 Hz), 124.45 (d, J_{C-F} = 3.4 Hz), 122.07 (s), 121.37 (s), 116.07 (d, J_{C-F} = 21.5 Hz), 81.56 (s), 79.49 (s), 50.91 (s), 49.90 (s), 28.98 (s), 14.96 (s); **HRMS** (ESI/IT-TOF) m/z: $[M + H]^+$ Calcd for $C_{25}H_{24}FN_4O$ 415.1926; found 415.1926.

2.2.7.28. (*S*)-8-Ethynyl-6-(2-fluorophenyl)-N,N,4-trimethyl-4*H*-benzo[*f*]imidazo[1,5-*a*][1,4]diazepine-3-carboxamide (GL-I-54, 30)

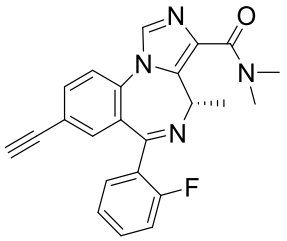

30 (GL-I-54)

The dimethyl amide **30** was prepared from **23** following the general procedure with dry dimethylamine as the nucleophile. The crude residue was purified by column chromatography (silica gel, EtOAc and 1% MeOH) to yield pure dimethyl amide **30** as a light yellow powder (0.15 g, 71%): mp 142-144 °C; $\mathbf{[\alpha]_D^{25}}$ = -16.0 (*c* 0.75, $CHCl_3$); **^{1}H NMR** (300 MHz, $CDCl_3$): δ 7.94 (s, 1H), 7.73 (d, *J* = 8.1 Hz, 1H), 7.63 (t, *J* = 7.4 Hz, 1H), 7.52 (d, *J* = 8.2 Hz, 1H), 7.48 – 7.41 (m, 2H), 7.26 (t, *J* = 7.5 Hz, 1H), 7.04 (t, *J* = 9.3 Hz, 1H), 4.33 (q, *J* = 6.0 Hz, 1H), 3.16 (s, 1H), 3.14 (s, 3H), 3.01 (s, 3H), 1.94 (d, *J* = 6.5 Hz, 3H); **^{13}C NMR** (75 MHz, $CDCl_3$): δ 166.14 (s), 162.60 (s), 160.25 (d, J_{C-F} = 252.3 Hz), 135.31 (s), 134.73 (d, J_{C-F} = 7.2 Hz), 133.83 (s), 133.73 (s), 132.79 (d, J_{C-F} = 12.7 Hz), 132.05 (d, J_{C-F} = 9.4 Hz), 131.78 (s), 131.28 (s), 129.25 (s), 127.69 (d, J_{C-F} = 10.8 Hz), 124.51 (d, J_{C-F} = 3.4 Hz), 122.83 (s), 121.50 (s), 116.17 (d, J_{C-F} = 21.7 Hz), 81.57 (s), 79.46 (s), 52.21 (s), 39.09 (s), 35.03 (s), 18.50 (s); **HRMS** (ESI/IT-TOF) m/z: $[M + H]^+$ Calcd for $C_{23}H_{20}FN_4O$ 387.1616; found 387.1624.

General Procedure for the Preparation of Oxadiazoles (31-33)

The ethyl ester **2** (200 mg, 0.52 mmol) was dissolved in dry THF (20 mL) at rt under argon. In a separate flask which contained 3Å molecular sieves, the corresponding oxime (2.08 mmol) was dissolved in dry THF (30 mL) under argon and treated with sodium hydride (60% dispersion in mineral oil, 0.57 mmol). The mixture, which resulted, was stirred for 15 min at which point the

solution containing the ethyl ester was added. The reaction mixture, which resulted, was stirred at rt for 2 h until the starting material was consumed as indicated on analysis by TLC (silica gel). The reaction mixture was quenched with a saturated aq $NaHCO_3$ solution (50 mL). Water (50 mL) was then added and the product was extracted with EtOAc (3 x 100 mL). The organic layers were combined, washed with brine (30 mL) and dried (Na_2SO_4). The solvent was removed under reduced pressure. The solid, which resulted, was purified by flash column chromatography (silica gel) to afford the pure corresponding oxadiazole, individually.

2.2.7.29. (*S*)-5-(8-Ethynyl-6-(2-fluorophenyl)-4-methyl-4*H*-benzo[*f*]imidazo[1,5-*a*][1,4]diazepin-3-yl)-3-methyl-1,2,4-oxadiazole (GL-I-65, 31)

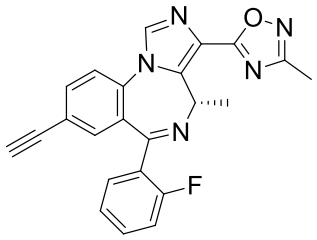

31 (GL-I-65)

The methyl oxadiazole **31** was prepared from **2** following the general procedure for oxadiazoles with the methyl oxime (0.154 g, 2.08 mmol). The crude residue was purified by flash column chromatography (silica gel, EtOAc/hexane 3:2) to yield pure methyl oxadiazole **31** as a white powder (0.174 g, 85%): mp 225-226 °C; $[\alpha]_D^{25}$ = +32.52 (*c* 2.86, $CHCl_3$); **^{1}H NMR** (300 MHz, $CDCl_3$): δ 8.08 (s, 1H), 7.74 (d, *J* = 8.2 Hz, 1H), 7.63 (d, *J* = 8.4 Hz, 2H), 7.48 (dd, *J* = 18.1, 11.6 Hz, 2H), 7.27 (t, *J* = 7.5 Hz, 1H), 7.06 (t, *J* = 9.2 Hz, 1H), 6.75 (q, *J* = 7.1 Hz, 1H), 3.18 (s, 1H), 2.47 (s, 3H), 1.35 (d, *J* = 7.2 Hz, 3H); **^{13}C NMR** (75 MHz, $CDCl_3$): δ 170.75 (s), 167.42 (s), 163.40 (s), 160.09 (d, $J_{C\text{-}F}$ = 250.5 Hz), 139.26 (s), 136.32 (s), 135.34 (s), 134.17 (s), 134.05 (s), 132.06

(d, $J_{C\text{-}F}$ = 8.5 Hz), 131.20 (s), 129.63 (s), 128.55 (d, $J_{C\text{-}F}$ = 12.3 Hz), 124.83 (s), 124.50 (d, $J_{C\text{-}F}$ = 3.2 Hz), 122.21 (s), 121.88 (s), 116.21 (d, $J_{C\text{-}F}$ = 21.4 Hz), 81.34 (s), 79.95 (s), 50.16 (s), 14.94 (s), 11.66 (s); **HRMS** (ESI/IT-TOF) m/z: $[M + H]^+$ Calcd for $C_{23}H_{17}FN_5O$ 398.1412; found 398.1419.

2.2.7.30. (*S*)-3-Ethyl-5-(8-ethynyl-6-(2-fluorophenyl)-4-methyl-4*H*-benzo[*f*]imidazo[1,5-*a*][1,4]diazepin-3-yl)-1,2,4-oxadiazole (GL-I-66, 32)

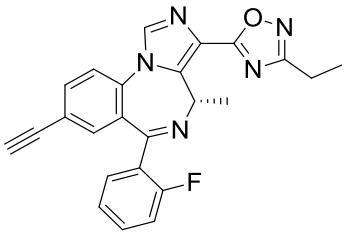

32 (GL-I-66)

The ethyl oxadiazole **32** was prepared from **2** following the general procedure for oxadiazoles with the ethyl oxime (0.183 g, 2.08 mmol). The crude residue was purified by flash column chromatography (silica gel, EtOAc/Hexane 3:2) to yield pure ethyl oxadiazole **32** as a white powder (0.168 g, 79%): mp 199-200 °C; $\mathbf{[\alpha]_D^{25}}$ = +50.00 (*c* 0.22, $CHCl_3$); **^{1}H NMR** (300 MHz, $CDCl_3$): δ 8.08 (s, 1H), 7.75 (d, *J* = 8.2 Hz, 1H), 7.63 (d, *J* = 8.3 Hz, 2H), 7.54 – 7.40 (m, 2H), 7.27 (t, *J* = 7.4 Hz, 1H), 7.06 (t, *J* = 9.2 Hz, 1H), 6.75 (q, *J* = 14.4, 7.2 Hz, 1H), 3.18 (s, 1H), 2.84 (q, *J* = 7.6 Hz, 2H), 1.40 (d, *J* = 7.6 Hz, 3H), 1.36 (t, *J* = 3.6 Hz, 3H); **^{13}C NMR** (75 MHz, $CDCl_3$): δ 171.88 (s), 170.70 (s), 163.41 (s), 160.10 (d, $J_{C\text{-}F}$ = 251.4 Hz), 139.22 (s), 136.26 (s), 135.33 (s), 134.22 (s), 134.07 (s), 132.04 (d, $J_{C\text{-}F}$ = 8.7 Hz), 131.15 (s), 129.58 (d, $J_{C\text{-}F}$ = 6.0 Hz), 128.58 (d, $J_{C\text{-}F}$ = 11.9 Hz), 124.99 (s), 124.51 (d, $J_{C\text{-}F}$ = 3.2 Hz), 122.18 (s), 121.88 (s), 116.22 (d, $J_{C\text{-}F}$ = 21.5 Hz), 81.34 (s), 79.90 (s), 50.23 (s), 19.74 (s), 14.97 (s), 11.51 (s); **HRMS** (ESI/IT-TOF) m/z: $[M + H]^+$ Calcd for $C_{24}H_{19}FN_5O$ 412.1568; found 412.1569.

2.2.7.31. (*S*)-5-(8-Ethynyl-6-(2-fluorophenyl)-4-methyl-4*H*-benzo[*f*]imidazo[1,5-*a*][1,4]diazepin-3-yl)-3-isopropyl-1,2,4-oxadiazole (GL-I-81, 33)

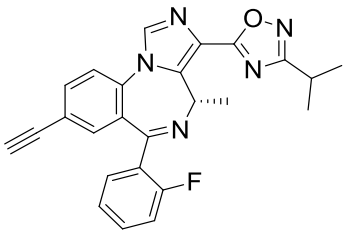

33 (GL-I-81)

The isopropyl oxadiazole **33** was prepared from **2** following the general procedure for oxadiazoles with the isopropyl oxime (0.212 g, 2.08 mmol). The crude residue was purified by flash column chromatography (silica gel, EtOAc/hexane 3:2) to yield pure isopropyl oxadiazole **33** as a white powder (0.180 g, 82%): mp 205-206 °C; $[\alpha]_D^{25}$ = +22.37 (*c* 0.76, $CHCl_3$); **^{1}H NMR** (300 MHz, $CDCl_3$): δ 8.06 (s, 1H), 7.66 (d, *J* = 8.3 Hz, 1H), 7.60 (d, *J* = 8.4 Hz, 1H), 7.53 (t, *J* = 7.3 Hz, 1H), 7.44 – 7.30 (m, 2H), 7.17 (t, *J* = 7.5 Hz, 1H), 6.96 (t, *J* = 9.2 Hz, 1H), 6.67 (q, *J* = 7.0 Hz, 1H), 3.14 (s, 1H), 3.09 (q, *J* = 7.0 Hz, 1H), 1.32 (d, *J* = 7.0 Hz, 6H), 1.28 (d, *J* = 7.5 Hz, 3H); **^{13}C NMR** (75 MHz, $CDCl_3$): δ 175.24 (s), 170.61 (s), 163.38 (s), 160.03 (d, J_{C-F} = 251.5 Hz), 139.17 (s), 136.34 (s), 135.36 (s), 134.17 (s), 133.98 (s), 132.01 (d, J_{C-F} = 8.3 Hz), 131.10 (s), 129.48 (s), 128.58 (d, J_{C-F} = 12.3 Hz), 124.96 (s), 124.48 (d, J_{C-F} = 3.1 Hz), 122.28 (s), 121.82 (s), 116.16 (d, J_{C-F} = 21.4 Hz), 81.30 (s), 80.03 (s), 50.22 (s), 26.70 (s), 20.57 (s), 20.51 (s), 14.94 (s); **HRMS** (ESI/IT-TOF) m/z: $[M + H]^+$ Calcd for $C_{25}H_{21}FN_5O$ 426.1725; found 426.1728.

2.2.7.32. (*S*)-8-Ethynyl-6-(2-fluorophenyl)-4-methyl-4*H*-benzo[*f*]imidazo[1,5-*a*][1,4]diazepine-3-carbonitrile (MP-III-018.A, 34)

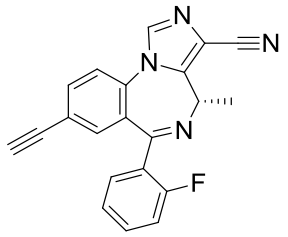

34 (MP-III-18.A)

The ethyl ester SH-053-2'F-*S*-CH_3 **2** (0.5 g, 1.40 mmol) was stirred in dry xylene (35 mL) at rt. Using a glass syringe and a metal needle, dimethylaluminum amine (0.67 M, 12.5 mL, 8.42 mmol) was carefully added to the solution of starting material **2**. The reaction was then heated to 80 ˚C in an oil bath and was monitored on analysis by TLC (silica gel) until the starting material had been consumed in 2 h. Once the reaction was complete, the mixture was cooled to rt and then quenched with cold water (15 mL). The product was extracted with EtOAc (5 x 50 mL) and the organic layers were combined, washed with brine and dried (Na_2SO_4). The solvent was removed under reduced pressure. The solid, which resulted, was purified by flash column chromatography (silica gel, EtOAc/hexane 1:1) which afforded the nitrile **34** as a white solid (0.331 g, 75.4%): mp 131-132 °C; **$[\alpha]_D^{25}$** = -165.16 (*c* 1.55, $CHCl_3$); **^{1}H NMR** (300 MHz, $CDCl_3$): δ 7.98 (s, 1H), 7.78 (d, *J* = 7.1 Hz, 1H), 7.67 (s, 1H), 7.62 – 7.53 (m, 1H), 7.49 (s, 2H), 7.28 (s, 1H), 7.04 (t, *J* = 8.7 Hz, 1H), 4.36 (d, *J* = 4.8 Hz, 1H), 3.20 (s, 1H), 2.18 (d, *J* = 4.6 Hz, 3H); **^{13}C NMR** (75 MHz, $CDCl_3$): δ 163.64 (s), 161.94 (d, J_{C-F} = 253.4 Hz), 143.66 (s), 135.75 (s), 135.69 (s), 133.97 (s), 133.35 (s), 132.89 (d, J_{C-F} = 9.7 Hz),131.37 (s), 129.22 (s), 126.85 (d, J_{C-F} = 13.0 Hz), 124.73 (d, J_{C-F} = 6.5 Hz), 122.88 (s), 122.64 (s), 116.50(d, J_{C-F} = 19.7 Hz), 114.54 (s), 110.74 (s), 81.13 (s), 80.33 (s), 51.68 (s), 18.09 (s); **HRMS** (ESI/IT-TOF) m/z: $[M + H]^+$ Calcd for $C_{21}H_{14}FN_4$ 341.1137; found 341.1142.

Preparation of the 0.67 M dimethylaluminum amine solution

The ammonia gas was bubbled into dry DCM (20 mL) at 0 °C until the solution was saturated. This took about 10-15 min. The trimethylaluminum (10 mL, 2.0 M in toluene) was then added to the solution. The solution was stirred at rt for 5 min and transferred directly for use in the reaction above using a glass syringe and metal needle.[120]

2.2.7.33. (*R*)-8-Ethynyl-6-(2-fluorophenyl)-N,4-dimethyl-4*H*-benzo[*f*]imidazo[1,5-*a*][1,4]diazepine-3-carboxamide (MP-III-022, 35)

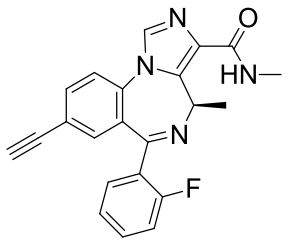

35 (MP-III-022)

The ethyl ester SH-053-2'F-*R*-CH_3 **1** (2 g, 5.2 mmol) was dissolved in DCM (10 mL) and was added to a sealed vessel fitted with a septum at -30 °C and treated with methyl amine (75 mL, 33% wt solution in EtOH). The vessel was sealed with a screw-cap and stirred at 55 °C for 18 h. The solution was then cooled to rt and the methyl amine and ethanol were removed under reduced pressure. The residue, which resulted, was purified by flash column chromatography (silica gel, EtOAc) to afford the pure methyl amide **35** as a pale white powder (1.7 g, 88.5 %): **^{1}H NMR** (300 MHz, $CDCl_3$) δ 7.81 (s, 1H), 7.60 (dd, *J* = 17.1, 7.6 Hz, 2H), 7.50 (d, *J* = 8.3 Hz, 1H), 7.43 – 7.32 (m, 2H), 7.26 – 7.12 (m, 2H), 6.96 (t, *J* = 9.3 Hz, 1H), 6.87 (q, *J* = 7.1 Hz, 1H), 3.14 (s, 1H), 2.91 (d, *J* = 5.0 Hz, 3H), 1.23 (d, *J* = 6.7 Hz, 3H); **^{13}C NMR** (75 MHz, $CDCl_3$) δ 163.27 (s), 162.79 (s), 160.07 (d, *J* = 250.3 Hz), 138.63 (s), 134.98 (s), 134.66 (s), 133.85 (s), 133.51 (s), 131.75 (s), 131.71 (s), 131.33 (s), 129.65 (s), 128.83 (d, *J* = 12.7 Hz), 124.40 (s), 122.10 (s), 121.32 (s), 116.02

(d, *J* = 21.5 Hz), 81.52 (s), 79.65 (s), 49.84 (s), 25.56 (s), 15.05 (s); **HRMS** (ESI/IT-TOF) m/z: $[M + H]^+$ Calcd for $C_{22}H_{18}FN_4O$ 373.1459, found: 373.1469.

2.2.7.34. (*R*)-8-Ethynyl-6-(2-fluorophenyl)-4-methyl-4*H*-benzo[*f*]imidazo[1,5-*a*][1,4] diazepine-3-carboxylic acid. (SH-053-2'F-*R*-CH_3-acid, 68)

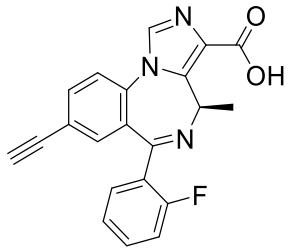

68 (SH-053-2'F-*R*-CH_3-acid)

The ethyl ester SH-053-2'F-*R*-CH_3 **1** (20.0 g, 51.6 mmol) was dissolved in EtOH (500 mL), after which solid NaOH (16.6 g, 412.8 mmol) was added to the solution. This reaction mixture was heated to 55 ˚C for 0.5 h and the EtOH was removed under reduced pressure. The remaining aq solution was stirred at 0 ˚C for 10 min and then aq HCl (1 M) was added dropwise to the solution until the pH was 5 (pH paper). A pale white precipitate which formed, was left in the solution for 10 min and was then collected by filtration, washed with cold water and the aq layer also allowed to stand at rt for 10 h to yield additional acid **68**. The combined solids were dried under vacuum for 7 h to provide the pure acid **68** as a white powder (18.4 g, 99.2 % yield): mp 196-198 °C; **$[\alpha]_D^{25}$** = +4 (*c* 0.46, $CHCl_3$); **^{1}H NMR** (300 MHz, DMSO-d^6) δ 8.42 (s, 1H), 7.94 (d, 1H, *J* = 8.4 Hz), 7.82 (d, 1H, *J* = 8.2 Hz), 7.56 (dt, 2H, *J* = 7.8, 6.5 Hz), 7.33 (t, 1H, *J* = 7.4 Hz), 7.22 (t, 2H, *J* = 9.3 Hz), 6.53 (d, 1H, *J* = 7.1 Hz), 2.51 (s, 1H), 1.16 (d, 3H, *J* = 6.8 Hz); **^{13}C NMR** (75 MHz, DMSO) δ 165.07 (s), 162.78 (s), 159.82 (d, *J* = 248.4 Hz), 140.49 (s), 136.40 (s), 135.52 (s), 134.78 (s), 133.18 (s), 132.62 (s), 131.87 (s), 129.35 (s), 128.95 (d, *J* = 12.6 Hz), 125.16 (s), 124.41

(s), 123.97 (s), 121.05 (s), 116.37 (d, *J* = 20.9 Hz), 83.37 (s), 82.01 (s), 49.77 (s), 15.00 (d, *J* = 15.1 Hz); **HRMS** (ESI/IT-TOF) m/z: $[M + H]^+$ Calcd for $C_{21}H_{15}FN_3O_2$ 360.1143; found 360.1140.

2.2.7.35. (*R*)-8-Ethynyl-6-(2-fluorophenyl)-*N*,*N*,4-trimethyl-4*H*-benzo[*f*]imidazo[1,5-*a*][1,4]diazepine-3-carboxam (GL-II-73, 36)

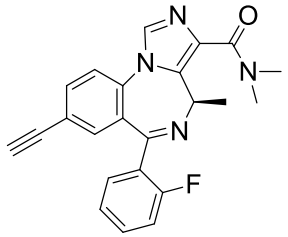

36 (GL-II-73)

The amide **36** was prepared from **68** following the general procedure for esters/thioester/amides, via the acid chloride, with dry dimethylamine as the nucleophile. The crude residue was purified by column chromatography (silica gel, EtOAc and 1% MeOH) to yield pure dimethyl amide **36** as a light yellow powder (1.5 g, 3.9 mmol, 70%): mp 189-190 °C; $[\alpha]_D^{25}$ = +40.98 (*c* 0.61, $CHCl_3$); **^{1}H NMR** (300 MHz, $CDCl_3$): δ 7.92 (s, 1H), 7.68 (d, *J* = 8.0 Hz, 1H), 7.59 (t, *J* = 7.3 Hz, 1H), 7.49 (d, *J* = 8.2 Hz, 1H), 7.45 – 7.35 (m, 2H), 7.21 (t, *J* = 7.5 Hz, 1H), 6.99 (t, *J* = 9.3 Hz, 1H), 4.28 (q, *J* = 6.0 Hz, 1H), 3.14 (s, 1H), 3.09 (s, 3H), 2.96 (s, 3H), 1.89 (d, *J* = 6.6 Hz, 3H); **^{13}C NMR** (75 MHz, CDCl3) δ 166.10 (s), 162.69 (s), 160.19 (d, *J* = 250.4 Hz), 135.34 (s), 134.62 (d, *J* = 9.0 Hz), 133.90 (s), 133.71 (s), 132.94 (d, *J* = 8.4 Hz), 132.47 (s), 132.12 (d, *J* = 9.1 Hz), 131.29 (s), 129.18 (s), 127.57 (d, *J* = 11.6 Hz), 124.51 (d, *J* = 2.2 Hz), 122.87 (s), 121.52 (s), 116.17 (d, *J* = 21.3 Hz), 81.52 (s), 79.63 (s), 52.13 (s), 39.09 (s), 35.04 (s), 18.37 (s); **HRMS** (ESI/IT-TOF) m/z: [M + H] Calcd for $C_{23}H_{20}FN_4O$ 387.1616; found 387.1626.

2.2.7.36. (*R*)-*N*-Ethyl-8-ethynyl-6-(2-fluorophenyl)-4-methyl-4*H*-benzo[*f*]imidazo[1,5-*a*][1,4]diazepine-3-carboxamide (GL-II-74, 37)

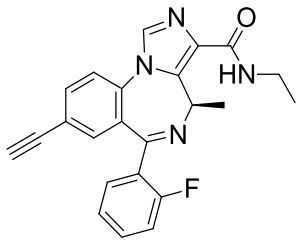

37 (GL-II-74)

The amide **37** was prepared from **68** following the general procedure for esters/thioester/amides, via the acid chloride, with dry ethylamine as the nucleophile. The crude residue was purified by column chromatography (silica gel, 3:2 EtOAc and hexane) to yield pure ethyl amide **37** as a white powder (1.6 g, 4.3 mmol, 78%): mp 215-216 °C; $[\alpha]_D^{25}$ = +44.07 (*c* 0.59, $CHCl_3$); **^{1}H NMR** (300 MHz, $CDCl_3$): δ 7.83 (s, 1H), 7.65 (dd, *J* = 16.8, 7.8 Hz, 2H), 7.53 (d, *J* = 8.3 Hz, 1H), 7.47 – 7.39 (m, 2H), 7.24 (t, *J* = 7.5 Hz, 1H), 7.17 (s, 1H), 7.01 (t, *J* = 9.3 Hz, 1H), 6.90 (q, *J* = 6.3 Hz, 1H), 3.61 – 3.34 (m, 2H), 3.15 (s, 1H), 1.26 (d, *J* = 9.0 Hz, 3H), 1.22 (t, *J* = 7.3 Hz, 3H); **^{13}C NMR** (75 MHz, $CDCl_3$) δ 162.81 (s), 162.51 (s), 160.13 (d, *J* = 250.7 Hz), 138.81 (s), 134.96 (s), 134.71 (s), 133.90 (s), 133.37 (s), 131.84 (s), 131.76 (s), 131.37 (s), 129.78 (s), 128.86 (d, *J* = 10.6 Hz), 124.44 (d, *J* = 3.4 Hz), 122.04 (s), 121.38 (s), 116.06 (d, *J* = 21.5 Hz), 81.55 (s), 79.52 (s), 49.89 (s), 33.70 (s), 15.02 (s), 15.01(s); **HRMS** (ESI/IT-TOF) m/z: [M + H] Calcd for $C_{23}H_{20}FN_4O$ 387.1616; found 387.1618.

2.2.7.37. (*R*)-*N*-Cyclopropyl-8-ethynyl-6-(2-fluorophenyl)-4-methyl-4*H*-benzo[*f*]imidazo [1,5-*a*][1,4]diazepine-3-carboxamide (GL-II-75, 38)

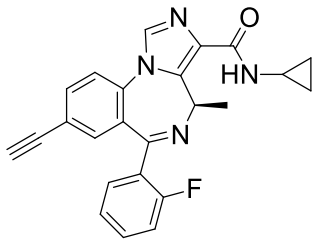

38 (GL-II-75)

The amide **38** was prepared from **68** following the general procedure for esters/thioester/amides, via the acid chloride, with dry cyclopropylamine as the nucleophile. The crude residue was purified by column chromatography (silica gel, 1:1 EtOAc and hexane) to yield pure cyclopropyl amide **38** as a white powder (1.8 g, 4.5 mmol, 82%): mp 231-232 °C; $\mathbf{[\alpha]_D^{25}}$ = +3.81 (*c* 0.46, $CHCl_3$); **^{1}H NMR** (300 MHz, $CDCl_3$): δ 7.80 (s, 1H), 7.64 (dd, *J* = 15.9, 7.6 Hz, 2H), 7.52 (d, *J* = 8.3 Hz, 1H), 7.47 – 7.37 (m, 2H), 7.30 – 7.19 (m, 2H), 7.01 (t, *J* = 9.3 Hz, 1H), 6.89 (q, *J* = 7.0 Hz, 1H), 3.15 (s, 1H), 2.93 – 2.67 (m, 1H), 1.26 (d, *J* = 6.8 Hz, 3H), 0.87 – 0.76 (m, 2H), 0.65 – 0.51 (m, 2H); **^{13}C NMR** (75 MHz, $CDCl_3$) δ 164.02 (s), 162.82 (s), 160.13 (d, *J* = 249.9 Hz), 138.91 (s), 134.97 (s), 134.65 (s), 133.89 (s), 133.37 (s), 131.80 (d, *J* = 9.0 Hz), 131.58 (s), 131.36 (s), 129.78 (s), 128.81 (d, *J* = 14.6 Hz), 124.45 (d, *J* = 3.4 Hz), 122.04 (s), 121.42 (s), 116.06 (d, *J* = 21.5 Hz), 81.53 (s), 79.55 (s), 49.88 (s), 22.10 (s), 14.99 (s), 6.54 (s), 6.50 (s); **HRMS** (ESI/IT-TOF) m/z: [M + H] Calcd for $C_{24}H_{20}FN_4O$ 399.1616; found 399.1621.

2.2.7.38. (*R*)-8-Ethynyl-6-(2-fluorophenyl)-*N*-isopropyl-4-methyl-4*H*-benzo[*f*]imidazo[1,5-*a*][1,4]diazepine-3-carboxamide (GL-III-66, 39)

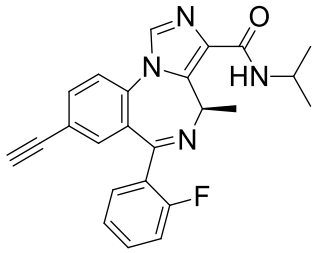

39 (GL-III-66)

The amide **39** was prepared from **68** following the general procedure for esters/thioester/amides, via the acid chloride, with dry isopropylamine as the nucleophile. The crude residue was purified by column chromatography (silica gel, 1:1 EtOAc and hexane) to yield a mixture of rotamers **39** as a white powder (2.9 g, 74.4 %): **^{1}H NMR** (300 MHz, $CDCl_3$) δ 7.83 (s, 1H), 7.64 (dd, *J* = 17.1, 8.0 Hz, 2H), 7.52 (d, *J* = 8.3 Hz, 1H), 7.43 (dd, *J* = 11.4, 5.8 Hz, 2H), 7.31 – 7.19 (m, 1H), 7.07 – 6.96 (m, 2H), 6.89 (q, *J* = 7.2 Hz, 1H), 4.54 – 3.92 (m, 1H), 3.15 (s, 1H), 1.33 – 1.16 (m, 9H); **^{13}C NMR** (75 MHz, $CDCl_3$) δ 162.92 (s), 161.76 (s), 159.42 (d, *J* = 144.0 Hz), 138.80 (s), 135.02 (s), 134.70 (s), 133.91 (s), 133.33 (s), 131.91 (s), 131.83 (d, *J* = 3.2 Hz), 131.38 (s), 129.74 (s), 128.78 (d, *J* = 11.6 Hz), 124.46 (d, *J* = 3.3 Hz), 122.08 (s), 121.41 (s), 116.07 (d, *J* = 21.5 Hz), 81.53 (s), 79.58 (s), 49.86 (s), 40.73 (s), 22.95 (s), 22.86 (s), 15.01 (s); **HRMS** (ESI/IT-TOF) m/z: [M + H] Calcd for $C_{24}H_{22}FN_4O$ 401.1772; found 401.1773.

2.2.7.39. (*R*)-(8-Ethynyl-6-(2-fluorophenyl)-4-methyl-4*H*-benzo[*f*]imidazo[1,5-*a*][1,4] diazepin-3-yl)(pyrrolidin-1-yl)methanone (GL-II-76, 40)

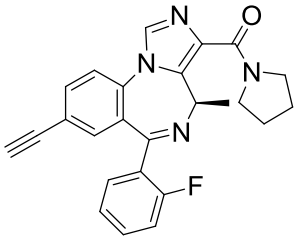

40 (GL-II-76)

The amide **40** was prepared from **68** following the general procedure for esters/thioester/amides, via the acid chloride, with dry pyrrolidine as the nucleophile. The crude residue was purified by column chromatography (silica gel, 6:4 EtOAc and hexane) to yield a mixture of rotamers **40** as a white powder (3:2 ratio by ^{1}H NMR, 1.8 g, 4.4 mmol, 80%): mp 173-174 °C; **$[\alpha]_D^{25}$** = -23.91 (*c* 0.70, $CHCl_3$); **^{1}H NMR Major rotamer** (300 MHz, $CDCl_3$): δ 7.90 (s, 1H), 7.73 – 7.58 (m, 2H), 7.51 (t, *J* = 9.0 Hz, 1H), 7.47 – 7.35 (m, 2H), 7.23 (t, *J* = 7.5 Hz, 1H), 7.01 (t, *J* = 9.3 Hz, 1H), 4.31 (q, *J* = 6.1 Hz, 1H), 3.66 – 3.56 (m, 4H), 3.14 (s, 1H), 1.95 (d, *J* = 6.4 Hz, 3H), 1.93 – 1.69 (m, 4H); **^{1}H NMR Minor rotamer** (300 MHz, $CDCl_3$): δ 7.85 (s, 1H), 7.74 – 7.57 (m, 2H), 7.51 (t, *J* = 9.0 Hz, 1H), 7.47 – 7.35 (m, 2H), 7.23 (t, *J* = 7.5 Hz, 1H), 7.01 (t, *J* = 9.3 Hz, 1H), 6.49 (q, *J* = 6.6 Hz, 1H), 3.82 (dd, *J* = 58.0, 32.3 Hz, 4H), 3.46 (d, *J* = 26.4 Hz, 4H), 3.14 (s, 1H), 1.28 (d, *J* = 6.4 Hz, 3H); **HRMS** (ESI/IT-TOF) m/z: [M + H] Calcd for $C_{25}H_{22}FN_4O$ 413.1772; found 413.1772.

General procedure with Lawesson's reagent (LR)[125-126] for the synthesis of thioamides (41-44)

The corresponding amide, and Lawesson's reagent (6 eq) was suspended in dry THF in a sealed tube. **Note, 5 mL THF is required for 1 mmol amide.** The reaction mixture was heated to 80 degrees for 36 h; a dark red clear solution was obtained. ***Caution, LR has a very unpleasant sulfur***

smell, it should be handled carefully in a fume hood. The reaction mixture was cooled down to rt, and the solvent was removed under reduced pressure. The residue, which resulted, was dissolved in DCM and passed through a column of silica gel to remove the LR byproducts as the first milky fraction. The later fractions contain the desired thioamide product. After removal of the eluent, the thioamide was purified as yellow solid. The other thioamides were prepared by applying this general thionation procedure with the corresponding starting amide.

2.2.7.40. (*R*)-8-Ethynyl-6-(2-fluorophenyl)-*N*,4-dimethyl-4*H*-benzo[*f*]imidazo[1,5-*a*][1,4] diazepine-3-carbothioamide (GL-III-84, 41)

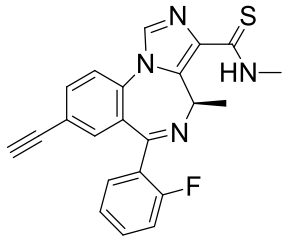

41 (GL-III-84)

The methyl thioamide **41** was prepared from **35** (214 mg, 0.57 mmol) in THF (2.87 mL) following the general thionation procedure for thioamides with the LR (1.38 g, 3.4 mmol). The crude residue was purified by flash column chromatography (silica gel, EtOAc/hexane 2:3) to yield pure methyl thioamide **41** as a yellow powder (133.9 mg, 60 %): **^{1}H NMR** (300 MHz, $CDCl_3$) δ 9.22 (s, 1H), 7.76 (s, 1H), 7.71 – 7.58 (m, 3H), 7.50 (d, *J* = 8.3 Hz, 1H), 7.47 – 7.35 (m, 2H), 7.22 (t, *J* = 7.5 Hz, 1H), 7.12 – 6.88 (m, 1H), 3.27 (d, *J* = 5.0 Hz, 3H), 3.15 (s, 1H), 1.27 (d, *J* = 7.3 Hz, 3H); **^{13}C NMR** (75 MHz, $CDCl_3$) δ 187.73 (s), 163.28 (s), 160.13 (d, *J* = 250.3 Hz), 140.04 (s), 136.33 (s), 135.04 (s), 134.75 (s), 133.71 (s), 132.50 (s), 131.88 (d, *J* = 8.3 Hz), 131.42 (d, *J* = 2.4 Hz), 129.85 (s), 128.64 (d, *J* = 12.5 Hz), 124.45 (d, *J* = 3.5 Hz), 122.30 (s), 121.54 (s), 116.02 (d, *J* = 21.6

Hz), 81.50 (s), 79.65 (s), 50.23 (s), 31.42 (s), 14.27 (s); **HRMS** (ESI/IT-TOF) m/z: [M + H] Calcd for $C_{22}H_{18}FN_4S$ 389.1231; found 389.1228.

2.2.7.41. (*R*)-8-Ethynyl-6-(2-fluorophenyl)-*N*,*N*,4-trimethyl-4*H*-benzo[*f*]imidazo[1,5-*a*][1,4] diazepine-3-carbothioamide (GL-III-85, 42)

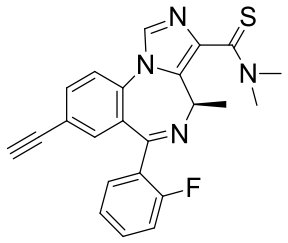

42 (GL-III-85)

The dimethyl thioamide **42** was prepared from **36** (234 mg, 0.6 mmol) in THF (3 mL) following the general thionation procedure for thioamides with the LR (1.46 g, 3.6 mmol). The crude residue was purified by flash column chromatography (silica gel, EtOAc/hexane 4:1) to yield pure dimethyl thioamide **42** as a yellow powder (170.6 mg, 70 %): the ratio of major and minor rotamers is 1.8:1. **^{1}H NMR Major rotamer** (300 MHz, CDCl3) δ 7.93 (s, 1H), 7.66 (s, 1H), 7.57 (td, *J* = 7.5, 1.6 Hz, 1H), 7.51 (d, *J* = 8.3 Hz, 1H), 7.44 – 7.33 (m, 2H), 7.20 (t, *J* = 7.4 Hz, 1H), 6.99 (t, *J* = 9.2 Hz, 1H), 4.26 (d, *J* = 5.7 Hz, 1H), 3.64 – 3.13 (m, 6H), 3.13 (s, 1H), 1.87 (d, *J* = 4.4 Hz, 3H); **^{1}H NMR Minor rotamer** (300 MHz, $CDCl_3$) δ 7.83 (s, 1H), 7.68 (s, 1H), 7.57 (td, *J* = 7.5, 1.6 Hz, 1H), 7.51 (d, *J* = 8.3 Hz, 1H), 7.44 – 7.33 (m, 2H), 7.20 (t, *J* = 7.4 Hz, 1H), 6.99 (t, *J* = 9.2 Hz, 1H), 6.37 – 6.11 (m, 1H), 3.64 – 3.13 (m, 6H), 3.13 (s, 1H), 1.26 (d, *J* = 4.4 Hz, 3H); **HRMS** (ESI/IT-TOF) m/z: [M + H] Calcd for $C_{23}H_{20}FN_4S$ 403.1387; found 403.1385.

2.2.7.42. (*R*)-*N*-Ethyl-8-ethynyl-6-(2-fluorophenyl)-4-methyl-4*H*-benzo[*f*]imidazo[1,5-*a*][1,4]diazepine-3-carbothioamide (GL-III-86, 43)

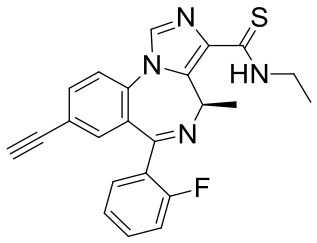

43 (GL-III-86)

The ethyl thioamide **43** was prepared from **37** (250 mg, 0.65 mmol) in THF (3.2 mL) following the general thionation procedure for thioamides with the LR (1.57 g, 3.9 mmol). The crude residue was purified by flash column chromatography (silica gel, EtOAc/hexane 2:3) to yield pure ethyl thioamide **43** as a yellow powder (161.4 mg, 62 %): **^{1}H NMR** (300 MHz, $CDCl_3$) δ 9.07 (s, 1H), 7.78 (s, 1H), 7.72 – 7.58 (m, 3H), 7.51 (d, *J* = 8.3 Hz, 1H), 7.47 – 7.37 (m, 2H), 7.23 (t, *J* = 7.4 Hz, 1H), 7.06 – 6.96 (m, 1H), 4.07 – 3.57 (m, 2H), 3.15 (s, 1H), 1.33 (t, *J* = 7.3 Hz,3H), 1.28 (d, *J* = 7.4 Hz, 3H); **^{13}C NMR** (75 MHz, $CDCl_3$) δ 186.59 (s), 163.27 (s), 160.13 (d, *J* = 250.3 Hz), 140.20 (s), 136.40 (s), 135.03 (s), 134.78 (s), 133.70 (s), 132.44 (s), 131.88 (d, *J* = 8.4 Hz), 131.43 (d, *J* = 2.4 Hz), 129.89 (s), 128.63 (d, *J* = 12.3 Hz), 124.45 (d, *J* = 3.4 Hz), 122.29 (s), 121.56 (s), 116.03 (d, *J* = 21.5 Hz), 81.50 (s), 79.64 (s), 50.25 (s), 39.26 (s), 14.26 (s), 13.39 (s); **HRMS** (ESI/IT-TOF) m/z: [M + H] Calcd for $C_{23}H_{20}FN_4S$ 403.1387; found 403.1381.

2.2.7.43. (*R*)-*N*-Cyclopropyl-8-ethynyl-6-(2-fluorophenyl)-4-methyl-4*H*-benzo[*f*]imidazo[1,5-*a*][1,4]diazepine-3-carbothioamide (GL-III-87, 44)

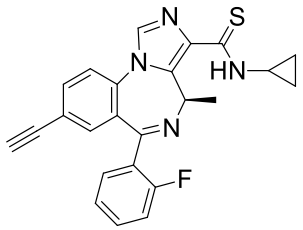

44 (GL-III-87)

The cyclopropyl thioamide **44** was prepared from **38** (223.6 mg, 0.56 mmol) in THF (2.8 mL) following the general thionation procedure for thioamides with the LR (1.36 g, 3.4 mmol). The crude residue was purified by flash column chromatography (silica gel, EtOAc/hexane 2:3) to yield the pure cyclopropyl thioamide **44** as a yellow powder (152.3 mg, 64 %): **^{1}H NMR** (300 MHz, $CDCl_3$) δ 9.05 (d, *J* = 3.7 Hz, 1H), 7.72 (s, 1H), 7.67 – 7.55 (m, 3H), 7.48 (d, *J* = 8.3 Hz, 1H), 7.45 – 7.33 (m, 2H), 7.21 (t, *J* = 7.5 Hz, 1H), 7.07 – 6.92 (m, 1H), 3.34 (td, *J* = 7.1, 4.2 Hz, 1H), 3.14 (s, 1H), 1.25 (d, *J* = 7.7 Hz, 3H), 0.94 (q, *J* = 7.2 Hz, 2H), 0.72 (td, *J* = 6.8, 4.4 Hz, 2H); **^{13}C NMR** (75 MHz, $CDCl_3$) δ 188.48 (s), 163.25 (s), 160.10 (d, *J* = 250.3 Hz), 140.08 (s), 136.15 (s), 135.03 (s), 134.71 (s), 133.67 (s), 132.40 (s), 131.86 (d, *J* = 8.4 Hz), 131.40 (d, *J* = 2.4 Hz), 129.83 (s), 128.64 (d, *J* = 12.5 Hz), 124.44 (d, *J* = 3.3 Hz), 122.32 (s), 121.55 (s), 116.01 (d, *J* = 21.6 Hz), 81.49 (s), 79.72 (s), 50.22 (s), 27.62 (s), 14.23 (s), 7.28 (s), 7.06 (s); **HRMS** (ESI/IT-TOF) m/z: [M + H] Calcd for $C_{24}H_{20}FN_4S$ 415.49861387; found 415.1392.

2.2.7.44. (*R*)-8-Bromo-6-(2-fluorophenyl)-*N*,*N*,4-trimethyl-4*H*-benzo[*f*]imidazo[1,5-*a*][1,4]diazepine-3-carboxamide (GL-III-69, 45)

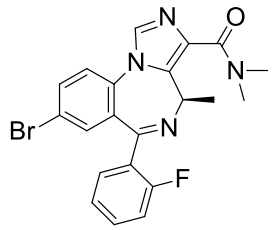

45 (GL-III-69)

The bromo dimethyl amide **45** was prepared from bromo ethyl ester **6** (8 g, 19.3 mmol) following the general procedure with dry dimethylamine as the nucleophile. The crude residue was purified by column chromatography (silica gel, EtOAc and 1% MeOH) to yield pure bromo dimethyl amide **45** as a light yellow powder (6 g, 70.6%): **^{1}H NMR** (300 MHz, $CDCl_3$) δ 7.91 (s, 1H), 7.72 (d, *J* = 8.2 Hz, 1H), 7.61 (t, *J* = 7.5 Hz, 1H), 7.49 – 7.36 (m, 3H), 7.24 (t, *J* = 7.5 Hz, 1H), 7.06 – 6.96 (m, 1H), 4.30 (s, 1H), 3.26 (s, 1H), 3.17 – 2.85 (m, 6H), 1.91 (s, 3H); **HRMS** (ESI/IT-TOF) m/z: [M + H] Calcd for $C_{21}H_{19}BrFN_4O$ 441.0721; found 441.0719.

2.2.7.45. (*R*)-8-Bromo-*N*-ethyl-6-(2-fluorophenyl)-4-methyl-4*H*-benzo[*f*]imidazo[1,5-*a*][1,4]diazepine-3-carboxamide (GL-III-67, 46)

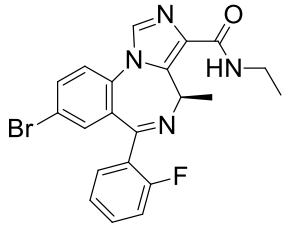

46 (GL-III-67)

The bromo ethyl amide **46** was prepared from the bromo ethyl ester **6** (7 g, 16.9 mmol) by following the general procedure for esters/thioester/amides with dry ethylamine as the nucleophile. The crude residue was purified by flash column chromatography (silica gel, EtOAc/hexane 1:1) to yield the pure bromo ethyl amide **46** as a white powder (5 g, 70 %): mp 255-256 °C; **^{1}H NMR** (300 MHz, $CDCl_3$) δ 7.82 (s, 1H), 7.69 (d, *J* = 7.9 Hz, 1H), 7.63 (t, *J* = 7.3 Hz, 1H), 7.50 – 7.37

(m, 3H), 7.23 (dd, *J* = 16.4, 8.9 Hz, 2H), 7.01 (t, *J* = 9.3 Hz, 1H), 6.90 (dd, *J* = 14.2, 7.0 Hz, 1H), 3.44 (dd, *J* = 8.7, 4.3 Hz, 2H), 1.27 (d, *J* = 7.2 Hz, 3H), 1.22 (t, *J* = 7.3 Hz, 3H); **^{13}C NMR** (75 MHz, $CDCl_3$) δ 162.45 (s), 162.32 (s), 160.10 (d, *J* = 248.8 Hz), 138.67 (s), 134.66 (s), 133.81 (s), 133.31 (s), 132.97 (s), 131.99 (d, *J* = 7.6 Hz), 131.78 (s), 131.37 (s), 131.25 (s), 128.58 (s), 124.51 (s), 123.54 (s), 120.72 (s), 116.10 (d, *J* = 21.5 Hz), 49.87 (s), 33.82 (d, *J* = 15.8 Hz), 15.02 (s), 15.01 (s); **HRMS** (ESI/IT-TOF) m/z: [M + H] Calcd for $C_{21}H_{19}BrFN_4O$ 441.0721; found 441.0719.

2.2.7.46. (*R*)-8-Cyclopropyl-6-(2-fluorophenyl)-*N*,*N*,4-trimethyl-4*H*-benzo[*f*]imidazo[1,5-*a*][1,4]diazepine-3-carboxamide (GL-III-70, 47)

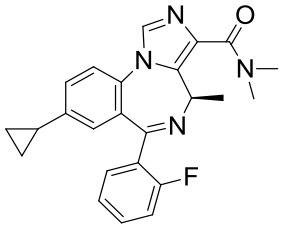

47 (GL-III-70)

To a solution of the bromo dimethyl amide **45** (3.0 g, 6.8 mmol) in toluene (50 mL) and water (1.58 mL), cyclopropyl boronic acid (3 g, 34.0 mmol), potassium phosphate (6.2 g, 29.2 mmol) and bis(triphenylphosphine)palladium(II) diacetate (1.53 g, 2.04 mmol) were added under argon. A reflux condenser was attached and the mixture was degassed under vacuum with argon. This process was repeated four times. The mixture, which was resulted, was stirred and heated to 100 °C. After 3 h the reaction was completed on analysis by TLC (silica gel) and it was then cooled to rt. Water (20 mL) was added and the mixture was extracted with EtOAc (3 × 20 mL), after which the filtrate was washed with brine (20 mL), dried (Na_2SO_4) and concentrated under reduced pressure. The black residue which resulted was purified by a wash column (silica gel, EtOAc/hexane 4:1 and 2 % MeOH) to afford the desired C(8)-cyclopropyl dimethyl amide **47** as a white solid (2.2 g,

81.5 %): mp 118-119 °C; **^{1}H NMR** (300 MHz, $CDCl_3$) δ 7.86 (s, 1H), 7.57 (t, *J* = 6.7 Hz, 1H), 7.38 (d, *J* = 7.6 Hz, 2H), 7.19 (t, *J* = 7.4 Hz, 2H), 7.04 – 6.86 (m, 2H), 4.26 (d, *J* = 6.6 Hz, 1H), 3.07 (s, 3H), 2.96 (s, 3H), 1.88 (d, *J* = 6.5 Hz, 3H), 1.22 (t, *J* = 7.0 Hz, 1H), 0.95 (d, *J* = 7.7 Hz, 2H), 0.77 – 0.45 (m, 2H); **^{13}C NMR** (75 MHz, $CDCl_3$) δ 166.41 (s), 163.60 (d, *J* = 18.7 Hz), 160.21 (d, *J* = 251.3 Hz), 143.59 (s), 134.67 (s), 133.72 (s), 132.87 (s), 132.23 (s), 132.05 (s), 131.73 (d, *J* = 7.9 Hz), 131.32 (s), 128.84 (s), 128.54 – 127.90 (m), 127.38 (s), 124.33 (s), 122.51 (s), 115.97 (d, *J* = 21.6 Hz), 52.11 (s), 39.10 (s), 34.98 (s), 18.50 (s), 15.01 (s), 9.74 (s); **HRMS** (ESI/IT-TOF) m/z: [M + H] Calcd for $C_{24}H_{24}FN_4O$ 403.1929; found 403.1928.

2.2.7.47. (*R*)-8-Cyclopropyl-*N*-ethyl-6-(2-fluorophenyl)-4-methyl-4*H*-benzo[*f*]imidazo[1,5-*a*][1,4]diazepine-3-carboxamide (GL-III-68, 48)

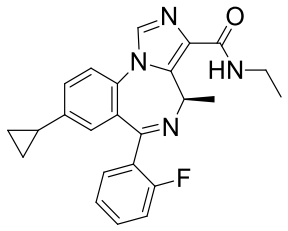

48 (GL-III-68)

To a solution of the bromo ethyl amide **46** (3.0 g, 6.8 mmol) in toluene (50 mL) and water (1.46 mL), cyclopropyl boronic acid (3 g, 34.0 mmol), potassium phosphate (6.3 g, 29.7 mmol) and bis(triphenylphosphine)palladium(II) diacetate (1.52 g, 2.0 mmol) were added under argon. A reflux condenser was attached and the mixture was degassed under vacuum with argon. This process was repeated four times. The mixture was stirred and heated to 100°C. After 12 h the reaction was completed on analysis by TLC (silica gel) and it was then cooled to rt. Water (20 mL) was added and the mixture was extracted with EtOAc (3 × 25 mL), after which the filtrate was washed with brine (20 mL), dried (Na_2SO_4) and concentrated under reduced pressure. The black

residue which resulted was purified by a wash column (silica gel, EtOAc/hexane 4:1) to afford the desired C(8)-cyclopropyl ethyl amide **48** as a white solid (2.3 g, 85 %): mp 189-190 °C; **^{1}H NMR** (300 MHz, $CDCl_3$) δ 7.79 (s, 1H), 7.61 (t, *J* = 6.6 Hz, 1H), 7.41 (t, *J* = 10.0 Hz, 2H), 7.31 – 7.14 (m, 3H), 7.09 – 6.91 (m, 2H), 6.86 (d, *J* = 7.0 Hz, 1H), 3.62 – 3.24 (m, 2H), 1.94 – 1.71 (m, 1H), 1.22 (dd, *J* = 15.1, 7.6 Hz, 6H), 0.98 (d, *J* = 7.9 Hz, 2H), 0.70 – 0.46 (m, 2H); **^{13}C NMR** (75 MHz, $CDCl_3$) δ 163.84 (s), 162.71 (s), 160.15 (d, *J* = 249.0 Hz), 143.60 (s), 138.69 (s), 133.31 (s), 132.27 (s), 131.57 (s), 131.40 (s), 129.35 (s), 129.29 (s), 128.49 (s), 128.29 (s), 127.85 (s), 124.28 (s), 121.79 (s), 115.89 (d, *J* = 21.8 Hz), 49.82 (s), 33.65 (s), 15.03 (s), 14.82 (s), 9.82 (s); **HRMS** (ESI/IT-TOF) m/z: [M + H] Calcd for $C_{24}H_{24}FN_4O$ 403.1929; found 403.1927.

2.2.7.48. 8-Bromo-6-(2-fluorophenyl)-*N*-methyl-4*H*-benzo[*f*]imidazo[1,5-*a*][1,4]diazepine-3-carboxamide (RV-II-04, 49)

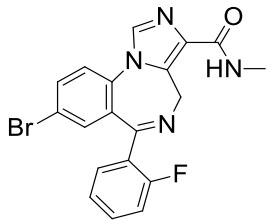

49 (RV-II-04) achiral

The bromo ethyl ester (2.0 g, 4.67 mmol) was dissolved in dry DCM (10 mL), which was added to a sealed vessel fitted with a septum at 0 ˚C and methylamine (20 mL; 33% by wt. solution in EtOH) was added. The vessel was sealed with a screw-cap and stirred at 60 ˚C for 15 h. The solution was then cooled to rt and the methylamine, DCM and ethanol were removed under reduced pressure. The residue which resulted was purified by a wash column (silica gel, EtOAc/hexane 7:3) to afford pure amide **49** as a yellow powder (1.35 g, 3.26 mmol, 70%); ^{1}H NMR (500 MHz, $CDCl_3$) δ 7.85 (s, 1H), 7.78 (dd, *J* = 8.5 Hz, 1.9 Hz, 1H), 7.73 (td, *J* = 7.7 Hz,

1.5 Hz, 1H), 7.50 -7.43 (m, 3H), 7.28 (t, *J* = 7.6 Hz, 1H), 7.12 (br s, 1H), 7.04 (t, *J* = 9.4 Hz, 1H), 6.33 (br s, 1H), 4.13 (br s, 1H), 2.99 (d, *J* = 4.9 Hz, 3H); HPLC-MS (ESI): *m/z* 413.15 $(M+H)^+$.

2.2.7.49. (*R*)-*Tert*-Butyl(1-((4-bromo-2-picolinoylphenyl)amino)-1-oxopropan-2-yl)carbamate (GL-II-04, 71)

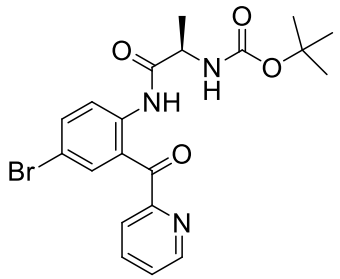

71 (GL-II-04)

The (2-amino-5-bromophenyl)(pyridin-2-yl)methanone **70** (100 g, 360.85 mmol) and Boc-D-alanine (95.6 g, 505.196 mmol) were dissolved in dry DCM (400 mL) and stirred at 0 ^oC. Dicyclohexylcarbodiimide (DCC; 96.8 g, 469.1 mmol) was dissolved in dry DCM (500 mL) to form a homogenous solution, which was added to the former mixture dropwise over a 30 min period at 0 ^oC. The solution, which resulted, was allowed to stir for 22 h at rt. The dicyclohexyl urea byproduct, which was formed, was filtered off and washed with DCM until the solid was colorless. The organic layers were combined and concentrated under reduced pressure. The resulted crude was dissolved in EtOAc, and hexane was added for recrystallization at 45 ^oC, and the Boc analog **71** was recrystallized when cooled down to rt after adding seed crystals. This solid was further washed with EtOAc/hexane (1:19) to afford the majority of the Boc analog **71.** The filtrate was combined, concentrated and purified by flash column chromatography (silica gel, EtOAc/hexane 2:3) to yield the additional amide **71** (159.5 g, 98.6 %): **^{1}H NMR** (300 MHz, $CDCl_3$) δ 11.37 (s, 1H), 8.72 (d, *J* = 4.7 Hz, 1H), 8.60 (d, *J* = 9.0 Hz, 1H), 7.96 (d, *J* = 2.3 Hz, 1H), 7.94

– 7.89 (m, 2H), 7.65 (dd, *J* = 9.0, 2.2 Hz, 1H), 7.51 (dd, *J* = 8.8, 4.8 Hz, 1H), 5.21 (d, *J* = 6.5 Hz, 1H), 4.35 (s, 1H), 1.63 – 1.15 (m, 12H); **HRMS** (ESI/IT-TOF) m/z: [M + H] Calcd for $C_{20}H_{23}BrFN_3O_4$ 448.0866; found 448.0877.

2.2.7.50. (*R*)-7-Bromo-3-methyl-5-(pyridin-2-yl)-1*H*-benzo[*e*][1,4]diazepin-2(3*H*)-one (GL-II-05, 72)

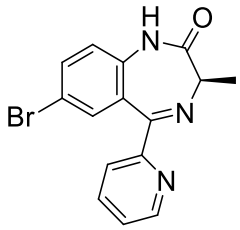

72 (GL-II-05)

Amide **71** (157.5 g, 351.32 mmol) was dissolved in dry DCM (800 mL) and cooled to 0 ºC. Anhydrous HCl (g) was slowly added until the solution was saturated, about 2 h, and the solution was allowed to stir overnight at rt. The reaction mixture was then washed with a sat aq solution of $NaHCO_3$ (2 x 500 mL) and water (2 x 300 mL). ***A mild exotherm was observed during the addition of a saturated aq NaHCO₃ during workup.*** The organic layer was concentrated under reduced pressure and the oil which resulted was dissolved in methanol-water (2:1, 1.5 L) and the pH was adjusted to 8.5 using a solution of 1 M aq NaOH (pH paper). The reaction mixture was allowed stir at rt for 48 h. The solution was concentrated under reduced pressure and water (100 mL) was added. The solution was extracted with DCM and the organic layer was washed with brine, dried (Na_2SO_4), and concentrated under reduced pressure. The majority of 1,4-benzodiazepine **72** precipitated out of solution as white solid, which was filtered off and washed with cold MeOH and water. The filtrated was combined and concentrated under reduced pressure,

and this was followed by the same washing procedure until no precipitate was left. The filtrate was then purified by flash column chromatography (silica gel, EtOAc/hexane 2:3) to yield additional 1,4-benzodiazepine **72** (109 g, 94 %): **^{1}H NMR** (300 MHz, $CDCl_3$) δ 9.67 (s, 1H), 8.61 (d, *J* = 4.2 Hz, 1H), 7.99 (d, *J* = 7.9 Hz, 1H), 7.79 (td, *J* = 7.8, 1.6 Hz, 1H), 7.55 (dd, *J* = 8.6, 2.2 Hz, 1H), 7.50 (d, *J* = 2.1 Hz, 1H), 7.39 – 7.31 (m, 1H), 7.04 (d, *J* = 8.6 Hz, 1H), 3.82 (q, *J* = 6.4 Hz, 1H), 1.76 (d, *J* = 6.5 Hz, 3H); **^{13}C NMR** (75 MHz, $CDCl_3$) δ 172.35, 166.34, 156.05, 148.86, 137.59, 136.86, 134.52, 133.72, 128.26, 124.62, 124.16, 122.92, 115.92, 59.06, 16.93; **HRMS** (ESI/IT-TOF) m/z: [M + H] Calcd for $C_{15}H_{13}BrN_3O$ 330.0236; found 330.0214.

2.2.7.51. (*R*)-Ethyl 8-bromo-4-methyl-6-(pyridin-2-yl)-4*H*-benzo[*f*]imidazo[1,5-*a*][1,4]diazepine-3-carboxylate (GL-II-06, 73)

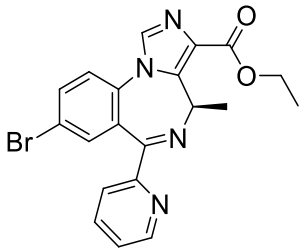

73 (GL-II-06)

The 1,4-benzodiazepine **72** (111.3 g, 337.1 mmol) was dissolved in dry THF (1.3 L) and cooled to -35 ^{o}C. The K-*t*-BuO (45.5 g, 404.5 mmol) was then added in one portion and the solution was allowed to warm to rt where the temperature was held for 1.5 h. The reaction was then cooled to -50 ^{o}C and diethyl chlorophosphate (82.85 g, 471.9 mmol) was added. The solution was allowed to warm to rt and the temperature was held there for 3 h. The reaction was then cooled to -78 ^{o}C and ethyl isocyanoacetate (53.38 g, 471.9 mmol) was added, followed by a second portion of K-*t*-BuO (45.5 g, 404.5 mmol). The reaction was allowed to warm to rt and stirred overnight, a dark red

solution was obtained. The reaction was quenched by addition of a cold sat aq solution of $NaHCO_3$ (1 L) and extracted with EtOAc. The organic layers were combined and washed with brine (2 x 250 mL), dried (Na_2SO_4) and the solvent was removed under reduced pressure to afford a brown solid. The majority of the bromide **73** can be recrystallized from methyl t-butyl ether or EtOAc after cooling from 60 ˚C. The solid **73** was then filtered and washed with large amount of water, and followed by ether until the solid was not pinkish in color. The filtrate was extracted with EtOAc, and concentrated under reduced pressure. This solid was further purified by flash column chromatography (silica gel, EtOAc:hexane, 3:2) to afford the pure bromo ethyl ester **73** as an off-white solid (97.5 g, 68 %): **^{1}H NMR** (300 MHz, $CDCl_3$) δ 8.56 (d, *J* = 4.6 Hz, 1H), 8.01 (d, *J* = 7.9 Hz, 1H), 7.82 (dd, *J* = 15.6, 6.3 Hz, 2H), 7.72 (dd, *J* = 8.5, 1.9 Hz, 1H), 7.46 (t, *J* = 6.0 Hz, 2H), 7.36 (dd, *J* = 6.7, 5.3 Hz, 1H), 6.69 (q, *J* = 7.3 Hz, 1H), 4.52 – 4.23 (m, 2H), 1.40 (t, *J* = 7.1 Hz, 3H), 1.27 (d, *J* = 7.3 Hz, 3H); **^{13}C NMR** (75 MHz, DMSO) δ 164.85, 157.38, 150.14, 148.57, 140.94, 137.60, 136.69, 135.06, 134.99, 134.60, 130.44, 129.58, 125.46, 125.40, 124.04, 123.79, 119.87, 119.49, 49.55, 14.75; **HRMS** (ESI/IT-TOF) m/z: [M + H] Calcd for $C_{20}H_{18}BrN_4O_2$ 425.0608; found 425.0610.

2.2.7.52. (*R*)-Ethyl 4-methyl-6-(pyridin-2-yl)-8-((trimethylsilyl)ethynyl)-4*H*-benzo[*f*]imidazo[1,5-*a*][1,4]diazepine-3-carboxylate (GL-II-18, 74)

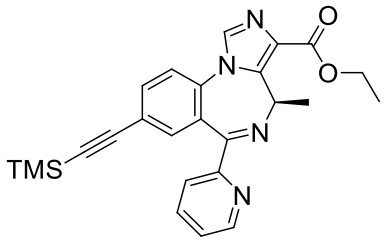

74 (GL-II-18)

The bromo ethyl ester **73** (24.77 g, 58.25 mmol) was dissolved in triethylamine (200 mL) and acetonitrile (300 mL). Trimethylsilylacetylene (8.58 g, 87.4 mmol) and bis(triphenylphosphine)-palladium (II) acetate (2.4 g, 3.2 mmol) were added. A reflux condenser was attached and the mixture was degassed under vacuum with argon; this process was repeated four times. The reaction mixture was heated to reflux under argon and stirred for 8 h. The solution was cooled to rt, filtered through celite, and washed with EtOAc. The filtrate was concentrated under reduced pressure. The black residue which resulted was purified by a wash column (silica gel, EtOAc/hexanes 1:2) to afford the TMS-analog **74** as an off-white solid (23.2 g, 90.3 %): **^{1}H NMR** (300 MHz, $CDCl_3$) δ 8.54 (d, *J* = 4.3 Hz, 1H), 7.94 (d, *J* = 7.8 Hz, 1H), 7.86 (s, 1H), 7.77 (t, *J* = 7.7 Hz, 1H), 7.64 (d, *J* = 8.1 Hz, 1H), 7.50 (t, *J* = 7.2 Hz, 1H), 7.37 (s, 1H), 7.32 (dd, *J* = 6.6, 5.6 Hz, 1H), 6.65 (q, *J* = 7.2 Hz, 1H), 4.49 – 4.25 (m, 2H), 1.37 (t, *J* = 7.1 Hz, 3H), 1.21 (t, *J* = 6.0 Hz, 3H), 0.19 (s, 9H); **^{13}C NMR** (75 MHz, $CDCl_3$) δ 165.28, 163.00, 157.60, 148.61, 141.71, 136.80, 135.45, 135.31, 134.95, 129.28, 127.88, 124.52, 123.97, 122.31, 121.98, 102.79, 96.91, 60.65, 49.79, 14.46, 14.39, -0.25; **HRMS** (ESI/IT-TOF) m/z: [M + H] Calcd for $C_{25}H_{27}N_4O_2Si$ 443.1898; found 443.1901.

2.2.7.53. (*R*)-Ethyl 8-ethynyl-4-methyl-6-(pyridin-2-yl)-4*H*-benzo[*f*]imidazo[1,5-*a*][1,4]diazepine-3-carboxylate (GL-II-19-2'N-*R*-CH_3, 75)

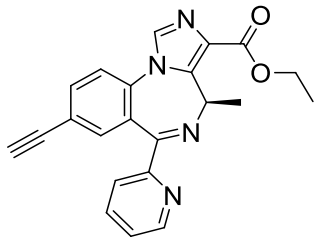

75 (GL-II-19-2'N-*R*-CH_3)

The intermediate **74** (18 g, 40.6 mmol) was dissolved in THF (300 mL) and cooled to -78 ^{o}C. This was treated with tetrabutylammonium fluoride hydrate (1 M solution in THF, 61 mmol), and this was followed by water (18 mL). The reaction mixture was stirred until the starting material was consumed as indicated by TLC (silica gel), about 1 h. The reaction mixture was allowed to warm to rt, and water (200 mL) was slowly added. The solution was extracted with EtOAc and the organic extracts were combined, washed with brine, dried (Na_2SO_4), and the solvent was removed under reduced pressure. The residue which resulted was recrystallized from DCM and MeOH after cooling down from 60 ^{o}C. The crystals were filtered and washed with cold MeOH. The filtrated was combined, concentrated and further purified by a wash column (silica gel, EtOAc/hexanes 3:2) to afford additional ethyl ester **75** as a white powder (14.9 g, 95 %): **^{1}H NMR** (300 MHz, $CDCl_3$) δ 8.58 (d, *J* = 4.4 Hz, 1H), 8.01 (d, *J* = 7.8 Hz, 1H), 7.89 (s, 1H), 7.83 (t, *J* = 7.6 Hz, 1H), 7.72 (d, *J* = 8.3 Hz, 1H), 7.55 (d, *J* = 8.3 Hz, 1H), 7.47 (s, 1H), 7.42 – 7.32 (m, 1H), 6.71 (q, *J* = 7.3 Hz, 1H), 4.56 – 4.28 (m, 2H), 3.15 (s, 1H), 1.43 (t, *J* = 7.1 Hz, 3H), 1.28 (d, *J* = 7.3 Hz, 3H); **^{13}C NMR** (75 MHz, $CDCl_3$) δ 165.14, 163.00, 157.52, 148.57, 141.71, 136.85, 135.82, 135.03, 134.99, 129.36, 127.92, 124.57, 124.00, 122.40, 120.95, 81.66, 79.47, 60.71, 49.82, 14.55, 14.40; **HRMS** (ESI/IT-TOF) m/z: [M + H] Calcd for $C_{22}H_{19}N_4O_2$ 371.1503; found 371.1502.

2.2.7.54. (*R*)-8-Ethynyl-*N*,4-dimethyl-6-(pyridin-2-yl)-4*H*-benzo[*f*]imidazo[1,5-*a*][1,4] diazepine-3-carboxamide (GL-II-31, 50)

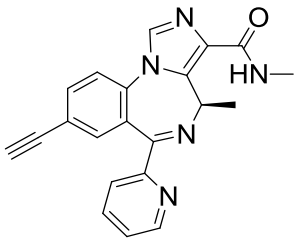

50 (GL-II-31)

The ethyl ester GL-II-19-2'N-*R*-CH_3 (**75**, 1.7 g, 4.59 mmol) was dissolved in dry DCM (15 mL), which was added to a sealed vessel fitted with a septum at 0 ˚C and methyl amine (25 mL; 33% by wt. solution in EtOH) was added. The vessel was sealed with a screw-cap and stirred at 60 ˚C for 18 hours. The solution was then cooled to r.t. and the methyl amine, DCM and ethanol were removed under reduced pressure. Then DCM (5 mL) was added to the crude mixture, and it was stirred at 35 ˚C for 5 min, after which then pure product was filtered off. The filtrate was further purified by flash column chromatography (silica gel, EtOAc/hexane 7:3) to afford an additional portion of pure amide **50** as a white powder (1.2 g, 72 %); **^{1}H NMR** (500 MHz, $CDCl_3$) δ 8.57 (d, *J* = 4.5 Hz, 1H), 8.07 (d, *J* = 7.9 Hz, 1H), 7.83 (t, *J* = 7.6 Hz, 1H), 7.77 (d, *J* = 3.3 Hz, 1H), 7.70 (d, *J* = 8.2 Hz, 1H), 7.53 (d, *J* = 8.3 Hz, 1H), 7.48 (s, 1H), 7.40 – 7.32 (m, 1H), 7.18 (s, 1H), 6.91 (q, *J* = 7.2 Hz, 1H), 3.15 (s, 1H), 2.97 (d, *J* = 5.0 Hz, 3H), 1.28 (d, *J* = 7.2 Hz, 3H); **^{13}C NMR** (75 MHz, MeOD) δ 165.47, 163.87, 157.41, 148.30, 138.74, 137.34, 135.81, 135.57, 135.25, 135.17, 134.26, 131.06, 127.84, 124.84, 124.22, 122.43, 121.10, 81.43, 79.66, 25.56, 14.45; **HRMS** (ESI/IT-TOF) m/z: [M + H] Calcd for $C_{21}H_{18}N_5O$ 356.1506; found 356.1504.

2.2.7.55. (*R*)-5-(8-Ethynyl-4-methyl-6-(pyridin-2-yl)-4*H*-benzo[*f*]imidazo[1,5-*a*][1,4]diazepin-3-yl)-3-methyl-1,2,4-oxadiazole (GL-II-33, 51)

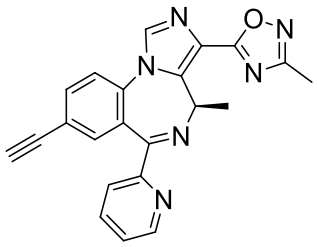

51 (GL-II-33)

The methyl oxadiazole **51** was prepared from the ethyl ester **75** (2 g, 5.4 mmol) following the general procedure with the required oxime (800 mg, 10.8 mmol) and sodium hydride (60% dispersion in mineral oil, 324 mg, 8.1 mmol) in dry THF (100 mL). The crude residue was purified by column chromatography (silica gel, EtOAc) to yield pure oxadiazole **51** as a white powder (1.58 g, 4.15 mmol, 77%); **^{1}H NMR** (300 MHz, $CDCl_3$) δ 8.57 (d, *J* = 4.4 Hz, 1H), 8.00 (d, *J* = 5.6 Hz, 2H), 7.81 (t, *J* = 7.8 Hz, 1H), 7.73 (d, *J* = 8.5 Hz, 1H), 7.59 (d, *J* = 8.4 Hz, 1H), 7.47 (s, 1H), 7.40 – 7.32 (m, 1H), 6.71 (d, *J* = 7.3 Hz, 1H), 3.16 (s, 1H), 2.46 (s, 3H), 1.34 (d, *J* = 7.3 Hz, 3H); **^{13}C NMR** (75 MHz, $CDCl_3$) δ 170.81, 167.42, 165.35, 157.45, 148.60, 139.28, 136.90, 136.45, 136.01, 135.77, 135.54, 135.19, 127.95, 124.68, 124.03, 122.37, 121.21, 81.61, 79.61, 49.97, 14.67, 11.66; **HRMS** (ESI/IT-TOF) m/z: [M + H] Calcd for $C_{22}H_{17}N_6O$ 381.1458; found 381.1461.

2.2.7.56. 5-(8-Ethynyl-6-(2-fluorophenyl)-4*H*-benzo[*f*]imidazo[1,5-*a*][1,4]diazepin-3-yl)-3-methyl-1,2,4-oxadiazole (GL-III-23, 52)

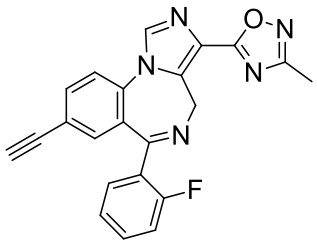

52 (GL-III-23) Achiral

The methyl oxadiazole **52** was prepared from the ethyl ester (3.0 g, 8.03 mmol), which contained the 2'F group, following the general procedure with the methyl oxime (1.2 g, 16.06 mmol) and sodium hydride (60% dispersion in mineral oil, 482 mg, 12.04 mmol) in dry THF (100 mL). The crude residue was purified by column chromatography (silica gel, 7:3 EtOAc and hexane) to yield pure product **52** as a white powder (1.6 g, 4.17 mmol, 52%): **^{1}H NMR** (500 MHz, $CDCl_3$): δ 8.11 (s, 1H), 7.80 (d, *J* = 8.6 Hz, 1H), 7.69 (t, *J* = 7.5 Hz, 1H), 7.64 (d, *J* = 8.6 Hz, 1H), 7.51 (br s, 1H), 7.49 (q, *J* = 6.4 Hz, 1H), 7.28 (t, *J* = 7.5 Hz, 1H), 7.06 (t, *J* = 9.1 Hz, 1H), 6.19 (br s, 1H), 4.52 (br s, 1H), 3.19 (s, 1H), 2.48 (s, 3H); **HRMS** (ESI/IT-TOF) m/z: [M + H] Calcd for $C_{22}H_{15}N_5O$ 384.1255; found 384.1273.

2.2.7.57. (R)-5-(8-Bromo-4-methyl-6-(pyridin-2-yl)-4*H*-benzo[*f*]imidazo[1,5-*a*][1,4] diazepin-3-yl)-3-methyl-1,2,4-oxadiazole (GL-II-54, 53)

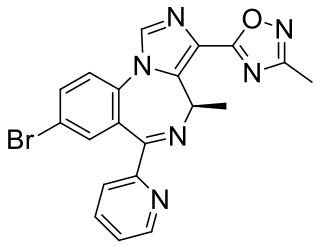

53 (GL-II-54)

The methyl oxadiazole **53** was prepared from the bromo ethyl ester **73** (2.0 g, 4.7 mmol) following the general procedure with the methyl oxime (1.3 g, 17.5 mmol) and sodium hydride (60%

dispersion in mineral oil, 282 mg, 7.1 mmol) in dry THF (100 mL). The crude residue was purified by column chromatography (silica gel, EtOAc and 1% MeOH) to yield pure methyl oxadiazole **53** as a white powder (1.7 g, 3.9 mmol, 85%); **^{1}H NMR** (500 MHz, $CDCl_3$) δ 8.60 (d, *J* = 4.3 Hz, 1H), 8.05 (d, *J* = 7.9 Hz, 1H), 8.00 (s, 1H), 7.84 (t, *J* = 7.0 Hz, 1H), 7.78 (d, *J* = 8.4 Hz, 1H), 7.52 (d, *J* = 8.2 Hz, 2H), 7.40 (dd, *J* = 6.7, 5.0 Hz, 1H), 6.73 (t, *J* = 7.3 Hz, 1H), 2.49 (s, 3H), 1.37 (d, *J* = 7.3 Hz, 3H); **^{13}C NMR** (126 MHz, $CDCl_3$) δ 170.81, 167.44, 164.77, 157.19, 148.60, 139.21, 137.00, 136.40, 135.17, 134.99, 134.90, 134.70, 129.42, 124.82, 124.07, 123.81, 120.59, 49.99, 14.70, 11.69; **HRMS** (ESI/IT-TOF) m/z: [M + H] Calcd for $C_{20}H_{16}BrN_6O$ 435.0564; found 435.0557.

2.2.7.58. (*R*)-5-(8-Cyclopropyl-4-methyl-6-(pyridin-2-yl)-4*H*-benzo[*f*]imidazo[1,5-*a*][1,4] diazepin-3-yl)-3-methyl-1,2,4-oxadiazole (GL-III-64, 54)

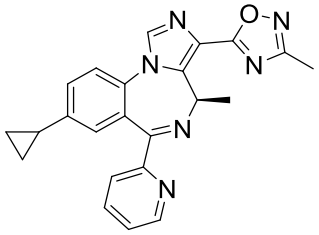

54 (GL-III-64)

To a solution of the bromo methyl oxadiazole **53** (4.0 g, 9.2 mmol) in toluene (100 mL) and water (7 mL), cyclopropyl boronic acid (1.98 g, 23.0 mmol), potassium phosphate (8.2 g, 38.6 mmol) and bis(triphenylphosphine)palladium(II) diacetate (1.38 g, 1.84 mmol) were added under argon. A reflux condenser was attached and the mixture was degassed under vacuum with argon; this process was repeated four times. The mixture was stirred and heated to 100 °C. After 3 h the reaction was completed on analysis by TLC (silica gel) and it was then cooled to rt. Then water

(20 mL) was added and the mixture was extracted with EtOAc (3 × 25 mL), after which the filtrate was washed with brine (20 mL), dried (Na_2SO_4) and concentrated under reduced pressure. The black residue which resulted was purified by a wash column (silica gel, EtOAc) to afford the desired C(8)-cyclopropyl methyl oxadiazole **54** as a white solid (2.18 g, 60 %): ^{1}H NMR (300 MHz, $CDCl_3$) δ 8.56 (d, *J* = 4.5 Hz, 1H), 7.96 (d, *J* = 7.6 Hz, 2H), 7.80 (t, *J* = 7.6 Hz, 1H), 7.49 (d, *J* = 8.3 Hz, 1H), 7.34 (t, *J* = 5.9 Hz, 1H), 7.26 (d, *J* = 9.3 Hz, 1H), 6.99 (s, 1H), 6.68 (q, *J* = 7.1 Hz, 1H), 2.44 (s, 3H), 1.89 (ddd, *J* = 13.0, 8.3, 4.9 Hz, 1H), 1.31 (d, *J* = 7.2 Hz, 3H), 1.00 (d, *J* = 7.4 Hz, 2H), 0.66 (d, *J* = 4.0 Hz, 2H); **^{13}C NMR** (75 MHz, $CDCl_3$) δ 171.04, 167.36, 166.39, 157.95, 148.54, 143.40, 139.26, 136.83, 136.45, 133.06, 129.64, 129.19, 128.88, 127.51, 124.51, 124.17, 122.11, 49.96, 15.16, 14.47, 11.68, 9.95, 9.89; **HRMS** (ESI/IT-TOF) m/z: [M + H] Calcd for $C_{23}H_{21}N_6O$ 397.1771; found 397.1770.

2.2.7.59. (*R*)-5-(8-Ethynyl-6-(2-fluorophenyl)-4-methyl-4*H*-benzo[*f*]imidazo[1,5-*a*][1,4] diazepin-3-yl)-3-isopropyl-1,2,4-oxadiazole (MP-IV-010, 57)

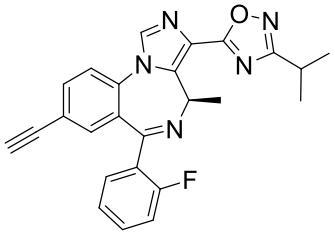

57 (MP-IV-010)

The isopropyl oxadiazole **57** was prepared from the ethyl ester **1** (390 mg, 1mmol) following the general procedure for oxadiazoles with the isopropyl oxime (411.3 mg, 4.03 mmol) and NaH (44.3 mg, 1.1 mmol). The crude residue was purified by flash column chromatography (silica gel, EtOAc/hexane 1:1) to yield pure isopropyl oxadiazole **57** as a white powder (373.6 mg, 87.2 %):

^{1}H NMR (300 MHz, CDCl3) δ 8.06 (s, 1H), 7.69 (d, J = 8.4 Hz, 1H), 7.58 (dd, J = 15.4, 7.8 Hz, 2H), 7.41 (ddd, J = 13.2, 6.2, 1.8 Hz, 2H), 7.21 (td, J = 7.5, 0.9 Hz, 1H), 7.00 (t, J = 9.2 Hz, 1H), 6.70 (q, J = 7.1 Hz, 1H), 3.24 – 2.89 (m, 2H), 1.36 (d, *J* = 6.9 Hz, 6H), 1.32 (d, *J* = 7.3 Hz, 3H). **^{13}C NMR** (75 MHz, $CDCl_3$) δ 175.28 (s), 170.61 (s), 163.43 (s), 160.06 (d, *J* = 250.5 Hz), 139.17 (s), 136.27 (s), 135.36 (s), 134.22 (s), 134.04 (s), 132.30 (s), 132.04 (d, *J* = 8.2 Hz), 131.12 (s), 129.51 (s), 128.56 (d, *J* = 12.8 Hz), 124.51 (d, *J* = 3.2 Hz), 122.24 (s), 121.85 (s), 116.20 (d, *J* = 21.4 Hz), 81.32 (s), 79.96 (s), 50.25 (s), 26.73 (s), 20.59 (s), 20.53 (s), 14.97 (s). **HRMS** (ESI/IT-TOF) m/z: [M + H] Calcd for $C_{25}H_{21}FN_5O$ 426.1725, found 426.1720.

2.2.7.60. (*R*)-5-(8-Bromo-6-(2-fluorophenyl)-4-methyl-4*H*-benzo[*f*]imidazo[1,5-*a*][1,4] diazepin-3-yl)-3-methyl-1,2,4-oxadiazole (GL-III-60, 58)

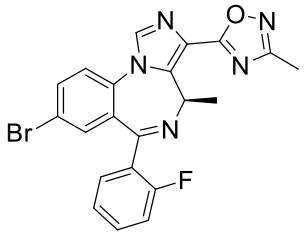

58 (GL-III-60)

The bromo methyl oxadiazole **58** was prepared from the bromo ethyl ester **6** (6 g, 13.5 mmol) following the general procedure for oxadiazoles with the methyl oxime (3 g, 40.5 mmol) and NaH (60% dispersion in mineral oil, 0.8 g, 14.9 mmol). The crude residue was purified by flash column chromatography (silica gel, EtOAc/Hexane 3:2) to yield the pure bromo methyl oxadiazole **58** as a white powder (5.6 g, 91.8 %): **^{1}H NMR** (500 MHz, $CDCl_3$) δ 8.08 (s, 1H), 7.76 (dd, *J* = 8.5, 1.9 Hz, 1H), 7.61 (t, *J* = 7.0 Hz, 1H), 7.55 (d, *J* = 8.6 Hz, 1H), 7.52 – 7.42 (m, 2H), 7.26 (td, *J* = 7.6, 0.9 Hz, 1H), 7.11 – 6.99 (m, 1H), 6.74 (q, *J* = 7.3 Hz, 1H), 2.45 (s, 3H), 1.35 (d, *J* = 7.3 Hz, 3H);

^{13}C NMR (126 MHz, $CDCl_3$) δ 170.69 (s), 167.46 (s), 161.09 (s), 161.06 (d, *J* = 495.1 Hz), 139.12 (s), 136.31 (s), 135.16 (s), 133.37 (s), 133.25 (s), 132.36 (d, *J* = 7.7 Hz), 131.26 (s), 131.02 (s), 128.15 (d, *J* = 11.0 Hz), 124.87 (s), 124.61 (d, *J* = 3.3 Hz), 123.71 (s), 121.26 (s), 116.29 (d, *J* = 21.4 Hz), 50.15 (s), 14.98 (s), 11.69 (s); **HRMS** (ESI/IT-TOF) m/z: [M + H] Calcd for $C_{21}H_{16}BrFN_5O$ 452.0517, found 452.0542.

2.2.7.61. (*R*)-5-(8-Bromo-6-(2-fluorophenyl)-4-methyl-4*H*-benzo[*f*]imidazo[1,5-*a*][1,4] diazepin-3-yl)-3-ethyl-1,2,4-oxadiazole (GL-III-98, 59)

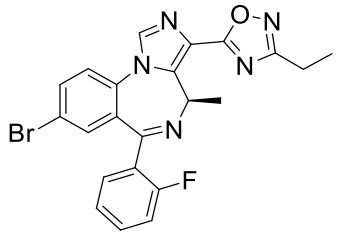

59 (GL-III-98)

The bromo ethyl oxadiazole **59** was prepared from the bromo ethyl ester **6** (2.5 g, 5.65 mmol) following the general procedure for oxadiazoles with the ethyl oxime (2.0 g, 22.6 mmol) and NaH (0.25 g, 6.2 mmol). The crude residue was purified by flash column chromatography (silica gel, EtOAc/Hexane 2:3) to yield pure bromo ethyl oxadiazole **59** as a white powder (2.2 g, 83.7 %): **^{1}H NMR** (300 MHz, $CDCl_3$) δ 8.05 (s, 1H), 7.71 (d, *J* = 8.6 Hz, 1H), 7.53 (d, *J* = 8.6 Hz, 2H), 7.44 – 7.31 (m, 2H), 7.19 (t, *J* = 7.5 Hz, 1H), 6.98 (t, *J* = 9.2 Hz, 1H), 6.69 (q, *J* = 7.1 Hz, 1H), 2.77 (q, *J* = 7.6 Hz, 2H), 1.32 (t, *J* = 7.6 Hz, 6H); **^{13}C NMR** (75 MHz, CDCl3) δ 171.82 (s), 170.67 (s), 162.84 (s), 160.03 (d, *J* = 250.7 Hz), 139.10 (s), 136.28 (s), 135.07 (s), 133.35 (s), 133.11 (s), 132.18 (d, *J* = 8.0 Hz), 131.16 (s), 131.00 (s), 128.30 (d, *J* = 12.4 Hz), 124.54 (d, *J* = 3.0 Hz),

123.75 (s), 121.13 (s), 116.20 (d, *J* = 21.4 Hz), 50.20 (s), 19.72 (s), 14.95 (s), 11.50 (s); **HRMS** (ESI/IT-TOF) m/z: [M + H] Calcd for $C_{22}H_{18}BrFN_5O$ 468.0655, found 468.0659.

2.2.7.62. (*R*)-5-(8-Bromo-6-(2-fluorophenyl)-4-methyl-4*H*-benzo[*f*]imidazo[1,5-*a*][1,4] diazepin-3-yl)-3-isopropyl-1,2,4-oxadiazole (GL-IV-01, 60)

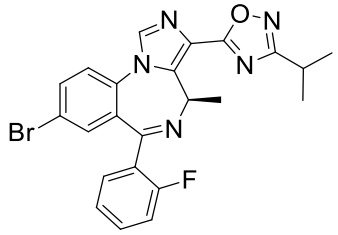

60 (GL-IV-01)

The bromo isopropyl oxadiazole **60** was prepared from the bromo ethyl ester **6** (3.5 g, 7.91 mmol) following the general procedure for oxadiazoles with the isopropyl oxime (3.2 g, 31.6 mmol) and NaH (60% dispersion in mineral oil, 0.35 g, 8.7 mmol). The crude residue was purified by flash column chromatography (silica gel, EtOAc/Hexane 1:1) to yield pure bromo isopropyl oxadiazole **60** as a white powder (3.0 g, 78.2 %): **^{1}H NMR** (300 MHz, $CDCl_3$) δ 8.04 (s, 1H), 7.70 (d, *J* = 8.8 Hz, 1H), 7.53 (d, *J* = 8.6 Hz, 2H), 7.43 – 7.31 (m, 2H), 7.19 (t, *J* = 7.5 Hz, 1H), 6.98 (t, *J* = 9.1 Hz, 1H), 6.69 (q, *J* = 7.0 Hz, 1H), 3.11 (dt, *J* = 13.8, 6.9 Hz, 1H), 1.33 (d, *J* = 7.0 Hz, 6H), 1.31 (d, *J* = 9.3 Hz, 3H); **^{13}C NMR** (75 MHz, CDCl3) δ 175.26 (s), 170.58 (s), 162.85 (s), 160.02 (d, *J* = 250.7 Hz), 139.06 (s), 136.26 (s), 135.08 (s), 133.37 (s), 133.11 (s), 132.60 (s), 132.18 (d, *J* = 8.0 Hz), 131.11 (s), 130.96 (s), 128.31 (d, *J* = 12.3 Hz), 124.57 (s), 123.75 (s), 121.11 (s), 116.20 (d, *J* = 21.4 Hz), 50.25 (s), 26.72 (s), 20.59 (s), 20.53 (s), 14.96 (s); **HRMS** (ESI/IT-TOF) m/z: [M + H] Calcd for $C_{23}H_{20}FN_5O$ 482.0812, found 482.0804.

2.2.7.63. (*R*)-5-(8-Cyclopropyl-6-(2-fluorophenyl)-4-methyl-4*H*-benzo[*f*]imidazo[1,5-*a*][1,4]diazepin-3-yl)-3-methyl-1,2,4-oxadiazole (GL-III-63, 61)

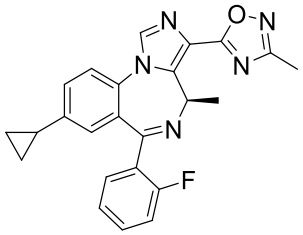

61 (GL-III-63)

To a solution of the bromo methyl oxadiazole **58** (1.6 g, 3.6 mmol) in toluene (100 mL) and water (1.3 mL), cyclopropyl boronic acid (0.55 g, 6.4 mmol), potassium phosphate (3.18 g, 15.0 mmol) and bis(triphenylphosphine)palladium(II) diacetate (0.56 g, 0.75 mmol) were added under argon. A reflux condenser was attached and the mixture was degassed under vacuum with argon; this process was repeated four times. The mixture was stirred and heated to 100 °C. After 4 h the reaction progress was complete on analysis by TLC (silica gel) and it was then cooled to rt. Then water (20 mL) was added and the mixture was extracted with EtOAc (3 × 25 mL), after which the filtrate was washed with brine (20 mL), dried (Na_2SO_4) and concentrated under reduced pressure. The black residue which resulted was purified by a wash column (silica gel, EtOAc) to afford the desired C(8)-cyclopropyl methyl oxadiazole **61** as a white solid (1.05 g, 72 %): **^{1}H NMR** (300 MHz, $CDCl_3$) δ 8.03 (s, 1H), 7.59 (t, *J* = 7.5 Hz, 1H), 7.51 (d, *J* = 8.3 Hz, 1H), 7.47 – 7.36 (m, 1H), 7.24 (dd, *J* = 14.9, 7.4 Hz, 2H), 7.08 – 6.95 (m, 2H), 6.69 (q, *J* = 7.3 Hz, 1H), 2.44 (s, 3H), 1.87 (dt, *J* = 12.6, 6.8 Hz, 1H), 1.32 (d, *J* = 7.2 Hz, 3H), 1.00 (d, *J* = 8.2 Hz, 2H), 0.64 (dd, *J* = 10.7, 4.7 Hz, 2H); **^{13}C NMR** (75 MHz, $CDCl_3$) δ 170.97 (s), 167.38 (s), 161.81 (s), 161.50 (d, *J* = 454.5 Hz), 144.23 (s), 139.19 (s), 136.30 (s), 131.91 (s), 131.80 (s), 131.30 (s), 129.12 (s), 128.99 (s), 128.69 (s), 128.11 (s), 127.32 (s), 124.38 (s), 121.93 (s), 116.06 (d, *J* = 21.8 Hz), 50.09 (s),

15.09 (s), 14.75 (s), 11.67 (s), 9.99 (s); **HRMS** (ESI/IT-TOF) m/z: [M + H] Calcd for $C_{24}H_{21}FN_5O$ 414.1725, found 414.1728.

2.2.7.64. (*R*)-5-(8-Cyclopropyl-6-(2-fluorophenyl)-4-methyl-4*H*-benzo[*f*]imidazo[1,5-*a*][1,4]diazepin-3-yl)-3-ethyl-1,2,4-oxadiazole (GL-IV-03, 62)

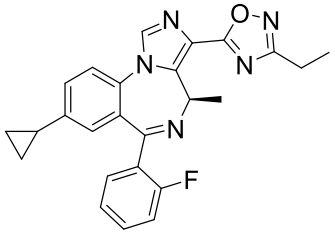

62 (GL-IV-03)

To a solution of the bromo ethyl oxadiazole **59** (1.1 g, 2.38 mmol), tri(O-tolyl)phosphine (85.5 mg, 0.28 mmol), cyclopropyl boronic acid (0.724 g, 8.43 mmol) and potassium phosphate (2.56 g, 12.1 mmol) in toluene (30 mL) and water (0.65 mL), $Pd(OAc)_2$ (31.5 mg, 0.14 mmol) was added under Ar at rt to form an orange cloudy solution. A reflux condenser was attached. The mixture was allowed to stir at rt for 5 min untill the color of the solution turned yellow, as an indication of the formation of the Pd complex generated *in situ*. The mixture was then placed into a pre-heated oil bath at 100 °C. After 2 h the reaction progress was complete on analysis by TLC (silica gel) and it was then cooled to rt. Then water (20 mL) was added and the mixture was extracted with EtOAc (3 × 25 mL), after which the filtrate was washed with brine (20 mL), dried (Na_2SO_4) and concentrated under reduced pressure. The black residue which resulted was purified by a wash column (silica gel, DCM and 5 % MeOH) to afford the desired C(8)-cyclopropyl ethyl oxadiazole **62** as a white solid (815.5 mg, 81.6 %): **^{1}H NMR** (300 MHz, CDCl3) δ 7.98 (s, 1H), 7.46 (d, *J* = 8.3 Hz, 2H), 7.38 – 7.25 (m, 1H), 7.13 (t, *J* = 7.5 Hz, 2H), 6.93 (t, *J* = 9.1 Hz, 2H), 6.63 (q, *J* =

7.0 Hz, 1H), 2.73 (q, *J* = 7.6 Hz, 2H), 1.84 – 1.65 (m, 1H), 1.27 (dd, *J* = 14.1, 6.6 Hz, 6H), 0.90 (d, *J* = 8.3 Hz, 2H), 0.54 (dd, *J* = 10.1, 4.8 Hz, 2H); **^{13}C NMR** (75 MHz, CDCl3) δ 171.70 (s), 170.95 (s), 164.32 (s), 160.06 (d, *J* = 250.5 Hz), 144.12 (s), 139.17 (s), 136.28 (s), 131.72 (s), 131.62 (s), 131.17 (s), 129.05 (t, *J* = 6.2 Hz), 128.61 (s), 127.96 (s), 127.20 (s), 124.36 (d, *J* = 8.0 Hz), 122.68 (s), 121.94 (s), 115.94 (d, *J* = 21.6 Hz), 50.13 (s), 19.69 (s), 15.02 (s), 14.68 (s), 11.49 (s), 9.89 (s); **HRMS** (ESI/IT-TOF) m/z: [M + H] Calcd for $C_{25}H_{23}FN_5O$ 428.1881, found 428.1889.

2.2.7.65. (*R*)-5-(8-Cyclopropyl-6-(2-fluorophenyl)-4-methyl-4*H*-benzo[*f*]imidazo[1,5-*a*][1,4]diazepin-3-yl)-3-isoproyl-1,2,4-oxadiazole (GL-IV-04, 63)

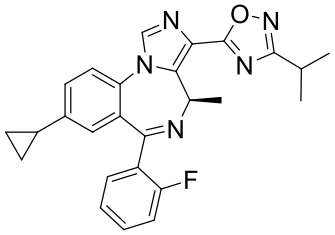

63 (GL-IV-04)

To a solution of the bromo isopropyl oxadiazole **60** (2.0 g, 4.16 mmol), tri(O-tolyl)phosphine (126.6 mg, 0.416 mmol), cyclopropyl boronic acid (1.07 g, 12.5 mmol) and potassium phosphate (3.8 g, 17.9 mmol) in toluene (40 mL) were added as well as water (0.96 mL). Then $Pd(OAc)_2$ (46.7 mg, 0.21 mmol) was added under Ar at rt to form an orange cloudy solution. A reflux condenser was attached. The mixture was allowed to stir at rt for 5 min untill the color of the solution turned yellow, as an indication for the formation of the Pd complex generated *in situ*. The mixture was then placed into a pre-heated oil bath at 100 °C. After 2.5 h the reaction progress was complete on analysis by TLC (silica gel) and it was then cooled to rt. Then water (20 mL) was added and the mixture was extracted with EtOAc (3 × 25 mL), after which the filtrate was washed

with brine (20 mL), dried (Na_2SO_4) and concentrated under reduced pressure. The black residue, which resulted, was purified by a wash column (silica gel, DCM and 5 % MeOH) to afford the desired C(8)-cyclopropyl isopropyl oxadiazole **63** as a white solid (1.45 g, 78.8 %): **^{1}H NMR** (300 MHz, CDCl3) δ 8.00 (s, 1H), 7.70 – 7.43 (m, 1H), 7.42 – 7.30 (m, 1H), 7.26 – 7.11 (m, 1H), 6.98 (d, *J* = 13.2 Hz, 1H), 6.65 (q, *J* = 7.1 Hz, 1H), 3.11 (dt, *J* = 13.8, 6.9 Hz, 1H), 1.81 (ddd, *J* = 13.1, 8.4, 5.0 Hz, 1H), 1.31 (dd, *J* = 15.3, 7.1 Hz, 4H), 0.95 (d, *J* = 8.2 Hz, 1H), 0.58 (dd, *J* = 10.3, 4.8 Hz, 1H); **^{13}C NMR** (75 MHz, $CDCl_3$) δ 175.19 (s), 170.88 (s), 164.35 (s), 160.09 (d, *J* = 250.5 Hz), 144.11 (s), 139.14 (s), 136.21 (s), 131.80 (s), 131.64 (s), 131.15 (s), 129.32 – 128.95 (m), 128.65 (s), 128.02 (s), 127.25 (s), 124.47 (d, *J* = 18.9 Hz), 122.68 (s), 121.92 (s), 116.00 (d, *J* = 21.5 Hz), 50.21 (s), 26.71 (s), 20.60 (s), 20.54 (s), 15.04 (s), 14.74 (s), 9.89 (s); **HRMS** (ESI/IT-TOF) m/z: [M + H] Calcd for $C_{26}H_{25}FN_5O$ 442.2038, found 442.2046.

2.2.7.66. (*R*)-8-Bromo-6-(2-fluorophenyl)-4-methyl-4*H*-benzo[*f*]imidazo[1,5-*a*][1,4]diazepine-3-carbaldehyde (GL-III-35, 78)

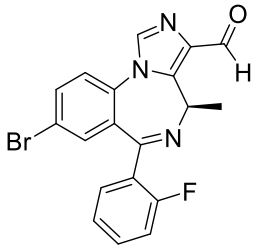

78 (GL-III-35)

The preparation of PDBBA: The potassium *tert*-butoxide (29.3 g, 261 mmol) was suspended in dry THF (261 mL). DIBALH (261 mL, 1.0 M in hexane, 261 mmol) was added dropwise to the solution of potassium *tert*-butoxide at 0 °C using an ice-water bath. The mixture was allowed to stir at rt for 2 h to achieve a colorless homogeneous solution. The concentration of PDBBA

solution in THF-hexanes was measured by GC analysis by hydrolysis of the solution with a mixture of *t*-butyl alcohol-THF (1:1) at 0 °C.[130, 161]

The reduction of bromo ethyl ester **6** to aldehyde **78**: The bromo ethyl ester **6** (5.6 g, 12.7 mmol) was dissolved in dry DCM (30 mL) at 0 °C. The ice-water bath was removed, and the PDBBA solution (0.42 M in THF-hexanes, 69 mL) was added in one portion with vigorous stirring. The reaction was monitored by TLC (silica gel) after each 3 min and was completed in 20 min, and this was followed by hydrolysis of the mixture in 1N aq HCl at 0 °C. Then water (50 mL) was added to the mixture, and it was stirred for 0.5 h. The aluminum salt was formed and filtered off on a celite pad. The filtrate was extracted with DCM (3 x 10 mL). The organic layers were combined and concentrated with reduced pressure, and this was followed by washing with brine and dried (Na_2SO_4). The solid residue was purified by flash chromatography (silica gel packed with DCM, eluent: DCM/EtOAc 3:2) to afford the bromo aldehyde **78** as a white solid (4.0 g, 79.4 % yield): **^{1}H NMR Major rotamer** (500 MHz, $CDCl_3$) δ 10.26 (s, 1H), 8.01 (s, 1H), 7.83 (d, *J* = 8.3 Hz, 1H), 7.69 (t, *J* = 7.2 Hz, 1H), 7.50 (dd, *J* = 23.6, 11.0 Hz, 2H), 7.32 – 7.26 (m, 2H), 7.07 (t, *J* = 9.3 Hz, 1H), 4.42 (d, *J* = 6.6 Hz, 1H), 2.22 (d, *J* = 6.7 Hz, 3H); **^{1}H NMR Minor rotamer** (500 MHz, $CDCl_3$) δ 10.07 (s, 1H), 8.01 (s, 1H), 7.83 (d, *J* = 8.3 Hz, 1H), 7.69 (t, *J* = 7.2 Hz, 1H), 7.50 (dd, *J* = 23.6, 11.0 Hz, 5H), 7.32 – 7.26 (m, 4H), 7.07 (t, *J* = 9.3 Hz, 2H), 6.60 (d, *J* = 7.2 Hz, 1H), 1.32 (d, *J* = 6.7 Hz, 3H).Ratio of rotamers is 2:1. **^{13}C NMR** (126 MHz, $CDCl_3$) δ 184.37 (d, *J* = 4.8 Hz), 162.64 (s), 160.21 (d, *J* = 251.8 Hz), 142.58 (s), 137.61 (s), 135.97 (s), 135.35 (s), 133.10 (s), 132.77 (s), 132.70 (s), 131.30 (s), 130.78 (s), 126.65 (d, *J* = 11.8 Hz), 124.69 (s), 124.65 (s),

121.73 (s), 116.32 (d, J = 21.3 Hz), 53.08 (s), 19.97 (s); **HRMS** (ESI/IT-TOF) m/z: [M + H] Calcd for $C_{19}H_{14}BrFN_3O$ 398.0299, found 398.0310.

2.2.7.67. (*R*)-5-(8-Bromo-6-(2-fluorophenyl)-4-methyl-4*H*-benzo[*f*]imidazo[1,5-*a*][1,4]diaze pin-3-yl)oxazole (GL-III-36, 78)

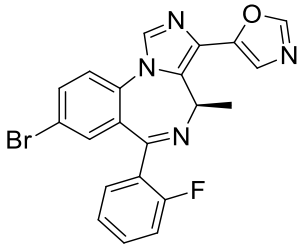

64 (GL-III-36)

The toluenesulfonylmethyl isocyanide (TosMIC, 1.6 g, 8.2 mmol), K_2CO_3 (3.12 g, 22.6 mmol) and the aldehyde **78** (3.0 g, 7.5 mmol) were placed in a dry two neck round bottom flask. Dry MeOH (200 mL) was added to the mixture under an argon atmosphere at rt. The reaction mixture was allowed to heat slowly to reflux for 3 h. After completion of the reaction on analysis by TLC (silica gel, DCM/EtOAc 3:2), the reaction mixture was quenched with cold water (200 mL) and additional saturated $NaHCO_3$ solution (400 mL) was added, after which the mixture was then stirred for 30 min. ***Dilution and additional base is needed to further neutralize the tosic acid formed in the reaction and reduce the possibility of the conversion to the [C(4)-N(5)] imine-migrated byproduct.*** The mixture was extracted with EtOAc (3 x 10 mL). The organic layers were combined and this was followed by washing with brine. The solution was then dried (Na_2SO_4) and concentrated under reduced pressure to dryness. The solid residue, which formed, was purified by flash chromatography (silica gel packed with DCM, eluent: DCM/EtOAc 3:2) to afford the bromo oxazole **64** as a white solid (2.7 g, 82 % yield): **^{1}H NMR Major rotomer** (500 MHz, $CDCl_3$) δ

8.00 (d, *J* = 8.0 Hz, 1H), 7.94 (d, *J* = 19.8 Hz, 1H), 7.78 (d, *J* = 7.9 Hz, 1H), 7.65 (t, *J* = 6.8 Hz, 1H), 7.54 – 7.43 (m, 3H), 7.39 (d, *J* = 23.7 Hz, 1H), 7.26 (t, *J* = 7.5 Hz, 1H), 7.06 (t, *J* = 7.9 Hz, 1H), 4.39 (d, *J* = 6.7 Hz, 1H), 1.89 (d, *J* = 6.6 Hz, 3H); **Minor rotomer:** δ 8.00 (d, *J* = 8.0 Hz, 1H), 7.94 (d, *J* = 19.8 Hz, 1H), 7.73 (d, *J* = 6.1 Hz, 1H), 7.59 (t, *J* = 6.5 Hz, 1H), 7.54 – 7.43 (m, 3H), 7.39 (d, *J* = 23.7 Hz, 1H), 7.26 (t, *J* = 7.5 Hz, 1H), 7.06 (t, *J* = 7.9 Hz, 1H), 6.24 (d, *J* = 7.1 Hz, 1H), 1.35 (d, *J* = 7.0 Hz, 3H). Ratio of major and minor rotomer 0.53:0.46. **HRMS** (ESI/IT-TOF) m/z: [M + H] Calcd for $C_{21}H_{15}BrFN_4O$ 437.0408, found 437.0420.

2.2.7.68. 5-(8-Bromo-6-(2-fluorophenyl)-4-methyl-6H-benzo[f]imidazo[1,5-a][1,4]diazepin-3-yl)oxazole (GL-III-36A/76A, 79)

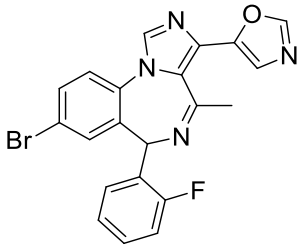

79 (GL-III-36A/76A)

This achiral imine-migrated oxazole byproduct [C(4)-N(5)] was formed during the workup of the desired chiral oxazole **64** and was purified by the same flash column (silica gel, DCM/EtOAc 3:2). The yield of **79** was minimized by dilution of the reaction mixture with water and addition of more aq $NaHCO_3$ solution. However, high temperature and strong acidic conditions resulted in the formation of this undesired byproduct **79**, as a white solid (0.4 g, 12 % yield from the optimized reaction for **64**). The byproduct GL-III-76A from the reaction of the enantiomer **65** was found to be the same compound as **79**, as expected. **^{1}H NMR** (500 MHz, $CDCl_3$) δ 8.29 (td, *J* = 7.3, 2.0 Hz, 1H), 8.15 (s, 1H), 8.00 (s, 1H), 7.57 (dt, *J* = 6.5, 3.2 Hz, 1H), 7.53 (s, 1H), 7.47 – 7.40 (m,

2H), 7.38 (d, *J* = 8.5 Hz, 1H), 7.17 – 7.07 (m, 1H), 6.97 (d, *J* = 1.7 Hz, 1H), 5.66 (s, 1H), 2.41 (s, 3H). **^{13}C NMR** (75 MHz, $CDCl_3$) δ 160.18 (d, *J* = 246.8 Hz), 158.92 (s), 150.81 (s), 145.65 (s), 138.30 (s), 137.11 (s), 133.25 (s), 132.02 (s), 131.01 (s), 130.67 (d, *J* = 3.6 Hz), 129.95 (s), 129.71 (d, *J* = 8.1 Hz), 126.00 (s), 125.77 (d, *J* = 8.8 Hz), 125.38 (s), 124.68 (d, *J* = 3.4 Hz), 123.54 (s), 122.60 (s), 115.56 (d, *J* = 21.0 Hz), 58.07 (d, *J* = 3.2 Hz), 25.51 (s). **HRMS** (ESI/IT-TOF) m/z: [M + H] Calcd for $C_{21}H_{15}BrFN_4O$ 437.0408, found 437.0405.

2.2.7.69. (*R*)-5-(6-(2-Fluorophenyl)-4-methyl-8-((trimethylsilyl)ethynyl)-4*H*-benzo[*f*]imidazo[1,5-*a*][1,4]diazepin-3-yl)oxazole (GL-III-72, 80)

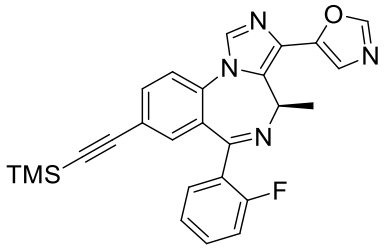

80 (GL-III-72)

The oxazole **64** (1.4 g, 3.2 mmol) was dissolved in triethylamine (30 mL) and acetonitrile (50 mL). Trimethylsilylacetylene (0.63 g, 6.4 mmol) and bis(triphenylphosphine)-palladium (II) acetate (0.132 g, 0.18 mmol) were added to the solution. A reflux condenser was attached and the mixture was degassed under vacuum with argon; this process was repeated four times. The reaction mixture was heated to reflux under argon and stirred for 8 hours. The solution was cooled to rt, filtered through celite, and washed with EtOAc. The filtrate was concentrated under reduced pressure. The black residue, which resulted, was purified by a wash column (silica gel, DCM/EtOAc 3:2) to afford the TMS-oxazole **80** as an off-white solid (1.08 g, 74.4 %): the ratio of rotamers was 1:1. **Rotamer 1: ^{1}H NMR** (300 MHz, $CDCl_3$) δ 7.98 (s, 1H), 7.89 (d, *J* = 10.1 Hz, 1H), 7.71 – 7.47

(m, 3H), 7.34 (d, *J* = 12.7 Hz, 3H), 7.19 (t, *J* = 7.3 Hz, 1H), 6.98 (t, *J* = 8.2 Hz, 1H), 6.17 (d, *J* = 6.7 Hz, 1H), 1.26 (d, *J* = 6.4 Hz, 3H), 0.18 (s, 9H). **Rotamer 2:** ^{1}H NMR (300 MHz, $CDCl_3$) δ 7.98 (s, 1H), 7.89 (d, *J* = 10.1 Hz, 1H), 7.71 – 7.47 (m, 3H), 7.34 (d, *J* = 12.7 Hz, 3H), 7.19 (t, *J* = 7.3 Hz, 1H), 6.98 (t, *J* = 8.2 Hz, 1H), 4.31 (d, *J* = 6.2 Hz, 1H), 1.82 (d, *J* = 5.7 Hz, 3H), 0.18 (s, 9H). **^{13}C NMR** (75 MHz, $CDCl_3$) δ 163.30, 162.79, 161.92, 161.76, 158.58, 158.45, 150.50, 149.85, 146.46, 145.62, 135.68, 135.43, 135.27, 134.72, 134.35, 134.14, 133.51, 133.17, 132.89, 132.19, 132.09, 131.89, 131.77, 131.29, 131.11, 129.36, 129.16, 128.92, 128.77, 127.47, 127.37, 125.90, 125.29, 124.45, 122.79, 122.72, 122.29, 121.95, 116.37, 116.09, 102.59, 97.22, 52.49, 50.62, 18.70, 15.55, -0.26; **HRMS** (ESI/IT-TOF) m/z: [M + H] Calcd for $C_{26}H_{24}FN_4OSi$ 455.1698, found 455.1697.

2.2.7.70. (*R*)-5-(8-Ethynyl-6-(2-fluorophenyl)-4-methyl-4*H*-benzo[*f*]imidazo[1,5-*a*][1,4]diazepin-3-yl)oxazole (GL-III-73, 66)

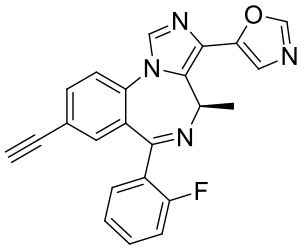

66 (GL-III-73)

The intermediate **80** (722 mg, 1.59 mmol) was dissolved in THF (15 mL) and cooled to 0 °C. This mixture was then treated with tetrabutylammonium fluoride hydrate (1 M solution in THF, 2.38 mmol), and this was followed by water (0.7 mL). The reaction mixture was stirred until the starting material was consumed as indicated by TLC (silica gel), about 20 min. The reaction mixture was allowed to warm to rt, and water (20 mL) was slowly added. The solution was extracted with

EtOAc and the organic extracts were combined, washed with brine, dried (Na_2SO_4), and the solvent was removed under reduced pressure. The residue which resulted was purified by a wash column (silica gel, EtOAc) to afford the pure 1,3-oxazole **66** as a white powder (591.5 mg, 97.4 %). **^{1}H NMR** (300 MHz, $CDCl_3$) δ 8.01 (s, 1H), 7.92 (d, *J* = 10.9 Hz, 1H), 7.69 (d, *J* = 11.3 Hz, 1H), 7.58 (t, *J* = 9.9 Hz, 2H), 7.39 (t, *J* = 12.8 Hz, 3H), 7.24 (dd, *J* = 14.6, 7.5 Hz, 1H), 7.03 (t, *J* = 8.3 Hz, 1H), 6.22 (d, *J* = 6.2 Hz, 0.5H), 4.37 (d, *J* = 5.3 Hz, 0.5H), 1.86 (d, *J* = 5.2 Hz, 1.5H), 1.32 (d, *J* = 5.8 Hz, 1.5H). **^{13}C NMR** (75 MHz, $CDCl_3$) δ 163.14, 162.68, 161.84, 158.49, 150.52, 149.87, 146.43, 145.58, 135.72, 135.28, 134.74, 134.47, 134.00, 133.65, 132.86, 132.14, 131.96, 131.27, 131.10, 129.33, 129.18, 128.82, 128.66, 127.44, 127.23, 125.90, 125.30, 124.47, 122.82, 122.03, 121.64, 121.24, 116.31, 116.03, 81.45, 79.83, 52.48, 50.60, 18.67, 15.63. **HRMS** (ESI/IT-TOF) m/z: [M + H] Calcd for $C_{23}H_{16}FN_4O$ 383.1303, found 383.1308.

2.2.7.71. (*S*)-8-Bromo-6-(2-fluorophenyl)-4-methyl-4*H*-benzo[*f*]imidazo[1,5-*a*][1,4]diazepine-3-carbaldehyde (GL-III-75, 81)

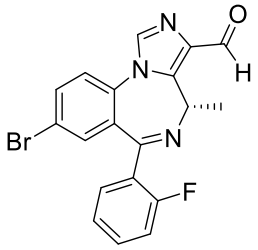

81 (GL-III-75)

The enantiomer **81** of **78** was synthesized as described in section 2.2.7.66., with the bromo ethyl ester **11** (7 g, 15.83 mmol) as the starting material and a solution of PDBBA (0.42 M in THF-hexanes, 48 mL) in DCM (200 mL) to afford **81** (5.3 g, 84.1 %) **^{1}H NMR Major rotamer** (300 MHz, $CDCl_3$) δ 10.22 (s, 1H), 7.99 (s, 1H), 7.80 (d, *J* = 8.1 Hz, 1H), 7.64 (d, *J* = 7.0 Hz, 1H), 7.58

– 7.38 (m, 3H), 7.31 – 7.18 (m, 1H), 7.03 (t, *J* = 9.3 Hz, 1H), 4.39 (d, *J* = 6.5 Hz, 1H), 2.18 (d, *J* = 6.4 Hz, 3H). **^{1}H NMR Minor rotamer** (300 MHz, $CDCl_3$) δ 10.03 (s, 1H), 7.99 (s, 1H), 7.80 (d, *J* = 8.1 Hz, 1H), 7.64 (d, *J* = 7.0 Hz, 1H), 7.58 – 7.38 (m, 3H), 7.31 – 7.18 (m, 1H), 7.03 (t, *J* = 9.3 Hz, 1H), 6.56 (d, *J* = 6.2 Hz, 1H), 1.29 (d, *J* = 5.3 Hz, 3H). Ratio of major and minor rotamer: 2:1. **Major rotamer ^{13}C NMR** (75 MHz, $CDCl_3$) δ 184.46 (s), 162.81 (s), 162.60 (s), 160.24 (d, *J* = 252.3 Hz), 142.41 (s), 137.70 (s), 135.91 (d, *J* = 16.8 Hz), 135.26 (s), 132.95 (d, *J* = 30.2 Hz), 132.75 (s), 131.26 (s), 126.68 (d, *J* = 16.2 Hz), 124.70 (s), 124.51 (s), 123.68 (s), 121.72 (s), 116.32 (d, *J* = 21.3 Hz), 53.11 (s), 19.96 (s); **HRMS** (ESI/IT-TOF) m/z: [M + H] Calcd for $C_{19}H_{14}BrFN_3O$ 398.0299, found 398.0298.

2.2.7.72. (*S*)-5-(8-Bromo-6-(2-fluorophenyl)-4-methyl-4*H*-benzo[*f*]imidazo[1,5-*a*][1,4]diazepin-3-yl)oxazole (GL-III-76, 65)

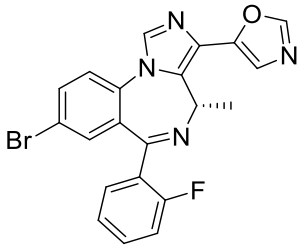

65 (GL-III-76)

The enantiomer of **64** was synthesized as described in section 2.2.7.67., with the bromo aldehyde as the starting aldehyde **81** (4.5 g, 11.3 mmol), TosMIC (2.43 g, 12.43 mmol), and K_2CO_3 (6.25 g, 45.2 mmol) in MeOH (250 mL) at reflux for 1.5 h to afford **81** (3.5 g, 71 %) and the byproduct **79** (1.3 g, 26.3 %). **^{1}H NMR Major rotamer** (300 MHz, $CDCl_3$) δ 7.98 (s, 1H), 7.92 (d, *J* = 8.6 Hz, 1H), 7.71 (t, *J* = 10.9 Hz, 1H), 7.64 – 7.56 (m, 1H), 7.52 – 7.34 (m, 4H), 7.24 (t, *J* = 7.4 Hz, 1H), 7.03 (t, *J* = 9.3 Hz, 1H), 4.37 (d, *J* = 6.1 Hz, 1H), 1.87 (d, *J* = 6.0 Hz, 3H). **^{1}H NMR Minor**

rotamer (300 MHz, $CDCl_3$) δ 7.98 (s, 1H), 7.92 (d, *J* = 8.6 Hz, 1H), 7.71 (t, *J* = 10.9 Hz, 1H), 7.64 – 7.56 (m, 1H), 7.52 – 7.34 (m, 4H), 7.24 (t, *J* = 7.4 Hz, 1H), 7.03 (t, *J* = 9.3 Hz, 1H), 6.22 (d, *J* = 6.6 Hz, 1H), 1.33 (d, *J* = 6.3 Hz, 3H). **^{13}C NMR** (75 MHz, $CDCl_3$) δ 162.62, 162.16, 161.80, 158.58, 150.54, 149.90, 146.42, 145.55, 135.57, 135.42, 135.02, 134.63, 133.87, 133.68, 133.13, 132.77, 132.33, 132.12, 131.26, 131.12, 130.79, 127.59, 127.21, 125.98, 125.45, 124.57, 124.30, 123.47, 122.91, 121.03, 120.61, 116.41, 116.13, 52.56, 50.69, 18.89, 18.68, 15.68. **HRMS** (ESI/IT-TOF) m/z: [M + H] Calcd for $C_{21}H_{15}BrFN_4O$ 437.0408, found 437.0407.

2.2.7.73. (*S*)-5-(6-(2-Fluorophenyl)-4-methyl-8-((trimethylsilyl)ethynyl)-4*H*-benzo[*f*]imidazo[1,5-*a*][1,4]diazepin-3-yl)oxazole (GL-III-77, 82)

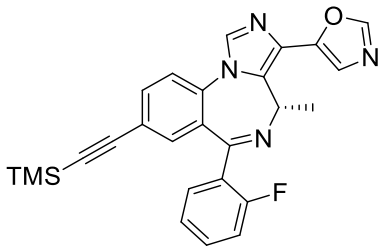

82 (GL-III-77)

The enantiomer **82** of **80** was synthesized as described in section 2.2.7.69., with the bromo oxazole **65** (2.9 g, 6.63 mmol) as the starting material, trimethylsilylacetylene (2.6 g, 26.5 mmol) and bis(triphenylphosphine)-palladium (II) acetate (0.54 g, 0.365 mmol) in triethylamine (60 mL) and acetonitrile (100 mL) at reflux for 1.5 h to afford the TMS-oxazole **82** as an off-white solid (2.7 g, 90 %): ^{1}H NMR (300 MHz, $CDCl_3$) δ 7.99 (s, 1H), 7.90 (d, *J* = 9.0 Hz, 1H), 7.72 – 7.47 (m, 3H), 7.43 – 7.28 (m, 3H), 7.21 (t, *J* = 7.4 Hz, 1H), 7.01 (t, *J* = 9.1 Hz, 1H), 6.19 (d, *J* = 6.7 Hz, 0.5H), 4.33 (d, *J* = 6.0 Hz, 0.5H), 1.84 (d, *J* = 5.5 Hz, 1.5H), 1.28 (d, *J* = 6.3 Hz, 1.5H), 0.20 (s, 9H). **^{13}C NMR** (75 MHz, $CDCl_3$) δ 163.29, 162.79, 161.86, 158.61, 150.50, 149.85, 146.45, 145.62,

135.65, 135.48, 135.27, 134.70, 134.38, 134.16, 133.54, 133.19, 132.91, 132.07, 131.87, 131.29, 131.14, 129.39, 129.21, 128.94, 128.80, 127.48, 125.93, 125.36, 124.46, 122.73, 122.32, 121.94, 116.39, 116.10, 102.59, 97.20, 52.52, 50.64, 18.70, 15.56, -0.26. **HRMS** (ESI/IT-TOF) m/z: [M + H] Calcd for $C_{26}H_{24}FN_4OSi$ 455.1698, found 455.1697.

2.2.7.74. (*S*)-5-(8-Ethynyl-6-(2-fluorophenyl)-4-methyl-4*H*-benzo[*f*]imidazo[1,5-*a*][1,4]diazepin-3-yl)oxazole (GL-III-78, 67)

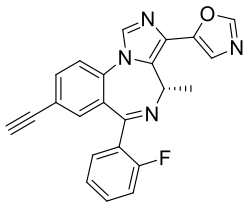

67 (GL-III-78)

The *S*-enantiomer **67** of **66** was synthesized as described in section 2.2.7.70., with the TMS-acetylene oxazole **82** (2.6 g, 5.72 mmol), tetrabutylammonium fluoride hydrate (1 M solution in THF, 8.58 mmol) in THF (100 mL) and water (2.5 mL) at 0 ^{o}C for 0.5 h to afford the ethinyl 1,3-oxazole **67** as an off-white solid (1.98 g, 91 %): **^{1}H NMR** (300 MHz, $CDCl_3$) δ 7.99 (s, 1H), 7.90 (d, *J* = 6.8 Hz, 1H), 7.68 (s, 1H), 7.55 (d, *J* = 8.3 Hz, 2H), 7.38 (dd, *J* = 12.0, 10.5 Hz, 3H), 7.21 (t, *J* = 7.5 Hz, 1H), 7.00 (t, *J* = 9.2 Hz, 1H), 6.20 (d, *J* = 6.0 Hz, 0.5H), 4.35 (d, *J* = 5.8 Hz, 0.5H), 1.84 (d, *J* = 5.0 Hz, 1.5H), 1.30 (d, *J* = 5.6 Hz, 1.5H);**^{13}C NMR** (75 MHz, $CDCl_3$) δ 163.15, 162.72, 161.85, 158.49, 150.54, 149.89, 146.41, 145.60, 135.68, 135.53, 135.30, 134.72, 134.08, 133.71, 132.91, 132.17, 131.98, 131.27, 129.27, 127.49, 125.97, 125.43, 124.50, 122.87, 122.03, 121.67, 121.33, 116.58, 116.36, 116.07, 81.53, 81.48, 79.93, 79.71, 52.52, 50.65, 18.70, 15.66; **HRMS** (ESI/IT-TOF) m/z: [M + H] Calcd for $C_{23}H_{16}FN_4O$ 383.1303, found 383.1302.

2.3. Asthma

2.3.1. Introduction

Asthma is well known as one of the most common long-term inflammatory, non-communicable diseases, which affects about 334 million people globally.[162] It is prominent in both adults and children of all ages, and is expected to reach a number of 400 million[163] effected in a decade. It is diagnosed by variable and recurring respiratory symptoms, reversible airflow limitation, increased mucus production, as well as bronchoconstriction.[164] The most common symptoms include wheezing, coughing, tightness or pain in the chest, and shortness of breath or trouble breathing.[162, 164-165] Asthma can be triggered by the interactions of a series of genetic and environmental factors, such as allergens, irritants, exercise, occupational hazards, air pollution, smoke, airway infections, cold air, and medical uses. [162, 164-165] Less care or non-efficient control at an early stage can lead to the development of severe asthma, which can cause airway remodeling, increase in the intensity of airway inflammation. It might eventually develop into chronic obstructive pulmonary disease (COPD),[162] which often can lead to death. In fact, because of the serious health concern and societal impact, the cost of asthma increases the economic burden daily, which grows steadily and is now up to about $56 billion annually in the US in 2011, and exceeds the total cost of AIDS and tuberculosis combined.[166]

The choice of the most effective approaches for different asthma patients is a significant challenge. Numerous potential targets for new asthma treatments are emerging readily and still suffer from side effects since asthma is such a highly complex disease. The initiation of asthmatic inflammation can include multiple factors and pathological processes. For instance, allergens interact with macrophages, dendritic cells and mast cells, which can activate the CD4T lymphocytes at lymph nodes and lead to eosinophilia as a character of asthmatic inflammation. A

series of pathological effects result from this inflammation such as swelling of the bronchial wall, decreased lumen diameter, airway remodeling, infiltration of immune cells, mucus overproduction, goblet cell hyperplasia, ASM thickening, and contracting (see Figure 71 for the structural comparison of normal and asthmatic bronchial walls).[163, 167-170] This complex development of asthma contains several pathways, mediators, inflammatory cells and proteins, which provide different targets for different therapies based on the patient's condition.

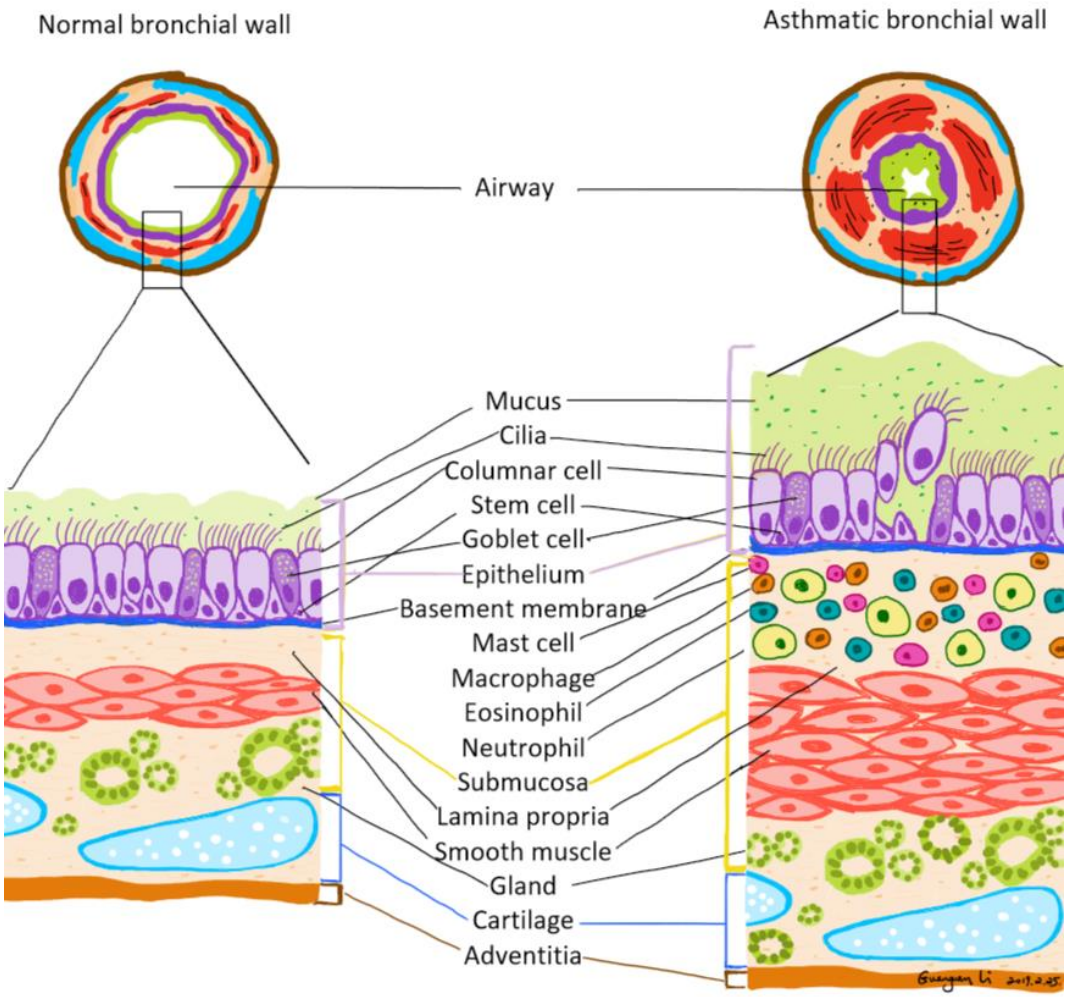

Figure 71. Anatomic structure of the normal and asthmatic bronchial wall. The asthmatic bronchial wall exhibits a series of pathological effects such as swelling, decreased lumen diameter, airway remodeling, infiltration of immune cells, mucus overproduction, goblet cell hyperplasia, ASM thickening, and contracting.[163, 167-170] (Drawing by Guanguan Li on iPad Pro, App: OneNote, version 16.11)

Unfortunately, current treatments for asthma do not cure the disease completely, but alleviate the symptoms and achieve only some control, and in other patients very poor control. This can lead eventually to COPD and death, as mentioned above. Bronchodilators, particularly β_2-adrenergic agonists, are the mainstay for relieving bronchoconstriction. Later, the anti-inflammatory medications, such as corticosteroids, have been used for the treatment of asthma after the identification of airway inflammation as one of the critical causes of asthma. Depending on the severity of asthma, the pharmacological treatment is stepwise[162] according to the Global Initiative for Asthma (GINA): step1, using short-acting β_2 agonists (SABA) as bronchodilators, such as salbutamol (Figure 72), for quick symptom relief. Step 2, a regular low dosage of inhaled corticosteroid (cortisol, see Figure 72) with the combination of SABA for better control of symptoms. Step 3, a low dosage of an inhaled corticosteroid as an anti-inflammatory agent together with a long-acting β_2 agonist (LABA), such as salmeterol (Figure 72). This is for patients with uncontrolled symptoms due to poor adherence, improper use of inhalers, and comorbidities. Step 4, the medium dosage of an inhaled corticosteroid together with LABA for the uncontrolled asthmatic with the other variables listed above addressed. Step 5 (or severe asthma), in addition to a high dosage of corticosteroid and LABA, specific injectable biologic therapies[162, 171] and other add-on therapies such as muscarinic antagonists,[172] leukotriene receptor antagonists,[173] theophylline,[174] immunosuppressants,[175] and bronchial thermoplasty[176] can be considered for treatment. **Although a series of emerging therapies have been approved over the years, patients with severe asthma respond poorly to the current therapies, moreover, long-term use and overuse of the medications cause numerous detrimental effects such as diabetes, cataracts, cardiovascular dysfunction, suppression of growth of children, CNS effects, etc.[162, 164-165, 171-176]** Therefore, there is an urgent unmet need for novel treatments for asthma that can

reduce inflammation, and mitigate the breathing problems with limited or no CNS side effects, cardiovascular issues or other side effects.

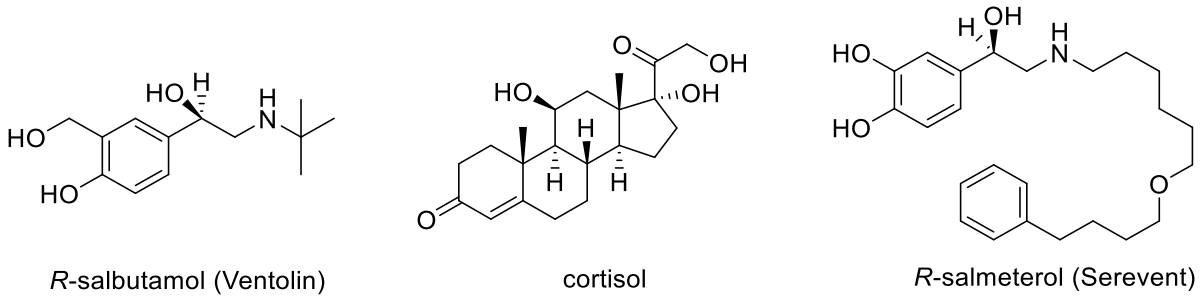

Figure 72. The structures of short-acting β2 agonist (salbutamol), corticosteroid (cortisol), and long-term β2 agonist (salmeterol).

2.3.2. Background

A large amount of pharmacological, and biochemical evidence has been identified, which indicates $GABA_ARs$ are not restricted to the brain and spinal neurons but are also found in the peripheral tissues and cells, such as the liver, heart, and lung.[1] An early study indicated that $GABA_ARs$ expressed in the lung were associated with the inhibition of cholinergic outflow,[177-178] which supports the muscle relaxant effects for asthma. However, there was not enough evidence to fully illustrate the specific location and function of $GABA_ARs$ in the lung tissue. Over the past few years, the expression of $GABA_ARs$ in the lung has attracted broad interest in the search for alternative treatments for asthma. It was first reported by the research group of Dr. Charles Emala that functional α4-, α5-, β3- and γ2- $GABA_ARs$ subtypes were expressed in the airway smooth muscle (ASM) in native human lungs and guinea pigs. The activation of $GABA_AR$ enhanced the β-agonist-regulated relaxation through calcium-activated potassium channels of both

precontracted ASM of human and guinea pig tracheal rings determined from organ bath studies.[56, 179-181]

In particular, evidence from Dr. Emala and others has shown that $GABA_AR$s expressed in the airway epithelium mediated the mucus overproduction,[182] which may be a detrimental effect for using $GABA_AR$ agonists to reduce ASM contraction. However, this mucus production was not mediated by α4β3γ2 or α5β3γ2 subtypes. Consequently, a balance of reduction of ASM contraction and inflammation, in the absence of over-excreting mucus, and the immune response should all be considered and emphasized in regard to the use of GABAergic signaling for the treatment of airway dysfunction and diseases, such as asthma. It must be emphasized that the subtypes that were found in the airway epithelium were β2-, β3- and π-containing $GABA_AR$,[182] whereas the subtypes in ASM are α4, α5, β3, and γ2.[180] Even if the β3 subtypes are expressed in both epithelium and ASM, the amount of its total receptor composition is much less than other subtypes. This balancing issue can be addressed by the design of subtype selective ligands for $GABA_AR$s that only interact with the subtypes in ASM to achieve ASM relaxation and decrease inflammation, but not induce an additional immune response or mucus overproduction. In this vein, PAMs for Bz/$GABA_AR$, especially an α4- or α5-subtype selective PAMs appear to be promising drug targets for asthma. This is not only because of their ability to increase ASM relaxation, but also because IMDZ ligands only bind at the interface of α and γ subunits, which eliminates the possible activation of the β2/3- and π-containing $GABA_AR$ pathway in the airway epithelium. This provides a potential therapy by using these α4- or α5 PAMs as improved bronchodilators or pills for asthma patients by targeting only ASM in the lungs, but not interacting with the subtypes in the brain to avoid CNS side effects nor the other subtypes in the epithelium to decrease the chance of an immune response and mucus production.

Over the last few years, the research on α4- or α5-subtype selective ligands for their SAR on ASM has been ongoing and produced a series of important results in regard to the development of novel treatments for asthma. Two α4 PAMs, XHe-III-74 and CMD-45 (Figure 73), were shown to exhibit the ability to relax the precontracted tracheal rings from guinea pig,[179] wild-type mouse, and human ASM at low doses.[183] These results were further confirmed when XHe-III-74 reduced the acute bronchospasm by inhalation in an *in vivo* murine asthma model of house dust mite (HDM) sensitization. This provided a direct approach to target only the lungs and limit the CNS effects due to systematic drug absorption.[183] A series of analogs of XHe-III-74 were later developed[184-185] to improve the PK profile and avoid side effects from the binding and efficacy of ligands at the $GABA_AR$ in the CNS. Two of the other two analogs, XHe-III-74EE and XHe-III-74A (Figure 73), alleviated the asthmatic symptoms such as inflammation, ASM contraction, airway eosinophilia, airway hyperresponsiveness (AHR) and mucus overproduction, partially.[185]

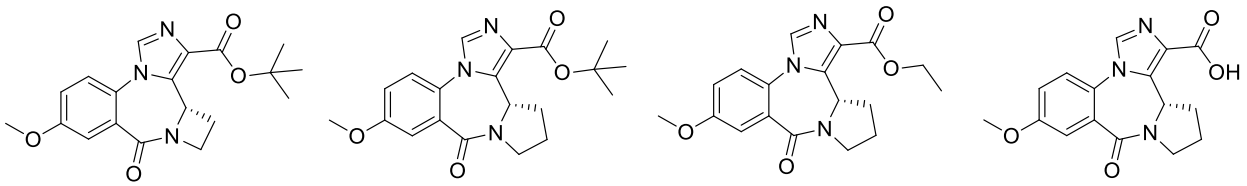

Figure 73. The structures of the α4 selective ligands, CMD-45, XHe-III-74, XHe-III-74EE (ethyl ester) and XHe-III-74A (acid).

In addition to the α4-subtype selective ligands for bronchorelaxation, targeting the α5β3γ2-containing receptors in the ASM in the lungs was investigated as well simultaneously. The question to answer was whether the α5 PAMs have a similar capacity to affect ASM relaxation as the α4 PAMs did since both α4 and α5 subtypes are expressed in human ASM. The first α5 PAM that was evaluated for effects on ASM relaxation was **1** (SH-053-2'F-*R*-CH_3), an α5 subtype

selective ligand[83] with a chiral (*R*)-methyl group at the C(4) position. This ligand alleviated the bronchoconstriction of precontracted ASM in both human ASM strips and guinea pig tracheal rings.[58] However, the ethyl ester **1** exhibited mild sedation at 200 mg/kg, which was due to activation of other BZD subtypes at the higher dose.[121] This was predictable since the ligand was originally designed to cross the BBB for CNS effects[18, 67] in the studies of treatment of other diseases such as schozophrenia[95-96] and MDD.[97] Despite the insignificant CNS effect of **1**, the effect on ASM relaxation provided a direction for further ligand design. This strategy was to maintain the backbone the "privileged structure" of **1** and the *R*-chirality, but modify other moieties on the molecule in order to avoid penetration through the BBB and minimize the possible unwanted CNS effects.

For this purpose, a series of structurally related ligands, Hz-166 (**76**), SH-I-048A (**10**) and α5 subtype selective ligands (Figure 74) SH-053-2'F-*R*-CH_3 (**1**), SH-053-2'F-*R*-CH_3-acid (**68**), MP-III-004 (**83**), MP-III-058 (**84**), were synthesized and evaluated for their electrophysiological $GABA_AR$ response in *Xenopus laevis* oocytes (unpublished results, Figure 75) and the effect on ASM relaxation in a study in an organ bath (unpublished results, Figure 76).

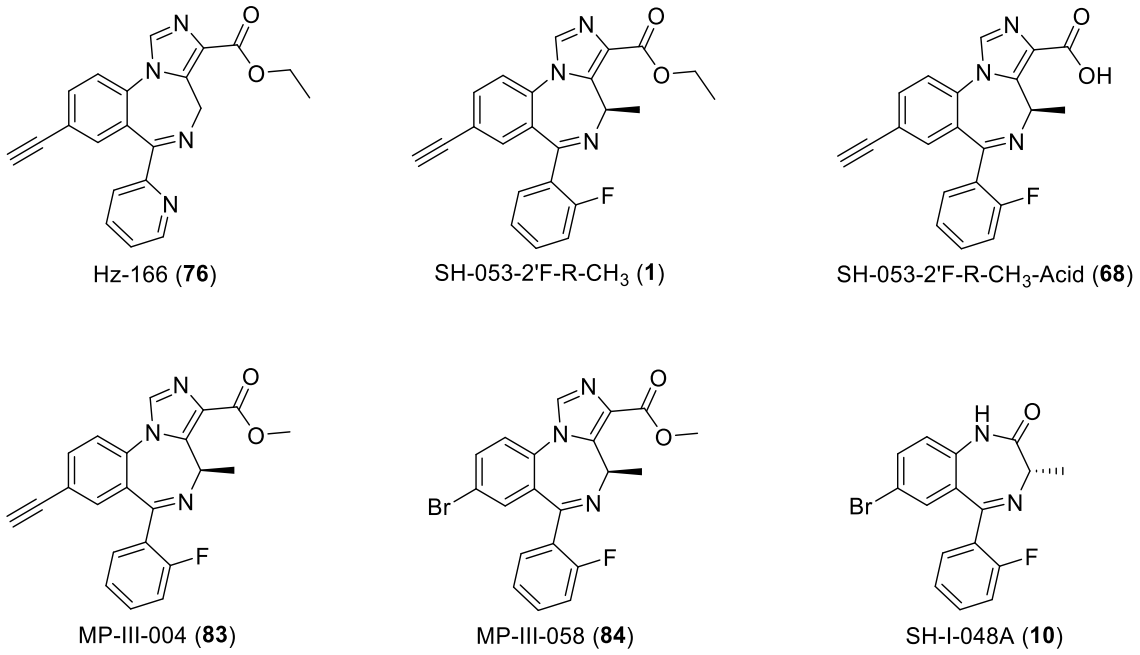

Figure 74. The structures of Hz-166 (76), SH-I-048A (10) and α5 subtype selective ligands SH-053-2'F-*R*-CH$_3$ (1), SH-053-2'F-*R*-CH$_3$-acid (68), MP-III-004 (83), MP-III-058 (84), that were evaluated in an organ bath assay for the effect of bronchorelaxation on guinea pig tracheal rings, and the study of electrophysiology.

As previously described, Hz-166 (**76**) is an α2/3 subtype selective ligand, which was used as a control for it was felt it would not induce ASM relaxation effects due to its very low efficacy at α5 subtypes. This was confirmed by the organ bath study; that there was no significant relaxation observed with **76**, as compared to the vehicle EtOH. The BZD so-called "super-agonist" SH-I-048A (**10**) contained the opposite chirality at the C(4) position did potentiate GABA$_A$R response at all α1-3,5 subtypes. Because of the high efficacy at α5 subtypes of **10**, it exerted the best effect on ASM relaxation. No further PK studies were done for this compound. This was because Dr. Savic showed **10** was sedating and ataxic, and did penetrate the BBB.[186] The structure of **10** was very close to diazepam, and some of the CNS effects induced by **10**, were not unexpected. The carboxylic acid of the ethyl ester, SH-053-2'F-*R*-CH$_3$-acid (**68**), was the best α5 subtype preferring compound up to this point; however, it only exhibited moderate ASM relaxation and was similar

to the parent ethyl ester **1**. The methyl ester analog MP-III-004 (**83)** of the ethyl ester **1**, and the C(8)-bromo methyl ester MP-III-058 (**84**) shared a similar efficacy profile; they were α5 subtype-selective, but both were less potent than the parent compound **1** at 100 nM. The C(8)-ethinyl methyl ester **83** improved the effect on ASM relaxation only a small amount, as compared to **1**. However, the C(8)-bromo methyl ester **84** was shown to exhibit a significant muscle force reduction (ASM) almost as potent as the non-selective super-agonist **10**.

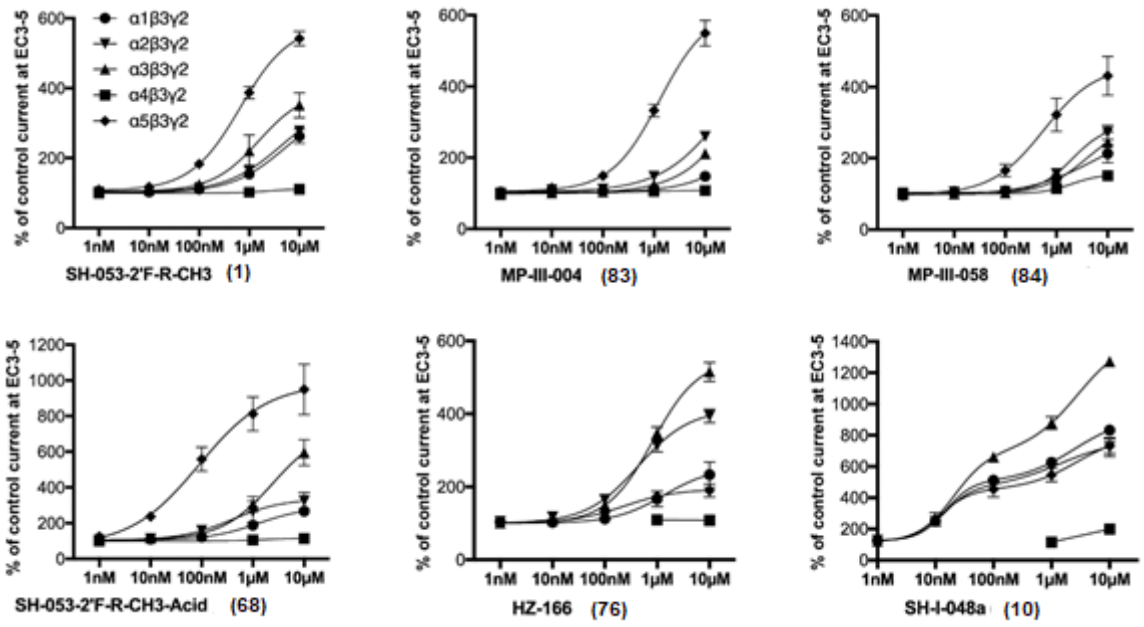

Figure 75. The oocyte efficacy of the Hz-166 (76), SH-I-048A (10), and the α5 subtype selective ligands. Concentration curves on $GABA_AR$ using an EC_3 GABA concentration (n = 3 – 5). (Unpublished results from the Ph. D. thesis of M. Poe, in collaboration with Dr. Ernst's group.)[120]

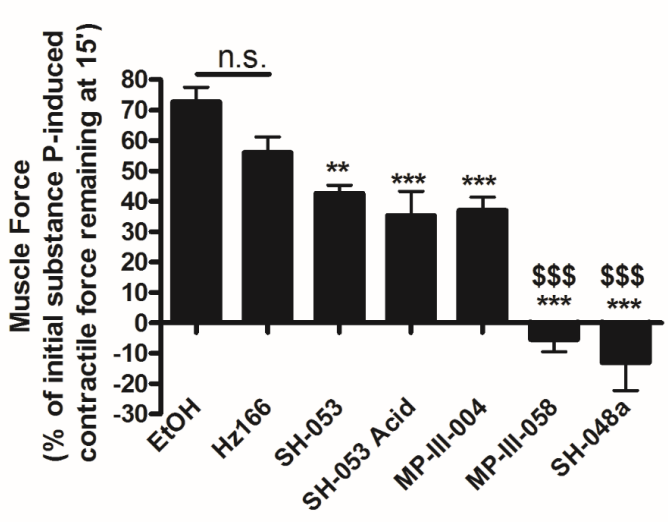

Figure 76. The results of Hz-166 (76), SH-I-048A (10) and α5 subtype selective ligands on the airway muscle relaxation effects from the precontracted guinea pig tracheal rings induced by substance P (1 μM). This was followed by vehicle (0.1% EtOH) or a test ligand (50 μM) in an organ bath, and the muscle force was measured. ** and * represent p< 0.01 and 0.001 as compared to vehicle control, respectively; $$$ p< 0.001 compared to SH-053, n = 6-17. SH-053 = SH-053-2'F-*R*-CH_3; SH-053 Acid = SH-053-2'F-*R*-CH_3-acid. (Unpublished results from the Ph. D. thesis of M. Poe, in collaboration with Dr. Ernst's group)[120]**

A PK study was carried out by Dr. Arnold, and the study demonstrated that three esters **1, 83** and **84** all penetrated the BBB, whereas the acid **68** was almost non-detectable in samples from rodent brain. It should be noted that the ester function will be hydrolyzed in the liver or blood by esterases to rapidly produce the acid as a metabolite, which indicated these esters could be used for the treatment of asthma since they will be, presumably, metabolized to the active acid. On the other hand, acid **68** will not exhibit CNS effects due to its high hydrophilicity. It has been shown not capable of passing through the BBB. In addition to low penetration into the brain, the acid **68**, which possessed good stability from PK studies and could potentially be administrated by oral administration.[99] This will be discussed in a later section. This acid could provide a better α5-preferring target for the treatment of asthma than the esters in regard to the reduction of CNS effects and both preferred routes of administration (aerosol and oral) to lower the possibility of off-target effects.

2.3.3. Chemistry and Results

Based on the results of SH-053-2'F-*R*-CH_3 (**1**) and previously made analogs, SH-053-2'F-*R*-CH_3-acid (**68**) and MP-III-058 (**84**) were resynthesized for follow-up experiments, such as PK studies, and studies of the mechanism of action of IMDZs in models of asthma.[99] Subsequentially, the novel analogs of **68**: GL-II-93 (**85**), GL-III-43 (**86**), GL-III-54 (**87**), GL-IV-14 (**88**), and tetrazoles were designed, synthesized and evaluated. From this study acid GL-II-93 (**85**) exhibited the highest efficacy on ASM relaxation *ex vivo* and significantly reduced AHR *in vivo* to nearly the control level.[187-188] Most importantly, CNS effects, which are always a significant concern for current asthma treatments, were not observed for GL-II-93 (**85**) in a long term study at high dosages on the rotarod and PK studies. Importantly, with acid **85,** (administrated orally), no mucus overproduction[187] or any adverse immunotoxicological effects in mice on oral administration were observed. These effects will be discussed in detail in the following sections.[189] This evidence, taken together, suggested acid **85** was a very promising orally active drug candidate for the treatment of asthma. Due to its high efficacy of the desired pharmacological effects, this ligand **85** is being investigated further as regards to phase I and II metabolites. Here the sodium salt form of acid **85** [GL-IV-18 (**89**)] and the open-ring form of acid **85** [GL-IV-19 (**90**)] from hydrolysis of the [C(6)-N(5)] imine bond are being studied as well.

2.3.3.1. SH-053-2'F-*R*-CH_3-acid (Follow-up Experiments)

Both SH-053-2'F-*R*-CH_3-acid (**68**) and MP-III-058 (**84**) exhibited the capacity to reduce precontracted ASM, as previously described. The acid **68** was chosen to study further due to the

concern for CNS effects of **84**. Although, the methyl ester **84**, at that time, exhibited the most significant effect on ASM relaxation.

The synthesis of SH-053-2'F-*R*-CH_3-acid **68** [99] was presented in the first part of this dissertation. As compared to the parent compound **1**, the acid analog **68,** significantly improved the metabolic stability of this series and also reduced AHR and inflammation with no side CNS effects. These studies were not carried out with the ethyl ester **1** because this ligand exhibited CNS effects at higher dose, which were not tested in **1** before, at which dose level it did not elicit any CNS effects, as compared to data in Table 20.

Table 20. Comparison of the essential pharmacological features of SH-053-2'F-*R*-CH_3 (1) and SH-053-2'F-*R*-CH_3-acid (68).[99]

Code number	SH-053-2'F-*R*-CH_3 (1)	SH-053-2'F-*R*-CH_3-acid (68)
Structure	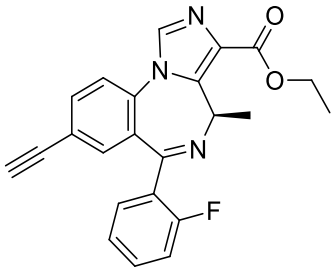	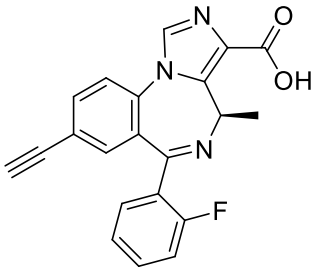
Microsomal stability	**Poor**	**Good**
PK	**Poor**	**Good**
CNS effects at high doses	**Yes**	**NO**
Smooth muscle relaxation	**Yes**	**Yes**
AHR	Not determined	**Reduced**
Inflammation	Not determined	**Reduced**

In order to further study the ability of SH-053-2'F-*R*-CH_3-acid **68** to relax the precontracted ASM, two asthma models were employed: the acetylcholine (ACh)-induced human ASM model

and the substance P-induced tracheal ring contraction in a guinea pig model. These experiments were carried out by Dr. Emala's research group, at Columbia University. In the first model, human tracheal ASM strips were precontracted by ACh at an EC_{50} concentration and then treated with 50 uM of acid **68**. The muscle force was then measured and recorded at four-time points: 15, 30, 45 and 60 minutes. Examination of the results indicated that the acid exhibited a time-dependent ASM relaxation response and it significantly reduced the muscle contractions after 15 min, as depicted in Figure 77A. In the second model, the tracheal rings of the guinea pig were pre-treated with a contractile agent, substance P, to induce muscle contraction. The acid **68** was applied at different concentrations after the contraction, and the muscle force was then measured and recorded. From a study of the data, the acid exerted a dose-dependent response and significant muscle relaxation on ASM was observed at 50 μM in the presence of the acid **68**, as shown in Figure 77B.

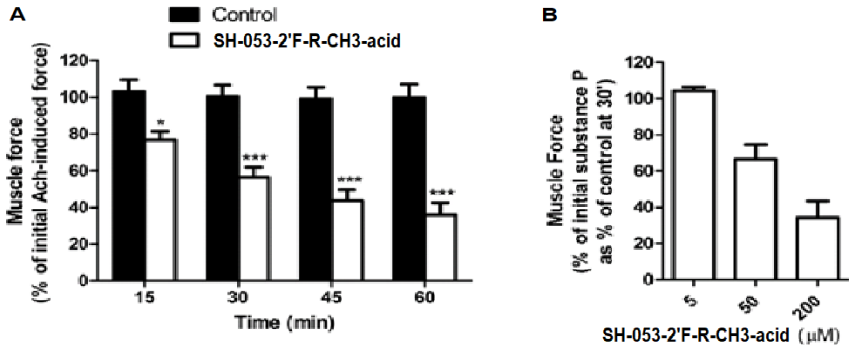

Figure 77. The contractile force of ASM measurement in the presence of 68. (A) The human tracheal airway smooth muscle strips were contracted with an EC_{50} concentration of acetylcholine (Ach) and then treated with 100 μM of the acid 68 or the vehicle 0.2% ethanol. The muscle force was measured at 15, 30, 45, and 60 minute time points after addition of 68. The percent of the initial Ach-induced contractile force was presented as shown. Individual muscle strips were used from at least seven humans. (B) Guinea pig tracheal rings were contracted with 1 μM substance P and then treated with different concentrations of 68. The percent of remaining contractile force was measured at 30 min and expressed as compared to the initial substance P-induced contractile force as a percent of control (N = 3). *, ** and * represents $p < 0.05$, $p < 0.01$ and $p < 0.001$, respectively, as compared to the vehicle control. (Modified from the figure in Forkuo et al.)[99]**

Since airway hyperresponsiveness (AHR) represents an important feature of asthma, the experiment to test the ability of the acid to reduce AHR was conducted by measuring the specific

airway resistance (sRaw), which was carried out by Dr. Arnold's research group (Gloria Forkuo), at UWM. Ova s/c mice were treated with the acid **68** at 100 mg/kg orally twice daily for 5 days during the challenge period. Mice were exposed to increasing concentrations of aerosolized methacholine, which led to bronchoconstriction and was used for the challenge test to assess the sensitivity of lung function. Then the AHR to methacholine at 1 minute was measured and recorded. As shown in Figure 78, the acid exhibited a decrease of sRaw, and successfully protected the animal against the AHR challenged by methacholine. The effect was significant at a high dosage (6.25 and 12.5 mg/mL) of the acid **68**, which almost brought the sRaw value down to the control level.

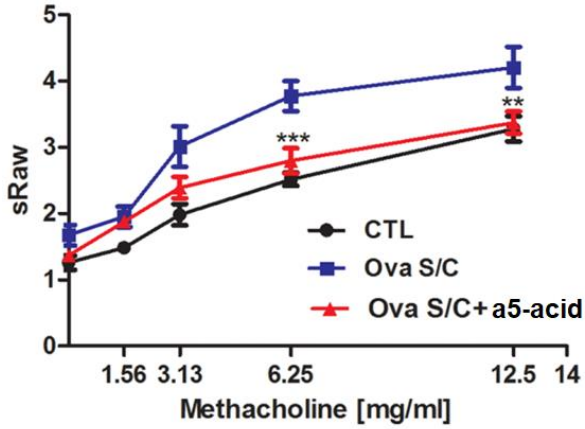

Figure 78. Effect of 68 on AHR. The sRaw was measured at an increasing dose of MCh by a DSI's Buxco FinePointe noninvasive airway mechanics instrument. Ligand 68 was orally administered in ova s/c BALB/c mice at 100 mg/kg twice daily for 5 days. Data represent mean ± SEM (n=10). *, **, and * represents significance $p < 0.05$, $p < 0.01$, and $p < 0.001$, respectively, as compared to the vehicle control. a5-acid = 68 (Modified from the Figure in Forkuo et al.)[99]**

A good pharmacokinetic (PK) profile is a crucial factor for any drug candidate. It illustrates how the drugs affect organs and vice versa and give information on distribution, absorption, metabolism, and excretion, as well as optimization of the dosage of the medication. The PK analysis data of the acid at 25 mg/kg *via* oral gavage is illustrated in Figure 79, which was carried out by Dr. Arnold's research group (Revathi, Kodali), at UWM. The acid was well absorbed and

distributed with a T_{max} of 60 min both in blood and lung AUC = 2648.9 and 1687.7 ug*min/g, respectively. The Cmax in blood and lung are high and similar. Moreover, the half-life of the acid is significantly longer in blood, about 15 h, and can still be detected after 8 h in both lung and blood. Most importantly, there is almost no detection of the acid in the brain, which indicated a perfect PK profile for an asthma drug candidate, which limits CNS effects with little or no distribution in the brain. To further confirm there were no CNS effects, the acid **68** was administrated orally at 100 mg/kg to mice on a rotarod. Their performance on the rotarod was recorded at 10, 30 and 60 min after the drug treatment, and diazepam was used as a negative control. This was carried out by Dr. Arnold's research group (Nick Zahn), at UWM. The results indicated there was no sedation nor ataxia observed, as shown in Figure 80, which correlated with the PK data and confirmed the lack of CNS effects of orally administrated SH-053-2'F-*R*-CH_3-acid (**68**).

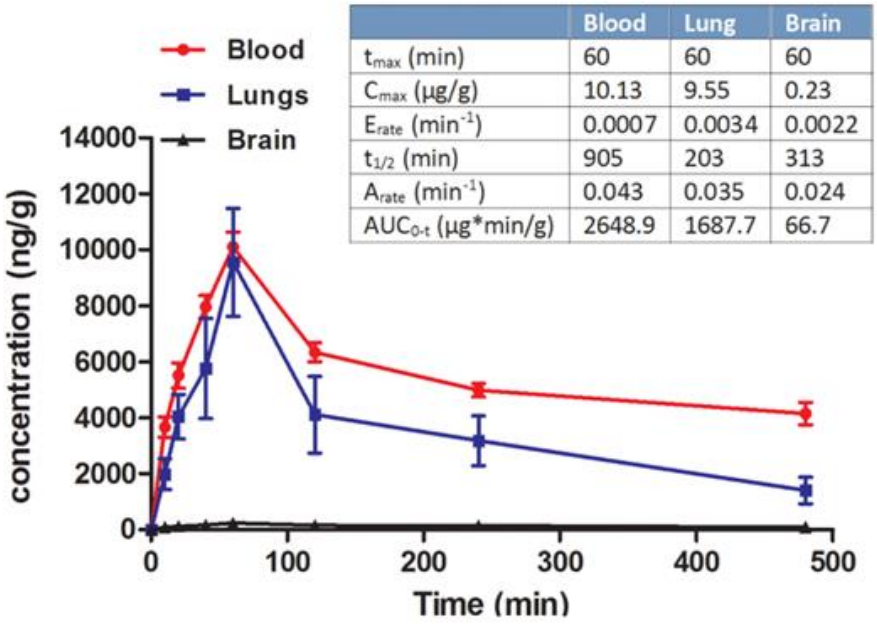

	Blood	Lung	Brain
t_{max} (min)	60	60	60
C_{max} (µg/g)	10.13	9.55	0.23
E_{rate} (min^{-1})	0.0007	0.0034	0.0022
$t_{1/2}$ (min)	905	203	313
A_{rate} (min^{-1})	0.043	0.035	0.024
AUC_{0-t} (µg*min/g)	2648.9	1687.7	66.7

Figure 79. The pharmacokinetic data of 68 in blood, lungs, and brain in mice. The time-dependent systemic distribution of 68 was determined at 25 mg/kg via oral gavage. (Modified from the Figure in Forkuo et al.)[99]

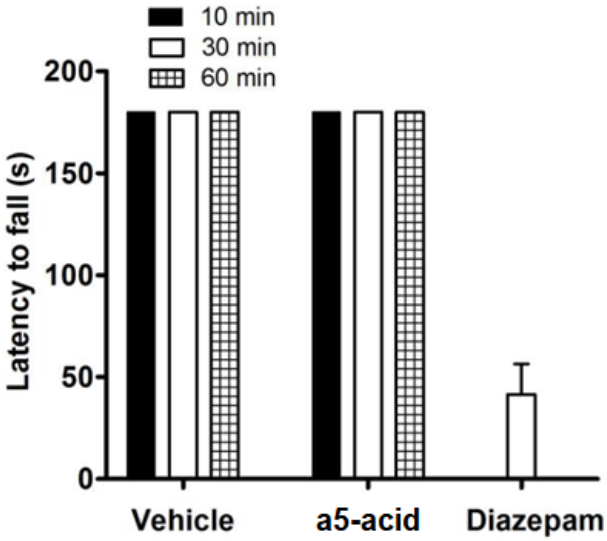

Figure 80. The effect of 68 on sensorimotor coordination *in vivo*. The Swiss Webster mice received a single intragastric gavage of the ligand at 100 mg/kg or diazepam (5 mg/kg i.p.) and were placed on a rotarod at 15 rpm for 3 minutes, and the performance was recorded after 10, 30 and 60 minute time points of drug administration. A fail was assigned to a mouse if they had fallen twice within 3 minutes. The latency to fall is presented as mean ± SEM (n = 9). The vehicle was used as the negative control, and diazepam as the positive control. a5-acid = 68. (Modified from the Figure in Forkuo et al.)[99]

In addition to the assays above for the acid, this key α5-agonist did not increase mucus production,[99] which is also a detrimental pharmacological feature of asthma. However, importantly this α5 PAM did not significantly affect the $CD4^+$ T cell response in broncho-alveolar lavage fluid (BALF) or the *ex vivo* response of current change.[99] The reason for no response may be due to the lack of α5 subtype expression in those immune cells,[190-191] or it might be because of other possible inflammatory signals. Consequently, the exact mechanism remains unclear.

To summarize the effect[99] of the acid SH-053-2'F-*R*-CH_3-acid (**68**): it reduced AHR, relaxed ASM *ex vivo*, exerted no observed CNS effects *in vivo*, exhibited a good PK profile, was an α5 subtype selective ligand, and was active against the effects of asthma *in vivo*. This key α5-$GABA_AR$ agonist acid is the first orally active asthma drug candidate from MIDD and was further optimized for improved pharmacological features on asthmatic inflammation.

2.3.3.2. GL-II-93 (MIDD0301)

2.3.3.2.1. Development and Synthesis

As previously demonstrated, it was discovered that a PAM of the α5-$GABA_AR$, SH-053-2'F-*R*-CH_3-acid (**68**), which exhibited the best α5 efficacy[99] among a library of over 650 IMDZ ligands,[18, 67] exhibited no CNS side effects. This was possible for this ligand did not penetrate the BBB and had a very good PK profile for a drug candidate for asthma.[99] However, the relaxation of contracted ASM only reached a moderate level. Meanwhile, another PAM of the α5-$GABA_AR$, MP-III-058 (**84**), exerted a better effect on ASM relaxation, as compared to **68**, but the α5 efficacy was not as potent as **68**. Moreover, the methyl ester **84** induced mild CNS effects, which disqualified it for an orally active asthma drug, but the presence of the C(8)-bromo group and the increased relaxation on ASM was significant, even though the C(8)-bromo analogs are normally sedating similar to diazepam.

In order to design a better ligand that retains the desired properties but reduces or avoids the drawbacks from the previously made ligands, it was critical to take an in-depth look at the SAR of the active ligands. From a structural point of view, when one functional group was altered at a time, it was clear that the ester and carboxylic acid function at the C(3) position did not improve the ASM relaxation effect significantly (see Figure 81 for a combined ASM Figure). However, the acid function remarkably increased the α5 subtype selectivity and efficacy as compared to both the ethyl and methyl esters (Figure 75 for efficacy). Furthermore, this acid **68** was hydrophilic and did not cross the BBB for CNS interactions. This is a fundamental PK feature required for these asthma drugs. Consequently, the carboxylic acid function should be taken into consideration during ligand

design to prevent CNS activity. Notwithstanding the acid function, comparison of the substituents at the C(8) position of the SH-series for example **83** and **84**, there was no perceptible difference efficacy-wise between these ligands. However, the C(8)-bromo ligand **84** significantly improved the relaxation effect on precontracted ASM, whereas the C(8)-ethinyl ligand **83** exhibited only a moderate effect. According to this difference, the bromine atom at the C(8) position appeared to exhibit a critical role for the purpose of better relaxation of pre-contracted ASM.

From an examination of the SAR, efficacy, and biology of the compounds above, it was deemed essential to keep the C(3)-carboxylic acid function and the C(8)-bromo substituent in the backbone of the IMDZ structure for future ligand design. Based on this hypothesis, MIDD0301 (**85**), originally termed GL-II-93, and a series of its analogs were designed, synthesized, and evaluated. Accumulative evidence[187-189] confirmed this hypothesis was rational for the design of ligands for asthma. Gratifyingly, it turns out that **85** is the best orally active asthma compound developed, to date (Figure 81). The performance of this compound in various *in vitro* studies and *in vivo* animal assays is presented in detail in the following sections.

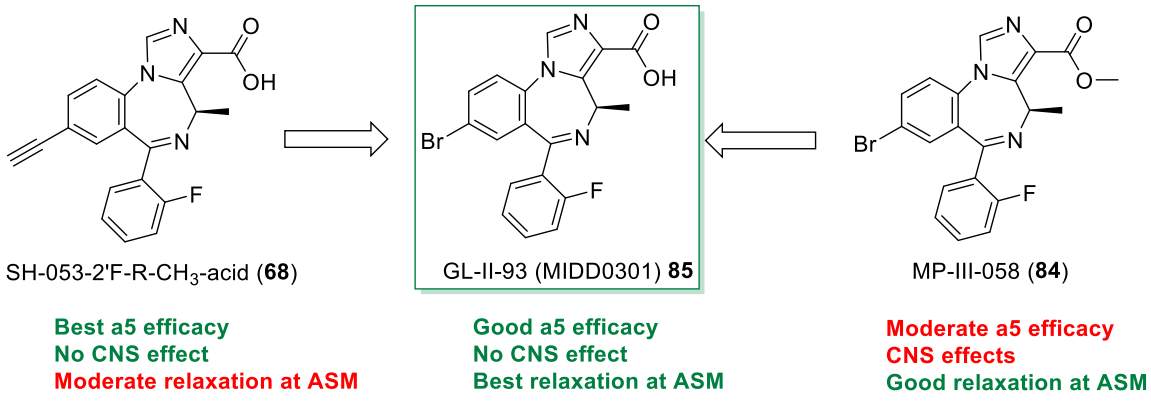

Figure 81. Development of GL-II-93 (85) and its key features, as compared to the previous ligands in this series.

The synthesis of GL-II-93 (**85**) was straight forward in high yield (Scheme 15) by hydrolyzing the C(8)-bromo ethyl ester SH-I-47 (**6**),[82, 120] which was the intermediate in the synthesis of the parent compound **1**. The reaction was conducted in ethanol with sodium hydroxide under refluxing conditions. The reaction progress was monitored by TLC (silica gel). After removal of the solvent, the acid precipitated out of solution after acidifying with an aqueous solution of hydrochloric acid. The precipitates, which formed, were filtered and were then washed with water. The remaining organic impurities can be washed away with ethyl acetate.

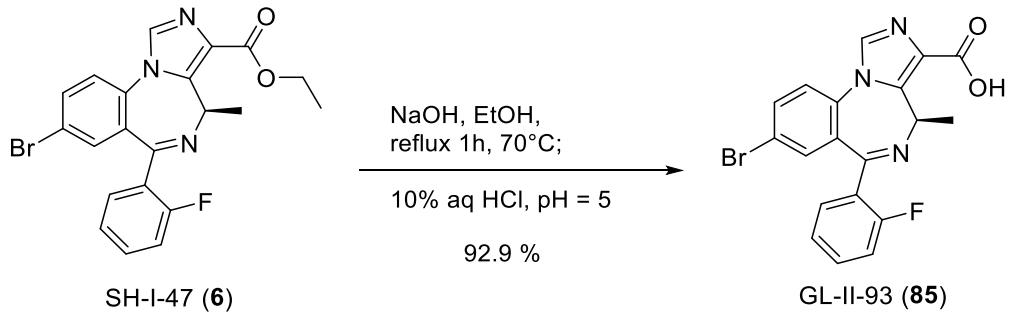

Scheme 15. Synthesis of GL-II-93 (85).

2.3.3.2.2. Efficacy on α1-5 $GABA_AR$ Subtypes and Receptor Binding

It was imperative to determine if GL-II-93 (**85**) exhibited good efficiency and selectivity for $GABA_ARs$. In order to answer this question, electrophysiological recordings were performed. Mammalian clones of $GABA_ARs$ with β3 and γ2 in addition to the indicated α subunits were transiently transfected into the HEK-293T cells, and voltage-clamp recordings were used to measure the currents in response to two concentrations of **85** (0.1 and 1 μM) and GABA (EC_{3-5}). The whole-cell configuration was carried out by Dr. Janet Fisher's research group, University of South Carolina School of Medicine. As illustrated in Figure 82, acid **85** as highly effective at potentiating $GABA_AR$ subtypes, however, it is only slightly selective at α4 subtypes at a lower

concentration and did not show subtype selective efficacy at 1 μM. Thus, by changing the C(8) acetylene function to a bromine atom overall, this resulted in the loss of selectivity in this molecule, but improved the efficacy at the other subtypes, as compared to acid **68**. On the other hand, comparison of the efficacy of **85** regardless of the substituents at C(8) resulted in an increase of the efficacy at α1-4 subtypes. Overall, despite the enhancement at the α1-4 subtypes, the α5 selectivity was decreased only in comparison with acid **68**. The efficacy of **85** at the α5 subtypes is actually improved, as compared to other ligands in the same 2'F-*R*-CH_3 series. Based on the results of the electrophysiology, the bromo acid **85** did potentiate α1-containing $GABA_A$Rs. This could become a significant concern for asthma drugs for the binding at the α1 subtype would result in CNS side effects. Fortunately, the α1 subtypes are not expressed in lung.[57-58, 180-181] Furthermore, by design, [99] this carboxylic acid **85** did not pass through the BBB negating any possible GABA-mediated CNS pharmacological effects. This data will follow in the section on PK. At this point, the bromo acid **85** exhibited high efficacy at both α4 and α5 subtypes both of which are found in the lungs and might be the reason for the more potent ASM relaxation for GL-II-93 (**85**).

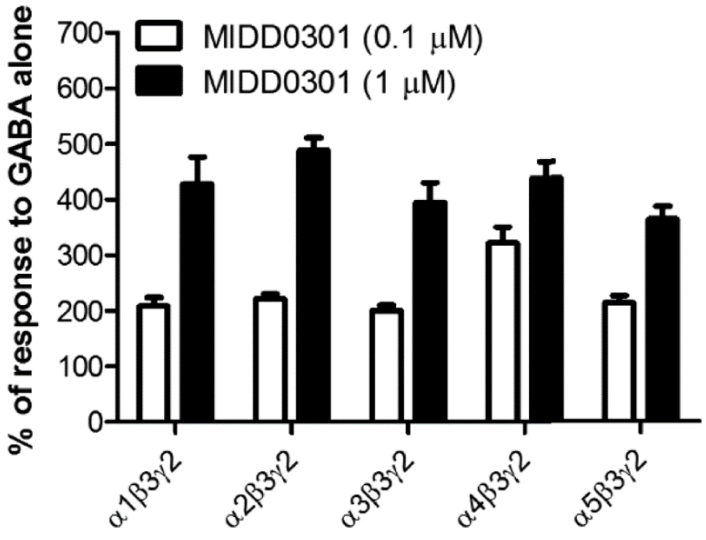

Figure 82. The potentiation of GL-II-93 (85) at α-containing $GABA_A$Rs. The transiently transfected HEK-293T cells with α subunits with β3 and γ2L subunits of $GABA_A$R were used to measure the average enhancement of

current evoked to GABA by 0.1 μM or 1 μM 85 by patch clamp. Data represented mean ± SEM (n = 5). (Adopted from the figure in Forkuo et al.)[187]

At present, it appears that GL-II-93 (**85**) acts through $GABA_A$Rs. In order to determine if any other receptor interactions with acid **85** would occur throughout the body, the ligand was sent to the National Institute of Mental Health (NIMH) Psychoactive Drug Screening Program (PDSP) for screening on a series of CNS receptors, ion channels, and transporters to determine any other possible receptor interactions.[137] The primary binding assay was conducted first to determine if there was any significant inhibition (over 50%), which PDSP would consider as a hit and be further tested in the secondary binding assay to obtain a K_i (nM) value. As shown in Table 21, **85** only bound at the BzR rat brain sites, as expected, with 72.5% inhibition in the primary binding assay and a K_i = 86 nM from the secondary binding assay. The binding affinity to the rat brain homogenized BzR sites was expected for it contains a mixture of all Bz/GABA(A) receptors. As requested, the secondary binding assay was also employed for the binding to both hERG and peripheral benzodiazepine receptors (PBR) for an accurate K_i value to eliminate possible heart issues and cholesterol disruptions. The ligands exhibited a deficient inhibition for hERG and PBR from the primary binding assay, 2.8% and -19.9% (negative value only represents stimulation of binding), respectively. **From the secondary binding assay, the K_i value for hERG and PBR was 8223.3 nM and over 10000 nM, respectively, which indicated very low or no binding interaction at hERG or PBR. This was extremely important in drug design for asthma.**

Table 21. Primary and secondary binding assay for GL-II-93 in a panel of CNS receptors, channels, and transporters. (PDSP code for GL-II-93 is 50109)

Binding Assay	Primary (% inhibition)	Secondary (nM)
5-HT1A	10.1	
5-HT1B	28.4	
5-HT1D	32.7	

Binding Assay	Primary (% inhibition)	Secondary (nM)
GABAA a6		
GABAB		
GPCRome		

5-ht1e	3.2		**H1**	-5.4	
5-HT2A	-4.7		**H2**	10.7	
5-HT2B	6.2		**H3**	-13.3	
5-HT2C	8.1		**H4**	26.2	
5-HT3	0.3		**HCA2**		
5-HT4			**HERG**		
5-ht5a	7.9		**HERG binding**	2.8	8,223.3(AVE)
5-HT6	2.4		**Imidazoline 1**		
5-HT7	6.5		**KA**		
A1			**KOR**	-9.1	
A2			**M1**	-7.3	
A2A			**M2**	-4.1	
A2A mouse			**M3**	-1.9	
A2B			**M3D**		
A2B2			**M4**	-5.6	
A2B4			**M4D**		
A3B2			**M5**	-4.6	
A3B4			**mGlur2**		
A4B2			**mGluR3**		
A4B2**			**mGlur4**		
A4B4			**mGlur5**		
A7			**mGluR5_Guinea pig**		
A7**			**mGluR5_RatBrain**		
Alpha1A	-4.9		**mGlur6**		
Alpha1B	14.3		**mGluR7**		
Alpha1D	-9		**mGluR8**		
Alpha2A	-18.2		**MOR**	-0.3	
Alpha2B	-14.1		**NET**	2	
Alpha2C	-16.2		**NK-1**		
AMPA			**NMDA**	20.2	
AT2			**NOP**		
B2			**NR2B**		
Beta1	-16		**NTS1**		
Beta2	-9.1		**NTS2**		
Beta3	-3.8		**Oxytocin**	-1	
BZP Rat Brain Site	72.5	86	**P2RY12**		
Calcium Channel	13.4		**PBR**	-19.9	>10,000
CB1			**PKCalpha**		
CB1 H			**PKCbeta**		
CB2			**PKCdelta**		

D1	4.4		**PKCepsilon**		
D2	14.8		**PKCgamma**		
D3	-3.5		**SERT**	26.1	
D4	-8.2		**Sigma 1**	11.2	
D5	2.4		**Sigma 1 GP**		
DAT	-15.9		**Sigma 2**	1.6	
DOR	-13.4		**Sigma 2 PC12**		
EP2			**Sodium Channel**		
EP3			**V1A**	19.6	
EP4			**V1B**	-1.5	
GABA a1			**V2**		
GABAA	12.7		**VMAT1**		
GABAa a2			**VMAT2**		
GABAa a3			**Y2**		
GABAa a5					

The data represent mean % inhibition (N = 4) for the tested compound at receptor panels. Significant inhibition is considered > 50 %. Negative inhibition (-) represents stimulation of binding. Occasionally, compounds at high concentrations will increase binding affinity non-specifically. The default concentration is 10 uM for the primary binding assay. Data represented as K_i (nM) values, which were obtained from non-linear regression of radioligand competition binding isotherms. The Ki values were calculated from best fit IC_{50} values by using the Cheng-Prusoff equation. A * next to a value number represents IC_{50}. Green indicates 1° Assay <50%.[137]

2.3.3.2.3. Pharmacokinetic Study, CNS Exposure as well as Cytotoxicity

Since the acid GL-II-93 (**85**) is structurally similar to SH-053-2'F-*R*-CH_3-acid (**68**), it was possible to predict a similar PK profile for both ligands. Indeed, this was confirmed by a 24 hour-period PK study in mice at a dose of 25 mg/kg of acid **85** on oral administration, see Figure 83. The experiment was carried out by Dr. Arnold's research group (Revathi, Kodali), at UWM. The compound was well absorbed within 40 min (T_{max}) in both blood and lung. The C_{max} of **85** was higher in blood than lung, with 8.24 vs 4.39 μg/g, respectively. The area under the curve (AUC) indicated that the distribution of the **85** was good in blood with 2807.1 μg*min/g and with 1390.5 μg*min/g in the lung. The elimination rate of the compound was very slow in the blood, slightly faster in the lung, at 0.001 and 0.003 min^{-1}, respectively. This led to a relatively long half-life of

836 min or 34.8 hours in blood than lung of 234 minutes or 9.8 hours, respectively. This was still a very good profile for GL-II-93 (**85**).

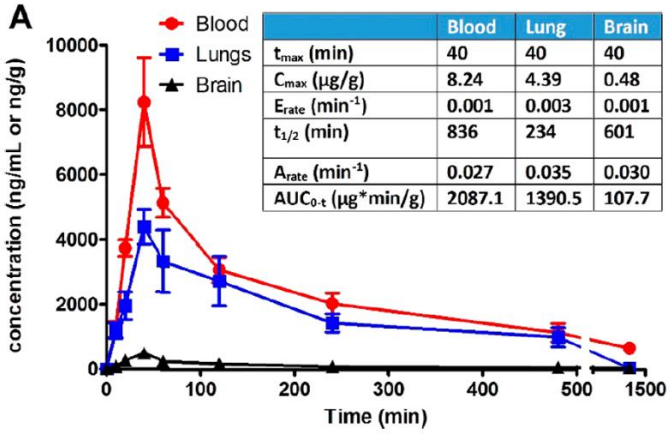

	Blood	Lung	Brain
t_{max} (min)	40	40	40
C_{max} (μg/g)	8.24	4.39	0.48
E_{rate} (min^{-1})	0.001	0.003	0.001
$t_{1/2}$ (min)	836	234	601
A_{rate} (min^{-1})	0.027	0.035	0.030
AUC_{0-t} (μg*min/g)	2087.1	1390.5	107.7

Figure 83. The pharmacokinetic data of GL-II-93 (85) in blood, lungs, and brain in mice. The time-dependent systemic distribution of GL-II-93 was determined at 25 mg/kg via oral gavage. (Adopted from the figure in Forkuo et al.)[187]

Examination of the *in vitro* microsomal stability study indicated (see Table 22) that acid **85** was much more stable in human liver microsomes (HLM) than in mouse liver microsomes (MLM), with a half-life of 64 and 23 hours, respectively (Table 22). The percentage of **85** remaining in HLM was 91% after 2 hours incubation, whereas it was only 83% in MLM. The metabolism rate was much slower in HLM than MLM, with 0.9261 and 2.624 nmol/min/mg, respectively. This is to be expected since mice liver enzymes are up-regulated ("they eat garbage"), and their metabolic rate is also faster than humans. In addition, from the examination of the data in Table 23, the plasma protein binding of **85** was 88.25% in the mouse, which was carried out by Dr. Arnold's research group (M. S. Rashid Roni), at UWM.

Table 22. Summary of microsomal stability studies for GL-II-93.

GL-II-93 (85)	HLM	MLM
Half-life (min)	1546 ± 501	549 ± 81
V_d (μL/mg)	2000	2000

Internal Clearance (μL/min/mg)	0.0463	0.1312
Metabolic Rate (nmol/min/mg)	0.9261	2.624
% remaining at end of 2 hrs. (%)	91 ± 0.25	83 ± 0.20

The acid GL-II-93 was incubated with human liver microsomes (HLM) or mouse liver microsomes (MLM) for 30 min at 37 ºC at a final concentration of 10 μM. The percentage of compound remaining after incubation was measured by LC-MS/MS. (Modified from the figure in Forkuo *et al.*)[187]

Table 23. Summary of plasma protein binding in mice.

Result %		
GL-II-93	Unbound drug	Bound drug
Average (n = 3)	11.75 ± 1.42	88.25 ± 1.42

The 5 μL of 1 mM GL-II-93 was added to the mouse plasma and this was shaking for 4 h; then the sample was transferred to tubes on ice to precipitate protein, which was vortexed and incubated for 30 min and then analyzed by LCMS/MS. (Modified from the figure in Forkuo *et al.*)[187]

The clearance of the acid **85** was further evaluated after a 28-day chronic immunotoxicity study. This data will be discussed in detail in a later section. In this PK study, the average concentration of acid **85** was quantified in urine and feces by LCMS/MS at day 28.[189] After the collection of urine and feces, intact **85** was recovered with a concentration of 113.0 ± 27.9 μM in urine, and 841.0 ± 188.6 μmol/kg in feces, which indicated that most of the compound was cleared through feces, accompanied by a relatively slow renal secretion rate.

Due to the carboxylic acid function of GL-II-93 (**85**), the penetration of the BBB did not occur to any significant level, which results in an extremely low C_{max} and AUC in the brain and indicated minimal or no CNS side effects. To further confirm this, the acid was tested in a rotarod study to see if any possible side effects, such as motor impairment or sedative effects, occurred in Dr. Arnold'g research group (Nick Zahn and Alec Huber), at UWM. In the initial rotarod study, mice were treated with vehicle, or a positive control diazepam at 5 mg/kg, or an increased dosage of **85** from 50 to 800 mg/kg orally. The performance of the mice on the rotarod was recorded. No fall from the rotarod was counted as a successful performance during the 3 minute test period for

15, 30, 60 minute time points. Examination of the data indicated the mice were able to stay on the rotarod during the test period and no motor impairment was observed, which demonstrated the absence of CNS effects after the treatment with **85.** This held true from doses, which ranged from 50 mg/kg to an extremely high dosage 800 of mg/kg, as presented in Figure 84. Moreover, there was no loss of righting response. The rotarod data eliminated the possible CNS side effects from the treatment with acid GL-II-93 (**85**).

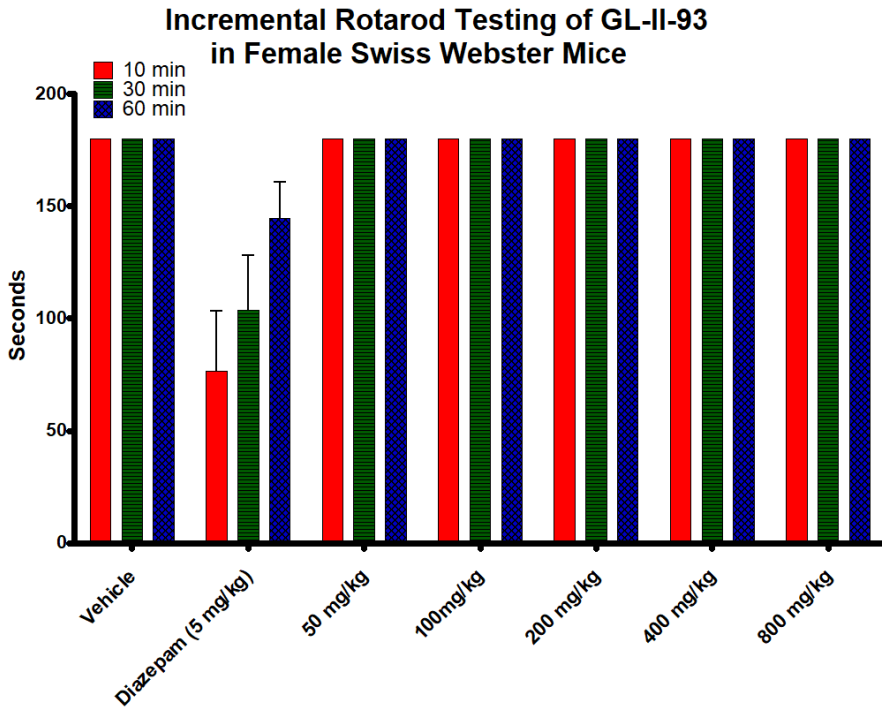

Figure 84. The incremental rotarod study of GL-II-93 (85) in mice. The Swiss Webster mice received a single intragastric gavage of GL-II-93 at an increased dosage 50-800 mg/kg rate or diazepam (5 mg/kg ip) and were placed on a rotarod at 15rpm for 3 minutes, and the performance was recorded after 10, 30 and 60 minutes. A fail was assigned to a mouse if they had fallen twice within 3 minutes. The latency to fall is presented as mean ± SEM (n = 9). The vehicle was used as the negative control and diazepam as positive control.

Examination of the rotarod study not only indicated the absence of possible CNS adverse effects but also provided some indication if the compound had any toxic metabolites that affect the performance of mice on the rotarod. Since the mice all successfully performed well on the

rotarod, it reflected the fact that GL-II-93 (**85**) did not produce toxic metabolites in mice and permitted its use for animal models. In addition to the rotarod study, the cytotoxicity study was conducted in both a human embryonic kidney cells (HEK293T) and human liver cancer cell line (HEPG2) to further investigate the toxicity of **85** at the cellular level. These experiments were run by Dr. Michael Stephen from Dr. Cook's group. The LD_{50} values of **85** in HEK293T and HEPG2 are both higher than 400 μM, as displayed in Figure 85, which demonstrated a very good safety profile for the acid **85**.

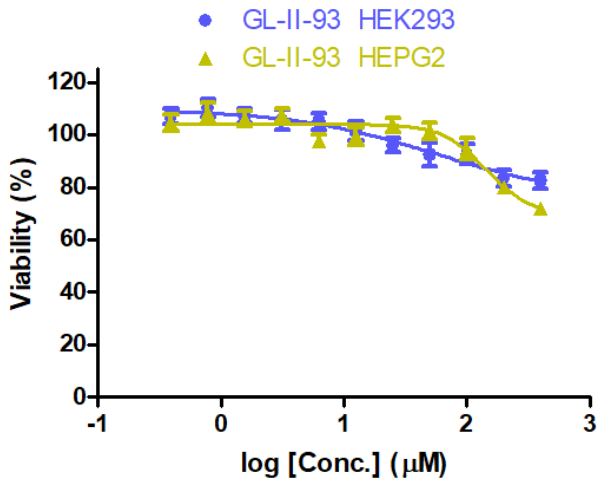

Figure 85. ***In vitro*** **cytotoxicity data of GL-II-93 (85). GL-II-93 was incubated with HEK293T cells and HEPG2 cells, respectively, for 48 hours followed by detection of cell viability using a Cell-Titer Glo (Promega). The results were normalized using DMSO as a negative control and 3-dibutylamino-1-(4-hexyl-phenyl)-propan-1-one (150 mM in DMSO final concentration, as a positive control. Data was determined by three independent experiments carried out in quadruplet.**

2.3.3.2.4. The Relaxation of Contracted Smooth Muscle *Ex Vivo* and *In Vivo*

As described above, acid **85** exhibited high potentiation at $GABA_ARs$ and possessed a very good PK profile for an asthma drug candidate; the next question was if the compound exhibited the desired pharmacological effects including the ability to relax precontracted ASM. The *ex vivo*

relaxation of ASM experiment was performed by Dr. Emala's research group at Columbia University. The tracheal rings from guinea pigs were removed and isolated. And then they were suspended in an organ bath. The EC_{50} of ACh was determined; the strips which had a similar EC_{50} were used for the experiments. The muscle contraction was achieved by applying 1 μM substance P from the resting tension, and this was, followed by the treatment of a series of increasing concentrations of **85** or vehicle. The percentage of remaining muscle force was recorded at four-time points: 15, 30, 45, 60 min. As shown in Figure 86, acid **85** successfully relaxed the precontracted ASM induced by substance P in a dosage-dependent and time-dependent manner. It exhibited the desired pronounced effect on ASM relaxation at 25 μM and higher dose. The significance of effect occurred at 15 min, and the effect was enhanced over the next 60-minute period. Moreover, the relaxation of **85** was much improved as compared to the C(8)-ethinyl acid **68**.

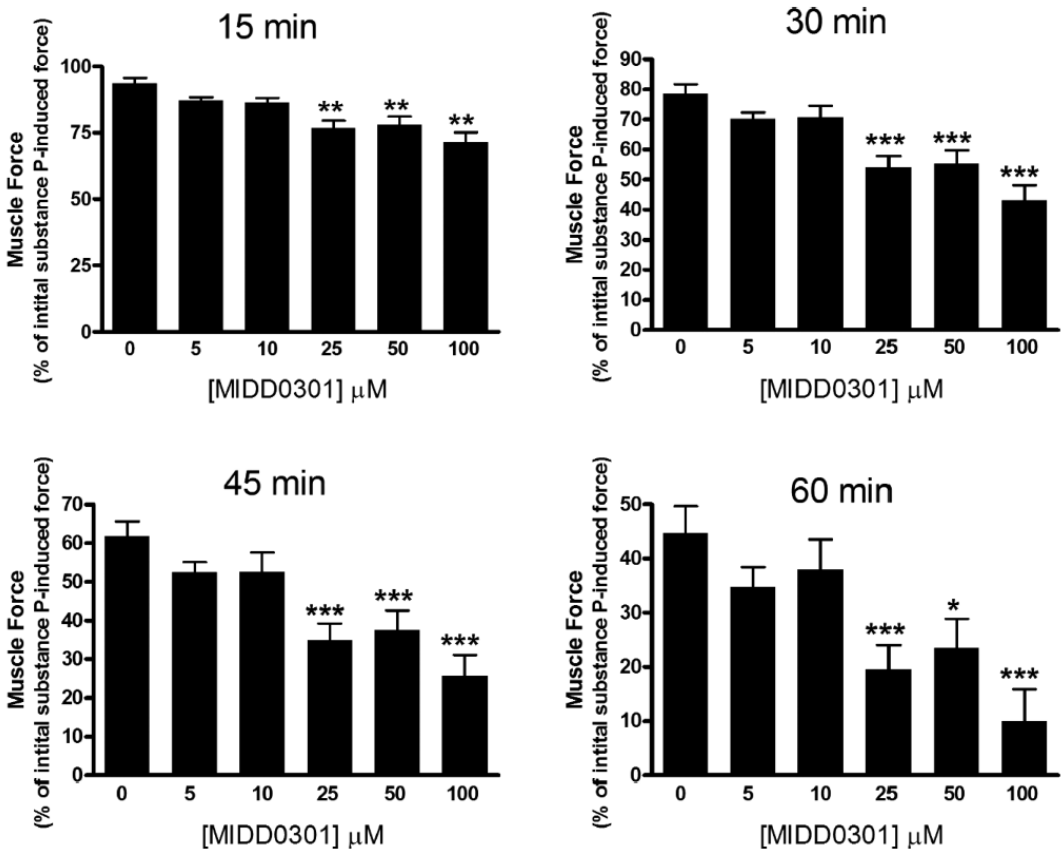

Figure 86. The GL-II-93 (85) relaxed the contracted muscle induced by substance P ex vivo. Muscle force in guinea pig ASM contracted with 1 μM substance P. GL-II-93 (25−100 μM) significantly produced a relaxation of substance P induced contraction of guinea pig tracheal rings, as compared to vehicle (0.1% DMSO). Muscle force is presented as a percent of the first muscle force remaining at different time points. The significance was determined by a two-way ANOVA repeated measures analysis. *, **, and * represents p < 0.05, 0.01, or 0.001, respectively, as compared to vehicle (n = 33). (Adopted from the Figures in Forkuo et al.)[187]**

In addition to the organ bath studies where substance P was employed to contract smooth muscle, histamine, which is usually involved in immune and inflammatory reponses[192] as a neurotransmitter, was also used as an alternative clinically relevant agent to induce muscle contraction in the organ bath. The guinea pig tracheal rings were suspended in organ baths, as previously described, and contraction was achieved by 10 μM histamine. After a steady contraction was achieved, the tracheal rings were then treated with acid **85** from an increasing concentration of 10 – 100 μM. The contractile force was measured and recorded. The bromo acid **85** again exhibited a significant dose-dependent relaxation at 25 μM and higher concentrations and

was consistent with the ASM relaxation data obtained from organ bath experiments, which employed substance P for muscle contraction, as illustrated in Figure 87. Furthermore, the effect was pronounced at 15 minutes and magnified over the 60 minute test period, as compared to the vehicle (DMSO).

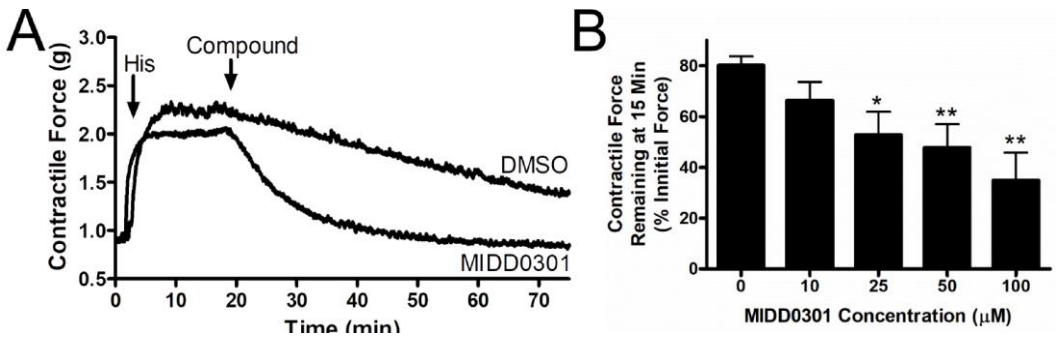

Figure 87. The GL-II-93 (85) relaxed the contracted muscle induced by histamine ex vivo. A: The contractile force of the guinea pig tracheal ring was presented as a percentage remaining versus time in an organ bath. The tracheal rings were exposed to 10 μM histamine, which was used to induce a rapid contractile force. Once a stable peak was achieved, GL-II-93, or DMSO as vehicle control, was added. B: GL-II-93 presented a dose-dependent decrease in the contractile force, and the significant effect was observed at 25, 50, and 100 μM at 15 minutes, as compared to the control DMSO. The significance was determined by a two-way ANOVA repeated measures analysis (n=6-9), $p<0.05$. (Adopted from the figure in Yocum et al.)[188]

The organ bath experiment was not only conducted on guinea pig tracheal rings but was also tested on human tracheal ASM strips obtained from 5 human donors, whom had lung surgery for another issue at Columbia University Hospital with Dr. Emala, an anesthesiologist. The assay employed the same procedure, as described above, only the resting tension was set to 1.5 g as compared to 1 g for the previous experiment. Histamine was again used to contract the human ASM strips at 10 μM. Once the contraction stabilized, then the strips were treated with vehicle DMSO or 100 μM of **85**. After exposure to **85**, the relaxation effect was measured at three time points and recorded. As expected, **85** was also able to reduce the contracted human ASM significantly with an average relaxation effect that was significant at 30 minutes in comparison with the vehicle, as presented in Figure 88.

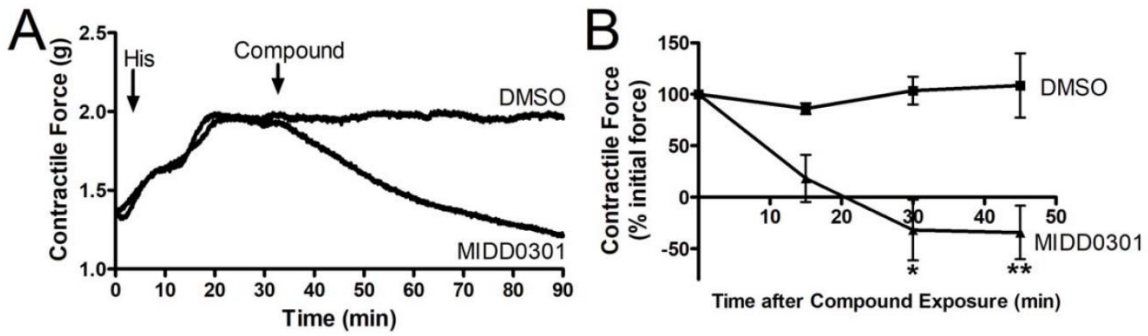

Figure 88. The human tracheal ASM strips were relaxed by GL-II-93 ex vivo. A: The contractile force of guinea pig tracheal ring was presented as a percentage remaining versus time in the organ bath. The tracheal rings were exposed to 10 µM of histamine. Once a stable peak was achieved, 100 µM GL-II-93 or DMSO as vehicle control, was added. B: The GL-II-93 at 100 uM relaxed ASM contractile force significantly by 30 minutes, as compared to the control DMSO. The significance was determined by a two-way ANOVA repeated measures analysis(n=6-10), *, and ** indicated $p<0.05$ and $p<0.01$, respectively. (Adopted from the Figure in Yocum et al.)[188]

The experiments, which employed *ex vivo* precision-cut lung slice (PCLS) from mouse peripheral airways were performed as well, in addition to the organ bath experiments. The PCLS experiment permits the observation of the ligand's effectiveness directly from the tissue section analysis. This airway diameter study was performed on the PCLS obtained from 3 mice. The airway lumenal area was calculated from a visualized microscopy image over time after 100 nM methacholine (MCh) exposure. This was followed by acid **85** treatment at 100 µM in the presence of MCh. As depicted in Figure 89, MCh reduced 34% of the airway lumen area as compared to the control, whereas acid **85** was able to relax the MCh induced-contraction to a 20% decrease of the airway lumen. It is clear that acid **85** dilated the lumenal area of the MCh-contracted airway significantly.

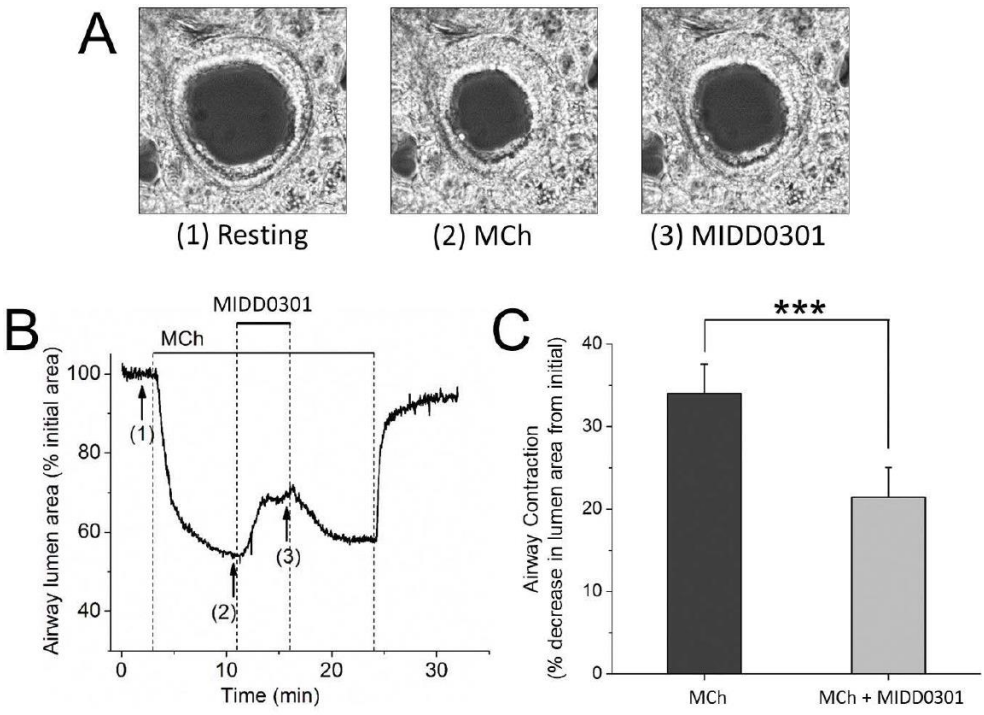

Figure 89. The mouse peripheral airways in PCLS was relaxed by GL-II-93 *ex vivo*. The 100 nM MCh was used to induce the contraction of the peripheral airways of an A/J mouse lung slices, which was exposed to 100 μM GL-II-93 subsequently, while the microscopy image of airway luminal was recorded continuously. A: The still photos tracing of airway luminal was presented over time during the experiments. B: The percentage of the overtime tracing of airway luminal area during the experiment. C: A significant reduction of MCh-induced ASM contraction was observed with GL-II-93 treatment. * indicates p<0.001, (n=3). (Adopted from the Figure in Yocum et al.)[188]**

2.3.3.2.5. Effects on Asthmatic Properties of Acid 85

Beside bronchoconstriction, there are a variety of other critical properties in asthma, such as airway inflammation, airway hyperresponsiveness (AHR), inflammatory cell recruitment, mucus hypersecretion, airway edema, epithelial desquamation, etc. To obtain a more comprehensive spectrum of GL-II-93 (**85**) in asthma, a series of assays for investigation of these effects of **85** on these features of asthma were performed. The results will now be discussed in detail. The experiments were conducted by Dr. Arnold's research group (Gloria Forkuo), at UWM, and Dr. Emala's group, Columbia University.

First of all, since the airway hyperresponsiveness (AHR) to allergens is one of the critical features of asthma, different doses of **85** were given to the ova s/c mice for 5 days and this was followed by a nebulized methacholine (MCh) challenge in an increasing concentration from 1.56 to 12.5 mg/mL. The specific airway resistance (sRaw) value was determined as quantification of AHR and compared with the control group. As illustrated in Figure 90, the treatment with **85** at 100 mg/kg significantly reduced the AHR at all concentrations of MCh. A similar effect was observed with 50 mg/kg of **85** treatment at only 12.5 mg/mL MCh, whereas sRaw values at other lower MCh concentrations were moderate in this study here. At a 20 mg/kg dosage of **85**, the effect of overcoming AHR was decreased at 12.5 mg/mL MCh challenge. Furthermore, 1 mg/kg of the approved LABA salmeterol was tested in the same model, however, it did not show the anti-AHR effect to protect the animal from MCh challenge at all concentrations.

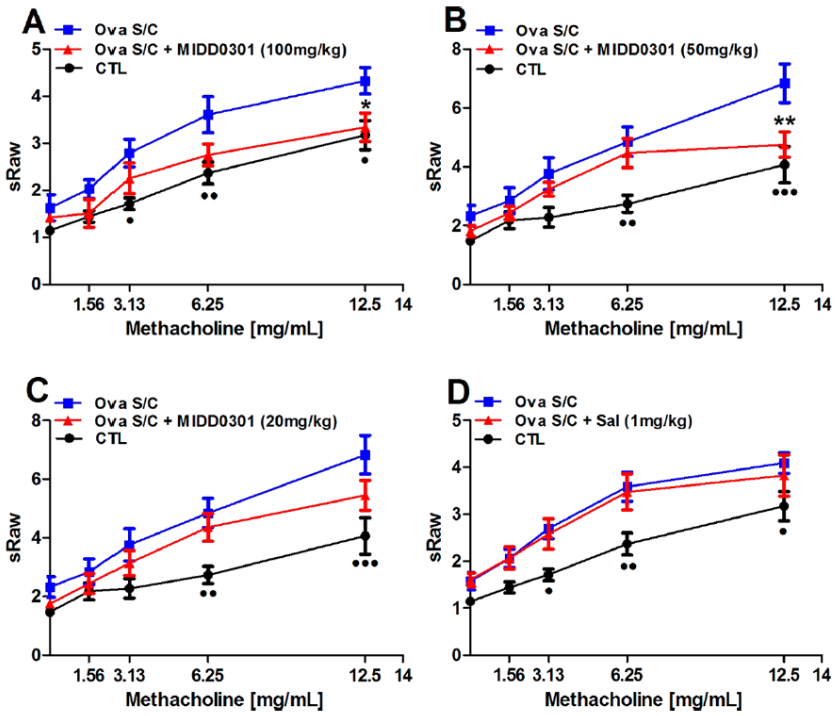

Figure 90. The examination of orally administered GL-II-93 and salmeterol on AHR. The sRaw was measured at an increasing dosage of MCh on a DSI's Buxco FinePointe noninvasive airway mechanics instrument. A, B, C: GL-II-93 was orally administered in ova s/c BALB/c mice twice daily for 5 days at a dosage of 100, 50, and 20 mg/kg, respectively. D: Salmeterol was administrated at 1 mg/kg twice daily for 5 days. Data represent mean

± SEM (n=10). The significance was determined by a two-way ANOVA repeated measures analysis. *, **, and * represents significance p < 0.05, p < 0.01, and p < 0.001, respectively. (Adapted from the figure in Forkuo et al.)[187]**

The assessment of the effect from orally administrated **85** on AHR demonstrated the capacity of the ligand to protect the animal from AHR in the MCh challenge assay. It would be interesting to investigate the effect of the compound as an aerosol, which is the common method of administration for the treatment of asthma. Therefore, the *in vivo* airway resistance experiment was performed in mice. Briefly, after receiving nebulized 5 mM **85**, the mice were given a nebulized MCh challenge in the apparatus with an increasing concentration (0-25 mg/mL), and the central lung resistance (R_n) values were measured and recorded. As displayed in Figure 91, acid **85** was able to reduce the R_n and protect the mice from the MCh challenge, which mimicked the effect of an inhaler on an asthma patient. Examination of the results indicated **85** is active not only when administrated orally but also effective as an aerosol. This expands the spectrum of use of **85** by employing effectively different methods of administration.

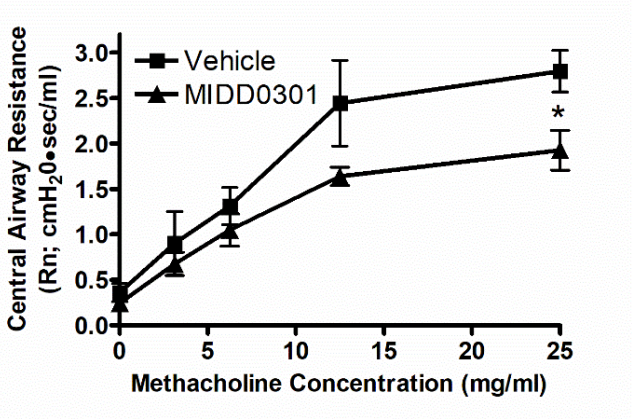

Figure 91. The bronchoconstriction in mice was reduced by GL-II-93 (85) treatment in vivo. The A/J mice were given an inhaled, MCh challenge, anesthetized and mechanically ventilated, then the mice received nebulized GL-II-93 at 5 mM, for 10 s nebulization (50 % duty cycle) or 25% ethanol in PBS as vehicle control. The resistance of mice receiving GL-II-93 was significantly reduced in regard to airway resistance during the MCh challenge with an increasing concentration. Data represent mean ± SEM (n=6). The significance was determined by a two-way ANOVA repeated measures analysis, * indicated p<0.05. (Adopted from the Figure in Yocum et al.)[188]

After the assessment of the airway resistance, and after the treatment with **85** for 10 seconds via nebulized administration, the concentration of **85** in brain, lung, and serum was determined at two time points: 10 minutes and 30 minutes from the mice. The average concentration of **85** after 10 and 30 minutes was 86 and 47 ng/g in serum, respectively; 1334 and 412 ng/g in the lung, respectively; 58 and 9.6 ng/g in the brain, respectively. As shown in Figure 92, the concentration of the acid **85** was significantly lower in both serum and brain tissue, whereas, the inhaled **85** concentration in the lung was extremely high in the first 10 minutes, and was eliminated at a very rapid rate after 30 minutes with about 70% clearance. These results indicate that the inhaled **85** can be used to alleviate ASM contractions in asthma and achieve a profound relaxation effect within 10 minutes acting much like a SABA inhaler.

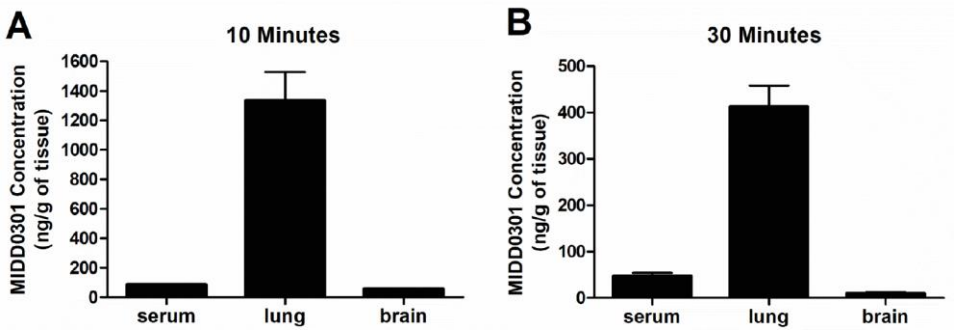

Figure 92. The concentrations of GL-II-93 (85) in serum, lung, and brain in mice after inhalation, was followed by the airway resistance assay. The concentration of GL-II-93 was determined in the serum, lung, and brain tissues from the A/J mice with GL-II-93 treatment after inhalation at 30 min. The mean concentrations (n=6 mice) were 412.8±44.8 ng/g in the lung, whereas 9.6±3.0 ng/g in the brain. (Adopted from the figure in Yocum et al.)[188]

Secondly, in addition to AHR, airway inflammation is another cardinal feature of asthma, which involves an over-expression of different types of immune cells, such as monocytes, eosinophils, neutrophils, basophils, lymphocytes, etc.[193] These immune cells infiltrate or migrate to the location where inflammation occurs to protect the body from external bacterias, allergens,

viruses, etc.[194] Therefore, **85** was tested to assess the ability to reduce inflammation by quantification of different types of mice immune cells in the bronchoalveolar lavage fluid (BALF). After treatment with 20, 50, 100 mg/kg **85**, or 1 mg/kg salmeterol for a continuous 5 day period via oral gavage, flow cytometry[195] was employed to quantify the amount of total inflammatory cells, CD4+T cells, F4/80 cells, and Siglec F cells by applying different antibodies. This included anti-mouse CD45 as a common leukocyte marker,[196] anti-mouse CD4 as a marker for a T cell subset,[197-198] anti-mouse F4/80 referenced mouse macrophage marker[199] and anti-mouse Siglec F as an eosinophils marker,[195] respectively. Ligand **85** was able to suppress the number of total inflammatory cells, and the effect was significant at 100 mg/kg, whereas the marketed drug salmeterol did not show a significant effect at 1 mg/kg, as illustrated in Figure 93A. Both **85** at all doses and salmeterol significantly decreased the CD4+ T cell numbers on oral administration, which indicated both were effective for reducing the lymphocyte population,[197-198] as shown in Examination of Figure 93 B. From Figure 93 C and D, **85** was shown to be effective to reduce the number of BALF F4/80 cells, and Siglec F cells and the significance was achieved at 100 mg/kg, which demonstrated the ability of **85** to suppress the macrophage[199] and eosinophils[195] types, respectively. However, salmeterol was not able to alter the numbers of these two cell types significantly.

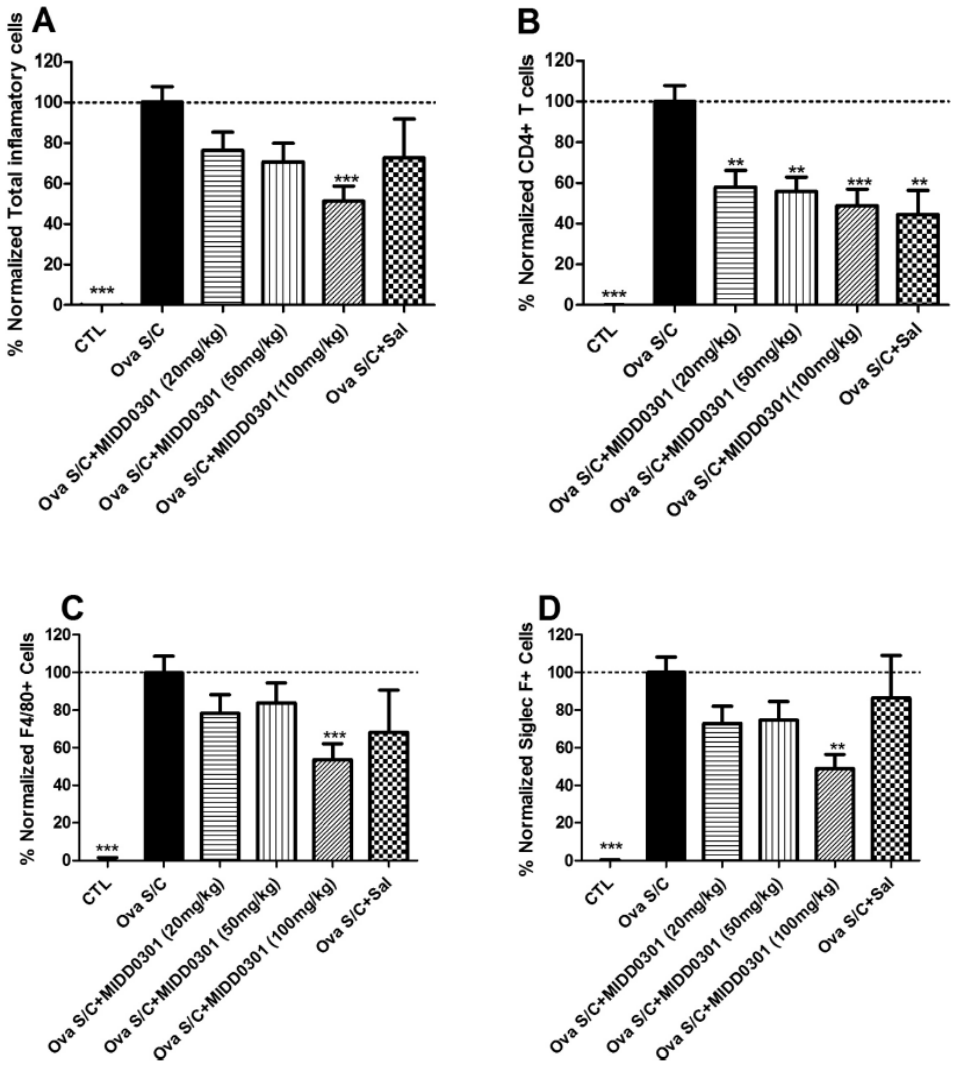

Figure 93. The influence of GL-II-93 and salmeterol on airway inflammatory cells. The vehicle, GL-II-93 (20, 50, or 100 mg/kg), or salmeterol (1 mg/kg) were orally administrated in the ova s/c mice twice daily for 5 days. BALF was obtained from each animal and analyzed for by flow cytometry (A) Quantification of total inflammatory cells using anti-CD45 APC antibody, (B) CD4+ T cell, (C) F4/80+ cell, and (D) Siglec F+ cell. Data represent mean ± SEM (n = 10). The significance was determined by a two-way ANOVA repeated measures analysis. *, **, and * indicated the significance $p < 0.05$, $p < 0.01$, and $p < 0.001$, respectively, as compared to vehicle control. (Adopted from the figure in Forkuo et al.)[187]**

Based on the results on the bromo acid **85**, which was able to reduce the numbers of airway inflammatory cells, the experiment for the visualization of this effect was performed by an EdU staining assay.[200] The EdU (5-ethynyl-2′-deoxyuridine) is an analog of thymidine, which can incorporate with the DNA in the cells that are undergoing the dividing stage, therefore EdU is used

to detect DNA synthesis. The visualization was achieved by click chemistry wherein the EdU labeled DNA reacts with the Alexa Fluor 488 azide in the presence of copper sulfate.[201] The formation of the covalent bond from azide and alkyne, produced a detectable fluorescence, which visualized the cells that were undergoing the DNA replication, as illustrated in Scheme 16. The lung of ova s/c mice treated with vehicle and **85** were both stained with EdU, as shown in Figure 94, column 1. All nuclei were stained by 5 μg/mL Hoechst 33342, see Figure 94, column 2. Examination of the data in column 3 depicts the superimposed images of columns 1 and 2. It is clear that the non-asthmatic mice in the negative control group did not show any cell staining (Figure 94 column 1 and row 1). The lung tissue of the asthmatic mice exhibited intense cell staining (Figure 94 column 1, and row 2), whereas the lung cells from the **85** treated mice stained to a much lower level (Figure 94 column 1, and row 3). The bronchiole alveolar cells and blood vessels were not stained, which indicated the mucosa, pneumocytes, and ASM cells did not proliferate fast enough in the asthmatic lung tissue. On the other hand, the leukocytes that infiltrate might be visualized, such as macrophages, eosinophils, and maybe lymphocytes. Consequently, reduction of the stained cells from the acid **85** treated group was visualized, the results of which were in agreement with the results from the inflammation cell count assay.

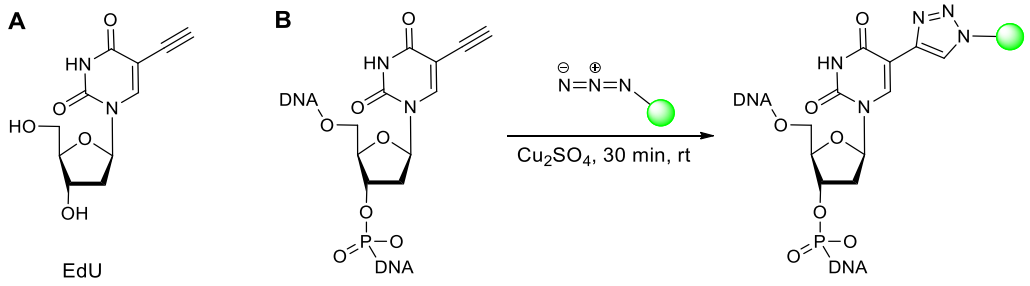

Scheme 16. A. The structure of EdU. B. The "click" chemistry between EdU labeled DNA and Alexa Fluor 488 azide. The alkyne of EdU reacted with the azide in the presence of a copper catalyst to form a detectable triazole ring.

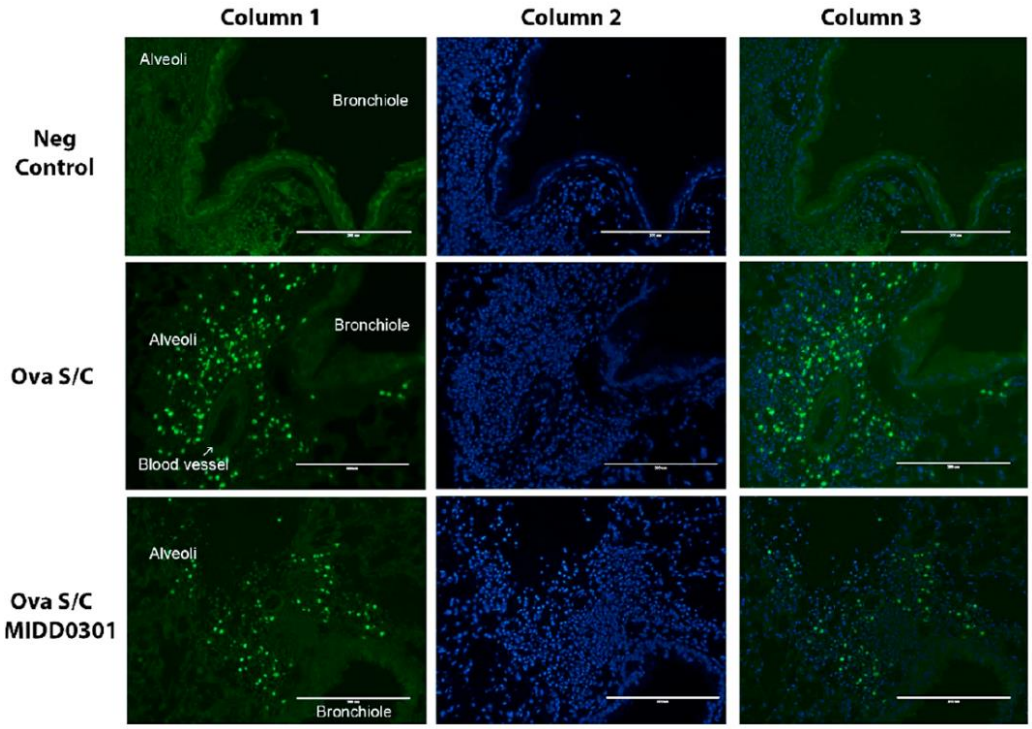

Figure 94. The effect of GL-II-93 treatment on the cellular difference of the asthmatic mouse lung. The EdU was injected i.p. into the mice lungs and they were harvested after 4 h. A fluorescent azide was applied to the lung section with "Click" chemistry to produce the conjugation of EdU to visualize cells that underwent the dividing stage in a 4 hour-period (column 1). The Hoechst 33342 (column 2) was used to counterstain the sections, and the images were superimposed images as shown in column 3. The lung images of control mice were shown in Row 1. The images of vehicle-treated ova s/c mice are presented in Row 2. The images of GL-II-93 (100 mg/kg) treated ova s/c mice were shown in Row 3. (Adopted from the figure in Forkuo et al.)[187]

Thirdly, mucus overproduction is another key feature of the asthma lung, in addition to AHR, and infiltration with inflammatory cells. Therefore, it was necessary to assess the effect of **85** on mucus accumulation, which was achieved by visualization of the epithelium of the lung tissue with periodic acid fluorescent Schiff's stain. The lung of asthmatic ova s/c mice exhibited a significant increase in mucosa than the control mice. Both salmeterol at 1 mg/kg and **85** at a dosage from 20 to 100 mg/kg did not induce a significant mucus volume change, as compared to the positive control mice after 5-day treatments, as presented in Figure 95.

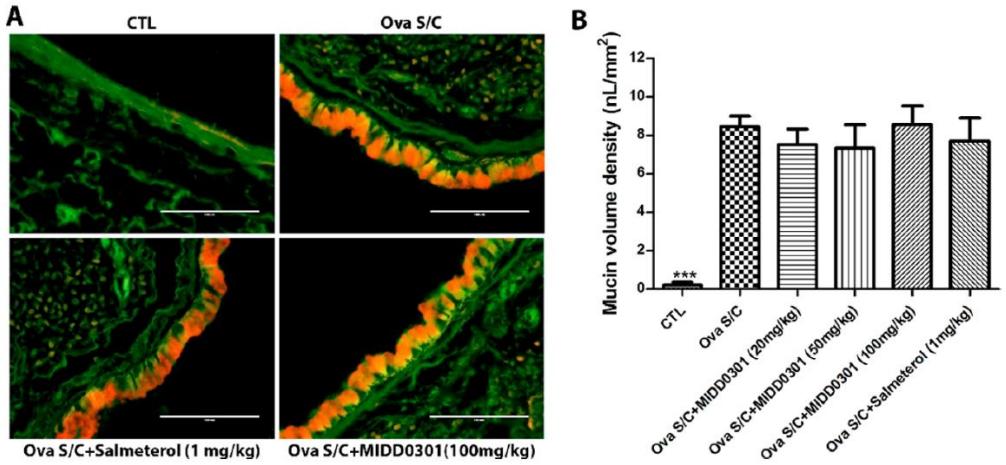

Figure 95. The effect on mucin production with GL-II-93 or salmeterol treatment. A: Images of lungs in control mice, ova s/c mice, salmeterol treated mice at 1 mg/kg, and GL-II-93 treated mice at 100 mg/kg twice daily for 5 days. Scale bar indicates 100 µm. Periodic acid fluorescent Schiff's stain agent was used to color the slides, and green represented the airway epithelium green, and mucin is in red. B: The mucin volume density of each group was measured. Data represent the mean ± SEM (n = 6). The significance was determined by a two-way ANOVA repeated measures analysis. (Adopted from the figure in Forkuo et al.)[187]

Finally, importantly, cytokines exhibit an essential role in chronic bronchial asthma due to their contribution to initiation, coordination, and persistence during the inflammatory process. It has been well documented that cytokines are extracellular signaling proteins involved in a series of interactions between cells through the surface receptors for both acute and chronic inflammatory responses.[202] Because of the pleiotropic and overlapping properties of cytokines, it is difficult to classify them easily. However, based on the knowledge of different abnormalities in features of asthma, cytokines might be divided into several groups, which result from the pathogenesis, such as lymphokines, pro-inflammatory cytokines, anti-inflammatory cytokines, chemotactic cytokines, and growth factors.[203] Since T-lymphocytes are the key enforcers of the immune response to external viruses, allergens, and bacterias, the cytokines that are related to lymphocytes draw much attention. The T-lymphocytes are classified into T helper 1 cells (Th1), T helper 2 cells (Th2), T helper 17 cells (Th17) and regulatory T cells (Treg).[204] To evaluate the cytokine expression with the treatment with acid **85**, the concentration of several T-lymphokines (TH1: IL-2, IFN-γ, and

TNFα; TH2: IL-4, IL-6, and IL-10; and TH17: IL-17A cytokines) were determined by flow cytometry. The results, as depicted in Figure 96, indicate that a remarkable increase was observed in the levels of IL-10, IL-17A, IL-4, and TNFα cytokine concentration in the ova s/c mice, as compared to the control group. Whereas there was no substantial change in IFN-γ, IL-6, IL-2. Despite IL-10 cytokines, acid **85** was able to reduce the expression of the lymphokines, which underwent a considerable increase in concentration than the control group. There was no significant effect of **85** on the other three cytokines that did not show a significant effect between the ova s/c mice and the control mice.

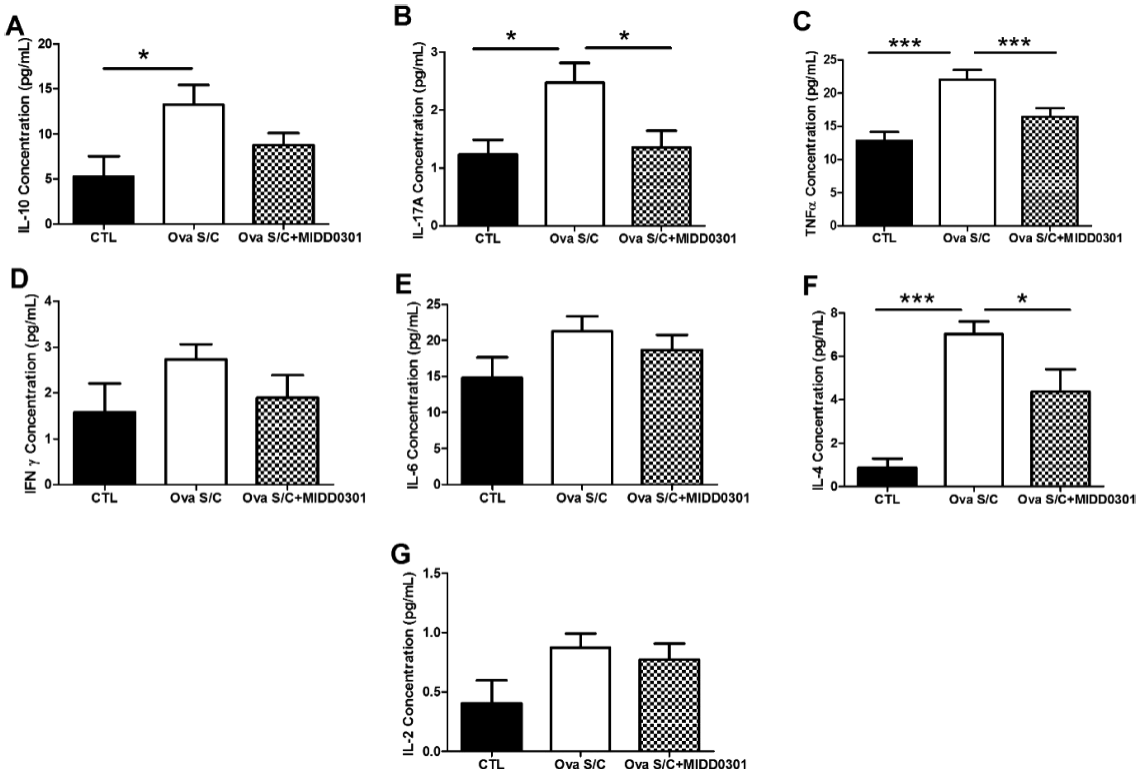

Figure 96. The evaluation of cytokine expression with GL-II-93 treatment in the lung. The quantification of mouse Th1/Th2/Th17 cytokines in mouse tissue homogenates was determined by applying the BD mouse Th1/Th2/Th17 cytometric bead array kit. Ova s/c mice were treated orally with 100 mg/kg GL-II-93 or vehicle twice a day for 5 days. The significance was determined by a two-way ANOVA repeated measures analysis. *, **, and * represented the significance $p < 0.05$, $p < 0.01$, and $p < 0.001$, respectively. Data represent mean ± SEM (n = 10). (Adopted from the figure in Forkuo et al.)[187]**

2.3.3.2.6. Immunotoxicity (Evaluation over a 28-Day Period) with Acid 85

The assessment of potential immunotoxicity of any new drug is required for the drug development process to eliminate the possible adverse effects from any off-target immune responsiveness reduction or suppression. The previous results of the 5-day treatment of **85** in mice at 100 mg/kg (orally administrated) indicated that **85** did not show any side effects during the treatment; therefore, a long-term immunotoxicity study could be performed. This was carried out to evaluate the pharmacological effects of **85** at 100 mg/kg with a twice-daily dosage over a 28-day test period. Both male and female mice, which was carried out by Dr. Arnold's research group (Nick Zahn, M. S. Rashid Roni, and Alec Huber), at UWM were employed. Before the test, the training of consuming peanut butter (the vehicle) was conducted at 100 mg/kg twice a day for a week to ensure the animal was used to the testing diet. These mice were then divided into two groups; the acid **85** treatment group and the peanut butter control group. The third group of mice did not receive either **85** nor peanut butter.

As presented in Figure 97, the average weight of the female mice in all three groups was lower than the male mice throughout the testing period, with about 26 and 32 grams, respectively. On the last day of the test, the average weight of female and male mice were about 28 and 36 grams, respectively, as expected in this strain of mice. During the 28-day course, there was no significant average weight change among the three groups in both male and female mice. At 21 days both weights were lower than the non treated control group, however, a similar weight was achieved at the end of the test for all groups. Furthermore, there was no gastrointestinal distress, nor abnormal behaviors observed, such as respiratory depression, impaired movement and aggressive behaviors, etc. Therefore, the data indicated that treatment with acid **85** did not affect the body weight nor actions of the test animals.

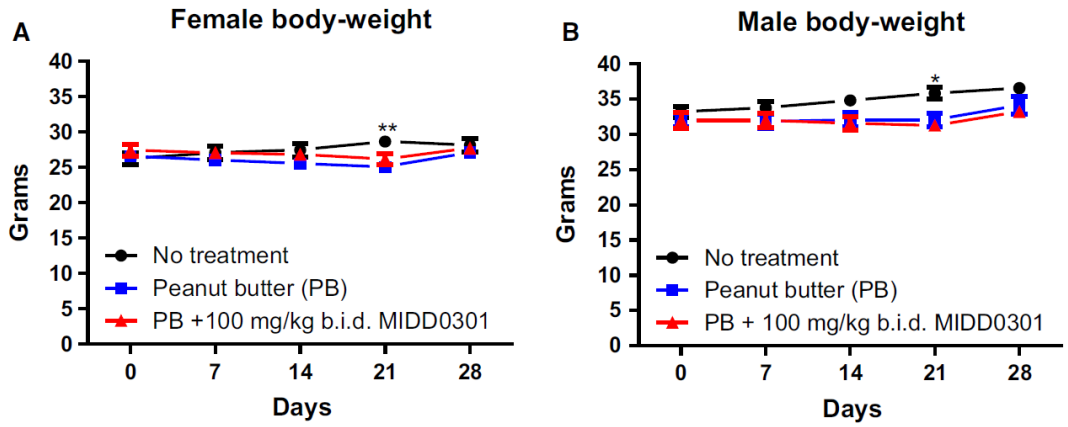

Figure 97. The effect of GL-II-93 on the average mouse body weights during the 28-day study. Peanut butter without or with 100 mg/kg MIDD0301 was administrated orally twice daily in both male and female Swiss Webster mice at the age of 8 weeks in a separate container. Mice without GL-II-93 treatment stayed in the same containers. Body weights were measured every week. Data represent mean ± SEM (n = 5). The significance was determined by a two-way ANOVA repeated measures analysis. *, and **, represented the significance p < 0.05, and p < 0.01, respectively. (Adopted from the figure in Zahn et al.)[189]

The effect of acid **85** on the immune response was determined by immunization of the Swiss Webster mice *in vivo* with 50 μg dinitrophenyl hapten-keyhole limpet hemocyanin (DNP-KLH), employed as a T cell-dependent antigen to induce an antigen-specific immune response,[205-207] on days 1 and 21. The average weight was measured on days 14 and 28. A high dose of the novel ligand **85** (100 mg/kg twice daily), and the asthma drug prednisone (5 mg/kg/day), which was used as corticosteroid, were administrated orally to the mice. The results of the average weight change are presented in Figure 98. All groups exhibited a percentage of positive weight increase during the four weeks. In both female and male mice, the change in weight with the peanut butter with and without DNP-KLH groups were not significant. The acid **85** treatment group did not induce considerable weight changes over the test period. However, the prednisone treatment group reduced the average weight slightly in female mice, and the effect was significant in male mice, as compared to the control group of male mice.

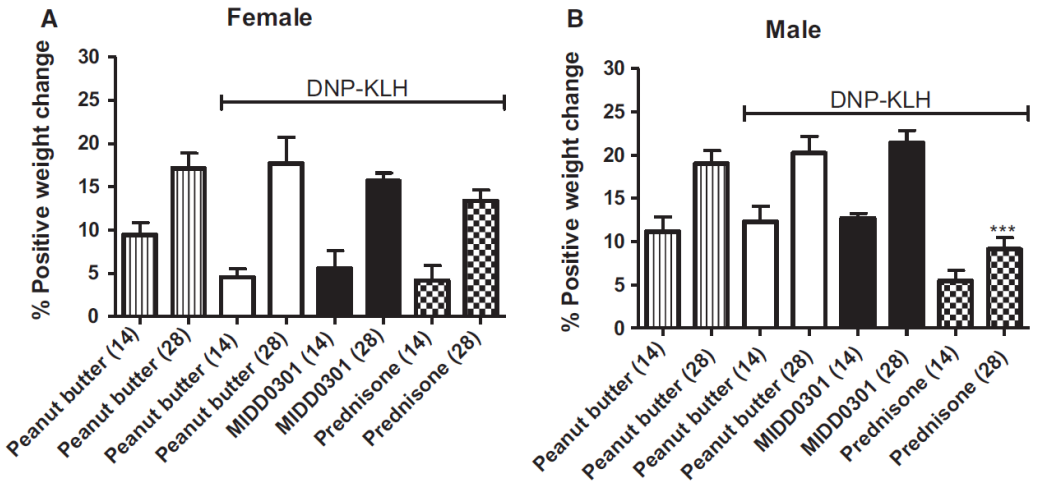

Figure 98. Evaluation of average body-weight with DNP-KLH immunization. Peanut butter without or with 100 mg/kg MIDD0301, or peanut butter + prednisone (5 mg/kg daily) was administrated orally twice daily to both male and female Swiss Webster mice at the age of 6 weeks in a separate container. DNP-KLH immunization was applied on days 1 and 21 for these 3 groups. Body weights were measured on day 14 and 28. Data represent mean ± SEM (n = 5). The significance was determined by a two-way ANOVA repeated measures analysis. * indicates P < 0.001. (Adopted from the figure in Zahn et al.)[189]**

At day 28, the small intestine, thymus, and spleen were dissected from the mice for each group. The weight of the organs was measured. The numbers of Peyer's patches from the intestine were counted, as illustrated in Figure 99. The weight of the thymus and spleen from the mice that were treated with or without DNP-KLH in both female and male mice were similar to each other. The acid **85** treated groups administrated 100 mg/kg twice daily in both sexes did not exhibit a remarkable change in weight of either the thymus or the spleen. However, the weight of the spleen and thymus from the prednisone-treated group in the female mice were both reduced, and the weight decrease was significant in male groups, as compared to the control group. The total numbers of Peyer's patches in the acid **85** or prednisone groups in both sexes were all similar to the control groups.

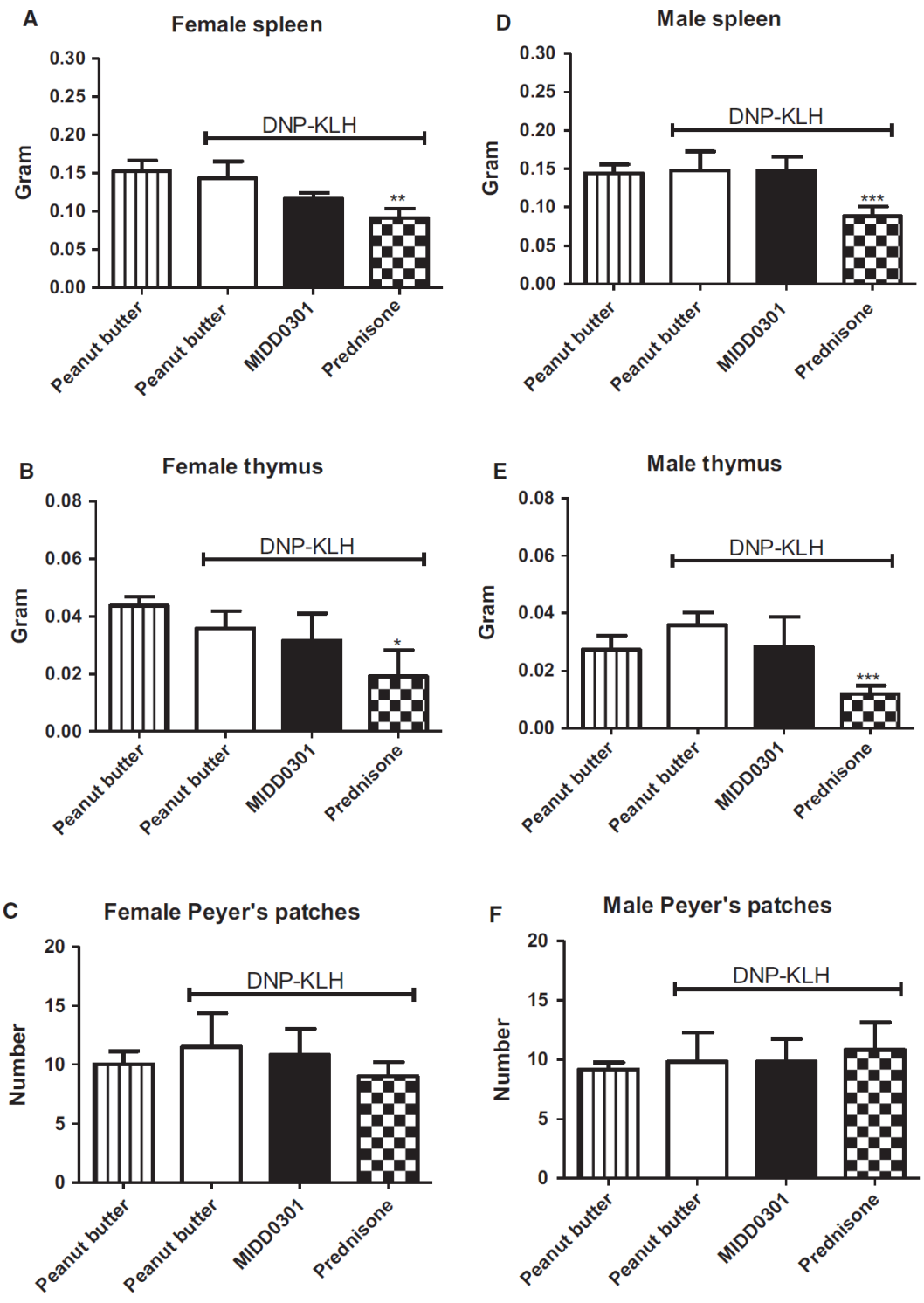

Figure 99. Effect of 28 days of treatment of GL-II-93 on lymphoid organs and Peyer's patches from Swiss Webster mice immunized with DNP-KLH. Peanut butter without or with 100 mg/kg MIDD0301, or peanut butter + prednisone (5 mg/kg daily) was administrated orally twice daily in both female (A-C) and male (D-F) Swiss Webster mice at the age of 6 weeks. The DNP-KLH immunization was applied on days 1 and 21 for these 3 groups. After the 28 day test period, organs were obtained and weighed, and small intestines were dissected

for the counting of Peyer's patches. Data represent mean ± SEM (n = 5). The significance was determined by a two-way ANOVA repeated measures analysis. *, **, and * represented the significance $p < 0.05$, $p < 0.01$, and $p < 0.001$, respectively. (Adopted from the figure in Zahn et al.)[189]**

Since it has been reported that the overuse or long-time use of a corticosteroid can cause changes in the spleen,[208], therefore, it was necessary to determine any possible histological change of the lymphoid organs after long term treatment with acid **85**, which led to the H&E-staining experiment for comparison. The experiment was performed after the spleen and thymus were removed and measured for the data shown in the Experiment above. As shown in Figure 100, the white and red pulp from the spleen did not exhibit a significant change with treatment with **85** in both sexes, except the mice, which received the treatment with prednisone, exhibited a smaller size of the white pulp (lymphoid follicles), which is in agreement with the reduction of spleen weight, as described above. There was no remarkable change in the thymus histology of all groups regardless of gender or treatment. Consequently, a high dosage of **85** treatment for 28 consecutive days did not alter the histological presence in the spleen or thymus in the animals versus control animals.

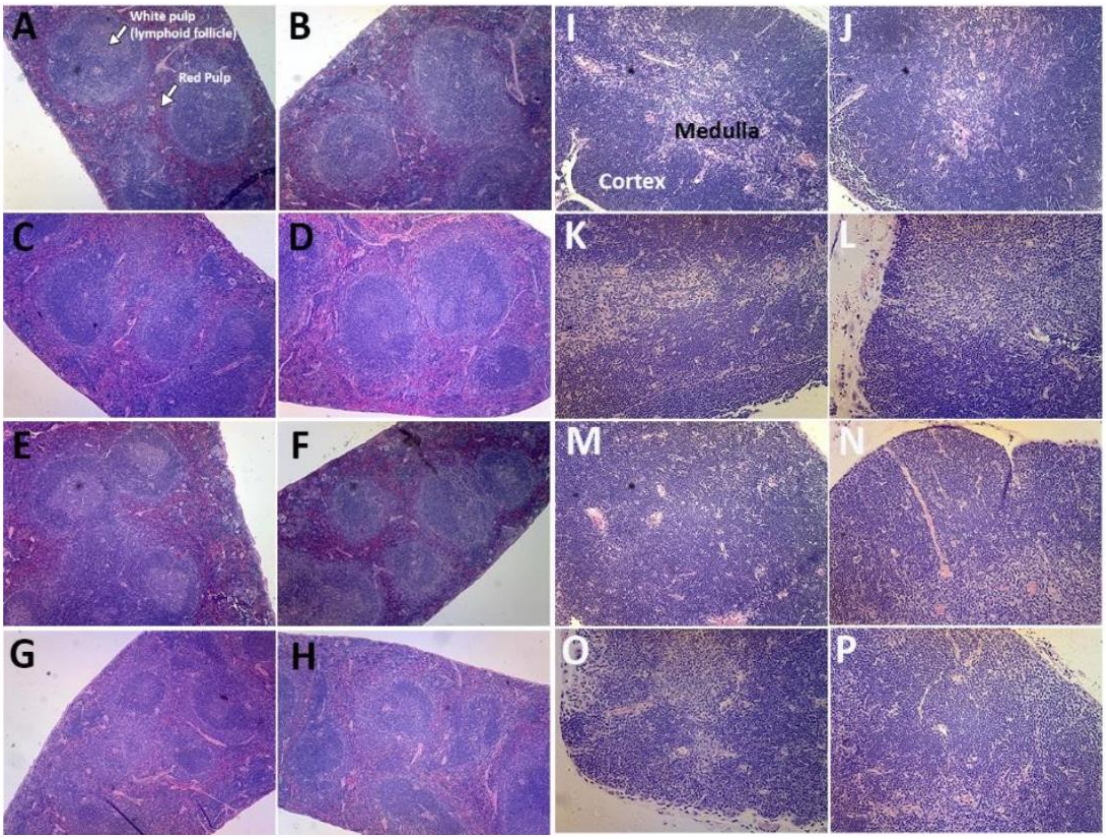

Figure 100. The mouse spleens (A-H, 40x) and thymus (I-P, 100x) H&E staining. A and I) male mice, peanut butter; B and J) female mice, peanut butter; C and K) DNP-KLH-immunized male mice, peanut butter; D and L) DNP-KLH-immunized female mice, peanut butter; E and M) DNP-KLH-immunized male mice, peanut butter with 100 mg/kg GL-II-93 twice daily for 28 days; F and N) DNP-KLH-immunized female mice, peanut butter with 100 mg/kg GL-II-93 twice daily for 28 days. G and O) DNP-KLH-immunized male mice, peanut butter with 5 mg/kg prednisone daily for 28 days; H and P) female DNP-KLH-immunized mice, peanut butter with 5 mg/kg prednisone daily for 28 days. (Adopted from the figure in Zahn et al.)[189]

In order to evaluate the pharmacological effect of acid **85** on the T-dependent humoral immune response, the serum DNP-immunoglobulin G (IgG)[209] quantification was investigated at day 28 by ELISA for all groups. As presented in Figure 101, the DNP-specific antibody IgG level was remarkably increased in both sexes in the DNP-KLH immunized group, as compared to the peanut butter the only group. The IgG level indicated there was no significant difference in both **85** nor the prednisone groups, which indicated that 28-day treatment with 100 mg/kg twice a day

with acid **85** did not suppress or interfere with the off-target systemic immune response by a common T-dependent antibody.

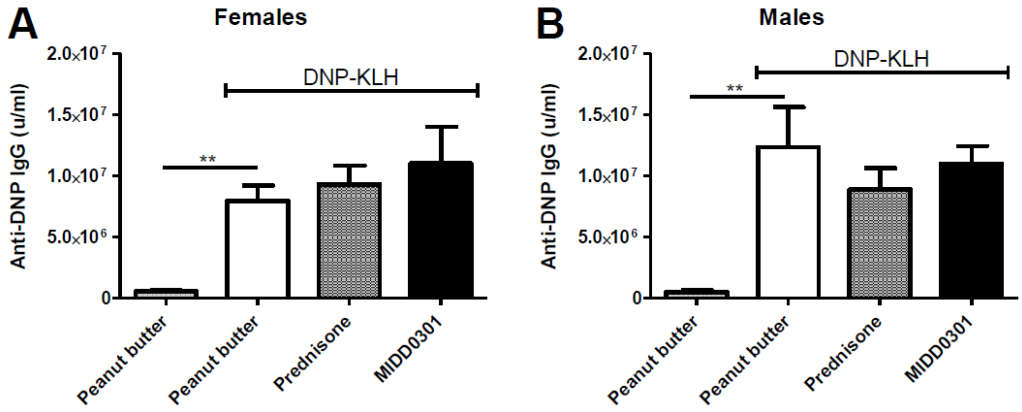

Figure 101. The mouse serum DNP IgG. The peanut butter without or with 100 mg/kg MIDD0301, or peanut butter + prednisone 5 mg/kg daily was administrated orally twice daily in both female (A) and male (B) Swiss Webster mice. The DNP-KLH immunization applied on days 1 and 21, and quantification of DNP-specific IgG was measured on day 28. Data represent mean ± SEM (n = 5). The significance was determined by a two-way ANOVA repeated measures analysis. ** represented the significance p < 0.01. (Adopted from the figure in Zahn et al.)[189]

2.3.3.2.7. Stability Studies

The bioavailability of a drug candidate is one of the critical pharmacokinetic properties for preclinical research, which provides information in regard to how much of the drug reaches the systemic circulation in its original form. The bioavailability is considered to be 100 % only by i.v. administration. The reason the route of administration is always a concern is because other routes of administration are usually not as efficient as an i.v. injection. Factors, such as an insufficient absorption time, low water solubility, and first-pass metabolism, can affect the bioavailability to a variable extent especially when given i.p. or p.o. Since the oral route was employed for the administration of **85**, the absorption of the drug must pass the digestive system before the first-pass metabolism takes place in the liver. The stability of **85** was critical for its absorption, therefore

the chemical stability of the ligand was determined under both acidic and basic conditions to mimic the drug stability in the stomach and intestine, respectively. In order to perform the experiment, the acid **85** was first converted into the open ring form and also the sodium salt form in the presence of 1 N aq HCl or 1 eq of sodium hydroxide, respectively, as shown in Scheme 17.

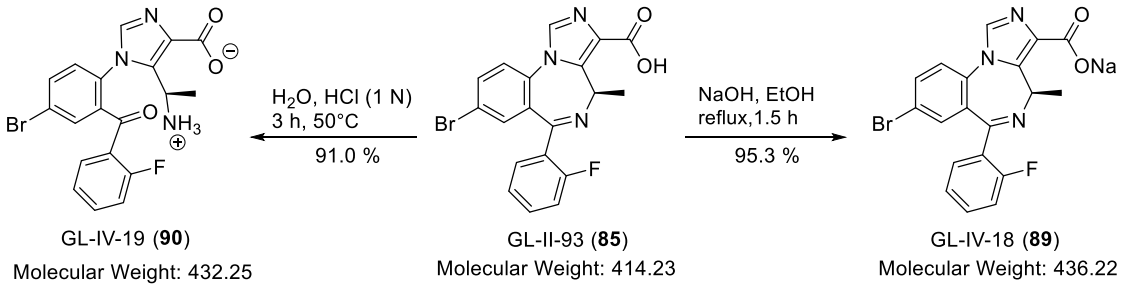

Scheme 17. Synthesis of the keto (ring-opened) form GL-IV-19 (90) and the sodium salt form GL-IV-18 (89) from GL-II-93 (85).

To perform the stability study, it was necessary to use a suitable solvent for the experiment. The solubility of the three ligands in different solvents at 37 °C is presented in Table 24.

Table 24. The solubility of GL-IV-19, GL-II-93 and GL-IV-18.

Solvent	GL-IV-19 (90)	GL-II-93 (85)	GL-IV-18 (89)
H_2O	No	No	Yes
MeOH	**Yes**	**Yes**	**Yes**
EtOH	partial	partial	Yes
ACN	No	No	No
DMSO	**Yes**	**Yes**	**Yes**
EtOAc	No	partial	No
Acetone	No	No	No
MTBE	No	No	No
DCM	No	partial	No

Based on examination of the solubility data in the table above, all three compounds were found soluble in MeOH and DMSO. Usually MeOH would be a convenient solvent for use due to the efficient compound recovery process. However, in this case MeOH was found unsuitable for

conduction of the experiment because the open ring keto form of **85** was converted back to its original cyclized 7-membered ring in MeOH. This was found by accident while measuring the mass spectrum by LCMS. The mass of both compound **85** (414, 416) and **90**(432, 434) were detected in the mass spectrum, however, the completion of the recyclization was monitored and confirmed by NMR. To evaluate this chemical stability with both compounds GL-II-93 (**85**) and GL-IV-19 (**90**) in MeOH, the experiment was conducted at 1, 20, 40, 60-minute time points. As presented in Figure 102, **90** started to convert back into **85** once the compound had been dissolved in MeOH at the first minute, and the conversion reached an equilibrium in about 1 hour. The spectra from longer time points were similar and are not shown here.

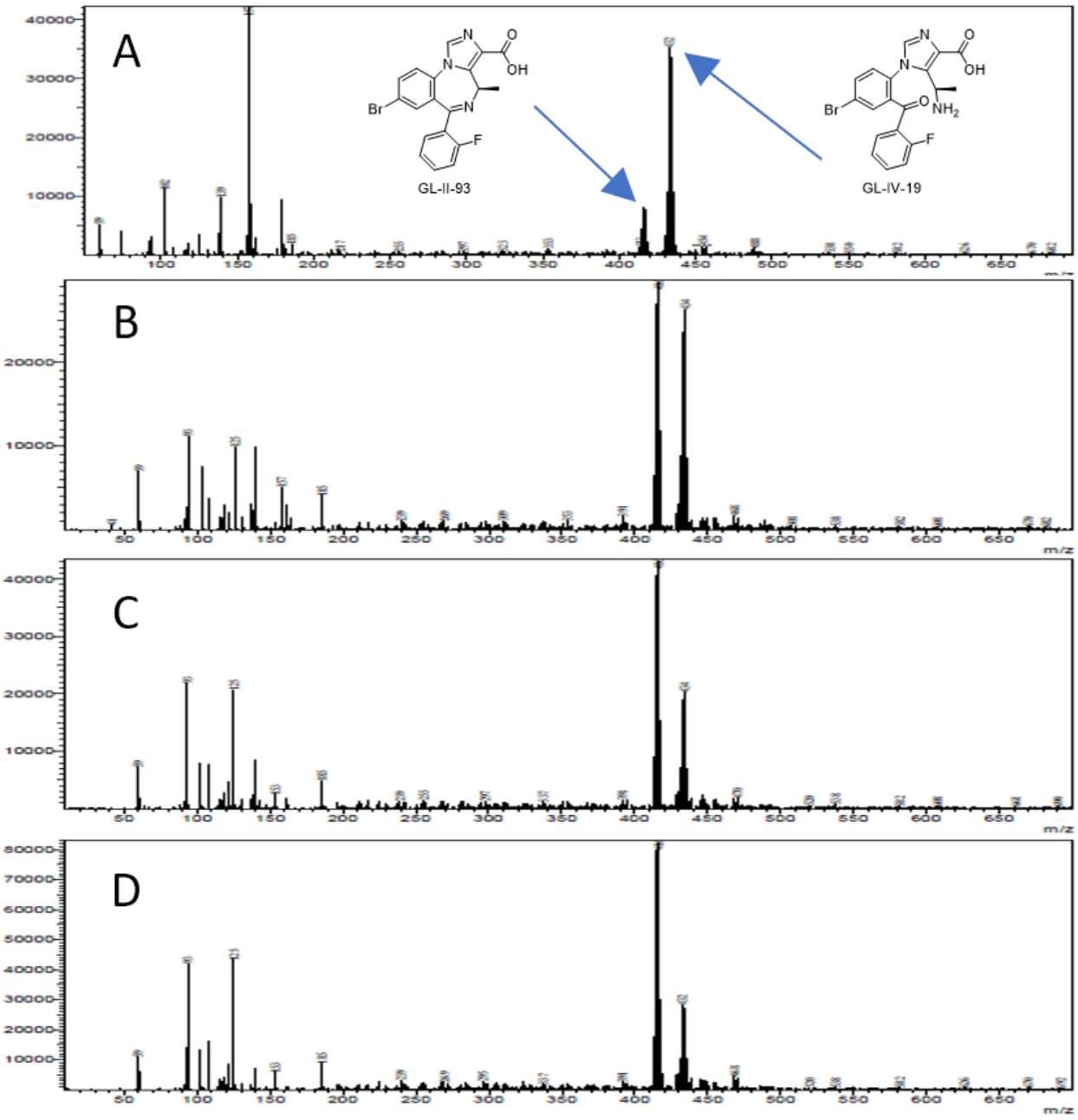

Figure 102. A, B, C, D: The mass spectra of GL-IV-19 (90) in 4-time points, respectively and examination of them indicated the conversion of GL-IV-19 to GL-II-93 took place in a time-dependent manner. The equilibrium was reached at 1 h, as compared to longer reaction times, which was very similar, data not shown here.

In addition to MeOH, the same experiment was repeated in DMSO. As compared to the instability of **90** in MeOH, the keto form **90** was much more stable in DMSO. The conversion into GL-II-93 (**85**) was very similar to each other at the 0.5 and 1 hour time points and the equilibrium

was achieved slowly only after 6 hours, as shown in Figure 103. Therefore, the data from the stability experiments indicated DMSO should be employed as the solvent for the experiment under acidic and basic conditions.

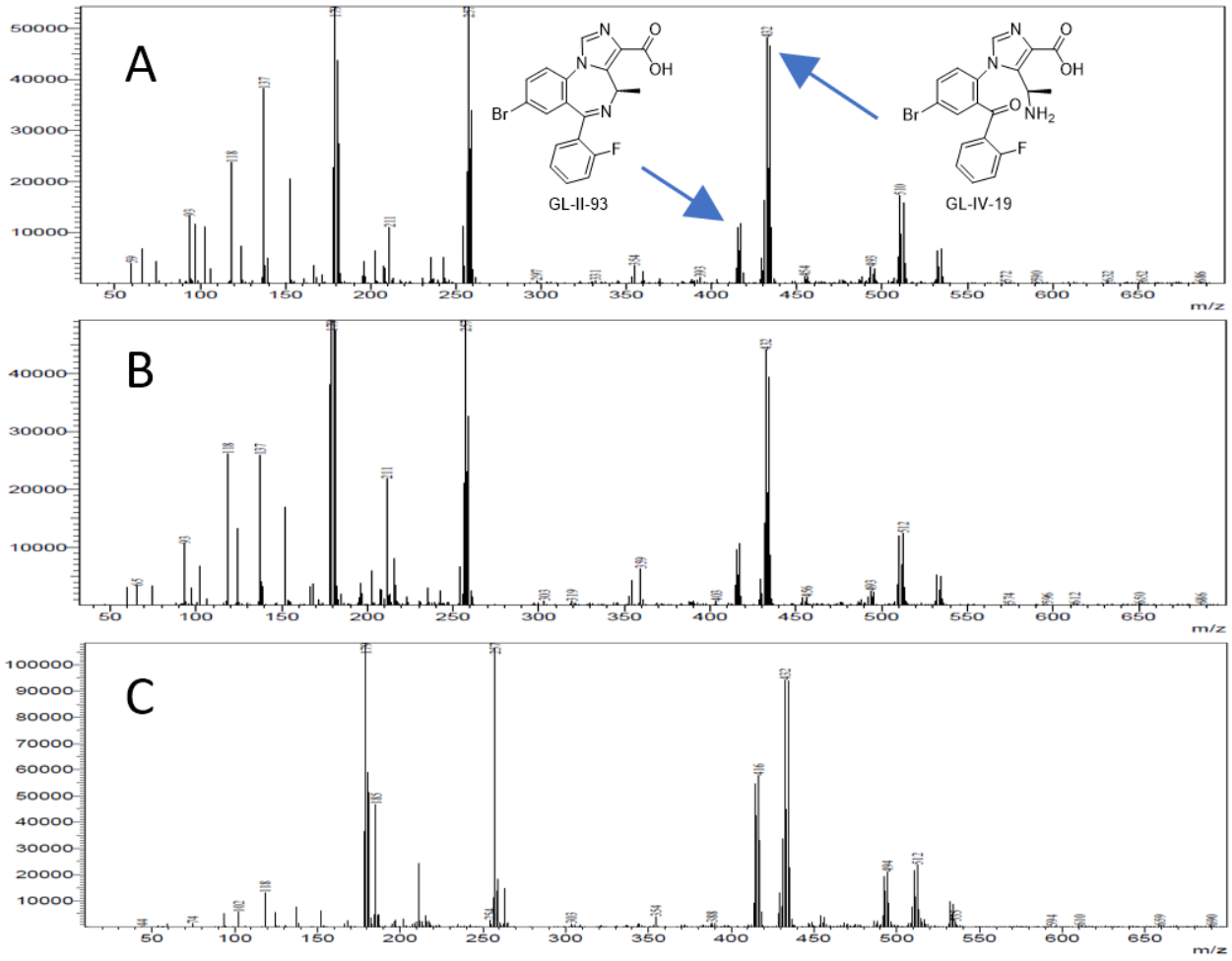

Figure 103. A, B, C: The mass spectra of GL-IV-19 (90) in DMSO at 0.5 min, 1 min, and 6 h time points, respectively. It indicated the conversion of GL-IV-19 to GL-II-93 in a time-dependent manner. The equilibrium was reached at 6 h, as compared to longer time points, data not shown here.

As presented in Figure104, the ^{1}H NMR spectra, comparison of **85** (upper spectra) and **90** (lower spectra) in a 1:1 mixture of DMSO and D_2O is depicted. The doublet of the C(4)-methyl group was shifted from 1.2 ppm to 1.4 ppm (two doublets because of the effect of the two rotamers on the C(4) methyl group in **90**), and the quartet of the C(4)-hydrogen atom shifted from 6.4 ppm

to 4.2 ppm. Since these sets of the peak had the highest intensity and clear splitting pattern, therefore, they were chosen to be monitored and quantified during the addition of acid and base in the NMR spectroscopy experiments.

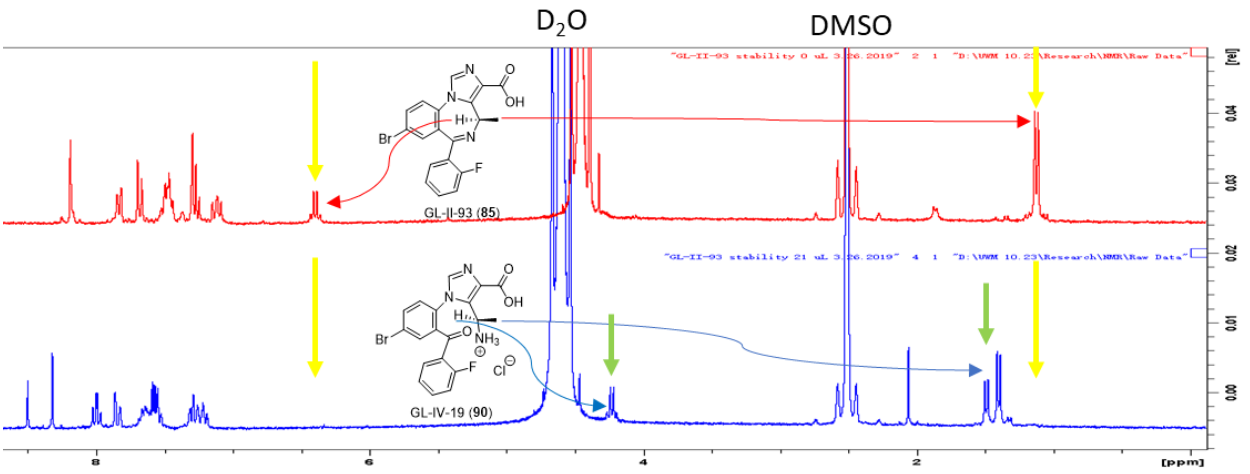

Figure 104. The ^{1}H NMR spectra comparison of GL-II-93 85 (upper spectra in red) and GL-IV-19 90 (lower spectra in blue). The doublet of the C(4)-methyl group was shifted from 1.2 ppm to 1.4 ppm (two double are the rotamers of the methyl group in 90), and quartet of the C(4)-hydrogen atom from 6.4 ppm to 4.2 ppm. The peaks disappeared in the spectra of 90 as indicated by yellow arrows, whereas the peak that appeared was colored in green. The DMSO peak was at 2.5 ppm; the D_2O peak was at 4.8 ppm.

The stability of acid **85** was conducted in a 1:1 mixture of DMSO and D_2O at a low concentration (1 mg/mL). The DCl/D_2O solution (5.125 M) was added by a micropipette in a small portion with the final volume of DCl as 0, 0.1, 1, 2, 3, 4, 5, 8, 11, 21 µL for a equilibrium study and also for the determination of the volume to conduct the kinetic study at pH = 2 (pH paper). In the equilibrium study, there was no change that occurred in the NMR spectra; the final spectra were saved for each addition of DCl. The bottom spectra is the ^{1}H NMR spectrum of GL-II-93 (**85**) in the DMSO/ D_2O mixture, and the spectra are presented with an increase of DCL (0.1, 1, 2, 3, 4, 5, 8, 11, 21 µL) in an order from bottom to the top of Figure 105. It appeared that the reaction reached equilibrium very rapidly, but the full conversion from **85** to **90** required harsh conditions and a large volume of DCl (21 µL). The desired pH at 2 can be achieved by the addition of 2 µL

of DCl (5.125 M), which was used for the next kinetic experiment with **85** under acidic conditions at pH = 2 to mimic the physiological pH in the stomach. The graphs were integrated by an area of an appearing or disappearing peak against the amount of acid added, as illustrated in Figure 106. The left panel of Figure 106 depicts the area-concentration curve of the C(4) methyl group at 1.4 ppm (the second rotamer for higher intensity), and 1.2 ppm for the right panel under acidic conditions. The concentration that resulted in a significant shift of peaks was consistent for both appearing and disappearing peaks in the proton NMR spectra, which was found at about 0.01 M of DCl in 1 mg/mL of **85** solution.

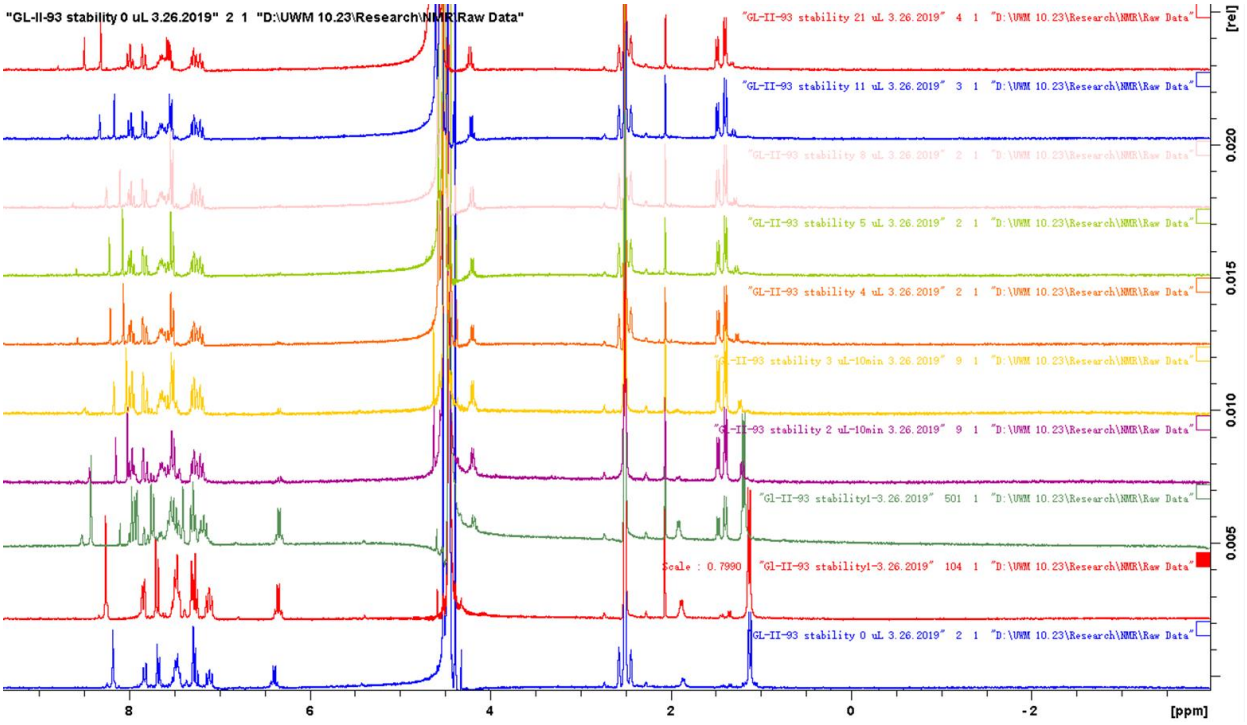

Figure 105. The ^{1}H NMR spectra for the equilibrium study of the conversion from GL-II-93 (85) into the open ring form GL-IV-19 (90) with a increased volume of DCl (5.125 M) from bottom to the top the spectra follow this order: 0, 0.1, 1, 2, 3, 4, 5, 8, 11, 21 µL.

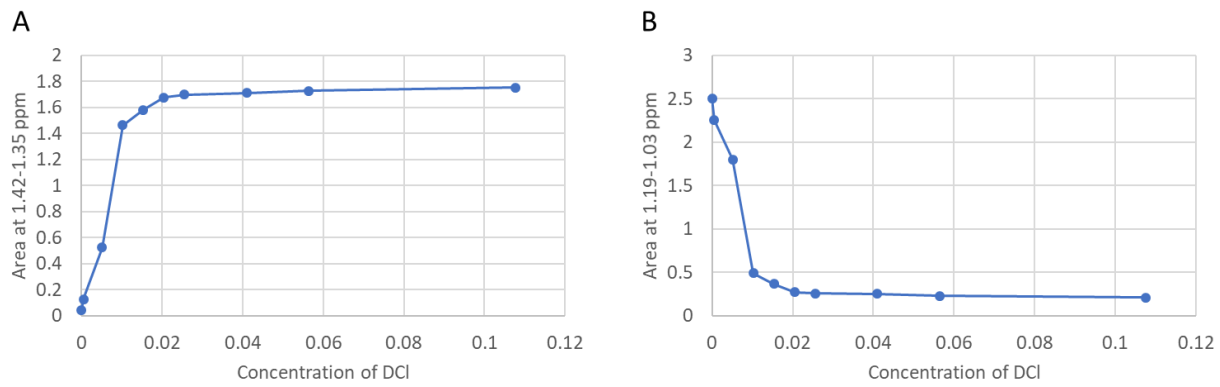

Figure 106. The area-concentration curve of the C(4) methyl group at (A) 1.4 ppm (the peak for the second rotamer was due to higher intensity), and (B) 1.2 ppm for the right panel under acidic conditions.

The kinetic study under acidic conditions was carried out by the addition of 2 μL of DCl solution in one portion. Once the desired concentration or pH was achieved, the NMR tube was shaken rapidly and vigorously to ensure a homogenous mixture. In the kinetic study, as shown in Figure 107, the ^{1}H NMR spectra were then obtained and saved for each time interval with one data point per minute for 1 hour under acidic conditions. Only 13 spectra were selected to show the obvious peak changes at 1, 2, 3, 4, 5, 6, 7, 8, 9, 11, 15, 20, 30, 40, 50, 62-minute time points. As described above, the peaks of the C(4) methyl group and the hydrogen atom were shifted from the position indicated with red arrows (peak decreased) to the position with green arrows (peak appeared). The graphs were integrated by an area of appearing or disappearing peak against time at certain concentrations for the desired pH to 2, as presented in Figure 108. This reaction reached equilibrium at about the 50 minute time point, and the half-life was about 20 minutes for both the appearing or disappearing peak. The results indicated that if given GL-II-93 (**85**) orally, it will not be stable in the original form in the stomach at pH to 2 and will start the conversion from the C(6)-N(5) imine form to the open keto form immediately. This will take about 20 minutes to hydrolyze

50 % of **85** to the open keto form **90.** The intensity-time curve and the half-lives were similar to the area-time curve (see details in Appendix VII).

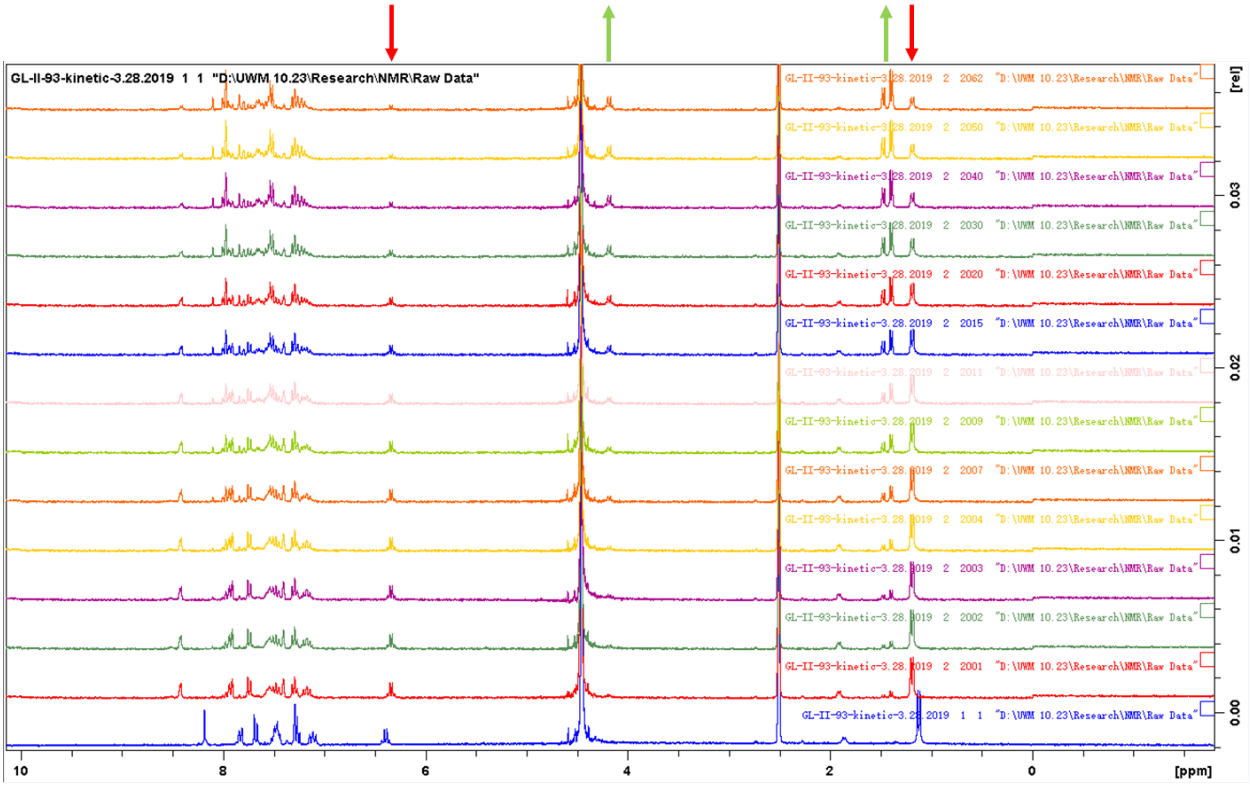

Figure 107. The ^{1}H NMR spectrum of 13 spectra in the kinetic study at pH = 2. The spectra were selected to show the obvious peak changes at specific time points. The bottom spectrum is the ^{1}H NMR spectrum of GL-II-93 (85) in the DMSO/ D_2O mixture, and the spectra with an increase of time points at 1, 2, 3, 4, 5, 6, 7, 8, 9, 11, 15, 20, 30, 40, 50, 62 minute time points in order from bottom to the top. As described above, the peaks for the C(4) methyl group and hydrogen atom were shifted from the position indicated with red arrows (peak decreased at 1.2 ppm and 6.4 ppm) to the position with green arrows (peak appeared at 1.4 ppm and 4.2 ppm).

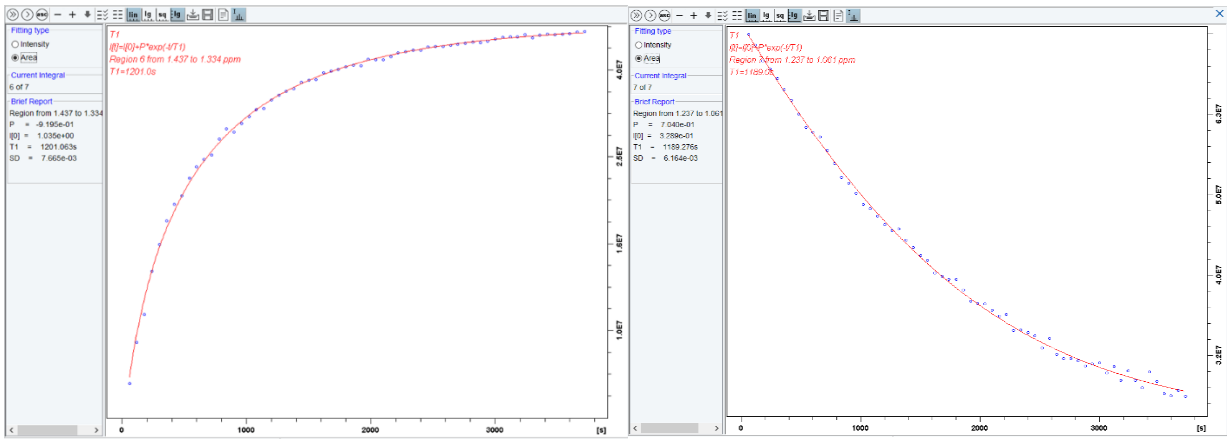

Figure 108. The area (lg)-time curve for the C(4) methyl group of GL-II-93 (85) at pH = 2. The panel on the left is the rotamer appearing at 1.4 ppm, and the right-hand panel is for the disappearing methyl group peak originally at 1.2 ppm. The half-life for these two peaks is 1201 seconds and 1189 seconds, respectively.

A second experiment based on the addition of NaOD was carried out in order to determine the time and concentration of the C(6)-N(5) imine reformation of keto GL-II-19 (**90**) back into its original C(6)-N(5) imine form GL-II-93 (**85**) and further to determine if the sodium salt form of the acid GL-IV-18 (**89**) would take place in more basic conditions. To the solution of GL-IV-19 (**90**) at 1 mg/mL in the mixture of 1:1 DMSO/D_2O, the NaOD/D_2O solution (7.32 M) was added in small portions (0.001, 0.005, 0.01, 0.02, 0.05, 0.075, 0.1, 0.2, 0.5, 1, 2 μL) for the equilibrium study. This mixture will be utilized for further determination of the volume of NaOD to create a pH = 8-9 solution to mimic the physiological pH in the intestine. In the equilibrium study, there was no change, which occurred in the NMR spectrum and the final spectrum was saved for each addition of NaOD. It was noticed that during the first three additions, the peak of the C(4) methyl group of keto GL-II-93 (**85**) had already appeared in high intensity without any addition of base and no significant change was observed when a small amount of base was added to first three-volume 0.001, 0.005, 0.01 μL, which was unexpected, as shown in Figure 109 for the last four spectra on the bottom. It was later found that GL-IV-19 (**90**) was actually a hydrochloric acid salt of the free amine. When it was dissolved in DMSO, it stayed in the salt form, therefore the C(4)-methyl group of **90** was the only the peak at the upper field in the NMR spectrum. However, it was ionized when D_2O was added as part of the solvent system, and the pH was found out to be around 4, as presented in Figure 110. The neutralization reaction had already begun the very second D_2O was added, therefore it explained the formation of the peak from the original imine GL-II-93 (**85**). The pH after each addition was measured on the further addition of NaOD. As shown in Figure 109, when the pH was 5 or slightly higher than 5, a significant amount of the

closed imine **85** was formed, which is consistent with the synthesis of **85** where the acidification of the salt GL-IV-18 (**89**) to pH = 5 would occur to form **85**. When the pH was even higher, the imine was hydrolyzed to the ring-opened form **90** and was completely eliminated and turned into its sodium salt.

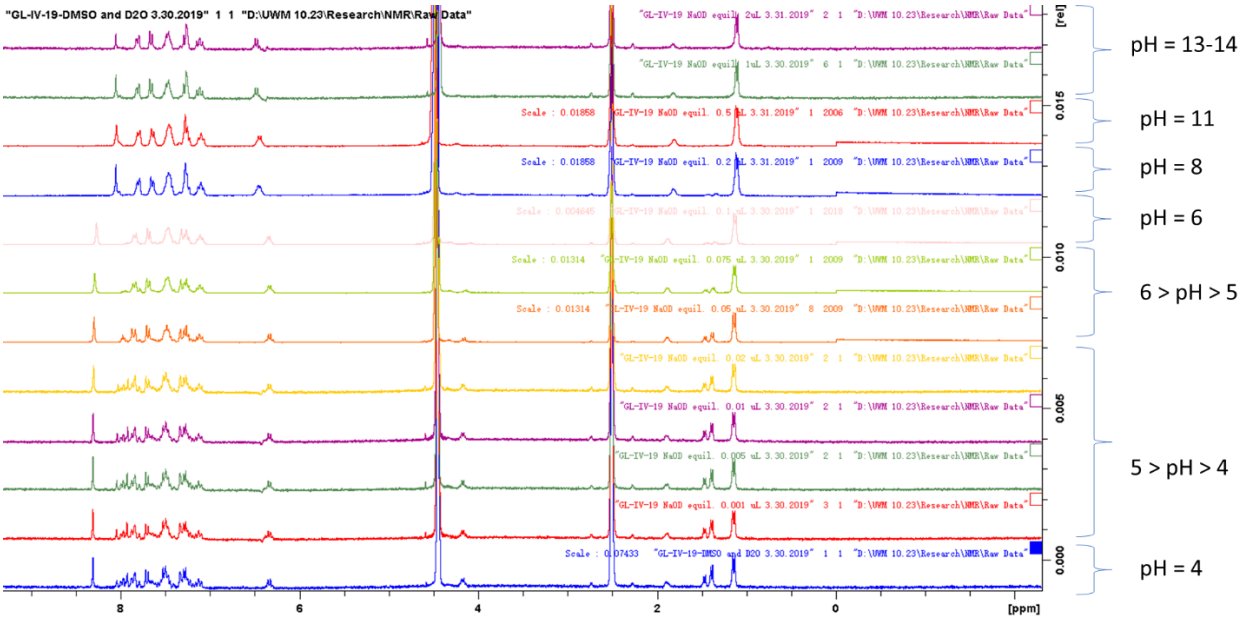

Figure 109. The ^{1}H NMR spectra of equilibrium study of the conversion from 1 mg/mL of GL-IV-19 (90) to the original form GL-II-93 (85) or its sodium salt GL-IV-18 (89) with an increased volume of NaOD (7.23 M) from bottom to the top spectra as following order: 0, 0.001, 0.005, 0.01, 0.02, 0.05, 0.075, 0.1, 0.2, 0.5, 1, 2 µL.The pH after each addition was indicated.

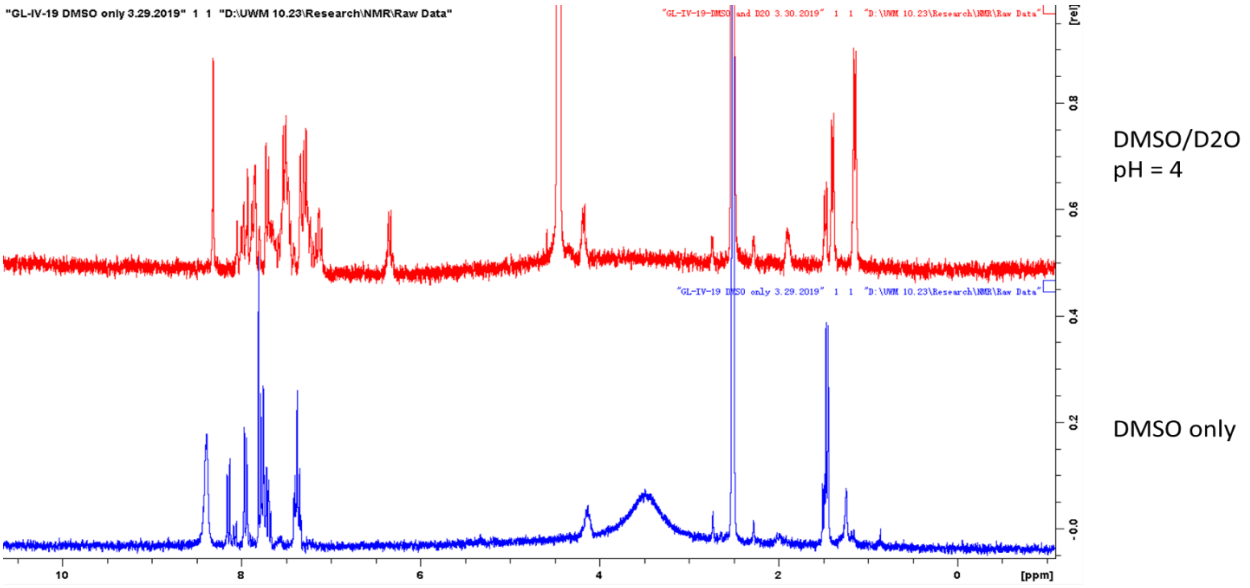

Figure 110. The ^{1}H NMR spectra of GL-IV-19 (90) in the DMSO/D_2O mixture and DMSO only. The pH in the mixture was about 4, and the peak of the product GL-II-93 (85) at 1.2 ppm had started to appear in the mixture, whereas this was not observed in the solution of DMSO only.

The graphs of the equilibrium study from NMR spectroscopy under basic conditions were integrated by the area of an appearing or disappearing peak against the amount of added base, as illustrated in Figure 111. The left panel shows the area-concentration curve of the C(4) methyl group at 1.4 ppm (the second rotamer for higher intensity), and 1.2 ppm for the right panel under acidic conditions. The red dot on the Y-axis represented the trials without any addition of base but just in the mixture of DMSO and D_2O. It is obvious that the reaction reacted rapidly when D_2O was added, and one was not able to monitor the mixture within one minute due to the time for sample preparation. The concentration that resulted in significant shifts of the peak was consistent for both the appearing and disappearing peaks, which was about 0-0.001 M of NaOD in 1 mg/mL of **90** solutions.

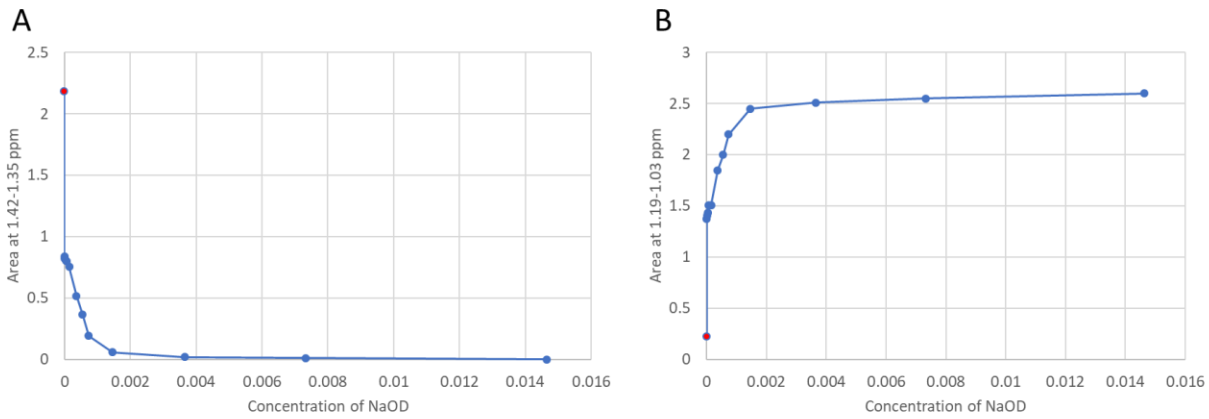

Figure 111. In panel A is represented the area-concentration curve of the C(4) methyl group at 1.4 ppm (the peak for the second rotamer due to higher intensity), and panel B represents 1.2 ppm under basic conditions. The red dot on the Y-axis represented the trials without any addition of base but just in the mixture of DMSO and D_2O.

The kinetic study under basic conditions was carried out by the addition of 0.025 µL of NaOD solution in one portion (initial pH = 8-9). Once the desired concentration or pH was achieved, the NMR tube was shaken rapidly and vigorously to ensure a homogenous mixture. In the kinetic study, as shown in Figure 112, the ^{1}H NMR spectra were then obtained and saved for each time interval with one data point per minute for 3 hours under basic conditions. Only 13 spectra were selected to show the obvious peak changes at 1, 9, 20, 30, 40, 50, 60, 80, 100, 120, 140, 160, 180-minute time points. As described above, the peaks of the C(4) methyl group and hydrogen atom were shifted back to its original C(6)-N(5) imine positions. The graphs of the kinetic study were integrated by the area of appearing or disappearing peak in the NMR spectra against a time point at certain concentrations for the desired initial pH to 8, as presented in Figure 113. The intensity-time curve and the half-lives were similar to the area-time curve (see details in Appendix VII). This reaction exhibited a half-life about 135 minutes for both the appearing (at 1.2 ppm) or disappearing (at 1.4 ppm) peak. This was tested when the final pH of the reaction was about 5-6 pH units. It should be noted that this is not exactly the pH conditions in the intestine that

has a stable balance of pH = 8-9 with a complex buffer conditions. Furthermore, the reaction began relatively fast after it was dissolved in D_2O. Therefore, the actual initial point was missing and undetectable due to the time for physical sample preparation, which time was very limited. All these factors influenced the determination of kinetic profile of the hydrolyzed form GL-IV-19 (**90**), especially the attempt to mimic the real conditions in the human body from the open ring keto form in the stomach and the recyclized form back to the seven-membered ring imine form in the intestine. However, these data revealed some insight into the kinetics and stability of the three forms of GL-II-93 (**85**) at different pH conditions (pH = 2, 5, and 8). The acid **85** was not stable under low pH conditions, and would be readily converted into the open ring keto form **90** and reaches to an equilibrium between the open ring keto form and the closed ring form **85.** This equilibrium would remain unless harsh conditions were applied such as heating and the presence of more acid. The open ring form **90** was also not stable; it would start to react in the presence of water only rapidly. At this point, any added base would only neutralize the hydrochloric acid salt to form the free amine first. When the solution reached a pH close to 5, the significant amount of the free amine would be cyclized back to the original form **85**. At higher pH, the sodium salt of **85** would form, and the open ring keto form **90** would be completely consumed.

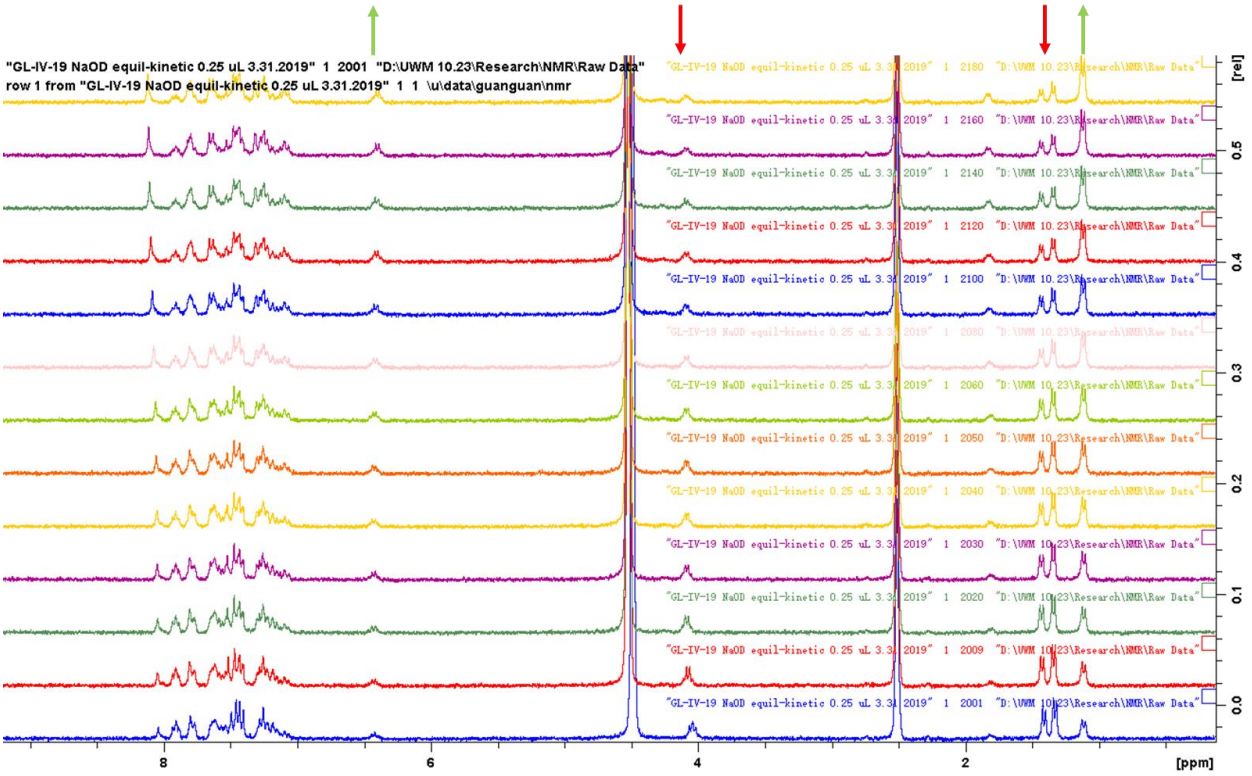

Figure 112. The ^{1}H NMR of 13 spectra in the kinetic study at pH = 8. The spectra were selected to show the obvious peak changes at time points. The spectra were presented with an increase in time point at 1, 9, 20, 30, 40, 50, 60, 80, 100, 120, 140, 160, 180 minutes in order from bottom to the top. As described above, the peaks of the C(4) methyl group and the C(4) hydrogen atom were shifted as indicated with green arrows (peak decreased at 1.2 ppm and 6.4 ppm) to the position with red arrows (peak appeared at 1.4 ppm and 4.2 ppm).

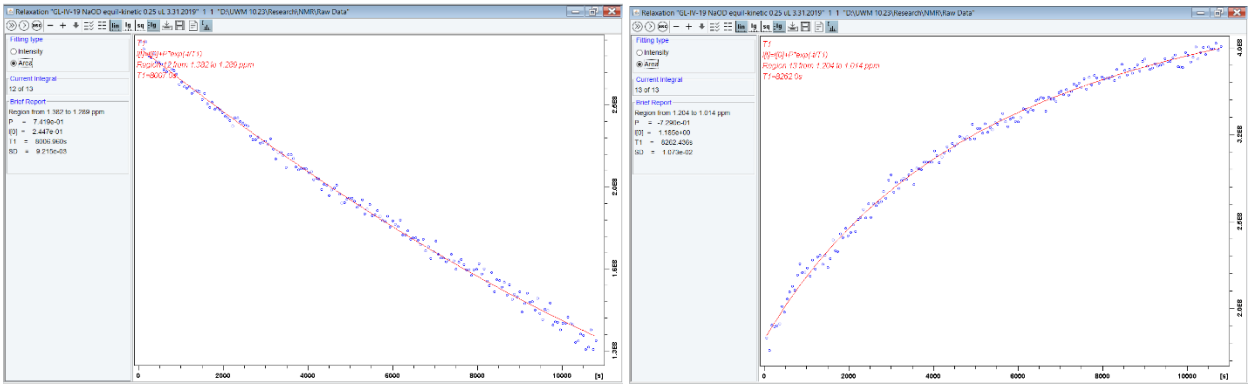

Figure 113. The area (lg)-time curve for the C(4) methyl group of GL-IV-19 (90) at pH = 8, the left panel is for the disappearing rotamer at 1.4 ppm, and the right panel is for the appearing methyl group peak originally at 1.2 ppm. The half-life for these two peaks is 8006 seconds and 8262 seconds, respectively.

2.3.3.3. Analog Research on GL-II-93

2.3.3.3.1. Synthesis of Analogs

To further explore the SAR based on the evidence accumulated on the lead compound Gl-II-93 (**85**) for the treatment of asthma, a series of carboxylic acid and tetrazole bioisosteres of **85** was designed and synthesized. Since the C(3)-acid function was critical for the high hydrophilicity to prevent penetration across the BBB to limit possible CNS effects, most of the analogs of **85** retain this acid moiety. With the exception of the "privileged IMDZ" backbone, the chirality at the C(4) position, the substituents at the 2 prime position, bioisosteres of the carboxylic acid function at the C(3) position as well as the functional group at the C(8) position were all considered for further modifications, as illustrated in Figure 114.

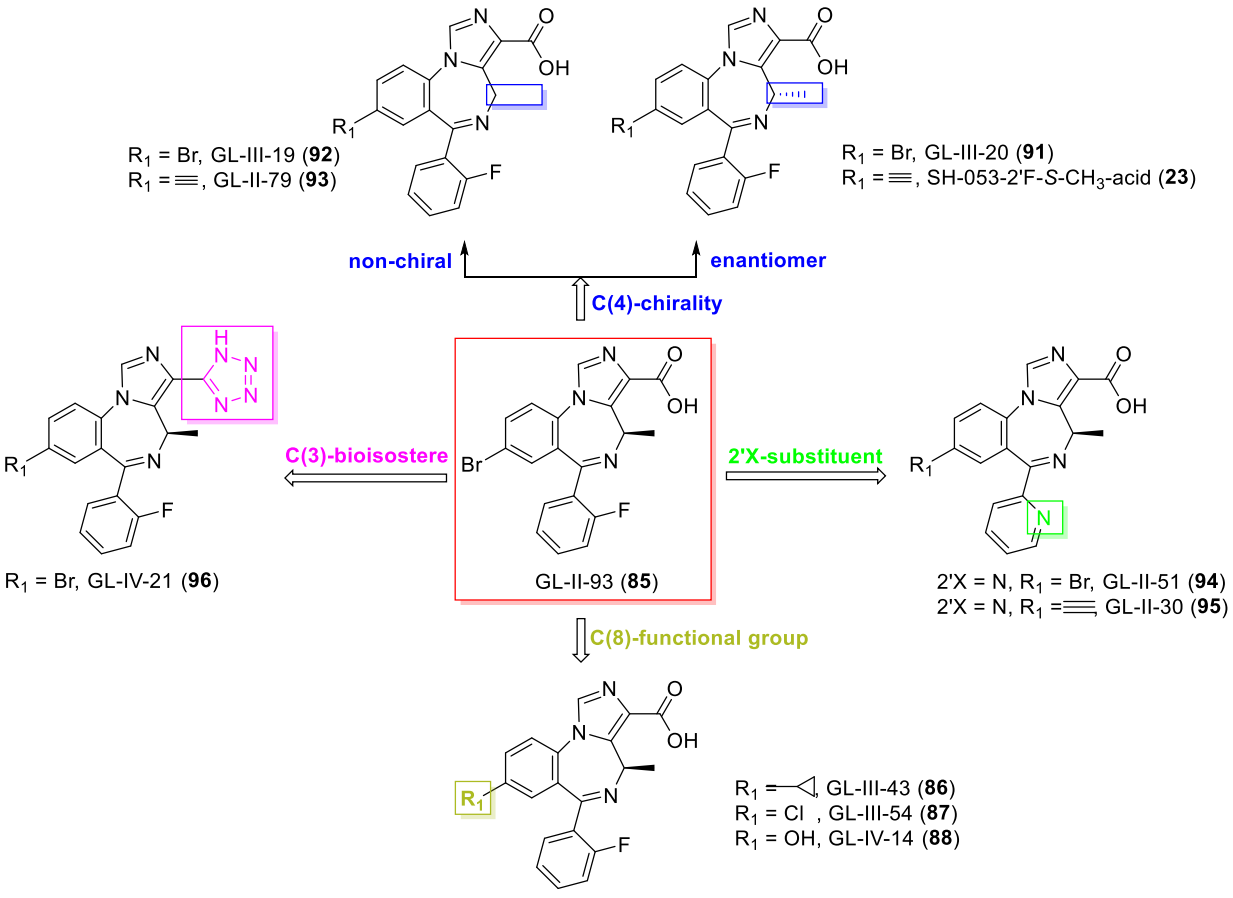

Figure 114. Analogs of 85 by modification of the substituents at the C(3), C(4), C(8) and 2'X positions.

It is reasonable to design the synthesis of the enantiomer of the most active compound GL-II-93 (**85**) if the target has a chiral center in the molecule. Moreover, the parent enantiomer (*S*-CH_3) **2** exhibited higher potency and better binding affinity[83] as compared to **1** not only at α5 subtypes but also at α2 and α3 subtypes. Therefore, the *S*-isomer GL-III-20 (**91**), the enantiomer of **85,** was synthesized as a negative control compound to evaluate the *S*-isomer in the animal models of asthma. Besides **91**, the *S*-isomer with the C(8)-ethinyl carboxylic acid was previously made as the enantiomer of the α5 agonist SH-053-2'F-*R*-CH_3-acid (**23**). This could also be screened for SAR to determine if a molecule with a different chiral center exhibit activity in asthma, as compared with the key *R*-isomer. These *S* isomers might be expected to cause inflammation and mucus overproduction confirming that the α4 and α5 subtypes are the targets of choice and supporting the approach to an (*R*) drug target here. Consequently, the synthesis of both **91** and **23** was carried out by hydrolyzing the ethyl ester of the *S*-isomers, which contained the C(8)-bromo or ethinyl substituent, respectively, into their corresponding carboxylic acids in excellent yield, as shown in Scheme 18.

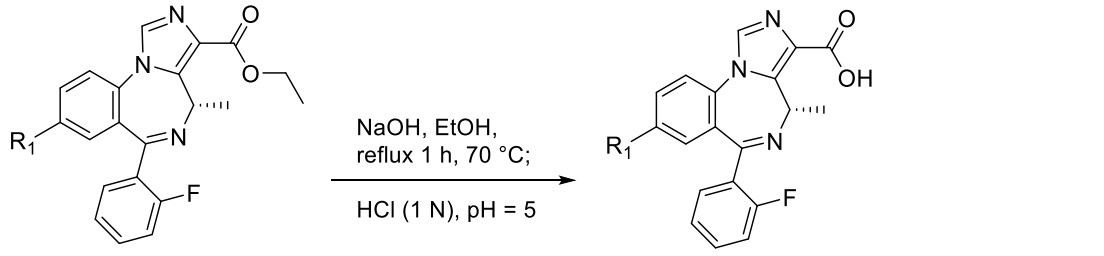

Scheme 18. Synthesis of GL-III-20 (91) and SH-053-2'F-*S*-CH_3-acid (23) from the corresponding ethyl esters in the 2'F-*S*-CH_3 series.

It is necessary always to use older valuable information from previous work. The data published a decade ago,[83] which demonstrated that the *in vitro* binding affinity at all subtypes from JY-XHe-053 were much higher than effects at **1, 2** and **85,** see Table 25. Furthermore, from the *in vitro* efficacy data, JY-XHe-053 exhibited the best efficacy compared to the other related compounds under study here including **1, 2** and even **85** at all subtypes at 100 nM, see Table 26. However, it did exhibit, the most potent efficacy (0.7 nM) at α5 subtypes observed to date. This concentration at 100 nM is the physiologically relevant concentration in clinical trials. The difference between JY-XHe-053 and **1 or 2** is the chirality at the C(4) position, wherein JY-XHe-053 does not contain a chiral methyl group. This makes it an ideal negative control compound. Initially, the chiral methyl group was introduced to reduce the binding at α1-subtypes for CNS disorders such as anxiety, epilepsy, and schizophrenia and patent protection. However, α1-containing $GABA_AR$ subtypes are not expressed in lung tissue. Moreover, since the carboxylic acid function greatly retards the penetration through the BBB, this further limits the effect of α1 subtypes on CNS-mediated side effects. Therefore, JY-XHe-053 was brought back into focus again. In this vein, the carboxylic acid analog of JY-XHe-053 could be an interesting ligand to investigate, due to its high efficacy and potent binding affinity pattern at α5 if it contained a C(3) acid function. Therefore, the C(8)-bromo acid analog, GL-III-19 (**92**), was synthesized via this hypothesis. The C(8)-ethinyl carboxylic acid, GL-II-79 (**93**), was made for this SAR study. The synthesis of these two acids was straight forward and performed with the same procedure for the synthesis of the acids, GL-III-19 (**92**) and GL-II-79 (**93**), as shown in Scheme 19.

Table 25. The binding affinity at α1-6β3γ2 $GABA_AR$ BzR. Measurements were generated in duplicate. K_i values are reported in nM. (Modified from the Figure in Fischer et al.)[83]

Compound	α1	α2	α3	α4	α5	α6
Diazepam	14.0	7.8	13.9	ND[a]	13.4	ND[a]
JY-XHe-053	22.0	12.3	34.9	ND[b]	0.7	ND[b]
XHe-II-053	247.0	40.0	90.0	>1000	13.0	>1000
HZ-166	300.0	160.0	527.0	ND[b]	82.0	>5000
SH-053-2′F-S-CH_3	468.2	33.3	291.5	ND[b]	19.2	>5000
SH-053-2′F-R-CH_3	759.1	948.2	768.8	ND[b]	95.2	ND [b]

[a] ND, not determined. [b] The binding affinity at α4-GABA$_A$Rs and α6-GABA$_A$Rs have not been determined, but since the 6-phenyl group is present, there will be no ligand binding to these receptors.

Table 26. Efficacy at α1-3,5β3γ2 GABA$_A$Rs as % of the control current at the concentration of 0.1 and 1 μM. Data are presented as 0.1μM/1 μM. (Modified from the Figure in Fischer et al.)[83] Data determined in the laboratory of Dr. Sieghart with an EC$_3$ GABA.

Compound	α1	α2	α3	α5
Diazepam	239/314	426/536	437/752	274/342
JY-XHe-053	169/248	307/410	365/596	220/246
XHe-II-053	130/194	209/329	265/513	150/186
HZ-166	113/167	165/313	149/346	130/174
SH-053-2′F-S-CH_3	116/164	170/348	138/301	218/389
SH-053-2′F-R-CH_3	111/154	124/185	125/220	183/387

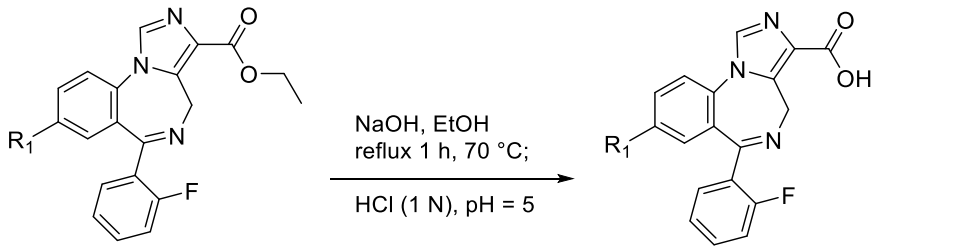

R_1 = Br,
R_1 = acetylene, JY-XHe-053

R_1 = Br, GL-III-19 (**92**), 92.8 %
R_1 = acetylene, GL-II-79 (**93**), 95.9 %

Scheme 19. Synthesis of GL-III-19 (92) and GL-II-79 (93) negative controls from the corresponding ethyl esters in the achiral 2'F series.

Since the 2'-F analogs from the *R*-isomer series were active in asthma and ligands in the 2'-N series were active in other assays, as described in the previous section for the treatment of schizophrenia and depression, it was logical to synthesize analogs from this 2'-N-*R*-CH_3 series for

a comprehensive SAR study for asthma as well. Therefore, at the 2 prime positions, instead of the C-F bond, a pyridine ring N was introduced for both C(8)-bromo and C(8)-ethinyl intermediates. The corresponding carboxylic acid analogs, GL-II-51 (**94**) and GL-II-30 (**95**), were synthesized applying the same procedure of saponification, as previously described. The synthesis is illustrated in Scheme 20.

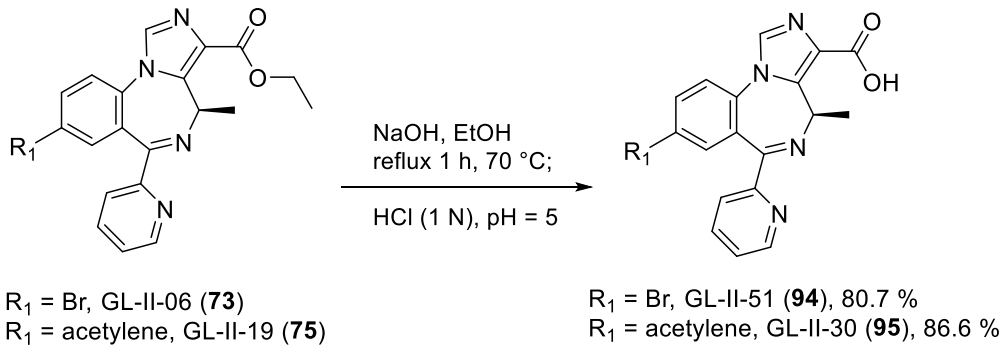

Scheme 20. Synthesis of GL-II-51 (94) and GL-II-30 (95) from the corresponding ethyl esters in the 2'N-*R*-CH_3 series.

In addition to the modifications at the C(3) and C(4) positions, the C(8)-substituents also play an essential role in terms of pharmacological effects, such as the Br vs. acetylene comparison as discussed in the previous sections. With a perspective from medicinal chemistry, Br, as one of the heavy halogens, usually is not the first choice of halogen-containing drugs due to several reasons: 1. A higher MW. 2. A possible undesired increase in lipophilicity. 3. The impact on the size of the molecule. 4. A possible lower solubility. 5. A weaker carbon aromatic bond as compared to chlorine or fluorine, which might lead to a shorter shelf-life than smaller size halogens.[210] 6. Also safety concerns such as photoreactivity, phototoxicity, and the formation of reactive metabolites,[211] which results from photoreactions with light. However, even with these possible issues listed above, there are still 70 drugs, which contain Br, approved for the drug market, and only 7 of them have been withdrawn due to the exhibition of toxicity. (Source https://www.drug

bank.ca/. by searching keyword “bromide”). Even though GL-II-93 (**85**) does not exhibit any side effects at the current stage, the concerns over the shelf stability of a Br atom should always be kept in mind. It is prudent to further explore the SAR with several other functional groups at the C(8) position.

As compared to Br, Cl is a safer halogen to use and might still possess the desired properties as bromine. If the C(8)-Cl ligand displays a similar effect as **85**, this analog might well be a good backup compound to **85** with less phototoxicity and provide a better shelf-life. This is because an aromatic C-Cl bond is stronger than a C-Br bond. The synthesis of the C(8)-Cl analog, GL-III-54 (**87**), was carried out in a procedure similar to that employed for **85** except that C(8)-Cl benzophenone **87** substrated for the C(8)-bromo benzophenone as the required building block, as shown in Scheme 21.

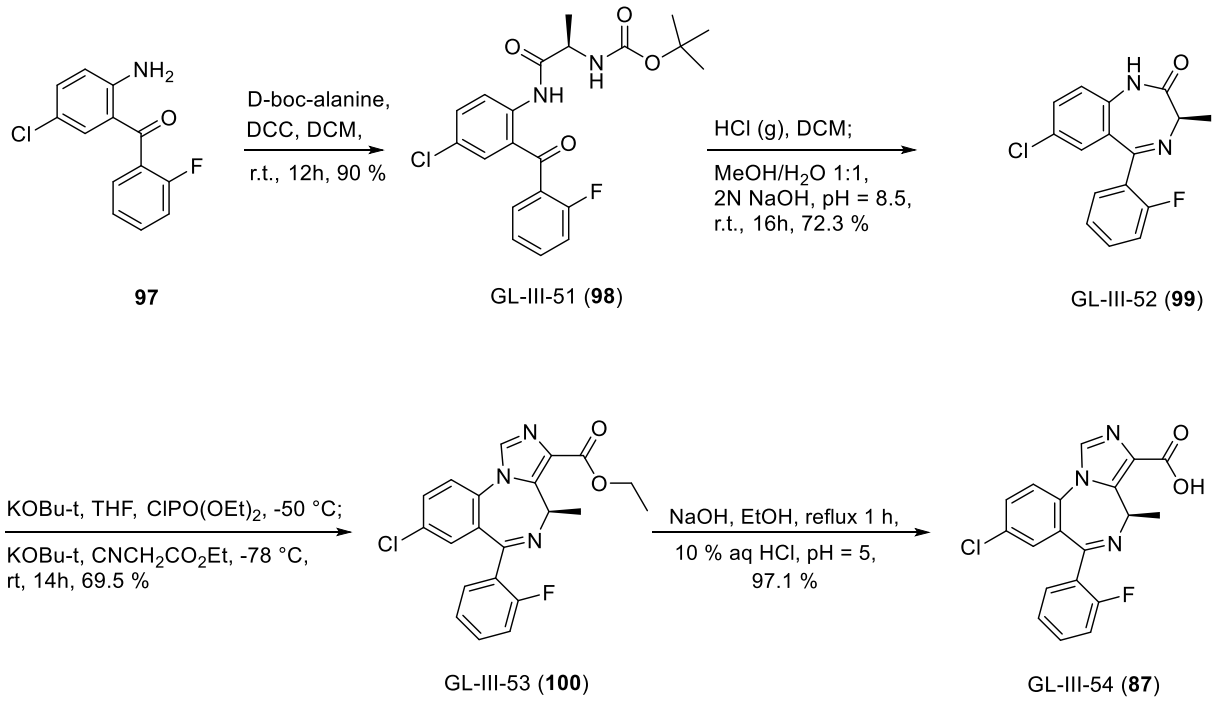

Scheme 21. Synthesis of GL-III-54 (87); the C(8)-Cl analog of 85.

Because the cyclopropyl group, occupied a similar van der Waals radii as an ethinyl function, the former group was introduced at the C(8) position. Since the cyclopropyl group can rotate at will at the C(8) position, the electron density map of a cyclopropyl group, ethinyl moiety and Br are very similar. Consequently, a C(8)-cyclopropyl group might exhibit the desired biological activity due to similar interactions in the binding pocket as acetylene. Moreover, the formation of a possible reactive metabolite from acetylene or bromine can be avoided by different metabolic pathways. Therefore, the C(8)-cyclopropyl analog, GL-III-43 (**86**) was synthesized based on this hypothesis. The aryl-bromide ethyl ester intermediate **6** was treated with cyclopropyl boronic acid in the presence of a Pd catalyst *via* a Suzuki cross-coupling reaction[110] to yield the C(8)-cyclopropyl ethyl ester. The ester at C(3) was then saponified to furnish the corresponding carboxylic acid, as shown in Scheme 22.

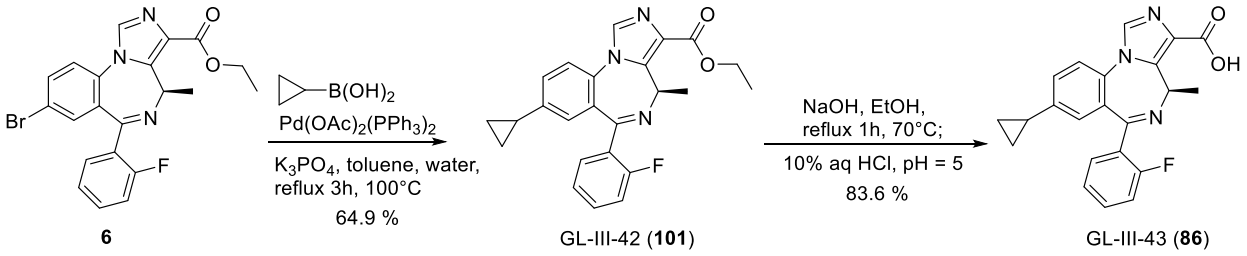

Scheme 22. Synthesis of GL-III-43 (86); the C(8)-cyclopropyl analog of 85.

A phenolic group is one of the most common constituents for pharmaceuticals and has been widely used in industrial synthesis. In addition to the replacement of the Cl and cyclopropyl groups at the C(8) position, the hydroxyl group was also used to substitute for a Br atom at the C(8) position. If active, the phenolic hydroxyl group would increase the hydrophilicity and further reduce the possible CNS effects due to its lower permeability across the BBB. Moreover, the C(8) OH analog might be a metabolite. The C(8)-OH analog, GL-IV-14 (**88**), was synthesized by a highly efficient copper-catalyzed one-pot SnAr reaction[212] of the bromo ethyl ester intermediate

with potassium hydroxide in PEG-4000 (polyethylene glycol) as the solvent at 120-Celsius degrees for 12 hours at low cost and in good yield, as illustrated in Scheme 23. The other advantage of this process rests on its compatibility because the ethyl ester can be hydrolyzed into the corresponding acid in the same process while replacing the bromine with a phenolic hydroxyl group. This provides the C(8)-phenolic analog of GL-II-93 (**85**) for metabolic studies if need be, as well as the guinea pig tracheal ring assay.

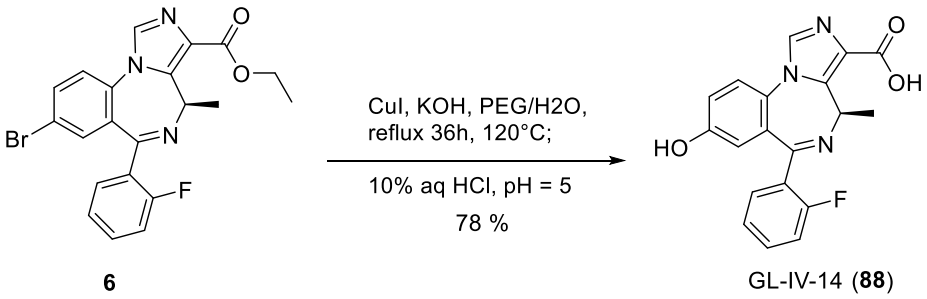

Scheme 23. Synthesis of GL-IV-14 (88); the C(8)-OH analog of 85.

The carboxylic acid function has proven to be extremely valuable for the design of IMDZs, which target $GABA_A$Rs for the novel treatment of asthma with limited CNS side effects due to its low permeability across the BBB. However, it has been reported that metabolism of a carboxylic acid might cause toxicity issues and adverse reactions which may result from the formation of reactive metabolic conjugates, such as acyl-coenzyme A thioesters derivatives (acyl-CoAs),[213] which might induce dysfunction of mitochondria as well as acyl glucuronides, which might trigger an immune response.[214] **It can not be concluded that the key carboxylic acid moiety should be avoided due to potential side effects or toxicity, since there are more than 450 approved drugs[215] on the market, which contains this moiety.** Moreover, people are actually exposed to food and products which contain the acid functional group, such as fatty acids or vinegar. However, attention should be paid to this structural alert and the possibility of reactive metabolites. Although

85 did not exhibit any side effects in recent *in vivo* rodent models and *in vitro* assays, it is reasonable to explore the surrogate structures of the carboxylic acid moiety while evaluating other properties of **85**.

One class of common surrogates for an atom or a functional group is bioisostere, which generally can be used as a primary strategy in medicinal chemistry. That is because bioisosteres have similar electron density, volume, and physiochemical properties as the functional group in question, which can result in similar pharmacological effects and perhaps a longer duration of action as well. Indeed, there are numerous bioisosteres of carboxylic acids due to its essential role in drug design. A recent structural-property relationship study reported the physiochemical parameters of 24 classes of carboxylic acid bioisosteres, such as acidity, lipophilicity, permeability, solubility, etc.[215] Based on this report, most of the bioisosteres are much more soluble than the carboxylic acid, itself, which provides another strategy to improve the solubility of **85** other than simple salt formation. Moreover, since a tetrazole is one of the carboxylic acid bioisosteres that has been studied in detail in the past few decades,[216] several parameters of the tetrazole and carboxylic acid were compared in this study. A tetrazole exhibits similar acidity and lipophilicity as compared to the carboxylic acid.[216] However, on the contrary to the previous studies that tetrazole showed remarkably less permeability across the BBB and much stronger hydrogen bonding interactions than the carboxylic acid. This finding indicated that a tetrazole might be a suitable replacement for the carboxylic acid moiety in **85** not only to further reduce the penetration across the BBB but also avoid possible reactive metabolites that the acid might produce. Therefore, the C(3)-tetrazole analog of **85**, GL-IV-21 (**96**) was synthesized.

The synthesis of a tetrazole moiety has been widely studied, most of which is by [3+2] cycloadditions between an azide and a nitrile. However, most of the nitriles are toxic, and sodium

azide is expensive and somewhat dangerous because of explosions. Therefore, the synthesis of the tetrazole analog GL-IV-21 (**96**), was conducted with a one-pot "click" synthesis[217] by the reaction of an aldehyde, hydroxylamine, and 1-butyl-3-methylimidazolium azide ([bmim]N_3) as a "green" azide source, in the presence of 20 mol% $Cu(OAc)_2$ as the catalyst, as shown in Scheme 24. **This chemistry was pioneered by Nobel Laureate Barry Sharpless.**

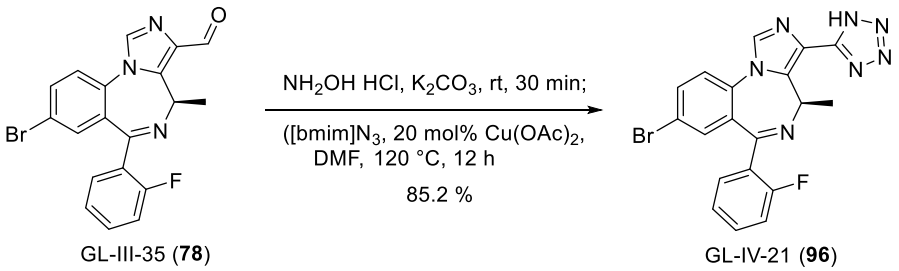

Scheme 24. Synthesis of GL-IV-21 (96); tetrazole analog of 85.

2.3.3.3.2. Evaluation of GL-II-93 Analogs, to Date

The analogs of **85** were sent to Dr. Michael R. Stephen at UWM for the assessment of cytotoxicity on both HEK293T and HEPG2 cell lines for a 48 h incubation time. As expected, the LD_{50} values of GL-II-93 analogs in HEK293T and HEPG2 are all higher than 400 µM, as illustrated in Table 27, which further indicates that the carboxylic acid function and its analogs have a very good safety profile in these two cell lines. This is regardless of any modifications in **85**. The further biological data on other analogs awaits the assays.

Table 27. Cytotoxicity of GL-II-93 (85) analogs.

No.	Compound	HEK293 LD_{50} (µM)	HEPG2 LD_{50} (µM)
1	**GL-II-93**	**>400**	**>400**
2	SH-053-2'F-R-CH3-acid	>400	>400
3	SH-053-2'F-S-CH3-acid	>400	>400
4	GL-II-30	>400	>400
5	GL-II-51	>400	>400

6	GL-II-79	>400	>400
7	GL-III-19	>400	>400
8	GL-III-20	>400	>400
9	GL-III-43	>400	>400
10	GL-III-54	>400	>400
11	GL-IV-14		
12	GL-IV-21		

The C(8)-cyclopropyl analog GL-III-43 (**86**) was evaluated in the airway hyperresponsiveness (AHR) assay at 100 mg/kg twice daily for 5 days in Dr. Arnold's group (Gloria Forkuo) to determine if the compound can induce any reduction on AHR reduction effect. Unfortunately, **86** presented a similar sRaw value, as compared to the ova s/c control, which indicated that **86** did not protect the MCh challenged mice at all concentrations and is an inactive compound in this asthma model, as depicted in Figure 115.

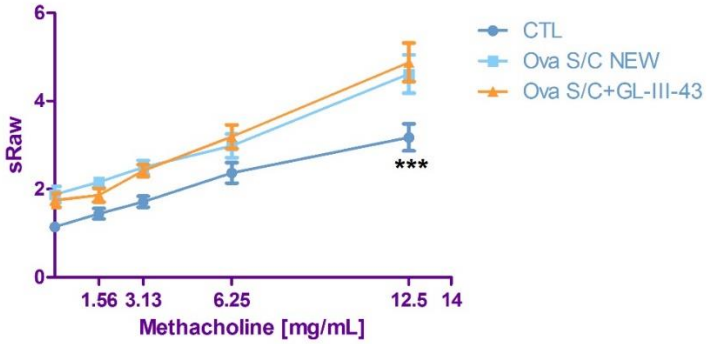

Figure 115. The effect of GL-III-43 (86) on AHR, orally administered. The sRaw was measured at an increasing dosage of MCh by a DSI's Buxco FinePointe noninvasive airway mechanics instrument. GL-III-43 was orally administered in ova s/c BALB/c mice at 100 mg/kg twice daily for 5 days. Data represent mean ± SEM (n=10). * represents significance p < 0.001.**

After the synthesis of GL-III-54 (**87**), the C(8)-Cl analog was sent to Dr. Janet Fisher's research lab at the University of South Carolina for the evaluation of efficacy by electrophysiological recordings. Illustrated below in Figure 116 is the efficacy data of **87** as compared to **85** at 0.1 and 1 μM. Overall, (data not received on α6 subtypes yet), the C(8)-Cl

analog **87** was able to potentiate all subtypes with the exception of α4 subtypes, which remained at the baseline GABA 100 %, but was slightly less potent than the C(8)-bromo **85.** It was interesting that the bromo acid **85** was more subtype selective at α4 subtype,s as compared to the other subtypes at 0.1 μM. However, the chloro and **87** did not show any α4 subtype selectivity at both 0.1 and 1 μM. At the higher concentration of 1 μM, the efficacy of **87** appeared similar to the normal efficacy pattern of diazepam, but with no potentiation at α4 subtypes. The diazepam related compounds with a pendant phenyl ring normally do not bind at DI (α4, α6) subtypes.

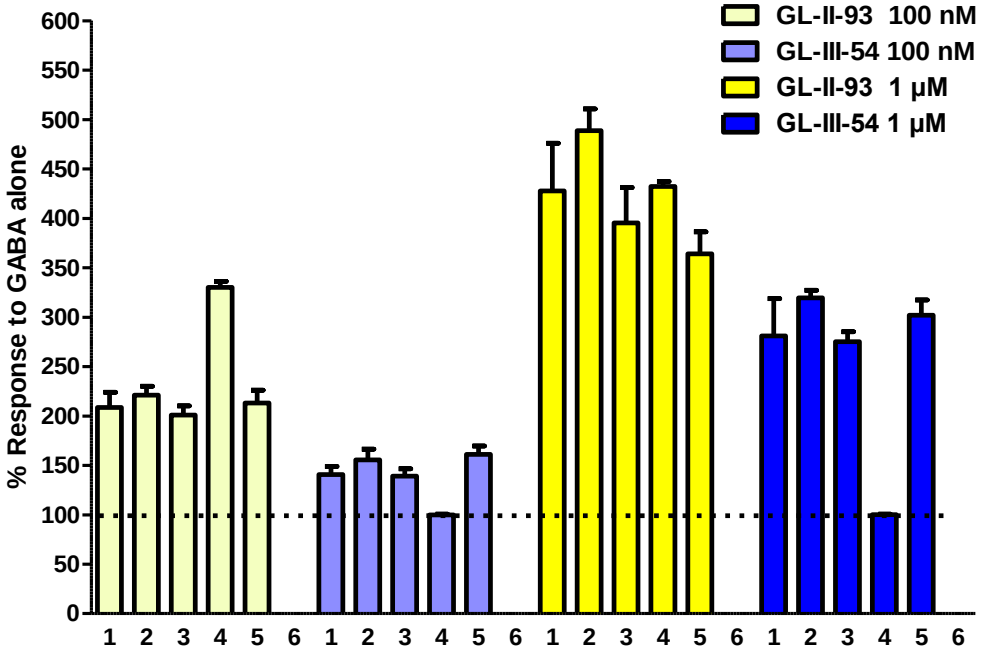

Figure 116. Potentiation of GL-III-54 and GL-II-93 in comparison at $\alpha_{1\text{-}5}$-containing $GABA_AR$s. The transiently transfected HEK-293T cells with α subunits of $GABA_AR$ were used to measure the average enhancement of current evoked to GABA EC3 by 0.1 μM or 1 μM GL-III-54 and GL-II-93 by patch clamp. Data represented mean ± SEM (n = 5).

Because **87** was able to potentiate most of the $GABA_AR$ subtypes and exhibited a structural similarity to **85**, this C(8)-Cl analog was expected to be active in the organ bath assay for relaxation of pre-contracted ASM. This was carried out by Dr. Emala's group, at Columbia University. In

order to confirm this hypothesis, **87** was examined in this asthma *ex vivo* model. Indeed chlrolide **87,** demonstrated in Figure 117 below, did relax the effect on ASM on a pre-existing substance P-induced contraction on guinea pig tracheal rings. The comparator **85** was run side-by-side in the same assay with tissue from the same animals and vehicle controls. There are a couple of observations regarding the data below. In this series of experiments, bromide **85** was much more potent than in our previous published data[187] (Furkuo GS, 2018, see Figure 86 for comparison). There are a number of explanations that could explain this increase in activity, such as handling the mice differently, the experience of the person who ran the assay, etc. Notably, **85** did exhibit a relatively larger relaxation effect on ASM in the most recent experiments, as compared to the earlier published findings.[187] Furthermore, the C(8)-chloro analog **87** was also able to reduce the ASM contraction at 25 μM similar to **85**, and it induced a significant relaxation at 50 and 100 μM, which was also observed from the previously published Figures on the bromo acid **85**. However, at the highest concentration (100 μM), **85** relaxed ASM much more, as compared to **87** at all 4 time points measured. This dose demonstrates the C(8)-bromo analog **85** is more potent in the ASM assay than the chloro analog **87.**

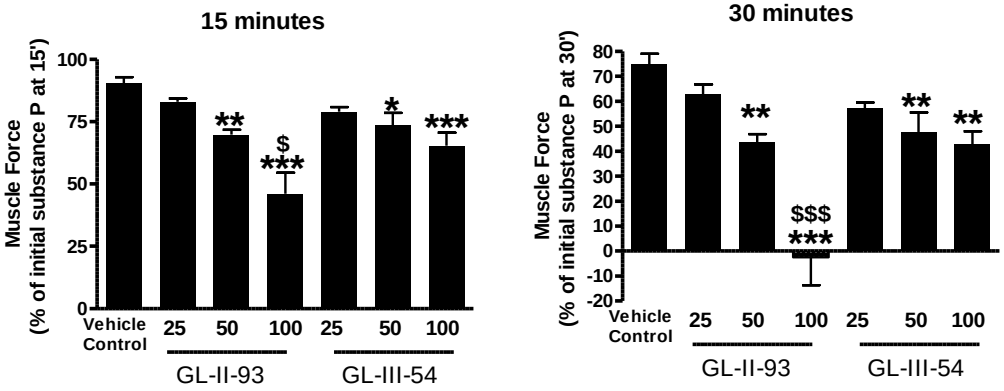

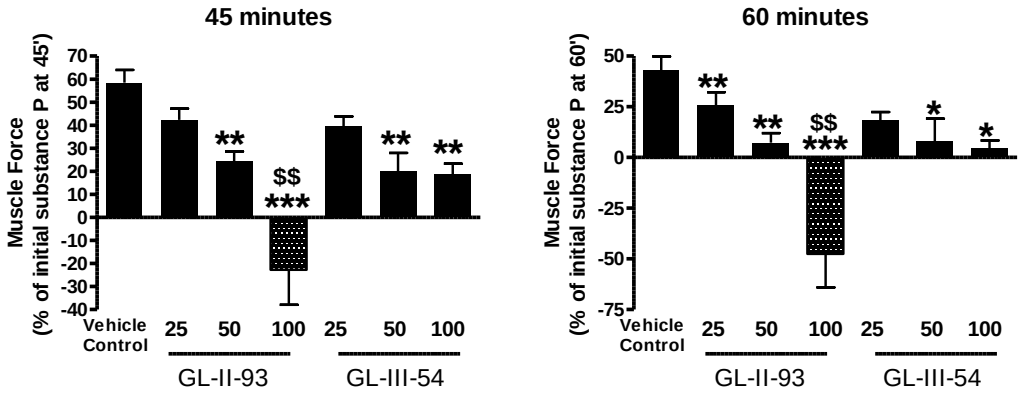

Figure 117. The ASM contractile force in guinea pig tracheal rings contracted with 1uM substance P and then treated with 25, 50 or 100 μM GL-II-93 (85) or GL-III-54 (87) in comparison. Data are expressed as the amount of muscle force remaining at 15, 30, 45 and 60 minutes, as compared to the initial substance P-induced contractile force. *, **, * represented the significance p < 0.05, 0.01, 0.001 as compared to vehicle control (0.1% DMSO), respectively. $, $$, $$$ represents p< 0.05, 0.01, 0.001 compared to 100 μM GL-III-54, respectively. The significance was determined by a two-way ANOVA repeated measures analysis with Bonferroni selected post-test comparisons n = 7 for GL compounds or 14 for vehicle controls.**

2.3.4. Discussion

Current treatments of asthma usually include the β_2-adrenergic agonists and corticosteroids. However, those therapies are either not very effective in some patients due to improper use of inhalers by children and the elderly, or the compounds induce severe adverse effects, which may be exacerbated with overuse or long-term use of the prescribed medications. Based on the discovery of the expression of α4/5-containing $GABA_AR$ subtypes in the lung by Emala et al., the investigation of a novel treatment for asthma with "privileged structure of IMDZ" has been underway for the last few years. This is ample preclinical data which indicate this is a novel and important approach.[57-58, 99, 180-181, 183, 185, 187-189]

The continued study of SH-053-2'F-*R*-CH_3-acid (**68**), the α5-agonist, has shown it exhibited mild ASM relaxation effects on guinea pig tracheal rings *ex vivo* but did not induce any CNS effects due to limited or no penetration of the BBB. Whereas its parent compound, the ethyl

ester **1**, caused mild sedation at higher doses.[185] Moreover, acid **68** demonstrated a good PK profile, as mentioned with nearly no brain distribution and very good metabolic stability. It also protected the mice *in vivo* from MCh induced airway inflammation after a 5-day treatment. The compound did not cause overproduction of mucus.[185]

From the unpublished results, the C(8)-bromo methyl ester MP-III-058 (**84**) demonstrated the most significant ASM relaxation, as compared to all compounds screened, yet the ester function was considered a problem for the molecule could pass through the BBB and trigger CNS effects. In order to keep the desired properties of both **84** and **68**, a new ligand **85** was designed, synthesized and evaluated in several asthma models. The carboxylic acid function was reinstated to prevent penetration through the BBB, while the C(8)-bromo atom was retained to improve the effect on ASM relaxation.

Consequently, the bromo acid **85** exhibited good *in vitro* properties on several parameters, which resulted in evaluation of the ligand in animal models. First of all, the electrophysiological recordings have demonstrated that **85** exhibited good potentiation at $\alpha_{1\text{-}5}$-containing $GABA_AR$ at both 0.1 and 1 μM, and it was slightly more potent at the α4 subtype at 0.1 μM, as compared to the other subtypes.[187] In addition to $GABA_ARs$, it did not bind to other receptors, channels or transport proteins. Importantly, there was no hERG or PBS affinity from the PDSP study (Dr. Roth, North Carolina). Secondly, due to the acid function, **85** was nearly non-detectable in the brain on PK studies, and had good tissue distribution, as well as a relatively long half-life in blood and lung. The low brain fraction indicates that the carboxylic acid function is too hydrophilic to pass across the lipophilic BBB. Examination of the data wherein no motor impairment nor sedation was observed from the rotarod study further confirmed the acid function was critical to avoid CNS side effects. Thirdly, the *in vitro* metabolism data indicated that **85** was metabolically very stable with

more than 90 % remaining after 2 hour-incubation in HLM.[187] Fourth, only 10 % of the original **85** was detected in mouse urine and feces after oral administration daily.[189] Finally, the compound demonstrated a safe cytotoxicity profile with an LD_{50} value higher than 400 μM in both HEK293T and HEPG2 cell lines.

Since bronchoconstriction is one of the essential hallmarks of asthma, GL-II-93 (MIDD0301) **85** was investigated in an ASM contraction model in different species. In an ASM relaxation organ bath assay, **85** exhibited the capacity to alleviate the pre-contracted ASM by substance P (1 μM) in guinea pig tracheal rings in a time-dependent (0 - 60 min) and dose-dependent (0 - 100 μM) manner. With the use of a different clinically relevant agent, histamine, employed for the induction of muscle contraction at 10 μM, and **85** again demonstrated a significant reduction of the muscle force in the same manner as in the substance P induced contraction assay. Additionally, the organ bath assay on human tracheal ASM strips was also conducted with histamine-induced contraction at 10 μM. The bromo acid **85** (100 mg/kg) exhibited a significant reduction of the ASM contraction within 30 min, as compared to the vehicle DMSO. Moreover, acid **85** dilated the lumenal area of the MCh-contracted (100 nM) airway significantly in the *ex vivo* precision-cut lung slice (PCLS) experiments from mouse peripheral airways. In all ASM relaxation assays, **85** was able to mitigate the muscle contraction significantly, regardless of animal species.

Besides the ability to relax bronchoconstriction, the **85** was also evaluated in other asthma models to determine its effects on several clinical features of asthma. First, an oral administration of **85** was able to protect mice from nebulized MCh challenge at an increasing concentration in a dosage-dependent manner, whereas the marketed drug salmeterol failed to do so in the AHR assay.[187] In addition, a similar test was performed, but with nebulized 5 nM **85** and the results

illustrated that **85** reduced the central lung resistance values significantly. After the resistance assay, the concentration of **85** was measured in serum, lung and brain. Examination of the results of **85** indicated high levels of **85** were found only in lung other than serum and brain, and it was rapidly eliminated within 30 minutes with only 30 % remaining.[188] These data expanded the use of **85** for not only can it be administrated as an orally active pill similar to the long-acting β_2 agonists for chronic asthma, but also as an aerosol similar to short-acting β_2 agonists for acute asthmatic attacks. Secondly, besides AHR, airway inflammation is also an important factor in asthma, which usually induces more immune cell over-expression. The acid **85** reduced the population of total immune cell numbers, CD4+ T cells, Siglec F+ cell (eosinophils) as well as F4/80+ cells (macrophages). The reduction of leukocytes was further visualized by EdU with "click chemistry." Thirdly, mucus over-expression is another essential feature of asthma; the 5-day treatment of **85** from 20 mg/kg to 100 mg/kg did not induce a significant change of mucus levels at all dosages. Fourth, **85** was able to decrease the expression of IL-17A, IL-4, and TNF-α, which are important lung cytokines in mice without affecting the expression of IL-10, an anti-inflammatory cytokine.[187]

In addition to the ability to relax contracted ASM and several other anti-asthmatic properties, immunotoxicity studies of **85** for possible off-target immune response reduction or side effects were conducted at 100 mg/kg with a twice-daily dose over a 28-day long-term period in both male and female mice.[189] The acid **85** treatment did not induce a change in animal weights; in organ weights such as the spleen, thymus, or Peyer's patches from the intestine, which have been reported to be reduced by other anti-inflammation drugs.[218] The consumption of **85** twice daily for 28 days did not decrease the systemic immune suppression induced by DNP-specific antibody after quantifying the IgG level. Analysis of the results from immunotoxicity studies

indicated there was no off-target immunotoxicity effects observed when orally administrated twice daily for a 28-day treatment with **85**.

Stability studies indicated that **85** was not stable under acidic conditions such as in the stomach due to the hydrolysis of the [C(6)-N(5)] imine and reached equilibrium rapidly. Subsequently, the open ring hydrochloric salt **90**, which was resulted, would be neutralized under basic conditions to the free imine, and further cylized back to the original form **85** at pH = 5. The higher pH such as the conditions in the intestines would produce the salt form of the **85.** Further investigation of the bioavailability of **85** is ongoing in Dr. Arnold's research group.

Based on the accumulated evidence on **85**, its analog research on analogs is underway as well. By modification of the chirality at the C(4) position, the S-isomer of **85** and the non-chiral analogs were synthesized to explore the role of the chirality in the structure to the anti-asthmatic activity. By changing substituents at the C(8) position, several analogs were made with a different functional group, such as a chlorine atom, a cyclopropyl group, and a hydroxyl group. A carboxylic acid bioisostere was also synthesized by introducing a tetrazole ring at the C(3) position. From the cytotoxicity data, the carboxylic acid bioisosteres are c non-toxic. To date, only two of the new analogs have been evaluated biologically. The C(8)-cyclopropyl analog **86** did not protect the animals from the MCh challenge in the AHR assay. The C(8)-Cl analog **87** was found to have a similar potentiation at α1/2/3/5 $GABA_A$Rs but did not show any efficacy at α4, whereas **85** was slightly more potent at the α4 subtypes at 0.1 μM. However, **87** was predicted to have a similar effect to **85** because a chlorine atom is very similar to a bromine atom. Therefore **87** was tested in the organ bath assay. This ligand exhibited significant ASM relaxation effects, as expected, but **85** exhibited a statistically significant more potent effect than **87** at the highest dose of 100 mg/kg in the newest data.

2.3.5. Conclusion

Taken together, GL-II-93 (**85**) is a novel ligand that acts through $GABA_AR$s, possesses good PK, safety and metabolic stability profiles. It also exhibited significant effects on ASM relaxation irregardless of animal species. It reduced airway hyperresponsiveness and airway inflammation significantly without any binding at the other 48 receptors at PDSP nor demonstrated any off-target detrimental immunotoxicity effects. It did not interact with PBR nor hERG receptors, which is very important. The QT issues in the heart should be minimized and cholesterol transport unaffected. All this evidence supports the identification of GL-II-93 (**85**) as a potential treatment for asthma for administration both as an orally active (pill) or as a constituent in an aerosol. Most importantly, there was little or none acid **85** in the brain due to the lack of BBB penetration. Therefore, it provides an asthma drug candidate without any CNS side effects observed, to date. The synthesis of **85** has been modified and presented to GMP companies, such as Alcami Corporation. Further evaluation of **85**, such as a Phase I/II metabolism studies, is ongoing, as well as analog optimization studies with the aid of molecular modeling programs. This ligand GL-II-93 (**85**) provides a potential novel treatment of asthma, which can be applied by both the oral route and as an aerosol without inducing any CNS side effects.

2.3.6. Methods

2.3.6.1. ASM Relaxation of SH-053-2'F-R-CH3-acid (Dr. Emala, Columbia University)[99]

These experiments were carried out by Dr. Emala's research group, Columbia University. All studies were run after approval of the Columbia University IACUC. Adult male Hartley guinea pigs were euthanized by i.p. injection of 100 mg/kg of pentobarbital. The tracheas with 2 cartilage rings were removed and transected, which was followed by rinsing for 1 h with 5 buffer exchanges to remove any remaining pentobarbital. A cotton swab was used to remove the epithelium, after which a 4 mL jacketed organ bath (Radnoti Glass Technology) was used to suspend the strips. One of the strips was attached to a stationary hook, and the other one was linked to an FT-03 force transducer (Grass-Telefactor, West Warwick, RI), and Acqknowledge 7.3.3 software (Biopac Systems, Goleta, CA) was used to couple it to the computer. The tracheal rings were bathed in 4 mL of KH buffer solution with the following compositions (in mM): 5.6 KCl, 1.3 NaH_2PO_4, 118 NaCl, 0.2 $MgSO_4$, 0.5 $CaCl_2$, 25 $NaHCO_3$, 5.6 D-glucose) with 10 μM indomethacin (DMSO vehicle final concentration of 0.01 %), which had 5% CO_2 and 95% O_2 at pH 7.4, and at 37 °C bubbled in continuously. The tracheal rings were equilibrated at 1 g of isotonic tension for 1 h with the addition of new KH buffer every 15 min. All tracheal rings were precontracted with 10 μM N-vanillylnonanamide and then two cycles of cumulatively increasing concentrations of ACh (0.1−100 μM) with a buffer wash extensively between and after the two cycles with 1.0 g of the resting tension. Pyrilamine (10 μM) and tetrodotoxin (1 μM) were then added to the buffer in the baths in order to eliminate the effects of airway nerves and histamine receptors. Once a stable peak line at 1.0 g resting tension was achieved, 1 μM of substance P was used to induce the contraction of the tracheal ring. After a stable contraction was established, the compound or vehicle (0.1% DMSO) was added to the organ bath mixture. After the exposure of compound, the percentage of

initial contractile force remaining at specific time points was obtained as compared to a percentage of the remaining force in tissues with the vehicle.

In other human ASM, strips were also dissected from the human trachea, which was obtained from lung transplantations incidentally from healthy donor lungs. The Columbia University IRB has reviewed the study protocol and confirmed it is not human subject research. ASM strips were suspended in organ baths, as described above in KH buffer, which was oxygenated at 37 °C, and reached 1.5 g of resting tension. The buffer exchanges were conducted for 1 h to reach equilibration at every 15 min, after which then the ASM strips were contracted by an increasing concentration of ACh (100 nM - 1 mM) for 3 cycles, which was followed by buffer exchanges extensively between and after these pre-contractions. The buffer was added with pyrilamine (10 μM), tetrodotoxin (1 μM) and MK571 (10 μM) before the contraction of each strip to calculate the EC_{50} concentration of ACh. Once a stable contractile force was established at 15 min, the buffer was added with 100 μM of a compound or the vehicle (0.2% ethanol), and the stable contractile force was measured over 1h continuously. The remaining contractile force at different time points 15, 30, 45 and 60 min was reported as a percentage of the initial ACh-mediated contractile force.

2.3.6.2. Evaluation of AHR of SH-053-2'F-*R*-CH_3-acid (Dr. Gloria Forkuo, UWM)[99]

These experiments were carried out by Gloria Forkuo from Dr. Arnold's research group, at UWM. The DSI's Buxco FinePointe Non-Invasive Airway Mechanics instrument was used to measure the AHR to MCh in conscious, spontaneously breathing mice. Before measurements, mice were trained to climb the chambers daily for 15 min for 5 days. Before data collection, the calibration of the chamber was conducted at each time. Briefly, a combination of the thoracic chamber and

the nasal chamber provides the computation of sRaw. The sRaw value was calculated by the FinePointe software with additional ventilatory parameters by the NAM analyzer. Mice were exposed to nebulized PBS (baseline), or MCh (1.5625 − 12.5 mg/mL) for 1 min. The readings were recorded and the average was calculated for 3 min for nebulization. Data were expressed as sRaw versus the MCh concentration (mg/mL), which was used to produce the aerosol.

2.3.6.3. Pharmacokinetic Study of SH-053-2'F-*R*-CH_3-acid (Revathi Kodali, UWM)[99]

These experiments were carried out by Revathi Kodali from Dr. Arnold's research group, at UWM. The Swiss Webster female mice received the test compound or vehicle in 2.5 % polyethylene glycol and 2% hydroxypropyl methylcellulose solution at 25 mg/kg by intragastric gavage. At each time point 10, 20, 40, 60, 120, 240 and 480 minutes, four mice were sacrificed by CO_2 anesthesia and this was followed by cervical dislocation. Blood was collected into heparinized tubes, whereas lungs and brain were obtained as well by disection. Liquid nitrogen was used to store the samples until analysis.

The sample preparation and LC/MS: Blood samples were thawed on ice, then vortexed for 10 s. A 100 μL sample was added to ACN (400 μL) and mixed with Hz-166 (100 nM) as an internal standard. The samples were vortexed for 30 s and then centrifuged for 10 min at 12,000 x g. The clean tubes were used for transferring the supernatant. The mixture, which resulted, was then concentrated by using a Speedvac concentrator. The residue was added to 400 μL of mobile phase solution and 0.22 μm nylon centrifugal filter units (Costar) were used for the required spin-filtration. After reconstitution, the samples were diluted properly, followed by addition of the verapamil control, then the injection of 5 μL the sample was performed into the LC-MS/MS. After

the brain and lung tissue samples were thawed, weighed, and homogenized by a Cole Palmer LabGen 7B Homogenizer, and they were added separately to a 400 μL ACN solution containing then internal standard. All samples were centrifuged at 12,000 x g for 10 min. The supernatant was recovered, and the sample preparation for LC-MS/MS analysis was the same protocol employed for the blood samples.

The high-performance liquid chromatography (HPLC) was conducted with a Shimadzu Nexera X2 LC30AD series pump (Shimadzu, Kyoto, Japan). Analytes were separated by a C18 column (2.1 mm × 100 mm, 5 um particle size, Restek, California, US) under a gradient elution at a flow rate of 0.4 mL/min for the compound. The ACN and water (both containing 0.1% formic acid) were used as the mobile phase. The time program followed in this order: 20 % B → 70 % B (3 min) → 99 % B (5 min), held at 99 % B (8 min), return to 10 % B (9 min), held (9.5 min) and 70 % B → 70 % B (6 min), and the column temperature was at 40 °C.

A Shimadzu 8040 triple quadrupole mass analyzer (Shimadzu, Kyoto, Japan) was used to monitor the analytes with electrospray; moreover, atmospheric pressure ionization runs were done in dual (DUIS) mode under the positive mode. A multiple reaction monitoring (MRM) mode was applied for monitoring the following transitions. The transition ion pairs for SH-053-2'F-*R*-CH_3-acid are at m/z 360.0 > m/z 342.10, m/z 360.0 > m/z 316.00, m/z 360.0 > m/z 301.10, m/z 360.0 > m/z 249.05, and m/z 360.0 > m/z 219.90. Hz-166 transition pairs are as follows: m/z 356.90 > m/z 311.15, m/z 356.90 > m/z 283.15, and m/z 356.90 > m/z 282.15. The transition pairs for verapamil were m/z 454.70 > m/z 165.05, m/z 454.70 > m/z 150, as well as m/z 454.70 > m/z 303.0. The optimal sensitivity was obtained by the optimization of the collision energy for each transition. The operation conditions of the mass spectrometer were at the heat block temperature of 400°C,

with a 15 L/min drying gas flow, with 250 °C as the desolvation line temperature, a 1.5 L/min nebulizing gas flow, and 4.5 kV for both needle and interface voltages. LabSolutions software was used to perform the response acquisition. A linear regression analysis was used to fit the standard curve, and the calibration curve was used to calculate the validation samples of that day. The calculation of the mean and the coefficient of variance was conducted accordingly. A comparison of calculated concentrations to the corresponding nominal was performed for the accuracy. PK solutions software 2.0 was used for the calculation of pharmacokinetic parameters and the calculation was fitted to the equation as following: c = A•e-at + B•e-bt + C•e-ct.

2.3.6.4. The Rotarod Study of SH-053-2'F-*R*-CH_3-acid (Revathi Kodali, Nick Zahn, and Alec Huber, UWM)[99]

These experiments were carried out by Revathi Kodali, Nick Zahn, and Alec Huber from Dr. Arnold's research group, at UWM. The Swiss Webster mice were trained to stay on the rotarod apparatus (Omnitech Electronics Inc., Nova Scotia, Canada) at a steady speed of 15 rpm in order to maintain balance until the mice performance was achieved for 3 min at 3 different time points. The 100 mg/kg test compounds or the vehicle (2.5% polyethylene glycol and 2% hydroxypropyl methylcellulose in about 200 μL) were administrated orally to groups of 9 mice. An i.p. injection of 5 mg/kg diazepam as a positive control was given in a solution of 40% propylene glycol, 50% PBS, and 10% DMSO. After the drugs were administrated, the mice were put on a rotarod apparatus at 3 time points of 10, 30, and 60 min separately. Briefly, if the mouse fell off the rotarod twice within 3 min, this was considered as a failure and was recorded for that time point. If the mice fell off the rotarod for one fall, this was considered not significant. One fall was common

after injection of vehicle. After 2 or 3 days of resting time, mice were then used to perform another rotarod test for a different test compound.

2.3.6.5. Patch Clamp Studies of GL-II-93 (Dr. Fisher, University of South Carolina School of Medicine)[187]

These experiments were carried out by Dr. Janet Fisher's research group, University of South Carolina School of Medicine. The human embryonic kidney HEK-293T cell line (GenHunter, Nashville, TN) was used for the transfection of full-length cDNAs for $GABA_AR$ subunits (generously provided by Dr. Robert Macdonald, Vanderbilt University and D David Weiss, University of Texas Health Science Center, San Antonio, TX) in mammalian expression vectors. All of the $GABA_AR$ subtypes were cloned in rat except for a human clone at α2 subtypes. The solution for cell maintenance conditions was 100 μg/mL streptomycin, 100 IU/mL penicillin, 10% fetal bovine serum and Dulbecco's modified Eagle's medium (DMEM). The calcium phosphate precipitation was used to perform the transient transfection of HEK-293T cells. A 1:1:1 ratio (α:β:γ) of 2 μg each of cDNAs was used for the cells, which received plasmids encoding $GABA_AR$ subtype cDNAs. A 1 μg of the plasmid pHook-1 (Invitrogen Life Technologies, Grand Island NY), which contained cDNA encoding the surface antibody sFv, was also used for the cell transfection in order to identify positively transfected cells. A 15% glycerol solution in PBS buffer [(50 mM BES(N,N-bis[2- hydroxyethyl]-2-aminoethanesulfonic acid), 280 mM NaCl, 1.5 mM Na_2HPO_4)] was added to the cells for 30 s after an incubation for 4 to 6 h at 3% CO_2. The pHook expression was conducted with the selection procedure after 18−52 h with 3−5 μL of magnetic beads, which were coated with antigen. These were used for the cell pass and mixture for 0.5 to 1 h for the pHook antibody with approximately 6 × 105 beads. A magnetic stand was used to isolate the bead-

coated cells. The supplemented DMEM was used to resuspend the selected cells, which were plated onto glass coverslips. The collagen was applied for recordings on the next day as well as poly L-lysine. The whole-cell recording configuration was used for the cell patch clamp at −50 mV. The bath solution contained the reagents as following (in mM): 6 $MgCl_2$, 1 $CaCl_2$, 8.1 KCl, and 142 NaCl, 10 HEPES [4-(2-hydroxyethyl)-1-piperazineethanesulfonic acid] at pH = 7.4 and 295−305 mOsm for osmolarity. A solution that contains (in mM) 10 HEPES, 1 $MgCl_2$, 153 KCl, and 5 K-EGTA (ethylene glycol-bis(β- aminoethyl ether N, N, N′, N′-tetraacetate), was used to fill the recording electrodes at pH = 7.4 and 295−305 mOsm for osmolarity. The frozen stocks in water or the freshly made bath solution was used for the dilution of GABA. The DMSO or diluted bath solution with the highest DMSO level of 0.01 % of cells, was used to dissolve the test compound. A two-stage puller (Narishige, Japan) was applied to pull the patch pipettes from borosilicate glass (World Precision Instruments, Sarasota, FL) with 5−10 MΩ of resistance. A computer-driven stepper motor (SF-77B, Harvard Apparatus, Holliston, MA, open tip exchange time of <50 ms) was applied to control the 3-barrelled solution delivery device for 5 s with the solutions containing GABA or GABA plus test compounds. A continuous flow of external solution was applied through the chamber. An Axon 200B (Foster City, CA) patch clamp amplifier was used to record the currents. The Prism (GraphPad, San Diego, CA) and programs Clampfit (pClamp9 suite, Axon Instruments, Foster City, CA) were applied for analyzing the whole cell currents.

2.3.6.6. Pharmacokinetic Study of GL-II-93 (Dr. Arnold, UWM)[187]

Refer to Section 2.3.6.3 for details.

2.3.6.7. Liver Microsomal Stability Study of GL-II-93 (Revathi Kodali, UWM)[187]

These experiments were carried out by Revathi Kodali from Dr. Arnold's research group, at UWM. A digital dry bath, which was able to shake and heat (Fischer Scientific, Pittsburgh, PA) was used for the pre-incubation of 4 µL of 1 mM test compound at 10 µM as the final concentration in DMSO at 37 °C for 5 min. This process was carried out in a total volume of 391.2 µL mixture, which contained 80 µL of phosphate buffer (0.5 M, pH 7.4), 20 µl of NADPH Regenerating System Solution A and 4 µL of NADPH Regenerating System Solution B (BD Bioscience, an Jose, CA), as well as water (282 µL). 8.8 µL of MLMs (Life technologies, Rockford, IL) or 8.8 µL of HLMs (BD Gentest, San Jose, CA) was added to the preincubation mixture, at a protein concentration of 0.5 mg/mL, to initiate the reaction. The time intervals at 0 (without microsomes), 10, 20, 40, 60, 90 and 120 min was the time point for taking 50 µL aliquots. A cold ACN solution (100 µL) containing 3 µM of 4,5-diphenylimidazole as an internal standard was used for the addition of each aliquot. After the addition, the mixture was sonicated for 10 seconds and then centrifuged for 5 min at 10,000 rpm. The Spin-X HPLC filter tubes (Corning Incorporated, NY) were employed for transferring the 100 µL of the supernatant layer, after which the tubes were centrifuged for 5 min at 13,000 rpm. A 100 fold dilution was carried out for the filtrate, and the mixture was analyzed by LC-MS/MS (Shimadzu LCMS 8040 instrument) subsequently. The calculation of the ratio of the peak areas of test compound and the internal standard was carried out at every time point, and the linear slope (k) was determined by plotting the natural log of the ratio against time. The calculation of the half-life (0.693/k), metabolic rate ($k*C_0/C$), as well as the internal clearance (V*k) were carried out, where V is the volume of incubation in µL per microsomal protein in mg, C is the concentration of microsomes, k is the slope, and C_0 is the initial

concentration of test compound. All experiments were carried out on two independent days and were repeated for three times to reach statistical significance.

2.3.6.8. Evaluation of Mouse Plasma Binding of GL-II-93 (M. S. Rashid Roni, UWM)[187]

These experiments were carried out by M. S. Rashid Roni from Dr. Arnold's research group, UWM. The 500 nM of 4,5-diphenylimidazole and 1 mM MIDD0301(GL-II-93) were added in the tube in methanol. An Eppendorf tube was used to dispense the 495 μL of thawed mouse plasma with 5 μL of 1 mM GL-II-93. A rapid equilibrium dialysis device (Thermo Scientific) which contained a marked red retainer well was used for transferring 400 μL of the previous solution, and this was followed by the addition of 600 μL of PBS buffer in the adjacent buffer chamber, which was repeated for 3 times at different wells in the plate. The sealed plate was placed onto a shaker for 4 h at 250 rpm. An Eppendorf tube was used to transfer the 50 μL of the sample from the red well combined with 50 μL PBS. The proteins were precipitated after the addition of 300 μL of cold methanol, which was then vortexed and incubated 30 minutes on ice, then centrifuged at 10000 rpm for 10 min. To a new tube, 50 μL of supernatant combined with 25 μL of a 500 nM 4,5-diphenyl imidazole solution, as internal standard, and 425 μL of methanol was added. A Shimadzu 8040 instrument was used for the LCMS/MS analysis of samples. A calibration curve was applied for quantification. Three experiments were repeated for statistical analysis.

2.3.6.9. Quantification of GL-II-93 by LCMS/MS (M. S. Rashid Roni, UWM)[189]

These experiments were carried out by M. S. Rashid Roni from Dr. Arnold's research group, at UWM. Urine collection: After feeding, the mouse was hung vertically by gently grasp on the back

of the neck of GL-II-93 treated mouse. Beneath the penis or female urethral orifice, a collection tube was placed to collect 50-100 μL urine without compulsion, which was used as a standard method for collecting urine after compound dosing. A solution containing 100 μL of urine, 400 μL methanol and SH-053-2'F-*R*-CH_3-acid as an internal standard was used for the quantification of GL-II-93. The solution was then centrifuged for 10 min at 10,000 x g. The solvent of the supernatant sample was removed and evaporated(speedvac). The solid, which was obtained, was added to a solution of 400 μL of methanol and 4,5-diphenyl imidazole as a second internal standard; and a 0.22 μm nylon centrifugal filter unit (Costar) was used to filter off the solid. LCMS/MS was applied on the liquid for the quantification of GL-II-93. Faeces collection: From the bedding, the expressed faecal pellets were collected on the last dosing day, and any adherent wood bedding shavings were removed after collection. After combining the faecal samples from each cage housing a mouse with GL-II-93 treatment, the sample was dried overnight under vacuum (15 torrs). The 100 mg of dried faeces was pulverized and combined with 400 μL methanol with SH-053-2'F-R-CH3-acid as an internal standard, and the same protocol for urine samples was employed for quantification of GL-II-93 in the faeces sample.

2.3.6.10. Rotarod Assay of GL-II-93 (Dr. Arnold, UWM)[187]

Refer to Section 2.3.6.4 for details.

2.3.6.11. Cytotoxicity Study of GL-II-93 (Dr. Michael R. Stephen, UWM)

These experiments were carried out by Dr. Michael R. Stephen from Dr. Cook's research group, at UWM. The human embryonic kidney 293T (HEK293T) and human liver hepatocellular

carcinoma (HEPG2) cell lines were purchased (ATCC) and cultured in 75 cm2 flasks (CellStar). A DMEM/High Glucose (Hyclone, #SH3024301) media was used for cell growth. In addition, 5 x 106 units of penicillin and streptomycin (Hyclone, #SV30010), 10 mM HEPES (Hyclone, #SH302237.01), 10% of heat-inactivated fetal bovine serum (Gibco, #10082147) and non-essential amino acids (Hyclone, #SH30238.01) were added to the media. Then 0.05% Trypsin (Hyclone, #SH3023601) was used to harvest the cells, and this was followed by PBS washing. A sterile white, optical bottom 384-well plate (NUNC, #142762) was used for dispensing the washed cells. After 2 h, a Tecan Freedom EVO liquid handling system, which was equipped with a 100 nL pin tool (V&P Scientific), was used for transferring the solution, which contained the compound. Then DMSO was used as a negative control, whereas the positive control was 3-dibutylamino-1-(4-hexyl-phenyl)-propan-1-one (25 mM in DMSO, positive control). After 48 h-incubation, the cells were tested on CellTiter-Glo™ (Promega, Madison, WI). A Tecan Infinite M1000 plate reader was applied for luminescence readings. The assay was performed in quadruplet with three repeats. The results were normalized to the control value, and GraphPad Prism was used for the nonlinear regression analysis.

2.3.6.12. *Ex Vivo* Guinea Pig Tracheal Ring Organ Bath Induced by Substance P (Dr. Emala, Columbia University)[188]

Refer to Section 2.3.6.1 for details.

2.3.6.13. *Ex Vivo* Guinea Pig Tracheal Ring Organ Bath with Histamine (Dr. Emala, Columbia University)[188]

These experiments were carried out by Dr. Emala's research group, at Columbia University. The guinea pigs were anesthetized by i.p. injection of 100 mg/kg pentobarbital. After removing the trachea, eight similar segments, which consisted of 2 cartilaginous rings were transected from each trachea under a dissecting microscope. The epithelium was denuded with a cotton swab from these segments, water jacketed (37°C) organ baths (Radnoti Glass Technology, Monrovia, CA) were used to suspend the two strings. One of them was attached to a stationary hook, and the other one was linked to an FT-03 force transducer (Grass-Telefactor, West Warwick, RI), and an Acqknowledge 7.3.3 software (Biopac Systems, Goleta, CA) was used to couple the computer to the transducer. The tracheal rings were bathed in 4 mL of KH buffer solution with the following composition (in mM): 5.6 KCl, 1.3 NaH_2PO_4, 118 NaCl, 0.2 $MgSO_4$, 0.5 $CaCl_2$, 25 $NaHCO_3$, 5.6 D-glucose) with 10 μM indomethacin (DMSO vehicle final concentration of 0.01 %). Then 5% CO_2 and 95% O_2 at pH 7.4, and at 37 °C was bubbled into the solution continuously. The tracheal rings were equilibrated at 1 g of isotonic tension for 1 h with the addition of new KH buffer at every 15 min before the assay.

Capsaicin (10 μM) was added to the buffer in the baths in order to eliminate the airway neural contribution to the effect of the contraction of ASM. All tracheal rings were contracted with two cycles of cumulatively increasing concentrations of ACh (0.1 μM - 0.1 mM) for the determination of the EC50 of each tracheal ring with the 6 KH buffer wash extensively to achieve 1.0 g of resting tension. In addition, 10 μM pyrilamine as an anti-histamine, 10 μM indomethacin as the inhibitor of prostaglandin synthesis, as well as 1 μM tetrodotoxin to inhibit neural transmission were added to the buffer to limit the interference factors.

Then 10 μM histamine was used to induce the contraction of the tracheal rings. After a stable contraction was established, 100 μM compound or vehicle (0.1% DMSO) was added to the organ

bath mixture, and the contractile force was monitored and recorded. The relaxation effect of tracheas treated with GL-II-93 and those treated with a vehicle on the rings at 15, 30, and 45 min were compared.

2.3.6.14. *Ex Vivo* Human Tracheal Airway Smooth Muscle Strip Organ Bath (Dr. Emala, Columbia University)[188]

These experiments were carried out by Dr. Emala's research group, at Columbia University. The ASM from human trachea was dissected into strips, and the epithelium was removed, and this was followed by suspending the strips in the organ bath as described above. However, 1.5 g was set as the resting tension. The determination of the ACh EC50 was carried out for each ASM strip. Also, 10 μM indomethacin, 10 μM MK571 as a leukotriene D4 receptor inverse agonist and 1 μM tetrodotoxin were added to the buffer to limit the interference factors. The10 μM histamine was used to induce the contraction of the tracheal rings. After the stable contraction was established, 100 μM compound or vehicle (0.1% DMSO) was added to the organ bath mixture, and the contractile force was monitored and recorded. The relaxation effect of GL-II-93 treated strips and vehicle-treated strips on the rings at 15, 30, and 45 min was compared.

2.3.6.15. *Ex Vivo* Mouse Precision-Cut Lung Slice Experiments (Dr. Emala, Columbia University)[188]

These experiments were carried out by Dr. Emala's research group, at Columbia University. The male A/J mice were euthanized, their thoracic cavities opened, and warm 2% agarose was used to inflate the lungs. The agarose was allowed to cool for 20 min at 4°C, and then the lungs were

harvested and immersed in ice-cold Hanks' balanced salt solution (HBSS) for 15 min. A 6% gelatin was employed to form a block, which was used to fully cover up the separated lung lobes. A vibratome (VF-300; Precision Instruments, Greenville, NC, USA) was used for dissecting the block into serial 130 μm sections. The overnight incubation of the lung slices, which contained a small peripheral airway was conducted in a solution that consisted of penicillin, low-glucose Dulbecco's modified Eagle's medium, L-glutamine, 1×antibiotic solution, and streptomycin (Thermo Fisher Scientific, Waltham, MA) with 10% CO_2 at 37 °C. The airway with a lumen diameter of 100–300 μm airways, which contained active (beating) ciliated epithelial cells were used as lung slices for the experiment. A custom-made perfusion chamber was applied for mounting the lung slices, and a 10X objective was used for visualization of the peripheral airways. During imaging at rt, the HBSS containing Hepes (20 mM) was used for slice superfusion at pH = 7.4. A charge-coupled device camera (KP-M1A; Hitachi), with a frame grabber (Piccolo; Euresys), and image-acquisition software (Video Savant; IO Industries) was employed for the digital image recording. The 100 nM MCh superfused in HBSS was used to induce airway contractions. Once a stable contraction was achieved, 100 μM GL-II-93 was added to the buffer in the continuous presence of MCh where PCLS were exposed. Each recorded image was used for the calculation of the lumenal area by using custom-written macros and normalization of the area before stimulation with MCh.

2.3.6.16. Evaluation of GL-II-93 on AHR (Dr. Gloria Forkuo, UWM)[187]

Refer to Section 2.3.6.2 for details.

2.3.6.17. Evaluation of *In Vivo* Mouse Airway Resistance (Dr. Emala, Columbia University)[188]

These experiments were carried out by Dr. Emala's research group, at Columbia University. The mice were anesthetized with pentobarbital, and this was followed by paralysis by i.p. injection of 10 mg/kg succinylcholine. A tracheostomy (tidal volume 10 mg/kg, 150 breaths/min, positive end-expiratory pressure 3 mmHg) was utilized to ventilate mice mechanically. Then nebulized vehicle (25% ethanol in PBS) or 5 mM GL-II-93 (10-sec nebulization, 50% duty cycle; ~25 μL delivered) was administrated to the mice 10 min before the central lung resistance measurement. This process was conducted by the forced oscillatory technique during the challenge from the increasing nebulized concentration of MCh (0-25 mg/ml). The temperature was monitored, as well as EKG, during the experiment. An average of 3 measurements were required to determine the resistance values for each mouse at each MCh dose.

After following the *in vivo* airway resistance experiment, the GL-II-93-treated mice were utilized for PK studies by a collection of the lung, brain and serum samples after 30 min of administration. The samples of serum were frozen at -20 ºC in a freezer and liquid nitrogen was used to snap freeze the samples from lung and brain. Then LCMS/MS was applied to determine the tissue concentration of GL-II-93.

2.3.6.18. Quantification of Airway Inflammatory Cells (Dr. Gloria Forkuo, UWM)[187]

These experiments were carried out by Gloria Forkuo from Dr. Arnold's research group, at UWM. The 1 mL of Ca^{2+} and Mg^{2+} free PBS was used as a solution to perform the bronchoalveolar lavage (BAL) on BALB/c mice. BD red blood cell lysis buffer (BD Pharmingen, San Jose, CA) was used

for the red blood cells lysis. Then 4 different tubes were utilized for BALF split, and 6 μg/mL of 2.4G2 mouse BD Fc Block (BD Pharmingen, San Jose, CA) was used to block the nonspecific binding to Fc receptors for 5 min. At this point, 100 μL of BSA stain buffer (BD Pharmingen, San Jose, CA) was applied for BALF cell staining at 4 °C for 30 min. The final concentrations of the following antibodies were contained in the buffer: FITC rat antimouse CD4 (1:500, RM4−5, BD Pharmingen, San Jose, CA), PE rat anti-mouse Siglec-F (1:500, E50-2440, BD Pharmingen, San Jose, CA), anti-mouse CD45 APC (1:1000, 30-F11, Affymetrix eBiosciences, San Diego, CA), and FITC anti-mouse F4/80 (1:200, M1/70 Affymetrix eBiosciences, San Diego, CA). The BD FACS Calibur (BD Pharmingen, San Jose, CA) was utilized for the flow cytometric studies. The live/dead propidium iodide viability stain (BD Pharmingen, San Jose, CA) was applied to exclude the dead cells. Now quest pro software (BD Pharmingen, San Jose, CA) was applied to analyze the data. All samples were run on high (60 μL/min) for 180 s to obtain the total inflammatory cell count. The calculation of the total inflammatory cell count as cells/mL was conducted by the gated anti-mouse CD45 positive events in the fourth channel (FL4). The differential cell populations were calculated from the multiplication of the total inflammatory cell count (cells/mL) with the frequencies of Siglec-F+ F4/80+, and CD4+cell populations.

2.3.6.19. EdU Staining (Dr. Gloria Forkuo, UWM)[187]

These experiments were carried out by Gloria Forkuo from Dr. Arnold's research group, at UWM. Before ketamine/xylazine overdose, a single i.p. injection of 100 mg/kg EdU (Invitrogen, Carlsbad, CA) was administrated to mice in separate treatment groups: 100 mg/kg GL-II-93 and vehicle-treated ova s/c mice. After the injection for 4 h, mice were euthanized, and lungs were removed, fixed in formalin, and embedded with paraffin. The Fisher Superfrost Plus Slides were employed

for mounting of the 6 μm lung sections. A Click-iT EdU imaging kit (Invitrogen, Carlsbad, CA) was applied for the EdU staining and followed the manufacturer's instructions. The deparaffinization of lungs was conducted in Histoclear, and graded ethanol was used for rehydration. Then 3% BSA (bovine serum albumin) in PBS was used to wash the tissue sections twice, and 0.5% Triton X-100 in PBS was further used to rinse the tissue for 20 min. The 3 % BSA in PBS was used for rinsing the permeabilized tissue slices twice, which was then incubated in the dark for 30 min with a Click-iT reaction cocktail that consisted of Alexa Fluor 488 azide, copper sulfate, and Click-iT reaction buffer. Then 3% BSA in PBS was used for the tissue slides after the previous step. The PBS wash was carried out once for the tissue slices, and 5 μg/mL Hoechst 33342 was used for incubation for 30 min which to stain the DNA. The sections were rinsed with PBS twice, and Permount mounting media was used for coverslipping. All these steps were performed at ambient temperature.

2.3.6.20. Histopathological Analysis of Lung Sections (Dr. Gloria Forkuo, UWM)[187]

These experiments were carried out by Gloria Forkuo from Dr. Arnold's research group, at UWM. After the collection of BALF using a tracheal cannula, 10% neutral buffered cold formalin was used for the lung perfusion. A suture was used to close the trachea which was removed from the mice and was further fixed at 4 °C for 2 days. The left lobe of the lung was dissected in cross-section, then the dehydration, paraffin embedding, and sectioning were carried out for the prepared samples. The 6 μm slices were placed onto a positively charged glass, and this was followed by Histoclear dewaxing. An ethanol/water mixture was used to rehydrate the slides. Then periodic acid (1%) was used to conduct oxidation, which was incubated for 20 min with fluorescent Schiff's reagent. The coverslip was washed by water then acidic alcohol by methyl salicylate and Canada

Balsam. A fluorescence microscope (EVOS, Invitrogen) was applied to stain slides. ImageJ software was used to analyze the quantification of the mucin volume density, which was determined by measuring the relationship between the stained area of glycoprotein and the length of the membrane basement. The same magnification scale was applied to all images.

2.3.6.21. Expression of Cytokines (Dr. Gloria Forkuo, UWM)[187]

These experiments were carried out by Gloria Forkuo from Dr. Arnold's research group, at UWM. The lungs of the BALB/c mouse were removed and frozen in liquid nitrogen and stored at −80 °C in the freezer until cytokine analysis. A 200 μL T-PER tissue protein extraction reagent (Thermo Fisher Scientific Inc., Rockford, IL) with 1× protease inhibitor cocktail was used for the whole lung homogenization by a hand-held tissue homogenizer. They were centrifuged for 5 min at 10,000 rpm and then transferred to pellet cell/tissue debris. A BD cytometric bead array mouse Th1/Th2/Th17 cytokine kit (BD Biosciences, San Jose, CA) was applied for the collection of tissue supernatant for further cytokine analysis using the manufacturer's instructions. A CELLQuest and FCAP Array Software (BD Bioscience, San Jose, CA), as well as FACSCalibur (BD Bioscience, San Jose, CA) flow cytometry, was applied for sample analysis. The fluorescence intensities were presented for individual cytokine concentrations.

2.3.6.22. The 28-Day Immunotoxicity Study of GL-II-93 (Nick Zahn, UWM)[189]

These experiments were carried out by Nick Zahn from Dr. Arnold's research group, at UWM. Specific pathogen-free conditions and standard conditions of humidity and temperature were applied for housing both the 8- and 6-week old male and female Swiss Webster mice (Charles

River Laboratory). The mice had free access to water and food under controlled 12-hr light and dark cycle. The University of Wisconsin−Milwaukee Institutional Animal Care and Use Committee (IACUC) had approved all animal experiments.

Oral gavage: the mice received an oral gavage administration of 0.2 ml of GL-II-93 in a 2.5% polyethylene glycol (Sigma-Aldrich, St. Louis, MO, USA) and 2% hydroxypropylmethylcellulose solution (Sigma-Aldrich, St. Louis, MO, USA) with 20G gavage needles (Kent Scientific Corporation, Torrington CT, USA) twice daily for 7 days. The formulation of a dose of 100 mg/kg GL-II-93 was prepared with 100 mg of peanut butter. Morever, 100 mg of peanut butter with or without 100 mg of the compound was put in separate boxes for mice to consume this in the boxes which were outside of their homecages every other day. The mice stayed in the boxes while consuming the peanut butter and test compound; once they finished the treatment after 30 min, they returned to their home cages.

2.3.6.23. Effect of GL-II-93 on DNP-KLH Immunization (Nick Zahn, UWM)[189]

These experiments were carried out by Nick Zahn from Dr. Arnold's research group, UWM. The 100 mg of solid DNP-KLH (Sigma, 324121-100 mg) was used to prepare the 1 mg/mL DNP-KLH aqueous solution. To a mixture with 7.5 ml of a 40 mg/mL $Al(OH)_3$ suspension (Thermo, Imject Alum 77161), 7.5 mL of the previously made solution was added. The immunization was carried out on days 1 and 21 by i.p. injection with 100 μL of this solution (50 μg DNP-KLH and 2 mg $Al(OH)_3$) in mice

2.3.6.24. Study of GL-II-93 on Lymphoid Organs and Peyer's Patches (Nick Zahn, UWM)[189]

These experiments were carried out by Nick Zahn from Dr. Arnold's research group, at UWM. Here CO_2 asphyxiation was used for euthanizing the mice, which was followed by cervical dislocation and the blood withdrawn by cardiac puncture. The EDTA was used for the analysis of blood cells and platelets with half of the collected blood. For DNP-specific IgG ELISA, the other half of the blood was coagulated at rt and centrifuged at 2,000 rpm for 10 min. A 10 % neutral buffered formalin was used for fixing the spleen and thymus, which had been removed from animals overnight at 4°C. After gross pathology, the organs were washed with water for three times and then stored in 70% ethanol. The small intestine section was removed, and this was followed by washing with water by a syringe, after which the clean intestine was further washed with a solution containing 7% (vol/vol) acetic acid/PBS, and the lumen was rinsed by a syringe. The Peyer's patches turned white after 5 min, and the visual examination was conducted.

2.3.6.25. The experiment of H&E-Staining (Wisconsin Children's Research Institute)[189]

The Wisconsin Children's Research Institute conducted the histology processing experiment, which included embedding, slicing, drying, as well as H&E staining. At the indicated magnification, light microscopy was applied for the visualization of the representative sections.

2.3.6.26. DNP IgG Quantification (Nick Zahn, UWM)[189]

These experiments were carried out by Nick Zahn from Dr. Arnold's research group, UWM. ELISA was applied for the quantification of DNP IgG, which used DNP coated wells (Kamiya Biomedical Company #KT-672). The dilution of Serum from non-immunized mice was set to 1:10,000, where 1:100,000 for the blood of the DNP-KLH-immunized mouse. The manufacturer's instructions were applied for conducting the assay.

2.3.6.27. Cytotoxicity Study of GL-II-93 Analogs (Dr. Michael R. Stephen, UWM)

Refer to Section 2.3.6.11 for details.

2.3.6.28. Evaluation of AHR of GL-III-43 (Dr. Gloria Forkuo, UWM)

Refer to Section 2.3.6.2 for details.

2.3.6.29. Patch Clamp Study of GL-III-54 (Dr. Fisher, University of South Carolina School of Medicine)

Refer to Section 2.3.6.5 for details.

2.3.6.30. Relaxation of ASM by GL-III-54 in Guinea Pig Tracheal Rings with Substance P (Dr. Emala, Columbia University)

Refer to Section 2.3.6.1 for details.

2.3.7. Experimental

General procedure for individual hydrolysis of esters 1, 6, 11, 73, 75, 100, 101, 108, and 109 into their corresponding carboxylic acids 68, 85-87, and 91-95, respectively.

The corresponding ethyl ester was dissolved in EtOH, after which sodium hydroxide pellets (8 eq, later changed to 4 eq) were added to the solution. This reaction mixture was heated to 70 ˚C for 0.5 - 1 h, and the EtOH was removed under reduced pressure. The remaining aq solution was stirred at 0 ˚C for 10 min and then aq HCl (1 N) was added dropwise to the solution until the pH was 5 (pH paper). A pale white precipitate, which formed, was left in the solution for 10 min and was then collected by filtration, washed with cold water and the aq layer also allowed to stand at rt for 10 h to yield additional acid. The combined solids were dried under vacuum for 8 h to provide the pure acid.

2.3.7.1. (*R*)-8-Ethynyl-6-(2-fluorophenyl)-4-methyl-4*H*-benzo[*f*]imidazo[1,5-*a*][1,4]diazepine-3-carboxylic acid. (SH-053-2'F-*R*-CH_3-acid, 68)

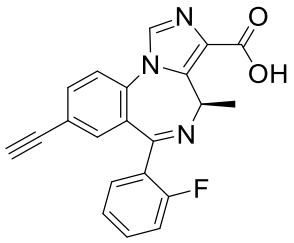

SH-05 3-2'F-*R*-CH_3-acid (**68**)

The ethyl ester **1** (20.0 g, 51.6 mmol) was dissolved in EtOH (500 mL), after which solid NaOH (16.6 g, 412.8 mmol) pellets were added to the solution. This reaction process then followed the general procedure for converting the ester into its corresponding acid. This hydrolysis provided the pure acid **68** as a white powder (18.4 g, 99.2 % yield): mp 196-198 °C; $[\alpha]_D^{25}$ = +4 (*c* 0.46, $CHCl_3$); **^{1}H NMR** (300 MHz, DMSO-d^6) δ 8.42 (s, 1H), 7.94 (d, 1H, *J* = 8.4 Hz), 7.82 (d, 1H, *J*

= 8.2 Hz), 7.56 (dt, 2H, *J* = 7.8, 6.5 Hz), 7.33 (t, 1H, *J* = 7.4 Hz), 7.22 (t, 2H, *J* = 9.3 Hz), 6.53 (d, 1H, *J* = 7.1 Hz), 2.51 (s, 1H), 1.16 (d, 3H, *J* = 6.8 Hz); **^{13}C NMR** (75 MHz, DMSO-d^6) δ 164.76, 162.81, 158.19, 140.57, 136.57, 135.54, 134.74, 133.18, 132.65, 131.88, 129.88, 129.35, 125.17, 123.98, 121.09, 116.53, 116.25, 83.42, 82.01, 49.79, 15.08; **HRMS** (ESI/IT-TOF) m/z: $[M + H]^+$ Calcd for $C_{21}H_{15}FN_3O_2$ 360.1143; found 360.1140.

2.3.7.2. (*R*)-8-Bromo-6-(2-fluorophenyl)-4-methyl-4*H*-benzo[*f*]imidazo[1,5-*a*][1,4]diazepine-3-carboxylic acid (GL-II-93, 85)

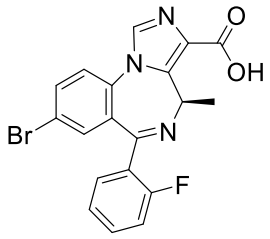

GL-II-93 (**85**)

The ethyl ester SH-I-47 [82, 120] **6** (20.0 g, 45.2 mmol) was dissolved in EtOH (400 mL) and DCM (50 mL), after which solid NaOH (7.2 g, 180.9 mmol) pellets were added to the solution. This reaction process then followed the general procedure for the conversion of the ester to its corresponding acid, and provided the pure acid **85** as a white powder (17.4 g, 92.9 % yield): mp 239-240 °C; **$[\alpha]_D^{25}$** = +12.9 (*c* 0.31, $CHCl_3$); **^{1}H NMR** (500 MHz, $CDCl_3$): δ 8.12 (s, 1H), 7.73 (d, *J* = 7.6 Hz, 1H), 7.63 (t, *J* = 6.9 Hz, 1H), 7.55 (d, *J* = 8.3 Hz, 1H), 7.45 (dd, *J* = 13.1, 6.7 Hz, 1H), 7.41 (s, 1H), 7.25 (t, *J* = 7.3 Hz, 1H), 7.06 (t, *J* = 9.3 Hz, 1H), 6.78 (q, *J* = 6.8 Hz, 1H), 1.27 (d, *J* = 6.3 Hz, 3H); **^{13}C NMR** (500 MHz, $CDCl_3$): δ 165.00 (s), 162.89 (s), 160.09 (d, *J* = 251.0 Hz), 141.25 (s), 135.04 (s), 134.89 (s), 133.59 (s), 133.08 (s), 132.54 (d, *J* = 6.7 Hz), 132.16 (d, *J* = 7.8 Hz), 131.34 (s), 131.11 (s), 128.25 (d, *J* = 11.2 Hz), 124.57 (s), 123.91 (s), 121.09 (s), 116.22 (d,

J = 21.3 Hz), 49.83 (s), 14.91 (s); **HRMS** (ESI/IT-TOF) m/z: $[M + H]^+$ Calcd for $C_{19}H_{14}BrFN_3O_2$ 414.0248 and 416.0230; found 414.0247 and 416.0246.

2.3.7.3. Sodium (*R*)-8-bromo-6-(2-fluorophenyl)-4-methyl-4*H*-benzo[*f*]imidazo[1,5-*a*][1,4]diazepine-3-carboxylate (GL-IV-18, 89)

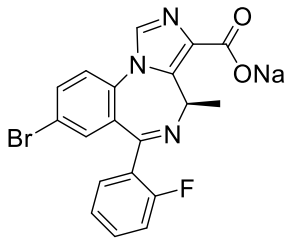

GL-IV-18 (**89**)

The acid GL-II-93 **85** (1.4 g, 3.5 mmol) and NaOH (0.14 g, 3.5 mmol) were added to EtOH (250 mL) and the mixture was heated to 70 °C for 1.5 h. The reaction mixture was cooled to 40 °C and then concentrated to dryness under reduced pressure. The solid, which resulted, was washed with EtOAc (3 × 25 mL) to furnish the sodium salt **89** (1.43 g, 95.3 % yield): **^{1}H NMR** (300 MHz, DMSO) δ 8.05 (s, 1H), 7.81 (d, J = 8.1 Hz, 1H), 7.66 (d, J = 8.4 Hz, 1H), 7.55 – 7.39 (m, 2H), 7.28 (d, J = 7.9 Hz, 2H), 7.10 (d, J = 9.3 Hz, 1H), 6.47 (q, J = 7.4 Hz, 1H), 1.11 (d, J = 7.2 Hz, 3H); **HRMS** (ESI/IT-TOF) m/z: $[M + H]^+$ Calcd for $C_{19}H_{13}BrFN_3NaO_2$ 436.0067; found 436.0079.

2.3.7.4. (*R*)-5-(1-Aminoethyl)-1-(4-bromo-2-(2-fluorobenzoyl)phenyl)-1*H*-imidazole-4-carboxylic acid (GL-IV-19, 90)

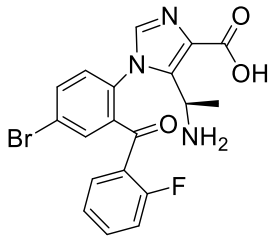

GL-IV-19 (**90**)

The acid GL-II-93 **85** (225.0 mg, 0.54 mmol) was suspended in water (2 mL), and this was followed by addition of 1 N aq HCl (2.16 mL). The reaction mixture was heated to 50 °C for 3 h, and the reaction progress was monitored by ^{1}H NMR spectroscopy. After the reaction mixture cooled to rt, a white precipitate formed, which was washed with water (3 × 50 mL) and EtOAc (3 × 70 mL). This solid was dried under high vacuum for 5 h to obtain the ring-opended analog **90** (213.8 mg, 91.0 % yield): **^{1}H NMR** (300 MHz, MeOD) δ 8.06 (td, *J* = 9.0, 2.1 Hz, 1H), 7.96 (d, *J* = 32.1 Hz, 1H), 7.89 (d, *J* = 6.9 Hz, 1H), 7.83 – 7.68 (m, 2H), 7.64 (dd, *J* = 8.3, 5.8 Hz, 1H), 7.39 (td, *J* = 7.7, 2.5 Hz, 1H), 7.30 (dd, *J* = 10.4, 8.8 Hz, 1H), 4.35 (dd, *J* = 16.8, 7.0 Hz, 1H), 1.65 (dd, *J* = 6.4 Hz, 3H); **HRMS** (ESI/IT-TOF) m/z: $[M + H]^+$ Calcd for $C_{19}H_{16}BrFN_3O_3$ 434.0335; found 434.0339.

2.3.7.5. (*S*)-8-Bromo-6-(2-fluorophenyl)-4-methyl-4*H*-benzo[*f*]imidazo[1,5-*a*][1,4]diazepine-3-carboxylic acid (GL-III-20, 91)

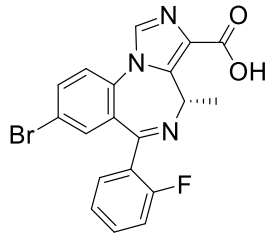

GL-III-20 (**91**)

The ethyl ester SH-I-48B **11** (1.0 g, 2.26 mmol) was dissolved in EtOH (40 mL), after which

sodium hydroxide pellets (0.72 g, 18.1 mmol) were added to the solution. This reaction mixture was then treated under the same conditions as the general procedure for conversion of an ester into its corresponding acid. This process provided the pure acid **91** as a white powder (0.9 g, 96.2 % yield): **^{1}H NMR** (500 MHz, $CDCl_3$): δ 8.11 (s, 1H), 7.74 (d, *J* = 7.6 Hz, 1H), 7.67 (t, *J* = 6.9 Hz, 1H), 7.51 (d, *J* = 8.3 Hz, 1H), 7.42 (dd, *J* = 13.1, 6.7 Hz, 1H), 7.40 (s, 1H), 7.23 (t, *J* = 7.3 Hz, 1H), 7.02 (t, *J* = 9.3 Hz, 1H), 6.76 (q, *J* = 6.8 Hz, 1H), 1.24 (d, *J* = 6.3 Hz, 3H); **^{13}C NMR** (500 MHz, $CDCl_3$): δ 165.03 (s), 162.88 (s), 160.03 (d, *J* = 251.0 Hz), 141.22 (s), 135.01 (s), 134.86 (s), 133.58 (s), 133.04 (s), 132.52 (d, *J* = 6.7 Hz), 132.11 (d, *J* = 7.8 Hz), 131.32 (s), 131.10 (s), 128.25 (d, *J* = 11.2 Hz), 124.54 (s), 123.90 (s), 121.04 (s), 116.22 (d, *J* = 21.3 Hz), 49.81 (s), 14.90 (s); **HRMS** (ESI/IT-TOF) m/z: $[M + H]^+$ Calcd for $C_{19}H_{14}BrFN_3O_2$ 414.0248 and 416.0230; found 414.0247 and 416.0242.

2.3.7.6. 8-Ethynyl-6-(2-fluorophenyl)-4*H*-benzo[*f*]imidazo[1,5-*a*][1,4]diazepine-3-carboxylic acid (GL-II-79, 93)

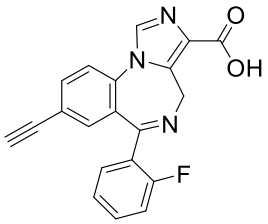

GL-II-79 (**93**)

The ethyl ester JY-XHe-053 (3.7 g, 9.9 mmol) was dissolved in EtOH (100 mL), after which sodium hydroxide pellets (1.6 g, 39.4 mmol) were added to the solution. This reaction mixture was heated and then followed the general procedure for conversion of the ester into its corresponding acid (the pH was adjusted to 6, not 5 for this compound). This process provided the pure acid **93** as a white powder (3.26 g, 95.9 % yield): mp °C; **^{1}H NMR** (300 MHz, DMSO) δ 8.43 (s, 1H),

7.91 (d, *J* = 7.9 Hz, 1H), 7.84 (d, *J* = 7.7 Hz, 1H), 7.70 – 7.47 (m, 2H), 7.32 (d, *J* = 7.6 Hz, 2H), 7.19 (t, *J* = 9.5 Hz, 1H), 5.83 (s, 1H), 4.36 (s, 1H), 4.12 (s, 1H); **HRMS** (ESI/IT-TOF) m/z: $[M + H]^+$ Calcd for $C_{21}H_{15}FN_3O_2$ 360.1143; found 360.1149.

2.3.7.7. (*R*)-8-Bromo-4-methyl-6-(pyridin-2-yl)-4*H*-benzo[*f*]imidazo[1,5-*a*][1,4]diazepine-3-carboxylic acid (GL-II-51, 94)

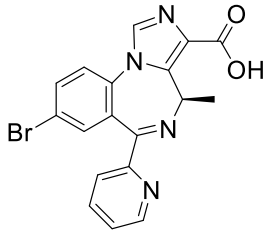

GL-II-51 (**94**)

The ethyl ester GL-II-06 **73** (1.5 g, 3.5 mmol) was dissolved in EtOH (100 mL) and DCM (15 mL), after which sodium hydroxide pellets (0.56 g, 14.1 mmol) were added to the solution. This reaction mixture was heated and then followed the general procedure for conversion of the ester into its corresponding acid. This process provided the pure acid **94** as a white powder (1.13 g, 80.7 % yield): **^{1}H NMR** (500 MHz, DMSO) δ 8.51 (s, 1H), 8.38 (s, 1H), 8.01 (d, *J* = 7.5 Hz, 1H), 7.98 – 7.88 (m, 2H), 7.84 (d, *J* = 7.6 Hz, 1H), 7.64 – 7.39 (m, 2H), 6.62 – 6.46 (m, 1H), 1.17 (d, *J* = 6.4 Hz, 3H); **^{13}C NMR** (75 MHz, DMSO) δ 164.85, 157.38, 150.14, 148.57, 140.94, 137.60, 136.69, 135.06, 134.60, 130.44, 129.58, 125.40, 124.04, 123.79, 119.87, 119.49, 49.55, 14.75; **HRMS** (ESI/IT-TOF) m/z: $[M + H]^+$ Calcd for $C_{18}H_{14}BrN_4O_2$ 397.0295 and 399.0276; found 397.0299 and 399.0318.

2.3.7.8. (*R*)-8-Ethynyl-4-methyl-6-(pyridin-2-yl)-4*H*-benzo[*f*]imidazo[1,5-*a*][1,4]diazepine-3-carboxylic acid (GL-II-30, 95)

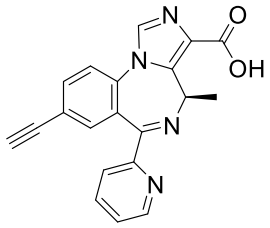

GL-II-30 (**95**)

The ethyl ester GL-II-19-2'F-*R*-CH_3 **75** (1.0 g, 2.7 mmol) was dissolved in EtOH (100 mL) and DCM (15 mL), after which sodium hydroxide pellets (0.43 g, 10.8 mmol) were added to the solution. This reaction mixture was heated and then the method followed the general procedure for conversion of the ester into its corresponding acid (the pH was adjusted to 6, not 5 for this compound). This process provided the pure acid **95** as a white powder (0.8 g, 86.6 % yield): **^{1}H NMR** (500 MHz, $CDCl_3$) δ 8.57 (d, *J* = 3.8 Hz, 1H), 8.08 – 7.98 (m, 2H), 7.84 (t, *J* = 6.6 Hz, 1H), 7.69 (d, *J* = 8.0 Hz, 1H), 7.57 (d, *J* = 8.2 Hz, 1H), 7.42 (s, 1H), 7.37 (t, *J* = 5.6 Hz, 1H), 6.72 (q, *J* = 7.0 Hz, 1H), 6.13 (s, 1H), 3.15 (s, 1H), 1.25 (d, *J* = 7.0 Hz, 3H). **^{13}C NMR** (75 MHz, DMSO) δ 165.18, 164.04, 163.98, 148.11, 140.78, 138.71, 137.00, 135.68, 135.57, 135.52, 128.45, 127.54, 125.96, 124.87, 124.12, 120.70, 83.37, 82.19, 49.42, 14.69; **HRMS** (ESI/IT-TOF) m/z: $[M + H]^+$ Calcd for $C_{20}H_{15}N_4O_2$ 343.1190; found 343.1190.

2.3.7.9. (*R*)-*Tert*-Butyl(1-((4-chloro-2-(2-fluorobenzoyl)phenyl)amino)-1-oxopropan-2-yl)carbamate (GL-III-51, 98)

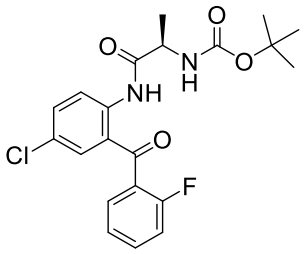

GL-III-51 (**98**)

The (2-amino-5-chlorophenyl)(2-fluorophenyl)methanone **97** (40.0 g, 160.2 mmol) and Boc-D-alanine (44.3 g, 233.9 mmol) were dissolved in dry CH_2Cl_2 (300 mL) and stirred at 0 °C. The dicyclohexylcarbodiimide (DCC; 46.3 g, 224.3 mmol) was dissolved in dry CH_2Cl_2 and was added dropwise over a 30 min period at 0 °C. The solution, which resulted, was allowed to stir for 15 h at rt, and the reaction was monitored by TLC (silica gel, EtOAc/hexanes, 1:5). The dicyclohexylurea byproduct, which formed, was filtered off and washed with CH_2Cl_2. The organic layers were combined and concentrated under reduced pressure. The solid, which formed, was recrystallized from the oily residue in hexanes at 0 °C. The crystals were filtered off and washed with hexanes until the yellow color (from starting benzophenone) was washed away. The filtrate was combined and concentrated under reduced pressure. Some additional product was isolated by repeating the washing steps. The Boc analog **98** was dried and used for the next step without further purification as white crystals (60.7 g, 90.0 % yield): **^{1}H NMR** (500 MHz, $CDCl_3$) δ 11.68 (s, 1H), 8.75 (d, *J* = 9.0 Hz, 1H), 7.56 (dd, *J* = 13.0, 6.9 Hz, 1H), 7.51 (dd, *J* = 9.0, 2.4 Hz, 1H), 7.43 (d, *J* = 2.0 Hz, 2H), 7.27 (d, *J* = 7.4 Hz, 1H), 7.18 (t, *J* = 8.7 Hz, 1H), 5.35 (s, 1H), 4.37 (s, 1H), 1.50 (d, *J* = 6.7 Hz, 3H), 1.44 (s, 9H); **^{13}C NMR** (126 MHz, $CDCl_3$) δ 195.45, 172.50, 160.53, 158.50, 155.37, 139.22, 135.02, 133.64, 133.57, 132.99, 130.28, 130.27, 127.61, 126.83, 126.72, 124.51, 124.48, 124.12, 122.34, 116.60, 116.43, 80.32, 51.85, 28.27, 18.44; **HRMS** (ESI/IT-TOF) m/z: $[M + H]^+$ Calcd for $C_{21}H_{23}ClFN_2O_4$ 421.1325; found 421.1356.

2.3.7.10. (*R*)-7-Chloro-5-(2-fluorophenyl)-3-methyl-1*H*-benzo[*e*][1,4]diazepin-2(3*H*)-one (GL-III-52, 99)

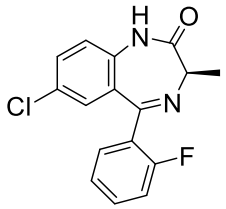

GL-III-52 (**99**)

The benzophenone GL-III-51 **98** (59.0 g, 140.2 mmol) was dissolved in dry DCM (400 mL) and cooled to -10 °C. Anhydrous HCl (g) was slowly purged through the mixture until the solution was saturated. The solution was allowed to stir until no starting material was left; it was monitored by TLC (silica gel, EtOAc/hexanes, 3:7), about every 1 h. A saturated aq solution of $NaHCO_3$ (2 x 100 mL) and water (2 x 100 mL) was added to the mixture, and the mixture was allowed to stir for 30 min until no more formation of CO_2 was observed. The reaction mixture was extracted with DCM. The organic layers were combined and concentrated under reduced pressure. The oily residue, which resulted, was dissolved in MeOH (200 mL), and this was followed by addition of water (150 mL). The pH was adjusted to 8 using a solution of 1 M aq NaOH. The reaction mixture was allowed to stir at rt overnight. The solution was concentrated under reduced pressure and water (400 mL) was added. The solution was extracted with DCM and the organic layer was washed with brine, dried (Na_2SO_4), and concentrated under reduced pressure. Hexanes (200 mL) were added to the solid, which resulted, and the mixture was heated to 60 °C. This was followed by concentration under reduced pressure down to ½ of the original volume to yield most of the amide crystals. The crystals were filtered off and washed with hexanes, and the filtrates were combined and then concentrated under reduced pressure. The residue was purified by repeating the recrystallization steps to yield additional amide **99** as a white solid (30.7 g, 72.3 % yield): **^{1}H**

NMR (500 MHz, CDCl3) δ 10.05 (s, 1H), 7.60 (td, *J* = 7.5, 1.5 Hz, 1H), 7.45 (dd, *J* = 8.7, 2.3 Hz, 2H), 7.27 – 7.20 (m, 3H), 7.06 (t, *J* = 9.0 Hz, 1H), 3.81 (q, *J* = 6.4 Hz, 1H), 1.80 (d, *J* = 6.5 Hz, 3H); **^{13}C NMR** (126 MHz, $CDCl_3$) δ 172.35, 164.74, 161.44, 159.44, 136.21, 132.26, 132.19, 131.97, 131.62, 129.59, 129.12, 129.01, 127.07, 126.98, 124.44, 124.41, 122.81, 116.37, 116.20, 58.86, 16.88; **HRMS** (ESI/IT-TOF) m/z: $[M + H]^+$ Calcd for $C_{16}H_{13}ClFN_2O$ 303.0695; found 303.0696.

2.3.7.11. (*R*)-Ethyl-8-chloro-6-(2-fluorophenyl)-4-methyl-4*H*-benzo[*f*]imidazo[1,5-*a*][1,4]diazepine-3-carboxylate (GL-III-53, 100)

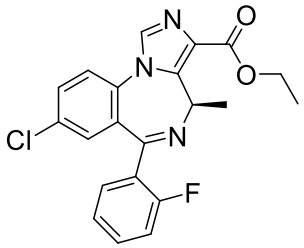

GL-III-53 (**100**)

The amide GL-III-52 **99** (25.0 g, 82.5 mmol) was dissolved in dry THF (300 mL), and cooled to -50 °C using a dry ice bath, after which potassium *t*-butoxide (12.0 g, 107.3 mmol) was added in one portion. The reaction mixture was stirred until it reached 0 °C and then stirred for 0.5 h at 0 °C. The mixture was then cooled to -50 °C, after which diethyl chlorophosphate (21.9 g, 125.0 mmol) was added dropwise with an addition funnel. The dry ice bath was removed to allow the temperature to rise to 0 °C, after which it was allowed to stir for 2 h with an ice-water bath. The solution was then cooled to -78 °C with a dry-ice bath and ethyl isocyanoacetate (14.1 g, 125.0 mmol) was added, and this was immediately followed by a second portion of potassium *t*-butoxide (12.0 g, 107.3 mmol). This solution was allowed to stir overnight during which period it was

allowed to warm to rt. The reaction progress was completed after 14 h on analysis by TLC (silica gel, EtOAc/hexanes, 1:1). The reaction mixture was quenched by the addition of a cold saturated aq solution of $NaHCO_3$ (500 mL) and extracted with EtOAc. The organic layers were combined; washed with brine (2 x 200 mL), and dried (Na_2SO_4). The solvent was removed under reduced pressure to obtain a dark brown solid residue. The solid was washed with Et_2O/EtOAc (9:1) to remove most of the impurities and the solid was further recrystallized from EtOAc and hexane (1:3), and this was followed by washing the solid with cold Et_2O to afford the majority of the pure ethyl ester. Alternative recrystallization method: the residue was dissolved in MTBE and the mixture was heated to 50 °C, after which the solvent was removed under reduced pressure to 1/3 of its original volume to obtain the precipitates. The solid was filtered off and washed with cold Et_2O. The remaining filtrate was combined and purified by flash chromatography to obtain additional ethyl ester (silica gel, EtOAc/ hexanes 3/2) as an off-white solid **100** (22.8 g, 69.5 % yield): **^{1}H NMR** (500 MHz, $CDCl_3$) δ 7.95 (s, 1H), 7.62 – 7.53 (m, 3H), 7.44 (td, *J* = 7.4, 1.4 Hz, 1H), 7.28 – 7.20 (m, 2H), 7.03 (t, *J* = 9.2 Hz, 1H), 6.69 (q, *J* = 7.2 Hz, 1H), 4.48 – 4.20 (m, 2H), 1.40 (t, *J* = 7.1 Hz, 3H), 1.27 (d, *J* = 7.3 Hz, 3H); **^{13}C NMR** (126 MHz, $CDCl_3$) δ 162.87, 161.07, 159.08, 141.49, 134.91, 133.29, 133.17, 132.19, 132.13, 132.00, 131.20, 130.82, 130.14, 129.46, 128.38, 128.28, 124.59, 124.56, 123.57, 116.31, 116.14, 60.81, 50.08, 14.86, 14.43; **HRMS** (ESI/IT-TOF) m/z: $[M + H]^+$ Calcd for $C_{21}H_{18}ClFN_3O_2$ 398.1066; found 398.1064.

2.3.7.12. (*R*)-8-Chloro-6-(2-fluorophenyl)-4-methyl-4*H*-benzo[*f*]imidazo[1,5-*a*][1,4]diazepine-3-carboxylic acid (GL-III-54, 87)

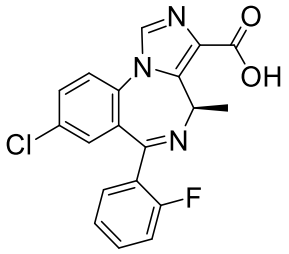

GL-III-54 (**87**)

The ethyl ester GL-III-53 **100** (3.0 g, 7.5 mmol) was dissolved in EtOH (200 mL) and DCM (3 mL), after which sodium hydroxide pellets (1.2 g, 30.2 mmol) were added to the solution. This reaction mixture was heated and then followed the general procedure for conversion of the ester into its corresponding acid. This process provided the pure acid **87** as a white powder (2.7 g, 97.1 % yield): **^{1}H NMR** (500 MHz, DMSO) δ 8.42 (s, 1H), 7.97 (d, *J* = 8.6 Hz, 1H), 7.83 (d, *J* = 8.2 Hz, 1H), 7.57 (dt, *J* = 19.4, 6.9 Hz, 2H), 7.34 (t, *J* = 7.4 Hz, 1H), 7.26 – 7.12 (m, 2H), 6.54 (d, *J* = 6.9 Hz, 1H), 1.17 (d, *J* = 7.1 Hz, 3H); **HRMS** (ESI/IT-TOF) m/z: $[M + H]^+$ Calcd for $C_{19}H_{14}ClFN_3O_2$ 370.0753; found 370.0752.

2.3.7.13. (*R*)-Ethyl-cyclopropyl-6-(2-fluorophenyl)-4-methyl-4*H*-benzo[*f*]imidazo[1,5-*a*][1,4]diazepine-3-carboxylate (GL-III-42, 101)

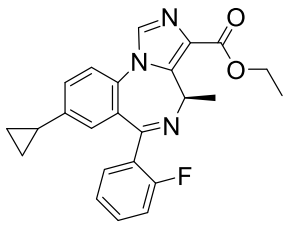

GL-III-42 (**101**)

To a solution of the bromo ethyl ester SH-I-47[82, 120] **6** (2.1 g, 4.8 mmol) in toluene (20 mL) and water (1.4 mL), cyclopropyl boronic acid (1.0 g, 12.0 mmol), potassium phosphate (4.1 g, 19.2 mmol) and bis(triphenylphosphine)palladium(II) diacetate (0.72 g, 0.96 mmol) were added under

argon. A reflux condenser was attached and the mixture was degassed under vacuum with argon; this process was repeated four times. The mixture was stirred and heated to 100 °C. After 12 h the reaction was completed on analysis by TLC (silica gel, DCM and 1% MeOH) and it was then cooled to rt. Water (10 mL) was added, and the mixture was extracted with EtOAc (3 × 15 mL), after which the filtrate was washed with brine (10 mL), dried (Na_2SO_4) and concentrated under reduced pressure. The black residue which resulted was purified by a wash column (silica gel, DCM and 1% MeOH. Note: no separation with the EtOAc/hexane solvent system) to afford the desired 8-cyclopropyl-imidazodiazepine **101** as a light yellow solid (1.26 g, 64.9 % yield): **^{1}H NMR** (500 MHz, $CDCl_3$) δ 7.88 (s, 1H), 7.55 (t, *J* = 7.1 Hz, 1H), 7.44 (d, *J* = 8.3 Hz, 1H), 7.42 – 7.32 (m, 1H), 7.19 (dd, *J* = 12.9, 6.1 Hz, 2H), 6.98 (dd, *J* = 18.9, 9.9 Hz, 2H), 6.64 (q, *J* = 7.2 Hz, 1H), 4.55 – 4.14 (m, 2H), 1.92 – 1.73 (m, 1H), 1.38 (t, *J* = 7.1 Hz, 3H), 1.24 (d, *J* = 7.3 Hz, 3H), 1.03 – 0.87 (m, 2H), 0.68 – 0.48 (m, 2H); **^{13}C NMR** (126 MHz, $CDCl_3$) δ 164.17, 163.12, 161.12, 159.12, 143.88, 141.58, 134.85, 132.09, 131.65, 131.58, 131.21, 129.22, 129.16, 129.04, 128.47, 127.87, 124.33, 121.95, 116.08, 115.91, 60.59, 50.05, 15.04, 14.64, 14.44, 9.91, 9.89; **HRMS** (ESI/IT-TOF) m/z: $[M + H]^+$ Calcd for $C_{24}H_{23}FN_3O_2$ 404.1769; found 404.1763.

2.3.7.14. (*R*)-8-Cyclopropyl-6-(2-fluorophenyl)-4-methyl-4*H*-benzo[*f*]imidazo[1,5-*a*][1,4]diazepine-3-carboxylic acid (GL-III-43, 86)

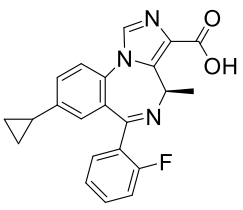

GL-III-43 (**86**)

The ethyl ester GL-III-42 **101** (0.9 g, 2.2 mmol) was dissolved in EtOH (12 mL), after which sodium hydroxide pellets (0.36 g, 8.9 mmol) were added to the solution. This reaction mixture was heated and then followed the general procedure for conversion of the ester into its corresponding acid (the pH was adjusted to 6, not 5 for this compound). This process provided the pure acid **86** as a white powder (0.7 g, 83.6 % yield): **^{1}H NMR** (500 MHz, $CDCl_3$) δ 8.04 – 7.99 (m, 1H), 7.63 (s, 1H), 7.50 (d, *J* = 7.9 Hz, 1H), 7.47 – 7.40 (m, 1H), 7.25 (dd, *J* = 13.6, 6.7 Hz, 2H), 7.03 (dd, *J* = 19.1, 10.1 Hz, 2H), 6.73 (q, *J* = 7.2 Hz, 1H), 3.96 (s, 1H), 1.95 – 1.76 (m, *J* = 25.4 Hz, 1H), 1.27 (d, *J* = 3.1 Hz, 3H), 1.02 (d, *J* = 7.8 Hz, 2H), 0.65 (d, *J* = 27.6 Hz, 2H); **HRMS** (ESI/IT-TOF) m/z: $[M + H]^+$ Calcd for $C_{22}H_{19}FN_3O_2$ 376.1456; found 376.1453.

2.3.7.15. (*R*)-6-(2-Fluorophenyl)-8-hydroxy-4-methyl-4*H*-benzo[*f*]imidazo[1,5-*a*][1,4]diazepine-3-carboxylic acid (GL-IV-14, 88)

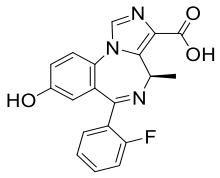

GL-IV-14

The ethyl ester SH-I-47[82, 120] **6** (2.0 g, 4.5 mmol), CuI (86 mg, 0.9 mmol), KOH pellets (1.78 g, 31.6 mmol), PEG 6000 (14.4 g), and water (3 mL) were added to a 100 mL sealed tube under Ar. The tube was degassed three times and backfilled with Ar and then the tube was quickly sealed and placed into a preheated oil bath at 100 °C under a positive pressure of Ar. The reaction was completed after 36 h, as confirmed by examination of the ^{1}H NMR spectrum. The solution, which was resulted, was cooled to rt, and this was followed by addition of water (10 mL). The acidification followed the general procedure by the addition of 10 % aq HCl dropwise, and the pH was adjusted to 5. A pale white precipitate, which formed, was left in the solution for 10 min and

was then collected by filtration, washed with cold water and the aq layer was allowed to stand at rt for 10 h to yield additional acid. The combined solids were dried under vacuum for 8 h to provide pure acid **88**(1.23 g, 78.0 % yield): **HRMS** (ESI/IT-TOF) m/z: $[M + H]^+$ Calcd for $C_{19}H_{15}FN_3O_3$ 352.1092; found 352.1107.

2.3.7.16. (*R*)-8-Bromo-6-(2-fluorophenyl)-4-methyl-3-(1*H*-tetrazol-5-yl)-4*H*-benzo[*f*]imidazo[1,5-*a*][1,4]diazepine (GL-IV-21, 96)

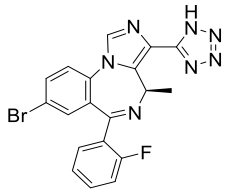

GL-IV-21 (**96**)

The hydroxylamine hydrocholoide salt (208.5 mg, 3.0 mmol), K_2CO_3 (483.7 mg, 3.5 mmol) and 3Å molecular sieves were added in DMF (50 mL) and the mixture was heated to 60 °C for 0.5 h. The aldehyde **78** (1 g, 2.5 mmol), [bmim]N_3 (1.66 g, 9.5 mmol), and $Cu(OAc)_2$ (90.8 mg, 0.5 mmol) were then added to the mixture, and it was heated to 120 °C for 12 h. After completion of the reaction, as indicated by analysis by TLC (silica gel), the reaction mixture was quenched with H_2O (50 mL) and extracted with EtOAc (2 × 50 mL). The aq layer was treated with 3 M HCl, until the pH was brought to 5. The mixture was extracted with EtOAc (2 × 50 mL). The organic layers were combined, washed with brine, dried (Na_2SO_4) and concentrated under reduced pressure. The residue, which resulted, was passed through a short pad of silica with 3% MeOH in DCM to yield the tetrazole **96** (0.94 g, 85.2 %): **HRMS** (ESI/IT-TOF) m/z: $[M + H]^+$ Calcd for $C_{19}H_{14}BrFN_7$ 438.2635 and 440.2660; found and 438.0473 and 438.0484.

Chapter 3. Design and Synthesis of Achiral α2/α3 Subtype-Selective Ligands and Their Use for the Treatment of Anxiety, Epilepsy, and Neuropathic Pain

Section 3.1. to Section 3.2. of this dissertation have been adopted from the following article:

- Li, G.; Golani, L. K.; Jahan, R.; Rashid, F.; Cook, J. M., Improved Synthesis of Anxiolytic, Anticonvulsant, and Antinociceptive alpha 2/alpha 3-GABA(A)-ergic Receptor Subtype Selective Ligands as Promising Agents to Treat Anxiety, Epilepsy, and Neuropathic. *Synthesis-Stuttgart* **2018,** *50* (20), 4124-4132.

3.1. Introduction

In the central nervous system (CNS) gamma-aminobutyric acid type A receptors (GABAARs) are transmembrane pentameric ligand-gated ionotropic channels.[219] They are the major inhibitory neurotransmitter receptors in the CNS and affect a wide variety of brain functions depending on the modulation of the GABAergic ligands at different subunits of the protein complex.[220] Benzodiazepines (BZDs), which bind at the α+γ2− extracellular interface of GABAARs,[18] are the classical psychoactive drugs prescribed for various CNS disorders including anxiety, convulsions, as well as insomnia.[46-47, 221-222] They have been employed to treat patients for over 50 years. However, these drugs, for example, diazepam, are not effective in all patients, moreover, they produce serious adverse effects including sedation, ataxia, amnesia, and addiction.[46] Consequently, there is an urgent need for improved treatments which are devoid of the above side effects.

Accumulating evidence suggests that α2β2/3γ2 and/or α3β2/3γ2 GABAAR subtype selective ligands exhibit agonist efficacy and are responsible for the anxiolytic, antinociceptive, and much of the anticonvulsant actions of the BZD when there is little or no efficacy at α1-subtypes.[47, 81-83, 107, 109, 223-226] These previous results indicated that GABA(A) α2 or α3 agonists can be used for the treatment of anxiety, epilepsy, as well as neuropathic pain with reduced side effects.

Previously, based on our BZD/GABA(A) pharmacophore model,[18, 227] a series of imidazodiazepine (IMDZ) agonists that are selective at GABA(A) α2/3-subunits were synthesized and investigated. Ligand Hz-166 (**76**), as listed in Figure 118, was one of the first and the initial lead for IBZs, which contained an acetylene group at the C(8) position in order to reduce α1-subtype efficacy and/or the binding affinity.[18, 227] In both mice and rats, the lead compound **76** exhibited antiseizure activity in a subcutaneous metrazole seizure (scMET) test in an animal model at ASP (NINDS) with both oral and i.p. administration.[228] Later in the Vogel conflict assay, **76** showed a non-sedating anxiolytic effect at 1 mg/kg in rhesus monkeys.[83] Moreover, **76** was also active in models of inflammatory and neuropathic pain exerting a dose-dependent antihyperalgesic effect without sedation, motor impairment or development of tolerance, as compared to the commonly used drug gabapentin for the management of neuropathic pain.[229] Although **76** was quite stable in human liver microsomes (HLMs), it was degraded very rapidly in mouse liver microsomes (MLMs) due to hydrolysis of the ester function to its carboxylic acid by enzymes in the liver.[230] The C(3) acid metabolite was not able to penetrate the blood-brain barrier and achieve the desired effects a long period of time. This limited the ability to do ADME toxicity studies in rodents. The pharmacokinetic profile of a ligand is one of the major concerns that can result in failure of promising candidates in clinical trials.

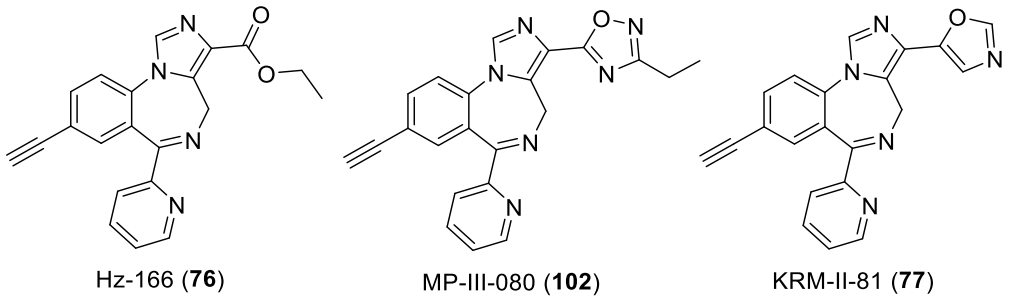

Figure 118. Structure of Hz-166 (76), MP-III-080 (102), and KRM-II-81 (77).

Currently, ester bioisosteres have been commonly used in drug development to increase metabolic stability and achieve better pharmacological effects.[113, 231-233] In order to prevent hydrolysis of the liable ester moiety and maintain the anxiolytic-like properties of lead ligand **76**, a number of bioisosteres to replace the C(3) ester functionality were designed, synthesized and evaluated.[80, 82, 234] The most potent analogs among these ligands were the 1,2,4-oxadiazole MP-III-080 (**102**) and the 1,3-oxazole KRM-II-81 (**77**), both of which markedly improved the pharmacokinetic properties in human, mouse, rat and god liver microsomes, as compared to the parent compound **76**. More recent results were reported indicating oxazole **77** exhibited anxiolytic effects in a rat Vogel conflict assay at 10 mg/kg when given i.p. Furthermore, in a mouse marble-burying assay,[107, 109, 226, 235] as a model of anxiety, ligand **102** significantly reduced the marble-burying activity at 10 mg/kg as an indication of anxiolytic-like effects, and both of the bioisosteres **102** and **77** exerted anxiolytic activity at 30 mg/kg.[107] All three ligands were shown to be α2/3 subtype selective ligands, as positive allosteric modulators (PAMs), with little or no agonist efficacy at α1-containing $GABA_ARs$.[83, 109, 236] In addition, ligand **77** exhibited potent antinociceptive activity in a model of acetic acid- and lactic acid-induced pain in mice.[236] Later in the motor function and anticonvulsant efficacy assays, **102** was an effective anticonvulsant versus

the GABAA negative modulator pentylenetetrazole (PTZ)-induced seizures with no observation of motor impairment at 30 mg/kg on i.p. administration.[109]

Taken together all these results suggested that instead of the rapidly metabolized parent compound **76** in rodents, ligands **102** and **77**, which are novel α2/3-subtype selective GABAARs PAMs, are stable in HLM, MLM, rat liver microsomes (RLM), and dog liver microsomes (DLM).[107] This permits further investigation of ligands **102** and **77** in models of anxiety, epilepsy, neuropathic pain, and respiration in rodents as well as primates.[83] Consequently, multigram quantities of both ligands were required for more critical evaluation in rodent models, as well as further important tests for ADME toxicity before human trials. As previously reported, the direct conversion from the ethyl ester **76** to the ethyl oxadiazole **102** earlier was only achieved in moderate yield from 40% to 71% [81-82, 107] on milligram scale. However, it was not possible to obtain a similar yield on gram scale. But the real major roadblock was the synthesis of the 1,3-oxazole **77**, the overall yield of which via the previous three-step procedure[107, 234] was only 28% on a maximum scale of 3 grams.[107] The most critical problem in the total synthesis of these two ligands was the low overall yield (17%) for the five-step route to the parent compound **76**, which was used directly as the starting material for both **77** and **102**. Therefore, the modification of the published routes or other efficient and inexpensive procedures were required. Herein, the optimization of the previous methods for the synthesis of **76** and **102**, and an improved route for the synthesis of **77** are reported. They are applicable for the scale-up process with improved yields, which is key for further studies of clinical potential.

3.2. Synthesis α2/α3 Subtype Selective Ligands

As demonstrated above, the improvement of the synthesis of Hz-166 (**76**) would play a critical role in the development of $GABA_A$ α2/3-subtype selective ligands since it was the parent compound for all analogs in this series. After many changes and modifications in each step in the synthetic route for Hz-166 (**76**), this provided a better 5-step overall yield of 56% (Scheme 25), as compared to the previous yield of 17%.[81]

The improved route began with the commercially available amine, 2-amino-5-bromo-benzyl-2'-pyridyl ketone **70**, which was acylated with bromoacetyl bromide in the presence of sodium bicarbonate. The intermediate **103**, which formed, without further purification, was directly treated with a saturated solution of ammonia (gas) in methanol and gradually increasing the temperature from 0 °C to reflux to provide the 1,4-benzodiazepine **104** in 78% overall yield (two-steps) on the 120-gram scale. The amide **104** can be purified by recrystallization in methanol and dichloromethane while avoiding any column chromatography on a large scale. The imidazole ring was introduced by applying the modified procedure[237] by treating the amide **104** with potassium *t*-butoxide and diethyl chlorophosphate at -50 °C for 2 h, after which the solution was allowed to warm up to 0 °C. Ethyl isocyanoacetate was then added to the reaction mixture, which was executed at -78 °C, and this was followed by addition of another equivalent of potassium *t*-butoxide to provide IMDZ **105** in 81% yield. The yield of the imidazole ring formation by a previous method using sodium hydride as the base by Ian Fryer at -10 °C was only 37%. This process was improved to 81% by replacing sodium hydride with potassium *t*-butoxide at a lower temperature.

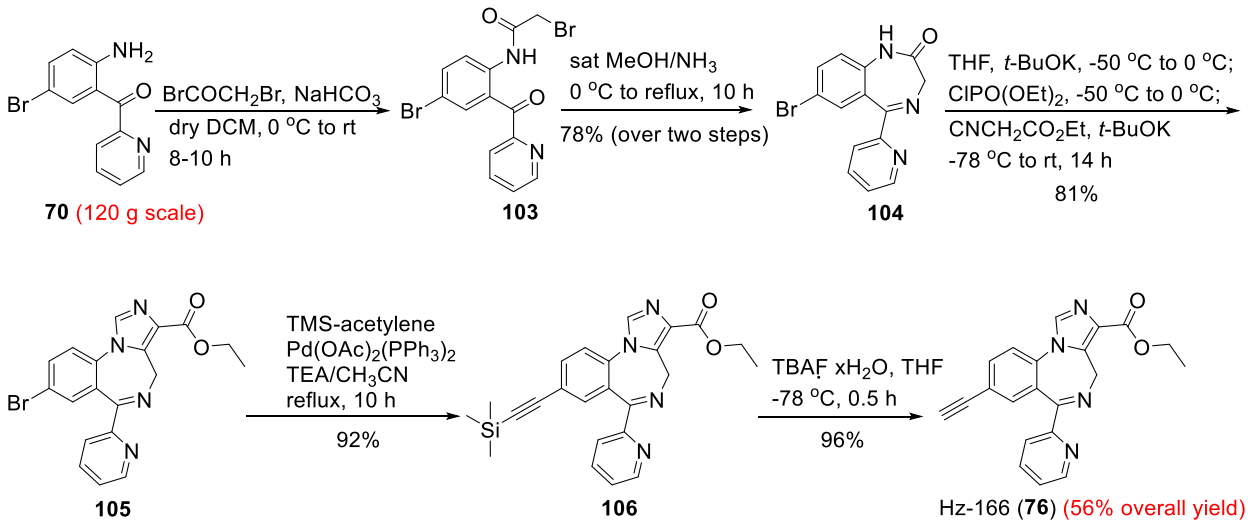

Scheme 25. Optimized total synthesis of Hz-166 (76).

The purification of **105** was easily executed by washing away the impurities with 10 % ethyl acetate in diethyl ether. The scale of this reaction was increased to 80 grams as compared to the previous one of 15 grams in the literature. A Heck-Cassar-Sonogashira type reaction was conducted with IMDZ **105** and trimethylsilylacetylene to provide the trimethylsilyl analog **106** in 92% yield. The lead ligand Hz-166 (**76**) was obtained by the deprotection of the analog **106** using tetrabutylammonium fluoride in 96% yield. After workup (see Experimental Section) the pure material **76** was recrystallized from methanol, which had been heated to 50 °C and allowed to cool.

With the optimized synthesis of the parent compound **76**, the overall yield was improved from 17% to 56%. The purification process in the case of ligands such as **76** was more difficult than the other ligands in the IMDZ series in the 2'-F, 2'-H, etc. due to the 2'-pyridine nitrogen, which can be a problem when using column chromatography on a large scale. In this new procedure, all the products can be isolated by either washing with specific solvents or by crystallization to avoid column chromatography. This is a more practical, efficient and scalable

synthesis of 2'-pyridine-containing substituted IMDZ (**76**) as the starting material for other important analogs.

The 1,2,4-oxadiazoles are well-known ester bioisosteres that ameliorate some of the problems of metabolism in the drug discovery process.[113, 230-232, 238] The oxadiazole MP-III-080 (**102**) was a very promising ligand in this series, which exhibited anxiolytic, anticonvulsant and antinociceptive effects in many animal models, as described above. The problems of inconsistent yields of **102** from **76** required a solution of scaleup. The development of efficient methods for the synthesis of 1,2,4-oxadiazoles has been ongoing for decades; however, most of the existing procedures either required harsh conditions or multiple steps from ester to the corresponding starting materials.[239] This was deemed not suitable for the present case with ligands containing multiple functionalities. Therefore, many attempts were made to improve the yield of the oxadiazole formation for the synthesis of grams quantities of ligand **102**.

For this purpose several experiments were conducted under different conditions. It was found that the equivalents of sodium hydride, the reaction time for the formation of amidoxime anion, dry reaction conditions, as well as the reaction temperature all played a critical role for good yields. Initially, the ratio of sodium hydride to the ethyl ester (**76**) was 2.5:1 on milligram scale and the yield of the byproduct, in which the imine [N(5)-C(6)] double bond had been reduced, was comparable to the desired oxadiazole **102**, as confirmed by analysis of the ^{1}H NMR spectrum. The formation of the major byproduct resulted from the extra equivalent of sodium hydride which reduced the [N(5)-C(6)] imine bond of the parent compound **76**. Hence, the amount of sodium hydride was lowered to 1.1[90] equivalents to avoid the unwanted imine reduction. Since esters are less reactive than the corresponding acyl chloride, the formation of the amidoxime anion was key and the only driving force for acylation; the first step toward oxadiazole formation. Therefore, the

reaction time of the amidoxime with sodium hydride should be adequate and ^{1}H NMR spectroscopy was required to monitor the reaction to completion due to the inability to analyze this step by TLC. Commonly, the thermal cyclization of *O*-acylamidoximes is the second step required to prepare the 1,2,4-oxadiazoles;[240] however, the higher temperature in the IMDZ series usually led to low yields (40-47%),[8] along with the formation of byproducts. Consequently, instead of using the usual conditions of reflux, the reactions were performed at room temperature. In addition, 3Å molecular sieves were added, the amount of which depended on the reaction scale. Efficient removal of water as an alternative method helped push the reaction at room temperature to completion. To date, with these optimizations, the yield of the one-step conversion from ester to oxadiazole was improved to 88%, as depicted in Scheme 26. It is consistent for gram scale processes.

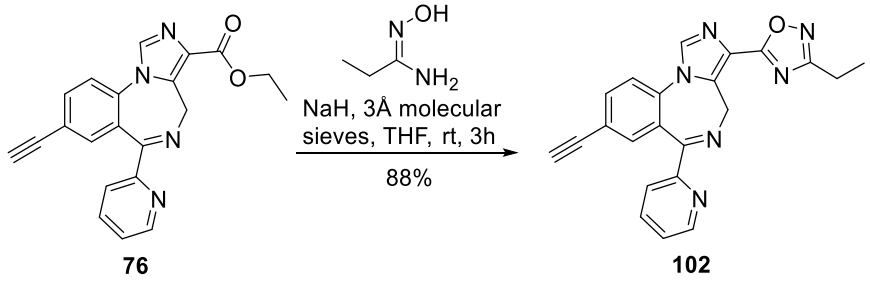

Scheme 26. Synthesis of MP-III-080 (102) from Hz-166 (76).

Beside 1,2,4-oxadiazoles as bioisosteres, 1,3-oxazoles are unique bioisosteres with a similar electron density map to that of an ester function. Oxazole-containing compounds have been reported with the desired pharmacological effects and promising therapeutic profiles in the past.[127-129] Accordingly, the 1,3-oxazole analogs of the parent compound **76**, which can be used as an alternative ester bioisostere, appeared to be a useful complement to **102**. The development of the synthesis of oxazoles has been employed for years, and numerous methods have been reported.[241]

In the case under study here a one or two-step synthetic route would be appropriate in order to avoid low overall yields from multi-step synthesis. As compared to other approaches, the Van Leusen oxazole synthesis,[242] which can be used to prepare 1,3-oxazoles by the direct conversion from the corresponding aldehyde, seemed advantageous because of the one-pot process and mild conditions. Indeed, this transformation provided good yields for oxazole formation in other series. However, the synthesis of the most potent oxazole bioisostere, KRM-II-81 (**77**), as described above (2'-N analog), was the most difficult bioisostere in the series of IMDZ analogs (i.e, compared to the 2'-F, 2'-H, 2'-Cl, isomers etc) to prepare. The problem was not from the formation of the oxazole, but the reduction reaction from the particular ester **76** to its corresponding aldehyde (**107**).

After many attempts with many reducing agents, which either reduced the [N(5)-C(6)] imine bond or reduced the aldehyde, so formed, at C(3) to the alcohol, diisobutylaluminium hydride (DIBAL), a commonly used reducing agent, was employed efficiently in good yield (75-80%) for the 2'-F and 2'-H series.[107, 234] The reduction with DIBAL for the ethyl ester **76**, however, failed to achieve the desired aldehyde in a temperature range of -78 °C to 25 °C due to the reduction to the corresponding alcohol and/or imine bond reduction as observed in the case of the oxadiazole synthesis. Moreover, the purification of this crude reaction mixture was tedious. After many attempts, it was found out it was difficult to stop the reduction in the 2'N case at the aldehyde stage. The next strategy was to employ lithium aluminum hydride (LAH) to reduce the ester to the alcohol and then reoxidize it to the aldehyde with activated manganese dioxide, or pyridinium dichromate. This mixture of alcohols (desired and imine-reduced), which formed, was then directly oxidized to a mixture of aldehydes with activated manganese dioxide in an overall two-step yield of 39%, as reported previously.[107] Even though the next step (the oxazole formation) was executed in

reasonable yield (73%), the three-step overall yield of **77** had fallen to 29%, which was not acceptable.

In order to overcome this problem, a number of weaker reducing agents were employed, such as lithium borohydride, sodium borohydride, potassium borohydride, or the bulkier lithium tri tert-butoxy aluminum hydride, however, none of these agents provided the desired aldehyde in good yield, as shown in Scheme 27. The solution to this issue was to find a bulkier reducing agent, but also a selective reducing agent to prevent imine reduction and permit the aldehyde to remain at this stage in the absence of alcohol formation.

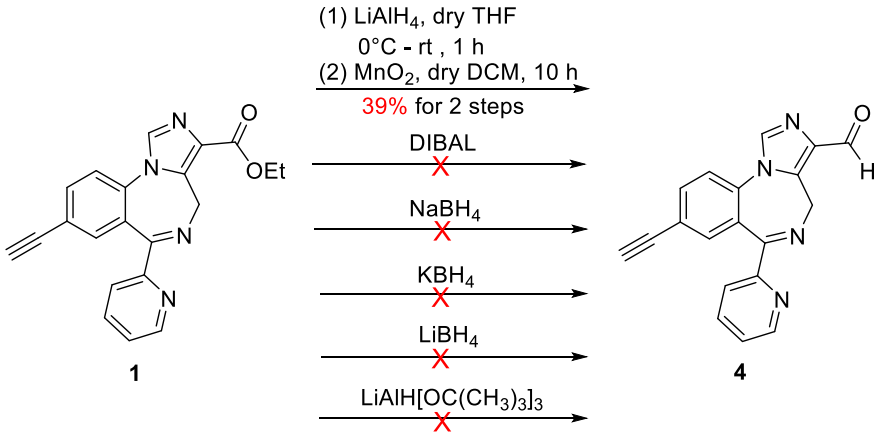

Scheme 27. Attempts to prepare aldehyde (4) from Hz-166 (1).

Because of work in another series, potassium diisobutyl-*t*-butoxy aluminum hydride (PDBBA)[161] seemed to be a suitable reducing agent for this series. The PDBBA can be easily prepared by addition of DIBAL in hexane dropwise into a solution of the same number of equivalents of potassium t-butoxide in THF at 0 °C for 2 h.[161] In theory, the PDBBA should not attack the imine double bond due to the three bulky groups; secondly, it can only offer one hydride atom in the reduction and might be easier to stop the reaction at the aldehyde stage, as compared to four hydride units provided by $LiAlH_4$. The reported mechanism is straightforward.[243-244] The

hydride from PDBBA attacks the carbonyl carbon forming a tetrahedral intermediate, and the elimination of the ethoxy group yields the desired aldehyde.

However, the first attempts were not successful under the reported conditions[161] or at lower temperatures (entries 1-4 in Table 28). The reactions were stopped at 3 hours due to more alcohol formation. The reactions were then conducted by using different equivalents of PDBBA from 1.5 to 2.5 at 0 °C at three time points 5, 30, 180 min, respectively (entries 5-14 in Table 28). The use of higher equivalents of PDBBA at 0 °C not only increased the yield of aldehyde but also the rate of reduction to the alcohol at the first 5 minute time point. Along with longer reaction times, the yields of aldehyde were not significantly improved and began to drop off at the 30 minute time point for 2 and 2.5 equivalents in trials of PDBBA (entries 9,10,12,13 in Table 28). The aldehyde, which formed, was immediately converted into the alcohol in this series of IMDZ, as observed at 0 °C. If the reactivity of the ester could be increased, then it could compete with the aldehyde and as a result, additional aldehyde and less alcohol could be predicted. With this in mind, a modification was made to increase the reaction temperature. As expected, more aldehyde and less alcohol formation were observed within the first 5 minute at room temperature for all equivalents of PDBBA; the yields of the aldehyde quickly dropped to provide more alcohol after reaching the maximum yield of aldehyde in 5 minutes (entries 14-23 in Table 28), as compared to the condition at 0 °C. The best yield of aldehyde (**107**) from all the trials was 79% (entry 18 in Table 28) with 1.5 equivalents of PDBBA at 25 °C; only 12% of the alcohol had formed. At 40 °C, the yield of aldehyde was worse, and the process rapidly formed the alcohol instead (entries 24, 25 in Table 28).

Table 28. Optimization of reduction conditions to form aldehyde 107.

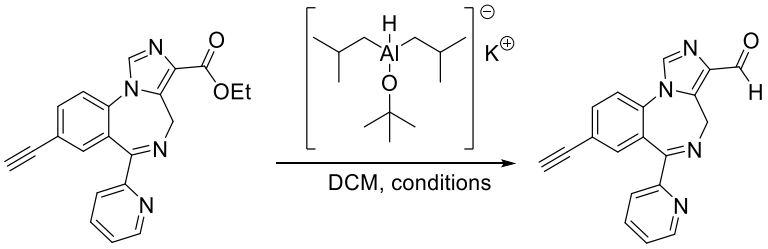

76 107

Entry	PDBBA eq.	Temp. (°C)	Time (min)	Yield (%) -CHO	Yield (%) -CH_2OH
1	1.3	-78	720	0	0
2	1.3	0	5	22	12
3	1.3	0	30	31	14
4	1.3	0	180	38	17
5	1.5	0	5	45	20
6	1.5	0	30	57	21
7	1.5	0	180	60	29
8	2.0	0	5	56	23
9	2.0	0	30	62	31
10	2.0	0	180	51	40
11	2.5	0	5	58	22
12	2.5	0	30	65	29
13	2.5	0	180	40	51
14	1.3	25	5	30	5
15	1.3	25	30	56	28
16	1.3	25	180	11	67
17	1.5	25	1	62	8
18	**1.5**	**25**	**5**	**79**	**12**
19	1.5	25	30	18	68
20	2.0	25	1	69	20
21	2.0	25	5	61	28
22	2.5	25	1	70	25
23	2.5	25	5	56	38
24	1.3	40	1	36	10
25	1.3	40	5	40	33

All reactions were conducted with 0.07 mmol of starting material (the ethyl ester 1) in dry DCM as the solvent of the reaction under different conditions listed above. The yields of aldehyde and alcohol were calculated after the isolation of the products.

From the results above, the best condition to obtain a good yield (79%) of aldehyde was with 1.5 equivalents of PDBBA, which was a bit higher than reported,[161] at room temperature. The reaction process had to be controlled carefully and monitored by TLC analysis for the first 5-10

min to avoid alcohol formation due to the very short reaction time. Most importantly, the imine bond was not reduced by PDBBA at all; the spectroscopy and properties of the aldehyde **107** match with the reported values as confirmed by NMR and LCMS. At lower temperatures such as at 0 °C, the ester was much less reactive than at 25 °C, the aldehyde, which formed at 0 °C, would favorably be reduced and resulted in a mixture of unreacted ester, desired aldehyde, and the alcohol byproduct. Moreover, longer reaction times should be avoided due to the reaction of aldehyde, as expected.

Even though the reaction time was very short, this procedure can be applied on a large scale if monitored every 5-10 minutes by TLC. To date, the largest scale for this reduction reaction under the optimized reaction conditions was 20 grams and in 80% yield, as illustrated in Scheme 28. The van Leusen reaction for the synthesis of the 1,3-oxazoles occurred smoothly. The oxazole **77** can be purified *via* crystallization in ethyl acetate to replace the earlier employed column chromatography, that was reported previously.[107]

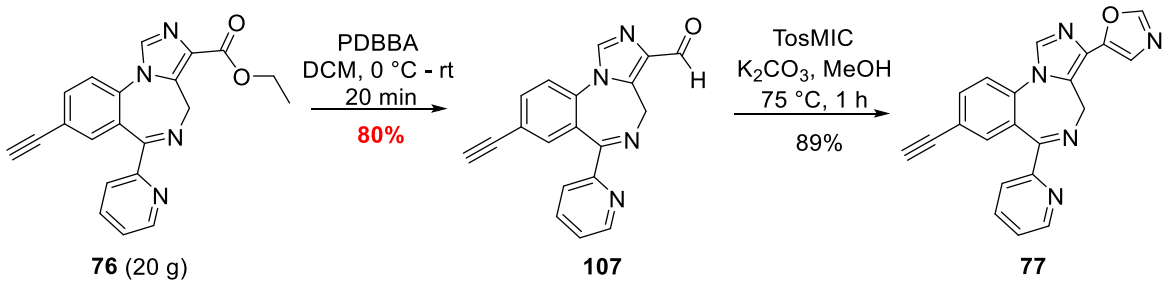

Scheme 28. The optimized synthesis of oxazole 77 with a significantly improved overall yield.

3.3. Results and Discussion of Biological Studies on KRM-II-81 (77)

With the aid of an improved and practical synthesis, the 1,3-oxazole KRM-II-81 (**77**) has been synthesized on a large scale for efficient supplies and evaluated further in many animal

models of anxiety, epilepsy, pain, and depression in rodents, as well as other *in vitro* and *in vivo* models.

The previous *in vitro* data of KRM-II-81 (**77**) including binding affinity, microsomal stability, cytotoxicity, and efficacy is briefly summarized here. The data obtained from PDSP has shown that **77** exhibited little to no binding affinity for a wide range of receptors, ion channels or transporters, including dopamine, calcium, histamine, opioid, adrenergic, serotonin, NMDA receptors, etc. Most importantly, **77** showed no hERG binding affinity, which reduced the possible influence on the heart QT problems. The oxazole **77** possesses a metabolically stable profile *in vitro*, as confirmed by the microsomal stability study on HLM and MLM after 30 minutes incubation at 37 degrees, more than 90 % of **77** remained in all human, mouse and rat liver microsomes *in vitro*. There was no cytotoxicity of oxazole **77** at 100 μM, which indicated the ligand was safe to use up to this concentration that is far above the dose level reached in a clinical therapeutic range.[107] The electrophysiological recording of **77** illustrated that it was a very potent α2/3 $GABA_AR$ subtype-selective ligand at 100 nM, and the potentiation at α1 or α5 was nearly at the baseline similar to the GABA current alone (EC3 GABA),[236] as depicted in Figure 119. This reduced the possibility of the development of tolerance to the antihyperalgesic and anticonvulsant side effects because the coupling of these two subtypes was diminished (Mohler, 2004).

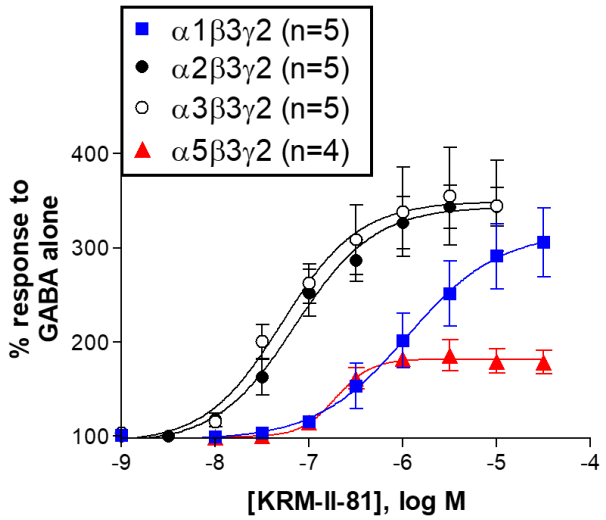

Figure 119. The dose-responsive efficacy data of KRM-II-81 (77) at α1,2,3,5-containing GABAARs. EC3–5 GABA value is presented in percentage of response to GABA alone.

In addition to the efficacy profile in $GABA_ARs$, GABA current of KRM-II-81 (**77**) was also evaluated in dorsal root ganglia isolated from the spinal cord of rats. The negative current displayed a rapid activation by saturating GABA (1 mM) potentiation, after which slow desensitization occurred, as shown in Figure 120A. The GABA at current from EC10 was only activated partially without significant desensitization from the low GABA concentration. With 10 μM of **77**, the GABA current (EC10) was partially activated at a level of 355 % in a concentration-dependent manner and at 32 nM achieved an efficacy of 421 % (EC50), as shown in Figure 120B.

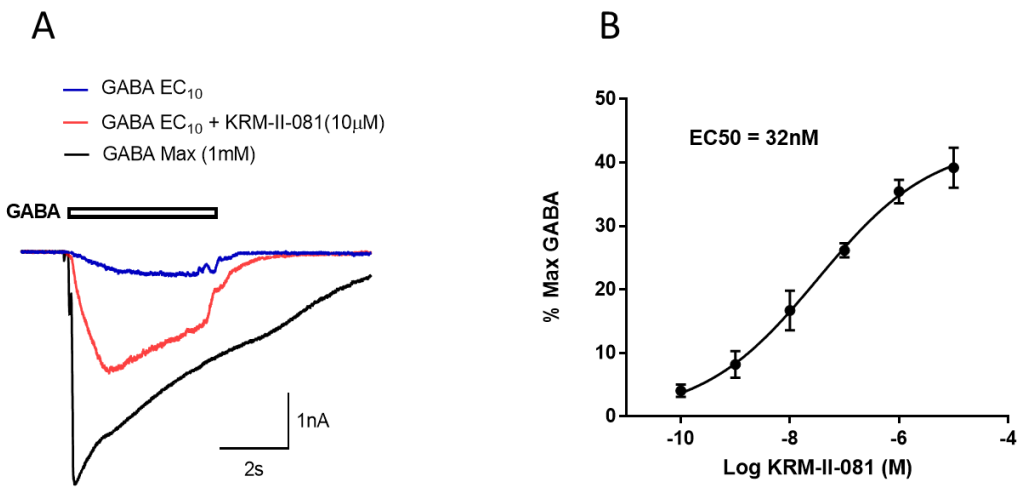

Figure 120. The effect of KRM-II-81 (77) on the potentiation of native GABA currents in cultured DRG neurons. A: Manual patch clamp recording of currents activated by saturating GABA concentration (1mM), and by EC10 concentration of GABA (5μM) and 10 μM of 77. GABA current activated with a low concentration of 5μM GABA was enhanced by 10μM of 77. B: Dose-response curve of 77 on currents activated with 5 μM GABA (EC10). The potentiation is represented as % of increase produced by saturating GABA-activated current. All values shown are mean ± SEM (n=4). (Adopted from Figure in Witkin et al., 2019) [245]

3.3.1. Anxiety

Anxiety is one of the most common mental disorders and affects over 18% of the US population.[246] It includes generalized anxiety disorder (GAD), obsessive-compulsive disorder (OCD), panic disorder, post-traumatic stress disorder (PTSD) and social phobia (or social anxiety disorder) among others, which can significantly dampen the quality of life for the patients and their families. The symptoms are usually characterized with the inability of letting go of worry or fear, stress that is more pronounced than the actual impact of the event, and restlessness. The standard treatment consists of a combination of psychotherapy, behavioral therapy, and medication. The common medications are classical BZDs, tricyclics, beta-blockers, and SSRI's. Classical BDZ has major side effects such as tolerance, addiction, sedation, ataxia, respiratory depression, adverse psychological and physical effects. Beta-blockers can cause blurred vision, insomnia, disorientation, CNS system effects, and serious heart problems. SSRI's takes 3-5 weeks to have

effect and also can cause sexual dysfunction.[247-248] Patient compliance is a problem with all these treatments. Therefore, there is an unmet need for improved treatments that possess desired anxiolytic-like properties but are devoid of sedation, ataxia, amnesia, addiction, and tolerance.

The marble burying assay has been widely used for its application to measure the possible anxiolytic properties of ligands on the text animal. It is based on the nature of the rodents that tend to bury any harmful or harmless objects underground due to fear or losing them or being anxious. A ligand which exerts anxiolytic-like properties will decrease this urge and will result in a reduced number of marbles, which are buried during the test period. This assay has been an effective method to evaluate the anxiolytic effects of the traditional BZDs, such as chlordiazepoxide (CDAP), and the novel IMDZ 1,3-oxazole KRM-II-81 (**77**), as illustrated in Figure 121. The male NIH Swiss mice (n=10/condition) were administrated either vehicle (1% carboxymethyl cellulose, CMC, a surfactant) or 30 mg/kg of CDAP or the 1,3-oxazole **77** i.p. They were then placed or a rotarod (spinning at 4 rpm) for assessment of motor impairment. After rotarod testing, mice were placed in a chamber with 20 marbles on the surface of sawdust bedding. The number of marbles buried (2/3 by sawdust) was counted after 30 minutes. Both oxazole **77** and CDAP at 30 mg/kg exhibited a significant effect on the reduction of the number of marbles buried, as compared to vehicle, which was considered an effect observed after acute dosing with anxiolytic and antidepressant drugs. In the rotarod test, CDAP induced 6 failures due to its sedative properties, as expected. In contrast to CDAP, **77** at 30 mg/kg did not impair motor performance during the 2-minute rotarod assay.

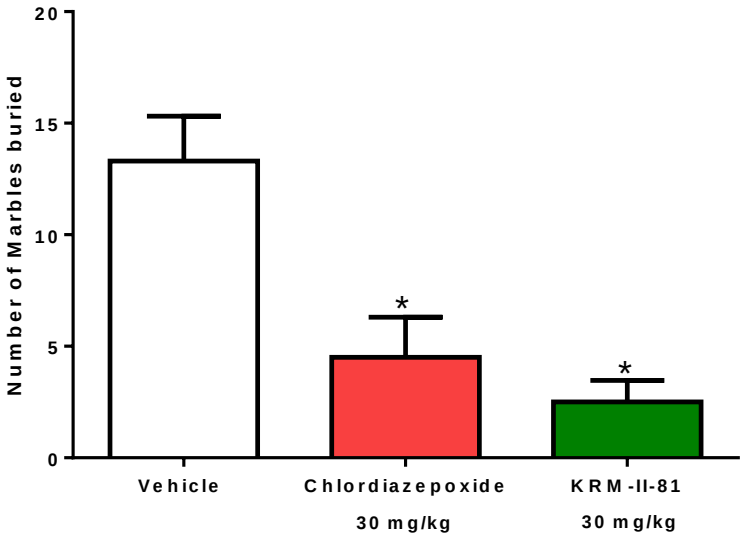

Compound (i.p.)	Failures
Vehicle	0/10
Chlordiazepoxide	6/10*
KRM-II-81	0/10

Failure = 2 times falling off rotarod during 2 min test

Figure 121. The evaluation of the anxiolytic-like activity of chlordiazepoxide and KRM-II-81 (77) in the marble burying assay. Male NIH Swiss Webster mice (n = 10) were administrated i.p. with either vehicle or chlordiazepoxide (CDAP) and KRM-II-81 (77) at 30 mg/kg 30 min prior to testing. The rotarod assay was performed (spinning at 4 rpm) for the assessment of motor impairment. Mice that fall off twice are scored as failures. Data were analyzed using ANOVA. Dunnett's test: (∗) P < 0.05 vs vehicle.

The Vogel conflict assay is another commonly used experimental method for the assessment of anxiolytic-like properties of test compounds. It is considered the gold standard as an assay. In general, the animal will be punished with a minimal electrical shock when they are trying to get water or food during the test by lever pressing, which will result in a reduction of the total number of times the press for water or food. If an anxiolytic is administrated, this number of times will be increased irregardless of the punishment. The parent ethyl ester Hz-166 (**76**), the 1,3-oxazole KRM-II-81 (**77**) and chlordiazepoxide (CDAP) as a positive control, were tested in the

Vogel conflict assay in rats for their ability to reduce anxiety of animals induced by the electrical shock punishment, as illustrated in Figure 122.[107] The ethyl ester **76** at 30 mg/kg did not exert any difference from the vehicle. On the other hand, as expected, the marketed anxiolytic CDAP at 20 mg/kg significantly increased the number of times the animal lever press for water during the punishment phase but did not show any effect during the non-punishment period. The 1,3-oxazole **77** did not induce any effect at the dose of 3 mg/kg, as compared to the vehicle. However, a significant increase in drinking behavior during the punishment phase was observed at 10 mg/kg ip dose with oxazole **77**, and the rate of response was increased by 240 %. The ligand **77** exhibited a similar anxiolytic effect at 30 and 60 mg/kg with an increasing rate of response about 220 % and 200 % in comparison to the control group, respectively. Again, CDAP exerted a significant increase of water licking behavior at 20 mg/kg and induced a 330 % responsive rate over the vehicle group. Moreover, **77** increased punished responding of rats without affecting un-punished responding, which suggested an anxiolytic property of **77** with no section nor ataxia. In contrast, CDAP produced a trend toward decreasing un-punished responding, which suggests sedation, as expected.

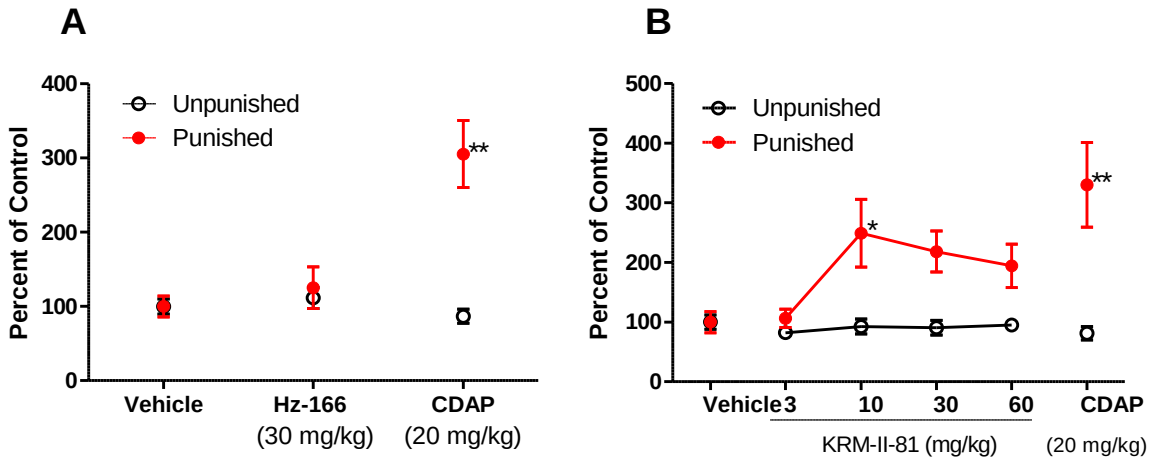

Figure 122. The Vogel Conflict assessment of anxiolytic-like properties with male Sprague-Dawley rats (n = 6-8). A. The evaluation of Hz-166 (76) and anxiolytic chlordiazepoxide (CDAP) administrated i.p. at 30 mg/kg and 20 mg/kg, respectively; B The dose response of KRM-II-81 (77) as compared to CDAP at 20 mg/kg. All

compounds were administered 30 minutes prior to testing. Results were analyzed using ANOVA. Each point represents the mean + SEM of 6-8 rats. * p<0.05, significantly different than vehicle control. (Dunnett's test: * P < 0.05; Student t-test: ** P < 0.05). (Modified from the Figure in Poe et al.) [107]

3.3.2. Epilepsy

Epilepsy is a chronic, life-threatening neurological disease that can occur at any age, which affects 2.3 million U.S. adults and 50 million people worldwide.[249] It is characterized by symptoms such as disturbances of movement, strange sensations, convulsions, muscle spasms, and loss of consciousness from a mild to a severe level over an extended period. The most common type of epilepsy is termed idiopathic epilepsy. It has unknown causes and is not preventable, while secondary epilepsy or symptomatic epilepsy has known causes, such as prenatal brain damage, a stroke, a brain tumor, a head injury or infection, etc. Diverse medications including benzodiazepines (BZDs), carbamazepine, phenytoin, valproate, felbamate, gabapentin, lamotrigine, levetiracetam, are used generally in combination in status epilepticus in emergency rooms since seizures are not well controlled. The surgical approaches are also utilized for the treatment of epilepsy to reset the section of the brain wherein the seizures emanate. This is the last resort. Even though some epileptic symptoms can be controlled at certain level, there is an urgent unmet need for improved antiepileptic drugs that are able to fully control the symptoms and are devoid of the side effects of current drugs.[250] This is especially important in medications given to children which can influence brain development, which lead to lifetime learning disabilities. This is a huge burden to the patients, the parents and the society as a whole. It has been widely reported that BZDs exhibit anticonvulsant activity through acting on both α1 and α2 $GABA_AR$/Bz subtypes.[251] The ligands that target α1 subtypes, as expected, are associated with the side effects, such as sedation, ataxia, addiction, tolerance, etc., which results in the greatest drawback of the application of BZDs to treat epilepsy. Only the ligands that target α2 or α2/3 subtypes are the ideal

candidates for the treatment of epilepsy due to their anticonvulsant activity with the elimination of the side effects from α1 efficacy, and the lack of possible tolerance from the coupling of α1 and α5 subtypes.[252] Therefore, in addition to the parent compound Hz-166 (**76**), which has been shown to exhibit anticonvulsant activity, without the development of tolerance to this anticonvulsant effect. However, it is rapidly metabolized in rodents,[120] consequently KRM-II-81 (**77**), was prepared as the metabolically much more stable bioisostere of **76**. It has also been evaluated in both acute and chronic seizure models (https://panache.ninds.nih.gov/CurrentModels.aspx) for its anticonvulsant-like properties by the NIH Epilepsy Therapy Screening Program (ETSP) under the guidance of Dr. Shalini Sharma. The original reports of test compounds from ETSP are included in Appendix V, and **77** was anticonvulsant in every model it was tested in. Lastly, the evaluation of the seizure protection in the resistant epileptic human brain tissue was conducted with **77**.

3.3.2.1. Acute Seizure Models

Three acute seizure models were utilized for the evaluation of the anticonvulsant activity of KRM-II-81 (**77**), which included the 6 Hz 44 mA seizure model in mice (i.p.), maximal electroshock seizure (MES) model, in rats (i.p.), and subcutaneous metrazol (pentylenetetrazole) seizure model (s.c. MET) in rats (p.o.). These "first-pass" animal models are critical and efficient for the fast identification of ligands that might exhibit anticonvulsant-like properties against therapy-resistant seizures.

The 6 Hz kindled seizure model is commonly used for the initial screening for possible anticonvulsant drugs that can dampen the induced seizures by a long-duration, low frequency (6 Hz) stimulation, which might not be detected by different screening methods. In brief, mice were

administrated p.o. with KRM-II-81 (**77**), and the 6 Hz stimulation was delivered for 3 seconds after 2 hours through corneal electrodes at 44 mA and the seizure activity in the animal was observed and recorded. A parallel group of mice was administrated with higher doses of **77** and observed for potential motor impairment and possible toxicity at 4 hours after dosing. At 10 mg/kg, KRM-II-81 (**77**) was unable to protect the mice (n = 8) that are subjected to 6 Hz stimulation. However, at the dose of 25 mg/kg, 3 out of 8 animals were protected by orally-administered **77**, and full protection was observed at 50 mg/kg at 2 hours after oral dosing, as presented in Table 29. At the most effective dose of 50 mg/kg, there was no motor impairment observed, which indicated no overt toxicity induced from **77.** Only mild tremors were observed at the dose of 100 mg/kg p.o. The loss of righting was observed at 150 mg/kg in 3/8 mice. More severe tremors were observed at a higher dose 200 mg/kg. Importantly, when 120 mg/kg of KRM-II-81 (**77**) was administrated to rats (p.o.) no side effects were observed. This may be because the metabolite level in rats is much lower than that in mice (Eli Lilly, Jeff Witkin et al.).

Table 29. The effects of KRM-II-81 (77) p.o. in the 6 Hz seizure model and the motor effects. (Adopted from Figure in Witkin, et al) [253]

Dose	**Number protected/number tested**	
10	0/8	
25	3/8	
50	**7/8**	
Dose	**Number with observed motor effects**	**Observation**
50	**0/8**	
100	3/8	tremor
150	5/8	tremor, unable to grasp
200	8/8	more severe tremor, loss of righting

The maximal electroshock (MES) assay is one of the most common choice ofs initial *in vivo* animal models in search of new antiepileptic drugs.[254] The 1,3-oxazole KRM-II-81 (**77**) was evaluated in the MES test, as compared with diazepam and Hz-166 (**76**).[253] The male CD-1 mice (n = 10) were administrated i.p. with vehicle (1% CMC), diazepam (1, 3 or 6 mg/kg), ester **76** (3, 10 or 30 mg/kg) or oxazole **77** (3, 10 or 30 mg/kg) 30 minutes prior to testing. During the testing, the tonic-clonic seizures were induced by a 10 uA electroshock for 0.2 seconds. The indication of the protection of an animal by the test compound is the observation of the abolition of tonic and/or clonic seizures at the hindlimb, which is considered an anticonvulsant effect. As illustrated in Figure 123, diazepam (DZP) was able to reduce MES-induced convulsions at 3 mg/kg and fully protected the animals at 6 mg/kg. The 1,3-oxazole KRM-II-81 (**77**) exhibited only a little effect at 3 mg/kg, however, a significant anticonvulsant effect was observed at 10 mg/kg and it also fully prevented the animals from seizures induced by MES at 30 mg/kg. However, the parent ethyl ester Hz-166 (**76**) was not active up to 30 mg/kg.

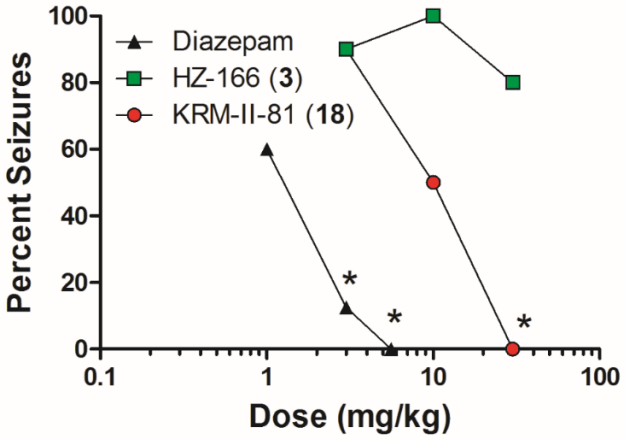

Figure 123. The evaluation of the anticonvulsant activity of Diazepam, HZ-166 (76) and KRM-II-81 (77) in the MES assay. Male CD-1 mice (n = 10) were administrated i.p. 30 minutes prior to being tested with either vehicle (1% CMC), diazepam (1, 3 or 6 mg/kg), KRM-II-81 (3, 10 or 30 mg/kg) or HZ-166 (3, 10 or 30 mg/kg). Analyzed using ANOVA (Dunnett's test versus vehicle: * P < 0.05). (Adopted from Figure in Witkin, et al) [253]

Pentylenetetrazole (PTZ), an antagonist of $GABA_AR$s, is commonly used for generalizing convulsions in animal models of seizures and epilepsy[255] in order to search for new anticonvulsant drugs. The 1,3-oxazole KRM-II-81 (**77**) was evaluated in the PTZ-induced seizure test, as compared with diazepam (DZP) and Hz-166 (**76**).[253] Thirty minutes after dosing DZP (3 or 10 mg/kg), **76** (30 mg/kg) or **77** (10, 30 or 60 mg/kg), PTZ was administered at a dose of 35 mg/kg to induce the seizures, and the effects on the animal were observed and recorded. As illustrated in Figure 124 A, DZP was able to produce some reduction of PTZ-induced seizures at 3 mg/kg and produced full protection at 10 mg/kg. The parent ethyl ester **76** only exhibited some anticonvulsant tendency toward efficacy up to 30 mg/kg. The 1,3-oxazole **77** exerted some reduction at 10 mg/kg and offered full protection at 30 and 60 mg/kg from PTZ-induced convulsions in rats. The efficacy of the full protection by DZP was 10x more potent than **77**. These results are consistent with the results obtained from the MES-induced seizure assay. The possible motor impairments of **76** and **77** were evaluated on the inverted screen. This assay was performed before the PTZ-induced seizure assay. The rats were evaluated on the inverted screen test after 25 min of dosing and were scored after 1 minute. As indicated in Figure 124 B, DZP had a minimal toxic dose (MTD) of 10 mg/kg, where sedation/ataxia was observed, whereas at 150 mg/kg for **77** (see more details in the ETSP report in Appendix V). There was no ataxia/sedation, even p.o. at a dose of 250 mg/kg. Thus, when calculating the protective index (PI) = ($MTD_{inverted\ screen}/MED_{PTZ\ convulsions}$), the PI value for DZP was 1 and that for **77** was 5, which indicated a wider safety therapeutic range of **77** than DZP.

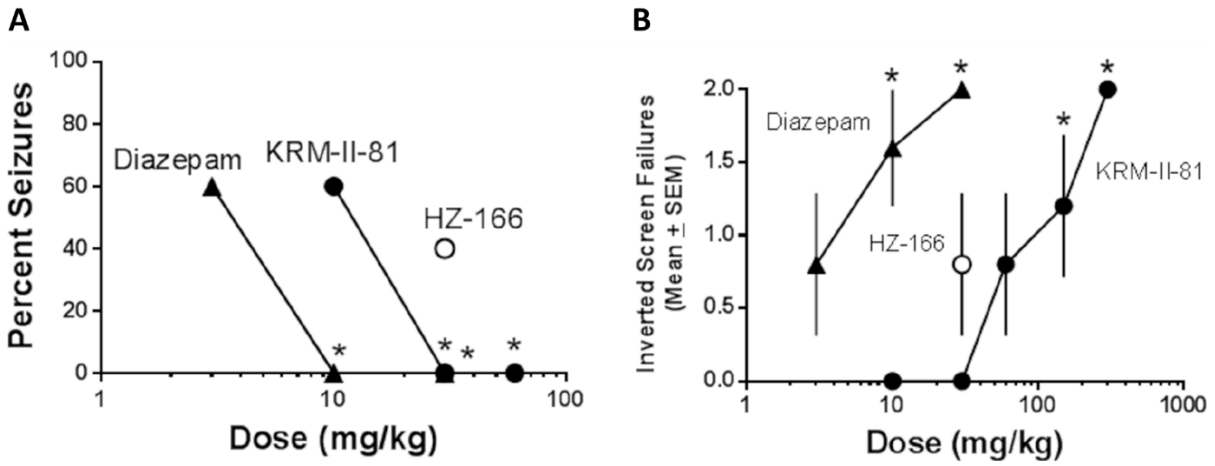

Figure 124. The anticonvulsant effects of Hz-166 (76), KRM-II-81 (77), and diazepam against (A) pentylenetetrazole (PTZ)-induced seizures (35 mg/kg, s.c.) and (B) their motor performances on an inverted screen in rats. Data represent mean ± SEM (n=5-8). Significant probability was analyzed by Fisher's Exact Probability test (*: p<0.05). For the motor score, n = 5 (diazepam, 3 mg/kg) or 8 (all other data) rats, 0=climbed over to the top of the screen, 1= hanging on to screen, 2= fell off. Data were analyzed by ANOVA followed by Dunnett's test with * p<0.05. PTZ alone produced convulsions in 96 ± 4%. The baseline motor scores were 0.12 ± 0.8. (Adopted from Figure in Witkin et al.) [253]

The pentylenetetrazole (PTZ)-induced seizure threshold test is used to determine the threshold limit of test compounds on the decrease of seizure threshold, as a follow-up experiment. During i.v. PTZ infusion, the threshold dose of PTZ to induce convulsions was assessed in rats with and without drug pretreatment. The dose of PTZ required to produce seizures was 35 mg/kg (PTZ threshold = 37.1 ± 1.9 mg/kg) given as a bolus, as described above. Examination of the results was illustrated in Figure 125 indicated that the pretreatment with diazepam (DZP), Hz-166 (**76**) and KRM-II-81 (**77**) all increased the dose of PTZ required to induce seizures. DZP at 1 mg/kg was able to increase the dose of PTZ to 49 mg/kg as the required dose. The ethyl ester **76** did not increase the required dose of PTZ up to 60 mg/kg, whereas the oxazole **77** at 10 mg/kg offered a significant increase of the amount of PTZ and required a 71 mg/kg dose to induce convulsions. This effect was significant and dose-dependent, and the 60 mg/kg of **77** administered increased the PTZ dose to 108 mg/kg and is much greater than the anticonvulsant drug, valproic

acid, that required 300 mg/kg of which to increase the PTZ dose to 81 mg/kg. Thus, it is obvious that DZP was much more potent than the **76** and **77** but was less efficacious, however, **77** exhibited a much wider range of efficacy to increase the dose of PTZ required to produce seizures (both ligands were equally efficacious against MES and acute PTZ-induced convulsions).

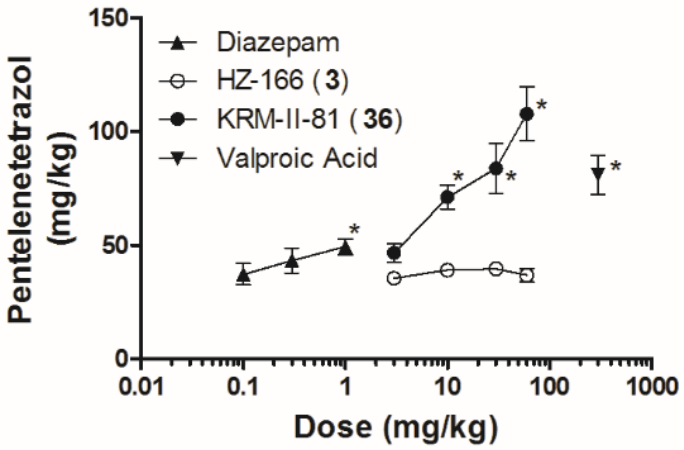

Figure 125. The threshold measurement of Hz-166 (76), KRM-II-81 (77), and diazepam (DZP) against PTZ-induced seizures. The threshold procedure (B) dosed diazepam, KRM-II-81, HZ-166 or valproic acid 30 minutes prior to an i.v. infusion of pentylenetetrazole until convulsions were observed in rats, n = 8. Analyzed using ANOVA (Dunnett's test: * P < 0.05). (Modified from Figure in Witkin, et al) [253]

As described above, the protective index (PI), can be calculated from the minimal dose that has a toxic effect (inverted screen) over its anticonvulsant potency in the PTZ-induced seizure model. The PI > 1 illustrated a margin between efficacy and side-effect doses; PI = 1 represents no separation between the side effects and as an anticonvulsant potency; whereas PI < 1 indicates that the potency to produce the desired effect is less than the potency to induce a toxic effect. A summary of the PI for DZP and **77** is listed in Table 30, which demonstrated that the oxazole **77** exhibited **a much wider safety margin** between the dose producing an anticonvulsant effect and the dose inducing motor impairment, as compared to DZP. In all of the acute seizure models, oxazole **77** demonstrated a robust anticonvulsant profile that was able to protect the animals from both chemical (PTZ) and electrical (6 Hz and MES) stimulus-induced seizures in rodent models.

Table 30. Protective indices (PI) for DZP and 77. (Modified from Figure in Witkin et al.)

Assay	KRM-II-81	Diazepam
Electroshock	15	3.3
PTZ Clonus	5	**1**
PTZ Threshold	15	10
After-Discharge Threshold	15	**1**
After-Discharge Duration	15	**<1**
Seizure Severity	15	**1**

[a]PI values were calculated as the minimal effective dose producing motor impairment /minimal effective doses producing efficacy. Values for HZ-166 could not be calculated for any measure due to lack of efficacy. Values of $\leq$1 are highlighted in bold.

3.3.2.2. Chronic Seizure Models

Up to date, four chronic seizure models, were used for further evaluation of the anticonvulsant effect of KRM-II-81 (**77**) in rodents. The four models, as discussed in this section, are the corneal kindled seizure model in mice (p.o.), lamotrigine (LTG) resistant amygdala-kindled seizure model in rats (i.p.), model of mesial temporal lobe epilepsy (mTLE) induced by focal chemoconvulsant injection in mice (p.o.), and chronic post-SE (KA) spontaneously seizing in rats: Stage 1 (i.p.). The results, obtained from the acute seizure models as described above, suggested a potential anticonvulsant ligand, KRM-II-81 (**77**), and this ligand was then carried on for further investigation in the chronic seizure models. It was important that the large scale synthesis of KRM-II-81 (**77**) and MP-III-080 (**102**) had been developed at this point.

The corneal kindled mouse model is a seizure model developed by repeated stimulation of an electrical shock or an epileptogenic drug. It is a rapid and low-cost initial screen for the development of potential anticonvulsant ligands at the ETSP. In addition, the anticonvulsant results obtained with a corneal kindled mouse is consistent with the pharmacological profile of the

test drugs from human partial epilepsy, which suggests this model is a reliable and effective method for the early stage screening for antiepileptic substances. In brief, the male CF-1 mice received a twice-daily kindled electrical 3-second stimulation, 3 mA, 60 Hz by corneal electrodes for 10-14 consecutive days to reach the criterion of Stage 5 seizures. The test started at 5-7 days post the last stimulation, after which stimulation was given to the mice to ensure the animals were with Stage 5 seizures. Mice (n = 8) were then administrated p.o. with the doses at 1, 3, 8, 15, 25, 30 mg/kg of KRM-II-81 (**77**), and the time of peak effect (TPE) was determined at the 2-hour time-point. As presented in Table 31, **77** exhibited moderate anticonvulsant effects at 3 mg/kg, and significant effects were observed at 8 mg/kg. The mice were fully protected by **77** at 15 mg/kg. The lower the seizure score, the better the anticonvulsant effect. Based on the previous results, the toxicity data was not determined at this point since **77** did not produce toxicity up to 50 mg/kg in mice nor 120 mg/kg in rats.

Table 31. The effect of KRM-II-81 in a corneal kindled mouse model. (Unpublished data)

Dose (mg/kg)	Time (hrs)	N / F	C	Individual Seizure Scores	Average Seizure Scores	Toxicity N / F
1	2	0 / 8		5,5,5,5,5,5,5,5	5	
3	2	2 / 8		5,5,5,5,0,5,5,0	3.75	
8	2	6 / 8		1,0,0,4,0,0,0,5	1.25	
15	2	8 / 8		0,0,0,0,0,0,0,0	0	
25	2	8 / 8		0,0,0,0,0,0,0,0	0	
30	2	8 / 8		0,0,0,0,0,0,0,0	0	
N: number of animals protected or toxic.			F : total number of animals tested.		C : Comment code.	

The lamotrigine (LTG)-resistant amygdala-kindled rat model is a useful method not only for the identification of substances that are active against symptomatic seizures **but also for the differentiation of drugs that may be active against resistant epilepsy.** It has been reported that,

during the seizure developmental stage, daily administration of lamotrigine (5 mg/kg) results in an LTG-resistant state rather than protecting the animal from the development of seizures. These research findings indicated that a subsequent resistance to Na+ channel blockers resulted from the presence of LTG during the kindling acquisition state, which suggests a useful model of resistant epilepsy. The 1,3-oxazole KRM-II-81 (**77**) was evaluated in this resistant epilepsy model. In brief, an electrode was implanted into the left amygdala in anesthetized male rats. After one week of recovery, animals started to receive a daily 200 μAmp stimulus until they all reached to stage 4 or 5 seizures. The LTG at 30 mg/kg was injected i.p. to the fully kindled animals to induce resistant seizures. After the washout of LTG for 3 days, animals were administrated with KRM-II-81 (**77**) at doses of 1, 5, 10, 20, and 40 mg/kg, then challenged with the stimulus at the predetermined time of peak effect at 1 hour. As depicted in Figure 126 A, **77** was able to protect the animals at a moderate level at 5 and 10 mg/kg, and it reached to 50 % protection at 20 mg/kg. The protection was significant at 40 mg/kg as compared to the vehicle; 6 out of 8 rats were protected by the administration of oxazole **77** after 1 hour. Furthermore, at the dose of 40 mg/kg, the seizure score of **77** was significantly reduced from 5 to 2.13, and the seizure duration was also decreased significantly from 123 seconds to 66 seconds, as compared to the vehicle, as demonstrated in Figure 126 B and C, which suggested that **77** was effective against LTG-induced resistant epilepsy at 40 mg/kg. **This is a severe epilepsy model!**

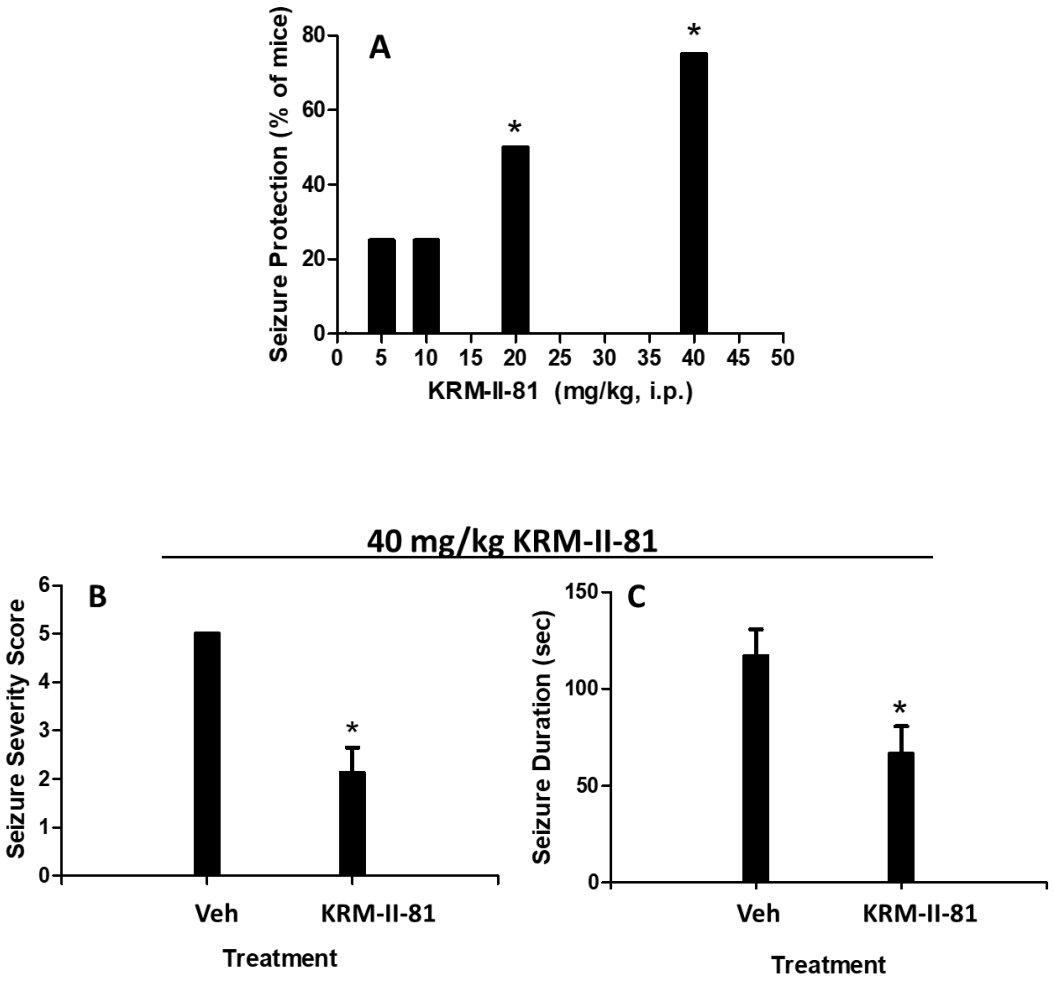

Figure 126. The effect of KRM-II-81 (77) in lamotrigine (LTG)-resistant amygdala-kindled rat model. (A)The percentage of seizure protection by 77 at the doses of 1, 5, 10, 20, and 40 mg/kg, (B) the seizure severity score of vehicle and 77 at 40 mg/kg, (C) the seizure duration of vehicle and 77 at 40 mg/kg, The average seizure scores ± S.E.M.and afterdischarge duration is noted, as are the number of animals protected from seizure (defined as a Racine score < 3) over the number of animals tested. (Unpublished data)

Mesial temporal lobe epilepsy (MTLE) makes up the largest rate of causes of human refractory epilepsy, which originates from the hippocampus of the brain in patients with epilepsy. The MTLE mouse model includes many features observed in human patients with temporal lobe epilepsy (TLE). In brief, the injection i.v. of kainic acid (KA) at 1 mmol in 100 mL of vehicles, as a neurotoxic and epileptogenic agent, into the dorsal hippocampus of a mouse, induces non-convulsive severe epilepsy (SE), which can last for hours. An electrode was implanted into the left part of the hippocampus in male rats. **After the KA injection for 4 weeks,**

spontaneous recurrent KA-induced seizures, which occur 30-60 times per hour and last about 15-20 seconds, can only be recorded in the hippocampus region, no paroxysmal hippocampal discharges (HPD) is detected in other regions in the brain of animals. A group of 4 or 5 MTLE mice was injected i.v. with 15 or 30 mg/kg of KRM-II-81 (**77**), respectively, and the behaviors of the animal were recorded by digital EEG recordings for 20 minutes before-injection and 90 minutes after-injection. The number of HPDs were recorded and analyzed during a 20 minute period for 10 minutes before and 10 minutes after the peak time of effect. As shown in the Table 32, at the dose of 15 mg/kg, **77** was able to reduce the KA-induced epilepsy in rats to 31.27 % as compared to the baseline HPD values, whereas a more significant suppression was observed to 8.69 % percent peak effect at dose of 30 mg/kg of **77**, which indicated the anticonvulsant effect of **77** in MTLE mice model was robust and provided a possible candidate for the treatment of the most common refractory epilepsy of human.

Table 32. The effect of KRM-II-81 (77) at 15 mg/kg on in MTLE mice model. (Unpublished data)

Dose and TPE	Recording Period	Mouse 1	Mouse 2	Mouse 3	Mouse 4	Mean	SEM
15 mg/kg	Baseline	11	18	23	15	16.75	2.53
peak	120 min	2	5	9	6	5.50	1.44
120 min	% peak effect	18.18	27.78	39.13	40.00	31.27	5.18

Table 33. The effect of KRM-II-81 (77) at 30 mg/kg on in MTLE mice model. (Unpublished data)

Dose and TPE	Recording Period	Mouse 1	Mouse 2	Mouse 3	Mouse 4	Mouse 5	Mean	SEM
30 mg/kg	Baseline	13	20	12	18	8	14.20	2.15
	110 - 130 min	5	1	0	0	0	1.20	0.97
Peak 120 min	% peak effect	38.46	5.00	0.00	0.00	0.00	8.69	7.51

Status epilepticus (SE) is a severe emergency characterized as a continuous seizure lasting more than 30 minutes, or at least two of them are too close without full recovery.

Seizure control mechanisms can be overwhelmed. In status-epilepticus, uncontrollable, recurrent generalized seizures occur. In order to evaluate the effect of KRM-II-81 (77) in SE, a SE-induced spontaneous recurrent seizure model in rats was utilized. In brief, chronic epilepsy in rats with status epilepticus was induced by a repeated low-dose of kainic acid (KA) at 7.5 mg/kg i.p. at every hour up to 4 hours until animals achieved Stage 5 seizures. After 10 weeks of chronic treatment, the rats were implanted with a wireless telemeter into the peritoneal space from the stomach to the head underneath the skin for the EEG monitor. Only the rats with the highest seizure burden scores were selected (n = 24). During the test period, a baseline seizure rate is determined in week 1. During week 2, the rats were administrated with 20 mg/kg of KRM-II-81 (**77**) over 5 days, Monday-Friday. Rats are split into groups of 12 for the vehicle group and another 12 for the drug-treated groups. Once the treatment was completed in week 2, rats were monitored during week 3 with only vehicle treatment (washout period). In order to avoid any possible design variations, the cross-over paradigm was utilized. Similar to the first group (n = 6), the second group (n = 6) received vehicle first, followed by the treatment of **77**. A list of potential detected events generated and listed. As illustrated in Figure 127, KRM-II-81 (**77**) significantly dampens KA-induced status epilepticus in regardless of treatment time either administrated in the second week or the third week. The daily seizure burden was significantly decreased to 1.6, as compared to the baseline 6.5, whereas the vehicle group exhibited a similar value as 6.7. **Half of the drug-treated rats (6 out of 12) were protected from KA-induced status epilepticus, the baseline and the vehicle did not show any difference in seizure freedom rate.** Overall, without the treatment of **77**, the generalized seizures were reoccurrence during the vehicle treatment period. **These results indicated that KRM-II-81 was able to reduce the KA-induced status epilepticus, which suggested a novel candidate for this life-threatening type of epilepsy.**

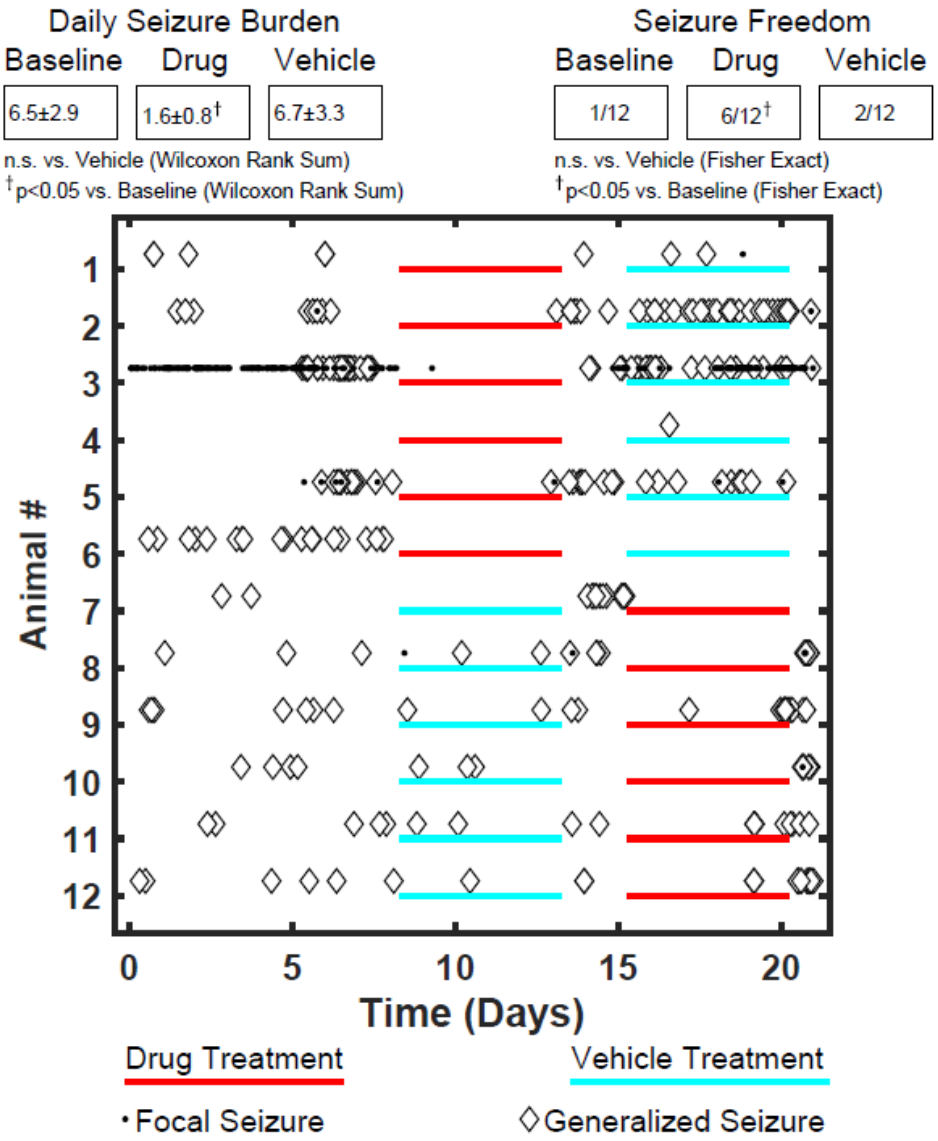

Figure 127. The effect of KRM-II-81 (77) in the SE-induced spontaneous recurrent seizures model in rats. During the test period, a baseline seizure rate is determined in week 1. An initial group of 12 rats enrolled in Stage 1 chronic monitoring were split into two (N=6/group) treatment groups. During week 2, the first group of rats was administrated with 20 mg/kg of KRM-II-81 (77) over 5 days, Monday-Friday. Once the treatment is completed in week 2, rats will be monitored during week 3 with only vehicle treatment. Similar to the first group (n = 6), the second group (n = 6) receives vehicle first, followed by the treatment of 77. Each data represents a seizure event. * p<0.05 as compared to the vehicle group. (Unpublished data)

3.3.2.3. Evaluation of Seizure Protection in Resistant Epileptic Human Cortical Tissue

Due to the improved anticonvulsant profile of KRM-II-81 (**77**), the effect of 1,3-oxazole **77** was evaluated to determine if there was any suppression of the firing rate in human cortical

tissue from two juveniles with intractable or resistance epilepsy after surgical treatment. The slices were prepared, and the electrophysiological recording was performed by using a 60-microelectrode array. The two neuronal stimulants, picrotoxin as a $GABA_AR$ antagonist, or 4-aminopyridine (AP-4) as the K^+ ligand, were utilized to induce the increase of firing rate frequency (Hz), as illustrated in Figure 121. Since the human epileptic tissue is usually not active without excitation, the slices was bathed in 10 μM picrotoxin. At least 30 channels of the array were able to be evoked for the test, which was monitored for 1 hour as the baseline with an average firing rate of 0.05 Hz ± 0.01. The 1,3-oxazole was added at 30 μM and the neuronal activity was recorded in the presence of picrotoxin for another hour. The average firing rate after **77** treatment was significantly reduced to 0.01 Hz ± 0.005, as illustrated in Figure 128 (left panel). On a separate slice, 50 μM of AP-4 (K+ channel-driven) was used as the neuroexcitant instead of picrotoxin, and all 60 channels were activated of the microelectrode array with an average firing rate of 0.08 Hz ± 0.01. With the oxazole **77** treatment at 30 μM, the neuronal activity was significantly attenuated to an average of 0.01 Hz ± 0.005, which indicated its anticonvulsant activity was not from the competition with picrotoxin at BzR bindint sites. **These results illustrated that KRM-II-81 (77) was able to significantly suppress the firing rate of epileptic seizures induced under both picrotoxin and AP-4 stimulation, which strengthens the confidence of the use of this ligand for further investigation for the treatment of epileptic seizures.**

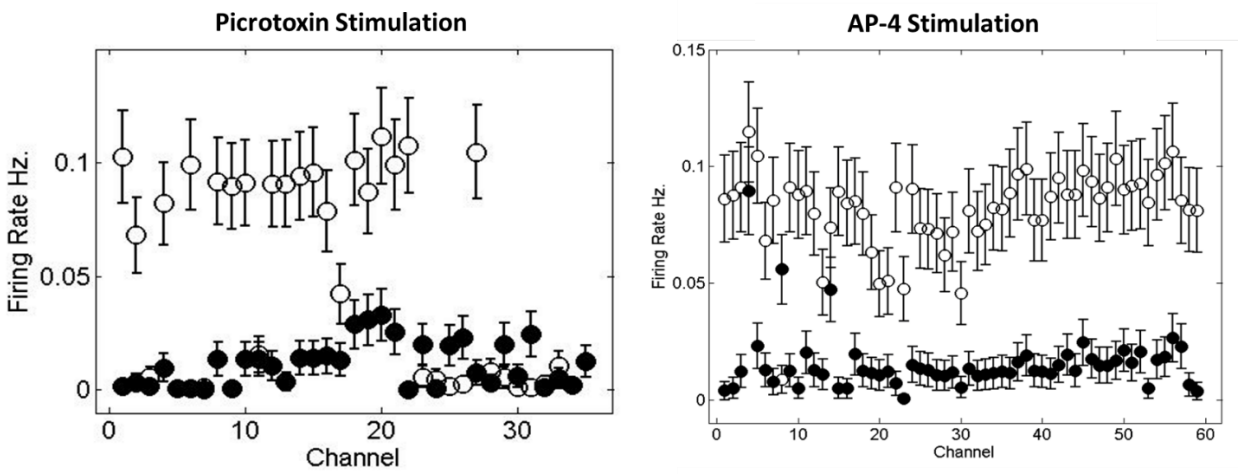

Figure 128. Functional blockade of the epileptic phenomenon in cortical slices of KRM-II-81 (77) from juvenile epileptic patients. Data of network firing rate frequency (Hz) was collected for 1 hour under each condition (unfilled circle EACSF, no 77 treatment; filled circle EACSF + 30 µM of 77) with either 10 µM of picrotoxin (left panel) or 50 µM AP-4 (right panel) as a neuronal stimulant. A 60-microelectrode array was used for recording. (paired t-test: $P < 0.05$). (Adopted from the Figure in Witkin et al.)

Taken all together with the preclinical findings on KRM-II-81 (**77**) in models of epilepsy, as summarized in Table 34, indicated significant suppression of firing rate induced by picrotoxin and AP-4 in human cortical tissue and enhanced the potentiation of GABA currents in dissociated dorsal root ganglion neurons. Although **77** was not active in the 6 Hz rat model, oxazole **77** produced robust anticonvulsant-like properties in all other rodents models. Together with the human tissue data, this effect significantly enhanced the confidence for pushing **77** forward to clinical trials for the treatment of refractory/resistant epilepsy in children as well as adults.

Table 34. Pre-clinical results of KRM-II-81 (77) in different animal models of epilepsy as well as in human cortical epileptic tissue. (Adopted from Table in Witkin et al. 2019)

Model	Species	Activity
Activated cultured cortical neurons	rat	+
Dissociated dorsal root ganglion neurons	rat	+
Electroshock convulsions	mouse	+
PTZ clonus	rat	+
PTZ seizure threshold	rat	+
Amygdala kindling - ADT	rat	+
Amygdala kindling - ADD	rat	+
Amygdala kindling – SS	rat	+
Amygdala kindling – 400 μA	rat	+
6 Hz stimulation – 44 mA	mouse	+

Data from Witkin et al., 2018 except dorsal root ganglion neurons (Witkin et al., 2019)

3.3.3. Activity of 1,3-oxazole (77) in Different Types of Pain Models

Pain disorder is a physical pain experience in one or several areas in the body. There are 100 million (U.S. adults) and 1.5 billion people worldwide who suffer from different extents of pain. The health cost is, up to date, is $560-635 billion a year in the U.S. (https://www.thegoodbody.com/ chronic-pain-statistics/) It deters the patient from proper function in life events for days or years. Pain disorders usually originate in several subtypes, such as chronic pain, complex regional pain syndrome, back pain, cancer pain, neuropathic pain, inflammatory pain, bladder pain, etc. The standard treatment consists of stress management, psychotherapy, behavioral therapy, acupuncture, and medication. The common medications used for the treatment of pain are addictive opioids, NSAIDs, acetaminophen, COX-2 inhibitors, tricyclic antidepressants, anti-epileptics SSRI's, and etc. Opioids antagonists are effective for severe pain; however, for every opioid on the market addiction, tolerance and constipation are serious problems (opioid epidemic).[256] The NSAIDS cause severe stomach pains, bleeding and can lead to death. Acetaminophen increases the risk of kidney damage and liver failure over time. COX-2 inhibitors, such as celecoxib, can cause kidney problems, fluid retention, increase the risk of heart attacks and

strokes, as well as high blood pressure.[257-258] Patient compliance is a problem with all these treatments. Indeed, an unmet urgent need is urgent for the development of novel non-opoid treatments of pain disorders. Over the past decade, there has been a large amount of growing evidence that an subtype selective ligand targeting α2-containing $GABA_AR$ can be applied in the treatment of pain disorders. The 1,3-oxazole KRM-II-81 (**77**), as an α2/3 $GABA_AR$ PAM, is active in animal models of pain due to its potency at these two subtypes, which are involved in the association of antihyperalgesic and antinociceptive effects. Therefore, oxazole **77** was evaluated to determine the efficacy of antinociceptive properties in a series of pain models, including visceral pain, inflammatory pain, and neuropathic pain.

3.3.3.1. Visceral Pain Model

Over the past few decades, a series of animal models of diseases have been established and developed in the area of antinociceptive activity. Visceral pain has been studied, which is induced by evoking the organs of the abdomen or pelvis with chemical, mechanical, or electrical noxious stimuli. One of the most common methods to study the nociceptors is the acetic acid writhing model,[259] which measures the spontaneous pain. KRM-II-81 (**77**) was evaluated in this acid-induced writhing test to determine if there was any antinociceptive-like effect. Acetic acid (0.6 %) was injected in mice, and the number of writhes (stretching, retracting, or pressing the belly against the floor) was recorded and counted with a mean of 46.29 ± 3.859. The opioid receptor agonist morphine, as the positive control, was able to reduce the acetic acid-induced writhing in a dose-dependent manner and the effect was significant at 0.32 mg/kg. Both KRM-II-18B and KRM-II-81 were able to attenuate the acetic acid-induced writhes. The significance was reached at 3.2 and 10 mg/kg of KRM-II-18B, whereas it was reached at 5.6 and 10 mg/kg of KRM-II-81, as compared

to the vehicle. No larger doses of both ligands were applied due to the sedative potentials at higher doses. A weaker chemical stimulus, 0.32 % of lactic acid, was used to induce writhes because both of the two PAMs only reduced 0.6% acetic acid-induced writhes partially, which might be too strong for the ligands. Under this condition, the vehicle group exhibited 27.33 ± 3.138 writhes. Morphine also able to attenuate the lactic-acid-induced writhing, which was more potent than in that of using 0.6% acetic acid and the significance was reached at 0.32 and 1.0 mg/kg. Both $GABA_AR$ PAMs reduced the 0.32 % lactic acid-induced writhes significantly at 10 mg/kg, as compared to the vehicle and 3.2 mg/kg treatment, as shown in Figure 129. The mechanism of this effect of mediating the antinociceptive effect through $GABA_AR$ was confirmed by the blockade of the antinociceptive effect of the two PAMs with the $GABA_AR$ antagonist flumazenil at a dose of 3.2 mg/kg, as depicted in Figure 130. These results suggested that the antinociceptive effects of both PAMs of Bz/$GABA_AR$ are acting at the BzR binding site of $GABA_ARs$.

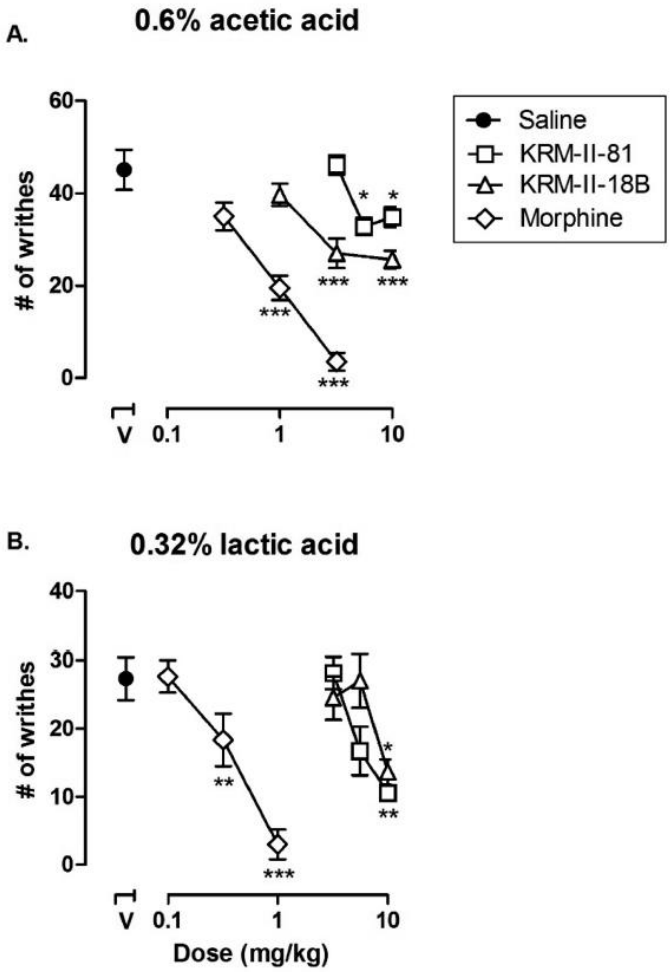

Figure 129. The assessment of antinociceptive effects of morphine, KRM-II-18B, and KRM-II-81 on (A) 0.6% acetic acid and (B) 0.32% lactic acid-induced writhing (n = 6−8 per group) observed in the 25 min observation period. *P < 0.05, ***p < 0.001. (Adopted from Figure in Lewter et al.) [236]

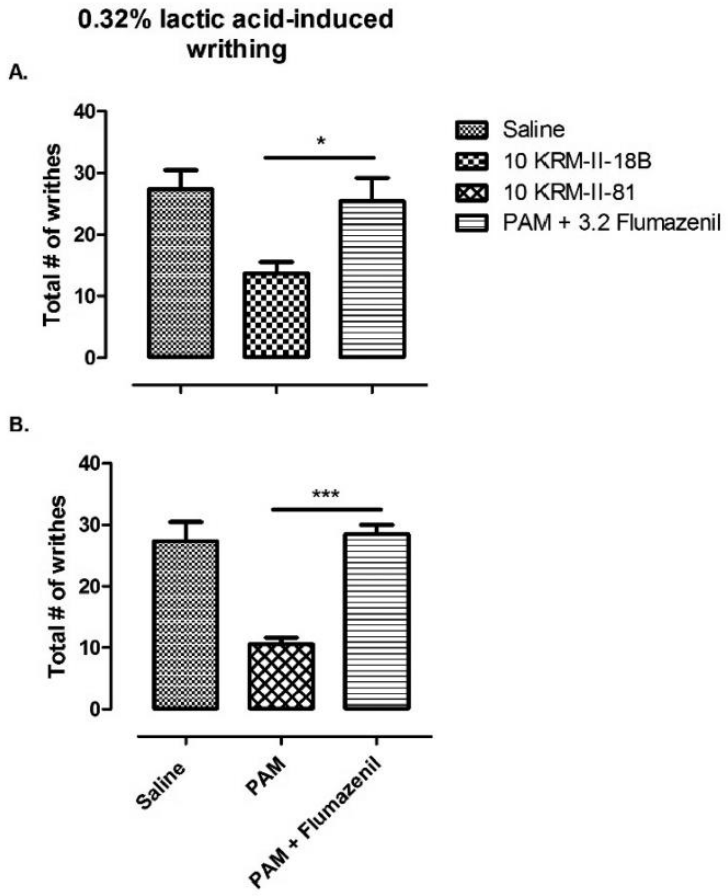

Figure 130. The assessment of flumazenil on the antinociceptive effects of KRM-II-18B- and KRM-II-81 in the acid-induced writhing model (n = 6−8 per group). Bars represent the mean and error bars show SEM. *P < 0.05, ***p < 0.001. (Adopted from Figure in Lewter et al.) [236]

3.3.3.2. Inflammatory Pain Models

The von Frey test is the gold standard for the evaluation of the mechanical allodynia in rodents and has been widely used in multiple animal models of diseases such as inflammatory pain, neuropathic pain, cancer pain, muscle pain, spinal injury and back pain, etc. In brief, rats (n = 6) are individually placed in cages with a wire grid floor or mesh. The induction of inflammation was achieved by the injection of 0.1 mL of complete Freund's adjuvant (CFA), a solution of antigen emulsified in mineral oil and used as an immunopotentiator, in the right hind paw of the rats. The left contralateral paw as unaffected and was the control paw. A filament was used to penetrate the

surface of the floor and poke the plantar surface of the hind paw until the fiber bends, which generates a constant force on the rat paw and is recorded.[260] Any exhibited response such as licking, withdraw or shaking of paw, is considered a positive response during the administration of the stimulus or immediately post the removal of the filament. The paw withdrawal threshold (PWT) was measured every 15 minutes. In the mechanical hyperalgesia study, rats received intermittent injections (every 20 min.) of increasing doses of flumazenil (or saline) immediately following pre-treatment with KRM-II-81 (**77**). The results of the CFA-induced inflammatory pain model in rats are illustrated in Figure 131. KRM-II-81 (i.p.) significantly increased pain thresholds in the Von-Frey test in rats after injection of the CFA in a dose-dependent and time-dependent manner. The withdrawal threshold reached a maximum effective dose at 5.6 mg/kg and at 60 minutes in all doses. The antinociceptive effects of treatment with **77** with a dose of 5.6 mg/kg can be completely attenuated by the $GABA_AR$ antagonist flumazenil at 10 mg/kg in the CFA-induced pain model via the von Frey test, as depicted in Figure 132.

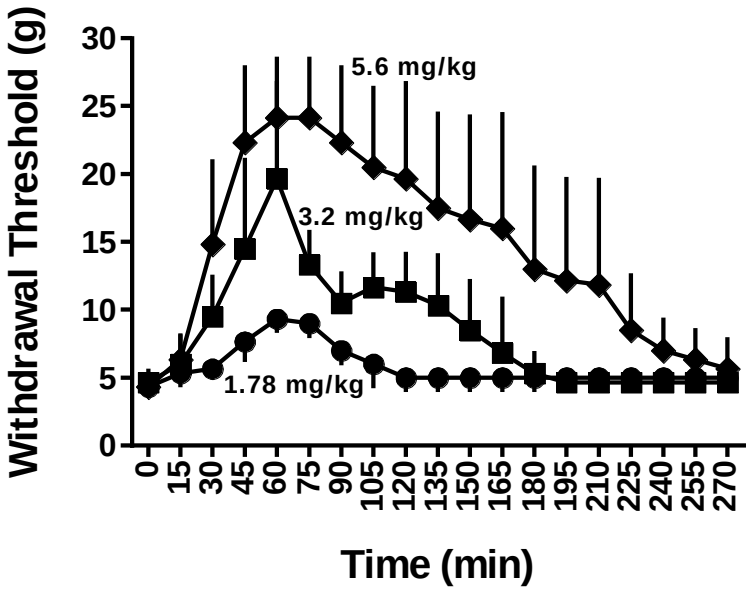

Figure 131. The withdrawal threshold by KRM-II-81 (77) treatment in the CFA-induced inflammatory pain in von Frey test in rats (n = 6) at 1.78, 3.2, 5.6 mg/kg up to 270 minutes test period. Each point represents the

mean + SEM of 6 rats. (Lewter, L., Cook, J.M. Li, J. The Behavioral effects of novel GABA(A) receptor positive allosteric modulators in rats. Biology, Behavior, and Chemistry Meeting, San Antonio, TX.,Mar. 2016)

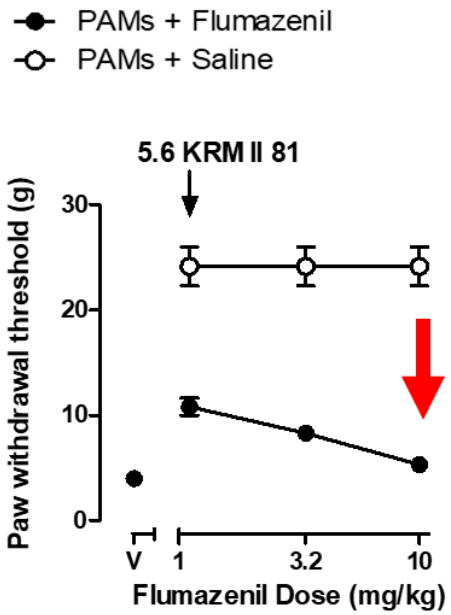

Figure 132. The assessment of flumazenil on the antinociceptive effects of KRM-II-81 (77) in CFA-induced inflammatory pain in rats (n = 6). The filled circle represented the PAM (5.6 mg/kg) + flumazenil group. The unfilled circles represent the PAM + saline group. The effect of KRM-II-81 (77) was completely blocked by flumazenil at 10 mg/kg. (Lewter, L., Cook, J.M. Li, J. The Behavioral effects of novel GABA(A) receptor positive allosteric modulators in rats. Biology, Behavior, and Chemistry Meeting, San Antonio, TX.,Mar. 2016)

The evaluation of possible tolerance to the antinociceptive effects of KRM-II-81 (**77**) was conducted in rats (n=6) that received 5.6 mg/kg (i.p.) of KRM-II-81 twice a day for 11 consecutive days in a CFA-induced inflammatory pain in the von Frey test versus the acute dose. Inflammatory pain was induced by Complete Freund's adjuvant (CFA) inoculations. The assay began 2 days after CFA treatment; mechanical hyperalgesia was measured on days 0, 4, 8, and 12. On days 1-3, 5-7, and 9-11 rats were treated with KRM-II-81 or saline twice a day (A.M. injections at 9:00-10:30 and P.M. injections at 5:00-6:30) in their home cages. On days 0, 4, and 8 rats will only receive P.M. injections due to the mechanical hyperalgesia test done in the A.M. The following doses of PAM were given at 5.6 mg/kg of KRM-II-81. In the acute study, they only received 5.6

mg/kg of KRM-II-81 (**77**) on day 12. On days that mechanical hyperalgesia was tested, cumulative dose-response curves included the following doses: KRM-II-81 (1.0-5.6 mg/kg). Tolerance to the antinociceptive effects of KRM-II-81 (**77**) did not develop in a 11 consecutive day study in CFA-induced inflammatory pain in von Frey test in rats, as illustrated in Figure 133 versus the control tests. The maximum percentage effect (MPE) of **77** treated group and vehicle group were nearly identical at all time, which indicated no tolerance of the antinociceptive effect of **77** had developed.

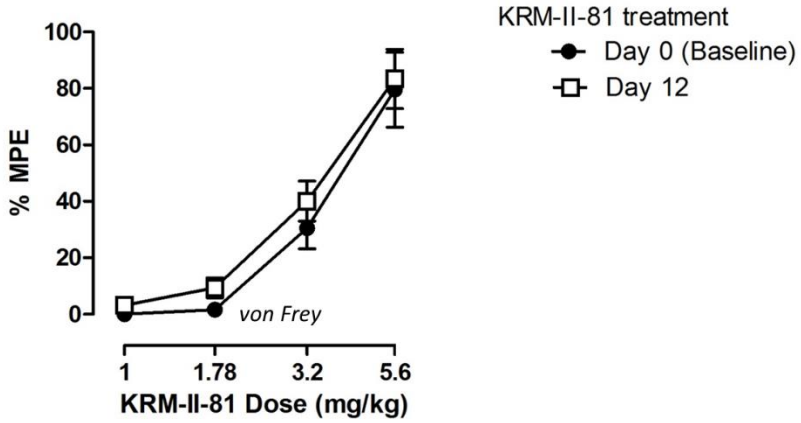

Figure 133. The evaluation of possible tolerance to the antinociceptive effects of KRM-II-81 (77) was conducted in rats (n=6) that received 5.6 mg/kg (i.p.) of KRM-II-81 twice a day for 11 consecutive days in CFA-induced inflammatory pain in von Frey test.Starting two days after CFA treatment, rats (n=6) were given 5.6 mg/kg of KRM-II-81, twice a day, for 11 consecutive days. On days 0, 4, and 8 rats will only receive P.M. injections due to the mechanical hyperalgesia test done in the A.M. (Unpublished data)

In addition to the CFA-induced inflammatory pain by the von Frey assay, KRM-II-81 (**77**) was also assessed in the formalin assay, which is a popular and reliable assay used as a chemical-induced inflammatory nociception model, to determine its ability to reduce the formalin-induced tactile hypersensitivity. The advantage of this assay over other inflammatory pain models is that it can produce both acute and chronic pain by a single dose of dilute formalin in a short period of time approximately 1 h. Briefly, rats were allowed to acclimate to the test chamber. The 50 μL of 5% formalin solution (in 0.9% saline) was given by i.p. injection to rats at the plantar surface of

the right hind paw. The response of the rat to the formalin-induced inflammatory pain was monitored and recorded for a period of 50 minutes. The behavioral response such as licking, resting or sniffing was observed and considered as the number of events. The response is the amount of time the animals spend licking the injected paw. Data were analyzed separately for two phases: the first 5 minutes and the later phase from 10-50 minutes. As illustrated in Figure 134, oxazole **77** was able to reduce the nociceptive response in the late phase of the test in a dose-dependent manner. The effect reached significance at 30 mg/kg, which was as efficacious as 80 mg/kg of the chronic used tramadol as the positive control. In the early phase of the test, only the positive control and **77** at 100 mg/kg significantly suppress the tactile-induced allodynia, as compared to the vehicle.

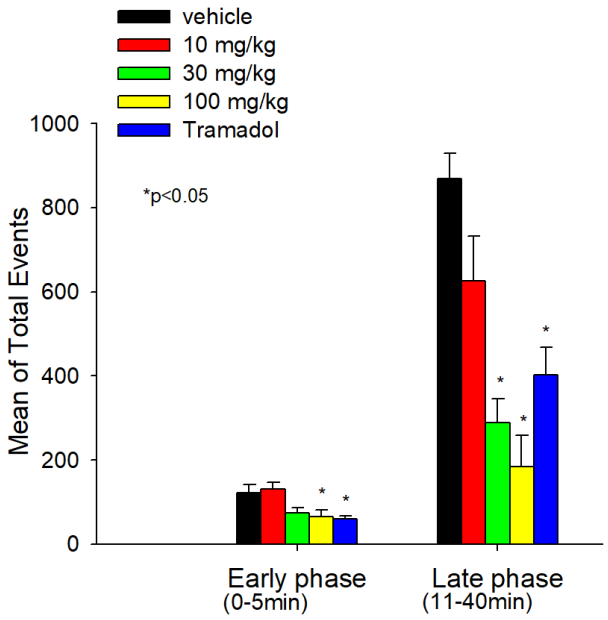

Figure 134. The assessment of antinociceptive effect of KRM-II-81 (77) in the formalin assay by reducing the paw-withdrawal thresholds. KRM-II-81 was given by i.p. injection to rats at a dose of 1-, 30, and 100 mg/kg, the positive control tramadol at 80 mg/kg. 77 (30 min prior) significantly reduced the nociceptive responses in the late phase at the dose of 30 mg/kg, whereas 100 mg/kg for the early stage. As a positive control, tramadol was active in both phases. Each point represents the mean±SEM of the same 8 rats *p<.05 compared to vehicle. (Modified from Figure in Witkin et al.) [245]

3.3.3.3. Neuropathic Pain Model

The spinal nerve ligation model is one of the direct peripheral nerve injury models for neuropathic pain.[259] In the spinal nerve ligation model, the L5 and L6 spinal nerves are separated and ligated with surgical silk strand tightly, which induces axonal degeneration and will affect all different types of axons in the area of the ligation. This leads to pronounced mechanical allodynia along with an unrecoverable spontaneous pain, which can last for months. The 1,3-oxazole KRM-II-81 (77) was evaluated in this spinal (L5/6) nerve-ligation (SNL)-induced neuropathic pain model for its potential analgesic effects. In brief, male rats went through SNL surgery 90 to 104 days prior to testing. After obtaining a baseline, rats were administrated i.p. with either vehicle (1% CMC), gabapentin (50 mg/kg) or **77** (30 mg/kg). During the test, the mechanical sensitization the rats underwent was measured with von Frey filaments to determine the paw withdrawal threshold (PWT) at every hour for a total of 4 hours of the test period. Gabapentin was used as a positive control since it is a commonly used medication for nerve pain and as an anticonvulsant. As illustrated in Figure 135, both the oxazole **77** and gabapentin reversed the SNL induced hyperalgesia at the 1 hour and 2-hour point after i.p. administration by increasing the PWT values. The oxazole **77** exhibited a greater reversal of antihyperalgesic effect than gabapentin with a lower dose, which would lower the possible concerns of side effect in higher doses resulting from the potentiation of off-target $GABA_AR$s or other receptors by gabapentin.

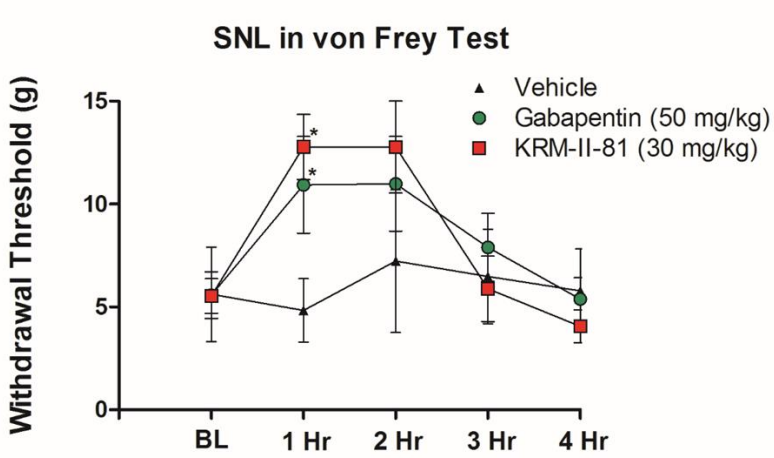

Figure 135. The assessment of KRM-II-81 (77) and gabapentin in the spinal (L5/6) nerve-ligation-induced neuropathic pain via the von Frey filament assay. Male Sprague-Dawley rats (n = 5) were administrated i.p. either vehicle, 77 (30 mg/kg), or gabapentin (50 mg/kg) and 30 minutes before testing. Analyzed using ANOVA (Dunnett's test: * P < 0.05). (Adopted from the Figure in Witkin et al, 2019)

A second SNL-induced pain experiment was performed using p.o. dosing rather than i.p. as the first experiment described above. As illustrated in Figure 129, the baseline levels of PWT were reduced to 0.65 ± 0.21 g by the sensitization methods of training before testing, as compared to the first experiment with a PWT value of 5.1 ± 2.8 g (Figure 136). Both 30 and 100 mg/kg of **77** administrated p.o., significantly increased PWT at 4 hour-point, whereas gabapentin tended to exhibit significance after 1 hour at 75 mg/kg, p.o. These results indicated a significant oral antihyperalgesic effect of **77** in the SNL-induced neuropathic pain model.

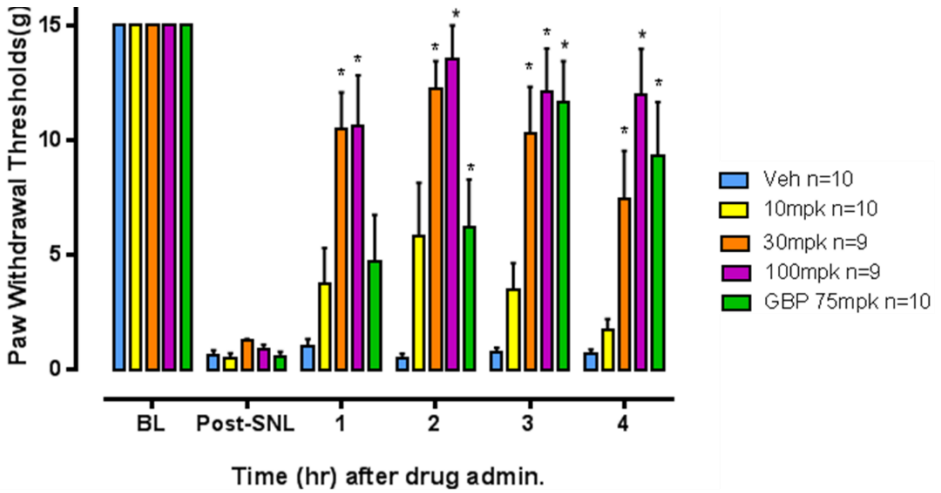

Figure 136. The assessment of KRM-II-81 (77) and gabapentin in the chronic spinal (L5/6) nerve-ligation-induced neuropathic pain in the von Frey filament assay under conditions of sensitization training. Male Sprague-Dawley rats (n = 5) were administrated p.o. either vehicle, 77 (10, 30, or 100 mg/kg), or gabapentin (75 mg/kg) and 30 minutes before testing. Analyzed using ANOVA (Dunnett's test: * P < 0.05).

The pain, that cancer patients suffer from, is not only from cancer itself but also from the treatments used against cancer. Chemotherapy-induced neuropathic pain (CINP) may occur during the treatment in cancer patients. In order to test the ability of possible alleviation of the pain from the chemotherapy-induced peripheral pain, KRM-II-81 (**77**) was further evaluated in the acute and chronic CINP model. In brief, vehicle or 4 mg/kg i.p. administration of the chemotherapy agent, Paclitaxel (PTX) used as a medication for cancer pain, was injected into mice to increased sensitivity to many sensory modalities such as mechanical and thermal hyperalgesia at day 0, 2, 4. On day 7, 11, 13 and on Day 15 (prior to the dose-response), mechanical hyperalgesia in the von Frey test, as described previously, and thermal allodynia (the length of the reaction) induced by acetone injection into the hind paw were measured. The dose-response was carried out at day 15 at the following cumulative doses: 0.1, 1, 5, 10, 15, 20 mg/kg with 6 injections, one every 30 min. After completing the dose-response study, treatments were decoded, and the ED 80 from mechanical data (Figure 137) was used to determine the dose for corresponding chronic treatment: 20 mg/kg for KRM-II-81 or 16 mg/kg for MP-III-080. From day 18, every even day up to day 40,

mice received an injection of their chronic treatment (vehicle, 20 mg/kg KRM-II-81 or 16 mg/kg MP-III-080) and then 30 minutes later, the measurements of mechanical hyperalgesia (3x per each hind paw) and thermal allodynia (2x per each hind paw) were recorded, as shown in Figure 138. Both KRM-II-81 and MP-III-080 are very effective in the CINP model at attenuating both mechanical and thermal allodynia. On odd days (19-30), the same processes were repeated, however, all measurements were taken prior to the chronic treatment injections, as presented in Figure 139. The results indicated that there was no tolerance to the anti-pain effects observed following chronic administration.

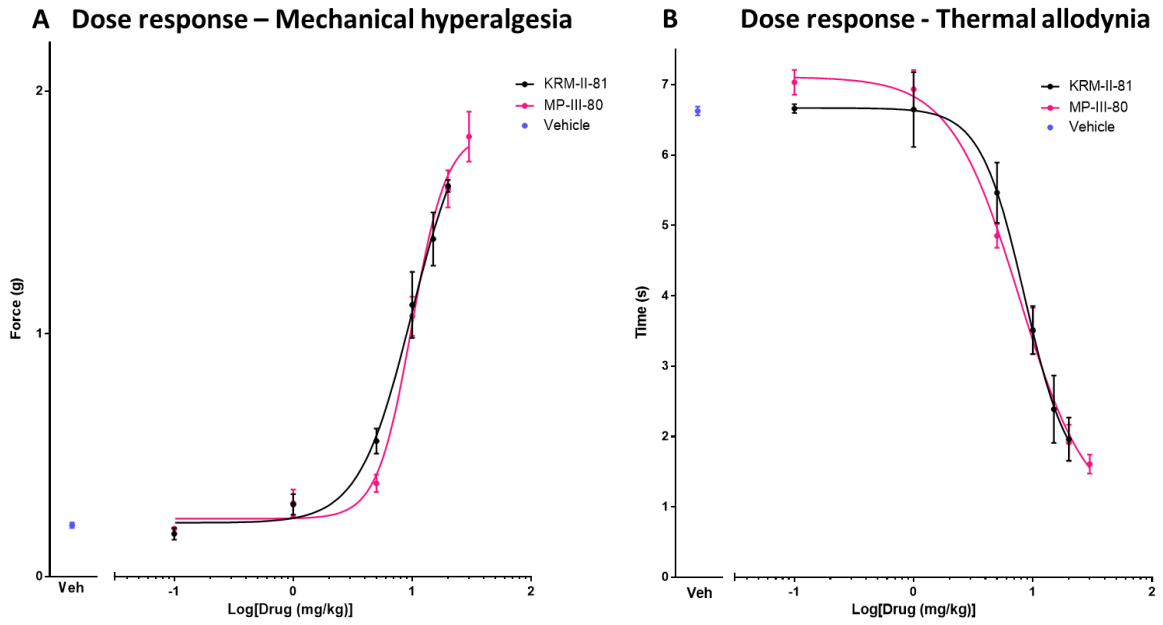

Figure 137. Acute dose-response effects of KRM-II-81 and MP-III-80 on (A) mechanical hyperalgesia and (B) thermal allodynia (n = 4). Veh represents mean of measurements from paclitaxel pre-treated animals in the vehicle dose response group (Mean ± SEM).

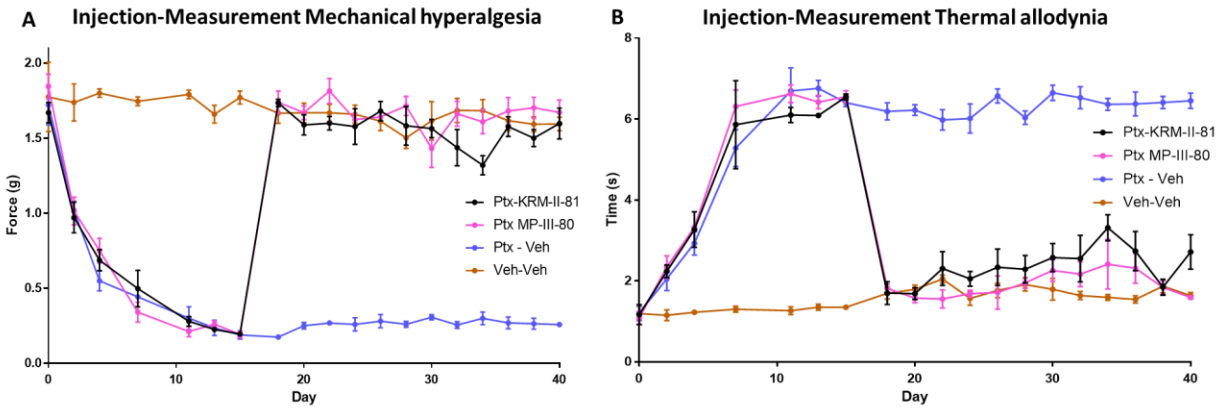

Figure 138. Effects of daily KRM-II-81 and MP-III-80 administration on chronic neuropathic pain (Day 18-40). Data for days 18-40 represent measurements of (A) mechanical hyperalgesia and (B) thermal allodynia (n = 4) 30 minutes after KRM-II-81, MP-III-80 or Vehicle administration. Ptx – Paclitaxel pre-treatment group, Veh – Vehicle pre-treatment or treatment groups. Error bars - ±SEM

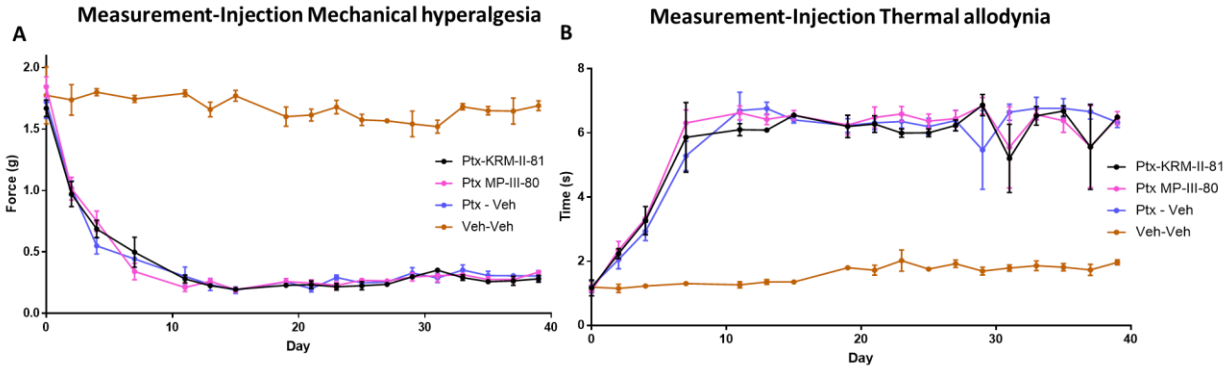

Figure 139. Effects of daily KRM-II-81 and MP-III-80 administration on chronic neuropathic pain (Day 19-39). Data for days 19-39 represent measurements of (A) mechanical hyperalgesia and (B) thermal allodynia (n = 4) before KRM-II-81, MP-III-80 or vehicle administration. Ptx – Paclitaxel pre-treatment group, Veh – Vehicle pre-treatment or treatment groups.

Take together all the data from different stimulus (chemical, thermal, mechanical) induced pain models; oxazole **77** was able to produce the desired antinociceptive or antihyperalgesic effects without the development of tolerance, which significantly widens the spectrum of oxazole **77** and its related analogs. No sedation, ataxia, amnesia loss of righting response no dependence was observed with **77,** and this was just confirmed by Steve Negus in the ICSS model with **77.**

3.3.4. Depression

Since depression is usually comorbid along with patients with anxiety, epilepsy, and pain, it is important to determine if the active drug can also produce an antidepressant effect as a beneficial property. As described in the previous chapter, the forced-swim test (FST), which is commonly used for the assessment of antidepressant-like effects of conventional and novel antidepressant drugs in pharmacological studies, was utilized for the possible desired effect of the 1,3-oxazole KRM-II-81 (**77**). It was administrated at its anxiolytic-producing doses, as an α2/3-selective PAM. This ligand was also tested in a related model, the tail-suspension test. Prior to the FST about 30 minutes, NIH Swiss mice were administrated i.p. with vehicle (1% CMC), oxazole **77** (3, 10 or 30 mg/kg) or the positive control imipramine at dose of 15 mg/kg, and placed in a chamber that was filled with water to a level that the mice can neither touch the bottom or escape. The reduction of immobility of mice indicates the animal was less depressed and would still continue to swim and search for a way to escape. The animal had not given up.

In the forced swim test, KRM-II-81 (**77**) exhibited an antidepressant effect at doses of 10 and 30 mg/kg by decreasing the immobility in a dose-dependent manner, as depicted in Figure 140. The marketed drug imipramine at 15 mg/kg ip, as expected, significantly reduced the immobility, as compared to vehicle ($F_{4,32}=8.19$, $p < 0.0001$). These results suggest there may be an alternative pathway, in addition to the serotonergic and/or noradrenergic systems,[261] for the treatment of depression by targeting at the α2-containing $GABA_AR$. It has also been reported that the α2 subunit might be involved in the antidepressant activity in a knockout study.[262] Furthermore, it was also suggested by Julian Mao (NIH). That antinociceptive agents that are both anxiolytic and antidepressant are considered much better therapies for a whole myriad of pain syndromes.

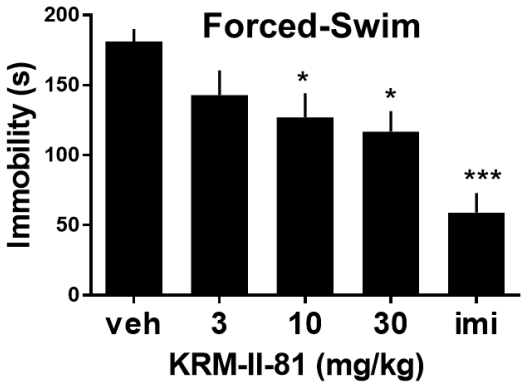

Figure 140. The antidepressant effect of KRM-II-81 (77) in male NIH Swiss mice in the FST. Mice were injected i.p. with vehicle (1% HEC, 0.25% Tween 80, 0.05% antifoam), KRM-II-81 (3, 10 or 30 mg/kg) or imipramine (15 mg/kg), n=6. *p < 0.05; ***p < 0.0001 as compared to vehicle by Dunnett's test.

3.3.5. Evaluation of the Lack of Side Effects in Other Animal Models

3.3.5.1. Respiratory Depression Effects

One of the critical side-effects of BZDR ligands, when combined with opioids, is respiratory depression, which significantly increases the emergency room visits as well as in overdose of BZDs combined with opioids or fentanyl. Therefore, KRM-II-81 (**77**) was evaluated for any possible respiratory depression effects. As presented in Figure 141, the non-selective $GABA_AR$ agonist, alprazolam, exhibited a significant decrease on the respiration rate at 0.32 mg/kg ($p < 0.01$) and 3.2 mg/kg ($p < 0.01$), whereas only at the highest tested dose 10.0 mg/kg of **77** actually have an effect on significantly reduced the respiration rate($p < 0.05$). All doses of both **77** and alprazolam did not exhibit a significant change in tidal volume. Alprazolam reduced the overall minute volume /kg value only at the highest dose at 3.2. mg/kg ($p < .05$), whereas no significant decrease was observed with the administration of **77** at any dose. Analysis of the oxygen consumption of KRM-II-81 (**77**) indicates there was no respiratory depression.

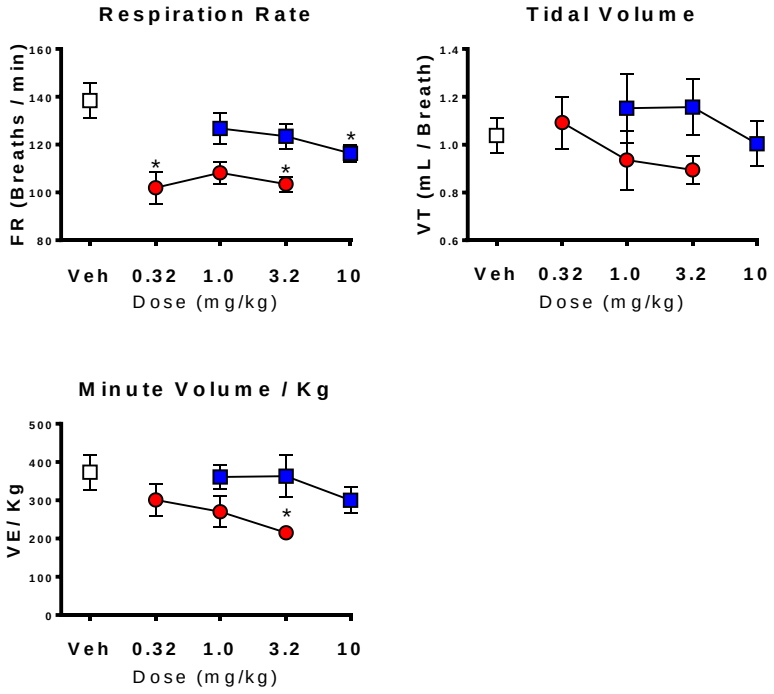

Figure 141. The effect comparison with administration i.p. of KRM-II-81 (30 min prior) and alprazolam (15 min prior) on measures of respiration in rats. a) Respiration rate, b) Tidal Volume c) Minute Volume / Kg. Data are means±S.E.M. (n = 8). *p < 0.05. (Adopted from Figure in Witkin et al., 2019)[245]

3.3.5.2. Drug Abuse Liability

Drug discrimination is a widely used method for determining the *in vivo* pharmacology of drugs abuse liability for by determining whether the known drug of abuse can be substituted by a new test ligand that produces a similar desired pharmacological effect as the known drug. In brief, rats are subjected to a 15-minute daily training. During the training section, lever pressing was reinforced by given a sugar pellet. Before the test session, rats are administrated with either 3.2 mg/kg midazolam, a known drug of abuse, or vehicle. Responses on pressing the "drug lever" are reinforced during drug training sessions; the same procedure was used for the training on pressing "vehicle lever" during vehicle training sections. Test ligand KRM-II-81 (**77**) at the antinociceptive dose of 5.6 mg/kg was injected into rats for the determination of its abuse ability by the responses

of rats that mimic or alter the response of midazolam. If the new ligand exhibited more than 80 % responding on the midazolam drug level, it would be considered as high risk of abuse potential, 20-80 % are partially generalized, less than 20 % indicates low abuse liability than the midazolam training drug. As an illustration in Figure 142, KRM-II-81 at 5.6 mg/kg, which produced a maximal analgesic effect in von Frey assay in the inflammatory chronic pain model, does not substitute for 3.2 mg/kg of midazolam in the drug discrimination assay. However, it elicited a moderate abuse liability at 17.8 mg/kg. The response rate was nearly at baseline at 32 mg/kg of **77**, which indicated a high potential of abuse, since higher doses of known drug of abuse do not produce a response. Examination of the data in this assay shows that at a dose that is anywhere near a clinical antinociceptive dose of **77**, there was no abuse potential.

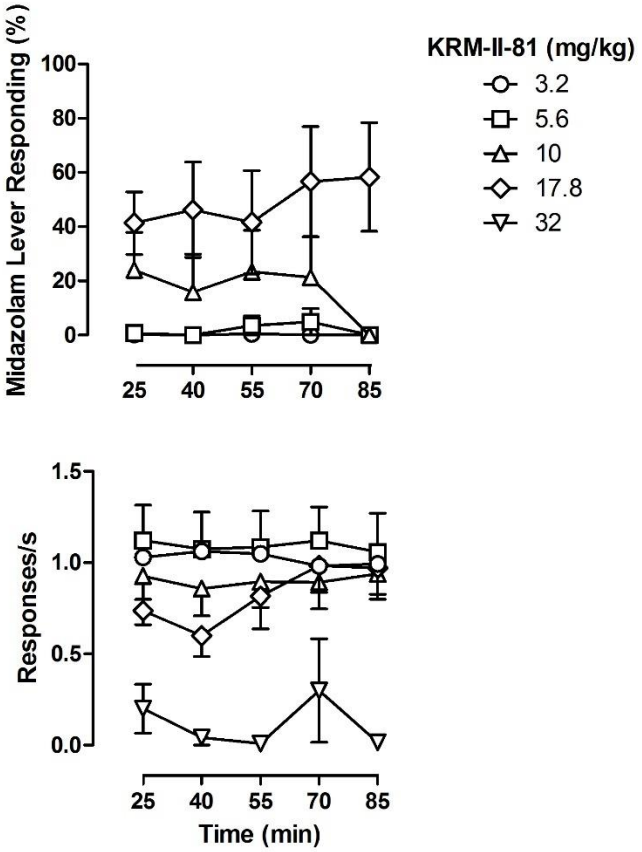

Figure 142. Drug discrimination assessment of increasing dose (3.2, 5.6, 10, 17.8, 32 mg/kg) of KRM-II-81 as compared to the known drug of abuse, midazolam at 3.2 mg/kg. Upper panel, midazolam lever responding percentage; lower panel, responses per second. KRM-II-81 at 5.6 mg/kg does not substitute for midazolam in the drug discrimination assay.

In addition to the drug discrimination test on KRM-II-81 (**77**), an assay of pain-depressed intracranial self-stimulation (ICSS) was also utilized to explore the potential abuse liability as a second approach, since it has been reported that the preclinical potential of drug liability can be indicated by drug-induced facilitation of ICSS in the absence of a noxious stimulus. In brief, rats were trained to press a level in response to the pulses of electrical brain stimulation. The ketorolac, an analgesic NSAID, was used as a positive control and diazepam as a negative control since it was not active in pain models but produced drug abuse potential. After a baseline was obtained, rats were administrated i.p. with either vehicle, or 0.32-10 mg/kg KRM-II-81 (n=8) and 0.1-10 mg/kg ketorolac (n=6) or 0.32-10 mg/kg diazepam (n=6) in the absence of the dilute lactic acid, as an acute visceral noxious stimulus, which produce an reduced response of ICSS and can be mitigated by clinically effective analgesics. A frequency-dependent increase in ICSS rates was achieved in the baseline condition by the electrical brain stimulation. As presented in Figure 143, neither ketorolac nor **77** at all tested doses significantly influenced ICSS rates, whereas a dose-dependent increase in ICSS rates was observed with diazepam treatment, especially at the dose of 1.0 and 3.2 mg/kg administration. These results suggest that both ketorolac and **77** did not affect the ICSS response in the absence of the noxious stimulus, which indicated a low potential of abuse liability; however, diazepam-induced facilitation which is consistent with its abuse potential.

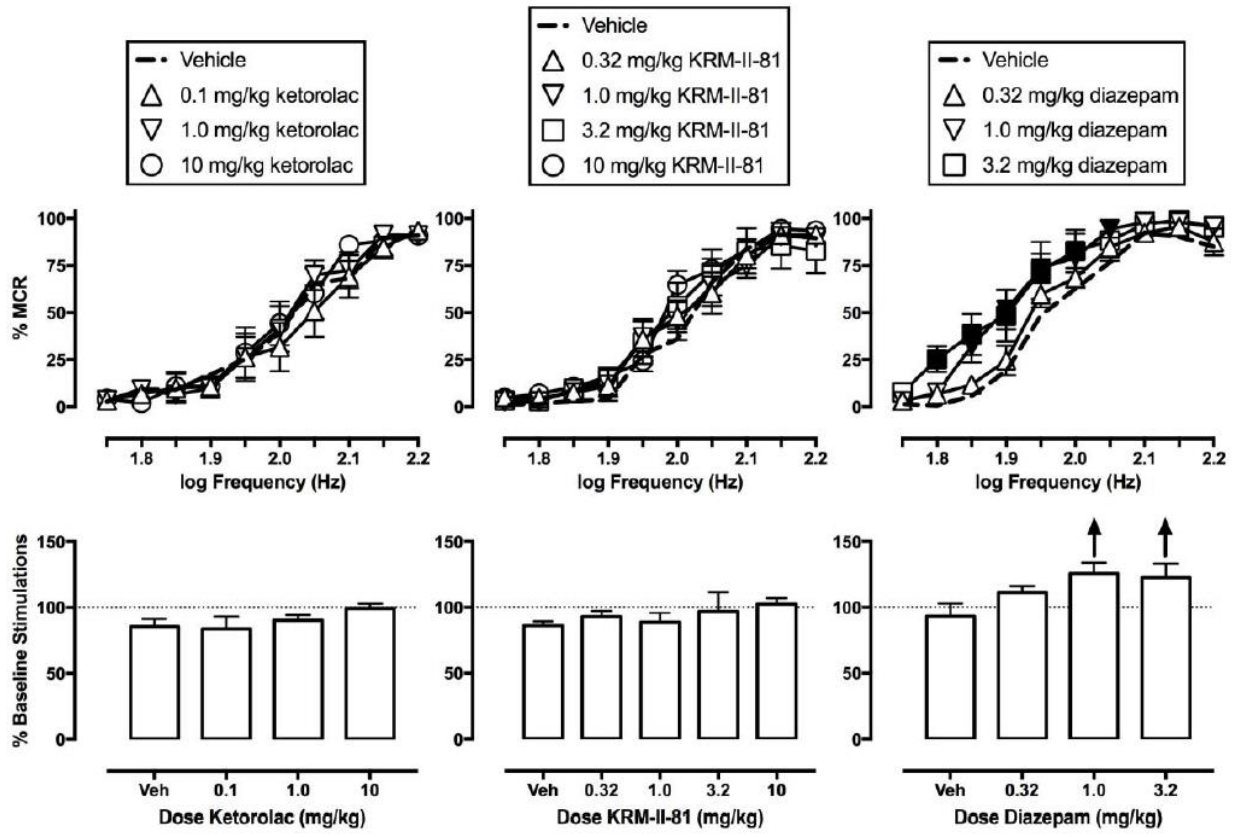

Figure 143. The effects of ketorolac (n=6), KRM-II-81 (n=8) or diazepam (n=6) effects on ICSS in the absence of the acid noxious stimulus in rats. Top panels show frequency-rate curves. Significance ($p<0.05$) is indicated by filled symbols, as compared to vehicle. Bottom panels show the total stimulations earned across all frequencies expressed as a baseline % for each frequency-rate curve on the top. Upward arrows indicate a significant increase in ICSS. All points and bars represent mean (± S.E.M.). (Adopted from the Figure in Moerke et al., 2018)

3.3.5.3. No Motor Impairment in the Rotarod Study

Since CNS side effects are major concerns for using imidazodiazepines (IMDZs) that bind to BzR site, KRM-II-81 (**77**) was evaluated in the rotarod test with a longer test period and higher doses to determine the possible toxicity-production dose and duration. As reported, **77** did not produce any sedative or ataxic effects on the rotarod at 30 mg/kg as the effective dose for anxiolytic effects. However, tremors, the latency of righting reflex and sedation were observed with p.o. administration of **77** at 120 mg/kg at the 2 hour-time point, as illustrated in Figure 144-146.

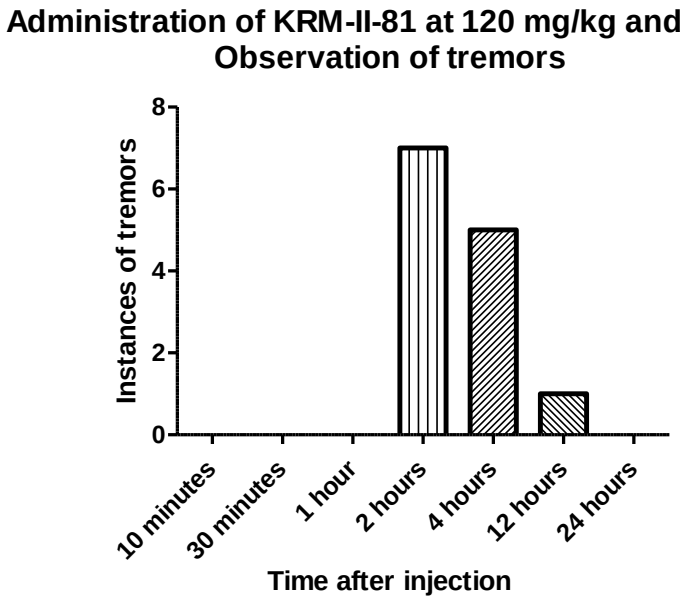

Figure 144. The observation of possible tremors of KRM-II-81 administrated p.o. at 120 mg/kg for 24 hours, n = 9.

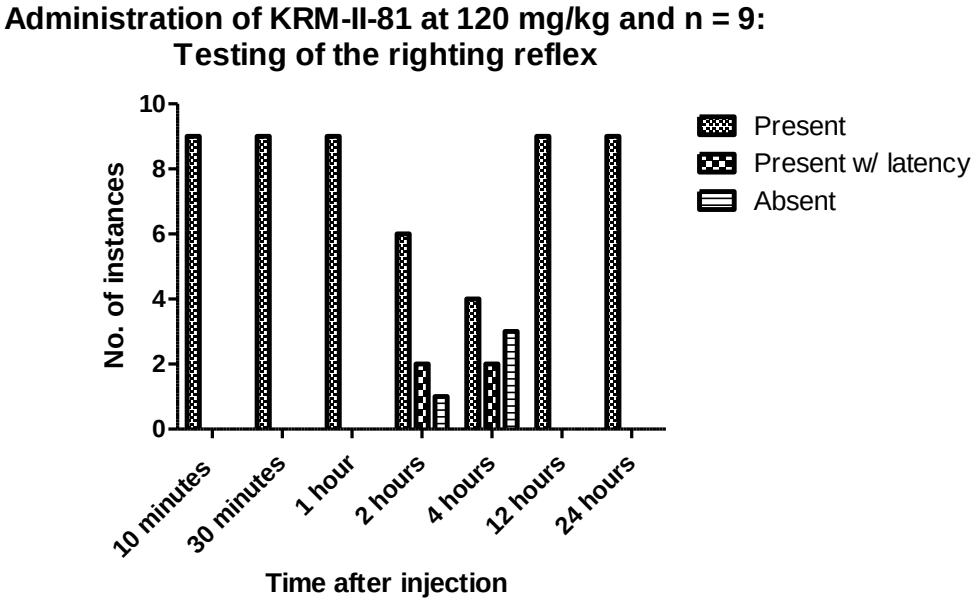

Figure 145. The observation of righting reflex of KRM-II-81 administrated p.o. at 120 mg/kg for 24 hours, n = 9.

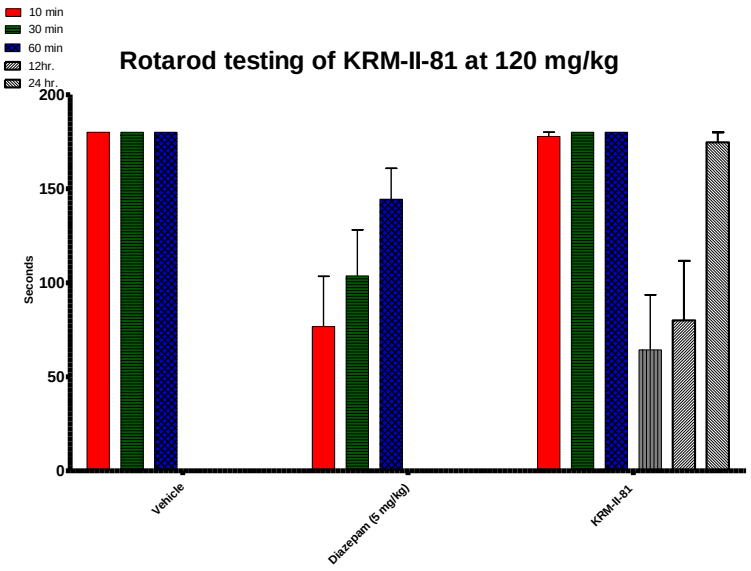

Figure 146. The observation of sedation of KRM-II-81 administrated p.o. at 120 mg/kg for 24 hours, n = 9, on rotarod test.

The study of metabolites in MLM (mouse), RLM (rat), MLM (monkey) and HML (human) from Eli Lilly on KRM-II-81 (Appendix VI) illustrated that the concentration of the metabolites in mice were much less in rats and nearly undetectable in monkey and not detectable in human liver microsomes, which suggested that the possible toxic metabolites induced tremor and latency, might not be produced in other species or only a trace of them was produced but too small an amount to induce a toxic effect. Importantly, ETSP/NINDS demonstrated that when the administrated 120 mg/kg in rats p.o., there were no side effects observed. This is a key result in regard to toxicity. Therefore, further identification of metabolites and their activity in mice or rats would be helpful to determine the exact toxic metabolites in mice, furthermore, the ligand design can be optimized from that data to avoid the metabolite-induced side effects observed in mice.

3.4. Conclusion

In conclusion, modifications of previous procedures for the synthesis of Hz-166 (**76**), MP-III-080 (**102**) and KRM-II-81 (**77**) are presented in this work under milder conditions and with much-improved yields. Moreover, an alternative method for the synthesis of the aldehyde (**107**) from ester (**76**) was optimized and overcame the long-standing problem of N(5)-C(6) imine bond reduction in good yield. These methods have been employed for larger scale reactions. In addition, there is no need for column chromatography for most of the compounds, which provided a much more practical route. With the improved synthesis, large quantities of these three α2/3-subtype selective $GABA_A$Rs PAMs, which exhibited anxiolytic, anticonvulsant and antinociceptive effects in many tests, can now be supplied with high-efficiency for investigation in many behavior assays including those in primates or other animal models for anxiety and epilepsy, pain as well as for depression.

Preclinical *in vitro* studies suggest that the 1,3-oxazole KRM-II-81 (**77**) represents a promising novel lead compound with the desired pharmacological profile, including α2/α3-$GABA_A$R subtype selectivity, no binding affinity for 46 other receptors (no hERG), an excellent PK profile, no cytotoxicity, metabolically stable on liver microsomes (human, rat, mice), and good lipophilicity (clogP = 2.3; ChemAxon program). In summary in the various animal models, 1,3-oxazole **77** demonstrated a wide range of beneficial behavioral effects, including the anxiolytic effect in marble bury assay and Vogel conflict assay; the excellent anticonvulsant effects from a series of both acute and chronic seizure models, resistant epilepsy as well as the ability to reduce the firing rate from human cortical epileptic tissues; the antinociceptive effect in acid-induced visceral pain model, the antihyperalgesic effect in the CFA induced mechanical allodynia in the von Frey test with no development of tolerance in the models of inflammatory pain. In addition,

oxazole **77** showed no SNL-induced hyperalgesia as well as no thermo-induced allodynia in the models of neuropathic pain. Importantly, the oxazole **77** had an antidepressant effect in the FST, no respiratory depression; no drug abuse potential (ICSS) as well as no sedation at all at important pharmacological concentrations. Taken together, all these evidence on 1,3-oxazole **77** strengthens the fact that an α2/3 $GABA_AR$ PAM **77** should be very valuable and efficient for the treatment of anxiety, epilepsy, and pain. Further investigations on metabolite studies, ADME-Tox studies, GMP synthesis and analog synthesis based on this oxazole, should provide better drugs for anxiety, pain, and respiratory/resistance epilepsy as well as depression.

3.5. Methods

3.5.1. Dorsal Root Ganglion Electrophysiology (Dr. Kevin Freeman, University of Mississippi Medical Center)

The culture of dorsal root ganglion neurons were prepared as described (Bleakman et al., 1996). Briefly, DRG were isolated from 2-month old rats (235–310 g) and enzymatically digested with 3 mg/mL of type II collagenase at 37 °C for 50 min. After 50 min of digestion, the tissue was mechanically dissociated with a series of sterile fire-polished glass pipettes of decreasing diameter. The dissociated neurons were plated directly on Nunc 35×10 tissue culture dishes and incubated in Nb Active1 (Brainbits LLC, Springfield, IL) supplemented with 5% dialyzed fetal bovine serum, 0.25% Glutamax (Gibco). Cell cultures were maintained in a tissue incubator (37 °C, 5% CO2) and used within seven days. DRG neurons were recorded at room temperature using conventional whole-cell voltage clamp methods as described (Cerne et al., 2016). Cells were voltage clamped at −80 mV for the duration of the experiment. GABA currents were activated by 4 s perfusion with

GABA at an EC10 concentration using a ValveBank II eight channel perfusion system (AutoMate Scientific, Berkley, CA). Stock solutions of test compounds were prepared in DMSO and diluted into the external solution or the GABA EC10 solution such that DMSO concentrations did not exceed 0.1% (v/v). The test compound was perfused for 2 min followed by 4 s co-administration with GABA. During the recording, the Nunc 35×10 tissue culture dishes were continuously perfused with an external solution using a gravity flow perfusion system, as described (Witkin et al., 2019). The data were normalized to the baseline GABA EC10–evoked current amplitude and reported as the mean ± standard error of the mean (SEM). The concentration-response data were fit using the four parameter Hill equation.

3.5.2. Marble Burying Assay (CRO)

The ligands were evaluated in the marble burying assay in mice using the previously published methods (Li, et al., *Life Sci.*, **2006**, *78*, 1933 – 1939). Mice were administrated i.p. with either vehicle (1% carboxymethyl cellulose) or a test compound 30 min prior to testing. Mice were then placed in a 17 x 28 x 12 cm high plastic tub with 5 mm sawdust shavings (Harlan Sani-Chips, Harlan-Teklad, Indianapolis, IN) on the floor. The 20 blue marbles (1.5 cm diameter) were placed in the center of the tub. Mice were left in the tub for 30 min. The marbles that were buried (2/3 covered with sawdust) by mice were counted and recorded.

3.5.3. Vogel Conflict Assay (Dr. Jeffrey M. Witkin, Wikin Consulting)

The ligands were evaluated in male Sprague-Dawley rats (Harlan Industries, Indianapolis, IN) weighing between 200-300 grams in the Vogel conflict assay using the previously published

methods (Alt, et al., *Neuropharmacology*, **2007**, *52*, 1482 – 1487). Operant behavior test chambers ENV-007 (Med Associates Inc., Georgia, Vermont, USA) 30.5 x 24.1 x 29.2 cm, were used for conducting the assay. The data were recorded by a Compaq computer running MED-PC Version IV (Med Associates Inc., Georgia, Vermont, USA)., Water was withheld for 24 h before the first training session. A 6 min drinking session after the first lick was considered of the training. The unpunished component was at the first 3 min, and the punished component was at the last three min of the assay. There was no shock given in the punished component during the first two training days. After training, rats were placed back into their homecages and water was accessible to the animal for 30 min before being deprived for the next 24 h prior to the next session. On the third day, 30 min prior to testing (n = 6 – 8), the rats were administrated i.p. with either vehicle (0.5% Tween 80, 1% hydroxyethyl cellulose, 0.05% Dow anti-foam administered at 3 mL/kg), chlordiazepoxide (20 mg/kg at 1 mL/kg), Hz-166 (30 mg/kg at 3 mL/kg) or KRM-II-81 (3, 10, 30, or 60 mg/kg; 3 and 10 mg/kg at 1 mL/kg, 30 mg/kg at 3 mL/kg, and 60 mg/kg at 6 mL/kg). During the punished section on the third day, rats received a minimal electrical shock (100 msec, 0.5 mA) after every 20th lick (FR20). The recorded value of the mean number of licks during both punished and unpunished were analyzed as compared to the control vehicle group. Dose-effect functions were analyzed by ANOVA followed by post-hoc Dunnett's test with vehicle treatment as the control standard. Statistical probabilities $\leqslant 0.05$ were considered significant.

3.5.4. 6 Hz 44mA Seizure Model (ETSP)

In briefly, mice were administrated p.o. with KRM-II-81 (**77**), and the 6 Hz stimulation was delivered for 3 seconds after 2 hours through corneal electrodes at 44 mA, and the seizure activity

in the animal was observed and recorded. A parallel group of mice was administrated with higher doses of **77** and observed for potential motor impairment and possible toxicity at 4 hours after dosing.

3.5.5. Maximal Electroshock Seizure (MES) Model (ETSP)

This assay detects the anticonvulsant effects of the test compounds that produced generalized seizures and those that alleviated seizure spread. Male, CD1 mice (Taconic Farms) were studied at weights of 21-32 g. The Wahlquist Model H stimulator with 0.2-sec stimulation with corneal electrodes was used in the assay. Diazepam was dissolved in 1% hydroxyethylcellulose/0.25% Tween- 80/0.05% Dow antifoam in water. KRM-II-81 and HZ-166 were suspended in carboxymethylcellulose. The dose volume for diazepam was 1 mL/kg for rats, and 10 ml/kg was used for mice. KRM-II-81 and HZ-166 were dosed in volumes of 10 mL/kg in mice. HZ-166 was dosed in a volume of 5 mL/kg in rats and KRM-II-81 was dosed at 1 mL/kg in rats below doses of 30 mg/kg; 30 mg/kg (dosed at 3 mL/kg), 60 mg/kg (dosed at 6 mL/kg). Mice were administrated i.p. with diazepam (1, 3 or 6 mg/kg), **76** (3, 10 or 30 mg/kg) or **77** (3, 10 or 30 mg/kg) 30 minutes prior to testing, and were observed for approximately 10 sec after administration of the electrical stimulus (10 uA) and the types of convulsions were recorded (0 = no convulsion, 1 = clonus, 2 = tonic flexion, 3 = tonic extension). Mice were euthanized immediately for the following test. The tonic extension at hindlimb was recorded as the primary endpoint. The Fisher's Exact probability test was used to analyze the percentage of animals exhibiting convulsions.

3.5.6. Inverted Screen Test (ETSP)

Male, Sprague Dawley rats (Harlan Sprague Dawley, Indianapolis, IN) were used, which weighed 90-110 g for this assay. The apparatus consisted of four 13 x 16 cm squares of a round hole, perforated stainless steel mesh (18 holes/square inch, 3/16 inch diameter, ¼ inch staggered centers, 50% open area) mounted 15 cm apart on a metal rod, 35 cm above the table top. Rats were administrated with test compounds p.o. with diazepam (3 or 10 mg/kg), **76** (30 mg/kg) or **77** (10 or 30 or 60 mg/kg), and returned to their home cage. The rats were evaluated on the inverted screen test after 25 min of dosing and were scored after 60 seconds as follows: 0=climbed over to the top of the screen, 1= hanging on to screen, 2= fell off).

3.5.7. Pentylenetetrazole (PTZ)-Induced Seizures (ETSP)

The rats were administrated i.p. with pentylenetetrazol (35 mg/kg, s.c.) in a volume of 1 ml/kg. A cage (40.6 x 20.3 x 15.2 cm) with a floor containing 0.25 inches of wood chip bedding material was used for placing the rats for observation. The dose of PTZ (35 mg/kg) was determined to be ~ EC97 for inducing the clonic seizures. The rats were then observed for 30 min post-PTZ for clonus seizures which the rat demonstrated loss of righting of fore- and hindlimbs or for tonic seizures as indication by loss of righting accompanied with tonic hindlimb extension. Fisher's Exact probability test was used to analyze the percentage of animals exhibiting convulsions.

3.5.8. Pentylenetetrazole (PTZ)-Induced Seizure Threshold (ETSP)

Male F-344 Harlan rats (Indianapolis, IN) were randomly assigned to treatment groups and administrated vehicle or test compounds. Rats were placed in a restrained container, and a winged infusion needle was inserted into the lateral tail vein. Intravenous infusion with 10 mg/ml PTZ at

a rate of 0.5 ml/min was initiated until a clonic seizure was observed, and the time to produce a seizure was recorded in sec or a maximum for four min was recorded and was calculated by the infusion rate concentration of PTZ, time to clonic convulsion, and animal weight. After the test of infusion, rats were euthanized.

3.5.9. Corneal Kindled Mouse Model (ETSP)

In brief, the male CF-1 mice are receiving a twice-daily kindled electrical 3-sec stimulation, 3 mA, 60 Hz by corneal electrodes for 10-14 consecutive days to reach the criterion of Stage 5 seizures. Mice were continuously given this twice daily stimulations until they achieved the criterion to ensure they were fully kindled. Any mouse not reaching the criterion was not included for the experiment for assessment of novel test compounds. The test started at 5-7 days post the last stimulation, after which stimulation was given to the mice to ensure the animals were at Stage 5 seizures. Mice (two groups, each group has 4 fully kindled mice) were then administrated p.o. with the doses at 1, 3, 8, 15, 25, 30 mg/kg of KRM-II-81 (**77**), and the time of peak effect (TPE) was determined at the 2 hour time-point. After the test, the corneal kindled mice were placed back into their home cage and were allowed to wash out the test compounds for 3-4 days.

3.5.10. Lamotrigine (LTG)-Resistant Amygdala Kindled Rat Model (ETSP)

In brief, an electrode was implanted into the left amygdala in anesthetized male Sprague-Dawley rats (250-300 g). After one week of recovery, animals started to receive a daily 200 μAmp stimulus until they all reached to the Stage 4 or 5 seizures. LTG at 30 mg/kg was injected i.p. to the fully kindled animals to induce resistant seizures, before being stimulated to confirm the LTG sensitivity

of the vehicle group, as well as the LTG-resistance group. After the washout of LTG for 3 days, animals were administrated with KRM-II-81 (**77**) at the doses of 1, 5, 10, 20, and 40 mg/kg, then challenged with the stimulus at the predetermined time of peak effect at 1 hour. After the test, the corneal kindled mice were placed back to their home cage and were allowed to wash out the test compounds for 3-4 days.

3.5.11. Model of Mesial Temporal Lobe Epilepsy (ETSP)

In brief, the injection i.v. of kainic acid (KA) at 1 mmol in 100 mL into the dorsal hippocampus of adult male C57/Bl6 mice, induces non-convulsive severe epilepsy. An electrode was implanted into the left hippocampus in male mice. After the KA injection for 4 weeks, a group of 4 MTLE mice was injected i.v. of 15 mg/kg of KRM-II-81, and the behaviors of the animal were recorded by digital EEG recordings for 20 minutes before-injection and 90 minutes after-injection. The number of HPDs were recorded and analyzed during a 20 minutes period for 10 minutes before and 10 minutes after the peak time of effect.

3.5.12. Chronic Post-SE (KA) Spontaneously Seizing Rats: Stage 1 with IP Administration (ETSP)

Chronic epilepsy in rats with status epilepticus was induced by a repeated low-dose of kainic acid (KA) at 7.5 mg/kg i.p. at every hour up to 4 hours until animal achieved Stage 5 seizures. The dose can be reduced as long as the animal retains lower-stage convulsions. Rats were received 3 mL of Ringers solution to keep them from dehydrating. After 10 weeks of chronic treatment, the rats were implanted a wireless telemeter into the peritoneal space from the stomach to the head

underneath the skin. In the EEG suites, an initial seizure rate is recorded over a week in rats. Only the rats with the highest seizure burden scores will be selected (n = 24). During the test period, a baseline seizure rate is determined in week 1. During week 2, the rats were administrated with 20 mg/kg of KRM-II-81 (**77**) over 5 days, Monday-Friday. Rats are split into groups of 12 for the vehicle group and another 12 for the drug-treated groups. Once the treatment is completed in week 2, rats will be monitored during week 3 with only vehicle treatment (washout period). In order to avoid any possible design variations, the cross-over paradigm was utilized. Similar to the first group (n = 6), the second group (n = 6) receives vehicle first, followed by the treatment of **77**. A list of potential detected events (focal seizures for the drug treatment, generalized seizures for the vehicle treatment) are automatically accumulated and generated by a seizure detection algorithm via a MATLAB GUI. The results were presented by seizure burden, frequency, and distribution of Racine scores.

3.5.13. Evaluation of Seizure Protection in Resistant Epileptic Human Brain Tissue (Dr. Jeffrey M. Witkin, Wikin Consulting)

The tissue was prepared as previously described (Zwart et al., 2014). Slices were perfused at 1.0 mL/min with normal ACSF (NACSF) solution for 1 h at 37 ° C. If there was no spontaneous activity developed after 1 h, the tissue was then bathed in excitable ACSF (EACSF) solution containing 5 mM K^+ to induce a robust local field potential (LFP) activity in cortical tissues, after which 10 µM of picrotoxin was added, and the activity was recorded for 1 h to establish a baseline. Then 30 µM of KRM-II-81 was added, and the tissue activity was recorded for another hour. A second experiment was carried out with 50 µM of AP-4 following the same procedure described above with all 60 channels activated. Time points were binned at 4 ms. Two-way ANOVA was

performed to ensure whether KRM-II-81 was effective and whether the drug effect was dependent upon different channels, as described in (Witkin et al., 2018).

3.5.14. Acetic Acid and Lactic Acid-Induced Writhing Model (Dr. Lakeisha A. Lewter and Jun-Xu Li, University at Buffalo)

Mice were administrated i.p. with either 0.32% lactic acid or 0.6% acetic acid. The number of acid-induced writhes was observed and counted in a 25 min period, starting 5 min after the injection of acetic acid or 10 min after the injection of lactic acid. Writhe was defined as a contraction of the abdomen following a stretch of the hind limbs. Mice in treatment groups received subcutaneous (s.c.) injections of either morphine (0.1−3.2 mg/kg, 10 min pretreatment), KRM-II-18B (1−10 mg/kg, 30 min pretreatment), or KRM-II-81 (3.2−10 mg/kg, 30 min pretreatment). In the flumazenil blockade experiment, mice received s.c.injections of flumazenil 15 min before the injections of each PAM.

3.5.15. CFA-Induced Inflammatory Pain Model by the Von Frey Test (Dr. Lakeisha A. Lewter and Jun-Xu Li, University at Buffalo)

Subjects: Adult male Sprague-Dawley rats (Harlan, Indianapolis, IN, USA) were housed individually on a 12/12 h light/dark cycle. Behavioral studies were conducted during the light period. Animals had free access to water and food except during experimental sessions. Animals were maintained and experiments will be conducted in accordance with guidelines of the International Association for the Study of Pain (Zimmermann, 1983A) and were approved by the Institutional Animal Care and Use Committee, University at Buffalo, the State University of New

York (Buffalo, NY), and with the 2011 Guide for the Care and Use of Laboratory Animals (Institute of Laboratory Animal Resources on Life Sciences, National Research Council, National Academy of Sciences, Washington, DC).

Induction of inflammatory pain: Inflammatory pain was induced by Complete Freund's adjuvant (CFA) inoculations, as previously described (Li et al., 2014). CFA contains approximately 0.05 mg of Mycobacterium butyricum, inducing inflammation and increasing paw thickness. 0.1 mL of CFA (Difco, Detroit, MI, USA) was injected in the right hind paw of Sprague Dawley male rats under isoflurane anesthesia (2% isoflurane mixed with 100% oxygen at a flow rate of 5 L/min). Mechanical nociception tests were conducted 48 hours after CFA inoculation.

Mechanical hyperalgesia: Mechanical hyperalgesia was measured using von Frey filaments (1.4 g - 26 g; North Coast Medical, Morgan Hill, CA), 2 days after CFA treatment. Rats (n=6 per group) were placed in elevated boxes with a mesh floor (IITC Life Science Inc., Woodland Hills, CA). The von Frey filaments were applied perpendicularly to the medial plantar surface of the hind paw, starting with the lowest filament (1.4 g), and then applied in ascending order until a behavioral response (withdrawal of the hind paw) was elicited. Filaments were applied until buckling of the filament occurred and was maintained for approximately 2 seconds. After each measurement, rats received the next dose of the drug (every 20 min) until the maximum threshold (26 g) was observed.

Tolerance development: Starting 2 days after CFA treatment, mechanical hyperalgesia was measured on days 0, 4, 8, and 12. On days 1-3, 5-7, and 9-11 rats were treated with PAMs (KRM-II-18B, KRM-II-81, or midazolam) or saline twice a day (AM injections (9:00-10:30) and P.M. injections (5:00-6:30)) in their home cages. On days 0, 4, and 8 rats will only receive PM injections due to the mechanical hyperalgesia test done in the A.M. The following doses of PAMs were given: Twice a day 3.2 mg/kg of KRM-II-18B, and 5.6 mg/kg KRM-II-81 and midazolam were given.

On days that mechanical hyperalgesia was tested, cumulative dose-response curves included the following doses: KRM-II-18B (1.0-5.6 mg/kg), KRM-II-81 (1.0-5.6 mg/kg) , and midazolam (1.78-10 mg/kg).

Drugs:

The following drugs were used: KRM-II-18B, KRM-II-81, and midazolam. KRM-II-18B and KRM-II-81 were dissolved in a mixture containing, 20% DMSO, 10% emulphor, and 70% saline. Midazolam (Akorn, Inc.) was dissolved in 0.9% saline. Doses were expressed as the weight of the drug in milligrams per kilogram of body weight, and drugs were administered intraperitoneally. In the antagonist, study rats received intermittent injections (every 20 min.) of increasing doses of flumazenil (or saline) immediately following pre-treatment of PAMs.

3.5.16. Formalin Assay (Dr. Jeffrey M. Witkin, Wikin Consulting)

Briefly, rats were allowed to acclimate to the test chamber (SR-Lab Startle Response System, San Diego Instruments, San Diego, CA). The 50 μL of 5% formalin solution (in 0.9% saline) was given by i.p. injection to rats at the plantar surface of the right hind paw. The response of the rat to the formalin-induced inflammatory pain were monitored and recorded for a period of 50 minutes by a force-transducer. The behavioral response such as licking, resting or sniffing was observed and considered as the number of events. The response is the amount of time the animals spend licking the injected paw. Data were analyzed separately for two phases: the first 5 minutes and later phase from 10-50 minutes by ANOVA followed by post-hoc Dunnett's test with $p < .05$ being considered statistically different than vehicle control values.

3.5.17. SNL-Induced Hyperalgesia Model of Neuropathic Pain (Dr. Jeffrey M. Witkin, Wikin Consulting)

Male Sprague-Dawley rats (Harlan Industries, Indianapolis, IN), weighing between 225 and 300 g went through SNL surgery (as described in Witkin et al., 2019) 90 to 104 days prior to testing. After obtaining a baseline, rats (n = 5 for all groups) were administrated i.p. with either vehicle (1% CMC), gabapentin (50 mg/kg) or **77** (30 mg/kg). During the test, mechanical sensitization was subjected to the rats with von Frey filaments to determine the paw withdrawal threshold (PWT) at every hour for a total of 4 hours test period. Any exhibited response such as licking, withdraw or shaking of paw, is considered a positive response during administration of the stimulus or immediately post the removing of the filament. Paw withdrawal threshold (PWT) was measured every 15 minutes. In the mechanical hyperalgesia study, rats received intermittent injections (every 20 min.) of increasing doses of flumazenil (or saline) immediately following pre-treatment of drugs. In the second study, rats (n = 5) were administrated p.o. either vehicle, **77** (10, 30, or 100 mg/kg), or gabapentin (75 mg/kg) and 30 minutes before testing.

3.5.18. Chemotherapy Induced Neuropathic Pain (CINP) Models (Dr. Bronwyn Kivell, Victoria University of Wellington)

All experimental work involving animals was conducted on male C57BL/6J mice in the Victoria University of Wellington Australia Animal facility.

Acute treatment

On day 0 mice were allocated to either paclitaxel (n=12) or vehicle (n=4) pre-treatment groups. The paclitaxel group received 4 mg/kg intraperitoneally (i.p.) paclitaxel in a vehicle of one part

1:1:18 mix of kolliphor EL, ethanol and saline and the vehicle group received vehicle only. These injections were repeated on Day 2, 4 and 6 to give a cumulative paclitaxel dose of 16 mg/kg/i.p.

Prior to any measurement, mice were acclimatized to the experimental room with the experimenter present for 1 hour and then to the experimental chambers for a minimum of 10 min. On Day 0, 2 and 4 (before the paclitaxel injections), on Day 7, 11, 13 and on Day 15 (before the dose-response) mechanical hyperalgesia and thermal allodynia were measured. These measurements were conducted in transparent raised enclosures with a grated floor to allow access to the underside of the animal's paws. Mechanical hyperalgesia was measured using an electronic von Frey anesthesiometer (IITC Inc., Life Science Instruments, Woodland Hills, CA, USA). A trained experimenter applied a slowly increasing force to the center of the underside of a rear hind paw through a filament until a sharp withdrawal response was observed. The force required to observe this reaction was recorded. Mechanical hyperalgesia measurements were recorded three times for both hind paws on each measurement day. Thermal allodynia was measured by applying acetone to the hind paw with a syringe, and the length of the reaction (raising, licking, shaking or biting of the paw) was recorded. Thermal allodynia measurements were recorded twice for both hind paws on each measurement day.

Dose-response study

On Day 15 the Paclitaxel pre-treated mice were allocated to each of the dose-response treatments: KRM-II-81, MP-III-80, and Vehicle (n=4). These treatments were blinded to the experimenter. During the dose-response all mice received six injections, one every 30 min. KRM-II-81 and MP-III-80 injections were at the following cumulative doses: 0.1, 1, 5, 10, 15, 20 mg/kg. Two measurements of mechanical hyperalgesia and one measurement of thermal allodynia for each hind paw were performed ~ 30 min after each injection.

Chronic neuropathic pain

Following the dose-response measurements on day 15, the treatment groups were decoded, and the ED_{80} dose from the mechanical hyperalgesia data was used to determine the chronic treatment doses for both KRM-II-81 and MP-III-80 in CINP. During the chronic experiment, KRM-II-81 and MP-III-80 or vehicle controls received a 1:2:7 ratio of drug or vehicle in tween 80: dimethyl sulfoxide: saline. The Paclitaxel pre-treated animals then received chronic treatments of either KRM-II-81, MP-III-80 or vehicle (n=4/group), with these treatments blinded to the experimenter.

On every even day from Day 18-40 mice received an injection of their chronic treatment and then 30 min later three measurements of mechanical hyperalgesia and two measurements of thermal allodynia were recorded for each hind paw. On odd days (Day 19-39) the same processes were performed as on even days. However all measurements were taken immediately prior to the chronic treatment injections.

3.5.19. Respiratory Depression (Dr. Kevin Freeman, University of Mississippi Medical Center)

Using a method adapted from Bassi et al. (2015), rats (n = 8) were allowed 60 min to acclimate to the recording chamber before being tested. Next, the chamber was opened, the animal was administered vehicle or drugs KRM-II-8 (1.0, 3.2, and 10 mg/kg, i.p., 30 min prior) or alprazolam (0.32, 1.0, and 3.2 mg/kg, i.p., 15 min prior). Subsequently, the chamber was filled with air (21% of O_2 and 0.04% CO_2), then sealed, and pressure fluctuations were measured for 1 min. One milliliter of air was then pumped into the chamber for pressure calibration. Pulmonary ventilation was measured by one-way ANOVA, with Dunnett's multiple comparisons and calculated using a

plethysmography method adapted from Bassi et al. (2015). Respiratory frequency (f) and tidal volume (VT) were determined for each baseline and drug condition by selecting data within the 1-min sampling period that contained rhythmic breathing using PowerLab data acquisition software. Minute Volume was determined by formulas adapted from Bassi et al. (2015). All statistical tests were performed with Prism 6 (GraphPad Software, San Diego, CA).

3.5.20. Pain-Depressed Intracranial Self-Stimulation (ICSS model, Dr. Megan Moerke and Dr. Steve Nuggus, Virginia Commonwealth University

Adult male Sprague-Dawley rats from Envigo (Indianapolis, IN), weighed 310-350 g were trained under a fixed-ratio 1 (FR 1) schedule of electrical brain stimulation using a reported procedure as described previously (Negus et al., 2012). After a baseline was obtained, rats were administrated i.p. with either vehicle, or 0.32-10 mg/kg KRM-II-81 (n=8) and 0.1-10 mg/kg ketorolac (n=6) or 0.32-10 mg/kg diazepam (n=6) in the absence of the dilute lactic acid. the reinforcement rate in stimulations per frequency trial was normalized and converted into percent Maximum Control Rate (% MCR), as the mean of the maximal rates observed as compared to the baseline, as described (Moerke et al., 2018.) % MCR = [(rate during a frequency trial) / (MCR)] x 100.

3.6. Experimental

3.6.1. 7-Bromo-5-(pyridin-2-yl)-1*H*-benzo[*e*][1,4]diazepin-2(3*H*)-one (104)

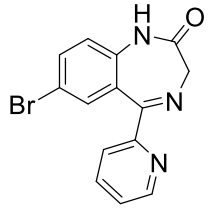

104

The 2'-pyridyl ketone **70** (120 g, 433.2 mmol) was dissolved in dry DCM (1.4 L) in a 3-neck round bottom flask and was stirred with an overhead mechanical stir for 15 min to obtain a homogenous solution. Then solid $NaHCO_3$ (72.8 g, 866.4 mmol) was added to the solution with vigorous stirring to avoid clogging of the stirrer, and the mixture was cooled to 0 °C using an ice bath. The bromoacetyl bromide (144.9 g, 714.8 mmol) was dissolved in dry DCM (200 mL) and was then added dropwise at 0 °C with an addition funnel. The reaction mixture was allowed to warm to rt and was stirred overnight until the starting material was consumed as monitored on analysis by TLC (silica gel, EtOAc/hexanes, 1:1). The reaction mixture was quenched with ice-water (500 mL) and stirred at rt for 30 min. The organic layer was then separated, and the aq layer was extracted with DCM (3 x 250 mL). The organic layers were combined, as well as washed (200 mL each) sequentially with a saturated aq solution of $NaHCO_3$, water, 10% HCl, brine and then dried (Na_2SO_4). The combined organic layer was then concentrated to $1/4^{th}$ of the original volume under reduced pressure. The intermediate **103**, which was prepared, was used for the next step without further purification.

Methanol (1.4 L) was cooled to 0 °C using an ice-water cooling bath and saturated with anhydrous ammonia gas. The DCM solution of intermediate **103** was added to the solution of saturated $MeOH/NH_3$ at 0 °C. The mixture was allowed to warm to rt and slowly heated to **reflux with**

caution (mild exotherm observed) until the starting material was consumed on analysis by TLC (silica gel) in 12 h. The reaction mixture was then cooled to rt and the solvent was removed under reduced pressure. The solid which remained was filtered and washed with water (3 x 150 mL), cold EtOAc (3 x 50 mL) and DCM (3 x 50 mL). The crude solid was dissolved in MeOH (600 mL) and DCM (100 mL) at 60 °C, and the solution was concentrated to 1/4th of the original volume. The amide **104** was crystallized at rt and filtered off, after which it was washed with DCM to obtain the majority of the pure amide **104** as white crystals. The filtrate was combined and concentrated under reduced pressure to an oily residue, which was further purified by flash chromatography on silica gel (EtOAc/hexanes, 1:1 and 1% of TEA) to afford additional amide **104** (108.6 g, 78% yield over the two steps): **mp** 228-229 °C; $\boldsymbol{R_f}$ = 0.4 (EtOAc-hexanes, 1:1 and 1% of TEA); **^{1}H NMR** (300 MHz, DMSO-d_6): δ = 10.63 (s, 1H), 8.55 (d, J = 4.1 Hz, 1H), 8.04 (d, J = 7.7 Hz, 1H), 7.93 (d, J = 7.4 Hz, 1H), 7.69 (d, J = 8.6 Hz, 1H), 7.54-7.44 (m, 1H), 7.42 (s, 1H), 7.18 (d, J = 8.7 Hz, 1H), 4.23 (s, 2H); **^{13}C NMR** (75 MHz, DMSO-d_6): δ = 170.3, 168.1, 156.3, 148.9, 139.3, 137.5, 134.4, 134.1, 127.9, 125.4, 123.9, 123.6, 114.5, 57.6; **HRMS** (ESI/IT-TOF): m/z $[M + H]^+$ calcd for $C_{14}H_{11}BrN_3O$: 316.0080; found: 316.0076.

3.6.2. Ethyl-8-bromo-6-(pyridin-2-yl)-4*H*-benzo[*f*]imidazo[1,5-*a*][1,4] diazepine-3-carboxyl ate (105)

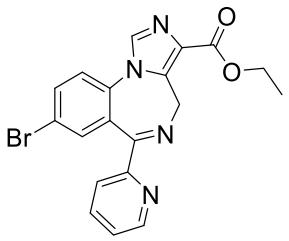

105

The amide **104** (80 g, 253.2 mmol) was suspended in dry THF (1.5 L), and cooled to -50 °C using a dry ice bath, after which potassium *t*-butoxide (34.1 g, 303.8 mmol) was added in one portion. The reaction mixture was stirred until it reached 0 °C and then stirred for 0.5 h at 0 °C. The mixture was then cooled to -50 °C, after which diethyl chlorophosphate (61.2 g, 354.5 mmol) was added dropwise with an addition funnel. The dry ice bath was removed to allow the temperature to rise to 0 °C, after which it was allowed to stir for 2 h with an ice-water bath. The solution was then cooled to -78 °C with a dry-ice bath and ethyl isocyanoacetate (40.1 g, 354.5 mmol) was added, immediately followed by a second portion of potassium *t*-butoxide (34.1 g, 303.8 mmol). This solution was allowed to stir overnight during which period it was allowed to warm to rt. The reaction was completed after 14 h on analysis by TLC (silica gel, EtOAc/hexanes/DCM, 2:2:1, and 1% TEA). The reaction mixture was quenched by addition of a cold saturated aq solution of $NaHCO_3$ (500 mL) and extracted with EtOAc. The organic layers were combined and washed with brine (2 x 200 mL), and dried (Na_2SO_4). The solvent was removed under reduced pressure to obtain a dark brown solid residue. The solid was washed with Et_2O/EtOAc (9:1) to remove most of the impurities and the solid was further recrystallized from EtOAc and hexane (1:4), and this was followed by washing the solid with cold Et_2O to afford the majority of the pure ethyl ester **105**. The remaining filtrate was combined and purified by flash chromatography to obtain additional ethyl ester **105** (silica gel, EtOAc/ hexanes/DCM 2/2:1 and 1% TEA) as an off-white solid (84.2 g, 81% yield): **mp** 212-213 °C; $\boldsymbol{R_f}$ = 0.3 (EtOAc-hexanes-DCM, 2:2:1 and 1% of TEA); **^{1}H NMR**

(300 MHz, $CDCl_3$): δ = 8.60 (d, *J* = 4.4 Hz, 1H), 8.11 (d, *J* = 7.9 Hz, 1H), 8.00 (s, 1H), 7.86 (td, *J* = 8.0, 1.7 Hz, 1H), 7.80 (dd, *J* = 8.6, 2.2 Hz, 1H), 7.60 (d, *J* = 2.1 Hz, 1H), 7.51 (d, *J* = 8.6 Hz, 1H), 7.41 (dd, *J* = 7.1, 5.2 Hz, 1H), 6.13 (d, *J* = 10.4 Hz, 1H), 4.51 – 4.33 (m, 2H), 4.17 (d, *J* = 11.6 Hz, 1H), 1.44 (t, *J* = 7.1 Hz, 3H); **^{13}C NMR** (75 MHz, $CDCl_3$): δ = 167.0, 162.9, 156.2, 148.7, 138.4, 136.9, 135.3, 135.0, 134.5, 134.4, 129.3, 128.5, 124.9, 124.3, 123.9, 120.5, 60.7, 45.0, 14.4; **HRMS** (ESI/IT-TOF): m/z $[M + H]^+$ calcd for $C_{19}H_{16}BrN_4O_2$: 411.0451; found: 411.0454.

3.6.3. Ethyl-6-(pyridin-2-yl)-8-((trimethylsilyl)ethynyl)-4*H*-benzo[*f*] imidazo[1,5*a*]-[1,4]diazepine-3-carboxylate (106)

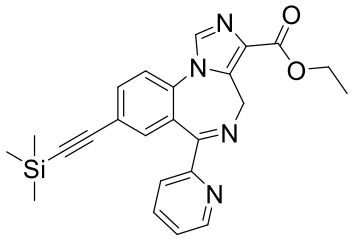

106

The ethyl ester **105** (63.8 g, 155.1 mmol) was dissolved in TEA (400 mL) and dry CH_3CN (600 mL) and placed in a 3-neck round bottom flask with a reflux condenser attached. The solution was then degassed three times under vacuum and argon. The trimethylsilylacetylene (22.9 g, 232.7 mmol) and bis(triphenyl phosphine)-palladium (II) acetate (6.4 g, 8.53 mmol) were added to the solution under argon, and the mixture was degassed four times (as above). The reaction mixture was then heated to reflux under argon and allowed to stir overnight. The reaction process was completed in 15 h as monitored on analysis by TLC (silica gel, EtOAc/hexanes, 7:3, and 1% TEA). The reaction mixture was then cooled to 0 °C and filtered through celite. This was followed by washing with EtOAc and drying (Na_2SO_4). The filtrate was concentrated under reduced pressure.

The black residue, which resulted, was loaded onto a silica plug (4 g of silica gel/1 g of the product) and washed with a mixture of EtOAc and hexanes (1:1 with 1% TEA) to remove the baseline impurities and the material was recrystallized from EtOAc. The crystals were filtered and washed with Et_2O to afford pure trimethylsilyl ethyl ester **106**. The filtrate was purified by flash chromatography to afford additional ester **106** as an off-white solid (61.1 g, 92% yield): **mp** 203-204 °C; $\boldsymbol{R_f}$ = 0.5 (EtOAc-hexanes, 1:1 and 1% of TEA); **^{1}H NMR** (300 MHz, $CDCl_3$): δ = 8.56 (d, *J* = 4.1 Hz, 1H), 8.02 (d, *J* = 7.8 Hz, 1H), 7.90 (s, 1H), 7.78 (t, *J* = 7.7 Hz, 1H), 7.70 (d, *J* = 8.3 Hz, 1H), 7.51 (d, *J* = 9.2 Hz, 2H), 7.34 (t, *J* = 5.9 Hz, 1H), 6.08 (d, *J* = 9.2 Hz, 1H), 4.47 – 4.31 (m, 2H), 4.10 (d, *J* = 6.9 Hz, 1H), 1.41 (t, *J* = 7.0 Hz, 3H), 0.21(s, 9H); **^{13}C NMR** (75 MHz, $CDCl_3$): δ = 167.8, 162.9, 156.6, 148.8, 138.5, 136.8, 135.7, 135.2, 135.1, 134.5, 129.3, 127.0, 124.7, 124.0, 122.7, 122.2, 102.8, 97.0, 60.7, 45.0, 14.4, -0.2; **HRMS** (ESI/IT-TOF): m/z [M + H]$^+$ calcd for $C_{24}H_{25}N_4O_2Si$: 429.1741; found: 429.1747.

3.6.4. Ethyl-8-ethynyl-6-(pyridin-2-yl)-4*H*-benzo[*f*]imidazo[1,5-*a*][1,4] diazepine-3-carboxy late (HZ-166, 76)

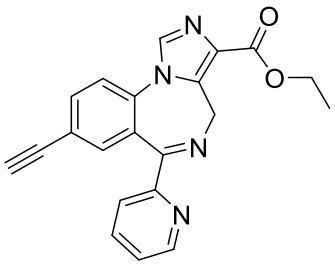

76 (Hz-166)

The trimethylsilyl ethyl ester **106** (50 g, 116.8 mmol) was dissolved in THF (1 L) and cooled to -78 °C. Tetrabutylammonium fluoride hydrate (1 M solution in THF, 175.1 mmol) was added to the solution, and this was followed by water (50 mL). The reaction mixture was stirred at -78 °C

until the starting material was consumed in 0.5 h, as indicated by TLC (silica gel). The reaction mixture was allowed to warm to 0 °C and quenched by a slow addition of water (500 mL). The organic layer was separated and the aq layer was extracted with EtOAc (5 x 300 mL). The combined organic layers were washed with brine (2 x 400 mL) and dried (Na_2SO_4). The solvent was removed under reduced pressure and the residue, which resulted, was dissolved in a mixture of DCM (100 mL) and MeOH (400 mL) at 50 °C and the solution was concentrated to 1/3rd of its original volume. The majority of the ethyl ester **76** was recrystallized at rt with addition of a seed crystal, and the solid was further washed with cold MeOH. The filtrate was combined and purified by a wash column (silica gel, EtOAc/hexanes/DCM 8:1:2, and 1% TEA) to afford additional ethyl ester **76** as a white powder (37.8 g, 96% yield): **mp** 243-244 °C; $\boldsymbol{R_f}$ = 0.4 (EtOAc-hexanes-DCM, 8:1:2 and 1% of TEA); **^{1}H NMR** (300 MHz, $CDCl_3$): δ = 8.59 (d, *J* = 4.6 Hz, 1H), 8.08 (d, *J* = 7.9 Hz, 1H), 7.96 (s, 1H), 7.83 (td, *J* = 7.8, 1.6 Hz, 1H), 7.77 (dd, *J* = 8.4, 1.7 Hz, 1H), 7.61 – 7.54 (m, 2H), 7.38 (dd, *J* = 7.0, 5.3 Hz, 1H), 6.12 (d, *J* = 10.6 Hz, 1H), 4.56 – 4.27 (m, 2H), 4.16 (d, *J* = 10.2 Hz, 1H), 3.17 (s, 1H), 1.44 (t, *J* = 7.1 Hz, 3H); **^{13}C NMR** (75 MHz, $CDCl_3$): δ = 167.6, 162.8, 156.2, 148.6, 138.4, 137.1, 136.2, 135.4, 135.4, 134.6, 129.2, 127.0, 124.9, 124.1, 122.9, 121.3, 81.6, 79.6, 60.9, 45.0, 14.4; **HRMS** (ESI/IT-TOF): m/z $[M + H]^+$ calcd for $C_{21}H_{17}N_4O_2$: 357.1346; found: 357.1344.

3.6.5. 3-Ethyl-5-(8-ethynyl-6-(pyridin-2-yl)-4*H*-benzo[*f*]imidazo[1,5-*a*] [1,4]diazepin-3-yl)-1,2,4-oxadiazole (MP-III-080, 102).

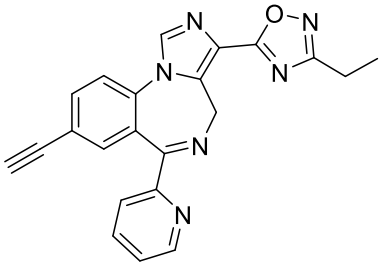

MP-III-080 (**102**)

The ethyl ester **76** (4.4 g, 12.4 mmol) was dissolved in dry THF (200 mL) at rt under argon. In a separate flask that contained 3Å molecular sieves, *N*-hydroxypropionimidamide (4.35 g, 49.4 mmol) was dissolved in dry THF (50 mL) under argon and then treated with sodium hydride (60% dispersion in mineral oil, 360 mg, 14.8 mmol). The mixture was allowed to stir for 1.5 h and was then added dropwise to the solution of ethyl ester **76**. The reaction was completed in 3 h as analyzed by TLC (silica gel). The reaction mixture was quenched with a saturated aq $NaHCO_3$ solution (10 mL) and extracted with EtOAc (3 x 250 mL). The organic layers were combined, washed with brine, and dried (Na_2SO_4). The solvent was removed under reduced pressure. The solid, which resulted, was purified by flash chromatography (silica gel, EtOAc/hexanes 4:1 and 1% TEA) to afford pure 1,2,4-oxadiazole **102** as a white powder (4.1 g, 88% yield); **mp** 204-205 °C; $\boldsymbol{R_f}$ = 0.6 (EtOAc-hexanes, 4:1 and 1% of TEA);[13] **^{1}H NMR** (500 MHz, $CDCl_3$): δ = 8.58 (d, *J* = 4.3 Hz, 1H), 8.07 (d, *J* = 8.0 Hz, 1H), 8.05 (s, 1H), 7.83 (dd, *J* = 11.8, 4.4 Hz, 1H), 7.78 (dd, *J* = 8.4, 1.3 Hz, 1H), 7.61 (d, *J* = 8.3 Hz, 1H), 7.57 (d, *J* = 1.0 Hz, 1H), 7.38 (dd, *J* = 6.7, 5.3 Hz, 1H), 6.16 (d, *J* = 11.4 Hz, 1H), 4.29 (d, *J* = 11.2 Hz, 1H), 3.19 (s, 1H), 2.85 (q, *J* = 7.6 Hz, 2H), 1.44 (t, *J* = 7.6 Hz, 3H); **^{13}C NMR** (126 MHz, $CDCl_3$): δ = 171.9, 170.8, 167.9, 156.3, 148.7, 137.1, 136.3, 136.2, 135.9, 135.5, 135.2, 127.1, 125.0, 124.8, 124.1, 122.9, 121.4, 81.6, 79.7, 44.9, 19.8, 11.6; **HRMS** (ESI/IT-TOF): m/z $[M + H]^+$ calcd for $C_{22}H_{17}N_6O$: 381.1458; found: 381.1461.

3.6.6. 8-Ethynyl-6-(pyridin-2-yl)-4*H*-benzo[*f*]imidazo[1,5-*a*][1,4] diazepine-3-carbaldehyde (GL-III-13, 107)

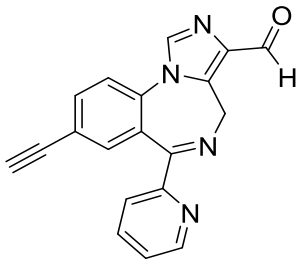

GL-III-13 (**107**)

The preparation of PDBBA. The potassium *tert*-butoxide (29.3 g, 261 mmol) was suspended in dry THF (261 mL). The DIBALH (261 mL, 1.0 M in hexane, 261 mmol) was added dropwise to the solution of potassium *tert*-butoxide at 0 °C using an ice-water bath. The mixture was allowed to stir at rt for 2 h to achieve a colorless homogeneous solution. The concentration of PDBBA solution in THF-hexanes was measured by GC analysis by hydrolysis of the solution with a mixture of *t*-butyl alcohol-THF (1:1) at 0 °C.[161]

The reduction of ethyl ester **76** to aldehyde **107**: The ethyl ester **76** (20 g, 56.1 mmol) was dissolved in dry DCM (500 mL) at 0 °C. The ice-water bath was removed, and the PDBBA solution (0.42 M in THF-hexanes, 200 mL) was added in one portion with vigorous stirring. The reaction was monitored by TLC (silica gel) after each 3 minutes and was completed in 20 min, and this was followed by hydrolysis of the mixture with 1N *aq* HCl at 0 °C. Water (200 mL) was added to the mixture, and it was stirred for 0.5 h. The aluminum salt was formed and filtered off on a celite pad. The filtrate was extracted with DCM (3 x 150 mL). The organic layers were combined and concentrated with reduced pressure, and this was followed by washing with brine and dried (Na_2SO_4). The solid residue was dissolved in a mixture of DCM (100 mL) and EtOAc (100 mL) at 50 °C. A seed crystal was added to the mixture and the solvent was reduced to $1/4^{th}$ of its original

volume. The aldehyde **107** was recrystallized from the mixture at rt and washed with cold Et_2O. The filtrate was combined and further purified by flash chromatography (silica gel, EtOAc and 1% each of TEA and MeOH) to afford additional aldehyde **107** as a white solid (14 g, 80% yield): **mp** 242-243 °C; $\boldsymbol{R_f}$ = 0.6 (EtOAc and 1% of TEA); **^{1}H NMR** (300 MHz, $CDCl_3$): δ = 10.04 (s, 1H), 8.54 (d, *J* = 4.1 Hz, 1H), 8.06 (d, *J* = 7.9 Hz, 1H), 7.96 (s, 1H), 7.78 (dd, *J* = 17.3, 8.8 Hz, 2H), 7.56 (dd, *J* = 4.6, 3.3 Hz, 2H), 7.35 (dd, *J* = 6.6, 5.1 Hz, 1H), 5.99 (s, 1H), 4.18 (s, 1H), 3.18 (s, 1H); **^{13}C NMR** (75 MHz, $CDCl_3$): δ = 186.8, 167.8, 156.3, 148.7, 137.9, 136.9, 136.7, 136.3, 135.5, 135.3, 135.0, 127.2, 124.9, 124.0, 122.8, 121.4, 81.6, 79.8, 44.4; **HRMS** (ESI/IT-TOF): m/z $[M + H]^+$ calcd for $C_{19}H_{13}N_4O$: 313.1084; found: 313.1087.

3.6.7. 5-(8-Ethynyl-6-(pyridin-2-yl)-4*H*-benzo[*f*]imidazo[1,5-*a*][1,4] diazepin-3-yl)oxazole (KRM-II-81, 77).

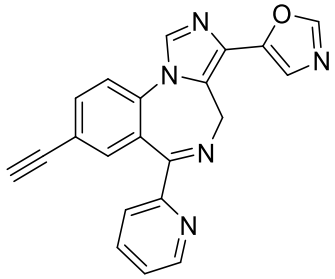

KRM-II-81 (**77**)

The toluenesulfonylmethyl isocyanide (TosMIC, 10.6 g, 54.6 mmol), K_2CO_3 (18.9 g, 136.5 mmol) and the aldehyde **107** (14.2 g, 45.5 mmol) were placed in a dry two neck round bottom flask. Dry MeOH (600 mL) was added to the mixture under an argon atmosphere at rt. The reaction mixture was allowed to heated slowly to reflux for 2 h. After completion of the reaction on analysis by TLC (silica gel, EtOAc and 1% each of TEA and MeOH), the reaction mixture was quenched with cold water (300 mL) and extracted with EtOAc (3 x 100 mL). The organic layers were combined

and this was followed by washing with brine. The solution was then dried (Na_2SO_4) and concentrated under reduced pressure to dryness. The solid residue, which formed, was dissolved in EtOAc (200 mL) at 60 °C, and the solvent was reduced to 1/4th of its original volume. A seed crystal was then added to the solution. The majority of oxazole **77** was crystallized at rt and filtered. This was followed by washing with cold Et_2O. The filtrate was combined and further purified by flash chromatography (silica gel, EtOAc and 1% each of TEA and MeOH) to afford additional oxazole **77** as a white solid (14.2 g, 89% yield): **mp** 241-242 °C; $\boldsymbol{R_f}$ = 0.3 (EtOAc and 1% each of MeOH and TEA);[13] **^{1}H NMR** (500 MHz, $CDCl_3$): δ = 8.55 (d, *J* = 4.5 Hz, 1H), 8.00 (d, *J* = 7.9 Hz, 1H), 7.95 (s, 1H), 7.92 (s, 1H), 7.78 (t, *J* = 7.4 Hz, 1H), 7.72 (d, *J* = 8.2, 0.8 Hz, 1H), 7.58-7.49 (m, 2H), 7.42 (s, 1H), 7.33 (dd, *J* = 6.9, 5.3 Hz, 1H), 5.72 (d, *J* = 11.9 Hz, 1H), 4.27 (d, *J* = 12.0 Hz, 1H), 3.16 (s, 1H); **^{13}C NMR** (126 MHz, $CDCl_3$): δ = 167.8, 156.6, 149.8, 148.8, 146.6, 136.9, 136.3, 135.7, 135.4, 135.2, 129.8, 127.4, 126.9, 124.8, 123.9, 122.7, 122.5, 120.9, 81.8, 79.5, 45.2; **HRMS** (ESI/IT-TOF): m/z $[M + H]^+$ calcd for $C_{21}H_{14}N_5O$: 352.1193; found: 352.1195.

References

1. Watanabe, M.; Maemura, K.; Kanbara, K.; Tamayama, T.; Hayasaki, H., GABA and GABA receptors in the central nervous system and other organs. In *Int. Rev. Cytol.*, Jeon, K. W., Ed. Academic Press: 2002; Vol. 213, pp 1-47.
2. Sieghart, W., Structure and pharmacology of gamma-aminobutyric acid A receptor subtypes. *Pharmacol. Rev.* **1995,** *47* (2), 181.
3. Twyman, R. E.; Rogers, C. J.; Macdonald, R. L., Differential regulation of gamma-aminobutyric acid receptor channels by diazepam and phenobarbital. *Ann. Neurol.* **1989,** *25* (3), 213-20.
4. Hyland, N. P.; Cryan, J. F., A gut feeling about gaba: focus on GABA(B) receptors. *Front. Pharmacol.* **2010,** *1*, 124-124.
5. Guidotti, A.; Auta, J.; Davis, J. M.; Dong, E.; Grayson, D. R.; Veldic, M.; Zhang, X.; Costa, E., GABAergic dysfunction in schizophrenia: new treatment strategies on the horizon. *Psychopharmacology (Berl.)* **2005,** *180* (2), 191-205.
6. Luscher, B.; Shen, Q.; Sahir, N., The GABAergic deficit hypothesis of major depressive disorder. *Mol. Psychiatry* **2011,** *16* (4), 383-406.
7. Sieghart, W.; Ernst, M., Heterogeneity of GABAA receptors: revived interest in the development of subtype-selective drugs. *Current Medicinal Chemistry - Central Nervous System Agents* **2005,** *5* (3), 217-242.
8. Bowser, D. N.; Wagner, D. A.; Czajkowski, C.; Cromer, B. A.; Parker, M. W.; Wallace, R. H.; Harkin, L. A.; Mulley, J. C.; Marini, C.; Berkovic, S. F.; Williams, D. A.; Jones, M. V.; Petrou, S., Altered kinetics and benzodiazepine sensitivity of a GABAA receptor subunit

mutation [gamma 2(R43Q)] found in human epilepsy. *Proc. Natl. Acad. Sci. U. S. A.* **2002,** *99* (23), 15170-5.

9. Munro, G.; Hansen, R. R.; Mirza, N. R., GABAA receptor modulation: Potential to deliver novel pain medicines? *Eur. J. Pharmacol.* **2013,** *716* (1), 17-23.

10. Barnard, E. A.; Skolnick, P.; Olsen, R. W.; Mohler, H.; Sieghart, W.; Biggio, G.; Braestrup, C.; Bateson, A. N.; Langer, S. Z., International Union of Pharmacology. XV. Subtypes of gamma-aminobutyric acidA receptors: classification on the basis of subunit structure and receptor function. *Pharmacol. Rev.* **1998,** *50* (2), 291-313.

11. Olsen, R. W.; Sieghart, W., GABA A receptors: subtypes provide diversity of function and pharmacology. *Neuropharmacology* **2009,** *56* (1), 141-8.

12. Wisden, W.; Laurie, D. J.; Monyer, H.; Seeburg, P. H., The distribution of 13 GABAA receptor subunit mRNAs in the rat brain. I. Telencephalon, diencephalon, mesencephalon. *J. Neurosci.* **1992,** *12* (3), 1040-62.

13. Fritschy, J. M.; Mohler, H., GABAA-receptor heterogeneity in the adult rat brain: differential regional and cellular distribution of seven major subunits. *J. Comp. Neurol.* **1995,** *359* (1), 154-94.

14. Sieghart, W.; Sperk, G., subunit composition, distribution and function of GABA-A receptor subtypes. *Curr. Top. Med. Chem.* **2002,** *2* (8), 795-816.

15. Nutt, D., GABAA receptors: subtypes, regional distribution, and function. *J. Clin. Sleep Med.* **2006,** *2* (2), S7-11.

16. Pirker, S.; Schwarzer, C.; Wieselthaler, A.; Sieghart, W.; Sperk, G., GABA(A) receptors: immunocytochemical distribution of 13 subunits in the adult rat brain. *Neuroscience* **2000,** *101* (4), 815-50.

17. Burt, D. R.; Kamatchi, G. L., GABAA receptor subtypes: from pharmacology to molecular biology. *The FASEB Journal* **1991,** *5* (14), 2916-2923.

18. Clayton, T.; Chen, J. L.; Ernst, M.; Richter, L.; Cromer, B. A.; Morton, C. J.; Ng, H.; Kaczorowski, C. C.; Helmstetter, F. J.; Furtmuller, R.; Ecker, G.; Parker, M. W.; Sieghart, W.; Cook, J. M., An updated unified pharmacophore model of the benzodiazepine binding site on gamma-aminobutyric acid(a) receptors: correlation with comparative models. *Curr. Med. Chem.* **2007,** *14* (26), 2755-75.

19. Keramidas, A.; Moorhouse, A. J.; Schofield, P. R.; Barry, P. H., Ligand-gated ion channels: mechanisms underlying ion selectivity. *Prog. Biophys. Mol. Biol.* **2004,** *86* (2), 161-204.

20. Ramerstorfer, J.; Furtmuller, R.; Sarto-Jackson, I.; Varagic, Z.; Sieghart, W.; Ernst, M., The GABAA receptor alpha+beta- interface: a novel target for subtype selective drugs. *J. Neurosci.* **2011,** *31* (3), 870-7.

21. Varagic, Z.; Ramerstorfer, J.; Huang, S.; Rallapalli, S.; Sarto-Jackson, I.; Cook, J.; Sieghart, W.; Ernst, M., Subtype selectivity of α+β- site ligands of GABAA receptors: identification of the first highly specific positive modulators at α6β2/3γ2 receptors. *Br. J. Pharmacol.* **2013,** *169* (2), 384-399.

22. Chiou, L.-C.; Tzeng, H.-R.; Fan, P.-C.; Sieghart, W.; Ernst, M.; Knutson, D. E.; Cook, J., A novel drug target for migraine: The GABAA receptor α6 subtype in trigeminal ganglia. *The FASEB Journal* **2019,** *33* (1_supplement), lb78-lb78.

23. Knutson, D. E.; Kodali, R.; Divović, B.; Treven, M.; Stephen, M. R.; Zahn, N. M.; Dobričić, V.; Huber, A. T.; Meirelles, M. A.; Verma, R. S.; Wimmer, L.; Witzigmann, C.; Arnold, L. A.; Chiou, L.-C.; Ernst, M.; Mihovilovic, M. D.; Savić, M. M.; Sieghart, W.; Cook, J. M., Design and synthesis of novel deuterated ligands functionally selective for the γ-

aminobutyric acid type a receptor (GABAAR) α6 subtype with improved metabolic stability and enhanced bioavailability. *J. Med. Chem.* **2018,** *61* (6), 2422-2446.

24. Vasović, D.; Divović, B.; Treven, M.; Knutson, D. E.; Steudle, F.; Scholze, P.; Obradović, A.; Fabjan, J.; Brković, B.; Sieghart, W.; Ernst, M.; Cook, J. M.; Savić, M. M., Trigeminal neuropathic pain development and maintenance in rats are suppressed by a positive modulator of α6 GABAA receptors. *European Journal of Pain* **2019,** *23* (5), 973-984.

25. Olsen, R. W.; Hanchar, H. J.; Meera, P.; Wallner, M., GABAA receptor subtypes: the "one glass of wine" receptors. *Alcohol* **2007,** *41* (3), 201-9.

26. Sawyer, E. K.; Moran, C.; Sirbu, M. H.; Szafir, M.; Van Linn, M.; Namjoshi, O.; Phani Babu Tiruveedhula, V. V. N.; Cook, J. M.; Platt, D. M., Little evidence of a role for the α1GABAA subunit-containing receptor in a rhesus monkey model of alcohol drinking. *Alcohol. Clin. Exp. Res.* **2014,** *38* (4), 1108-1117.

27. Ernst, M.; Brauchart, D.; Boresch, S.; Sieghart, W., Comparative modeling of GABA(A) receptors: limits, insights, future developments. *Neuroscience* **2003,** *119* (4), 933-43.

28. Haefely, W., The biological basis of benzodiazepine actions. *J. Psychoactive Drugs* **1983,** *15* (1-2), 19-39.

29. Hillestad, L.; Hansen, T.; Melsom, H.; Drivenes, A., Diazepam metabolism in normal man I. Serum concentrations and clinical effects after intravenous, intramuscular, and oral administrations. *Clin. Pharmacol. Therapeutics* **1974,** *16*, 479 - 484.

30. Stevenson, I. H.; Browning, M.; Crooks, J.; O'Malley, K., Changes in human drug metabolism after long-term exposure to hypnotics. *Br. Med. Journal* **1972,** *4*, 322 - 324.

31. Garattini, S.; Mussini, E.; Marucci, F.; Guaitani, A., Metabolic studies on benzodiazepines in various animal species. In *The Benzodiazepines*, Garattini, S.; Mussini, E.; Randall, L. O., Eds. Raven Press: New York, 1973; pp 75 - 97.

32. Rutherford, D. M.; Okoko, A.; Tyrer, P. J., Plasma concentrations of diazepam and desmethyldiazepam during chronic diazepam therapy. *Br. J. Clin. Pharmacol.* **1978,** *1978* (6).

33. Bond, A. J.; Hailey, D. M.; Lader, M. H., Plasma concentrations of benzodiazepines. *Br. J. Clin. Pharmacol.* **1977,** *4*, 51 - 56.

34. Haefely, W.; Facklam, M.; Schoch, P.; Martin, J. R.; Bonetti, E. P.; Moreau, J. L.; Jenck, F.; Richards, J. G., Partial agonists of benzodiazepine receptors for the treatment of epilepsy, sleep, and anxiety disorders. *Advances in biochemical psychopharmacology* **1992,** *47*, 379-394.

35. Moss, G. P., Nomenclature of fused and bridged fused ring systems (IUPAC Recommendations 1998). In *Pure Appl. Chem.*, 1998; Vol. 70, p 143.

36. Hadingham, K. L.; Wingrove, P. B.; Wafford, K. A.; Bain, C.; Kemp, J. A.; Palmer, K. J.; Wilson, A. W.; Wilcox, A. S.; Sikela, J. M.; Ragan, C. I.; et al., Role of the beta subunit in determining the pharmacology of human gamma-aminobutyric acid type A receptors. *Mol. Pharmacol.* **1993,** *44* (6), 1211-8.

37. Khom, S.; Baburin, I.; Timin, E. N.; Hohaus, A.; Sieghart, W.; Hering, S., Pharmacological properties of GABAA receptors containing gamma1 subunits. *Mol. Pharmacol.* **2006,** *69* (2), 640-9.

38. Bencsits, E.; Ebert, V.; Tretter, V.; Sieghart, W., A significant part of native gamma-aminobutyric AcidA receptors containing alpha4 subunits do not contain gamma or delta subunits. *J. Biol. Chem.* **1999,** *274* (28), 19613-6.

39. Yang, W.; Drewe, J. A.; Lan, N. C., Cloning and characterization of the human GABAA receptor alpha 4 subunit: identification of a unique diazepam-insensitive binding site. *Eur. J. Pharmacol.* **1995,** *291* (3), 319-25.

40. Korpi, E. R.; Seeburg, P. H., Natural mutation of GABAA receptor alpha 6 subunit alters benzodiazepine affinity but not allosteric GABA effects. *Eur. J. Pharmacol.* **1993,** *247* (1), 23-27.

41. Macdonald, R. L.; Olsen, R. W., GABAA receptor channels. *Annu. Rev. Neurosci.* **1994,** *17* (1), 569-602.

42. Study, R. E.; Barker, J. L., Diazepam and (--)-pentobarbital: fluctuation analysis reveals different mechanisms for potentiation of gamma-aminobutyric acid responses in cultured central neurons. *Proc. Natl. Acad. Sci. U. S. A.* **1981,** *78* (11), 7180-7184.

43. MacDonald, R. L., Benzodiazepine mechanisms of action. In *Antiepileptic Drugs*, Levy, R. H.; Mattson, R. H.; Meldrum, B. S.; Perucca, E., Eds. Lippincott Williams and Wilkins: Philadelphia, 2002; pp 179 - 186.

44. Killam, E. K.; Suria, A., Benzodiazepines. In *Antiepileptic Drugs: Mechanisms of Action*, Glaser, G. H.; Penry, J. K.; Woodbury, D. M., Eds. Raven Press: New York, 1980; pp 597 - 615.

45. Rogawski, M. A., Principles of antiepileptic drug action. In *Antiepileptic Drugs*, 5th ed.; Levy, R. H.; Mattson, R. H.; Meldrum, B. S.; Perucca, E., Eds. Lippincott Williams and Wilkins: Philadelphia, 2002; pp 3 - 22.

46. Rudolph, U.; Crestani, F.; Benke, D.; Brunig, I.; Benson, J. A.; Fritschy, J. M.; Martin, J. R.; Bluethmann, H.; Mohler, H., Benzodiazepine actions mediated by specific gamma-aminobutyric acid(A) receptor subtypes. *Nature* **1999,** *401* (6755), 796-800.

47. Low, K.; Crestani, F.; Keist, R.; Benke, D.; Brunig, I.; Benson, J. A.; Fritschy, J. M.; Rulicke, T.; Bluethmann, H.; Mohler, H.; Rudolph, U., Molecular and neuronal substrate for the selective attenuation of anxiety. *Science* **2000,** *290* (5489), 131-4.

48. Collinson, N.; Kuenzi, F. M.; Jarolimek, W.; Maubach, K. A.; Cothliff, R.; Sur, C.; Smith, A.; Otu, F. M.; Howell, O.; Atack, J. R.; McKernan, R. M.; Seabrook, G. R.; Dawson, G. R.; Whiting, P. J.; Rosahl, T. W., Enhanced learning and memory and altered GABAergic synaptic transmission in mice lacking the alpha 5 subunit of the GABAA receptor. *J. Neurosci.* **2002,** *22* (13), 5572-80.

49. Paul, J.; Yévenes, G. E.; Benke, D.; Di Lio, A.; Ralvenius, W. T.; Witschi, R.; Scheurer, L.; Cook, J. M.; Rudolph, U.; Fritschy, J.-M.; Zeilhofer, H. U., Antihyperalgesia by α2-GABAA receptors occurs via a genuine spinal action and does not involve supraspinal sites. *Neuropsychopharmacology : official publication of the American College of Neuropsychopharmacology* **2014,** *39* (2), 477-487.

50. McKernan, R. M.; Rosahl, T. W.; Reynolds, D. S.; Sur, C.; Wafford, K. A.; Atack, J. R.; Farrar, S.; Myers, J.; Cook, G.; Ferris, P.; Garrett, L.; Bristow, L.; Marshall, G.; Macaulay, A.; Brown, N.; Howell, O.; Moore, K. W.; Carling, R. W.; Street, L. J.; Castro, J. L.; Ragan, C. I.; Dawson, G. R.; Whiting, P. J., Sedative but not anxiolytic properties of benzodiazepines are mediated by the GABAA receptor α1 subtype. *Nat. Neurosci.* **2000,** *3*, 587.

51. Morris, H. V.; Dawson, G. R.; Reynolds, D. S.; Atack, J. R.; Stephens, D. N., Both alpha2 and alpha3 GABAA receptor subtypes mediate the anxiolytic properties of benzodiazepine site ligands in the conditioned emotional response paradigm. *Eur. J. Neurosci.* **2006,** *23* (9), 2495-504.

52. Dias, R.; Sheppard, W. F.; Fradley, R. L.; Garrett, E. M.; Stanley, J. L.; Tye, S. J.; Goodacre, S.; Lincoln, R. J.; Cook, S. M.; Conley, R.; Hallett, D.; Humphries, A. C.; Thompson, S. A.; Wafford, K. A.; Street, L. J.; Castro, J. L.; Whiting, P. J.; Rosahl, T. W.; Atack, J. R.; McKernan, R. M.; Dawson, G. R.; Reynolds, D. S., Evidence for a significant role of alpha 3-containing GABAA receptors in mediating the anxiolytic effects of benzodiazepines. *J. Neurosci.* **2005,** *25* (46), 10682-8.

53. Yee, B. K.; Keist, R.; von Boehmer, L.; Studer, R.; Benke, D.; Hagenbuch, N.; Dong, Y.; Malenka, R. C.; Fritschy, J. M.; Bluethmann, H.; Feldon, J.; Möhler, H.; Rudolph, U., A schizophrenia-related sensorimotor deficit links α3-containing GABAA receptors to a dopamine hyperfunction. *Proc. Natl. Acad. Sci. U. S. A.* **2005,** *102* (47), 17154.

54. Crestani, F.; Keist, R.; Fritschy, J. M.; Benke, D.; Vogt, K.; Prut, L.; Blüthmann, H.; Möhler, H.; Rudolph, U., Trace fear conditioning involves hippocampal alpha5 GABA(A) receptors. *Proc. Natl. Acad. Sci. U. S. A.* **2002,** *99* (13), 8980-8985.

55. Ralvenius, W. T.; Benke, D.; Acuna, M. A.; Rudolph, U.; Zeilhofer, H. U., Analgesia and unwanted benzodiazepine effects in point-mutated mice expressing only one benzodiazepine-sensitive GABAA receptor subtype. *Nature communications* **2015,** *6*, 6803.

56. Mizuta, K.; Xu, D.; Pan, Y.; Comas, G.; Sonett, J. R.; Zhang, Y.; Panettieri, R. A., Jr.; Yang, J.; Emala, C. W., Sr., GABAA receptors are expressed and facilitate relaxation in airway smooth muscle. *Am. J. Physiol. Lung Cell Mol. Physiol.* **2008,** *294* (6), L1206-16.

57. Gallos, G.; Yim, P.; Chang, S.; Zhang, Y.; Xu, D.; Cook, J. M.; Gerthoffer, W. T.; Emala, C. W., Sr., Targeting the restricted alpha-subunit repertoire of airway smooth muscle GABAA receptors augments airway smooth muscle relaxation. *Am. J. Physiol. Lung Cell Mol. Physiol.* **2012,** *302* (2), L248-56.

58. Gallos, G.; Yocum, G. T.; Siviski, M. E.; Yim, P. D.; Fu, X. W.; Poe, M. M.; Cook, J. M.; Harrison, N.; Perez-Zoghbi, J.; Emala, C. W., Sr., Selective targeting of the alpha5-subunit of GABAA receptors relaxes airway smooth muscle and inhibits cellular calcium handling. *Am. J. Physiol. Lung Cell Mol. Physiol.* **2015,** *308* (9), L931-42.

59. Cook, J. M.; Edwankar, R.; Poe, M. M.; Tiruveedhula, V. V. N. P. B.; Witzigmann, C., Synthesis of natural products and related heterocyclic compounds. Search for agents to treat neuropathic pain, epilepsy and anxiety disorders as well as simple molecules to treat TB and MRSA infections. In *Mona Symposium on Natural Products and Medicinal Chemistry*, Kingston, Jamaica, 2014.

60. Davies, M.; Bateson, A. N.; Dunn, S. M. J., Structural requirements for ligand interactions at the benzodiazepine recognition site of the GABAA receptor. *J. Neurochem.* **1998,** *70* (5), 2188-2194.

61. Dunn, S. M. J.; Davies, M.; Muntoni, A. L.; Lambert, J. J., Mutagenesis of the Rat α1 Subunit of the γ-aminobutyric acid receptor reveals the importance of residue 101 in determining the allosteric effects of benzodiazepine site ligands. *Mol. Pharmacol.* **1999,** *56* (4), 768.

62. Sigel, E.; Schaerer, M. T.; Buhr, A.; Baur, R., The benzodiazepine binding pocket of recombinant α1β2γ2 γ-aminobutyric acid receptors: relative orientation of ligands and amino acid side chains. *Mol. Pharmacol.* **1998,** *54* (6), 1097.

63. Whitwam, J. G.; Amrein, R., Pharmacology of flumazenil. *Acta Anaesthesiol. Scand. Suppl.* **1995,** *108*, 3-14.

64. Clayton, T. S. Ph.D. Thesis, Part I. Unified Pharmacophoric Protein Models of the Benzodiazepine Receptor Subtypes. Part II. Subtype Selective Ligands for a5 $GABA_A$/Bz Receptors. University of Wisconsin-Milwaukee, 2011.

65. He, X.; Huang, Q.; Ma, C.; Yu, S.; McKernan, R.; Cook, J. M., Pharmacophore/receptor models for $GABA_A$/BzR a2b3g2, a3b3g2 and a4b3g2 recombinant subtypes. Included volume analysis and comparison to a1b3g2, a5b3g2 and a6b3g2 subtypes. *Drug Des. Discov.* **2000,** *17*, 131 - 171.

66. Huang, Q.; He, X.; Ma, C.; Liu, R.; Yu, S.; Dayer, C. A.; Wenger, G. R.; McKernan, R.; Cook, J. M., Pharmacophore/Receptor Models for GABAA/BzR Subtypes (α1β3γ2, α5β3γ2, and α6β3γ2) via a Comprehensive Ligand-Mapping Approach. *J. Med. Chem.* **2000,** *43* (1), 71-95.

67. Clayton, T.; Poe, M. M.; Rallapalli, S.; Biawat, P.; Savic, M. M.; Rowlett, J. K.; Gallos, G.; Emala, C. W.; Kaczorowski, C. C.; Stafford, D. C.; Arnold, L. A.; Cook, J. M., A Review of the updated pharmacophore for the alpha 5 GABA(A) benzodiazepine receptor model. *Int J Med Chem* **2015,** *2015*, 430248.

68. Gu, Z. Q.; Wong, G.; Dominguez, C.; de Costa, B. R.; Rice, K. C.; Skolnick, P., Synthesis and evaluation of imidazo[1,5a][1,4]benzodiazepine esters with high affinities and

selectivities at diazepam insensitive (DI) benzodiazepine receptors. *J. Med. Chem* **1993,** *36*, 1001 - 1006.

69. Wong, G.; Koehler, K. F.; Skolnick, P.; Gu, Z. Q.; Ananthan, S.; Schonholze, P.; Hunkeler, W.; Zhang, W.; Cook, J. M., Synthetic and computer-assisted analysis of the structural requirements for selective, high affinity ligand binding to 'diazepam-insensitive' benzodiazepine receptors. *J. Med. Chem* **1993,** *36*, 1820 - 1830.

70. Lippke, K. P.; Schunack, W. G.; Wenning, W.; Muller, W. E., b-Carbolines as benzodiazepine receptor ligands. I. Synthesis and benzodiazepine receptor interactino of esters of b-carboline-3-carboxylic acid. *J. Med. Chem* **1983,** *26*, 499 - 503.

71. Haefely, W.; Martin, J. R.; Schoch, P., Novel anxiolytics that act as partial agonists at benzodiazepine receptors. *Trends Pharmacol. Sci.* **1990,** *11*, 452 - 456.

72. Hagen, T. J.; Guzman, F.; Schultz, C.; Cook, J. M., Synthesis of 3,6-disubstituted b-carbolines which possess either benzodiazepine antagonist or agonist activity. *Heterocycles* **1986,** *24*, 2845 - 855.

73. Gee, K. W.; Brinton, R. E.; Yamamura, H. I., CL-218872 antagonism of diazepam induced loss of righting reflex: Evidence for partial agonistic activity at the benzodiazepine receptor. *Life Sci.* **1983,** *32*, 1037 - 1040.

74. Allen, M. S.; Hagen, T. J.; Trudell, M. L.; Codding, P. W.; Skolnick, P.; Cook, J. M., Synthesis of novel 3-substituted b-carbolines as benzodiazepine receptor ligands: probing the benzodiazepine receptor pharmacophore. *J. Med. Chem* **1988,** *31*, 1854 - 1861.

75. Trudell, M. L.; Lifer, S. L.; Tan, Y. C.; Martin, M. J.; Deng, T.; Skolnick, P.; Cook, J. M., Synthesis of substituted 7,12-dihydropyrido[3,2-*b*:5,4-*b*'] diindoles: rigid planar

benzodiazepine receptor ligands with inverse agonist/antagonist properties. *J. Med. Chem* **1990,** *33*, 2412 - 2420.

76. Arbilla, S.; Depoortere, H.; Geroge, P.; Langer, S. Z., Pharmacological profile of the imidazopyridine zolpidem at benzodiazepine receptors and electrocorticogram in rats. *Naunym Schmiederbergs Arch. Pharmacol.* **1985,** *330*, 248 - 251.

77. Yokoyama, N.; Ritter, B.; Neubert, A. D., 2-Arylpyrazolo[4,3-*c*]quinolin-3-ones: novel agonist, partial agonist, and antagonist of benzodiazepines. *J. Med. Chem* **1982,** *25*, 337 - 339.

78. Huang, Q.; Zhang, W.; Liu, R.; McKernan, R. M.; Cook, J. M., Benzo-fused benzodiazepines employed as topological probes for the study of benzodiazepine receptor subtypes. *Med. Chem. Res.* **1996,** *6*, 384 - 391.

79. van Rijnsoever, C.; Täuber, M.; Choulli, M. K.; Keist, R.; Rudolph, U.; Mohler, H.; Fritschy, J. M.; Crestani, F., Requirement of α5GABA receptors for the development of tolerance to the sedative action of diazepam in mice. *The Journal of Neuroscience* **2004,** *24* (30), 6785.

80. Cook, J.; Huang, S.; Edwankar, R.; Namjoshi, O. A.; Wang, Z. J. Selective agents for pain suppression. Patent: US 8835424 B2. Date: Sep. 16, 2014.

81. Cook, J. M.; Huang, Q.; He, X.; Li, X.; Yu, J.; Han, D.; Lelas, S.; McElroy, J. F. Anxiolytic agents with reduced sedative and ataxic effects. Patent: US7119196 B2. Date: Oct. 10, 2006.

82. Cook, J. M.; Zhou, H.; Huang, S.; Sarma, P. V. V. S.; Zhang, C., Stereospecific anxiolytic and anticonvulsant agents with reduced muscle-relaxant, sedative-hypnotic and ataxic effects. Patent: US 7618958 B2. Date: Nov. 17, 2009.

83. Fischer, B. D.; Licata, S. C.; Edwankar, R. V.; Wang, Z. J.; Huang, S.; He, X.; Yu, J.; Zhou, H.; Johnson, E. M., Jr.; Cook, J. M.; Furtmuller, R.; Ramerstorfer, J.; Sieghart, W.; Roth, B. L.; Majumder, S.; Rowlett, J. K., Anxiolytic-like effects of 8-acetylene imidazobenzodiazepines in a rhesus monkey conflict procedure. *Neuropharmacology* **2010,** *59* (7-8), 612-8.

84. Blaser, H.-U., Chirality and its implications for the pharmaceutical industry. *Rendiconti Lincei* **2013,** *24* (3), 213-216.

85. Maher, T. J.; Johnson, D. A., Review of chirality and its importance in pharmacology. *Drug Development Research* **1991,** *24* (2), 149-156.

86. Nguyen, L. A.; He, H.; Pham-Huy, C., Chiral drugs: an overview. *International journal of biomedical science : IJBS* **2006,** *2* (2), 85-100.

87. Mellin, G. W.; Katzenstein, M., The saga of thalidomide. *N. Engl. J. Med.* **1962,** *267* (23), 1184-1193.

88. Landoni, M. F.; Soraci, A., Pharmacology of chiral compounds: 2-arylpropionic acid derivatives. *Current drug metabolism* **2001,** *2* (1), 37-51.

89. Patocka, J.; Ales, D., *Biomedical aspects of chiral molecules*. 2004; Vol. 2.

90. Li, G.; Stephen, M. R.; Kodali, R.; Zahn, N. M.; Poe, M. M.; Tiruveedhula, V. V. N. P. B.; Huber, A. T.; Schussman, M. K.; Qualmann, K.; Panhans, C. M.; Raddatz, N. J.; Baker, D. A.; Prevot, T. D.; Banasr, M.; Sibille, E.; Arnold, L. A.; Cook, J. M., Synthesis of chiral GABAA receptor subtype selective ligands as potential agents to treat schizophrenia as well as depression. *ARKIVOC* **2018,** *iv*, 158-183.

91. Frangou, S., Schizophrenia. *Medicine* **2008,** *36* (8), 405-409.

92. Kapur, S.; Mamo, D., Half a century of antipsychotics and still a central role for dopamine D2 receptors. *Prog. Neuropsychopharmacol. Biol. Psychiatry* **2003,** *27* (7), 1081-90.

93. Leucht, S.; Corves, C.; Arbter, D.; Engel, R. R.; Li, C.; Davis, J. M., Second-generation versus first-generation antipsychotic drugs for schizophrenia: a meta-analysis. *The Lancet* **2009,** *373* (9657), 31-41.

94. Longo, L. P.; Johnson, B., Addiction: Part I. Benzodiazepines--side effects, abuse risk and alternatives. *Am. Fam. Physician* **2000,** *61* (7), 2121-8.

95. Gill, K. M.; Cook, J. M.; Poe, M. M.; Grace, A. A., Prior antipsychotic drug treatment prevents response to novel antipsychotic agent in the methylazoxymethanol acetate model of schizophrenia. *Schizophr. Bull.* **2014,** *40* (2), 341-350.

96. Gill, K. M.; Lodge, D. J.; Cook, J. M.; Aras, S.; Grace, A. A., A novel α5GABA(A)R-positive allosteric modulator reverses hyperactivation of the dopamine system in the mam model of schizophrenia. *Neuropsychopharmacology* **2011,** *36* (9), 1903-1911.

97. Piantadosi, S. C.; French, B. J.; Poe, M. M.; Timic, T.; Markovic, B. D.; Pabba, M.; Seney, M. L.; Oh, H.; Orser, B. A.; Savic, M. M.; Cook, J. M.; Sibille, E., Sex-dependent anti-stress effect of an alpha5 subunit containing gabaa receptor positive allosteric modulator. *Front. Pharmacol.* **2016,** *7*, 446.

98. Batinic, B.; Santrac, A.; Jancic, I.; Li, G.; Vidojevic, A.; Markovic, B.; Cook, J. M.; Savic, M. M., Positive modulation of alpha5 GABAA receptors in preadolescence prevents reduced locomotor response to amphetamine in adult female but not male rats prenatally exposed to lipopolysaccharide. *Int. J. Dev. Neurosci.* **2017,** *61*, 31-39.

99. Forkuo, G. S.; Nieman, A. N.; Yuan, N. Y.; Kodali, R.; Yu, O. B.; Zahn, N. M.; Jahan, R.; Li, G.; Stephen, M. R.; Guthrie, M. L.; Poe, M. M.; Hartzler, B. D.; Harris, T. W.; Yocum,

G. T.; Emala, C. W.; Steeber, D. A.; Stafford, D. C.; Cook, J. M.; Arnold, L. A., Alleviation of multiple asthmatic pathologic features with orally available and subtype selective GABAA receptor modulators. *Mol. Pharm.* **2017,** *14* (6), 2088-2098.

100. Fischer, B. D.; Licata, S. C.; Edwankar, R. V.; Wang, Z.-J.; Huang, S.; He, X.; Yu, J.; Zhou, H.; Johnson, E. M.; Cook, J. M.; Furtmüller, R.; Ramerstorfer, J.; Sieghart, W.; Roth, B. L.; Majumder, S.; Rowlett, J. K., Anxiolytic-like effects of 8-acetylene imidazobenzodiazepines in a rhesus monkey conflict procedure. *Neuropharmacology* **2010,** *59* (7-8), 612-618.

101. Savić, M. M.; Majumder, S.; Huang, S.; Edwankar, R. V.; Furtmüller, R.; Joksimović, S.; Clayton, T.; Ramerstorfer, J.; Milinković, M. M.; Roth, B. L.; Sieghart, W.; Cook, J. M., Novel positive allosteric modulators of gabaa receptors: do subtle differences in activity at α1 plus α5 versus α2 plus α3 subunits account for dissimilarities in behavioral effects in rats? *Prog. Neuropsychopharmacol. Biol. Psychiatry* **2010,** *34* (2), 376-386.

102. Richetto, J.; Labouesse, M. A.; Poe, M. M.; Cook, J. M.; Grace, A. A.; Riva, M. A.; Meyer, U., Behavioral effects of the benzodiazepine-positive allosteric modulator SH-053-2'F-S-CH3 in an immune-mediated neurodevelopmental disruption model. *Int. J. Neuropsychopharmacol.* **2015,** *18* (4), pyu055-pyu055.

103. Takai, S.; Matsuda, A.; Usami, Y.; Adachi, T.; Sugiyama, T.; Katagiri, Y.; Tatematsu, M.; Hirano, K., Hydrolytic profile for ester- or amide-linkage by carboxylesterases pi 5.3 and 4.5 from human liver. *Biol. Pharm. Bull.* **1997,** *20* (8), 869-873.

104. Sanberg, P. R.; Bunsey, M. D.; Giordano, M.; Norman, A. B., The catalepsy test: its ups and downs. *Behav. Neurosci.* **1988,** *102* (5), 748-59.

105. Bakshi, V. P.; Geyer, M. A., Antagonism of phencyclidine-induced deficits in prepulse inhibition by the putative atypical antipsychotic olanzapine. *Psychopharmacology (Berl.)* **1995,** *122* (2), 198-201.

106. Batinić, B.; Santrač, A.; Jančić, I.; Li, G.; Vidojević, A.; Marković, B.; Cook, J. M.; Savić, M. M., Positive modulation of α5 GABAA receptors in preadolescence prevents reduced locomotor response to amphetamine in adult female but not male rats prenatally exposed to lipopolysaccharide. *Int. J. Dev. Neurosci.* **2017,** *61* (Supplement C), 31-39.

107. Poe, M. M.; Methuku, K. R.; Li, G.; Verma, A. R.; Teske, K. A.; Stafford, D. C.; Arnold, L. A.; Cramer, J. W.; Jones, T. M.; Cerne, R.; Krambis, M. J.; Witkin, J. M.; Jambrina, E.; Rehman, S.; Ernst, M.; Cook, J. M.; Schkeryantz, J. M., Synthesis and characterization of a novel γ-aminobutyric acid type a (GABAA) receptor ligand that combines outstanding metabolic stability, pharmacokinetics, and anxiolytic efficacy. *J. Med. Chem.* **2016,** *59* (23), 10800-10806.

108. Fischer, B. D.; Schlitt, R. J.; Hamade, B. Z.; Rehman, S.; Ernst, M.; Poe, M. M.; Li, G.; Kodali, R.; Arnold, L. A.; Cook, J. M., Pharmacological and antihyperalgesic properties of the novel α2/3 preferring GABAA receptor ligand MP-III-024. *Brain Res. Bull.* **2017,** *131* (Supplement C), 62-69.

109. Witkin, J. M.; Cerne, R.; Wakulchik, M.; S, J.; Gleason, S. D.; Jones, T. M.; Li, G.; Arnold, L. A.; Li, J. X.; Schkeryantz, J. M.; Methuku, K. R.; Cook, J. M.; Poe, M. M., Further evaluation of the potential anxiolytic activity of imidazo[1,5-a][1,4]diazepin agents selective for α2/3-containing GABAA receptors. *Pharmacology Biochemistry and Behavior* **2017,** *157* (Supplement C), 35-40.

110. Wallace, D. J.; Chen, C.-y., Cyclopropylboronic acid: synthesis and Suzuki cross-coupling reactions. *Tetrahedron Lett.* **2002,** *43* (39), 6987-6990.

111. Otera, J., Transesterification. *Chemical Reviews* **1993,** *93* (4), 1449-1470.

112. Cook, J. M.; Clayton, T. S.; Jain, H. D.; Johnson, Y. T.; Yang, J.; Rallipalli, S. K.; Wang, Z. J.; Namjoshi, O. A.; Poe, M. M. J., Gabaergic receptor subtype selective ligands and their uses. Google Patents: 2015.

113. Patani, G. A.; LaVoie, E. J., Bioisosterism: A rational approach in drug design. *Chemical Reviews* **1996,** *96* (8), 3147-3176.

114. Namjoshi, O. A.; Wang, Z.-j.; Rallapalli, S. K.; Johnson, E. M.; Johnson, Y.-T.; Ng, H.; Ramerstorfer, J.; Varagic, Z.; Sieghart, W.; Majumder, S.; Roth, B. L.; Rowlett, J. K.; Cook, J. M., Search for α3β2/3γ2 subtype selective ligands that are stable on human liver microsomes. *Bioorganic & Medicinal Chemistry* **2013,** *21* (1), 93-101.

115. Fleming, F. F.; Yao, L.; Ravikumar, P. C.; Funk, L.; Shook, B. C., Nitrile-containing pharmaceuticals: efficacious roles of the nitrile pharmacophore. *Journal of medicinal chemistry* **2010,** *53* (22), 7902-7917.

116. Wood, J. L.; Khatri, N. A.; Weinreb, S. M., A direct conversion of esters to nitriles. *Tetrahedron Letters* **1979,** *20* (51), 4907-4910.

117. Prevot, T. D.; Li, G.; Vidojevic, A.; Misquitta, K. A.; Fee, C.; Santrac, A.; Knutson, D. E.; Stephen, M. R.; Kodali, R.; Zahn, N. M.; Arnold, L. A.; Scholze, P.; Fisher, J. L.; Marković, B. D.; Banasr, M.; Cook, J. M.; Savic, M.; Sibille, E., Novel benzodiazepine-like ligands with various anxiolytic, antidepressant, or pro-cognitive profiles. *Molecular Neuropsychiatry* **2019**.

118. Savić, M. M.; Milinković, M. M.; Rallapalli, S.; Clayton, T., Sr.; Joksimović, S.; Van Linn, M.; Cook, J. M., The differential role of alpha1- and alpha5-containing GABA(A) receptors in mediating diazepam effects on spontaneous locomotor activity and water-maze learning and memory in rats. *The international journal of neuropsychopharmacology* **2009,** *12* (9), 1179-1193.

119. Richetto, J.; Labouesse, M. A.; Poe, M. M.; Cook, J. M.; Grace, A. A.; Riva, M. A.; Meyer, U., Behavioral effects of the benzodiazepine-positive allosteric modulator SH-053-2'F-S-CH_3 in an immune-mediated neurodevelopmental disruption model. *The international journal of neuropsychopharmacology* **2015,** *18* (4), 10.1093/ijnp/pyu055 pyu055.

120. Poe, M. M., Ph. D. Thesis: Synthesis of Subtype Selective Bz/GABAA Receptor Ligands for the Treatment of Anxiety, Epilepsy and Neuropathic Pain, as well as Schizophrenia and Asthma. University of Wisconsin Milwaukee. **2016**.

121. Stamenic, T. T.; Poe, M. M.; Rehman, S.; Santrac, A.; Divovic, B.; Scholze, P.; Ernst, M.; Cook, J. M.; Savic, M. M., Ester to amide substitution improves selectivity, efficacy and kinetic behavior of a benzodiazepine positive modulator of GABAA receptors containing the alpha5 subunit. *Eur. J. Pharmacol.* **2016,** *791*, 433-443.

122. Batinić, B.; Santrač, A.; Jančić, I.; Li, G.; Vidojević, A.; Marković, B.; Cook, J. M.; Savić, M. M., Positive modulation of α5 GABAA receptors in preadolescence prevents reduced locomotor response to amphetamine in adult female but not male rats prenatally exposed to lipopolysaccharide. *Int. J. Dev. Neurosci.* **2017,** *61*, 31-39.

123. Wiberg, K. B.; Rablen, P. R., Why does thioformamide have a larger rotational barrier than formamide? *J. Am. Chem. Soc.* **1995,** *117* (8), 2201-2209.

124. Wiberg, K. B., The interaction of carbonyl groups with substituents. *Acc. Chem. Res.* **1999,** *32* (11), 922-929.

125. Ozturk, T.; Ertas, E.; Mert, O., Use of Lawesson's reagent in organic syntheses. *Chem. Rev.* **2007,** *107* (11), 5210-5278.

126. Curphey, T. J., Thionation with the reagent combination of phosphorus pentasulfide and hexamethyldisiloxane. *The Journal of Organic Chemistry* **2002,** *67* (18), 6461-6473.

127. Drach, S. V.; Litvinovskaya, R. P.; Khripach, V. A., Steroidal 1,2-oxazoles. Synthesis and biological activity. (Review). *Chemistry of Heterocyclic Compounds* **2000,** *36* (3), 233-255.

128. Greenblatt, D. J.; Matlis, R.; Scavone, J. M.; Blyden, G. T.; Harmatz, J. S.; Shader, R. I., Oxaprozin pharmacokinetics in the elderly. *Br. J. Clin. Pharmacol.* **1985,** *19* (3), 373-378.

129. Mussoni, L.; Poggi, A.; De Gaetano, G.; Donati, M. B., Effect of ditazole, an inhibitor of platelet aggregation, on a metastasizing tumour in mice. *Br. J. Cancer* **1978,** *37* (1), 126-129.

130. Li, G.; Golani, L. K.; Jahan, R.; Rashid, F.; Cook, J. M., Improved synthesis of anxiolytic, anticonvulsant, and antinociceptive alpha 2/alpha 3-GABA(A)-ergic receptor subtype selective ligands as promising agents to treat anxiety, epilepsy, and neuropathic. *Synthesis-Stuttgart* **2018,** *50* (20), 4124-4132.

131. Mandrioli, R.; Mercolini, L.; Raggi, M. A., Benzodiazepine metabolism: an analytical perspective. *Current drug metabolism* **2008,** *9* (8), 827-44.

132. Borchers, F.; Achtert, G.; Hausleiter, H. J.; Zeugner, H., Metabolism and pharmacokinetics of metaclazepam (Talis®), Part III: Determination of the chemical structure of metabolites in dogs, rabbits and men. *Eur. J. Drug Metab. Pharmacokinet.* **1984,** *9* (4), 325-346.

133. Garattini, S.; Marcucci, F.; Mussini, E., Benzodiazepine metabolism in vitro. *Drug Metab. Rev.* **1972,** *1* (1), 291-309.

134. Szatkowska, P.; Koba, M.; Kośliński, P.; Wandas, J.; Bączek, T., Analytical methods for determination of benzodiazepines. A short review. *Central European Journal of Chemistry* **2014,** *12* (10), 994-1007.

135. Perrin, L.; Loiseau, N.; André, F.; Delaforge, M., Metabolism of N-methyl-amide by cytochrome P450s. *The FEBS Journal* **2011,** *278* (12), 2167-2178.

136. Fan, P. W.; Gu, C.; Marsh, S. A.; Stevens, J. C., Mechanism-based inactivation of cytochrome P450 2B6 by a novel terminal acetylene inhibitor. *Drug Metab. Dispos.* **2003,** *31* (1), 28-36.

137. Besnard, J.; Ruda, G. F.; Setola, V.; Abecassis, K.; Rodriguiz, R. M.; Huang, X.-P.; Norval, S.; Sassano, M. F.; Shin, A. I.; Webster, L. A.; Simeons, F. R. C.; Stojanovski, L.; Prat, A.; Seidah, N. G.; Constam, D. B.; Bickerton, G. R.; Read, K. D.; Wetsel, W. C.; Gilbert, I. H.; Roth, B. L.; Hopkins, A. L., Automated design of ligands to polypharmacological profiles. *Nature* **2012,** *492*, 215.

138. Catterall, W. A., Voltage-gated calcium channels. *Cold Spring Harb. Perspect. Biol. 3* (8), a003947-a003947.

139. Carvajal, F. J.; Mattison, H. A.; Cerpa, W., Role of NMDA receptor-mediated glutamatergic signaling in chronic and acute neuropathologies. *Neural Plast.* **2016,** *2016*, 2701526-2701526.

140. Casellas, P.; Galiegue, S.; Basile, A. S., Peripheral benzodiazepine receptors and mitochondrial function. *Neurochem. Int.* **2002,** *40* (6), 475-486.

141. Galiegue, S.; Tinel, N.; Casellas, P., The peripheral benzodiazepine receptor: a promising therapeutic drug target. *Curr. Med. Chem.* **2003,** *10* (16), 1563-72.

142. Barron, H.; Hafizi, S.; Andreazza, A. C.; Mizrahi, R., Neuroinflammation and Oxidative Stress in Psychosis and Psychosis Risk. *Int. J. Mol. Sci.* **2017,** *18* (3), 651.

143. Boerrigter, D.; Weickert, T. W.; Lenroot, R.; O'Donnell, M.; Galletly, C.; Liu, D.; Burgess, M.; Cadiz, R.; Jacomb, I.; Catts, V. S.; Fillman, S. G.; Weickert, C. S., Using blood cytokine measures to define high inflammatory biotype of schizophrenia and schizoaffective disorder. *J. Neuroinflammation* **2017,** *14* (1), 188.

144. Chen, W.-W.; Zhang, X.; Huang, W.-J., Role of neuroinflammation in neurodegenerative diseases (Review). *Mol. Med. Report.* **2016,** *13* (4), 3391-3396.

145. De Picker, L. J.; Morrens, M.; Chance, S. A.; Boche, D., Microglia and Brain Plasticity in Acute Psychosis and Schizophrenia Illness Course: A Meta-Review. *Frontiers in Psychiatry* **2017,** *8* (238).

146. Prata, J.; Santos, S. G.; Almeida, M. I.; Coelho, R.; Barbosa, M. A., Bridging autism spectrum disorders and schizophrenia through inflammation and biomarkers - pre-clinical and clinical investigations. *J. Neuroinflammation* **2017,** *14* (1), 179.

147. Lee, M.; Schwab, C.; McGeer, P. L., Astrocytes are GABAergic cells that modulate microglial activity. *Glia* **2011,** *59* (1), 152-65.

148. Jones, C. A.; Watson, D. J. G.; Fone, K. C. F., Animal models of schizophrenia. *Br. J. Pharmacol.* **2011,** *164* (4), 1162-1194.

149. Abekawa, T.; Ito, K.; Nakagawa, S.; Koyama, T., Prenatal exposure to an NMDA receptor antagonist, MK-801 reduces density of parvalbumin-immunoreactive GABAergic neurons in the medial prefrontal cortex and enhances phencyclidine-induced hyperlocomotion but

not behavioral sensitization to methamphetamine in postpubertal rats. *Psychopharmacology (Berl.)* **2007,** *192* (3), 303-16.

150. Kalinichev, M.; Bate, S. T.; Coggon, S. A.; Jones, D. N., Locomotor reactivity to a novel environment and sensitivity to MK-801 in five strains of mice. *Behav. Pharmacol.* **2008,** *19* (1), 71-5.

151. Walf, A. A.; Frye, C. A., The use of the elevated plus maze as an assay of anxiety-related behavior in rodents. *Nat. Protoc.* **2007,** *2* (2), 322-328.

152. Lin, L.-C.; Sibille, E., Reduced brain somatostatin in mood disorders: a common pathophysiological substrate and drug target? *Front. Pharmacol.* **2013,** *4*, 110-110.

153. Fee, C.; Banasr, M.; Sibille, E., Somatostatin-positive gamma-aminobutyric acid interneuron deficits in depression: cortical microcircuit and therapeutic perspectives. *Biol. Psychiatry* **2017,** *82* (8), 549-559.

154. Geng, Y.; Bush, M.; Mosyak, L.; Wang, F.; Fan, Q. R., Structural mechanism of ligand activation in human GABA(B) receptor. *Nature* **2013,** *504* (7479), 254-9.

155. Behlke, L. M.; Foster, R. A.; Liu, J.; Benke, D.; Benham, R. S.; Nathanson, A. J.; Yee, B. K.; Zeilhofer, H. U.; Engin, E.; Rudolph, U., A pharmacogenetic 'restriction-of-function' approach reveals evidence for anxiolytic-like actions mediated by α5-containing GABAA receptors in mice. *Neuropsychopharmacology* **2016,** *41*, 2492.

156. Botta, P.; Demmou, L.; Kasugai, Y.; Markovic, M.; Xu, C.; Fadok, J. P.; Lu, T.; Poe, M. M.; Xu, L.; Cook, J. M.; Rudolph, U.; Sah, P.; Ferraguti, F.; Lüthi, A., Regulating anxiety with extrasynaptic inhibition. *Nat. Neurosci.* **2015,** *18*, 1493.

157. Joksimović, S.; Divljaković, J.; Van Linn, M. L.; Varagic, Z.; Brajković, G.; Milinković, M. M.; Yin, W.; Timić, T.; Sieghart, W.; Cook, J. M.; Savić, M. M., Benzodiazepine-

induced spatial learning deficits in rats are regulated by the degree of modulation of α1 GABA(A) receptors. *European neuropsychopharmacology : the journal of the European College of Neuropsychopharmacology* **2013,** *23* (5), 390-399.

158. Joksimović, S.; Varagic, Z.; Kovačević, J.; Van Linn, M.; Milić, M.; Rallapalli, S.; Timić, T.; Sieghart, W.; Cook, J. M.; Savić, M. M., Insights into functional pharmacology of α_1 GABA(A) receptors: how much does partial activation at the benzodiazepine site matter? *Psychopharmacology (Berl.)* **2013,** *230* (1), 113-123.

159. Dunham, N. W.; Miya, T. S., A note on a simple apparatus for detecting neurological deficit in rats and mice. *J. Am. Pharm. Assoc. Am. Pharm. Assoc.* **1957,** *46* (3), 208-9.

160. Huang, S. Ph.D. Thesis, Synthesis of Optically Active Subtype Selective Benzodiazepine Receptor Ligands. University of Wisconsin-Milwaukee, 2007.

161. Chae, M. J.; Song, J. I.; An, D. K., Chemoselective reduction of esters to aldehydes by potassium diisobutyl-t-butoxyaluminum hydride (PDBBA). *Bull. Korean Chem. Soc.* **2007,** *28* (28), 2517-2518.

162. Papi, A.; Brightling, C.; Pedersen, S. E.; Reddel, H. K., Asthma. *The Lancet* **2018,** *391* (10122), 783-800.

163. Adcock, I. M.; Caramori, G.; Chung, K. F., New targets for drug development in asthma. *The Lancet* **2008,** *372* (9643), 1073-1087.

164. Trevor, J. L.; Chipps, B. E., Severe asthma in primary care: identification and management. *The American Journal of Medicine* **2018,** *131* (5), 484-491.

165. McCracken, J. L.; Veeranki, S. P.; Ameredes, B. T.; Calhoun, W. J., Diagnosis and management of asthma in adults: a review. *JAMA* **2017,** *318* (3), 279-290.

166. Nunes, C.; Pereira, A. M.; Morais-Almeida, M., Asthma costs and social impact. *Asthma research and practice* **2017,** *3*, 1-1.

167. Shimizu, T., Mucus, Goblet Cell, Submucosal Gland. In *Nasal Physiology and Pathophysiology of Nasal Disorders*, Önerci, T. M., Ed. Springer Berlin Heidelberg: Berlin, Heidelberg, 2013; pp 1-14.

168. Rydell-Törmänen, K.; Risse, P.-A.; Kanabar, V.; Bagchi, R.; Czubryt, M. P.; Johnson, J. R., Smooth muscle in tissue remodeling and hyper-reactivity: Airways and arteries. *Pulm. Pharmacol. Ther.* **2013,** *26* (1), 13-23.

169. Barnes, P. J., Pharmacology of airway smooth muscle. *Am. J. Respir. Crit. Care Med.* **1998,** *158* (5 Pt 3), S123-32.

170. Pascoe, C. D.; Wang, L.; Syyong, H. T.; Par; , P. D., A brief history of airway smooth muscle's role in airway hyperresponsiveness. *J. Allergy* **2012,** *2012*, 8.

171. Bush, A.; Pedersen, S.; Hedlin, G.; Baraldi, E.; Barbato, A.; de Benedictis, F.; Lødrup Carlsen, K. C.; de Jongste, J.; Piacentini, G., Pharmacological treatment of severe, therapy-resistant asthma in children: what can we learn from where? *Eur. Respir. J.* **2011,** *38* (4), 947.

172. Kew, K. M.; Dahri, K., Long-acting muscarinic antagonists (LAMA) added to combination long-acting beta2-agonists and inhaled corticosteroids (LABA/ICS) versus LABA/ICS for adults with asthma. *The Cochrane database of systematic reviews* **2016,** (1), Cd011721.

173. D'Urzo, A. D.; Chapman, K. R., Leukotriene-receptor antagonists. Role in asthma management. *Canadian family physician Medecin de famille canadien* **2000,** *46*, 872-879.

174. Barnes, P. J., Theophylline. *Am. J. Respir. Crit. Care Med.* **2013,** *188* (8), 901-906.

175. Polosa, R.; Morjaria, J., Immunomodulatory and biologic therapies for severe refractory asthma. *Respir. Med.* **2008,** *102* (11), 1499-1510.

176. Laxmanan, B.; Hogarth, D. K., Bronchial thermoplasty in asthma: current perspectives. *J. Asthma Allergy* **2015,** *8*, 39-49.

177. Shirakawa, J.; Taniyama, K.; Tanaka, C., gamma-Aminobutyric acid-induced modulation of acetylcholine release from the guinea pig lung. *J. Pharmacol. Exp. Ther.* **1987,** *243* (1), 364-9.

178. Moore, C. T.; Wilson, C. G.; Mayer, C. A.; Acquah, S. S.; Massari, V. J.; Haxhiu, M. A., A GABAergic inhibitory microcircuit controlling cholinergic outflow to the airways. *Journal of applied physiology (Bethesda, Md. : 1985)* **2004,** *96* (1), 260-70.

179. Gallos, G.; Yim, P.; Chang, S.; Zhang, Y.; Xu, D.; Cook, J. M.; Gerthoffer, W. T.; Emala, C. W., Sr., Targeting the restricted α-subunit repertoire of airway smooth muscle GABAA receptors augments airway smooth muscle relaxation. *American journal of physiology. Lung cellular and molecular physiology* **2012,** *302* (2), L248-L256.

180. Gallos, G.; Townsend, E.; Yim, P.; Virag, L.; Zhang, Y.; Xu, D.; Bacchetta, M.; Emala, C. W., Airway epithelium is a predominant source of endogenous airway GABA and contributes to relaxation of airway smooth muscle tone. *Am. J. Physiol. Lung Cell Mol. Physiol.* **2013,** *304* (3), L191-7.

181. Gallos, G.; Gleason, N. R.; Zhang, Y.; Pak, S. W.; Sonett, J. R.; Yang, J.; Emala, C. W., Activation of endogenous GABAA channels on airway smooth muscle potentiates isoproterenol-mediated relaxation. *Am. J. Physiol. Lung Cell Mol. Physiol.* **2008,** *295* (6), L1040-7.

182. Xiang, Y. Y.; Wang, S.; Liu, M.; Hirota, J. A.; Li, J.; Ju, W.; Fan, Y.; Kelly, M. M.; Ye, B.; Orser, B.; O'Byrne, P. M.; Inman, M. D.; Yang, X.; Lu, W. Y., A GABAergic system in airway epithelium is essential for mucus overproduction in asthma. *Nat. Med.* **2007,** *13* (7), 862-7.

183. Yocum, G. T.; Gallos, G.; Zhang, Y.; Jahan, R.; Stephen, M. R.; Varagic, Z.; Puthenkalam, R.; Ernst, M.; Cook, J. M.; Emala, C. W., Targeting the gamma-aminobutyric acid a receptor alpha4 subunit in airway smooth muscle to alleviate bronchoconstriction. *Am. J. Respir. Cell Mol. Biol.* **2016,** *54* (4), 546-53.

184. Jahan, R.; Stephen, M. R.; Forkuo, G. S.; Kodali, R.; Guthrie, M. L.; Nieman, A. N.; Yuan, N. Y.; Zahn, N. M.; Poe, M. M.; Li, G.; Yu, O. B.; Yocum, G. T.; Emala, C. W.; Stafford, D. C.; Cook, J. M.; Arnold, L. A., Optimization of substituted imidazobenzodiazepines as novel asthma treatments. *Eur. J. Med. Chem.* **2017,** *126* (Supplement C), 550-560.

185. Forkuo, G. S.; Guthrie, M. L.; Yuan, N. Y.; Nieman, A. N.; Kodali, R.; Jahan, R.; Stephen, M. R.; Yocum, G. T.; Treven, M.; Poe, M. M.; Li, G.; Yu, O. B.; Hartzler, B. D.; Zahn, N. M.; Ernst, M.; Emala, C. W.; Stafford, D. C.; Cook, J. M.; Arnold, L. A., Development of GABAA receptor subtype-selective imidazobenzodiazepines as novel asthma treatments. *Mol. Pharm.* **2016,** *13* (6), 2026-2038.

186. Obradovic, A. L.; Joksimovic, S.; Batinic, B.; Radulovic, T.; Poe, M. M.; Namjoshi, O. A.; Cook, J. M.; Ramerstorfer, J.; Varagic, Z.; Sieghart, W.; Karovic, B.; Roth, B.; Savic, M. M., SH-I-048A, an *in vitro* nonselective super-agonist at the benzodiazepine site of $GABA_A$ receptors: the approximated activation of receptor subtypes may explain behavioral effects. *Brain Res.* **2014,** *1554*, 36 - 48.

187. Forkuo, G. S.; Nieman, A. N.; Kodali, R.; Zahn, N. M.; Li, G.; Rashid Roni, M. S.; Stephen, M. R.; Harris, T. W.; Jahan, R.; Guthrie, M. L.; Yu, O. B.; Fisher, J. L.; Yocum, G. T.; Emala, C. W.; Steeber, D. A.; Stafford, D. C.; Cook, J. M.; Arnold, L. A., A novel orally available asthma drug candidate that reduces smooth muscle constriction and inflammation by targeting GABAA receptors in the lung. *Mol. Pharm.* **2018,** *15* (5), 1766-1777.

188. Yocum, G. T.; Perez-Zoghbi, J. F.; Danielsson, J.; Kuforiji, A. S.; Zhang, Y.; Li, G.; Roni, M. S. R.; Kodali, R.; Stafford, D. C.; Arnold, L. A.; Cook, J. M.; Emala, C. W., Sr., A novel gabaa receptor ligand MIDD0301 with limited blood-brain barrier penetration relaxes airway smooth muscle ex vivo and in vivo. *Am. J. Physiol. Lung Cell Mol. Physiol.* **2018**.

189. Zahn, N. M.; Huber, A. T.; Mikulsky, B. N.; Stepanski, M. E.; Kehoe, A. S.; Li, G.; Schussman, M.; Rashid Roni, M. S.; Kodali, R.; Cook, J. M.; Stafford, D. C.; Steeber, D. A.; Arnold, L. A., MIDD0301 - A first-in-class anti-inflammatory asthma drug targets GABAA receptors without causing systemic immune suppression. *Basic Clin. Pharmacol. Toxicol.* **2019**.

190. Tian, J.; Lu, Y.; Zhang, H.; Chau, C. H.; Dang, H. N.; Kaufman, D. L., Gamma-aminobutyric acid inhibits T cell autoimmunity and the development of inflammatory responses in a mouse type 1 diabetes model. *J. Immunol.* **2004,** *173* (8), 5298-304.

191. Bjurstöm, H.; Wang, J.; Ericsson, I.; Bengtsson, M.; Liu, Y.; Kumar-Mendu, S.; Issazadeh-Navikas, S.; Birnir, B., GABA, a natural immunomodulator of T lymphocytes. *J. Neuroimmunol.* **2008,** *205* (1-2), 44-50.

192. Rosa, A. C.; Fantozzi, R., The role of histamine in neurogenic inflammation. *Br. J. Pharmacol.* **2013,** *170* (1), 38-45.

193. Chaplin, D. D., Overview of the immune response. *The Journal of allergy and clinical immunology* **2010,** *125* (2 Suppl 2), S3-S23.

194. Yatim, K. M.; Lakkis, F. G., A brief journey through the immune system. *Clinical journal of the American Society of Nephrology : CJASN* **2015,** *10* (7), 1274-1281.

195. Stevens, W. W.; Kim, T. S.; Pujanauski, L. M.; Hao, X.; Braciale, T. J., Detection and quantitation of eosinophils in the murine respiratory tract by flow cytometry. *J. Immunol. Methods* **2007,** *327* (1-2), 63-74.

196. Nakano, A.; Harada, T.; Morikawa, S.; Kato, Y., Expression of leukocyte common antigen (CD45) on various human leukemia/lymphoma cell lines. *Acta Pathol. Jpn.* **1990,** *40* (2), 107-15.

197. Zhu, J.; Paul, W. E., CD4 T cells: fates, functions, and faults. *Blood* **2008,** *112* (5), 1557.

198. Corrigan, C. J.; Haczku, A.; Gemou-Engesaeth, V.; Doi, S.; Kikuchi, Y.; Takatsu, K.; Durham, S. R.; Kay, A. B., CD4 T-Lymphocyte activation in asthma is accompanied by increased serum concentrations of interleukin-5: effect of glucocorticoid therapy. *Am. Rev. Respir. Dis.* **1993,** *147* (3), 540-547.

199. Lin, H.-H.; Faunce, D. E.; Stacey, M.; Terajewicz, A.; Nakamura, T.; Zhang-Hoover, J.; Kerley, M.; Mucenski, M. L.; Gordon, S.; Stein-Streilein, J., The macrophage F4/80 receptor is required for the induction of antigen-specific efferent regulatory T cells in peripheral tolerance. *The Journal of experimental medicine* **2005,** *201* (10), 1615-1625.

200. Zeng, C.; Pan, F.; Jones, L. A.; Lim, M. M.; Griffin, E. A.; Sheline, Y. I.; Mintun, M. A.; Holtzman, D. M.; Mach, R. H., Evaluation of 5-ethynyl-2'-deoxyuridine staining as a sensitive and reliable method for studying cell proliferation in the adult nervous system. *Brain Res.* **2010,** *1319*, 21-32.

201. Cavanagh, B. L.; Walker, T.; Norazit, A.; Meedeniya, A. C., Thymidine analogues for tracking DNA synthesis. *Molecules* **2011,** *16* (9), 7980-93.

202. Barnes, P. J., The cytokine network in asthma and chronic obstructive pulmonary disease. *The Journal of Clinical Investigation* **2008,** *118* (11), 3546-3556.

203. Chung, K. F.; Barnes, P. J., Cytokines in asthma. *Thorax* **1999,** *54* (9), 825.

204. Wei, H.; Tan, K.; Sun, R.; Yin, L.; Zhang, J.; Pu, Y., Aberrant production of Th1/Th2/Th17-related cytokines in serum of C57BL/6 mice after short-term formaldehyde exposure. *Int. J. Environ. Res. Public Health* **2014,** *11* (10), 10036-10050.

205. Tonomura, N.; Habiro, K.; Shimizu, A.; Sykes, M.; Yang, Y.-G., Antigen-specific human T-cell responses and T cell-dependent production of human antibodies in a humanized mouse model. *Blood* **2008,** *111* (8), 4293-4296.

206. Kojima, F.; Frolov, A.; Matnani, R.; Woodward, J. G.; Crofford, L. J., Reduced T cell-dependent humoral immune response in microsomal prostaglandin E synthase-1 null mice is mediated by nonhematopoietic cells. *J. Immunol.* **2013,** *191* (10), 4979-88.

207. Swaminathan, A.; Lucas, R. M.; Dear, K.; McMichael, A. J., Keyhole limpet haemocyanin - a model antigen for human immunotoxicological studies. *Br. J. Clin. Pharmacol.* **2014,** *78* (5), 1135-1142.

208. Hassan, N. M.; Neiman, R. S., The pathology of the spleen in steroid-treated immune thrombocytopenic purpura. *Am. J. Clin. Pathol.* **1985,** *84* (4), 433-8.

209. Weir, H.; Chen, P. L.; Deiss, T. C.; Jacobs, N.; Nabity, M. B.; Young, M.; Criscitiello, M. F., DNP-KLH yields changes in leukocyte populations and immunoglobulin isotype use with different immunization routes in zebrafish. *Front. Immunol.* **2015,** *6*, 606-606.

210. Machado, D.; Girardini, M.; Viveiros, M.; Pieroni, M., Challenging the drug-likeness dogma for new drug discovery in tuberculosis. *Front. Microbiol.* **2018,** *9* (1367).

211. Pal, P.; Zeng, H.; Durocher, G.; Girard, D.; Li, T.; Gupta, A. K.; Giasson, R.; Blanchard, L.; Gaboury, L.; Balassy, A.; Turmel, C.; Laperrière, A.; Villeneuve, L., Phototoxicity of some bromine-substituted rhodamine dyes: synthesis, photophysical properties and application as photosensitizers. *Photochem. Photobiol.* **1996,** *63* (2), 161-168.

212. Chen, J.; Yuan, T.; Hao, W.; Cai, M., Simple and efficient CuI/PEG-400 system for hydroxylation of aryl halides with potassium hydroxide. *Catalysis Communications* **2011,** *12* (15), 1463-1465.

213. Lassila, T.; Hokkanen, J.; Aatsinki, S.-M.; Mattila, S.; Turpeinen, M.; Tolonen, A., toxicity of carboxylic acid-containing drugs: the role of acyl migration and coa conjugation investigated. *Chem. Res. Toxicol.* **2015,** *28* (12), 2292-2303.

214. Skonberg, C.; Olsen, J.; Madsen, K. G.; Hansen, S. H.; Grillo, M. P., Metabolic activation of carboxylic acids. *Expert Opin. Drug Metab. Toxicol.* **2008,** *4* (4), 425-438.

215. Lassalas, P.; Gay, B.; Lasfargeas, C.; James, M. J.; Tran, V.; Vijayendran, K. G.; Brunden, K. R.; Kozlowski, M. C.; Thomas, C. J.; Smith, A. B.; Huryn, D. M.; Ballatore, C., Structure Property Relationships of Carboxylic Acid Isosteres. *J. Med. Chem.* **2016,** *59* (7), 3183-3203.

216. Ballatore, C.; Huryn, D. M.; Smith, A. B., 3rd, Carboxylic acid (bio)isosteres in drug design. *ChemMedChem* **2013,** *8* (3), 385-95.

217. Heravi, M. M.; Fazeli, A.; Oskooie, H. A.; Beheshtiha, Y. S.; Valizadeh, H., Click synthesis of 5-substituted 1h-tetrazoles from aldehydes, hydroxyl-amine, and [bmim]N3 via one-pot, three-component reaction. *Synlett* **2012,** *23* (20), 2927-2930.

218. Wang, W.; Xu, A.; Zhou, G.; Leng, M.; Zhou, H.; Yan, J., Proliferation and apoptosis of Peyer's patches and its lymphocytes in experimental terminal ileitis. *Int. J. Clin. Exp. Pathol.* **2014,** *7* (12), 8583-8592.

219. Richter, L.; de Graaf, C.; Sieghart, W.; Varagic, Z.; Morzinger, M.; de Esch, I. J.; Ecker, G. F.; Ernst, M., Diazepam-bound GABAA receptor models identify new benzodiazepine binding-site ligands. *Nat. Chem. Biol.* **2012,** *8* (5), 455-64.

220. Rudolph, U.; Mohler, H., GABA-based therapeutic approaches: GABAA receptor subtype functions. *Curr. Opin. Pharmacol.* **2006,** *6* (1), 18-23.

221. Mendelson, W. B.; Owen, C.; Skolnick, P.; Paul, S. M.; Martin, J. V.; Ko, G.; Wagner, R., Nifedipine blocks sleep induction by flurazepam in the rat. *Sleep* **1984,** *7* (1), 64-8.

222. Ninan, P. T.; Insel, T. M.; Cohen, R. M.; Cook, J. M.; Skolnick, P.; Paul, S. M., Benzodiazepine receptor-mediated experimental "anxiety" in primates. *Science* **1982,** *218* (4579), 1332-4.

223. Atack, J. R.; Wafford, K. A.; Street, L. J.; Dawson, G. R.; Tye, S.; Van Laere, K.; Bormans, G.; Sanabria-Bohorquez, S. M.; De Lepeleire, I.; de Hoon, J. N.; Van Hecken, A.; Burns, H. D.; McKernan, R. M.; Murphy, M. G.; Hargreaves, R. J., MRK-409 (MK-0343), a GABAA receptor subtype-selective partial agonist, is a non-sedating anxiolytic in preclinical species but causes sedation in humans. *Journal of psychopharmacology (Oxford, England)* **2011,** *25* (3), 314-28.

224. Mirza, N. R.; Larsen, J. S.; Mathiasen, C.; Jacobsen, T. A.; Munro, G.; Erichsen, H. K.; Nielsen, A. N.; Troelsen, K. B.; Nielsen, E. O.; Ahring, P. K., NS11394 [3'-[5-(1-hydroxy-1-methyl-ethyl)-benzoimidazol-1-yl]-biphenyl-2-carbonitrile], a unique subtype-selective

GABAA receptor positive allosteric modulator: in vitro actions, pharmacokinetic properties and in vivo anxiolytic efficacy. *J. Pharmacol. Exp. Ther.* **2008,** *327* (3), 954-68.

225. Munro, G.; Lopez-Garcia, J. A.; Rivera-Arconada, I.; Erichsen, H. K.; Nielsen, E. O.; Larsen, J. S.; Ahring, P. K.; Mirza, N. R., Comparison of the novel subtype-selective GABAA receptor-positive allosteric modulator NS11394 [3'-[5-(1-hydroxy-1-methyl-ethyl)-benzoimidazol-1-yl]-biphenyl-2-carbonitrile] with diazepam, zolpidem, bretazenil, and gaboxadol in rat models of inflammatory and neuropathic pain. *J. Pharmacol. Exp. Ther.* **2008,** *327* (3), 969-81.

226. Fischer, B. D.; Schlitt, R. J.; Hamade, B. Z.; Rehman, S.; Ernst, M.; Poe, M. M.; Li, G.; Kodali, R.; Arnold, L. A.; Cook, J. M., Pharmacological and antihyperalgesic properties of the novel α2/3 preferring GABAA receptor ligand MP-III-024. *Brain Res. Bull.* **2017,** *131*, 62-69.

227. Clayton, T.; Poe, M. M.; Rallapalli, S.; Biawat, P.; Savic, M. M.; Rowlett, J. K.; Gallos, G.; Emala, C. W.; Kaczorowski, C. C.; Stafford, D. C.; Arnold, L. A.; Cook, J. M., A review of the updated pharmacophore for the alpha 5 GABA(A) benzodiazepine receptor model. *International journal of medicinal chemistry* **2015,** *2015*, 430248.

228. Rivas, F. M.; Stables, J. P.; Murphree, L.; Edwankar, R. V.; Edwankar, C. R.; Huang, S.; Jain, H. D.; Zhou, H.; Majumder, S.; Sankar, S.; Roth, B. L.; Ramerstorfer, J.; Furtmüller, R.; Sieghart, W.; Cook, J. M., Antiseizure activity of novel γ-aminobutyric acid (a) receptor subtype-selective benzodiazepine analogues in mice and rat models. *J. Med. Chem.* **2009,** *52* (7), 1795-1798.

229. Di Lio, A.; Benke, D.; Besson, M.; Desmeules, J.; Daali, Y.; Wang, Z. J.; Edwankar, R.; Cook, J. M.; Zeilhofer, H. U., HZ166, a novel GABAA receptor subtype-selective

benzodiazepine site ligand, is antihyperalgesic in mouse models of inflammatory and neuropathic pain. *Neuropharmacology* **2011,** *60* (4), 626-32.

230. Namjoshi, O. A.; Wang, Z.-j.; Rallapalli, S. K.; Johnson, E. M.; Johnson, Y.-T.; Ng, H.; Ramerstorfer, J.; Varagic, Z.; Sieghart, W.; Majumder, S.; Roth, B. L.; Rowlett, J. K.; Cook, J. M., Search for α3β(2/3)γ2 subtype selective ligands that are stable on human liver microsomes. *Bioorg. Med. Chem.* **2013,** *21* (1), 93-101.

231. Boström, J.; Hogner, A.; Llinàs, A.; Wellner, E.; Plowright, A. T., Oxadiazoles in medicinal chemistry. *J. Med. Chem.* **2012,** *55* (5), 1817-1830.

232. Burger, A., Isosterism and bioisosterism in drug design. *Progress in drug research. Fortschritte der Arzneimittelforschung. Progres des recherches pharmaceutiques* **1991,** *37*, 287-371.

233. Langmuir, I., Isomorphism, isosterism and covalence. *J. Am. Chem. Soc.* **1919,** *41* (10), 1543-1559.

234. Cook, J.; POE, M. M. J.; METHUKU, K. R.; LI, G. GABAergic ligands and their uses. WO2016154031 A1, Sep 29, 2016, 2016.

235. Shimazaki, T.; Iijima, M.; Chaki, S., Anxiolytic-like activity of MGS0039, a potent group II metabotropic glutamate receptor antagonist, in a marble-burying behavior test. *Eur. J. Pharmacol.* **2004,** *501* (1-3), 121-125.

236. Lewter, L. A.; Fisher, J. L.; Siemian, J. N.; Methuku, K. R.; Poe, M. M.; Cook, J. M.; Li, J.-X., Antinociceptive effects of a novel α2/α3-subtype selective GABAA receptor positive allosteric modulator. *ACS Chem. Neurosci.* **2017,** *8* (6), 1305-1312.

237. Yang, J.; Teng, Y.; Ara, S.; Rallapalli, S.; Cook, J. M., An Improved Process for the Synthesis of 4H-Imidazo[1,5-a][1,4]benzodiazepines. *Synthesis* **2009,** *40* (32), nihpa145687-nihpa145687.

238. Watjen, F.; Baker, R.; Engelstoff, M.; Herbert, R.; MacLeod, A.; Knight, A.; Merchant, K.; Moseley, J.; Saunders, J., Novel benzodiazepine receptor partial agonists: oxadiazolylimidazobenzodiazepines. *J. Med. Chem.* **1989,** *32* (10), 2282-2291.

239. Kayukova, L. A., Synthesis of 1,2,4-oxadiazoles (a review). *Pharmaceutical Chemistry Journal* **2005,** *39* (10), 539-547.

240. Fylaktakidou, K. C.; Hadjipavlou-Litina, D. J.; Litinas, K. E.; Varella, E. A.; Nicolaides, D. N., Recent developments in the chemistry and in the biological applications of amidoximes. *Curr. Pharm. Des.* **2008,** *14* (10), 1001-47.

241. Turchi, I. J.; Dewar, M. J. S., Chemistry of oxazoles. *Chem. Rev.* **1975,** *75* (4), 389-437.

242. van Leusen, A. M.; Hoogenboom, B. E.; Siderius, H., A novel and efficient synthesis of oxazoles from tosylmethylisocyanide and carbonyl compounds. *Tetrahedron Lett.* **1972,** *13* (23), 2369-2372.

243. Boussonnière, A.; Bénéteau, R.; Lebreton, J.; Dénès, F., Aluminum acetals in organic synthesis. *European J. Org. Chem.* **2013,** *2013* (35), 7853-7866.

244. Zakharkin, L. I.; Khorlina, I. M., Reduction of esters of carboxylic acids into aldehydes with diisobutylaluminium hydride. *Tetrahedron Lett.* **1962,** *3* (14), 619-620.

245. Witkin, J. M.; Cerne, R.; Davis, P. G.; Freeman, K. B.; do Carmo, J. M.; Rowlett, J. K.; Methuku, K. R.; Okun, A.; Gleason, S. D.; Li, X.; Krambis, M. J.; Poe, M.; Li, G.; Schkeryantz, J. M.; Jahan, R.; Yang, L.; Guo, W.; Golani, L. K.; Anderson, W. H.; Catlow, J. T.; Jones, T. M.; Porreca, F.; Smith, J. L.; Knopp, K. L.; Cook, J. M., The alpha2,3-

selective potentiator of GABAA receptors, KRM-II-81, reduces nociceptive-associated behaviors induced by formalin and spinal nerve ligation in rats. *Pharmacol. Biochem. Behav.* **2019,** *180*, 22-31.

246. Kessler, R. C.; Chiu, W. T.; Demler, O.; Walters, E. E., Prevalence, severity, and comorbidity of 12-month *DSM-IV* disorders in the National Comorbidity Survey Replication. *Arch. Gen. Psychiatry* **2005,** *62*, 617 - 627.

247. Baldwin, D. S.; Polkinghorn, C., Evidence-based pharmacotherapy of generalized anxiety disorder. *Int. J. Neuropsychopharmacol.* **2005,** *8*, 293 - 302.

248. Nutt, D. J., Overview of diagnosis and drug treatments of anxiety disorders. *CNS Spectrums* **2005,** *10*, 49 - 56.

249. Krisberg, K., New research: More Americans have epilepsy than ever before. *The Nation's Health* **2017,** *47* (8), 10.

250. Zaccara, G.; Schmidt, D., Antiepileptic drugs in clinical development: differentiate or die? *Curr. Pharm. Des.* **2017,** *23* (37), 5593-5605.

251. Möhler, H.; Fritschy, J. M.; Rudolph, U., A new benzodiazepine pharmacology. *J. Pharmacol. Exp. Ther.* **2002,** *300* (1), 2.

252. van Rijnsoever, C.; Tauber, M.; Choulli, M. K.; Keist, R.; Rudolph, U.; Mohler, H.; Fritschy, J. M.; Crestani, F., Requirement of alpha5-GABAA receptors for the development of tolerance to the sedative action of diazepam in mice. *J. Neurosci.* **2004,** *24* (30), 6785-90.

253. Witkin, J. M.; Smith, J. L.; Ping, X.; Gleason, S. D.; Poe, M. M.; Li, G.; Jin, X.; Hobbs, J.; Schkeryantz, J. M.; McDermott, J. S.; Alatorre, A. I.; Siemian, J. N.; Cramer, J. W.; Airey, D. C.; Methuku, K. R.; Tiruveedhula, V.; Jones, T. M.; Crawford, J.; Krambis, M. J.; Fisher,

J. L.; Cook, J. M.; Cerne, R., Bioisosteres of ethyl 8-ethynyl-6-(pyridin-2-yl)-4H-benzo[f]imidazo [1,5-a][1,4]diazepine-3-carboxylate (HZ-166) as novel alpha 2,3 selective potentiators of GABAA receptors: Improved bioavailability enhances anticonvulsant efficacy. *Neuropharmacology* **2018,** *137*, 332-343.

254. Castel-Branco, M. M.; Alves, G. L.; Figueiredo, I. V.; Falcao, A. C.; Caramona, M. M., The maximal electroshock seizure (MES) model in the preclinical assessment of potential new antiepileptic drugs. *Methods Find. Exp. Clin. Pharmacol.* **2009,** *31* (2), 101-6.

255. Velisek, L.; Kubova, H.; Pohl, M.; Stankova, L.; Mares, P.; Schickerova, R., Pentylenetetrazol-induced seizures in rats: an ontogenetic study. *Naunyn Schmiedebergs Arch. Pharmacol.* **1992,** *346* (5), 588-91.

256. Benyamin, R.; Trescot, A. M.; Datta, S.; Buenaventura, R.; Adlaka, R.; Sehgal, N.; Glaser, S. E.; Vallejo, R., Opioid complications and side effects. *Pain Physician* **2008,** *11*, S105 - S120.

257. Antman, E. M.; Bennett, J. S.; Daugherty, A.; Furberg, C.; Roberts, H.; Taubert, K. A., Use of nonsteroidal antiinflammatory drugs: an update for clinicians: a scientific statement from the American Heart Association. *Circulation* **2007,** *115*, 1634 - 1642.

258. Kearney, P. M.; Baigent, C.; Godwin, J.; Halls, H.; Emberson, J. R.; Patrono, C., Do selective cyclo-oxygenase-2 inhibitors and traditional non-steroidal anti-inflammatory drugs increase the risk of atherothrombosis? Meta-analysis of randomised trials. *Brit. Med. J.* **2006,** *332*, 1302 - 1308.

259. Gregory, N. S.; Harris, A. L.; Robinson, C. R.; Dougherty, P. M.; Fuchs, P. N.; Sluka, K. A., An overview of animal models of pain: disease models and outcome measures. *J. Pain* **2013,** *14* (11), 1255-69.

260. Deuis, J. R.; Dvorakova, L. S.; Vetter, I., Methods used to evaluate pain behaviors in rodents. *Front. Mol. Neurosci.* **2017,** *10*, 284-284.

261. Rudolph, U.; Knoflach, F., Beyond classical benzodiazepines: novel therapeutic potential of GABAA receptor subtypes. *Nature reviews. Drug discovery* **2011,** *10* (9), 685-697.

262. Vollenweider, I.; Smith, K. S.; Keist, R.; Rudolph, U., Antidepressant-like properties of alpha2-containing GABA(A) receptors. *Behav. Brain Res.* **2011,** *217* (1), 77-80.

Appendix

Appendix I: HPLC/PDA

UWM Shimadzu LabSolutions HPLC.PDA Analysis Report

Sample Name : 2'F-R-3 crude
Sample ID : 2'F-R-3 crude
Data Filename : 2'F-R-3 crude_5_Gradient2 GL_006.lcd
Method Filename : Gradient2 GL.lcm
Batch Filename : 2.1.2018 QH-66 GLIII59 SH-2'F-3 analysis.lcb
Vial # : 3-5 Sample Type : Unknown
Injection Volume : 2 uL
Date Acquired : 2/1/2018 6:30:23 PM Acquired by : Guanguan Li
Date Processed : 2/1/2018 8:11:54 PM Processed by : Guanguan Li

<Sample Summary>

MASS Peak Table TIC
2'F-R-3 crude

Peak#	Ret. Time	Area%	Base Peak m/z	Base Peak Intensity
1	6.330	27.615	449.40	1487330
2	6.387	18.730	449.45	316833
3	6.812	9.438	296.00	656396
4	7.335	26.266	411.05	972683
5	7.850	17.951	396.35	721823
6	6.345	4.156	286.05	63040
7	6.502	2.602	241.05	11194
8	7.348	72.930	464.95	805827
9	7.855	10.060	457.25	149617
10	8.506	10.252	410.15	104173
Total		200.000		

Method
<<Pump>>
Mode : Binary gradient
Pump A : LC-30AD
Pump B : LC-30AD
Total Flow : 0.7000 mL/min
B Conc. : 15.0 %
B Curve : 0
PressMax : 16000 psi
PressMin : 0 psi
Solenoid Valve A Name : FCV-15AL
Solenoid Valve A : A
Solenoid Valve B Name : FCV-15AL
Solenoid Valve B : B
Compressibility Setting : On
Pump A Compressibility : 0.45 /GPa
Pump B Compressibility : 1.25 /GPa

<<LC Time Program>>

Time	Module	Command	Value	Comment
8.00	Pumps	Pump B Conc.	100	
9.00	Pumps	Pump B Conc.	100	
9.10	Pumps	Pump B Conc.	15	
12.00	Controller	Stop		

<<Data Acquisition>>
LC Stop Time : 12.00 min
PDA Detector Name : PDA
PDA Sampling Frequency : 4.16667 Hz
PDA Start Time : 0.00 min
PDA End Time : 12.00 min
PDA Time Constant : 0.480 sec

<<Mobile Phase Name>>
Pump A Mobile Phase A : Water

<<PDA>>
PDA Model : SPD-M30A
Start Wavelength : 200 nm
End Wavelength : 500 nm
Lamp : D2

C:\LabSolutions\Data\GLi\Data\2.1.2018\2'F-R-3 crude_5_Gradient2 GL_006.lcd

<Sample Report>

<PDA Chromatogram>

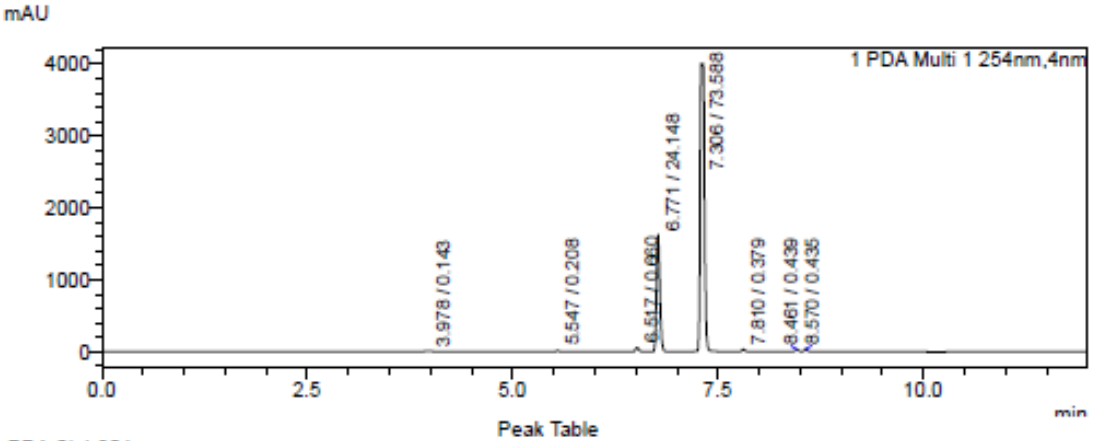

Peak Table

PDA Ch1 254nm

Peak#	Ret. Time	Area	Area%	Height
1	3.978	28189	0.143	5857
2	5.547	41073	0.208	16015
3	6.517	130227	0.660	49040
4	6.771	4765725	24.148	1582099
5	7.306	14523137	73.588	3994842
6	7.810	74839	0.379	27438
7	8.461	86606	0.439	30327
8	8.570	85946	0.435	34500
Total		19735743	100.000	5740120

<UV Spectrum>

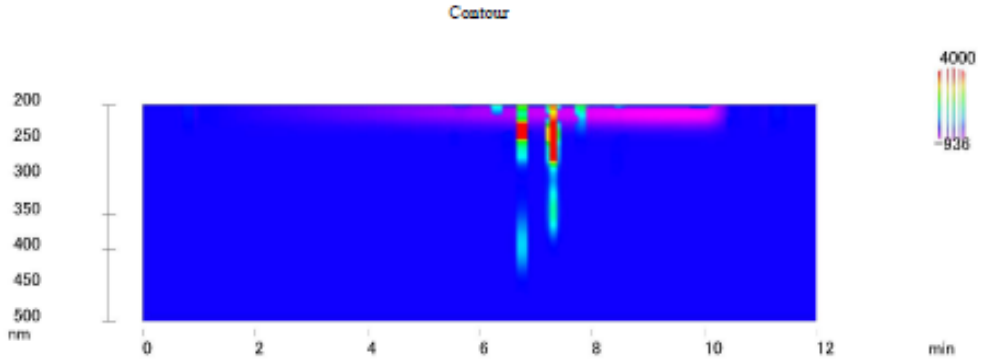

UV Spectrum

Peak# : 1
Retention Time : 3.978 min

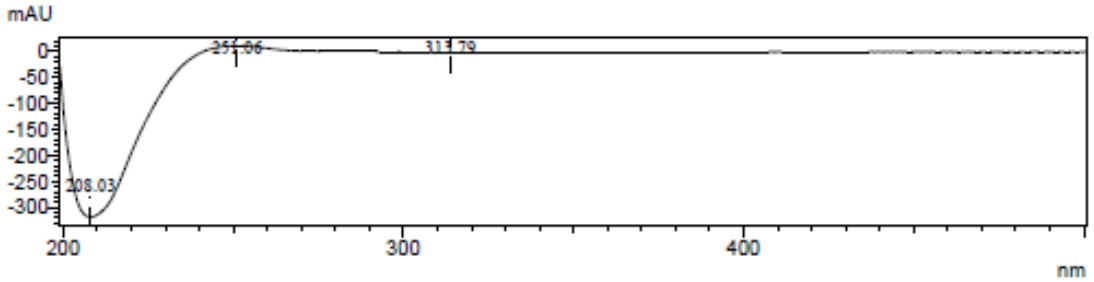

C:\LabSolutions\Data\GLi\Data\2.1.2018\2'F-R-3 crude_5_Gradient2 GL_006.lcd

Peak# : 2
Retention Time : 5.547 min

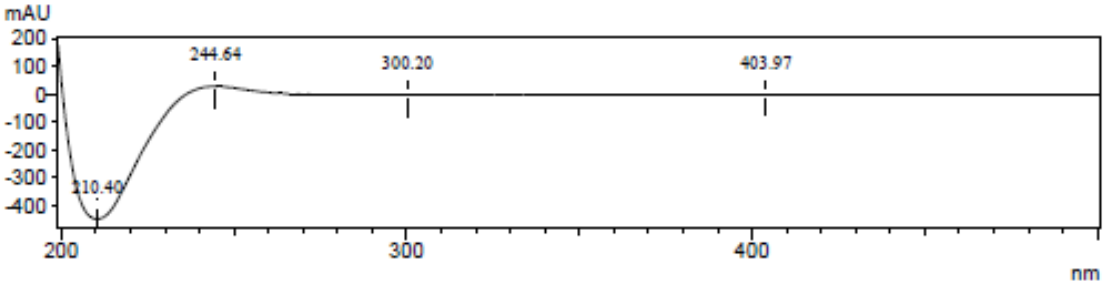

Peak# : 3
Retention Time : 6.517 min

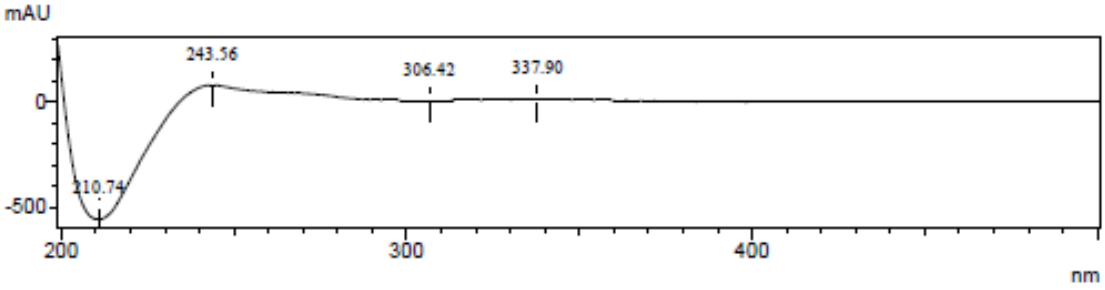

Peak# : 4
Retention Time : 6.771 min

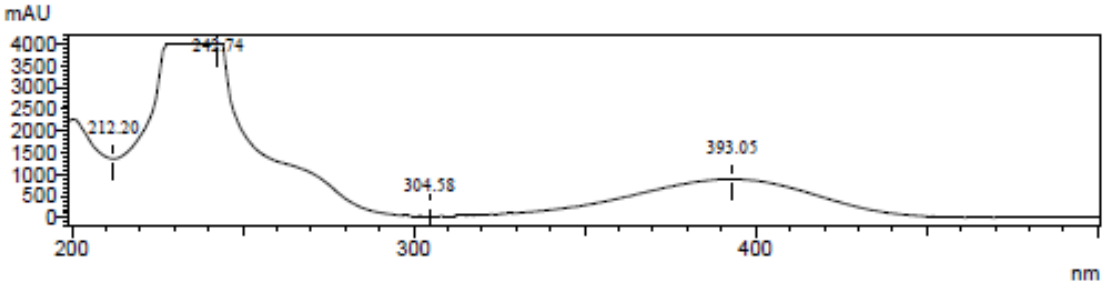

Peak# : 5
Retention Time : 7.306 min

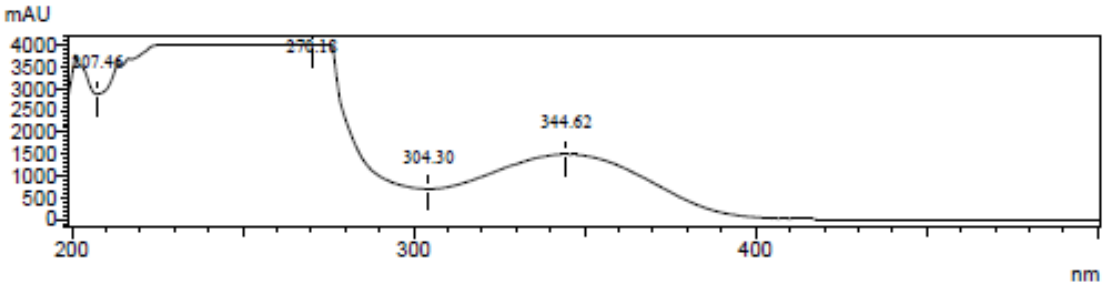

C:\LabSolutions\Data\GLi\Data\2.1.2018\2'F-R-3 crude_5_Gradient2 GL_006.lcd

Peak# : 6
Retention Time : 7.810 min

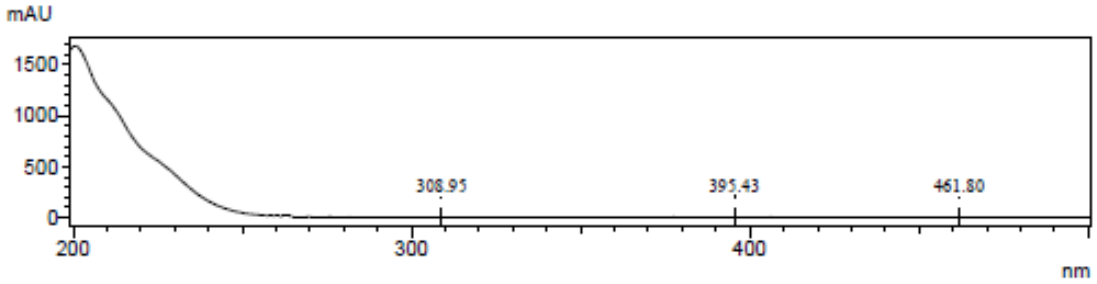

Peak# : 7
Retention Time : 8.461 min

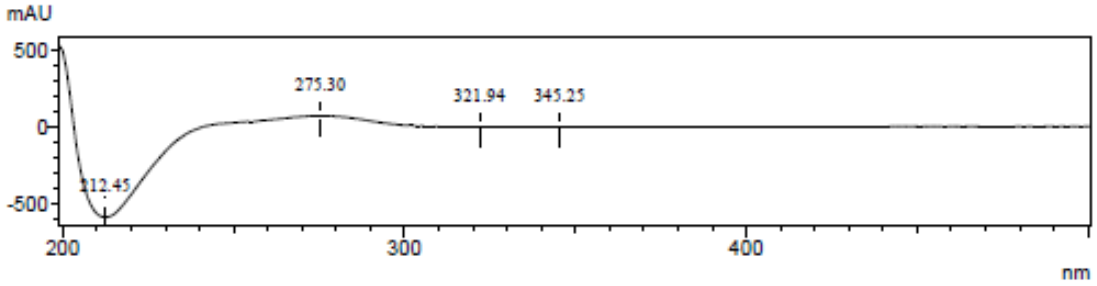

Peak# : 8
Retention Time : 8.570 min

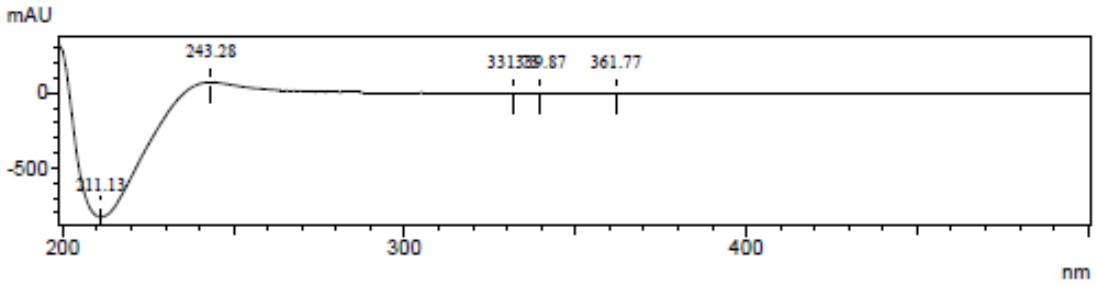

C:\LabSolutions\Data\GLi\Data\2.1.2018\2'F-R-3 crude_5_Gradient2 GL_006.lcd

<LCMS Chromatogram>

MS Chromatogram

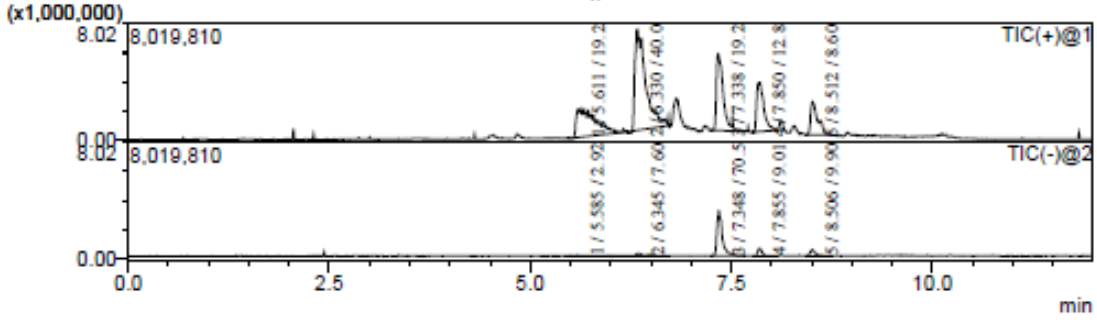

MASS Peak Table TIC(Event)

TIC(1-1)

Peak#	Ret. Time	Area%	Base Peak m/z	ase Peak Intensi
1	6.330	27.615	449.40	1487330
2	6.387	18.730	449.45	316833
3	6.812	9.438	296.00	656396
4	7.338	26.266	411.05	972683
5	7.850	17.951	396.35	721823
Total		100.000		

TIC(1-2)

Peak#	Ret. Time	Area%	Base Peak m/z	ase Peak Intensi
1	6.345	4.156	286.05	63040
2	6.502	2.602	241.05	11194
3	7.348	72.930	464.95	805827
4	7.855	10.060	457.25	149617
5	8.506	10.252	410.15	104173
Total		100.000		

MS Spectrum

Peak#:1 R.Time:6.330(Scan#:3797)
MassPeaks:380
Spectrum Mode:Averaged 6.323-6.330(3795-3799)
BG Mode:Calc Segment 1 - Event 1

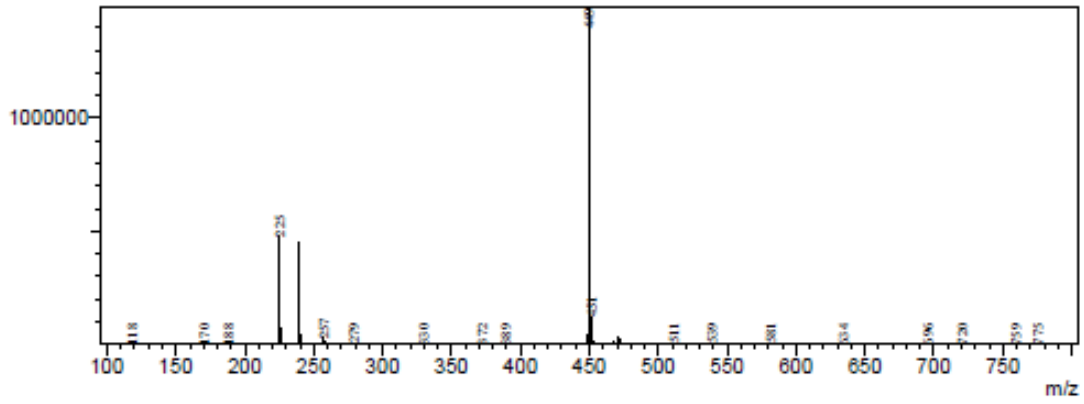

C:\LabSolutions\Data\GLhData\2.1.2018\2 P-R-3 crude_5_Gradient2 GL_006.lcd

Peak#:1 R.Time:6.345(Scan#:3808)
MassPeaks:360
Spectrum Mode:Averaged 6.341-6.348(3806-3810)
BG Mode:Calc Segment 1 - Event 2

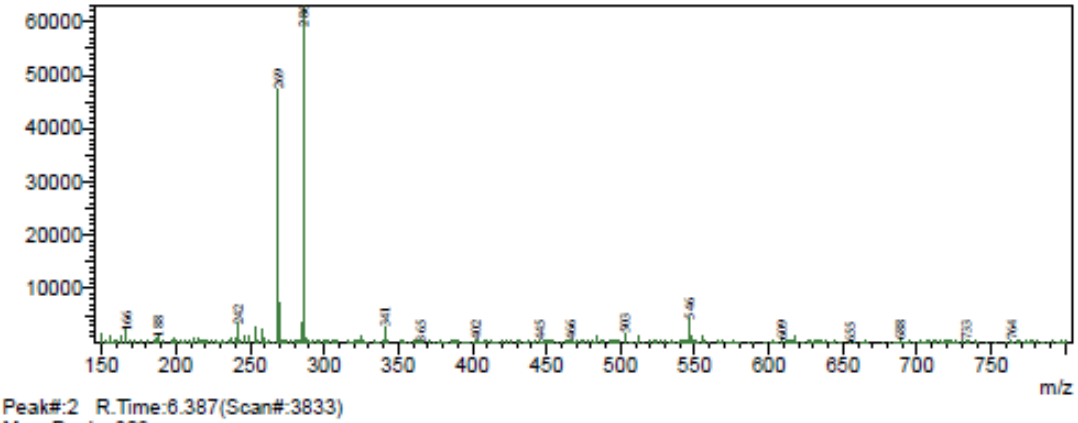

Peak#:2 R.Time:6.387(Scan#:3833)
MassPeaks:329
Spectrum Mode:Averaged 6.383-6.390(3831-3835)
BG Mode:Calc Segment 1 - Event 1

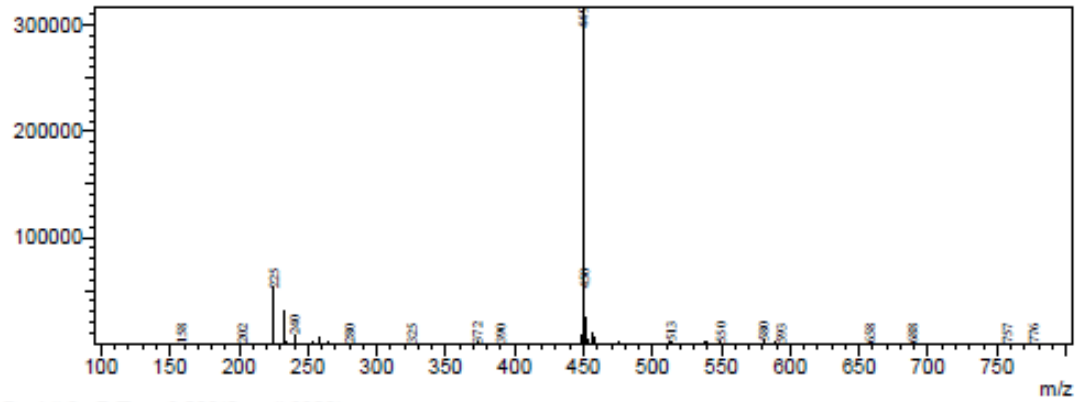

Peak#:2 R.Time:6.502(Scan#:3902)
MassPeaks:363
Spectrum Mode:Averaged 6.498-6.505(3900-3904)
BG Mode:Calc Segment 1 - Event 2

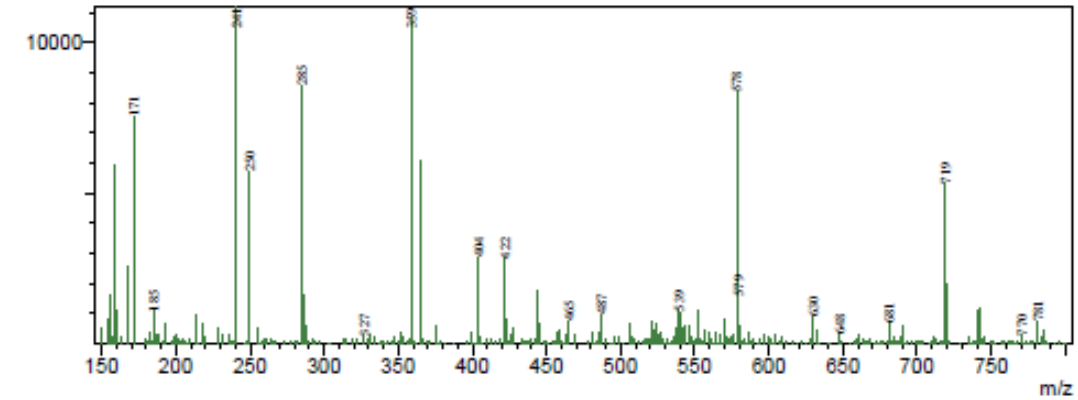

C:\LabSolutions\Data\GLHData\2.1.2018\2 F-R-3 crude_3_Gradient2 GL_006.lcd

Peak#:3 R.Time:6.812(Scan#:4087)
MassPeaks:354
Spectrum Mode:Averaged 6.807-6.813(4085-4089)
BG Mode:Calc Segment 1 - Event 1

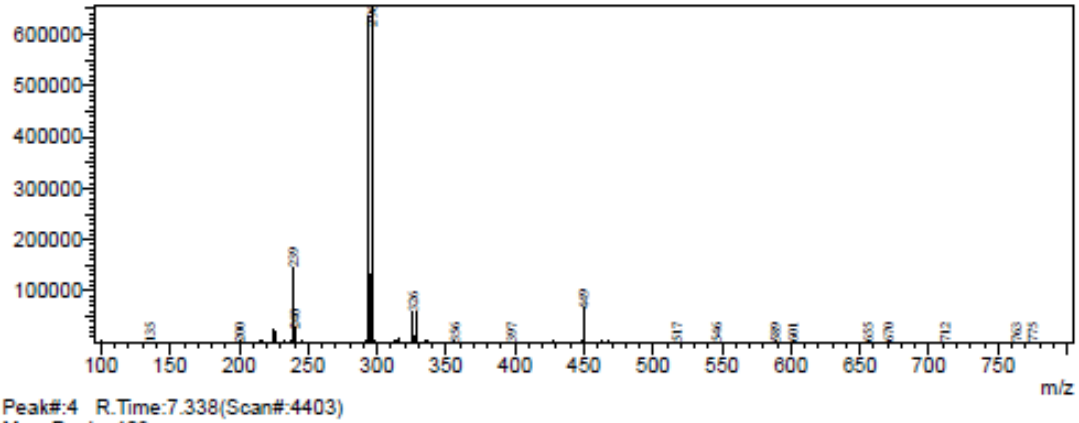

Peak#:4 R.Time:7.338(Scan#:4403)
MassPeaks:429
Spectrum Mode:Averaged 7.333-7.340(4401-4405)
BG Mode:Calc Segment 1 - Event 1

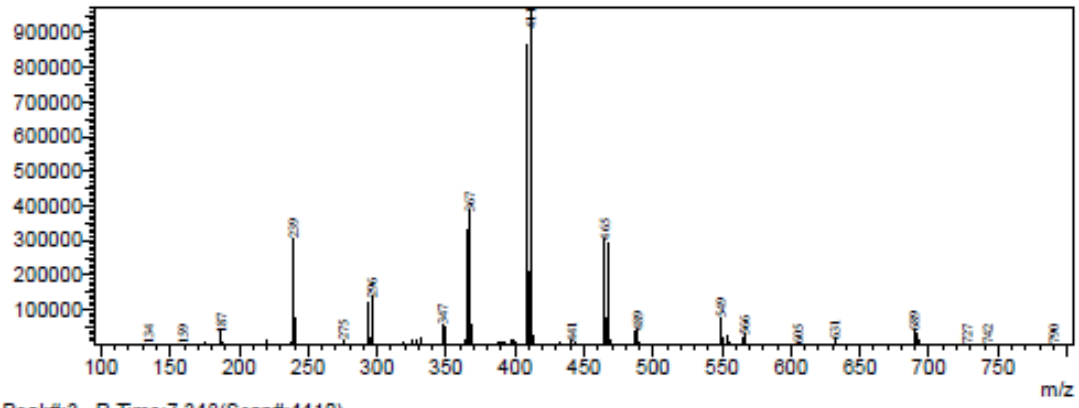

Peak#:3 R.Time:7.348(Scan#:4410)
MassPeaks:421
Spectrum Mode:Averaged 7.345-7.351(4408-4412)
BG Mode:Calc Segment 1 - Event 2

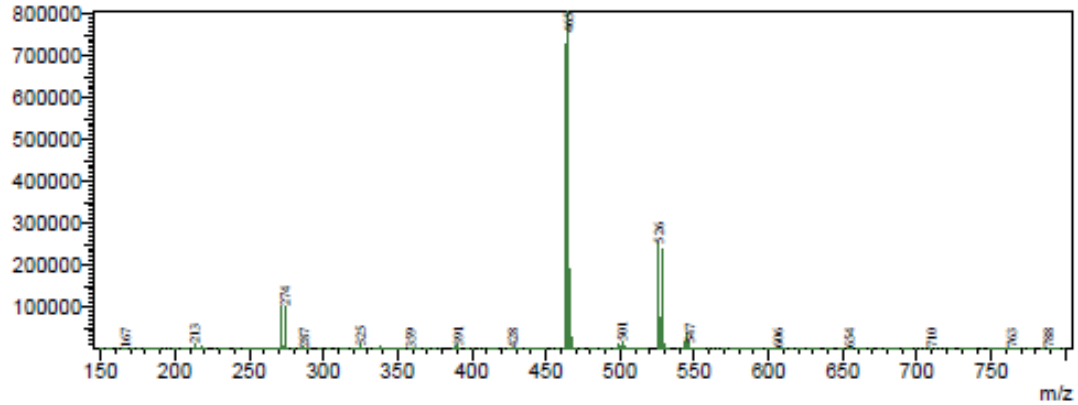

C:\LabSolutions\Data\GLData\2.1.2018\2 P-R-3 crude_5_Gradient2 GL_006.lcd

Peak#:5 R.Time:7.850(Scan#:4709)
MassPeaks:378
Spectrum Mode:Averaged 7.843-7.850(4707-4711)
BG Mode:Calc Segment 1 - Event 1

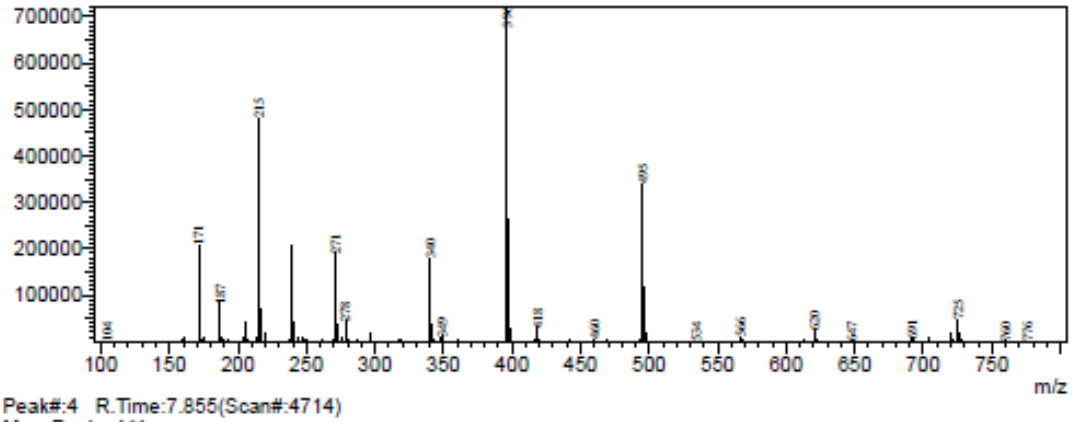

Peak#:4 R.Time:7.855(Scan#:4714)
MassPeaks:411
Spectrum Mode:Averaged 7.851-7.858(4712-4716)
BG Mode:Calc Segment 1 - Event 2

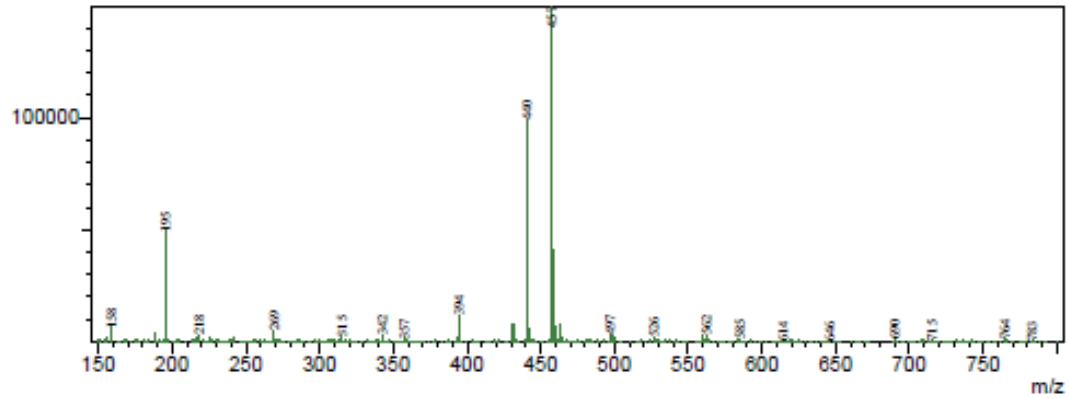

Peak#:5 R.Time:8.506(Scan#:5104)
MassPeaks:366
Spectrum Mode:Averaged 8.501-8.508(5102-5106)
BG Mode:Calc Segment 1 - Event 2

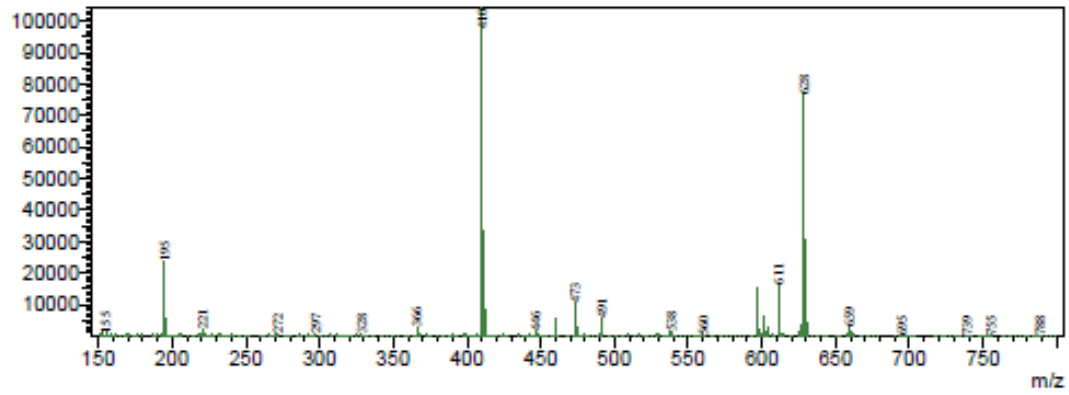

C:\LabSolutions\Data\GLi\Data\2.1.2018\2'F-R-3 crude_5_Gradient2 GL_006.lcd

Appendix II: PDSP Data

Table 35. PDSP compound list.

Compound #	Name	Molecular Weight	Formula	Received Date
30611	SH-053-2'F-R-CH3	387.41	C23H18FN3O2	30-Oct-13
30612	SH-053-2'F-S-CH3	387.41	C23H18FN3O2	30-Oct-13
30613	MP-III-004	373.38	C22H16FN3O2	30-Oct-13
30614	MP-III-021	373.38	C22H16FN3O2	30-Oct-13
30615	MP-III-019	340.35	C21H13FN4	30-Oct-13
30616	MP-III-018.A	340.35	C21H13FN4	30-Oct-13
30617	MP-III-022	372.39	C22H17FN4O	30-Oct-13
30618	MP-III-023	372.39	C22H17FN4O	30-Oct-13
30619	SH-I-85	423.24	C20H12BrFN4O	30-Oct-13
37713	MP-III-068	358.39	(not set)	1-Jul-15
37714	MP-III-080	380.4	(not set)	1-Jul-15
37715	MP-III-085	366.38	(not set)	1-Jul-15
37717	SH-053-2'F-R-CH3-Acid	359.35	(not set)	1-Jul-15
37718	SH-053-2'F-S-CH3-Acid	359.35	(not set)	1-Jul-15
37719	MP-III-018.B	358.37	(not set)	1-Jul-15
37720	MP-III-019.B	358.37	(not set)	1-Jul-15
37721	MP-IV-004	397.4	(not set)	1-Jul-15
37722	GL-I-65	397.4	(not set)	23-Oct-17
37723	MP-IV-005	411.43	(not set)	1-Jul-15
37724	GL-I-66	411.43	(not set)	1-Jul-15
37725	MP-IV-010	425.46	(not set)	1-Jul-15
37726	GL-I-81	425.46	(not set)	23-Oct-17

37728	SH-I-085	423.23	(not set)	1-Jul-15
37729	KRM-II-18B	368.36	(not set)	1-Jul-15
37730	KRM-II-73	405.24	(not set)	1-Jul-15
37731	KRM-II-82	350.37	(not set)	1-Jul-15
37732	KRM-II-97	406.23	(not set)	1-Jul-15
37733	KRM-II-81	351.36	(not set)	1-Jul-15
37734	KRM-II-68	336.34	(not set)	1-Jul-15
37735	KRM-II-08	292.3	(not set)	1-Jul-15
37736	KRM-II-3B	307	(not set)	1-Jul-15
42621	KRM-III-59	437.26	C21H14BrFN4O	23-Oct-17
42622	KRM-III-65	382.38	C23H15FN4O	23-Oct-17
42623	KRM-III-66	419.27	C21H15BrN4O	23-Oct-17
42624	KRM-III-67	364.39	C23H16N4O	23-Oct-17
42625	KRM-III-79	365.38	C22H15N5O	23-Oct-17
42626	KRM-III-70	275.3	C17H13N3O	23-Oct-17
42627	KRM-III-77	308.76	C18H13ClN2O	23-Oct-17
42628	KRM-III-78	420.26	C20H14BrN5O	23-Oct-17
42633	Ro5-4846	319.19	C16H12Cl2N2O	23-Oct-17
42634	Ro7-9277	335.18	C16H12Cl2N2O2	23-Oct-17
42635	GL-I-74	305.16	C15H10Cl2N2O	23-Oct-17
42636	GL-II-39	377.22	C18H14Cl2N2O3	23-Oct-17
42637	GL-II-05	330.18	C15H12BrN3O	23-Oct-17
42638	GL-II-06	425.28	C20H17BrN4O2	23-Oct-17
42639	GL-II-18	442.59	C25H26N4O2Si	23-Oct-17
42640	GL-II-19	370.4	C22H18N4O2	23-Oct-17
42641	GL-II-30	342.35	C20H14N4O2	23-Oct-17
42642	GL-II-31	355.39	C21H17N5O	23-Oct-17

42643	GL-II-32	356.38	C21H16N4O2	23-Oct-17
42644	GL-II-33	380.4	C22H16N6O	23-Oct-17
42645	GL-II-51	397.23	C18H13BrN4O2	23-Oct-17
42647	GL-II-53	410.27	C19H16BrN5O	23-Oct-17
42648	GL-II-54	435.28	C20H15BrN6O	23-Oct-17
42651	GL-II-57	394.43	C23H18N6O	23-Oct-17
42653	GL-II-59	344.21	C16H14BrN3O	23-Oct-17
42654	GL-II-60	361.51	C21H23N3OSi	23-Oct-17
42655	GL-II-61	289.33	C18H15N3O	23-Oct-17
42656	GL-I-30	415.46	C25H22FN3O2	23-Oct-17
42657	GL-I-31	401.43	C24H20FN3O2	23-Oct-17
42658	GL-I-32	401.43	C24H20FN3O2	23-Oct-17
42659	GL-I-33	429.49	C26H24FN3O2	23-Oct-17
42660	GL-I-38	399.42	C24H18FN3O2	23-Oct-17
42661	GL-I-36	441.38	C23H15F4N3O2	23-Oct-17
42662	GL-I-43	386.42	C23H19FN4O	23-Oct-17
42663	GL-I-41	414.47	C25H23FN4O	23-Oct-17
42664	GL-I-55	398.43	C24H19FN4O	23-Oct-17
42665	GL-I-54	386.42	C23H19FN4O	23-Oct-17
42666	GL-I-77	403.47	C23H18FN3OS	23-Oct-17
42667	GL-I-78	403.45	C24H22FN3O2	23-Oct-17
50093	SH-I-044	347.18	C16H12BrFN2O	2-Nov-17
50094	SH-I-047	442.28	C21H17BrFN3O2	2-Nov-17
50095	SH-I-060	459.59	C26H26FN3O2Si	2-Nov-17
50096	MP-III-058	428.25	C20H15BrFN3O2	2-Nov-17
50097	SH-I-048A	347.18	C16H12BrFN2O	2-Nov-17
50098	SH-I-048B	442.28	C21H17BrFN3O2	2-Nov-17

50099	SH-I-055	459.59	C26H26FN3O2Si	2-Nov-17
50101	YT-III-31	340.38	C21H16N4O	2-Nov-17
50102	YT-III-271	730.72	C43H28F2N6O4	2-Nov-17
50103	SR-II-54	328.32	C19H12N4O2	2-Nov-17
50104	GL-II-73	386.42	C23H19FN4O	2-Nov-17
50105	GL-II-74	386.42	C23H19FN4O	2-Nov-17
50106	GL-II-75	398.43	C24H19FN4O	2-Nov-17
50107	GL-II-76	412.46	C25H21FN4O	2-Nov-17
50108	GL-I-50	382.21	C18H12BrN3O2	2-Nov-17
50109	GL-II-93	414.23	C19H13BrFN3O2	2-Nov-17
50110	GL-I-65	397.4	C23H16FN5O	2-Nov-17
50111	GL-I-81	425.46	C25H20FN5O	2-Nov-17
50112	GL-III-19	427.27	C20H16BrFN4O	2-Nov-17
50114	GL-I-61	364.49	C21H21FN2OSi	2-Nov-17
50117	GL-I-63	364.49	C21H21FN2OSi	2-Nov-17
50120	GL-III-26	347.48	C20H21N3OSi	2-Nov-17
50121	GL-III-27	275.3	C17H13N3O	2-Nov-17
50122	GL-III-59	260.29	C17H12N2O	2-Nov-17
50123	GL-III-57	333.459	C19H19N3OSi	2-Nov-17
50124	GL-III-58	261.27	C16H11N3O	2-Nov-17
50125	GL-III-35	398.23	C19H13BrFN3O	2-Nov-17
50126	GL-III-36	437.26	C21H14BrFN4O	2-Nov-17
50127	KRM-III-18A	437.26	C21H14BrFN4O	2-Nov-17
50128	GL-III-38	343.35	C21H14FN3O	2-Nov-17
50129	GL-III-72	454.57	C26H23FN4OSi	2-Nov-17
50130	GL-III-73	382.39	C23H15FN4O	2-Nov-17
50132	GL-III-42	403.45	C24H22FN3O2	2-Nov-17

50133	GL-III-43	375.4	C22H18FN3O2	2-Nov-17
50134	GL-III-52	302.73	C16H12ClFN2O	2-Nov-17
50135	GL-III-53	397.83	C21H17ClFN3O2	2-Nov-17
50136	GL-III-54	369.78	C19H13ClFN3O2	2-Nov-17
50137	GL-III-60	452.28	C21H15BrFN5O	2-Nov-17
50138	GL-III-63	413.45	C24H20FN5O	2-Nov-17
50139	GL-III-64	396.44	C23H20N6O	2-Nov-17
50140	GL-III-66	400.45	C24H21FN4O	2-Nov-17
50141	GL-III-67	441.3	C21H18BrFN4O	2-Nov-17
50142	GL-III-68	402.46	C24H23FN4O	2-Nov-17
50143	GL-III-69	441.3	C21H18BrFN4O	2-Nov-17
50144	GL-III-70	402.46	C24H23FN4O	2-Nov-17
50145	GL-III-75	398.23	C19H13BrFN3O	2-Nov-17
50146	GL-III-76	437.26	C21H14BrFN4O	2-Nov-17
50147	GL-III-76A	437.26	C21H14BrFN4O	2-Nov-17
50148	GL-III-77	454.57	C26H23FN4OSi	2-Nov-17
50149	GL-III-78	382.39	C23H15FN4O	2-Nov-17

Table 36. PDSP primary binding data for 5-HT1A, 5-HT1B, 5-HT1D, 5-ht1e, 5-HT2A, and 5-HT2B.

Compound #	Name	5-HT1A	5-HT1B	5-HT1D	5-ht1e	5-HT2A	5-HT2B
30611	SH-053-2'F-R-CH3	18	9.3	16.4	-8.8	-10.7	17.3
30612	SH-053-2'F-S-CH3	8.5	4.8	12.8	-4.6	19.4	20.4
30613	MP-III-004	37.5	0.6	32.5	-3.3	9.4	44.2
30614	MP-III-021	18.8	3.3	34.4	-12.5	-0.9	36.6
30615	MP-III-019	-1.4	2.1	37	-9.5	-9.6	50
30616	MP-III-018.A	8.3	2.4	23.1	-5.8	38.5	47.3

30617	MP-III-022	1.7	0.9	9.6	-2	8.8	10.4
30618	MP-III-023	6.9	2.3	20.1	-0.3	12.4	44.5
30619	SH-I-85	22.9	9.4	14	-12	7	54.7
37713	MP-III-068	2.4	5.6	-0.7	3.1	-20	-16.8
37714	MP-III-080	18.8	11	-3.5	2.2	-11.7	1.3
37715	MP-III-085	7.3	2.8	2.4	3.5	-16	-6.4
37717	SH-053-2'F-R-CH3-Acid	0.8	5.4	-2.3	1.6	-7.2	-9.7
37718	SH-053-2'F-S-CH3-Acid	7.1	14.2	-2.9	-1	4.8	-8.9
37719	MP-III-018.B	12	3.1	-2.5	1.6	-0.2	-8.4
37720	MP-III-019.B	1.5	14.2	-9.2	2.7	17.3	0.8
37721	MP-IV-004	8.7	8.2	-7	0.7	32.8	-8.2
37722	GL-I-65	9.3	-2.8	-15.1	-10.4	-10.5	-7
37723	MP-IV-005	19.6	17.3	2.2	-1.1	18.9	1.4
37724	GL-I-66	24	16.5	-0.6	-2.3	4.6	12.6
37725	MP-IV-010	19.4	28.7	6	-6.7	-0.6	0.2
37726	GL-I-81	16.3	41.5	37.6	-14.9	29	50.2
37728	SH-I-085	43.4	28.8	13.9	-9.6	-3.1	5.9
37729	KRM-II-18B	51.2	27.6	16	-2.9	3.5	-8.5
37730	KRM-II-73	43.4	29.3	15.7	-6.8	-3.7	-8.9
37731	KRM-II-82	56.6	38.8	20.1	-2.7	7.7	-11.3
37732	KRM-II-97	22.9	5.9	-0.4	-3.3	16.8	-5.5
37733	KRM-II-81	29.5	-1.6	-0.3	4.9	16	-1.5
37734	KRM-II-68	15.5	-5.2	3.6	10	20.1	-3.1
37735	KRM-II-08	9.6	3.6	9.2	1.1	-2.3	8
37736	KRM-II-3B	17.8	1.2	6.9	-2.7	11	88.9
42621	KRM-III-59	29.6	-12.5	-5	-14	4	5.6

42622	KRM-III-65	39.1	13.4	-9.9	9.2	21.2	0.6
42623	KRM-III-66	22.2	19.2	-3	-9.2	10.5	10.9
42624	KRM-III-67	30.6	32.8	9.7	12.4	27.6	6.8
42625	KRM-III-79	7.4	32.2	1.2	7.8	6.6	8.6
42626	KRM-III-70	19.3	19.2	15.9	7.1	16.8	10.3
42627	KRM-III-77	14.4	6.5	8	-4.9	12.7	9.5
42628	KRM-III-78	20.7	20.9	6.1	-2.6	15.1	15.2
42633	Ro5-4846	10.4	3.7	-13.5	-9.8	-4.5	-2.1
42634	Ro7-9277	-4.9	-11.5	-13.1	-1.1	-5.4	2.1
42635	GL-I-74	16.2	24.7	-5.2	-5.1	6.3	15.3
42636	GL-II-39	-0.5	20.4	-6	0.3	5.1	17.8
42637	GL-II-05	12.8	24.3	-5.1	4.1	4.1	13.3
42638	GL-II-06	28.3	23.5	-2.3	3.9	4.8	10.6
42639	GL-II-18	9.4	27.9	9.8	-9.2	16.3	28.7
42640	GL-II-19	-1.5	29.7	3.4	1.8	6.6	13.5
42641	GL-II-30	-8.1	21	3.9	14.1	9.5	10.3
42642	GL-II-31	-3.4	-5	6.6	3.9	-3.9	17.2
42643	GL-II-32	8.1	6.4	2.8	-4.2	-14.5	2.4
42644	GL-II-33	5.4	24.8	-6.3	-2.4	4.3	11.2
42645	GL-II-51	-1.6	22.5	-1.7	-7	-0.2	9.2
42647	GL-II-53	-6.9	18.8	-9.9	-13.5	-1.2	11.2
42648	GL-II-54	19.6	-4	-14.4	-4.4	13.3	10
42651	GL-II-57	-0.4	10.4	-5.2	-10	-4.7	16.7
42653	GL-II-59	2.4	11.9	-2.3	-5	-6.4	14.1
42654	GL-II-60	0.3	2.4	-0.9	-7.5	4.5	18
42655	GL-II-61	2.9	-19.8	-4.3	-2.1	2.3	18.7
42656	GL-I-30	12.9	1.1	0.3	-14.3	-6.4	4.2

42657	GL-I-31	5.9	-2.8	-0.6	-3.5	0	-4.1
42658	GL-I-32	1.5	21	5.7	9.2	-1.3	2.9
42659	GL-I-33	2.6	30.3	20	5.2	19.4	13
42660	GL-I-38	3.3	17.6	8.8	8.2	-0.2	7.3
42661	GL-I-36	6.7	18.4	14.6	13.5	4.2	20.9
42662	GL-I-43	2.7	17.1	19.9	9.3	-2.4	6.9
42663	GL-I-41	5.1	14.4	12.4	2.3	8.8	9.9
42664	GL-I-55	-1.2	26.1	3.7	2.3	7.6	9.6
42665	GL-I-54	-7.3	0.6	6.4	12.6	9.9	19.5
42666	GL-I-77	1	-10.6	19.2	-15.6	1	2.8
42667	GL-I-78	6.8	3.4	-12.2	-17.2	25.1	7.8
50093	SH-I-044	-2.5	16.5	16.8	-12.1	2.2	29.3
50094	SH-I-047	2.2	16.4	4.4	6.6	22.6	31.2
50095	SH-I-060	13.4	32.5	44.9	7.8	60.8	30.6
50096	MP-III-058	16.5	27.9	12.8	-13.1	-17.3	-8.7
50097	SH-I-048A	10.1	31.9	16.2	-13.8	-8.5	8.9
50098	SH-I-048B	3.5	31.8	21.3	-10.1	-7.9	11.6
50099	SH-I-055	23.6	8.5	66.6	14.3	57.2	44.6
50101	YT-III-31	32.8	23.5	43	1.5	-1.2	8.6
50102	YT-III-271	15.2	12.6	53.5	-0.6	11.3	11.1
50103	SR-II-54	6.9	15	54.2	16.3	1.4	17.7
50104	GL-II-73	7.5	16.1	34.1	26.9	10.1	31.5
50105	GL-II-74	15	18.3	0.9	5.8	11.2	35.3
50106	GL-II-75	11.3	25.3	10.4	6.4	-11.5	6.3
50107	GL-II-76	6.5	23.7	6.7	-2	-13	14.2
50108	GL-I-50	10	24	21.1	2.6	-3.2	16.5
50109	GL-II-93	10.1	28.4	32.7	3.2	-4.7	6.2

50110	GL-I-65	16	-4.8	48.1	12.9	3.2	13.7
50111	GL-I-81	-3.8	-11.9	53.2	9.2	22.2	48.8
50112	GL-III-19	-8.7	-9.9	43	11.6	1.9	15.6
50114	GL-I-61	15.9	2.4	40	-6.5	45.6	30.9
50117	GL-I-63	-1.3	4.3	14.9	-5.5	59.5	39.2
50120	GL-III-26	-10.3	2.2	-17.4	-13.5	20.9	31.2
50121	GL-III-27	-10.4	13.1	-8.7	0.6	-5.9	5.5
50122	GL-III-59	-3.9	31	-8.3	-18.7	0.8	9.7
50123	GL-III-57	-6.4	14.6	1	2.8	5.6	14.1
50124	GL-III-58	-7.9	11.8	-4.1	4.5	-3.4	0.8
50125	GL-III-35	-5.5	-14.8	-10.3	-17.1	-0.3	0.1
50126	GL-III-36	16.5	-1.7	-3.7	-9.5	-3.7	5.5
50127	KRM-III-18A	39.3	6.5	9	-31.5	14.7	15.2
50128	GL-III-38	11.9	13.2	1.3	-13.6	-1.5	15.3
50129	GL-III-72	37.4	22.7	27.4	20.7	62.9	28.9
50130	GL-III-73	17.3	23.1	-9	-13.1	-2.4	0.5
50132	GL-III-42	11.7	21.2	-13	-8.8	-1.6	22
50133	GL-III-43	-2.3	4.4	-2.7	-10.4	-19.3	0.8
50134	GL-III-52	-2.5	24.5	-4.4	-6	-9.2	4.9
50135	GL-III-53	20	-14	-3.1	6.1	-24.1	8.5
50136	GL-III-54	1.2	22	3.4	-0.4	7.7	15.2
50137	GL-III-60	-0.4	5.9	1.2	8.2	5.7	8
50138	GL-III-63	15	-2.2	-0.3	4.3	4.3	12.3
50139	GL-III-64	-7.6	3.2	6.2	10.9	-10.2	7.1
50140	GL-III-66	-2.1	15.2	20.4	19.8	-0.8	2.2
50141	GL-III-67	-3.6	14.1	-5.2	8.8	-3.6	-2.8
50142	GL-III-68	-8.5	14.4	7.9	8.5	18.3	48.4

50143	GL-III-69	-16	5.7	8.1	0.9	-0.4	6.3
50144	GL-III-70	-16.3	10.8	0.2	3.7	-5.3	23.8
50145	GL-III-75	-7.2	7.7	0.7	-15.1	3.4	-2.1
50146	GL-III-76	9.7	7.3	8.1	-11.8	0.6	1.4
50147	GL-III-76A	30.5	5.8	8	-2.9	8.4	6.3
50148	GL-III-77	38.2	-53.5	66.9	19.5	67.5	51.3
50149	GL-III-78	28.3	2.1	0.3	-7.7	8.2	8.8

Table 37. PDSP primary binding data for 5-HT2C, 5-HT3, 5-ht5a, 5-HT6, 5-HT7, and Alpha1A.

Compound #	Name	5-HT2C	5-HT3	5-ht5a	5-HT6	5-HT7	Alpha1A
30611	SH-053-2'F-R-CH3	17.4	-3.8	11.5(AVE)	16.8	8.2	4.8
30612	SH-053-2'F-S-CH3	23.4	-10.7	4.9(AVE)	8.6	7.9	3.9
30613	MP-III-004	24.5	36.6	-3.9(AVE)	11.1	24.4	7.7
30614	MP-III-021	14.6	1.1	1.4(AVE)	4.1	47.8	1.7
30615	MP-III-019	19.6	-6.5	7.7(AVE)	18.5	32.9	1.3
30616	MP-III-018.A	17.2	-2.9	11.6(AVE)	4.8	38.2	2
30617	MP-III-022	15.8	-1.7	3.5(AVE)	14.1	-1.8	-5.3
30618	MP-III-023	35	6.1	9.5(AVE)	20.3	3.2	-11.4
30619	SH-I-85	14.8	-5.3	12.2(AVE)	18.8	18.6	-11
37713	MP-III-068	-4.7	-15.3	-9.2	-15.2	2.6	15.3
37714	MP-III-080	92.6	-11.4	11.9	-17.6	18.9	11
37715	MP-III-085	-3.7	-6.6	-0.9	2.8	14.7	5.1
37717	SH-053-2'F-R-CH3-Acid	8.6	-14.4	-1.1	-9.6	0	11.1
37718	SH-053-2'F-S-CH3-Acid	-0.6	-1.2	-6.8	-5	-7.1	2.2

37719	MP-III-018.B	10.2	6.3	3.7	11.2	-1.9	9.3
37720	MP-III-019.B	14	0.9	9.4	2.2	4.5	16.7
37721	MP-IV-004	10.4	0.8	12.2	21.1	3.1	12.9
37722	GL-I-65	-4.8	-1.5	-19.3	1.9	5.5	0.4
37723	MP-IV-005	11.2	-0.3	11.8	21.6	7	13.2
37724	GL-I-66	7	-1.8	19.3	15.1	7	23.8
37725	MP-IV-010	-1.9	12.8	11.3	21.2	-5.4	2.1
37726	GL-I-81	-2.2	1.2	-5.4	-0.6	17	8.6
37728	SH-I-085	24.1	3.9	14.6	-0.3	10.2	4.2
37729	KRM-II-18B	21.8	4.9	18.4	8.2	-4.5	4.3
37730	KRM-II-73	24.2	17.3	18.9	-1.7	8.1	-0.2
37731	KRM-II-82	16.4	11.5	14	-5.4	1.8	2.2
37732	KRM-II-97	21.9	13.3	8.1	-1.5	5.4	5.2
37733	KRM-II-81	17.3	6.7	9.4	-1.3	4.3	-9.6
37734	KRM-II-68	10.7	12.5	3.9	7.3	1.7	7.4
37735	KRM-II-08	15.3	18	17.6	11.6	10.9	10.2
37736	KRM-II-3B	65.9	-6.7	26.3	20.8	13	2.5
42621	KRM-III-59	6.9	10.8	-2.6	-0.8	-5.1	-6.1
42622	KRM-III-65	6.2	9.1	7.1	8	0.2	6.4
42623	KRM-III-66	5.7	14	5.9	3.4	7	5.3
42624	KRM-III-67	0.7	10.4	12.4	4.1	-6.9	7.2
42625	KRM-III-79	0.8	5.7	3.5	5.9	-3.7	3.4
42626	KRM-III-70	0.5	-1.7	4.1	14.5	7.5	11
42627	KRM-III-77	-5.1	1.9	13.6	8.9	7.9	-2.4
42628	KRM-III-78	-5.9	11.9	2.8	-2.8	-15.4	0.7
42633	Ro5-4846	-2.3	-0.7	-6.8	6.6	-12.2	1.9
42634	Ro7-9277	-0.5	-0.5	-3.1	-2.8	-2.2	2

42635	GL-I-74	5.8	-0.8	-2.8	0.7	3.9	7.8
42636	GL-II-39	15.8	5.8	-1	8.2	6.9	-3
42637	GL-II-05	-3.1	6.4	-3.1	4.6	2.2	-5.4
42638	GL-II-06	-0.8	6.8	6.5	0.3	-0.4	5.9
42639	GL-II-18	5.1	19.2	18.2	-6.6	7.4	1.9
42640	GL-II-19	-6.2	13.6	16.5	-8.8	2.2	3.9
42641	GL-II-30	-4.4	16.7	6.5	-6.3	-1.3	-5.4
42642	GL-II-31	-12.2	23	-0.8	-14	-10.5	4.7
42643	GL-II-32	6.1	-8.8	-18.5	-3.1	-19	9.5
42644	GL-II-33	-10	-5.6	6.3	-5.3	-6.9	-3.9
42645	GL-II-51	2.8	-12	-0.4	-0.9	6.4	-10.8
42647	GL-II-53	-2.8	-8.6	4.1	6.7	-1.8	-4
42648	GL-II-54	-1.8	-3.4	11	-0.1	0.6	-7.5
42651	GL-II-57	-3.6	3.3	14.5	11.1	3.4	-8.1
42653	GL-II-59	-2.2	-3	8.3	-3.3	6.1	-7.7
42654	GL-II-60	11.7	2.1	16.1	-5.2	6	-3.6
42655	GL-II-61	-8.4	20.8	10.3	-2.2	-4.9	-7.2
42656	GL-I-30	-10.4	11.1	-8.5	-7.4	-13.7	7.5
42657	GL-I-31	-4.3	6.5	-6.3	-3.9	1.8	4
42658	GL-I-32	-8.2	-4.1	-2.4	2.2	-14	-3.2
42659	GL-I-33	-2.6	17	14.3	-2.4	14.5	-5.5
42660	GL-I-38	2.4	7.4	0.9	7.5	9.5	-0.9
42661	GL-I-36	14	2.3	7.5	2.3	16	1.2
42662	GL-I-43	2.4	10.5	8	8.8	12.7	-8.8
42663	GL-I-41	4.6	2.5	9.2	9.9	4	-6.5
42664	GL-I-55	6.9	19.4	17.1	0.9	11.3	2.4
42665	GL-I-54	7.6	60.1	15.7	-6.4	1	-12.3

42666	GL-I-77	2.4	-2.6	-16	0.9	3.8	-5.8
42667	GL-I-78	-17.8	20.4	-16.9	9.2	-8.3	13.5
50093	SH-I-044	0.7	28.5	-5.6	14.8	24.4	-16.7
50094	SH-I-047	5.6	48.7	-10.7	7.4	16.6	2.3
50095	SH-I-060	10.4	16.4	31.6	10.5	-11.3	3.7
50096	MP-III-058	-5.2	14.7	-16.6	-11.8	-5.8	-2.6
50097	SH-I-048A	-2.3	-0.1	3.9	-15.9	-8.5	-6.9
50098	SH-I-048B	3.9	-11.2	-12.2	-6.9	-2.8	2.7
50099	SH-I-055	-6.3	8.5	19.8	-5.5	2.6	8.3
50101	YT-III-31	-5.5	9.3	-19.6	-7.7	3.5	-10.7
50102	YT-III-271	-6.3	29.8	-3.6	0.4	-0.9	-3.6
50103	SR-II-54	-10.8	18.4	-11.8	-7.6	5	-18.4
50104	GL-II-73	-10.5	44.1	-8.4	0.7	-1.4	-13.7
50105	GL-II-74	-16.8	56.1	-8.1	-3.5	1.3	4.1
50106	GL-II-75	-3.9	1	-14.9	2.4	-2.7	15.8
50107	GL-II-76	6.4	-16.9	-17.9	0.3	-2.5	-5.4
50108	GL-I-50	11.3	32.6	-15.1	-2.8	-5.6	1.1
50109	GL-II-93	8.1	0.3	7.9	2.4	6.5	-4.9
50110	GL-I-65	1	29.6	-0.9	6.4	2.3	-1.2
50111	GL-I-81	8.4	10.5	25.4	2.8	8.4	0.5
50112	GL-III-19	7	5	1.5	7.3	18.7	12.1
50114	GL-I-61	15.9	37.3	12.3	0	-7.5	-1.3
50117	GL-I-63	16.4	44.6	25.2	0.2	4.2	0.1
50120	GL-III-26	-1.6	51.6	-8.9	-8.2	11.6	88.3
50121	GL-III-27	4.5	-0.3	-11.9	-16.9	-69.8	30.1
50122	GL-III-59	0.6	-3.9	3.9	-15.6	13.4	77.8
50123	GL-III-57	0.1	-1.3	-6.3	8.4	-34.4	87.2

50124	GL-III-58	4.4	13.2	-8.3	-5.8	14.3	53.3
50125	GL-III-35	5.4	1.2	-0.4	-10.3	23.4	74.1
50126	GL-III-36	-1.8	23.6	9.9	47.5	5	62.3
50127	KRM-III-18A	-0.8	1.4	9.4	-2.2	7.2	61.9
50128	GL-III-38	1.4	-8.9	4.9	8.7	8.9	53.3
50129	GL-III-72	19.7	-13.4	13.5	21.1	-3.4	55.9
50130	GL-III-73	-1.5	6.9	7.4	38.1	8.4	1.6
50132	GL-III-42	-3	15.7	13.2	30.7	-18.6	46.8
50133	GL-III-43	2.3	-6.9	37.2	-0.1	4.2	-2.4
50134	GL-III-52	-8.1	-1.1	1.5	-1.3	5.9	4.1
50135	GL-III-53	13.3	-1.6	-2.3	11.8	-3.8	-2.9
50136	GL-III-54	-2.9	-8.2	3.3	6.9	-9	-11.4
50137	GL-III-60	-0.9	11.1	0.1	-1.9	-2.7	-12.7
50138	GL-III-63	-9.4	11	14.5	28.8	14.6	24.9
50139	GL-III-64	-3.4	7.6	-3.1	2.8	-0.4	-5.6
50140	GL-III-66	-10.6	12	-3.8	6.2	2.8	-7.5
50141	GL-III-67	-18.6	-7.5	2	17.7	9.6	-4.4
50142	GL-III-68	23.2	-1.3	25.6	66	12.4	49.3
50143	GL-III-69	-13.6	-8.9	-1.5	10.1	-0.7	2.5
50144	GL-III-70	-12	9.2	7.5	9.4	13.4	28.8
50145	GL-III-75	-19.5	-15.6	0.3	2.5	15.1	3.9
50146	GL-III-76	5.8	-11	3.3	18.4	-6.6	7.3
50147	GL-III-76A	15.5	-14.7	2.8	7	10.9	3.1
50148	GL-III-77	37.3	11.5	34.4	22.3	-1.2	60
50149	GL-III-78	-2.7	6.7	7.8	22.9	18.3	13.5

Table 38. PDSP primary binding data for Alpha1B, Alpha1D, Alpha2A, Alpha2B, Alpha2C, and Beta1.

Compound #	Name	Alpha1B	Alpha1D	Alpha2A	Alpha2B	Alpha2C	Beta1
30611	SH-053-2'F-R-CH3	-3.7	13.6(AVE)	9.4	9.6(AVE)	18.2(AVE)	30.6(AVE)
30612	SH-053-2'F-S-CH3	-7.1	10.7(AVE)	16.6	18.9(AVE)	18.9(AVE)	19.4(AVE)
30613	MP-III-004	2.4	7.5(AVE)	14.4	13.6(AVE)	19.3(AVE)	14.5(AVE)
30614	MP-III-021	-7	5.4(AVE)	8	10.5(AVE)	1.7(AVE)	21.4(AVE)
30615	MP-III-019	-4.7	8.5(AVE)	-4.8	3.3(AVE)	-4.3(AVE)	21.4(AVE)
30616	MP-III-018.A	-3.6	12.8(AVE)	11.6	17.1(AVE)	2.9(AVE)	42.9(AVE)
30617	MP-III-022	39.6	6.7(AVE)	1.9	0.7(AVE)	1.8(AVE)	32.2(AVE)
30618	MP-III-023	23.4	-1.2(AVE)	-1.0	4.3(AVE)	27.5(AVE)	26.5(AVE)
30619	SH-I-85	22	26.8(AVE)	8.5	28.3(AVE)	12.8(AVE)	19.2(AVE)
37713	MP-III-068	15.8	2.5	5	23.8	-5.2	-19.4
37714	MP-III-080	3.5	-10.5	23	35	1.2	-19.9
37715	MP-III-085	-5.6	-18.4	11.7	23.8	-7.3	-16.7
37717	SH-053-2'F-R-CH3-Acid	-17.4	-17.9	13.4	-1.7	-10.4	13.2
37718	SH-053-2'F-S-CH3-Acid	-15.2	-9.1	21.2	16.2	0.9	-5.9
37719	MP-III-018.B	12.3	-8.9	5	21.1	-5.3	-14.1
37720	MP-III-019.B	-3.9	-4.6	29.4	18.3	19.3	-2.1
37721	MP-IV-004	1.5	4.5	22	9.7	3.8	-3.7
37722	GL-I-65	4.7	-10.3	4.3	21	10.2	13
37723	MP-IV-005	8.3	5.9	30.5	20.5	20.9	5.6
37724	GL-I-66	23.9	11.4	12.9	30.2	27	8
37725	MP-IV-010	14.6	9	14.1	28.8	30.9	6.4
37726	GL-I-81	4.7	8.1	23.1	25	8.9	17.3
37728	SH-I-085	27	3.6	14.9	37.8	11	-17.1

37729	KRM-II-18B	26.1	12	13.4	23.7	2.6	11.6
37730	KRM-II-73	18.7	8.6	17	50	20	6.9
37731	KRM-II-82	27.4	6.8	16.3	36.3	13.1	-6.6
37732	KRM-II-97	17.8	13.5	15	79.5	17.6	-4.6
37733	KRM-II-81	22.3	0.1	20.9	55	0.1	-12.2
37734	KRM-II-68	9.7	-6.1	14.7	12.2	4.2	-9.6
37735	KRM-II-08	27.9	-11.6	27.7	2.6	-6.7	-13.3
37736	KRM-II-3B	8.1	-4.7	37.1	26.2	23.7	-6.1
42621	KRM-III-59	24.5	-7.2	17.6	55.6	4.1	15.8
42622	KRM-III-65	30.1	-5.9	15.7	40	9.6	-5.9
42623	KRM-III-66	21.1	-10.3	28.1	65.1	21.7	9.3
42624	KRM-III-67	21	-7.2	23.2	37.2	21.4	2.8
42625	KRM-III-79	24.2	-10	25.2	49.8	6	4.7
42626	KRM-III-70	11.8	-1.1	20.3	14.2	2.9	10.4
42627	KRM-III-77	6.5	-18.8	20.5	13.3	6.8	4
42628	KRM-III-78	24.6	-15.8	21.8	77.4	26.9	15.5
42633	Ro5-4846	-4.3	-11.2	11.2	13.2	15.8	23
42634	Ro7-9277	-4.1	0.5	5.9	17.8	-18.9	3.5
42635	GL-I-74	3.3	2.4	11.9	19.1	2	-2.1
42636	GL-II-39	-0.6	-9.2	12.5	24.8	-4	1.1
42637	GL-II-05	14.8	-2.1	13.1	7	-3	3
42638	GL-II-06	4.9	-10.3	18.1	64.7	5.2	5.7
42639	GL-II-18	6.7	-9.7	57.4	40.1	35.3	-2
42640	GL-II-19	4.4	-10.3	27.4	38.7	4.6	17.1
42641	GL-II-30	8.8	-12.2	18.4	2.6	-5.5	19.3
42642	GL-II-31	12.5	-5.6	16.2	16.6	10.3	19.2
42643	GL-II-32	-18.4	-17.1	-8.7	35.7	12.6	17.5

42644	GL-II-33	-1.2	-7.9	-8.4	18.1	-4.3	18.8
42645	GL-II-51	-8.1	-5	0.7	11	-5.3	14.5
42647	GL-II-53	-9.7	-12.7	-4.1	26.9	-9.3	2.3
42648	GL-II-54	-19.2	-12.2	6	45.7	5.5	16.3
42651	GL-II-57	-9.9	-10.2	5.5	9.8	1.8	13.9
42653	GL-II-59	-7.8	-1.8	4.6	12.4	18.4	25.9
42654	GL-II-60	-1.3	-13.4	2	11.6	19.5	23.6
42655	GL-II-61	-2.8	-11.7	5.9	20.6	7.4	6.8
42656	GL-I-30	12.7	6.9	15.7	25.1	18.4	15.3
42657	GL-I-31	-5.1	-6	-4	30.7	22.7	-4.8
42658	GL-I-32	21.7	5.3	7.8	47.6	3.6	42.9
42659	GL-I-33	11.4	-1.8	18.4	42.2	19.9	-2.6
42660	GL-I-38	15	-1.5	0.9	36.4	9.5	-11
42661	GL-I-36	14.9	5.4	5.5	9.6	23.6	-9.9
42662	GL-I-43	20.8	4.4	9.5	5.4	5.5	-3.6
42663	GL-I-41	1.3	9.9	16.6	18	5.6	2.3
42664	GL-I-55	-4.2	-14.1	5.8	15.9	4.8	8
42665	GL-I-54	3.3	-4.8	9.4	-2.1	6.2	-1.3
42666	GL-I-77	20.9	-7.4	25.3	21.6	42.3	12
42667	GL-I-78	16.8	4.6	22.9	52.3	23.2	18.1
50093	SH-I-044	-5.8	-11	19	1.1	1	-12
50094	SH-I-047	-19.5	-4	-16.7	4.6	6.9	-0.9
50095	SH-I-060	-0.5	9.5	44.5	61.5	64.9	20.8
50096	MP-III-058	12	-8.1	0	36.8	2.7	-9.2
50097	SH-I-048A	-0.3	-5	9.8	-2.1	-0.9	-15.1
50098	SH-I-048B	14.5	-15.3	7.3	16	-14.6	-10.2
50099	SH-I-055	12.7	15.7	45	48.6	38.3	13.1

50101	YT-III-31	14.4	-8.6	16.7	-1.6	-7.6	-7.7
50102	YT-III-271	14.5	10	25.2	-7.9	-0.3	-1.5
50103	SR-II-54	2.7	-1	1.9	-18.2	-2.2	-14.7
50104	GL-II-73	-8	0.1	6.2	6.5	-17.6	7.2
50105	GL-II-74	-15.3	-0.5	-13.9	-4.6	-19	10.1
50106	GL-II-75	7.9	-4.3	-19.1	-4.6	-6.7	0.1
50107	GL-II-76	21.8	2.5	-5.8	26.3	-11.7	-7.5
50108	GL-I-50	20.3	-5.7	-7.6	-0.7	-4	-15.6
50109	GL-II-93	14.3	-9	-18.2	-14.1	-16.2	-16
50110	GL-I-65	14	2.8	-3.7	5	-11.6	15.8
50111	GL-I-81	10.7	-0.6	8	29.9	6.4	-19
50112	GL-III-19	23.1	-13.4	-2.5	3.6	-10.1	-12.4
50114	GL-I-61	15.7	-10.1	18.4	44.8	45.4	6.5
50117	GL-I-63	-11.4	-1.5	42.7	35.7	53.4	22.5
50120	GL-III-26	-13.4	-16	-1.6	34.6	29.1	3.3
50121	GL-III-27	-15.2	-15.1	-16.5	-2.8	4.5	-9.6
50122	GL-III-59	-3.7	11.5	-19.7	-11.2	-10.1	1.9
50123	GL-III-57	-4.3	-4.3	5.3	13.1	2.7	0.4
50124	GL-III-58	18.5	-7.1	-14.4	1.9	-5.2	-9.4
50125	GL-III-35	6.5	0.7	-4.5	25.6	-11.8	-5.6
50126	GL-III-36	19.6	-11.3	-9.6	37.1	7	-2.1
50127	KRM-III-18A	15.9	-6	27.1	94	65.6	5.9
50128	GL-III-38	9.4	-12.9	-5.8	17.2	4	-17.1
50129	GL-III-72	44	18.4	64.4	63.6	61.4	22.5
50130	GL-III-73	17.1	-18.3	12.1	9.9	-4.1	4.6
50132	GL-III-42	12.1	16.9	6	22.9	13.5	6.1
50133	GL-III-43	-4.3	-11.3	17.5	7.7	-3	8.3

50134	GL-III-52	-15.7	-8.3	31.3	10.9	13	10.8
50135	GL-III-53	4.3	-6.1	5.8	-1.8	-0.4	-8.5
50136	GL-III-54	7.2	-5.7	15	-1.1	-15.2	-4.2
50137	GL-III-60	3.9	-13.8	5.1	1.9	1.2	37.2
50138	GL-III-63	29.2	22.2	31.6	24.2	4.1	4.9
50139	GL-III-64	6.3	-16.7	5.9	59.9	-12.8	-7
50140	GL-III-66	3.9	-15.4	-5.8	-4	32.1	6.7
50141	GL-III-67	1.3	-13.4	64.8	73.3	-6.9	26.5
50142	GL-III-68	16	47.1	8.8	35.5	-3.1	33.8
50143	GL-III-69	9.6	-18.1	-2.9	55.2	-14.1	19.4
50144	GL-III-70	4.2	15.7	1.4	15.1	-12.8	9.5
50145	GL-III-75	4	-6.1	34.9	7.2	0.4	17
50146	GL-III-76	19.6	29.8	14.9	22.3	-7.1	20
50147	GL-III-76A	9.7	13.5	9.9	82.1	28.5	-20.3
50148	GL-III-77	36.9	65.1	73.3	74.4	57.4	26.9
50149	GL-III-78	22.2	15.3	14.7	18.2	4.8	-0.7

Table 39. PDSP primary binding data for Beta2, Beta3, BZP Rat Brain Site, Calcium Channel, D1, and D2.

Compound #	Name	Beta2	Beta3	BZP Rat Brain Site	Calcium Channel	D1	D2
30611	SH-053-2'F-R-CH3	-1.2	-7.2(AVE)	83.7(AVE)		12.3	9.6(AVE)
30612	SH-053-2'F-S-CH3	-1.8	0.3(AVE)	91.5(AVE)		11.2	7.9(AVE)
30613	MP-III-004	16.8	-12.4(AVE)	76.3(AVE)		16	22.7(AVE)
30614	MP-III-021	22.9	-11.0(AVE)	87.3(AVE)		33.2	20.1(AVE)
30615	MP-III-019	31.1	1.0(AVE)	49.0(AVE)		15.2	14.3(AVE)

30616	MP-III-018.A	19	7.9(AVE)	93.1(AVE)		14.2	3.7(AVE)
30617	MP-III-022	18	0.2(AVE)	93.5(AVE)		9.7	12.6(AVE)
30618	MP-III-023	5.6	18.5(AVE)	97.0(AVE)		2.4	14.8(AVE)
30619	SH-I-85	5.2	15.7(AVE)	98.2(AVE)		26.7	13.6(AVE)
37713	MP-III-068	29.4	-2.5	87.6	-7.7	-4.6	-10.3
37714	MP-III-080	8.2	15.4	88.2	-10.6	11.1	-5.8
37715	MP-III-085	-8.2	-1.3	81.7	2.9	4	5.7
37717	SH-053-2'F-R-CH3-Acid	93.6	-6.5	93.4	-3.5	-10.4	-14.8
37718	SH-053-2'F-S-CH3-Acid	19.7	-16.2	92.9	-8.1	-4.3	-8.4
37719	MP-III-018.B	19.2	6.5	96.6	6.3	4.9	1.3
37720	MP-III-019.B	3.1	16.6	94.1	10	10	-4.8
37721	MP-IV-004	7.8	14.8	63.4	-2.3	9.3	-1.1
37722	GL-I-65	-10.1	-9.9	78.6	1.8	-3.9	-8.5
37723	MP-IV-005	22.2	29.6	67.7	-17.1	20.5	-0.8
37724	GL-I-66	9.7	25.6	80.2	18.9	15.7	8.2
37725	MP-IV-010	20.5	38.2	64.1	14.9	27.8	25.1
37726	GL-I-81	-2	-1.4	83.1	43.1	23.4	-15.9
37728	SH-I-085	26.7	-0.5	97	18.7	19.5	29.4
37729	KRM-II-18B	-8.2	-1.4	96.8	15.3	12.9	13.9
37730	KRM-II-73	-18	-8.5	96.9	10.7	26.4	21.6
37731	KRM-II-82	-10.5	-2.9	94.6	23.8	18	15.4
37732	KRM-II-97	-18.7	-5.8	93.4	41.8	8.1	23.6
37733	KRM-II-81	-28.4	-14	85.6	23.1	14.3	13.6
37734	KRM-II-68	-12.2	-7.4	74.8	20.5	0.6	16.4
37735	KRM-II-08	-7.2	-12.4	94.8	-4.1	5.5	19.1
37736	KRM-II-3B	-5.2	5.9	69.4	-19.8	25.3	-1.7

42621	KRM-III-59	-9.3	-18.9	96.3		-2.2	3.2
42622	KRM-III-65	-4.1	-17.2	96		7.7	11.2
42623	KRM-III-66	-1.2	-4.6	85.6		7	12.5
42624	KRM-III-67	-13.9	-8.8	70.7		-4	14.7
42625	KRM-III-79	-19.8	-13.4	80.7		5.1	11.2
42626	KRM-III-70	-17.1	-13.1	79.7		-2.9	10.5
42627	KRM-III-77	-18.8	-7.3	85.5		-7.7	16.1
42628	KRM-III-78	-13.1	32.8	83.9		23.5	2.6
42633	Ro5-4846	-17.2	18.5	52.7		-0.3	-0.1
42634	Ro7-9277	-19.5	7.7	47		-2.6	-8.5
42635	GL-I-74	-11.8	13	55.5		8.4	13.6
42636	GL-II-39	-4.2	28.7	40.6		4.1	16.5
42637	GL-II-05	8.7	30.6	50		2.5	16.1
42638	GL-II-06	-1.8	30.9	81.3		8.9	15.2
42639	GL-II-18	-2.2	33.7	55		16.6	17.2
42640	GL-II-19	-1.3	8.5	70.9		4.2	22
42641	GL-II-30	-5	-2.7	65.2		-0.3	12
42642	GL-II-31	-5.6	-3.8	72.2		16.8	-10.6
42643	GL-II-32	-6.1	-12.2	62.5		13.8	-12.9
42644	GL-II-33	-0.1	0.1	98.2		10.5	-12.9
42645	GL-II-51	-9	-14.5	84.4		3.1	-13.6
42647	GL-II-53	-0.2	11.9	79		-1.7	-19.2
42648	GL-II-54	19	7.5	66.3		2.8	-6.4
42651	GL-II-57	-4.4	21.5	86.6		3.9	-8.4
42653	GL-II-59	-7.5	20.3	88.3		-4.3	0.1
42654	GL-II-60	0.2	-11.2	88.1		11.5	3.4
42655	GL-II-61	-12.2	15.7	80.7		14.3	-10.6

42656	GL-I-30	-18.7	-4	96.2		16.9	-14.7
42657	GL-I-31	0	40.3	97		-10.1	-14.7
42658	GL-I-32	-18.6	1.5	98.3		-2.6	-5.4
42659	GL-I-33	-1.8	32.1	96		6.9	-11.7
42660	GL-I-38	1.9	-1.2	95.5		-5.1	-14.7
42661	GL-I-36	35.6	-6.5	77.2		-1	-15.2
42662	GL-I-43	-3.8	-18.4	93.8		-9.3	-9.2
42663	GL-I-41	-14.8	-10	89.9		-3.9	-7.8
42664	GL-I-55	-7.5	-4.8	95		-11.1	0.7
42665	GL-I-54	-7.6	-6.6	93.7		-6.5	-4.3
42666	GL-I-77	0.3	-2	92.3		5.6	-12.1
42667	GL-I-78	-5.1	11.1	76		-5.3	-14.9
50093	SH-I-044	1.4	32.1	72.8	5.8	-16.2	-17.9
50094	SH-I-047	-6.8	41.1	83.9	-10.5	-8.6	2.9
50095	SH-I-060	3.5	63.8	75.7	33.2	34.1	0.9
50096	MP-III-058	6	31.3	86.4	22.5	-8.2	-17.4
50097	SH-I-048A	-4.4	54.1	68.6	32.4	-14.1	-9.6
50098	SH-I-048B	-5.1	49.2	61.4	24.1	0.3	1.8
50099	SH-I-055	3.5	63.5	52.1	35.6	23.3	11.5
50101	YT-III-31	13.2	33.9	81.9	11.9	-4	6.5
50102	YT-III-271	8.7	38.1	72.6	-18.2	14.7	15.3
50103	SR-II-54	1.9	35	79.9	24.3	7.7	18
50104	GL-II-73	-13.7	18.5	74.6	-18.5	4.9	27.2
50105	GL-II-74	-16.6	7.3	84.2	3	17.5	11.6
50106	GL-II-75	-2.8	3.5	85	-5	8.4	0
50107	GL-II-76	-5.2	-0.7	43.3	-13.8	-2.5	4
50108	GL-I-50	-8.5	8.7	42.2	-14.9	-2.7	6.1

50109	GL-II-93	-9.1	-3.8	72.5	13.4	4.4	14.8
50110	GL-I-65	8.6	10.9	33.2	17.3	3.3	16.7
50111	GL-I-81	7.1	4.8	81.4	28.1	15.3	29.1
50112	GL-III-19	11.7	-18.5	79.5	11.9	7	24.5
50114	GL-I-61	12.8	28.1	76.6	0.9	31.3	14.8
50117	GL-I-63	1.3	11.2	82	30	23.1	29.4
50120	GL-III-26	-2.8	-6.7	71	16.4	17.3	30.4
50121	GL-III-27	2.1	-11.3	80.2	9.5	-3.4	-17.5
50122	GL-III-59	5.8	-8.9	85.7	38.8	-0.3	10.1
50123	GL-III-57	-9.6	1	56.3	39.8	4.5	-17.2
50124	GL-III-58	-9.5	14.7	58.9	22.2	3.3	-14
50125	GL-III-35	1.5	25.1	78.6	7.6	-8.2	-5.8
50126	GL-III-36	8.8	4.2	85.7	10.6	-3.2	-12
50127	KRM-III-18A	18.2	16.7	54.5	41.9	10.6	-19.8
50128	GL-III-38	11.5	-1.6	61.6	28	3.5	-11.3
50129	GL-III-72	-0.1	61.4	82.8	-0.1	31.4	-3
50130	GL-III-73	-6.1	-4.9	65.1	1.9	-7	-15
50132	GL-III-42	-2.1	18.1	62.1	21.4	24.1	-7.8
50133	GL-III-43	1.6	13.3	45.6	1.4	-3.2	-15.7
50134	GL-III-52	-2.7	33.6	52.4	20.3	2.9	-16.5
50135	GL-III-53	3.1	22.2	63.6	12.9	-4.8	-19
50136	GL-III-54	21.1	4.7	139.1	37.9	-18.3	6.3
50137	GL-III-60	7.6	12.7	109.4	45.6	-18.1	-15.8
50138	GL-III-63	3.3	-2.5	28.1	49.6	68.8	27.3
50139	GL-III-64	-10.5	-0.5	92.4	15.8	46.7	-12.5
50140	GL-III-66	-10	0.2	87.5	4	-5.1	10.7
50141	GL-III-67	-16.3	1.1	106.9	-9.3	-3.8	7.9

50142	GL-III-68	-1.1	-3.4	136.5	17.2	46.5	8
50143	GL-III-69	12.5	-14.5	118.1	21.2	20.9	13.3
50144	GL-III-70	19	2.9	113.7	28.5	31.9	13.3
50145	GL-III-75	21.5	9.6	95.2	38.8	35.7	10
50146	GL-III-76	18.5	30	121.8	41.2	39.5	11.2
50147	GL-III-76A	15.1	42.4	83	46	-5.8	-3.6
50148	GL-III-77	14.5	39.9	50	59.9	50	14.5
50149	GL-III-78	-4	43.3	100.7	66.3	11.2	10

Table 40. PDSP primary binding data for D3, D4, D5, DAT, DOR, and GABAA.

Compound #	Name	D3	D4	D5	DAT	DOR	GABAA
30611	SH-053-2'F-R-CH3	2.4(AVE)	23.1	5.9(AVE)	35.3(AVE)	22.4(AVE)	-12.2(AVE)
30612	SH-053-2'F-S-CH3	6.8(AVE)	3.1	25.1(AVE)	38.1(AVE)	25.2(AVE)	-12.6(AVE)
30613	MP-III-004	9.6(AVE)	-5.5	19.6(AVE)	32.3(AVE)	21.0(AVE)	-6.0(AVE)
30614	MP-III-021	7.5(AVE)	4.9	21.7(AVE)	36.9(AVE)	20.2(AVE)	-13.4(AVE)
30615	MP-III-019	-9.8(AVE)	42.5	20.6(AVE)	65.4(AVE)	13.6(AVE)	-11.1(AVE)
30616	MP-III-018.A	12.9(AVE)	-7.4	8.1(AVE)	34.0(AVE)	27.1(AVE)	-10.4(AVE)
30617	MP-III-022	11.1(AVE)	-7.1	1.0(AVE)	48.6(AVE)	16.9(AVE)	-19.5(AVE)
30618	MP-III-023	6.2(AVE)	-15.7	14.1(AVE)	41.6(AVE)	15.0(AVE)	-24.4(AVE)
30619	SH-I-85	4.2(AVE)	2	13.9(AVE)	33.6(AVE)	35.2(AVE)	-17.7(AVE)
37713	MP-III-068	-5	-4.7	-17.2	7.8	18.7	9.4
37714	MP-III-080	12.1	-0.3	11.7	-6.4	0	-0.6
37715	MP-III-085	-0.3	-3.1	-17.2	-2.9	-3.9	-18.2
37717	SH-053-2'F-R-CH3-Acid	-4.3	-4.6	-16.2	-1.5	-3.9	-15.2

37718	SH-053-2'F-S-CH3-Acid	-2.8	-3.7	-13.3	3.6	17.6	-3.8
37719	MP-III-018.B	2.3	-6.5	-9.1	11	9.7	-14.4
37720	MP-III-019.B	20.4	-6.2	-0.4	21.8	-9.9	-19.4
37721	MP-IV-004	6.9	-2.9	11.6	32.2	9.8	-8.5
37722	GL-I-65	-11.8	-10.5	26.5		6.6	-4.6
37723	MP-IV-005	10	4.7	30.7	26.6	23.4	-5.6
37724	GL-I-66	13.2	0.6	26.1	10.7	1.5	-5.7
37725	MP-IV-010	15	4.8	28.7	13.5	5.1	-7.6
37726	GL-I-81	-16.3	6	19.8	4.2	24.7	14.7
37728	SH-I-085	1.5	-4.5	13.3	17.8	11	-1.2
37729	KRM-II-18B	4.6	-1.8	5.9	18.9	20.1	-11.2
37730	KRM-II-73	3.3	5	9	19.3	31.7	-17.5
37731	KRM-II-82	9.4	7.6	1	20.3	19.6	-15.3
37732	KRM-II-97	9.9	3.2	14	21.3	8.3	-14.8
37733	KRM-II-81	6.6	-2.8	-7	26.9	15.2	-7.9
37734	KRM-II-68	11.2	-1	-8.7	39.5	-6	-0.6
37735	KRM-II-08	17	4.3	5.1	-15.2	-7.2	-19.8
37736	KRM-II-3B	35.8	-12	-2.9	-17.7	11.9	-16.1
42621	KRM-III-59	-3.9	-20.2	23.7		10.5	39.2
42622	KRM-III-65	1.4	19.8	22.2	-6.8	15.8	40.2
42623	KRM-III-66	0.4	25	18.7	1.4	11.4	17.8
42624	KRM-III-67	-2.5	26.6	21.1	-8	2.6	27.9
42625	KRM-III-79	8.5	32.4	17.5		1.4	32.2
42626	KRM-III-70	11.8	33.8	17.4		-9.7	9.9
42627	KRM-III-77	23.4	24	12.5		-12.5	9.8
42628	KRM-III-78	11	31.7	15	-8.2	-1.5	3.6

42633	Ro5-4846	-3	-15.1	4.3	11.3	7.5	10.7
42634	Ro7-9277	-5.5	-8	7.5	-0.8	-8.2	14.8
42635	GL-I-74	9.1	13.7	14.6	6.2	5.4	26.8
42636	GL-II-39	11.7	11.3	8.9	8.9	2	15.4
42637	GL-II-05	9.5	16.5	5.1	1.1	0.3	30.8
42638	GL-II-06	16.3	28.1	6.9	-3.3	8.8	25.9
42639	GL-II-18	36.2	35.9	17.5	28.2	74.5	31
42640	GL-II-19	32.1	3.6	6.1	6.3	1.8	0.7
42641	GL-II-30	18.7	13.8	9.6	7.6	3.8	-5.4
42642	GL-II-31	-19.7	31.5	-9.4	5.5	2.6	14.8
42643	GL-II-32	-11.3	-10	-15.6	-34.1	-7.1	21.2
42644	GL-II-33	-9	-2	-5.1	-67.6	9.9	33
42645	GL-II-51	-12	-3.8	-7.1	-28.3	-6.7	36.6
42647	GL-II-53	-13.5	-2.3	-4.1	-8.6	1.1	45.8
42648	GL-II-54	-10.3	-13	5.1	-16.2	-1.8	38.6
42651	GL-II-57	-4.3	-6.1	-1.8	-4.1	4.6	27.8
42653	GL-II-59	3.1	-2.4	1.2	9.4	-3.5	44.3
42654	GL-II-60	5.2	12.3	5.7	-0.6	11.7	16
42655	GL-II-61	-5.1	-0.8	8.6	5.9	9.3	1
42656	GL-I-30	-0.5	-13.6	5	-2.5	7.4	-1.1
42657	GL-I-31	-10.6	-12.9	15.5	-23.4	8.2	18.3
42658	GL-I-32	-17.6	-9	18	-9.5	13.9	19.5
42659	GL-I-33	1.2	-6.3	23.9	-0.3	25.3	18.3
42660	GL-I-38	-4.4	-7.8	17.6	-5.4	15.8	29.7
42661	GL-I-36	-5.2	0.6	23.6	-11.4	-0.6	33.3
42662	GL-I-43	-4.5	-5.6	5.1	-2.8	2.8	48.5
42663	GL-I-41	7.2	1.2	10.1	7.3	9.6	45.2

42664	GL-I-55	13.1	5.4	12	9.8	23.8	23.7
42665	GL-I-54	2.5	5.5	16.5	5.6	11.3	6.5
42666	GL-I-77	-13.4	4.7	-8.6	-2.6	4.1	20.4
42667	GL-I-78	-7.6	4.5	-16.5		40.5	18.4
50093	SH-I-044	5.4	18.5	-4	9.3	-6.6	-0.4
50094	SH-I-047	6.5	21.8	-2.6	7.4	-9.5	-2.2
50095	SH-I-060	25.5	16.1	61.7	32.2	47.7	-0.4
50096	MP-III-058	-11.4	-15.3	2.4	7	3.5	25
50097	SH-I-048A	-5.1	-2	-1.3	-6.7	0.6	32.4
50098	SH-I-048B	-13.6	-1.5	-3.5	7.5	-0.7	27.8
50099	SH-I-055	17.3	-1.9	54.1	30	16.7	18.5
50101	YT-III-31	-12	-3	1.4	-22.2	-2.9	11.4
50102	YT-III-271	3.5	-14.1	12.7	-8.9	16.8	21
50103	SR-II-54	16.6	-1.7	9.4	-1.8	1.4	12.7
50104	GL-II-73	7.8	-9.4	-5.7	-11.4	-12.4	-10.4
50105	GL-II-74	8.4	1.2	1	-38.2	-7.1	-4.4
50106	GL-II-75	-12.4	3.6	-2.6	-14	3.3	0.8
50107	GL-II-76	-18.9	1.3	0	-7.1	-6	12.5
50108	GL-I-50	-17.2	-9.6	-2.6	-11.2	-9.1	11.5
50109	GL-II-93	-3.5	-8.2	2.4	-15.9	-13.4	12.7
50110	GL-I-65	10	5.6	22	-0.4	35	16.7
50111	GL-I-81	6.7	-2.9	4.6	11.7	4.7	5.9
50112	GL-III-19	18.6	-11	-6.5	23.7	3.6	21.7
50114	GL-I-61	26.7	-4.1	50	41.8	29.2	-4.1
50117	GL-I-63	55.1	4	43.8	-11	10.9	-6.2
50120	GL-III-26	50	16.9	4.4	-4.5	64.6	5.2
50121	GL-III-27	-16.6	-0.4	12.3	-15	-1.9	-1.7

50122	GL-III-59	-9.1	-17.6	2.7	-4.5	-5.3	11.1
50123	GL-III-57	2	-19.7	5.4	10.9	23	35.1
50124	GL-III-58	2.7	-12.5	4.1	7.6	0.1	31.4
50125	GL-III-35	1.9	1.1	11.1	12.6	-14.4	19.9
50126	GL-III-36	1.9	-10.3	8.4	17.8	12.4	12.3
50127	KRM-III-18A	7.2	-0.4	17.6	48.1	27.2	19.2
50128	GL-III-38	-6.4	-10.5	11.8	38	14	0.1
50129	GL-III-72	52.3	16	29.2	44.2	82.8	-45.8
50130	GL-III-73	-7.7	7.4	4.4	-20.3	3.5	-18.7
50132	GL-III-42	-13	15.6	2.2	18	13.3	-17.2
50133	GL-III-43	-7.1	-1.8	7.8	8	21.5	1.1
50134	GL-III-52	-8.5	-5.4	6.9	3.8	19.6	3.6
50135	GL-III-53	-5.5	-6.8	10.8	-4.4	1	15
50136	GL-III-54	-19.4	-12.5	-19	-39	-5.8	6.5
50137	GL-III-60	1.3	-3.1	-8.9	-18.4	18.3	-6.3
50138	GL-III-63	-18.8	-10.1	33	-9.8	31.3	17.9
50139	GL-III-64	-2.7	14.4	44	-7.1	13.6	-12.8
50140	GL-III-66	-6.5	-4	1.8	-9.8	-5.8	11.7
50141	GL-III-67	-7.4	-2.9	23.8	0.4	-8	-1.8
50142	GL-III-68	8.7	21.8	41.5	1.5	9.7	-4.5
50143	GL-III-69	0.6	22.2	21.3	5.8	10	-3.8
50144	GL-III-70	-2.8	25.5	24.2	6.3	49.5	-4.8
50145	GL-III-75	0.8	19.7	25.3	10.9	-17.3	-10.9
50146	GL-III-76	-7.4	6.1	-16.2	11.7	-2.6	-13
50147	GL-III-76A	-4	-16.5	-4.5	5.9	0.3	-16.3
50148	GL-III-77	43.9	-2.5	70.7	59.4	77.9	-3.3
50149	GL-III-78	-4.6	-4.3	14.7	12.9	9.2	-4.7

Table 41. PDSP primary binding data for H1, H2, H3, H4, HERG binding, and KOR.

Compound #	Name	H1	H2	H3	H4	HERG binding	KOR
30611	SH-053-2'F-R-CH3	35.6	1	-2.6	9.7(AVE)	10.6	90.9(AVE)
30612	SH-053-2'F-S-CH3	50.0	-7	0.4	13.9(AVE)	15.3	95.7(AVE)
30613	MP-III-004	44.5	-9	-6.6	12.9(AVE)	21.7	80.3(AVE)
30614	MP-III-021	44.8	-5.8	-1.8	12.1(AVE)	16.1	97.5(AVE)
30615	MP-III-019	59.5	8.6	-19.1	20.5(AVE)	15	45.5(AVE)
30616	MP-III-018.A	53.7	-2.7	-1.2	16.5(AVE)	27.6	71.1(AVE)
30617	MP-III-022	25.5	5.5	12.5	10.4(AVE)	25.3	87.0(AVE)
30618	MP-III-023	17.3	-3.2	12	14.1(AVE)	9.4	96.1(AVE)
30619	SH-I-85	3.2	-5.5	4.8	-6.3(AVE)	4.1	95.6(AVE)
37713	MP-III-068	24.9	12.4	2.3	-3.2	-10.5	28.5
37714	MP-III-080	89.3	2.6	7.9	7.1	5.3	46.6
37715	MP-III-085	90.2	-1.9	-5.9	-3.1	-6.4	40.2
37717	SH-053-2'F-R-CH3-Acid	86.7	-5.4	-1.3	14	0.7	16.4
37718	SH-053-2'F-S-CH3-Acid	78	7.7	8	-7.6	-4.4	20.1
37719	MP-III-018.B	71.3	1.2	3	-1.1	0.4	50.9
37720	MP-III-019.B	58.3	-0.8	-0.2	-0.1	2	62.1
37721	MP-IV-004	44.1	-6.9	-5.5	8.4	18.6	86
37722	GL-I-65	-9.8	7.1	-12.5	-4.1	-8.8	88.4
37723	MP-IV-005	20.8	0.7	-1.2	5.6	18.5	89.3
37724	GL-I-66	19.6	6.1	-29.9	13.5	37.8	91.7
37725	MP-IV-010	19	28.2	-17.9	5.7	28.8	93.6
37726	GL-I-81	8	21.7	-11.9	3.4	8.8	92.9

37728	SH-I-085	19.3	11.6	16.2	15.5	17.8	91.3
37729	KRM-II-18B	5.1	9.6	22.2	19	17.6	88.9
37730	KRM-II-73	-8.1	0.7	16.6	14.8	17.9	83.1
37731	KRM-II-82	-11.3	19.6	13.1	32.8	16.3	77.9
37732	KRM-II-97	-32.6	-4.7	2.4	15.2	20	61.6
37733	KRM-II-81	-13.5	-11.7	8.6	11.7	-16.4	45.9
37734	KRM-II-68	4.2	79.1	-1	4.9	6.1	20.3
37735	KRM-II-08	89	1.7	-11.4	20.5	3	80.2
37736	KRM-II-3B	42.9	-0.7	-6.8	-4.9	-9.2	54.7
42621	KRM-III-59	-5	20.1	5.5		9.3	73.4
42622	KRM-III-65	0.8	8.9	-2.2	-1.1	7.7	64.1
42623	KRM-III-66	-15.6	22.3	13.4		11.4	66.5
42624	KRM-III-67	-11.6	15.9	9		4.3	48.1
42625	KRM-III-79	-12.8	2.8	-13.2	4.3	-14.2	8.9
42626	KRM-III-70	0.3	-3.6	1.3		-6.2	-4.6
42627	KRM-III-77	-8.4	7.4	-1.3	6.8	-2.3	59.1
42628	KRM-III-78	-5.4	14.6	13		2.9	42
42633	Ro5-4846	-10	11.6	-10.8		4.6	57.5
42634	Ro7-9277	0.5	7.5	-4.3		-1.5	19.4
42635	GL-I-74	16.1	16.5	-2.2	15.8	14.2	62.4
42636	GL-II-39	4.7	3.2	17.6	17.8	8.6	31.4
42637	GL-II-05	28.4	1.8	11.2	33.6	-2.9	25.8
42638	GL-II-06	27.6	0.9	10.6	18.3	3.3	78.8
42639	GL-II-18	28.1	10.6	14	15.8	58.5	7.3
42640	GL-II-19	2.5	0.1	31.4	16.4	4.6	43.5
42641	GL-II-30	12.4	0.2	28.1	9.3	-0.2	-15.6
42642	GL-II-31	17.6	6.9	9.4	13.7	-15.6	22.9

42643	GL-II-32	-5	22.7	31.2	4.2	-12.7	35.2
42644	GL-II-33	-18.1	18.3	1.1	9.1	-2.8	88.8
42645	GL-II-51	-14.4	11.1	2.3	14.8	1.4	11.2
42647	GL-II-53	-6	11.5	5.6	7.4	-3.8	78.1
42648	GL-II-54	-19.5	14.7	-12.1	17.2	3.1	80
42651	GL-II-57	-11.7	30.3	-7	12.8	5.8	96
42653	GL-II-59	-4.1	21.1	8.8	8.6	6.7	93.6
42654	GL-II-60	-16.8	26.5	2.9	11.2	13.3	89.9
42655	GL-II-61	-6.8	16.9	7.1	7.5	18.7	3.5
42656	GL-I-30	7.2	29.7	4.7	-37.1	-6.9	94.9
42657	GL-I-31	11.4	22.8	-19.3	-9.6	-15.8	94.2
42658	GL-I-32	2	73.1	8.4	0.2	14.6	94.5
42659	GL-I-33	10.5	21.7	-4.6	24.7	27.3	93.7
42660	GL-I-38	14.9	12.8	0.1	-4.6	6.8	95.2
42661	GL-I-36	7.6	12.1	1	36.6	15	84.9
42662	GL-I-43	10	13.8	10.9	3.8	12.3	95.2
42663	GL-I-41	2.1	19.3	36	-7.1	14.4	97
42664	GL-I-55	2.6	21.5	4.3	0.4	23.8	93.1
42665	GL-I-54	1	7.1	17.4	0.9	14.7	77.9
42666	GL-I-77	23.7	29.3	1.6	4.6	-12.9	95
42667	GL-I-78	15.8	57.7	11	-5	-7.6	95.7
50093	SH-I-044	-15.6	20	1.2	8.9	-16.1	31.3
50094	SH-I-047	-10.3	-6.9	-9.6	-16.7	-1.5	82.4
50095	SH-I-060	15.3	40	17.6	3.7	69.1	2.5
50096	MP-III-058	-1.5	12.5	-7.8	-9.9	-1.2	83.6
50097	SH-I-048A	1.7	16.4	-9.4	5.6	-13.7	6.3
50098	SH-I-048B	2.6	19.6	-2.9	14.1	-0.3	95.2

50099	SH-I-055	24.3	40.8	4.5	30	68.5	38.9
50101	YT-III-31	-10.7	-2.6	34.8	68.1	13.4	89.2
50102	YT-III-271	-3.4	13.9	21.6	6.7	13	58.3
50103	SR-II-54	-12.8	2.7	0.7	28.3	-15.9	8.9
50104	GL-II-73	0.1	2.2	-1	2.7	-9.3	58.1
50105	GL-II-74	-8	32	-8.5	-11.1	2.8	86
50106	GL-II-75	9.8	16.1	0.9	-16.6	4.8	80.9
50107	GL-II-76	-5.1	13.2	-13.4	24.3	5.8	80.4
50108	GL-I-50	-13.6	33	2.4	27.8	8.1	-11.1
50109	GL-II-93	-5.4	10.7	-13.3	26.2	2.8	-9.1
50110	GL-I-65	-8	19.9	-18.3	-1.5	13.7	79.3
50111	GL-I-81	10	19.2	-0.2	41.9	37.1	86.9
50112	GL-III-19	0.9	11.3	0.2	13.6	20.9	81.5
50114	GL-I-61	19.2	56.2	21.7	-10.2	34.7	-18.1
50117	GL-I-63	15.6	66.5	26.5	-18.2	63.8	-6.7
50120	GL-III-26	14.7	56.1	15.8	-6.1	23.1	12.2
50121	GL-III-27	26.4	42.5	24.6	-5	-4.8	-13.1
50122	GL-III-59	4.8	11.4	19.6	-13.2	-5.7	15.8
50123	GL-III-57	16.8	14.5	4.1	6.8	7.1	13
50124	GL-III-58	2	11.3	13.2	0.7	-12.3	15.5
50125	GL-III-35	-4	9.5	-11.5	-7.2	-4.3	77
50126	GL-III-36	6.5	16.8	18.7	2.4	-6.5	87.8
50127	KRM-III-18A	-2.7	31.2	-14.7	-12.6	1.1	62
50128	GL-III-38	2.1	1.5	-15.8	-6.2	-14.8	38.2
50129	GL-III-72	-0.3	67.2	0.8	-14.4	44	3.3
50130	GL-III-73	3.4	54.9	5.8	-0.2	-14.5	74.3
50132	GL-III-42	29	47.5	8.5	-0.9	6.1	86.1

50133	GL-III-43	1	15.6	11	11.8	-0.5	50.2
50134	GL-III-52	-12.1	18.2	13.3	13.7	-17.8	39.9
50135	GL-III-53	-7.9	25.6	9.4	11.3	-19.7	91.7
50136	GL-III-54	12.3	-14.9	-14.7	-8.6	-16.8	22
50137	GL-III-60	50	-5.9	-18.6	10.7	-5.1	87.4
50138	GL-III-63	40.8	16.9	25.7	-83.1	12.2	77.5
50139	GL-III-64	53.7	-7.1	-7.5	19.4	6.4	60.2
50140	GL-III-66	39.4	-4.7	-7.6	25.2	0.5	62.9
50141	GL-III-67	11.4	0.2	-13.6	-6.4	-8.1	87.3
50142	GL-III-68	64.2	71.9	-4.7	16.3	23.4	88.3
50143	GL-III-69	-12.7	16	3	-7.2	1.8	75.1
50144	GL-III-70	-12.5	19.1	-4.6	-10.3	-14.9	67.7
50145	GL-III-75	-11.7	7.7	15.5	18.9	-2.9	61.2
50146	GL-III-76	-13.4	-16.9	18.3	-9.2	0.8	83.2
50147	GL-III-76A	0.8	1.7	-16.2	-10.1	2.6	39.4
50148	GL-III-77	54.1	60.7	4.1	-10.3	57.4	10.4
50149	GL-III-78	31.2	11.6	-6	-4.7	-1.3	74.1

Table 42. PDSP primary binding data for M1, M2, M3, M4, M5, and mGlur5.

Compound #	Name	M1	M2	M3	M4	M5	mGlur5
30611	SH-053-2'F-R-CH3	-4.9	17.9	26.1(AVE)	7.7(AVE)	0	31.7
30612	SH-053-2'F-S-CH3	-8.5	11.7	12.8(AVE)	12.6(AVE)	-1.9	24.8
30613	MP-III-004	-7.8	-0.7	7.9(AVE)	1.0(AVE)	3.6	4.8
30614	MP-III-021	-6.2	2.9	9.3(AVE)	5.8(AVE)	0.8	-5.1
30615	MP-III-019	-4.5	2.1	1.7(AVE)	9.2(AVE)	6	-7.3
30616	MP-III-018.A	-7.2	-3.2	2.3(AVE)	43.3(AVE)	8.3	54.4

30617	MP-III-022	-11.4	4.7	-0.9(AVE)	-3.9(AVE)	5.7	29.1
30618	MP-III-023	-2.2	10	9.1(AVE)	-2.3(AVE)	2.6	-0.6
30619	SH-I-85	-10.2	0.6	10.8(AVE)	1.4(AVE)	2.4	28.6
37713	MP-III-068	7.2	19.5	15.4	18.2	-2.7	
37714	MP-III-080	4	25.9	7.8	26.6	11.5	
37715	MP-III-085	6.2	16.3	3.3	29.4	-5.9	
37717	SH-053-2'F-R-CH3-Acid	11.9	21.1	8.6	29	-3.9	
37718	SH-053-2'F-S-CH3-Acid	5.8	20.7	12.3	20.7	-0.1	
37719	MP-III-018.B	10.6	50	16.7	29.7	6.6	
37720	MP-III-019.B	4.2	50	8.1	28.6	14.1	
37721	MP-IV-004	-9.8	26.5	-5.5	27.7	12.4	
37722	GL-I-65	-7.5	-8.6	36.5	38.8	-2.8	
37723	MP-IV-005	-11.3	22.3	7.3	22.2	12	
37724	GL-I-66	-16	50	-4.7	37.7	20.8	
37725	MP-IV-010	-11.2	10.5	-0.4	8.4	26.2	
37726	GL-I-81	-1.4	-17	47.7	22.5	4.9	
37728	SH-I-085	-3.4	17.1	-3.9	14.2	28.2	
37729	KRM-II-18B	-1.4	4.9	7.7	9	30.5	
37730	KRM-II-73	-4.5	6.6	4.9	15.4	50	
37731	KRM-II-82	-4.3	0	3.8	13.5	33.5	
37732	KRM-II-97	10.1	3.5	6.7	12	38.3	
37733	KRM-II-81	3.2	2.4	-8.9	11.2	37.5	
37734	KRM-II-68	6.9	0.1	-8.3	12.8	26.2	
37735	KRM-II-08	11.8	3.5	-0.1	18	25.4	
37736	KRM-II-3B	-5	-1.3	15.2	-7.5	10.3	
42621	KRM-III-59	-9	-18.3	-18.3	-4	2.3	

42622	KRM-III-65	-17	-8.8	-0.1	-0.1	-2	
42623	KRM-III-66	-8.7	-12.5	24.9	0.1	3	
42624	KRM-III-67	-6.2	-9.9	23.8	3.3	-3.9	
42625	KRM-III-79	11.8	3.7	23	-6.1	7.7	
42626	KRM-III-70	3.9	-9.4	18.4	-4.8	2	
42627	KRM-III-77	3.5	-13.7	1.3	18.1	-3.3	
42628	KRM-III-78	3.5	0.8	3.6	9.2	6.1	
42633	Ro5-4846	-4	-7.5	8	7.8	16.7	
42634	Ro7-9277	5	4.4	32.8	11.4	9.3	
42635	GL-I-74	-2.2	6	39.6	-11.9	0	
42636	GL-II-39	2.8	11.9	29.6	-10.5	7.9	
42637	GL-II-05	19.2	7.1	21.8	16.7	-10.3	
42638	GL-II-06	11	2.8	16.4	30.6	-11.2	
42639	GL-II-18	-0.7	-1.2	-1.1	2.6	-1.7	
42640	GL-II-19	-13.9	-0.6	8.6	5.7	8.2	
42641	GL-II-30	2.3	-0.7	-7.7	-3	-3.8	
42642	GL-II-31	-6.6	0.4	-12.6	-2.3	-10.2	
42643	GL-II-32	-1.9	2.8	-7.1	-4	-9.4	
42644	GL-II-33	-4.1	1.3	16.9	0.6	-6.2	
42645	GL-II-51	3.3	-6.4	18.5	-8.9	-1.2	
42647	GL-II-53	-14.3	4.2	1.3	23	-6.5	
42648	GL-II-54	-8.1	2.1	8.3	-2.2	-10.8	
42651	GL-II-57	-4.4	3.9	-0.1	3.1	-13.8	
42653	GL-II-59	-15.5	-3.9	4.2	-13.5	-2	
42654	GL-II-60	0.2	5.9	-1	2.4	-4.4	
42655	GL-II-61	-6.4	2.4	-5.6	-9.7	-10.5	
42656	GL-I-30	-7.1	8.9	-8.6	-2.3	-4.7	

42657	GL-I-31	-7.6	11.3	-0.2	1.3	-6.6	
42658	GL-I-32	-13.2	-13.4	0.9	17.2	-2.1	
42659	GL-I-33	-2.4	-9	-6.2	-12.2	-8.6	
42660	GL-I-38	-0.5	2.2	-13.1	-18.4	-11	
42661	GL-I-36	6.5	3.2	3.7	-8.1	-6.7	
42662	GL-I-43	5.3	-3.3	-16.6	-15.6	-6.5	
42663	GL-I-41	-9.3	-5.6	-11.4	43.6	2.6	
42664	GL-I-55	4.9	-7.9	-10	32.5	4.6	
42665	GL-I-54	5.1	-2.4	-10.6	22.5	-4.9	
42666	GL-I-77	11.4	-0.2	-19.9	38.2	2.6	
42667	GL-I-78	3.1	15.3	-16.6	14	-3.5	
50093	SH-I-044	-1.2	-14.1	-4	1.6	13.2	
50094	SH-I-047	-6.3	-11	9.5	-13.4	1.3	
50095	SH-I-060	2.5	-13.3	-4.7	1.5	-1.6	
50096	MP-III-058	3.1	4.3	-16	-8.1	2.7	
50097	SH-I-048A	-13	1	-9.3	-0.3	2.6	
50098	SH-I-048B	-16.3	4.3	4.8	3.7	6.6	
50099	SH-I-055	-5.6	25.2	22.6	12.2	3.4	
50101	YT-III-31	-2.7	-4.9	4.2	-1	4.6	
50102	YT-III-271	0	-7.3	-5.3	-8.4	10.9	
50103	SR-II-54	-17.9	3.5	5.6	-5.9	6.3	
50104	GL-II-73	-5.2	-2.9	1.4	4.8	11.7	
50105	GL-II-74	-1.8	4.2	-2	-13.7	-6.4	
50106	GL-II-75	0.9	-0.6	8.7	-13.6	-16.9	
50107	GL-II-76	-0.6	11.8	-4.8	-5.5	-10.1	
50108	GL-I-50	-8.2	1.7	-7.7	-8.8	-2.5	
50109	GL-II-93	-7.3	-4.1	-1.9	-5.6	-4.6	

50110	GL-I-65	-1.2	1.4	7.8	-17.7	-0.2	
50111	GL-I-81	16.2	5.6	-3.5	-11.7	-1.9	
50112	GL-III-19	2.8	0.9	-0.7	-14.3	8.6	
50114	GL-I-61	-8.2	0.8	-5.8	-2.8	15.2	
50117	GL-I-63	9.7	-5.4	-3.3	-1.5	23.6	
50120	GL-III-26	-3.5	-6.3	-3.7	1.7	12.7	
50121	GL-III-27	4.8	5.8	-6.6	2.1	-6.5	
50122	GL-III-59	10.9	13.8	-13.1	8.1	6.6	
50123	GL-III-57	-4.3	9.8	1.9	11	3.1	
50124	GL-III-58	-7.7	8.9	-5.8	13.2	5.8	
50125	GL-III-35	-0.5	7.7	23.9	10.4	11.2	
50126	GL-III-36	0.6	10.4	-9.6	-2.9	3.8	
50127	KRM-III-18A	-13.8	8.2	-10.4	6.3	10.1	
50128	GL-III-38	-15.3	0.8	-5.8	1.2	17	
50129	GL-III-72	-3.6	3.1	11.4	12.8	19.6	
50130	GL-III-73	-17.6	-0.6	0.7	-4.7	-7.4	
50132	GL-III-42	-18.2	5.1	3.9	-2.2	-14.4	
50133	GL-III-43	-14.1	-13.2	-6.1	8.3	-12.8	
50134	GL-III-52	-18.2	-4.5	-0.1	7.9	-10.8	
50135	GL-III-53	-17.1	15.3	-6.5	5.3	-11.8	
50136	GL-III-54	80.1	20.1	14.7	11.3	53.6	
50137	GL-III-60	73.5	-20	-18.5	13.2	48.5	
50138	GL-III-63	-3.7	19.4	-18.1	-17.3	-18	
50139	GL-III-64	56.2	-8.6	24.1	23.1	44.7	
50140	GL-III-66	40.5	-7.6	25.2	14.6	51.4	
50141	GL-III-67	4.7	1.1	40.5	27.7	59.6	
50142	GL-III-68	0.1	-5.5	62.4	15.4	50.1	

50143	GL-III-69	-9.3	-6.3	50.1	3.7	35.9	
50144	GL-III-70	-17	7.4	38.2	-5.7	21.7	
50145	GL-III-75	0.7	11	50	15.9	-0.6	
50146	GL-III-76	16.1	22.8	76.9	-8.3	16.4	
50147	GL-III-76A	5.9	17.2	-7.4	-12.5	57.6	
50148	GL-III-77	0.3	-17.6	11.3	17.6	7.8	
50149	GL-III-78	-1.8	-13.3	50	22.8	10.3	

Table 43. PDSP primary binding data for MOR, NET, NMDA, Oxytocin, PBR, and SERT.

Compound #	Name	MOR	NET	NMDA	Oxytocin	PBR	SERT
30611	SH-053-2'F-R-CH3	15.7(AVE)	-11.3		13.9	12.3(AVE)	-14.3
30612	SH-053-2'F-S-CH3	15.6(AVE)	-5.5		18.1	18.2(AVE)	-9.5
30613	MP-III-004	-2.2(AVE)	-14.2		42.1	30.1(AVE)	-12.5
30614	MP-III-021	2.1(AVE)	-11.8		16.8	25.5(AVE)	-9
30615	MP-III-019	2.7(AVE)	-22		15.9	22.5(AVE)	-4.2
30616	MP-III-018.A	8.8(AVE)	-6.4		7.6	1.9(AVE)	5.4
30617	MP-III-022	4.1(AVE)	-11.4		12.5	16.6(AVE)	-6.1
30618	MP-III-023	-5.7(AVE)	7.9		21.8	15.1(AVE)	-10
30619	SH-I-85	10.8(AVE)	-26.8		30.2	60.4(AVE)	1.1
37713	MP-III-068	24.8	-11.3			61.8	-12.7
37714	MP-III-080	-1.1	-3.4			84.8	-13.4
37715	MP-III-085	-4.3	-17.8			75.2	40.7
37717	SH-053-2'F-R-CH3-Acid	-9.2	11.4			12.8	-26.8
37718	SH-053-2'F-S-CH3-Acid	-2.5	38.9			17.7	2.1
37719	MP-III-018.B	2	38.5			22.3	-5.4

37720	MP-III-019.B	2	32.8			34.4	-2
37721	MP-IV-004	7	19			47.6	10.9
37722	GL-I-65	2.4	-8.1			30.2	-5.6
37723	MP-IV-005	20.6	27.2			38.2	13.3
37724	GL-I-66	28.1	19.7			49.7	23.7
37725	MP-IV-010	32.7	-2.2			27.7	21.7
37726	GL-I-81	63.7	5.8			-16.7	0
37728	SH-I-085	10.9	-12.1			80.3	6.4
37729	KRM-II-18B	10.9	-2.2			38.4	11.5
37730	KRM-II-73	10.5	16.6			67.9	3.5
37731	KRM-II-82	5.4	9.8			42.7	21.1
37732	KRM-II-97	18.1	26.6			93.4	0.7
37733	KRM-II-81	6.5	41.1			93.1	-9.1
37734	KRM-II-68	6.1	37.3			37.8	-3.7
37735	KRM-II-08	5	38.3			81.6	7.7
37736	KRM-II-3B	-12.3	39.4			66.5	33.4
42621	KRM-III-59	-0.6	-9.9			71.4	-11.3
42622	KRM-III-65	-5.9	-4			21.2	-14.5
42623	KRM-III-66	11.7	-9.7			59	-9.9
42624	KRM-III-67	30.4	1.2			26	-2.2
42625	KRM-III-79	32.4	-2.7			85.6	0.6
42626	KRM-III-70	5.1	-18.5			9.4	-15.2
42627	KRM-III-77	29.8	3.1			56	-9.7
42628	KRM-III-78	29	9.7			63.2	12.8
42633	Ro5-4846	19.1	-9.1			83.7	7.2
42634	Ro7-9277	-11.5	-11.5			73.2	9.2
42635	GL-I-74	-17.3	4			62.6	19.2

42636	GL-II-39	1.1	-5.7			86.7	14.6
42637	GL-II-05	5.5	-8.4			12	15.4
42638	GL-II-06	10.6	-1.6			76.4	15.2
42639	GL-II-18	25.4	20.4			39.3	24.3
42640	GL-II-19	16.6	-6.7			73.5	22
42641	GL-II-30	19.9	14.1			17.5	14.7
42642	GL-II-31	17.1	14			70.2	-3.3
42643	GL-II-32	31.7	13			50	3.6
42644	GL-II-33	-15	17.6			18.5	9.4
42645	GL-II-51	-11.6	23.4			20.8	0.1
42647	GL-II-53	-1.3	13.6			19.8	0.5
42648	GL-II-54	-10.7	9.5			97.2	6.1
42651	GL-II-57	11.7	11.6			14.1	11.1
42653	GL-II-59	8	4.1			5.7	17.1
42654	GL-II-60	6.5	12.1			7.4	18.2
42655	GL-II-61	2.1	23.5			-5.3	19.3
42656	GL-I-30	53.7	16.4			28.9	0
42657	GL-I-31	31.6	0.1			16.8	4.7
42658	GL-I-32	9.2	2.6			16.4	7.4
42659	GL-I-33	30.2	11.3			74.7	4.1
42660	GL-I-38	18	-4.8			22.9	1.2
42661	GL-I-36	8.1	4.3			12.1	4.3
42662	GL-I-43	22	-2.6			13	4.2
42663	GL-I-41	40.2	5			27.2	3.8
42664	GL-I-55	16.6	-1.2			8.1	17.9
42665	GL-I-54	17.9	12.3			-2.1	19.7
42666	GL-I-77	41.3	22.3			33.7	18.9

42667	GL-I-78	31.9	-13.3			83.4	21.9
50093	SH-I-044	7.5	33.2	69.2	-0.9	15	18.9
50094	SH-I-047	16.4	-5.4	68.4	3.1	33.3	-7.4
50095	SH-I-060	9.8	44.4	54	32.1	28.2	14.6
50096	MP-III-058	-3.8	-1.9	-0.1	18.9	63.3	5.6
50097	SH-I-048A	-7.2	19.4	-0.2	-6.3	7	3.4
50098	SH-I-048B	0.3	-4.7	5.1	3.6	21.5	12.9
50099	SH-I-055	21.3	24.3	9.3	16.5	1.1	1.1
50101	YT-III-31	17.5	9	-6.8	13.1	-6.5	-24.3
50102	YT-III-271	24.1	-0.4	2.8	12.5	3.6	-17.4
50103	SR-II-54	7.6	24.1	13.8	13.3	7.2	-19.7
50104	GL-II-73	5.8	4.6	31.8	7.8	8.7	-20.7
50105	GL-II-74	10.2	11.8	21	8.9	28.8	-13.6
50106	GL-II-75	-9.3	-2.1	13	45.1	11.5	6.4
50107	GL-II-76	-0.8	-2.4	-11.6	29.7	-13.9	21.8
50108	GL-I-50	0.7	10.8	13.9	0	-11.4	35.7
50109	GL-II-93	-0.3	2	20.2	-1	-19.9	26.1
50110	GL-I-65	0.9	1.5	37.9	5.8	7.9	7.4
50111	GL-I-81	29.9	17.9	15.8	9.3	1.3	-6.5
50112	GL-III-19	-4.9	4.4	44.1	-1.7	-2.1	-9.8
50114	GL-I-61	24.4	38.9	30.1	9.7	29	3.4
50117	GL-I-63	21.6	31	22.3	8.8	10.7	25.9
50120	GL-III-26	16.7	20.9	31.7	27.9	25	28
50121	GL-III-27	-8.4	-4.7	31.8	15.7	5.1	27.1
50122	GL-III-59	0	0.7	16.5	20.1	3.7	46.6
50123	GL-III-57	-10.7	22.9	25.7	13	34	41
50124	GL-III-58	8.7	-0.4	36.6	-0.7	-4.8	35.1

50125	GL-III-35	4.1	-0.5	5.2	2.3	3.3	19.9
50126	GL-III-36	-4.1	17.6	30.8	7.3	40	27.2
50127	KRM-III-18A	-9.9	4.4	39.1	11.9	43.3	8.5
50128	GL-III-38	10.1	3.8	7.2	10.3	7.7	4.6
50129	GL-III-72	25.1	49.7	16.2	20.5	7.5	33.3
50130	GL-III-73	12.1	-6.2	45	3.8	33.5	-5.4
50132	GL-III-42	-7.9	-8.5	38.7	8.6	72.1	-1
50133	GL-III-43	-16.6	2	-6	9.2	40.5	-4.6
50134	GL-III-52	-5.5	9.7	22.9		6.8	-7.4
50135	GL-III-53	-9.1	-6.4	5.7		-9.5	-3.5
50136	GL-III-54	-2	-7.9	-11.8		44.7	-1.1
50137	GL-III-60	25.7	29	-10.2		61	-2.4
50138	GL-III-63	8.1	16.7	7.7		60	-3.6
50139	GL-III-64	6.6	8	33.6		55.1	-15
50140	GL-III-66	-17.4	9.1	43.2		24.5	-15.2
50141	GL-III-67	-4.4	10.2	46.7		29.5	-16.4
50142	GL-III-68	-4.5	22.6	48.3		61	-5.1
50143	GL-III-69	-3.5	20.7	-13.8		25	-4.5
50144	GL-III-70	-16.9	27	-18.6		33.1	-10.6
50145	GL-III-75	-8.7	22.2	-2.3		32.7	-17.6
50146	GL-III-76	3.2	29.7	-2.1		25	-12.7
50147	GL-III-76A	8	-8.5	-10.1		10.2	1.8
50148	GL-III-77	37.1	58.9	-14.4		12.6	44
50149	GL-III-78	10.4	21	43		2.6	-4.7

Table 44. PDSP primary binding data for Sigma 1, Sigma 1 GP, Sigma 2, Sigma 2 PC12, V1A, V1B, and V2.

Compound #	Name	Sigma 1	Sigma 1 GP	Sigma 2	Sigma 2 PC12	V1A	V1B	V2
30611	SH-053-2'F-R-CH3		-5.3(AVE)		-2.8	9.2	31.3	2
30612	SH-053-2'F-S-CH3		-3.0(AVE)		-5.0	10.7	32.3	7.5
30613	MP-III-004		7.5(AVE)		-7.1	4.7	18.1	5.6
30614	MP-III-021		8.9(AVE)		5.5	9.7	13.2	9.1
30615	MP-III-019		3.2(AVE)		-22.5(AVE)	7.1	10	6.6
30616	MP-III-018.A		-0.7(AVE)		-8.4	17.4	-2.5	8.6
30617	MP-III-022		-8.1(AVE)		-7.6	5.4	17.9	15.7
30618	MP-III-023		-15.3(AVE)		-9.9	10	23.1	14.1
30619	SH-I-85		-12.7(AVE)		30.3	14.6	44.7	4.2
37713	MP-III-068		25.5		-16.6			
37714	MP-III-080		36.3		24.1			
37715	MP-III-085		25		59.1			
37717	SH-053-2'F-R-CH3-Acid		0.5		-3.3			
37718	SH-053-2'F-S-CH3-Acid		12.6		-3.8			
37719	MP-III-018.B		18.5		11.6			
37720	MP-III-019.B		28		26.2			
37721	MP-IV-004		22.2		62.4			
37722	GL-I-65	28.1						
37723	MP-IV-005		25.3		63.2			
37724	GL-I-66		23.8		64.8			
37725	MP-IV-010		34.9		64.2			
37726	GL-I-81	5						
37728	SH-I-085		11.6		44.8			
37729	KRM-II-18B		-1.5		45.8			

37730	KRM-II-73		6.3		58.1			
37731	KRM-II-82		-5.5		47.5			
37732	KRM-II-97		-13.1		30.7			
37733	KRM-II-81		-14.9		34.5			
37734	KRM-II-68		-8.2		14.9			
37735	KRM-II-08		-6.3		41.5			
37736	KRM-II-3B		17.5		54.6			
42621	KRM-III-59	29		39.5				
42622	KRM-III-65	87.6		24.7				
42623	KRM-III-66	92.4		70.1				
42624	KRM-III-67	33.8		67.5				
42625	KRM-III-79	-7.2		45.1				
42626	KRM-III-70	88.6		20.4				
42627	KRM-III-77	74.9		13.8				
42628	KRM-III-78	88.6		41.7				
42633	Ro5-4846	18.7		34.9				
42634	Ro7-9277	34.4		9.4				
42635	GL-I-74	6.4		30.7				
42636	GL-II-39	50		29.4				
42637	GL-II-05	4.1		13.7				
42638	GL-II-06	24.8		33.6				
42639	GL-II-18	50		63.9				
42640	GL-II-19	-14.3		30.9				
42641	GL-II-30	-5.7		-16				
42642	GL-II-31	94.1		-12				
42643	GL-II-32	-3		15.7				
42644	GL-II-33	-8.7		60				

42645	GL-II-51	-17.5		-0.9				
42647	GL-II-53	-12.7		29.6				
42648	GL-II-54	1.1		58.9				
42651	GL-II-57	3.2		50.3				
42653	GL-II-59	-12.3		28.3				
42654	GL-II-60	-8.4		39.2				
42655	GL-II-61	-5.1		16				
42656	GL-I-30	-0.4		72.3				
42657	GL-I-31	10.4		55.6				
42658	GL-I-32	17.4		65				
42659	GL-I-33	6		67.3				
42660	GL-I-38	7.2		46.7				
42661	GL-I-36	-2.7		26.3				
42662	GL-I-43	12.4		35.2				
42663	GL-I-41	-1		44.9				
42664	GL-I-55	0.3		40.9				
42665	GL-I-54	-3		26.9				
42666	GL-I-77	-4.7		60.9				
42667	GL-I-78	9.6		67.1				
50093	SH-I-044	0.2		28.7				
50094	SH-I-047	11.8		53.7				
50095	SH-I-060	26.8		73.3				
50096	MP-III-058	-4.1		42.5				
50097	SH-I-048A	7		38.3				
50098	SH-I-048B	7		40.6				
50099	SH-I-055	21.7		75.5				
50101	YT-III-31	9		18.3				

50102	YT-III-271	10.5		33.7				
50103	SR-II-54	1.4		10.5				
50104	GL-II-73	12.2		18.4		2.9	16.4	
50105	GL-II-74	19.6		45.6		27.7	-7.8	
50106	GL-II-75	16.1		53		10.4	2.6	
50107	GL-II-76	13		33.5		5.5	-1.3	
50108	GL-I-50	18		-9.4		6.3	-0.7	
50109	GL-II-93	11.2		1.6		19.6	-1.5	
50110	GL-I-65	25.8		52.4		11.9	-1.6	
50111	GL-I-81	30.7		69.2		11.5	2.2	
50112	GL-III-19	5		39.9		12	6.2	
50114	GL-I-61	33.5		75.8		22.3	10.2	
50117	GL-I-63	36		74.6		16.2	-2.9	
50120	GL-III-26	44.3		54.3		-2.7	-3.7	
50121	GL-III-27	40.4		3.7		0.2	2.4	
50122	GL-III-59	27.7		6.4		23.5	1	
50123	GL-III-57	47.2		50.5		13.1	6.7	
50124	GL-III-58	28		5.9		8.3	4.3	
50125	GL-III-35	25.1		33.6		2.5	9.8	
50126	GL-III-36	40.8		68.4		7.1	3	
50127	KRM-III-18A	43.2		72.8		6.8	11.2	
50128	GL-III-38	26		39.3		6.6	10.8	
50129	GL-III-72	44.8		85.5		8.9	-16.6	
50130	GL-III-73	41.9		68.7		4.5	-7.5	
50132	GL-III-42	34.5		82.3		15.8	2.7	
50133	GL-III-43	27.2		43.8		23.7	4.3	
50134	GL-III-52	39.8		49.5		23.1	8.8	

50135	GL-III-53	37.1		29.9		17.2	7.2	
50136	GL-III-54	3.5		-44.2		8.9	3.6	
50137	GL-III-60	81.1		76.4		13.9	0.4	
50138	GL-III-63	64.3		36.6		13.5	4.9	
50139	GL-III-64	46.3		35.3		41.7	12.9	
50140	GL-III-66	9.2		-9		23.9	3.4	
50141	GL-III-67	-0.8		9.3		-0.3	6.8	
50142	GL-III-68	-13.6		48.5		5.4	10.8	
50143	GL-III-69	-13.7		24.3		17	12.9	
50144	GL-III-70	5		32.4		5.2	11.2	
50145	GL-III-75	17.6		25		17.3	9.7	
50146	GL-III-76	25.7		47.6		2.5	7.5	
50147	GL-III-76A	13		13.7		3.1	1.7	
50148	GL-III-77	26.4		49.1		14.6	7.2	
50149	GL-III-78	10.8		34.1		27.7	-13.5	

Table 45. PDSP secondary binding data for 5-HT1A, 5-HT1B, 5-HT1D, 5-ht1e, 5-HT2A, and 5-HT2B.

Compound #	Name	5-HT1A	5-HT1B	5-HT1D	5-ht1e	5-HT2A	5-HT2B
30611	SH-053-2'F-R-CH3						
30612	SH-053-2'F-S-CH3						
30613	MP-III-004						
30614	MP-III-021						
30615	MP-III-019						>10,000
30616	MP-III-018.A						
30617	MP-III-022						
30618	MP-III-023						

30619	SH-I-85						>10,000
37713	MP-III-068						
37714	MP-III-080						
37715	MP-III-085						
37717	SH-053-2'F-R-CH3-Acid						
37718	SH-053-2'F-S-CH3-Acid						
37719	MP-III-018.B						
37720	MP-III-019.B						
37721	MP-IV-004						
37722	GL-I-65						
37723	MP-IV-005						
37724	GL-I-66						
37725	MP-IV-010						
37726	GL-I-81						5,927.00
37728	SH-I-085						
37729	KRM-II-18B	3,372.0(AVE)					
37730	KRM-II-73						
37731	KRM-II-82	2,383.7(AVE)					
37732	KRM-II-97						
37733	KRM-II-81						
37734	KRM-II-68						
37735	KRM-II-08						
37736	KRM-II-3B						852.5(AVE)
42621	KRM-III-59						

42622	KRM-III-65						
42623	KRM-III-66						
42624	KRM-III-67						
42625	KRM-III-79						
42626	KRM-III-70						
42627	KRM-III-77						
42628	KRM-III-78						
42633	Ro5-4846						
42634	Ro7-9277						
42635	GL-I-74						
42636	GL-II-39						
42637	GL-II-05						
42638	GL-II-06						
42639	GL-II-18						
42640	GL-II-19						
42641	GL-II-30						
42642	GL-II-31						
42643	GL-II-32						
42644	GL-II-33						
42645	GL-II-51						
42647	GL-II-53						
42648	GL-II-54						
42651	GL-II-57						
42653	GL-II-59						
42654	GL-II-60						
42655	GL-II-61						
42656	GL-I-30						

42657	GL-I-31						
42658	GL-I-32						
42659	GL-I-33						
42660	GL-I-38						
42661	GL-I-36						
42662	GL-I-43						
42663	GL-I-41						
42664	GL-I-55						
42665	GL-I-54						
42666	GL-I-77						
42667	GL-I-78						
50093	SH-I-044						
50094	SH-I-047						
50095	SH-I-060					1,809.5(AVE)	
50096	MP-III-058						
50097	SH-I-048A						
50098	SH-I-048B						
50099	SH-I-055			6,471.0(AVE)		885	
50101	YT-III-31						
50102	YT-III-271			6,631.5(AVE)			
50103	SR-II-54			2,838.0(AVE)			
50104	GL-II-73						
50105	GL-II-74						
50106	GL-II-75						

50107	GL-II-76						
50108	GL-I-50						
50109	GL-II-93						
50110	GL-I-65						
50111	GL-I-81			2,876.5(AVE)			
50112	GL-III-19						
50114	GL-I-61						
50117	GL-I-63					6,365.00	
50120	GL-III-26						
50121	GL-III-27						
50122	GL-III-59						
50123	GL-III-57						
50124	GL-III-58						
50125	GL-III-35						
50126	GL-III-36						
50127	KRM-III-18A				10,000.0(AVE)		
50128	GL-III-38						
50129	GL-III-72					1,416.00	
50130	GL-III-73						
50132	GL-III-42						
50133	GL-III-43						
50134	GL-III-52						
50135	GL-III-53					>10,000	
50136	GL-III-54						
50137	GL-III-60						
50138	GL-III-63						

50139	GL-III-64						
50140	GL-III-66						
50141	GL-III-67						
50142	GL-III-68						
50143	GL-III-69						
50144	GL-III-70						
50145	GL-III-75						
50146	GL-III-76						
50147	GL-III-76A						
50148	GL-III-77		3172	2,216.0(AVE)		838	3,694.00
50149	GL-III-78						

Table 46. PDSP secondary binding data for 5-HT2C, 5-HT3, 5-ht5a, 5-HT6, 5-HT7, and Alpha1A.

Compound #	Name	5-HT2C	5-HT3	5-ht5a	5-HT6	5-HT7	Alpha1A
30611	SH-053-2'F-R-CH3						
30612	SH-053-2'F-S-CH3						
30613	MP-III-004						
30614	MP-III-021						
30615	MP-III-019						
30616	MP-III-018.A						
30617	MP-III-022						
30618	MP-III-023						
30619	SH-I-85						

37713	MP-III-068						
37714	MP-III-080	3,660.0(AVE)					
37715	MP-III-085						
37717	SH-053-2'F-R-CH3-Acid						
37718	SH-053-2'F-S-CH3-Acid						
37719	MP-III-018.B						
37720	MP-III-019.B						
37721	MP-IV-004						
37722	GL-I-65						
37723	MP-IV-005						
37724	GL-I-66						
37725	MP-IV-010						
37726	GL-I-81						
37728	SH-I-085						
37729	KRM-II-18B						
37730	KRM-II-73						
37731	KRM-II-82						
37732	KRM-II-97						
37733	KRM-II-81						
37734	KRM-II-68						
37735	KRM-II-08						
37736	KRM-II-3B	1,643.7(AVE)					
42621	KRM-III-59						
42622	KRM-III-65						

42623	KRM-III-66						
42624	KRM-III-67						
42625	KRM-III-79						
42626	KRM-III-70						
42627	KRM-III-77						
42628	KRM-III-78						
42633	Ro5-4846						
42634	Ro7-9277						
42635	GL-I-74						
42636	GL-II-39						
42637	GL-II-05						
42638	GL-II-06						
42639	GL-II-18						
42640	GL-II-19						
42641	GL-II-30						
42642	GL-II-31						
42643	GL-II-32						
42644	GL-II-33						
42645	GL-II-51						
42647	GL-II-53						
42648	GL-II-54						
42651	GL-II-57						
42653	GL-II-59						
42654	GL-II-60						
42655	GL-II-61						
42656	GL-I-30						
42657	GL-I-31						

42658	GL-I-32						
42659	GL-I-33						
42660	GL-I-38						
42661	GL-I-36						
42662	GL-I-43						
42663	GL-I-41						
42664	GL-I-55						
42665	GL-I-54		>10,000				
42666	GL-I-77						
42667	GL-I-78						
50093	SH-I-044						
50094	SH-I-047						
50095	SH-I-060						
50096	MP-III-058						
50097	SH-I-048A						
50098	SH-I-048B						
50099	SH-I-055						
50101	YT-III-31						
50102	YT-III-271						
50103	SR-II-54						
50104	GL-II-73						
50105	GL-II-74		10,000.0(AVE)				
50106	GL-II-75						
50107	GL-II-76						
50108	GL-I-50						
50109	GL-II-93						
50110	GL-I-65						

50111	GL-I-81						
50112	GL-III-19						
50114	GL-I-61						
50117	GL-I-63						
50120	GL-III-26		10,000.0(AVE)				8,239.00
50121	GL-III-27					6,499.5(AVE)	
50122	GL-III-59						>10,000
50123	GL-III-57					2652	>10,000
50124	GL-III-58						>10,000
50125	GL-III-35						5,616.00
50126	GL-III-36						6,150.00
50127	KRM-III-18A						4,745.00
50128	GL-III-38						7,686.00
50129	GL-III-72						946
50130	GL-III-73						
50132	GL-III-42						
50133	GL-III-43						
50134	GL-III-52						
50135	GL-III-53						
50136	GL-III-54						
50137	GL-III-60						
50138	GL-III-63						
50139	GL-III-64						
50140	GL-III-66						
50141	GL-III-67						
50142	GL-III-68				2,089.00		

50143	GL-III-69						
50144	GL-III-70						
50145	GL-III-75						
50146	GL-III-76						
50147	GL-III-76A						
50148	GL-III-77						>10,000
50149	GL-III-78						

Table 47. PDSP secondary binding data for Alpha1D, Alpha2A, Alpha2B, Alpha2C, Beta1, and Beta2.

Compound #	Name	Alpha1D	Alpha2A	Alpha2B	Alpha2C	Beta1	Beta2
30611	SH-053-2'F-R-CH3						
30612	SH-053-2'F-S-CH3					7,214.00	
30613	MP-III-004						
30614	MP-III-021					>10,000	
30615	MP-III-019					>10,000	
30616	MP-III-018.A					>10,000	
30617	MP-III-022						
30618	MP-III-023				>10,000		
30619	SH-I-85						
37713	MP-III-068						
37714	MP-III-080						
37715	MP-III-085						
37717	SH-053-2'F-R-CH3-Acid						>10,000

37718	SH-053-2'F-S-CH3-Acid						
37719	MP-III-018.B						
37720	MP-III-019.B						
37721	MP-IV-004						
37722	GL-I-65						
37723	MP-IV-005						
37724	GL-I-66						
37725	MP-IV-010						
37726	GL-I-81						
37728	SH-I-085						
37729	KRM-II-18B						
37730	KRM-II-73			4,565.7(AVE)			
37731	KRM-II-82						
37732	KRM-II-97			834.3(AVE)			
37733	KRM-II-81			2,876.7(AVE)			
37734	KRM-II-68						
37735	KRM-II-08						
37736	KRM-II-3B						
42621	KRM-III-59			1,059.00			
42622	KRM-III-65						
42623	KRM-III-66			845			
42624	KRM-III-67						
42625	KRM-III-79						
42626	KRM-III-70						
42627	KRM-III-77						
42628	KRM-III-78			293			

42633	Ro5-4846						
42634	Ro7-9277						
42635	GL-I-74						
42636	GL-II-39						
42637	GL-II-05						
42638	GL-II-06			313			
42639	GL-II-18		3,837.00				
42640	GL-II-19						
42641	GL-II-30						
42642	GL-II-31						
42643	GL-II-32						
42644	GL-II-33						
42645	GL-II-51						
42647	GL-II-53						
42648	GL-II-54						
42651	GL-II-57						
42653	GL-II-59						
42654	GL-II-60						
42655	GL-II-61						
42656	GL-I-30						
42657	GL-I-31						
42658	GL-I-32						
42659	GL-I-33						
42660	GL-I-38						
42661	GL-I-36						
42662	GL-I-43						
42663	GL-I-41						

42664	GL-I-55						
42665	GL-I-54						
42666	GL-I-77						
42667	GL-I-78			1,785.00			
50093	SH-I-044						
50094	SH-I-047						
50095	SH-I-060			774	10,000.0(AVE)		
50096	MP-III-058						
50097	SH-I-048A						
50098	SH-I-048B						
50099	SH-I-055						
50101	YT-III-31						
50102	YT-III-271						
50103	SR-II-54						
50104	GL-II-73						
50105	GL-II-74						
50106	GL-II-75						
50107	GL-II-76						
50108	GL-I-50						
50109	GL-II-93						
50110	GL-I-65						
50111	GL-I-81						
50112	GL-III-19						
50114	GL-I-61						
50117	GL-I-63				10,000.0(AVE)		
50120	GL-III-26						
50121	GL-III-27						

50122	GL-III-59						
50123	GL-III-57						
50124	GL-III-58						
50125	GL-III-35						
50126	GL-III-36						
50127	KRM-III-18A			149.5(AVE)	8,411.3(AVE)		
50128	GL-III-38						
50129	GL-III-72		2,278.00	1,027.5(AVE)	10,000.0(AVE)		
50130	GL-III-73						
50132	GL-III-42						
50133	GL-III-43						
50134	GL-III-52						
50135	GL-III-53						
50136	GL-III-54						
50137	GL-III-60						
50138	GL-III-63						
50139	GL-III-64			1,530.0(AVE)			
50140	GL-III-66						
50141	GL-III-67		7,941.00	10,000.0(AVE)			
50142	GL-III-68						
50143	GL-III-69			1,701.0(AVE)			
50144	GL-III-70						
50145	GL-III-75						
50146	GL-III-76						
50147	GL-III-76A			310.0(AVE)			
50148	GL-III-77	1,686.00	1,566.00	1,670.0(AVE)	6,076.8(AVE)		
50149	GL-III-78						

Table 48. PDSP secondary binding data for Beta3, BZP Rat Brain Site, D1, D3, D5, and DAT.

Compound #	Name	Beta3	BZP Rat Brain Site	D1	D3	D5	DAT
30611	SH-053-2'F-R-CH3		379				>10,000
30612	SH-053-2'F-S-CH3		111				>10,000
30613	MP-III-004		445				
30614	MP-III-021		219				
30615	MP-III-019		3,246.00				6,482.00
30616	MP-III-018.A		139				5,857.00
30617	MP-III-022		83				>10,000
30618	MP-III-023		37				>10,000
30619	SH-I-85		11				>10,000
37713	MP-III-068		244.7(AVE)				
37714	MP-III-080		263.3(AVE)				
37715	MP-III-085		339.0(AVE)				
37717	SH-053-2'F-R-CH3-Acid		32.3(AVE)				
37718	SH-053-2'F-S-CH3-Acid		52.7(AVE)				
37719	MP-III-018.B		27.7(AVE)				
37720	MP-III-019.B		88.3(AVE)				
37721	MP-IV-004		941.0(AVE)				
37722	GL-I-65		1,147.00				

37723	MP-IV-005		710.0(AVE)				
37724	GL-I-66		589.0(AVE)				
37725	MP-IV-010		1,051.0(AVE)				
37726	GL-I-81		839				
37728	SH-I-085		10.8(AVE)				
37729	KRM-II-18B		38				
37730	KRM-II-73		56.0(AVE)				
37731	KRM-II-82		134.7(AVE)				
37732	KRM-II-97		150.3(AVE)				
37733	KRM-II-81		382.0(AVE)				
37734	KRM-II-68		475.7(AVE)				
37735	KRM-II-08		6.4(AVE)				
37736	KRM-II-3B		1,114.0(AVE)				
42621	KRM-III-59		20				
42622	KRM-III-65		45				
42623	KRM-III-66		49				
42624	KRM-III-67		144				
42625	KRM-III-79		308				
42626	KRM-III-70		157				
42627	KRM-III-77		6.6				
42628	KRM-III-78		157				
42633	Ro5-4846		4,284.00				
42634	Ro7-9277						
42635	GL-I-74		4,797.00				
42636	GL-II-39						
42637	GL-II-05		1,237.00				

42638	GL-II-06		556				
42639	GL-II-18		>10,000				
42640	GL-II-19		1,143.00				
42641	GL-II-30		431				
42642	GL-II-31		1,697.00				
42643	GL-II-32		1,427.00				6062
42644	GL-II-33		36				>10,000
42645	GL-II-51		181				>10,000
42647	GL-II-53		1,041.00				
42648	GL-II-54		2,037.00				
42651	GL-II-57		54				
42653	GL-II-59		43				
42654	GL-II-60		57				
42655	GL-II-61		485				
42656	GL-I-30		177				
42657	GL-I-31		245				2,094.0(AVE)
42658	GL-I-32		148				
42659	GL-I-33		117				
42660	GL-I-38		127				
42661	GL-I-36		418				
42662	GL-I-43		44				
42663	GL-I-41		140				
42664	GL-I-55		20				
42665	GL-I-54		90				
42666	GL-I-77		124				
42667	GL-I-78		352				
50093	SH-I-044		1,195.00				

50094	SH-I-047		238				
50095	SH-I-060	353	1,958.00			2,967.00	
50096	MP-III-058		290				
50097	SH-I-048A	6125	3.3				
50098	SH-I-048B		96				
50099	SH-I-055	1671	1,662.00			4,425.00	
50101	YT-III-31		45				>10,000
50102	YT-III-271		36				
50103	SR-II-54		69				
50104	GL-II-73		506				
50105	GL-II-74		68				>10,000
50106	GL-II-75		93				
50107	GL-II-76						
50108	GL-I-50						
50109	GL-II-93		86				
50110	GL-I-65						
50111	GL-I-81		780				
50112	GL-III-19		23				
50114	GL-I-61		1,368.00			4,759.00	
50117	GL-I-63		501		2,726.00		
50120	GL-III-26		1,350.00		>10,000		
50121	GL-III-27		250				
50122	GL-III-59		19				
50123	GL-III-57		665				
50124	GL-III-58		60				
50125	GL-III-35		311				
50126	GL-III-36		319				

50127	KRM-III-18A		3,148.00				
50128	GL-III-38		1,146.00				
50129	GL-III-72	2,814.00	748		1,714.00		
50130	GL-III-73		602				>10,000
50132	GL-III-42		726				
50133	GL-III-43						
50134	GL-III-52		233				
50135	GL-III-53		449				
50136	GL-III-54		42				>10,000
50137	GL-III-60		784				
50138	GL-III-63			3,523.00			
50139	GL-III-64		1,490.00				
50140	GL-III-66		271				
50141	GL-III-67		116				
50142	GL-III-68		452				
50143	GL-III-69		647.5(AVE)				
50144	GL-III-70		3,395.00				
50145	GL-III-75		114				
50146	GL-III-76		120				
50147	GL-III-76A		4,026.00				
50148	GL-III-77		1,608.00	>10,000		1,271.00	>10,000
50149	GL-III-78		261				

Table 49. PDSP secondary binding data for DOR, H1, H2, H3 , H4, and HERG binding.

Compound #	Name	DOR	H1	H2	H3	H4	HERG binding

30611	SH-053-2'F-R-CH3						
30612	SH-053-2'F-S-CH3		>10,000				
30613	MP-III-004						
30614	MP-III-021						
30615	MP-III-019		>10,000				
30616	MP-III-018.A		>10,000				
30617	MP-III-022						
30618	MP-III-023						
30619	SH-I-85						
37713	MP-III-068						
37714	MP-III-080		8,737.0(AVE)				
37715	MP-III-085		9,169.8(AVE)				
37717	SH-053-2'F-R-CH3-Acid		10,000.0(AVE)				
37718	SH-053-2'F-S-CH3-Acid		8,480.8(AVE)				
37719	MP-III-018.B		924.3(AVE)				

37720	MP-III-019.B		10,000.0(AVE)				
37721	MP-IV-004						
37722	GL-I-65						
37723	MP-IV-005						
37724	GL-I-66						
37725	MP-IV-010						
37726	GL-I-81						
37728	SH-I-085						
37729	KRM-II-18B						
37730	KRM-II-73						
37731	KRM-II-82						
37732	KRM-II-97						
37733	KRM-II-81						
37734	KRM-II-68			3,516.00			
37735	KRM-II-08		9,333.3(AVE)				
37736	KRM-II-3B		1.2				
42621	KRM-III-59						
42622	KRM-III-65						

42623	KRM-III-66						
42624	KRM-III-67						
42625	KRM-III-79						
42626	KRM-III-70						
42627	KRM-III-77						
42628	KRM-III-78						
42633	Ro5-4846						
42634	Ro7-9277						
42635	GL-I-74						
42636	GL-II-39						
42637	GL-II-05						
42638	GL-II-06						
42639	GL-II-18	2,313.0(AVE)					>10,000
42640	GL-II-19						
42641	GL-II-30						
42642	GL-II-31						
42643	GL-II-32						
42644	GL-II-33						
42645	GL-II-51						
42647	GL-II-53						
42648	GL-II-54						
42651	GL-II-57						
42653	GL-II-59						

42654	GL-II-60						
42655	GL-II-61						
42656	GL-I-30					5,818.0(AVE)	
42657	GL-I-31						
42658	GL-I-32			1,208.00			
42659	GL-I-33						
42660	GL-I-38						
42661	GL-I-36						
42662	GL-I-43						
42663	GL-I-41						
42664	GL-I-55						
42665	GL-I-54						
42666	GL-I-77						
42667	GL-I-78			2,278.00			
50093	SH-I-044						
50094	SH-I-047						
50095	SH-I-060						1,658.00
50096	MP-III-058						
50097	SH-I-048A						
50098	SH-I-048B						
50099	SH-I-055						1,268.00
50101	YT-III-31					4,775.7(AVE)	
50102	YT-III-271						
50103	SR-II-54						

50104	GL-II-73						>10,000
50105	GL-II-74						>10,000
50106	GL-II-75						>10,000
50107	GL-II-76						
50108	GL-I-50						
50109	GL-II-93						8,223.3(AVE)
50110	GL-I-65						
50111	GL-I-81						
50112	GL-III-19						
50114	GL-I-61			3,692.00			
50117	GL-I-63			>10,000			>10,000
50120	GL-III-26	1,168.8(AVE)		4,183.00			
50121	GL-III-27						
50122	GL-III-59						
50123	GL-III-57						
50124	GL-III-58						
50125	GL-III-35						
50126	GL-III-36						
50127	KRM-III-18A						
50128	GL-III-38						
50129	GL-III-72	3,152.0(AVE)		2,301.00			
50130	GL-III-73			7,991.00			
50132	GL-III-42						
50133	GL-III-43						
50134	GL-III-52						
50135	GL-III-53						

50136	GL-III-54						
50137	GL-III-60		6,387.00				
50138	GL-III-63					1,445.5(AVE)	
50139	GL-III-64		3,164.00				
50140	GL-III-66						
50141	GL-III-67						
50142	GL-III-68		543	413			
50143	GL-III-69						
50144	GL-III-70						
50145	GL-III-75						
50146	GL-III-76						
50147	GL-III-76A						
50148	GL-III-77	2,315.5(AVE)	1,492.00	1,108.00			659
50149	GL-III-78						

Table 50. PDSP secondary binding data for KOR, M1, M2, M3, M4, M5 and mGlur5.

Compound #	Name	KOR	M1	M2	M3	M4	M5	mGlur5
30611	SH-053-2'F-R-CH3	240						
30612	SH-053-2'F-S-CH3	90						
30613	MP-III-004	599						
30614	MP-III-021	122						
30615	MP-III-019	3,367.00						
30616	MP-III-018.A	1,182.00				>10,000		1,358.0(AVE)
30617	MP-III-022	381						

30618	MP-III-023	119						
30619	SH-I-85	162						
37713	MP-III-068							
37714	MP-III-080							
37715	MP-III-085							
37717	SH-053-2'F-R-CH3-Acid							
37718	SH-053-2'F-S-CH3-Acid							
37719	MP-III-018.B	3,072.0(AVE)		10,000.0(AVE)				
37720	MP-III-019.B	2,621.0(AVE)		10,000.0(AVE)				
37721	MP-IV-004	637.0(AVE)						
37722	GL-I-65	222						
37723	MP-IV-005	379.5(AVE)						
37724	GL-I-66	295.5(AVE)		10,000.0(AVE)				
37725	MP-IV-010	149.0(AVE)						
37726	GL-I-81	127						
37728	SH-I-085	219.5(AVE)						
37729	KRM-II-18B	375.5(AVE)						
37730	KRM-II-73	900.5(AVE)					10,000.0(AVE)	
37731	KRM-II-82	1,084.0(AVE)						
37732	KRM-II-97	2,102.5(AVE)						
37733	KRM-II-81							

37734	KRM-II-68							
37735	KRM-II-08	713.0(AVE)						
37736	KRM-II-3B	3,627.0(AVE)						
42621	KRM-III-59	408						
42622	KRM-III-65	879						
42623	KRM-III-66	756						
42624	KRM-III-67							
42625	KRM-III-79							
42626	KRM-III-70							
42627	KRM-III-77	921						
42628	KRM-III-78							
42633	Ro5-4846	1,323.00						
42634	Ro7-9277							
42635	GL-I-74	1,404.00						
42636	GL-II-39							
42637	GL-II-05							
42638	GL-II-06	401						
42639	GL-II-18							
42640	GL-II-19							
42641	GL-II-30							
42642	GL-II-31							
42643	GL-II-32							
42644	GL-II-33	193						
42645	GL-II-51							
42647	GL-II-53	680						
42648	GL-II-54	504						

42651	GL-II-57	59						
42653	GL-II-59	90						
42654	GL-II-60	239						
42655	GL-II-61							
42656	GL-I-30	27						
42657	GL-I-31	65						
42658	GL-I-32	64						
42659	GL-I-33	34						
42660	GL-I-38	68						
42661	GL-I-36	411						
42662	GL-I-43	102						
42663	GL-I-41	39						
42664	GL-I-55	150						
42665	GL-I-54	788						
42666	GL-I-77	125						
42667	GL-I-78	48						
50093	SH-I-044							
50094	SH-I-047	110.0(AVE)						
50095	SH-I-060							
50096	MP-III-058	249.0(AVE)						
50097	SH-I-048A							
50098	SH-I-048B	63.5(AVE)						
50099	SH-I-055							
50101	YT-III-31	3,434.3(AVE)						
50102	YT-III-271	451.5(AVE)						
50103	SR-II-54							

50104	GL-II-73	1,402.0(AVE)						
50105	GL-II-74	228.5(AVE)						
50106	GL-II-75	353.5(AVE)						
50107	GL-II-76	418.0(AVE)						
50108	GL-I-50							
50109	GL-II-93							
50110	GL-I-65	362.5(AVE)						
50111	GL-I-81	752.0(AVE)						
50112	GL-III-19	264.5(AVE)						
50114	GL-I-61							
50117	GL-I-63							
50120	GL-III-26							
50121	GL-III-27							
50122	GL-III-59							
50123	GL-III-57							
50124	GL-III-58							
50125	GL-III-35	912.0(AVE)						
50126	GL-III-36	252.5(AVE)						
50127	KRM-III-18A	2,397.5(AVE)						
50128	GL-III-38							
50129	GL-III-72							
50130	GL-III-73	452.0(AVE)						
50132	GL-III-42	213.0(AVE)						
50133	GL-III-43	1,926.5(AVE)						
50134	GL-III-52							

50135	GL-III-53	226.5(AVE)						
50136	GL-III-54		7,081.00			>10,000	5,981.00	
50137	GL-III-60	391.3(AVE)	4,822.0(AVE)					
50138	GL-III-63	795.7(AVE)						
50139	GL-III-64	2,639.7(AVE)	8,807.3(AVE)					
50140	GL-III-66	240.5(AVE)					>10,000	
50141	GL-III-67	181.0(AVE)					>10,000	
50142	GL-III-68	211.5(AVE)			>10,000		>10,000	
50143	GL-III-69	626.5(AVE)			>10,000			
50144	GL-III-70	1,079.5(AVE)						
50145	GL-III-75	1,568.5(AVE)			1,033.00			
50146	GL-III-76	459.5(AVE)			6,226.00			
50147	GL-III-76A						>10,000	
50148	GL-III-77							
50149	GL-III-78	571.0(AVE)			2,928.00			

Table 51. PDSP secondary binding data for MOR, NET, NMDA, PBR, Sigma 1, Sigma 2, and Sigma 2 PC12.

Compound #	Name	MOR	NET	NMDA	PBR	Sigma 1	Sigma 2	Sigma 2 PC12

30611	SH-053-2'F-R-CH3							
30612	SH-053-2'F-S-CH3							
30613	MP-III-004							
30614	MP-III-021							
30615	MP-III-019							
30616	MP-III-018.A							
30617	MP-III-022							
30618	MP-III-023							
30619	SH-I-85				1,226.00			
37713	MP-III-068				2,501.3(AVE)			
37714	MP-III-080				943.5(AVE)			
37715	MP-III-085				2,241.5(AVE)			6,994.3(AVE)
37717	SH-053-2'F-R-CH3-Acid							
37718	SH-053-2'F-S-CH3-Acid							
37719	MP-III-018.B							
37720	MP-III-019.B							
37721	MP-IV-004							1,730.0(AVE)
37722	GL-I-65							
37723	MP-IV-005							2,054.3(AVE)
37724	GL-I-66							3,116.0(AVE)
37725	MP-IV-010							2,070.5(AVE)

37726	GL-I-81	2,916.00						
37728	SH-I-085				1,338.0(AVE)			
37729	KRM-II-18B							
37730	KRM-II-73				3,318.0(AVE)			1,579.7(AVE)
37731	KRM-II-82							
37732	KRM-II-97				311.0(AVE)			
37733	KRM-II-81				560.0(AVE)			
37734	KRM-II-68							
37735	KRM-II-08				1,055.0(AVE)			
37736	KRM-II-3B				3,757.7(AVE)			3,061.3(AVE)
42621	KRM-III-59				580.5(AVE)			
42622	KRM-III-65					>10,000		
42623	KRM-III-66				1,753.5(AVE)	7,523.00	715	
42624	KRM-III-67						1,271.00	
42625	KRM-III-79				519.0(AVE)			
42626	KRM-III-70					>10,000		
42627	KRM-III-77				1,313.0(AVE)	>10,000		
42628	KRM-III-78				278.5(AVE)	8,057.00		
42633	Ro5-4846				53.0(AVE)			
42634	Ro7-9277				400.0(AVE)			
42635	GL-I-74				2,186.5(AVE)			

42636	GL-II-39				196.0(AVE)	8,486.00		
42637	GL-II-05							
42638	GL-II-06				591.5(AVE)			
42639	GL-II-18					5,305.00	1,155.00	
42640	GL-II-19				1,397.5(AVE)			
42641	GL-II-30							
42642	GL-II-31				734.5(AVE)	>10,000		
42643	GL-II-32				3,787.5(AVE)			
42644	GL-II-33						1,100.00	
42645	GL-II-51							
42647	GL-II-53							
42648	GL-II-54				397.0(AVE)		2,059.00	
42651	GL-II-57						2,019.00	
42653	GL-II-59							
42654	GL-II-60							
42655	GL-II-61							
42656	GL-I-30	2,331.7(AVE)					867	
42657	GL-I-31						995	
42658	GL-I-32						1,177.00	
42659	GL-I-33				1,791.0(AVE)		1,985.00	
42660	GL-I-38							

42661	GL-I-36							
42662	GL-I-43							
42663	GL-I-41							
42664	GL-I-55							
42665	GL-I-54							
42666	GL-I-77						1,297.00	
42667	GL-I-78				595.0(AVE)		1,286.00	
50093	SH-I-044			7,825.00				
50094	SH-I-047			5,700.3(AVE)			1,565.00	
50095	SH-I-060			3214			386	
50096	MP-III-058							
50097	SH-I-048A							
50098	SH-I-048B							
50099	SH-I-055						610	
50101	YT-III-31							
50102	YT-III-271							
50103	SR-II-54							
50104	GL-II-73				>10,000			
50105	GL-II-74				8,429.00			
50106	GL-II-75				7,249.00		1,788.00	
50107	GL-II-76							
50108	GL-I-50							
50109	GL-II-93				>10,000			
50110	GL-I-65						1,323.00	

50111	GL-I-81						1,129.00	
50112	GL-III-19							
50114	GL-I-61						1,051.00	
50117	GL-I-63						1,047.00	
50120	GL-III-26						984	
50121	GL-III-27							
50122	GL-III-59							
50123	GL-III-57						1,003.00	
50124	GL-III-58							
50125	GL-III-35							
50126	GL-III-36						998	
50127	KRM-III-18A						565	
50128	GL-III-38							
50129	GL-III-72						432	
50130	GL-III-73						1,189.00	
50132	GL-III-42				966		614	
50133	GL-III-43							
50134	GL-III-52							
50135	GL-III-53							
50136	GL-III-54							
50137	GL-III-60				2,389.00	9,586.7(AVE)	468	
50138	GL-III-63				364	8,488.0(AVE)		

50139	GL-III-64				29			
50140	GL-III-66							
50141	GL-III-67							
50142	GL-III-68				1,273.00			
50143	GL-III-69							
50144	GL-III-70							
50145	GL-III-75							
50146	GL-III-76							
50147	GL-III-76A							
50148	GL-III-77		4983					
50149	GL-III-78							

Appendix III: The master data file for anti-depression project

Table 52. Pharmacokinetic parameters in mice and rats calculated for GL-II-73, GL-II-74, GL-II-75, RV-II-04, GL-II-31, MP-III-023, GL-I-54, GL-III-23, GL-II-33, GL-II-54 and GL-I-65.

Compound	Animal species and dosing	Tissue	Route of admini-stration	C_{max} (Mean ± SEM, ng/ml – plasma, ng/g - brain)	T_{max}(Mean ± SEM, h)	AUC_{0-12} (Mean ± SEM, ng*h/ml – plasma, ng*h/g – brain)	$AUC_{0-\infty}$ (Mean ± SEM, ng*h/ml – plasma, ng*h/g – brain)	$T_{1/2}$ (Mean ± SEM, h)	β (Mean ± SEM, 1/h)
RV-II-04	Mouse 3 mg/kg	Plasma	IV	1910.44 ± 190.95	0 ± 0.00	2974.93 ± 429.88	2981.44 ± 436.01	1.13 ± 0.24	0.66 ± 0.12
			PO	528.54 ± 129.42	1.78 ± 1.13	3573.79 ± 667.43	3714.7 ± 642.36	2.76 ± 0.41	0.26 ± 0.04
			IP	1412.33 ± 152.97	0.25 ± 0.08	4876.15 ± 503.26	4883.35 ± 502.87	1.13 ± 0.24	0.67 ± 0.12
		Brain	IV	1816.24 ± 227.80	0.25 ± 0.08	3414.7 ± 815.13	3416.05 ± 815.27	1.1 ± 0.06	0.63 ± 0.03
			PO	554.17 ± 51.12	0.55 ± 0.22	2897.87 ± 765.81	2902.37 ± 764.41	2.11 ± 0.86	0.43 ± 0.13
			IP	1626.66 ± 22.20 ± 22.20	0.33± 0.00 ± 0.00	5631.75 ± 644.15 ± 644.15	5632.1 ± 644.27 ± 644.27	0.91 ± 0.03 ± 0.03	0.76 ± 0.02 ± 0.02
	Rat 3 mg/kg	Plasma	IV	981.66 ± 184.23	0 ± 0.00	450.49 ± 46.77	456.25 ± 45.97	1.61 ± 0.15	0.42 ± 0.04
			PO	13.27 ± 5.27	2.33 ± 0.67	75.76 ± 32.18	94.28 ± 21.19	5.67 ± 3.02	0.2 ± 0.08
			IP	452.21	0.17	976.3	979.41	1.4	0.46

				± 36.63	± 0.08	± 353.51	± 354.60	± 0.07	± 0.01
		Brain	IV	3343.61 ± 463.84	0.08 ± 0.00	1761.11 ± 143.44	1788.35 ± 139.97	1.78 ± 0.07	0.39 ± 0.01
			PO	136.34 ± 61.97	1.44 ± 0.80	631.71 ± 298.55	649.36 ± 294.93	3.13 ± 1.26	0.29 ± 0.08
			IP	959.19 ± 162.83	0.25 ± 0.08	4745.2 ± 1385.08	5368.98 ± 786.53	3.79 ± 2.64	0.43 ± 0.18
GL-II-31	Mouse 3 mg/kg	Plasma	IV	340.07 ± 73.23	0 ± 0.00	630.86 ± 297.47	631.16 ± 297.52	1.12 ± 0.01	0.62 ± 0.01
			PO	195.4 ± 41.41	1 ± 0.00	894.63 ± 187.36	902.16 ± 190.71	1.42 ± 0.35	0.54 ± 0.11
			IP	381.96 ± 45.02	0.78 ± 0.22	1143.66 ± 67.30	1145.95 ± 65.82	1.3 ± 0.21	0.56 ± 0.09
		Brain	IV	418.68 ± 24.31	0.25 ± 0.08	389.02 ± 179.73	389.33 ± 179.66	1.26 ± 0.12	0.56 ± 0.06
			PO	47.74 ± 10.09	0.69 ± 0.31	122.77 ± 64.36	123.31 ± 64.13	1.87 ± 0.54	0.43 ± 0.11
			IP	168.6 ± 5.83	0.33 ± 0.00	382.88 ± 78.33	383.2 ± 78.42	1.2 ± 0.07	0.58 ± 0.04
	Rat 3 mg/kg	Plasma	IV	639.33 ± 204.62	0 ± 0.00	620.61 ± 36.43	635.33 ± 37.88	2.04 ± 0.04	0.34 ± 0.01
			PO	58.33 ± 13.71	3 ± 0.00	386.97 ± 81.52	394.82 ± 80.48	2.08 ± 0.20	0.34 ± 0.03
			IP	180.44 ± 7.76	0.33 ± 0.00	819.66 ± 147.89	849.45 ± 149.74	2.38 ± 0.38	0.31 ± 0.04
		Brain	IV	708.92	0.08	732.82	795.57	2.67	0.28

				± 167.01	± 0.00	± 145.63	± 120.25	± 0.45	± 0.06
			PO	25.2 ± 9.18	6 ± 3.00	184.38 ± 48.92	234.32 ± 29.38	4.55 ± 0.96	0.17 ± 0.04
			IP	116.4 ± 12.71	0.25 ± 0.08	501.55 ± 65.11	595.01 ± 114.54	2.71 ± 0.39	0.27 ± 0.04
MP-III-023	Mouse 3 mg/kg	Plasma	IV	1053.42 ± 178.15	0 ± 0.00	1324.67 ± 72.10	1325.81 ± 72.41	1.1 ± 0.12	0.64 ± 0.06
			PO	495.79 ± 92.02	1 ± 0.00	1419.4 ± 288.19	1431.44 ± 286.06	1.73 ± 0.16	0.41 ± 0.04
			IP	914.38 ± 54.14	0.08 ± 0.00	1069.2 ± 141.30	1073.74 ± 143.84	1.5 ± 0.15	0.47 ± 0.04
		Brain	IV	1041.87 ± 204.05	0.08 ± 0.00	936.37 ± 81.20	936.41 ± 81.20	0.85 ± 0.01	0.81 ± 0.01
			PO	163.97 ± 21.32	0.25 ± 0.08	364.6 ± 108.18	364.89 ± 108.25	1.18 ± 0.08	0.59 ± 0.04
			IP	708.5 ± 23.43	0.25 ± 0.08	1236.64 ± 127.71	1236.78 ± 127.67	0.85 ± 0.10	0.84 ± 0.10
	Rat 3 mg/kg	Plasma	IV	740.38 ± 132.13	0 ± 0.00	487.3 ± 42.55	500.45 ± 47.09	1.81 ± 0.30	0.4 ± 0.06
			PO	17.77 ± 7.92	1.44 ± 0.80	69.63 ± 18.64	91.31 ± 6.23	6.6 ± 4.06	0.22 ± 0.11
			IP	256.08 ± 43.26	0.17 ± 0.08	240.18 ± 8.63	250.65 ± 7.25	2.37 ± 0.37	0.31 ± 0.06
		Brain	IV	2720.98 ± 356.62	0.08 ± 0.00	1404.13 ± 60.66	1430.22 ± 58.02	1.82 ± 0.09	0.38 ± 0.02
			PO	45.62 ± 32.85	5.11 ± 3.53	100.93 ± 30.80	142.39 ± 46.10	5.54 ± 2.66	0.2 ± 0.09

			IP	502.48 ± 168.89	0.25 ± 0.08	553.6 ± 192.31	568.4 ± 189.21	1.74 ± 0.65	0.63 ± 0.32
GL-I-54	Mouse 3 mg/kg	Plasma	IV	1390.42 ± 222.26	0 ± 0.00	2039.56 ± 50.53	2039.68 ± 50.56	0.88 ± 0.02	0.79 ± 0.02
			PO	339.7 ± 29.77	0.55 ± 0.22	1511.09 ± 287.14	1511.18 ± 187.17	0.9 ± 0.06	0.78 ± 0.05
			IP	1283.79 ± 46.18	0.08 ± 0.00	2445.94 ± 401.30	2445.96 ± 401.30	0.74 ± 0.01	0.94 ± 0.01
		Brain	IV	464.81 ± 117.94	0.08 ± 0.00	400.91 ± 21.65	400.95 ± 21.65	0.91 ± 0.04	0.77 ± 0.04
			PO	83.43 ± 6.75	0.33 ± 0.00	199.71 ± 38.48	199.77 ± 38.47	1 ± 0.05	0.7 ± 0.04
			IP	320.13 ± 2.22	0.25 ± 0.08	467.03 ± 36.06	467.05 ± 36.06	0.82 ± 0.03	0.84 ± 0.03
	Rat 3 mg/kg	Plasma	IV	1389.45 ± 257.98	0 ± 0.00	537.21 ± 70.83	578.24 ± 70.22	1.62 ± 0.06	0.43 ± 0.02
			PO	77.48 ± 35.02	0.33 ± 0.00	142.98 ± 43.91	149.82 ± 44.25	3.05 ± 0.42	0.24 ± 0.04
			IP	979.87 ± 196.66	0.17 ± 0.08	487.07 ± 27.52	490.08 ± 28.49	1.72 ± 0.03	0.4 ± 0.01
		Brain	IV	916.08 ± 196.67	0.08 ± 0.00	458.63 ± 64.25	485.71 ± 59.34	2.34 ± 0.17	0.3 ± 0.02
			PO	114.97 ± 55.53	0.33 ± 0.00	322.24 ± 30.29	347.25 ± 29.89	0.37 ± 0.01	1.9 ± 0.05
			IP	186.5 ± 65.09	0.17 ± 0.08	406.85 ± 69.29	444.7 ± 79.70	0.4 ± 0.02	1.76 ± 0.09
GL-III-23	Mouse	Plasma	IV	164.27	0	392.05	457.81	3.37	0.29

	3 mg/kg			± 32.71	± 0.00	± 56.38	± 86.29	± 1.09	± 0.14
			PO	109.84 ± 30.55	3 ± 1.00	827.77 ± 263.74	1317.38 ± 626.00	5.91 ± 2.59	0.34 ± 0.25
			IP	242.45 ± 30.57	0.78 ± 0.22	1199.56 ± 142.88	1386.94 ± 158.65	4.14 ± 0.12	0.17 ± 0.01
		Brain	IV	524.04 ± 102.71	0.08 ± 0.00	931.76 ± 192.73	974.14 ± 191.48	2.5 ± 0.58	0.31 ± 0.07
			PO	191.42 ± 60.45	3 ± 1.00	1170.4 ± 340.95	1285.24 ± 263.90	3.61 ± 1.97	0.32 ± 0.12
			IP	479.03 ± 7.53	2 ± 1.00	3056.79 ± 274.84	3284.04 ± 342.75	2.67 ± 1.00	0.47 ± 0.28
	Rat 3 mg/kg	Plasma	IV	195.59 ± 42.20	0 ± 0.00	215.37 ± 23.64	216.19 ± 23.64	1.48 ± 0.02	0.47 ± 0.01
			PO	103.65 ± 34.15	0.78 ± 0.22	245.99 ± 119.30	246.85 ± 119.21	1.56 ± 0.17	0.45 ± 0.05
			IP	63.62 ± 7.85	0.39 ± 0.31	281.37 ± 32.48	334.37 ± 17.65	4.42 ± 0.77	0.17 ± 0.03
		Brain	IV	356.14 ± 72.29	0.4 ± 0.31	783.91 ± 117.03	872.52 ± 99.94	3.38 ± 0.64	0.22 ± 0.05
			PO	128.73 ± 24.94	5.33 ± 3.38	822.11 ± 147.77	1276.76 ± 260.35	5 ± 1.73	0.18 ± 0.07
			IP	175.58 ± 3.40	0.08 ± 0.00	952.11 ± 129.97	1213.43 ± 65.82	5.19 ± 1.31	0.15 ± 0.03
GL-II-33	Mouse 3 mg/kg	Plasma	IV	111.24 ± 34.45	0 ± 0.00	175.3 ± 34.25	212.91 ± 35.01	4.4 ± 0.41	0.16 ± 0.01
			PO	59.54 ± 15.91	3 ± 1.00	442.5 ± 88.97	803.7 ± 180.17	10.73 ± 6.96	0.3 ± 0.23

			IP	134.63 ± 3.29	0.78 ± 0.22	701.76 ± 51.78	1019.78 ± 126.91	7.61 ± 2.16	0.1 ± 0.02
		Brain	IV	298.17 ± 67.12	0.08 ± 0.00	372.27 ± 189.23	550.31 ± 263.79	5.46 ± 2.13	0.21 ± 0.12
			PO	85.81 ± 25.49	3 ± 1.00	508.42 ± 207.87	631.34 ± 307.79	3.11 ± 1.37	0.36 ± 0.18
			IP	240.73 ± 49.80	2 ± 1.00	1386.97 ± 270.11	1487.33 ± 266.22	3.01 ± 0.08	0.23 ± 0.01
	Rat 3 mg/kg	Plasma	IV	104.15 ± 42.00	0 ± 0.00	50.61 ± 10.03	51.77 ± 10.00	2.12 ± 0.07	0.33 ± 0.011
			PO	39.24 ± 21.86	1.67 ± 0.67	58.27 ± 27.70	59.87 ± 27.34	2.91 ± 0.73	0.27 ± 0.05
			IP	4.75 ± 1.50	0.17 ± 0.08	9.5 ± 1.11	12.7 ± 1.32	5.83 ± 0.40	0.12 ± 0.01
		Brain	IV	172.47 ± 28.89	0.17 ± 0.08	613.23 ± 55.69	1944.91 ± 688.72	17.95 ± 6.41	0.05 ± 0.02
			PO	68.56 ± 21.58	0.69 ± 0.31	296.85 ± 18.10	1361.21 ± 985.70	25.35 ± 22.02	0.2 ± 0.14
			IP	97.18 ± 19.76	0.17 ± 0.08	422.85 ± 28.86	1003.05 ± 415.06	15 ± 10.05	0.2 ± 0.15
GL-II-54	Mouse 3 mg/kg	Plasma	IV	954.6 ± 134.45	0 ± 0.00	738.85 ± 85.08	798.85 ± 85.82	3.23 ± 0.27	0.22 ± 0.02
			PO	137.05 ± 23.14	3 ± 1.00	872.15 ± 156.31	993.08 ± 148.20	3.61 ± 1.07	0.23 ± 0.08
			IP	370.78 ± 61.82	0.78 ± 0.22	1672.11 ± 104.67	1811.11 ± 99.47	3.3 ± 0.04	0.21 ± 0.00

		Brain	IV	877.97 ± 155.12	0.08 ± 0.00	1458.62 ± 47.18	1459.02 ± 47.12	1.07 ± 0.02	0.65 ± 0.01
			PO	107.05 ± 30.65	3 ± 1.00	538.84 ± 225.47	539.88 ± 225.23	1.31 ± 0.40	0.63 ± 0.17
			IP	352.86 ± 62.32	2 ± 1.00	2105.67 ± 307.62	2119.37 ± 313.13	1.53 ± 0.29	0.49 ± 0.12
	Rat 3 mg/kg	Plasma	IV	592.56 ± 79.89	0 ± 0.00	884.99 ± 131.29	885.77 ± 131.28	1.25 ± 0.02	0.56 ± 0.01
			PO	230.93 ± 43.53	1.67 ± 0.67	939.87 ± 361.59	947.33 ± 357.39	1.58 ± 0.47	0.51 ± 0.13
			IP	146.92 ± 3.71	0.56 ± 0.22	867 ± 101.00	1021.54 ± 77.54	4.46 ± 1.13	0.18 ± 0.04
		Brain	IV	290.14 ± 36.86	0.17 ± 0.08	859.22 ± 60.61	1284.87 ± 17.83	6.51 ± 0.57	0.11 ± 0.01
			PO	105.66 ± 13.92	1.67 ± 0.67	859.69 ± 97.79	1600.41 ± 348.96	9.13 ± 4.23	0.17 ± 0.11
			IP	118.75 ± 5.80	0.56 ± 0.22	799.87 ± 48.21	1988.85 ± 484.63	14.49 ± 4.13	0.06 ± 0.02
GL-I-65	Mouse 3 mg/kg	Plasma	IV	101.89 ± 34.49	0 ± 0.00	156.09 ± 29.81	181.7 ± 37.05	3.69 ± 0.87	0.21 ± 0.04
			PO	51.35 ± 10.68	3 ± 1.00	363.06 ± 84.22	575.32 ± 140.25	7.2 ± 3.80	0.32 ± 0.24
			IP	151.1 ± 8.67	0.78 ± 0.22	619.41 ± 46.29	871.09 ± 34.30	6.25 ± 0.65	0.11 ± 0.01
		Brain	IV	230.63 ± 50.40	0.08 ± 0.00	286.56 ± 174.85	288.39 ± 175.90	1.65 ± 0.09	0.42 ± 0.02
			PO	65.51	3	304.52	312.22	1.74	0.57

				± 11.60	± 1.00	± 106.53	± 99.28	± 0.85	± 0.19
			IP	182.58 ± 37.57	2 ± 1.00	1029.72 ± 192.47	1126.95 ± 203.15	3.16 ± 0.44	0.23 ± 0.03
	Rat 3 mg/kg	Plasma	IV	116.77 ± 40.89	0 ± 0.00	150.23 ± 15.11	151.23 ± 15.11	1.74 ± 0.03	0.4 ± 0.01
			PO	46.81 ± 20.78	1.67 ± 0.67	105.25 ± 20.10	106.25 ± 20.07	1.74 ± 0.06	0.4 ± 0.01
			IP	24.71 ± 1.36	0.33 ± 0.00	76.83 ± 8.40	78.03 ± 8.38	2.09 ± 0.02	0.33 ± 0.00
		Brain	IV	152.07 ± 29.08	0.08 ± 0.00	530.05 ± 83.18	2031.38 ± 1099.74	20.31 ± 10.35	0.06 ± 0.03
			PO	62.1 ± 18.05	1.67 ± 0.67	310.43 ± 16.93	531.37 ± 110.46	7.93 ± 2.74	0.11 ± 0.03
			IP	92.43 ± 19.98	0.17 ± 0.08	447.07 ± 79.99	730.43 ± 100.40	8.46 ± 1.48	0.09 ± 0.02
GL-II-73	Mouse 10 mg/kg	Plasma	IP	5384.54 ± 838.04	0.08 ± 0.00	4620.09 ± 323.21	4626.35 ± 322.80	1.2 ± 0.02	0.58 ± 0.01
		Brain	IP	1195.94 ± 51.75	0.17 ± 0.08	1311.86 ± 85.86	1397.47 ± 119.30	2.44 ± 0.20	0.29 ± 0.02
	Rat 3 mg/kg	Plasma	IV	777.76 ± 31.34	0 ± 0.00	434.48 ± 63.02	435.03 ± 62.92	1.21 ± 0.07	0.58 ± 0.03
			PO	79.43 ± 50.72	0.25 ± 0.08	68.54 ± 19.28	144.52 ± 65.73	7.16 ± 1.82	2.7 ± 2.58
		Brain	IV	239.7 ± 11.83	0.08 ± 0.00	103.79 ± 7.18	110.44 ± 7.05	2.35 ± 0.26	0.3 ± 0.03

			PO	20.5 ± 13.49	1.22 ± 0.89	54.09 ± 8.58	68.79 ± 13.69	7.2 ± 3.94	0.16 ± 0.06
GL-II-74	Mouse 10 mg/kg	Plasma	IP	2840.74 ± 404.87	0.08 ± 0.00	2053.17 ± 297.11	2102.62 ± 298.38	1.84 ± 0.17	0.38 ± 0.03
		Brain	IP	3246.23 ± 184.90	0.08 ± 0.00	2218.83 ± 177.52	2231.34 ± 177.69	1.47 ± 0.07	0.48 ± 0.02
	Rat 3 mg/kg	Plasma	IV	426.55 ± 77.06	0 ± 0.00	292.69 ± 4.72	294.25 ± 4.15	1.5 ± 0.13	0.47 ± 0.04
		Brain	IV	690.92 ± 23.66	0.08 ± 0.00	339.54 ± 11.53	344.94 ± 11.28	1.75 ± 0.09	0.4 ± 0.02
GL-II-75	Mouse 10 mg/kg	Plasma	IP	2151.323 ± 81.07	0.25 ± 0.08	4845.31 ± 118.92	4856.48 ± 111.76	0.53 ± 0.06	0.16 ± 0.06
		Brain	IP	1410.23 ± 136.71	0.33 ± 0.00	3895.8 ± 114.08	3907.26 ± 112.51	1.43 ± 0.09	0.49 ± 0.03

Table 53. PK parameters for GL-III-68 and GL-III-70.

		Time point	Mean ± SEM (nmol/l or nmol/kg)	Mean ± SEM (ng/ml or ng/g)
GL-III-68	Plasma	5 min	6968.64 ± 1031.64	2804.60 ± 415.19
		20 min	5445.90 ± 148.67	2191.75 ± 59.83
		1 h	3092.50 ± 1122.90	1244.61 ± 451.92
		4 h	134.59 ± 97.20	54.17 ± 39.12
		12 h	1.48 ± 0.36	0.60 ± 0.14
	Brain	5 min	2380.16 ± 169.19	957.92 ± 68.09
		20 min	2591.14 ± 131.13	1042.83 ± 52.77
		1 h	2096.90 ± 495.51	843.92 ± 199.42
		4 h	63.36 ± 38.99	25.50 ± 15.69
		12 h	13.80 ± 3.98	5.56 ± 1.60
GL-III-70	Plasma	5 min	9817.54 ± 2027.70	3951.17 ± 816.07
		20 min	6311.95 ± 825.85	2540.31 ± 332.37
		1 h	2086.17 ± 717.95	838.60 ± 288.95
		4 h	31.14 ± 1.50	12.63 ± 0.61
		12 h	3.11 ± 0.89	1.25 ± 0.36
	Brain	5 min	3033.75 ± 276.71	1220.96 ± 111.36
		20 min	1604.61 ± 123.08	645.79 ± 49.53
		1 h	417.23 ± 95.02	167.92 ± 38.24
		4 h	26.98 ± 0.37	10.86 ± 0.15
		12 h	18.17 ± 6.47	7.31 ± 2.60

	Pharmacokinetic parameters	Mean ± SEM (plasma)	Mean ± SEM (brain)
GL-III-68	Cmax (ng/ml; ng/g)	2900.234 ± 320.147	1089.565 ± 53.400
	Tmax (h)	0.166 ± 0.083	0.555 ± 0.222
	AUC0_12 (ng*h/ml; ng*h/g)	3937.793 ± 692.277	2307.679 ± 259.262
	AUC0_∞ (ng*h/ml; ng*h/g)	3938.646 ± 692.497	2321.181 ± 262.839
	T1/2 (h)	0.979 ± 0.026	1.624 ± 0.123
	β (1/h)	0.709 ± 0.019	0.432 ± 0.035
	Kp	0.59	
GL-III-70	Cmax (ng/ml)	3992.139 ± 789.028	1220.965 ± 111.365
	Tmax (h)	0.166 ± 0.083	0.083 ± 0.000
	AUC0_12 (ng*h/ml)	3271.958 ± 363.428	845.571 ± 74.067
	AUC0_∞ (ng*h/ml)	3273.913 ± 362.911	865.594 ± 65.275
	T1/2 (h)	1.063 ± 0.036	1.776 ± 0.171
	β (1/h)	0.654 ± 0.022	0.397 ± 0.035
	Kp	0.26	

BRIEF DESCRIPTION OF THE DRAWINGS

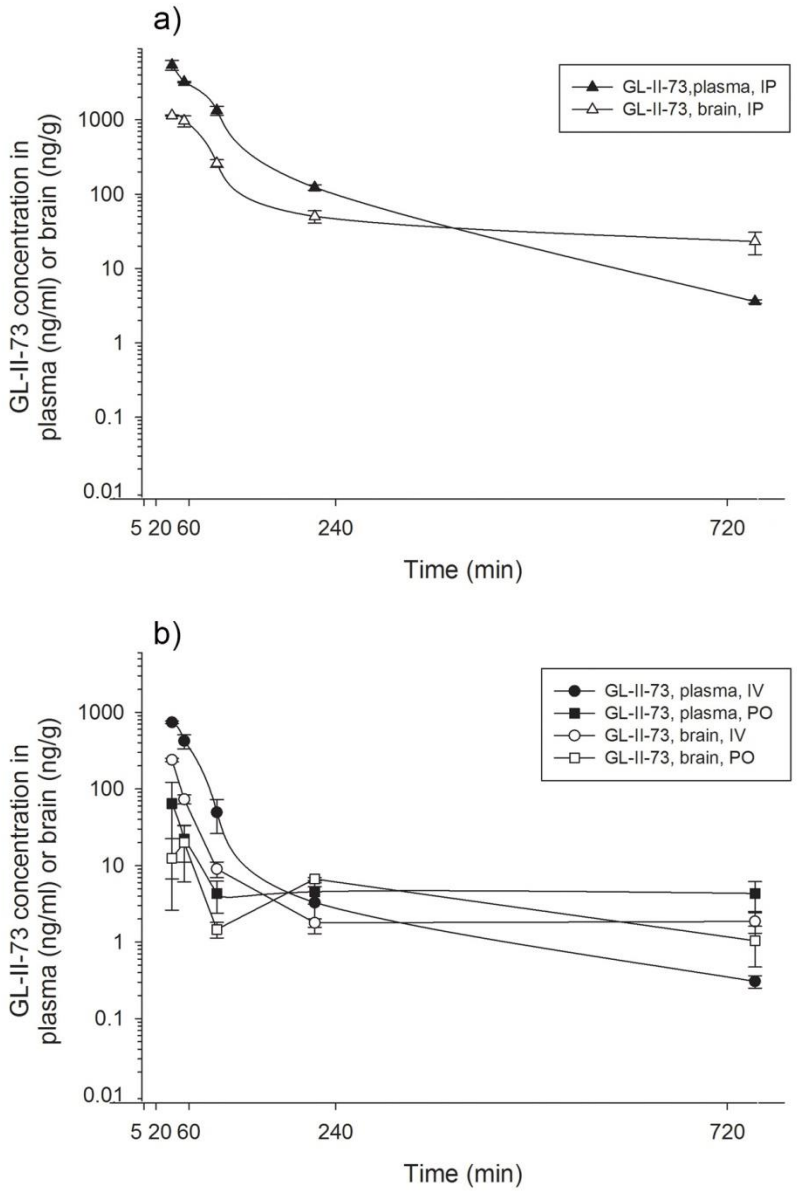

Figure 1. The concentration–time profile of GL-II-73 after intraperitoneal (IP) administration of the 10 mg/kg dose in mouse plasma and brain (a) and after intravenous (IV) and peroral (PO) administration of the 3 mg/kg dose in rat plasma and brain (b). n=3 per time point.

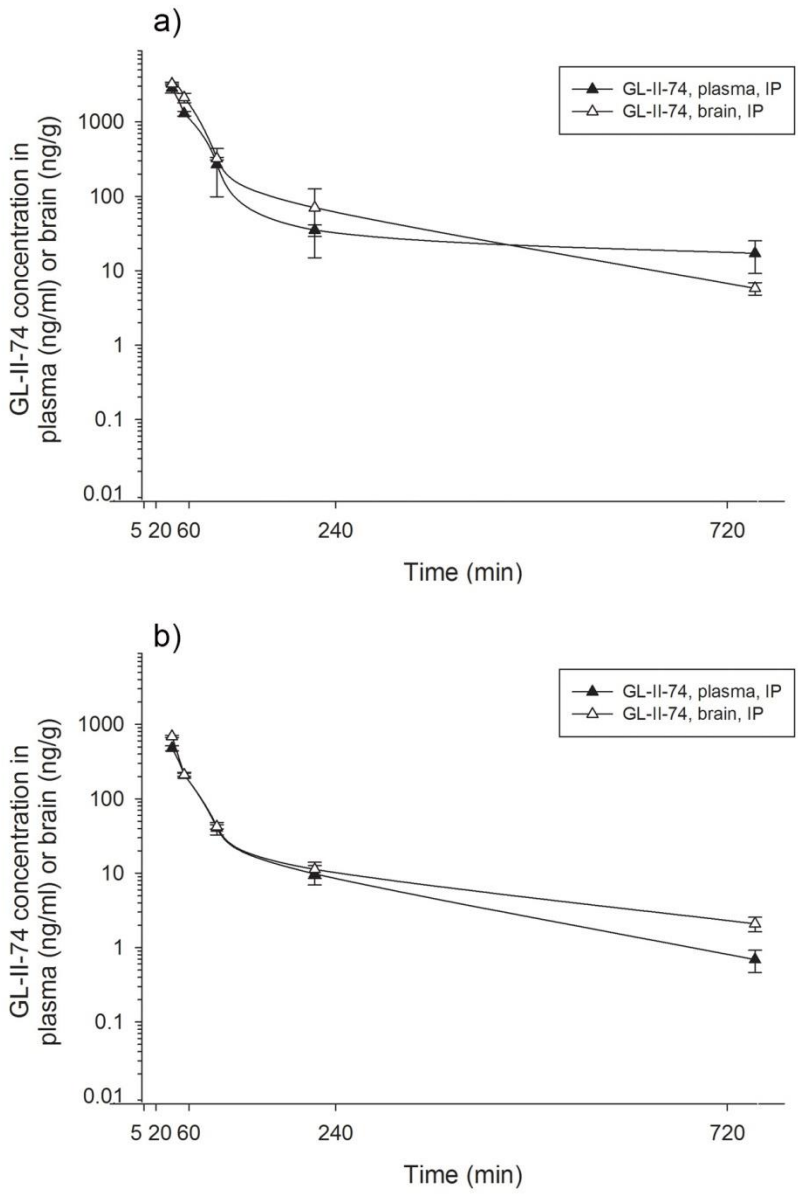

Figure 2. The concentration–time profile of GL-II-74 after intraperitoneal (IP) administration of the 10 mg/kg dose in mouse plasma and brain (a) and after intravenous (IV) administration of the 3 mg/kg dose in rat plasma and brain (b). n=3 per time point.

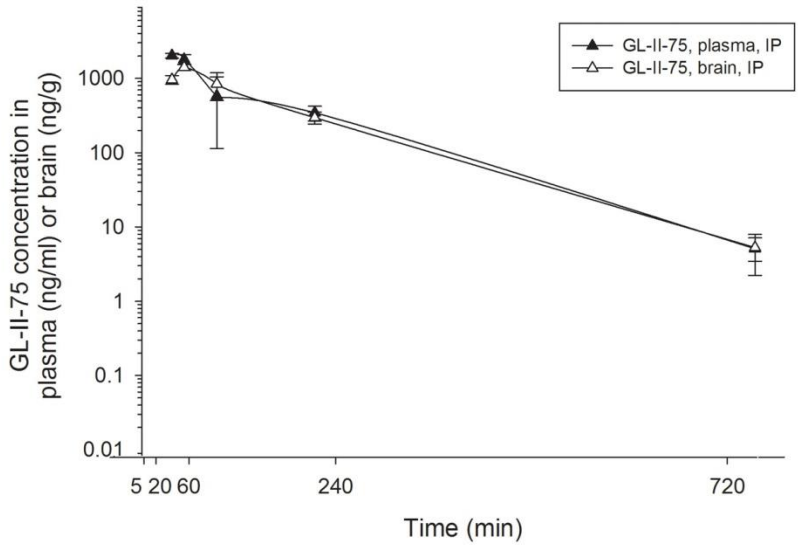

Figure 3. The concentration–time profile of GL-II-75 after intraperitoneal (IP) administration of the 10 mg/kg dose (n=3 per time point) in mouse plasma and brain.

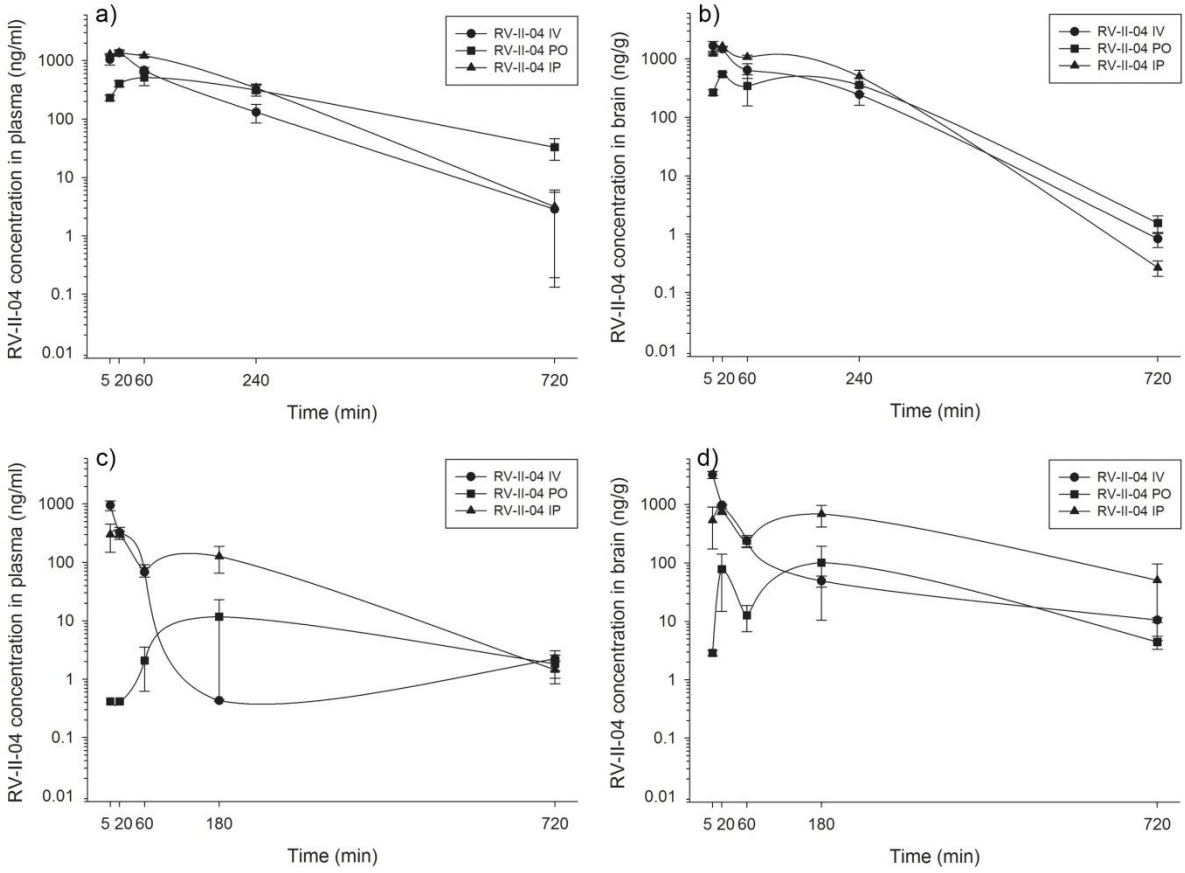

Figure 4. The concentration–time profile of RV-II-04 after intravenous (IV), peroral (PO) or intraperitoneal (IP) administration of the 3 mg/kg dose (n=3 per time point) in mouse plasma (a) and brain (b), as well as in rat plasma (c) and brain (d).

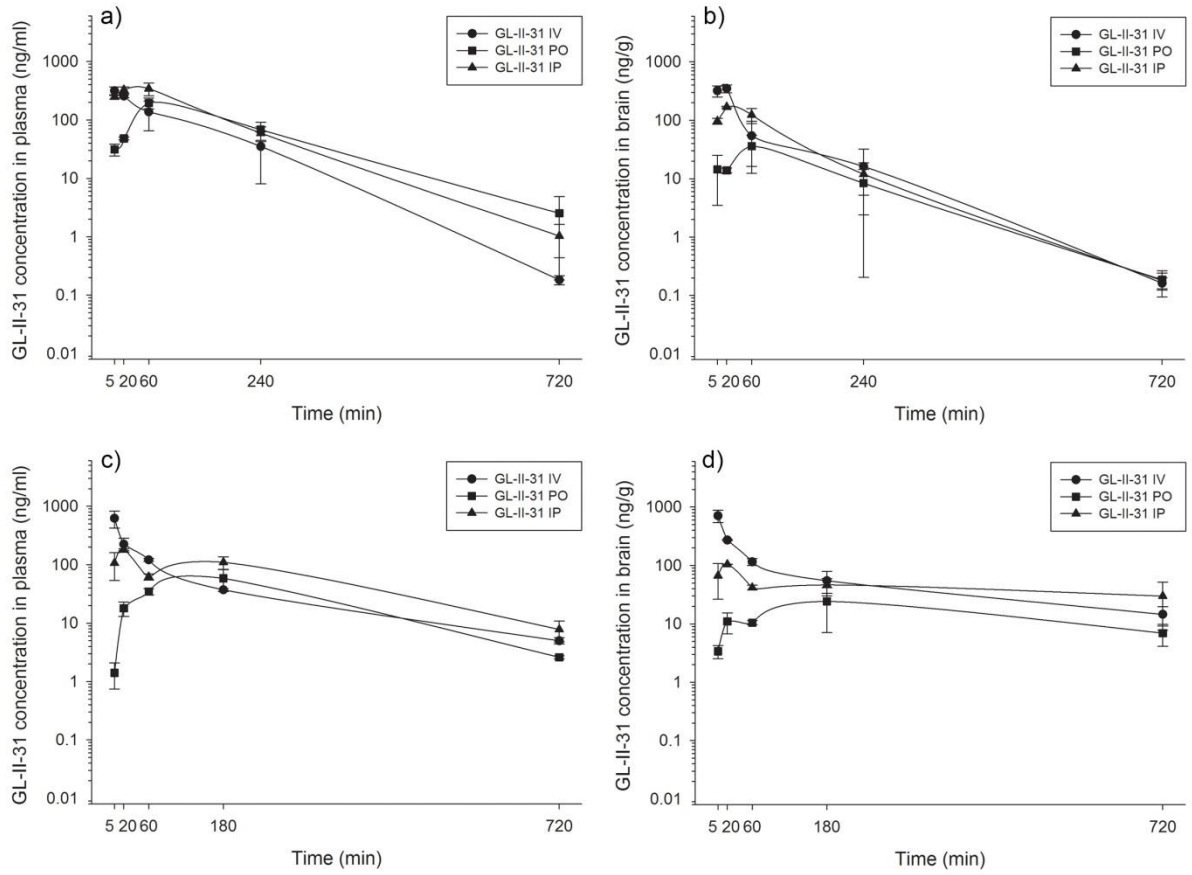

Figure 5. The concentration–time profile of GL-II-31 after intravenous (IV), peroral (PO) or intraperitoneal (IP) administration of the 3 mg/kg dose (n=3 per time point) in mouse plasma (a) and brain (b), as well as in rat plasma (c) and brain (d).

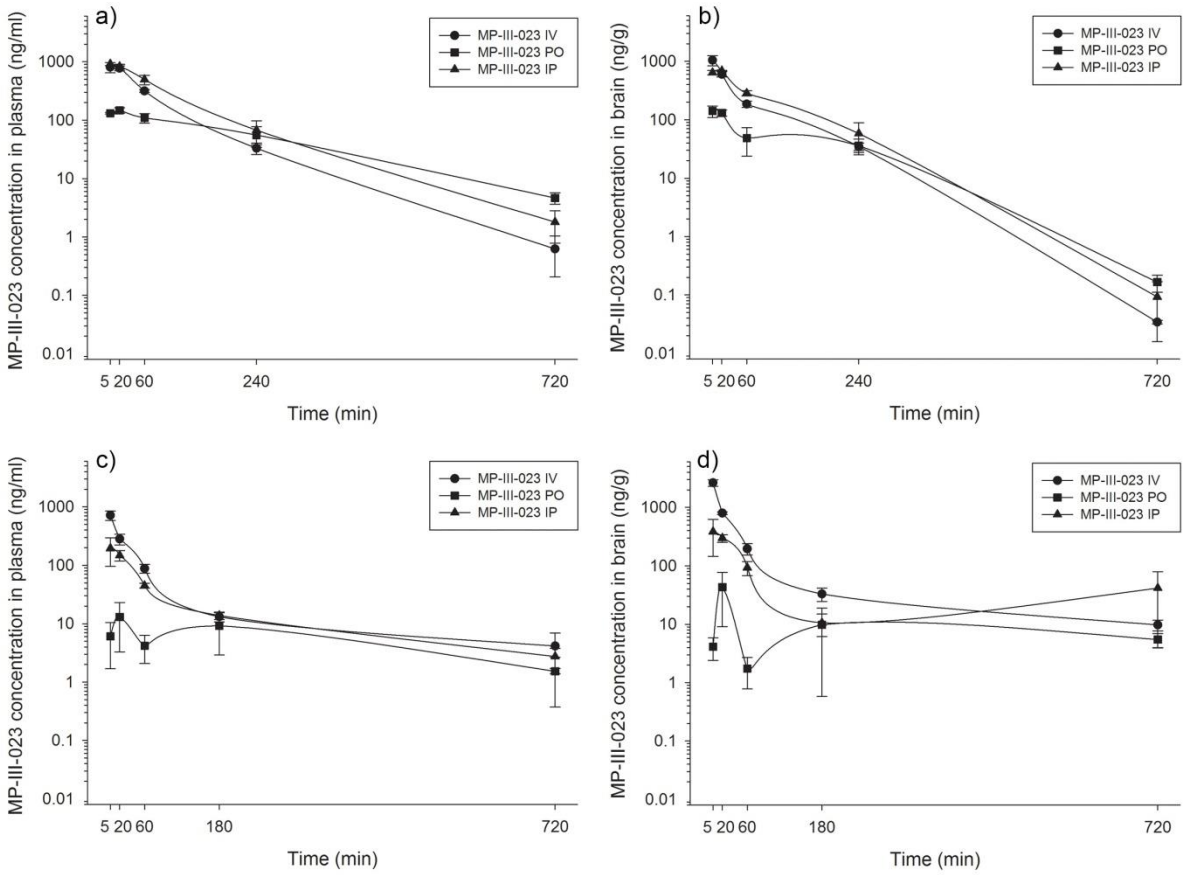

Figure 6. The concentration–time profile of MP-III-023 after intravenous (IV), peroral (PO) or intraperitoneal (IP) administration of the 3 mg/kg dose (n=3 per time point) in mouse plasma (a) and brain (b), as well as in rat plasma (c) and brain (d).

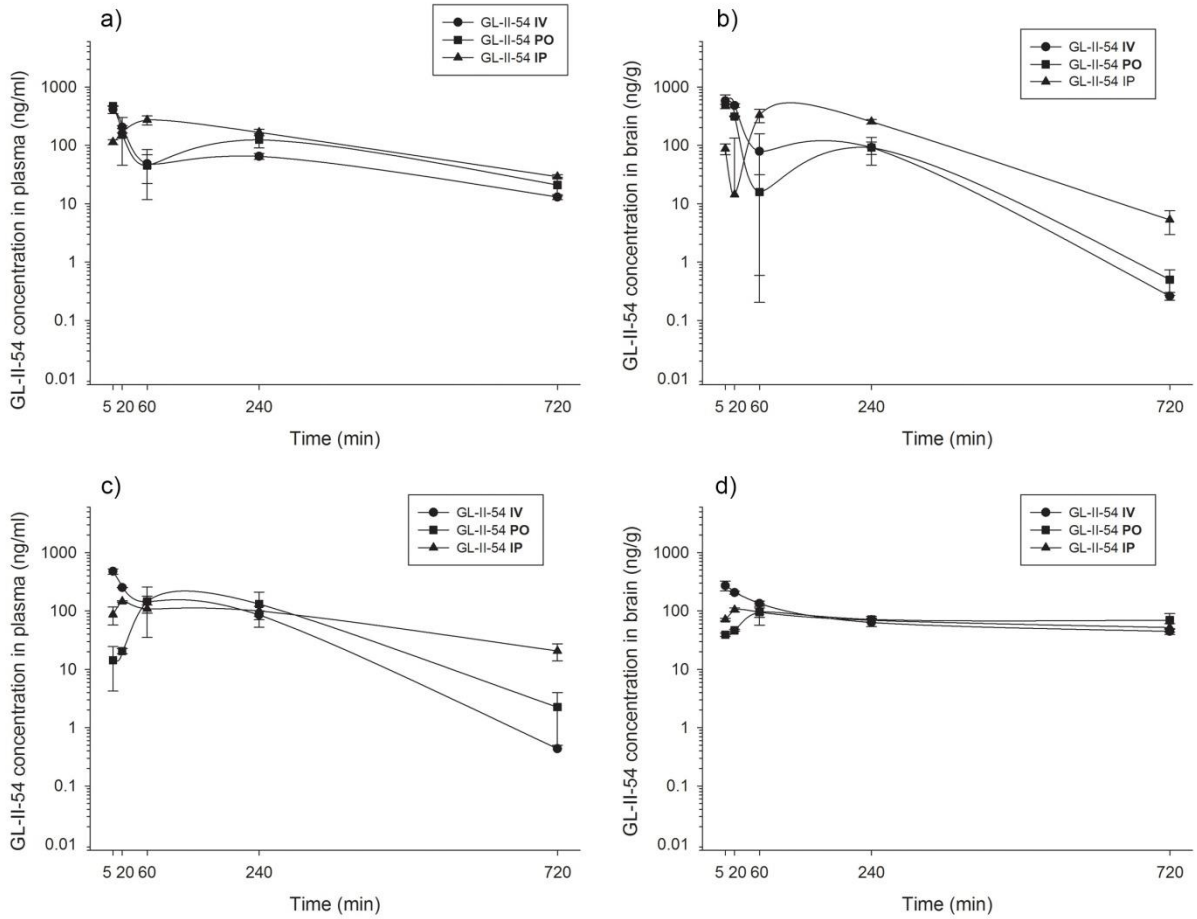

Figure 7. The concentration–time profile of GL-I-54 after intravenous (IV), peroral (PO) or intraperitoneal (IP) administration of the 3 mg/kg dose (n=3 per time point) in mouse plasma (a) and brain (b), as well as in rat plasma (c) and brain (d).

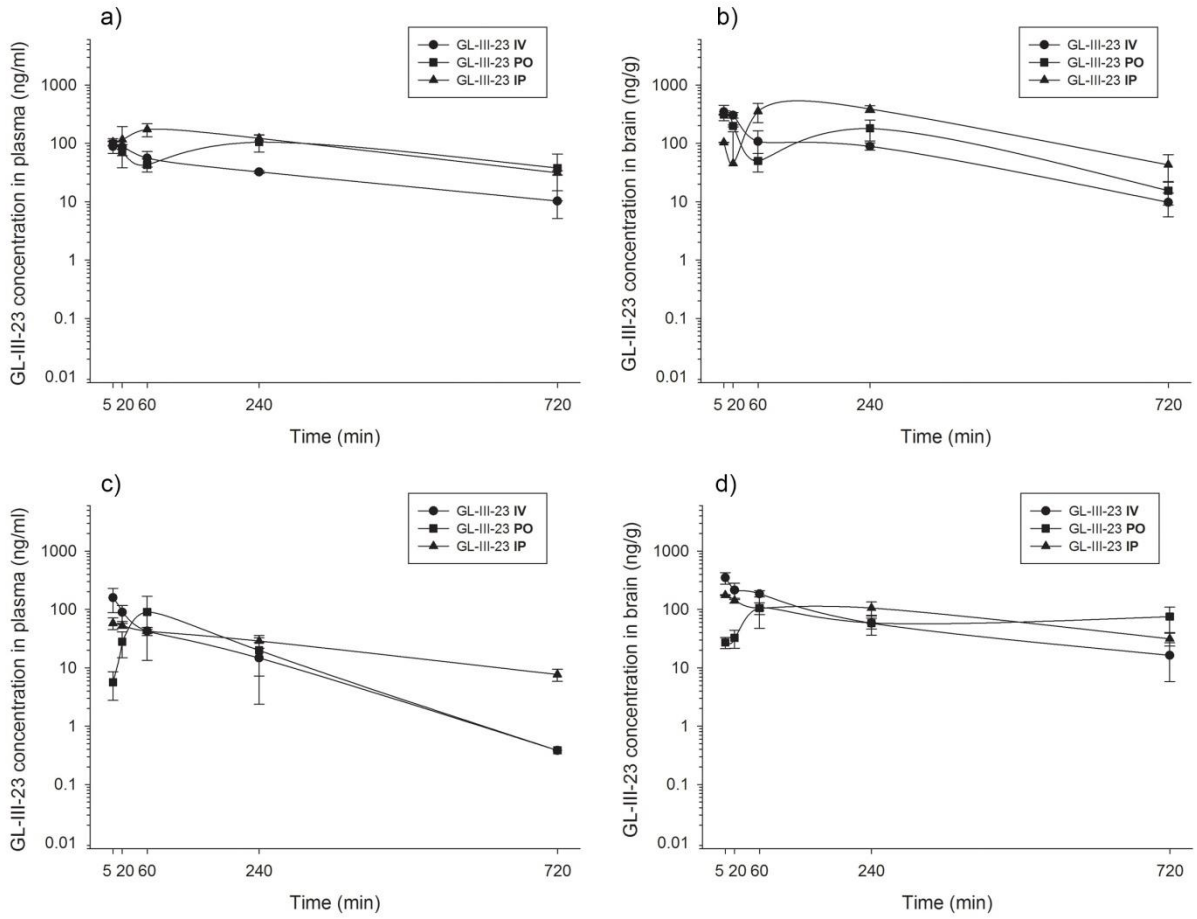

Figure 8. The concentration–time profile of GL-III-23 after intravenous (IV), peroral (PO) or intraperitoneal (IP) administration of the 3 mg/kg dose (n=3 per time point) in mouse plasma (a) and brain (b), as well as in rat plasma (c) and brain (d).

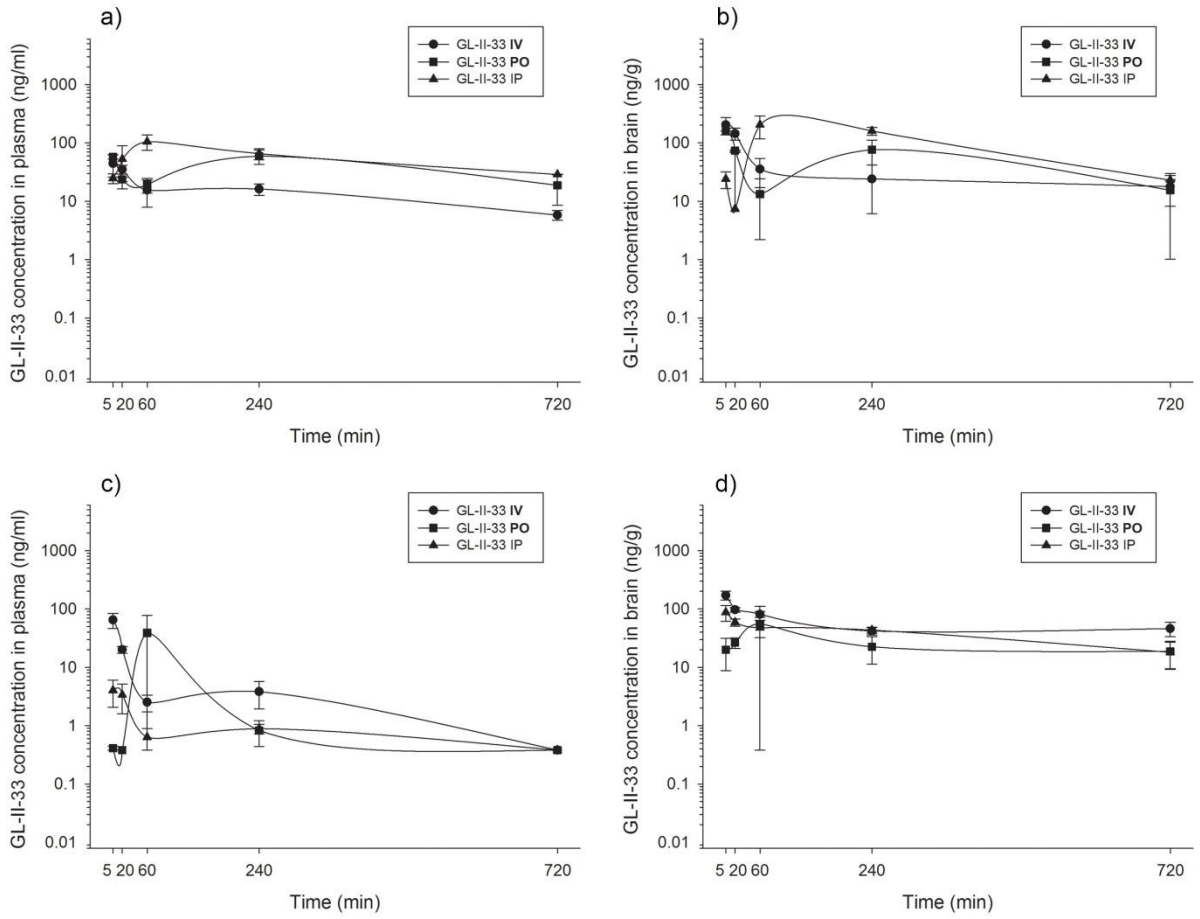

Figure 9. The concentration–time profile of GL-II-33 after intravenous (IV), peroral (PO) or intraperitoneal (IP) administration of the 3 mg/kg dose (n=3 per time point) in mouse plasma (a) and brain (b), as well as in rat plasma (c) and brain (d).

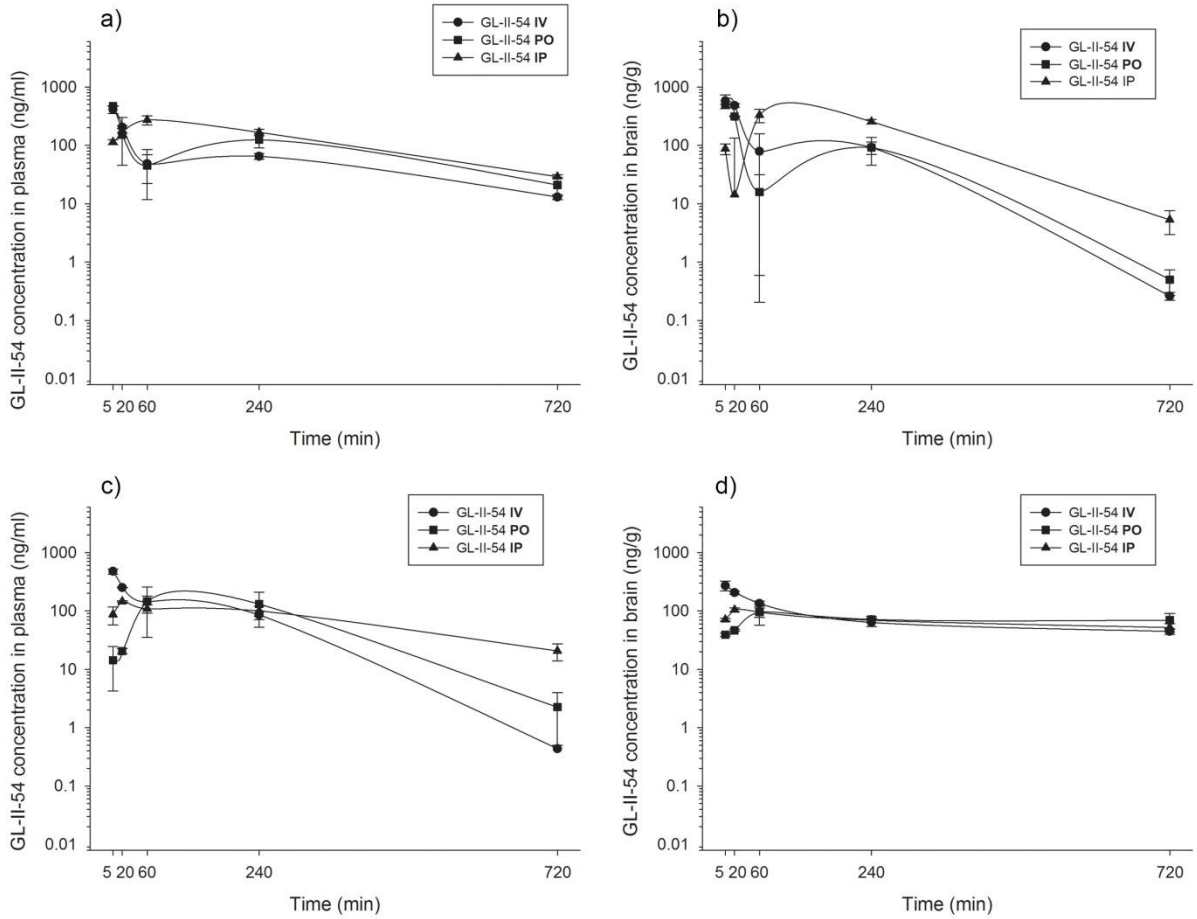

Figure 10. The concentration–time profile of GL-II-54 after intravenous (IV), peroral (PO) or intraperitoneal (IP) administration of the 3 mg/kg dose (n=3 per time point) in mouse plasma (a) and brain (b), as well as in rat plasma (c) and brain (d).

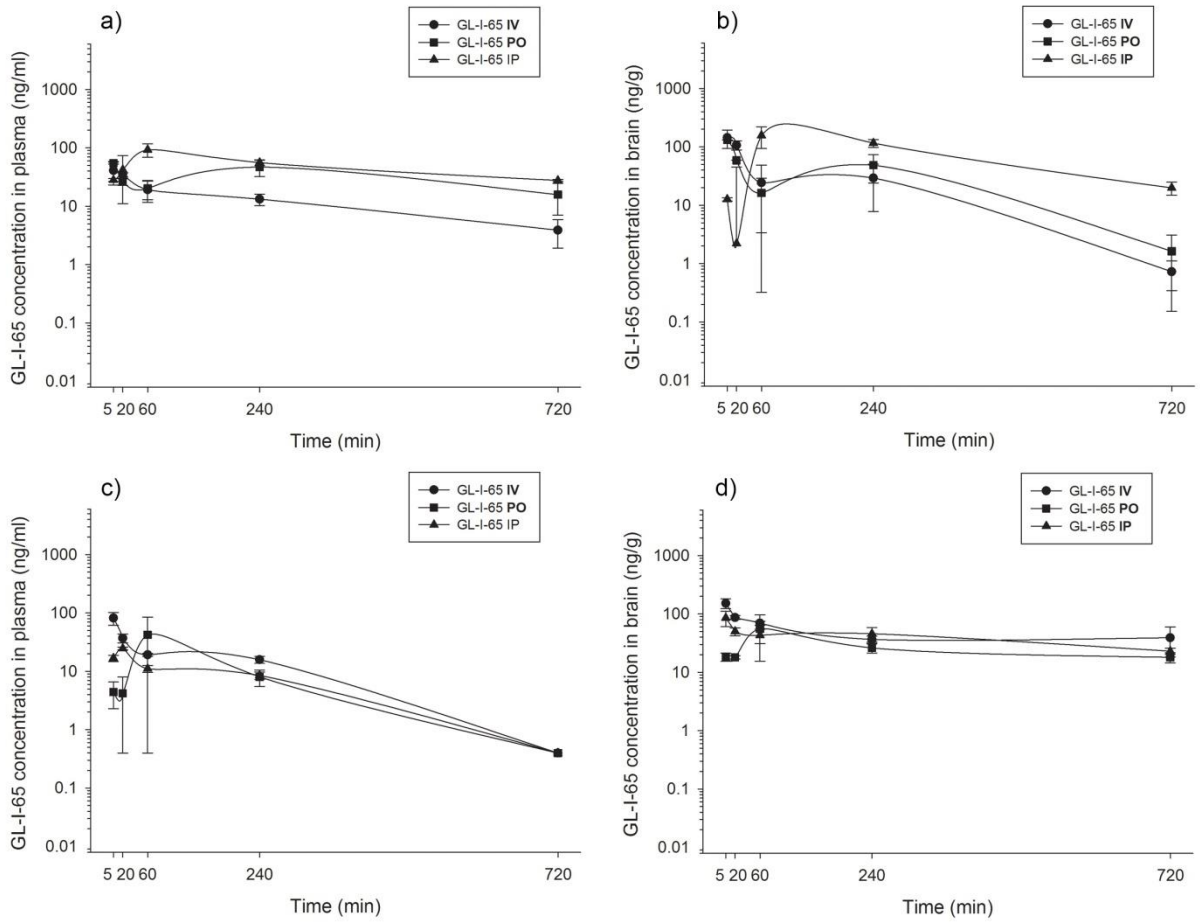

Figure 11. The concentration–time profile of GL-I-65 after intravenous (IV), peroral (PO) or intraperitoneal (IP) administration of the 3 mg/kg dose (n=3 per time point) in mouse plasma (a) and brain (b), as well as in rat plasma (c) and brain (d).

Plasma	Mean	SEM
Cmax (ng/ml)	91.049	11.272
Tmax (h)	2.000	1.000
AUC0_12 (ng*h/ml)	635.684	51.066
AUC0_∞ (ng*h/ml)	733.442	75.937
t1/2 (h)	8.884	1.406
β (1/h)	0.082	0.014

Brain	Mean	SEM
Cmax (ng/ml)	278.115	51.698
Tmax (h)	0.083	0.000
AUC0_12 (ng*h/ml)	1240.876	63.685
AUC0_∞ (ng*h/ml)	1698.191	107.291
t1/2 (h)	6.437	0.194
β (1/h)	0.108	0.003

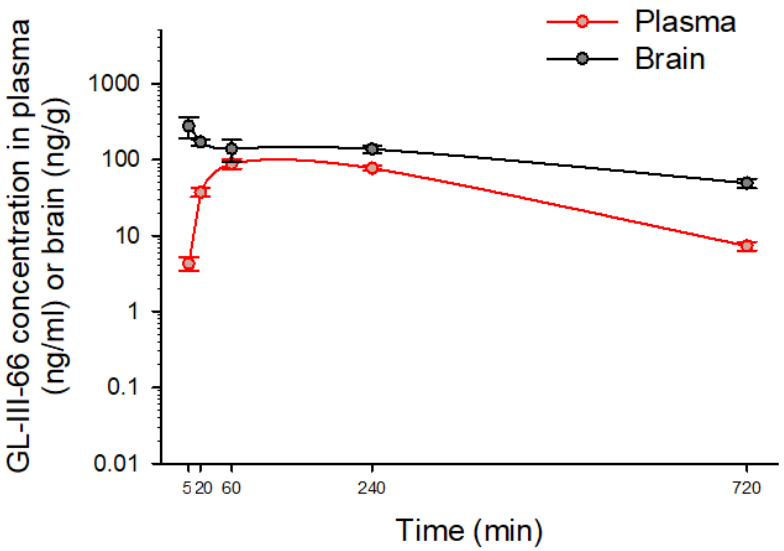

Figure 12. Plasma and brain concentration–time profiles of GL-III-66 and calculated pharmacokinetic parameters in male C57BL/6 mice (n = 3 per time point) after intraperitoneally administration of the cassette solution containing 3 mg/kg of each GL-III-66, GL-III-67, GL-III-68 and GL-III-63. C_{max} = maximum concentration in plasma or brain; T_{max} = time of maximum concentration in plasma or brain; AUC_{0-12} = area under the plasma or brain concentration–time curve from 0 to 12 h; $AUC_{0-\infty}$ = area under the plasma or brain concentration–time curve from 0 to extrapolated infinite time; $t_{1/2}$ = elimination half-life from plasma or brain; β = elimination constant rate from plasma or brain. All values are represented as a mean ± standard error of the mean.

Plasma	Mean	SEM
Cmax (ng/ml)	408.486	13.750
Tmax (h)	0.166	0.083
AUC0_12 (ng*h/ml)	387.985	36.451
AUC0_∞ (ng*h/ml)	389.037	36.842
t1/2 (h)	1.206	0.095
β (1/h)	0.583	0.050

Brain	Mean	SEM
Cmax (ng/ml)	1227.251	372.721
Tmax (h)	0.083	0.000
AUC0_12 (ng*h/ml)	751.337	120.652
AUC0_∞ (ng*h/ml)	787.670	108.260
t1/2 (h)	1.985	0.249
β (1/h)	0.361	0.045

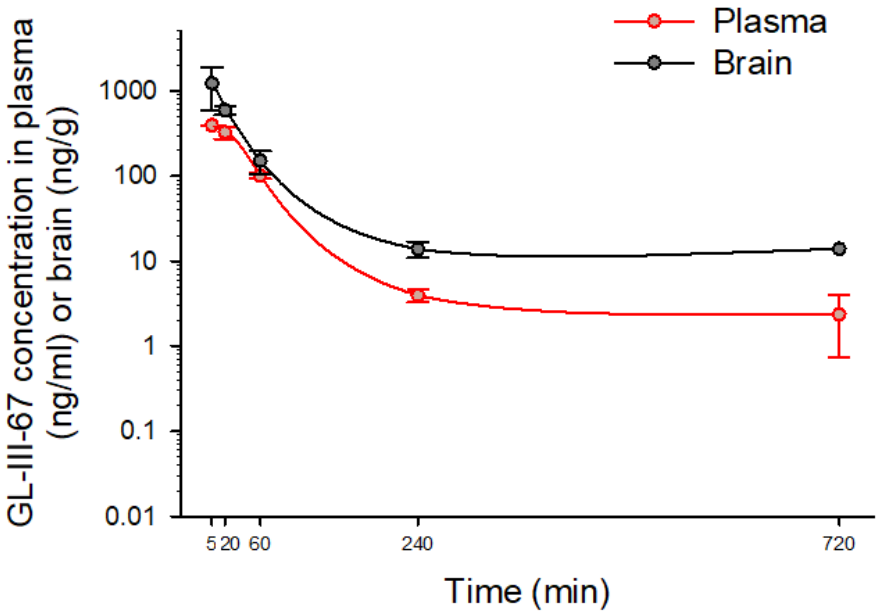

Figure 13. Plasma and brain concentration–time profiles of GL-III-67 and calculated pharmacokinetic parameters in male C57BL/6 mice (n = 3 per time point) after intraperitoneally administration of the cassette solution containing 3 mg/kg of each GL-III-66, GL-III-67, GL-III-68 and GL-III-63. C_{max} = maximum concentration in plasma or brain; T_{max} = time of maximum concentration in plasma or brain; AUC_{0-12} = area under the plasma or brain concentration–time curve from 0 to 12 h; $AUC_{0-\infty}$ = area under the plasma or brain concentration–time curve from 0 to extrapolated infinite time; $t_{1/2}$ = elimination half-life from plasma or brain; β = elimination constant rate from plasma or brain. All values are represented as a mean ± standard error of the mean.

Plasma	Mean	SEM
Cmax (ng/ml)	883.562	30.845
Tmax (h)	0.083	0.000
AUC0_12 (ng*h/ml)	536.691	46.793
AUC0_∞ (ng*h/ml)	565.585	46.567
t1/2 (h)	2.093	0.021
β (1/h)	0.331	0.003

Brain	Mean	SEM
Cmax (ng/ml)	1201.050	181.201
Tmax (h)	0.250	0.083
AUC0_12 (ng*h/ml)	947.671	69.805
AUC0_∞ (ng*h/ml)	1065.871	65.414
t1/2 (h)	2.721	0.144
β (1/h)	0.256	0.013

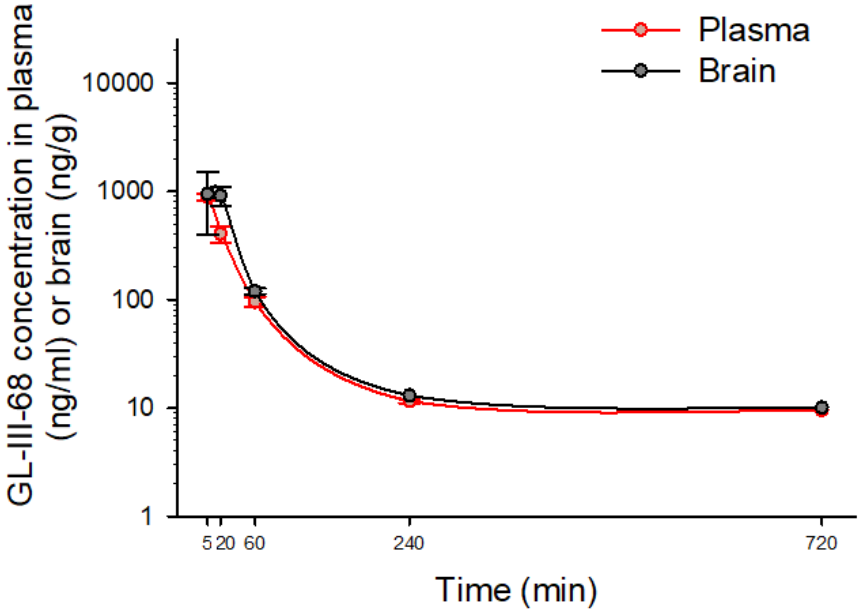

Figure 14. Plasma and brain concentration–time profiles of GL-III-68 and calculated pharmacokinetic parameters in male C57BL/6 mice (n = 3 per time point) after intraperitoneally administration of the cassette solution containing 3 mg/kg of each GL-III-66, GL-III-67, GL-III-68 and GL-III-63. C_{max} = maximum concentration in plasma or brain; T_{max} = time of maximum concentration in plasma or brain; AUC_{0-12} = area under the plasma or brain concentration–time curve from 0 to 12 h; $AUC_{0-\infty}$ = area under the plasma or brain concentration–time curve from 0 to extrapolated infinite time; $t_{1/2}$ = elimination half-life from plasma or brain; β = elimination constant rate from plasma or brain. All values are represented as a mean ± standard error of the mean. GL-III-68 and GL-III-70 are stereoisomers and some issues in analytical separation were encountered, so pharmacokinetic data for these compounds is approximated.

Plasma	Mean	SEM
Cmax (ng/ml)	883.562	30.845
Tmax (h)	0.083	0.000
AUC0_12 (ng*h/ml)	536.691	46.793
AUC0_∞ (ng*h/ml)	565.585	46.567
t1/2 (h)	2.093	0.021
β (1/h)	0.331	0.003

Brain	Mean	SEM
Cmax (ng/ml)	1201.050	181.201
Tmax (h)	0.250	0.083
AUC0_12 (ng*h/ml)	947.671	69.805
AUC0_∞ (ng*h/ml)	1065.871	65.414
t1/2 (h)	2.721	0.144
β (1/h)	0.256	0.013

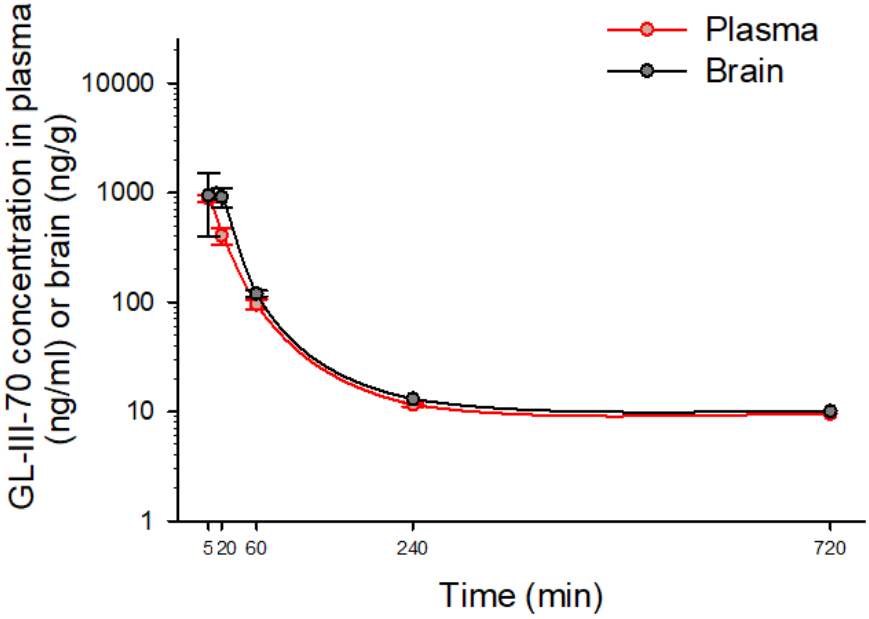

Figure 15. Plasma and brain concentration–time profiles of GL-III-70 and calculated pharmacokinetic parameters in male C57BL/6 mice (n = 3 per time point) after intraperitoneally administration of the cassette solution containing 3 mg/kg of each GL-III-70, GL-III-64 and GL-III-60. C_{max} = maximum concentration in plasma or brain; T_{max} = time of maximum concentration in plasma or brain; AUC_{0-12} = area under the plasma or brain concentration–time curve from 0 to 12 h; $AUC_{0-\infty}$ = area under the plasma or brain concentration–time curve from 0 to extrapolated infinite time; $t_{1/2}$ = elimination half-life from plasma or brain; β = elimination constant rate from plasma or brain. All values are represented as a mean ± standard error of the mean. GL-III-68 and GL-III-70 are stereoisomers and some issues in analytical separation were encountered, so pharmacokinetic data for these compounds is approximated.

Plasma	Mean	SEM
Cmax (ng/ml)	657.843	42.606
Tmax (h)	0.166	0.083
AUC0_12 (ng*h/ml)	2463.243	50.896
AUC0_∞ (ng*h/ml)	2495.755	32.930
t1/2 (h)	1.892	0.340
β (1/h)	0.395	0.081

Brain	Mean	SEM
Cmax (ng/ml)	1975.949	192.629
Tmax (h)	0.250	0.083
AUC0_12 (ng*h/ml)	5674.886	368.181
AUC0_∞ (ng*h/ml)	6202.476	640.257
t1/2 (h)	3.073	0.490
β (1/h)	0.238	0.040

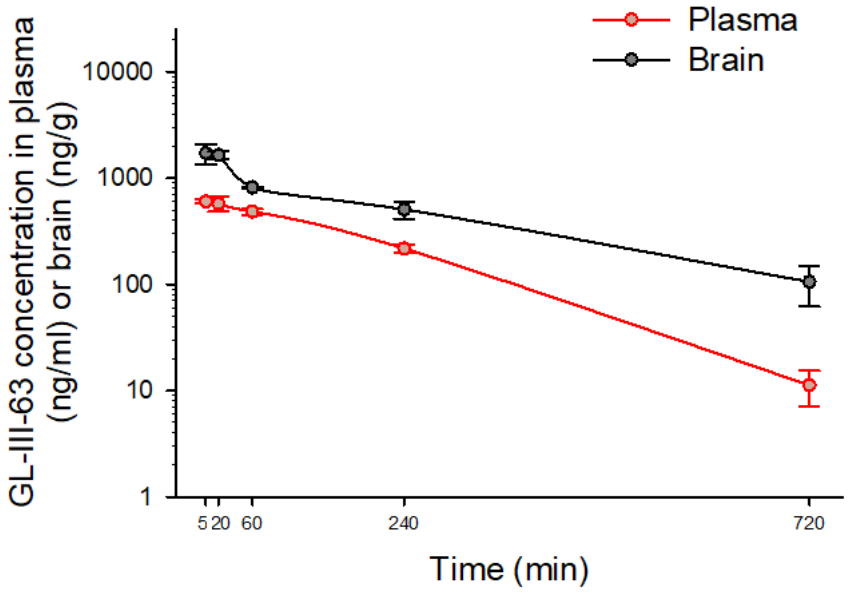

Figure 16. Plasma and brain concentration–time profiles of GL-III-63 and calculated pharmacokinetic parameters in male C57BL/6 mice (n = 3 per time point) after intraperitoneally administration of the cassette solution containing 3 mg/kg of each GL-III-66, GL-III-67, GL-III-68 and GL-III-63. C_{max} = maximum concentration in plasma or brain; T_{max} = time of maximum concentration in plasma or brain; AUC_{0-12} = area under the plasma or brain concentration–time curve from 0 to 12 h; $AUC_{0-\infty}$ = area under the plasma or brain concentration–time curve from 0 to extrapolated infinite time; $t_{1/2}$ = elimination half-life from plasma or brain; β = elimination constant rate from plasma or brain. All values are represented as a mean ± standard error of the mean.

Plasma	Mean	SEM
Cmax (ng/ml)	362.957	7.570
Tmax (h)	0.166	0.083
AUC0_12 (ng*h/ml)	1437.872	121.183
AUC0_∞ (ng*h/ml)	1464.937	111.962
t1/2 (h)	2.043	0.350
β (1/h)	0.361	0.065

Brain	Mean	SEM
Cmax (ng/ml)	605.255	97.689
Tmax (h)	0.166	0.083
AUC0_12 (ng*h/ml)	2302.144	307.403
AUC0_∞ (ng*h/ml)	3494.815	1072.093
t1/2 (h)	6.042	2.094
β (1/h)	0.143	0.043

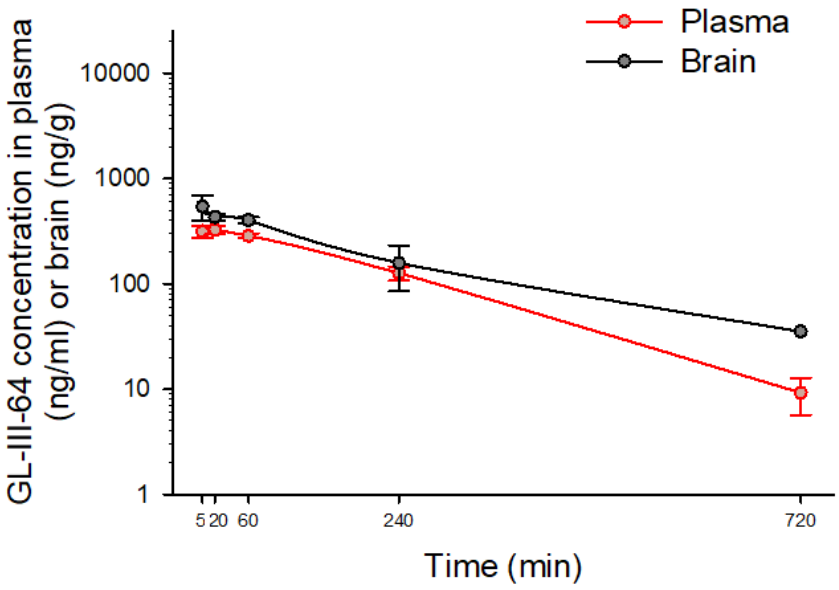

Figure 17. Plasma and brain concentration–time profiles of GL-III-64 and calculated pharmacokinetic parameters in male C57BL/6 mice (n = 3 per time point) after intraperitoneally administration of the cassette solution containing 3 mg/kg of each GL-III-70, GL-III-64 and GL-III-60. C_{max} = maximum concentration in plasma or brain; T_{max} = time of maximum concentration in plasma or brain; AUC_{0-12} = area under the plasma or brain concentration–time curve from 0 to 12 h; $AUC_{0-\infty}$ = area under the plasma or brain concentration–time curve from 0 to extrapolated infinite time; $t_{1/2}$ = elimination half-life from plasma or brain; β = elimination constant rate from plasma or brain. All values are represented as a mean ± standard error of the mean.

Plasma	Mean	SEM
Cmax (ng/ml)	128.600	10.097
Tmax (h)	0.555	0.222
AUC0_12 (ng*h/ml)	748.607	101.675
AUC0_∞ (ng*h/ml)	789.627	127.234
t1/2 (h)	2.937	0.711
β (1/h)	0.270	0.071

Brain	Mean	SEM
Cmax (ng/ml)	451.067	46.356
Tmax (h)	1.000	0.000
AUC0_12 (ng*h/ml)	2529.863	183.395
AUC0_∞ (ng*h/ml)	3078.920	326.580
t1/2 (h)	5.497	0.885
β (1/h)	0.133	0.022

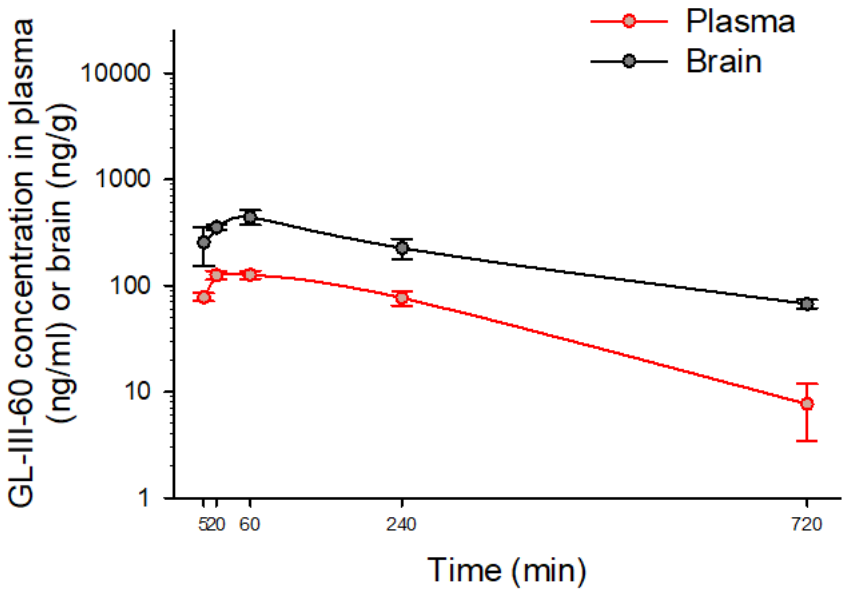

Figure 18. Plasma and brain concentration–time profiles of GL-III-60 and calculated pharmacokinetic parameters in male C57BL/6 mice (n = 3 per time point) after intraperitoneally administration of the cassette solution containing 3 mg/kg of each GL-III-70, GL-III-64 and GL-III-60. C_{max} = maximum concentration in plasma or brain; T_{max} = time of maximum concentration in plasma or brain; AUC_{0-12} = area under the plasma or brain concentration–time curve from 0 to 12 h; $AUC_{0-\infty}$ = area under the plasma or brain concentration–time curve from 0 to extrapolated infinite time; $t_{1/2}$ = elimination half-life from plasma or brain; β = elimination constant rate from plasma or brain. All values are represented as a mean ± standard error of the mean.

Table 54. Summary table (occupancy, efficacy, binding)

Compound	Dose	$GABA_A$ subtype	Occ.	Eff.	Ki
DZP	1.5 mg/kg	α1	67.70 %	212.82 % (207 %)*	22 nM
		α2	77.79 %	/, (333 %)	13 nM
		α3	69.71 %	/, (345 %)	20 nM
		α5	79.51 %	172.19 %, (266 %)	12 nM
SH-053-2'F-RCH3	30 mg/kg	α1	21.13 %	120%	759 nM
		α2	17.66 %	125%	948 nM
		α3	20.92 %	135%	768 nM
		α5	68.12 %	230%	95 nM
MP-III-022	10 mg/kg	α1	6.27 %	100%	850 µM
		α2	13.63 %	150%	55µM
GL-II-73	10 mg/kg	α1	0.57 %	131.68 %	55 µM
		α2	1.04 %	124.25 %	30 µM
		α3	0.50 %	129.08 %	63 µM
		α5	5.95 %	179.62 %	5 µM
GL-II-74	10 mg/kg	α1	19.45 %	146.18 %	1060 nM
		α2	24.03 %	150.02 %	809 nM
		α3	16.99 %	154.85 %	1250 nM
		α5	75.51 %	256.67 %	194 nM
GL-II-75	10 mg/kg	α1	8.34 %	162.90 %	542 nM
		α2	5.88 %	153.24 %	789 nM
		α3	9.31 %	139.49 %	480 nM
		α5	38.42 %	136.76 %	79 nM
RV-II-04	10 mg/kg	α1			
		α2			
		α3			
		α5			
GL-II-31	10 mg/kg	α1			
		α2			
		α3			
		α5			
MP-III-023	10 mg/kg	α1			
		α2			

		α3			
		α5			
GL-I-54	10 mg/kg	α1			
		α2			
		α3			
		α5			
GL-III-66	10 mg/kg	α1			
		α2			
		α3			
		α5			
GL-III-67	10 mg/kg	α1			
		α2			
		α3			
		α5			
GL-III-68	10 mg/kg	α1			
		α2			
		α3			
		α5			
GL-III-70	10 mg/kg	α1			
		α2			
		α3			
		α5			
GL-II-33	10 mg/kg	α1			
		α2			
		α3			
		α5			
GL-II-54	10 mg/kg	α1			
		α2			
		α3			
		α5			
GL-I-65	10 mg/kg	α1			
		α2			
		α3			
		α5			
GL-III-60	10 mg/kg	α1			
		α2			
		α3			
		α5			
GL-III-63	10 mg/kg	α1			

		α2			
		α3			
		α5			
GL-III-64	10 mg/kg	α1			
		α2			
		α3			
		α5			
MRK-016 (NAM)	3 mg/kg	α1			
		α2			
		α3			
		α5			

Table 55. Summary table (microsomal stability, FST, Y-maze)

Compound	Hum Liver Microsome	Mo Liver Microsome	Half-Life Pl	Half Life Br	FST	YM CRS
DZP					prodepr.	no infl.
SH-053-2'F-RCH3			1,2 hr	1,4 hr	antistress, females, UCMS	/
MP-III-022	141 min (70% /1hr)	164 min (77%)	0.6 hr	1.2 hr	/	/
GL-II-73	280 min (73%)	472 min (81%)	1,2 hr	2,4 hr	antidepr.	procogn.

GL-II-74	403 min (82%)	72 min (32%)	1,8 hr	1,5 hr	antidepr.	no infl.
GL-II-75	163 min (62%)	106 min (50%)	1,3 hr	1,4 hr	antidepr.	procogn.
RV-II-04	595 min (80%)	302 min (74%)	1.13 hr	0.9 hr	No eff	No eff
GL-II-31	1870 min (92%)	1840 min (93%)	1.3 hr	1.2 hr	No eff	No eff
MP-III-023	1790 min (92%)	846 min (85%)	1.5 hr	0.8hr	No eff	No eff
GL-I-54	100 min (36%)	53 min (15%)	0.7 hr	0.8 hr	antidepr. (5mg/kg)	
GL-III-66			8.8 hr	6.4 hr	/	No eff

GL-III-67			1.2 hr	1.9 hr	/	No eff
GL-III-68			2.1 hr	2.7 hr	/	procogn.
GL-III-70			2.1 hr	2.7 hr	/	procogn.
GL-II-33					/	procogn.
GL-II-54					/	/
GL-I-65					/	procogn.

GL-III-60			2.9 hr	5.5 hr	/	/
GL-III-63			1.9 hr	3 hr	/	/
GL-III-64			2. hr	6 hr	/	/
MRK-016 (NAM)					/	/

Table 56. Summary table (Y-maze, SLA, RR, EPM).

Compound	YM no stress	YM Aging	YM CRS Chro	SLA	RR	EPM
DZP	anticogn.	/	no infl. (30 mg/kg)	hypo	hypo	anxl.
	/	/	/	hypo	no infl.	no infl.

SH-053-2'F-RCH3						
MP-III-022	/	/	/	no infl. (rats)	no infl.	no infl.
GL-II-73	no infl.	procogn.	procogn. (30 mg/kg)	no infl.	no infl.	anxl.
GL-II-74	anticogn.	no infl.	/	hyper	hypo	anxl.
GL-II-75	no infl.	procogn.	/	hypo	hypo	anxl.
RV-II-04	/	/	/	hypo	hypo	/
GL-II-31	/	/	/	No eff	No eff	/
MP-III-023	/	/	/	hypo	hypo	/

GL-I-54	/	/	/	No eff	No eff	/
GL-III-66	/	/	/	No eff (Hypo >15mgkg [rat])	No eff (Hypo @40mgkg [rat])	No eff
GL-III-67	/	/	/	No eff (Hypo >15mgkg [rat])	No eff (Hypo @20mgkg [rat])	Potential anxiolytic
GL-III-68	/	/	/	No eff (Hypo >15mgkg [rat])	No eff (Hypo @30mgkg [rat])	Potential anxiolytic
GL-III-70	/	/	/	No eff (Hypo >15mgkg [rat])	No eff	No eff
GL-II-33	/	/	/	No eff		/

GL-II-54	/	/	/	No eff		/
GL-I-65	/	/	/	No eff		/
GL-III-60	/	/	/	No eff (Hypo >15mgkg [rat])	No eff	No eff
GL-III-63	/	/	/	No eff (Hypo >15mgkg [rat])	No eff	No eff
GL-III-64	/	/	/	No eff (Hypo >15mgkg [rat])	No eff	No eff
MRK-016 (NAM)	/	/	/	/	/	No eff

Appendix IV: Additional Data for Anti-schizophrenic like Behavioral Study Induced by MK-801

Total immobile episodes

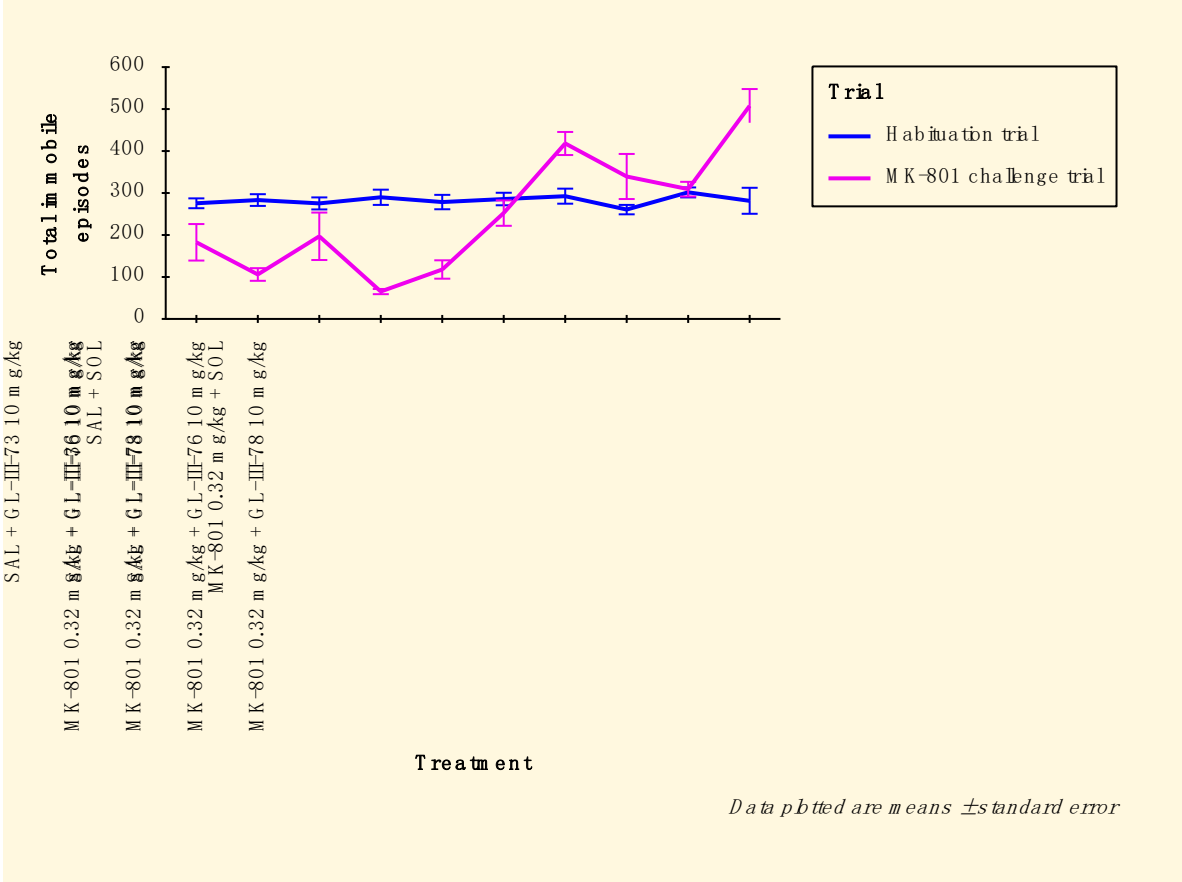

Figure 1. Total immobile episodes. The data analysed has been limited in the following way: Treatment = SAL + SOL, SAL + GL-III-36 10 mg/kg, SAL + GL-III-73 10 mg/kg, SAL + GL-III-76 10 mg/kg, SAL + GL-III-78 10 mg/kg, MK-801 0.32 mg/kg + SOL, MK-801 0.32 mg/kg + GL-III-36 10 mg/kg, MK-801 0.32 mg/kg + GL-III-73 10 mg/kg, MK-801 0.32 mg/kg + GL-III-76 10 mg/kg or MK-801 0.32 mg/kg + GL-III-78 10 mg/kg and Trial = Habituation trial or MK-801 challenge trial.

Maximum speed (m/s)

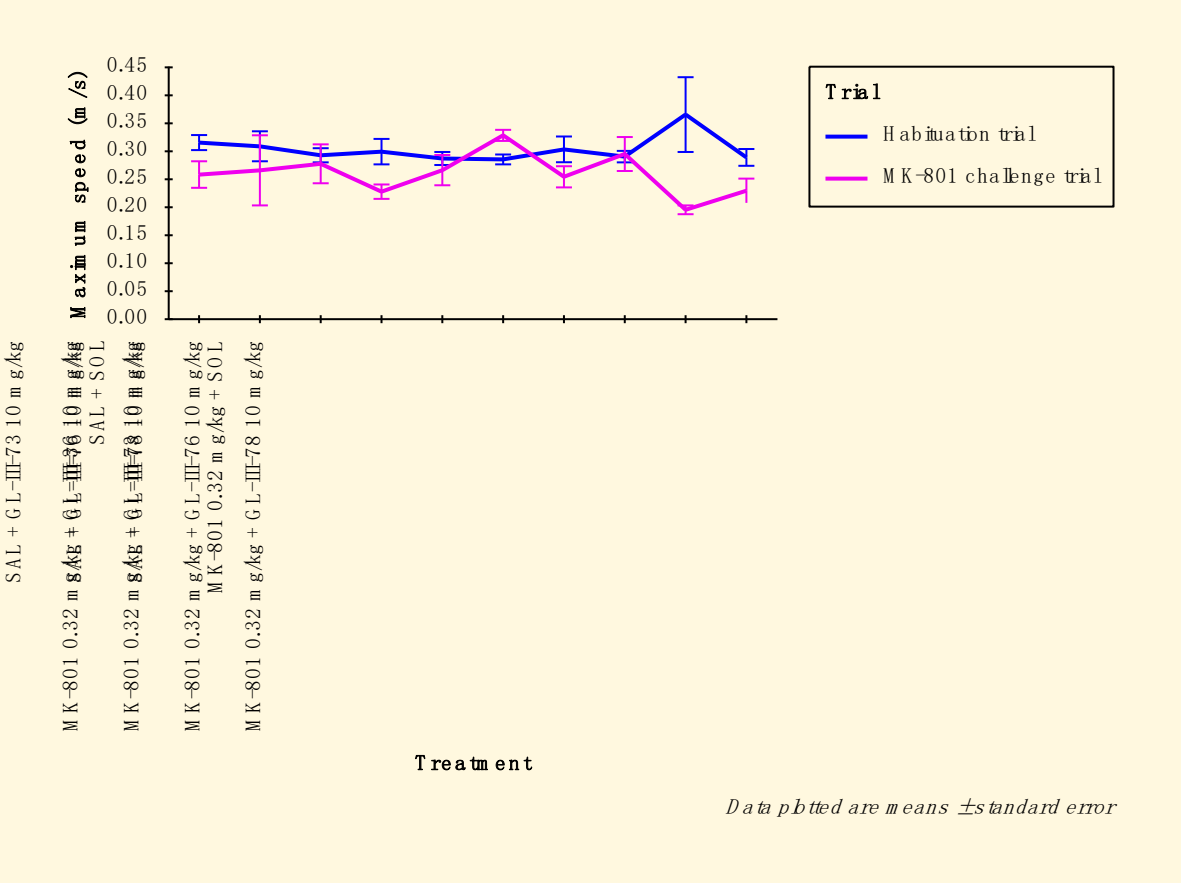

Figure 2. Maximum speed. The data analysed has been limited in the following way: Treatment = SAL + SOL, SAL + GL-III-36 10 mg/kg, SAL + GL-III-73 10 mg/kg, SAL + GL-III-76 10 mg/kg, SAL + GL-III-78 10 mg/kg, MK-801 0.32 mg/kg + SOL, MK-801 0.32 mg/kg + GL-III-36 10 mg/kg, MK-801 0.32 mg/kg + GL-III-73 10 mg/kg, MK-801 0.32 mg/kg + GL-III-76 10 mg/kg or MK-801 0.32 mg/kg + GL-III-78 10 mg/kg and Trial = Habituation trial or MK-801 challenge trial.

Rotations of the animal's body

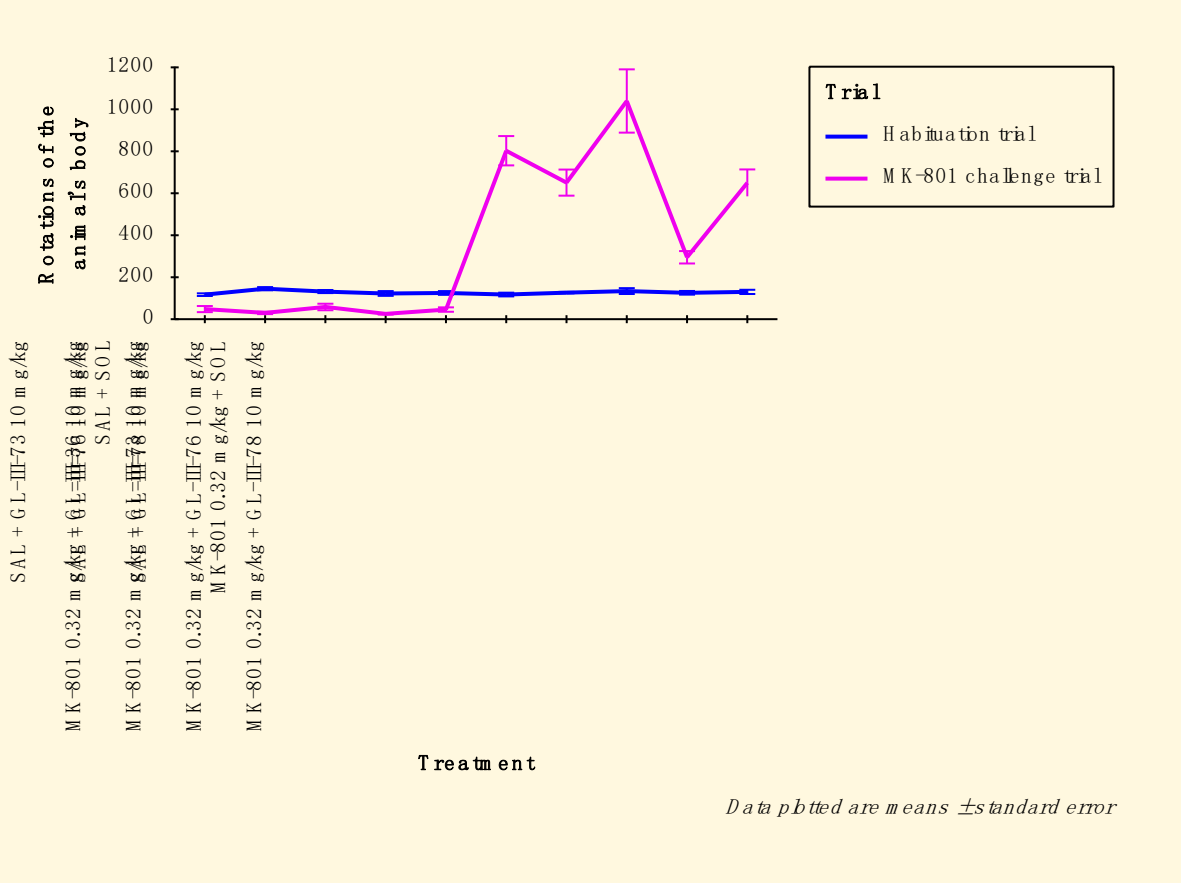

Figure 3. Rotations of the animal's body. The data analysed has been limited in the following way: Treatment = SAL + SOL, SAL + GL-III-36 10 mg/kg, SAL + GL-III-73 10 mg/kg, SAL + GL-III-76 10 mg/kg, SAL + GL-III-78 10 mg/kg, MK-801 0.32 mg/kg + SOL, MK-801 0.32 mg/kg + GL-III-36 10 mg/kg, MK-801 0.32 mg/kg + GL-III-73 10 mg/kg, MK-801 0.32 mg/kg + GL-III-76 10 mg/kg or MK-801 0.32 mg/kg + GL-III-78 10 mg/kg and Trial = Habituation trial or MK-801 challenge trial.

Clockwise rotations of the animal's body

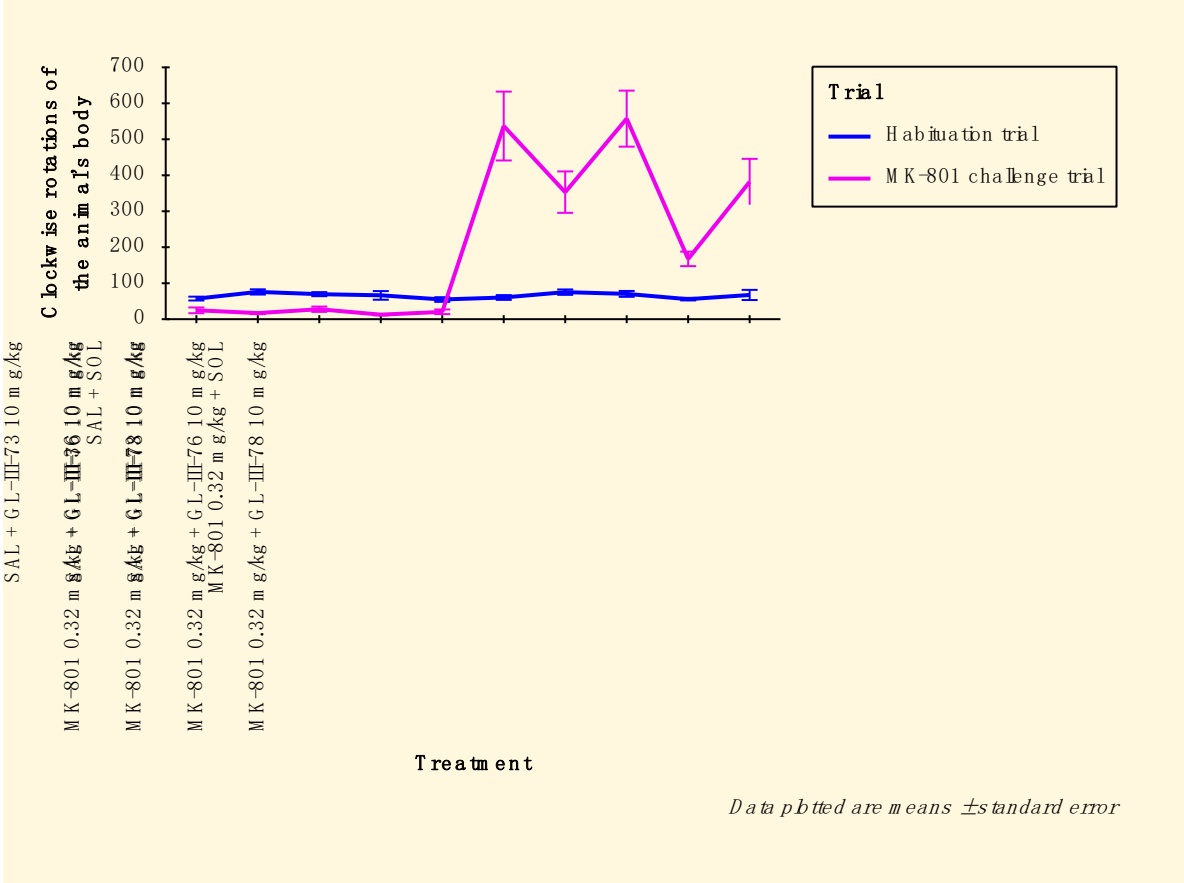

Figure 4. Clockwise rotations of the animal's body. The data analysed has been limited in the following way: Treatment = SAL + SOL, SAL + GL-III-36 10 mg/kg, SAL + GL-III-73 10 mg/kg, SAL + GL-III-76 10 mg/kg, SAL + GL-III-78 10 mg/kg, MK-801 0.32 mg/kg + SOL, MK-801 0.32 mg/kg + GL-III-36 10 mg/kg, MK-801 0.32 mg/kg + GL-III-73 10 mg/kg, MK-801 0.32 mg/kg + GL-III-76 10 mg/kg or MK-801 0.32 mg/kg + GL-III-78 10 mg/kg and Trial = Habituation trial or MK-801 challenge trial.

Anticlockwise rotations of the animal's body

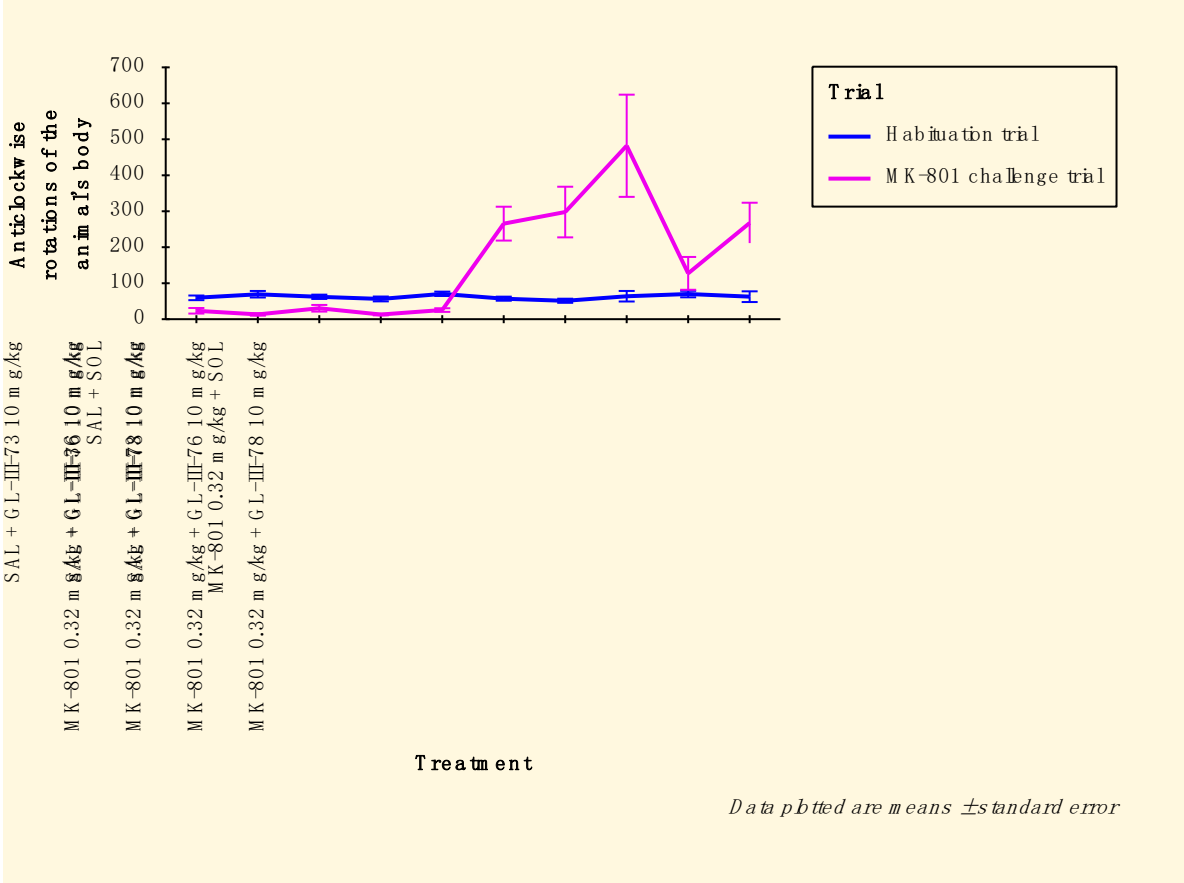

Figure 5. Anticlockwise rotations of the animal's body. The data analysed has been limited in the following way: Treatment = SAL + SOL, SAL + GL-III-36 10 mg/kg, SAL + GL-III-73 10 mg/kg, SAL + GL-III-76 10 mg/kg, SAL + GL-III-78 10 mg/kg, MK-801 0.32 mg/kg + SOL, MK-801 0.32 mg/kg + GL-III-36 10 mg/kg, MK-801 0.32 mg/kg + GL-III-73 10 mg/kg, MK-801 0.32 mg/kg + GL-III-76 10 mg/kg or MK-801 0.32 mg/kg + GL-III-78 10 mg/kg and Trial = Habituation trial or MK-801 challenge trial.

Total freezing episodes

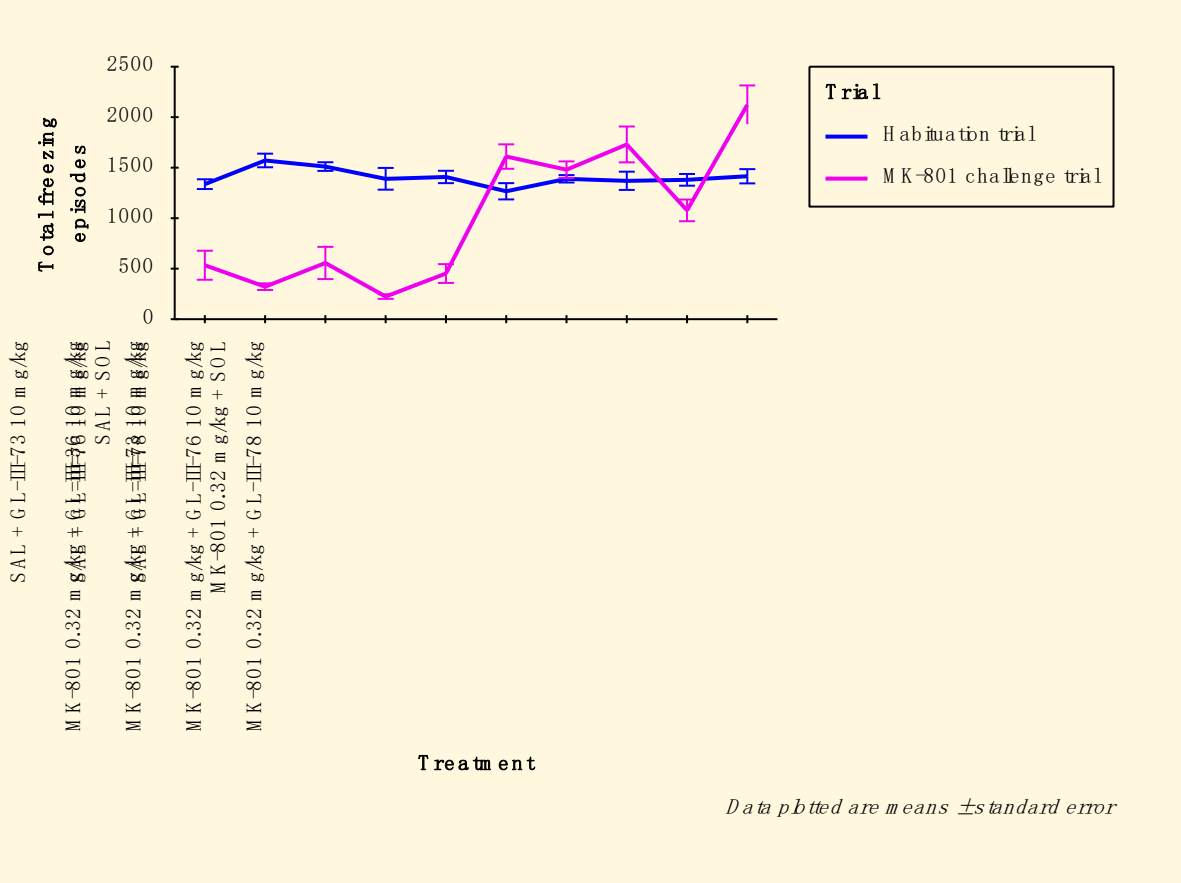

Figure 6. Total freezing episodes. The data analysed has been limited in the following way: Treatment = SAL + SOL, SAL + GL-III-36 10 mg/kg, SAL + GL-III-73 10 mg/kg, SAL + GL-III-76 10 mg/kg, SAL + GL-III-78 10 mg/kg, MK-801 0.32 mg/kg + SOL, MK-801 0.32 mg/kg + GL-III-36 10 mg/kg, MK-801 0.32 mg/kg + GL-III-73 10 mg/kg, MK-801 0.32 mg/kg + GL-III-76 10 mg/kg or MK-801 0.32 mg/kg + GL-III-78 10 mg/kg and Trial = Habituation trial or MK-801 challenge trial.

Total time freezing (s)

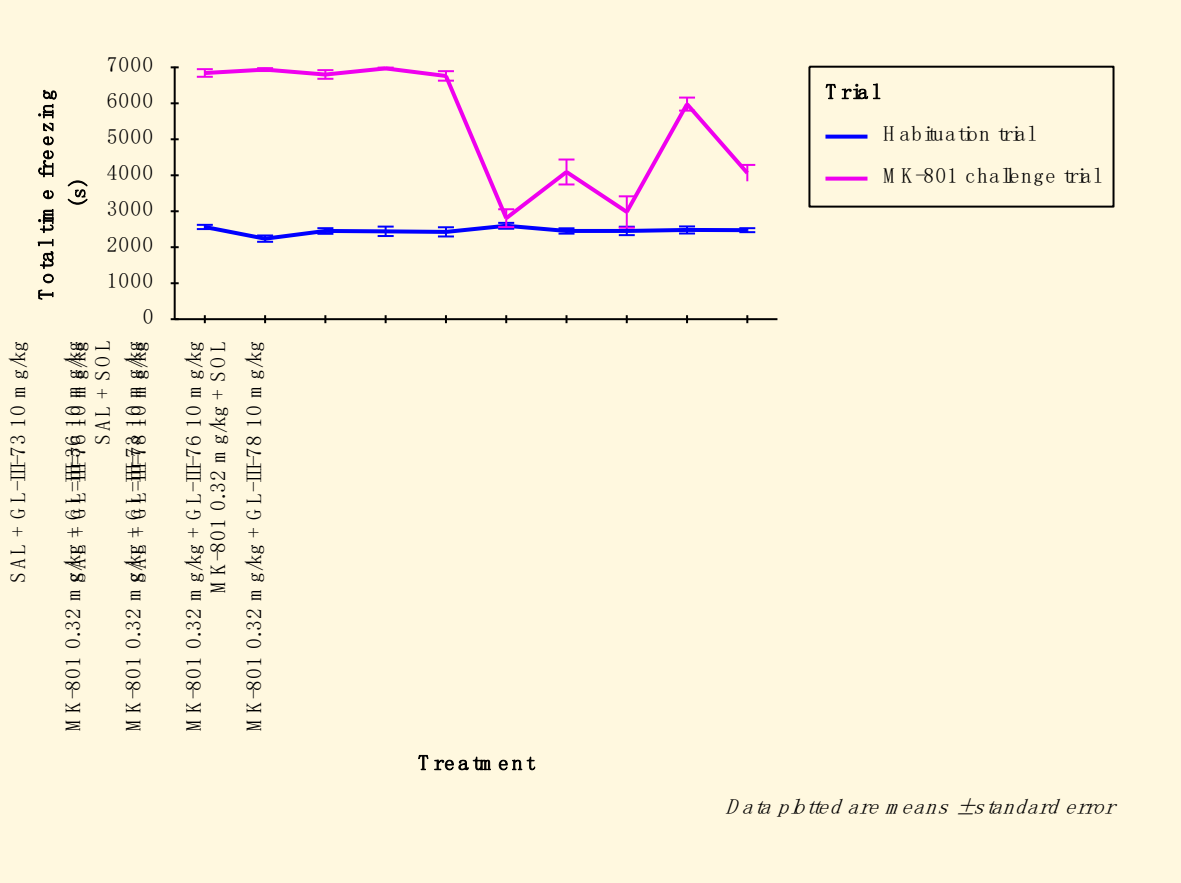

Figure 7. Total time freezing. The data analysed has been limited in the following way: Treatment = SAL + SOL, SAL + GL-III-36 10 mg/kg, SAL + GL-III-73 10 mg/kg, SAL + GL-III-76 10 mg/kg, SAL + GL-III-78 10 mg/kg, MK-801 0.32 mg/kg + SOL, MK-801 0.32 mg/kg + GL-III-36 10 mg/kg, MK-801 0.32 mg/kg + GL-III-73 10 mg/kg, MK-801 0.32 mg/kg + GL-III-76 10 mg/kg or MK-801 0.32 mg/kg + GL-III-78 10 mg/kg and Trial = Habituation trial or MK-801 challenge trial.

Total distance travelled (m)

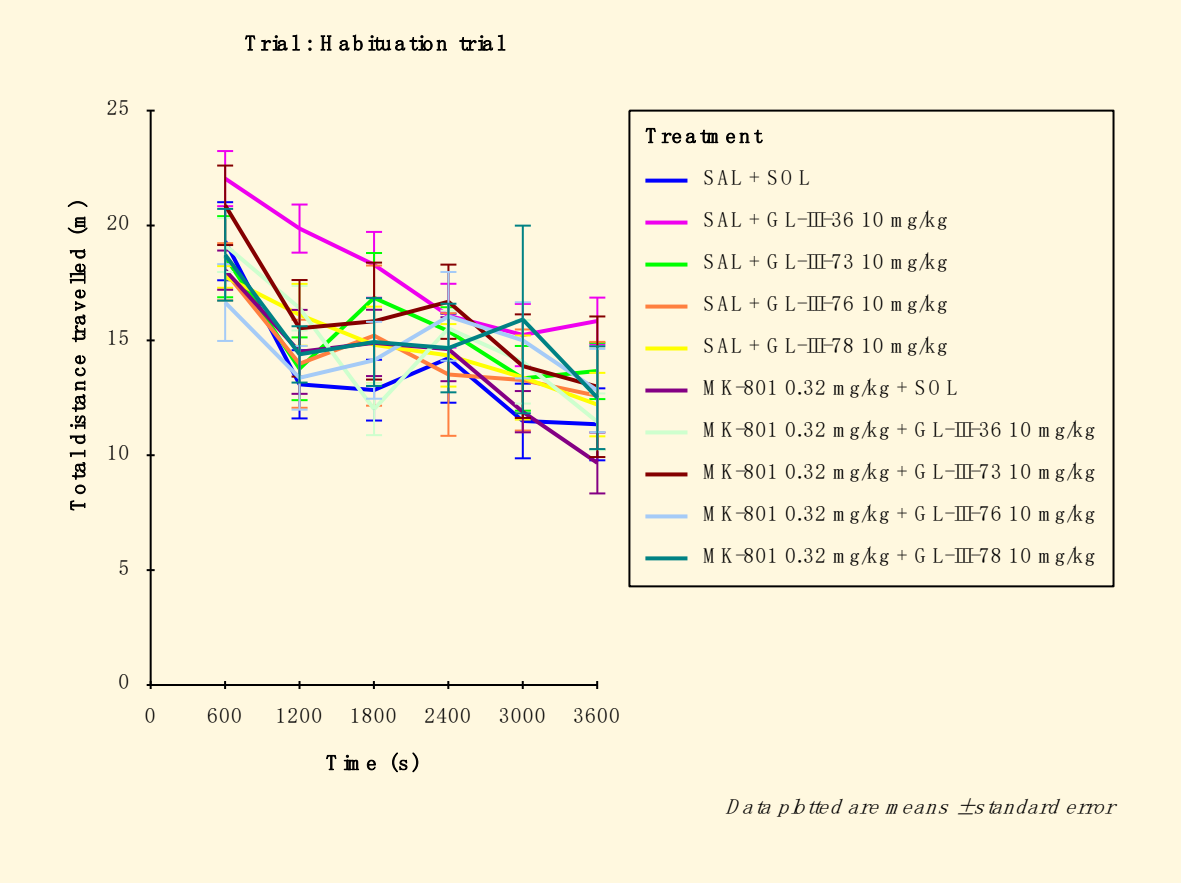

Figure 8. Total distance travelled for tests where Trial is Habituation trial. The data analysed has been limited in the following way: Treatment = SAL + SOL, SAL + GL-III-36 10 mg/kg, SAL + GL-III-73 10 mg/kg, SAL + GL-III-76 10 mg/kg, SAL + GL-III-78 10 mg/kg, MK-801 0.32 mg/kg + SOL, MK-801 0.32 mg/kg + GL-III-36 10 mg/kg, MK-801 0.32 mg/kg + GL-III-73 10 mg/kg, MK-801 0.32 mg/kg + GL-III-76 10 mg/kg or MK-801 0.32 mg/kg + GL-III-78 10 mg/kg and Trial = Habituation trial or MK-801 challenge trial.

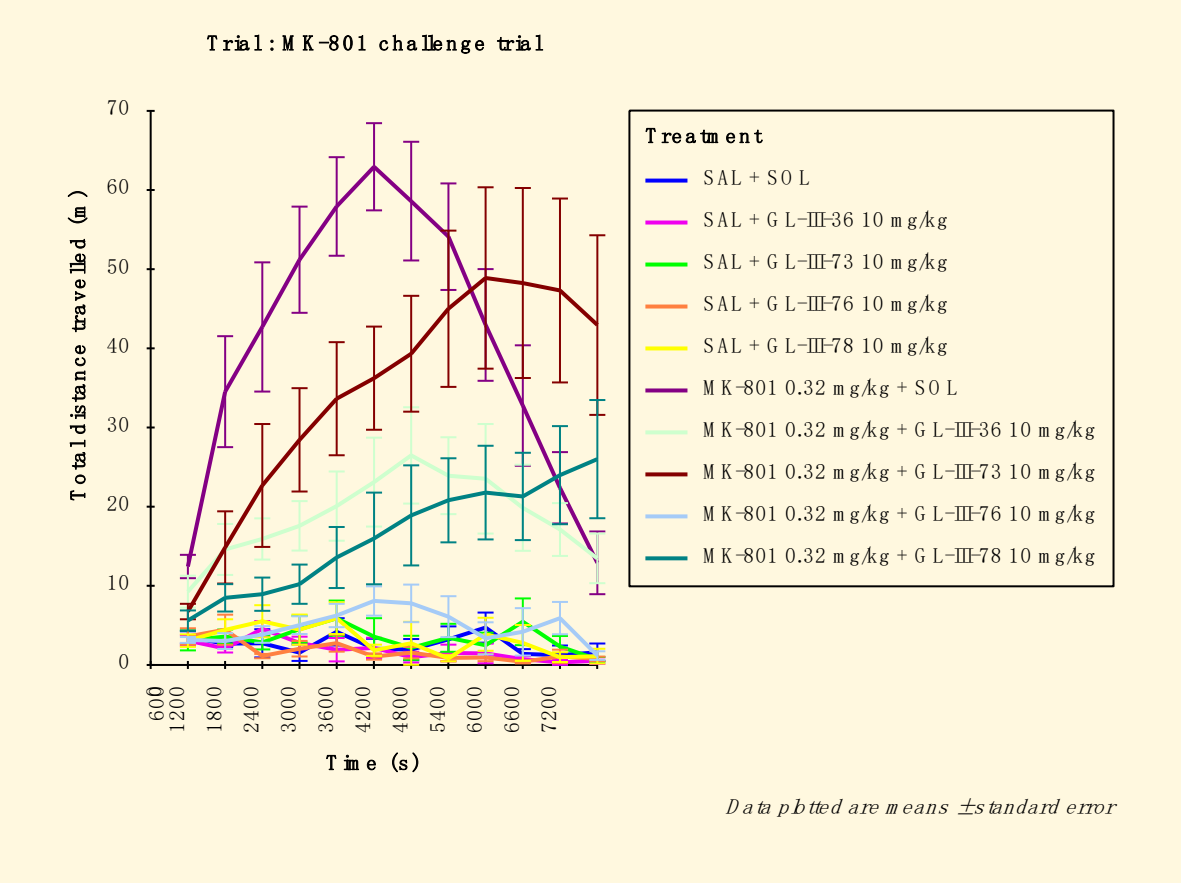

Figure 9. Total distance travelled for tests where Trial is MK-801 challenge trial. The data analysed has been limited in the following way: Treatment = SAL + SOL, SAL + GL-III-36 10 mg/kg, SAL + GL-III-73 10 mg/kg, SAL + GL-III-76 10 mg/kg, SAL + GL-III-78 10 mg/kg, MK-801 0.32 mg/kg + SOL, MK-801 0.32 mg/kg + GL-III-36 10 mg/kg, MK-801 0.32 mg/kg + GL-III-73 10 mg/kg, MK-801 0.32 mg/kg + GL-III-76 10 mg/kg or MK-801 0.32 mg/kg + GL-III-78 10 mg/kg and Trial = Habituation trial or MK-801 challenge trial.

Average speed (m/s)

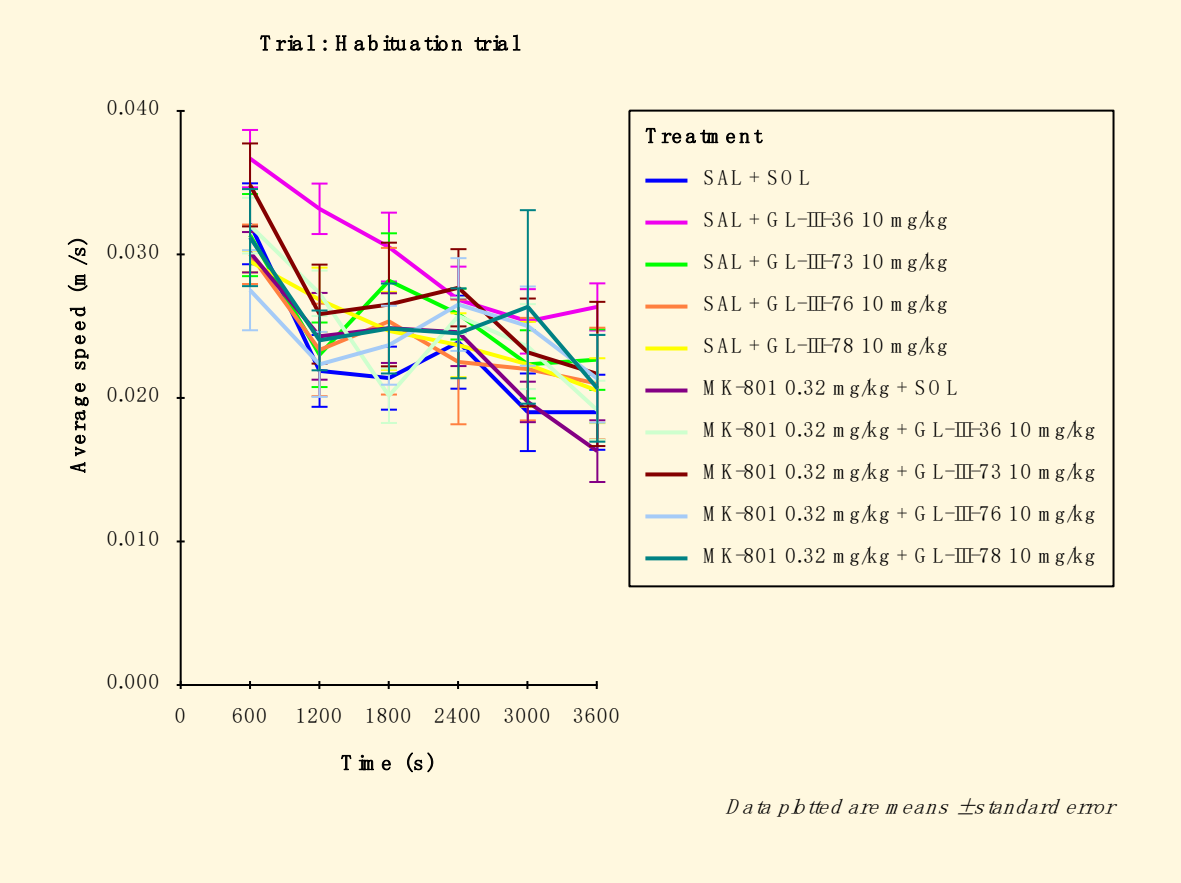

Figure 10. Average speed for tests where Trial is Habituation trial. The data analysed has been limited in the following way: Treatment = SAL + SOL, SAL + GL-III-36 10 mg/kg, SAL + GL-III-73 10 mg/kg, SAL + GL-III-76 10 mg/kg, SAL + GL-III-78 10 mg/kg, MK-801 0.32 mg/kg + SOL, MK-801 0.32 mg/kg + GL-III-36 10 mg/kg, MK-801 0.32 mg/kg + GL-III-73 10 mg/kg, MK-801 0.32 mg/kg + GL-III-76 10 mg/kg or MK-801 0.32 mg/kg + GL-III-78 10 mg/kg and Trial = Habituation trial or MK-801 challenge trial.

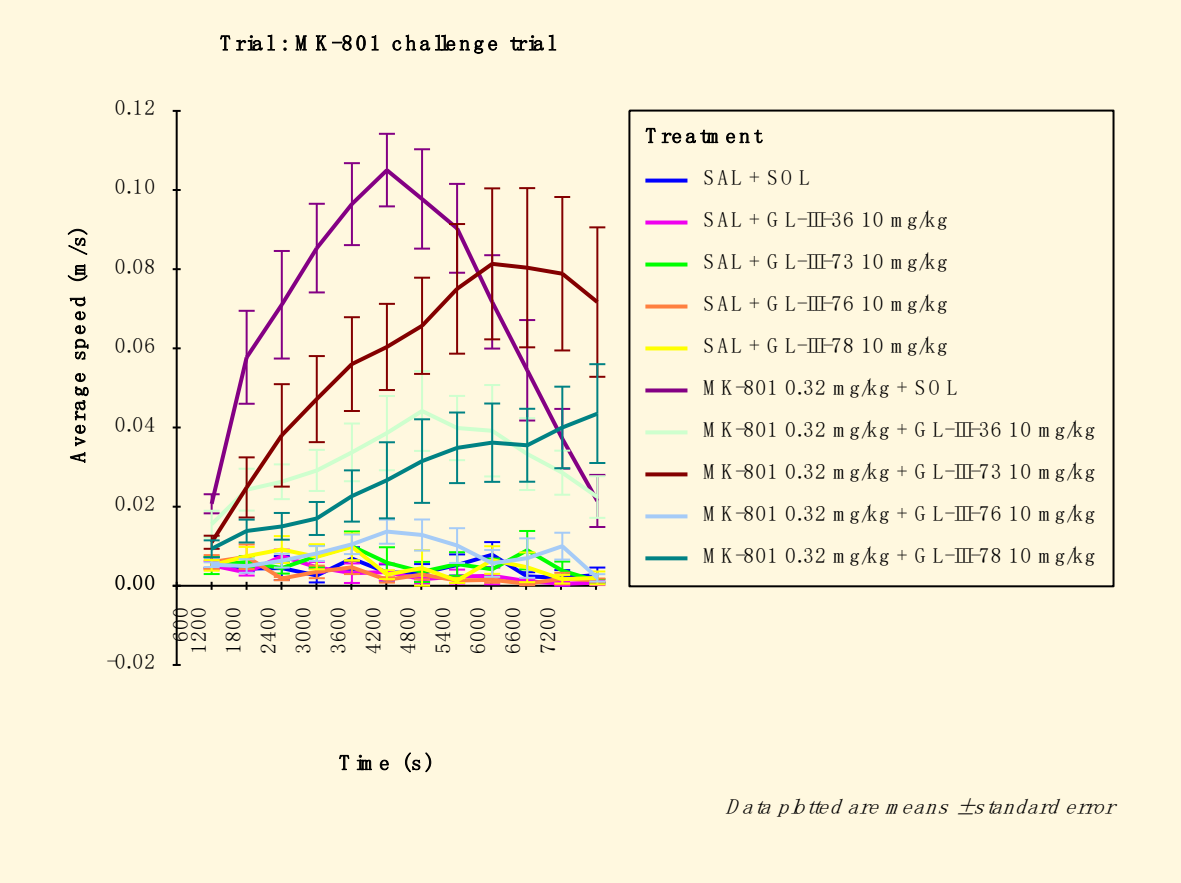

Figure 11. Average speed for tests where Trial is MK-801 challenge trial. The data analysed has been limited in the following way: Treatment = SAL + SOL, SAL + GL-III-36 10 mg/kg, SAL + GL-III-73 10 mg/kg, SAL + GL-III-76 10 mg/kg, SAL + GL-III-78 10 mg/kg, MK-801 0.32 mg/kg + SOL, MK-801 0.32 mg/kg + GL-III-36 10 mg/kg, MK-801 0.32 mg/kg + GL-III-73 10 mg/kg, MK-801 0.32 mg/kg + GL-III-76 10 mg/kg or MK-801 0.32 mg/kg + GL-III-78 10 mg/kg and Trial = Habituation trial or MK-801 challenge trial.

Total time mobile (s)

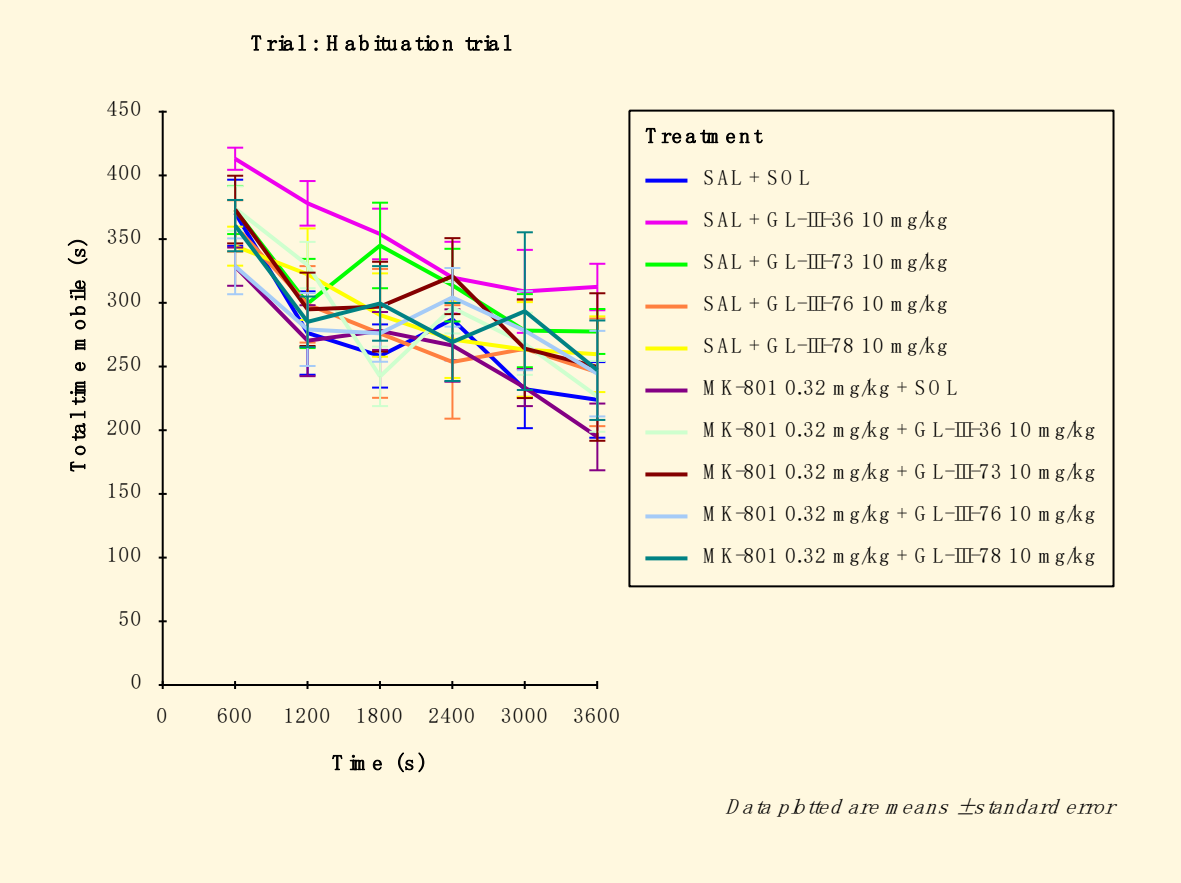

Figure 12. Total time mobile for tests where Trial is Habituation trial. The data analysed has been limited in the following way: Treatment = SAL + SOL, SAL + GL-III-36 10 mg/kg, SAL + GL-III-73 10 mg/kg, SAL + GL-III-76 10 mg/kg, SAL + GL-III-78 10 mg/kg, MK-801 0.32 mg/kg + SOL, MK-801 0.32 mg/kg + GL-III-36 10 mg/kg, MK-801 0.32 mg/kg + GL-III-73 10 mg/kg, MK-801 0.32 mg/kg + GL-III-76 10 mg/kg or MK-801 0.32 mg/kg + GL-III-78 10 mg/kg and Trial = Habituation trial or MK-801 challenge trial.

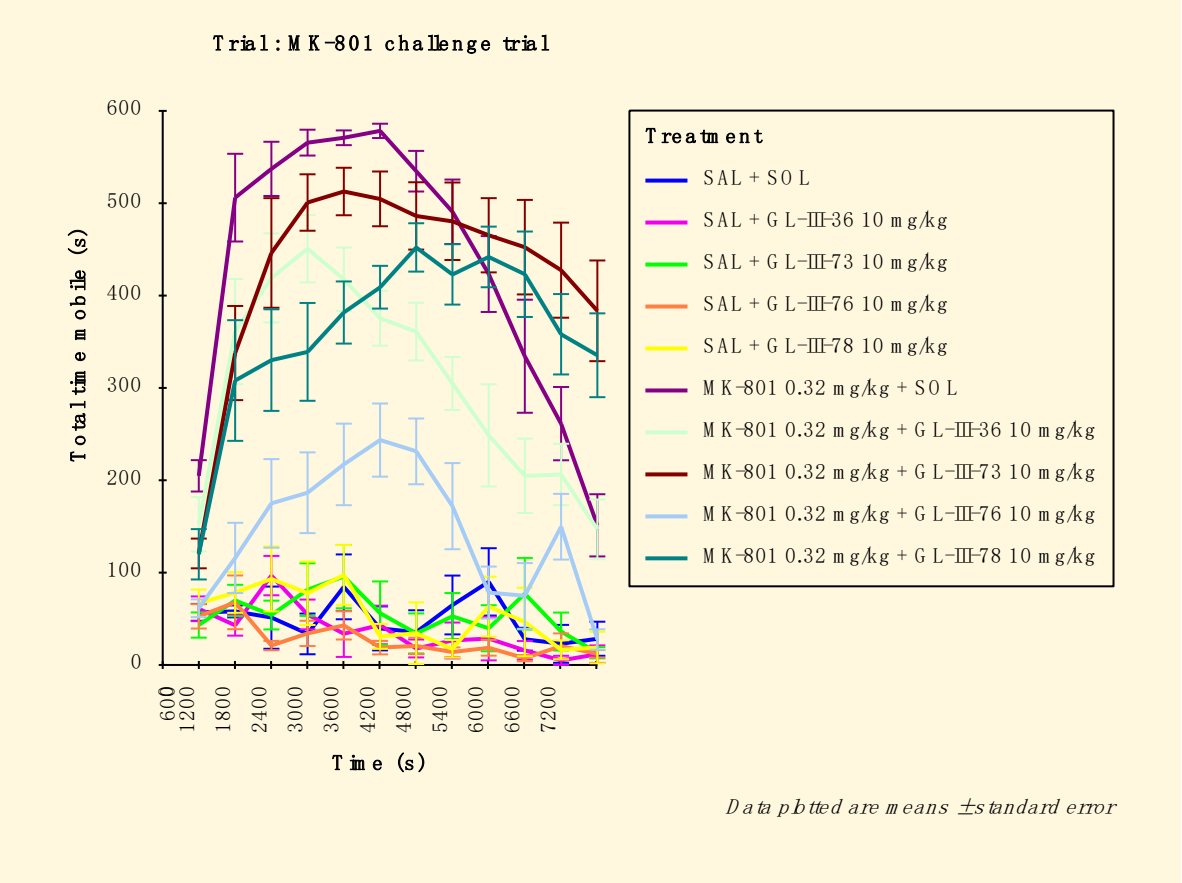

Figure 13. Total time mobile for tests where Trial is MK-801 challenge trial. The data analysed has been limited in the following way: Treatment = SAL + SOL, SAL + GL-III-36 10 mg/kg, SAL + GL-III-73 10 mg/kg, SAL + GL-III-76 10 mg/kg, SAL + GL-III-78 10 mg/kg, MK-801 0.32 mg/kg + SOL, MK-801 0.32 mg/kg + GL-III-36 10 mg/kg, MK-801 0.32 mg/kg + GL-III-73 10 mg/kg, MK-801 0.32 mg/kg + GL-III-76 10 mg/kg or MK-801 0.32 mg/kg + GL-III-78 10 mg/kg and Trial = Habituation trial or MK-801 challenge trial.

Total time immobile (s)

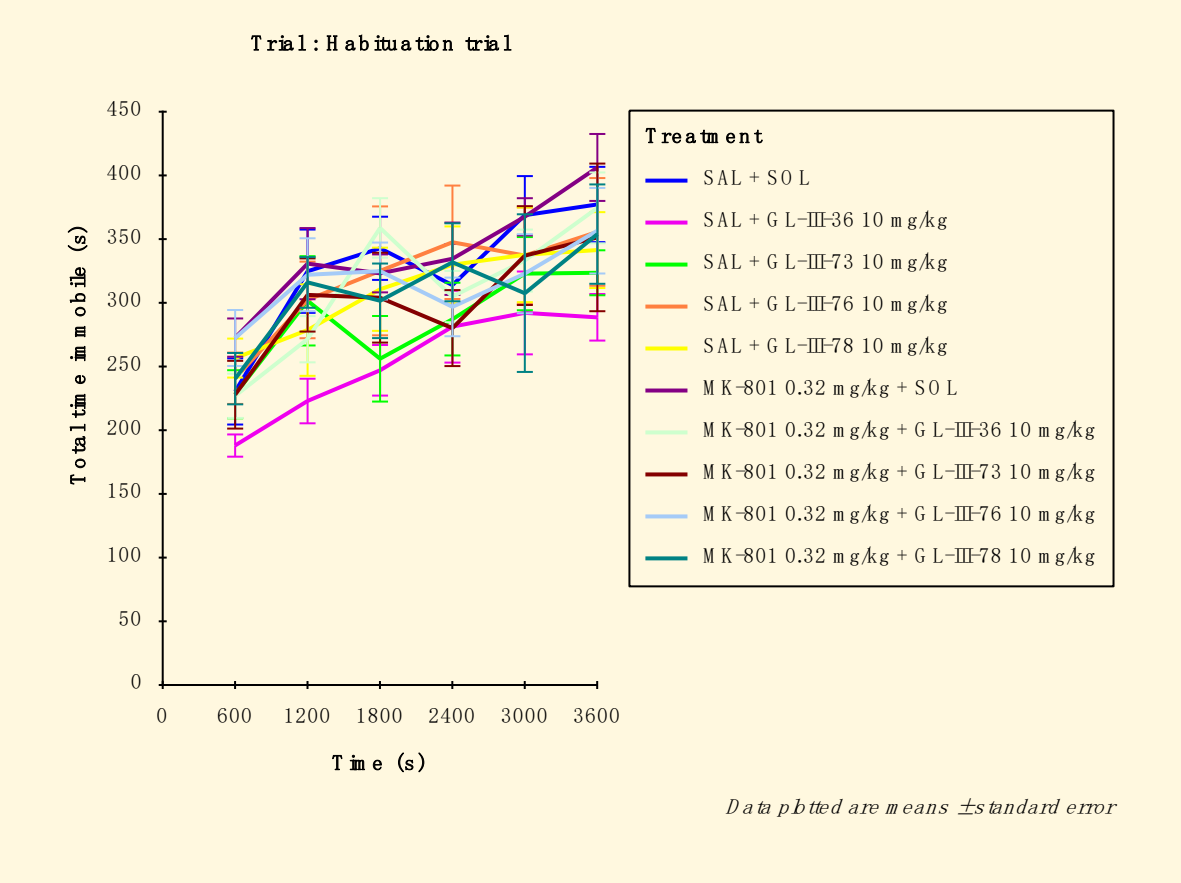

Figure 14. Total time immobile for tests where Trial is Habituation trial. The data analysed has been limited in the following way: Treatment = SAL + SOL, SAL + GL-III-36 10 mg/kg, SAL + GL-III-73 10 mg/kg, SAL + GL-III-76 10 mg/kg, SAL + GL-III-78 10 mg/kg, MK-801 0.32 mg/kg + SOL, MK-801 0.32 mg/kg + GL-III-36 10 mg/kg, MK-801 0.32 mg/kg + GL-III-73 10 mg/kg, MK-801 0.32 mg/kg + GL-III-76 10 mg/kg or MK-801 0.32 mg/kg + GL-III-78 10 mg/kg and Trial = Habituation trial or MK-801 challenge trial.

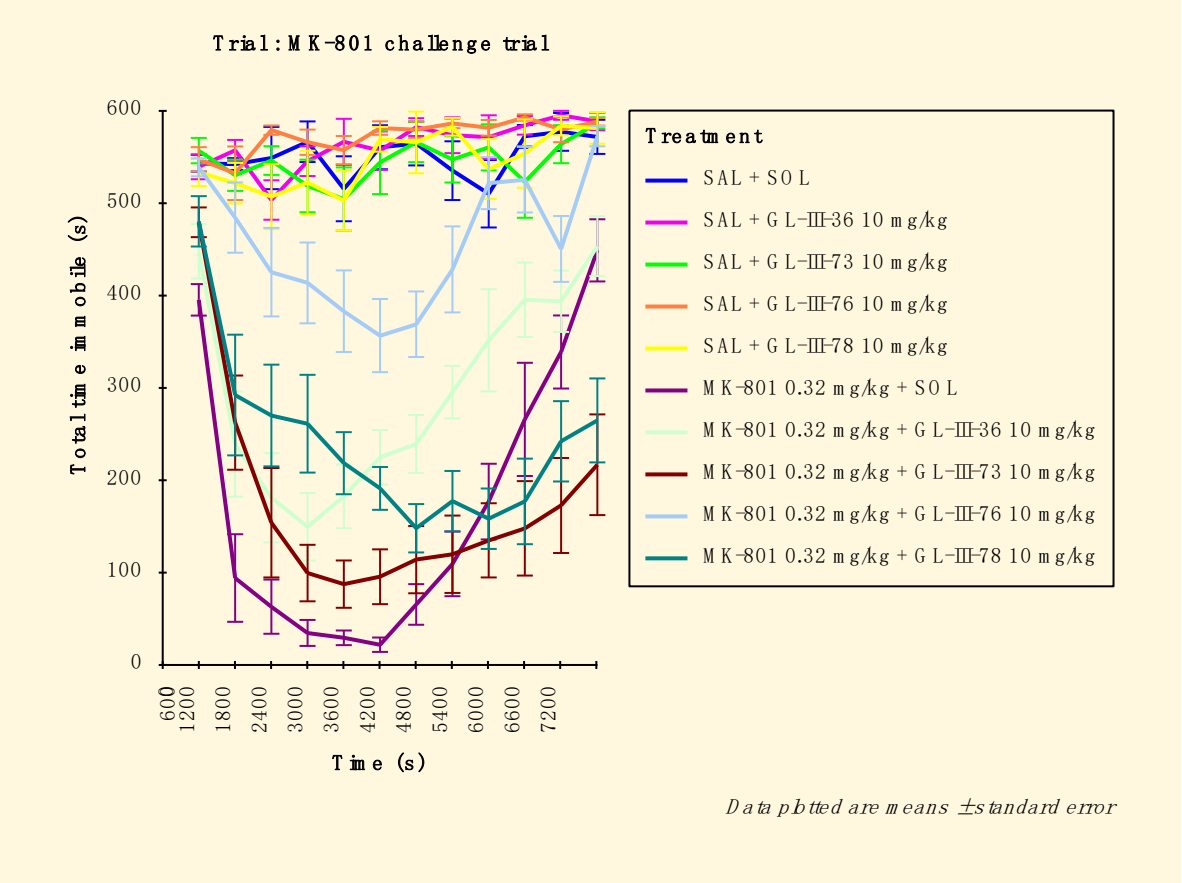

Figure 15. Total time immobile for tests where Trial is MK-801 challenge trial. The data analysed has been limited in the following way: Treatment = SAL + SOL, SAL + GL-III-36 10 mg/kg, SAL + GL-III-73 10 mg/kg, SAL + GL-III-76 10 mg/kg, SAL + GL-III-78 10 mg/kg, MK-801 0.32 mg/kg + SOL, MK-801 0.32 mg/kg + GL-III-36 10 mg/kg, MK-801 0.32 mg/kg + GL-III-73 10 mg/kg, MK-801 0.32 mg/kg + GL-III-76 10 mg/kg or MK-801 0.32 mg/kg + GL-III-78 10 mg/kg and Trial = Habituation trial or MK-801 challenge trial.

Total mobile episodes

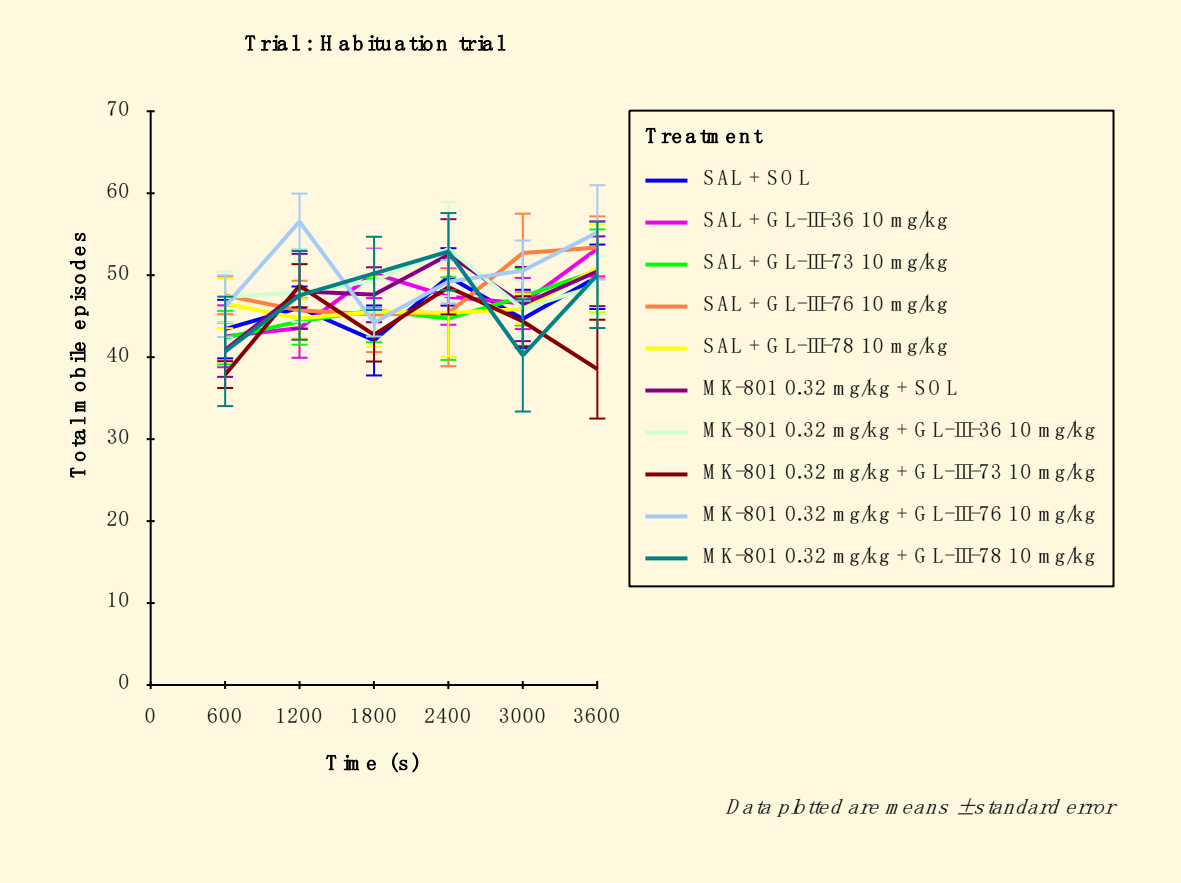

Figure 16. Total mobile episodes for tests where Trial is Habituation trial. The data analysed has been limited in the following way: Treatment = SAL + SOL, SAL + GL-III-36 10 mg/kg, SAL + GL-III-73 10 mg/kg, SAL + GL-III-76 10 mg/kg, SAL + GL-III-78 10 mg/kg, MK-801 0.32 mg/kg + SOL, MK-801 0.32 mg/kg + GL-III-36 10 mg/kg, MK-801 0.32 mg/kg + GL-III-73 10 mg/kg, MK-801 0.32 mg/kg + GL-III-76 10 mg/kg or MK-801 0.32 mg/kg + GL-III-78 10 mg/kg and Trial = Habituation trial or MK-801 challenge trial.

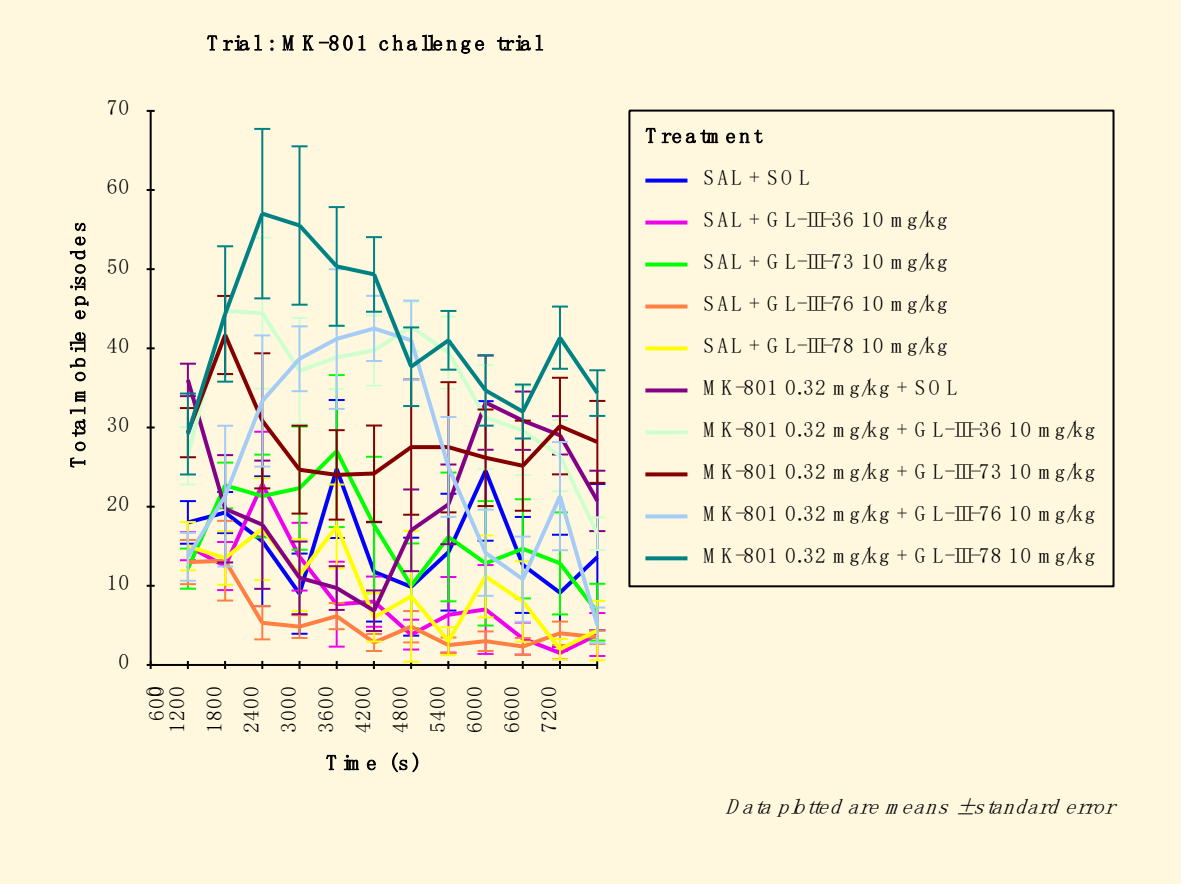

Figure 17. Total mobile episodes for tests where Trial is MK-801 challenge trial. The data analysed has been limited in the following way: Treatment = SAL + SOL, SAL + GL-III-36 10 mg/kg, SAL + GL-III-73 10 mg/kg, SAL + GL-III-76 10 mg/kg, SAL + GL-III-78 10 mg/kg, MK-801 0.32 mg/kg + SOL, MK-801 0.32 mg/kg + GL-III-36 10 mg/kg, MK-801 0.32 mg/kg + GL-III-73 10 mg/kg, MK-801 0.32 mg/kg + GL-III-76 10 mg/kg or MK-801 0.32 mg/kg + GL-III-78 10 mg/kg and Trial = Habituation trial or MK-801 challenge trial.

Total immobile episodes

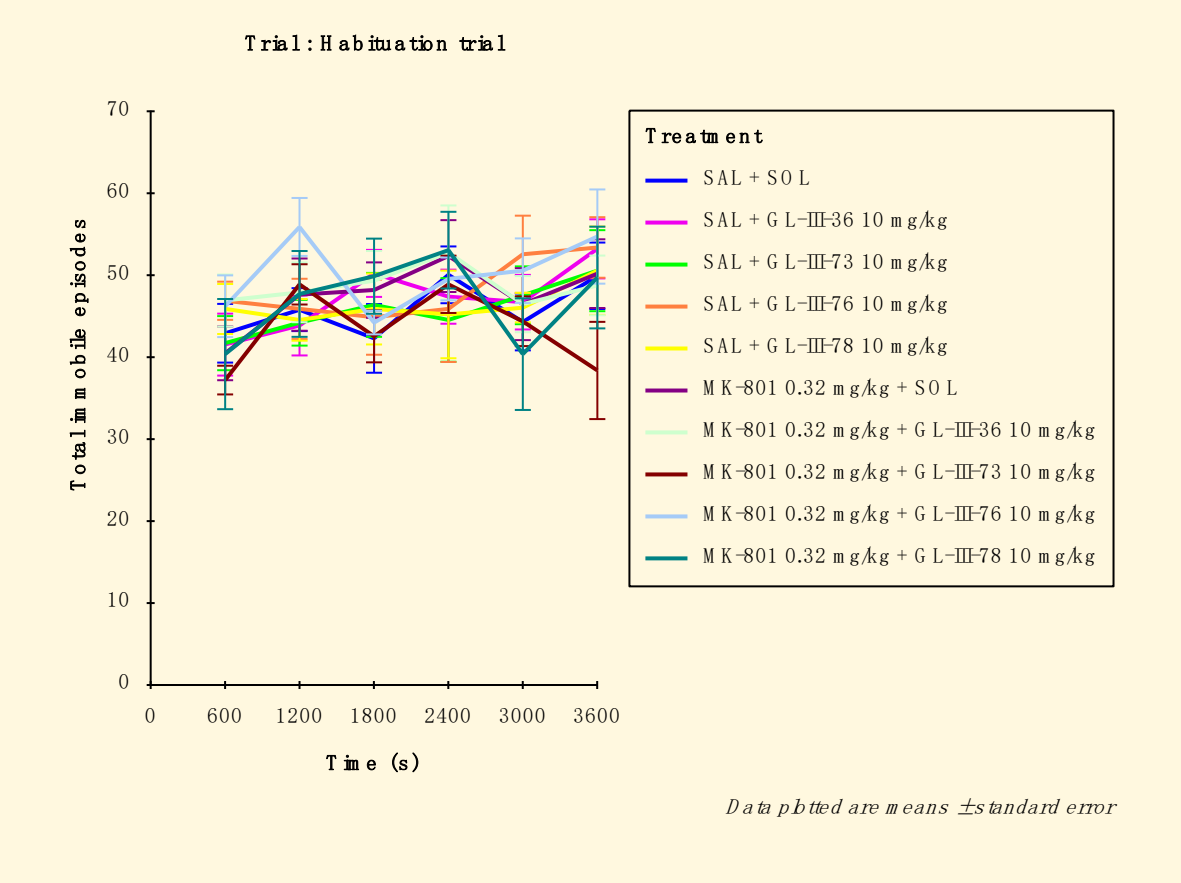

Figure 18. Total immobile episodes for tests where Trial is Habituation trial. The data analysed has been limited in the following way: Treatment = SAL + SOL, SAL + GL-III-36 10 mg/kg, SAL + GL-III-73 10 mg/kg, SAL + GL-III-76 10 mg/kg, SAL + GL-III-78 10 mg/kg, MK-801 0.32 mg/kg + SOL, MK-801 0.32 mg/kg + GL-III-36 10 mg/kg, MK-801 0.32 mg/kg + GL-III-73 10 mg/kg, MK-801 0.32 mg/kg + GL-III-76 10 mg/kg or MK-801 0.32 mg/kg + GL-III-78 10 mg/kg and Trial = Habituation trial or MK-801 challenge trial.

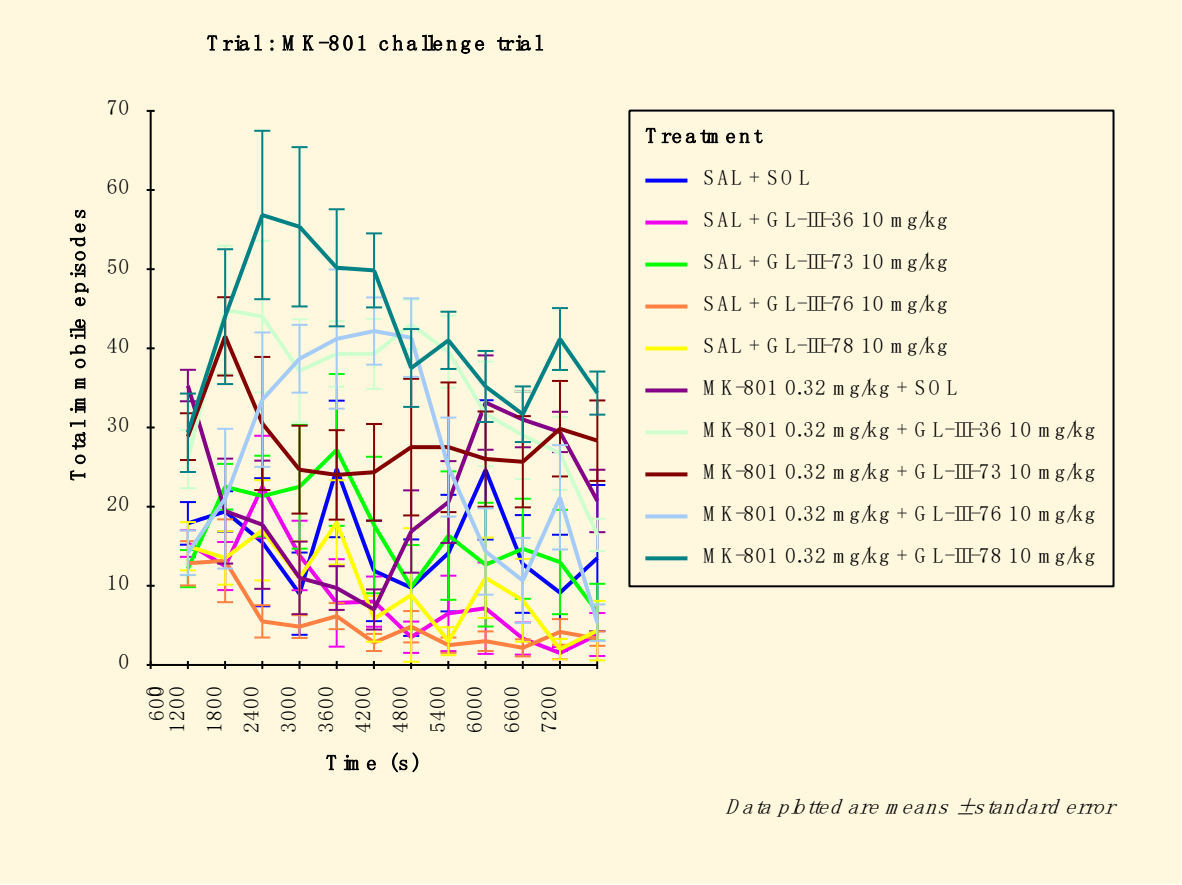

Figure 19. Total immobile episodes for tests where Trial is MK-801 challenge trial. The data analysed has been limited in the following way: Treatment = SAL + SOL, SAL + GL-III-36 10 mg/kg, SAL + GL-III-73 10 mg/kg, SAL + GL-III-76 10 mg/kg, SAL + GL-III-78 10 mg/kg, MK-801 0.32 mg/kg + SOL, MK-801 0.32 mg/kg + GL-III-36 10 mg/kg, MK-801 0.32 mg/kg + GL-III-73 10 mg/kg, MK-801 0.32 mg/kg + GL-III-76 10 mg/kg or MK-801 0.32 mg/kg + GL-III-78 10 mg/kg and Trial = Habituation trial or MK-801 challenge trial.

Maximum speed (m/s)

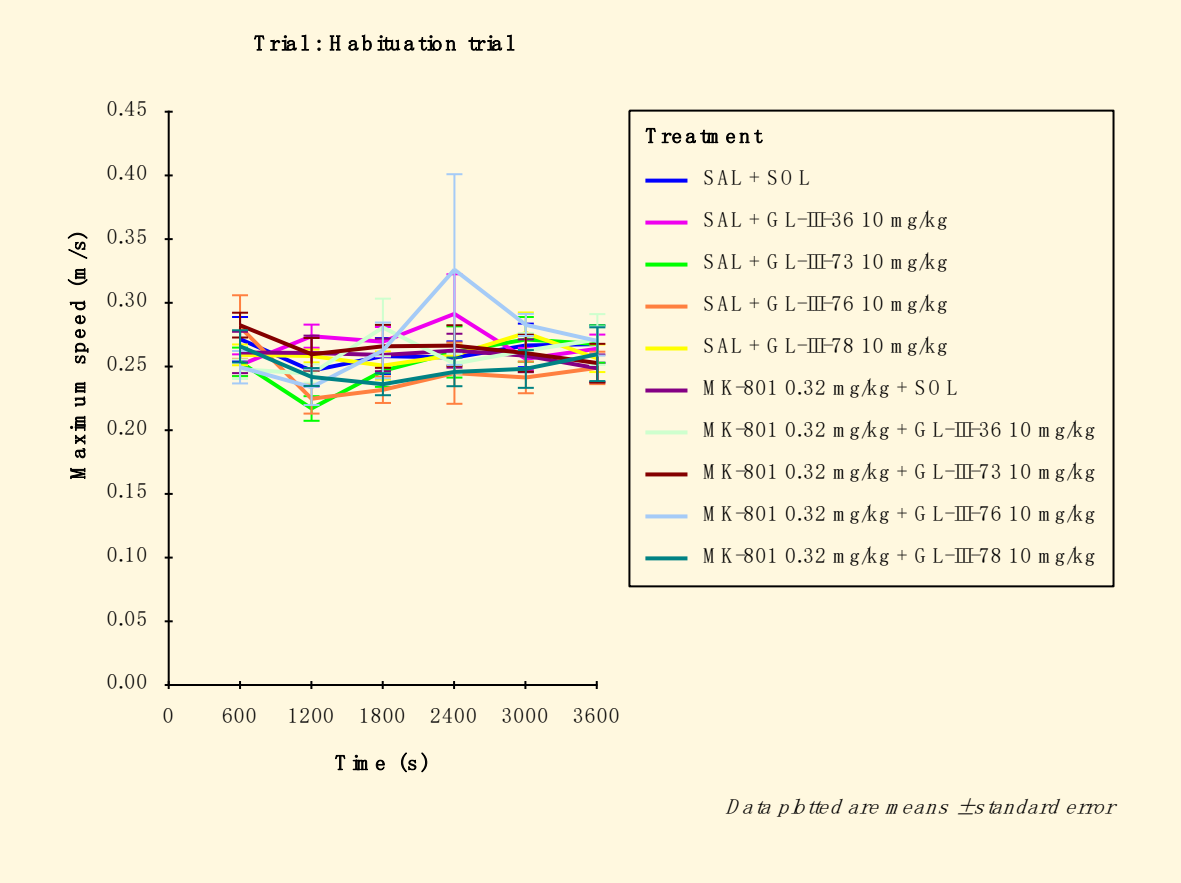

Figure 20. Maximum speed for tests where Trial is Habituation trial. The data analysed has been limited in the following way: Treatment = SAL + SOL, SAL + GL-III-36 10 mg/kg, SAL + GL-III-73 10 mg/kg, SAL + GL-III-76 10 mg/kg, SAL + GL-III-78 10 mg/kg, MK-801 0.32 mg/kg + SOL, MK-801 0.32 mg/kg + GL-III-36 10 mg/kg, MK-801 0.32 mg/kg + GL-III-73 10 mg/kg, MK-801 0.32 mg/kg + GL-III-76 10 mg/kg or MK-801 0.32 mg/kg + GL-III-78 10 mg/kg and Trial = Habituation trial or MK-801 challenge trial.

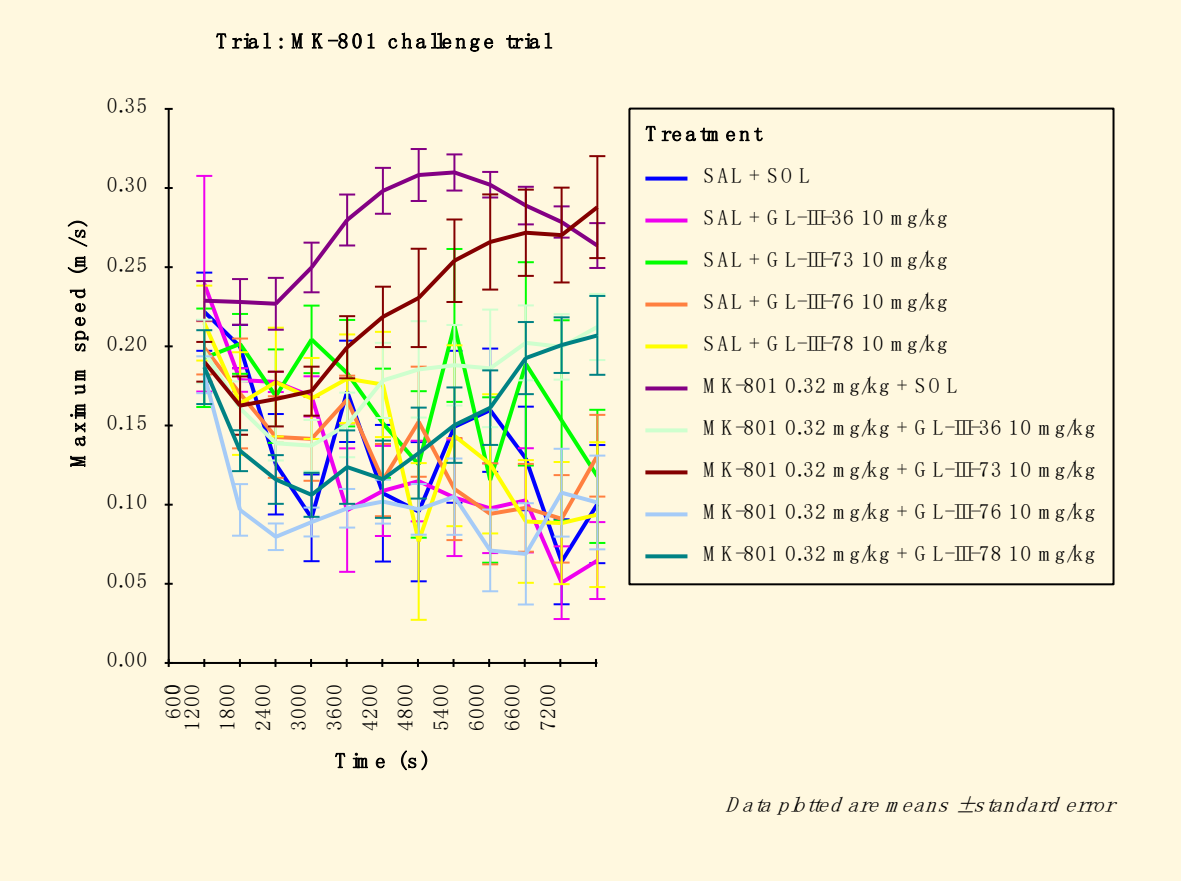

Figure 21. Maximum speed for tests where Trial is MK-801 challenge trial. The data analysed has been limited in the following way: Treatment = SAL + SOL, SAL + GL-III-36 10 mg/kg, SAL + GL-III-73 10 mg/kg, SAL + GL-III-76 10 mg/kg, SAL + GL-III-78 10 mg/kg, MK-801 0.32 mg/kg + SOL, MK-801 0.32 mg/kg + GL-III-36 10 mg/kg, MK-801 0.32 mg/kg + GL-III-73 10 mg/kg, MK-801 0.32 mg/kg + GL-III-76 10 mg/kg or MK-801 0.32 mg/kg + GL-III-78 10 mg/kg and Trial = Habituation trial or MK-801 challenge trial.

Rotations of the animal's body

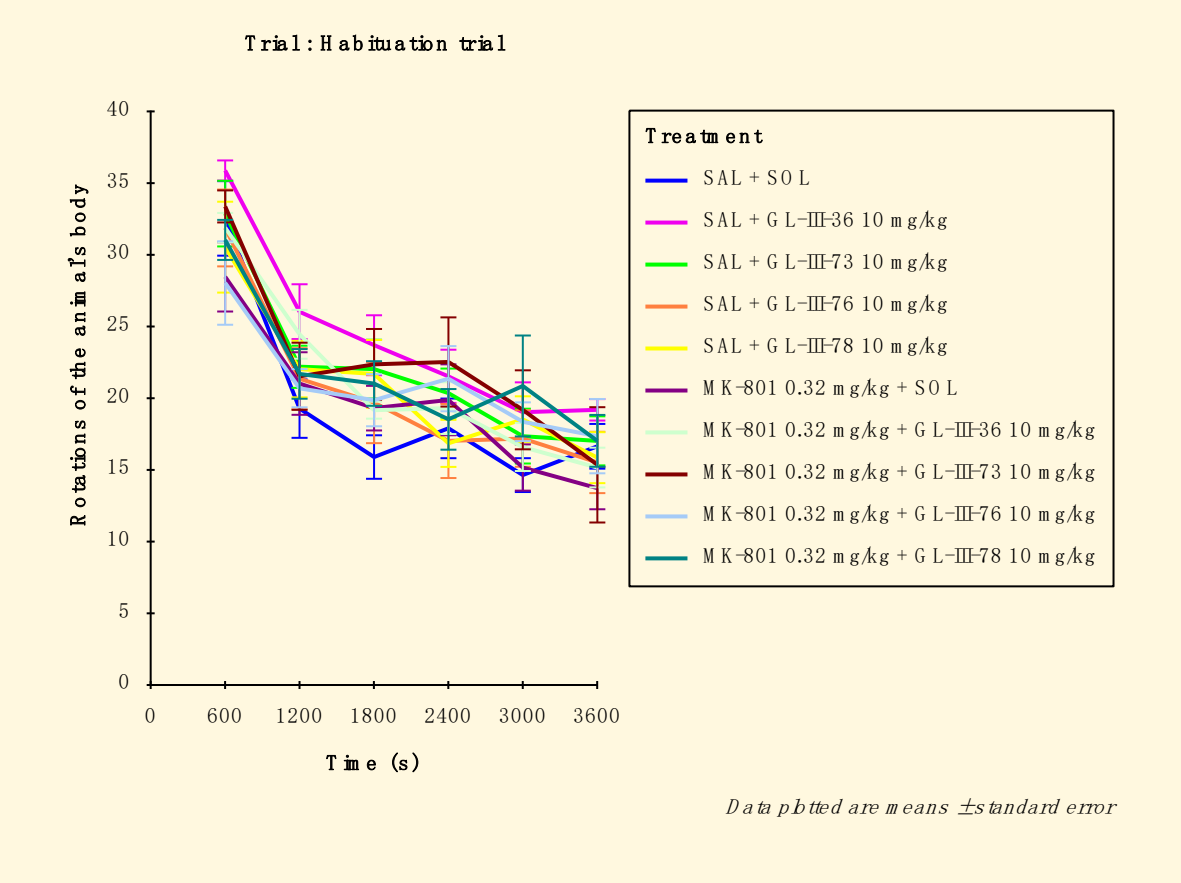

Figure 22. Rotations of the animal's body for tests where Trial is Habituation trial. The data analysed has been limited in the following way: Treatment = SAL + SOL, SAL + GL-III-36 10 mg/kg, SAL + GL-III-73 10 mg/kg, SAL + GL-III-76 10 mg/kg, SAL + GL-III-78 10 mg/kg, MK-801 0.32 mg/kg + SOL, MK-801 0.32 mg/kg + GL-III-36 10 mg/kg, MK-801 0.32 mg/kg + GL-III-73 10 mg/kg, MK-801 0.32 mg/kg + GL-III-76 10 mg/kg or MK-801 0.32 mg/kg + GL-III-78 10 mg/kg and Trial = Habituation trial or MK-801 challenge trial.

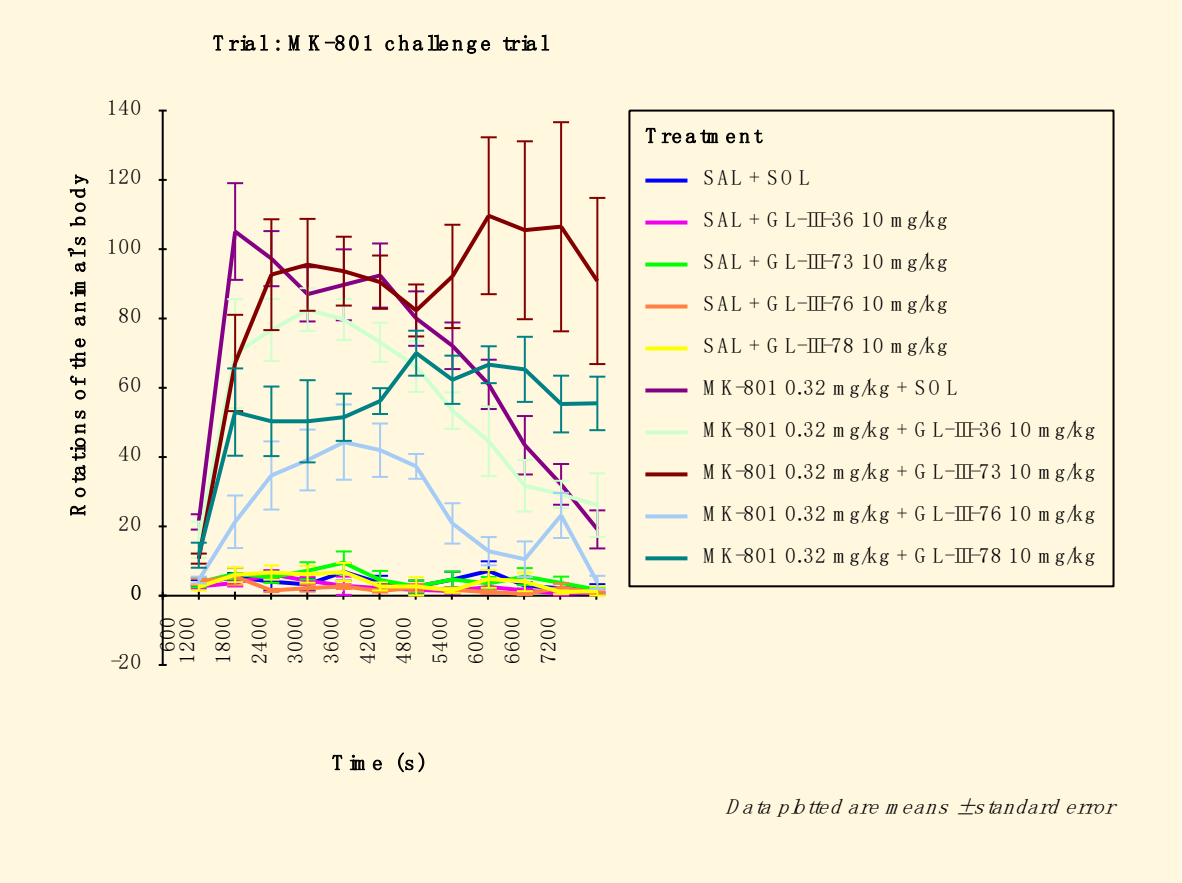

Figure 23. Rotations of the animal's body for tests where Trial is MK-801 challenge trial. The data analysed has been limited in the following way: Treatment = SAL + SOL, SAL + GL-III-36 10 mg/kg, SAL + GL-III-73 10 mg/kg, SAL + GL-III-76 10 mg/kg, SAL + GL-III-78 10 mg/kg, MK-801 0.32 mg/kg + SOL, MK-801 0.32 mg/kg + GL-III-36 10 mg/kg, MK-801 0.32 mg/kg + GL-III-73 10 mg/kg, MK-801 0.32 mg/kg + GL-III-76 10 mg/kg or MK-801 0.32 mg/kg + GL-III-78 10 mg/kg and Trial = Habituation trial or MK-801 challenge trial.

Clockwise rotations of the animal's body

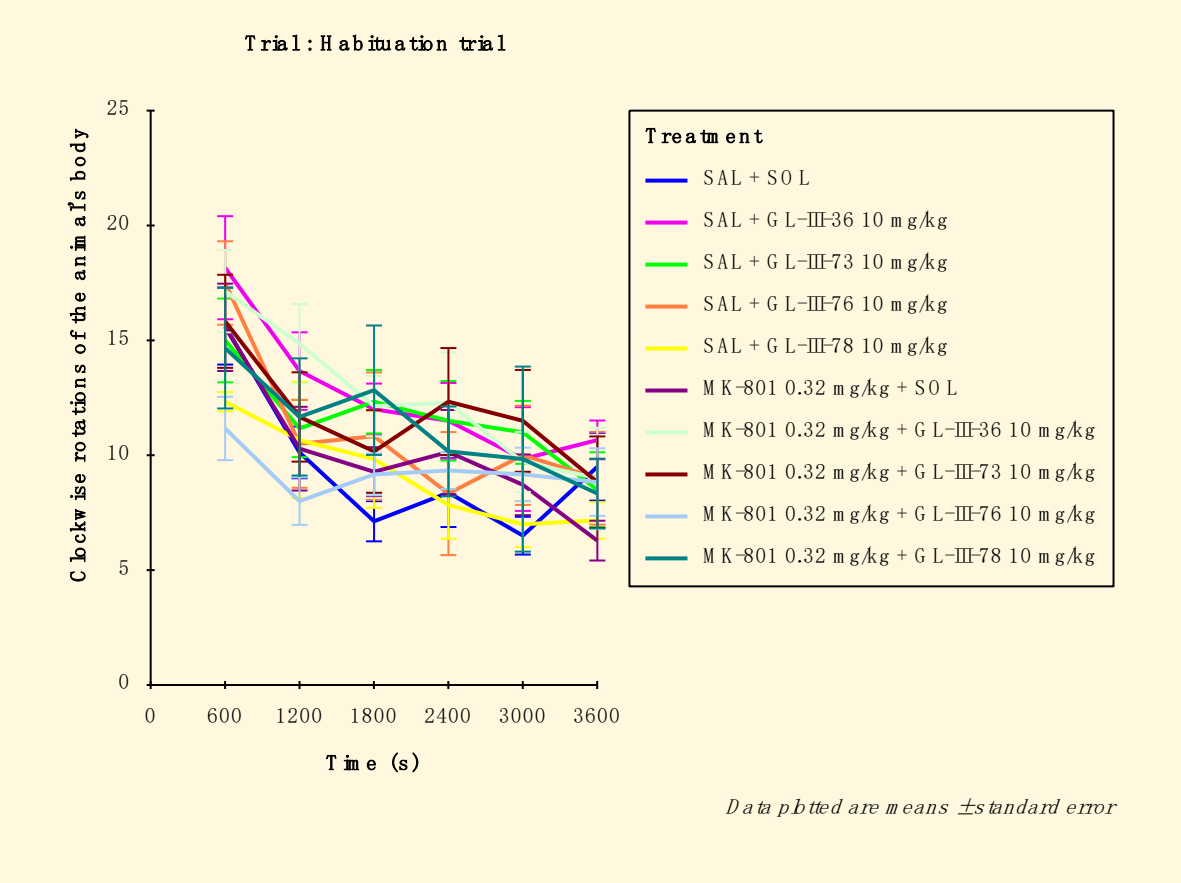

Figure 24. Clockwise rotations of the animal's body for tests where Trial is Habituation trial. The data analysed has been limited in the following way: Treatment = SAL + SOL, SAL + GL-III-36 10 mg/kg, SAL + GL-III-73 10 mg/kg, SAL + GL-III-76 10 mg/kg, SAL + GL-III-78 10 mg/kg, MK-801 0.32 mg/kg + SOL, MK-801 0.32 mg/kg + GL-III-36 10 mg/kg, MK-801 0.32 mg/kg + GL-III-73 10 mg/kg, MK-801 0.32 mg/kg + GL-III-76 10 mg/kg or MK-801 0.32 mg/kg + GL-III-78 10 mg/kg and Trial = Habituation trial or MK-801 challenge trial.

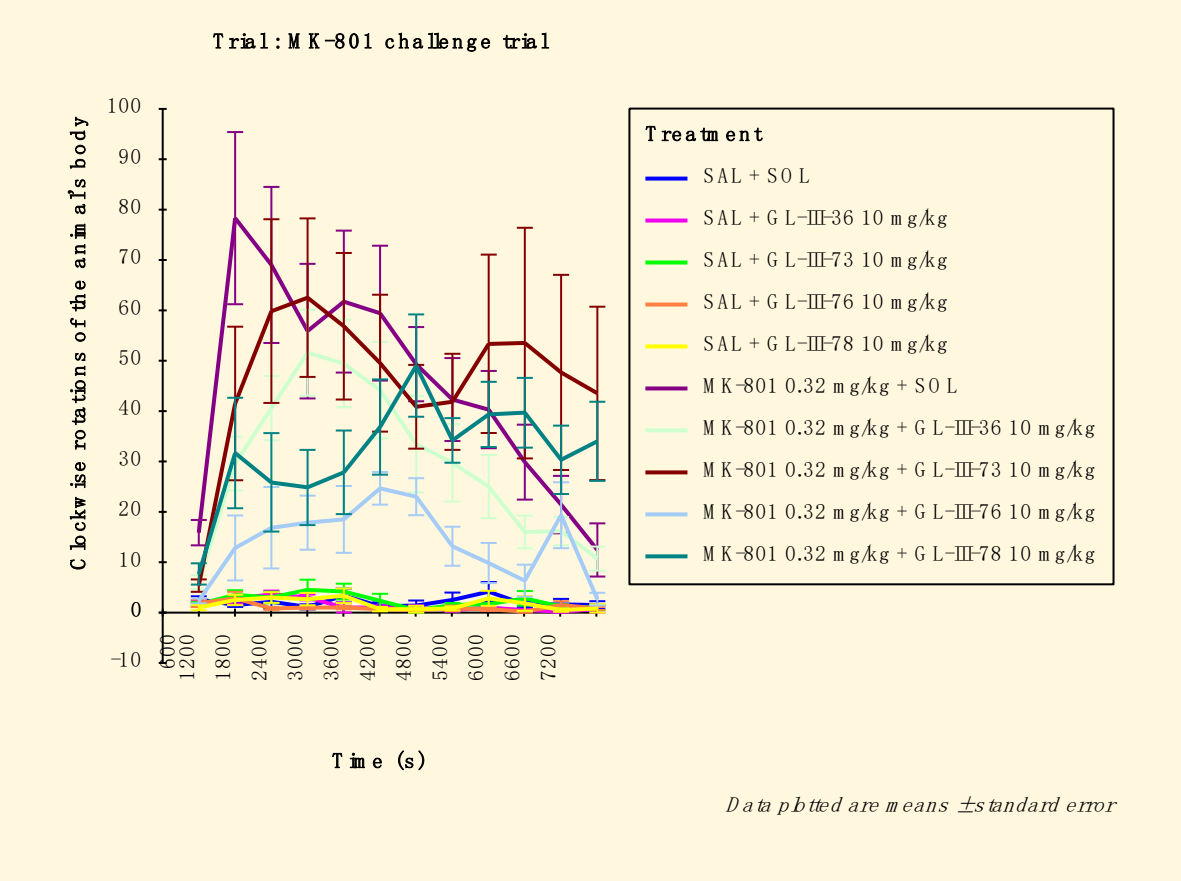

Figure 25. Clockwise rotations of the animal's body for tests where Trial is MK-801 challenge trial. The data analysed has been limited in the following way: Treatment = SAL + SOL, SAL + GL-III-36 10 mg/kg, SAL + GL-III-73 10 mg/kg, SAL + GL-III-76 10 mg/kg, SAL + GL-III-78 10 mg/kg, MK-801 0.32 mg/kg + SOL, MK-801 0.32 mg/kg + GL-III-36 10 mg/kg, MK-801 0.32 mg/kg + GL-III-73 10 mg/kg, MK-801 0.32 mg/kg + GL-III-76 10 mg/kg or MK-801 0.32 mg/kg + GL-III-78 10 mg/kg and Trial = Habituation trial or MK-801 challenge trial.

Anticlockwise rotations of the animal's body

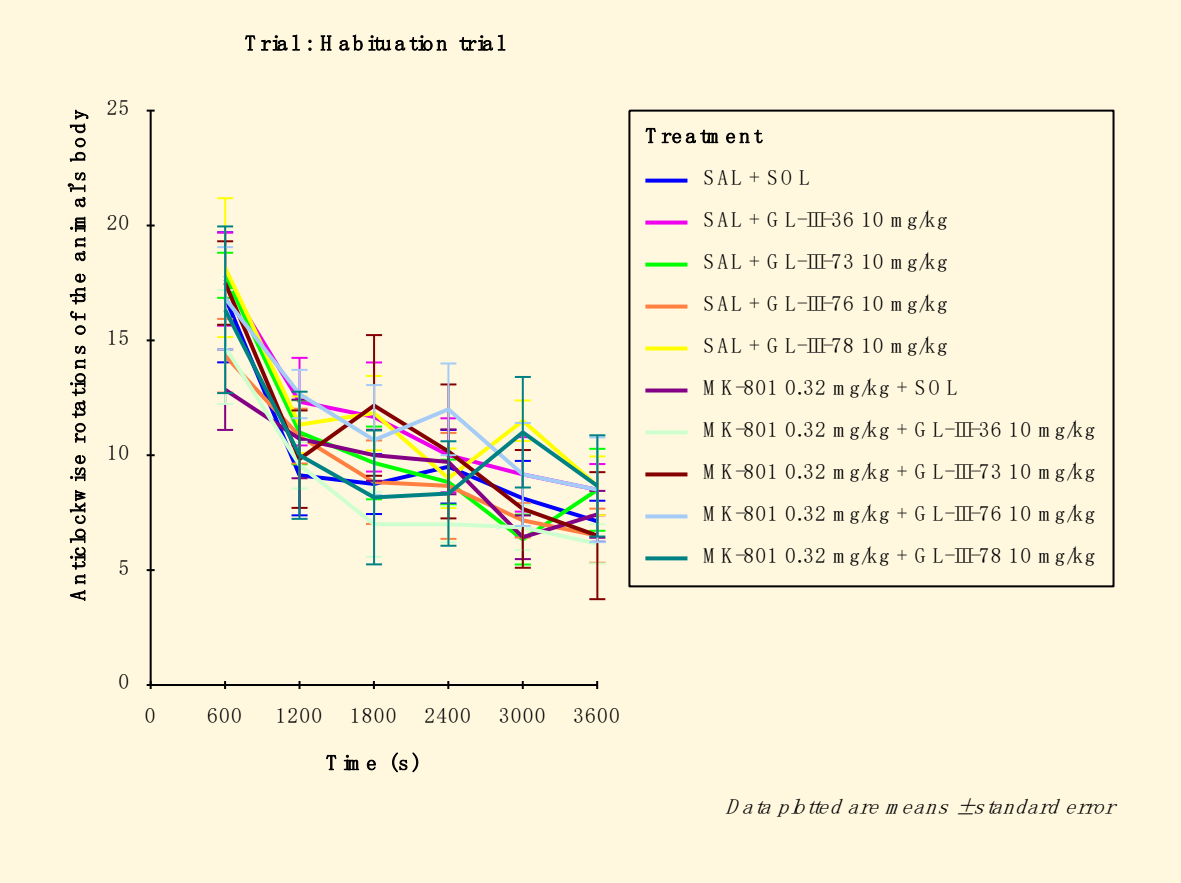

Figure 26. Anticlockwise rotations of the animal's body for tests where Trial is Habituation trial. The data analysed has been limited in the following way: Treatment = SAL + SOL, SAL + GL-III-36 10 mg/kg, SAL + GL-III-73 10 mg/kg, SAL + GL-III-76 10 mg/kg, SAL + GL-III-78 10 mg/kg, MK-801 0.32 mg/kg + SOL, MK-801 0.32 mg/kg + GL-III-36 10 mg/kg, MK-801 0.32 mg/kg + GL-III-73 10 mg/kg, MK-801 0.32 mg/kg + GL-III-76 10 mg/kg or MK-801 0.32 mg/kg + GL-III-78 10 mg/kg and Trial = Habituation trial or MK-801 challenge trial.

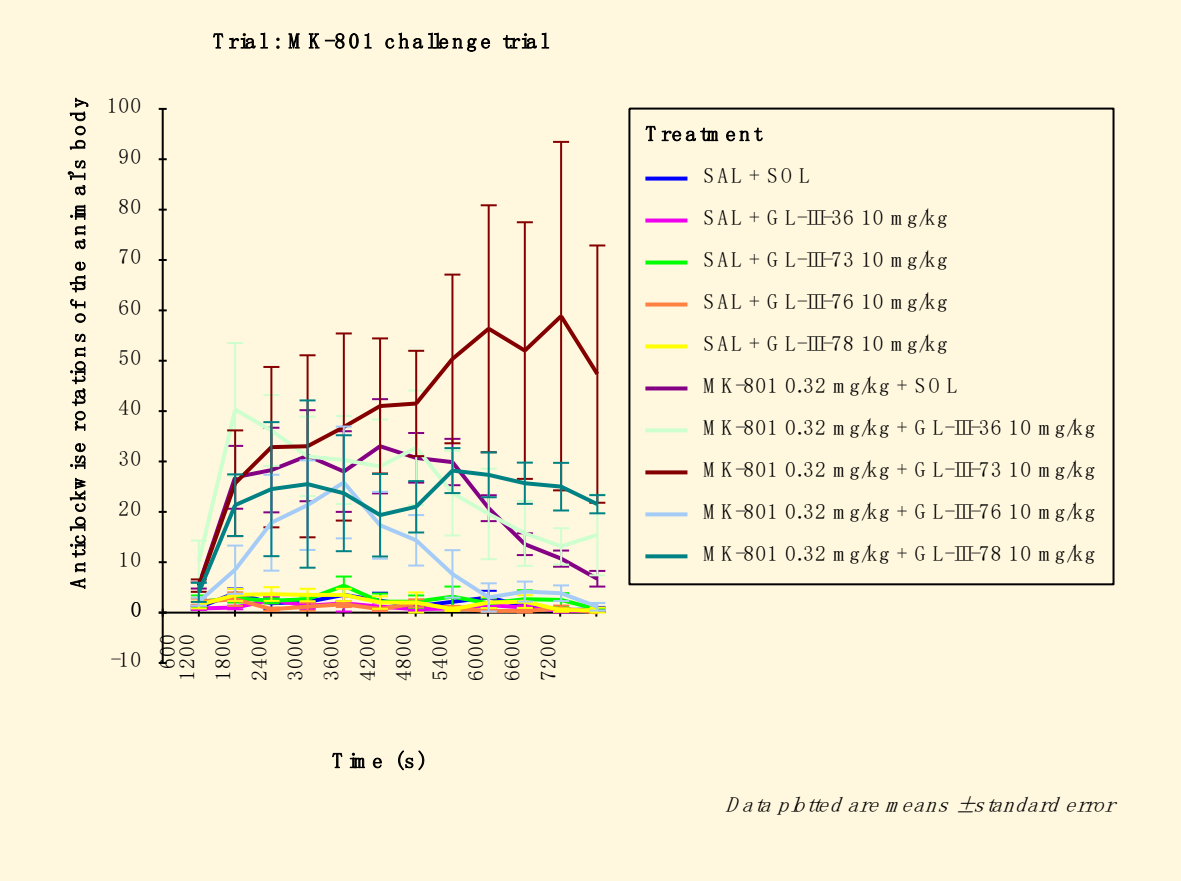

Figure 27. Anticlockwise rotations of the animal's body for tests where Trial is MK-801 challenge trial. The data analysed has been limited in the following way: Treatment = SAL + SOL, SAL + GL-III-36 10 mg/kg, SAL + GL-III-73 10 mg/kg, SAL + GL-III-76 10 mg/kg, SAL + GL-III-78 10 mg/kg, MK-801 0.32 mg/kg + SOL, MK-801 0.32 mg/kg + GL-III-36 10 mg/kg, MK-801 0.32 mg/kg + GL-III-73 10 mg/kg, MK-801 0.32 mg/kg + GL-III-76 10 mg/kg or MK-801 0.32 mg/kg + GL-III-78 10 mg/kg and Trial = Habituation trial or MK-801 challenge trial.

Total freezing episodes

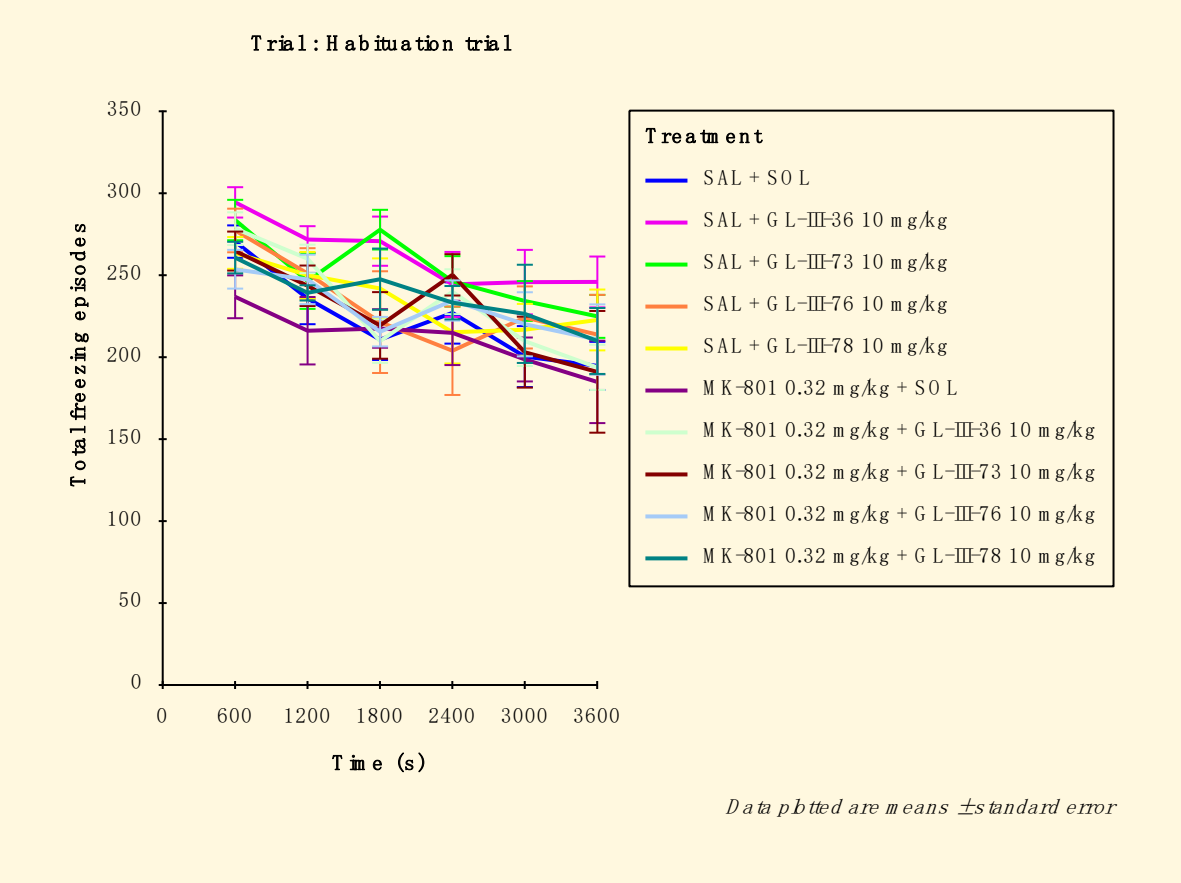

Figure 28. Total freezing episodes for tests where Trial is Habituation trial. The data analysed has been limited in the following way: Treatment = SAL + SOL, SAL + GL-III-36 10 mg/kg, SAL + GL-III-73 10 mg/kg, SAL + GL-III-76 10 mg/kg, SAL + GL-III-78 10 mg/kg, MK-801 0.32 mg/kg + SOL, MK-801 0.32 mg/kg + GL-III-36 10 mg/kg, MK-801 0.32 mg/kg + GL-III-73 10 mg/kg, MK-801 0.32 mg/kg + GL-III-76 10 mg/kg or MK-801 0.32 mg/kg + GL-III-78 10 mg/kg and Trial = Habituation trial or MK-801 challenge trial.

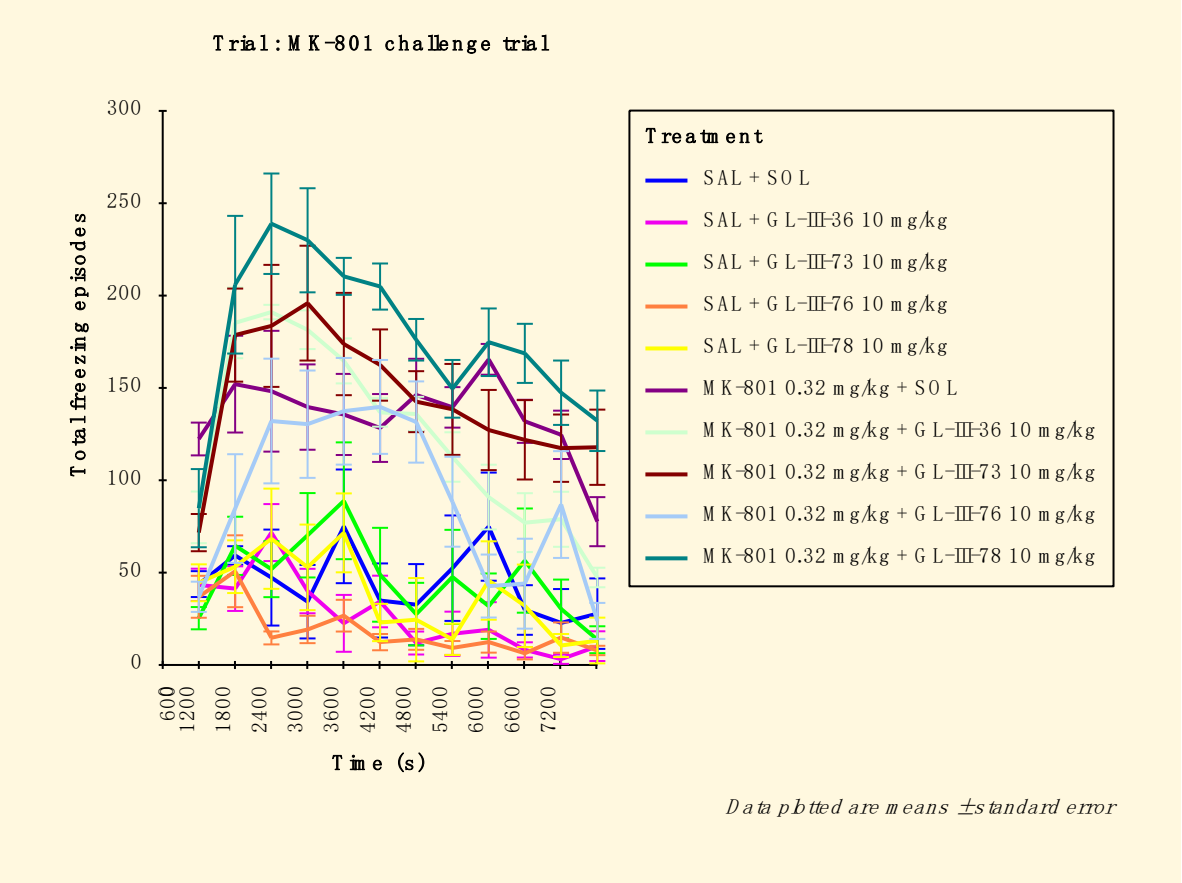

Figure 29. Total freezing episodes for tests where Trial is MK-801 challenge trial. The data analysed has been limited in the following way: Treatment = SAL + SOL, SAL + GL-III-36 10 mg/kg, SAL + GL-III-73 10 mg/kg, SAL + GL-III-76 10 mg/kg, SAL + GL-III-78 10 mg/kg, MK-801 0.32 mg/kg + SOL, MK-801 0.32 mg/kg + GL-III-36 10 mg/kg, MK-801 0.32 mg/kg + GL-III-73 10 mg/kg, MK-801 0.32 mg/kg + GL-III-76 10 mg/kg or MK-801 0.32 mg/kg + GL-III-78 10 mg/kg and Trial = Habituation trial or MK-801 challenge trial.

Total time freezing (s)

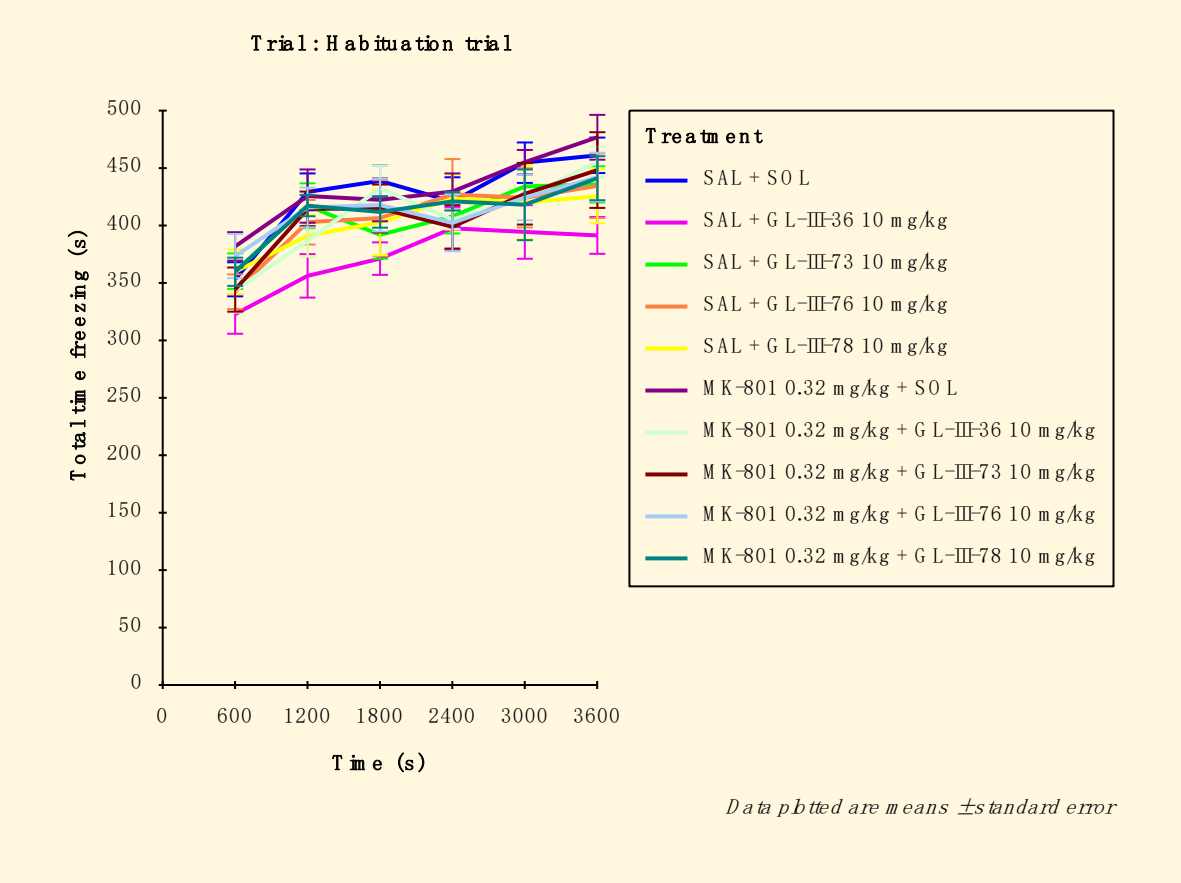

Figure 30. Total time freezing for tests where Trial is Habituation trial. The data analysed has been limited in the following way: Treatment = SAL + SOL, SAL + GL-III-36 10 mg/kg, SAL + GL-III-73 10 mg/kg, SAL + GL-III-76 10 mg/kg, SAL + GL-III-78 10 mg/kg, MK-801 0.32 mg/kg + SOL, MK-801 0.32 mg/kg + GL-III-36 10 mg/kg, MK-801 0.32 mg/kg + GL-III-73 10 mg/kg, MK-801 0.32 mg/kg + GL-III-76 10 mg/kg or MK-801 0.32 mg/kg + GL-III-78 10 mg/kg and Trial = Habituation trial or MK-801 challenge trial.

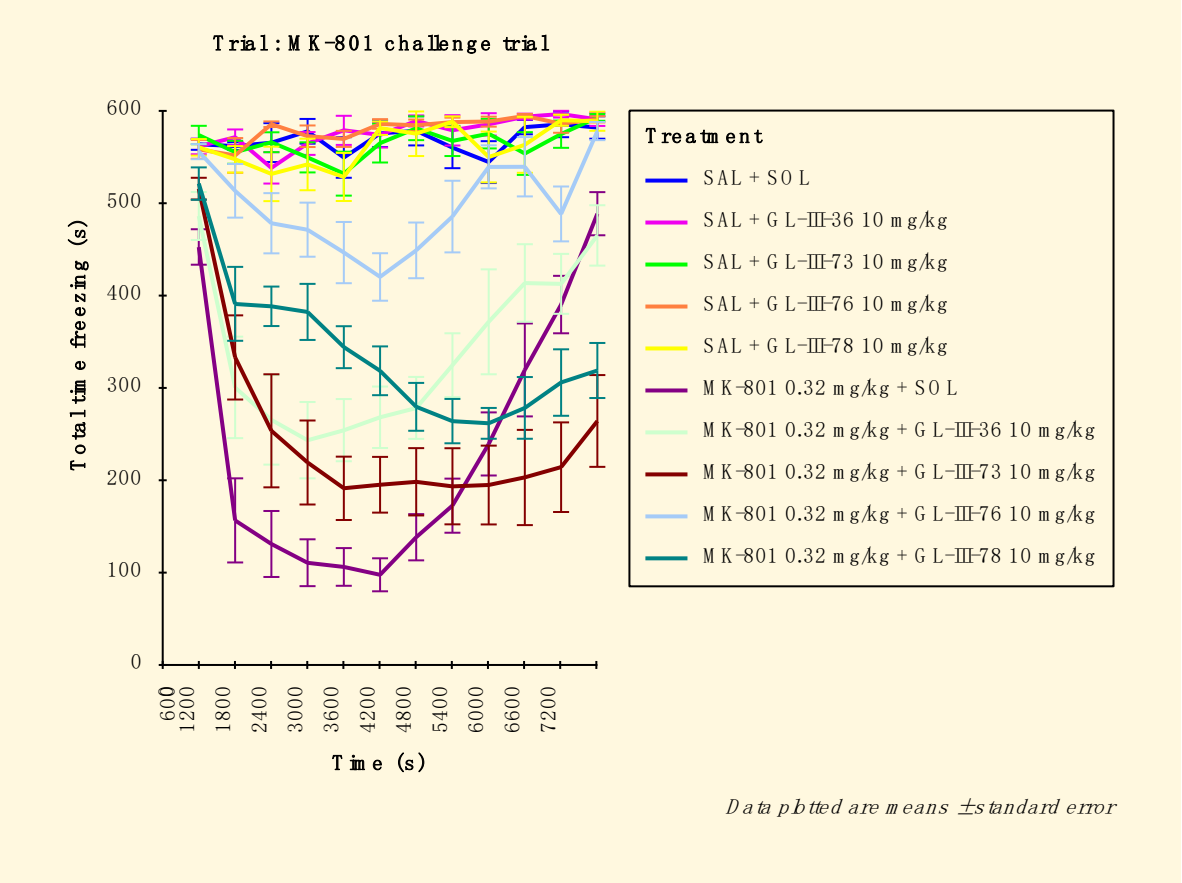

Figure 31. Total time freezing for tests where Trial is MK-801 challenge trial. The data analysed has been limited in the following way: Treatment = SAL + SOL, SAL + GL-III-36 10 mg/kg, SAL + GL-III-73 10 mg/kg, SAL + GL-III-76 10 mg/kg, SAL + GL-III-78 10 mg/kg, MK-801 0.32 mg/kg + SOL, MK-801 0.32 mg/kg + GL-III-36 10 mg/kg, MK-801 0.32 mg/kg + GL-III-73 10 mg/kg, MK-801 0.32 mg/kg + GL-III-76 10 mg/kg or MK-801 0.32 mg/kg + GL-III-78 10 mg/kg and Trial = Habituation trial or MK-801 challenge trial.

Table 57. Raw data of anti-schizophrenia model.

Animal	Treatment (SORTED)	Stage	Distance (m)	Mean speed (m/s)	Time mobile (s)	Time immobile (s)	Mobile episodes	Immobile episodes
1	SAL + SOL	Habituation	118.410	0.033	2169.7	1430.3	206	205
15	SAL + SOL	Habituation	82.770	0.023	1718.9	1881.1	302	302
26	SAL + SOL	Habituation	93.715	0.026	2005.2	1594.8	261	260

40	SAL + SOL	Habituation	57.969	0.016	1184.8	2415.2	280	280
46	SAL + SOL	Habituation	82.517	0.023	1790.0	1810.0	290	289
51	SAL + SOL	Habituation	84.018	0.023	1672.3	1927.7	317	317
61	SAL + SOL	Habituation	73.295	0.020	1380.4	2219.6	272	272
64	SAL + SOL	Habituation	65.808	0.018	1242.1	2357.9	276	275
1	SAL + SOL	MK-801 challenge	69.530	0.010	1355.7	5844.3	335	335
15	SAL + SOL	MK-801 challenge	65.374	0.009	1238.6	5961.4	314	314
26	SAL + SOL	MK-801 challenge	21.290	0.003	457.6	6742.4	144	144
40	SAL + SOL	MK-801 challenge	9.304	0.001	185.0	7015.0	72	72
46	SAL + SOL	MK-801 challenge	10.971	0.002	240.0	6960.0	83	82
51	SAL + SOL	MK-801 challenge	5.982	0.001	109.4	7090.6	55	55
61	SAL + SOL	MK-801 challenge	45.446	0.006	837.3	6362.7	330	330
64	SAL + SOL	MK-801 challenge	18.519	0.003	321.2	6878.8	126	126
2	SAL + GL-III-36 10 mg/kg	Habituation	121.637	0.034	2082.0	1518.0	285	285
13	SAL + GL-III-36 10 mg/kg	Habituation	91.649	0.025	1738.4	1861.6	289	289
23	SAL + GL-III-36 10 mg/kg	Habituation	96.470	0.027	2129.8	1470.2	229	228
36	SAL + GL-III-36 10 mg/kg	Habituation	111.018	0.031	2137.2	1462.8	262	261
41	SAL + GL-III-36 10 mg/kg	Habituation	124.912	0.035	2364.0	1236.0	324	323
59	SAL + GL-III-36 10 mg/kg	Habituation	98.491	0.027	2045.1	1554.9	310	310
2	SAL + GL-III-36 10 mg/kg	MK-801 challenge	31.496	0.004	607.0	6593.0	168	169
13	SAL + GL-III-36 10 mg/kg	MK-801 challenge	24.685	0.003	436.9	6763.1	80	80

23	SAL + GL-III-36 10 mg/kg	MK-801 challenge	16.232	0.002	327.0	6873.0	77	77
36	SAL + GL-III-36 10 mg/kg	MK-801 challenge	14.427	0.002	309.2	6890.8	76	76
41	SAL + GL-III-36 10 mg/kg	MK-801 challenge	16.955	0.002	391.0	6809.0	107	107
59	SAL + GL-III-36 10 mg/kg	MK-801 challenge	28.677	0.004	553.5	6646.5	125	126
3	SAL + GL-III-73 10 mg/kg	Habituation	114.987	0.032	2192.3	1407.7	266	266
16	SAL + GL-III-73 10 mg/kg	Habituation	79.433	0.022	1590.5	2009.5	317	317
22	SAL + GL-III-73 10 mg/kg	Habituation	90.716	0.025	1891.0	1709.0	229	229
33	SAL + GL-III-73 10 mg/kg	Habituation	91.391	0.025	1730.2	1869.7	309	309
45	SAL + GL-III-73 10 mg/kg	Habituation	82.213	0.023	1643.0	1957.0	284	284
58	SAL + GL-III-73 10 mg/kg	Habituation	91.413	0.025	2253.2	1346.8	244	243
3	SAL + GL-III-73 10 mg/kg	MK-801 challenge	31.411	0.004	489.9	6710.1	101	101
16	SAL + GL-III-73 10 mg/kg	MK-801 challenge	21.265	0.003	461.8	6738.2	182	182
22	SAL + GL-III-73 10 mg/kg	MK-801 challenge	101.466	0.014	1481.7	5718.3	444	444
33	SAL + GL-III-73 10 mg/kg	MK-801 challenge	53.770	0.007	925.9	6274.1	261	261
45	SAL + GL-III-73 10 mg/kg	MK-801 challenge	11.197	0.002	180.2	7019.8	94	95
58	SAL + GL-III-73 10 mg/kg	MK-801 challenge	21.398	0.003	379.5	6820.5	96	96

4	SAL + GL-III-76 10 mg/kg	Habituation	100.605	0.028	1964.0	1636.0	327	326
14	SAL + GL-III-76 10 mg/kg	Habituation	52.082	0.014	1209.7	2390.3	239	239
29	SAL + GL-III-76 10 mg/kg	Habituation	72.818	0.020	1429.7	2170.3	320	320
35	SAL + GL-III-76 10 mg/kg	Habituation	124.710	0.035	2154.1	1445.9	229	229
47	SAL + GL-III-76 10 mg/kg	Habituation	58.923	0.016	1218.5	2381.5	297	296
60	SAL + GL-III-76 10 mg/kg	Habituation	110.328	0.031	2193.9	1406.1	326	325
4	SAL + GL-III-76 10 mg/kg	MK-801 challenge	17.985	0.002	279.3	6920.7	64	64
14	SAL + GL-III-76 10 mg/kg	MK-801 challenge	29.250	0.004	454.1	6746.0	87	86
29	SAL + GL-III-76 10 mg/kg	MK-801 challenge	14.840	0.002	276.5	6923.5	56	56
35	SAL + GL-III-76 10 mg/kg	MK-801 challenge	16.061	0.002	285.5	6914.5	43	43
47	SAL + GL-III-76 10 mg/kg	MK-801 challenge	18.000	0.002	275.8	6924.2	67	67
60	SAL + GL-III-76 10 mg/kg	MK-801 challenge	27.547	0.004	407.1	6792.9	76	76
5	SAL + GL-III-78 10 mg/kg	Habituation	83.550	0.023	1539.2	2060.8	319	318
12	SAL + GL-III-78 10 mg/kg	Habituation	73.970	0.021	1590.6	2009.4	290	289
30	SAL + GL-III-78 10 mg/kg	Habituation	80.947	0.022	1589.4	2010.6	251	250
34	SAL + GL-III-78 10 mg/kg	Habituation	101.779	0.028	2084.1	1515.9	278	278

43	SAL + GL-III-78 10 mg/kg	Habituation	111.773	0.031	2298.3	1301.7	212	211
52	SAL + GL-III-78 10 mg/kg	Habituation	79.788	0.022	1389.0	2211.0	322	321
5	SAL + GL-III-78 10 mg/kg	MK-801 challenge	37.686	0.005	562.2	6637.8	124	124
12	SAL + GL-III-78 10 mg/kg	MK-801 challenge	23.076	0.003	405.1	6795.0	81	81
30	SAL + GL-III-78 10 mg/kg	MK-801 challenge	29.425	0.004	445.3	6754.7	61	61
34	SAL + GL-III-78 10 mg/kg	MK-801 challenge	36.985	0.005	745.9	6454.1	155	155
43	SAL + GL-III-78 10 mg/kg	MK-801 challenge	76.698	0.011	1302.8	5897.3	202	202
52	SAL + GL-III-78 10 mg/kg	MK-801 challenge	21.463	0.003	384.3	6815.7	83	83
6	MK-801 0.32 mg/kg + SOL	Habituation	94.877	0.026	1776.3	1823.7	241	240
11	MK-801 0.32 mg/kg + SOL	Habituation	88.069	0.024	1715.1	1884.9	338	337
25	MK-801 0.32 mg/kg + SOL	Habituation	91.339	0.025	1609.8	1990.2	282	281
39	MK-801 0.32 mg/kg + SOL	Habituation	96.167	0.027	1564.9	2035.1	257	257
48	MK-801 0.32 mg/kg + SOL	Habituation	69.307	0.019	1261.9	2338.1	322	321
57	MK-801 0.32 mg/kg + SOL	Habituation	87.071	0.024	1800.7	1799.3	315	314
62	MK-801 0.32 mg/kg + SOL	Habituation	58.651	0.016	1251.6	2348.4	245	245
6	MK-801 0.32 mg/kg + SOL	MK-801 challenge	674.169	0.094	6048.2	1151.8	146	146

11	MK-801 0.32 mg/kg + SOL	MK-801 challenge	536.922	0.075	4891.2	2308.8	281	281
25	MK-801 0.32 mg/kg + SOL	MK-801 challenge	331.255	0.046	4537.1	2663.0	284	284
39	MK-801 0.32 mg/kg + SOL	MK-801 challenge	618.611	0.086	5650.1	1549.9	169	169
48	MK-801 0.32 mg/kg + SOL	MK-801 challenge	271.965	0.038	4055.2	3144.8	385	384
57	MK-801 0.32 mg/kg + SOL	MK-801 challenge	483.603	0.067	5112.3	2087.7	272	272
62	MK-801 0.32 mg/kg + SOL	MK-801 challenge	480.560	0.067	5801.9	1398.1	227	227
7	MK-801 0.32 mg/kg + GL-III-36 10 mg/kg	Habituation	104.045	0.029	1896.8	1703.2	263	263
17	MK-801 0.32 mg/kg + GL-III-36 10 mg/kg	Habituation	81.126	0.023	1626.3	1973.7	308	308
28	MK-801 0.32 mg/kg + GL-III-36 10 mg/kg	Habituation	86.459	0.024	1737.9	1862.1	358	358
38	MK-801 0.32 mg/kg + GL-III-36 10 mg/kg	Habituation	85.601	0.024	1809.5	1790.5	269	269
44	MK-801 0.32 mg/kg + GL-III-36 10 mg/kg	Habituation	97.086	0.027	1943.3	1656.7	214	213
53	MK-801 0.32 mg/kg + GL-III-36 10 mg/kg	Habituation	87.084	0.024	1713.2	1886.8	309	309
63	MK-801 0.32 mg/kg + GL-III-36 10 mg/kg	Habituation	78.832	0.022	1406.6	2193.4	324	323
7	MK-801 0.32 mg/kg + GL-III-36 10 mg/kg	MK-801 challenge	376.727	0.052	4354.5	2845.5	320	321
17	MK-801 0.32 mg/kg + GL-III-36 10 mg/kg	MK-801 challenge	263.060	0.037	3925.5	3274.5	333	332
28	MK-801 0.32 mg/kg + GL-III-36 10 mg/kg	MK-801 challenge	344.040	0.048	4374.5	2825.5	491	491

38	MK-801 0.32 mg/kg + GL-III-36 10 mg/kg	MK-801 challenge	89.512	0.012	2694.1	4505.9	416	415
44	MK-801 0.32 mg/kg + GL-III-36 10 mg/kg	MK-801 challenge	125.727	0.017	2648.3	4551.7	514	514
53	MK-801 0.32 mg/kg + GL-III-36 10 mg/kg	MK-801 challenge	152.032	0.021	3113.1	4086.9	409	409
63	MK-801 0.32 mg/kg + GL-III-36 10 mg/kg	MK-801 challenge	221.942	0.031	4420.3	2779.7	438	437
8	MK-801 0.32 mg/kg + GL-III-73 10 mg/kg	Habituation	62.613	0.017	1211.3	2388.6	210	210
18	MK-801 0.32 mg/kg + GL-III-73 10 mg/kg	Habituation	140.500	0.039	2561.6	1038.4	264	264
27	MK-801 0.32 mg/kg + GL-III-73 10 mg/kg	Habituation	120.039	0.033	2043.9	1556.1	254	253
37	MK-801 0.32 mg/kg + GL-III-73 10 mg/kg	Habituation	89.436	0.025	1631.8	1968.2	292	291
50	MK-801 0.32 mg/kg + GL-III-73 10 mg/kg	Habituation	86.492	0.024	1829.9	1770.1	269	268
55	MK-801 0.32 mg/kg + GL-III-73 10 mg/kg	Habituation	75.719	0.021	1500.9	2099.1	274	274
8	MK-801 0.32 mg/kg + GL-III-73 10 mg/kg	MK-801 challenge	703.302	0.098	6235.5	964.5	176	175
18	MK-801 0.32 mg/kg + GL-III-73 10 mg/kg	MK-801 challenge	299.045	0.042	3766.8	3433.2	393	393
27	MK-801 0.32 mg/kg + GL-III-73 10 mg/kg	MK-801 challenge	629.346	0.087	5866.6	1333.4	245	244
37	MK-801 0.32 mg/kg + GL-III-73 10 mg/kg	MK-801 challenge	376.363	0.052	5947.0	1253.0	257	257
50	MK-801 0.32 mg/kg + GL-III-73 10 mg/kg	MK-801 challenge	255.332	0.035	4640.8	2559.2	478	477
55	MK-801 0.32 mg/kg + GL-III-73 10 mg/kg	MK-801 challenge	221.365	0.031	4240.7	2959.3	487	486

9	MK-801 0.32 mg/kg + GL-III-76 10 mg/kg	Habituation	81.879	0.023	1302.8	2297.2	339	338
19	MK-801 0.32 mg/kg + GL-III-76 10 mg/kg	Habituation	116.572	0.032	2090.9	1509.1	264	263
21	MK-801 0.32 mg/kg + GL-III-76 10 mg/kg	Habituation	81.742	0.023	1635.3	1964.7	299	298
32	MK-801 0.32 mg/kg + GL-III-76 10 mg/kg	Habituation	86.410	0.024	1636.9	1963.1	323	322
42	MK-801 0.32 mg/kg + GL-III-76 10 mg/kg	Habituation	89.913	0.025	1946.9	1653.1	313	313
56	MK-801 0.32 mg/kg + GL-III-76 10 mg/kg	Habituation	71.675	0.020	1632.8	1967.2	272	271
9	MK-801 0.32 mg/kg + GL-III-76 10 mg/kg	MK-801 challenge	72.305	0.010	1945.9	5254.0	286	287
19	MK-801 0.32 mg/kg + GL-III-76 10 mg/kg	MK-801 challenge	29.615	0.004	1445.9	5754.1	295	295
21	MK-801 0.32 mg/kg + GL-III-76 10 mg/kg	MK-801 challenge	34.851	0.005	949.4	6250.6	277	278
32	MK-801 0.32 mg/kg + GL-III-76 10 mg/kg	MK-801 challenge	53.357	0.007	1879.5	5320.5	289	289
42	MK-801 0.32 mg/kg + GL-III-76 10 mg/kg	MK-801 challenge	39.306	0.005	1807.0	5393.0	308	309
56	MK-801 0.32 mg/kg + GL-III-76 10 mg/kg	MK-801 challenge	117.862	0.016	2366.0	4834.0	393	393
10	MK-801 0.32 mg/kg + GL-III-78 10 mg/kg	Habituation	134.519	0.037	2253.3	1346.7	194	194
20	MK-801 0.32 mg/kg + GL-III-78 10 mg/kg	Habituation	77.400	0.022	1611.6	1988.4	344	343
24	MK-801 0.32 mg/kg + GL-III-78 10 mg/kg	Habituation	79.378	0.022	1603.5	1996.5	338	337
31	MK-801 0.32 mg/kg + GL-III-78 10 mg/kg	Habituation	52.150	0.014	1091.5	2508.5	253	253

49	MK-801 0.32 mg/kg + GL-III-78 10 mg/kg	Habituation	92.216	0.026	1811.9	1788.1	362	361
54	MK-801 0.32 mg/kg + GL-III-78 10 mg/kg	Habituation	111.170	0.031	2139.6	1460.4	197	197
10	MK-801 0.32 mg/kg + GL-III-78 10 mg/kg	MK-801 challenge	174.143	0.024	5198.8	2001.2	415	414
20	MK-801 0.32 mg/kg + GL-III-78 10 mg/kg	MK-801 challenge	141.461	0.020	4651.2	2548.8	570	569
24	MK-801 0.32 mg/kg + GL-III-78 10 mg/kg	MK-801 challenge	181.833	0.025	4641.7	2558.4	510	509
31	MK-801 0.32 mg/kg + GL-III-78 10 mg/kg	MK-801 challenge	134.103	0.019	3245.6	3954.4	661	662
49	MK-801 0.32 mg/kg + GL-III-78 10 mg/kg	MK-801 challenge	436.112	0.061	5151.6	2048.4	402	403
54	MK-801 0.32 mg/kg + GL-III-78 10 mg/kg	MK-801 challenge	105.118	0.015	3028.5	4171.5	482	481

Table 58. Raw data of anti-schizophrenia model. Continued.

Animal	Treatment (SORTED)	Stage	Max speed (m/s)	Rotations	Clockwise rotations	Anticlockwise rotations	Freezing episodes	Time freezing (s)
1	SAL + SOL	Habituation	0.307	135	49	86	1493	2477.7
15	SAL + SOL	Habituation	0.351	140	73	67	1491	2401.6
26	SAL + SOL	Habituation	0.338	128	68	60	1479	2449.4
40	SAL + SOL	Habituation	0.265	87	40	47	1223	2712.6
46	SAL + SOL	Habituation	0.311	121	73	48	1281	2556.6
51	SAL + SOL	Habituation	0.293	115	37	78	1355	2346.7
61	SAL + SOL	Habituation	0.277	109	48	61	1220	2823.1
64	SAL + SOL	Habituation	0.377	99	70	29	1159	2698.8

1	SAL + SOL	MK-801 challenge	0.364	117	47	70	1044	6472.0
15	SAL + SOL	MK-801 challenge	0.323	94	63	31	1160	6329.6
26	SAL + SOL	MK-801 challenge	0.267	31	14	17	440	6946.7
40	SAL + SOL	MK-801 challenge	0.185	16	4	12	233	7046.4
46	SAL + SOL	MK-801 challenge	0.195	22	8	14	157	7069.7
51	SAL + SOL	MK-801 challenge	0.188	6	5	1	133	7110.1
61	SAL + SOL	MK-801 challenge	0.297	75	41	34	778	6664.3
64	SAL + SOL	MK-801 challenge	0.244	25	16	9	331	6961.4
2	SAL + GL-III-36 10 mg/kg	Habituation	0.292	149	69	80	1436	2461.9
13	SAL + GL-III-36 10 mg/kg	Habituation	0.275	120	61	59	1423	2537.3
23	SAL + GL-III-36 10 mg/kg	Habituation	0.439	133	93	40	1444	2090.3
36	SAL + GL-III-36 10 mg/kg	Habituation	0.264	159	103	56	1633	2091.1
41	SAL + GL-III-36 10 mg/kg	Habituation	0.279	171	68	103	1831	2196.7
59	SAL + GL-III-36 10 mg/kg	Habituation	0.300	139	61	78	1662	2026.1
2	SAL + GL-III-36 10 mg/kg	MK-801 challenge	0.238	58	30	28	427	6854.3
13	SAL + GL-III-36 10 mg/kg	MK-801 challenge	0.233	22	11	11	296	6935.7

23	SAL + GL-III-36 10 mg/kg	MK-801 challenge	0.573	22	15	7	295	6953.7
36	SAL + GL-III-36 10 mg/kg	MK-801 challenge	0.187	25	18	7	268	7002.6
41	SAL + GL-III-36 10 mg/kg	MK-801 challenge	0.169	23	13	10	229	7026.5
59	SAL + GL-III-36 10 mg/kg	MK-801 challenge	0.192	32	15	17	419	6754.3
3	SAL + GL-III-73 10 mg/kg	Habituation	0.319	145	69	76	1667	2107.6
16	SAL + GL-III-73 10 mg/kg	Habituation	0.313	117	57	60	1500	2525.6
22	SAL + GL-III-73 10 mg/kg	Habituation	0.289	145	64	81	1366	2593.8
33	SAL + GL-III-73 10 mg/kg	Habituation	0.317	144	95	49	1535	2491.5
45	SAL + GL-III-73 10 mg/kg	Habituation	0.274	104	60	44	1437	2621.1
58	SAL + GL-III-73 10 mg/kg	Habituation	0.241	135	72	63	1565	2344.7
3	SAL + GL-III-73 10 mg/kg	MK-801 challenge	0.285	51	16	35	402	6813.4
16	SAL + GL-III-73 10 mg/kg	MK-801 challenge	0.231	49	23	26	578	6883.4
22	SAL + GL-III-73 10 mg/kg	MK-801 challenge	0.438	121	49	72	1215	6283.9
33	SAL + GL-III-73 10 mg/kg	MK-801 challenge	0.280	83	52	31	759	6626.9
45	SAL + GL-III-73 10 mg/kg	MK-801 challenge	0.217	19	9	10	171	7100.8
58	SAL + GL-III-73 10 mg/kg	MK-801 challenge	0.211	27	18	9	217	7001.9

4	SAL + GL-III-76 10 mg/kg	Habituation	0.305	137	66	71	1571	2304.5
14	SAL + GL-III-76 10 mg/kg	Habituation	0.242	99	63	36	1007	2854.1
29	SAL + GL-III-76 10 mg/kg	Habituation	0.397	108	34	74	1299	2646.6
35	SAL + GL-III-76 10 mg/kg	Habituation	0.301	156	90	66	1495	2023.4
47	SAL + GL-III-76 10 mg/kg	Habituation	0.249	87	36	51	1229	2623.9
60	SAL + GL-III-76 10 mg/kg	Habituation	0.298	148	108	40	1740	2174.6
4	SAL + GL-III-76 10 mg/kg	MK-801 challenge	0.197	21	12	9	181	6978.0
14	SAL + GL-III-76 10 mg/kg	MK-801 challenge	0.265	35	14	21	290	6922.6
29	SAL + GL-III-76 10 mg/kg	MK-801 challenge	0.214	18	8	10	180	7018.7
35	SAL + GL-III-76 10 mg/kg	MK-801 challenge	0.215	23	9	14	189	6972.8
47	SAL + GL-III-76 10 mg/kg	MK-801 challenge	0.204	21	13	8	212	6964.4
60	SAL + GL-III-76 10 mg/kg	MK-801 challenge	0.269	37	20	17	296	6865.2
5	SAL + GL-III-78 10 mg/kg	Habituation	0.316	117	51	66	1284	2693.6
12	SAL + GL-III-78 10 mg/kg	Habituation	0.271	110	34	76	1557	2537.6
30	SAL + GL-III-78 10 mg/kg	Habituation	0.327	148	59	89	1187	2559.2
34	SAL + GL-III-78 10 mg/kg	Habituation	0.259	136	79	57	1514	2423.6

43	SAL + GL-III-78 10 mg/kg	Habituation	0.265	147	63	84	1532	1802.2
52	SAL + GL-III-78 10 mg/kg	Habituation	0.281	94	43	51	1379	2522.5
5	SAL + GL-III-78 10 mg/kg	MK-801 challenge	0.399	46	14	32	375	6854.2
12	SAL + GL-III-78 10 mg/kg	MK-801 challenge	0.246	31	16	15	330	6920.6
30	SAL + GL-III-78 10 mg/kg	MK-801 challenge	0.246	30	7	23	250	6907.2
34	SAL + GL-III-78 10 mg/kg	MK-801 challenge	0.234	41	25	16	562	6761.8
43	SAL + GL-III-78 10 mg/kg	MK-801 challenge	0.246	97	50	47	866	6109.3
52	SAL + GL-III-78 10 mg/kg	MK-801 challenge	0.223	32	12	20	335	6917.2
6	MK-801 0.32 mg/kg + SOL	Habituation	0.278	146	80	66	1269	2577.1
11	MK-801 0.32 mg/kg + SOL	Habituation	0.285	129	65	64	1465	2380.2
25	MK-801 0.32 mg/kg + SOL	Habituation	0.300	131	68	63	1438	2513.9
39	MK-801 0.32 mg/kg + SOL	Habituation	0.324	129	72	57	1212	2428.9
48	MK-801 0.32 mg/kg + SOL	Habituation	0.283	85	27	58	1186	2708.2
57	MK-801 0.32 mg/kg + SOL	Habituation	0.276	116	49	67	1438	2522.1
62	MK-801 0.32 mg/kg + SOL	Habituation	0.248	86	61	25	864	3012.0
6	MK-801 0.32 mg/kg + SOL	MK-801 challenge	0.359	1163	896	267	1445	2053.8

11	MK-801 0.32 mg/kg + SOL	MK-801 challenge	0.354	697	419	278	1320	2736.5
25	MK-801 0.32 mg/kg + SOL	MK-801 challenge	0.334	780	671	109	1659	3441.8
39	MK-801 0.32 mg/kg + SOL	MK-801 challenge	0.324	794	390	404	1129	1925.9
48	MK-801 0.32 mg/kg + SOL	MK-801 challenge	0.285	634	233	401	1903	3660.1
57	MK-801 0.32 mg/kg + SOL	MK-801 challenge	0.333	642	340	302	1858	3046.4
62	MK-801 0.32 mg/kg + SOL	MK-801 challenge	0.305	895	801	94	1962	2749.8
7	MK-801 0.32 mg/kg + GL-III-36 10 mg/kg	Habituation	0.366	136	81	55	1432	2213.6
17	MK-801 0.32 mg/kg + GL-III-36 10 mg/kg	Habituation	0.276	131	83	48	1246	2667.6
28	MK-801 0.32 mg/kg + GL-III-36 10 mg/kg	Habituation	0.251	126	75	51	1526	2354.9
38	MK-801 0.32 mg/kg + GL-III-36 10 mg/kg	Habituation	0.239	136	109	27	1363	2659.9
44	MK-801 0.32 mg/kg + GL-III-36 10 mg/kg	Habituation	0.318	125	46	79	1473	2203.3
53	MK-801 0.32 mg/kg + GL-III-36 10 mg/kg	Habituation	0.399	120	71	49	1385	2589.6
63	MK-801 0.32 mg/kg + GL-III-36 10 mg/kg	Habituation	0.270	111	61	50	1307	2446.3

7	MK-801 0.32 mg/kg + GL-III-36 10 mg/kg	MK-801 challenge	0.315	896	336	560	1155	3234.4
17	MK-801 0.32 mg/kg + GL-III-36 10 mg/kg	MK-801 challenge	0.302	646	474	172	1533	3922.8
28	MK-801 0.32 mg/kg + GL-III-36 10 mg/kg	MK-801 challenge	0.281	705	472	233	1857	3356.2
38	MK-801 0.32 mg/kg + GL-III-36 10 mg/kg	MK-801 challenge	0.266	567	547	20	1503	5510.8
44	MK-801 0.32 mg/kg + GL-III-36 10 mg/kg	MK-801 challenge	0.223	455	169	286	1312	4666.4
53	MK-801 0.32 mg/kg + GL-III-36 10 mg/kg	MK-801 challenge	0.193	474	165	309	1475	4746.6
63	MK-801 0.32 mg/kg + GL-III-36 10 mg/kg	MK-801 challenge	0.197	803	303	500	1533	3138.7
8	MK-801 0.32 mg/kg + GL-III-73 10 mg/kg	Habituation	0.262	95	66	29	1075	2771.8
18	MK-801 0.32 mg/kg + GL-III-73 10 mg/kg	Habituation	0.309	191	67	124	1735	2172.3
27	MK-801 0.32 mg/kg + GL-III-73 10 mg/kg	Habituation	0.326	153	77	76	1439	2057.9
37	MK-801 0.32 mg/kg + GL-III-73 10 mg/kg	Habituation	0.297	112	36	76	1317	2681.5
50	MK-801 0.32 mg/kg + GL-III-73 10 mg/kg	Habituation	0.274	134	96	38	1406	2583.7

55	MK-801 0.32 mg/kg + GL-III-73 10 mg/kg	Habituation	0.271	120	80	40	1252	2424.4
8	MK-801 0.32 mg/kg + GL-III-73 10 mg/kg	MK-801 challenge	0.345	1281	842	439	1254	1523.8
18	MK-801 0.32 mg/kg + GL-III-73 10 mg/kg	MK-801 challenge	0.279	675	335	340	1352	4091.4
27	MK-801 0.32 mg/kg + GL-III-73 10 mg/kg	MK-801 challenge	0.415	1386	652	734	1692	2082.2
37	MK-801 0.32 mg/kg + GL-III-73 10 mg/kg	MK-801 challenge	0.239	1442	417	1025	1995	2625.9
50	MK-801 0.32 mg/kg + GL-III-73 10 mg/kg	MK-801 challenge	0.276	697	648	49	2437	4014.8
55	MK-801 0.32 mg/kg + GL-III-73 10 mg/kg	MK-801 challenge	0.213	742	443	299	1653	3511.6
9	MK-801 0.32 mg/kg + GL-III-76 10 mg/kg	Habituation	0.331	118	66	52	1195	2789.7
19	MK-801 0.32 mg/kg + GL-III-76 10 mg/kg	Habituation	0.312	164	53	111	1451	2071.3
21	MK-801 0.32 mg/kg + GL-III-76 10 mg/kg	Habituation	0.694	122	65	57	1360	2500.7
32	MK-801 0.32 mg/kg + GL-III-76 10 mg/kg	Habituation	0.288	126	49	77	1380	2414.7
42	MK-801 0.32 mg/kg + GL-III-76 10 mg/kg	Habituation	0.305	126	56	70	1610	2466.7

56	MK-801 0.32 mg/kg + GL-III-76 10 mg/kg	Habituation	0.259	97	45	52	1287	2613.9
9	MK-801 0.32 mg/kg + GL-III-76 10 mg/kg	MK-801 challenge	0.215	353	188	165	1106	5737.4
19	MK-801 0.32 mg/kg + GL-III-76 10 mg/kg	MK-801 challenge	0.191	237	222	15	1159	6253.4
21	MK-801 0.32 mg/kg + GL-III-76 10 mg/kg	MK-801 challenge	0.189	194	185	9	615	6536.5
32	MK-801 0.32 mg/kg + GL-III-76 10 mg/kg	MK-801 challenge	0.163	366	110	256	984	5632.5
42	MK-801 0.32 mg/kg + GL-III-76 10 mg/kg	MK-801 challenge	0.199	267	196	71	1210	6233.6
56	MK-801 0.32 mg/kg + GL-III-76 10 mg/kg	MK-801 challenge	0.214	350	103	247	1394	5389.6
10	MK-801 0.32 mg/kg + GL-III-78 10 mg/kg	Habituation	0.297	159	123	36	1421	2316.9
20	MK-801 0.32 mg/kg + GL-III-78 10 mg/kg	Habituation	0.315	106	56	50	1553	2394.6
24	MK-801 0.32 mg/kg + GL-III-78 10 mg/kg	Habituation	0.238	112	74	38	1454	2495.4
31	MK-801 0.32 mg/kg + GL-III-78 10 mg/kg	Habituation	0.274	106	47	59	1082	2692.8
49	MK-801 0.32 mg/kg + GL-III-78 10 mg/kg	Habituation	0.266	140	82	58	1544	2540.6

54	MK-801 0.32 mg/kg + GL-III-78 10 mg/kg	Habituation	0.340	157	23	134	1440	2376.8
10	MK-801 0.32 mg/kg + GL-III-78 10 mg/kg	MK-801 challenge	0.211	641	412	229	2543	4170.1
20	MK-801 0.32 mg/kg + GL-III-78 10 mg/kg	MK-801 challenge	0.261	681	520	161	2712	3581.7
24	MK-801 0.32 mg/kg + GL-III-78 10 mg/kg	MK-801 challenge	0.206	784	560	224	2208	3931.2
31	MK-801 0.32 mg/kg + GL-III-78 10 mg/kg	MK-801 challenge	0.198	419	131	288	1754	4155.7
49	MK-801 0.32 mg/kg + GL-III-78 10 mg/kg	MK-801 challenge	0.321	837	306	531	2055	3456.0
54	MK-801 0.32 mg/kg + GL-III-78 10 mg/kg	MK-801 challenge	0.177	527	358	169	1465	5019.0

Appendix V: NIH Epilepsy Therapy Screening Program (ETSP) Test Results of KRM-II-81

Test 3 Results - Rat P.O.

ETSP ID: 490011 **Screen ID: 4** **Batch ID: D**

Solvent Code : MC **Solvent Prep : MPSB**
Route Code : PO
Date Started : 11-Sep-2018 **Date Completed : 11-Sep-2018**
Reference : 488:139 **Strain / Supplier :**

Time to peak effect

Time (Hours)				0.25		0.5		1.0		2.0		4.0		6.0		8.0		24		72	
Test	Dose (mg/kg)	Form	Deaths	N / F	C	N / F	C	N / F	C	N / F	C	N / F	C	N / F	C	N / F	C	N / F	C	N / F	C
TOX	300	SUS		0 / 8		0 / 8		0 / 8		0 / 8		0 / 8		0 / 8							

N: number of animals protected or toxic. **F : total number of animals tested.** **C : Comment code.**

Form : Formulation. **SUS : Suspension.**

Anticonvulsant Screening Program
Test 3 Results - Rat P.O. Quantification

ASP ID: 490011 B Screen ID: 1

Solvent Code:	**MC**	**Solvent Prep:**	**M&P,SB**
Animal Weight:	**100.0 - 150.0 g**		
Date Started:	**03-Oct-2017**	**Date Completed:**	**18-Oct-2017**
Reference:	**526:25-27**		

ED50 Biological Response

Test	Time (hr)	Dose (mg/kg)	Dths	N / F C
MES	1.0	15		1 / 8
MES	1.0	30		2 / 8
MES	1.0	60		2 / 8
MES	1.0	120		2 / 8
MES	1.0	240		0 / 8 Z

Note: Presence of an asterisk (*) indicates that there are multiple comment codes.

ED50 Biological Response Comments

Test	Dose (mg/kg)	Time (Hrs)	Code	Comment
MES	240	1	Z	1/8 toxic

Time to Peak Effect

Time (Hours)				0.25	0.5	1.0	2.0	4.0	6.0	8.0	24	3.0
Test	Dose		Dths	N / F C	N / F C	N / F C	N / F C	N / F C	N / F C	N / F C	N / F C	N / F C
MES	30			0 / 4	0 / 4	2 / 4	1 / 4	0 / 4	/	/	/	/
TOX	30			0 / 4	0 / 4	0 / 4	0 / 4	0 / 4	/	/	/	/

Note: N/F = number of animals active or toxic over the number tested.

C= Comment code. Presence of an asterisk (*) indicates that there are multiple comment codes.

Epilepsy Therapy Screening Program

Test 3 Results - Rat P.O.

ETSP ID: 490011 **Screen ID: 2** **Batch ID: C**

Solvent Code : MC **Solvent Prep : MPSB**
Route Code : PO
Date Started : 22-Feb-2018 **Date Completed : 22-Feb-2018**
Reference : 488:116 **Strain / Supplier :**

Time to peak effect

Time (Hours)				0.25		0.5		1.0		2.0		4.0		6.0		8.0		24		72	
Test	Dose (mg/kg)	Form	Deaths	N / F	C	N / F	C	N / F	C	N / F	C	N / F	C	N / F	C	N / F	C	N / F	C	N / F	C
SCM ET	100	SUS		4 / 4		4 / 4		4 / 4		3 / 4		3 / 4									

N: number of animals protected or toxic. F : total number of animals tested. C : Comment code.

Form : Formulation. SUS : Suspension.

Anticonvulsant Screening Program
Test 4 Results - Mice I.P. Quantification

ASP ID: 490011 U Screen ID: 1

Solvent Code: MC **Solvent Prep:** M&P,SB

Animal Weight: - g

Date Started: 30-Nov-2015 **Date Completed:** 06-Jan-2016

Reference: 517: 22 & 31-32

ED50 Value

Test	Time(Hrs)	ED50	95% Confidence Interval	Slope	STD Err	PI Value
SCMET	0.5	10.94	7.13 - 16.65	1.26	4.23	
TOX	0.5	46.77	29.11 - 76.17	3.29	1.02	

ED50 Biological Response

Test	Time (hr)	Dose (mg/kg)	Dths	N / F C
SCMET	0.50	5		0 / 8
SCMET	0.50	10		5 / 8
SCMET	0.50	25		7 / 8
SCMET	0.50	50		8 / 8
TOX	0.50	10		0 / 8
TOX	0.50	25		2 / 8
TOX	0.50	50		4 / 8
TOX	0.50	100		7 / 8 33

Note: Presence of an asterisk (*) indicates that there are multiple comment codes.

ED50 Biological Response Comments

Test	Dose (mg/kg)	Time (Hrs)	Code	Comment
TOX	100	0.5	33	Tremors

Time to Peak Effect

Time (Hours)				0.25	0.5	1.0	2.0	4.0	6.0	8.0	24	3.0
Test	Dose		Dths	N / F C	N / F C	N / F C	N / F C	N / F C	N / F C	N / F C	N / F C	N / F C
MES	100			0 / 4	2 / 8	1 / 8	0 / 4	0 / 4	/	/	/	/
TOX	100			3 / 4	7 / 8	4 / 8	1 / 4	0 / 4	/	/	/	/

Anticonvulsant Screening Program
Test 4 Results - Mice I.P. Quantification

ASP ID: 490011 U Screen ID: 1

Note: N/F = number of animals active or toxic over the number tested.

C= Comment code. Presence of an asterisk (*) indicates that there are multiple comment codes.

Comments to Supplier:	MES ED50 not determined, toxicity exceed efficacy

Anticonvulsant Screening Program

Test 7 Results - Anticonvulsant Evaluation (6Hz, Mice)

ASP ID: 490011 A Screen ID: 1

Solvent Code:	**MC**	**Solvent Prep:**	**M&P,SB**	**Route Code:**	**PO**
Animal Weight:	**- g**			**Current(mA):**	**44**
Date Started:	**13-Jun-2017**	**Date Completed:**	**20-Jun-2017**		
Reference:	**519:146-149**				

ED50 Value

Test	Time(Hrs)	ED50	95% Confidence Interval	Slope	STD Err	PI Value
6HZ	2	29.9	18.47 - 43.74	5.31	1.94	
TOX	4	119.38	85.87 - 146.42	6.97	2.25	

ED50 Biological Response

Test	Time (hr)	Dose (mg/kg)	Dths	N / F	C
6HZ	2.0	10		0 / 8	
6HZ	2.0	25		3 / 8	
6HZ	2.0	50		7 / 8	
TOX	4.0	50		0 / 8	
TOX	4.0	100		3 / 8	33
TOX	4.0	150		5 / 8	*
TOX	4.0	200		8 / 8	*

Note: Presence of an asterisk (*) indicates that there are multiple comment codes.

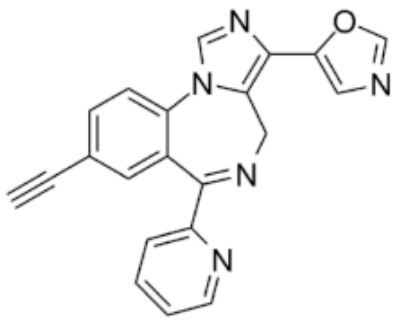

KRM-II-81

ED50 Biological Response Comments

Test	Dose (mg/kg)	Time (Hrs)	Code	Comment
TOX	100	4	33	Tremors
TOX	150	4	13	Loss of righting reflex
TOX	150	4	14	Unable to grasp rotorod
TOX	150	4	33	Tremors
TOX	200	4	13	Loss of righting reflex
TOX	200	4	31	Severe Tremors
TOX	200	4	33	Tremors

Epilepsy Therapy Screening Program

Test 8 Results - Rats I.P.

ETSP ID: 490011 **Screen ID: 1** **Batch ID: D**

Solvent Code : MC **Solvent Prep : MPSB**
Route Code : IP
Date Started : 12-Sep-2018 **Date Completed : 20-Sep-2018**
Reference : 488:138-139; 527:13 **Strain / Supplier :**

Time to peak effect

Time (Hours)				0.25		0.5		1.0		2.0		4.0		6.0		8.0		24		72	
Test	Dose (mg/kg)	Form	Deaths	N / F	C	N / F	C	N / F	C	N / F	C	N / F	C	N / F	C	N / F	C	N / F	C	N / F	C
SCMET	5	SOL		5 / 8		4 / 8		1 / 4		0 / 4		0 / 4									
TOX	50	SOL		2 / 8	12	3 / 8	12	2 / 8	12	0 / 8		0 / 8									
TOX	100	SOL		8 / 8	12	8 / 8	12	7 / 8	12	7 / 8	12	7 / 8	12	0 / 8							

N: number of animals protected or toxic. | F : total number of animals tested. | C : Comment code.

Form : Formulation. | SOL : Solution.

Response Comments

Test	Dose (mg/kg)	Time (hrs)	Code	Description	How many
TOX	50	0.25	12	Ataxia	2
TOX	50	0.5	12	Ataxia	3
TOX	50	1	12	Ataxia	2
TOX	100	0.25	12	Ataxia	8
TOX	100	0.5	12	Ataxia	8
TOX	100	1	12	Ataxia	7
TOX	100	2	12	Ataxia	7
TOX	100	4	12	Ataxia	7

Epilepsy Therapy Screening Program

Test 10 Results - Rats I.P.

ETSP ID: 490011 **Screen ID: 1** **Batch ID: D**

Solvent Code : MC **Solvent Prep : MPSB**
Route Code : IP
Date Started : 12-Sep-2018 **Date Completed : 20-Sep-2018**
Reference : 488:138-140; 527:11-13 **Strain / Supplier :**

ED50

Test	Time (hrs)	ED50	95% Confidence Interval	Slope	Std Err
SCMET	0.25	3.6	1.99 - 5.37	2.6	0.73

ED50 Biological Response

Test	Time (hrs)	Dose (mg/kg)	Deaths	N / F	C
SCMET	0.25	1		1 / 8	
SCMET	0.25	2.5		2 / 8	
SCMET	0.25	5		5 / 8	
SCMET	0.25	7.5		7 / 8	
SCMET	0.25	10		7 / 8	

N: number of animals protected or toxic. **F : total number of animals tested.** **C : Comment code.**

Epilepsy Therapy Screening Program

Test 18 Results - Flexible Format

ETSP ID: 490011 **Screen ID: 1** **Batch ID: E**

Solvent Code : MC **Solvent Prep : TTSB**
Route Code : IP
Gender : **Species : MICE**
Date Started : 15-Nov-2018 **Date Completed : 13-Dec-2018**
Reference : 529; 28, 29, 34, 35, 36, 42, 43, 50, 51 **Strain / Supplier : CF-1 / Charles River**

ED50

Test	Time (hrs)	ED50	95% Confidence Interval	Slope	Std Err
SCMET	0.5	12.49	5.9 - 19.65	2.05	0.67
TOX	0.25	207.77	151.19 - 302.55	5.03	1.45

ED50 Biological Response

Test	Time (hrs)	Dose (mg/kg)	Deaths	N / F	C
SCMET	0.5	2.5		0 / 8	
SCMET	0.5	8		3 / 8	
SCMET	0.5	15		2 / 8	
SCMET	0.5	19		6 / 8	
SCMET	0.5	23		5 / 8	
SCMET	0.5	30		8 / 8	
TOX	0.25	100		0 / 8	
TOX	0.25	150		3 / 8	14
TOX	0.25	300		5 / 7	
TOX	0.25	600		8 / 8	12
TOX	0.5	300		0 / 8	
N: number of animals protected or toxic.		F : total number of animals tested.			C : Comment code.

ED50 Biological Response Comments

Test	Dose (mg/kg)	Time (hrs)	Code	Description	How many
TOX	150	0.25	14	Unable to grasp rotorod	3
TOX	600	0.25	12	Ataxia	8

Epilepsy Therapy Screening Program

Test Result

Test	Time (hrs)	Dose (mg/kg)	Deaths	N / F	C
SCMET	0.25	15		1 / 4	
SCMET	0.5	15		3 / 4	
SCMET	1	15		1 / 4	
SCMET	2	15		1 / 4	
SCMET	4	15		1 / 4	
TOX	0.25	150		3 / 8	
TOX	0.5	150		1 / 8	
TOX	1	150		0 / 8	
TOX	2	150		1 / 8	
TOX	4	150		0 / 8	
TOX	6	150		0 / 8	
TOX	24	150		0 / 8	
N: number of animals protected or toxic.		**F : total number of animals tested.**			**C : Comment code.**

Epilepsy Therapy Screening Program

Test 25 Results - LTG-Resistant Amygdala Kindled Rat

ETSP ID: 490011 **Screen ID: 1** **Batch ID: C**

Solvent Code : MC **Solvent Prep : MPSB**
Route Code : IP
Date Started : 20-Apr-2018 **Date Completed : 18-May-2018**
Reference : 525:69-73 **Strain / Supplier :**

ED50

Test	Time (hrs)	ED50	95% Confidence Interval	Slope	Std Err
*LTG-K	1	19.21	9.62 - 56.18	1.75	0.6

ED50 Biological Response

Test	Dose (mg/kg)	Time (hrs)	N / F	C
LTG-K	1	1	0 / 8	
LTG-K	5	1	2 / 8	
LTG-K	10	1	2 / 8	
LTG-K	20	1	4 / 8	
LTG-K	40	1	6 / 8	
N: number of animals protected or toxic.		F : total number of animals tested.		C : Comment code.

Test Result

Dose (mg/kg)	Time (hrs)	Seizure Score +/- SEM		Duration (sec) +/- S.D	Protected	Tested
Control	0	5 +/- 0		117.25 +/- 13.8	0	8
10	1	3.75 +/- 0.65		87.38 +/- 10.56	2	8
Control	0	5 +/- 0		84.63 +/- 13.94	0	8
40	1	2.13 +/- 0.52	*	66.75 +/- 14.46	6	8
Control	0	5 +/- 0		123.75 +/- 19.39	0	8
20	1	3.25 +/- 0.59	*	106.75 +/- 18.67	4	8
Control	0	5 +/- 0		123.38 +/- 17.13	0	8
5	1	4.25 +/- 0.49		123.13 +/- 14.75	2	8
Control	0	5 +/- 0		107.5 +/- 18.03	0	8
1	1	5 +/- 0		103.13 +/- 8.18	0	8
* indicates data is significantly different from control.						

Epilepsy Therapy Screening Program

Test 26 Results - Corneal Kindled Mouse

ETSP ID: 490011 **Screen ID: 1** **Batch ID: E**

Solvent Code : MC
Solvent Prep : TTSB
Route Code : PO
Date Started : 05-Apr-2019
Date Completed : 10-Apr-2019
Reference : 524:268,269
Strain / Supplier : CF-1 / Charles River

ED50

Test	Time (hrs)	ED50	95% Confidence Interval	Slope	Std Err
CKM	2	3.96	2.11 - 6.05	2.79	0.66

ED50 Biological Response

Dose (mg/kg)	Time (hrs)	N / F	C	Individual Seizure Scores	Average Seizure Scores	Toxicity N / F
1	2	0 / 8		5,5,5,5,5,5,5,5	5	
3	2	2 / 8		5,5,5,5,0,5,5,0	3.75	
8	2	6 / 8		1,0,0,4,0,0,0,5	1.25	
15	2	8 / 8		0,0,0,0,0,0,0,0	0	
25	2	8 / 8		0,0,0,0,0,0,0,0	0	
30	2	8 / 8		0,0,0,0,0,0,0,0	0	

N: number of animals protected or toxic. **F : total number of animals tested.** **C : Comment code.**

Anticonvulsant Screening Program

Test 33 Results - Mice MES 6Hz 44mA Identification

ASP ID: 490011 U **Screen ID:** 1

Solvent Code: MC **Solvent Prep:** M&P,SB **Route Code:** IP

Animal Weight: 23.0 - 29.0 g **6Hz Current (mA):** 44mA

Reference: 512:272-273

Response

Time (Hours)				0.5	2.0	0.25	1.0	4.0	6.0	3.0	8.0	24
Test	Dose	Form	Dths	N / F C	N / F C	N / F C	N / F C	N / F C	N / F C	N / F C	N / F C	N / F C
6HZ	30	SUS		1 / 4	0 / 4	/	/	/	/	/	/	/
6HZ	100	SUS		3 / 4	3 / 4	/	/	/	/	/	/	/
6HZ	300	SUS		4 / 4	4 / 4	/	/	/	/	/	/	/
MES	30	SUS		0 / 4	0 / 4	/	/	/	/	/	/	/
MES	100	SUS		2 / 4	0 / 4	/	/	/	/	/	/	/
MES	300	SUS		4 / 4	0 / 4	/	/	/	/	/	/	/
TOX	30	SUS		0 / 8	0 / 8	/	/	/	/	/	/	/
TOX	100	SUS		2 / 8	0 / 8 33	/	/	/	/	/	/	/
TOX	300	SUS		2 / 8	8 / 8 *	/	/	/	/	/	/	/
72HR	300	SUS	5	2 / 8 1	3 / 8 1	/	/	/	/	/	/	/

Note: N/F = number of animals active or toxic over the number tested.

C= Comment code. Presence of an asterisk (*) indicates that there are multiple comment codes.

Response Comments

Test	Dose (mg/kg)	Time	Code	Comments
72HR	300	0.5	1	Death
72HR	300	2	1	Death
TOX	100	2	33	Tremors
TOX	300	2	31	Severe Tremors

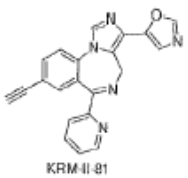

TOX	300	2	33	Tremors

Epilepsy Therapy Screening Program

Test 34 Results - 6Hz, Rats

ETSP ID: 490011 **Screen ID: 1** **Batch ID: ***

Solvent Code	: MC	**Solvent Prep**	: M&P,SB
Route Code	: PO	**Current(mA)**	: 2xCC97
Date Started	: 11-Dec-2017	**Date Completed**	: 11-Dec-2017
Reference	: 514:296	**Strain / Supplier**	:

Time to peak effect

Time (Hours)				0.25		0.5		1.0		2.0		4.0		6.0		8.0		24		72	
Test	Dose (mg/kg)	Form	Deaths	N / F	C	N / F	C	N / F	C	N / F	C	N / F	C	N / F	C	N / F	C	N / F	C	N / F	C
6HZ	120			0 / 4		0 / 4		0 / 4		0 / 4		0 / 4									

N: number of animals protected or toxic. **F : total number of animals tested.** **C : Comment code.**

Form : Formulation.

Epilepsy Therapy Screening Program

Test 35 Results - Post-KA Epileptic Rat Phase 1

ETSP ID: 490011 **Screen ID: 1** **Batch ID: E**

Solvent Code : MC **Solvent Prep : MPSB**
Route Code : IP
Date Started : 28-Jan-2019 **Date Completed : 15-Feb-2019**
Reference : KA Chronic Model Stage 1 **Strain / Supplier :**
Binder 2

Epilepsy Therapy Screening Program

Test 35 - Chronic Post-SE (KA) Spontaneously Seizing Rats: Stage 1 (IP Administration)

ETSP: 490011	Batch: E
Dose: 20 m/k	Frequency: TID

Daily Seizure Burden

Baseline	Drug	Vehicle
6.5±2.9	1.6±0.8†	6.7±3.3

n.s. vs. Vehicle (Wilcoxon Rank Sum)

†p<0.05 vs. Baseline (Wilcoxon Rank Sum)

Seizure Freedom

Baseline	Drug	Vehicle
1/12	6/12†	2/12

n.s. vs. Vehicle (Fisher Exact)

†p<0.05 vs. Baseline (Fisher Exact)

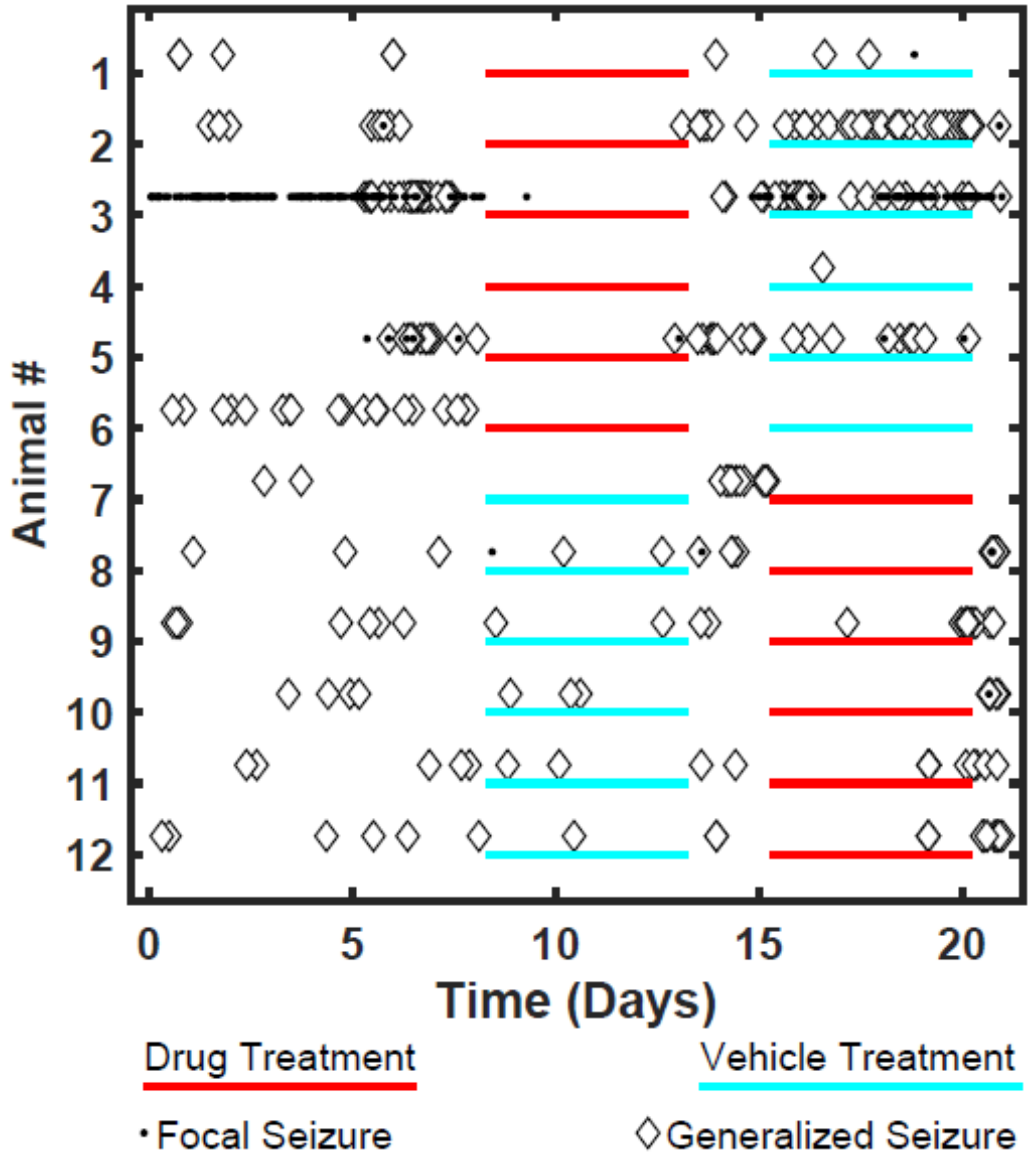

Epilepsy Therapy Screening Program

Test 37 Results - Mesial Temporal Lobe Epilepsy

ETSP ID: 490011 **Screen ID: 1** **Batch ID: U,A,C**

Solvent Code : **Solvent Prep :**
Route Code : PO
Date Started : 09-Jan-2018 **Date Completed : 14-Mar-2018**
Reference : Report sent by email (see Cameron) **Strain / Supplier :**

Test 37 Results - MTLE Mouse Acute Screen Evaluation

ASP ID: 490011 A **Screen ID: 1**
Solvent Code: MC **Route Code: PO**
Date Started: 09 Jan 18 **Date Completed: 14 Mar 18**

Dose and TPE	Recording Period	Mouse 1	Mouse 2	Mouse 3	Mouse 4	Mouse 5	Mean	SEM
30 mg/kg	Baseline	13	20	12	18	8	14.20	2.15
	110 - 130 min	5	1	0	0	0	1.20	0.97
Peak 120 min	% peak effect	38.46	5.00	0.00	0.00	0.00	8.69	7.51

Comments to Supplier:

Test 37 Results - Mesial Temporal Lobe Epilepsy

ETSP ID: 490011 **Screen ID: 2** **Batch ID: C**

Solvent Code : MC
Solvent Prep : TTSB
Route Code : PO
Date Started : 01-Apr-2018
Date Completed : 30-Jun-2018
Reference : Results sent by email, see cameron
Strain / Supplier :

ASP ID: 490011 C **Screen ID: 2**
Solvent Code: MC **Route Code: PO**
Date Started: April 2018 **Date Completed: June 2018**

Dose and TPE	Recording Period	Mouse 1	Mouse 2	Mouse 3	Mouse 4	Mean	SEM
15 mg/kg	Baseline	11	18	23	15	16.75	2.53
peak	120 min	2	5	9	6	5.50	1.44
120 min	% peak effect	18.18	27.78	39.13	40.00	31.27	5.18

Comments to Supplier:

Appendix VI: Metabolites Study from Eli Lilly of KRM-II-81 and MP-III-080

Report 1. *In Vitro* Metabolism of Compound (KRM-II-81) LSN3310515 in Mouse Hepatocytes

Q² Solutions
a Quintiles Quest Joint Venture

Discovery Metabolism

Report Title

In Vitro Metabolism of Compound LSN3310515 in Mouse Hepatocytes

Study

H2100188M171012

Study Completion Date

October 23, 2017

Sponsor

Eli Lilly and Company

Testing Facility

Q Squared Solutions BioSciences LLC
Purdue Research Park
5225 Exploration Drive
Indianapolis, IN 46241

This report has been reviewed for completeness and accuracy.

Responsible investigator:

Xiaochun (Sean) Zhu, Ph.D. Date: October 23, 2017

Title: Director

Q^2 Solutions – Discovery Metabolism

Tel: 317-548-5180

Email: Xiaochun.Zhu@q2labsolutions.com

Reviewed by:

Richard Burton, Ph.D. Date: October 23, 2017

Title: Research Investigator

Q^2 Solutions – Discovery Metabolism

Tel: 317-548-5120

Email: Richard.Burton@q2labsolutions.com

Discovery Biotransformation Summary

Tentatively Identified Metabolites of LSN3310515 in Mouse Hepatocytes
(2 μM incubation for 4 hours)

Metabolite Table:

Peak ID	Tentative Metabolite Identification	*m/z*	RT (min)	Species/Matrix
3310515	Parent (P)	352	2.71	MH
A	P + 2O + 2H	386	1.67	MH
C	P + O + 2H	370	2.03	MH
E	P + 2O + 2H	386	2.42	MH

MH = mouse hepatocytes

Comments: All following summary is based on the MS intensity. Extent of metabolism for LSN3310515: Extensive– MH. LSN3310515 was the major component observed in MH.

Additional metabolites were observed but considered minor (as judged by ion intensity) and therefore not reported in this study report.

Proposed Metabolite Structures of LSN3310515

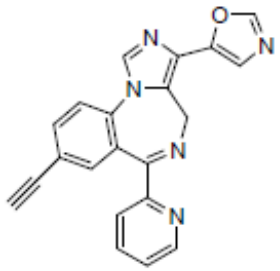

LSN3310515, Parent, m/z 352

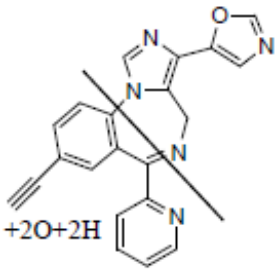

A, m/z 386

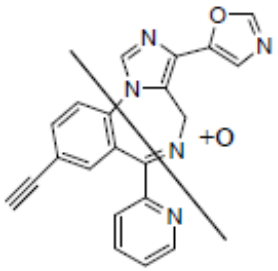

B, D, m/z 368

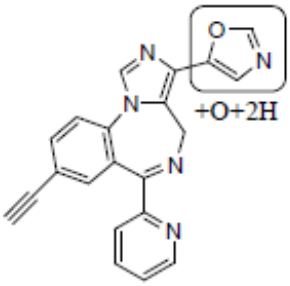

C, m/z 370

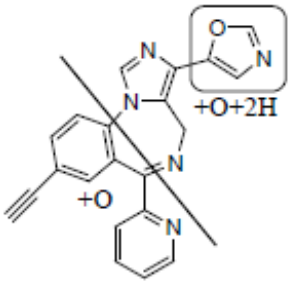

E, m/z 386

Extracted Ion Chromatograms:

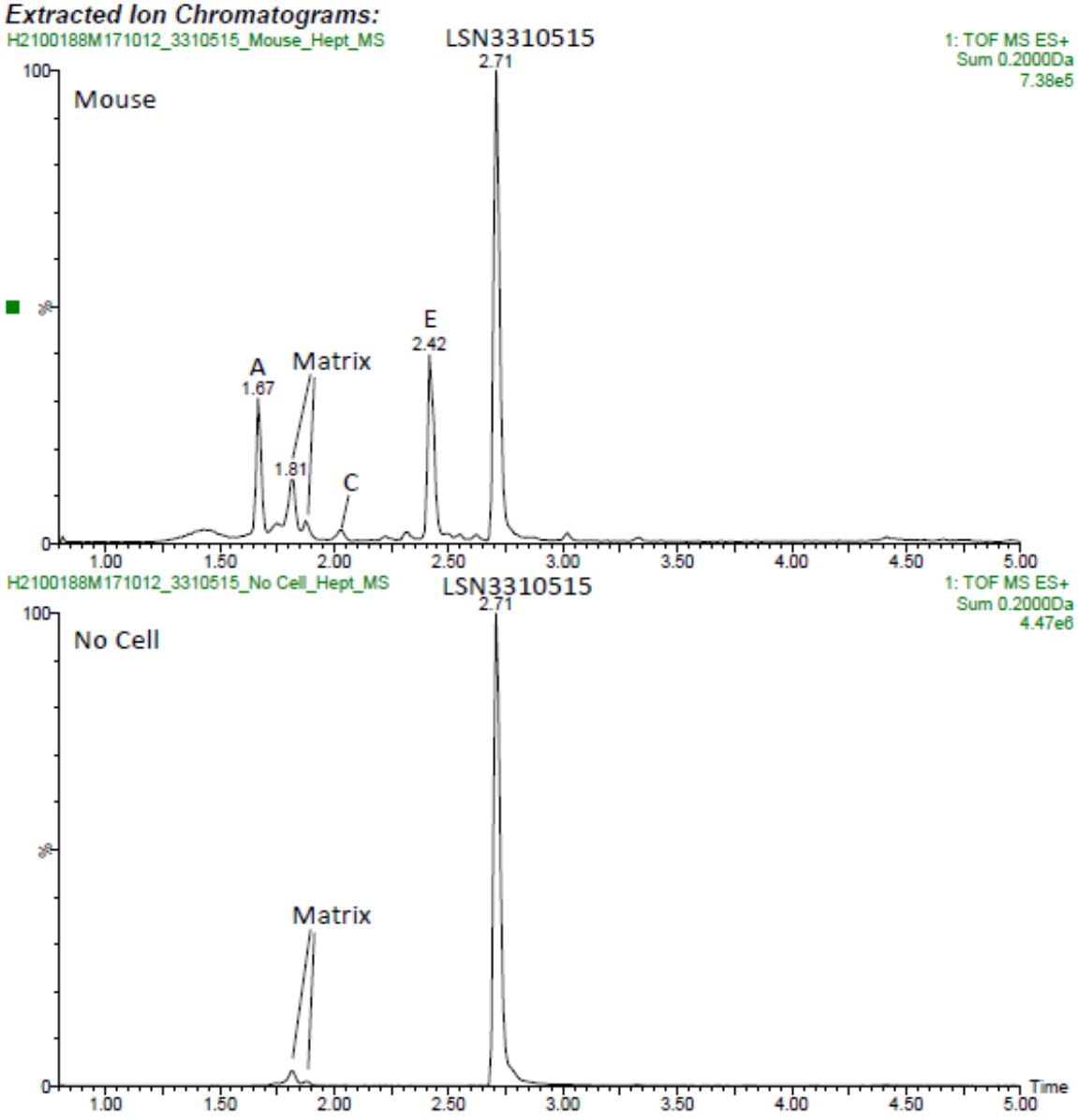

Ions monitored:

352.12+386.12+370.13+354.06+354.10+354.14+366.10+366.14+368.11+370.09+374.10+377.11+382.09+382.13+384.11+390.08+394.13+400.10+409.14+432.08+448.07+455.13+459.12+471.12+473.14+500.16+512.03+513.13+515.15+514.17+528.14+528.15+544.15+655.17+657.19+659.20+673.18+704.18+352.08+350.10+338.10+336.12+336.09+334.11+326.10+324.09+310.11+310.07+308.13+307.13+296.06

Experimental Summary

Instrumentation

UPLC System: Waters Acquity System (SN's: D12USM306G, D12BUR530M, E12CMP754G)
Mass Spectrometer: Waters Synapt G2-S (SN UEB102)
Detector: Waters PDA (SN E12UPD105A)

UPLC Conditions

Mobile Phase A: 10 mM Ammonium Bicarbonate
Mobile Phase B: Acetonitrile
Gradient: M2 (0/5, 0.4/5, 3.5/75, 4/90, 4.25/90, 4.5/5, 6/stop)
HPLC Column: Waters Acquity BEH C18, 2.1 x 100 mm, 1.7 µm particle size. Column Temp: 60°C
Flow Rate (mL/min): 0.5 Injection Volume (µL): 5 Divert: 0.8 min

Mass Spec Conditions

Ionization: Positive ESI
Capillary: 1.0 kV
Source Temperature: 120 °C
Desolvation: 500 °C
Sample cone: 50 V
MS/MS Collision Energy: 25 V

Sample Preparation

Compound: 3310515 Lot #: MH3-E14861-050

Hepatocyte incubations were prepared by adding thawed cryopreserved hepatocytes to hepatocyte maintenance media. Dilute stock solution of compound was added to media to give a final incubated concentration of 2 µM. After 4 hours of incubation at 37 °C in a humidified CO_2 incubator, the incubations were quenched with an equal volume of acetonitrile. Samples were centrifuged at 4,000 rpm for 10 minutes and the supernatant transferred to a 96-well plate. Hepatocyte samples were analyzed as received.

Hepatocyte incubation conditions and procedures are recorded in notebook IND-INVM-00004, which is stored at the Indianapolis site of Q Squared Solutions. LC-MS/UV raw data files and the Discovery Biotransformation Summary Reports are electronically stored on the Q Squared Solutions server.

Data Processing

The LC/MS full scan data was processed by Metabolynx to identify metabolites. Manual data mining was also used to search for unique biotransformations. Product ion spectra were acquired by a separate LC/MS/MS analysis to confirm the metabolites.
Species/Gender Information:
MH – CD-1 male mouse

Representative MS/MS Spectra of Parent and Metabolites

ID	MS/MS Spectra
P	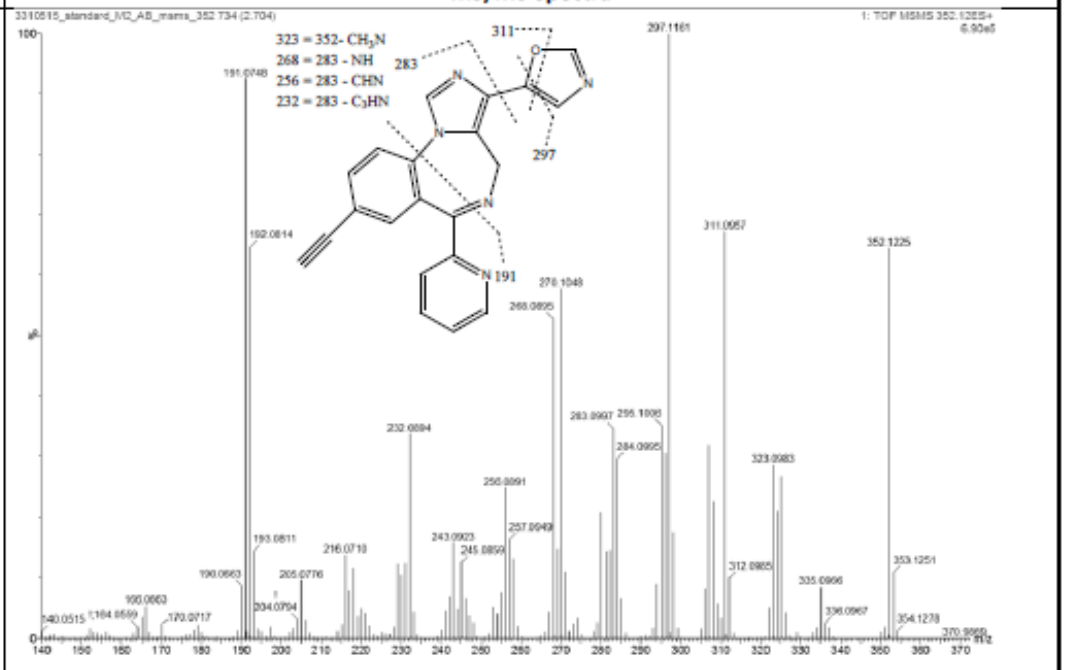
A	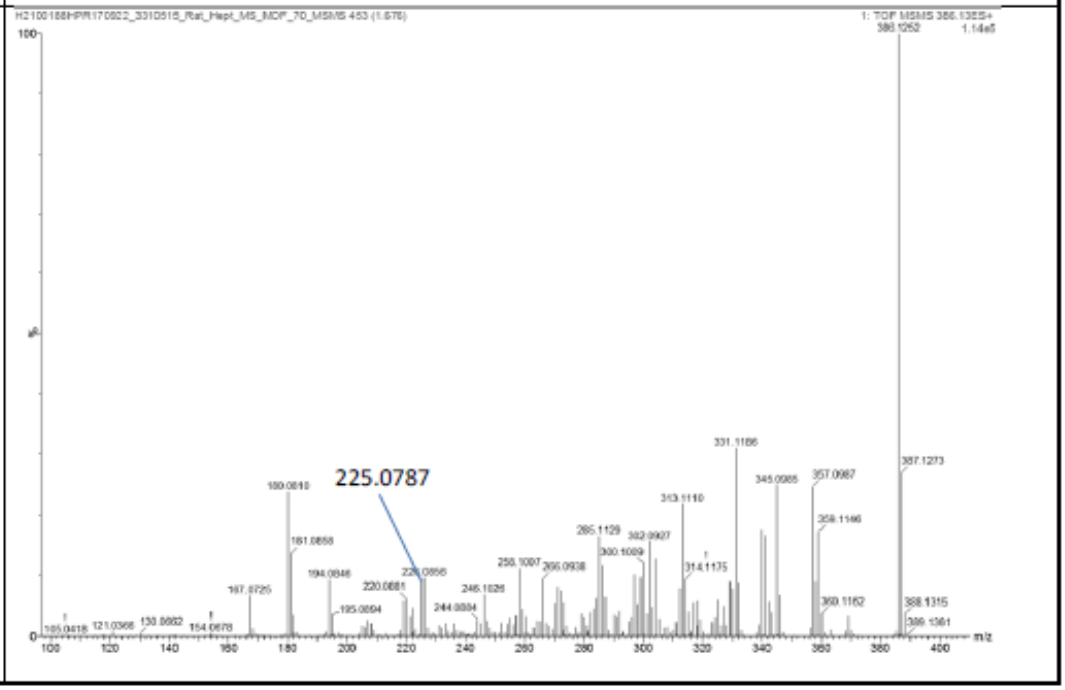

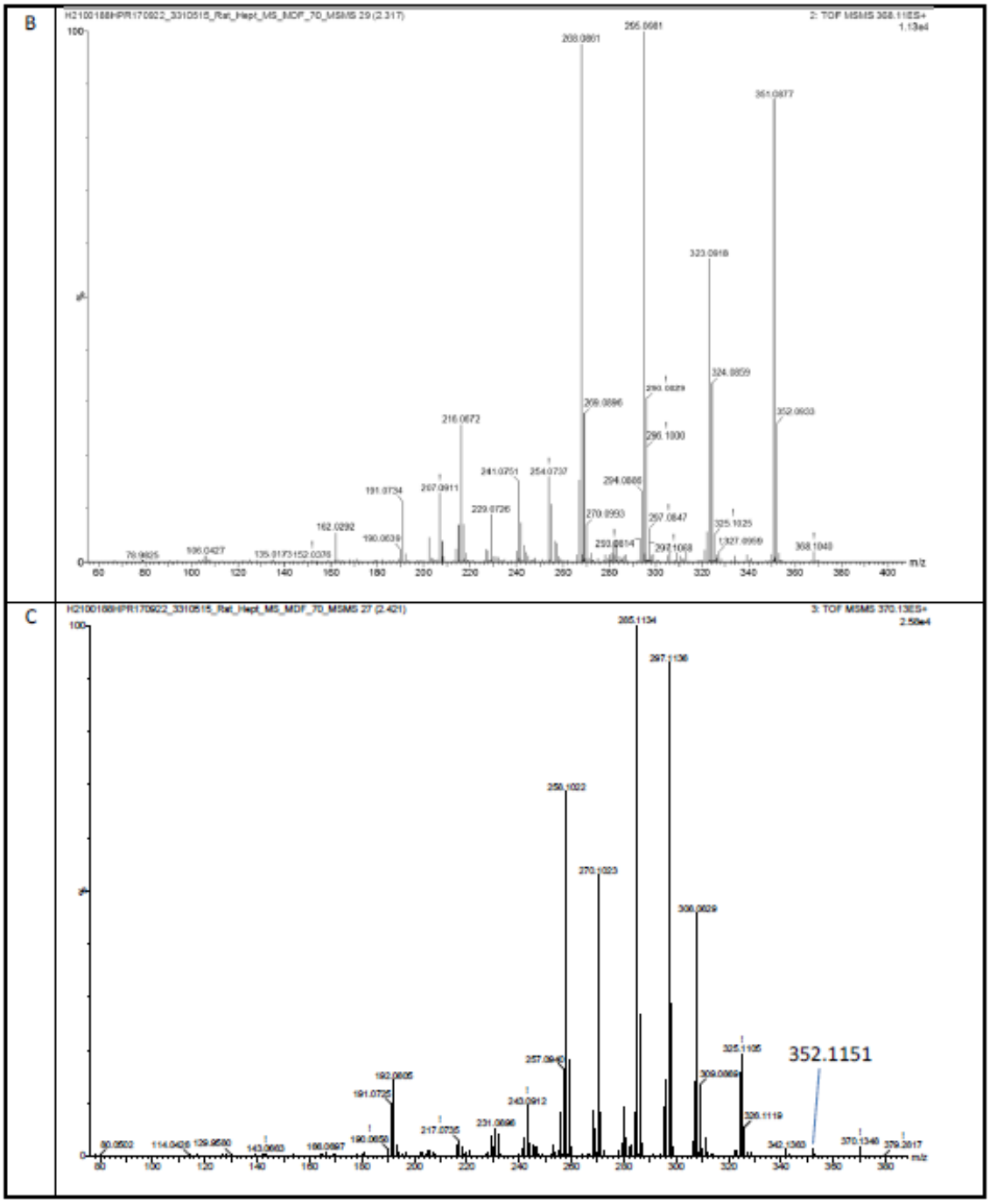
B
C
352.1151

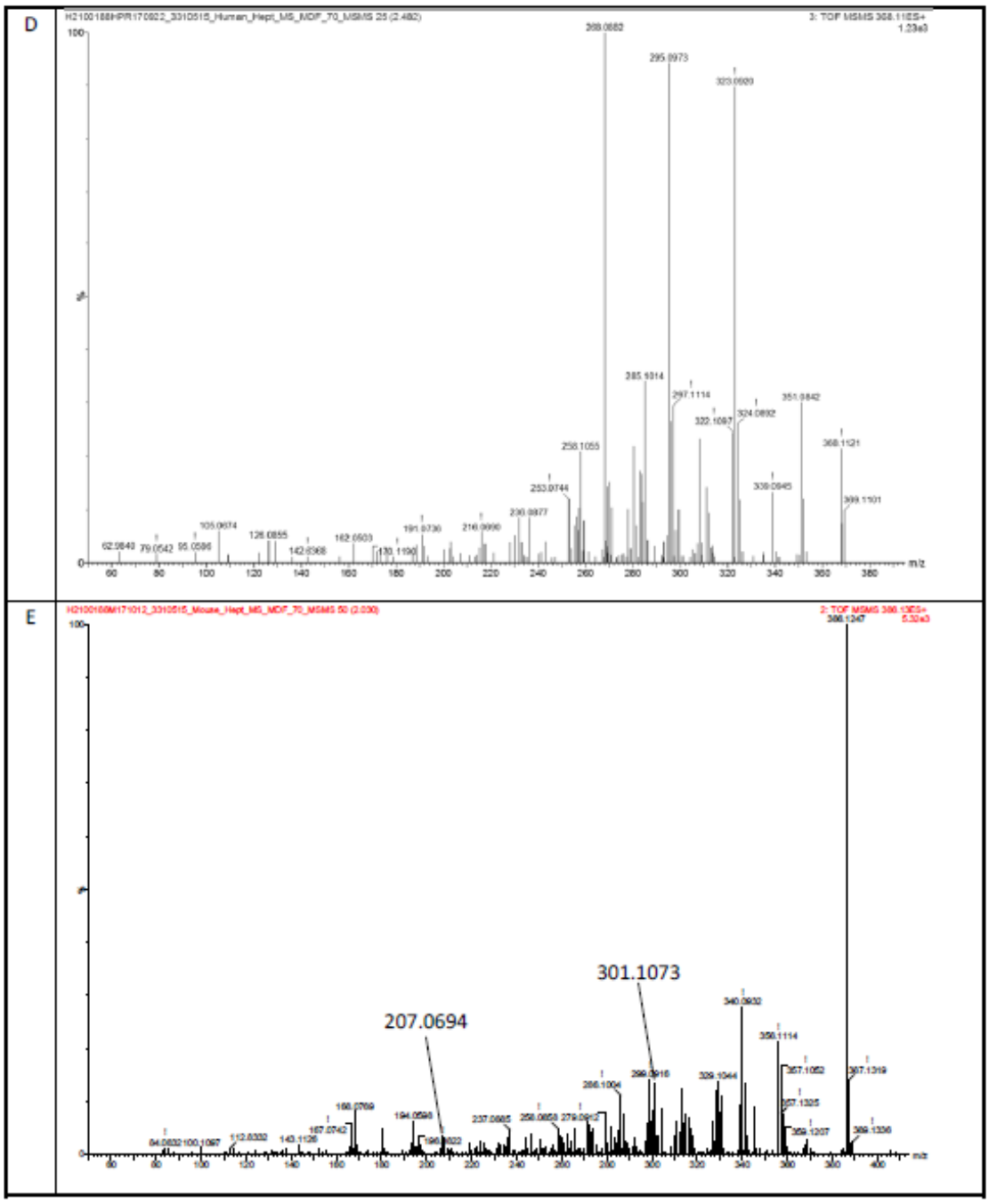

Note: The MS/MS spectra are representative only and may be from a matrix different than from this report.

PROMIS Predicted Sites of Metabolism of LSN3310515

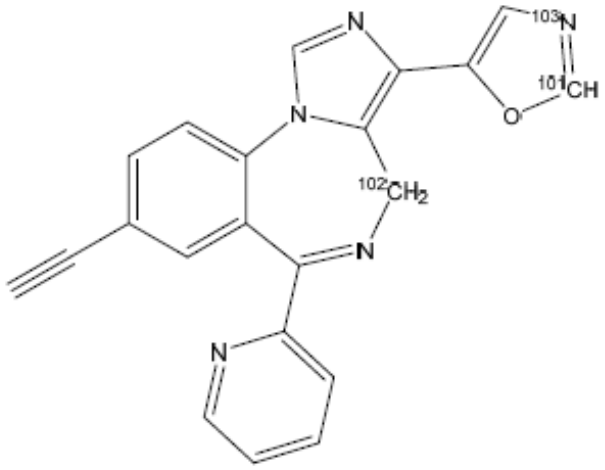

PROMIS (Version 1.0) site of metabolism (SOM) predicts the three most likely sites of metabolism on the molecule.

101= most likely site, 102= 2nd most likely site, 103= 3rd most likely site

Key considerations when comparing the SOM predicted by PROMIS with experimental results:

1. **PROMIS only predicts human CYP-mediated SOM.** Software does not predict any other metabolic pathway (e.g. amide hydrolysis, AO oxidation, glucuronidation, etc.)
2. PROMIS only predicts the sites of metabolism, not the rate of metabolism or the CYP enzyme involved.

Report 2. *In Vitro* Metabolism of Compound (KRM-II-81) LSN3310515 in Rat, Monkey and Human Hepatocytes

Q² Solutions
a Quintiles Quest Joint Venture

Discovery Metabolism

Report Title

In Vitro Metabolism of Compound LSN3310515 in Rat, Monkey and Human Hepatocytes

Study

H2100188HPR170922

Study Completion Date

October 4, 2017

Sponsor

Eli Lilly and Company

Testing Facility

Q Squared Solutions BioSciences LLC
Purdue Research Park
5225 Exploration Drive
Indianapolis, IN 46241

This report has been reviewed for completeness and accuracy.

Responsible investigator:

Xiaochun (Sean) Zhu, Ph.D. Date: October 3, 2017

Title: Director

Q^2 Solutions – Discovery Metabolism

Tel: 317-548-5180

Email: Xiaochun.Zhu@q2labsolutions.com

Reviewed by:

Richard Burton, Ph.D. Date: October 4, 2017

Title: Research Investigator

Q^2 Solutions – Discovery Metabolism

Tel: 317-548-5120

Email: Richard.Burton@q2labsolutions.com

Discovery Biotransformation Summary

Tentatively Identified Metabolites of LSN3310515 in Rat, Monkey and Human Hepatocytes
(2 μM incubation for 4 hours)

Metabolite Table:

Peak ID	Tentative Metabolite Identification	*m/z*	RT (min)	Species/Matrix
3310515	Parent (P)	352	2.70	RH, PH, HH
A	P + 2O + 2H	386	1.68	RH, PH, HH
B	P + O	368	2.31	RH
C	P + O + 2H	370	2.42	RH, PH, HH
D	P + O	368	2.50	RH, PH, HH

RH = rat hepatocytes, PH = monkey hepatocytes, HH = human hepatocytes

Comments: All following summary is based on the MS intensity. Extent of metabolism for LSN3310515: Low – HH; Moderate – RH, PH. LSN3310515 was the major component observed in all three species.

Additional metabolites were observed but considered minor (as judged by ion intensity) and therefore not reported in this study report.

Proposed Metabolite Structures of LSN3310515

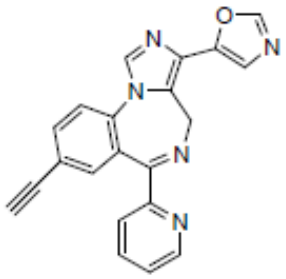

LSN3310515, Parent, m/z 352

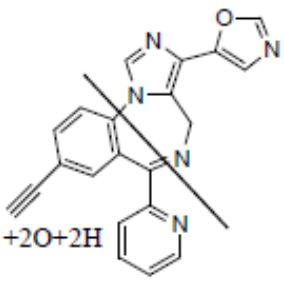

A, m/z 386

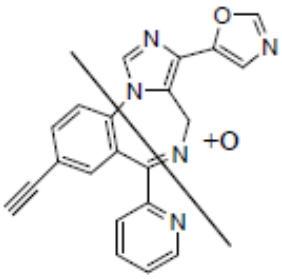

B, D, m/z 368

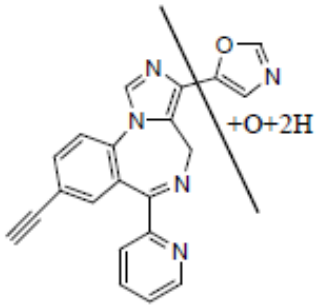

C, m/z 370

Extracted Ion Chromatograms:

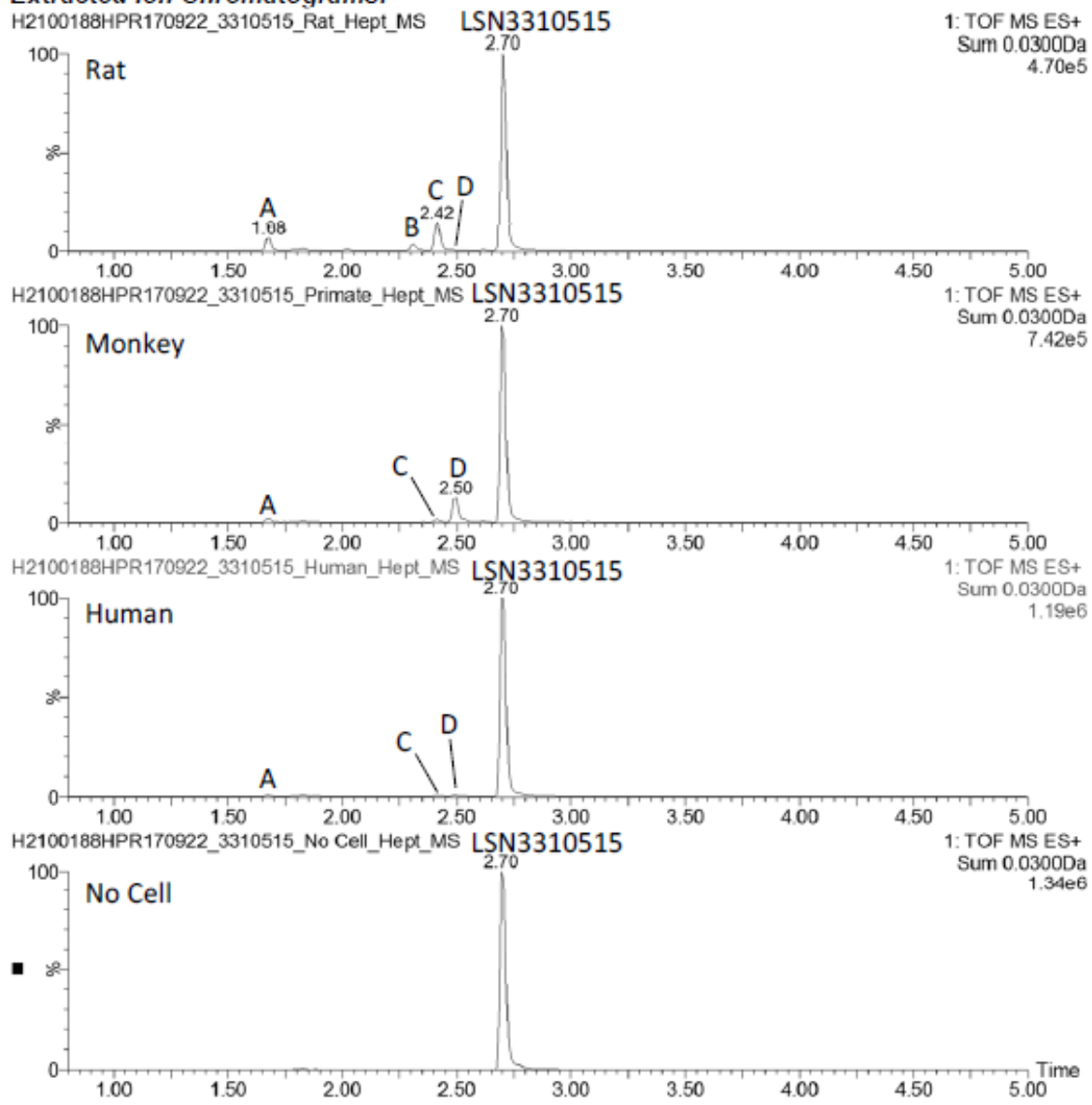

Ions monitored:

352.12+386.12+368.11+370.13+354.06+354.10+354.14+366.10+366.14+370.09+374.10+377.11+382.09+382.13+384.11+390.08+394.13+400.10+409.14+432.08+448.07+455.13+459.12+471.12+473.14+500.16+512.03+513.13+515.15+514.17+528.14+528.15+544.15+655.17+657.19+659.20+673.18+704.18+352.08+350.10+338.10+336.12+336.09+334.11+326.10+324.09+310.11+310.07+308.13+307.13+296.06

Experimental Summary

Instrumentation

UPLC System: Waters Acquity System (SN's: D12USM306G, D12BUR530M, E12CMP754G)
Mass Spectrometer: Waters Synapt G2-S (SN UEB102)
Detector: Waters PDA (SN E12UPD105A)

UPLC Conditions

Mobile Phase A: 10 mM Ammonium Bicarbonate
Mobile Phase B: Acetonitrile
Gradient: M2 (0/5, 0.4/5, 3.5/75, 4/90, 4.25/90, 4.5/5,6/stop)
HPLC Column: Waters Acquity BEH C18, 2.1 x 100 mm, 1.7 µm particle size. Column Temp: 60°C
Flow Rate (mL/min): 0.5 Injection Volume (µL): 5 Divert: 0.8 min

Mass Spec Conditions

Ionization: Positive ESI
Capillary: 1.0 kV
Source Temperature: 120 °C
Desolvation: 500 °C
Sample cone: 50 V
MS/MS Collision Energy: 25 V

Sample Preparation

Compound: 3310515 Lot #: MH3-E14861-050

Hepatocyte incubations were prepared by adding thawed cryopreserved hepatocytes to hepatocyte maintenance media. Dilute stock solution of compound was added to media to give a final incubated concentration of 2 µM. After 4 hours of incubation at 37 °C in a humidified CO_2 incubator, the incubations were quenched with an equal volume of acetonitrile. Samples were centrifuged at 4,000 rpm for 10 minutes and the supernatant transferred to a 96-well plate. Hepatocyte samples were analyzed as received.

Hepatocyte incubation conditions and procedures are recorded in notebook IND-INVM-00004, which is stored at the Indianapolis site of Q Squared Solutions. LC-MS/UV raw data files and the Discovery Biotransformation Summary Reports are electronically stored on the Q Squared Solutions server.

Data Processing

The LC/MS full scan data was processed by Metabolynx to identify metabolites. Manual data mining was also used to search for unique biotransformations. Product ion spectra were acquired by a separate LC/MS/MS analysis to confirm the metabolites.
Species/Gender Information:
RH – Sprague-Dawley male rat, PH – Cynomolgus male monkey, HH – mixed gender human

Representative MS/MS Spectra of Parent and Metabolites

ID	MS/MS Spectra
P	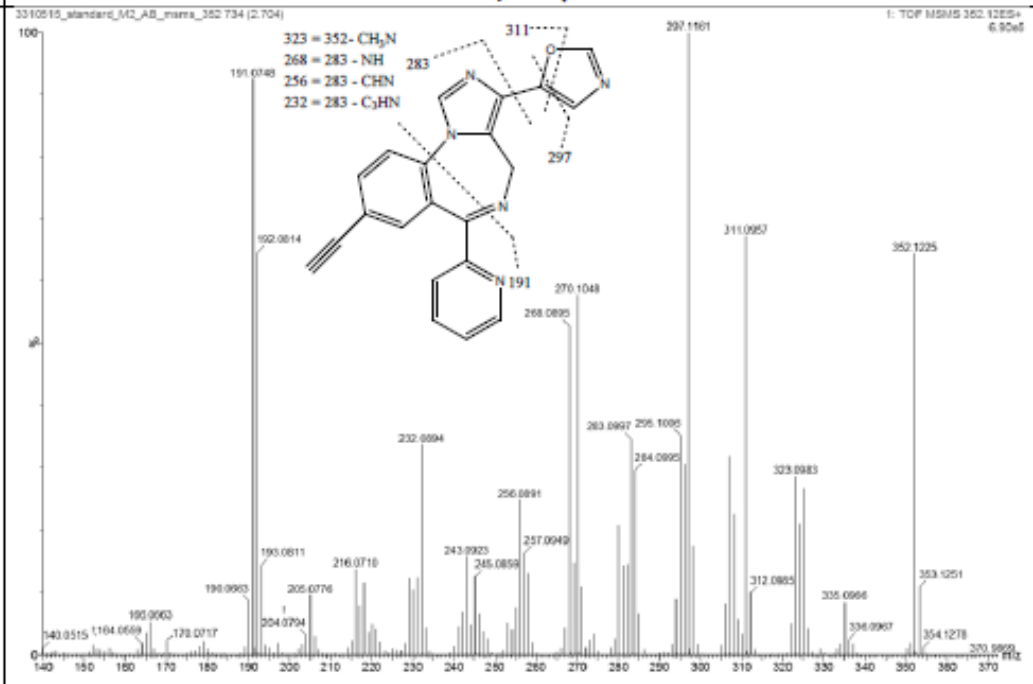
A	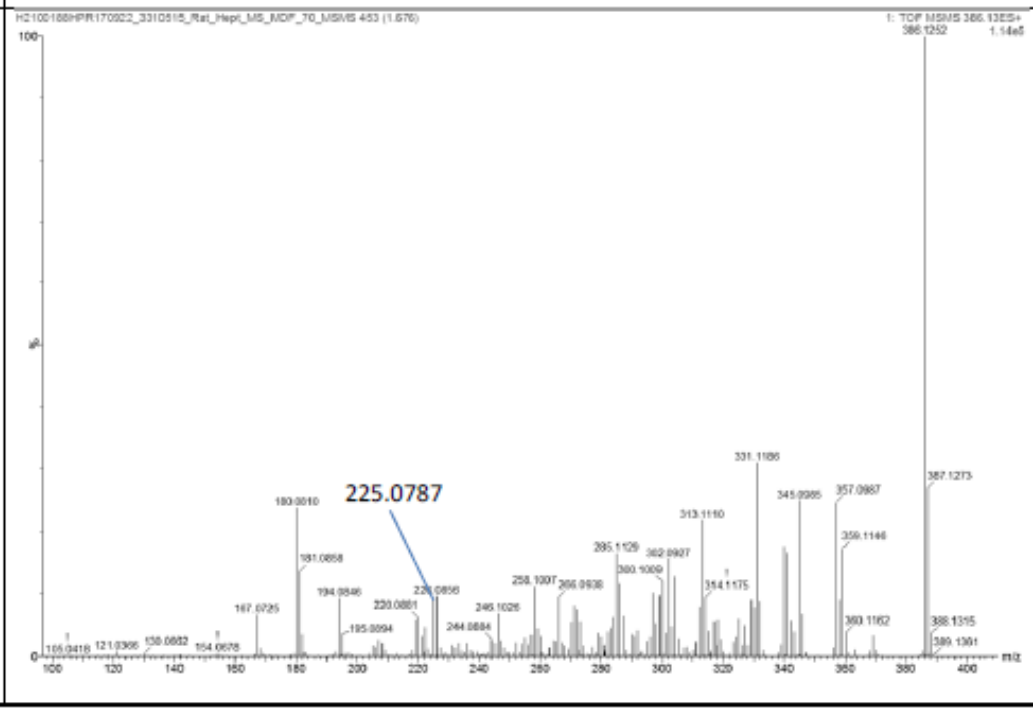

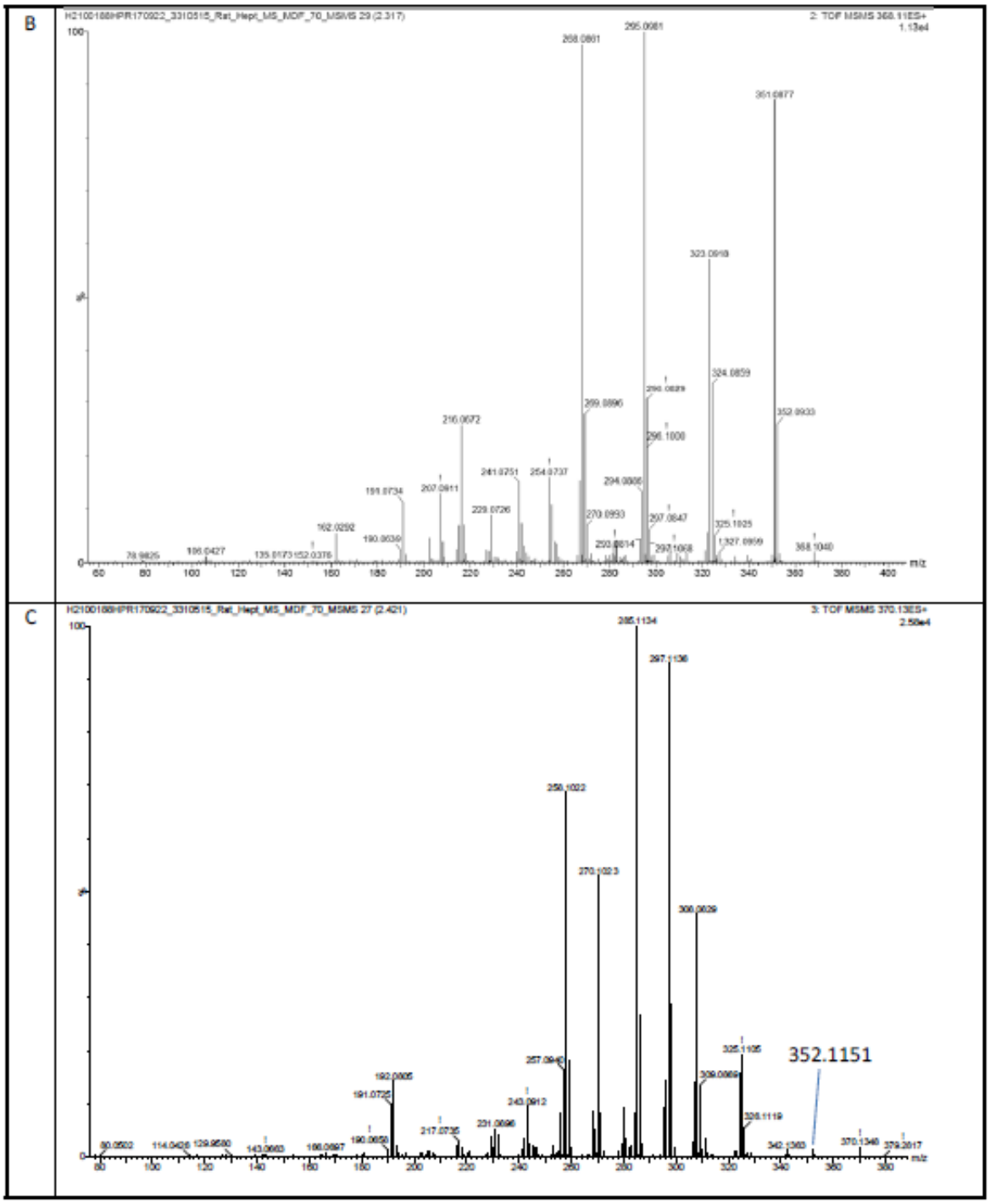
B
C
352.1151

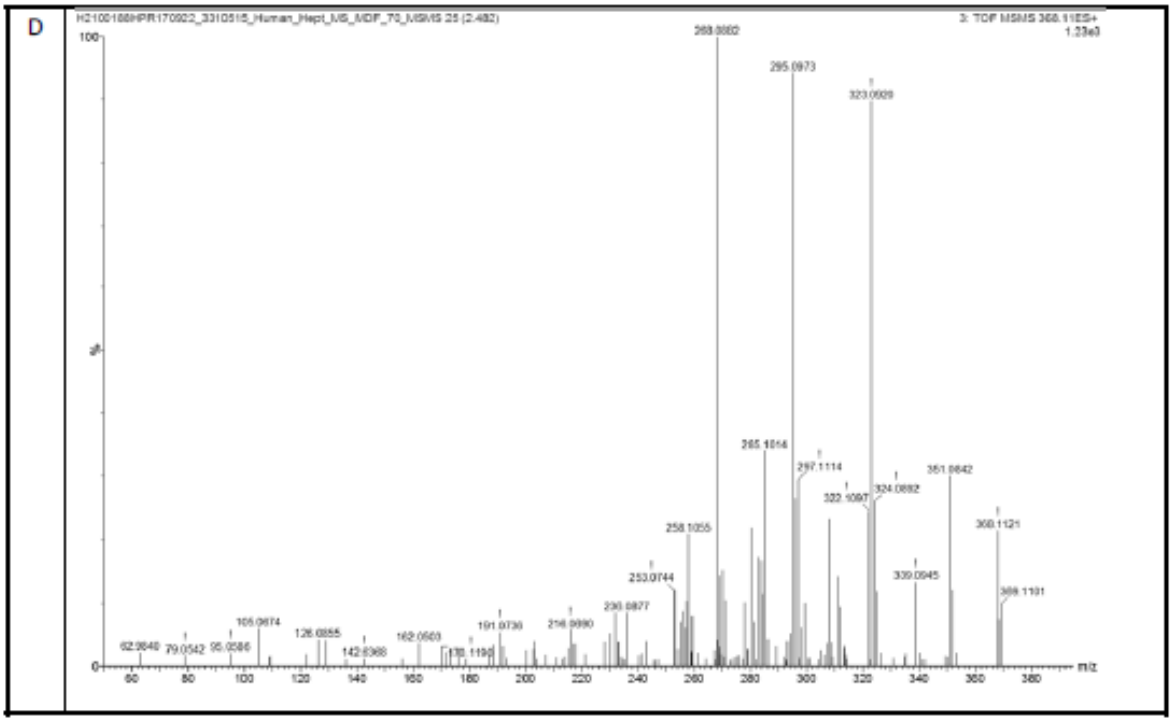

Note: The MS/MS spectra are representative only and may be from a matrix different than from this report.

PROMIS Predicted Sites of Metabolism of LSN3310515

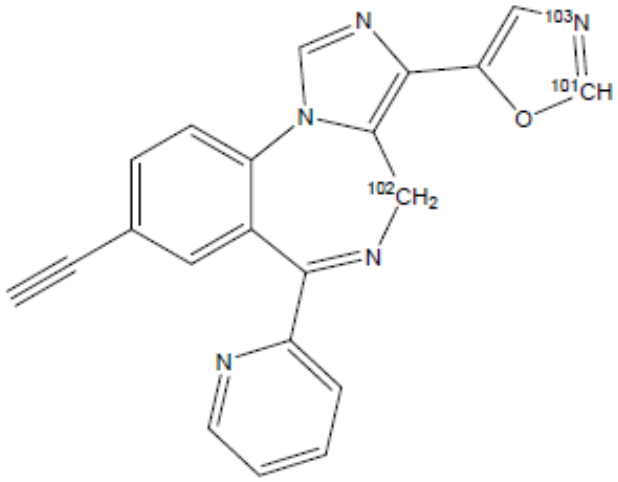

PROMIS (Version 1.0) site of metabolism (SOM) predicts the three most likely sites of metabolism on the molecule.

101= most likely site, 102= 2nd most likely site, 103= 3rd most likely site

Key considerations when comparing the SOM predicted by PROMIS with experimental results:

1. **PROMIS only predicts human CYP-mediated SOM.** Software does not predict any other metabolic pathway (e.g. amide hydrolysis, AO oxidation, glucuronidation, etc.)
2. PROMIS only predicts the sites of metabolism, not the rate of metabolism or the CYP enzyme involved.

Report 3. *In Vitro* Metabolism of Compound (MP-III-080) LSN3310516 in Mouse Hepatocytes

Q² Solutions
a Quintiles Quest Joint Venture

Discovery Metabolism

Report Title

In Vitro Metabolism of Compound LSN3310516 in Mouse Hepatocytes

Study

H2100188M171012

Study Completion Date

October 20, 2017

Sponsor

Eli Lilly and Company

Testing Facility

Q Squared Solutions BioSciences LLC
Purdue Research Park
5225 Exploration Drive
Indianapolis, IN 46241

This report has been reviewed for completeness and accuracy.

Responsible investigator:

Xiaochun (Sean) Zhu, Ph.D. Date: October 20, 2017

Title: Director

Q² Solutions – Discovery Metabolism

Tel: 317-548-5180

Email: Xiaochun.Zhu@q2labsolutions.com

Reviewed by:

Richard Burton, Ph.D. Date: October 20, 2017

Title: Research Investigator

Q² Solutions – Development Metabolism

Tel: 317-548-5120

Email: Richard.Burton@q2labsolutions.com

Discovery Biotransformation Summary

Tentatively Identified Metabolites of LSN3310516 in Mouse Hepatocytes
(2 µM incubation for 4 hours)

Metabolite Table:

Peak ID	Tentative Metabolite Identification	*m/z*	RT (min)	Species/Matrix
3310516	Parent (P)	381	3.25	MH
A	P + 2O + 2H	415	2.04	MH
B	P + 2O + 2H	415	2.57	MH
C	P + O	397	2.70	MH

MH = mouse hepatocytes

Comments: All following summary is based on the MS intensity. Extent of metabolism for LSN3310516: Extensive – MH. LSN3310516 and A (P + 2O + 2H) were the major components observed in MH.

Additional metabolites were observed but considered minor (as judged by ion intensity) and therefore not reported in this study report.

Proposed Metabolite Structures of LSN3310516

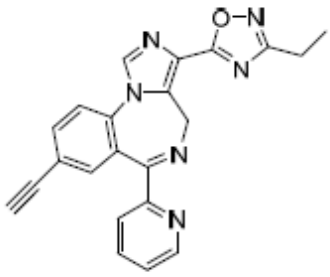

LSN3310516, Parent, m/z 381

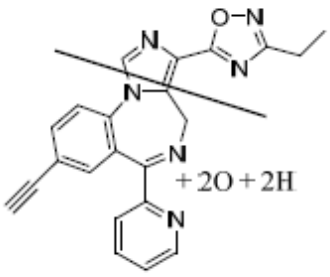

A, m/z 415

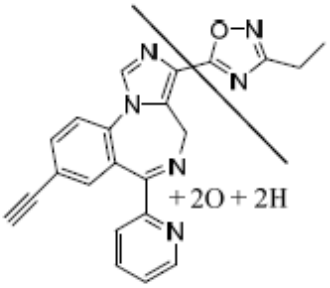

B, m/z 415

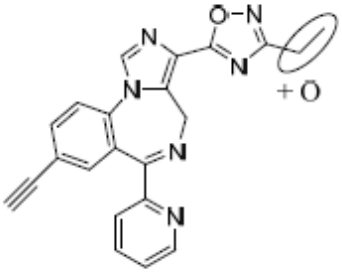

C, m/z 397

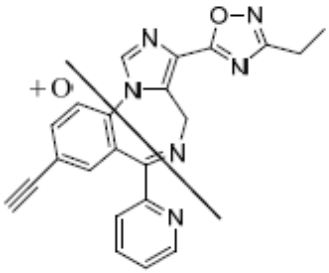

D, m/z 397

Extracted Ion Chromatograms:

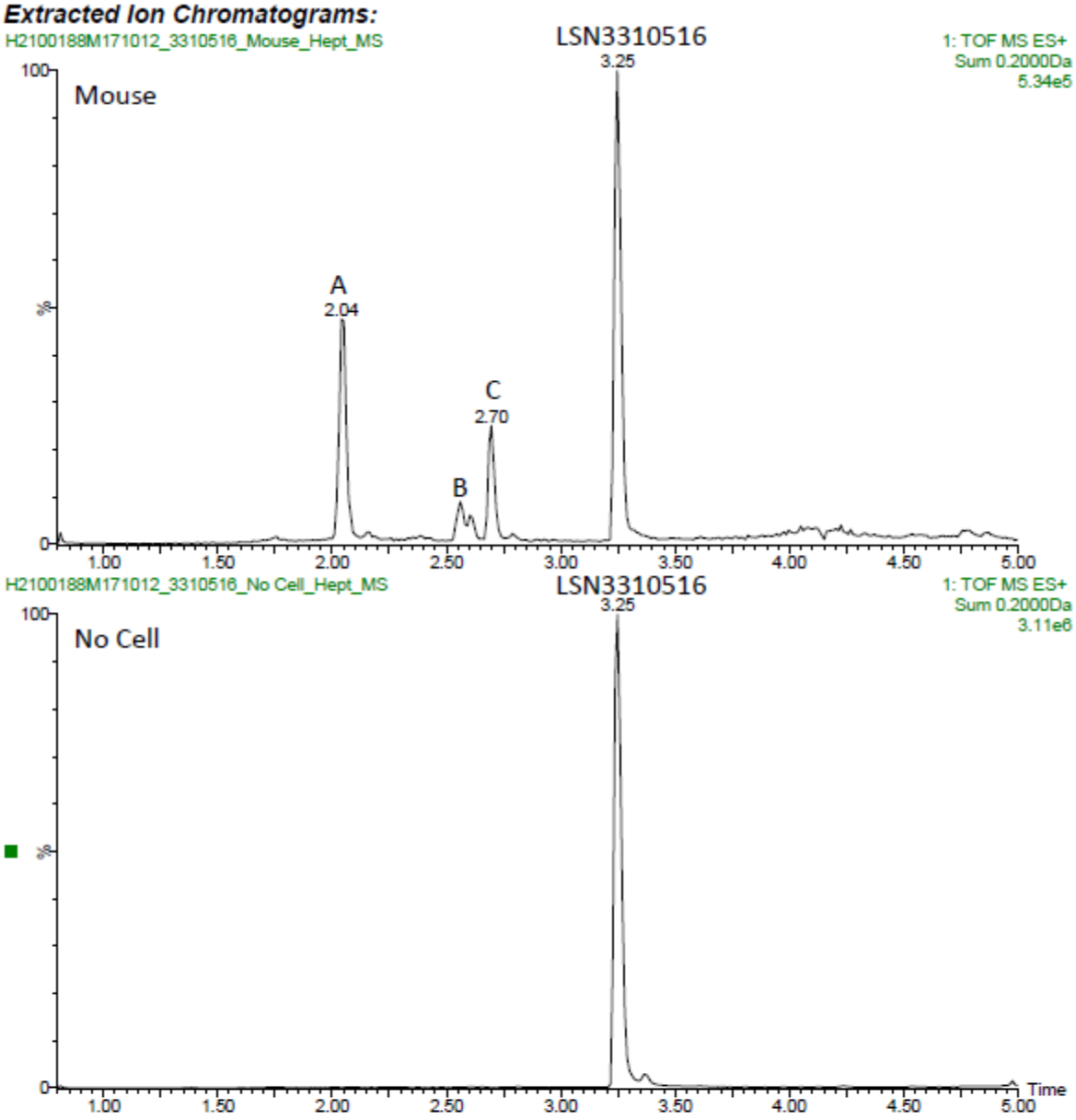

Ions monitored:

381.15+415.15+397.14+383.09+383.13+383.16+395.13+395.16+399.12+399.16+403.13+406.14+411.12+411.16+413.14+419.10+423.16+429.13+438.17+461.10+477.10+484.16+488.15+500.15+502.17+529.18+541.06+542.16+544.18+543.20+557.17+557.18+573.17+684.20+686.21+688.23+702.21+733.21+381.11+379.13+367.13+365.15+365.11+363.14+355.13+353.11+339.14+339.10+337.16+336.16+325.08

Experimental Summary

Instrumentation

UPLC System: Waters Acquity System (SN's: D12USM306G, D12BUR530M, E12CMP754G)
Mass Spectrometer: Waters Synapt G2-S (SN UEB102)
Detector: Waters PDA (SN E12UPD105A)

UPLC Conditions

Mobile Phase A: 10 mM Ammonium Bicarbonate
Mobile Phase B: Acetonitrile
Gradient: M2 (0/5, 0.4/5, 3.5/75, 4/90, 4.25/90, 4.5/5,6/stop)
HPLC Column: Waters Acquity BEH C18, 2.1 x 100 mm, 1.7 µm particle size. Column Temp: 60°C
Flow Rate (mL/min): 0.5 Injection Volume (µL): 5 Divert: 0.8 min

Mass Spec Conditions

Ionization: Positive ESI
Capillary: 1.0 kV
Source Temperature: 120 °C
Desolvation: 500 °C
Sample cone: 50 V
MS/MS Collision Energy: 25 V

Sample Preparation

Compound: 3310516 Lot #: MH3-E13095-023-B

Hepatocyte incubations were prepared by adding thawed cryopreserved hepatocytes to hepatocyte maintenance media. Dilute stock solution of compound was added to media to give a final incubated concentration of 2 µM. After 4 hours of incubation at 37 °C in a humidified CO_2 incubator, the incubations were quenched with an equal volume of acetonitrile. Samples were centrifuged at 4,000 rpm for 10 minutes and the supernatant transferred to a 96-well plate. Hepatocyte samples were analyzed as received.

Hepatocyte incubation conditions and procedures are recorded in notebook IND-INVM-00004, which is stored at the Indianapolis site of Q Squared Solutions. LC-MS/UV raw data files and the Discovery Biotransformation Summary Reports are electronically stored on the Q Squared Solutions server.

Data Processing

The LC/MS full scan data was processed by Metabolynx to identify metabolites. Manual data mining was also used to search for unique biotransformations. Product ion spectra were acquired by a separate LC/MS/MS analysis to confirm the metabolites.
Species/Gender Information:
MH – CD-1 male mouse

Representative MS/MS Spectra of Parent and Metabolites

ID	MS/MS Spectra
P	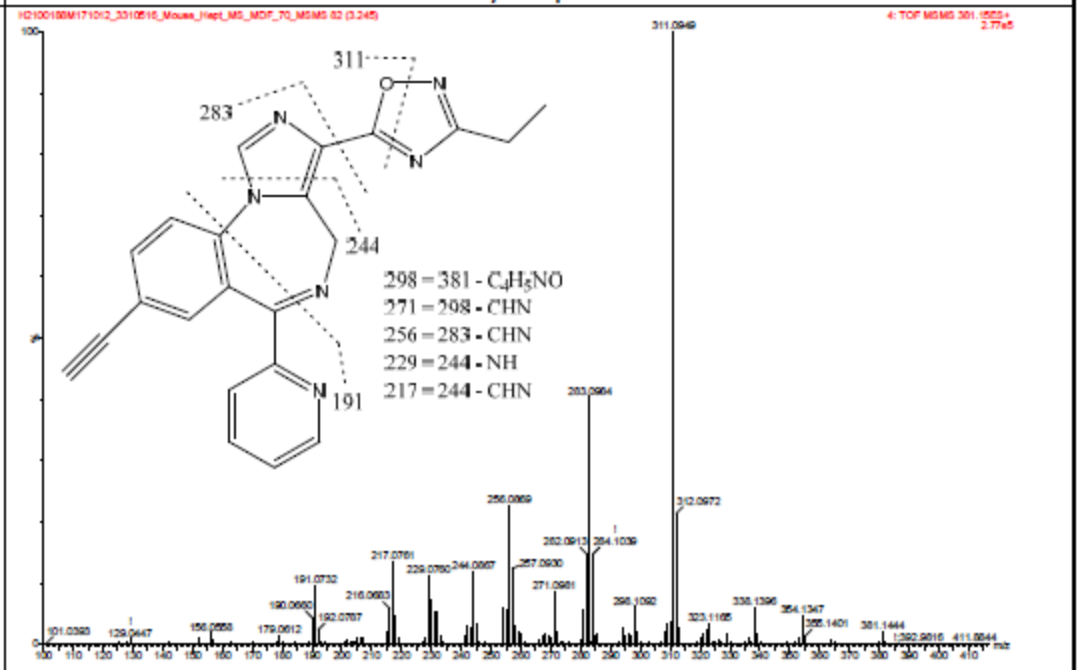
A	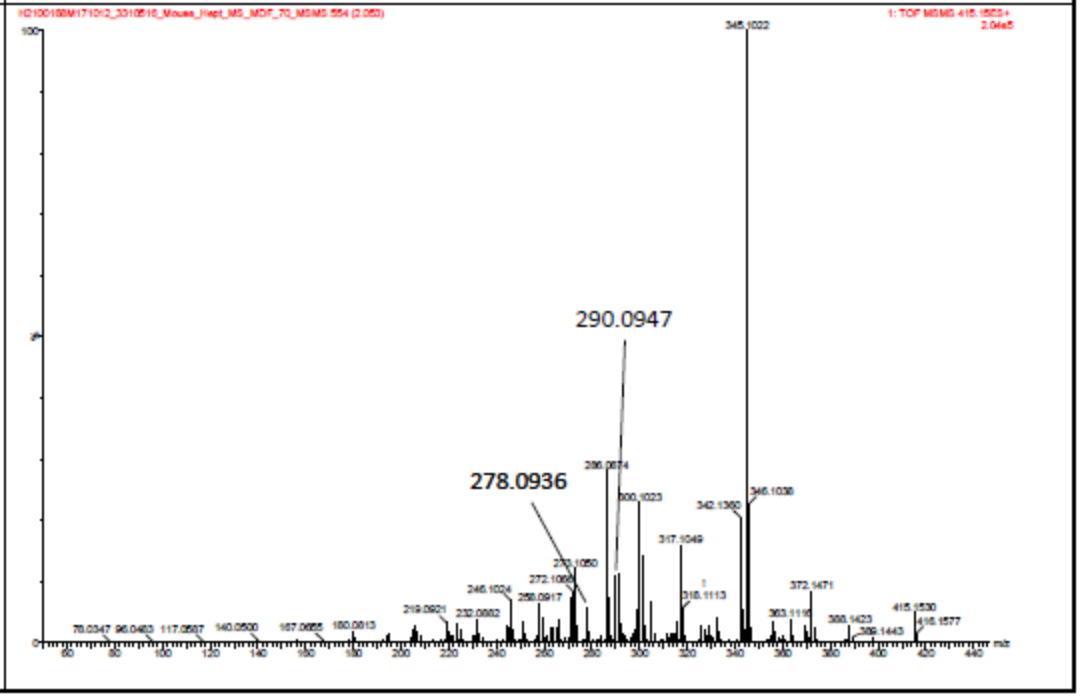

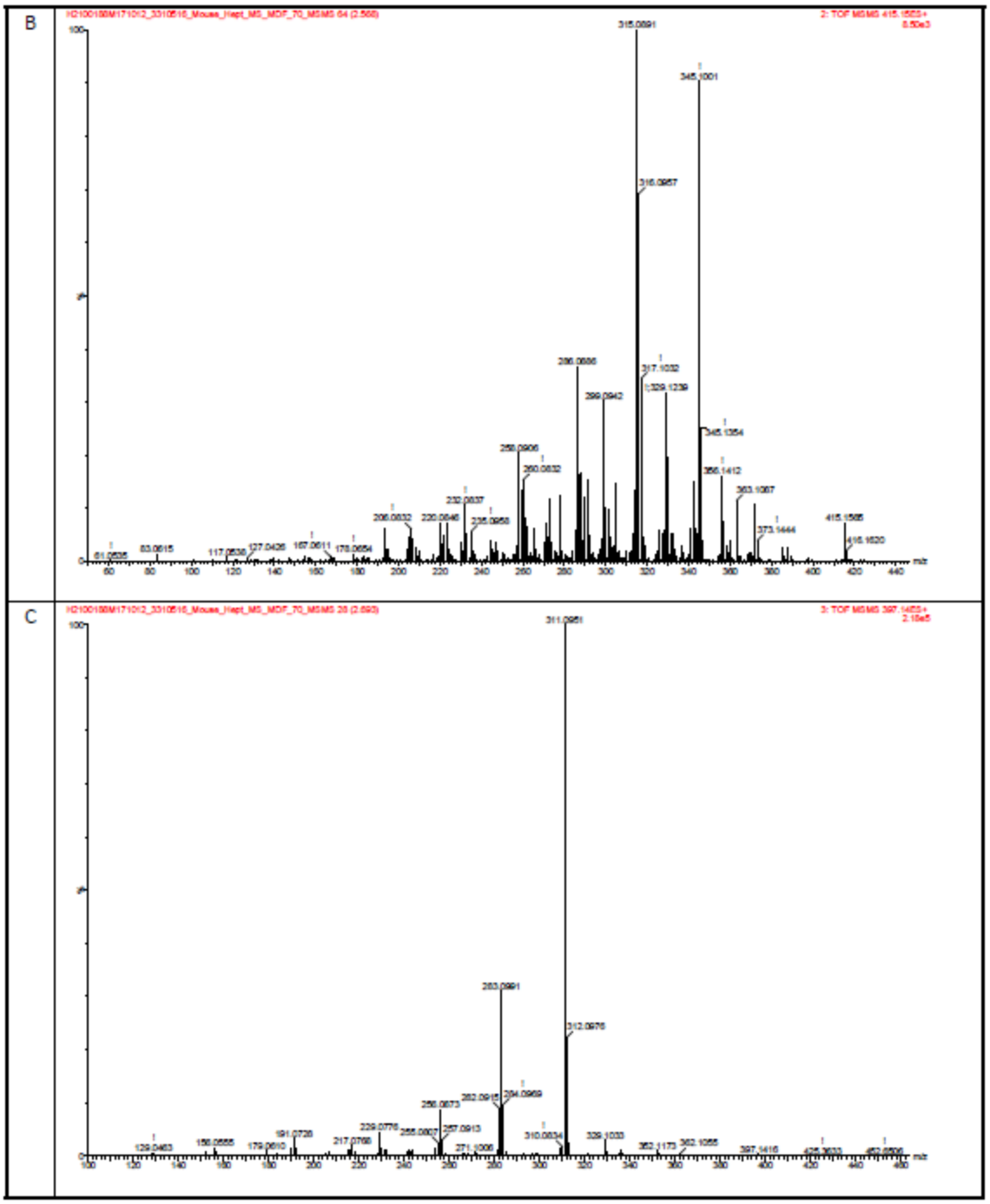
B
C

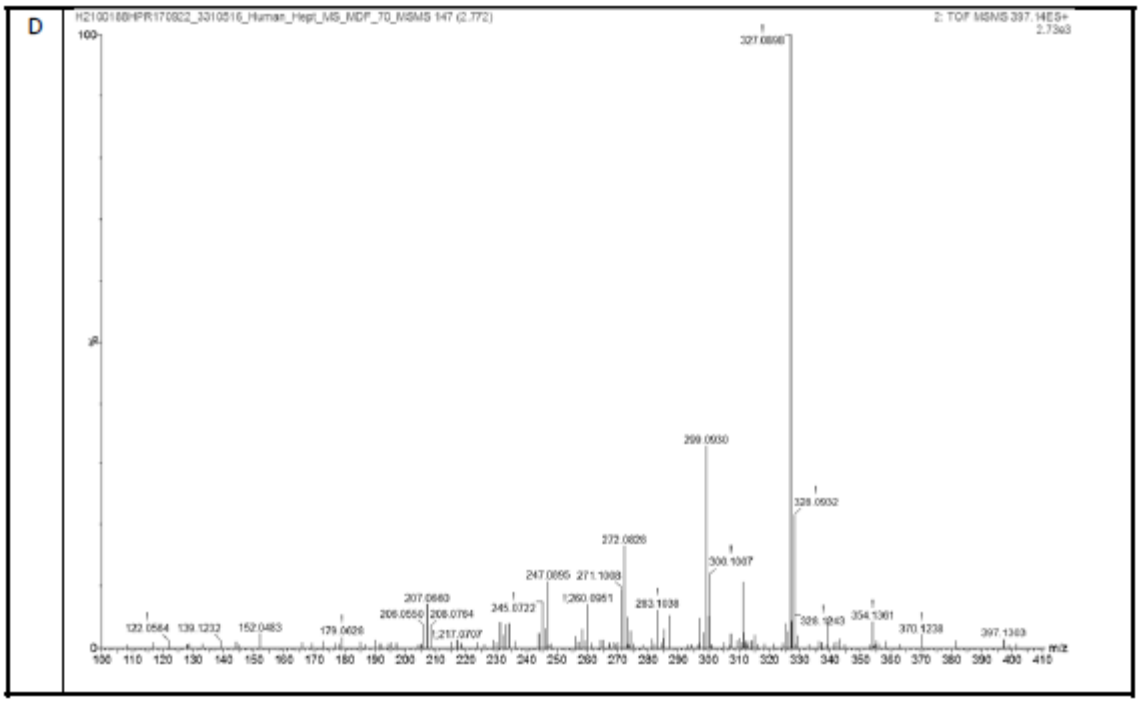

Note: The MS/MS spectra are representative only and may be from a matrix different than from this report.

PROMIS Predicted Sites of Metabolism of LSN3310516

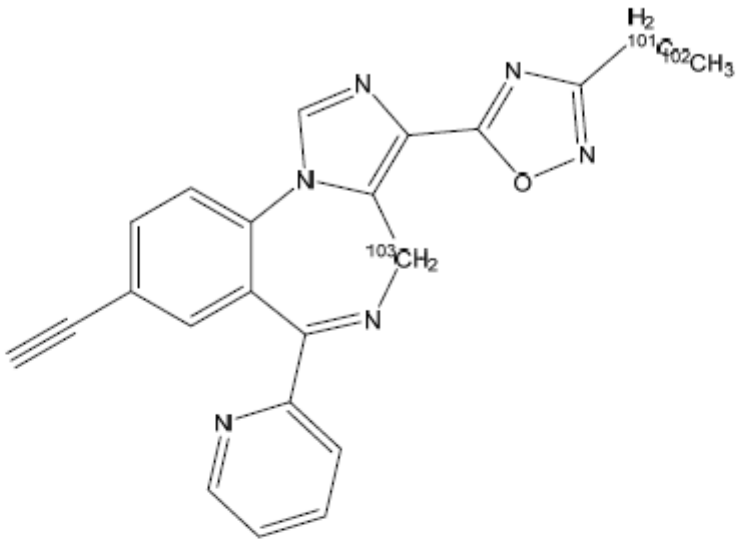

PROMIS (Version 1.0) site of metabolism (SOM) predicts the three most likely sites of metabolism on the molecule.

101= most likely site, 102= 2nd most likely site, 103= 3rd most likely site

Key considerations when comparing the SOM predicted by PROMIS with experimental results:

1. **PROMIS only predicts human CYP-mediated SOM.** Software does not predict any other metabolic pathway (e.g. amide hydrolysis, AO oxidation, glucuronidation, etc.)
2. PROMIS only predicts the sites of metabolism, not the rate of metabolism or the CYP enzyme involved.

Report 4. *In Vitro* Metabolism of Compound (MP-III-080) LSN3310516 in Rat, Monkey and Human Hepatocytes

Q² Solutions
a Quintiles Quest Joint Venture

Discovery Metabolism

Report Title

In Vitro Metabolism of Compound LSN3310516 in Rat, Monkey and Human Hepatocytes

Study

H2100188HPR170922

Study Completion Date

October 4, 2017

Sponsor

Eli Lilly and Company

Testing Facility

Q Squared Solutions BioSciences LLC
Purdue Research Park
5225 Exploration Drive
Indianapolis, IN 46241

This report has been reviewed for completeness and accuracy.

Responsible investigator:

Xiaochun (Sean) Zhu, Ph.D. Date: October 3, 2017

Title: Director

Q² Solutions – Discovery Metabolism

Tel: 317-548-5180

Email: Xiaochun.Zhu@q2labsolutions.com

Reviewed by:

Richard Burton, Ph.D. Date: October 4, 2017

Title: Research Investigator

Q² Solutions – Discovery Metabolism

Tel: 317-548-5120

Email: Richard.Burton@q2labsolutions.com

Discovery Biotransformation Summary

Tentatively Identified Metabolites of LSN3310516 in Rat, Monkey and Human Hepatocytes
(2 μM incubation for 4 hours)

Metabolite Table:

Peak ID	Tentative Metabolite Identification	*m/z*	RT (min)	Species/Matrix
3310516	Parent (P)	381	3.24	RH, PH, HH
A	P + 2O + 2H	415	2.05	RH, PH, HH
B	P + 2O + 2H	415	2.56	RH, PH, HH
C	P + O	397	2.69	RH, PH, HH
D	P + O	397	2.80	RH, PH, HH

RH = rat hepatocytes, PH = monkey hepatocytes, HH = human hepatocytes

Comments: All following summary is based on the MS intensity. Extent of metabolism for LSN3310516: Low – HH; Moderate – PH; Extensive – RH. LSN3310516 and metabolite C (P + O) were the major components observed in RH. LSN3310516 was the major component observed in both PH and HH.

Additional metabolites were observed but considered minor (as judged by ion intensity) and therefore not reported in this study report.

Proposed Metabolite Structures of LSN3310516

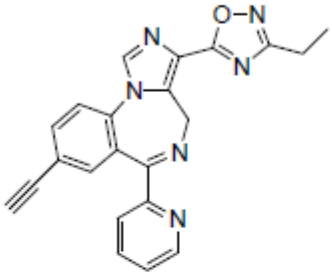

LSN3310516, Parent, m/z 381

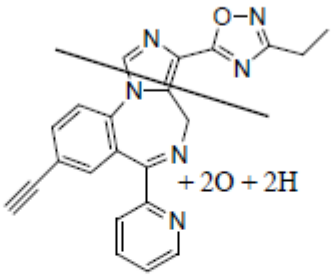

A, m/z 415

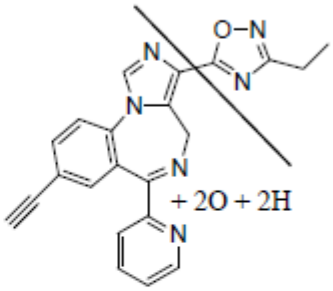

B, m/z 415

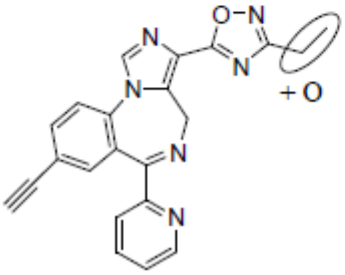

C, m/z 397

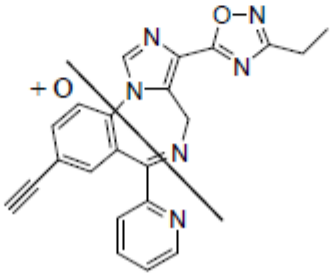

D, m/z 397

Extracted Ion Chromatograms:

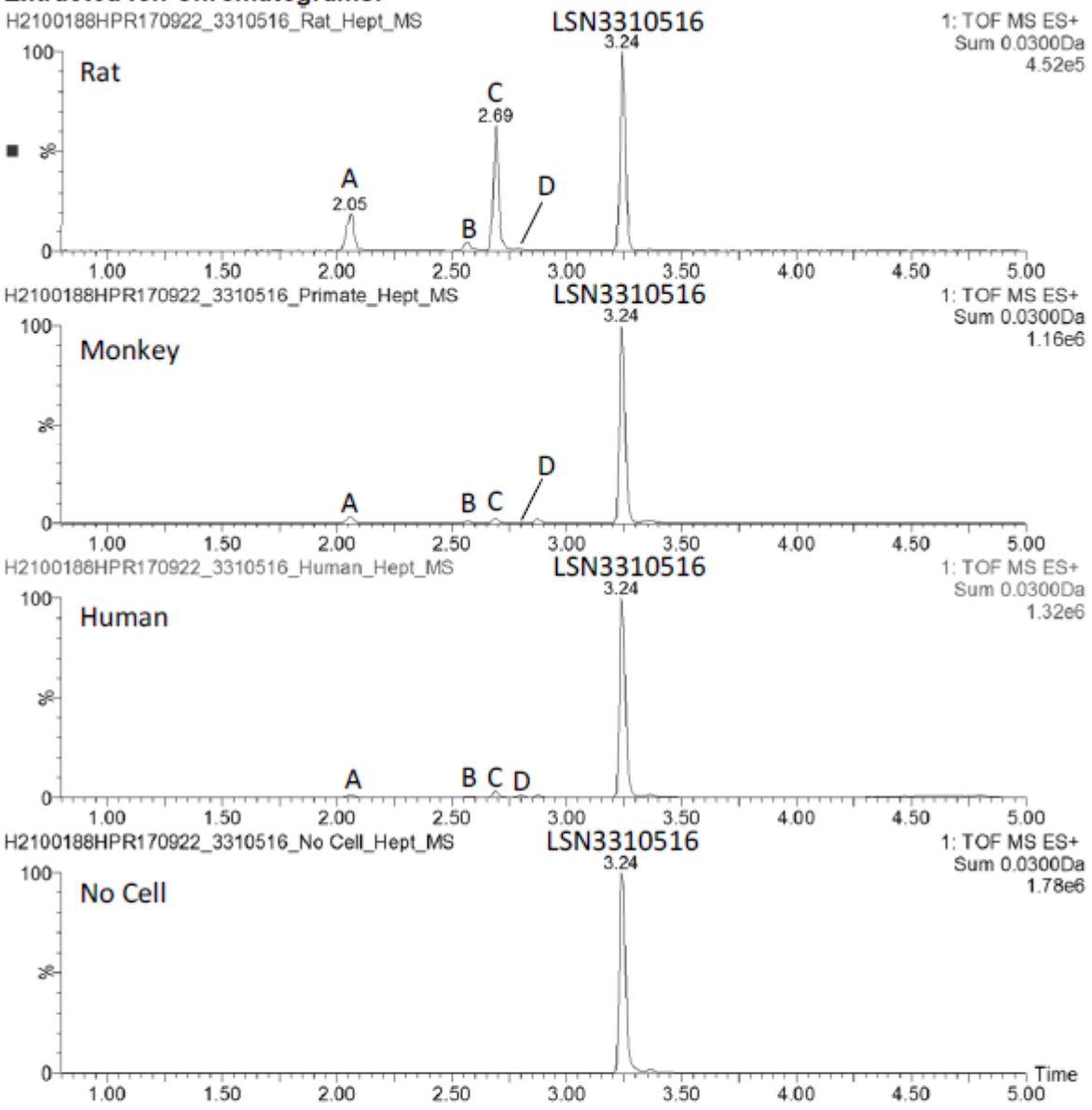

Ions monitored:

381.15+415.15+397.14+383.09+383.13+383.16+395.13+395.16+399.12+399.16+403.13+406.14+411.12+411.16+413.14+419.10+423.16+429.13+438.17+461.10+477.10+484.16+488.15+500.15+502.17+529.18+541.06+542.16+544.18+543.20+557.17+557.18+573.17+684.20+686.21+688.23+702.21+733.21+381.11+379.13+367.13+365.15+365.11+363.14+355.13+353.11+339.14+339.10+337.16+336.16+325.08

Experimental Summary

Instrumentation

UPLC System: Waters Acquity System (SN's: D12USM306G, D12BUR530M, E12CMP754G)
Mass Spectrometer: Waters Synapt G2-S (SN UEB102)
Detector: Waters PDA (SN E12UPD105A)

UPLC Conditions

Mobile Phase A: 10 mM Ammonium Bicarbonate
Mobile Phase B: Acetonitrile
Gradient: M2 (0/5, 0.4/5, 3.5/75, 4/90, 4.25/90, 4.5/5,6/stop)
HPLC Column: Waters Acquity BEH C18, 2.1 x 100 mm, 1.7 µm particle size. Column Temp: 60°C
Flow Rate (mL/min): 0.5 Injection Volume (µL): 5 Divert: 0.8 min

Mass Spec Conditions

Ionization: Positive ESI
Capillary: 1.0 kV
Source Temperature: 120 °C
Desolvation: 500 °C
Sample cone: 50 V
MS/MS Collision Energy: 25 V

Sample Preparation

Compound: 3310516 Lot #: MH3-E13095-023-B

Hepatocyte incubations were prepared by adding thawed cryopreserved hepatocytes to hepatocyte maintenance media. Dilute stock solution of compound was added to media to give a final incubated concentration of 2 µM. After 4 hours of incubation at 37 °C in a humidified CO_2 incubator, the incubations were quenched with an equal volume of acetonitrile. Samples were centrifuged at 4,000 rpm for 10 minutes and the supernatant transferred to a 96-well plate. Hepatocyte samples were analyzed as received.

Hepatocyte incubation conditions and procedures are recorded in notebook IND-INVM-00004, which is stored at the Indianapolis site of Q Squared Solutions. LC-MS/UV raw data files and the Discovery Biotransformation Summary Reports are electronically stored on the Q Squared Solutions server.

Data Processing

The LC/MS full scan data was processed by Metabolynx to identify metabolites. Manual data mining was also used to search for unique biotransformations. Product ion spectra were acquired by a separate LC/MS/MS analysis to confirm the metabolites.
Species/Gender Information:
RH – Sprague-Dawley male rat, PH – Cynomolgus male monkey, HH – mixed gender human

Representative MS/MS Spectra of Parent and Metabolites

ID	MS/MS Spectra
P	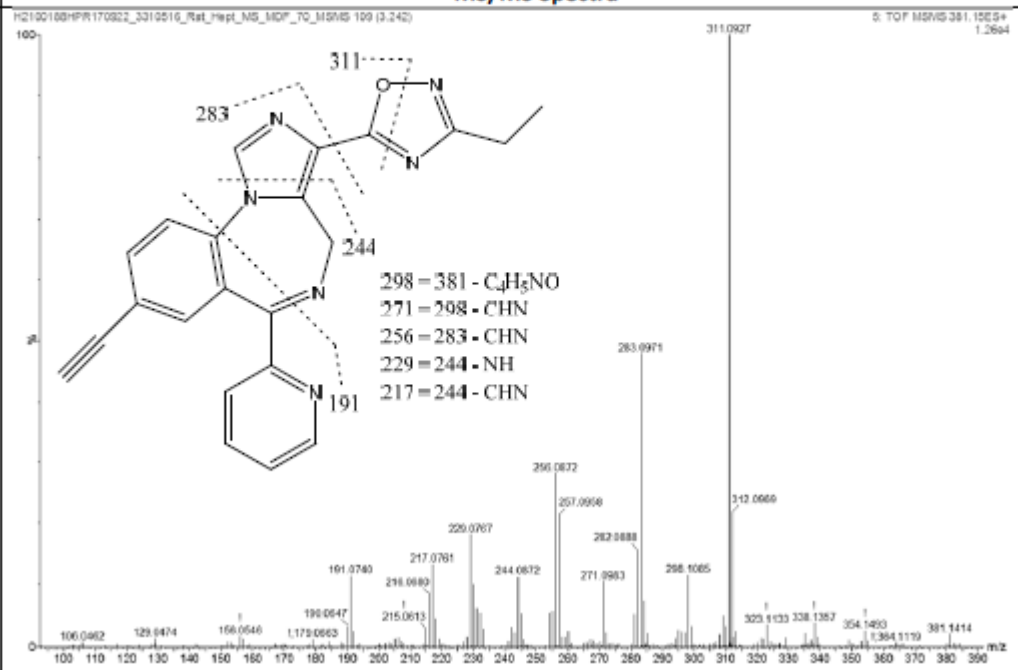
A	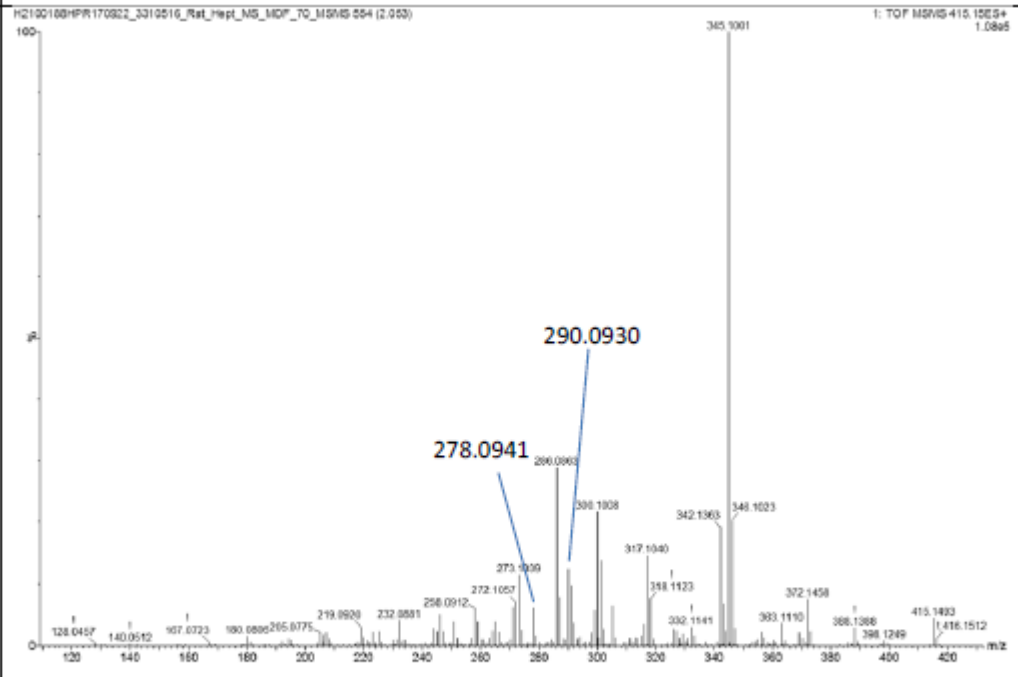

B

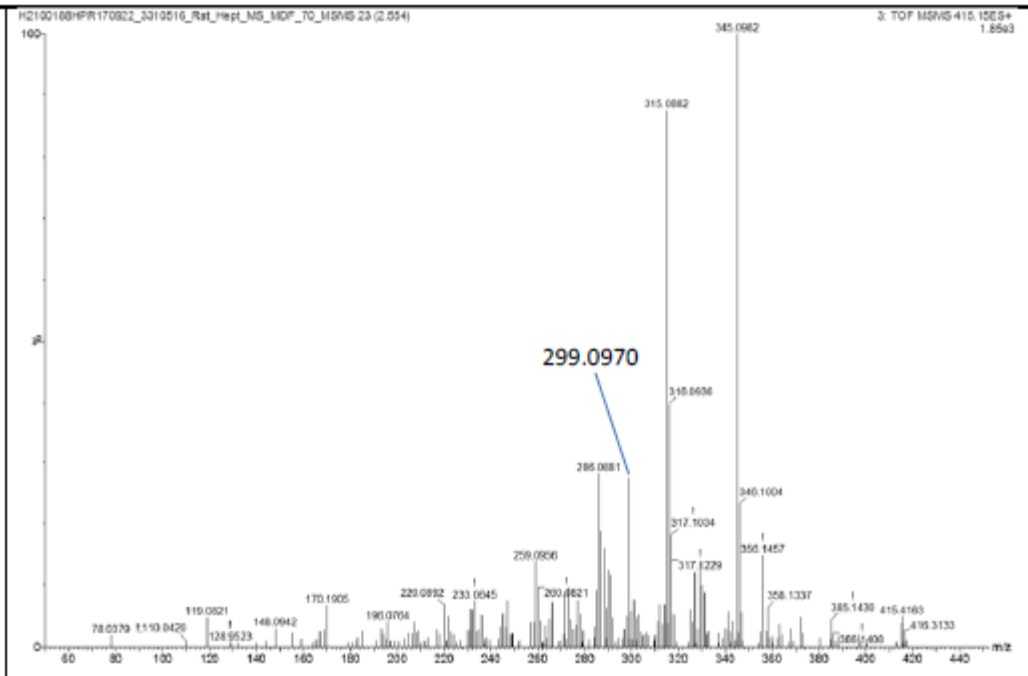

C

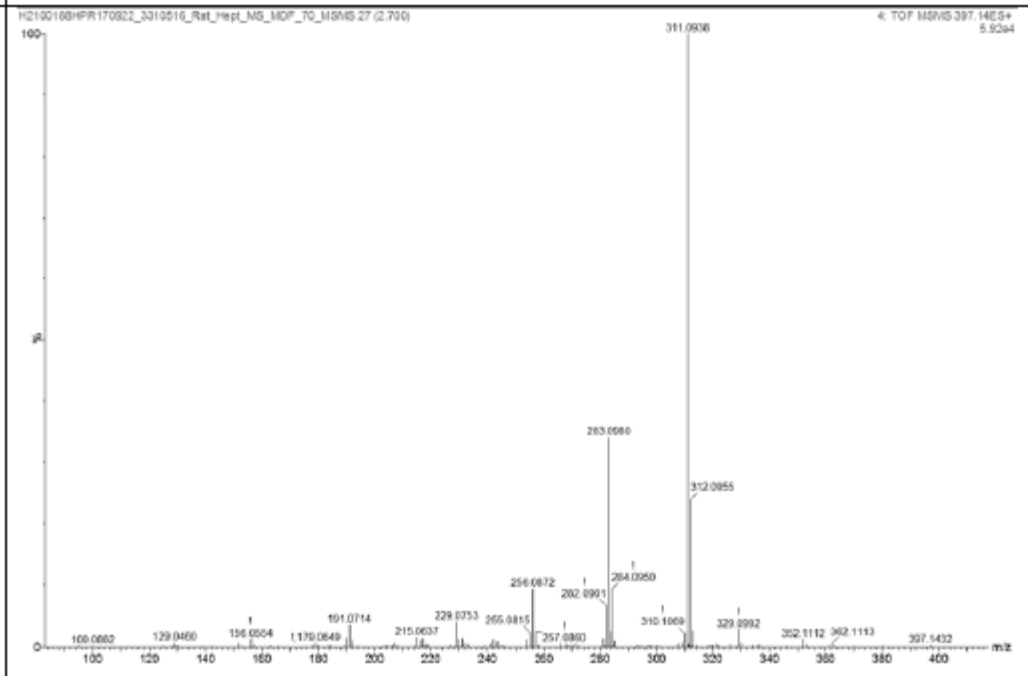

D

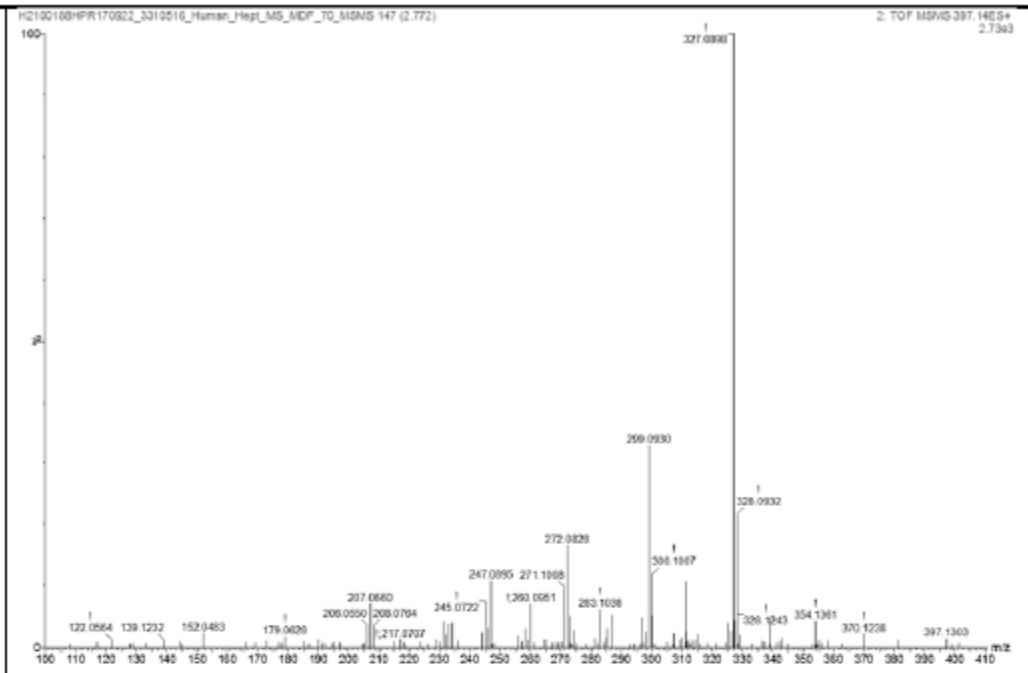

Note: The MS/MS spectra are representative only and may be from a matrix different than from this report.

PROMIS Predicted Sites of Metabolism of LSN3310516

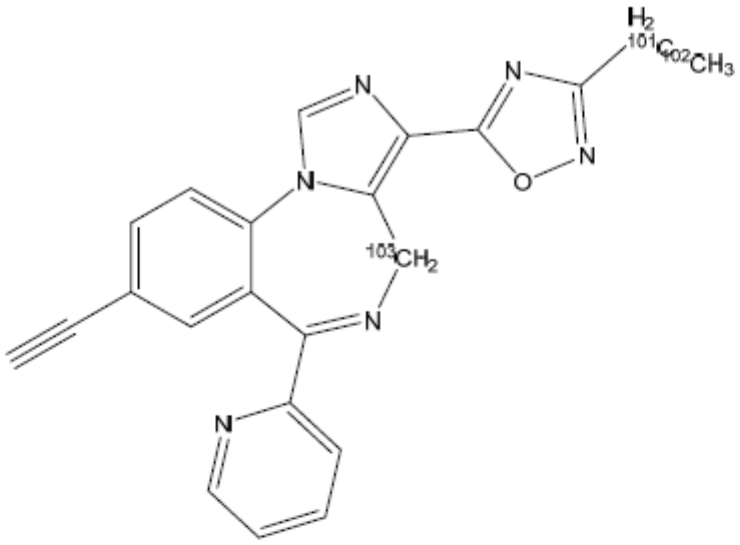

PROMIS (Version 1.0) site of metabolism (SOM) predicts the three most likely sites of metabolism on the molecule.

101= most likely site, 102= 2nd most likely site, 103= 3rd most likely site

Key considerations when comparing the SOM predicted by PROMIS with experimental results:

1. **PROMIS only predicts human CYP-mediated SOM.** Software does not predict any other metabolic pathway (e.g. amide hydrolysis, AO oxidation, glucuronidation, etc.)
2. PROMIS only predicts the sites of metabolism, not the rate of metabolism or the CYP enzyme involved.

Appendix VII: Kinetic and Stability Studies of GL-II-93 in Acidic and Basic Condition.

1. 2D NMR experiment (DCl addition)

1.1. DCl addition at pH = 2, at all range

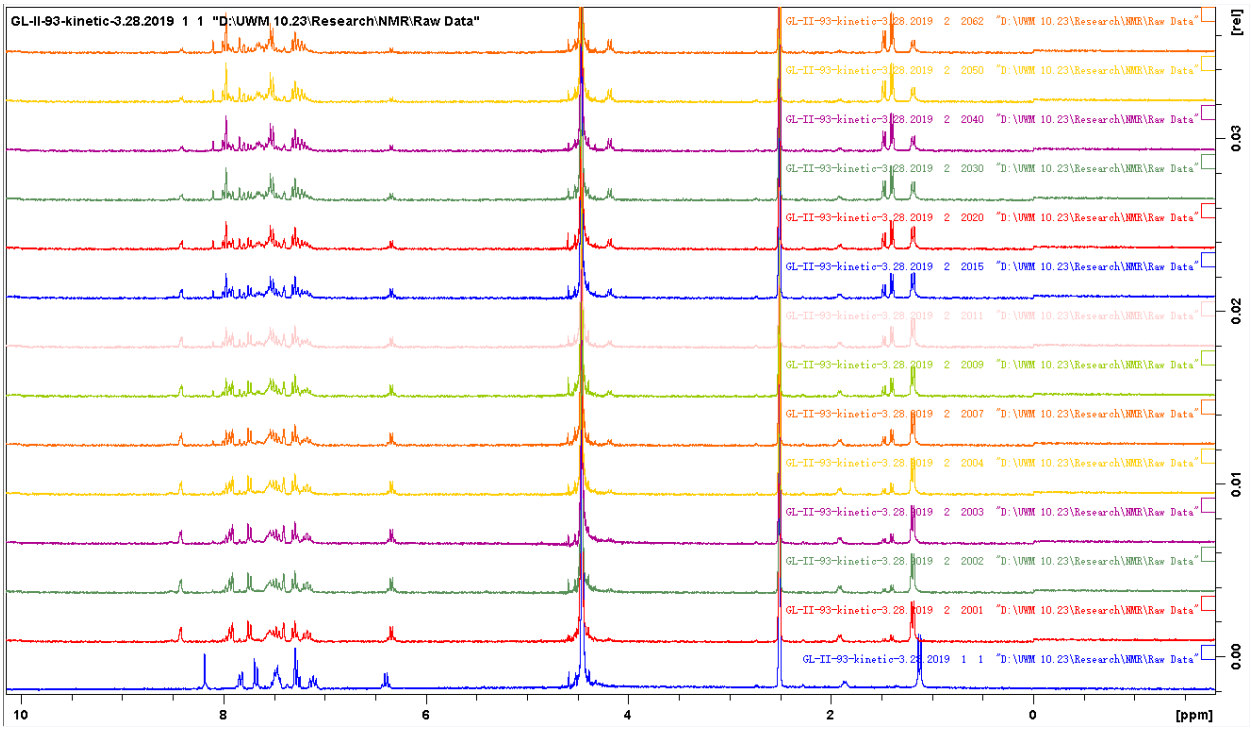

1.2. DCl addition at pH = 2, at 1.1-2.0 ppm

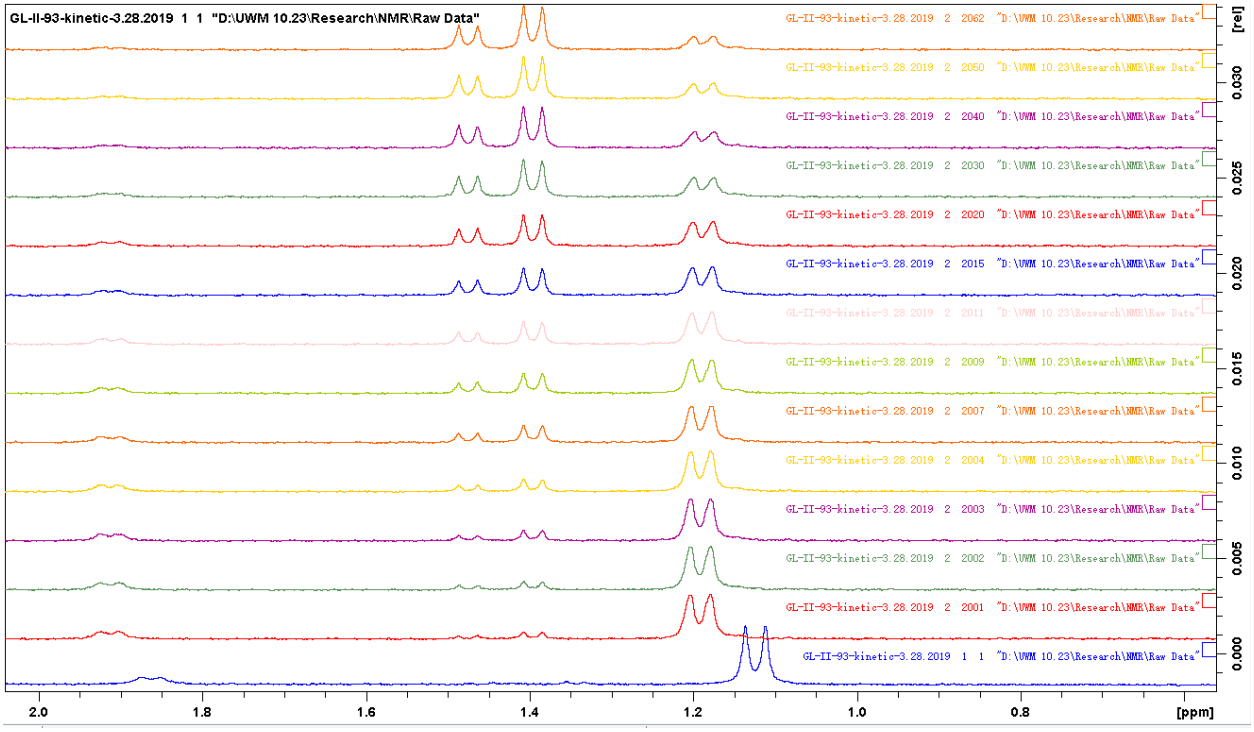

1.3. DCl addition at pH = 2, at 4.0-6.5 ppm

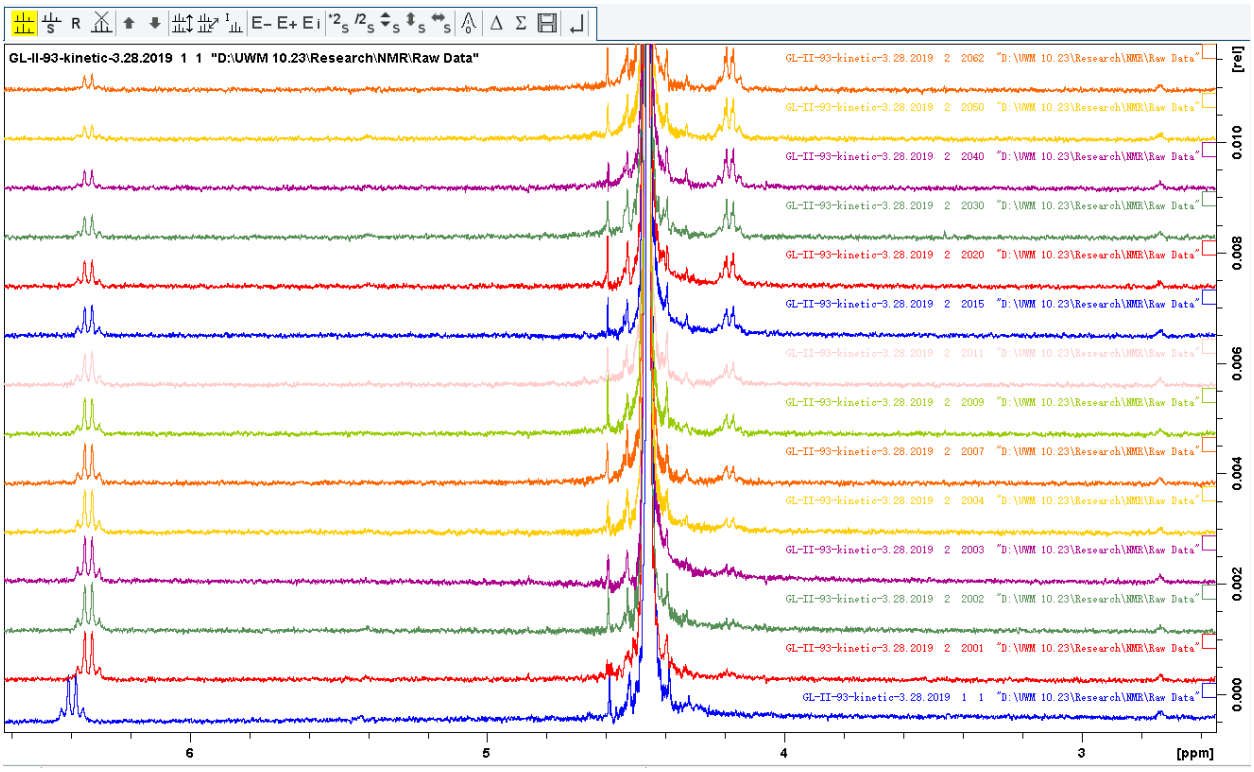

1.4. DCl addition at pH = 2, at 6.0-8.5 ppm

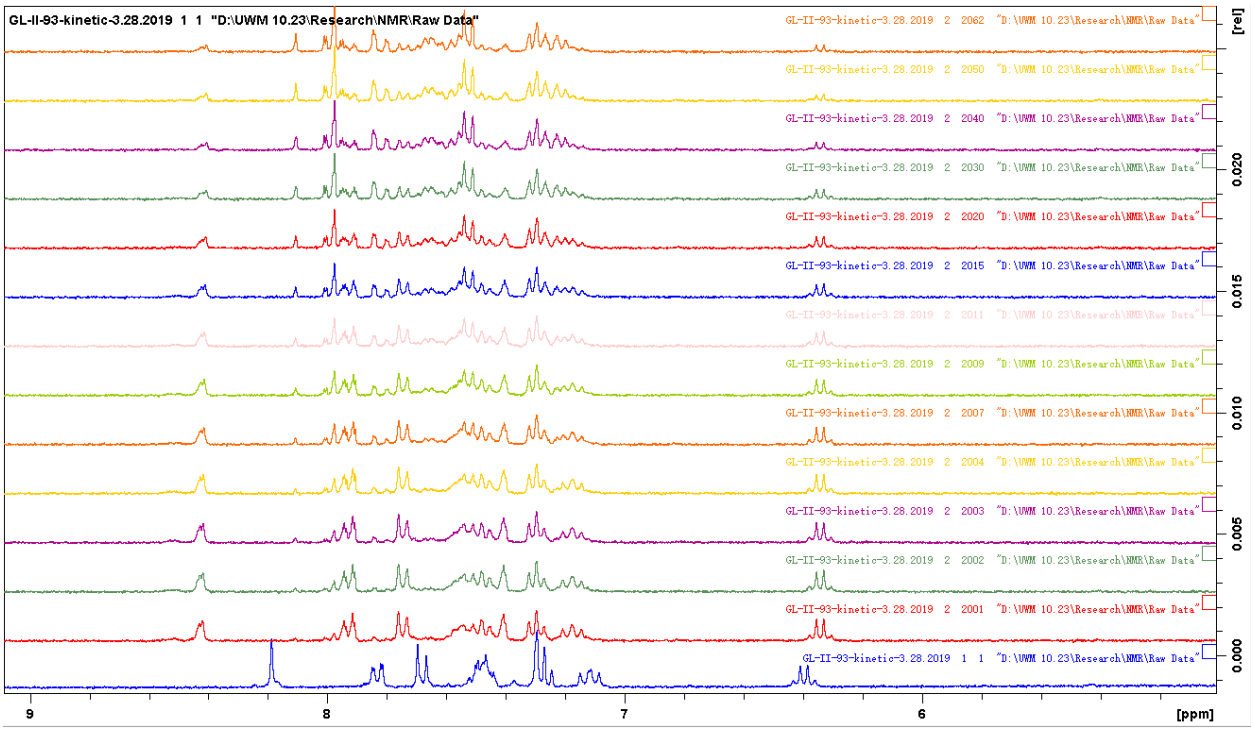

2. The area (lg)-time curve of DCl addition at pH = 2

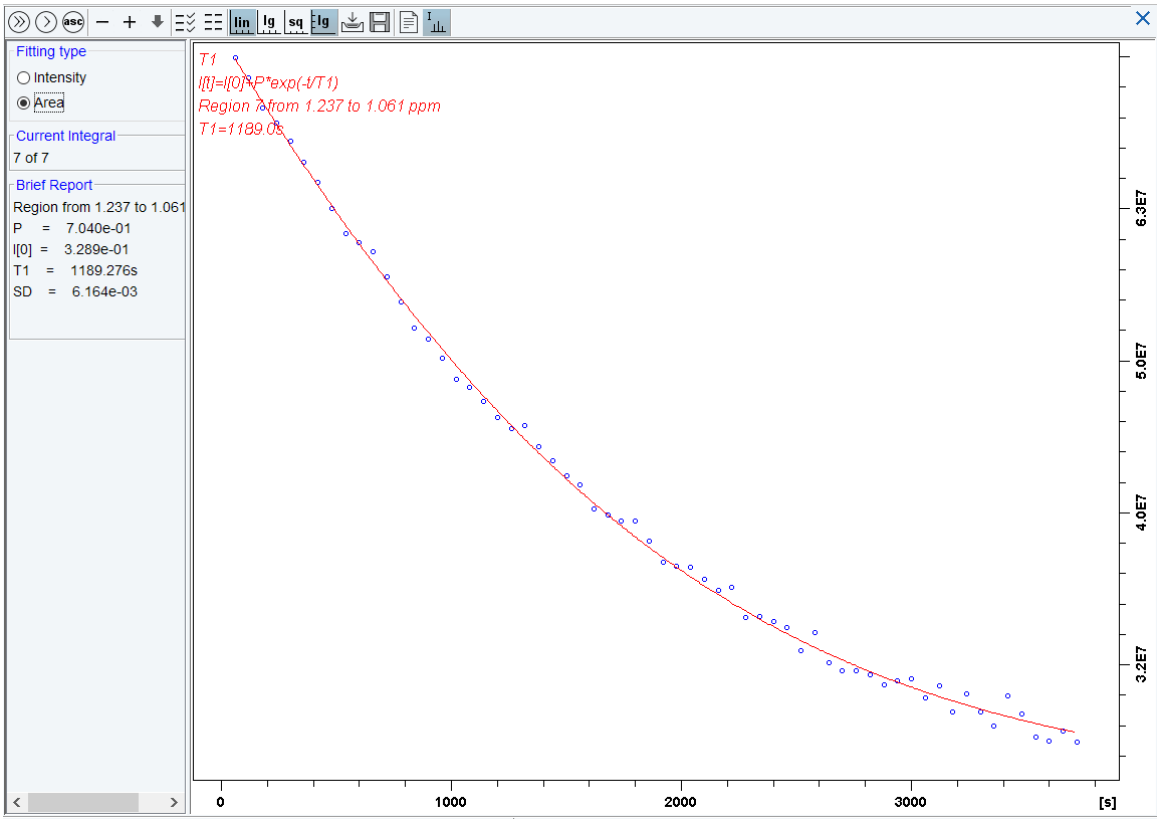

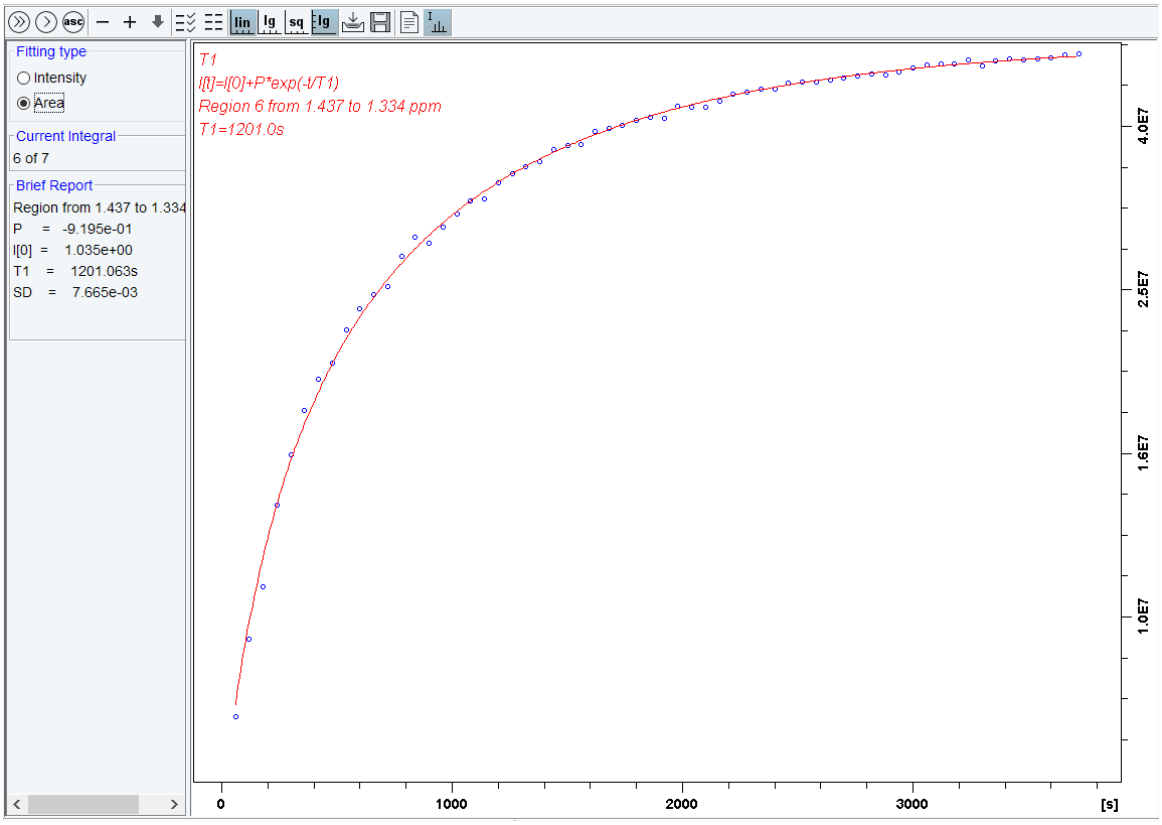

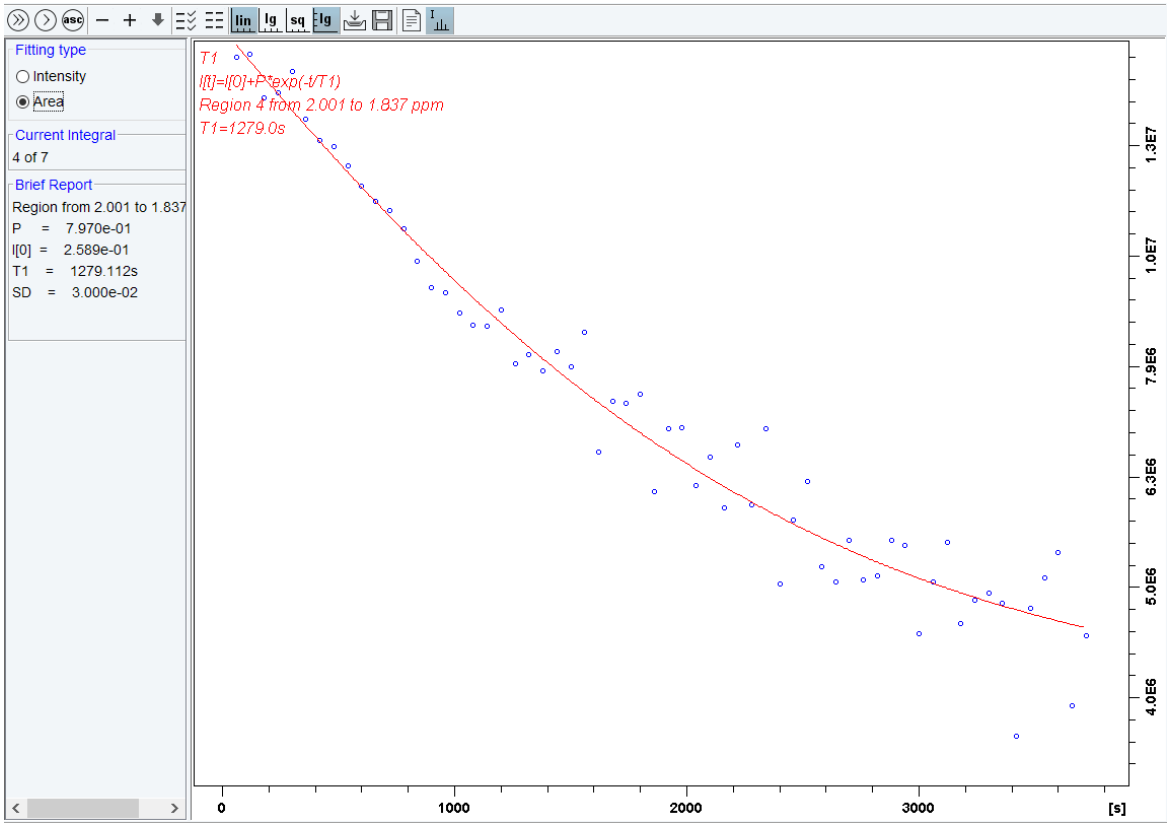
Fitting type
Intensity
Area
Current Integral
4 of 7
Brief Report
Region from 2.001 to 1.837
P = 7.970e-01
I[0] = 2.589e-01
T1 = 1279.112s
SD = 3.000e-02
T1
I[t]=I[0]+P*exp(-t/T1)
Region 4 from 2.001 to 1.837 ppm
T1=1279.0s
1.3E7
1.0E7
7.9E6
6.3E6
5.0E6
4.0E6
0
1000
2000
3000
[s]

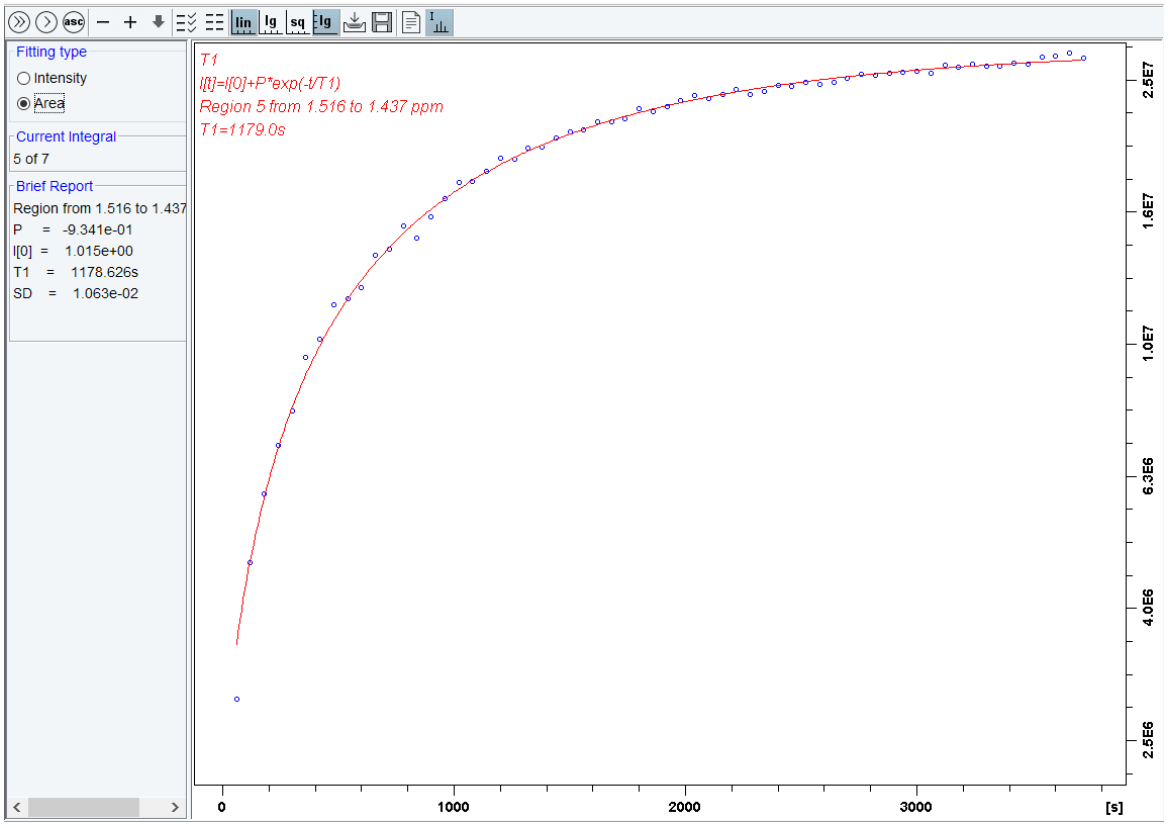
Fitting type
Intensity
Area
Current Integral
5 of 7
Brief Report
Region from 1.516 to 1.437
P = -9.341e-01
I[0] = 1.015e+00
T1 = 1178.626s
SD = 1.063e-02
T1
I[t]=I[0]+P*exp(-t/T1)
Region 5 from 1.516 to 1.437 ppm
T1=1179.0s
2.5E7
1.6E7
1.0E7
6.3E6
4.0E6
2.5E6
0
1000
2000
3000
[s]

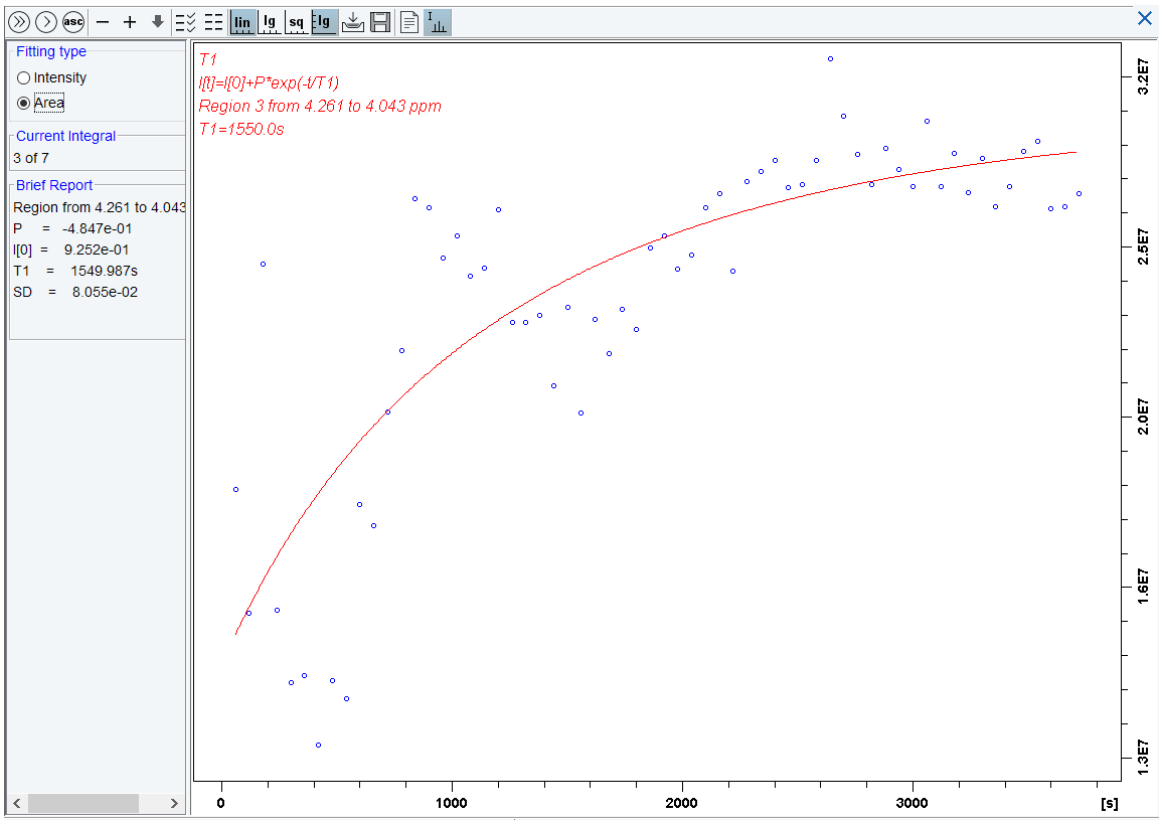
Fitting type
Intensity
Area
Current Integral
3 of 7
Brief Report
Region from 4.261 to 4.043
P = -4.847e-01
I[0] = 9.252e-01
T1 = 1549.987s
SD = 8.055e-02
T1
I[t]=I[0]+P*exp(-t/T1)
Region 3 from 4.261 to 4.043 ppm
T1=1550.0s
3.2E7
2.5E7
2.0E7
1.6E7
1.3E7
0
1000
2000
3000
[s]

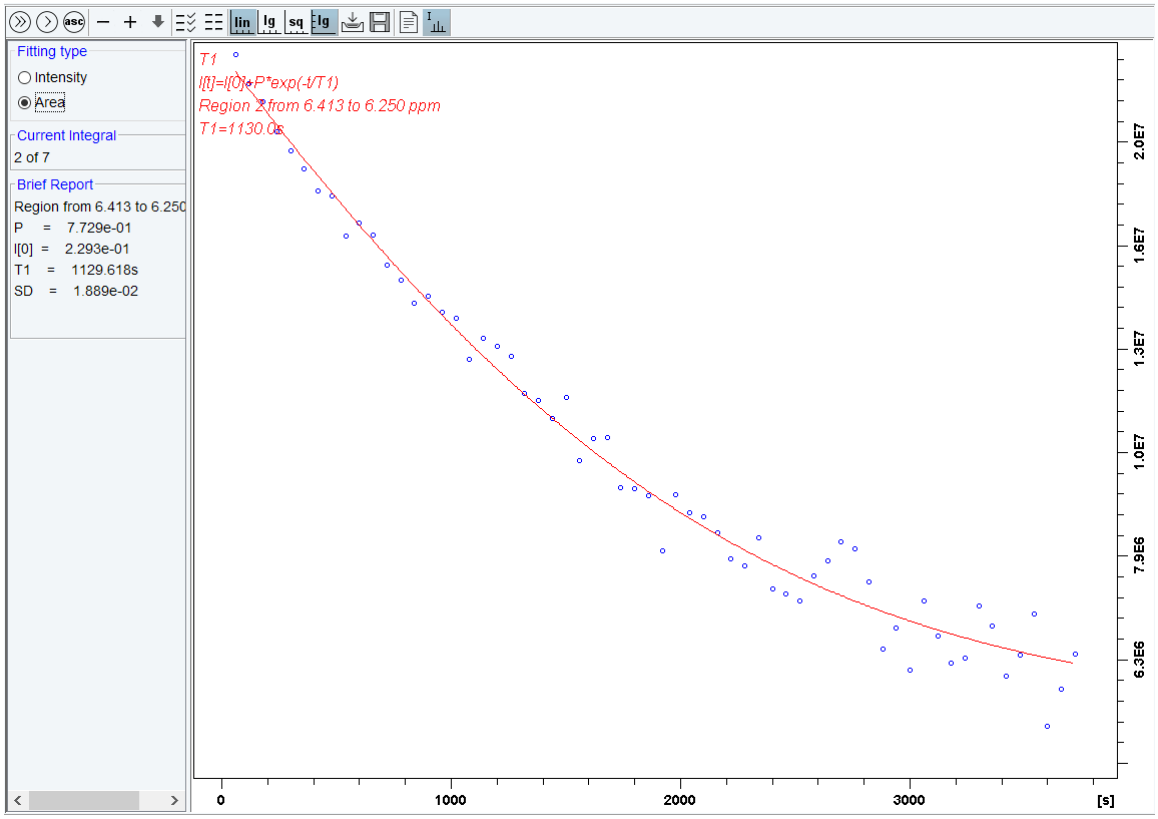
Fitting type
Intensity
Area
Current Integral
2 of 7
Brief Report
Region from 6.413 to 6.250
P = 7.729e-01
I[0] = 2.293e-01
T1 = 1129.618s
SD = 1.889e-02
T1
I[t]=I[0]+P*exp(-t/T1)
Region 2 from 6.413 to 6.250 ppm
T1=1130.0s
2.0E7
1.6E7
1.3E7
1.0E7
7.9E6
6.3E6
0
1000
2000
3000
[s]

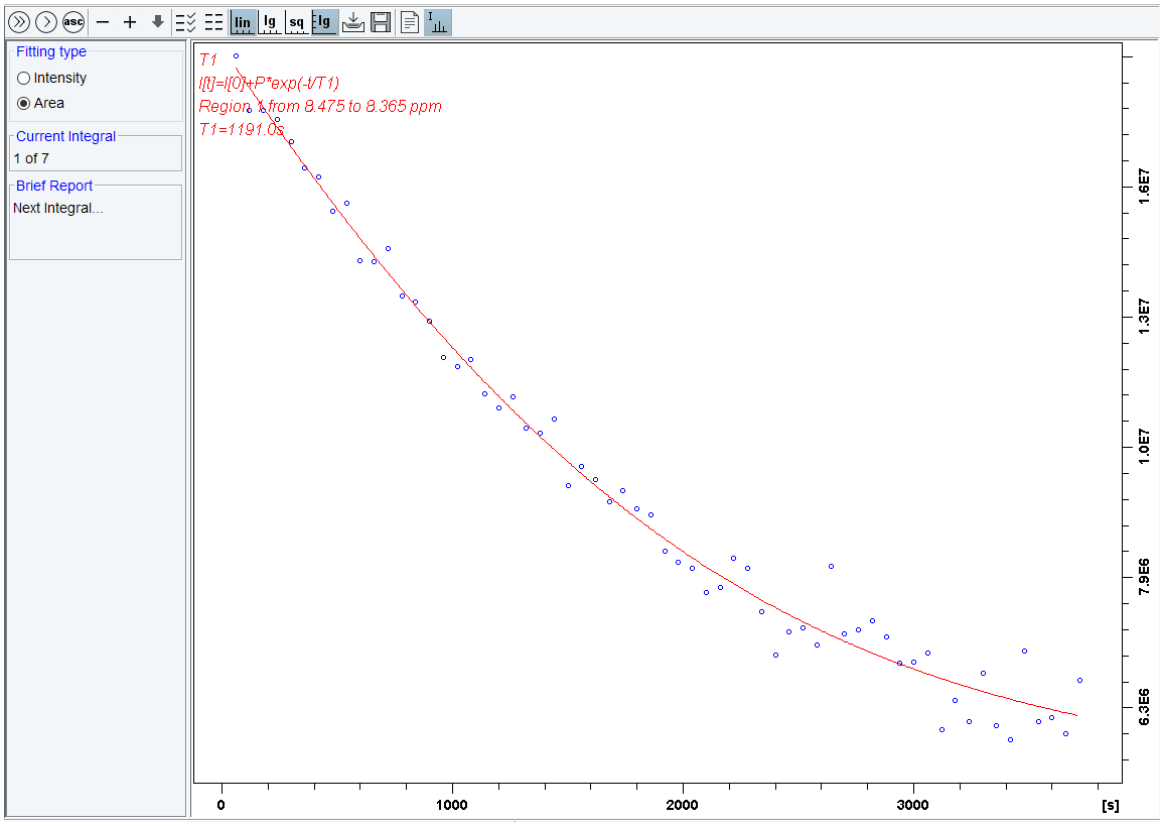
Fitting type
Intensity
Area
Current Integral
1 of 7
Brief Report
Next Integral...
T1
I[t]=I[0]+P*exp(-t/T1)
Region 1 from 8.475 to 8.365 ppm
T1=1191.0s
1.6E7
1.3E7
1.0E7
7.9E6
6.3E6
0
1000
2000
3000
[s]

3. The intensity (lg)-time curve of DCl addition at pH = 2

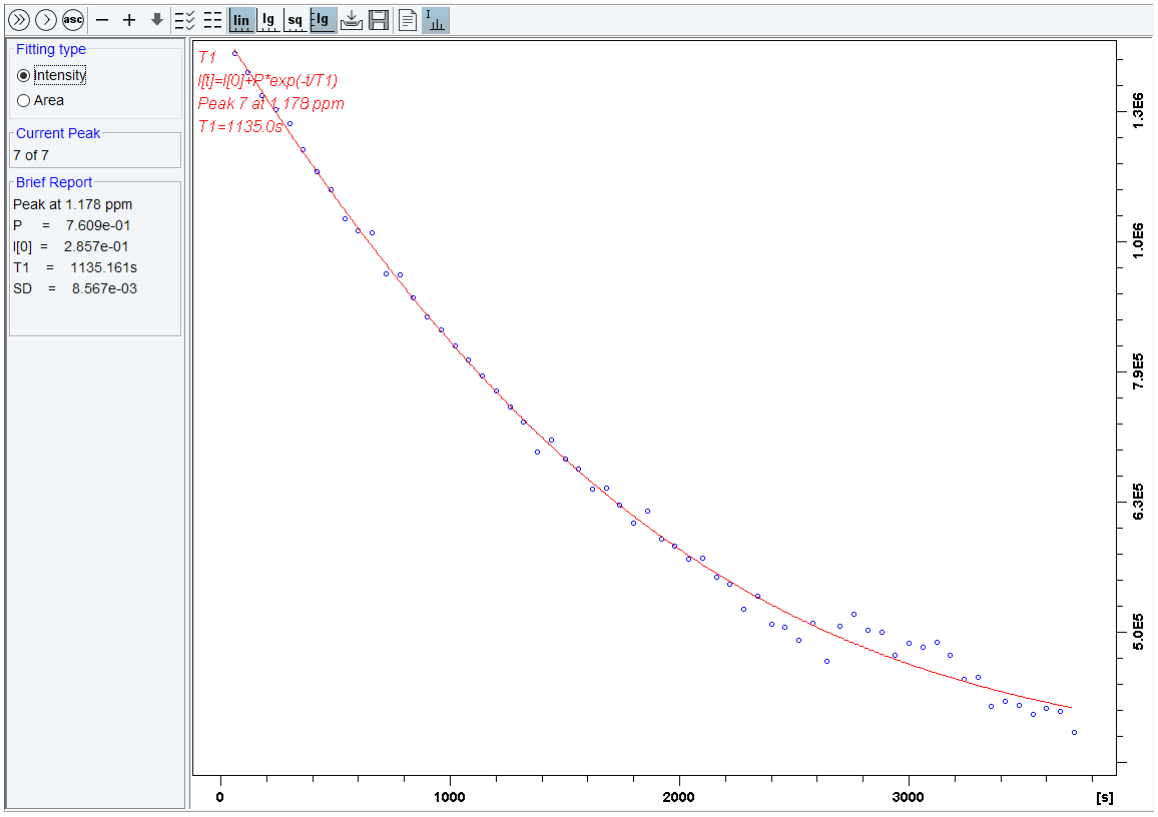

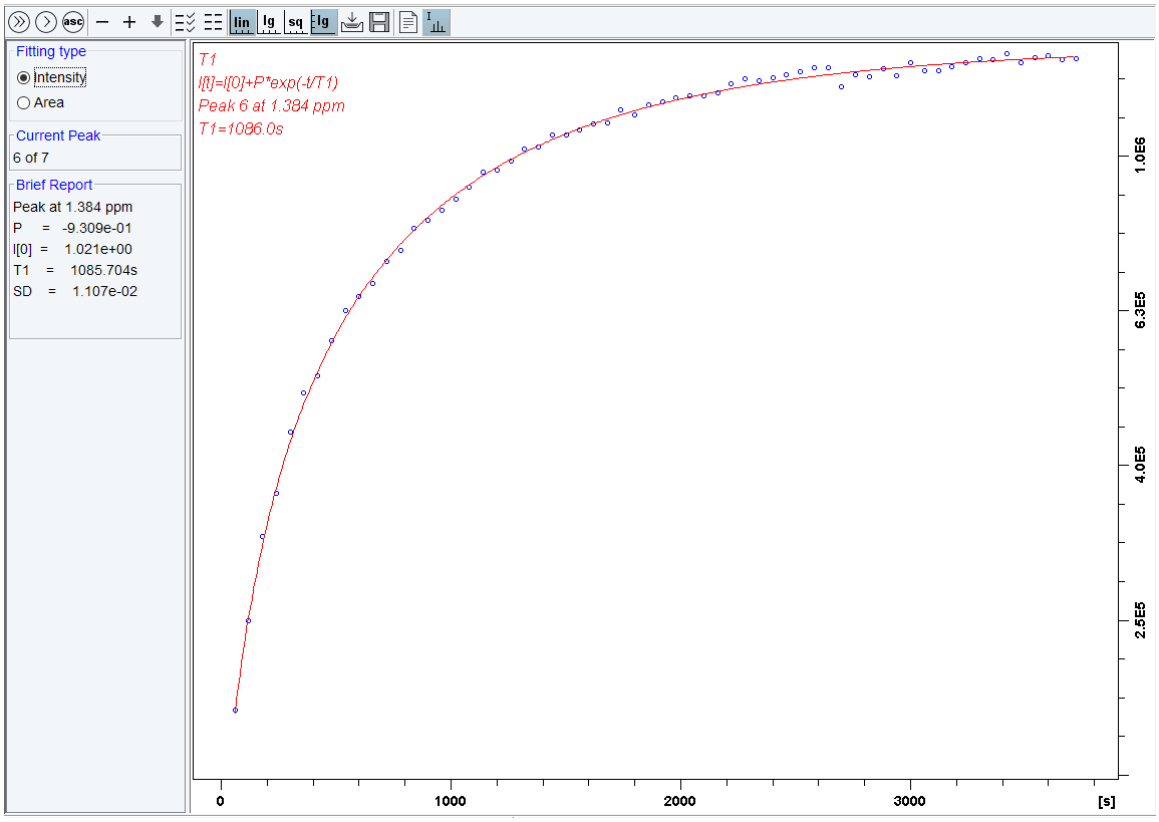

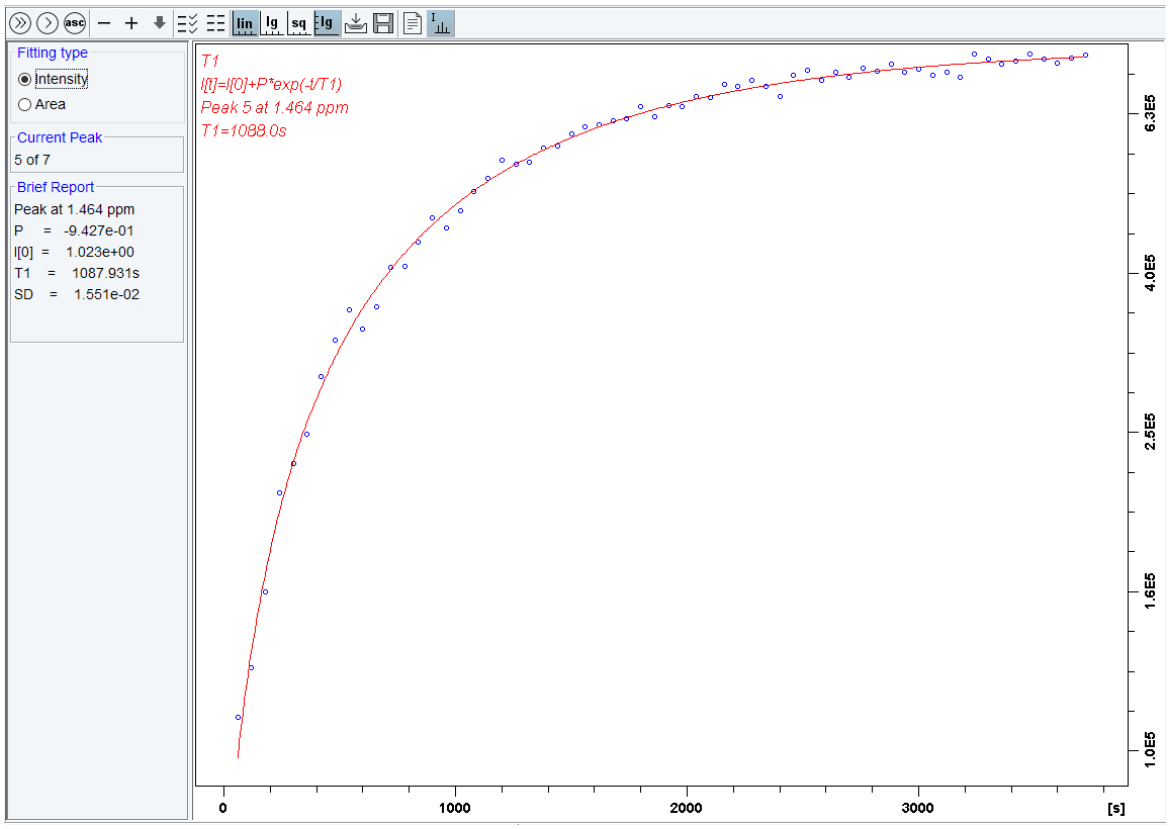
Fitting type
Intensity
Area
Current Peak
5 of 7
Brief Report
Peak at 1.464 ppm
P = -9.427e-01
I[0] = 1.023e+00
T1 = 1087.931s
SD = 1.551e-02
T1
I[t]=I[0]+P*exp(-t/T1)
Peak 5 at 1.464 ppm
T1=1088.0s
6.3E5
4.0E5
2.5E5
1.6E5
1.0E5
0
1000
2000
3000
[s]

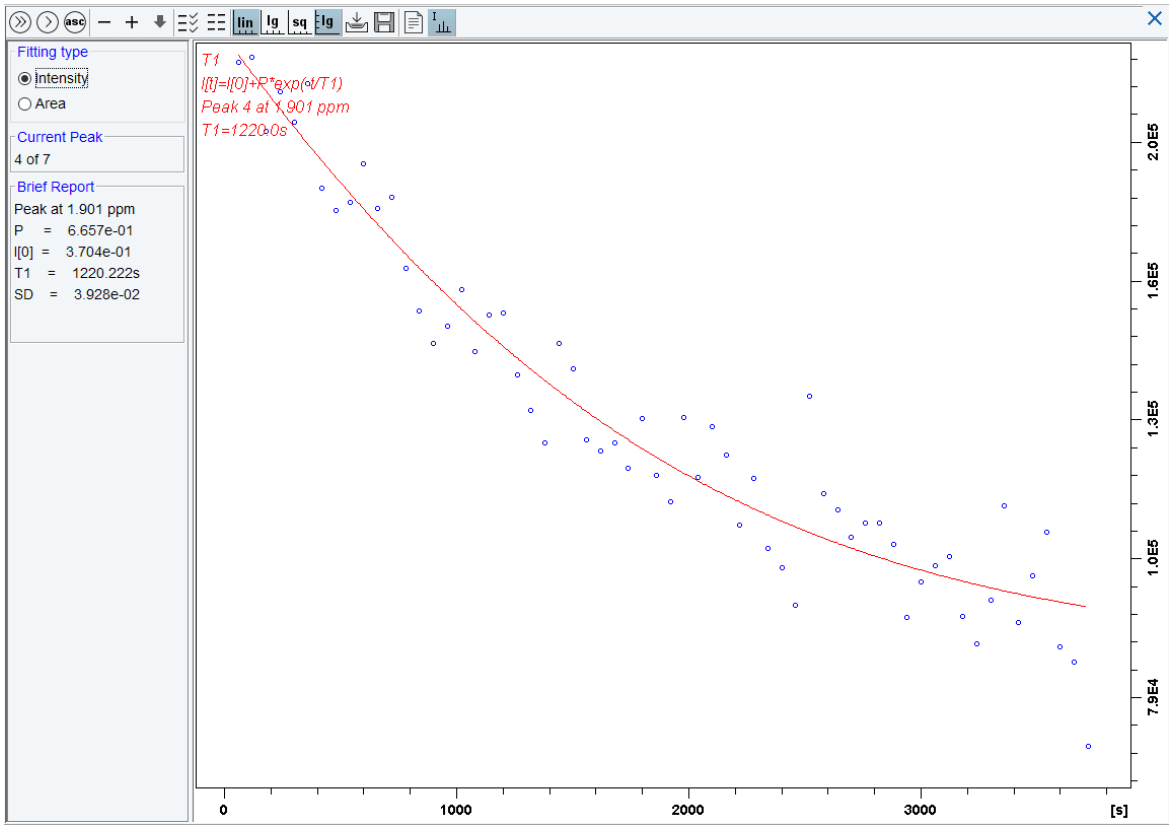
Fitting type
Intensity
Area
Current Peak
4 of 7
Brief Report
Peak at 1.901 ppm
P = 6.657e-01
I[0] = 3.704e-01
T1 = 1220.222s
SD = 3.928e-02
T1
I[t]=I[0]+P*exp(-t/T1)
Peak 4 at 1.901 ppm
T1=1220.0s
2.0E5
1.6E5
1.3E5
1.0E5
7.9E4
0
1000
2000
3000
[s]

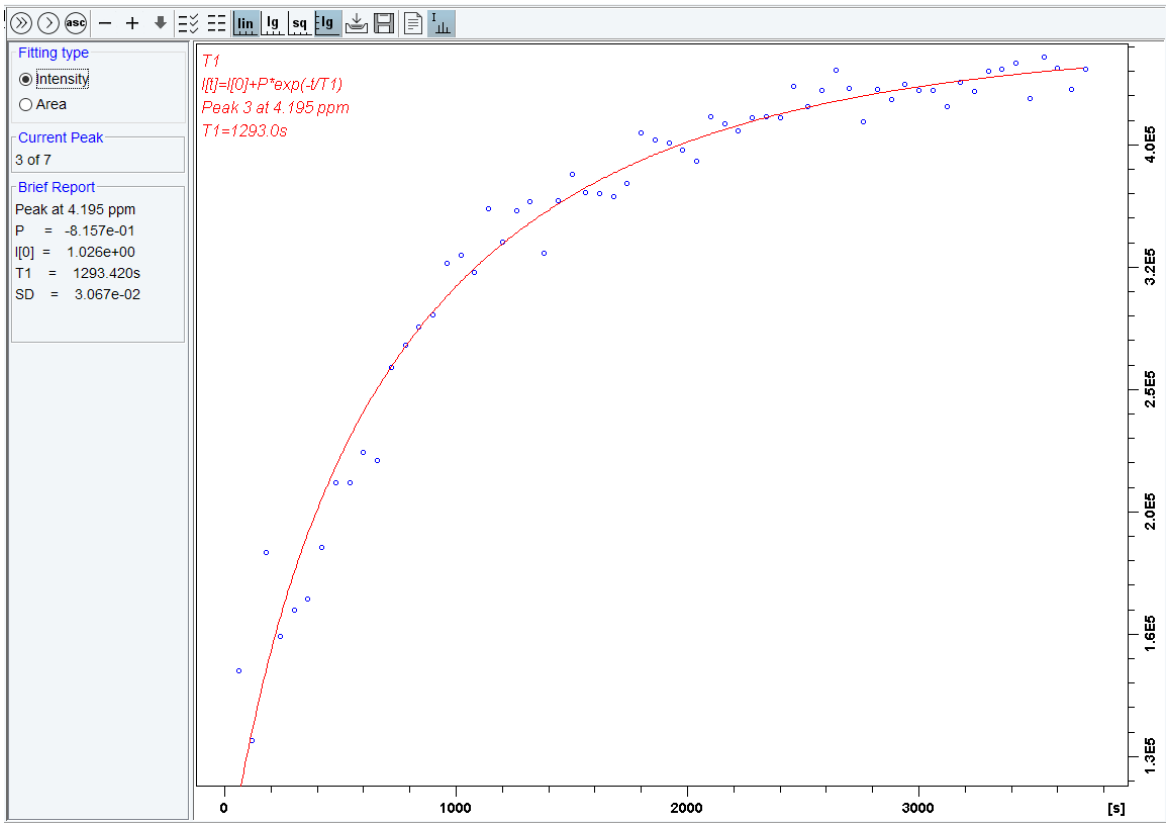
Fitting type
Intensity
Area
Current Peak
3 of 7
Brief Report
Peak at 4.195 ppm
P = -8.157e-01
I[0] = 1.026e+00
T1 = 1293.420s
SD = 3.067e-02
T1
I[t]=I[0]+P*exp(-t/T1)
Peak 3 at 4.195 ppm
T1=1293.0s
4.0E5
3.2E5
2.5E5
2.0E5
1.6E5
1.3E5
0
1000
2000
3000
[s]

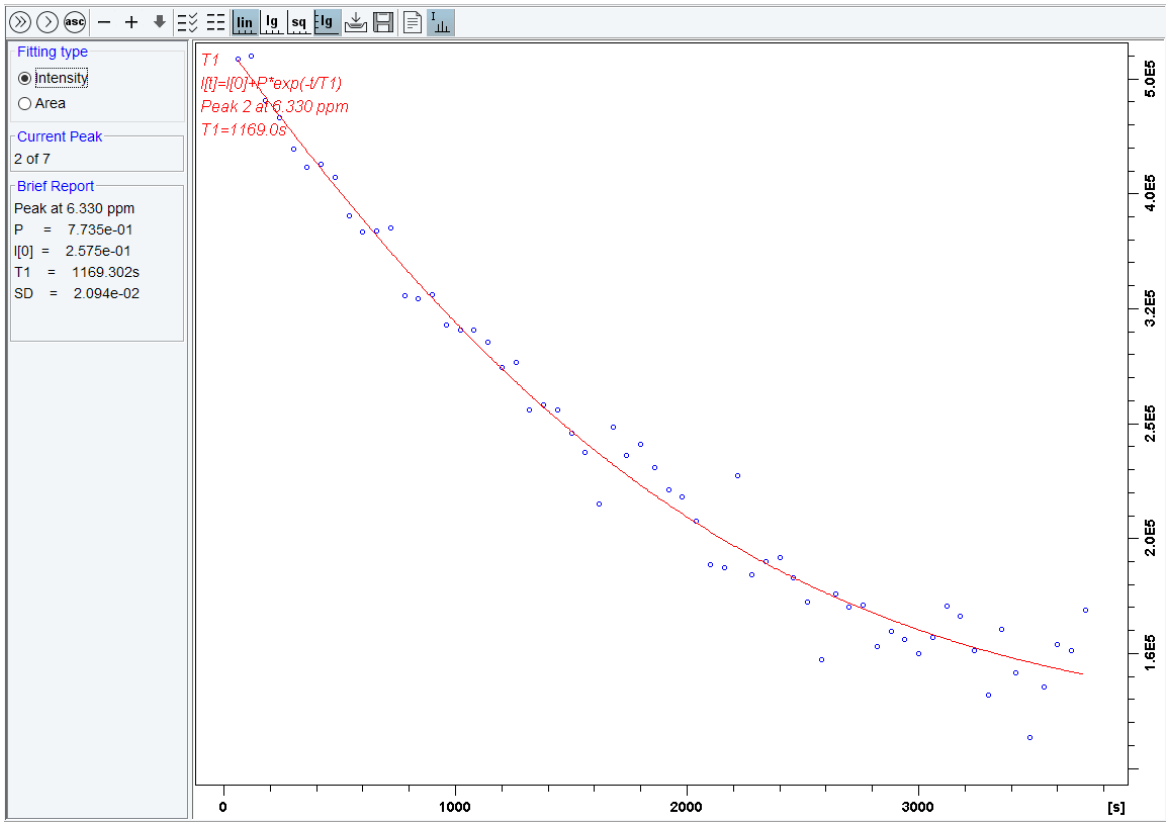
Fitting type
Intensity
Area
Current Peak
2 of 7
Brief Report
Peak at 6.330 ppm
P = 7.735e-01
I[0] = 2.575e-01
T1 = 1169.302s
SD = 2.094e-02
T1
I[t]=I[0]+P*exp(-t/T1)
Peak 2 at 6.330 ppm
T1=1169.0s
5.0E5
4.0E5
3.2E5
2.5E5
2.0E5
1.6E5
0
1000
2000
3000
[s]

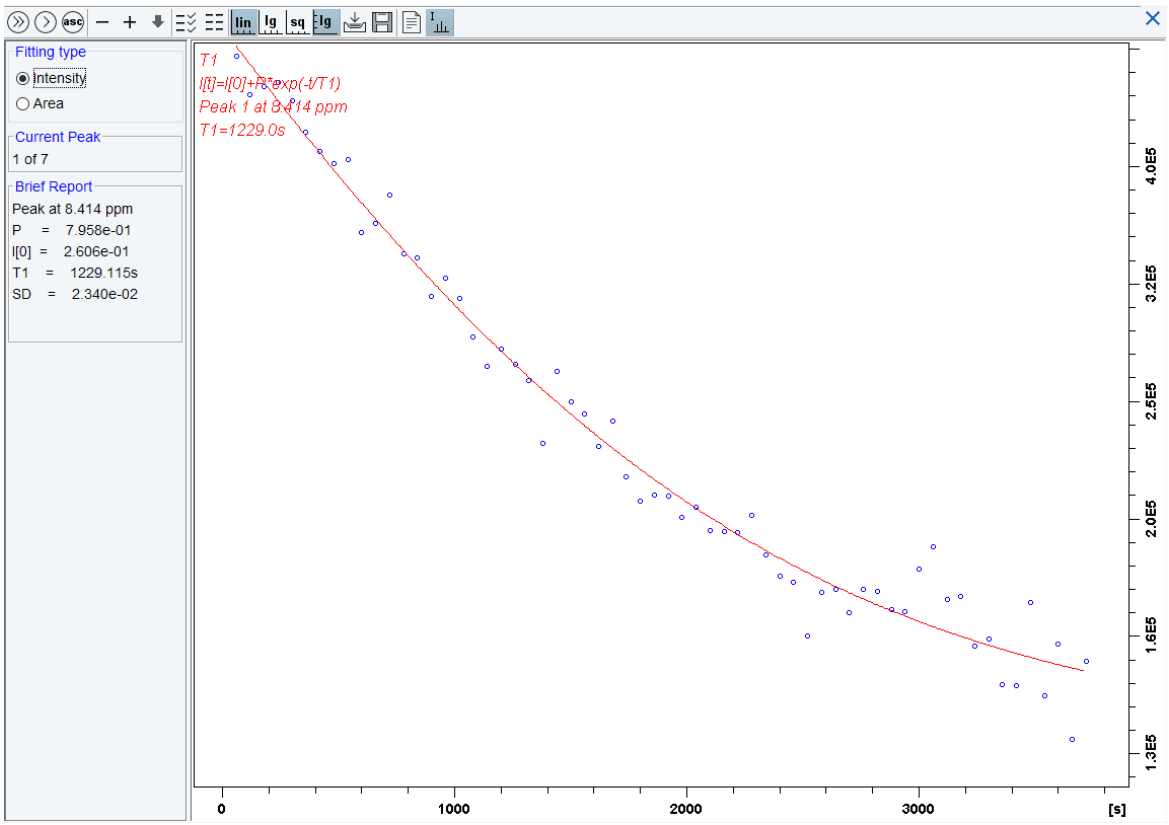

4. DCl addition t1/2 list [area (lg)-time curve]

Brief Report

Region 1 from 8.475 to 8.365 ppm
T1 = 1191.128s
Region 2 from 6.413 to 6.250 ppm
T1 = 1129.618s
Region 3 from 4.261 to 4.043 ppm
T1 = 1549.987s
Region 4 from 2.001 to 1.837 ppm
T1 = 1279.112s
Region 5 from 1.516 to 1.437 ppm
T1 = 1178.626s
Region 6 from 1.437 to 1.334 ppm
T1 = 1201.063s
Region 7 from 1.237 to 1.061 ppm
T1 = 1189.276s

5. DCl addition t1/2 list [intensity (lg)-time curve]

Brief Report

Peak 1 at 8.414 ppm
T1 = 1229.115s
Peak 2 at 6.330 ppm
T1 = 1169.302s
Peak 3 at 4.195 ppm
T1 = 1293.420s
Peak 4 at 1.901 ppm
T1 = 1220.222s
Peak 5 at 1.464 ppm
T1 = 1087.931s
Peak 6 at 1.384 ppm
T1 = 1085.704s
Peak 7 at 1.178 ppm
T1 = 1135.161s

6. 2D NMR experiment (NaOD addition)

6.1. NaOD addition at pH = 8, at all range

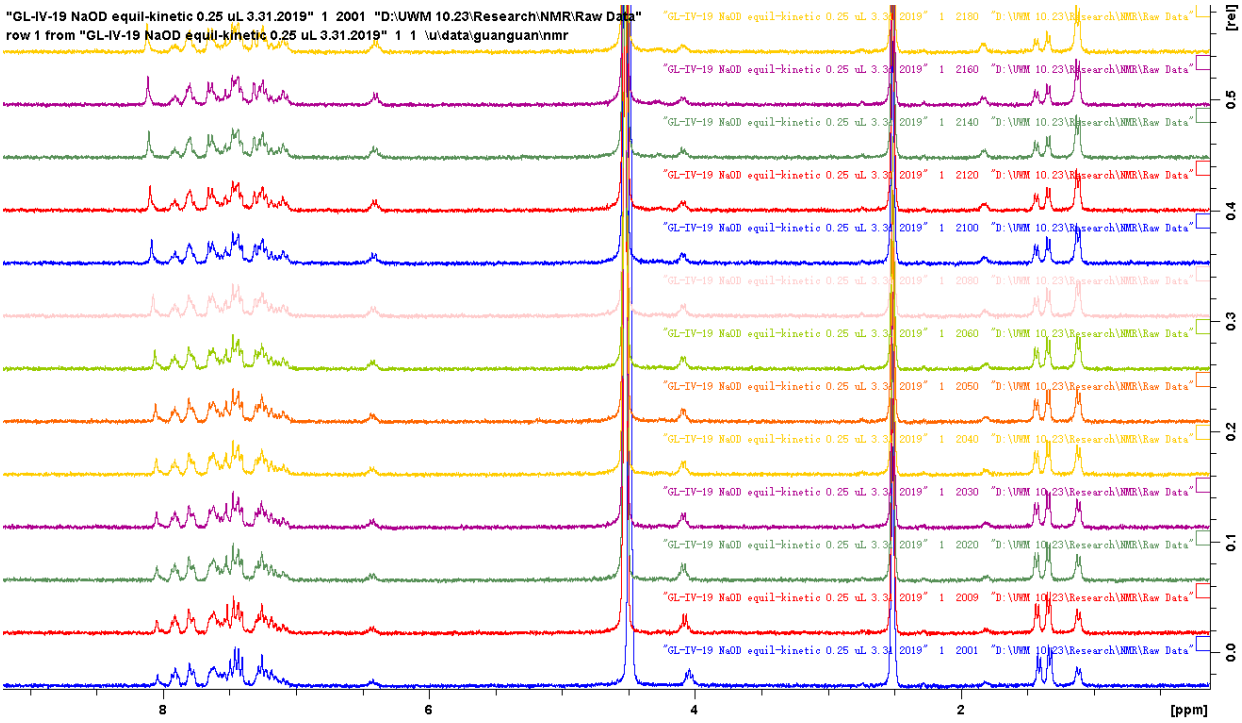

6.2. NaOD addition at pH = 8, at 0.4-2.0 ppm

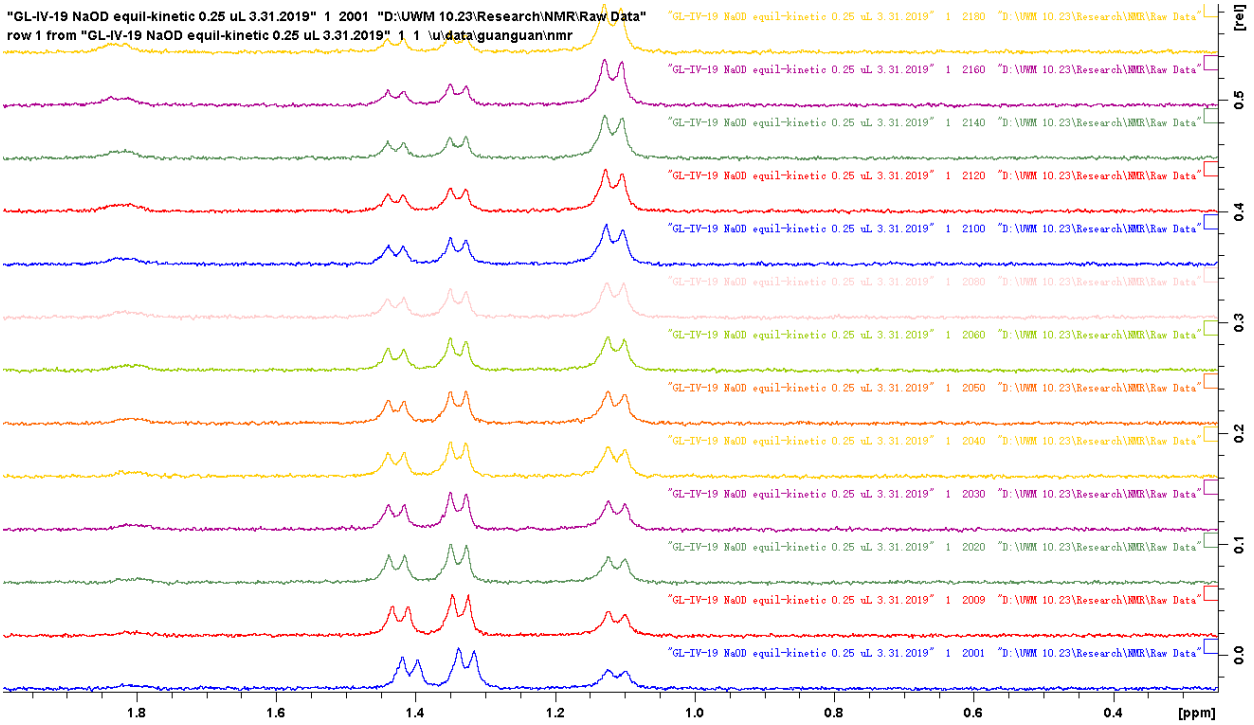

6.3. NaOD addition at pH = 8, at 6.0-8.0 ppm

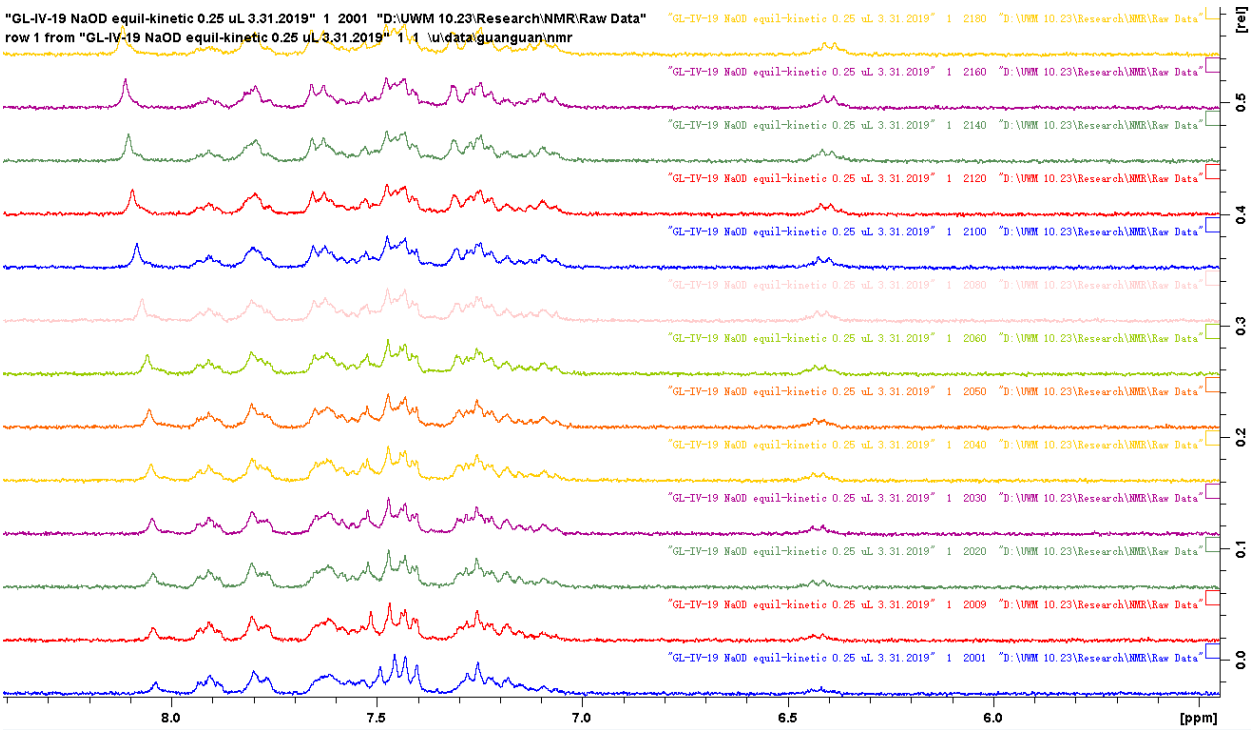

6.4.NaOD addition at all concentration, at all range

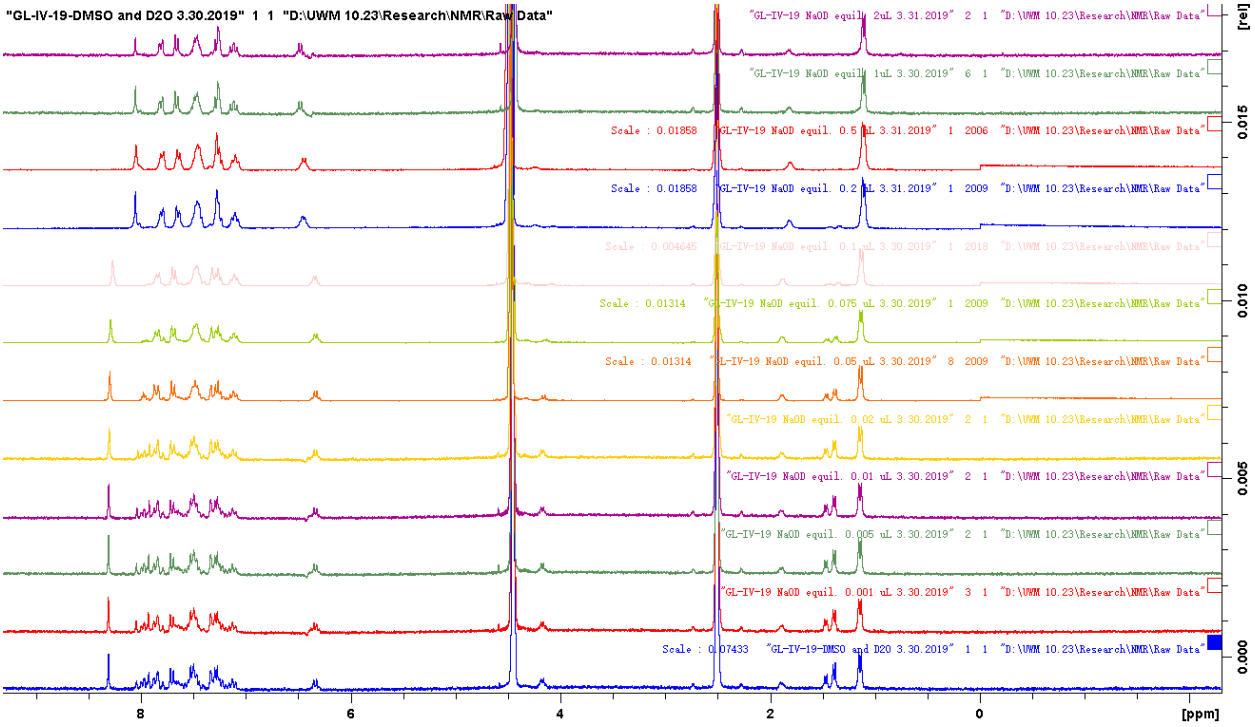

6.5.NaOD addition at all concentration, at 1.0-7.0 ppm

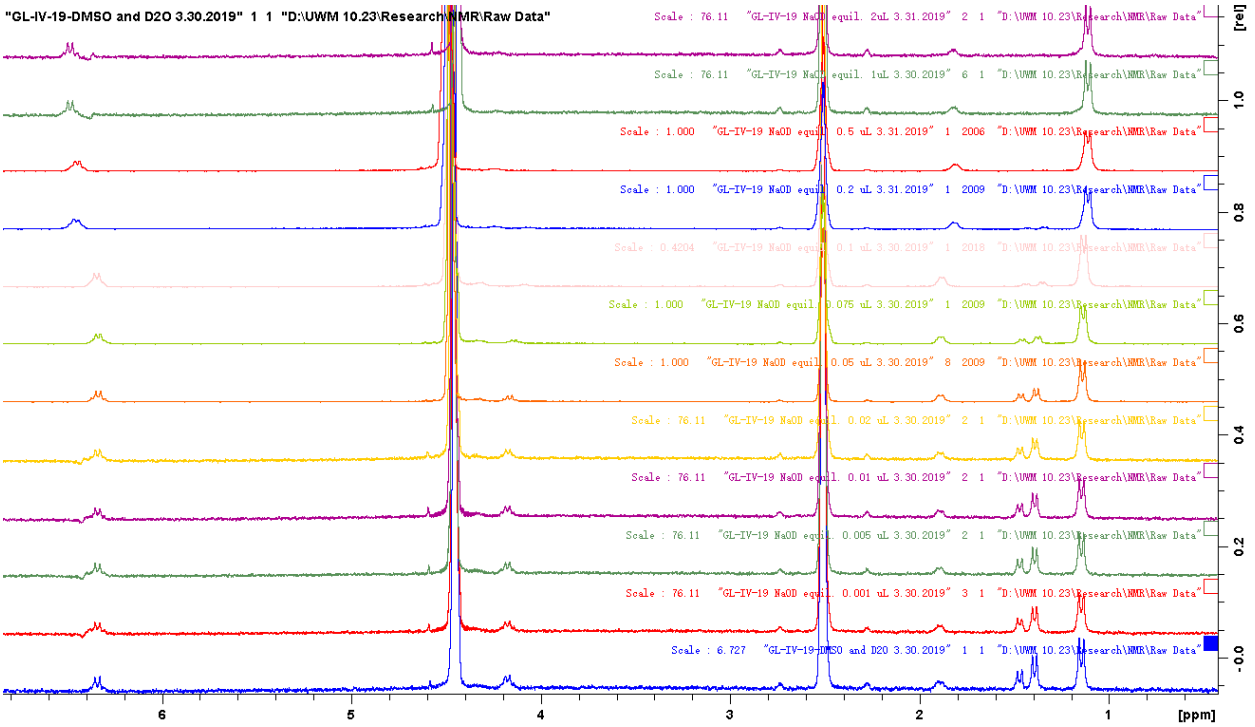

6.6.NaOD addition at all concentration, at 7.0-8.0 ppm

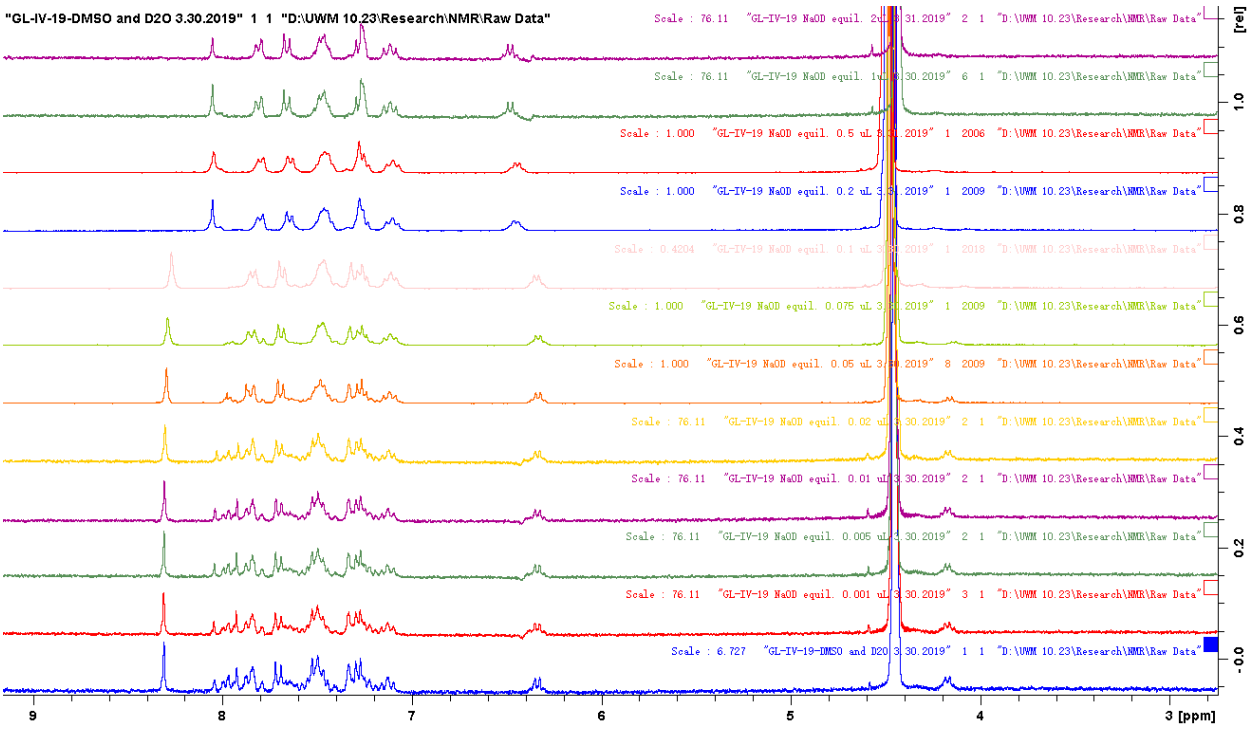

7. The area (lg)-time curve of NaOD addition at pH = 8

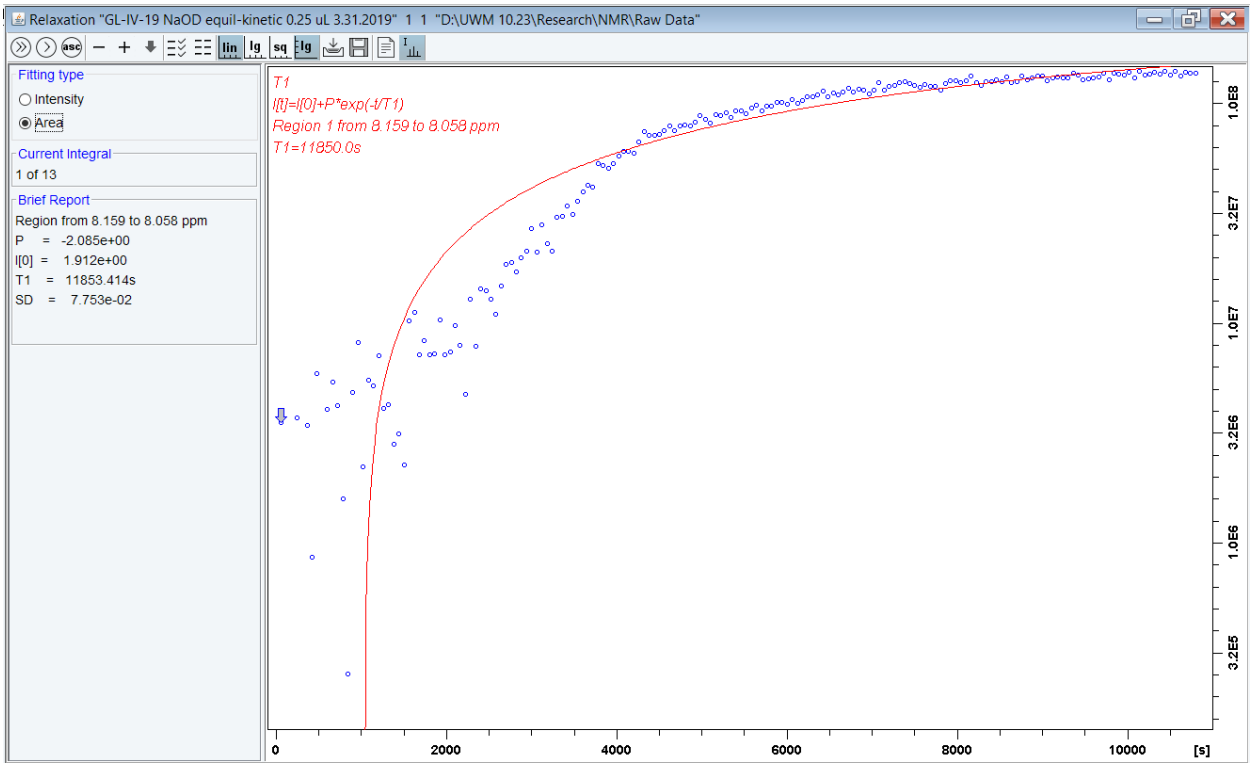

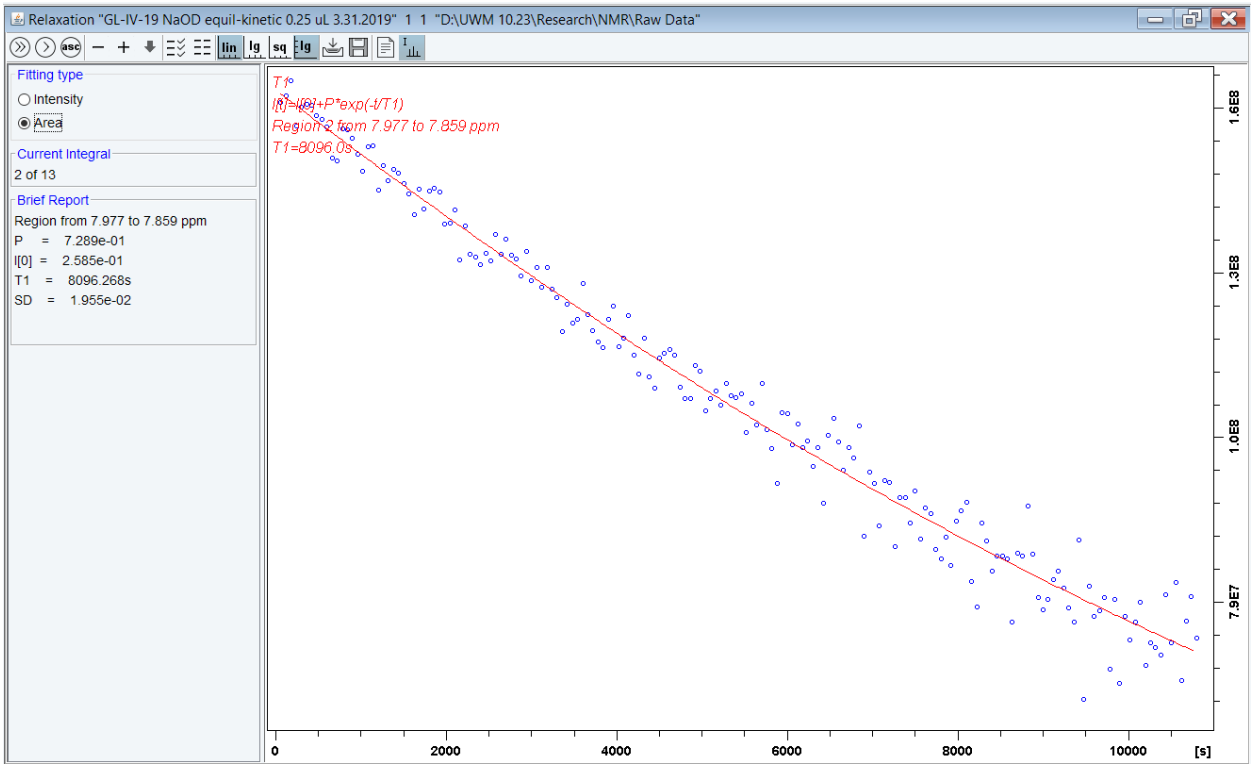
Relaxation "GL-IV-19 NaOD equil-kinetic 0.25 uL 3.31.2019" 1 1 "D:\UWM 10.23\Research\NMR\Raw Data"
Fitting type
Intensity
Area
Current Integral
2 of 13
Brief Report
Region from 7.977 to 7.859 ppm
P = 7.289e-01
I[0] = 2.585e-01
T1 = 8096.268s
SD = 1.955e-02
T1
I[t]=I[0]+P*exp(-t/T1)
Region 2 from 7.977 to 7.859 ppm
T1=8096.0s
1.6E8
1.3E8
1.0E8
7.9E7
0
2000
4000
6000
8000
10000
[s]

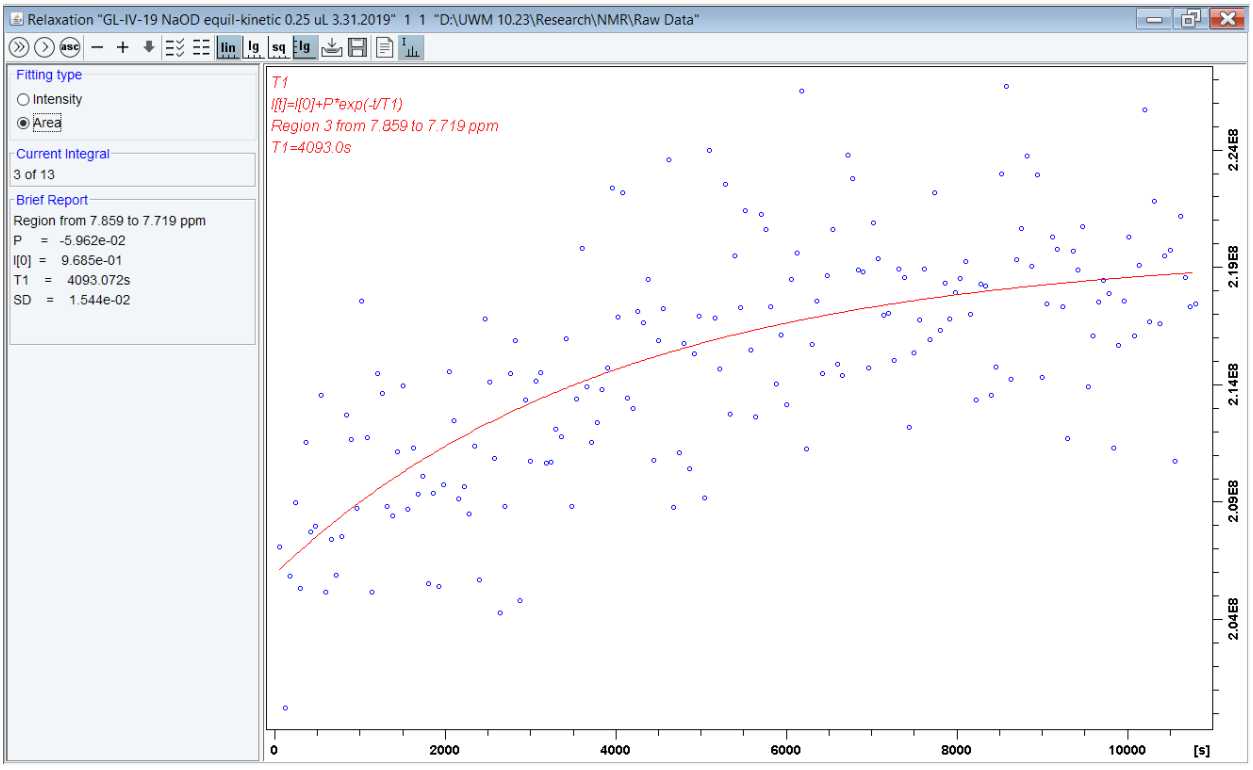
Relaxation "GL-IV-19 NaOD equil-kinetic 0.25 uL 3.31.2019" 1 1 "D:\UWM 10.23\Research\NMR\Raw Data"
Fitting type
Intensity
Area
Current Integral
3 of 13
Brief Report
Region from 7.859 to 7.719 ppm
P = -5.962e-02
I[0] = 9.685e-01
T1 = 4093.072s
SD = 1.544e-02
T1
I[t]=I[0]+P*exp(-t/T1)
Region 3 from 7.859 to 7.719 ppm
T1=4093.0s
2.24E8
2.19E8
2.14E8
2.09E8
2.04E8
0
2000
4000
6000
8000
10000
[s]

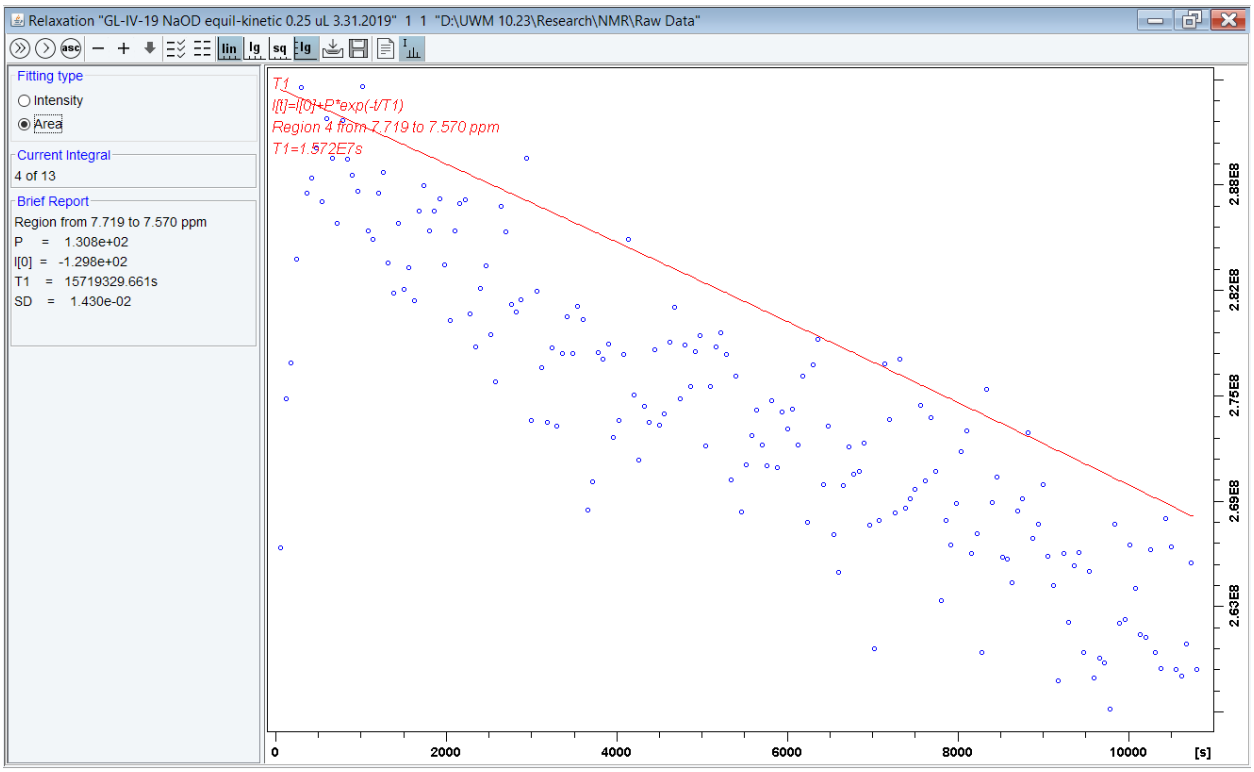
Relaxation "GL-IV-19 NaOD equil-kinetic 0.25 uL 3.31.2019" 1 1 "D:\UWM 10.23\Research\NMR\Raw Data"
Fitting type
Intensity
Area
Current Integral
4 of 13
Brief Report
Region from 7.719 to 7.570 ppm
P = 1.308e+02
I[0] = -1.298e+02
T1 = 15719329.661s
SD = 1.430e-02
T1
I[t]=I[0]+P*exp(-t/T1)
Region 4 from 7.719 to 7.570 ppm
T1=1.572E7s
2.88E8
2.82E8
2.75E8
2.69E8
2.63E8
0
2000
4000
6000
8000
10000
[s]

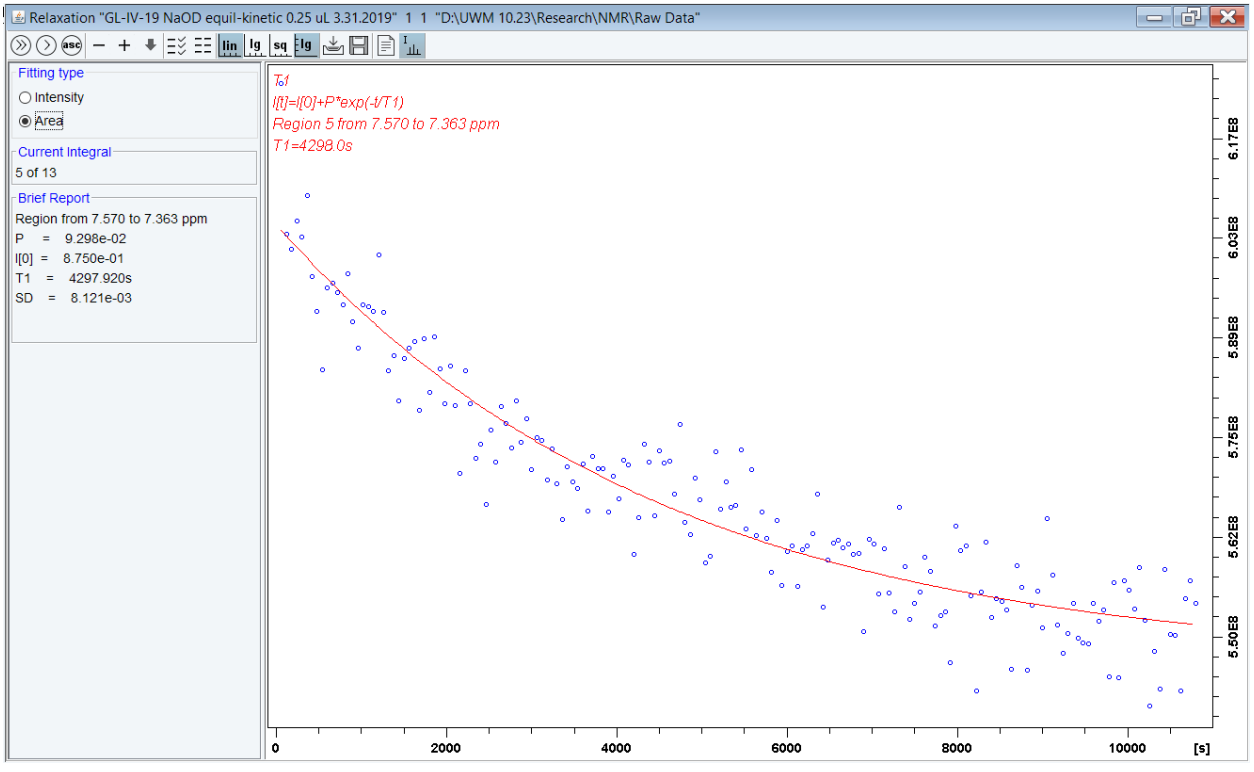
Relaxation "GL-IV-19 NaOD equil-kinetic 0.25 uL 3.31.2019" 1 1 "D:\UWM 10.23\Research\NMR\Raw Data"
Fitting type
Intensity
Area
Current Integral
5 of 13
Brief Report
Region from 7.570 to 7.363 ppm
P = 9.298e-02
I[0] = 8.750e-01
T1 = 4297.920s
SD = 8.121e-03
T1
I[t]=I[0]+P*exp(-t/T1)
Region 5 from 7.570 to 7.363 ppm
T1=4298.0s
6.17E8
6.03E8
5.89E8
5.75E8
5.62E8
5.50E8
0
2000
4000
6000
8000
10000
[s]

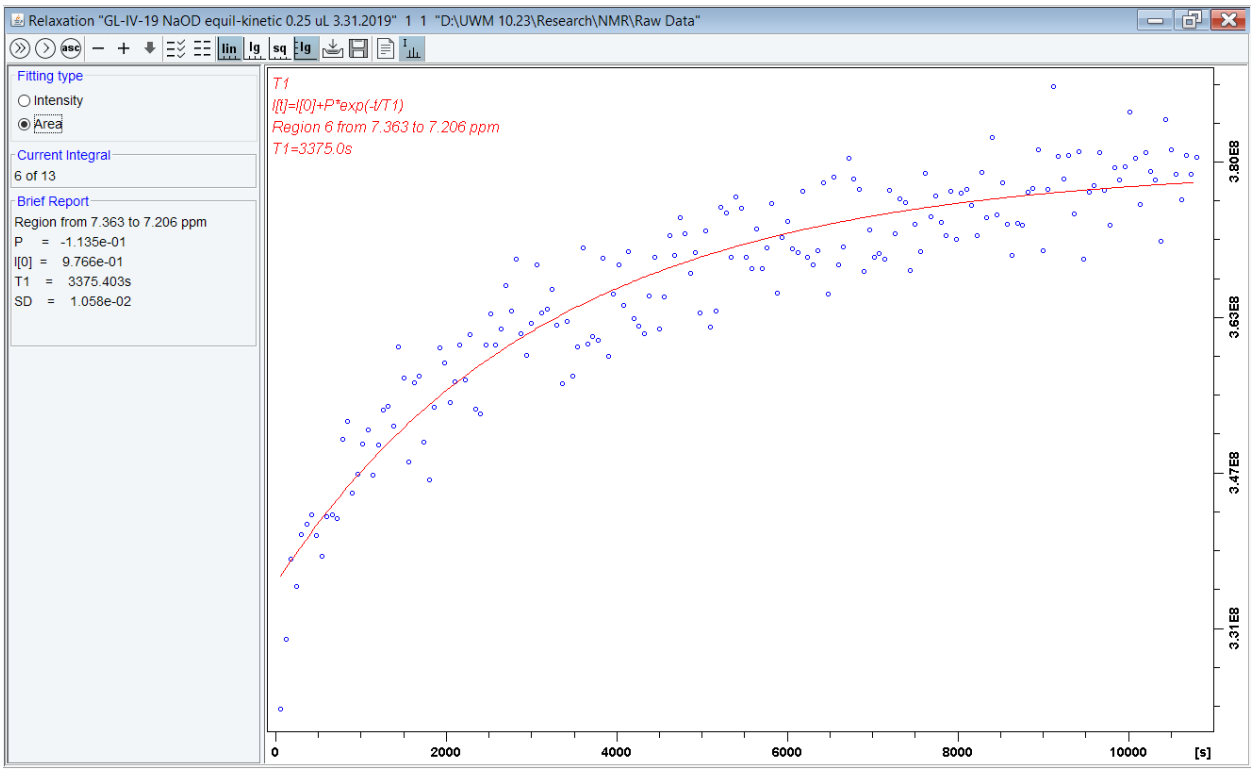
Relaxation "GL-IV-19 NaOD equil-kinetic 0.25 uL 3.31.2019" 1 1 "D:\UWM 10.23\Research\NMR\Raw Data"
Fitting type
Intensity
Area
Current Integral
6 of 13
Brief Report
Region from 7.363 to 7.206 ppm
P = -1.135e-01
I[0] = 9.766e-01
T1 = 3375.403s
SD = 1.058e-02
T1
I[t]=I[0]+P*exp(-t/T1)
Region 6 from 7.363 to 7.206 ppm
T1=3375.0s
3.80E8
3.63E8
3.47E8
3.31E8
0
2000
4000
6000
8000
10000
[s]

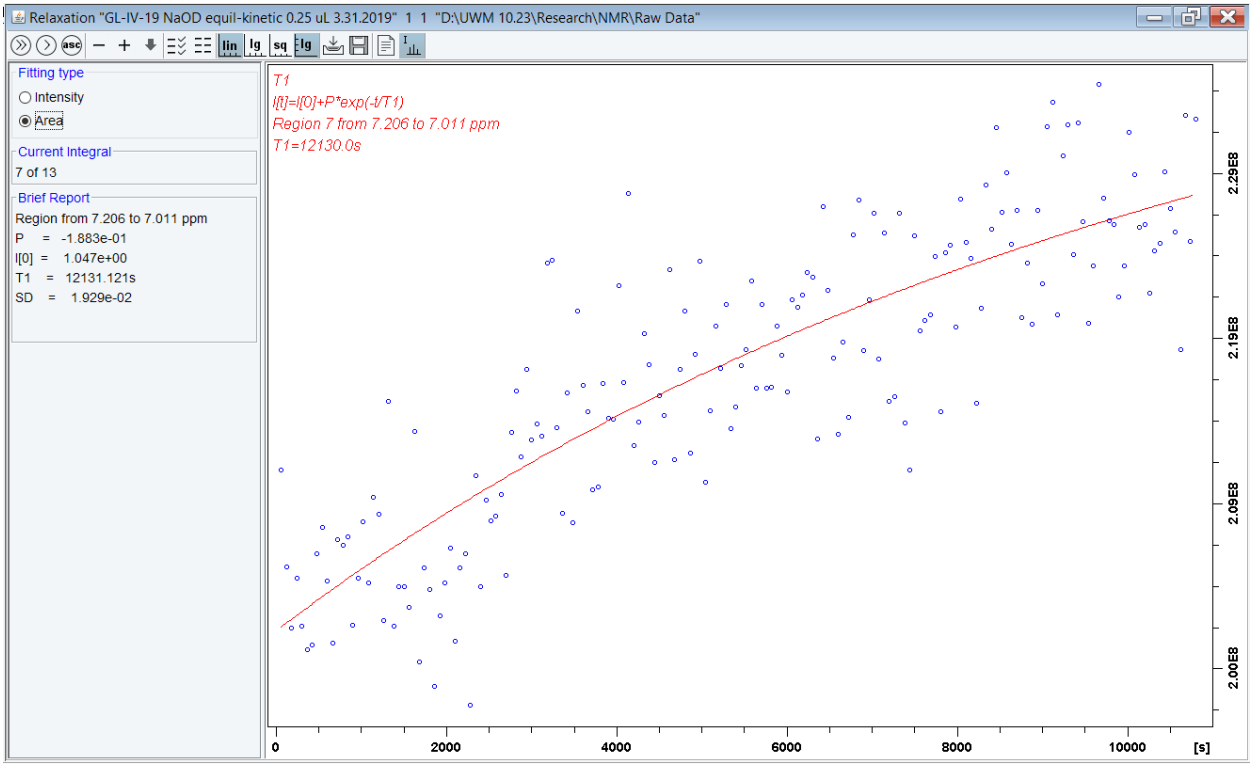
Relaxation "GL-IV-19 NaOD equil-kinetic 0.25 uL 3.31.2019" 1 1 "D:\UWM 10.23\Research\NMR\Raw Data"
Fitting type
Intensity
Area
Current Integral
7 of 13
Brief Report
Region from 7.206 to 7.011 ppm
P = -1.883e-01
I[0] = 1.047e+00
T1 = 12131.121s
SD = 1.929e-02
T1
I[t]=I[0]+P*exp(-t/T1)
Region 7 from 7.206 to 7.011 ppm
T1=12130.0s
2.29E8
2.19E8
2.09E8
2.00E8
0
2000
4000
6000
8000
10000
[s]

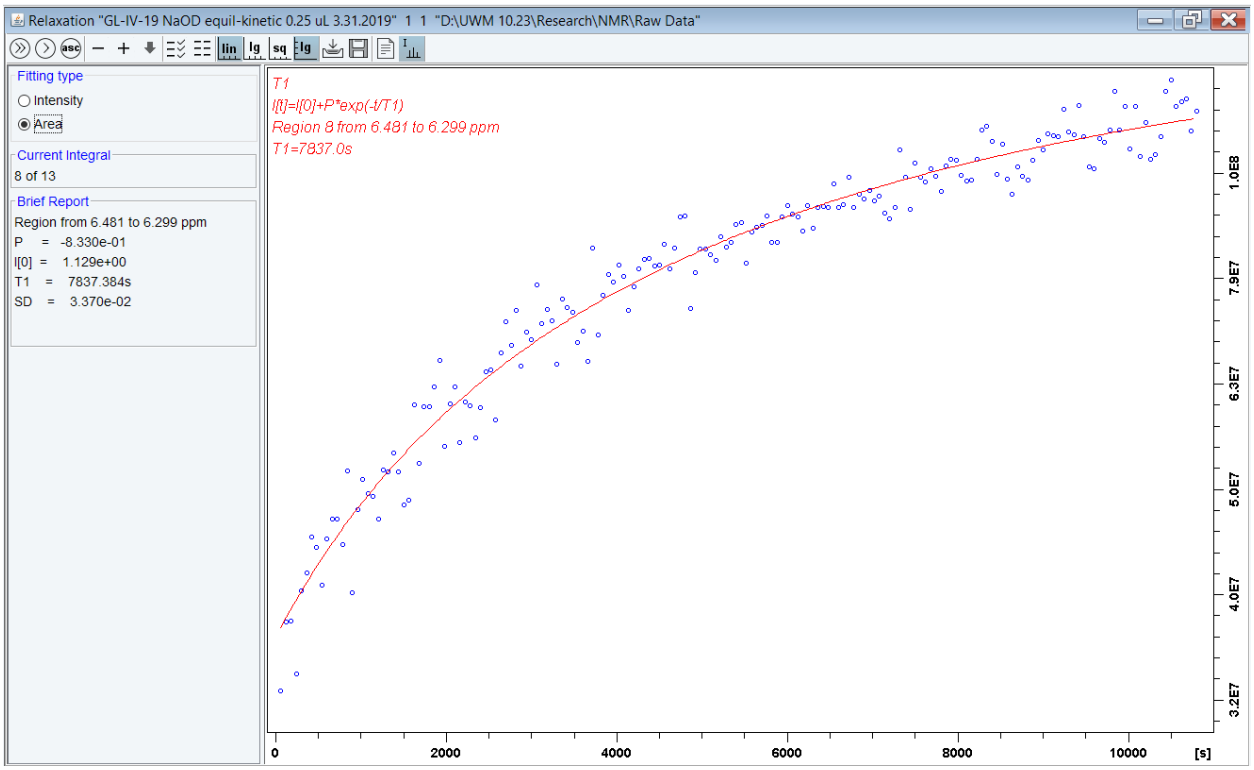
Relaxation "GL-IV-19 NaOD equil-kinetic 0.25 uL 3.31.2019" 1 1 "D:\UWM 10.23\Research\NMR\Raw Data"
Fitting type
Intensity
Area
Current Integral
8 of 13
Brief Report
Region from 6.481 to 6.299 ppm
P = -8.330e-01
I[0] = 1.129e+00
T1 = 7837.384s
SD = 3.370e-02
T1
I[t]=I[0]+P*exp(-t/T1)
Region 8 from 6.481 to 6.299 ppm
T1=7837.0s
1.0E8
7.9E7
6.3E7
5.0E7
4.0E7
3.2E7
0
2000
4000
6000
8000
10000
[s]

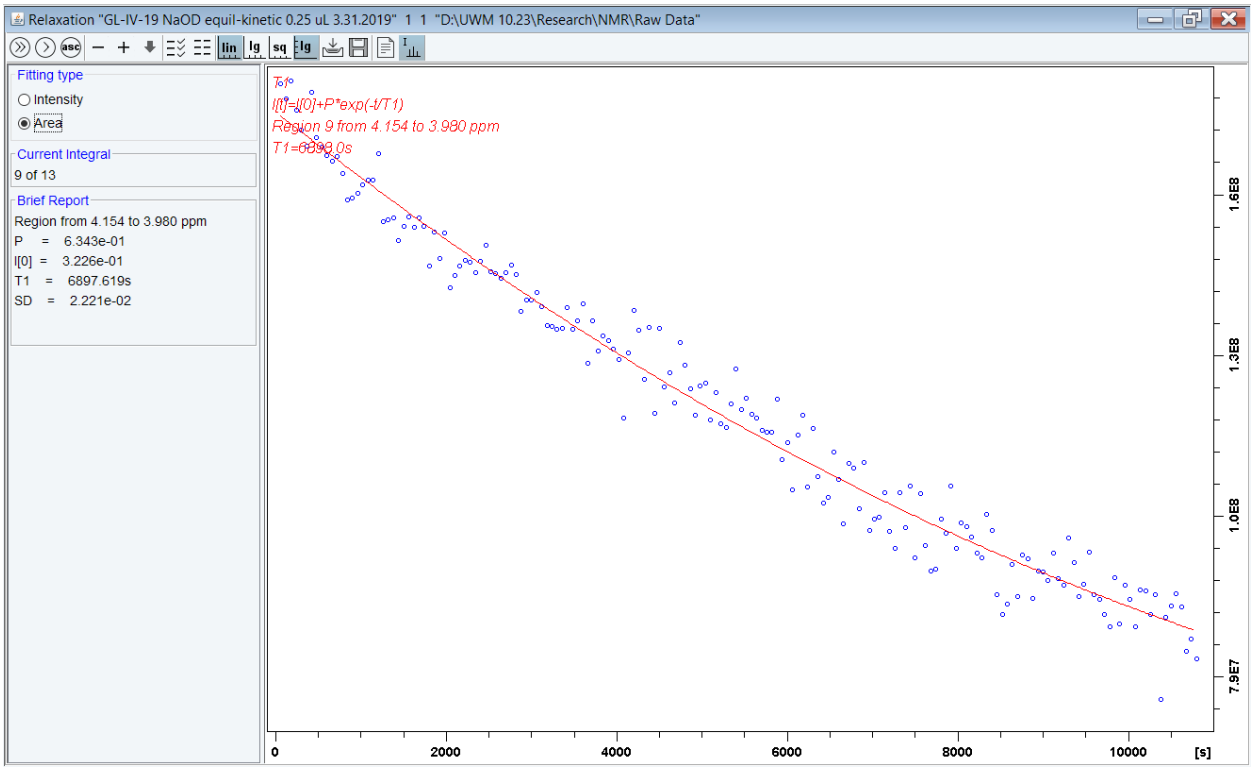
Relaxation "GL-IV-19 NaOD equil-kinetic 0.25 uL 3.31.2019" 1 1 "D:\UWM 10.23\Research\NMR\Raw Data"
Fitting type
Intensity
Area
Current Integral
9 of 13
Brief Report
Region from 4.154 to 3.980 ppm
P = 6.343e-01
I[0] = 3.226e-01
T1 = 6897.619s
SD = 2.221e-02
T1
I[t]=I[0]+P*exp(-t/T1)
Region 9 from 4.154 to 3.980 ppm
T1=6898.0s
1.6E8
1.3E8
1.0E8
7.9E7
0
2000
4000
6000
8000
10000
[s]

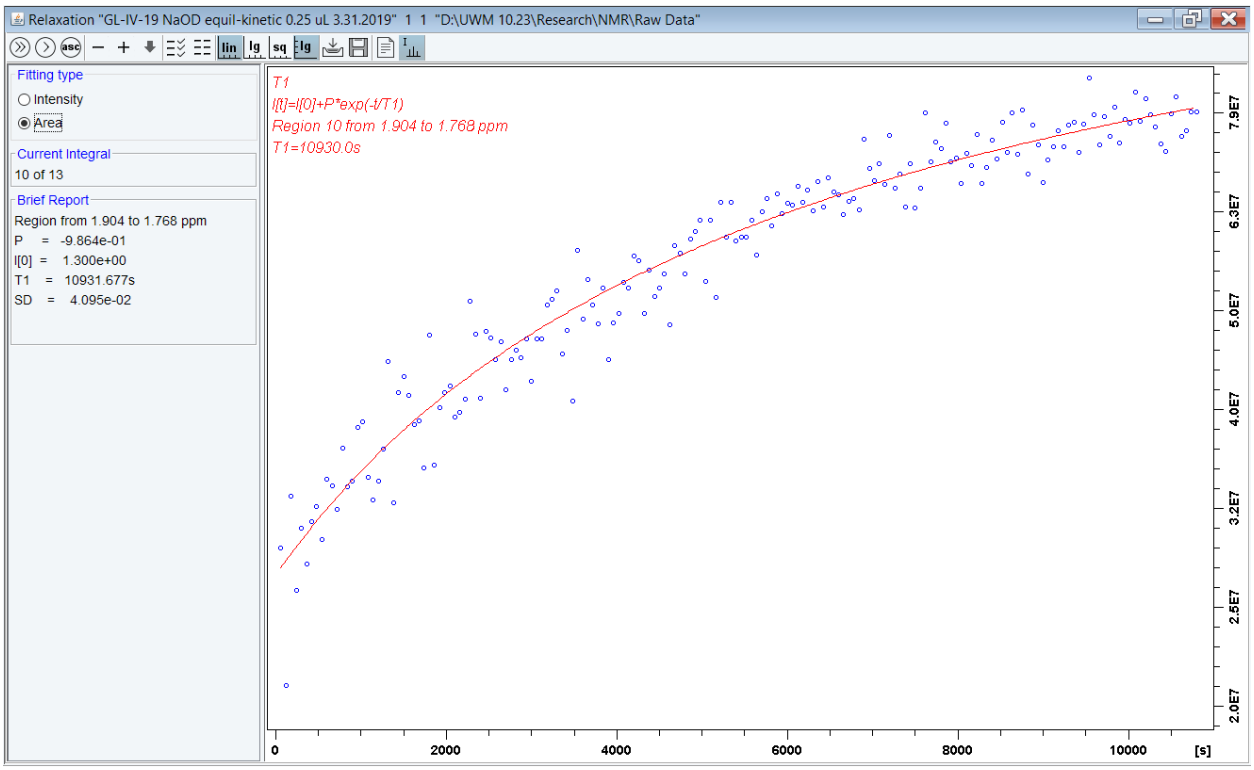
Relaxation "GL-IV-19 NaOD equil-kinetic 0.25 uL 3.31.2019" 1 1 "D:\UWM 10.23\Research\NMR\Raw Data"
Fitting type
Intensity
Area
Current Integral
10 of 13
Brief Report
Region from 1.904 to 1.768 ppm
P = -9.864e-01
I[0] = 1.300e+00
T1 = 10931.677s
SD = 4.095e-02
T1
I[t]=I[0]+P*exp(-t/T1)
Region 10 from 1.904 to 1.768 ppm
T1=10930.0s
7.9E7
6.3E7
5.0E7
4.0E7
3.2E7
2.5E7
2.0E7
0
2000
4000
6000
8000
10000
[s]

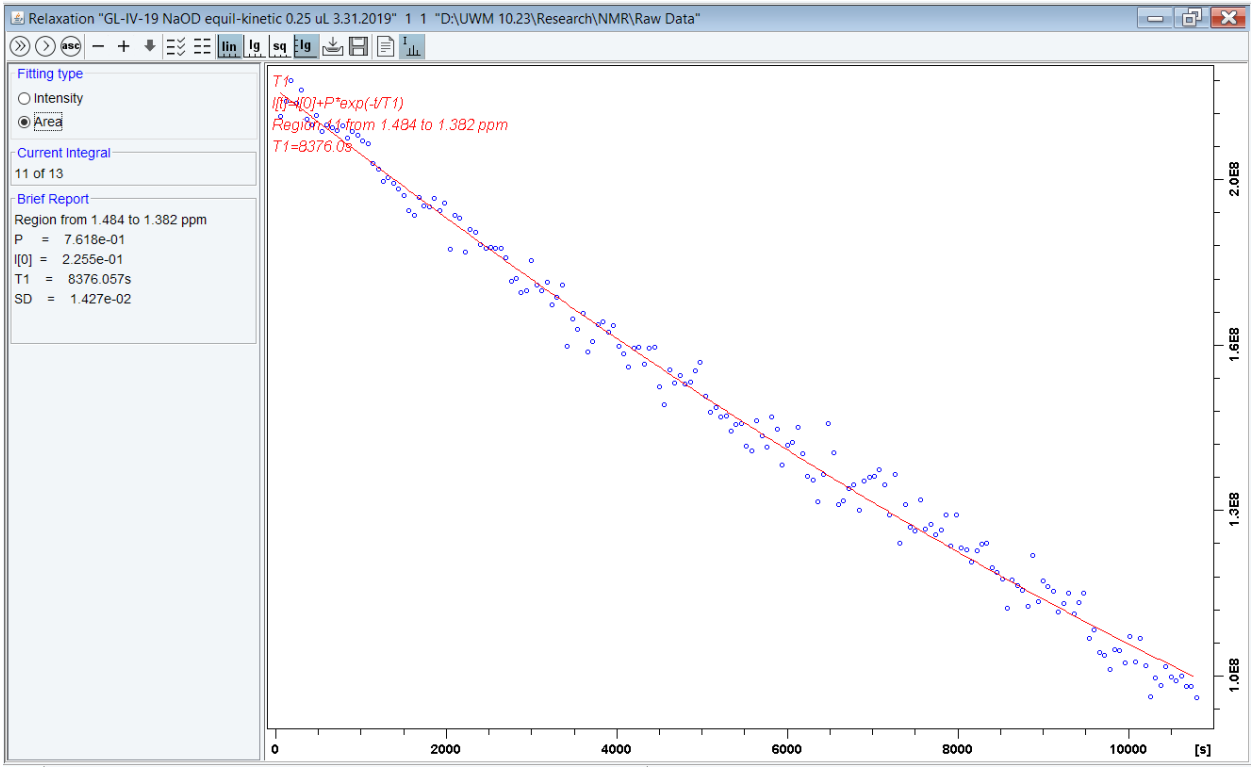
Relaxation "GL-IV-19 NaOD equil-kinetic 0.25 uL 3.31.2019" 1 1 "D:\UWM 10.23\Research\NMR\Raw Data"
Fitting type
Intensity
Area
Current Integral
11 of 13
Brief Report
Region from 1.484 to 1.382 ppm
P = 7.618e-01
I[0] = 2.255e-01
T1 = 8376.057s
SD = 1.427e-02
T1
I[t]=I[0]+P*exp(-t/T1)
Region 11 from 1.484 to 1.382 ppm
T1=8376.0s
2.0E8
1.6E8
1.3E8
1.0E8
0
2000
4000
6000
8000
10000
[s]

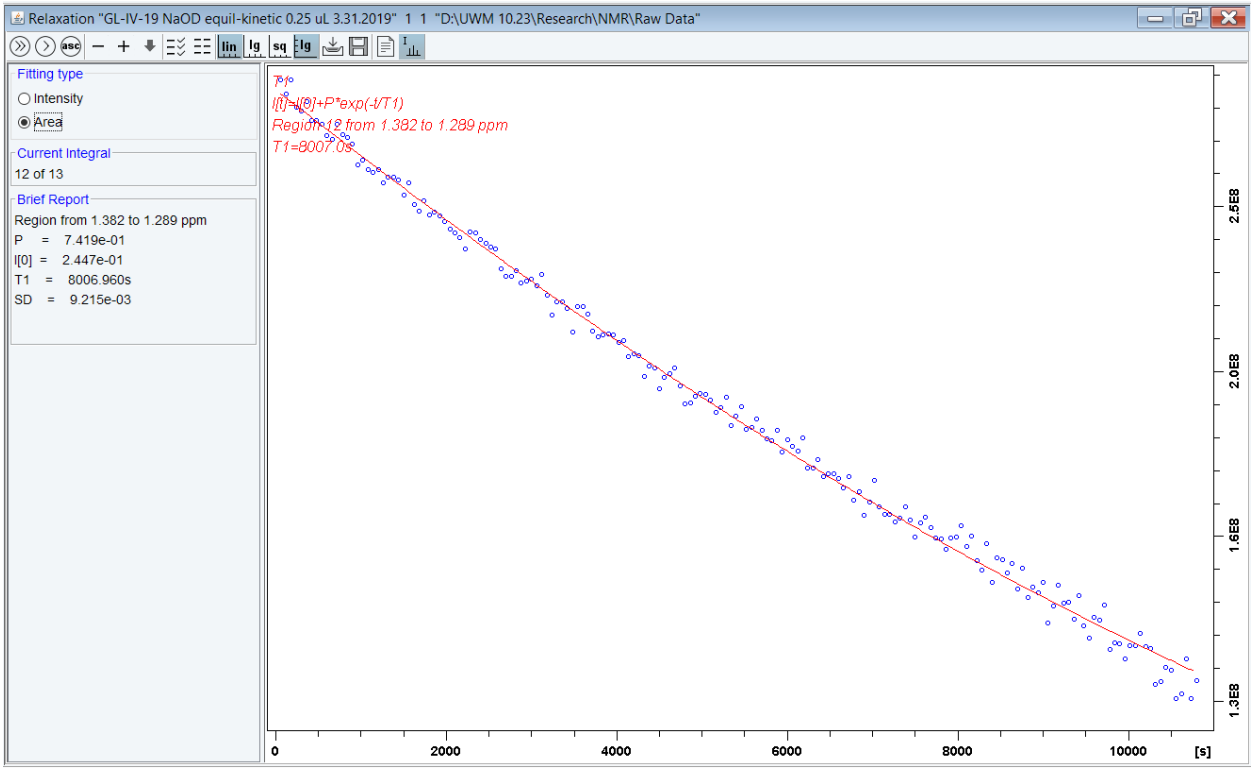
Relaxation "GL-IV-19 NaOD equil-kinetic 0.25 uL 3.31.2019" 1 1 "D:\UWM 10.23\Research\NMR\Raw Data"
Fitting type
Intensity
Area
Current Integral
12 of 13
Brief Report
Region from 1.382 to 1.289 ppm
P = 7.419e-01
I[0] = 2.447e-01
T1 = 8006.960s
SD = 9.215e-03
T1
I[t]=I[0]+P*exp(-t/T1)
Region 12 from 1.382 to 1.289 ppm
T1=8007.0s
2.5E8
2.0E8
1.6E8
1.3E8
0
2000
4000
6000
8000
10000
[s]

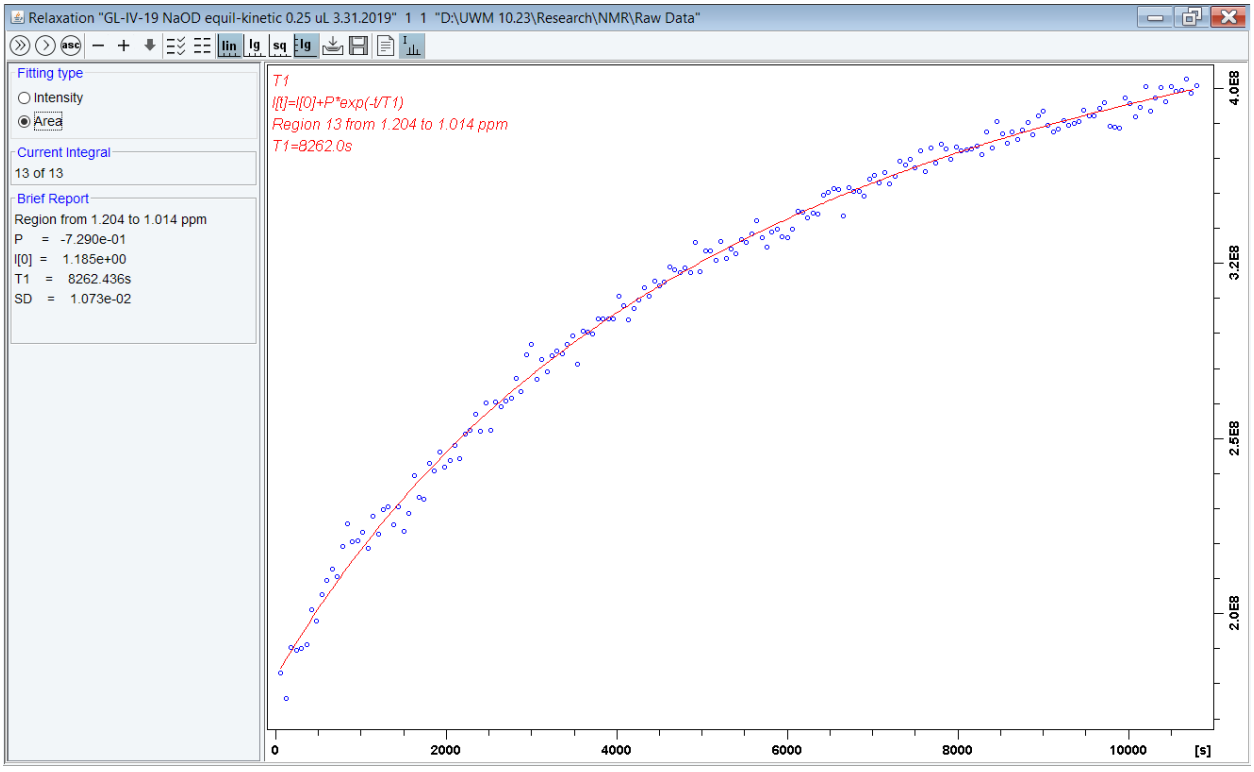
Relaxation "GL-IV-19 NaOD equil-kinetic 0.25 uL 3.31.2019" 1 1 "D:\UWM 10.23\Research\NMR\Raw Data"
Fitting type
Intensity
Area
Current Integral
13 of 13
Brief Report
Region from 1.204 to 1.014 ppm
P = -7.290e-01
I[0] = 1.185e+00
T1 = 8262.436s
SD = 1.073e-02
T1
I[t]=I[0]+P*exp(-t/T1)
Region 13 from 1.204 to 1.014 ppm
T1=8262.0s
4.0E8
3.2E8
2.5E8
2.0E8
0
2000
4000
6000
8000
10000
[s]

8. The intensity (lg)-time curve of NaOD addition at pH = 8

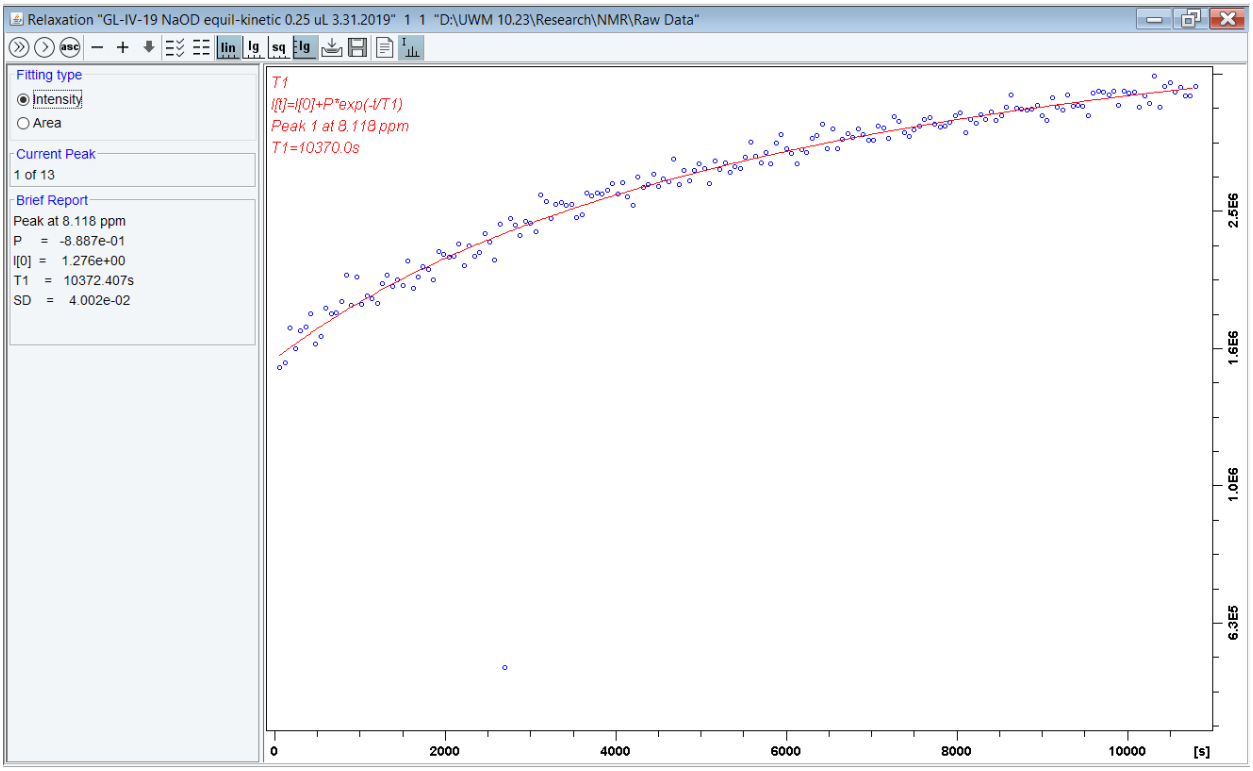

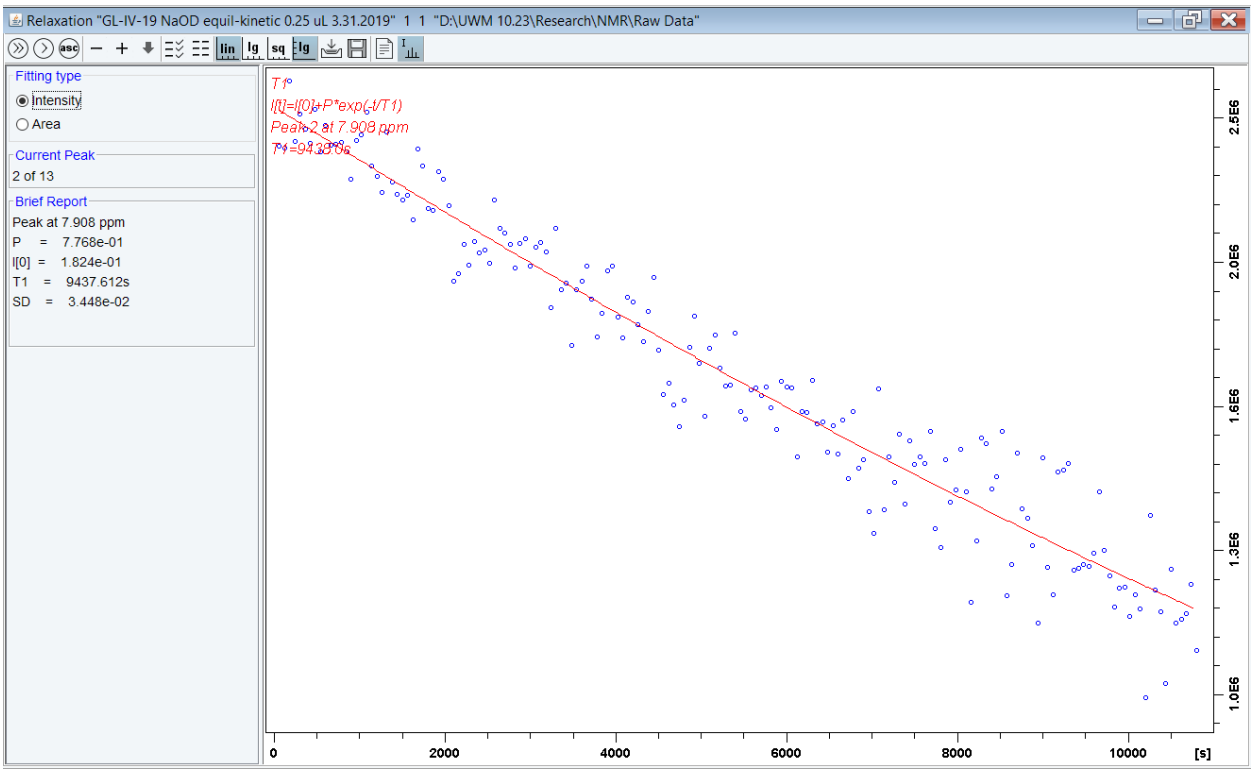

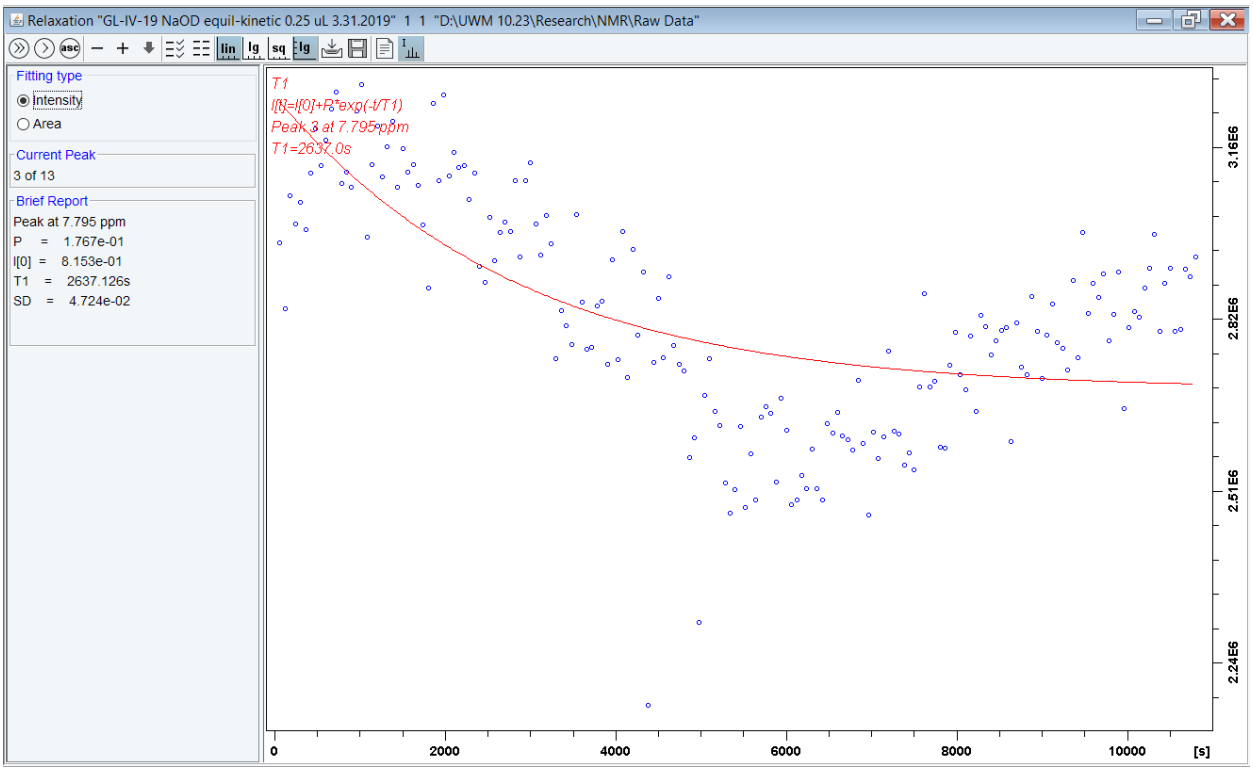
Relaxation "GL-IV-19 NaOD equil-kinetic 0.25 uL 3.31.2019" 1 1 "D:\UWM 10.23\Research\NMR\Raw Data"
Fitting type
Intensity
Area
Current Peak
3 of 13
Brief Report
Peak at 7.795 ppm
P = 1.767e-01
I[0] = 8.153e-01
T1 = 2637.126s
SD = 4.724e-02
T1
I[t]=I[0]+P*exp(-t/T1)
Peak 3 at 7.795 ppm
T1=2637.0s
3.16E6
2.82E6
2.51E6
2.24E6
0
2000
4000
6000
8000
10000
[s]

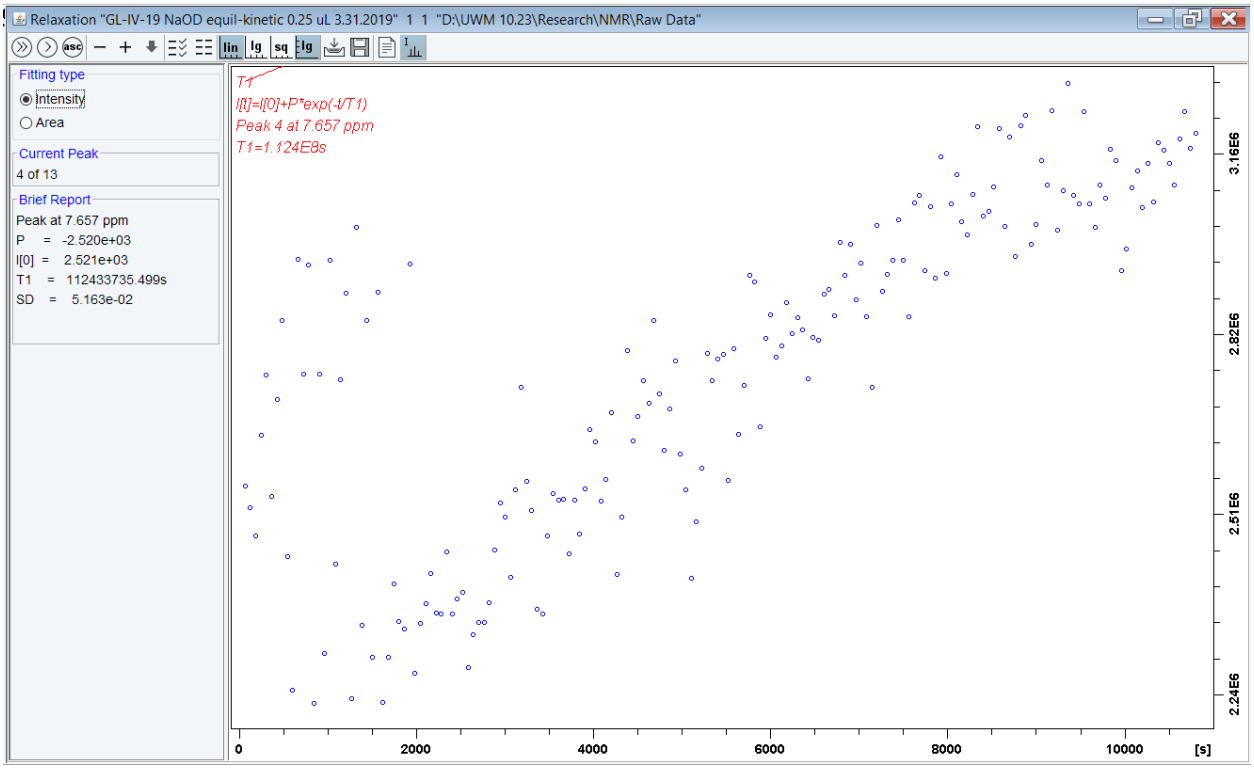
Relaxation "GL-IV-19 NaOD equil-kinetic 0.25 uL 3.31.2019" 1 1 "D:\UWM 10.23\Research\NMR\Raw Data"
Fitting type
Intensity
Area
Current Peak
4 of 13
Brief Report
Peak at 7.657 ppm
P = -2.520e+03
I[0] = 2.521e+03
T1 = 112433735.499s
SD = 5.163e-02
T1
I[t]=I[0]+P*exp(-t/T1)
Peak 4 at 7.657 ppm
T1=1.124E8s
3.16E6
2.82E6
2.51E6
2.24E6
0
2000
4000
6000
8000
10000
[s]

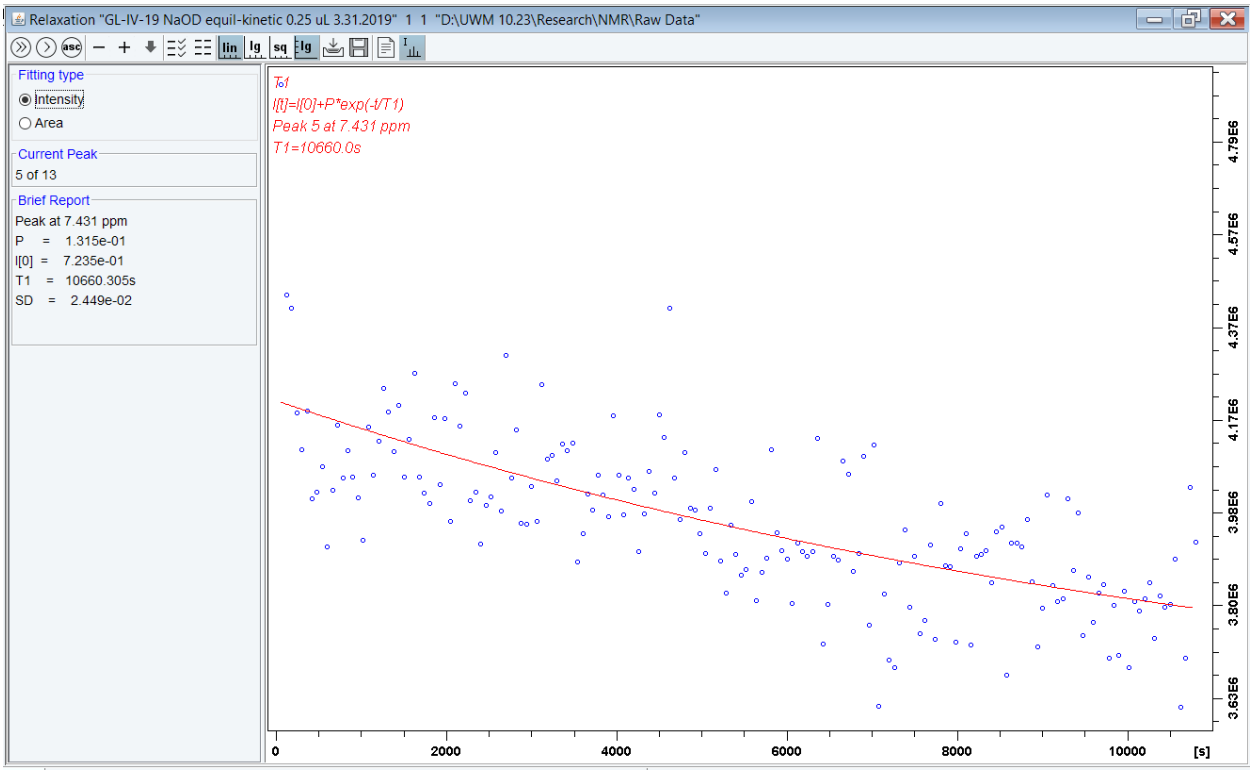
Relaxation "GL-IV-19 NaOD equil-kinetic 0.25 uL 3.31.2019" 1 1 "D:\UWM 10.23\Research\NMR\Raw Data"
Fitting type
Intensity
Area
Current Peak
5 of 13
Brief Report
Peak at 7.431 ppm
P = 1.315e-01
I[0] = 7.235e-01
T1 = 10660.305s
SD = 2.449e-02
T1
I[t]=I[0]+P*exp(-t/T1)
Peak 5 at 7.431 ppm
T1=10660.0s
4.79E6
4.57E6
4.37E6
4.17E6
3.98E6
3.80E6
3.63E6
0
2000
4000
6000
8000
10000
[s]

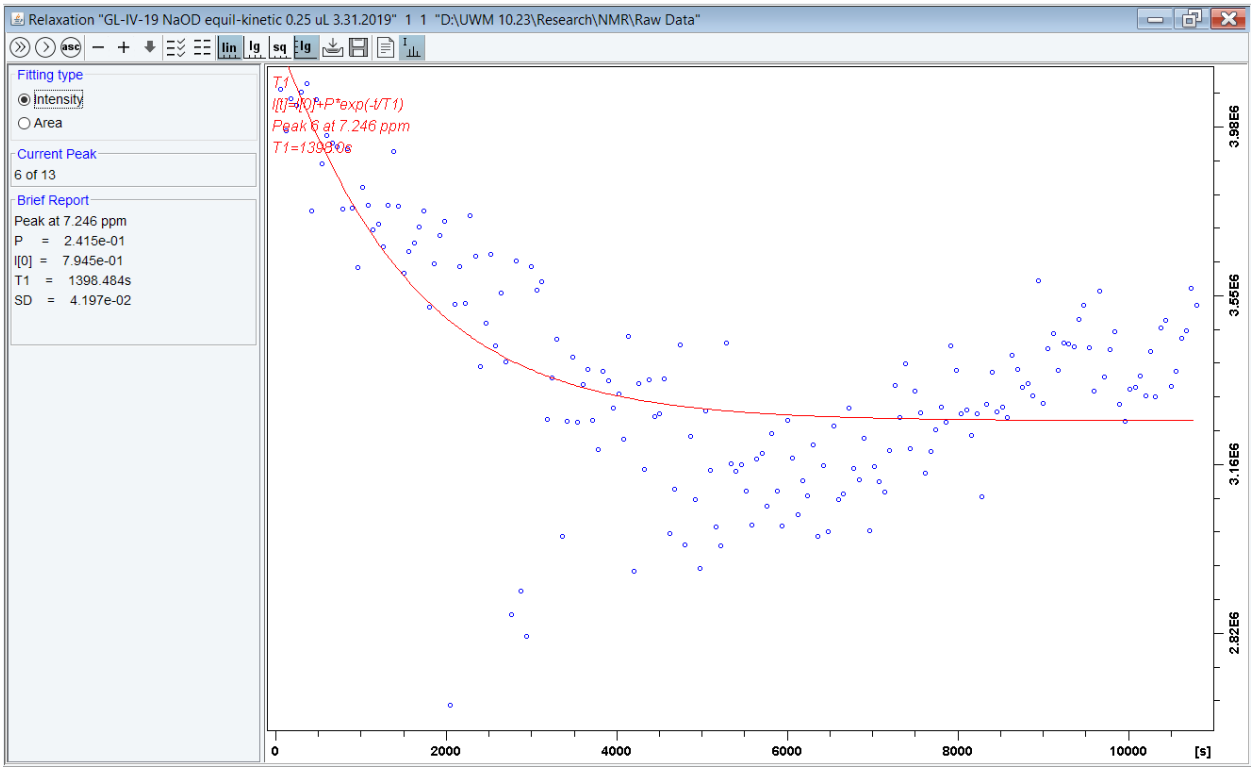
Relaxation "GL-IV-19 NaOD equil-kinetic 0.25 uL 3.31.2019" 1 1 "D:\UWM 10.23\Research\NMR\Raw Data"
Fitting type
Intensity
Area
Current Peak
6 of 13
Brief Report
Peak at 7.246 ppm
P = 2.415e-01
I[0] = 7.945e-01
T1 = 1398.484s
SD = 4.197e-02
T1
I[t]=I[0]+P*exp(-t/T1)
Peak 6 at 7.246 ppm
T1=1398.0s
3.98E6
3.55E6
3.16E6
2.82E6
0
2000
4000
6000
8000
10000
[s]

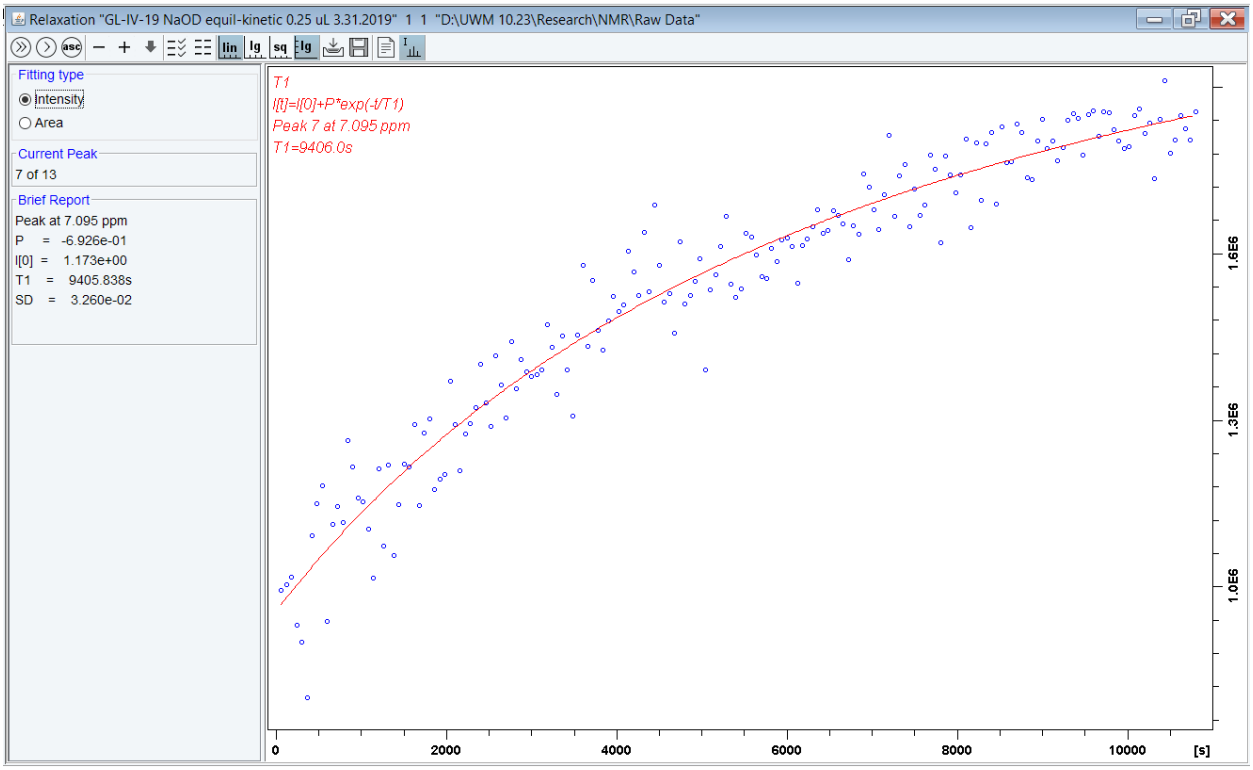
Relaxation "GL-IV-19 NaOD equil-kinetic 0.25 uL 3.31.2019" 1 1 "D:\UWM 10.23\Research\NMR\Raw Data"
Fitting type
Intensity
Area
Current Peak
7 of 13
Brief Report
Peak at 7.095 ppm
P = -6.926e-01
I[0] = 1.173e+00
T1 = 9405.838s
SD = 3.260e-02
T1
I[t]=I[0]+P*exp(-t/T1)
Peak 7 at 7.095 ppm
T1=9406.0s
1.6E6
1.3E6
1.0E6
0
2000
4000
6000
8000
10000
[s]

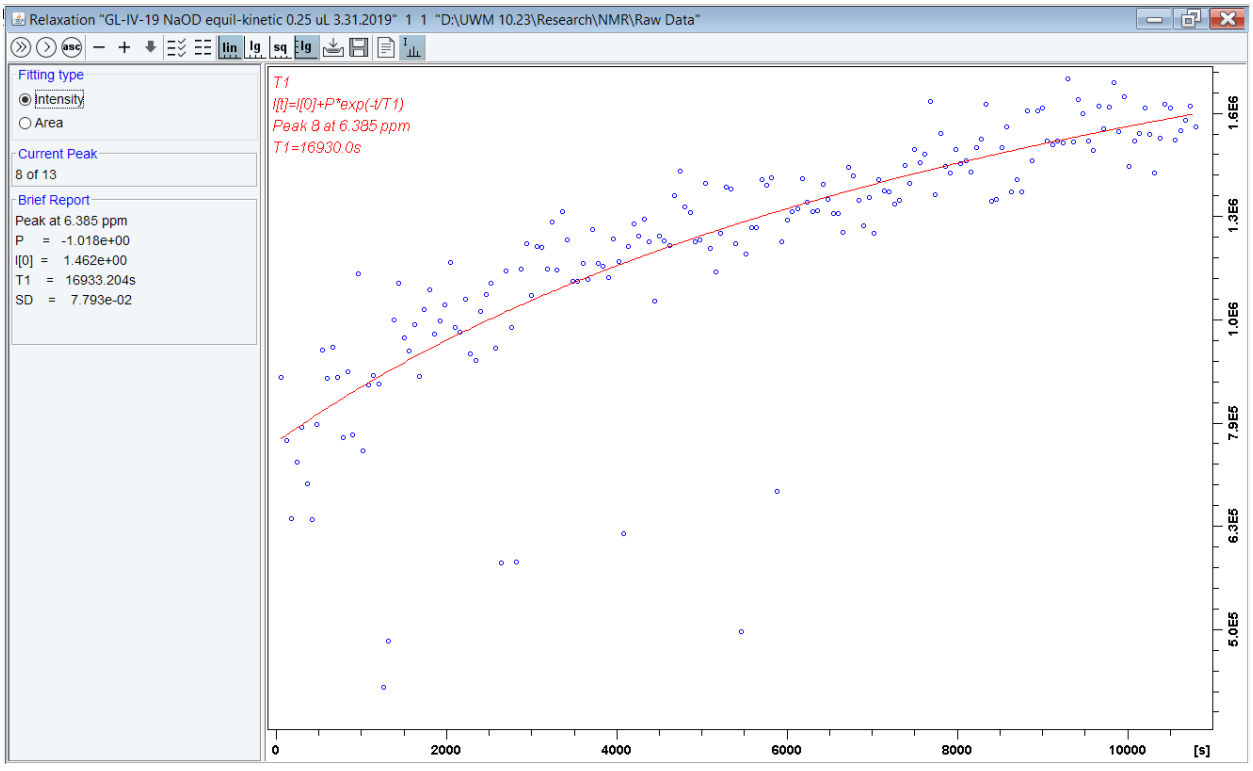
Relaxation "GL-IV-19 NaOD equil-kinetic 0.25 uL 3.31.2019" 1 1 "D:\UWM 10.23\Research\NMR\Raw Data"
Fitting type
Intensity
Area
Current Peak
8 of 13
Brief Report
Peak at 6.385 ppm
P = -1.018e+00
I[0] = 1.462e+00
T1 = 16933.204s
SD = 7.793e-02
T1
I[t]=I[0]+P*exp(-t/T1)
Peak 8 at 6.385 ppm
T1=16930.0s
1.6E6
1.3E6
1.0E6
7.9E5
6.3E5
5.0E5
0
2000
4000
6000
8000
10000
[s]

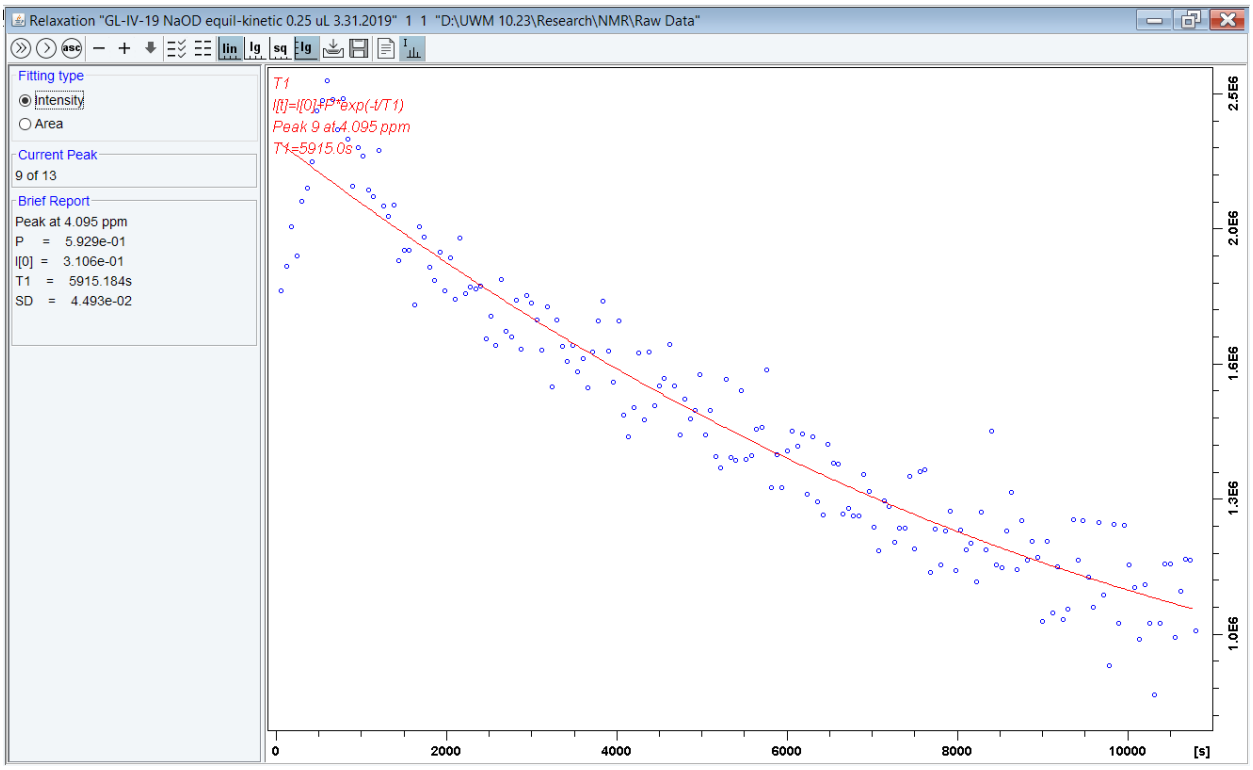
Relaxation "GL-IV-19 NaOD equil-kinetic 0.25 uL 3.31.2019" 1 1 "D:\UWM 10.23\Research\NMR\Raw Data"
Fitting type
Intensity
Area
Current Peak
9 of 13
Brief Report
Peak at 4.095 ppm
P = 5.929e-01
I[0] = 3.106e-01
T1 = 5915.184s
SD = 4.493e-02
T1
I[t]=I[0]+P*exp(-t/T1)
Peak 9 at 4.095 ppm
T1=5915.0s
2.5E6
2.0E6
1.6E6
1.3E6
1.0E6
0
2000
4000
6000
8000
10000
[s]

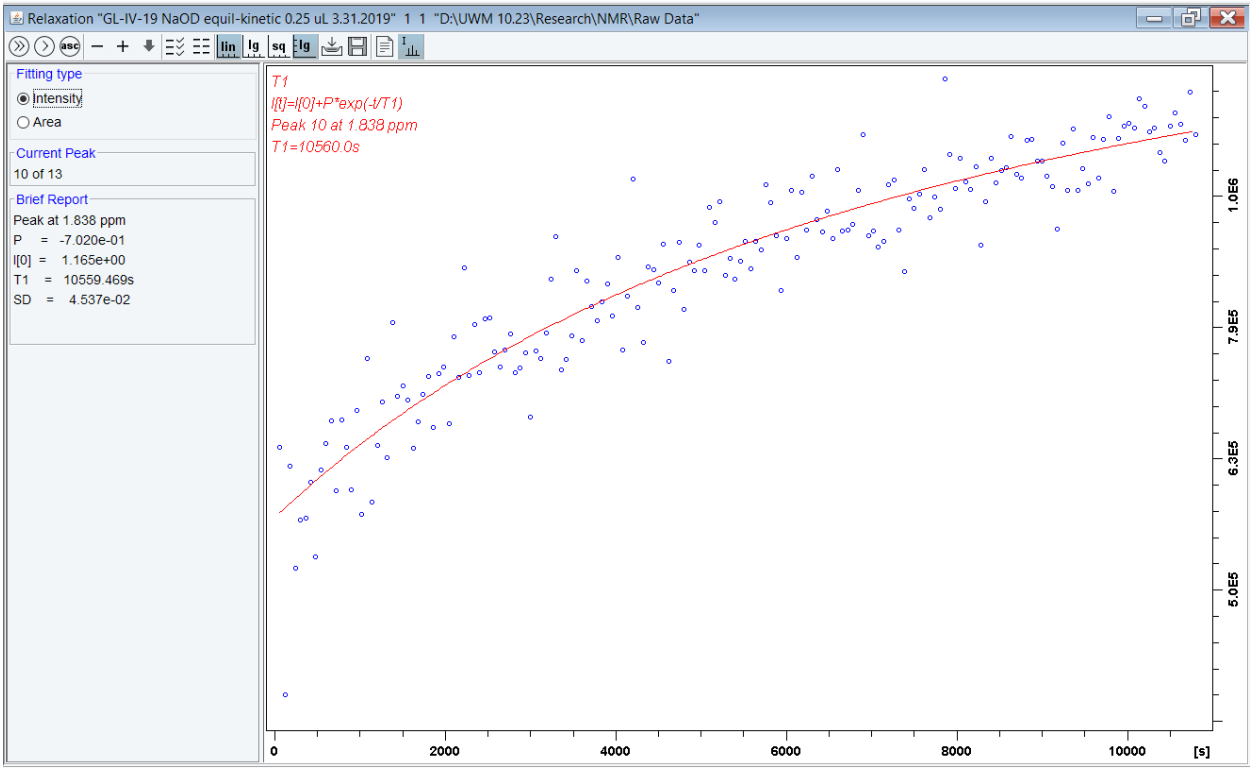
Relaxation "GL-IV-19 NaOD equil-kinetic 0.25 uL 3.31.2019" 1 1 "D:\UWM 10.23\Research\NMR\Raw Data"
Fitting type
Intensity
Area
Current Peak
10 of 13
Brief Report
Peak at 1.838 ppm
P = -7.020e-01
I[0] = 1.165e+00
T1 = 10559.469s
SD = 4.537e-02
T1
I[t]=I[0]+P*exp(-t/T1)
Peak 10 at 1.838 ppm
T1=10560.0s
1.0E6
7.9E5
6.3E5
5.0E5
0
2000
4000
6000
8000
10000
[s]

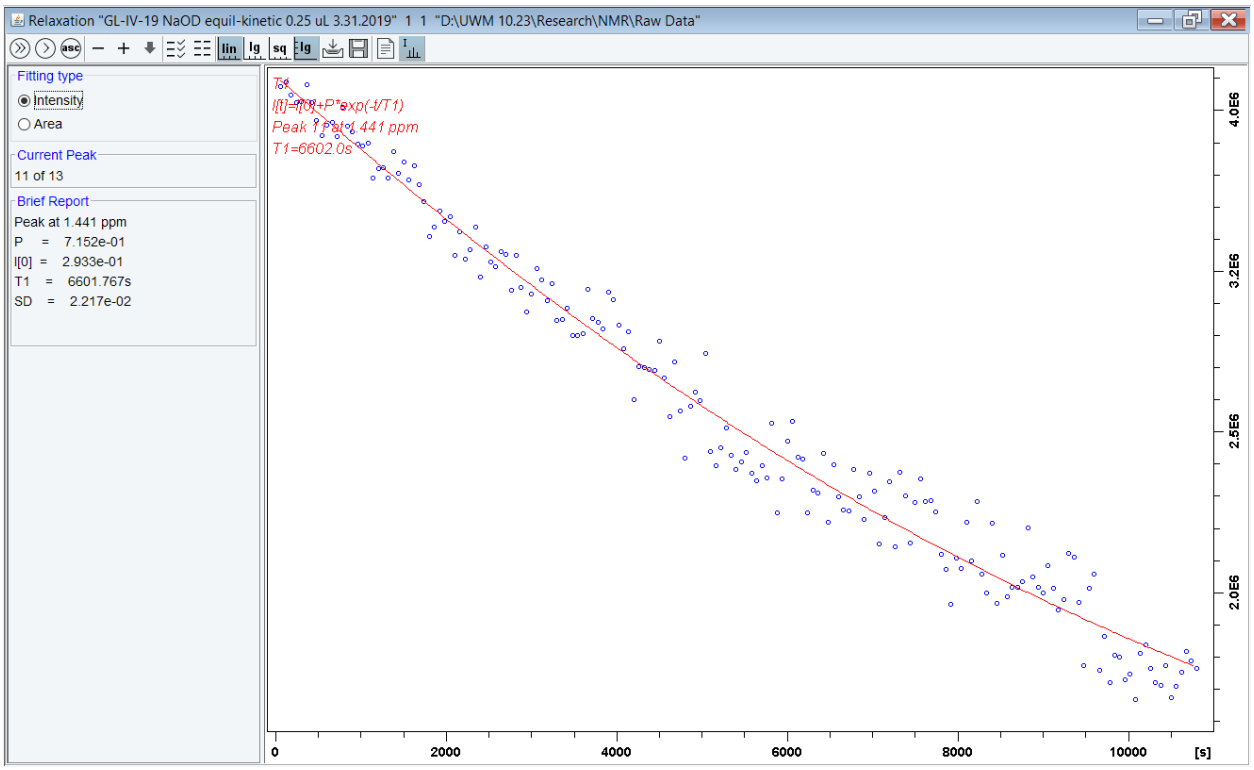
Relaxation "GL-IV-19 NaOD equil-kinetic 0.25 uL 3.31.2019" 1 1 "D:\UWM 10.23\Research\NMR\Raw Data"
Fitting type
Intensity
Area
Current Peak
11 of 13
Brief Report
Peak at 1.441 ppm
P = 7.152e-01
I[0] = 2.933e-01
T1 = 6601.767s
SD = 2.217e-02
T1
I[t]=I[0]+P*exp(-t/T1)
Peak 11 at 1.441 ppm
T1=6602.0s
4.0E6
3.2E6
2.5E6
2.0E6
0
2000
4000
6000
8000
10000
[s]

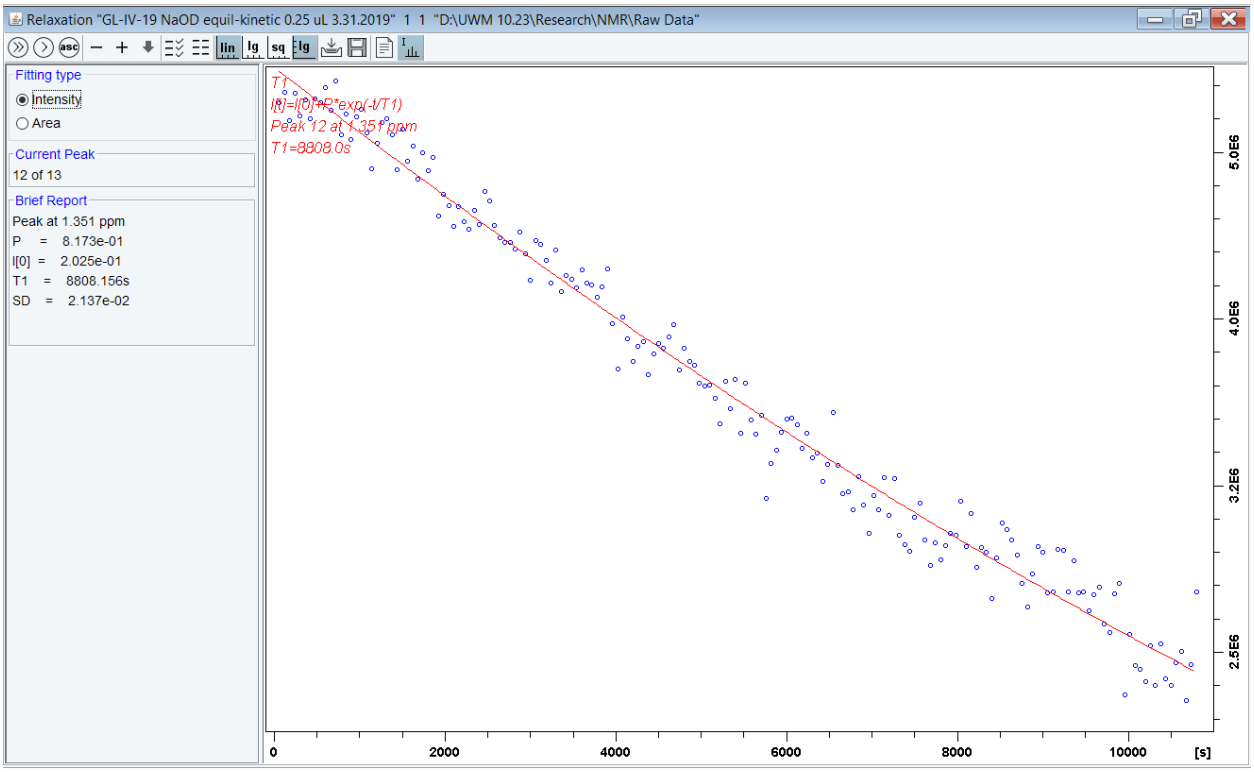
Relaxation "GL-IV-19 NaOD equil-kinetic 0.25 uL 3.31.2019" 1 1 "D:\UWM 10.23\Research\NMR\Raw Data"
Fitting type
Intensity
Area
Current Peak
12 of 13
Brief Report
Peak at 1.351 ppm
P = 8.173e-01
I[0] = 2.025e-01
T1 = 8808.156s
SD = 2.137e-02
T1
I[t]=I[0]+P*exp(-t/T1)
Peak 12 at 1.351 ppm
T1=8808.0s
5.0E6
4.0E6
3.2E6
2.5E6
0
2000
4000
6000
8000
10000
[s]

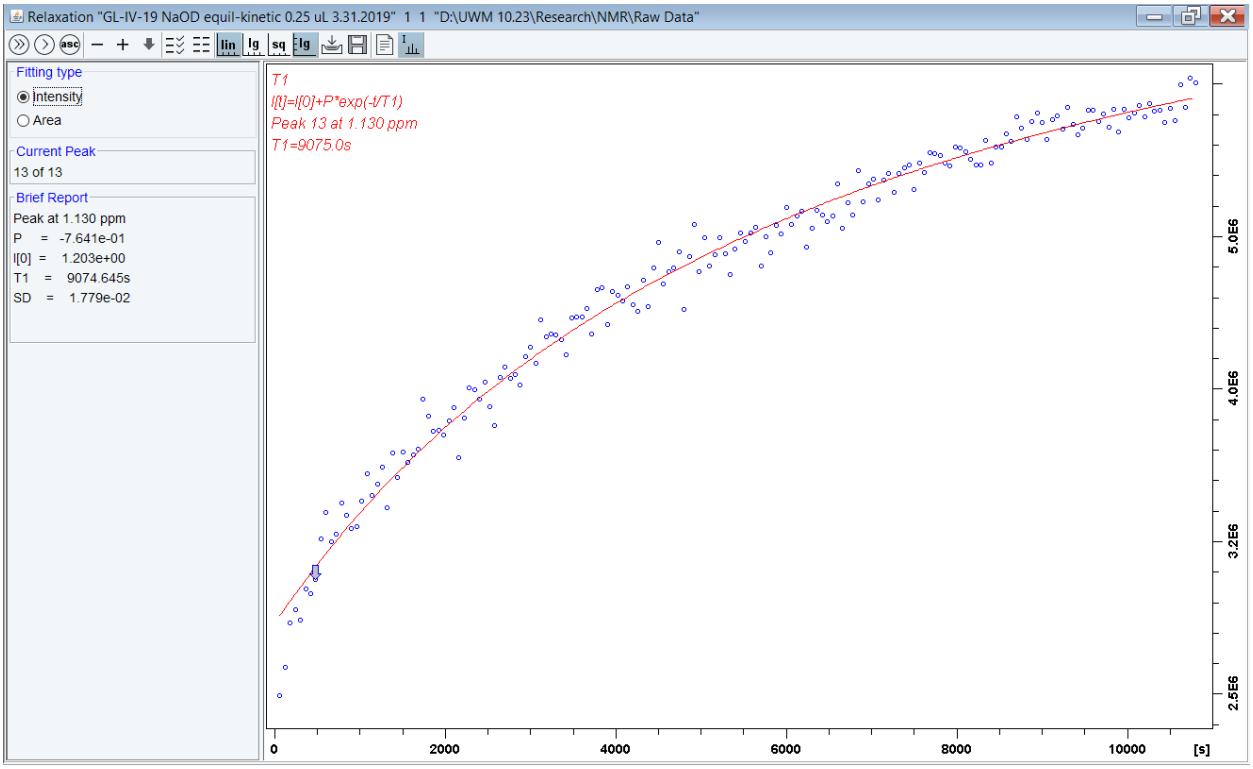
Relaxation "GL-IV-19 NaOD equil-kinetic 0.25 uL 3.31.2019" 1 1 "D:\UWM 10.23\Research\NMR\Raw Data"
Fitting type
Intensity
Area
Current Peak
13 of 13
Brief Report
Peak at 1.130 ppm
P = -7.641e-01
I[0] = 1.203e+00
T1 = 9074.645s
SD = 1.779e-02
T1
I[t]=I[0]+P*exp(-t/T1)
Peak 13 at 1.130 ppm
T1=9075.0s
5.0E6
4.0E6
3.2E6
2.5E6
0
2000
4000
6000
8000
10000
[s]

9. NaOD addition t1/2 list [area (lg)-time curve]

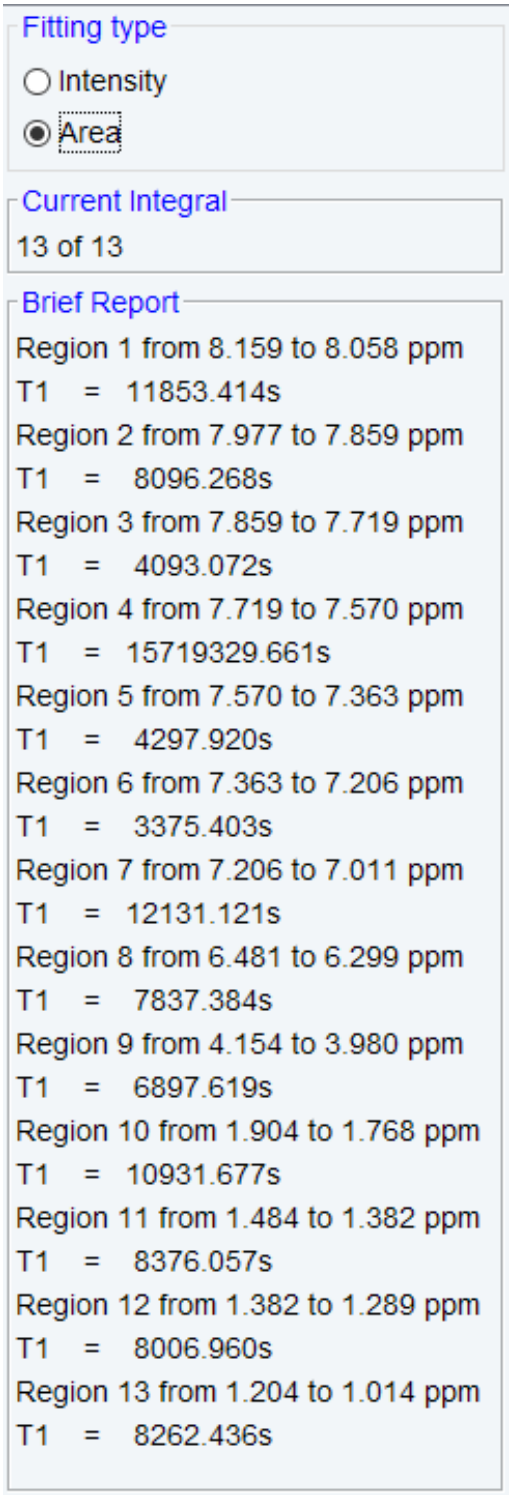

10. NaOD addition t1/2 list [intensity (lg)-time curve]

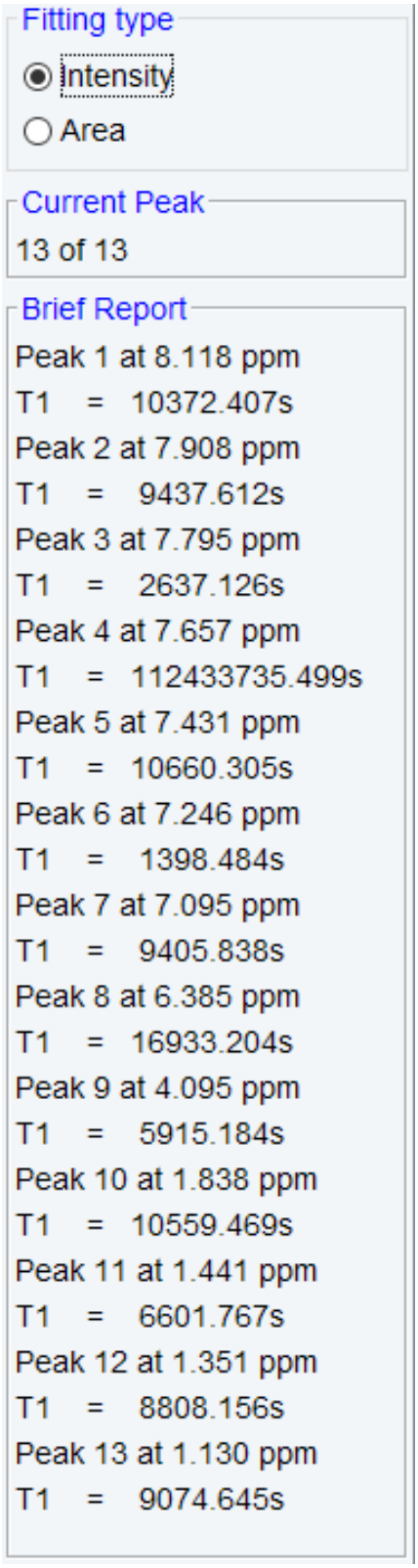

Appendix VIII: BZD-related drugs reduced methamphetamine-related behaviors in rats via BZD-induced TSPO activation

Our research has demonstrated that certain specific benzodiazepine-related drugs can powerfully reduce methamphetamine-related behaviors in rats, a finding which is likely related to benzodiazepine-induced TSPO activation. Other benzodiazepines may also activate TSPO and, therefore, may be useful in reducing methamphetamine–related behaviors. Structure-activity relationships suggest that benzodiazepines with a halogen moiety in the 4' position possess higher affinity for TSPO 1,2. Several such possible drug candidates are described in the table below. We are currently testing Ro5-4864 for efficacy against methamphetamine self-administration in rats. While dosing parameters for these compounds are not currently available, we expect that doses of these compounds will be similar to other clinically-relevant benzodiazepines (rats: 1-50 mg/kg, intraperitoneally; humans: 1-20 mg, orally).

Structural Position

	Structural Position						
Drug	**1**	**7**	**4'**	**2'**	**3**	**6'**	**4**
Ro5-5115	CH3	H	Cl	H	H	H	-
Ro5-5119	CH3	H	Cl	H	H	H	CH3
Ro5-5120	CH3	NO2	Cl	H	H	H	-
Ro5-5122	CH3	H	F	H	H	H	-
Ro5-5888	CH3	Cl	Cl	H	H	H	H
Ro5-4864	CH3	Cl	Cl	H	H	H	-
Ro5-6524	CH3	F	Cl	H	H	H	CH3
Ro5-6528	CH3	F	Cl	H	H	H	H
Ro5-6531	CH3	F	Cl	H	H	H	-
Ro5-6900	CH3	Cl	Cl	Cl	H	H	-
Ro5-6902	CH3	Cl	Cl	H	H	H	H
Ro5-6945	CH2CH=CH2	Cl	Cl	H	H	H	-
Ro5-6993	CH2CH3	Cl	Cl	H	H	H	-
Ro7-9277	CH3	Cl	Cl	H	OH	H	-

We propose that these compounds will decrease methamphetamine-seeking and methamphetamine-taking behaviors by decreasing the activation of brain circuits involved in methamphetamine craving. We also propose that these compounds will reduce other cognitive and behavioral effects of methamphetamine. Methamphetamine users often exhibit neurocognitive impairments and are more likely to engage in risky sexual behaviors that promote sexual-transmitted infections such as HIV 3–8. Chronic methamphetamine and HIV infection both induce a neuroinflammatory response characterized by a marked increase in TSPO binding and microglial activation9–17. TSPO activation is known to decrease sexual behavior and enhance memory functions, especially in animal models of neuroinflammation or neurodegeneration18–21. Therefore, targeting TSPO activation may decrease the neuroinflammatory response and alleviate the neurocognitive effects associated with prolonged methamphetamine use.

To summarize:

- We are proposing the development of compounds with the basic benzodiazepine structure, but with a halogen moiety (e.g., chlorine, fluorine) in the 4' position instead of hydrogen. These are referred to herein as TSPO compounds. Ro5-4864 is the prototype TSPO compound currently under investigation.
- TSPO compounds will reduce craving (seeking) for methamphetamine.
- TSPO compounds will halt and potentially reverse the cognitive deficits produced by methamphetamine.
- TSPO compounds will reduce the increased risky sexual behaviors induced by methamphetamine.
- By reducing the occurrence of methamphetamine-induced sexual behaviors, and by decreasing the neuroinflammatory response associated with HIV, TSPO compounds may reduce the consequences of HIV/AIDS in methamphetamine users.

REFERENCES

1. Wang, J. K., Taniguchi, T. & Spector, S. Structural requirements for the binding of benzodiazepines to their peripheral-type sites. Mol. Pharmacol. 25, 349–351 (1984).

2. Johnson, M. D., Wang, J. K., Morgan, J. I. & Spector, S. Downregulation of [3H]Ro5-4864 binding sites after exposure to peripheral-type benzodiazepines in vitro. J. Pharmacol. Exp. Ther. 238, 855–859 (1986).

3. Garvey, L. J. et al. Increased microglia activation in neurologically asymptomatic HIV-infected patients receiving effective ART. AIDS 28, 67–72 (2014).

4. Coughlin, J. M. et al. Regional brain distribution of translocator protein using [(11)C]DPA-713 PET in individuals infected with HIV. J. Neurovirol. 20, 219–32 (2014).

5. Semple, S. J., Patterson, T. L. & Grant, I. Motivations associated with methamphetamine use among HIV+ men who have sex with men. J. Subst. Abuse Treat. 22, 149–56 (2002).

6. Scott, J. C. et al. Neurocognitive effects of methamphetamine: a critical review and meta-analysis. Neuropsychol. Rev. 17, 275–97 (2007).

7. Rippeth, J. D. et al. Methamphetamine dependence increases risk of neuropsychological impairment in HIV infected persons. J. Int. Neuropsychol. Soc. 10, 1–14 (2004).

8. Cheng, W. S. et al. Increased drug use and STI risk with injection drug use among HIV-seronegative heterosexual methamphetamine users. J. Psychoactive Drugs 42, 11–8 (2010).

9. Thomas, D. M., Walker, P. D., Benjamins, J. A., Geddes, T. J. & Kuhn, D. M. Methamphetamine neurotoxicity in dopamine nerve endings of the striatum is associated with microglial activation. J. Pharmacol. Exp. Ther. 311, 1–7 (2004).

10. Cadet, J. L. & Krasnova, I. N. Interactions of HIV and methamphetamine: cellular and molecular mechanisms of toxicity potentiation. Neurotox. Res. 12, 181–204 (2007).

11. Hammoud, D. A. et al. Imaging glial cell activation with [11C]-R-PK11195 in patients with AIDS. J. Neurovirol. 11, 346–55 (2005).

12. Escubedo, E. et al. Microgliosis and down-regulation of adenosine transporter induced by methamphetamine in rats. Brain Res. 814, 120–6 (1998).

13. Thomas, D. M. et al. Microglial activation is a pharmacologically specific marker for the neurotoxic amphetamines. Neurosci. Lett. 367, 349–54 (2004).

14. Fantegrossi, W. E. et al. A comparison of the physiological, behavioral, neurochemical and microglial effects of methamphetamine and 3,4-methylenedioxymethamphetamine in the mouse. Neuroscience 151, 533–43 (2008).

15. Pubill, D. et al. Different glial response to methamphetamine- and methylenedioxymethamphetamine-induced neurotoxicity. Naunyn. Schmiedebergs. Arch. Pharmacol. 367, 490–9 (2003).

16. Sekine, Y. et al. Methamphetamine causes microglial activation in the brains of human abusers. J. Neurosci. 28, 5756–61 (2008).

17. Bae, K.-R., Shim, H.-J., Balu, D., Kim, S. R. & Yu, S.-W. Translocator protein 18 kDa negatively regulates inflammation in microglia. J. Neuroimmune Pharmacol. 9, 424–37 (2014).

18. Frye, C. A. & Petralia, S. M. Mitochondrial benzodiazepine receptors in the ventral tegmental area modulate sexual behaviour of cycling or hormone-primed hamsters. J. Neuroendocrinol. 15, 677–86 (2003).

19. Freeman, F. M. & Young, I. G. The mitochondrial benzodiazepine receptor and avoidance learning in the day-old chick. Pharmacol. Biochem. Behav. 67, 355–62 (2000).

20. Holmes, P. V & Drugan, R. C. Differential effects of anxiogenic central and peripheral benzodiazepine receptor ligands in tests of learning and memory. Psychopharmacology (Berl). 104, 249–54 (1991).

21. Petralia, S. M. & Frye, C. A. In the ventral tegmental area picrotoxin blocks FGIN 1-27-induced increases in sexual behavior of rats and hamsters. Psychopharmacology (Berl). 178, 174–82 (2005).

Other classes of drugs which may potentiate the actions of TSPO compounds when used in combination:

1. Agonists (activators) of potassium-chloride co-transporter 2 (KCC2) – These compounds activate the chloride extrusion pump in neurons (KCC2) to modify the driving force for chloride ions across the neuronal membrane. These agonists enhance the activity of other GABAergic drugs, including neurosteroids and benzodiazepines. The combination of KCC2 agonist and TSPO compound may enhance therapeutic effects by increasing the efficacy of downstream signaling events including GABA-gated chloride influx.1–4

a. Specific KCC2 activators may include CLP257 [(5Z)-5-[(4-Fluoro-2-hydroxyphenyl)methylene]-2-(tetrahydro-1-(2H)-pyridazinyl)-4(5H)-thiazolone] no other compounds identified.

2. Inhibitors (antagonists) of 20alpha-hydroxysteroid dehydrogenase (20alpha-HSD) – This enzyme is responsible for the catabolism of GABA-active neurosteroids. A combination of 20alpha-HSD inhibitor and TSPO compound may further enhance the levels of therapeutic neurosteroids by both enhancing the early steps of neurosteroid biosynthesis and preventing enzymatic breakdown by 20alpha-HSD.5–9

a. Specific 20alpha-HSD inhibitors may include STZ26 (D-homo-16-oxa-4-androstene-3,16alpha-dione), 3-chloro-5-phenylsalicylic acid or 3-bromo-5-phenylsalicylic acid.

Compound	Structure	CAS #
Ro5-5115	4'-chloro-1,3-dihydro-1-methyl-5-phenyl-2H-1,4-benzodiazepin-2-one	N/A
Ro5-5119	4'-chloro-1,3-dihydro-1,4-dimethyl-5-phenyl-2H-1,4-benzodiazepin-2-one	N/A
Ro5-5120	4'-chloro-1,3-dihydro-1-methyl-7-nitro-5-phenyl-2H-1,4-benzodiazepin-2-one	N/A
Ro5-5122	4'-Fluoro-1,3-dihydro-1-methyl-5-phenyl-2H-1,4-benzodiazepin-2-one	N/A
Ro5-5888	4',7-Dichloro-1,3,4-trihydro-1-methyl-5-phenyl-2H-1,4-benzodiazepin-2-one	N/A
Ro5-4864	4',7-Dichloro-1,3-dihydro-1-methyl-5-phenyl-2H-1,4-benzodiazepin-2-one	N/A
Ro5-6524	4'-Chloro-7-fluoro-1,3-dihydro-1,4-dimethyl-5-phenyl-2H-1,4-benzodiazepin-2-one	N/A
Ro5-6528	4'-Chloro-7-fluoro-1,3,4-trihydro-1,4-dimethyl-5-phenyl-2H-1,4-benzodiazepin-2-one	N/A
Ro5-6531	4'-Chloro-7-fluoro-1,3-dihydro-1-methyl-5-phenyl-2H-1,4-benzodiazepin-2-one	N/A
Ro5-6900	2',4',7-trichloro-1,3-dihydro-1-methyl-5-phenyl-2H-1,4-benzodiazepin-2-one	N/A
Ro5-6902	4',6',7-Trichloro-1,3,4-trihydro-1-methyl-5-phenyl-2H-1,4-benzodiazepin-2-one	N/A
Ro5-6945	1-allyl-4',7-dichloro-1,3-dihydro-5-phenyl-2H-1,4-benzodiazepin-2-one	N/A
Ro5-6993	4',7-dichloro-1-ethyl-1,3-dihydro-5-phenyl-2H-1,4-benzodiazepin-2-one	N/A
Ro7-9277	4',7-dichloro-1-hydro-3-hydroxy-1-methyl-5-phenyl-2H-1,4-benzodiazepin-2-one	N/A
Diazepam	7-chloro-1,3-dihydro-1-methyl-5-phenyl-2H-1,4-benzodiazepin-2-one	439-14-5
Oxazepam	7-chloro-1,3-dihydro-3-hydroxy-5-phenyl-2H-1,4-benzodiazepin-2-one	604-75-1
Alprazolam	8-chloro-1-methyl-5-phenyl-4H-(1,2,4)triazolo-1,4-benzodiazepine	28981-97-7

1. Kahle, K. T., Khanna, A., Clapham, D. E. & Woolf, C. J. Therapeutic Restoration of Spinal Inhibition via Druggable Enhancement of Potassium-Chloride Cotransporter KCC2-Mediated Chloride Extrusion in Peripheral Neuropathic Pain. JAMA Neurol. 71, 640–5 (2014).

2. Gagnon, M. et al. Chloride extrusion enhancers as novel therapeutics for neurological diseases. Nat. Med. 19, 1524–8 (2013).

3. Smith, S. S. The influence of stress at puberty on mood and learning: Role of the ??4???? GABAA receptor. Neuroscience 249, 192–213 (2013).

4. Löscher, W., Puskarjov, M. & Kaila, K. Cation-chloride cotransporters NKCC1 and KCC2 as potential targets for novel antiepileptic and antiepileptogenic treatments. Neuropharmacology 69, 62–74 (2013).

5. Higaki, Y. et al. Selective and potent inhibitors of human 20alpha-hydroxysteroid dehydrogenase (AKR1C1) that metabolizes neurosteroids derived from progesterone. Chem. Biol. Interact. 143-144, 503–513 (2003).

6. Dhagat, U., Endo, S., Sumii, R., Hara, A. & El-Kabbani, O. Selectivity determinants of inhibitor binding to human 20alpha-hydroxysteroid dehydrogenase: crystal structure of the

enzyme in ternary complex with coenzyme and the potent inhibitor 3,5-dichlorosalicylic acid. J. Med. Chem. 51, 4844–8 (2008).

7. Endo, S. et al. Substrate specificity and inhibitor sensitivity of rabbit 20α-hydroxysteroid dehydrogenase. Biol. Pharm. Bull. 36, 1514–8 (2013).

8. Yoshida, S., Shiota, K., Nishihara, M. & Takahashi, M. A novel steroid inhibitor for a rat 20alpha-hydroxysteroid dehydrogenase isozyme. Biol. Reprod. 57, 1433–7 (1997).

9. Usami, N. et al. Substrate specificity of human 3(20)alpha-hydroxysteroid dehydrogenase for neurosteroids and its inhibition by benzodiazepines. Biol. Pharm. Bull. 25, 441–445 (2002).

1. 2016 poster (Ro5-4846)

Control/Tracking Number: 2016-S-13783-SfN
Activity: Scientific Abstract
Current Date/Time: 5/5/2016 1:46:06 PM
Effects of Ro5-4864 on methamphetamine self-administration in male and female rats
AUTHOR BLOCK: *G. F. GUERIN[1], S. M. HAROLD[1], S. R. PORTER[1], C. D. SCHMOUTZ[1], G. LI[2], J. M. COOK[2], N. E. GOEDERS[1];
[1]LSUHSC-S, Shreveport, LA; [2]Univ. of Wisconsin-Milwaukee, Milwaukee, WI
Abstract:
Methamphetamine abuse continues to be a serious and growing problem with no approved treatment. We have previously demonstrated differential effects of benzodiazepines on various methamphetamine-related behaviors based upon their relative affinities for either the "central" benzodiazepine (BZD) binding site associated with the $GABA_A$ receptor or the "peripheral" BZD binding site associated with the translocator protein of 18kDa (TSPO). Specifically, oxazepam, which binds to both receptors, decreases methamphetamine self-administration, conditioned place preference and drug discrimination. In contrast, alprazolam, which binds only to the central BZD binding site, augments the effects of methamphetamine at certain dose combinations. The current experiment was designed to investigate the effects of Ro5-4864 on methamphetamine self-administration in rats. Ro5-4864 is a potent selective ligand for TSPO that does not bind to the $GABA_A$ receptor complex and lacks typical "central" benzodiazepine-like effects. Male and female Wistar rats were trained to self-administer methamphetamine (0.05 mg/kg/infusion) during daily two-hour sessions. After responding stabilized, several doses of Ro5-4864 were administered intraperitoneally 30 minutes before the start of the sessions. Self-administration was dose dependently decreased in both males and females; however, female rats were more sensitive to these effects. The TSPO receptor has an integral role in the ability of certain benzodiazepines to decrease methamphetamine self-administration and could be important in developing novel treatments for stimulant addiction.
Presentation Preference (Complete): Poster Only
Nanosymposium Information (Complete):
Theme and Topic (Complete): G.08.j. Amphetamines: Reinforcement, seeking, and reinstatement ; G.08.l. Amphetamines: Neural mechanisms of addiction
Linking Group (Complete): None selected
Keyword (Complete): METHAMPHETAMINE ; SELF ADMINISTRATION ; BENZODIAZEPINE
Support (Complete): No
Special Requests (Complete):
Would you be interested in being considered for a dynamic poster?: No, I am not interested in presenting a Dynamic Poster
Is the submitting author of this abstract also a senior author?: No
Is the first (presenting) author of this abstract a high school or undergraduate student?: None
Religious Conflict?: No Religious Conflict
Additional Conflict?: No

Status: Complete

Effects of Ro5-4864 on methamphetamine self-administration in male and female rats

G. F. Guerin[1], S. M. Harold[1], S. R. Porter[1], C. D. Schmoutz[1],
G. Li[2], J. M. Cook[2], N. E. Goeders[1]

[1]*Pharmacology, Toxicology & Neuroscience, LSU Health Sciences Center, Shreveport LA*
[2]*Chemistry & Biochemistry, University of Wisconsin-Milwaukee*

457.05

LSU Health Sciences Center

INTRODUCTION

The misuse of methamphetamine continues to be a serious and growing problem with no approved treatment. We have previously demonstrated differential effects of benzodiazepines on various methamphetamine-related behaviors based upon their relative affinities for either the "central" benzodiazepine (BZD) binding site associated with the $GABA_A$ receptor or the "peripheral" BZD binding site associated with the translocator protein of 18kDa (TSPO). Specifically, oxazepam, which binds to both receptors, decreases methamphetamine self-administration, conditioned place preference and drug discrimination. In contrast, alprazolam, which binds only to the central BZD binding site, augments the effects of methamphetamine at certain dose combinations. The current experiment was designed to investigate the effects of Ro5-4864 on methamphetamine self-administration in rats. Ro5-4864 is a potent selective ligand for TSPO that does not bind to the $GABA_A$ receptor complex and lacks typical "central" benzodiazepine-like effects. Two other TSPO ligands, PK11195 and Ro7-9277, were also tested. The TSPO receptor has an integral role in the ability of certain drugs to decrease methamphetamine reinforcement, suggesting this mechanism in the development of novel treatments for methamphetamine use disorder.

METHAMPHETAMINE SELF-ADMINISTRATION

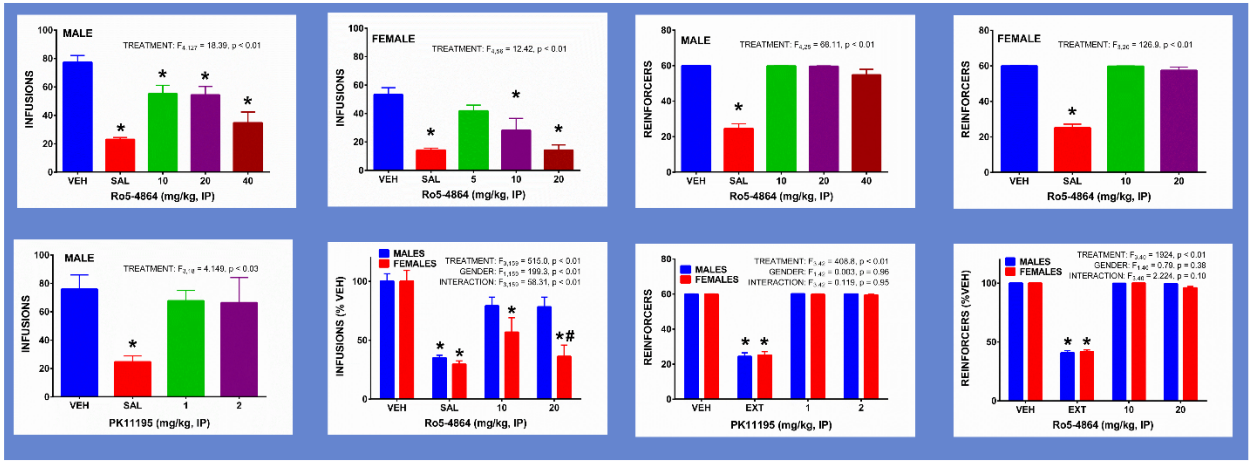

FOOD SELF-ADMINISTRATION

METHODS

Animals: Male and female Wistar rats aged 60-90 days old were individually housed in a climate-controlled colony and were maintained on a reversed light-dark cycle. All procedures were approved by the LSUHSC-S IACUC.

Surgery: Self-administration rats were implanted with chronic indwelling jugular catheters under pentobarbital anesthesia.

Behavioral apparatus and training: Each rat was initially trained to respond under a continuous reinforcement (fixed-ratio 1 or FR1) schedule during sessions conducted five days a week in standard operant sound-attenuated chambers. Separate groups of rats were trained to self-administer METH (0.06 mg/kg/infusion) or 45mg food pellets. Following initial METH self-administration training during daily six-hour sessions, the sessions were shortened to two hours in duration. The number of food reinforcers was limited to 60/session to prevent satiation. Stable behavior was defined as three consecutive sessions with less than 10% variability. Extinction sessions (saline substitution or no food delivery) ensured that lever responding was contingent on the delivery of the appropriate reinforcer.

Drug administration and testing: Once stable responding was established, each rat was pretreated with a selective TSPO ligand (Ro5-4864, 5-40 mg/kg IP; PK11195, 1-2 mg/kg IP; Ro7-9277, 10-40 mg/kg IP) or vehicle, 30 minutes prior to the test session.

RESULTS AND FUTURE DIRECTIONS

- Ro5-4864 reduced methamphetamine self-administration; Female rats were more sensitive to this effect.
- Ro5-4864 did not significantly affect food self-administration in male or female rats.
- PK11195 had marginal effects on methamphetamine self-administration in males.
- PK11195 had no effects on food self-administration.
- Ro7-9277 had no effects on methamphetamine self-administration.
- In the future, we will characterize the pathological and behavioral contributions of TSPO using genetic manipulations.

2. 2018 poster (Ro5-4846)

Abstract Control Number: 13411
Abstract Title: The effects of a TSPO agonist (Ro5-4864) on cocaine and methamphetamine drug-primed and cue-reactivity in rats
Session Title: Behavioral Studies of Amphetamines
Session Number: 079
Session Time: 11/3/2018 1:00:00 PM - 11/3/2018 5:00:00 PM

Presentation Number: 079.24
Presentation Time: Sat, Nov. 3, 2018, 4:00 PM - 5:00 PM
Posterboard Number: DDD12

***G. F. GUERIN**[1], C. M. KELLER[1], S. M. HAROLD[1], A. MEAUX[1], L. HERNDON[1], K. BJORNSON[2], G. LI[3], J. M. COOK[3], N. E. GOEDERS[1];
[1]LSUHSC-S, Shreveport, LA; [2]Hobart and William Smith Colleges, Geneva, NY; [3]Univ. of Wisconsin-Milwaukee, Milwaukee, WI

Neuro Abstract 2018

Research has shown that stress and the activation of the HPA axis play a major role in reward and drug reinforcement. Benzodiazepines, such as alprazolam and oxazepam, interact with α1 subunits of $GABA_A$ receptors to increase dopaminergic activity in the VTA. However, oxazepam also has an affinity for a second binding site, the translocator protein 18 kDa (TSPO), also known as the peripheral benzodiazepine receptor. Binding at TSPO increases neurosteroid levels, which can reduce dopamine levels in regions associated with reward. Previous research has shown that oxazepam reduces cocaine self-administration as well as two measures of cocaine craving (i.e., cue reactivity and reinstatement) in rats. Another experiment showed that Ro5-4864, a benzodiazepine derivative of diazepam with selective affinity for TSPO, dose dependently decreased methamphetamine self-administration in male and female rats without affecting food self-administration. The current study tested the effects of selective TSPO binding on cocaine and methamphetamine drug-primed reactivity and cue-reactivity. Male and female Wistar rats were trained to self-administer cocaine or methamphetamine. After stabilization of responding and a two-week abstinence period, rats were pretreated with Ro5-4864 or vehicle before testing in either a drug-primed reactivity or cue-reactivity session that measured drug-seeking behavior. The rats were once again trained to self-administer cocaine or methamphetamine, placed into abstinence, and pretreated with vehicle or Ro5-4864 before reactivity testing. Drug-primed responding with cocaine and methamphetamine was reduced by Ro5-4864 in both male and female rats. However, cue-reactivity was reduced only in rats trained with methamphetamine. These data suggest that selective binding to TSPO may be a potential treatment for methamphetamine relapse. This research also demonstrates the potential for the development of other TSPO variants for use in future experiments.

The Effects of a TSPO Receptor Agonist (Ro5-4864) on Cocaine and Methamphetamine Drug-Primed and Cue Reactivity in Rats

G. F. Guerin[1], C. M. Keller[1], S. M. Harold[1], A. Meaux[1], L. Herndon[1], K. Bjornson[3], G. Li[2], J. M. Cook[2], N. E. Goeders[1]

[1]Pharmacology, Toxicology & Neuroscience, LSU Health Sciences Center, Shreveport LA, [2]Chemistry & Biochemistry, University of Wisconsin-Milwaukee
[3]Hobart and William Smith Colleges, Geneva, NY

LSU Health SHREVEPORT

778

INTRODUCTION

Cocaine and methamphetamine use continues to be a prevalent issue in the United States. However, there is currently no FDA-approved treatment for dependence. Stress and activation of the HPA axis play a major role in reward and drug reinforcement. Decreasing HPA axis activation may be an avenue for reducing stimulant relapse. Benzodiazepines, such as alprazolam and oxazepam, interact with the α_1 subunits of $GABA_A$ receptor. However, oxazepam also has an affinity for the translocator protein of 18 kDa (TSPO), previously known as the peripheral benzodiazepine receptor. Oxazepam has been shown to reduce cocaine self-administration as well as responding in two models of cocaine craving (cue reactivity and reinstatement) in rats. Binding on TSPO is thought to increase neurosteroid levels. Cue reactivity and drug-primed reactivity can be used to model the human experience associated with relapse. After a two week period of abstinence, cue reactivity simulates re-exposure to cues that may induce relapse whereas drug-primed reactivity simulates re-exposure to the drug itself. In order to test the effects of selective TSPO binding on cocaine and methamphetamine drug-primed reactivity and cue reactivity, Ro5-4864, a benzodiazepine derivative of diazepam with selective affinity for TSPO, was used.

METHAMPHETAMINE

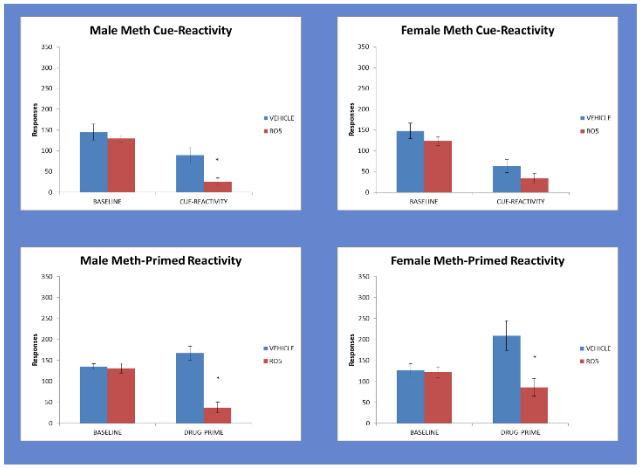

COCAINE

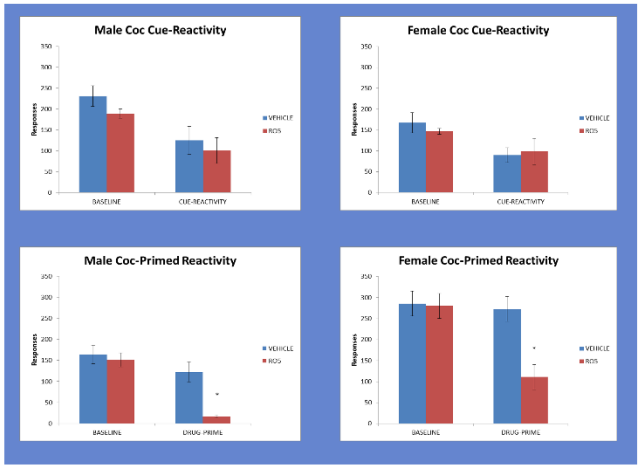

METHODS

Animals: Male and female Wistar rats 75-100 days old were individually housed in a climate-controlled animal care facility and maintained on a reversed light-dark cycle. All procedures were approved by the LSUHSC-S ACUC. N = 6-8 per group.
Surgery: Rats were implanted with chronic indwelling jugular catheters.
General training: Rats were trained to self-administer methamphetamine (0.06 mg/kg/inf) or cocaine (0.25 mg/kg/inf) during 2 hr sessions 5 days a week in standard operant sound-attenuated chambers. Rats were initially trained under a fixed-ratio 1 (FR1) schedule of reinforcement so that 1 response resulted in a drug infusion. The response requirement was gradually increased to FR2, and finally FR4. Following a minimum of 10 days at FR4 with the achievement of a stable baseline of responding (less than 10% variation for 3 consecutive sessions), rats were placed into a two-week period of abstinence.
Cue reactivity training conditions: The light above the response lever was illuminated when cocaine or methamphetamine was available for self-administration. Following completion of the FR, the lever light was extinguished and the rats received an intravenous infusion of drug (0.2 mL over 5.6 seconds), which was paired with the presentation of a house light and tone compound stimulus. After a 20-s timeout period in which no drug was available, the stimulus light was illuminated.
Drug-primed reactivity training conditions: A similar design was used except there was no house light or tone compound stimulus.
Drug administration and testing: Following abstinence, rats were pretreated with Ro5-4864 (20 mg/kg) or vehicle, i.p., 30 minutes before testing. Conditions for testing cue reactivity and drug-primed reactivity were similar to those used for self-administration, except cocaine and methamphetamine were not delivered through the implanted IV catheters.
For **drug-primed reactivity**, rats received an intraperitoneal injection of cocaine (15 mg/kg) or methamphetamine (1 mg/kg) immediately before the session began. After the first test, rats were re-trained to self-administer drug, placed into abstinence, and pretreated with vehicle or Ro5-4846 before being tested again. Each animal received both treatments.
For **cue reactivity**, rats were placed into the chambers, and responding resulted in the presentation of the house light and tone compound stimulus (conditioned reinforcer), but no drug was delivered. Rats were pretreated with vehicle or Ro5-4846 before testing, and each animal received both treatments.

RESULTS AND FUTURE DIRECTIONS

- Ro5-4864 reduces methamphetamine and cocaine seeking during drug-primed reactivity.
- Selective TSPO binding reduces the effects of drug exposure on drug seeking after a period of abstinence.
- Ro5-4864 also reduces methamphetamine but not cocaine seeking during cue reactivity.
- Selective TSPO binding may be more salient in the rewarding effects of methamphetamine versus cocaine.
- Selective binding to TSPO may be a potential treatment for methamphetamine and cocaine Substance Use Disorder.
- These results indicate the potential for a novel pharmacotherapy that may help prevent relapse during recovery.

Appendix IX: Angelman syndrome (in collaboration with Kiyoshi Egawa, Japan)

GL, PUT THIS EMAIL IN THESIS APPENDIX ,PLUS HIS DATA IN ATTACHMENT ///IMPORTANT....JIM.C.....: MTA with UWM for GABA alpha 5

James M Cook

Tue 5/1/2018 9:04 AM

To:Guanguan Li <guanguan@uwm.edu>;

1 attachments (27 KB)

MTA16-135 Hokkaido amendment 5-1-18.doc;

Using Angelman syndrome model mice and am ready to apply MP-III-022 *in vivo*. I will contact an officer in the intellectual property to renew the contract.

Research progress:
Last year, Angelman Syndrome Foundation (U.S.) kindly founded me for two years, which accelerated the research progress.

1. Patch-clamp recordings indicated that tonic inhibition in the hippocampal pyramidal neuron was significantly reduced in AS mice, while not in the thalamic relay neuron (see pdf 1), in line with our hypothesis.
2. I confirmed aberrant EEG and impaired learning memory in AS mice (pdf 2), which might be caused by the regional discrepancy of tonic inhibition mentioned above and might be improved by PAM GABAA5.

I would like to evaluate the efficacy of chronic administration of low dose MP-III-022 by using Alzet osmotic pump. As you know, this pump allows continuous and consistent application of compounds, but I wonder it is difficult for me to determine an adequate rate for administration. I think target concentration should correspond to the peak concentration after 1~2.5mg/kg i.p. injection of MP-III-022. I would be most grateful if you could kindly indicate me the ideal administration rate (i.e. X μg/kg/h) from the pharmacokinetics data in the 2016 paper to obtain the target concentration ?

Please let me know if you have any questions or comments.
Thank you.

Kiyoshi Egawa M.D., Ph.D
Pediatric Dept., Hokkaido Univ. Graduate Sch. of Med.

----- Original Message -----
From: James M Cook <capncook@uwm.edu>
To: Jessica Silvaggi <jessica@uwmrf.org>; "egakiyo@huhp.hokudai.ac.jp" <egakiyo@huhp.hokudai.ac.jp>

KIYOSHI,THANKS FOR THE GREAT NEWS.....JESSICA,DO THE MTA FOR FIVE YEARS TO PROTECT KYOSHI AMND ME...JIM...: MTA with UWM for GABA alpha 5

James M Cook

Mon 4/23/2018 10:38 AM

To:Jessica Silvaggi <jessica@uwmrf.org>; egakiyo@huhp.hokudai.ac.jp <egakiyo@huhp.hokudai.ac.jp>; 江川 潔 <egakiyoda@yahoo.co.jp>; Guanguan Li <guanguan@uwm.edu>;

2 attachments (728 KB)

1_ AS tonic_inhibition.pdf; 2_AS-Phenotype.pdf;

KIYOSHI, THANK YOU. JIM...GREAT NEWS.....GUANGUAN SEND KIYOSHI SAVICS PAPER ON MP-III-22.....KIYOSHI,WHAT WE KNOW RIGHT NOW,IF YOU GET A REALLY POTENT ALP 5 AGONIST,IT IS NOT AS ACTIVE AS A WEAKER ANTIDEPRESSANT/PROCOGNITIVE LIGAND,SO I SUGGEST TO START WITH REALLY LOW DOSES OF MP-III-022;YOU CAN ALWAYS RAISE THEM.....(OR THE REVERSE).....SECONDLY,WE ARE CHEMISTS,WE HAVE NO CLUE AS TO HOW MUCH YOU SHOULD GIVE/MINUTE; ALL WE CAN DO IS RESEND YOU THE SAVIC PAPER ON MP-III-022.....WE BELIEVE HIS DOSES MAY BE TO HIGH FOR YOU,WE JUST DONT KNOW. ANGELMAN'S SYNDROME MAY REQUIRE HIGHER DOSES THAN MAJOR DEPRESSION.....(GUANGUAN,SEND HIM SEANS PAPER TO ON SH-053-2'F-R-CH3 TO).....WE HAVE AN MDD PAPER SUBMITTED,THAT I WILL SEND YOU AS SOON AS ITS OUT DOI,PHARMACOLOGISTS WANT TO KEEP IT CONFIDENTIAL,UNTIL ITS OUT DOI.....YOU COULD START WITH HIGH DOSE OF MP-III-022,THEN IF ITS NOT ACTIVE,GO TO A VERY LOW DOSE.....WE WILL SEND YOU THE BEST ANTIDEPRESSANT/PROCOGNITIVE ALP 5 CPD,ONCE PAPER IN PRESS.....I AM REALLY LOOKNG FORWARD TO READING YOU DATA.....BEST REGARDS,JIM.....CAPS NOT FOR EMPHASIS(I TYPE TO SLOW OTHERWISE)

From: 江川 潔 <egakiyoda@yahoo.co.jp>
Sent: Saturday, April 21, 2018 12:52 PM
To: James M Cook; Jessica Silvaggi; egakiyo@huhp.hokudai.ac.jp
Subject: Re: MTA with UWM for GABA alpha 5

Dear Dr. Silvaggi and Dr. Cook

I apologize for not contacting you so long and thank you for giving me a kind remind.
> are you still working with Dr. Cook's compounds for GABA alpha 5?
Yes, I am still working for the project using Angelman syndrome model mice and am ready to apply MP-III-022 *in vivo*. I will contact an officer in the intellectual property to renew the contract.

Research progress:
Last year, Angelman Syndrome Foundation (U.S.) kindly founded me for two years, which accelerated the research progress.

1. Patch-clamp recordings indicated that tonic inhibition in the hippocampal pyramidal neuron was significantly reduced in AS mice, while not in the thalamic relay neuron (see pdf 1), in line with our hypothesis.

2. I confirmed aberrant EEG and impaired learning memory in AS mice (pdf 2), which might be caused by the regional discrepancy of tonic inhibition mentioned above and might be improved by PAM GABAA5.

I would like to evaluate the efficacy of chronic administration of low dose MP-III-022 by using Alzet osmotic pump. As you know, this pump allows continuous and consistent application of compounds, but I wonder it is difficult for me to determine an adequate rate for administration. I think target concentration should correspond to the peak concentration after 1~2.5mg/kg i.p. injection of MP-III-022. I would be most grateful if you could kindly indicate me the ideal administration rate (i.e. X μg/kg/h) from the pharmacokinetics data in the 2016 paper to obtain the target concentration ?

Please let me know if you have any questions or comments.
Thank you.

Kiyoshi Egawa M.D., Ph.D
Pediatric Dept., Hokkaido Univ. Graduate Sch. of Med.

----- Original Message -----
From: James M Cook <capncook@uwm.edu>
To: Jessica Silvaggi <jessica@uwmrf.org>; "egakiyo@huhp.hokudai.ac.jp" <egakiyo@huhp.hokudai.ac.jp>
Date: 2018/4/20, Fri 05:23
Subject: Re: MTA with UWM for GABA alpha 5

RENEW IF HES STILL INTERESTED JESS. BEST,JIM...

From: Jessica Silvaggi <jessica@uwmrf.org>
Sent: Thursday, April 19, 2018 10:59 AM
To: egakiyo@huhp.hokudai.ac.jp; James M Cook
Subject: MTA with UWM for GABA alpha 5

Dear Kiyoshi,

Our MTA signed in 2106 will expire in May. Are you still working with Dr. Cook's compounds for GABA alpha 5?

Thank you,

Jessica

Jessica M. Silvaggi, PhD, CLP
Senior Licensing Manager
UWM Research Foundation, Inc.
1440 East North Avenue
Milwaukee, WI 53202
jessica@uwmrf.org
Office: 414-906-4654
Cell: 508-769-5171
https://uwmrf.org/

Brain region-dependent deregulation of tonic inhibition in Angelman syndrome.

Kiyoshi Egawa[1], Yoshiaki Hirata[1], Yukitoshi Takahashi[2], Daisuke Satoh[1], Hideaki Shiraishi[1], Atsuo Fukuda[3]

1. Department of Pediatrics, Faculty of Medicine and Graduate School of Medicine, Hokkaido University
2. Department of Pediatrics, Shizuoka Institute of Epilepsy and Neurological Disorders
3. Department of Neurophysiology, Hamamatsu University School of Medicine

Authors declare no COI.

1. Rationale: Angelman Syndrome (AS)

- Genetically confirmed autism spectrum disorder
- Incidence 1 : 15,000 – 20,000
- The major clinical manifestations
  1. Severe developmental delay
  2. Speech impairment
  3. Movement and balance problems
  4. Peculiar face, paroxysmal laughter
  5. Epilepsy (Williams et al., 1995)

Casual gene: maternally imprinted UBE3A

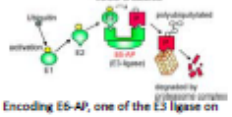

Encoding E6-AP, one of the E3 ligase on protein-proteasome pathway

Pathophysiological mechanisms are still under elucidated, but GABAergic dysfunction has been proposed as one of the main feature of dysfunction.

2. Our pervious finding: Decreased tonic inhibition in cerebellar granule cells

We has recently shown that non-synaptic form of inhibition, "**tonic inhibition**" is significantly decreased in the cerebellum of Ube3a knockout mice.

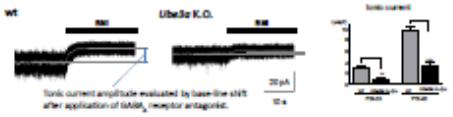

Tonic current amplitude evaluated by base-line shift after application of $GABA_A$ receptor antagonist.

As its mechanism, we have also shown that UBE3A binds to neuronal GABA transporter 1 (GAT1). UBE3A deficiency induces a surplus GAT1 and decreased GABA levels of extrasynaptic space.

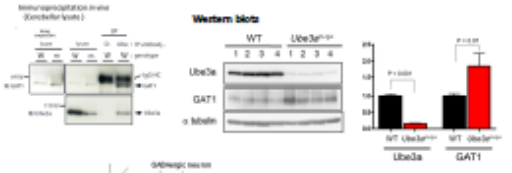

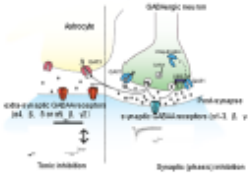

The decrement of tonic inhibition may contribute to the pathophysiology of AS because Gaboxadol, which increases tonic inhibition globally in the brain, improved motor dysfunction in Ube3a knock-out mice

3. Open Questions and study design

Is tonic inhibition similarly decreased in other brain regions?

Methods

An acute brain slice was prepared from *Ube3a* K.O. mice or littermate wild type (postnatal day 21-28)

GABA-mediated tonic inhibition has been analyzed in CA1 hippocampal pyramidal neurons or in thalamic relay neuron utilized by voltage-clamp patch clamp recordings .

We also performed immunostaining for GAT1, GAT3 and UBE3A in the hippocampus and thalamus

4. Result (1): Tonic inhibition was decreased in CA1 hippocampal pyramidal neuron of *Ube3a* K.O. mice.

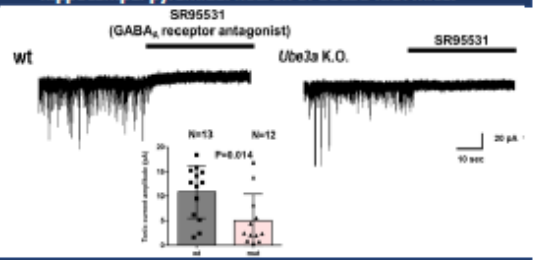

4. Result (2): Tonic inhibition was NOT decreased in thalamic relay neuron of *Ube3a* K.O. mice.

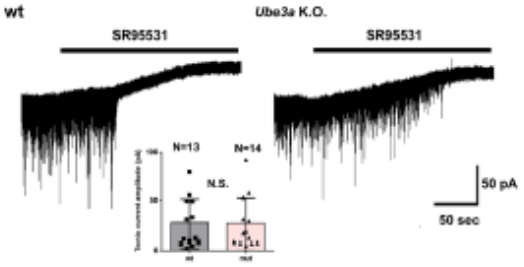

4. Result (3): Diverse deregulation of GAT1 expression among brain region in *Ube3a* K.O. mice

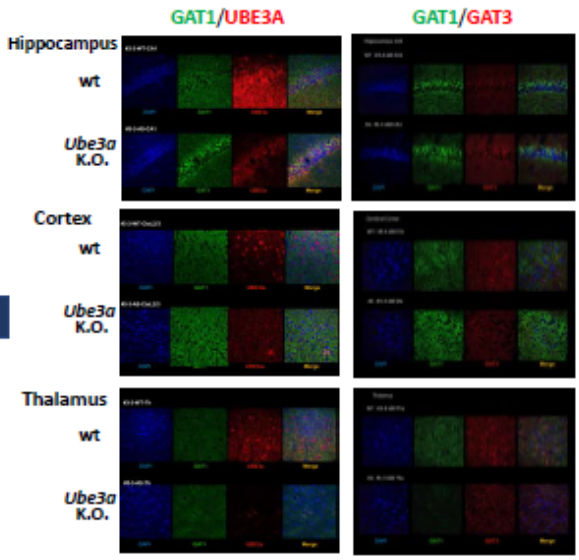

5. Conclusion and Prospective

GABA-mediated Tonic inhibition is specifically decreased in UBE3A deficiency, while phasic (synaptic) inhibition is preserved.

The degree of reduction differs region by region. A reason for unchanged tonic inhibition in the thalamus may be explained by lack of neuronal GAT1 expression in this region (De Biasi,1998).

We hypothesized that this discrepancy rather than a global decrement of tonic inhibition may contribute to some of the neurological dysfunctions such as epilepsy or sleep disorder by disrupting usual network activity across the brain. Increase, rather than decrease, of tonic inhibition in thalamic relay neurons has been shown as a mechanism for absence seizure in model mice (Cope et al., 2009), which supports the above "imbalanced tonic inhibition" hypothesis.

Subunit α5 is predominantly expressed in the cortex or hippocampus and comprises extrasynaptic receptors. Recently developed positive allosteric modulator for subunit α5 containing GABAa receptor (PAM-α5GABAaR) might be a preferable treatment to Gaboxadol by correcting the "gap" of inhibition.

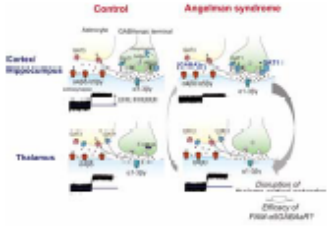

Phenotypic evaluation in Angelman syndrome (AS) models

A

EEG recordings in the V1 area indicates that AS mice have frequent spikes or poly spikes as an epileptic discharge

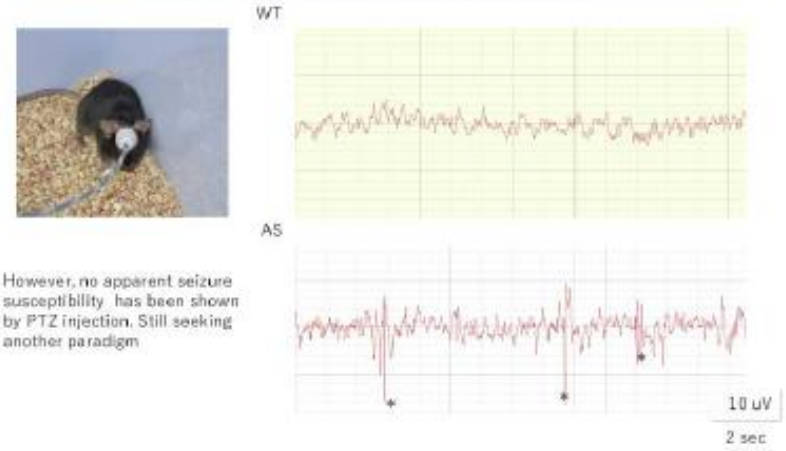

However, no apparent seizure susceptibility has been shown by PTZ injection. Still seeking another paradigm

B

Impairment of learning memory in AS mice evaluated by Novel-Objection test

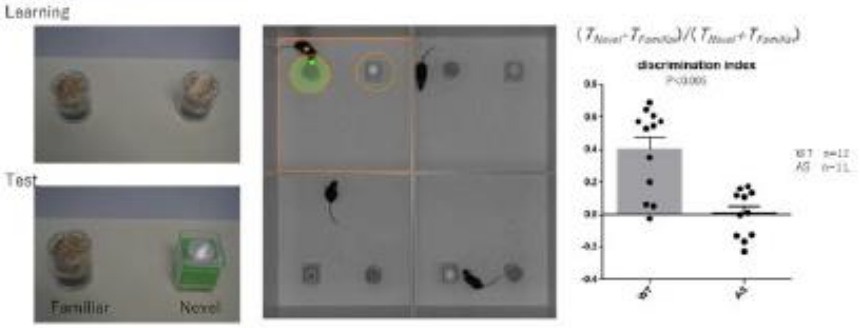

C

Accelerating Rotarod test

4-40 /min 5分

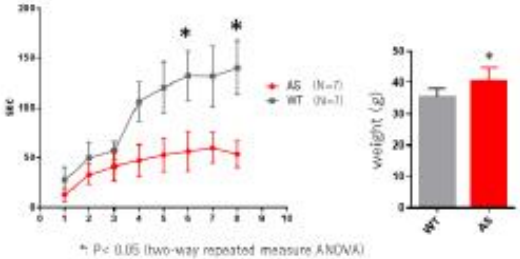

* P< 0.05 (two-way repeated measure ANOVA)
Day 1: trial 1-4, Day 2: trial 5-8

Plasma samples	nM	time point		
1	421.2504	animal sacrificed after 8 days		
2	347.269	animal sacrificed after 8 days		
3	1128.311	animal sacrificed after 72 h		
Brain samples	nmol/kg	free fraction (nmol/kg)	ng/g	time point
1	2872.282	189.5706064	1069.609	animal sacrificed after 8 days
2	2005.054	132.3335313	746.6619	animal sacrificed after 8 days
3	12689.84	837.5293412	4725.569	animal sacrificed after 72 h

Appendix X: Modulating GABAA receptors in medulloblastoma with BZD derivatives

1. Poster: Targeting medulloblastoma with benzodiazepines delivered using tunable biodegradable hydrogels

TARGETING MEDULLOBLASTOMA WITH BENZODIAZAPINES DELIVERED USING TUNABLE BIODEGRADABLE HYDROGELS

Laura Kallay[1], Daniel Pomeranz Krummel[1], Kashi Reddy Methuku[2], Guanguan Li[2], Alexandra Ross[1], Zhaobin Zhang[1], Jeffrey Olson[1], Daniel Brat[1], Tobey MacDonald[1], Stefanie Sydlik[3], James Cook[2], Soma Sengupta[1]

[1]Winship Cancer Institute, Emory School of Medicine; [2]Chemistry & Biochemistry, Univ. Wisconsin-Madison; [3]Dept. Chemistry, Carnegie-Mellon

INTRODUCTION

Medulloblastoma (MB) is a common pediatric malignant primary brain tumor and classified into four subgroups: WNT; Sonic Hedgehog, SHH; photoreceptor/GABA$_A$ergic, Group 3; neuronal/glutamatergic, Group 4 (1,2). Group 3 is refractory to treatment, has a survival rate of ~20%, and associated with higher rates of relapse and metastasis. Group 3 exhibits a molecular signature that includes over expression of GABRA5, an isoform of the GABA$_A$ neurotransmitter. GABA$_A$ is composed of five subunits: two α, two β, and a single γ-subunit (**Figure 1**). There are several isoforms of the α-subunit, including α-5 (GABRA5). GABA$_A$ is a target of the benzodiazepine class of allosteric modulators. Its binding site is located at the interface of the γ-subunit and one of two α-subunits. Benzodiazepines function to enhance the effect of GABA and increase cellular chloride ion influx.

We have shown that GABRA5 is active in Group 3 MB and that a benzodiazepine positive allosteric modulator enhances effectiveness of radiation for Group 3 MB and can function as a synergistic enhancer of the chemotherapeutic cisplatin (3). Recently, we screened a newly synthesized class of benzodiazepines in a mouse model system and identified as particularly effective against Group 3 MB, the benzodiazepine KRM-II-08 (**Figure 2**) (4). We propose that KRM-II-08 leads to cell death by its tight binding to the over expressed GABRA5 resulting in significant accumulation of chloride ion in the cell. We hypothesize that this results in a compensatory influx of sodium ions and water (experiments underway), which leads to apoptosis through the intrinsic pathway (3).

AIMS

MB treatment consists of conventional cranio-spinal radiotherapy and chemotherapy, which results in significant morbidity in children. Brain tumors are challenging to treat as the therapeutic must overcome the blood-brain barrier and survive first pass metabolism. Treatment of Group 3 MB must therefore entail identification of an effective therapeutic and its targeted delivery. We aim to:

- Obtain mechanistic understancing of how a benzodiazepine may kill or sensitize cells to radiation and/or chemotherapy;
- Develop a new approach to deliver a therapeutic that does not elicit an immune response, is biocompatible, biodegradable, and affords the potential for controlled release.

We hypothesize that group 3 MB can be targeted and killed with benzodiazepine(s) in conjunction with a tunable biodegradable hydrogel formulation.

Model of Benzodiazepine Mediated Cell Death

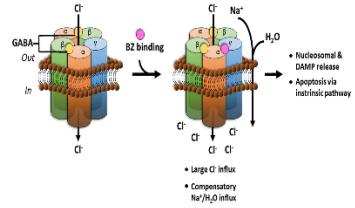

Figure 1. GABA$_A$ receptor structure and model of BZ mediated cell death. GABA$_A$ neurotransmitter receptor is composed of five subunits: two α, two β, and a single γ-subunit. There are several isoforms of the α-subunit, including α-5 (GABRA5). GABRA5 has binding sites for GABA and a benzodiazepine (BZ). We hypothesize that the binding of a BZ to GABRA5 elicits a large cellular influx of chloride ion, followed by compensatory influx of sodium and water which triggers nucleosomal and DAMP release, then apoptosis via the intrinsic pathway.

Benzodiazepine Structure

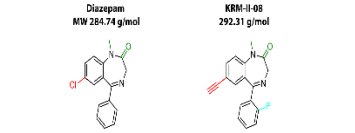

Figure 2. Benzodiazepines. Chemical structure of benzodiazepines diazepam (valium) and KRM-II-08. We previously reported on results of a screen of benzodiazepines that functioned as GABRA5 modulators (Jonas et al., 2016). This study identifies KRM-I-08 as particularly efficacious against Group 3 medulloblastoma.

MATERIALS & METHODS

Diazepam was obtained from Sigma-Aldrich. Benzodiazepines QH-II-066 and KRM-II-08 were synthesized as described (5). Medulloblastoma cell lines were provided by S. Pomeroy (Children's Hospital, Boston). Dose response curves were performed as described (3). Confocal light microscopy was performed to examine cellular apoptosis in combination with anti-BAD and DAPI staining, as previously described (3). A 'hydrogel' polymer consisting of chondroitin sulfate is synthesized according to published protocols (6-8).

RESULTS

Dose response curve

The half maximal inhibitory concentration (IC_{50}) of the benzodiazepine compounds were obtained using an MTS cell proliferation assay. We identified the benzodiazepine KRM-II-08 as particularly effective when screening efficacy of benzodiazepines against group 3 MB (**Figure 3**). The same benzodiazepine as well as QH-II-066 has no effect on the control medulloblastoma cell line, DAOY (data not shown). KRM-II-08 has an IC_{50} of 0.1 μM. We had previously reported QH-II-066's activity against Group 3 MB (3), it has an IC_{50} of 1.0 μM.

Benzodiazepine Dose Response Curve

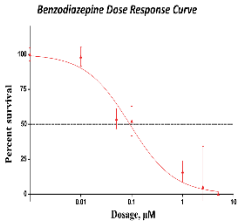

Figure 3. KRM-II-08 dose response curve. KRM-II-08 is effective in killing D425 medulloblastoma cells, IC_{50} of 0.1 μM. D425 cells over express the GABA$_A$ receptor GABRA5, mimicking Group 3 MB cells. KRM-II-08 has no effect on DAOY, which does not express GABRA5.

Microscopy

To provide insight into the mechanism of cell mediated death by one of our synthesized benzodiazepines, we used QH-II-066 as the therapeutic. By confocal microscopy we observed strong staining for Bcl-2-associated promoter (BAD) which is an indicator for apoptosis via the intrinsic pathway (**Figure 4**).

Benzodiazepine Induces Apoptosis

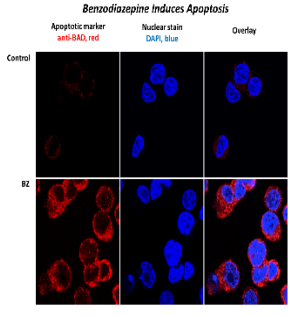

Figure 4. Benzodiazepine induces apoptosis in Group 3 medulloblastoma cells. The observed apoptosis is specific to Group 3 medulloblastoma cells. Cells are stained for the pro-apoptotic protein Bcl-2-associatec promoter (BAD) using an anti-BAD antibody (red) and nucleus using 4',6-diamidino-2-phenylindole or 'DAPI stain' (blue) after treatment (1.0 μM, 24 hours) with vehicle control (top) or benzodiazepine (bottom).

RESULTS

Hydrogels for brain tumor targeted delivery

KRM-II-08 is particularly efficacious against group 3 MB, an order of magnitude greater than QH-II-066 – the chemical 'parent' benzodiazepine. An effective approach to delivery needs to be established for use of this benzodiazepine in clinic. We are exploring hydrogel formulations for delivery, due to their being biodegradable, biocompatible, and offering an avenue for tunable release. Specifically, we are designing biomimetic hydrogels with tunable mechanical properties and covalent modifications to allow for controlled release of the benzodiazepine KRM-II-08. Using an intracranial xenograft mouse model, we will focus initially on KRM-II-08 chemically conjugated to a modified chondroitin sulfate (**Figure 5**).

Biocompatible, Biodegradable Hydrogel

BZ, KRM-II-08

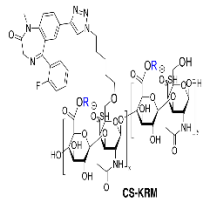

Figure 5. Hydrogel composition. Chemical structure of two linked chondroitin sulfate units (each in brackets) covalently modified or 'clicked' to include the benzodiazepine (BZ) KRM-II-08. R-groups (blue) can be altered for use in cross-linking chemistry so as to tune gel polymer properties.

CONCLUSIONS

- Dose response curve reveals that KRM-II-08 is more effective than QH-II-065 against Group 3 MB cells. In a mouse flank model system, we were also able to reproduce this result (5).
- Confocal microscopy shows upregulation of the intrinsic pathway of apoptosis following benzodiazepine administration. We are in the process of further characterizing this pathway.
- Our aim is to employ GABRA5 agonists to kill an aggressive subtype of pediatric brain cancer and hydrogels for their delivery in a surgical setting. Such a drug-hydrogel approach may establish a paradigm for how to target a brain tumor.

REFERENCES

1. Pugh TJ, Weeraratne SD, Archer TC et al. (2012) Medulloblastoma exome sequencing uncovers subtype-specific somatic mutations with a broad landscape of genetic heterogeneity. Nature. 488: 106-110.
2. Cho Y-J, Tsherniak A, Tamayo P et al. (2011) Integrative genomic analysis of medulloblastoma identifies a molecular subgroup that drives poor clinical outcome. J. Clinical Oncology. 29: 1424-1430.
3. Sengupta S, Weeraratne SD, Sun H et al. (2014) Alpha5 GABAA receptors negatively regulate MYC-amplified medulloblastoma growth. Acta Neuropathol. 127: 593-609.
4. Jones C, Calligaris D, Methuku KR et al. (2016) First in vivo testing of compounds targeting Group 3 medulloblastoma using an implantable microdevice as a new paradigm for drug development. J. Biomedical Nanotechnology. 12(8): 1297-1302.
5. Huang Q, Zhang W, Liu R, McKernan RM, and Cook JM (1996) Benzo-fused benzodiazepines employed as topological probes for the study of benzodiazepine receptor subtypes. Medicinal Chem. Res. 6(3): 384-391.
6. Lutz J-F, and Zarafshani Z (2008) Efficient construction of therapeutics, bioconjugates, biomaterials and bioactive surfaces using azide–alkyne 'click' chemistry. Adv. Drug Deliv. Rev. 60: 958-970.
7. Wang D-A, Varghese S, Sharma B et al. (2007) Multifunctional chondroitin sulphate for cartilage tissue-biomaterial integrati on. Nat. Mater. 6: 385-392.
8. Tomihata K and Ikada Y (1997) Crosslinking of hyaluronic acid with glutaraldehyde. J. Polym. Sci. Part A Polym. Chem. 35: 3553-3559.

ACKNOWLEDGEMENTS

This work was funded in part by the NIH/DS-008 (award ID NS083626) to S. Sengupta.

Contact Information:

Funding:

PDTB-28

2. Poster: Understanding the mechanism of benzodiazepine mediated cell death in GABRA5 overexpressing medulloblastomas

Understanding the mechanism of benzodiazepine mediated cell death in GABRA5 overexpressing medulloblastomas

Laura Kallay[1], Alexandra Ross[1], Olivia Moody[2], Guanguan Li[3], Tobey MacDonald[4], James Cook[3], Andrew Jenkins[2], Daniel Pomeranz Krummel[1], Soma Sengupta[1]

[1]Winship Cancer Institute, Emory School of Medicine; [2]Department of Pharmacology, Emory School of Medicine; [3]Chemistry & Biochemistry, Univ. Wisconsin-Madison; [4]Department of Pediatrics, Children's Hospital of Atlanta

INTRODUCTION

Medulloblastoma (MB) is a common pediatric malignant primary brain tumor, in the past classified into four subgroups: WNT; Sonic Hedgehog, SHH; Group 3; Group 4 (1,2). Group 3 patients are refractory to treatment, have a survival rate of ~70%, and associated with higher rates of relapse and metastasis.

Group 3 MB exhibits a molecular signature that includes high expression of GABRA5, an isoform of the $GABA_A$ neurotransmitter. $GABA_A$ receptor is composed of five subunits; two α, two β, and a γ (**Fig. 1**). There are several isoforms of the α-subunit, including α-5 (GABRA5). Two molecules of the neurotransmitter GABA bind $GABA_A$ receptors at the interface between α and β subunits. $GABA_A$ receptors are a target of the benzodiazepine class of allosteric modulators. Its binding site located at the interface of the γ-subunit and one of two α-subunits. Benzodiazepines can function to enhance the effect of GABA and increase cellular chloride ion influx.

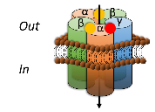

Figure 1. $GABA_A$ receptor. $GABA_A$ receptor is composed of five subunits: two α, two β, and a γ. $GABA_A$ has two binding sites for the neurotransmitter GABA (orange spheres) and a single benzodiazepine site (red sphere).

We have shown that a benzodiazepine positive allosteric modulator can kill Group 3 MB cells, enhance effectiveness of radiation for Group 3 MB, and function as a synergistic enhancer of the chemotherapeutic cisplatin (3).

AIM

MB treatment consists of conventional cranio-spinal radiotherapy and chemotherapy, which results in significant morbidity in children. Brain tumors are challenging to treat as the therapeutic must overcome the blood-brain barrier and survive first pass metabolism. Benzodiazepines are safe and pass the blood-brain barrier. Our Aim is to obtain mechanistic understanding of how a benzodiazepine may arrest Group 3 MB cells.

MATERIALS & METHODS

Benzodiazepines were synthesized as described (5). Medulloblastoma cell line D283 was obtained from ATCC. Effect of benzodiazepines on D283 growth was assessed using an MTS assay, performed as described (3). Confocal light microscopy was performed to examine TP53 and cellular apoptosis in combination with anti-BAD and DAPI staining, as previously described (3). Whole cell patch clamp electrophysiology techniques were standard.

RESULTS

Presence of a GABRA5 message does not mean it is translated into a GABRA5 protein and if there is protein produced, that it localizes to the membrane and contributes to assembly of a functional $GABA_A$ receptor. We report that in Group 3 MB cells GABRA5 protein localizes to the plasma membrane as assessed by IF microscopy, distributed diffusely (**Fig. 2A**), and as determined by electrophysiology, contributes to ~1,000 functional receptors that are α5-β3-γ3-like and have a basal chloride efflux rate of ~$2x10^3$ ions/second (**Fig. 2B**).

Group 3 MB cells have a functional $GABA_A$ receptor

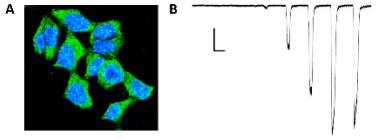

Figure 2. $GABA_A$ receptor is functional in medulloblastoma cells. (A) Localization of GABRA5 in D283 MB cells shows diffuse staining at the cell membrane. (B) Whole-cell patch clamp recording of D283 MB cells shows an active α5-β3-γ3-like receptor with increasing GABA (calibration bar: 100 pA, 5 sec).

RESULTS

Drug cytoxicity studies of benzodiazepines, positive allosteric modulators

Benzodiazepines are generally modified at three sites (R^1, R^2, R^7, R'; **Fig. 3A**). We screened benzodiazepines which had an ethylene group at R^7 in place of a halogen (Chloride in diazepam), with or without a CH_3 at R^1, and with or without a halogen (F, Cl, Br) at R' (**Fig. 3B**). The effect of these benzodiazepine variants on D283 MB cell growth was assessed by an MTS proliferation assay. Measurement of the half maximal inhibitory concentration (IC_{50}) of the benzodiazepine variants revealed that benzodiazepine **KRM-II-08** which has a fluoride at R' was particularly potent (IC_{50} of 0.17 μM). We had previously reported that Valium (**Fig. 3B**) has an IC_{50} of 10.0 μM (3). Thus, small chemical change has a large effect on efficacy. We conducted whole-cell patch clamp recordings of D283 MB cells in presence of KRM-II-08. These studies revealed that KRM-II-08 is GABRA5-selective; has a maximal activation with 1 μM GABA present; and has an EC_{50} for enhancement of 0.8 μM.

Cytotoxicity screen of benzodiazepines identifies critical chemical changes

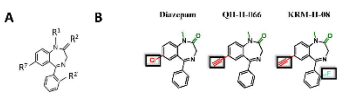

Figure 2. Benzodiazepines. Chemical structure of benzodiazepines diazepam (valium) and KRM-I-08. We previously reported on results of a screen of benzodiazepines that functioned as GABRA5 modulators (Jonas et al., 2016). This study identified KRM-II-08 as particularly efficacious against Group 3 medulloblastoma.

Determination of EC_{50} for enhancement of drug

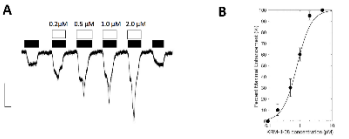

Figure 3. Whole-cell patch clamp recording of D283 MB cells with KRM-II-08. (A) Receptors activated with 1 μM GABA; (B) EC_{50} for enhancement is 0.8 μM (Max. enhancement: 180%; Calbar: 100 pA and 2 sec).

Transcription factor upregulated

To provide insight into the mechanism of cell mediated death by one of our synthesized benzodiazepines (KRM-II-08), we performed IF microscopy based on initial observations of RNA-seq data. We observed staining for the transcription factor TP53 upon after D238 MB cells were exposed to KRM II-08 (**Fig. 4.**).

Benzodiazepine Upregulates TP53

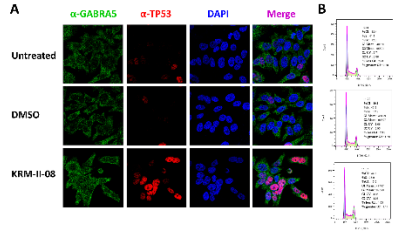

Figure 4. Benzodiazepine upregulates TP53. (A) Benzodiazepine causes an increase in nuclear staining for the protein TP53 as assessed using an anti-TP53 antibody (red) and nucleus using 4',6-diamidino-2-phenylindole or 'DAPI stain' (blue) after treatment (0.7 μM KRM-I-08; 6 hours). (B) There is only a slight accumulation of cells in G2 phase of the cell cycle when incubated with benzodiazepine, see bottom cell sorting graph and data analysis.

RESULTS

Study of apoptosis

KRM II-08 is particularly efficacious arresting D238 MB cells. We conducted various assays to determine if KRM-II-08 arrested cells by evoked or triggering cell senescence or apoptosis (intrinsic or extrinsic pathways). Our analysis indicates that KRM-II-08 activates the intrinsic pathway of apoptosis. This is most clearly demonstrated by IF microscopy and staining for the pro-apoptotic protein Bcl-2-associated promoter (BAD).

Benzodiazepine Induces Apoptosis

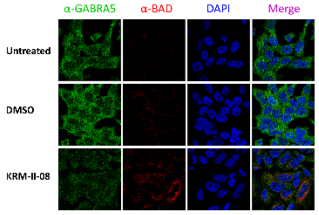

Figure 5. Benzodiazepine induces apoptosis. The observed apoptosis is specific to Group 3 medulloblastoma cells. Cells are stained for the pro apoptotic protein Bcl 2 associated promoter (BAD) using an anti-BAD antibody (red) and nucleus using 4',6-diamidino-2-phenylindole or 'DAPI stain' (blue) after treatment (0.7 μM drug; 24 hours).

CONCLUSIONS

- GABRA5 contributes to assembly of ~1,000 functional $GABA_A$ receptors per medulloblastoma cell;
- Medulloblastoma cell growth is arrested by a new class of benzodiazepines with EC_{50} ~0.7 μM;
- Small chemical changes in benzodiazepine structure, have large effects in cytotoxicity;
- Once the benzodiazepine binds to the native receptor it leads to TP53 upregulation;
- Drug binding does not effect cell cycle;
- Changes induced by benzodiazepine binding to receptor leads to apoptosis via the intrinsic pathway.

REFERENCES

1. Pugh TJ, Weeraratne SD, Archer TC et al. (2012) Medulloblastoma exome sequencing uncovers subtype-specific somatic mutations within a broad landscape of genetic heterogeneity. Nature. 488: 106-110.
2. Cho YJ, Tsherniak A, Tamayo P et al. (2011) Integrative genomic analysis of medulloblastoma identifies a molecular subgroup that drives poor clinical outcome. J. Clin Oncology. 29: 1424-1430.
3. Sengupta S, Weeraratne SD, Sun H et al. (2014) alpha5-GABAA receptors negatively regulate MYC-amplified medulloblastoma growth. Acta Neuropathol. 127: 583-601.
4. Jonas O, Celiker D, Methuku KR et al. (2016) First in vivo testing of compounds targeting Group 3 medulloblastoma using an implantable microdevice as a new paradigm for drug development. J. Biomed Nanotechnol. 12(6): 1237-1252.
5. Huang Q, Zhang W, Liu R, McKernan RM, and Cook JM (1996) 4-azido-furo[3,2-c]benzodiazepines analogs as topological probes for the study of benzodiazepine receptor subtypes. Medicinal Chem. Res. 6(3): 384-391.

ACKNOWLEDGEMENTS

This project was supported in part by funding awarded to S. Sengupta from NIH/NINDS (R01 NS089626), American Cancer Society IRG, and B*CURED Foundation.

Contacts: Daniel Pomeranz Krummel: pomeranz.krummel@emory.edu
Soma Sengupta: soma.sengupta@emory.edu
James Cook: capncook@uwm.edu
Andrew Jenkins: ajenki2@emory.edu

3. **Poster: Modulating GABA$_A$ receptors in medulloblastoma with benzodiazepine derivatives induces cell death**

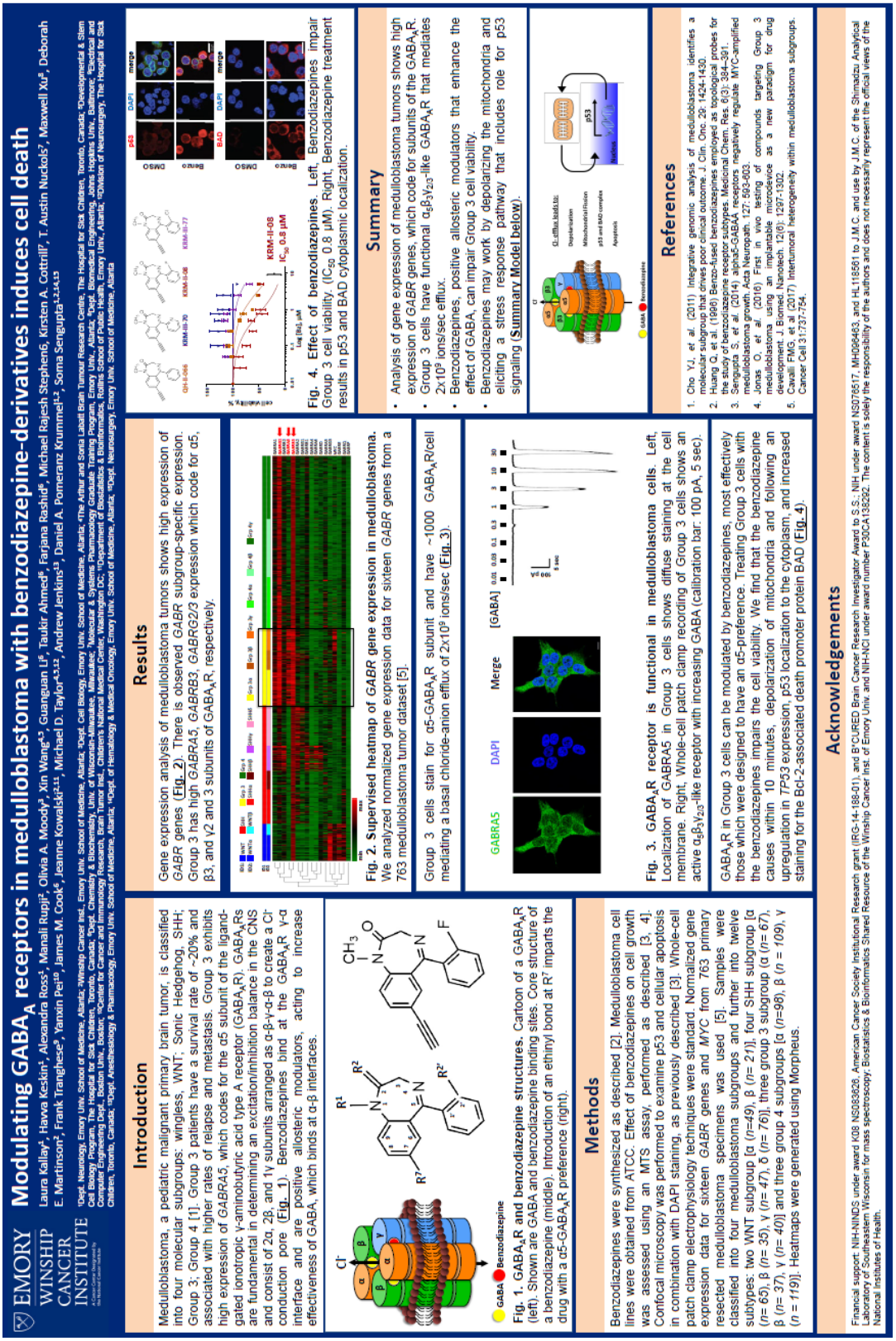

4. **Paper: Modulating native -GABAA receptors in medulloblastoma with positive allosteric benzodiazepine-derivatives induces cell death**

Modulating native $GABA_A$ receptors in medulloblastoma with positive allosteric benzodiazepine-derivatives induces cell death

Laura Kallay, Havva Keskin, Alexandra Ross, Manali Rupji, Olivia A. Moody, Xin Wang, Guanguan Li, Taukir Ahmed, Farjana Rashid, et al.

Journal of Neuro-Oncology

ISSN 0167-594X

J Neurooncol
DOI 10.1007/s11060-019-03115-0

Springer

Your article is published under the Creative Commons Attribution license which allows users to read, copy, distribute and make derivative works, as long as the author of the original work is cited. You may self-archive this article on your own website, an institutional repository or funder's repository and make it publicly available immediately.

Journal of Neuro-Oncology
https://doi.org/10.1007/s11060-019-03115-0

LABORATORY INVESTIGATION

Modulating native $GABA_A$ receptors in medulloblastoma with positive allosteric benzodiazepine-derivatives induces cell death

Laura Kallay[1] · Havva Keskin[1] · Alexandra Ross[1] · Manali Rupji[2] · Olivia A. Moody[3] · Xin Wang[4,5] · Guanguan Li[6] · Taukir Ahmed[6] · Farjana Rashid[6] · Michael Rajesh Stephen[6] · Kirsten A. Cottrill[7] · T. Austin Nuckols[7] · Maxwell Xu[8] · Deborah E. Martinson[2] · Frank Tranghese[9] · Yanxin Pei[10] · James M. Cook[6] · Jeanne Kowalski[2,11] · Michael D. Taylor[4,5,12] · Andrew Jenkins[13] · Daniel A. Pomeranz Krummel[1,2,16] · Soma Sengupta[1,2,14,15,16]

Received: 2 November 2018 / Accepted: 31 January 2019
© The Author(s) 2019

Abstract

Purpose Pediatric brain cancer medulloblastoma (MB) standard-of-care results in numerous comorbidities. MB is comprised of distinct molecular subgroups. Group 3 molecular subgroup patients have the highest relapse rates and after standard-of-care have a 20% survival. Group 3 tumors have high expression of *GABRA5*, which codes for the α5 subunit of the γ-aminobutyric acid type A receptor ($GABA_AR$). We are advancing a therapeutic approach for group 3 based on $GABA_AR$ modulation using benzodiazepine-derivatives.

Methods We performed analysis of *GABR* and *MYC* expression in MB tumors and used molecular, cell biological, and whole-cell electrophysiology approaches to establish presence of a functional 'druggable' $GABA_AR$ in group 3 cells.

Results Analysis of expression of 763 MB tumors reveals that group 3 tumors share high subgroup-specific and correlative expression of *GABR* genes, which code for $GABA_AR$ subunits α5, β3 and γ2 and 3. There are ~ 1000 functional α5-$GABA_ARs$ per group 3 patient-derived cell that mediate a basal chloride-anion efflux of 2×10^9 ions/s. Benzodiazepines, designed to prefer α5-$GABA_AR$, impair group 3 cell viability by enhancing chloride-anion efflux with subtle changes in their structure having significant impact on potency. A potent, non-toxic benzodiazepine ('KRM-II-08') binds to the α5-$GABA_AR$ (0.8 μM EC_{50}) enhancing a chloride-anion efflux that induces mitochondrial membrane depolarization and in response, *TP53* upregulation and p53, constitutively phosphorylated at S392, cytoplasmic localization. This correlates with pro-apoptotic Bcl-2-associated death promoter protein localization.

Conclusion *GABRA5* expression can serve as a diagnostic biomarker for group 3 tumors, while α5-$GABA_AR$ is a therapeutic target for benzodiazepine binding, enhancing an ion imbalance that induces apoptosis.

Keywords Benzodiazepine · Medulloblastoma · $GABA_A$ receptor · Apoptosis · *TP53*

Introduction

Medulloblastoma is a significant cause of cancer-related morbidity and mortality in children [1]. Its standard-of-care consists of surgical resection, followed by radiotherapy and chemotherapy, which cause neurocognitive side effects [2–4]. Medulloblastoma molecular profiling delineated four subgroups, by consensus termed wingless (WNT), sonic hedgehog (SHH), group 3, and group 4 [5–7]. WNT and SHH exhibit anomalous expression of genes associated with the Wnt and Shh pathways, consistent with genomic alterations [8–10]. Groups 3 and 4, which account for ~ 60% of medulloblastomas and include those with poorest prognosis, do not have shared subgroup-specific genomic alterations

Havva Keskin and Alexandra Ross have contributed equally to this work.

Electronic supplementary material The online version of this article (https://doi.org/10.1007/s11060-019-03115-0) contains supplementary material, which is available to authorized users.

✉ Daniel A. Pomeranz Krummel
pomeranz.krummel@emory.edu

✉ Soma Sengupta
soma.sengupta@emory.edu

Extended author information available on the last page of the article

Published online: 06 February 2019

[10]. Group 3 is often referenced as *MYC*-driven, however *MYC* expression is seen in only a subset of group 3 tumors [11]. Group 3 tumors are typically *TP53* wild-type and its high expression is associated with poor prognosis [12, 13]. Group 3 tumors share high expression of *GABRA5*, which codes for the α5-subunit of the ligand-gated ionotropic γ-aminobutyric acid type A receptor ($GABA_AR$) [6].

$GABA_ARs$ are fundamental in determining an excitation/inhibition balance in the CNS. As an ionotropic receptor mediating chloride-anion flux, $GABA_ARs$ predominantly function to hyperpolarize neural cells following binding of γ-aminobutyric acid (GABA), thereby decreasing the likelihood of generating an action potential. $GABA_AR$ usually consists of two α, two β, and γ subunits arranged as α–β–γ–α–β (Fig. 1a). Nineteen genes encode $GABA_AR$ subunits, including of six α (*GABRA1-6*), three β (*GABRB1-3*), and three γ (*GABRG1-3*) [14]. Benzodiazepines bind at the γ-α interface and are positive allosteric modulators, acting to increase GABA effectiveness and thus chloride-anion flux. Benzodiazepines consist commonly of fusion of diazepine and benzene rings (1,4-benzodiazepine) and a phenol ring (5-phenyl-1*H*-benzo[*e*]) (Fig. 1a). Changes to its chemical structure can alter its $GABA_AR$-subtype preference. For example, introducing an ethinyl bond to the diazepine ring at R^7 results in a α5-$GABA_AR$ preference [15, 16].

Investigating $GABA_AR$ in group 3, we showed that Gabra5 (or α5) was present in patient-derived group 3 cells and tumor tissue and contributed to assembly of a functional $GABA_AR$ [17]. An α5-$GABA_AR$ preferring benzodiazepine was capable of impairing group 3 cell viability in vitro [17] and its potency in a mouse model was greater than standard-of-care chemotherapeutic [18] and agents proposed as potential medulloblastoma therapeutics [19, 20]. The most efficacious α5-$GABA_AR$ preferring benzodiazepine tested ('QH-II-066') caused cell cycle arrest and its effectiveness in inducing apoptosis abrogated by loss in expression

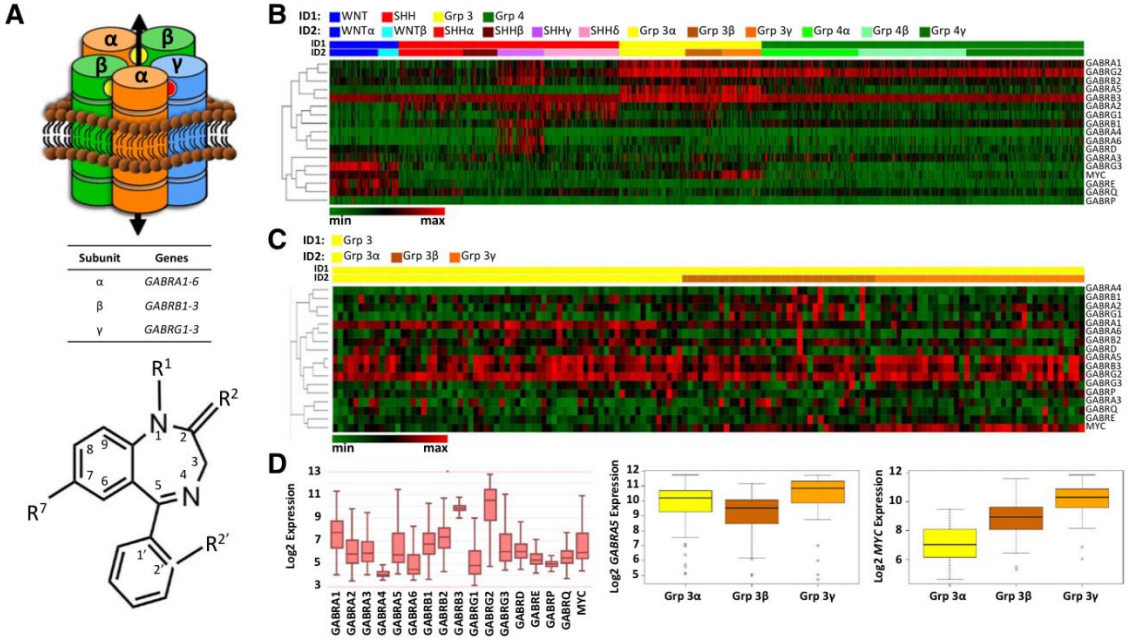

Fig. 1 $GABA_A$ receptor subunit gene (*GABR*) and *MYC* expression across 763 primary medulloblastoma tumors. **a** Top, $GABA_A$ receptor ($GABA_AR$), αβαβγ subunit stoichiometry, consists of five subunit transmembrane segments which create the chloride-anion conduction pore. Inter-subunit binding sites for GABA and benzodiazepine are shown as yellow and red spheres, respectively. Bottom, common core structure of a 'benzodiazepine'. Indicated are sites frequently modified (R^1, R^2, $R^{2'}$, R^7), which may impart a $GABA_AR$ subtype-preference. Introduction of an ethinyl bond at R^7 imparts an α5-$GABA_AR$ preference. **b** Supervised heatmap clustering analysis across medulloblastoma molecular subgroups using z-score scaling, 1-Pearson correlation distance, and average clustering. The relationship between genes is indicated by the dendrogram (left). Shown bottom, left is a color palette where color scaling indicates low (green) to high (red) expression. Samples were classified into four subgroups (ID1) and further into twelve subtypes (ID2). **c** Supervised heatmap clustering analysis of group 3 only using z-score scaling, 1-Pearson correlation distance, and complete clustering. Shown bottom, left is a color palette where color scaling indicates low (green) to high (red) expression. ID1: group 3, yellow; ID2 within group 3: α, yellow; β, brown; γ, orange. **d** Boxplots of *GABR* and *MYC* expression across subgroups (left) and separately *GABRA5* (middle) and *MYC* (right) expression of group 3

of HOXA5, a homeobox transcription factor that regulates p53 expression [17]. Further, QH-II-066 sensitized group 3 cells to radiation and cisplatin in a p53-dependent manner. Thus, p53 appears important in group 3 cells' response to $GABA_AR$ mediated chloride-anion flux.

We report on analysis of $GABA_AR$ and *MYC* expression in 763 primary medulloblastoma patient tumors, characterization of $GABA_AR$ in a patient-derived cell line, identification of chemical features critical to α5-$GABA_AR$ preferring benzodiazepine potency, and examination of how such benzodiazepines may impair group 3 cell viability.

Materials and methods

Gene expression analysis

Normalized gene expression data for sixteen *GABR* genes and *MYC* from 763 primary resected medulloblastoma specimens was used [11]. Samples were classified into four medulloblastoma subgroups and further into twelve subtypes: two WNT subgroup [α (*n* = *49*), β (*n* = *21*)], four SHH subgroup [α (*n* = *65*), β (*n* = *35*), γ (*n* = *47*), δ (*n* = *76*)], three group 3 subgroup [α (*n* = *67*), β (*n* = *37*), γ (*n* = *40*)] and three group 4 subgroups [α (*n* = *98*), β (*n* = *109*), γ (*n* = *119*)]. Heatmaps for analysis of expression across all four subgroups and among group 3 subtypes were generated using Morpheus (https://software.broadinstitute.org/morpheus). Boxplots for expression analysis were created in R.

Cell lines

Daoy (SHH cell line) and D283 (group 3 cell line) were purchased from ATCC. D425 (group 3 cell line) was obtained through a MTA between Emory and Duke.

Cell proliferation

Benzodiazepines were synthesized as described [21, 22], kept lyophilized at room temperature, and suspended prior to use in dimethyl sulfoxide (DMSO; 0.125%). D283 cell viability was assayed using the CellTiter 96® AQueous One Solution Assay (Promega) as described [17]. D283 cells (7500) added per well of a Falcon® 96 well flat bottom TC-treated polystyrene cell culture plate (Corning) in pentaplicates and incubated 4–5 h, 37 °C. DMEM (Thermo-Fisher), lacking phenol-red, HEPES, and penicillin/streptomycin but with 20% FBS and 4 mM L-glutamine, was used for plating. Benzodiazepines were diluted in DMSO (0.125%) to a 4 mM working stock for drug dilution in DMEM. After 48 h at 37 °C, 20 µL CellTiter 96® AQueous One Solution (Promega) was added per well, plate incubated 1 h at 37 °C, and absorbance (490 nm) measured. To obtain a reading, media control (average reading of wells containing only media) was subtracted from DMSO control and drug-treated values. Drug-treated values were divided by DMSO values to normalize data. IC_{50} values were obtained using the '[Inhibitor] versus normalized response' nonlinear regression function in Prism 7 software (GraphPad).

Electrophysiology

Recordings used methods similar to those described [23]. Experiments were performed 24–72 h post-plating at 22 °C and across multiple days (controlling for cell health and expression efficiency). All reagents were purchased from Sigma, unless otherwise noted. Patch pipettes were fabricated from thin-walled borosilicate glass (World Precision Instruments) using a horizontal puller (Sutter Instruments) to give a resistance of 2–8 MΩ when filled with intracellular solution (120 mM KCl/2 mM $MgCl_2$/10 mM EGTA/10 mM HEPES, NaOH adjusted to pH 7.2, 315 mOsm). Extracellular solution contained: 161 mM NaCl/3 mM KCl/1 mM $MgCl_2$/1.5 mM $CaCl_2$/10 mM HEPES/6 mM D-glucose, NaOH adjusted to pH 7.4 (320–330 mOsm). A rapid solution changer (BioLogic Science Instruments) connected to a infusion pump (KD Scientific) delivered GABA and benzodiazepine solutions.

Mitochondria structure–function

Mitochondrial membrane potential was measured using the TMRE Mitochondrial Membrane Potential Assay Kit (Abcam). D283 cells were treated with drug or control solutions (10 min, 37 °C), 50 nM TMRE added (20 min, 37 °C), and TMRE fluorescence visualized (Leica SP8) and quantified (LAS X platform, Leica).

Quantitative RT-PCR

Total RNA was extracted from cells (RNeasy Mini Kit, Qiagen), converted into cDNA by PCR (Cloned AMV First-strand Synthesis Kit, Invitrogen; primers shown in Online Table 1), analyzed using SYBR dye (SYBR Green PCR Master Mix, Applied Biosystems).

Microscopy

Cells plated on poly-D-lysine coated glass coverslips fixed 1 h in 4% (w/v) paraformaldehyde (Electron Microscopy Sciences, EMS), washed in PBS (6×, 5 min/wash), blocked 1 h (PBS, 0.8% Triton X-100, 10% normal goat serum), incubated overnight with antibody. Cells washed in PBS (6×, 5 min/wash) and goat anti-rabbit and goat anti-mouse secondary [Ig-Alexa-488 (green) or Ig-Alexa-555 (red), Invitrogen] added. Cells washed in PBS (6×, 5 min/wash),

coverslips mounted on slides (Immuno Mount DAPI and DABCO Mounting Media, EMS), and fluorescence visualized (Leica SP8) and images prepared (LAS X platform, Leica).

Western blots

D283 whole-cell extracts were prepared as described [17]. Nuclear and cytoplasmic fractions were prepared using NE-PER Nuclear Cytoplasmic Extraction Reagent kit (Thermo-Scientific). Pierce BCA Protein Assay (Thermo-Scientific) was used to quantify protein in lysates. Protein (20 µg whole-cell; 15 µg cytoplasmic/nuclear fractions) were resolved by PAGE using 10% pre-cast gels (Bio-Rad), transferred to 0.45 µM PVDF or 0.45 µM nitrocellulose (for BAD and Caspase-9 antibodies) membranes. Membranes blocked in PBS containing 0.1% Tween 20 and either 5% non-fat dry milk or 5% BSA and probed with primary (anti-p53, anti-PTEN, anti-Caspase-9, anti-GAPDH, anti-β-actin, Lamin B1, PARP, Cell Signaling; anti-MDM2, Abcam). Additionally, Abcam's p53 Antibody Sampler Panel [S20, S46, S392, phospho-p53 (K382), and p53 (DO)] was used. Membranes washed 3× (10 min/wash) with 0.1% PBST or 0.1% TBST (for phospho-p53 antibodies) and incubated in HRP-conjugated secondary anti-rabbit or anti-mouse (GE). Membranes washed (3×, 10 min/wash) with 0.1% PBST or 0.1% TBST and visualized using ECL Western Blotting Detection Reagent (Amersham) or SuperSignal™ West Pico PLUS Chemiluminescent Substrate (Thermo-Scientific) and film.

Results

Medulloblastoma gene expression

We analyzed *GABR* and *MYC* expression across all subgroups in 763 resected primary medulloblastoma tumors [11] (Fig. 1b, c; Online Resource 1, 2; Online Tables 2, 3). This analysis reveals that: (1) all subgroups have shared high expression of select *GABR* genes; (2) there is subgroup-specific high expression of some *GABR* genes and some subgroups have *GABR* expression that is specific to only a subset of patients within the subgroup; (3) there is a positive correlation in expression of *GABRA5* and *MYC* in a subset of group 3 and more surprisingly WNT tumors.

GABRB3 expression is high across all four subgroups, with subtle differences in the degree of expression across subgroups (Fig. 1b, c). Expression is also high for *GABRG2*, but there is greater variability in degree of expression between subgroups. Groups 3 and 4 have highest expression of *GABRG2*.

GABR expression between subgroups and within some subgroups is variable: (i) WNT subgroup subtypes (α and β) have high expression of *GABRG3* and *GABRE*; (ii) SHHγ subtype has high expression of several *GABR* genes that distinguish it from SHHα, SHHβ, SHHδ, while all SHH subgroup patients have high expression of *GABRA2* and *GABRG1*. Medulloblastoma patients with poorest prognosis are group 3. Group 3 patients have high *GABRA5* expression. *GABRA5* expression is consistently the highest in the group 3γ subtype, which carries the poorest prognosis.

Supervised heatmaps and boxplots show expression differences for both *GABRA*5 and *MYC* within group 3 and WNT subgroups. Correlation between *MYC* and *GABRA5* is not statistically significant in group 3 ($p = 0.202$). However, there is a significant positive correlation in expression between *GABRA5* and *MYC* in the group 3α subtype ($p = 0.006$), where it was reported that *MYC* loss is more frequent [9], but not in group 3β ($p = 0.336$). Group 3γ has the highest level of *MYC* expression [11]. We do not find a significant correlation ($p = 0.634$) between *MYC* and *GABRA5* expression in the group 3γ subtype. As well as group 3γ, WNT subgroup patients have high *MYC* expression (Fig. 1b). There is a significant positive correlation of *MYC* and *GABRA5* ($p < 0.001$) in the WNT subgroup (Online Resource 1; Online Table 2), but *GABRA5* expression is significantly lower than in group 3 tumors.

GABR expression consistent with assembly of α5-GABRAR

To identify the probable composition of a $GABA_AR$ in medulloblastoma tumors that would be sensitive to benzodiazepine modulation, we examined correlation in expression of $GABA_AR$ subunits in subgroups using the normalized gene expression dataset of 763 medulloblastoma tumors [11] (Online Resource 2). Using a Spearman's correlation test (where $p < 0.01$) we find that: (1) there is a positive correlation in all subgroups in expression of *GABR* genes that may form a functional $GABA_AR$ sensitive to benzodiazepine modulation; and (2) group 3 has a high and correlative expression that includes *GABRA5*. In WNT, SHH, group 3, and group 4 there is a shared correlation in expression of two groups of genes that suggest assembly of a functional $GABA_AR$ and its composition. The *GABR* gene groups in WNT, SHH, group 3, and group 4 are: (1) *GABRA1, GABRB2*, and *GABRG2*, which code for α1, β2, and γ2 subunits, respectively; and (2) *GABRA2, GABRB1*, and *GABRG1*, which code for α2, β1, and γ1 subunits, respectively. In group 3 there is a set of *GABR* genes that exhibit high expression and have a significant correlation in expression: *GABRA5, GABRB3*, and *GABRG2 or GABRAG3*, which code for α5, β3, γ2 and γ3 subunits, respectively.

To investigate how benzodiazepines may impair group 3 cell viability requires use of a cell line(s) that reflects the molecular profile of group 3 patient tumors. A significant

difference in expression between group 3 subtypes and other subgroups is the degree of *GABRA5* expression. Further, group 3 tumors typically have low *N-MYC* and high *MYC* expression [11]. We analyzed expression by qRT-PCR patient-derived lines Daoy, D283 and D425 for *N/C-MYC* and *GABRA5*. Daoy is reported as SHH subgroup derived [24], while D283 is a group 3 medulloblastoma line, *TP53*-wildtype [25], and D425 is a group 3 medulloblastoma line, *TP53*-mutated [26]. qRT-PCR reveals that Daoy, D283, and D425 have a low and similar degree of expression of *N-MYC* (Fig. 2a). Daoy has no significant expression of *MYC*. In contrast, D283 and D425 have high *MYC* expression, characteristic of some WNT and group 3 tumors. As noted, group 3 tumors have high correlative expression of *GABRA5, GABRB3*, and *GABRG2*, which cluster on chromosome/locus 15q12. In addition, group 3α patient tumors have high *GABRA1* expression. D283 has very high *GABRA5* expression, relative to other *GABRA* genes, and higher *GABRB3* and *GABRG2* than other *GABRB* and *GABRG* genes, respectively (Fig. 2b). There is a consistency in expression between group 3 tumors and D283 cells. Most likely, D283 cell line is representative of group 3β or 3γ, given the lower *GABRA1* expression detected by qRT-PCR, which is more reflective of group 3α.

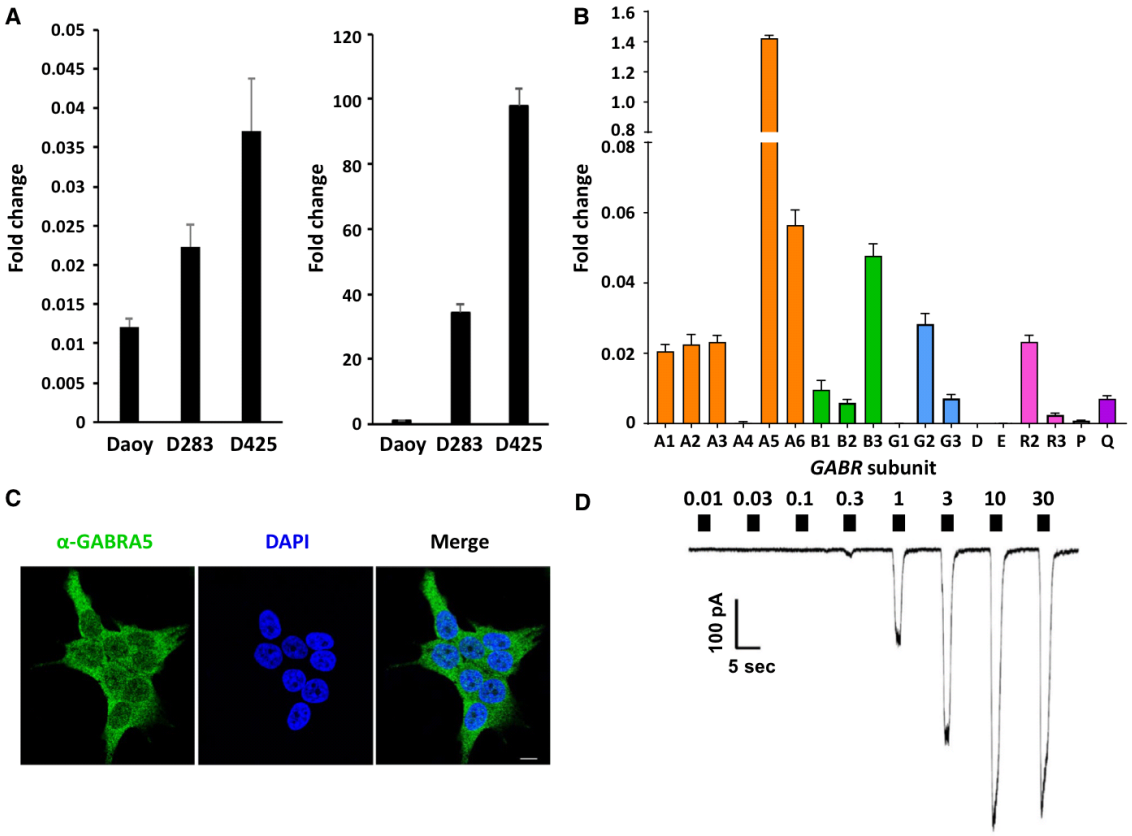

Fig. 2 *MYC* and *GABR* expression in medulloblastoma and evidence for a functional α5-$GABA_A$ receptor. **a** qRT-PCR of *N-MYC* (left) and *MYC* (right) in patient-derived lines Daoy, D283, and D425. **b** qRT-PCR of *GABR* expression in D283. Data are represented as a fold-change value with respect to expression of the housekeeping gene *TBP*, TATA Box binding protein. Values in all panels are presented as the mean and standard deviation of three experiments. Primer sequences listed in Online Resource Table 1. **c** The *GABRA5* protein product (or α5 subunit) localizes to the cell membrane in patient-derived cell line D283 with diffuse staining over the plasma membrane, as visualized by immunofluorescence microscopy using an antibody specific to the α5 subunit (green). Nucleus of cells is stained with 4′,6-diamidino-2-phenylindole (DAPI). Scale bar, 10 microns. **d** Representative current trace from a whole-cell patch clamp electrophysiology recording of a D283 cell, clamped at −60 mV. Filled boxes above the current trace denote the period of GABA exposure (2 s) and are labeled with the concentration applied (0.01–30 μM)

A functional α5-GABRAR in D283 cells

Immuno-staining for the α5-subunit shows diffuse staining that appears localized to the plasma membrane (Fig. 2c). To establish that D283 cells express functional $GABA_AR$s, we obtained whole-cell patch clamp recordings. If functional $GABA_AR$s were expressed on the cell surface, then its agonist GABA should elicit a concentration-dependent chloride-anion flux. For D283 cells the average maximal current, EC_{50}, and Hill slope of GABA responses in D283 cells was -480 ± 120 pA, 1.26 ± 0.05 μM, and 1.37 ± 0.07 respectively (where $n = 8$) (Fig. 2d), demonstrating a concentration-dependent chloride-anion flux commensurate with GABA concentration. The electrophysiology recordings also provide insight into $GABA_AR$ subtype, chloride-anion flux rate, and number of functional receptors per D283 cell. The low GABA EC_{50} of the native GABA-sensitive receptor in D283 cells is consistent with expression of a $\alpha_5\beta_3\gamma_2$ or γ_3-like $GABA_AR$, supported by qRT-PCR analysis as well as *GABR* expression in group 3 tumors. The basal chloride-anion efflux rate is $\sim 2 \times 10^9$ ions/s, consistent with the rate of recombinant expressed $GABA_AR$. We estimate that there are ~ 1000 functional α5-$GABA_AR$s per D283 cell.

Benzodiazepines are potent α5-GABAAR modulators

We screened benzodiazepines to identify aspects of the chemical structure critical to potency (Fig. 3). All benzodiazepines examined were synthesized to be α5-$GABA_AR$ preferring and differed chemically at R^1, endocyclic 2′, or exocyclic $R^{2'}$. The most potent benzodiazepines have a hydrogen at R^1 and no modification at the endocyclic 2′ or exocyclic $R^{2'}$ (NOR-QH-II-066) or fluoride at the exocyclic $R^{2'}$ (KRM-II-08 and NOR-KRM-II-08). Benzodiazepines with a larger halide (e.g. chloride) at exocyclic $R^{2'}$ (KRM-III-77 and NOR-KRM-III-77) are poorer ligands for α5-$GABA_AR$. The 2′-F at the exocyclic $R^{2'}$ on KRM-II-08 may form a better three-centered hydrogen bond in the α5-$GABA_AR$ binding site, consistent with in silico modeling [27, 28]. We note an apparent increase in cell growth for KRM-III-70, which has an exocyclic nitrogen at $R^{2'}$. This benzodiazepine may bind to an alternative target such as the peripheral benzodiazepine channel TSPO (see below), which could enhance mitochondrial function and cell proliferation.

Benzodiazepine enhances chloride-anion efflux

We pursued for greater analysis QH-II-066 and KRM-II-08, which have IC_{50} values of 3.4 ± 0.3 and 0.8 ± 0.1 μM,

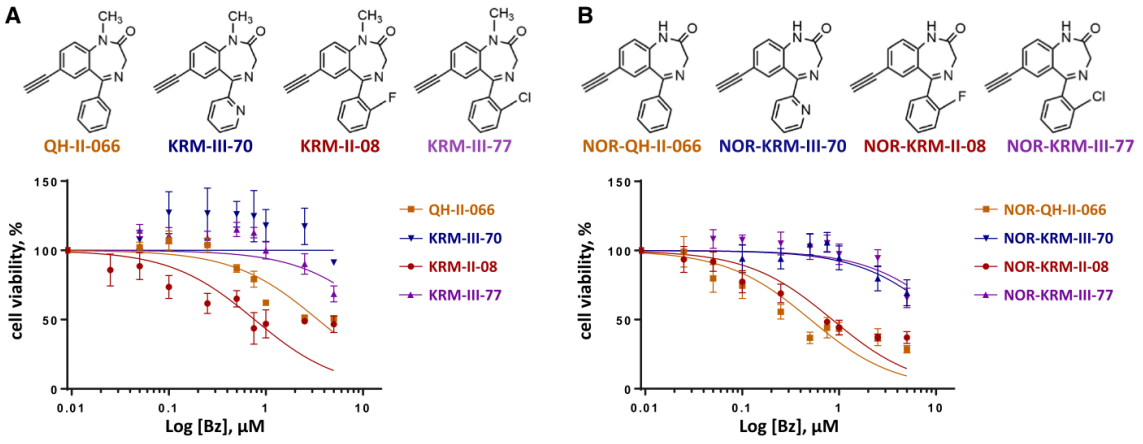

Bz	IC_{50} (μM)
QH-II-066	3.4 ± 0.3
KRM-III-70	-
KRM-II-08	0.8 ± 0.1
KRM-III-77	16.3 ± 3.4

Bz	IC_{50} (μM)
NOR-QH-II-066	0.51 ± 0.06
NOR-KRM-III-70	12.16 ± 1.85
NOR-KRM-II-08	0.85 ± 0.09
NOR-KRM-III-77	14.97 ± 2.54

Fig. 3 Cell viability impaired by α5-preferring benzodiazepines. Chemical structures of α5-selective benzodiazepines (**a**) and NOR variants (**b**) tested (top), dose–response curves from MTS cell proliferation assay at 48 h (middle) presented as semi-log plots and derived IC_{50} values (bottom)

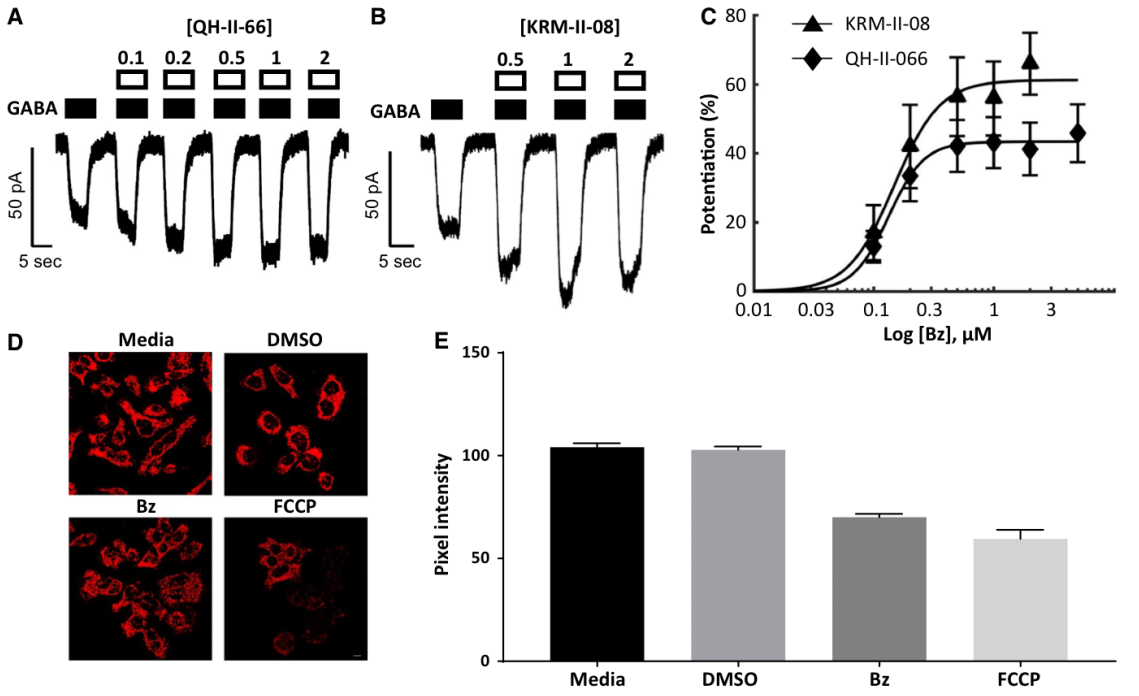

Fig. 4 Early chemical and physiological response of group 3 medulloblastoma cells treated with α5-selective benzodiazepines. **a**, **b** D283 cells, clamped at −60 mV, responses to GABA by α5-selective benzodiazepines QH-II-066 (**a**) and KRM-II-08 (**b**). Filled boxes above current trace denote duration of GABA application. Open boxes denote the period of benzodiazepine exposure and are labeled with the concentration applied. **c** Both QH-II-066 and KRM-II-08 (Bz) show enhanced submaximal (EC_5–EC_{10}) responses in a concentration-dependent manner: PC_{50}: 43 ± 7 versus 61 ± 9, Hill slope 2.7 ± 5 versus 2.9 ± 5 and PC_{50} 0.13 ± 0.09 versus 0.14 ± 0.07 µM, respectively. The effects of QH-II-066 and KRM-II-08 were not significantly different from one another ($p > 0.05$, Student's *t*-test). **d** Fluorescence microscopy imaging of live D283 cells stained with tetramethylrhodamine ethyl ester (TMRE) following a 10-min treatment with dimethyl sulfoxide (DMSO; 0.125%), carbonyl cyanide 4-(trifluoromethoxy) phenylhydrazone (FCCP, 20 µM), or KRM-II-08 (Bz) (0.7 µM). Media alone had no DMSO. Peak: λ_{ex}, 549 nm; λ_{em}, 575 nm. **e** Quantitation of TMRE staining with the Leica Application Suite X (LAS X) software platform. Data are presented as standard error from mean of thirty or more cells (media, n = 30; DMSO, n = 43; KRM, n = 39; FCCP, n = 35). Scale bar in panel (**d**) image for FCCP is 10 microns

respectively. Whole-cell recordings were obtained of the effect of these benzodiazepines on $GABA_AR$ function in D283 cells (Fig. 4a–c; Online Resource 3). QH-II-066 and KRM-II-08 enhanced EC_{10} responses in a concentration-dependent manner: PC_{50}: 43 ± 7 versus 61 ± 9, hill slope 2.7 ± 5 versus 2.9 ± 5 and PC_{50} 0.13 ± 0.09 versus 0.14 ± 0.07 µM, respectively. The high apparent affinity for GABA in D283 cells is consistent with the presence of functional α5-$GABA_ARs$. The EC_{50} values for QH-II-066 and KRM-II-08 are similar in all assays performed, $p > 0.05$ Student's *t*-test, in contrast to their IC_{50} values. In all cases, the modulation peaks below 2 µM and has a maximum effect of ~ 50%.

Given the lower IC_{50} of KRM-II-08 as well as greater solubility than QH-II-06 and its potential for future therapeutic use, we assessed its hepatocyte toxicity profile. LD_{50} for KRM-II-08 in vitro is > 100 µM, tested in two cell lines (HEK293 and HEPG2) (Online Resource 4). KRM-II-08 is non-toxic until the concentration is less than or equal to 100 µM, a concentration higher than IC_{50} and EC_{50} values.

Benzodiazepine induces changes in mitochondria

Since we expected that benzodiazepine binding to $GABA_AR$ in group 3 cells might alter ionic flux rapidly assuming exogenous GABA is ≥ 0.3 µM, we examined changes to mitochondria and its membrane potential. Staining for $GABA_AR$ at the plasma membrane remains similar and constant in DMSO and KRM-II-08 treated cells as well as untreated cells over 48 h (Online Resource 5), suggesting that the receptor remains intact and possibly then functional. We examined changes in mitochondrial morphology using the cationic stain tetramethylrhodamine ethyl ether (TMRE), which is taken-up by functioning mitochondria. Ten-minutes

following benzodiazepine treatment, mitochondria have undergone fission but continue to take-up TMRE (Fig. 4d). Fission of mitochondria is not observed in DMSO but is when a protonophore, carbonyl cyanide-4-(trifluoromethoxy) phenylhydrazone (FCCP) is added.

FCCP disrupts mitochondrial ATP synthesis, depolarizing mitochondria or causing loss of ΔΨm [29]. FCCP is used as a positive control for monitoring change in mitochondria membrane potential, as it causes reduced TMRE staining. We quantified the degree of TMRE staining of thirty or more cells in all treatment groups (Fig. 4e). KRM-II-08 causes a depolarization of mitochondrial membrane potential within 10 min, but not DMSO.

There is, as noted above, a chloride-anion efflux in D283 cells commensurate with benzodiazepine administration that mediates membrane depolarization. Present in the outer mitochondrial membrane is the peripheral benzodiazepine metabotropic receptor TSPO to which diazepam has reported to bind and whose activity can reduce mitochondrial membrane potential [30]. We tested if TSPO agonist emapunil has an effect on viability of Daoy and D283 cells to determine if the observed potency of KRM-II-08 was a consequence of its binding to TSPO (Online Resource 6). Emapunil does not impair viability of Daoy or D283 cells. This observation supports the contention that the primary and effective binding site of KRM-II-08 that induces apoptosis is not TSPO.

p53 response to benzodiazepine

Previously we demonstrated that benzodiazepines were capable of impairing group 3 cell viability, including of cell line D425, which has a *TP53* exon 4 single-nucleotide polymorphism (R72P) that has been reported to impact the apoptotic response to some types of stress [31]. Since D425 response to the benzodiazepines tested was not impacted by the *TP53* polymorphism, this supports p53 not being critical to the cell death response. However, this point mutation may not impair all functions of p53 and the apoptotic response of some types of stress are not impacted [32]. We also previously observed that benzodiazepines were capable of sensitizing group 3 cells to either radiation or a chemotherapeutic, abrogated by a p53 knockdown [17], which supports the role of p53 in the apoptotic response mediated by benzodiazepines.

Since p53 appears to play a critical role in the stress-response to benzodiazepine mediated chloride-anion efflux and its DNA-binding domain contributes to this role, we examined the impact of the benzodiazepine KRM-II-08 on expression of genes that participate in the *PTEN-TP53-AKT-MDM2* signaling axis [33]: PI3K molecules (Class I regulatory and catalytic subunits, Class II, and Class III); serine/threonine kinases *AKT1*, *AKT2*, and *AKT3*; *PTEN*, the phosphatase which negatively regulates the PI3K/Akt signaling pathway, stabilizes p53, and whose expression is regulated by p53; and *MDM2*, which codes for the E3 ubiquitin ligase that functions as a negative regulator of p53. We examined changes in expression of these genes as well as *TP53* in D283 cells at 6 and 24 h post-incubation with KRM-II-08. *MDM2*, *PTEN*, *AKT1-3* as well as *TP53* are upregulated in KRM-II-08 treated cells, which is benzodiazepine-specific, as DMSO causes no change in *TP53* and *PTEN* levels while *MDM2 and AKT1-3* expression are down-regulated (Online Resource 7). Of *PI3K* genes, only Class I catalytic and regulatory subunits PI3CA and PIK3R1, respectively, are significantly upregulated. *MDM2* protein levels also appear to increase moderately between 6 and 24 h post-KRM-II-08 treatment, while p53 levels increase significantly at 24 h and in both nuclear and cytoplasmic fractions (Fig. 5a). As well as an increase in p53 by Western blot, we observe an increase in p53 by immunofluorescence with the most intense staining in the nucleus (Fig. 5b).

Previously we observed that a less potent benzodiazepine studied here (see QH-II-066, IC_{50} 3.4 μM), caused cell cycle arrest [17]. We therefore repeated an analysis on the cell cycle of D283 cells of the more potent benzodiazepine KRM-II-8 (IC_{50} 0.8 μM). KRM-II-08 does not arrest the cell cycle of D283 cells at 24 or 48 h (Online Resource 8). This suggests that the less potent benzodiazepine tested earlier may have a secondary or 'off-target' effect in group 3 cells. However, arresting the cell cycle is not critical to benzodiazepine-mediated apoptosis.

Activation of cell death

There are early changes in mitochondrial structure–function, which may precipitate events that result in D283 cell death. However, cell death is not immediate and may require p53 transcriptional activity as well as its migration to the cytoplasm. We initially examined whether D283 cells underwent senescence. Analysis of senescence-associated β-galactosidase of DMSO and KRM-II-08 treated cells reveals that in 48 h at most ~ 12% of cells may be undergoing senescence (Online Resource 9), which does not account for loss in cell viability observed using KRM-II-08. We subsequently utilized an immune-blotting approach to identify change in levels and/or post-translational modification of proteins that have a role in apoptosis in D283 cells incubated with DMSO or KRM-II-08. There is a modest change in the degree of p53 post-translational modification, specifically phosphorylation of Serine392 (pS392) (Online Resource 10). We confirmed by Western that p53 is phosphorylated at S392 (Fig. 5a). While S392 exhibits increased phosphorylation in KRM-II-08 treated cells, it's also modified in

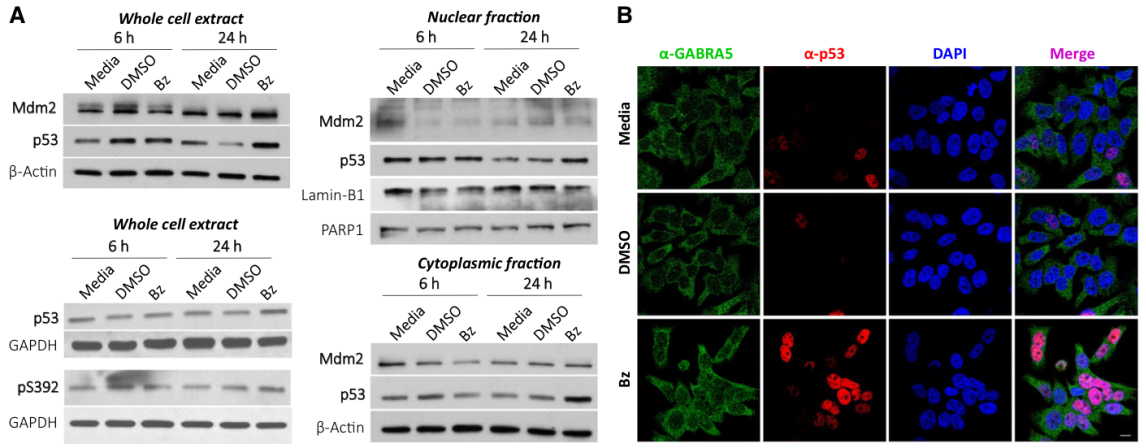

Fig. 5 Contribution of p53 to response of α5-preferring benzodiazepine KRM-II-08. **a** Western blot of Mdm2 and p53 at 6 and 24 h post-treatment with KRM-II-08. Western blots of whole cell (top), cytoplasmic (middle), and nuclear (bottom) extracts. Loading controls for blots are beta-actin, Lamin-B1, and/or PARP1. Western blot of p53 using antibodies that recognize the protein regardless of post-translational modification and specific to phosphorylation of p53 Serine392 (pS392). GAPDH is the loading control. **b** Immunofluorescence microscopy imaging of D283 cells at 24 h following incubation with media alone, DMSO, or KRM-II-08 (Bz, 0.8 μM). Cells were stained using antibodies specific to α5 (green) and p53 (red). Nucleus of cells were stained with 4′,6-diamidino-2-phenylindole (DAPI). Scale bar in bottom, right image is 10 microns

control cells (DMSO and media). Thus, pS392 appears to be a constitutive modification in D283 cells.

Since senescence did not account for the death of most benzodiazepine treated cells, we examined by immunofluorescence KRM-II-08 treated D283 cells for change in amount and/or localization of pro-apoptotic Bcl-2 family members Bax, Puma, Bcl-2, Bcl-xL, and BAD [34]. Only BAD protein exhibits a change in intensity detected by immunofluorescence in KRM-II-08 treated D283 cells and there is a slight increase in BAD protein levels between 6 and 24 h (Online Resource 11). It's been reported that BAD and p53 do complex at mitochondria to induce apoptosis [35].

Discussion

In medulloblastomas we find that *GABR* genes are expressed in all subgroups. Interestingly, we find that WNT subgroup patients appear to have a unique shared *GABR* expression signature. In contrast, not all SHH subgroup patients have a shared *GABR* expression signature, however, there is a specific subset of SHH subgroup patients (the SHHγ subtype) that do. These observations may be connected to activation of distinct signaling pathways in these subgroups and warrant further analysis. In this study, we have also explored in detail the *GABR* signature in group 3 patients and the functional and therapeutic implications of the signature. We report that the group 3 cell line D283 has a functional $\alpha_5\beta_3\gamma_2$ or γ_3-like $GABA_AR$ and have shown the physical, chemical, and molecular changes to group 3 cells that precede their death, as a consequence of α5-$GABA_AR$ preferring benzodiazepine enhancing the activity of GABA.

In a non-neural cell, $GABA_AR$ may polarize a cell by creating a chloride-anion flux, which may drive cell proliferation [36]. Alternatively, a chloride-anion flux may elicit a stress-response, if it significantly perturbs ionic homeostasis [37]. We have shown that the $\alpha_5\beta_3\gamma_2$ or γ_3-like $GABA_AR$ in group 3 cells mediates a significant chloride-anion efflux to depolarize mitochondria, when an α5-$GABA_AR$ preferring benzodiazepine binds in the presence of GABA, such that the cell activates a stress-response involving p53 and that this sustained effect induces apoptosis.

In our analysis of p53 response to benzodiazepine, we find that p53 is constitutively phosphorylated at S392. S392 phosphorylation stabilize p53's tetrameric state, which decreases its turnover and increases its DNA-binding affinity [38]. We have not examined the oligomeric state of cytoplasmic p53, but it may serve a role in determining its cytoplasmic function that includes an increased affinity for the pro/anti-apoptotic protein BAD. In addition, S392 hyperphosphorylation is correlated with poor prognosis in several cancers [39–41], and this may be the case in medulloblastoma.

Conclusion

Altered GABA levels or high expression of $GABA_AR$ subunits has been observed in pediatric as well as adult cancers

[42–46]. Ion channels have potential to be promising anticancer therapeutic targets [47] and a significant number of FDA approved drugs target $GABA_A$Rs. α5-$GABA_A$R preferring benzodiazepine KRM-II-08 is like other benzodiazepines predicted to be non-toxic and capable of crossing the blood–brain barrier. While we have shown in cell culture that KRM-II-08 is non-toxic, further testing in vivo is warranted. KRM-II-08 may be an effective therapeutic to be included in treating medulloblastoma and other cancers. Moving in this direction will require more extensive studies in an appropriate animal model, possibly exploring impact of administration of benzodiazepine in combination with radiation and/or other therapeutics.

Acknowledgements We thank Scott Pomeroy, Tobey MacDonald, and Yoon-Jae Cho for helpful discussions.

Funding Financial support for this study was provided by: National Institutes of Health-NINDS under award number K08 NS083626, an American Cancer Society Institutional Research grant (IRG-14-188-01), and B*CURED Brain Cancer Research Investigator Award to S.S.; National Institutes of Health-NINDS under award number NS089719 to A.J.; National Institutes of Health under award numbers NS076517, MH096463, and HL118561 to J.M.C. and use by J.M.C. of the Shimadzu Analytical Laboratory of Southeastern Wisconsin for mass spectroscopy. Research reported in this publication was also supported in part by the Biostatistics & Bioinformatics and the Integrated Cellular Imaging Shared Resources of the Winship Cancer Institute of Emory University and National Institutes of Health/National Cancer Institute under award number P30CA138292. The content is solely the responsibility of the authors and does not necessarily represent the official views of the National Institutes of Health.

Compliance with ethical standards

Conflict of interest All authors declare they have no conflict of interest with the present study.

Open Access This article is distributed under the terms of the Creative Commons Attribution 4.0 International License (http://creativecommons.org/licenses/by/4.0/), which permits unrestricted use, distribution, and reproduction in any medium, provided you give appropriate credit to the original author(s) and the source, provide a link to the Creative Commons license, and indicate if changes were made.

References

1. Sengupta S, Pomeranz Krummel D, Pomeroy S (2017) The evolution of medulloblastoma therapy to personalized medcine. F1000Research 6:490. https://doi.org/10.12688/f1000research.10859.1
2. Sturm D, Pfister SM, Jones DTW (2017) Pediatric gliomas: current concepts on diagnosis, biology, and clinical management. J Clin Oncol 35:2370–2377. https://doi.org/10.1200/JCO.2017.73.0242
3. Marini BL, Benitez LL, Zureick AH, Salloum R, Gauthier AC, Brown J et al (2017) Blood–brain barrier-adapted precision medicine therapy for pediatric brain tumors. Transl Res 188:e1–e27. https://doi.org/10.1016/j.trsl.2017.08.001
4. Wu L, Li X, Janagam DR, Lowe TL (2014) Overcoming the blood–brain barrier in chemotherapy treatment of pediatric brain tumors. Pharm Res 31:531–540. https://doi.org/10.1007/s11095-013-1196-z
5. Schwalbe EC, Lindsey JC, Nakjang S, Crosier S, Smith AJ, Hicks D et al (2017) Novel molecular subgroups for clinical classification and outcome prediction in childhood medulloblastoma: a cohort study. Lancet Oncol 18:958–971. https://doi.org/10.1016/S1470-2045(17)30243-7
6. Cho YJ, Tsherniak A, Tamayo P, Santagata S, Ligon A, Greulich H et al (2011) Integrative genomic analysis of medulloblastoma identifies a molecular subgroup that drives poor clinical outcome. J Clin Oncol 29:1424–1430. https://doi.org/10.1200/JCO.2010.28.5148
7. Northcott PA, Korshunov A, Witt H, Hielscher T, Eberhart CG, Mack S et al (2011) Medulloblastoma comprises four distinct molecular variants. J Clin Oncol 29:1408–1414. https://doi.org/10.1200/JCO.2009.27.4324
8. Kool M, Korshunov A, Remke M, Jones DTW, Schlanstein M, Northcott PA et al (2012) Molecular subgroups of medulloblastoma: a international meta-analysis of transcriptome, genetic aberrations, and clinical data of WNT, SHH, Group 3, and Group 4 medulloblastomas. Acta Neuropathol 123:473–484. https://doi.org/10.1007/s00401-012-0958-8
9. Northcott PA, Shih DJ, Peacock J, Garzia L, Morrissy AS, Zichner T et al (2012) Subgroup-specific structural variation across 1,000 medulloblastoma genomes. Nature 488:49–56. https://doi.org/10.1038/nature11327
10. Pugh TJ, Weeraratne SD, Archer TC, Pomeranz Krummel DA, Auclair D, Bochicchio J et al (2012) Medulloblastoma exome sequencing uncovers subtype-specific somatic mutations within a broad landscape of genetic heterogeneity. Nature 488:106–110. https://doi.org/10.1038/nature11329
11. Cavalli FMG, Remke M, Rampasek L, Peacock J, Shi DJH, Luu B et al (2017) Intertumoral heterogeneity within medulloblastoma subgroups. Cancer Cell 31:737–754. https://doi.org/10.1016/j.ccell.2017.05.005
12. Gessi M, von Bueren AO, Rutkowski S, Pietsch T (2012) p53 expression predicts dismal outcome for medulloblastoma patients with metastatic disease. J Neuro Oncol 106:135–141. https://doi.org/10.1007/s11060-011-0648-8
13. Northcott PA, Buchhalter I, Morrissy AS, Hovestadt V, Weischenfeldt J, Ehrenberger T et al (2017) The whole-genome landscape of medulloblastoma subtypes. Nature 547:311–317. https://doi.org/10.1038/nature22973
14. Sigel E, Steinmann ME (2012) Structure, function, and modulation of GABAA receptors. J Biol Chem 287:40224–40231. https://doi.org/10.1074/jbc.R112.386664
15. Huang Q, Liu R, Zhang P, He X, McKernan R, Gan T, Bennett DW, Cook JM (1998) Predictive models for GABAA/benzodiazepine receptor subtypes: studies of quantitative structure – activity relationships for imidazobenzodiazepines at five recombinant GABAA/benzodiazepine receptor subtypes [αxβ3γ2 (x = 1–3, 5, and 6)] via comparative molecular field analysis. J Med Chem 41:4130–4142. https://doi.org/10.1021/jm980317y
16. Huang Q, He X, Ma C, Liu R, Yu S, Dayer CA, Wenger GR, McKernan R, Cook JM (2000) Pharmacophore/receptor models for GABA(A)/BzR subtypes (alpha1beta3gamma2, alpha5beta3gamma2, and alpha6beta3gamma2) via a comprehensive ligand-mapping approach. J Med Chem 43:71–95. https://doi.org/10.1021/jm990341r
17. Sengupta S, Weeraratne SD, Sun H, Phallen J, Rallapalli SK, Teider N et al (2014) α5-GABAA receptors negatively regulate MYC-amplified medulloblastoma growth. Acta Neuropathol 127:593–603. https://doi.org/10.1007/s00401-013-1205-7

18. Jonas O, Calligaris D, Methuku KR, Poe MM, Francois JP, Tranghese F et al (2016) First in vivo testing of compounds targeting Group 3 medulloblastoma using an implantable microdevice as a new paradigm for drug development. J Biomed Nanotechnol 12:1297–1302. https://doi.org/10.1166/jbn.2016.2262
19. Bandopadhayay P, Bergthold G, Nguyen B, Schubert S, Gholamin S, Tang Y et al (2014) BET bromodomain inhibition of MYC-amplified medulloblastoma. Clin Cancer Res 20:912–925. https://doi.org/10.1158/1078-0432.CCR-13-2281
20. Bai RY, Staedtke V, Rudin CM, Bunz F, Riggins GJ (2015) Effective treatment of diverse medulloblastoma models with mebendazole and its impact on tumor angiogenesis. Neuro Oncol 17:545–554. https://doi.org/10.1093/neuonc/nou234
21. Cook JM, Huang Q, He X, Li X, Yu J, Han D, Lelas S, McElroy JF (2006) US Patent 7119196 B2
22. Cook JM, Huang S, Edwankar R, Namjoshi OA, Wang ZJ (2014) US Patent 8835424 B2
23. Williams CA, Bell SV, Jenkins A (2010) A residue in loop 9 of the beta2-subunit stabilizes the closed state of the GABAA receptor. J Biol Chem 285:7281–7287. https://doi.org/10.1074/jbc.M109.050294
24. Jacobsen PF, Jenkyn DJ, Papadimitriou JM (1985) Establishment of a human medulloblastoma cell line and its heterotransplantation into nude mice. J Neuropathol Exp Neurol 44:472–485
25. Friedman HS, Burger PC, Bigner SH, Trojanowski JQ, Wikstrand CJ, Halperin EC, Bigner DD (1985) Establishment and characterization of the human medulloblastoma cell line and transplantable xenograft D283. Med J Neuropathol Exp Neurol 44:592–605
26. Bigner SH, Friedman HS, Vogelstein B, Oakes WJ, Bigner DD (1990) Amplification of the c-myc gene in human medulloblastoma cell lines and xenografts. Cancer Res 50:2347–2350
27. Clayton T, Chen JL, Ernst M, Richter L, Cromer BA, Morton CJ et al (2007) An updated unified pharmacophore model of the benzodiazepine binding site on gamma-aminobutyric acid(a) receptors: correlation with comparative models. Curr Med Chem 14:2755–2775. https://doi.org/10.2174/092986707782360097
28. Clayton T, Poe MM, Rallapalli S, Biawat P, Savić MM, Rowlett JK et al (2015) A review of the updated pharmacophore for the alpha 5 GABA (A) benzodiazepine receptor model. Int J Med Chem 2015:430248. https://doi.org/10.1155/2015/430248
29. Maro B, Marty MC, Bornens M (1982) In vivo and in vitro effects of the mitochondrial uncoupler FCCP on microtubules. EMBO J 1:1347–1352
30. Costa B, Da Pozzo E, Martini C (2012) Translocator protein as a promising target for novel anxiolytics. Curr Top Med Chem 12:270–285. https://doi.org/10.1111/j.1365-2826.2011.02166.x
31. Zhu F, Dollé ME, Berton TR, Kuiper RV, Capps C, Espejo A et al (2010) Mouse models for the p53 R72P polymorphism mimic human phenotypes. Cancer Res 70:5851–5859. https://doi.org/10.1158/0008-5472.CAN-09-4646
32. Domínguez ER, Orona J, Lin K, Pérez CJ, Benavides F, Kusewitt DF, Johnson DG (2017) The p53 R72P polymorphism does not affect the physiological response to ionizing radiation in a mouse model. Cell Cycle 16:1153–1163. https://doi.org/10.1080/15384101.2017.1312234
33. Abraham AG, O'Neill E (2014) PI3K/Akt-mediated regulation of p53 in cancer. Biochem Soc Trans 42:798–803. https://doi.org/10.1042/BST20140070
34. Chipuk JE, Green DR (2008) How do BCL-2 proteins induce mitochondrial outer membrane permeabilization? Trends Cell Biol 18:157–164. https://doi.org/10.1016/j.tcb.2008.01.007
35. Charlot JF, Prétet JL, Haughey C, Mougin C (2004) Mitochondrial translocation of p53 and mitochondrial membrane potential (Delta Psi m) dissipation are early events in staurosporine-induced apoptosis of wild type and mutated p53 epithelial cells. Apoptosis 9:333–343. https://doi.org/10.1023/B:APPT.0000025810.58981.4c
36. Blackiston DJ, McLaughlin KA, Levin M (2009) Bioelectric controls of cell proliferation: ion channels, membrane voltage and the cell cycle. Cell Cycle 8:3519–3528. https://doi.org/10.4161/cc.8.21.9888
37. Yu SP, Canzoniero LM, Choi DW (2001) Ion homeostasis and apoptosis. Curr Opin Cell Biol 13:405–411. https://doi.org/10.1016/S0955-0674(00)00228-3
38. Sakaguchi K, Sakamoto H, Lewis MS, Anderson CW, Erickson JW, Appella E, Xie D (1997) Phosphorylation of serine 392 stabilizes the tetramer formation of tumor suppressor protein p53. Biochemistry 36:10117–10124. https://doi.org/10.1021/bi970759w
39. Bar JK, Słomska I, Rabczyński J, Noga L, Gryboś M (2009) Expression of p53 protein phosphorylated at serine 20 and serine 392 in malignant and benign ovarian neoplasms: correlation with clinicopathological parameters of tumors. Int J Gynecol Cancer 19:1322–1328. https://doi.org/10.1111/IGC.0b013e3181b70465
40. Matsumoto M, Furihata M, Kurabayashi A, Ohtsuki Y (2004) Phosphorylation state of tumor-suppressor gene p53 product overexpressed in skin tumors. Oncol Rep 12:1039–1043. https://doi.org/10.3892/or.12.5.1039
41. Matsumoto M, Furihata M, Kurabayashi A, Sasaguri S, Araki K, Hayashi H, Ohtsuki Y (2004) Prognostic significance of serine 392 phosphorylation in overexpressed p53 protein in human esophageal squamous cell carcinoma. Oncology 67:143–150. https://doi.org/10.1159/000081001
42. Young SZ, Bordey A (2009) GABA's control of stem and cancer cell proliferation in adult neural and peripheral niches. Physiology 24:171–185. https://doi.org/10.1152/physiol.00002.2009
43. Smits A, Jin Z, Elsir T, Pedder H, Nistér M, Alafuzoff I et al (2012) GABA-A channel subunit expression in human glioma correlates with tumor histology and clinical outcome. PLoS ONE 7:e37041. https://doi.org/10.1371/journal.pone.0037041
44. Gumireddy K, Li A, Kossenkov AV, Sakurai M, Yan J, Li Y, Xu H, Wang J, Zhang PJ, Zhang L, Showe LC, Nishikura K, Huang Q (2016) The mRNA-edited form of GABRA3 suppresses GABRA3-mediated Akt activation and breast cancer metastasis. Nat Commun 7:10715. https://doi.org/10.1038/ncomms10715
45. Liu L, Yang C, Shen J, Huang L, Lin W, Tang H, Liang W, Shao W, Zhang H, He J (2016) GABRA3 promotes lymphatic metastasis in lung adenocarcinoma by mediating upregulation of matrix metalloproteinases. Oncotarget 7:32341–32350. https://doi.org/10.18632/oncotarget.8700
46. Long M, Zhan M, Xu S, Yang R, Chen W, Zhang S, Shi Y, He Q, Mohan M, Liu Q, Wang J (2017) miR-92b-3p acts as a tumor suppressor by targeting Gabra3 in pancreatic cancer. Mol Cancer 16:167. https://doi.org/10.1186/s12943-017-0723-7
47. Kale VP, Amin SG, Pandey MK (2015) Targeting ion channels for cancer therapy by repurposing the approved drugs. Biochem Biophys Acta 1848:2747–2755. https://doi.org/10.1016/j.bbamem.2015.03.0347

Affiliations

Laura Kallay[1] · Havva Keskin[1] · Alexandra Ross[1] · Manali Rupji[2] · Olivia A. Moody[3] · Xin Wang[4,5] · Guanguan Li[6] · Taukir Ahmed[6] · Farjana Rashid[6] · Michael Rajesh Stephen[6] · Kirsten A. Cottrill[7] · T. Austin Nuckols[7] · Maxwell Xu[8] · Deborah E. Martinson[2] · Frank Tranghese[9] · Yanxin Pei[10] · James M. Cook[6] · Jeanne Kowalski[2,11] · Michael D. Taylor[4,5,12] · Andrew Jenkins[13] · Daniel A. Pomeranz Krummel[1,2,16] · Soma Sengupta[1,2,14,15,16]

1 Department of Neurology, Emory University School of Medicine, Atlanta, GA, USA

2 Winship Cancer Institute, Emory University School of Medicine, Atlanta, GA, USA

3 Department of Cell Biology, Emory University School of Medicine, Atlanta, GA, USA

4 The Arthur and Sonia Labatt Brain Tumour Research Centre, The Hospital for Sick Children, Toronto, Canada

5 Developmental & Stem Cell Biology Program, The Hospital for Sick Children, Toronto, Canada

6 Department of Chemistry and Biochemistry, University of Wisconsin-Milwaukee, Milwaukee, WI, USA

7 Molecular and Systems Pharmacology Graduate Training Program, Graduate Division of Biological and Biomedical Sciences, Laney Graduate School, Emory University, Atlanta, GA, USA

8 Department of Biomedical Engineering, Johns Hopkins University, Baltimore, MD, USA

9 Electrical and Computer Engineering Department, Boston University, Boston, MA, USA

10 Center for Cancer and Immunology Research, Brain Tumor Institute, Children's National Medical Center, Washington, DC, USA

11 Department of Biostatistics & Bioinformatics, Rollins School of Public Health, Emory University, Atlanta, GA, USA

12 Division of Neurosurgery, The Hospital for Sick Children, Toronto, Canada

13 Departments of Anesthesiology & Pharmacology, Emory University School of Medicine, Atlanta, GA, USA

14 Department of Hematology & Medical Oncology, Emory University School of Medicine, Atlanta, GA, USA

15 Department of Neurosurgery, Emory University School of Medicine, Atlanta, GA, USA

16 Winship Cancer Institute, Emory University Hospital, 1365C Clifton Road, Suite C5086, Atlanta, GA, USA

Appendix XI: Additional poster presentations

1. Poster: Novel α5 selective benzodiazepine site ligands

Medical Neuroscience Cluster
IG Neuropsychopharmacology

MEDICAL UNIVERSITY OF VIENNA

Novel α5 selective benzodiazepine site ligands

[1]Sabah Rehman, [1]Roshan Puthenkalam, [1]Petra Scholze, [1]Friederike Steudle, [2]Michael M. Poe, [2]Guanguan Li, [2]James M. Cook, [3]Miroslav Savić, [3]Tamara Timić Stamenić, [4]Charles Emala, [4]George Gallos, [1]Margot Ernst

[1]Center for Brain Research, Medical University of Vienna;
[2]Department of Chemistry and Biochemistry, University of Wisconsin-Milwaukee;
[3]Faculty of Pharmacy, University of Belgrade;
[4]Department of Anesthesiology, Columbia University

Introduction

$GABA_A$ receptors are the most prominent inhibitory receptors in the CNS and belong to the superfamily of pentameric ligand-gated ion channels. These receptors are assembled from a selection of 19 subunits and the most common receptors are composed of two β, two α and one γ subunit. **The benzodiazepine binding site** is located at the interface between α1,2,3,5 and γ2 subunits.

$GABA_A$ receptors containing the **α5 subunit** are primarily distributed in the hippocampus and are associated with the regulation of learning and memory and cognitive functions. α5 selective ligands have been proposed for the treatment of schizophrenia and autism spectrum disorder (Grace et al. 2011; Nutt et al. 2013). Furthermore, α5 selective compounds also have been introduced into clinical trials for reducing cognitive disabilities in patients with Down syndrome. Interestingly, α5 containing $GABA_A$ receptors can also be found in peripheral tissue. In a recent study it was demonstrated that selective targeting of α5 containing receptors leads to relaxation of airway smooth muscle which has been proposed as a novel approach for treating asthma symptoms (Gallos et al. 2015). **Here, we present novel compounds which show improved selectivity for the α5 subtype of the benzodiazepine binding site.**

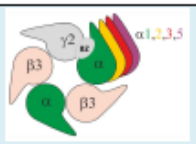

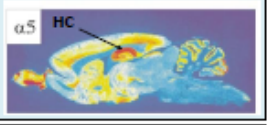

Results

1) *in vitro* results: electrophysiology data

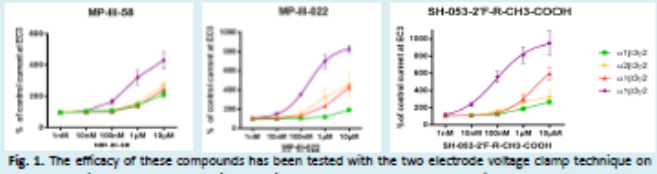

Fig. 1. The efficacy of these compounds has been tested with the two electrode voltage clamp technique on *Xenopus laevis* oocytes. Concentrations ranging from 1nM to 10μM were applied to the α1β3γ2, α2β3γ2, α3β3γ2 and α5β3γ2 subtypes. All three compounds show a high maximum efficacy (430-950%) of the α5β3γ2 receptor upon compound application, and lower EC50 (potency) for this subtype. Radioligand binding experiments revealed higher affinity for α5β3γ2 as well. Thus, the compounds are functionally and binding selective.

Methods
- Two electrode voltage clamp electrophysiology

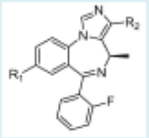

Compound	R1	R2
MP-III-004	Ethinyl-	$COOCH_3$
MP-III-022	Ethinyl-	$CONCH_3$
MP-III-058	Br	$COOCH_3$
SH-053-2'F-R-CH3-COOH	Ethinyl-	COOH

Fig.2. Table 1. Basic structure of the tested compounds.

2) *ex vivo* results: effects of α5-selective compounds on ASM

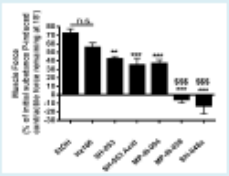

Methods
organ tissue bath experiments
- guinea pig tracheal rings suspended in physiological salt solution
- tracheal rings pre-contracted with 1 μM substance P
- 50 μM of α5 selective ligands added to the buffer to measure relaxation

Fig. 3. **Airway smooth muscle relaxation.** α5- selective compounds, the unselective SH-048a, and the α5- inactive Hz166 have been tested on pre-contracted guinea pig airway smooth muscle. The percent of the initial muscle force remaining 15 minutes after the addition of the $GABA_A$ ligands is shown. 0.1% ethanol was the vehicle for SH-053, 0.1% DMSO was vehicle for all others.

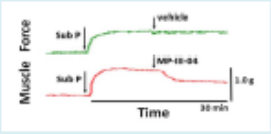

Fig. 4. Representative muscle force tracings of guinea pig trachea rings suspended in organ baths contracted with 1μM substance P (Sub P) and then treated with vehicle (0,2% ethanol) or 50 μM of the $GABA_A$ α5-selective ligand MP III 004.

Pharmacokinetic data
For the pharmacokinetic experiments, male Wistar rats were given a 10mg/kg IP dose of either MP-III-004 or MP-III-058 or MP-III-022 or SH-053-2'F-R-CH3-COOH. Plasma and brain samples were analysed after 20 min (n=3).
The results revealed that most of the α5- selective compounds are detectable in the plasma as well as in the brain. Pharmacokinetic data for SH-053-2'F-R-CH3-COOH show that this ligand is possibly not able to penetrate the blood brain barrier.

3) *in vivo* results: effects of MP-III-022 on behaviour

Treatment	Mean±SEM	N
MP-III022 10 mg/kg	180	3
MP-III022 15 mg/kg	69,09 ± 25,58	9
MP-III022 20 mg/kg	6,67 ± 4,81	3
MP-III022 15 mg/kg + XLI-093 20 mg/kg	74,61 ± 34,04	6
MP-III022 15 mg/kg + Flumazenil 15 mg/kg	175,17 ± 4,83	6

Methods
Behavioural tests:
- Rotarod test
- Morris water maze

Table 2. **Rotarod test.** Three days of rotarod training (15rpm; three daily sessions of 2 min. duration and 30 min breaks) prior to testing led to the control value of 180s in untreated selected animals. Different doses of MP III 022 (10 mg/kg, 15mg/kg, 20mg/kg) were given to animals. 10mg/kg did not have any effect on animals whereas 15mg/kg and 20mg/kg induced dose dependent incapacitation. Flumazenil inhibits the MP-III-022 induced high dose incapacitation, the α5-selective antagonist XLI-093 did not.

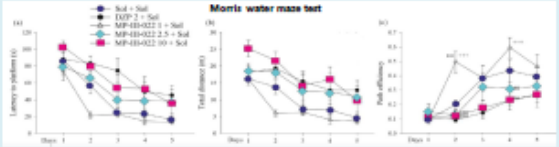

Fig. 5. Morris water maze test was conducted on 5 consecutive days. Rats received the appropriate treatment 20 min before a swimming block, each block consisted of 4 trials, lasting a maximum time of 120s, the inter-trial interval being 60s. Starting positions were determined randomly and the rats were permitted to remain on the escape platform for 15s once they found and mounted it. The results show that at the highest dose selective for α5 $GABA_A$ receptors (10 mg/kg, causing no rotarod incapacitation), MP-III-022 elicited spatial learning incapacitation indistinguishable from that induced by diazepam 2 mg/kg used as a positive control.

References

Grace et al., A novel α5GABA$_A$R-positive allosteric modulator reverses hyperactivation of the dopamine system in the MAM model of Schizophrenia. Neuropsychopharmacology (2011) 36, 1903–1911
Nutt et al., The brain GABA-benzodiazepine receptor alpha-5 subtype in autism spectrum disorder: A pilot [11C]Ro15-4513 positron emission tomography study. Neuropharmacology 68 (2013) 195e201
Rudolph and Möhler, $GABA_A$ Receptor Subtypes: Therapeutic Potential in Down syndrome, Affective Disorders, Schizophrenia, and Autism. Annu Rev Pharmacol Toxicol. 2014 ; 54: 483–507. doi:10.1146
Gallos et al., Selective targeting of the α$_5$-subunit of $GABA_A$ receptors relaxes airway smooth muscle and inhibits cellular calcium handling. Am J Physiol Lung Cell Mol Physiol 308: L931–L942, 2015

Acknowledgements
FWF project P 27746 and DK W1232

Discussion

- Novel compounds show dramatically improved selectivity for the α5-containing benzodiazepine binding site on the $GABA_A$ receptor
- MP III 058 performs best at the airway smooth muscle relaxation
- SH-053-2'F-R-CH3-COOH shows the highest selectivity for α5 and has poor brain penetration
- MP-III-022 can be used as an excellent experimental tool for investigating selective potentiation of α5- containing $GABA_A$ receptors

2. Poster: Design and synthesis of anxiolytic, anticonvulsant and antinociceptive benzodiazepine/GABA(a)ergic receptor subtype selective ligands as potential nonsedating treatment for anxiety disorders, epilepsy and pain disorders (ACS 2018)

ABSTRACT SYMPOSIUM NAME: General Poster Session (Poster)

ABSTRACT SYMPOSIUM PROGRAM AREA NAME: MEDI

CONTROL ID: 2994271

PRESENTATION TYPE: Poster Preferred : Consider for Sci-Mix

TITLE: Design and Synthesis of Anxiolytic, Anticonvulsant and Antinociceptive Benzodiazepine/GABA(A)ergic Receptor Subtype Selective Ligands as Potential Nonsedating Treatment for Anxiety Disorders, Epilepsy and Pain Disorders

AUTHORS (FIRST NAME, LAST NAME): Guanguan Li2, Jeffrey Witkin3, Jeffrey Schkeryantz3, Rok Cerne3, Jun-Xu Li4, Lakeisha Lewter4, Kevin Freeman5, Douglas Stafford2, Leggy Arnold1, James M. Cook2

INSTITUTIONS (ALL):

1. University of Wisconsin Milwaukee, Milwaukee, WI, United States.

2. Univ of Wisconsin, Milwaukee, WI, United States.

3. Eli Lilly and Company, Indianapolis, IN, United States.

4. Pharmacology and Toxicology, University at Buffalo, Buffalo, NY, United States.

5. Psychiatry and Human Behavior, University of Mississippi Medical Center, Jackson, MS, United States.

ABSTRACT BODY:

Abstract: Benzodiazepines (BZD) are a common class of psychoactive medications for the treatment of CNS disorders such as anxiety, epilepsy, neuropathic pain, schizophrenia, depression and other diseases. However, not all patients have a positive response to BZDs, as well as the presence of serious side effects including amnesia, sedation, addiction, ataxia, withdraw and drug resistance. An alpha 2/alpha 3 GABA(A)R subtype-selective ligand Hz-166 (1) was the initial lead imidazobenzodiazepine (IBZ, Zeilhofer et al.) and was found to be anxiolytic in primates (Fischer et al.), an anticonvulsant in rats and mice (Rivas et al.), antihyperalgesia in a pain model (Paul et al.) with no tolerance and less sedative or ataxia effects were observed. However, the ester moiety in 1 was metabolized very rapidly in rodents to its corresponding carboxylic acid, which did not readily pass the blood-brain barrier, which would interfere with ADME TOX in rodents. Therefore, a series of novel ester bioisosteres at C-3 in place of the labile ester group were then designed and synthesized to improve the metabolic stability and achieve enhanced pharmacological effects. Among the series of novel bioisosteres, one of the most promising ligands, a 1,3-oxazole KRM-II-81 (2), was identified as an alpha 2/alpha 3 GABA(A)R subtype-selective ligand very little or no alpha 1 nor alpha

5 efficacy. KRMII- 81 had an excellent metabolic profile in vitro in human, mice, and rat liver microsomes, as compared to the parent ligand 1. The ligand 2 exhibited an anxiolytic effect in a rat Vogel conflict test and a mouse marble-burying assay without rotorod failures. Most recently, the ligand 2 (30 micro M) significantly attenuated the firing rates in human epileptic cortical tissue on a 60 microelectrode array and has a wider margin of effect compared to motor-impairment than diazepam. Moreover, 2 reduces tactile-induced allodynia after CFA-induced pain in rats, and the behavior effects can be attenuated by the BZD receptor antagonist flumazenil. In addition, 2 did not develop tolerance to the antinociceptive effects in rats, nor decreased the respiration rate. The results here indicated that the oxazole 2 could be a potential anxiolytic, anticonvulsant and analgesic for the treatment of anxiety disorders, epilepsy and pain disorders. This work was supported by NIH grants, NS076517 and MH096463. Recent results will be presented.

(No Image Selected)

Design and Synthesis of Anxiolytic, Anticonvulsant and Antinociceptive Benzodiazepine/GABA(A)ergic Receptor Subtype Selective Ligands as Potential Nonsedating Treatment for Anxiety Disorders, Epilepsy and Pain Disorders

Guanguan Li[1], Jeffrey M. Witkin[1], Jeffrey M. Schkeryantz[1], Rok Cerne[1], Janet Fisher[2], Jun-Xu Li[3], Lakeisha Lewter[3], Kevin B. Freeman[4], Patrick Davis[4], Douglas C. Stafford[1], Leggy A. Arnold[1] and James M. Cook[1]

[1] Department of Chemistry & Biochemistry, University of Wisconsin-Milwaukee, Milwaukee, WI 53211; [2] Department of Biomedical Sciences, Pharmacology, Physiology & Neuroscience, University of South, Columbia, SC 29209; [3] Department of Pharmacology and Toxicology, University at Buffalo, Buffalo, NY 14214; [4] Department of Psychiatry and Human Behavior, University of Mississippi Medical Center, Jackson, MS 39216

Abstract

Benzodiazepines (BZD) are a common class of psychoactive medications for the treatment of CNS disorders such as anxiety, epilepsy, and sleep disorders. However, not all patients have a positive response to BZDs, as well as the presence of serious side effects including amnesia, sedation, addiction, ataxia, withdraw and dependence. An alpha 2/alpha 3 GABA(A)R subtype-selective ligand Hz-166 (**1**) was an initial lead imidazobenzodiazepine (IBZ, Zeilhofer et al.) and was found to be anxiolytic in primates (Fischer et al.), an anticonvulsant in rats and mice (Rivas et al.), antihyperalgesia in a pain model (Paul et al.) with no tolerance and no sedative or ataxia effects were observed. However, the ester moiety in **1** was metabolized very rapidly in rodents into its corresponding carboxylic acid, which did not readily pass the blood-brain barrier, which would interfere with ADME TOX studies in rodents. Therefore, a series of novel ester bioisosteres at C-3 in place of the labile ester group were then designed and synthesized to improve the metabolic stability and achieve enhanced pharmacological effects. Among the series of novel bioisosteres, one of the most promising ligands, a 1,3-oxazole KRM-II-81 (**2**), was identified as an alpha 2/alpha 3 GABA(A)R subtype-selective ligand with very little or no efficacy at alpha 1 nor alpha 5 subtypes. KRM-II-81 had an excellent metabolic profile in vitro in human, mice, and rat liver microsomes, as compared to the parent ligand **1**. The ligand **2** exhibited an anxiolytic effect in a rat Vogel conflict test and a mouse marble-burying assay without rotorod failures. Most recently, the ligand **2** (30 micro M) significantly attenuated the firing rates in human epileptic cortical tissue on a 60 microelectrode array and has a wider margin of effect compared to motor-impairment than diazepam. Moreover, **2** reduces tactile-induced allodynia after CFA-induced pain in rats, and the behavioral effects can be attenuated by the BZD receptor antagonist flumazenil. In addition, **2** did not develop tolerance to the antinociceptive effects in rats, nor decreased the respiration rate. The results here indicated that the oxazole **2** could be a potential anxiolytic, anticonvulsant and analgesic for the treatment of anxiety disorders, epilepsy and pain disorders. This work was supported by NIH grants, NS076517 and MH096463. Recent results will be presented.

GABA/BzR Chloride Ion Complex

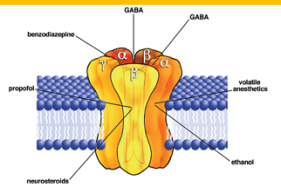

Modified form Lovinger, Comm. Networks in the *Brain, Neurons, Receptors, Neurotransmitters and Alcohol*, NIAAA Publications.

Action at $\alpha_{1\text{-}6}\beta_{2/3}\gamma_2$ $GABA_AR$ Subtypes

Subtype	Associated Effect
α1	Sedation, ataxia, anterograde amnesia, anticonvulsant action (some), and addiction
α2	Anxiolytic (very good), antinociceptive activity (very good), anticonvulsant action (some), may be hypnotic (EEG) (at higher doses), may be some muscle relaxation (at much higher doses)
α3	Anxiolytic (some), may be some muscle relaxation (at much higher doses)
α4	Diazepam-insensitive site
α5	Cognition, temporal and spatial memory
α6	Diazepam-insensitive site

Mohler, Mckernan, Walford, Rudolph, Rowlett, et al.

Synthesis of 1,3-Oxazole Bioisostere

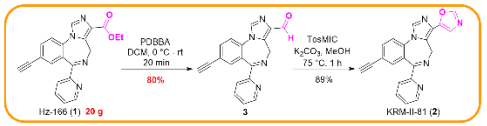

Note: $LiAlH_4$ reduction followed by treatment with activated MnO_2 provided aldehyde **3** in only 39% yield.

In Vitro Data of Compounds 1 and 2

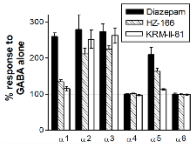

Figure 1. Average enhancement of the current evoked to GABA by 0.1 μM (α1, α2, α3, α5) or 1 μM (α4, α6) of the modulator indicated (EC_2 GABA in HEK cells). Baseline control was 100% potentiation in the presence of GABA only. It is clear diazepam is a very potent against at α1 and α5 subtypes (tolerance, addiction) while ligand **2** is not.

	Liver microsomal stability (% remaining) [a]			Cytotoxicity [b]
	Human	Mouse	Rat	LD_{50} (μM)
1	86	57	58	> 100
2	91	90	90	> 100

Table 1. Liver microsomal stability and cytotoxicity.
[a] Compounds were incubated with liver microsomes for 0.5 h, 37 °C, 4 μM:
[b] Compounds (n = 4) were incubated with HEK293T cells for 18 h followed by the quantification of viable cells.

Behavior Testing – Antinociceptive and Respiration Effect

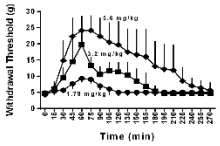

Figure 2. Ligand **2** reduces tactile-induced allodynia after complete Freund's adjuvant (CFA)-induced pain in rats in a von Frey test.

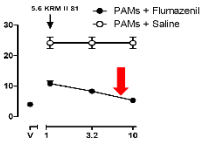

Figure 3. The behavioral effects can be completely attenuated by the benzodiazepine receptor antagonist flumazenil in a CFA-induced von Frey test.

Figure 4 **Respiration Rate**

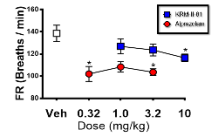

Figure 5 **Tidal Volume**

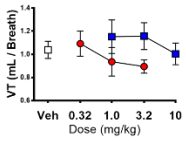

Figure 6 **Minute Volume / Kg**

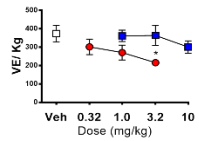

Figure 4 and 5. Traditional $GABA_A$ ligand alprazolam significantly decreased respiration rate at 0.32 mg/kg (p= 0.0060) and 3.2 mg/kg (p=0.0018). **2** significantly decreased respiration rate at 10.0 mg/kg (p=0.0361).
Figure 6. Overall oxygen consumption is significantly decreased at 3.2 mg/kg of alprazolam (p=0.0234). At the highest dose of **2**, no decrease in overall oxygen consumption is observed (p = 0.3842), which indicates no respiratory depression at the therapeutic dose (higher doses under study).

Biological Testing – Anxiolytic and Anticonvulsant Activity

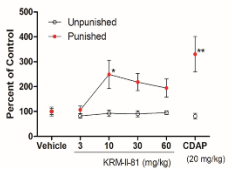

Figure 7. Vogel Conflict assay of anxiolytic -like activity. In contrast to clordiazepoxide (CDAP), **2** increased punished responding of rats (n = 6-8) without affecting un-punished responding. There was no sedation with ligand **2**.

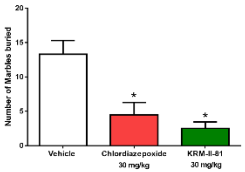

Figure 8. In marble-burying assay, both **2** and chlordiazepoxide decreased marble-burying, which elicit anxiolytic-like activity in mice. The number of marbles buried (2/3 by sawdust) is counted after 30 min.

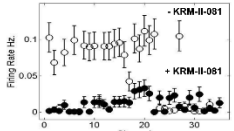

Figure 9. Resistance epilepsy tested in human epileptic cortical tissue on a 60 microelectrode array. Ligand **2** (30 μM) significantly attenuated the firing rates in the brain tissue removed from two children suffering from resistance/refractory epilepsy seizures.

Compound (i.p.)	Failures
Vehicle	0/10
Chlordiazepoxide	6/10*
KRM-II-81	0/10

Failure = 2 times falling off rotarod during 2 min test

Table 2. Rotorod screen (30 mg/kg), in contrast to chlordiazepoxide, Ligand **2** did not impair motor performance.

Assay	KRM-II-81 (2)	Diazepam
PTZ Clonus	5	1
PTZ Threshold	15	10
After-Discharge Threshold	15	1
After-Discharge Duration	15	<1
Seizure Severity	15	1
Electroshock	15	3.3

Table 3. Protective indices (PI) for **2** and diazepam.
* PI values were calculated as the minimal effective dose producing motor impairment /minimal effective doses producing efficacy. Values for HZ-166 could not be calculated for any measure due to lack of efficacy. Values of <1 are highlighted in bold. Ligand **2** has a much better therapeutic index in agreement with the efficacy in HEK cells.

Results and Conclusion

Results presented here indicate that 1,3-oxazole **2** has potential as an anxiolytic agent devoid of adverse effects, such as sedation, ataxia, amnesia, tolerance, and dependence. Consequently, it represents a unique and promising lead compound with attributes that include a desirable α2/α3-$GABA_AR$ subtype selective profile with little to no efficacy at the α1 and α5 subtypes, and an excellent pharmacokinetic and safety profile at pharmacologically relevant doses (10-100nM). The Vogel conflict assay and marble-burying assay indicated that ligand **2** exhibited an anxiolytic-like effect; **2** was active in seizure models in mice, and its protective indices were better than diazepam; antinociceptive activity was observed in the CFA-induced pain model in rats, and the effect can be attenuated by the $GABA_AR$ antagonist flumazenil. Furthermore, **2** did not develop tolerance to the antinociceptive effects in rats, nor decreased the respiration rate. All these recent data suggest that 2 can be further investigated in vivo activity in pre-clinical models of anxiety, epilepsy and neuropathic pain.

Acknowledgments

We thank the NIH (NS076517 and MH096463) for financial support. We also thank the Shimadzu Laboratory for Advanced Applied and Analytical Chemistry, and the Milwaukee Institute of Drug Discovery (MIDD) for spectroscopy.

References

1.Clayton, et al. *Curr. Med. Chem.* **2007**,*14*, 2755.
2.Poe, et al. *J. Med. Chem.* **2016**, *59*, 10800.
3.Witkin, et al. *Pharmacol. Biochem. Behav.* **2017**, *157*, 35.
4.Lewter, et al. *ACS Chem. Neurosci.*, **2017**, 8 (6), 1305.
5.Cook, et al. US Patent Appl: US 2018/0065967 A1, Pub. Date Mar. 8, 2018.
6. Witkin, et al. *Neuropharmacology*, manuscript submitted.

CURRICULUM VITAE

Guanguan Li

Place of Birth: Shanxi, China

Education

2012 – 2019 **Ph. D.** in Organic and Medicinal Chemistry
Advisor: Professor Dr. James M. Cook, FRSC,
University of Wisconsin-Milwaukee, WI, USA
Dissertation title: Design and synthesis of achiral and chiral imidazodiazepine (IMDZ) GABA(A)R subtype selective ligands for the treatment of CNS disorders, as well as asthma

2007 - 2011 **B.Sc.**, Chemistry, Xinzhou Teachers (Normal) University, China

Research Experience

2012 - 2019 Design and synthesis of benzodiazepine ligands for the treatment of CNS Disorders as well as asthma in Dr. James Cook's organic research lab, University of Wisconsin Milwaukee.

- Antidepressant drug development, in collaborating with Dr. Etienne Sibille, University of Toronto, Canada; Dr. Miroslav Savic, University of Belgrade, Serbia; Dr. Petra Scholze, Medical University of Vienna, Austria, Dr. Catherine Belzung, University of Tours, France.
- Anxiolytics research, in collaborating with Dr. Jeff Witkin, Eli Lilly and Company, USA; Dr. Junxu Li, University at Buffalo, USA.
- Asthma drug development, in collaborating with Dr. Leggy A. Arnold, UWM, USA; Dr. Charles W. Emala, Columbia University, USA.
- Alcohol abuse, in collaborating with Dr. Donna Platt, University of Mississippi Medical Center, USA.
- Medulloblastoma research, in collaborating Dr. Soma Sengupta, Emory University, USA.

2011 - 2012 Synthesize the parent compound (E)-1-(2,4-dihydroxy-5-(3-methyl butyl-2-enyl) phenyl)-3-(3,4-dihydroxyphenyl)prop-2-en-1-one isolated from Broussonetia Papyvifera and its analog research for the treatment for breast cancer, Creighton University, USA.

2009 - 2010 Purification of Chinese herbal medicine, Shanxi University.

2007 - 2011 Research of carbazoles, Xinzhou Teachers (Normal) University.

Work Experience

2018/8/15 Judge of UWM Undergraduate Research Symposium in the Department Chemistry and Biochemistry, UW-Milwaukee

2018/4/7 Event Supervisor in the Physical Science & Chemistry category, Science Olympiad

2012 – 2019 Research Assistant/Teaching Assistant, Department of Chemistry and Biochemistry, UW-Milwaukee (Courses: Chem 100: Introduction of Chemistry, Chem 104: General Chemistry and Qualitative, Chem 344: Organic Chemistry lab)

2009 - 2010 Volunteer teacher of the Aid-the-Poor Practice of Teaching Program for 6th-grade students, Donglou Elementary School, Xinzhou, Shanxi, China (Courses: Chinese, English, mathematics and physical training)

2008/8/8-24 Volunteer, Beijing 2008 Olympic Games, China

2007 - 2011 Part-time tutor for high school students, Xinzhou, Shanxi, China (Courses: English, mathematics, chemistry, and physics)

Honors / Awards

2019 Spring UWM Chemistry and Biochemistry Department Research Award

"Sosnovsky Award for Excellence in Graduate Research"

2018 Spring UWM Department of Chemistry and Biochemistry Travel Grant

2017 Spring 1st Price Winner of graduate research poster award, UWM Department of Chemistry & Biochemistry, Awards Day and Symposium, 2018

2017 Spring UWM Department of Chemistry and Biochemistry Travel Grant

2016 Spring UWM Department of Chemistry and Biochemistry Travel Grant

2016 Spring Chemistry and Biochemistry Graduate Student Council Travel Grant

2016 Spring UWM Graduate School Travel Grant

2012-2018 UWM Chancellor's Graduate Student Award (received every semester appointed as a TA from 2012-2018)

Publications

Published papers (29)

1. Prevot, T.; **Li, G**.; Cook, J. M.; Sibille, E. Insight into novel treatment for cognitive dysfunctions across disorders. *ACS Chemical Neuroscience*, **2019**, *in press*.

2. Berro, L. F.; Rüedi-Bettschen, D.; Cook, J. E.; Golani, L. K.; **Li, G.;** Jahan, R.; Rashid, F.; Cook, J. M.; Rowlett, J. K. and Platt, D. M. Role of alpha2/3 $GABA_A$ receptor subtypes in the abuse-related effects of ethanol in rhesus monkeys, *Alcoholism: Clinical and Experimental Research*, **2019**, *in press*.

3. Zahn, N. M.; Huber, A.T.; Mikulsky, B. N.; Stepanski, M. E.; Kehoe, A. S.; **Li, G.;** Schussman, M.; Roni, M. S. R.; Kodali, R.; Cook, J.M.; Stafford, D. C.; Steeber, D. A. and Arnold, L.A. MIDD0301 – A first-in-class anti-inflammatory asthma drug targets GABAA receptors without causing systemic immune suppression, *Basic & Clinical Pharmacology & Toxicology*, **2018**, *in press.*

4. Witkin, J. M.; Davis, P. G.; Freeman, K. B.; do Carmo, J. M.; Rowlett, J. K.; Methuku, K. R.; Okun, A.; Gleason, S. D.; Li, X.; Krambis, M. J.; Cerne, R.; Poe, M.; **Li, G.;** Schkeryantz, J. M.; Jahan, R.; Yang, L.; Guo, W.; Golani, L. K.; Anderson, W. H.; Catlow, J.T.; Jones, T. M.; Porreca, F; Smith, J. L.; Knopp, K. L.; and Cook, J. M.;. The 2,3-selective potentiator of $GABA_A$ receptors, KRM-II-81, is active in multiple rodent models that detect potential pain therapeutics. *Pharmacology Biochemistry and Behavior*, **2018,** *in press.*

5. Kallay, L.; Keskin, H.; Ross, A.; Rupji, M.; Moody, O. A.; Wang, X.; **Li, G.**; Ahmed, T.; Rashid, F.; Stephen, M. R.; Cottrill, K. A.; Nuckols, T. A.; Xu, M.; Martinson, D. E.; Tranghese, F.; Cook, J.M.; Pei, Y.; Kowalski, J.; Taylor, M.; Jenkins, A.; Krummel, D. A. P. and Sengupta, S. Modulating native GABAA receptors in medulloblastoma with positive allosteric benzodiazepine-derivatives induces cell death, *Neuro-Oncology*, **2018,** *in press.*

6. Neumann, E.; Rudolph, U.; Knutson, D. E.; **Li, G.**; Cook, J. M.; Hentschke, H.; Antkowiak, B.; Drexler, B., Zolpidem Activation of Alpha 1-Containing GABAA Receptors Selectively Inhibits High-Frequency Action Potential Firing of Cortical Neurons. *Front. Pharmacol.* **2019,** *9* (1523), *in press.*

7. Moerke, M. J.; **Li, G.**; Golani, L. K.; Cook, J.; Negus, S. S., Effects of the α2/α3-subtype-selective GABAA receptor positive allosteric modulator KRM-II-81 on pain-depressed behavior in rats: comparison with ketorolac and diazepam. *Behav. Pharmacol.* **2019,** *in press*.

8. Chandler, C. M.; Reeves-Darby, J.; Jones, S. A.; McDonald, J. A.; **Li, G.**; Rahman, M. T.; Cook, J. M.; Platt, D. M., a5GABAA subunit-containing receptors and sweetened alcohol cue-induced reinstatement and active sweetened alcohol self-administration in male rats. *Psychopharmacology.* **2019**, *in press.* (*Doi.org/10.1007/s00213-018-5163-6)*

9. Yocum, G. T.; Perez-Zoghbi, J. F.; Danielsson, J.; Kuforiji, A. S.; Zhang, Y.; **Li, G.**; Roni, M. S. R.; Kodali, R.; Stafford, D. C.; Arnold, L. A.; Cook, J. M.; Emala, C. W., Sr., A Novel GABAA Receptor Ligand MIDD0301 with Limited Blood-Brain Barrier Penetration Relaxes Airway Smooth Muscle Ex Vivo and In Vivo. *Am. J. Physiol. Lung Cell Mol. Physiol.* **2018**, *in press.*

10. Xu, N. Z.; Ernst, M.; Treven, M.; Cerne, R.; Wakulchik, M.; Li, X.; Jones, T. M.; Gleason, S. D.; Morrow, D.; Schkeryantz, J. M.; Rahman, M. T.; **Li, G.**; Poe, M. M.; Cook, J. M.; Witkin, J. M., Negative allosteric modulation of alpha 5-containing GABAA receptors engenders antidepressant-like effects and selectively prevents age-associated hyperactivity in tau-depositing mice. *Psychopharmacology (Berl.)* **2018,** *235* (4), 1151-1161.

11. Witkin, J. M.; Smith, J. L.; Ping, X.; Gleason, S. D.; Poe, M. M.; **Li, G.**; Jin, X.; Hobbs, J.; Schkeryantz, J. M.; McDermott, J. S.; Alatorre, A. I.; Siemian, J. N.; Cramer, J. W.; Airey, D. C.; Methuku, K. R.; Tiruveedhula, V. V. N. P. B.; Jones, T. M.; Crawford, J.; Krambis, M. J.; Fisher, J. L.; Cook, J. M.; Cerne, R., Bioisosteres of ethyl 8-ethynyl-6-(pyridin-2-yl)-4H-benzo[f]imidazo [1,5-a][1,4]diazepine-3-carboxylate (HZ-166) as novel alpha 2,3 selective potentiators of GABA(A) receptors: Improved bioavailability enhances anticonvulsant efficacy. *Neuropharmacology* **2018,** *137*, 332-343.

12. Prevot, T.; **Li, G**.; Vidojevic, A.; Santrac, A.; Misquitta, K.; Fee, C.J.; Knutson, D.; Stephen, M. R.; Kodali, R.; Zahn, N.; Arnold, A.; Scholze, P.; Fisher, J.; Banasr, M.; Cook, J. M.; Savic, M.; Sibille, E., Novel benzodiazepine-like ligands with various anxiolytic, antidepressant or pro-cognitive profiles. *Molecular Neuropsychiatry* **2018,** *in press.* (*Doi: 10.1159/000496086)*

13. Methuku, K. R.; Li, X.; Cerne, R.; Gleason, S. D.; Schkeryantz, J. M.; Tiruveedhula, V. V. N. P. B.; Golani, L. K.; **Li, G.**; Poe, M. M.; Rahman, M. T.; Cook, J. M.; Fisher, J. L.; Witkin, J. M., An antidepressant-related pharmacological signature for positive allosteric modulators of alpha 2/3-containing GABA(A) receptors. *Pharmacology Biochemistry and Behavior* **2018,** *170*, 9-13.

14. **Li, G.**; Stephen, M. R.; Kodali, R.; Zahn, N. M.; Poe, M. M.; Tiruveedhula, V. V. N. P. B.; Huber, A. T.; Schussman, M. K.; Qualmann, K.; Panhans, C. M.; Raddatz, N. J.; Baker, D. A.; Prevot, T. D.; Banasr, M.; Sibille, E.; Arnold, L. A.; Cook, J. M., Synthesis of chiral GABA(A) receptor subtype selective ligands as potential agents to treat schizophrenia as well as depression. *ARKIVOC* **2018**, 158-182.

15. **Li, G.**; Golani, L. K.; Jahan, R.; Rashid, F.; Cook, J. M., Improved Synthesis of Anxiolytic, Anticonvulsant, and Antinociceptive alpha 2/alpha 3-GABA(A)-ergic Receptor Subtype Selective Ligands as Promising Agents to Treat Anxiety, Epilepsy, and Neuropathic. *Synthesis-Stuttgart* **2018,** *50* (20), 4124-4132.

16. Forkuo, G. S.; Nieman, A. N.; Kodali, R.; Zahn, N. M.; **Li, G.**; Roni, M. S. R.; Stephen, M. R.; Harris, T. W.; Jahan, R.; Guthrie, M. L.; Yu, O. B.; Fisher, J. L.; Yocum, G. T.; Emala, C. W.; Steeber, D. A.; Stafford, D. C.; Cook, J. M.; Arnold, L. A., A Novel Orally

Available Asthma Drug Candidate That Reduces Smooth Muscle Constriction and Inflammation by Targeting GABA(A) Receptors in the Lung. *Mol. Pharm.* **2018,** *15* (5), 1766-1777.

17. Elgarf, A. A.; Siebert, D. C. B.; Steudle, F.; Draxler, A.; **Li, G.**; Huang, S. M.; Cook, J. M.; Ernst, M.; Scholze, P., Different Benzodiazepines Bind with Distinct Binding Modes to GABA(A) Receptors. *ACS Chem. Biol.* **2018,** *13* (8), 2033-2039.

18. Duke, A. N.; Meng, Z.; Platt, D. M.; Atack, J. R.; Dawson, G. R.; Reynolds, D. S.; Tiruveedhula, V. V. N. P. B.; **Li, G.**; Stephen, M. R.; Sieghart, W.; Cook, J. M.; Rowlett, J. K., Evidence That Sedative Effects of Benzodiazepines Involve Unexpected GABA_A Receptor Subtypes: Quantitative Observation Studies in Rhesus Monkeys. *J. Pharmacol. Exp. Ther.* **2018,** *366* (1), 145-157.

19. Batinic, B.; Stankovic, T.; Stephen, M. R.; Kodali, R.; Tiruveedhula, V. V.; **Li, G.**; Scholze, P.; Markovic, B. D.; Obradovic, A. L.; Ernst, M.; Cook, J. M.; Savic, M. M., Attaining in vivo selectivity of positive modulation of alpha 3 ss gamma 2 GABA(A) receptors in rats: A hard task! *Eur. Neuropsychopharmacol.* **2018,** *28* (8), 903-914.

20. Witkin, J. M.; Cerne, R.; Wakulchik, M.; S, J.; Gleason, S. D.; Jones, T. M.; **Li, G.**; Arnold, L. A.; Li, J. X.; Schkeryantz, J. M.; Methuku, K. R.; Cook, J. M.; Poe, M. M., Further evaluation of the potential anxiolytic activity of imidazo[1,5-a][1,4]diazepin agents selective for α2/3-containing GABAA receptors. *Pharmacology Biochemistry and Behavior* **2017,** *157*, 35-40.

21. Schwienteck, K. L.; **Li, G.**; Poe, M. M.; Cook, J. M.; Banks, M. L.; Stevens Negus, S., Abuse-related effects of subtype-selective GABAA receptor positive allosteric modulators in an assay of intracranial self-stimulation in rats. *Psychopharmacology (Berl.)* **2017,** *234* (14), 2091-2101.

22. Meyer, M. A. A.; Corcoran, K. A.; Chen, H. J.; Gallego, S.; **Li, G.**; Tiruveedhula, V. V.; Cook, J. M.; Radulovic, J., Neurobiological correlates of state-dependent context fear. *Learn. Mem.* **2017,** *24* (9), 385-391.

23. Kannampalli, P.; Babygirija, R.; Zhang, J.; Poe, M. M.; **Li, G.**; Cook, J. M.; Shaker, R.; Banerjee, B.; Sengupta, J. N., Neonatal bladder inflammation induces long-term visceral pain and altered responses of spinal neurons in adult rats. *Neuroscience* **2017,** *346* (Supplement C), 349-364.

24. Jahan, R.; Stephen, M. R.; Forkuo, G. S.; Kodali, R.; Guthrie, M. L.; Nieman, A. N.; Yuan, N. Y.; Zahn, N. M.; Poe, M. M.; **Li, G.**; Yu, O. B.; Yocum, G. T.; Emala, C. W.; Stafford, D. C.; Cook, J. M.; Arnold, L. A., Optimization of substituted imidazobenzodiazepines as novel asthma treatments. *Eur. J. Med. Chem.* **2017,** *126* (Supplement C), 550-560.

25. Forkuo, G. S.; Nieman, A. N.; Yuan, N. Y.; Kodali, R.; Yu, O. B.; Zahn, N. M.; Jahan, R.; **Li, G.**; Stephen, M. R.; Guthrie, M. L.; Poe, M. M.; Hartzler, B. D.; Harris, T. W.; Yocum, G. T.; Emala, C. W.; Steeber, D. A.; Stafford, D. C.; Cook, J. M.; Arnold, L. A., Alleviation

of Multiple Asthmatic Pathologic Features with Orally Available and Subtype Selective GABAA Receptor Modulators. *Mol. Pharm.* **2017,** *14* (6), 2088-2098.

26. Fischer, B. D.; Schlitt, R. J.; Hamade, B. Z.; Rehman, S.; Ernst, M.; Poe, M. M.; **Li, G.**; Kodali, R.; Arnold, L. A.; Cook, J. M., Pharmacological and antihyperalgesic properties of the novel α2/3 preferring GABAA receptor ligand MP-III-024. *Brain Res. Bull.* **2017,** *131*, 62-69.

27. Batinić, B.; Santrač, A.; Jančić, I.; **Li, G.**; Vidojević, A.; Marković, B.; Cook, J. M.; Savić, M. M., Positive modulation of α5 GABAA receptors in preadolescence prevents reduced locomotor response to amphetamine in adult female but not male rats prenatally exposed to lipopolysaccharide. *Int. J. Dev. Neurosci.* **2017,** *61*, 31-39.

28. Poe, M. M.; Methuku, K. R.; **Li, G.**; Verma, A. R.; Teske, K. A.; Stafford, D. C.; Arnold, L. A.; Cramer, J. W.; Jones, T. M.; Cerne, R.; Krambis, M. J.; Witkin, J. M.; Jambrina, E.; Rehman, S.; Ernst, M.; Cook, J. M.; Schkeryantz, J. M., Synthesis and Characterization of a Novel γ-Aminobutyric Acid Type A (GABAA) Receptor Ligand That Combines Outstanding Metabolic Stability, Pharmacokinetics, and Anxiolytic Efficacy. *J. Med. Chem.* **2016,** *59* (23), 10800-10806.

29. Forkuo, G. S.; Guthrie, M. L.; Yuan, N. Y.; Nieman, A. N.; Kodali, R.; Jahan, R.; Stephen, M. R.; Yocum, G. T.; Treven, M.; Poe, M. M.; **Li, G.**; Yu, O. B.; Hartzler, B. D.; Zahn, N. M.; Ernst, M.; Emala, C. W.; Stafford, D. C.; Cook, J. M.; Arnold, L. A., Development of GABAA Receptor Subtype-Selective Imidazobenzodiazepines as Novel Asthma Treatments. *Mol. Pharm.* **2016,** *13* (6), 2026-2038.

Submitted Papers

1. Meng, Z,; Berro, L.F.; Sawyer, E.K.; Rüedi-Bettschen, D.; Cook, J.E.; **Li, G.;** Platt, D.M.; Cook, J.M. and Rowlett, J.K. Evaluation of the anxiolytic-like, reinforcing, and sedative effects of YT-III-31, a ligand functionally selective for alpha 3 subunit-containing GABAA receptors. *Journal of Psychopharmacology,* **2019**, *submitted.*

2. Witkin, J.M.; Ping, X.; Cerne, R.; Mouser, C.; Jin, X.; Hobbs, J.; Tiruveedhula, V. V. N. P. B.; **Li, G.**; Jahan, R.; Rashid, F.; Golani, L.K.; Cook, J.M. and Smith, J.L. The value of human epileptic tissue in the discovery of novel antiepileptic drugs: The example of CERC-611 and KRM-II-81. *Brain Research,* **2019**, *submitted.*

3. Puthenkalam, R.; Treven, M.; Ramerstorfer, J.; Steudle, F.; Scholze, P.; Gallos, G.; Poe, M.M.; Methuku, K.R.; **Li, G.**; Arnold, L.A.; Seighert, W.; Santrac, Anja.; Savic, M.; Emala, C.; Cook, J.M.; Ernst, M. Benzodiazepine Ligands with Improved α5 Selectivity and Their Airway Smooth Muscle Relaxant Effect. *Mol. Pharmacology,* **2017**, *submitted.*

Manuscripts in preparation

1. **Li, G.**; Kodali, R.; Zahn, N. M; Huber, A.T.; Niemen, A. N.; Stafford, D. C.; Arnold, L. A., and Cook, J. M. Metabolism study on imidazobenzodiazepines. *Manuscript in preparation.*
2. **Li, G.**; Golani, L. K.; Jahan, R.; Knutson, D.; Witkin, J. and Cook, J. M. MP-III-080, an Alpha 2,3-selective potentiator of $GABA_A$ receptors, is Active in Epilepsy Model. *Manuscript in preparation.*
3. Nieman, A. N.; **Li, G.**; Kodali, R.; Zahn, N. M; Huber, A.T.; Mikulsky, B. N.; Stafford, D. C.; Cook, J. M. and Arnold, L. A., The capability of modulating the inflammatory response from microglia by imidazobenzodiazepines for the treatment of neuropathic pain. *Manuscript in preparation.*
4. Guerin, G.; **Li, G.;** Harold, S.; Porter, S.; Schmitz, C. D.; Cook, J.M.; Goeders, N. E. Effects of Ro5-4864 on methamphetamine self-administration in male and female rats. *Neuroscience, Manuscript in preparation.*

Patents

1. Cook, J. M.; Poe, M. M. J.; Methuku, K. R.; **Li, G.** Gabaergic ligands and their uses. PCT Patent filed on March 20,2015; application # PCTUS2016/023209; Patent: WO2016154031 A1, Sep 29, 2016; Patent Application Publication No: US20180065967 A1, Mar 8, 2018.
2. Cook, J. M.; **Li, G.**; Poe, M. M. J.; Savic, M. M.; Sibille, E. Treatment of cognitive and mood symptoms in neurodegenerative and neuropsychiatric disorders with alpha5-containing GABA receptor agonists. PCT Patent filed on March 18,2016; application # PCT/US2017/023206; Patent: WO2017161370 A1, Sep 21, 2017.
3. Arnold, A. E.; Stafford, D.; Cook, J. M.; Emala, C. W.; Forkuo, G.; Jahan, R.; Kodali, R.; **Li, G.;** Stephen, M. R. GABA(A) Receptor Modulators and Methods to Control Airway Hyperresponsiveness and Inflammation in Asthma. PCT Patent filed on August 16,2017; application # PCTUS2017/047185; Patent: WO2018035246 A1, Feb 22, 2018.
4. Cook, J. M.; Ahmed, T.; Tiruveedhula, V. V. N. P. B.; Jahan, R.; Golani, L. K.; **Li, G.;** Rashid, F.; GABA(A)ergic Subtype Selective Ligands as Anxiolytic, Antinociceptive, Anticonvulsant and Antidepressant Agents *via* Deuterium Exchange. PCT Patent filed on January 3, 2019.

Conference Paper Presentations:

1. Witkin, J. M.; Methuku, K. R.; Schkeryantz, J. M.; Gleason, S. D.; Okun, A.; Porreca, F.; Cramer, J. W.; Jones, T. M.; Catlow, J. T.; Li, X.; Poe, M. M.; **Li, G.**; Arnold, A.; Cook,

J. M., A novel, a-2, 3-selective GABAA receptor modulator with improved central penetrability and associated antiepileptic and anti-pain efficacy. *The FASEB Journal* **2016,** *30* (1 Supplement), 705.1.

2. Kallay, L.; Krummel, D. P.; Methuku, K. R.;**Li, G.**; Ross, A.; Zhang, Z.; Cook, J.; Olson, J.; Brat, D.; MacDonald, T.; Sydlik, S.; Sengupta, S., PDTB-28. Targeting medulloblastoma with benzodiazepines delivered using tunable biodegradable hydrogels. *Neuro-Oncology* **2016,** *18* (suppl_6), vi156-vi156.

3. Yocum, G. T.; Yim, P. D.; Zhang, Y.; **Li, G.**; Jahan, R.; Perez-Zoghbi, J.; Arnold, A.; Cook, J.; Stafford, D. C.; Emala, C. W., A novel GABAA receptor α5 subunit-selective allosteric modulator that does not cross the blood-brain barrier relaxes airway smooth muscle contracted with diverse ligands. In *D19. NOVEL THERAPEUTIC TARGETS IN OBSTRUCTIVE LUNG DISEASE*, American Thoracic Society: 2017; pp A7045-A7045.

4. Chandler, C.; Reeves, J.; Jones, S.; **Li, G.**; Rahman, Md; Cook, J.; Platt, D. (2017). Alpha5 gabaa receptors, a potential therapeutic target for the treatment of alcohol-related disorders: evidence from rodent studies. Alcoholism, Clinical and Experimental Research., 41, 117A.

5. Platt, D.; Ruedi-Bettschen, D.; **Li, G.**; Poe, M.; Methuku, K. R.; Cook, J.; (2017). Contribution of alpha 2/3 GABA-a receptors tothe abuse-related effects of ethanol in rhesus monkeys. Alcoholism, Clinical and Experimental Research., 41, 116A.

6. Arnold, L.; Forkuo, G.S.; Yuan, N.Y.; Kodali, R.; Yu, O.B.; Zahn, N.M.; Jahan, R.; **Li, G.;** Stephen, M.R.; Guthrie, M.; Nieman, A.N.; Poe, M.M.; Yocum, G.T.; Emala, C.W.; Stafford, D.C.; Steeber, D.A.; Cook, J.M. Development of new therapies for asthma based on compounds that specifically target GABA(A) receptors in the lung. 253rd ACS National Meeting, San Fransico, CA, April 2-6, (Abst. MEDI 19), 2017.

Posters Presented at National Meetings

1. Guerin, G.; Keller, C. M.; Harold, S.; Meaux, A.; Herndon, L.; Bjornson, K.; Li, G.; Cook, J. M.; Goeders, N. "The effects of a TSPO agonist (Ro5-4864) on cocaine and methamphetamine drug-primed and cue-reactivity in rats", Society for Neuroscience, San Diego, CA, November 3-7 (Session: Behavioral Studies of Amphetamines, (Abst. 13411), 2018.

2. Kallay, L.; Keskin, H.; Ross, A.; Moody, O.; Cottrill, K.; Nuckols, A.; Li, G.; Ahmed, T.; Rashid, F.; Stephen. M. R.; Xu, M.; Martinson, D.; Macdonald, T.; Kowalski, J.; Wang, X.; Taylor, M.; Cook, J.; Jenkins, A.; Krummel, D. P.; Sengupta, S., PDTM-45. Positive modulation of native gabaa receptors in medulloblastoma cancer cells with benzodiazepines induces rapid mitochondrial fragmentation and tp53-dependent, cell cyclin dependent apoptosis. Neuro Oncol. 2018, 20 (suppl_6), vi213.

3. Li, G.; Methuku, K. R.; Poe, M. M.; Witkin, J. M.; Schkeryantz, J. M.; Ernst, M.; Cook, J. M. "Synthesis of novel imidazobenzodiazepine oxazole bioisosteres as potential alpha 2, 3

subtype selective GABA(A) receptors agonists with excellent metabolic stability, pharmacokinetics, and anxiolytic efficacy." 253rd ACS National Meeting, San Fransico, CA, April 2-6, (Abst. MEDI 99), 2017.

4. Guthrie, M.; Li, G.; et al. "Imaging the distribution of selective GABAA receptor modulators in the asthmatic lung using MALDI assisted mass spectrometry." 253rd ACS National Meeting, San Fransico, CA, April 2-6, (Abst. ANYL 148), 2017.

5. Kallay, L.; Ross, A.; Moody, O.; Li, G.; Cook, J.; MacDonald, T.; Jenkins, A.; Krummel, D. P.; Sengupta, S., PATH-50. Understanding the mechanism of benzodiazepine mediated cell death in gabra5 overexpressing group 3 medulloblastomas. Neuro Oncol. 2017, 19 (suppl_6), vi182-vi182.

6. Li, G.; Methuku, K. R.; Poe, M. M.; Witkin, J. M.; Schkeryantz, J. M.; Ernst, M.; Cook, J. M. "Synthesis of novel imidazobenzodiazepine oxazole bioisosteres as potential alpha 2, 3 subtype selective GABA(A) receptors agonists with excellent metabolic stability, pharmacokinetics, and anxiolytic efficacy." UWM annual symposium, Milwaukee, WI, May 23, (Abst. 1), 2017.

7. Li, G.; Poe, M. M.; Raddatz, J. N.; Baker, D. A.; Ernst, M.; Cook, J. M. "potential novel targets for schizophrenia: stereospecific GABAA receptor subtype selective imidazobenzodiazepines." 251st ACS National Meeting, San Diego, CA, March 13-17, (Abst. MEDI 325), 2016.

8. Scholze, P.; Elgarf, A.; Steudle, F.; Li, G.; Cook, J.M.; Ernst, M.; "Different benzodiazepines seen to interact differently with GABAA receptors," Society for Neuroscience (2016).

9. Guerin, G.; Harold, S.; Porter, S.; Schmoutz, C.; Cook, J. M.; Li, G.; Goeders, N. "Effects of Ro5-4864 on methamphetamine self- administration in male and female rats". Society for Neuroscience (2016).

10. Rehman, S.; Puthenkalam, R.; Scholze, P.; Steudle. F.; Poe, M.; Li, G.; Cook, J. M.; Savic; M.; Stamenic, T.; Emala, C.; Gallos, G.; Ernst, M. "Novel α5 selective benzodiazepine site ligands", Medical Neuroscience Cluster, IG Neuropsychopharmacology (2016).

11. Li, G.; Methuku, K. R.; Poe, M. M.; Witkin, J. M.; Schkeryantz, J. M.; Cook, J. M. "Synthesis of Nonsedating and selective α2- or α3-GABAAR agonists as potential novel anxiolytics against neuropathic pain". 5th Annual International Chemical Biology Society Conference, Madison WI, October 24-26, (Abst. 121), 2016.

12. Rehman, S.; Puthenkalam, R.; Scholze, P.; Steudle, F.; Poe, M.; Li, G.; Cook, J. M.; Savic, M.; Stamenic, T.; Emala, C.; Gallos, G.; Ernst, M. "Novel α5 selective benzodiazepine site ligands." Austrian Society of Neurosciences Metting, Austria (2015).

Professional Affiliations

2015 - present Member of the American Chemical Society – Med. Chem. Division